European Nuclear Young Generation Forum 2021

Book of Proceedings

Tarragona, Spain 26 - 30 September 2021

Organized by Jóvenes Nucleares

The Spanish Nuclear Young Generation

ENYGF

TARRAGONA'21

APRIL 26TH - 30TH

EL SEMINARI CENTRE TARRACONENS

TARRAGONA, SPAIN

ENYGF
TGN2021

European Nuclear Young Generation Forum 2021

26th – 30th September 2021

Tarragona, Spain

Book of Proceedings

Sponsored by

ROSATOM

TECHNICAL COMMITTEE

Carlos Vázquez-Rodriguez
Technical Committee Chair
Universidad Politécnica de Madrid

Antonio Jiménez Carrascosa
Technical Program Chair
Universidad Politécnica de Madrid

Alba Valls
Hot Topic Manager and Workshops
AMPHOS 21 Consulting SL

Alex Carrasco
Hot Topic Manager
ENUSA Industrias Avanzadas S.A.

Antonella Labarille
Poster Contest Manager
Universidad Politécnica de Valencia

David Cobos
Hot Topic Manager and Workshops
AMPHOS 21 Consulting SL

Roberto García-Baonza
Hot Topic Manager
Universidad Politécnica de Madrid

Samanta Estévez-Albuja
Hot Topic Manager
Studsvik Nuclear AB

ENYGF TGN2021

This book of proceedings compiles the articles of the European Nuclear Young Generation Forum 2021. The conference organizers did not ask for any intellectual property or exclusive use of the articles include herein. The materials in the articles have been used under the responsibility of the authors.

Graphic design, layout, compilation and editing:

- Carlos Vázquez-Rodriguez - Technical Comittee Chair/ UPM Spain
- Antonio Jiménez Carrascosa - Technical Program Chair/ UPM Spain
- Samanta Estevez Albuja - Hot Topic Manager/ Studsvik Nuclear Sweden
- Luis Felipe Duran Vinuesa – Comunication Manager/ UPM Spain

ISBN-13: 978-84-09-24743-1

INDEX

Our ENYGF

For more than 20 years, the European Nuclear Young Generation Forum (ENYGF) has been seen as the main opportunity for young people to be heard on a global stage. It provides an international platform for knowledge transfer, discussion, and sharing of best practices. The 2021 event was hosted by the Spanish Young Generation Network and took place in Tarragona, a Mediterranean city full of history. Eventually, more than 150 professionals attended the physical event, whereas another 100 followed the forum from home due to the COVID19 pandemic restrictions.

The motto of the Technical Program of ENYGF21 was "*It is time to look ahead*", a claim of the vital role to play for the young generations in dealing with all the challenges that nuclear will face this decade. Indeed, the technical program was built on the basis of four "Hot Topics", issues selected by senior experts of industry and academia that will shape the future of nuclear. However, a conference welcoming all the nuclear young generations could not be limited to four topics, and thus the technical program included five additional technical tracks.

After a comprehensive reviewing process, 132 of the more than 200 submissions were accepted by the Technical Committee, and thus included in this proceedings book.

From the ENYGF Organizing Team, we hoped you enjoy this little piece of our conference.

ACKNOWLEDGEMENTS

The Conference Organizers gratefully acknowledge the efforts of the more than 50 volunteers who collaborated with the reviewing process of the articles included herein, specially to Tanja Goricanec, Yann Morvan, Ilieva Ilizástigui, John Kickhofel, and Saralyn Thomas, our outstanding technical tracks managers.

Last but not least, we are especially thankful to Alba Valls, Alex Carrasco, David Cobos, Roberto García-Baonza and Samanta-Estévez Albuja, our hot topics managers, who have helped to shape and execute all the items of the technical program.

Antonio and Charlie

ACKNOWLEDGEMENTS: REVIEWERS

Hot Topic 1 – Small Modular Reactors

Samanta Estévez-Albuja (Manager)	**Studsvik AB (Sweden)**
Assil Halimi	ENGIE (Belgium)
Ekaterina Solntceva	Rosatom (Russia)
Samantha Larriba	Universidad Politécnica de Madrid (Spain)
Florent Charvet	General Electric (France)
Ignacio Gomez	CEA (France)
Edwin Privas	Technicatome (France)
Jacob Home	UK YGN (United Kingdom)

Hot Topic 2 – Energy Transition: The Role of Nuclear

Roberto García-Baonza (Manager)	**Universidad Politécnica de Madrid (Spain)**
Laura Martín Huete	IDOM (Spain)
Azucena Bello Fernández	CNAT (Spain)
Ana González Felgueroso	Aseguradores de Riesgos Nucleares (Spain)
Clément Vincent	EDF (France)
Umar Farouk Ahmad	Centre for Renewable Energy Research (Nigeria)
Malinda Ranaweera	Sri Lanka Atomic Energy Board (Sri Lanka)
Usama Abdulkader	CEA (France)

Hot Topic 3 – Radioactive Waste: Closing the circle

Alba Valls (Manager)	**AMPHOS21 (Spain)**
David García (Manager)	**AMPHOS21 (Spain)**
Antonio Di Buono	University of Manchester (United Kingdom)
Kota Kawai	Mitsubishi Research Institute (Japan)
Elsa Lemaitre	CEA (France)
Hannah Paterson	Sellafield Ltd (United Kingdom)
Thomas Barral	Marcoule Institute for Separation Chemistry (France)
James Begg	AMPHOS21 (Spain)
Olga Riba	AMPHOS21 (Spain)
Fidel Grandia	AMPHOS21 (Spain)
Elisenda Colas	AMPHOS21 (Spain)

Marta López-García	AMPHOS21 (Spain)
James Hylko	JJE, LLC (United States)

Hot Topic 4 – Breakthroughs in Nuclear Fuel and Materials

Alejandro Carrasco (Manager)	ENUSA (Spain)
Ariel Alejandro Chavez	CNEA (Argentina)
Pau Aragón Grabiel	CIEMAT (Spain)
Xavier van Heule	University of Bristol (United Kingdom)
Tawei Lin	Studsvik AB (Sweden)
Fidelma Di Lemma	INL (US)
Allan Simpson	National Nuclear Laboratory (United Kingdom)

Technical Track 1 – Reactor physics, Thermal-hydraulics and Simulation

Tanja Goričanec (Manager)	**Jožef Stefan Institute (Slovenia)**
Luis Felipe Durán Vinuesa	Universidad Politécnica de Madrid (Spain)
Antonio Jiménez-Carrascosa	Universidad Politécnica de Madrid (Spain)
Đorđe Petrović	SCK CEN (Belgium)
Timothée Kooyman	CEA (France)
Antonella Labarile	Universitat Politècnica de València (Spain)
Alban Martinez Delcayrou	Framatome (France)
Jesús Saiz de Omeñaca Tijero	ENSA (Spain)
David Catalán	IDOM (Spain)

Technical Track 2 – Nuclear Safety and Security

Yann Morvan (Manager)	**Electricité De France (France)**
Olivier Wantz	Nuxam (Belgium)
Geoffroy Blesbois	EDF (France)
Emily Newton	University of Birmingham (United Kingdom)
Koen Vints	The Binding Energy (Belgium)
Raul Marques	Assystem (University institution : KTH / INSTN) (France)
Kevin Fernandez-Cosials	Universidad Politécnica de Madrid (Spain)
Thomas Romming	Sanmed GmbH (Germany)

Technical Track 3 – Radioactivity and Radiation Protection

Ilieva Ilizastigui (Manager)	**Nuclear Safety Division (Cuba)**
Aina Noverques Medina	Universitat Politècnica de València (Spain)
Maxime Karst	EDF/UNIE/GPEX (France)
Andrea Kozlowski	University of Strathclyde (UK)
John Lindberg	World Nuclear Association (United Kingdom)
Zamazizi Dlamini	South African Nuclear Energy Corporation (South Africa)
Prasoon Raj	Khalifa University (UAE)
Kaitlyn Gunderson-Briggs	ANSTO (Australia)
Behzad Khosrowpour	OCE (Iran)

Technical Track 4 – NPP Engineering, Operation, Maintenance and Digitalization

John Kickhofel (Manager)	**Apollo Plus GmbH (Switzerland)**
Lorenzo Michelotti	EDF (France)
Pavel Aksenov	JSC Atomproekt (Russia)
Francisco Suárez	ENEN (Belgium)
Laetitia Vernoud	Framatome (France)
Miriam Díaz Hernández	Tecnatom (Spain)
Carsten Hölderlin	TÜV SÜD Energietechnik GmbH BW (Germany)
Devanshu Jha	MVJCE (India)

Technical Track 5 – Communication, Teaching & Learning and Knowledge Management

Saralyn Thomas (Manager)	**Abbott Risk Consulting Ltd (United Kingdom)**
Rachael Clayton	IMechE, NI (United Kingdom)
Pierre Morvan	Thomas Thor Associates (The Netherlands)
Pedram Masoudi	Geovariances (France)
Paweł Gajda	AGH University of Science and Technology (Poland)
Laura Ortega	IE University (Spain)
Víctor Expósito	CIEMAT (Spain)
Abiodun Ogunbiyi	Aerospace Palace International (Nigeria)

SUMMARIES

Hot Topics were selected based on an extensive expert judgement process. Around 50 recognized experts from academia, research centers and industry have kindly provided their opinion about the topics to be addressed during the conference. European countries were well represented along the process and opinions also came from countries outside Europe. The Technical Committee was responsible for coordinating the selection process towards defining 4 Hot Topics. Experts' opinions were classified into 11 different categories and the corresponding 7 topics showing most votes were discussed by the Committee. The Hot Topics finally selected were:

Hot Topic 1 - Small Modular Reactors

The Small Modular Reactors (SMR), which includes designs producing electricity up to 300 MWe per module, can be used to generate process heat, ancillary services and work in harmony with intermittent energy sources. Among the many advantages offered by their flexibility and multiple designs they could adequately fit the needs of remote regions with less developed infrastructures. SMRs claim to offer the potential for a viable, robust, and dependable source of electric generation that can help meet the economic, energy security, and environmental goals by replacing retiring fossil fuel plants. Will SMRs be a game changer?

Hot Topic 2 - Energy Transition: The Role of Nuclear

Expanding energy access and responding to a growing energy demand is one of the most significant challenges that the world faces in this century. Simultaneously, the importance of reducing drastically the greenhouse gases emitted by the energy sector is a necessity to provide a future to the next generations. These concerns are clearly highlighted by the United Nations in the Sustainable Development Goals. Nuclear energy should be of paramount importance at least during the energy transition, tackling climate change and discarding low-carbon sources would be rowing in opposite directions. If all these arguments are supported by basic logic, what is missing for nuclear to rock n'role?

Hot Topic 3 - Radioactive Waste: Closing the Circle

Radioactive wastes have been generated by human society since the XIX century. The nature and activity level of radioactive wastes is variable depending on their origin: hospitals, universities, research centers, industry, mining, NORM, operation and decommissioning of nuclear power plants, etc. Several waste management strategies have been studied during the last 60 years to ensure the long-term protection of people and environment. Given the spectrum of wastes and strategies, joining the dots presents its challenges. Furthermore, bringing sustainability into the balance would require to manage the present without compromising the future. Can we fully close this circle?

Hot Topic 4 - Breakthroughs in Nuclear Fuel and Materials

Innovation in materials science and technology is a primary driver and basis for increasing development in nuclear energy. New insights in this field can improve safety margins, reduce costs and permit to push the current boundaries in nuclear energy production to new levels. By definition, a breakthrough is "any significant or sudden advance, development or achievement that removes a barrier to progress" which seems tailor-made for what's cooking in advanced nuclear fuels and materials nowadays.

The list of technical tracks of the conference dedicated to integrally cover all the topics related to nuclear technology were as follows:

Technical Track 1 - Reactor physics, Thermal-hydraulics and Simulation

This track covers topics related to recent developments in reactor physics, neutronics, thermal-hydraulics and multi physics coupling. Core characterization and performance for both existing reactors and advanced fission systems. Thermal-hydraulics code developments, phenomena identification, single and two phase flow heat transfer and CFD for single and multi-phase systems. Advances in computer codes, verification, validation techniques, sensitivity and uncertainty quantification and data science for numerical analysis.

Technical Track 2 - Nuclear Safety and Security

This track is focused on nuclear plants safety and security topics. Probabilistic Risk Assessments, Design Basis Accident, Beyond Design Basis Accident and mitigation, Safety Assessment and Emergency management and response. Transient and accident performance during accidental scenarios and their associated risks.

Technical Track 3 - Radioactivity and Radiation Protection

This track is focused on topics related to radioactivity and radiation protection. Dosimetry and detectors applications, radiation data science and Monte Carlo Methods and applications. Radon and thoron exposure, terrestrial and cosmic radiation, environmental measurements, protection standards and emergency action plans.

Technical Track 4 - NPP Engineering, Operation, Maintenance and Digitalization

This track covers topics related to innovative predictive maintenance methodologies and digitalization in the nuclear sector. Plant systems, structures and components reliability analyses. Operators training and control rooms issues, operational experiences, instrumentation and control, human factors and human-machine interface, major components repair and replacement and inspection techniques.

Technical Track 5 - Communication, Teaching & Learning and Knowledge Management

This track is focused on nuclear communication campaigns, social media, social acceptance and public debate as well as novelties in the training and learning fields. Current best practices in teaching and learning, innovative pedagogical approaches and methodologies, capacity building, talent developing and knowledge transfer. Networking interrelations between the nuclear stakeholders, governments and society, human resource development and best practices in knowledge transfer.

Hot Topic 1 - Small Modular Reactors

Economic and technical analysis of the non-electrical applications for a High Temperature Small Modular Reactor.
Authors: Larriba del Apio, Samantha; de Pablo, Guillermo; Jiménez, Gonzalo

Towards a NuScale BEPU analysis: numerical biases estimation and uncertainty analysis in lattice calculations.
Authors: Durán-Vinuesa, Luis-Felipe; Cuervo, Diana

The advantages of lead bismuth as a coolant for small modular reactors.
Authors: Agafonov, Denis; Talabanov, Maksim

Floating Nuclear Units: approaches to economic efficiency assessment when compared to LNG generation.
Authors: Roslaya, Mariya; Salnikova, Nadezhda; Shmelev, Igor

Assessing Small Modular Sodium-Cooled Fast Reactors characteristics for fuel cycle closure in a PWR-SMR symbiotic fleet.
Authors: Tirel, Kévin (1); Kooyman, Timothée (2); Coquelet-Pascal, Christine (2); Merle, Elsa (3)

Applicability of local heat transfer correlations for residual heat removal via loop thermosyphons in small modular reactors (SMRs).
Authors: Rincon Soto, Nelson Felipe; Ramírez Carrasco, Fernando; Buck, Michael; Starflinger, Jörg

Case-study analysis of the potential for implementation of a small modular reactor in spain.
Authors: Martín Huete, Laura (1); González Navarro, Miguel Ángel (2); Suárez Ortiz, Francisco (3)

Application of digital twin technology in the calculation justification of SMR.
Authors: Zotova, Maria; Zotov, Igor; Ushatikov, Anton; Bolnov, Vladimir

Small Modular Reactor for Small NPP.
Authors: Krapivin, Anton (1); Kukhtevich, Daria (2)

Innovating UK Nuclear to support Net Zero by 2050.
Authors: Ray, Daisy; Home, Jacob

Improving the physical characteristics of the fast-neutron SMR by using Radiogenic Lead.
Authors: Sufiyarov, Ildar

The specific aspects of the New Generation SMLWRs taking into account EUR requirements.
Authors: Simonov, Pavel E. (1); Chetverikov, Alexander E. (1); Soldatov, Alexey I. (2)

Boron dilution sequence analysis in NuScale SMR using TRACE.
Authors: Sanchez Torrijos, Jorge; Queral, César

Main control room staffing of small modular reactors: analysis and validation.
Authors: Hervas, Borja

Proceedings of the European Nuclear Young Generation Forum
ENYGF'21
September 27-30, 2021, Tarragona, Spain

Economic and technical analysis of the non-electrical applications for a High Temperature Small Modular Reactor

Larriba, Samantha[1*]; de Pablo, Guillermo[1] and Jimenez, Gonzalo[1]

[1] Universidad Politécnica de Madrid (UPM), Spain

*Corresponding author: *samantha.larriba@upm.es*

I. INTRODUCTION

Small modular nuclear reactors (SMRs) are getting attractive for several reasons, and everything seems to indicate that they could be a good alternative to traditional nuclear reactors. Several studies [1] highlight different advantages, among them: its cheaper initial investment compared with bigger nuclear plants; its flexible capacity to increase the number of reactors to get more power, with an easily depreciation thanks to the possibility of escalate the investment; its factory construction, which impacts in the cost; the option of building these reactors in isolated areas without expensive infrastructure works; and its improves in safety systems, usually passive systems. Despite its cheaper initial investment, they have a more expensive unit cost of generation in comparison with common NPP. Furthermore, SMRs represent a good alternative for industrial applications that require high temperatures [2]. These non-electrical applications range from district heating to the production of green hydrogen.

The non-electrical applications depend on the temperature that the reactor could achieve. Light water reactors (LWR) could be used to give support for district heating or desalination. However, others industrial applications for petrochemical industry or hydrogen production need higher outer reactor temperatures, which correspond better with the Generation IV reactors temperatures range, thanks to the use of different coolers with better thermal properties and/or higher outlet temperatures during full power

So far, the projects based on nuclear cogeneration have covered the possibility of employ different types of non-electrical applications. Some studies [3] have presented the theoretical bases for analysed which applications could be more profitable considering the technology and the type of nuclear reactor.

District heating or desalination are the technologies with the most experience in nuclear cogeneration [3]. This is explained because these two applications need a lower temperature, which could be supply by LWR (the most extended reactors type in the actual world), as mentioned earlier. China, Russia, and Canada are the states with most accumulated experience in these uses.

Canada has been studied the cogeneration for the ACR-700 reactor [4], in particular, for hydrogen production and oil refining. On the other hand, China is interested in the applications of Very High Temperature Reactor to reduce the price of the oil industry [4].

High Temperature Gas Reactors could produce methanol reducing the CO2 emissions usually associated to this process [5]. United States of America, Japan and South Korea have been working in this possibility, and in bioethanol production by biomass using the vapor of a nuclear power plant [5]. The last application needs a high mass rate vapor, but less temperature.

A Very High Temperature Reactor design has been selected for this study because of its extensive operative experience, its technological improvements in safety, and the high temperatures reached, which allows a wide range of applications, including hydrogen production. Furthermore, the use of helium as a coolant enables more electrical efficiency and reduces the cost for the plant.

This study looks for improve gas cycles, in a Generation IV SMR, with the goal of compare the plant efficiency for each application and the cost (or benefit) of implement these technologies.

With all these characteristics, Gas Turbine High Temperature Reactor 300 (GTHTR300) [6] is the ultimate choice for this study. It is a reactor developed by JAERI (Japan Atomic Energy Research Institute), which is cooled by helium and moderated by graphite. In addition, its safety systems are passive. Its Brayton cycle is analysed with the EES ((Engineering Equation Solver) software. This study takes into account the utilization of the residual heat for some applications and several modifications on the original cycle for the purpose of adapt it for the high temperature applications. Also, the economic impacts could be calculated considering the electricity prices or the selling price of the final product.

II. NON-ELECTRICAL APLICATIONS STUDY

In this section, different cogeneration alternatives are described and analysed. Due to the limited extension for this paper, only the most representative processes are selected.

A. District heating and sanitary hot water

The non-electrical application for nuclear power plants which accumulate the most years of operative experience is district heating or sanitary hot water. For GTHTR3000, several studies have been done to assess the viability of this application [7]. The conclusion was that the GTHTR3000 could be used in this application if the reactor only proportionate electricity and low pressure and temperature steam for cogeneration, with an efficiency of 81.8%.

An interesting alternative is the simultaneous production of low pressure (and temperature) and high pressure (and temperature) steam for two different applications. This could be the case for a reactor cycle which produces steam for district heating and electricity generation and hydrogen. The hydrogen production will be described later in the paper. The conclusions drawn from this analysis indicate that while the highest efficiency is reached when more steam is dedicated to high pressure applications. This give us the possibility to change production of electricity with the goal of proportionate more district heat is the winter or more hydrogen (for example) in summer or when the electricity demand is cover by other energy sources cheaper, as renewables.

B. Desalination

Another non-electrical application with a high experience for nuclear power plants is desalination [4]. In the case of LWRs, the necessary temperature for doing the process involve a reduction of electricity generation. However, for gas reactors, the higher temperature at the turbine outlet allows to couple a desalination plant without an electricity generation reduction.

For the GTHTR300, the called "Multi-Stage Flash distillation" (MSF) have been selected for its high performance and operative experience in comparative with others desalination technologies. Usually, only the first phase receive heat, but GTHTR300 have enough residual heat for contributing to all the phases. This allows convert 9.85 $\frac{m^3_{water}}{MW_{th}}$, with an efficiency of the 88 % in the desalination process. In addition, the performance of the cycle improves until 72.61% if we consider a maximum temperature for the MSF process of 110 ºC and a minimum temperature of the 50 ºC, to do the process viable.

Just like in the district heating, simultaneous production of low pressure (and temperature) and high pressure (and temperature) steam for two different applications is considered. For this case, it is found that the efficiency increases with respect to install only a cogeneration for hydrogen. However, the performance with respect to install only a desalination plan decreases the efficiency. This fact raises the next question: which are the scenarios when it will be cost-effective? For this case, the previous scenario, it was not need low pressure applications during one season, can not be considered (because the water is necessary all time). If we know the price of buying and selling of the desalination water and the hydrogen prices, the cost of MW_{th} could be calculated. Thanks to this, we know that the higher benefits are obtained implementing these two non-electrics applications, and the lower benefits are obtained if the nuclear power plant only produces electricity.

C. Oil refining

The oil refining industry demands high amount of electricity and heat [8]. For this study, the called "Steam Assisted Gravity Drainage" (SAGD) process have been chosen. This application has a steam demand between 6 to 9 MPa and 275 to 310 ºC depending on the land type. These conditions could be obtained installing an intermediate heat exchanger.

Knowing that GTHTR300 reactor produces 600 MWth and the minimum temperature for turbine entry is 730ºC, this reactor could contribute with 386 MWth to SAGD process. To calculate the bitumen extracted with these capacities, a SOR value must be considered [8]. The SOR is the ratio of conversion of steam to bitumen, and usually is between 2 and 4. Witch all this dates, a maximum and minimum bitumen extracted is calculated for different conditions Table 1.

Table 1: Bitumen extracted for different conditions

QIHX	T2	Steam conditions	Steam produced	Bitumen removed SOR=2	Bitumen removed SOR=4
170 MWt	850°C	310 °C y 9 MPa	17824 bbl/day	8912 bbl/day	4456 bbl/day
170 MWt	850°C	310 °C y 6 MPa	29619 bbl/day	14809 bbl/day	7404 bbl/day
386 MWt	730°C	310 °C y 9 MPa	40447 bbl/day	20224 bbl/day	10112 bbl/day
386 MWt	730°C	310 °C y 6 MPa	67250 bbl/day	33635 bbl/day	16813 bbl/day

In another scenario, the steam production for more common necessities in this industry could be calculated. The Table 2 shows the conditions (temperature and pressure) and its corresponding steam production [9].

Table 2: Steam production for different conditions

Oil refining demanding	Conditions	Production
Very high-pressure steam	500 °C y 11 MPa	179 $\frac{T}{h}$
High-pressure steam	450°C y 4,8 MPa	181 $\frac{T}{h}$
Medium-pressure steam	350 °C y 3,6 MPa	194 $\frac{T}{h}$
Low-pressure steam	280 °C y 1 MPa	200 $\frac{T}{h}$

In the last scenario, a plan of ethylene production and refinery are simulated for the same reactor [10]. The plant chosen needs 10 $\frac{MT_{oil}}{year}$ and 1 $\frac{MT_{ethylene}}{year}$. For ethylene production, a high-pressure steam is needed, while for refined a medium- and high-pressure steam is required. It is concluded that 564.2 $\frac{T}{h}$ high-pressure steam and 22.4 $\frac{T}{h}$ medium-pressure steam is demanded by this plant. Only one unit of GTHTR300 could not produce this amount of steam,

and therefore is conclude that 4 reactors, which would generate 832 MW_e, are needed for this specific application.

D. Hydrogen production

Regarding to hydrogen production, we may be considered the concept of green hydrogen and the first step is to identify its true meaning [11]. Some different definitions could be foundin the literature, and there appears to be an agreement with the idea that hydrogen produced from renewable energy technology is considered green hydrogen. But, what about the hydrogen from nuclear reactors? There is no consensus about how to categorise it. In literature, sometimes nuclear-produced hydrogen is called “clean”, “blue” and, also “green”. In fact, this green adjective always refers to the same idea: carbon-emissions free. Hence, green hydrogen is made with free CO_2 emission sources and that is the case for the nuclear power.

A good question at this point is which the optimal hydrogen production technology is [12]. The first step is identifying the demands for different processes. For example, some processes only need heat, but others require electricity, such as electrolysis. Before defining these methods, it is important to know that although Steam Methane Reforming is the most extended hydrogen production technology, it has been discarded as green hydrogen because of its greenhouse gas emissions, although it is included in the study for comparison purposes. However, the technologies based on water electrolysis, thermomechanical water splitting, or hybrid water splitting have some processes with enough commercial development to be considered as a good option. For instance, this is the case of the alkaline electrolysis or the sulfur-iodine cycle (S-I).

For the sulfur-iodine cycle (S-I), three different cases are compared [13]. First, a GTHTR300 which only produces electricity. Second, a reactor unit of GTHTR300 which supplies 170 MW_{th} for hydrogen production. And the last one, like the previous one but with 370 MWth for S-I cycle. This allows the study (Figure 1) of the relation between hydrogen production in m^3/h and electricity production in MW_e considering a outer reactor temperature of 900ºC, a 55% of efficiency and a 250 MJ for each kilogram of hydrogen. The orange vertical lines represent the three scenarios described (in order).

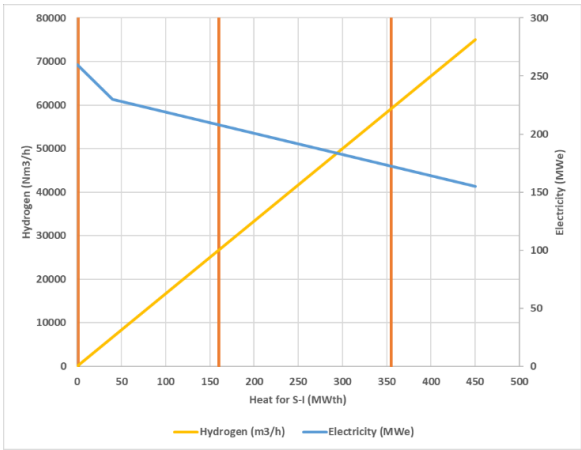

Figure 1: Relation between hydrogen production and electricity production for S-I cycle

The electrolysis is also considerer, and It is found that due to the high electricity demands of this process the efficiency is lower than another cogeneration process [14], this has a small CO2 footprint. The electrolysis process is considered for temperatures between 400 and 1000 ℃, but for the future comparisons the temperature in the heat exchanger is assumed as 900 ℃. The efficiency increases with higher hydrogen production, but this is limited because of the minimum operate capacity of the turbine, meaning it is not possible to reduce too much the steam temperature at the inlet of the turbine. This cycle has a high impact in the electricity lead to the grid, which involves a high price of hydrogen production than other technologies.

As mentioned earlier, Steam Methane Reforming is considered [15] with the goal of compare the cost-efficiency with the previous process. Beside the use of a gas-powered boiler, the employ of a nuclear power plant for the process significantly reduces the CO_2 emissions with the consequence of reduce the efficiency to, which goes from 85% to 78%. Even then, the efficiency is higher than S-I process, however the goal of reduce the CO_2 emissions involve that the costs are not the enough competitive for a free emissions market.

Meanwhile, the cost of implement these technologies must be analysed too. To get a good understanding of the real costs, some variables have been analysed, such as the time of depreciation of the nuclear reactor and the hydrogen production plant, the electricity prices or hydrogen market prize. Considering the above, in the Figure 2 different profits are compared according to hydrogen production. Benefits for GTHTR300 if only electricity is produced is represented, considering an electricity price of 0.037 $/kWh [16] and a hydrogen sell price of 3 $/(kg_(H_2))[17], which is the minimum considerer.

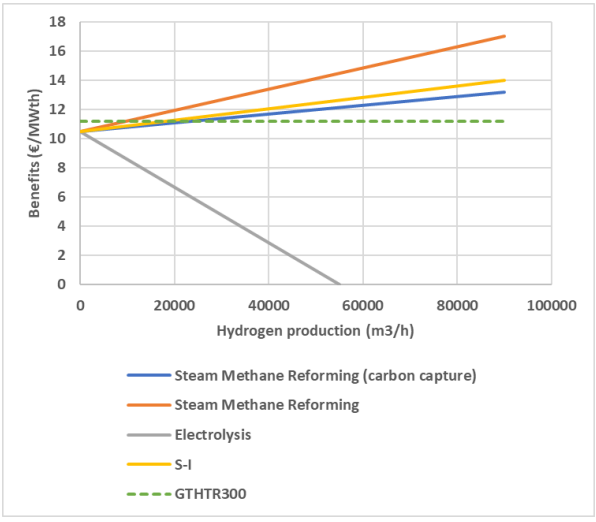

Figure 2: Economics profits for hydrogen production with different technologies

The comparison concludes that the most cost-effective is the Steam Methane Reforming, which produce the higher financial incomes as the hydrogen production is increasing. The reason behind it is that it allows more electricity production for the same hydrogen production because its heat demand is lower. Both processes are cost effective as of approximately 1800 $\frac{m^3_{H_2}}{h}$, comparing with GTHTR300 if

only electricity is produced. However, electrolysis is not cost-effective for the hydrogen price considerer. This process could be profitable if the hydrogen price is the maximum in the literature ($10\ \frac{\$}{kg_{H_2}}$).

III. CONCLUSIONS

GTHTR300 SMR nuclear reactor is designed to work with temperatures between 950 to 730 ºC to turbine inlet, maintaining a temperature of 950ºC in reactor outlet. Thanks to this capacity, all the cogeneration models raised in this study are possible.

For low pressure applications, we only found a improve of the efficiency, but the real interesting scenario is when two applications are included. This allows to improve the efficiency and to adapt the different products to the necessities. For oil refining industries a CO_2 reduction is possible, adding to the electricity demand (and cost) reduction.

In addition, although green hydrogen could be produced by nuclear reactors, Steam Methane Reforming still is the most cost-effective method. However, S-I is competitive with Steam Methane Reforming technology if it is considered that S-I is CO_2 free. Indeed, the benefit is higher even than Steam Methane Reforming with carbon capture, which be a more sustainable process.

IV. Acknowledgements

This work was partly granted by the "Programa Propio UPM" of the Universidad Politécnica de Madrid.

V. References

[1] R. Rosner y S. Goldberg, «Small Modular Reactors – Key to Future Nuclear Power Generation in the U.S.1,2», p. 81.

[2] IAEA, «Advanced in Small Modular Reactor Design and Technology Development». 2018.

[3] IAEA, «Industrial Applications of Nuclear Energy». 2017.

[4] International Conference on Non-electric Applications of Nuclear Power, Ed., *Non-electric applications of nuclear power: seawater desalination, hydrogen production and other industrial applications*. Vienna: International Atomic Energy Agency, 2009.

[5] R. Candeli, E. Arndt, y H. Barnert, «Status of the high-temperature reactor (HTR) — applications», *Nucl. Eng. Des.*, vol. 121, n.º 2, pp. 249-258, jul. 1990, doi: 10.1016/0029-5493(90)90110-J.

[6] X. L. Yan *et al.*, «GTHTR300 cost reduction through design upgrade and cogeneration», *Nucl. Eng. Des.*, vol. 306, pp. 215-220, sep. 2016, doi: 10.1016/j.nucengdes.2016.02.023.

[7] S. Kasahara *et al.*, «Heat transport analysis in a district heating system applying waste heat from GTHTR300, a commercial design of high-temperature gas-cooled reactor», *Mech. Eng. J.*, vol. 3, n.º 3, pp. 15-00616-15-00616, 2016, doi: 10.1299/mej.15-00616.

[8] Finan, Ashley E., «Integration of Nuclear Energy Into Oil Sands Projects», *J. Eng. Gas Turbines Power*, p. 8.

[9] D. H. Salimy y National Nuclear Energy Agency, «Application of High Temperature Nuclear Reactor for Petrochemical Industry», *Int. J. Eng. Res.*, vol. V7, n.º 10, p. IJERTV7IS100102, dic. 2018, doi: 10.17577/IJERTV7IS100102.

[10] C. Fang, «Process heat applications of HTR-PM600 in Chinese petrochemical industry: Preliminary study of adaptability and economy», *Ann. Nucl. Energy*, p. 6, 2017.

[11] A. Velazquez Abad y P. E. Dodds, «Green hydrogen characterisation initiatives: Definitions, standards, guarantees of origin, and challenges», *Energy Policy*, vol. 138, p. 111300, mar. 2020, doi: 10.1016/j.enpol.2020.111300.

[12] R. Pinsky, P. Sabharwall, J. Hartvigsen, y J. O'Brien, «Comparative review of hydrogen production technologies for nuclear hybrid energy systems», *Prog. Nucl. Energy*, vol. 123, p. 103317, may 2020, doi: 10.1016/j.pnucene.2020.103317.

[13] S. Kubo *et al.*, «A pilot test plan of the thermochemical water-splitting iodine–sulfur process», *Nucl. Eng. Des.*, vol. 233, n.º 1-3, pp. 355-362, oct. 2004, doi: 10.1016/j.nucengdes.2004.08.018.

[14] Kazuhiko Kunitomi, «JAEA'S VHTR FOR HYDROGEN AND ELECTRICITY COGENERATION GTHTR300C». 2007.

[15] Department of Advanced Nuclear Heat Technology, Japan Atomic Energy Research Institute, «PRESENT STATUS OF JAERI'S R&D ON HYDROGEN PRODUCTION SYSTEMS IN HTGR.» 2000.

[16] X. Yan, K. Kunitomi, T. Nakata, y S. Shiozawa, «GTHTR300 design and development», *Nucl. Eng. Des.*, vol. 222, n.º 2-3, pp. 247-262, jun. 2003, doi: 10.1016/S0029-5493(03)00030-X.

[17] P. Nikolaidis y A. Poullikkas, «A comparative overview of hydrogen production processes», *Renew. Sustain. Energy Rev.*, vol. 67, pp. 597-611, ene. 2017, doi: 10.1016/j.rser.2016.09.044.

.

Proceedings of the European Nuclear Young Generation Forum
ENYGF'21
September 27-30, 2021, Tarragona, Spain

Towards a NuScale BEPU analysis: numerical biases estimation and uncertainty analysis in lattice calculations

Duran-Vinuesa, L.*, Cuervo, D.

Universidad Politécnica de Madrid (UPM), Spain

*Corresponding author: *luisfelipe.duran@upm.es*

I. INTRODUCTION

Small Modular Reactors (SMR) appear on the scene to solve many problems that the nuclear industry is facing now, such as the capitalised cost reduction and the Levelized Cost of Energy to compete with other energy sources and secure low-carbon energy supply. SMR's overall make an impact on the reduction of the capitalised costs, easing financing. In this context, SMRs designs translate the traditional design of water-cooled reactors to their small size "equivalents" (i.e., NuScale, BWRX-300, and VK-300) and bring other innovative designs: high-temperature gas-cooled reactors, fast neutron spectrum reactors, molten salt reactors, among other [1]. The NuScale Power Module (NPM) is one of the most promising SMR designs. It has become the first SMR design receiving approval from the USNRC in August 2020 because of its PWR proven design, with other European countries investigating a NuScale SMR fleet deployment during the upcoming years. With this business forecast, there's a high interest in testing and validating the traditional simulation tools for the SMR safety analysis.

Research on the NuScale first core has been focused on the equilibrium cycle design [2, 3] and burn-up analysis [4]. In addition, the capabilities of system codes to address the SMR accident analysis are being tested in the frame of the McSafer EU project and similar research for reactivity-initiated accidents in the SMART SMR design [5, 6]. UPM work on core simulation includes a multi-physics, multi-scale core simulation platform that relies on the standard two-step approach: fuel assembly cross-section preparation (lattice calculation) and entire core coupled modelling (core simulation). The UPM platform is applied to the NPM core design and reactivity-initiated accident analysis using a Best Estimate Plus Uncertainty (BEPU) approach to the deterministic safety analysis, currently under deployment.

The BEPU analysis comprises BE and PU parts: code-to-code verification and numerical bias insights are investigated in the companion of an uncertainty analysis that consists of uncertainty quantification and sensitivity analysis. This work performs the fuel assembly cross-sections preparation, verification, and uncertainty analysis through the lattice calculation step necessary to address the NPM safety analysis adequately.

II. UPM SIMULATION PLATFORM

The UPM simulation platform relies on the standard two-step approach to the reactor core analysis. First, a lattice calculation solves the 2D neutron transport equation for each fuel assembly in the core. This step keeps the neutron flux energy and spatial dependencies and the resonance self-shielding effect to obtain accurate homogenised and two-group collapsed cross-sections at pin-by-pin resolution. The second step performs the full core 3D coupled simulation through the diffusion code using the cross-sections, accounting for the thermal-hydraulic feedback. The UPM simulation platform is shown in Figure 1.

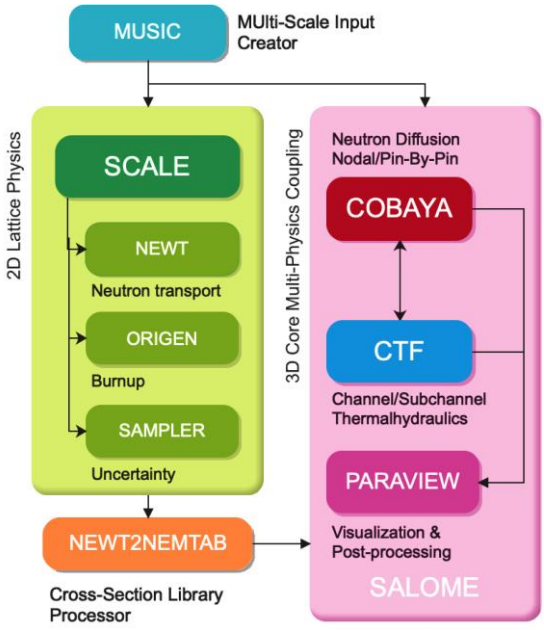

Figure 1. UPM core simulation platform: codes and tools.

- **COBAYA** is the UPM multi-group neutron diffusion code to solve the reactor domain at nodal scale based on the Analytic Coarse-Mesh Finite-Difference (ACMFD) method and pin-by-pin resolution with the Fine-Mesh Finite-Difference (FMFD) solver.

- **SCALE** [7] codes system to perform lattice calculations. NEWT is used for 2D transport solutions, ORIGEN for inventory calculations in the TRITON sequence for reactor burn-up, and finally, the SAMPLER module for uncertainty propagation.
- **CTF** [8] solves the thermal-hydraulic subchannel approach to the Navier-Stokes equations for the entire reactor at subchannel and fuel assembly scales, providing thermal-hydraulic feedback to COBAYA.
- **SALOME** environment [9] is used to couple COBAYA and CTF through external coupling with the Operator Splitting coupling scheme.
- **MUSIC** (MUlti-Scale Input Creator) is an in-home python tool to generate coherent multi-scale SCALE, COBAYA, and CTF inputs. MUSIC deals with the consistent uncertainty propagation in multi-physics avoiding user effect by automatisation.
- **NEWT2NEMTAB** is an in-home tool developed to generate cross-sections NEMTAB-like format libraries from SCALE outputs suitable for COBAYA.

III. FUEL ASSEMBLY MODELS

The NPM core consists of 37 fuel assemblies based on an array of 17 x 17 fuel rods. Fuel assembly data is shown in Table 2, available in the NuScale Standard Plant Design Certification Application [10]. Fuel rod arrangements are shown in Figure 2. This work reproduces the geometry and compositions used in references [2-3]. Therefore, materials' density and fuel assembly compositions are shown in Table 3 and Figure 3 accordingly.

The "out-in" loading pattern is optimised to reduce uranium enrichment and Gd_2O_3 burnable poison load, following the loading pattern depicted in Figure 3.

Table 2. Fuel assembly geometry design and HFP avg. conditions

Parameter	Value	Parameter	Value
Assembly pitch	215.036 mm	Pin pitch	12.598 mm
Height	2435.6 mm	Active Height	2000 mm
Pellet diameter	8.1153 mm	Relative density	96 %
Cladding ID	8.2804 mm	Cladding OD	9.4996 mm
Guide tube ID	10.0838 mm	Guide tube OD	12.2428 mm
Fuel temp.	700 K	Mod. Temp.	531.5 K
Mod. density	0.7529 g/cm^3	Boron conc.	0 ppm

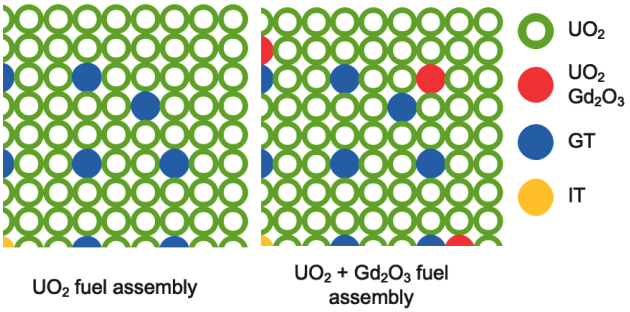

Figure 2. Quarter fuel assembly array with/without Gd pins.

Table 3. Materials Density

Element(s)	Material	Density
Fuel rods	UO_2	10.257 g/cm^3
Gd fuel rods	UO_2 + Gd_2O_3	10.111 g/cm^3
Fuel cladding	M5-alloy	6.500 g/cm^3
Guide tube	Zircaloy-4	6.560 g/cm^3

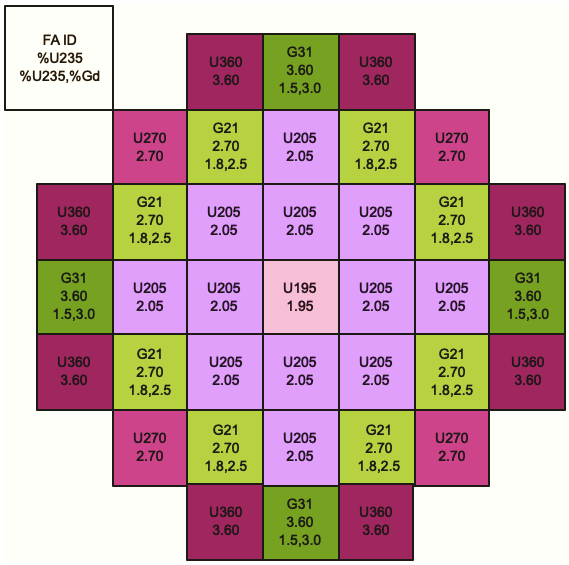

Figure 3. Core loading pattern "out-in".

IV. VERIFICATION AND UNCERTAINTY ANALYSIS METHODS

This work performs a code-to-code model verification for an initial boron-free hot full power state with no Xe equilibrium and numerical bias quantification. In addition, the effective multiplication factor (k_{eff}) is analysed in the lattice calculation phase for each fuel assembly type.

NEWT results are compared with continuous energy (CE) Serpent [11] and 252-group Polaris [3] codes using infinite lattice cell calculation using ENDF/B VII.1 library. The principal codes characteristics are shown in Table 4.

Table 4. Characteristics of the codes used for verification

	Serpent	Polaris	NEWT
Library processing code	NJOY	AMPX	AMPX
Library	ENDFB VII.1	ENDFB VII.1	ENDFB VII.1
Code type	Stochastic	Deterministic	Deterministic
Energy disc.	CE	252 MG	252/56 MG
Transport solution method	Monte-Carlo	2D Method of Characteristics	2D Discrete ordinates S_N
Self-shielding model	-	ESSM	CENTRM 2D MOC & 1D S_N
XS preparation	-	Nodal	Nodal/PBP

Uncertainties are propagated through the stochastic uncertainty propagation technique: PDFs are sampled to create NEWT inputs. Sample size 146 were chosen to comply with the two-sided 95/95 interval statistical conditions [12]. The output uncertainty is quantified using the 95/95 tolerance regions based on Wilks' theory [13] and the standard deviation. The sensitivity analysis is based on Spearman's Rank Correlation Coefficient (SRCC) to measure the strength and direction of association input/output within an interval [-1, 1].

Input manufacturing uncertainties are taken from the NuScale subchannel analysis methodology [14] and the OECD/NEA Uncertainty Analysis in Modelling Benchmark [18] in the form of probability density functions (PDFs). These uncertainties are shown in Table 5 in terms of their nominal values and ranges or standard deviations. Nuclear data uncertainties have been taken from the ENDF/B-VII.1 library through precomputed microscopic cross-section perturbation factors with SCALE SAMPLER. Nuclear data and manufacturing uncertainties are propagated through the lattice calculation phase. Both perturbation types must coincide for all fuel assembly types in each perturbation to guarantee a coherent uncertainty propagation.

Table 5. Manufacturing uncertainties PDFs

Geometry	PDF	Nominal	Range/Std.Dev.
Assembly pitch [a]	Uniform	215.0364mm	± 0.127 mm
Pin pitch [a]	Uniform	12.5984 mm	± 0.0508 mm
Pellet diameter [b]	Normal	8.1153 mm	± 0.0083 mm
Fuel cladding OD [a]	Uniform	9.4995 mm	± 0.0508 mm
Fuel cladding thk. [b]	Normal	0.6096 mm	1.37 %
Guide tube OD [a]	Uniform	12.2428 mm	± 0.0508 mm
Guide tube thk. [b]	Normal	1.0795 mm	± 0.0083 mm
Composition	**PDF**	**Parameters**	**Values**
Enrichment [b]	Normal	-	0.001
Fuel density [b]	Normal	96 %	0.50

[a] *NuScale subchannel analysis methodology uncertainties* [14].

[b] *Uncertainty in Analysis and Modelling Phase II-1 (Case 2a)* [15].

V. RESULTS AND CONCLUSIONS

Results demonstrate the NEWT employed modelling options are consistent with a non-calibrated model, and the uncertainty analysis with the developed tools to investigate the inputs' uncertainty contribution to k_{eff} uncertainty.

A. Pin-cell discretisation error

When building the NEWT transport input, the user can choose the mesh resolution for each fuel pin, in other words, the number of divisions of each pin domain (see Figure 4). The pin-cell mesh analysis has been carried out to quantify the discretisation bias from the coarsest mesh (2x2) to the most refined mesh (36x36), where the asymptotical k_{eff} value is reached. Figure 4 shows k_{eff} deviation from its asymptotical value is defined as follows:

$$k_{eff}^{dev} = \left(k_{eff}^{X} - k_{eff}^{36x36}\right) \cdot 10^5 \ [pcm]$$

Resolutions greater than 12x12 limit the discretisation bias under 20 pcm to save computational effort, from 37.5 h (36x36) to 8.5 h (12x12) in CPU time for 252 energy groups. It is remarkable the time-saving at 56 groups, from 37.5 h to 11.4 h, and from 8.5 h to 1.7 h, accordingly with identical convergence ratios.

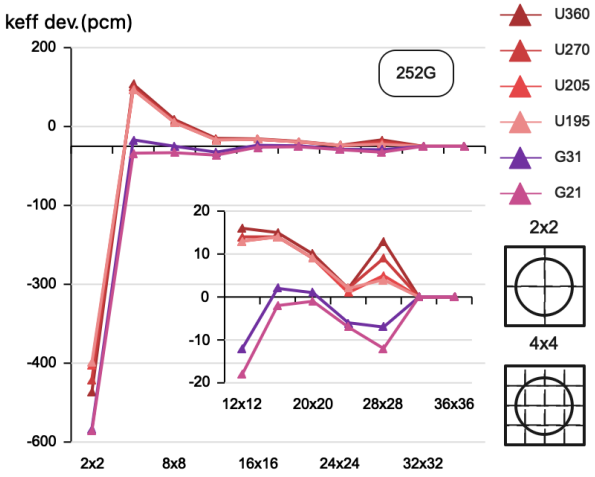

Figure 4. k-eff deviation from its asymptotic value (36x36).

B. Code-to-code comparison

The asymptotic k_{eff} results for a 36x36 pin lattice are used to compare NEWT, Polaris, and Serpent k_{eff} values in Figure 5 to remove the discretisation error from the comparison. The k_{eff} differences are defined as:

$$\Delta k_{eff} = \left(k_{eff}^{X} - k_{eff}^{serpent}\right) \cdot 10^5 \ [pcm]$$

Differences versus Serpent are a few hundred pcm. Gd cases show differences up to 332 pcm underestimation. The differences can be explained by nuclear data processing codes, multi-group approximation (and self-shielding models), deterministic transport method, and user effect.

The observed differences are likely caused by user effect, considering Polaris and Serpent models, equivalent and negligible user-effect differences. The k_{eff} differences mean around 30 ppm of boron concentration.

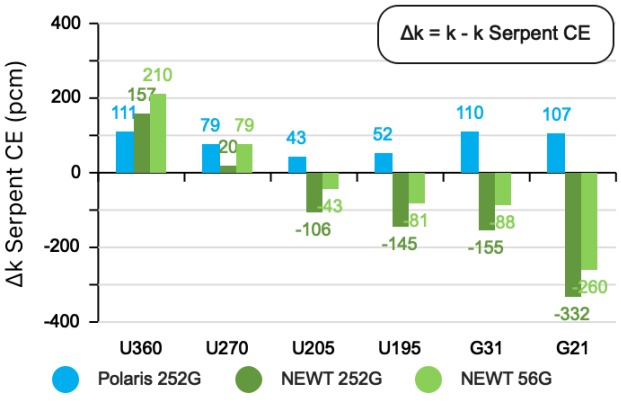

Figure 5. k-eff differences vs Serpent CE solution.

C. Multi-group approach and number of groups

Direct comparison between NEWT and Serpent results doesn't allow a quantification of the multi-group approach bias because of the number of intermediate approaches and steps that haven't been analysed separately. However, differences between NEWT 252 and 56 groups have been quantified in Figure 6 by direct comparison between equivalent calculations in 252 and 56 energy groups.

The 56 groups library systematically overestimate k_{eff} about 60 pcm (around 6 boron ppm) respect the 252 groups solution preserving the same bias direction. This fact explains the 56-group simulation's better results for U205, U195, G31, and G21 fuel assembly types because of the fortunate error cancellation. The 56 groups calculation saves up to 5 times of CPU time that could improve the fuel assembly lattice calculation when the other intermediate approaches underestimate the k_{eff} calculation.

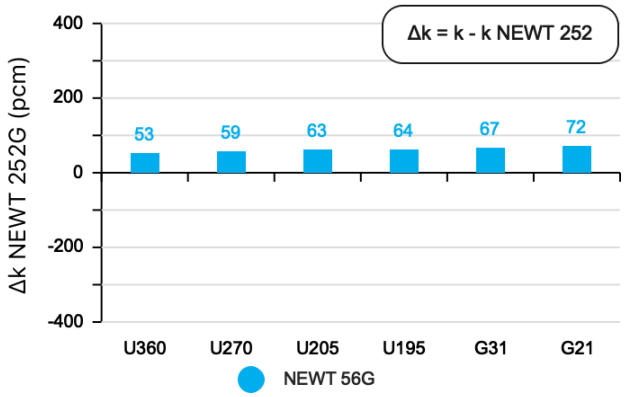

Figure 6. k-eff differences in the 252 to 56 MG NEWT solution.

D. Uncertainty analysis

Uncertainty quantification has been performed with a 16x16 pin-cell resolution and 56 energy groups to optimise the computational effort reducing biases. Results show **Δ**k-eff $^{95/95}$ tolerance intervals are about 3600 pcm and a standard deviation of 750 pcm in Figure 10, more significant than the 20 pcm discretisation bias. Although uncertainty ranges are more critical than code biases, it is a priority to reduce as many as possible biases that must be considered in the BEPU analysis as they still affect the safety limits.

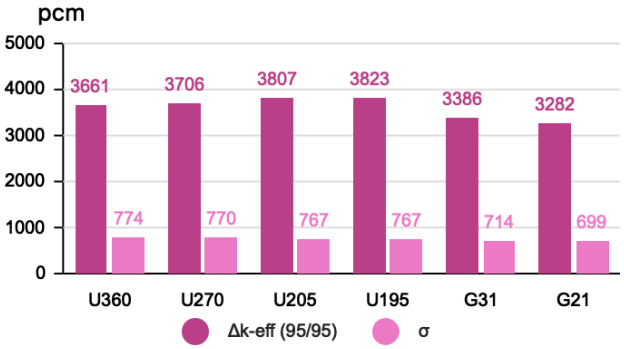

Figure 10. k-eff tolerance region and population standard deviation.

A separate effects analysis has been performed to quantify the sensitivity to manufacturing uncertainties through the reactivity differences defined as follows:

$$\rho = \frac{k_{eff}-1}{k_{eff}} \cdot 10^5\ [pcm];\quad \Delta\rho = \rho^* - \rho_0\ [pcm]$$

The most sensitive parameter is the cladding thickness around 100 pcm per standard deviation with a slight dependence on the composition (see Figure 11). Sensitivity to assembly pitch and guide tube geometry is the lowest regardless of the composition. k_{eff} shows no sensitivity to the pin pitch when the 2D MOC self-shielding method is used, but sensitivity up to 15 pcm appears with the 1D SN method for the poisoned assemblies.

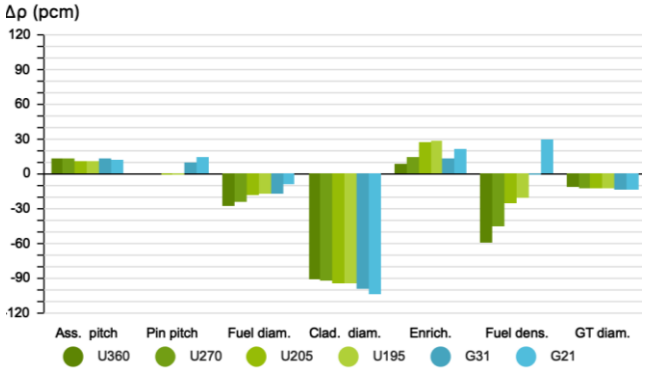

Figure 11. Different reactivity sensitivity to manufacturing tolerances.

Last, a local sensitivity analysis with the SRCC infers the contributions to k_{eff} uncertainty in the presence of nuclear data uncertainty contribution in Figure 12. Manufacturing uncertainties show a "very weak" correlation (less than 0.2) with a negligible contribution to the k_{eff} uncertainty. The only manufacturing parameter indicating a "weak" correlation coefficient is the cladding diameter. Based on the results shown in this section and Subsection V-D, one can conclude that k_{eff} uncertainty is mainly explained by the lack of knowledge on nuclear data.

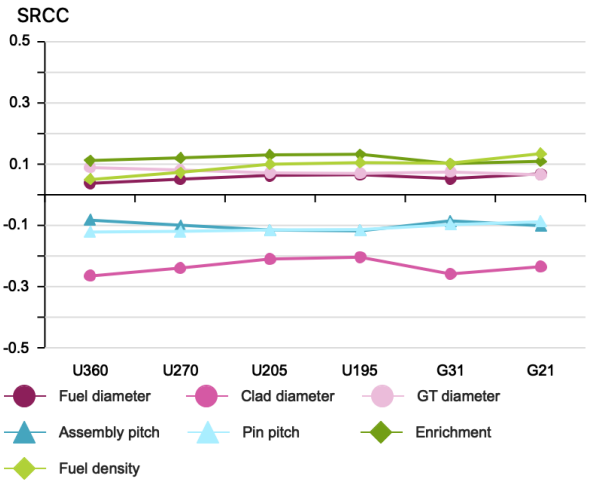

Figure 12. Sensitivity analysis with nuclear data uncertainty.

VI. CONCLUSIONS

UQ and a preliminary numerical bias assessment have been carried out as a first step to the whole NPM core simulation. These analyses are focused on the lattice calculation phase and include a lot of information and data to continue the BEPU analysis of the NPM core.

The discretisation bias analysis reflects that a 16x16 pin-cell resolution limits the fuel assembly k_{eff} bias under 20 pcm with computational effort savings around 400% in CPU time. Numerical discretisation could be used for model calibration to compensate for other bias sources. However, further research on the effect over other parameters such as power distribution or delayed neutron fraction should be investigated.

A systematic bias from the ENDF/B-VII.1 library in 56 energy groups has been estimated around 60 pcm of k-effective overestimation respect the 252 groups solution. This overestimation cancels the deterministic transport bias improving the results with a computational time saving up to 5 times. Better results can be obtained with 16x16 pin-cell discretisation and the 56 energy group libraries.

UQ with k-effective 95/95 tolerance interval throws 3600 pcm of uncertainty with 760 pcm of standard deviation, covering the differences between NEWT and Serpent results produced by user effect. It is also necessary to undertake the Monte-Carlo (KENO) simulation of the model used in this work to perform a deeper bias analysis in future research. Furthermore, the full reactor simulation will suffer from biases coming from the reflector modelling, the operation history effect, and the fuel assembly neighbourhood, as the cross-sections were prepared with infinite lattice calculation.

The reactivity sensitivity analysis to the manufacturing uncertainties revealed that in the presence of nuclear data uncertainty. The only visible effect is the outer cladding diameter sensitivity. The under-moderated nature of the system explains this fact: as that the moderator -to-fuel ratio decreases with larger cladding diameter, k_{eff} drops.

Finally, the analysis with KENO would be necessary to make a rigorous analysis of the code biases to generate a solid base to perform code-to-code verification, addressing the NEWT and multi-group biases properly, and going deeper into the different bias sources and their quantities for the sake of the whole core BEPU analysis optimization.

VII. ACKNOWLEDGEMENTS

The author thanks the Programa Propio of the Universidad Politécnica de Madrid for the funding without which this work would not have been possible.

VIII. REFERENCES

[1] IAEA, *Advances in Small Modular Reactors and Technology Developments*. Austria: IAEA, 2020.

[2] M. Hines, M. Underwood, A. Naylor, M. Burrell, L. Clowers, y K. Knecht, «Equilibrium Core Design of a NuScale Designed Small Modular Reactor Using CASL's Virtual Environment for Reactor Applications (VERA)», University of Tennesse, Knoxville, 2019.

[3] P. Suk, O. Chvála, G. I. Maldonado, y J. Frýbort, «Simulation of a NuScale core design with the CASL VERA code», *Nuclear Engineering and Design*, vol. 371, p. 110956, ene. 2021, doi: 10.1016/j.nucengdes.2020.110956.

[4] A. Sadegh-Noedoost, F. Faghihi, A. Fakhraei, y M. Amin-Mozafari, «Investigations of the fresh-core cycle-length and the average fuel depletion analysis of the NuScale core», *Annals of Nuclear Energy*, vol. 136, p. 106995, feb. 2020, doi: 10.1016/j.anucene.2019.106995.

[5] R. Akbari-Jeyhouni, D. Rezaei Ochbelagh, y A. Gharib, «Assessment of an integral small modular reactor during rod ejection accident using DRAGON/PARCS codes», *Progress in Nuclear Energy*, vol. 108, pp. 136-143, sep. 2018, doi: 10.1016/j.pnucene.2018.05.010.

[6] A. Pourrostam, S. Talebi, y O. Safarzadeh, «Core analysis of accident tolerant fuel cladding for SMART reactor under normal operation and rod ejection accident using DRAGON and PARCS», *Nuclear Engineering and Technology*, vol. 53, n.º 3, pp. 741-751, mar. 2021, doi: 10.1016/j.net.2020.08.025.

[7] B. T. Rearden y M. A. Jessee, *SCALE Code System, Version 6.2.3*. Oak Ridge, Tennessee: Oak Ridge National Laboratory, 2018.

[8] R. Salko y M. Avramova, *CTF Theory Manual*. 2015.

[9] A. Ribes y C. Caremoli, «Salome platform component model for numerical simulation», en *31st Annual International Computer Software and Applications Conference - Vol. 2 - (COMPSAC 2007)*, Beijing, China, jul. 2007, pp. 553-564. doi: 10.1109/COMPSAC.2007.185.

[10] NuScale LLC., *NuScale Standard Plant Design Certification Application. Chapter 4. Reactor*. 2019.

[11] J. Leppänen, M. Pusa, T. Viitanen, V. Valtavirta, y T. Kaltiaisenaho, «The Serpent Monte Carlo Code: Status, Development and Applications in 2013», en *SNA + MC 2013 - Joint International Conference on Supercomputing in Nuclear Applications + Monte Carlo*, Paris, France, 2014, p. 06021. doi: 10.1051/snamc/201406021.

[12] I. Hong, D. Oh, y I. Kim, «Generic application of Wilks' tolerance limit evaluation approach to nuclear safety», Barcelona, 2013, pp. 16-25.

[13] S. Wilks, «Determination of Sample Sizes for Setting Tolerance Limits», *The Annals of Mathematical Statistics*, vol. 12, n.º 1, pp. 91-96, 1941, doi: 10.1214/aoms/1177731788.

[14] «NuScale Power, LLC Submittal of "Subchannel Analysis Methodology," TR-0915-17564, Revision 2.», p. 143.

[15] J. Hou *et al.*, «Benchmarks for Uncertainty Analysis in Modelling (UAM) for Design, Operation and Safety Analysis of LWRs. Volume II: Specification and Support Data for the Core Cases (Phase II)», *Nuclear Science. NEA/NSC/DOC(2014)*, pp. 100-102, 2017.

Proceedings of the European Nuclear Young Generation Forum
ENYGF'21
September 27-30, 2021, Tarragona, Spain

The Advantages of Lead Bismuth as a Coolant for Small Modular Reactors

Agafonov Denis[1*], Talabanov Maksim[1]

[1] Rosatom Technical Academy, Russian Federation;

*Corresponding author: *DNAgafonov@rosatomtech.ru*

I. INTRODUCTION

Currently, the idea of usage of small modular reactors (SMR) in remote areas to supply power and heat is becoming popular. Moreover, such type of reactor can be used by countries located near the sea for water desalination. Obviously, the scope of SMR application is wide nevertheless may be increased if liquid metals will be implemented as coolant. This new feature allows applying the reactor in the regions with a lack of the fresh water and in the areas with a negative average annual temperature. The secondary circuit coolant is considered the natural air.

This paper considers a design of a small nuclear power plant including the reactor facility with a heavy liquid-metal coolant lead-bismuth, which advantages are low pressure (due to the fact that the Pb-Bi has a very high boiling temperature the primary circuit pressure can be almost atmospheric) in the primary circuit and zero change in volume during passing the melting point. Nuclear power plant with such characteristics keeps operational capacity during the outage even the temperature drops below zero. As far as refueling is concerned fuel refreshment is envisioned after no less 10 years. It provides for the delivery of ready-made modules to the nuclear power plant site as result the reduction of the construction and installation work. Technologies applied in the plant allows to reduce the number and the qualification of the personnel to the extent does not influence the safety. These technologies are following:

- applying of referenced or scaled with small coefficients of design and circuit-technological solutions, proven by the operating experience of the submarine reactor plants and other reactor facilities;
- use of referenced operating parameters for the primary and secondary circuits;
- the reactor mono unit with a safety casing is placed in the water tank of the passive heat removal system (PHRS), which also serves as an earthquake-resistant support structure. The rest of the reactor equipment is located above the PHRS tank and is closed from above by a sealed steel shell;
- a double-circuit heat removal scheme and a steam generator with multiple natural water circulation along the evaporator circuit are used;
- the natural circulation of coolants, sufficient to cool down the reactor without dangerous overheating of the core in the heat-removing circuits of the reactor mono unit is provided;
- the main components of the reactor mono unit and the reactor installation are constructed in the form of separate modules, while providing the possibility of their replacement and repair

The considered reactor facility as a part of the described above nuclear power plant is close in a scale to the submarines' reactor plants with lead-bismuth coolant such as Russian designed SVBR. For that reason, a conservative approach was used to choose the design and arrangement of that type of reactor, as a result, it considerably reduces technical and financial risks, error likelihood, volume, cost, and time for R&D being performed.

The paper considers the possibility of realizing the critical state of the reactor plant with a lead-bismuth coolant of 8 MW thermal power as well as it also gives calculations of the initial reactivity margin and the change in the isotopic composition of the fuel during burnup. The fuel is uranium dioxide (UO_2).

Three versions of the geometric design of the core were calculated during the survey. The initial parameters for calculation are:

- the reactor has a fast neutron spectrum,
- type of fuel is uranium dioxide UO_2
- required campaign is ten years.

The survey's main results show that for all three versions of the core geometry design as well as the fuel volume fractions, coolant and structural materials both in its composition and in the composition of physical zones adjacent to it (reflectors, protective shields, fuel rods, etc.) achieving of the criticality by this reactor is theoretically possible. In addition, initial margin sufficient to compensate reduction of reactivity through a campaign is able to realized [1].

II. MODELING

The reactor neutronics was calculated using the REACTOR-GP software package with the BNAB-93 system of 26-group constants [2].

The REACTOR-GP package is intended for calculating a reactor during a campaign in a multi-group diffusion approximation, in two-dimensional cylindrical (R-Z) and three-dimensional hexagonal (HEX-Z) geometries (including those with an arbitrarily distributed external source).

The REACTOR-GP code was developed by the employees of the Keldysh Institute of Applied Mathematics (Russian Academy of Sciences) in cooperation with State Scientific Centre of the Russian Federation – Leypunsky Institute for Physics and Power Engineering, Joint-Stock Company (IPPE JSC). The code is intended to diffusion calculation of a fast reactor for each fuel-element during a campaign with a system of multi-group constants BNAB-93 [2] and a constant preparation system CONSYST. At IPPE JSC, the REACTOR-GP code has been operating since 2001 as a working tool for calculating the design neutronics of fast reactors cooled with a lead-bismuth coolant and operating without partial refueling.

Immediately prior to carrying out the neutronics calculation, it is necessary to perform the procedure for calculating the nuclear and physical composition of all physical zones of the reactor, modeled in the software package, and to homogenize all materials that make up the reactor core.

The homogenization procedure was carried out by the mixing method. This technique makes it possible to obtain sufficiently correct data for performing the neutron and physics calculation with a fast spectrum in the core.

In Figure 1 a diagram of the homogenized zones and their sizes are shown, the volume fractions of the materials of the physical zones are presented, and the nuclear concentrations of the main nuclides are shown. The zone number on figure 1 corresponds to the zone number in the corresponding table 1.

The active zone is a cylinder. The fuel assembly consists of 198 fuel elements, the diameter of the fuel element is 12 mm, the diameter of the fuel pellet is 10.9 mm, the diameter of the inner hole is 1.9 mm, and the lattice spacing of the fuel elements is 13.6 mm.

The calculations were carried out with three versions for the core size represented in table 2.

In all calculations and geometric designs of the core, the fuel was uranium dioxide UO_2, the coolant was the eutectic lead-bismuth Pb-Bi alloy, and the fuel element cladding was stainless steel.

Further, the results of calculations on campaign duration and changes of isotope composition in the core during burnup follow. As shown in table 2 the calculations were performed with three versions of core size (0.5 m, 0.6 m, 0.7 m) in constant height. When diameter was 0.5 m the calculation was performed with one profiling zone on enrichment and 25 zones on burnup, when diameter was 0.6 m – 1 zone on enrichment and 100 zones on burnup, when diameter was 0.7 m – 3 profiling zones on enrichment and 100 zones on burnup.

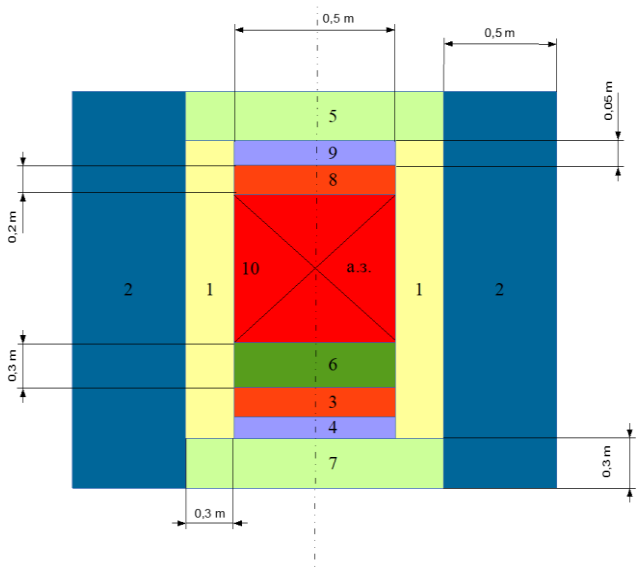

Figure 1. Diagram of homogenized physical zones.

Table 1. Types of homogenized zones.

Zone's number	Name
1	Steel side reflector
2	Side protective shield
3	Bottom reflector in the fuel element
4	Bottom grids
5	Upper coolant chamber
6	Compensation volume (without accounting gas volume fraction)
7	Filter and inlet chamber
8	Upper reflector in the fuel element
9	Upper grids
10	Core (without the gas gap)

Table 2. Types of homogenized cores.

Height H, m	Diameter D, m	Ratio H/D
0.5	0.5	1
0.5	0.6	0.833
0.5	0.7	0.714

The calculation was performed in 10 steps with duration of one year. There was a condition that duration of the campaign is not less than 10 years. In turn, each step of calculation was divided into 5 micro steps. The computational time for each micro step was 4 seconds. Thus the total computational time was about 3 minutes and 20 seconds using the two-dimensional cylindrical geometry for calculation.

In each three cases with the different geometry the average enrichment was increased through the core to achieve the necessary reactivity margin with accounting burnup during the reactor operation which parameters can be found in table 3. The initial reactivity margin was estimated as 42, 38 and 34 β for the core with a diameter of 0.5, 0.6 and 0.7 respectively.

Table 3. Enrichment with accounting margin on burnup.

Height H, m	Enrichment on U-235, %
0.5	83.5
0.6	61.5
0.7	48.0

Table 4 reflects the change in K_{eff} during the reactor operation.

Table 4. Change of K_{eff} during the campaign

Time, years	K_{eff} (D=0.5 m)	K_{eff} (D=0.6 m)	K_{eff} (D=0.7 m)
1	1.369	1.318	1.278
2	1.337	1.285	1.239
3	1.300	1.255	1.196
4	1.263	1.220	1.159
5	1.224	1.179	1.134
6	1.177	1.144	1.114
7	1.138	1.105	1.082
8	1.092	1.072	1.055
9	1.047	1.039	1.033
10	1.009	1.008	1.008

In the calculation of the campaign and the change of the isotope content during the burnup with a core diameter 0.7 m, the core is split into 100 zones on burnup and 3 profiling zones on enrichment. All three enrichment zones have the same geometry size. Enrichment on U-235 in the central zone – 38%, in the intermediate zone – 48%, in the peripheral one – 58%. Hence, the average enrichment through the core is 48%.

The profiling on enrichment is carried out to flat the power density field and to get the aceptable value of radial peaking factor Kr which is necessary for the safe operation of the reactor plant.

III. CONCLUSIONS

The paper presents the results of a neutronics calculation of the reactor plant with a lead-bismuth coolant, considered as part of small nuclear power plant. The calculation is performed using the design code REACTOR-GP. The purpose of the calculation was to obtain a reactor characteristic as effective neutron multiplication factor, as well as to calculate the campaign and the initial reactivity margin for fuel burnup. The work was carried out with three versions of the core geometry, namely, diameters of 0.5 m, 0.6 m and 0.7 m, and a constant height of 0.5 m. Fuel type - uranium dioxide UO_2.

The calculation results showed that in all three versions of the core geometric design with the assumed volume fractions of fuel, coolant and structural materials both in its composition and in the composition of physical zones adjacent to it (reflectors, protective shields, fuel rods, etc.) the critical state is theoretically achievable and initial margin sufficient to compensate reduction of reactivity through a campaign is able to realized. The campaign has a duration of at least 10 years. The sensitivity analysis by increasing the thermal power is an ongoing work at this moment.

In order for the reactor to operate through the campaign with 10-year duration, the average enrichment on U-235 in the core shall be at least:

- 83.5% when diameter of the core is 0.5 m

- 61.5% when diameter of the core is 0.6 m

- 48.0% when diameter of the core is 0.7 m

With a core diameter of 0.7 m, enrichment profiling was performed. The core had three enrichment zones, the average enrichment trough the core was 48%.

Nevertheless, such high fuel enrichment in the core is not acceptable in the case of commercial use of this type of reactor plant and a small nuclear power plant as a whole. The compensation of such high reactivity margin is a separate additional task.

Therefore, at this moment, it is planned to develop the concept of a reactor with a lead-bismuth coolant using a hydride-zirconium moderator in order to soften the neutron spectrum to thermal or intermediate one and, accordingly, reduce the fuel enrichment to values below 20%. This type of moderator has been successfully tested in aircraft reactors, in particular, satellites.

Reduction of the fuel enrichment in U-235 in the core will satisfy the IAEA's nonproliferation requirement and allow to consider this concept of a small nuclear power plant and a reactor plant in its composition from the point of view of the prospects for commercial use both in Russia and abroad.

IV. References

[1] D.N. Agafonov, G.I. Toshinskii “The concept of using the nuclear reactor with a lead-bismuth coolant as an equipment of an ultra-small power NPP “Arktika-M,” Academic science: problems and achievements, North Charleston, SC, USA, May 15-16, 2017, vol. 1, p.134.

[2] M.N. Nikolaev, G.N. Manturov, A.M. Tsibulia, “BNAB-93 group constants system. Part 1: neutron and photon nuclear constants”, Nuclear science and technics issues, vol. 1, no. 1, 1996

Proceedings of the European Nuclear Young Generation Forum
ENYGF'21
September 27-30, 2021, Tarragona, Spain

Floating Nuclear Power Units: Approaches to Economic Efficiency Assessment When Compared to LNG Generation

Roslaya, Mariya[1*], Shmelev, Igor[1] and Salnikova, Nadezhda[1]

[1] JSC "Afrikantov OKBM", Russia

*Corresponding author: *roslaiamk@okbm.nnov.ru*

I. INTRODUCTION

Today our civilization depends on electric power generation. The need for affordable and clean energy is one of the goals aimed at transforming our world that was adopted by all United Nations (UN) Member States in 2015 as part of the 2030 Agenda for Sustainable Development, which sets out a 15-year plan to achieve them[1]. To date, there has been some progress in many aspects of the plan, but the actions aimed at implementing the Goals and targets have not yet reached the necessary pace and scale. In terms of power industry in particular, a sustainable electricity supply is needed to promote a higher standard of living. A flexible and load-following energy source with reduced construction period than that of a large power plant is needed to develop areas remote from the central power grids; and sometimes it is preferable when such an energy source is transportable.

This trend does not signify the end of the large-scale projects' era; they still have their target sector. At the same time, in response to the challenges of the present, the topic of small power plants, in particular, small modular nuclear power units (SMRs), is currently being actively discussed by the global community. Despite the existing interest, especially among the developing countries, there are difficulties in launching such projects. The issues of SMR economic competitiveness are of primary concern for the customers, although the safety assessment of new technologies is not less important and SMRs have a system solution regarding the available reference experience in the operation of such systems [2].

As for the SMRs the economy of scale is a basic factor that influences negatively the levelized cost of electricity (LCOE). Nevertheless the full one-time costs per unit for SMRs are expected to be lower than for the large NPPs. i.e., in the long term it can be cheaper to build one SMR unit and, if necessary, to build another one or more than to spend a large sum at once on a large NPP because of the exchange rate fluctuations and SMR equipment series production.. Moreover, the phased construction allows for a kind of partial self-financing based on the profits received from the sale of electricity generated by the existing power units.

Floating power units round the world predominantly run on petroleum products and liquefied natural gas (LNG). Given the trend of tightening hydrocarbon emission limits in the shipping sector, LNG energy sources are covering a growing number of countries.

With regard to floating nuclear power units, the ROSATOM's first-of-a-kind nuclear floating power unit (FPU) *Akademik Lomonosov* has been successfully operating in the north of Russia since 2020.

The purpose of this article is to analyze the economic efficiency and competitiveness of the nuclear power generation as compared to the LNG energy sources.

The article proposes to consider:

- advantages and applications of floating power units;
- ROSATOM's nuclear floating power units and parameters of competitor designs that apply LNG;
- approaches to the cost-effectiveness analysis and justification of competitive advantages of nuclear power generation over gas power generation;
- analysis results of competitive ability and prospects for further development of the floating power units.

II. Advantages and applications of floating power units

At the moment there are more than 75 floating co-generation units around the world, and as it has already been mentioned above, most of those units use petroleum products or LNG for power generation.

Floating units are designed for niche markets in order to meet the need for flexible power generation for a wide range of users in the following conditions:

- as an alternative to construction of stationary generating capacities unmarketable after completion of the energy-consuming activities;

- power supply at a competitive price for the territories with a weak power supply system or the territories where the construction of conventional large-sized nuclear plants (such as hydroelectric power plants, co-generation plants, etc.) is impossible;
- power supply for remote territories and industrial facilities that have to use autonomous power generation.

From an economic perspective there is also potential interest in floating power units on isolated islands and in small settlements not connected to the central power system, in densely populated developing countries and island States, such as Indonesia and the Philippines.

There are a number of key advantages of floating power units over land-based energy sources:

- a compact size, allowing deployment in remote areas and on limited sites,
- a high maneuverability,
- reduced major construction activities at the site.

Nuclear generation projects in the small power segment are at the development stage. The development of SMRs is a priority task in most countries around the world such as: China (CNNC project), South Korea (SMART project), the USA (NuScale project), etc.

The development stage of those projects is not higher than TRL-6. In Russia, a floating power unit (FPU) was put into commercial operation in 2020, and a decision has been made to construct a land-based SMR in the northeastern Siberia, which will give a qualitative impetus to the development of Russia's Arctic regions.

The following advantages of small floating nuclear power plants of Russian design, as compared to those using LNG energy sources, are worth mentioning:

- long service life without refueling,
- no fuel handling activities at the operation site,
- fuel handling, qualified maintenance and decommissioning of the plant upon the end of its operational life shall be performed by the operator.

III. ROSATOM's floating nuclear power units and parameters of competitor designs that apply LNG

One of the new and priority business areas of the Rosatom State Atomic Energy Corporation is the development of the floating nuclear power units.

The first design to be mentioned is the FPU *Academik Lomonosov* (Pevek, in the north of the Russian Federation). The FPU *Akademik Lomonosov* is equipped with two reference KLT-40S reactors developed by JSC "Afrikantov OKBM". Similar reactor plants have extensive experience of successful operation on nuclear icebreakers. The electric output of the unit is 70 MW.

The 144 meter long floating power unit is commercially constructed at the shipyard and delivered to the operation site by sea in a ready-to-operate state. Only the auxiliary facilities shall be constructed at the operation site to ensure the positioning of the floating unit and the transfer of heat and electric power to the shore. The exceptional strengths of the project involve: "turnkey" production, well-established cooperation scheme of all the production participants, reduced project schedule; the design is self-sustainable, reliable and safe with a small footprint.

The detailed design of the optimized floating power unit (OFPU) with improved technical and economic indicators is currently underway taking into account the successful experience in the FPU *Academik Lomonosov* design development and operation. Two upgraded RITM-200M reactor units are going to be installed in the OFPU. This will increase the capacity of the floating power unit up to 100 MW with the refueling period of up to 9-10 years. The set of equipment intended for fresh and spent fuel handling operations, fuel storage, as well as the accommodation block have been excluded from the OFPU design, and shipboard systems and equipment have been optimized resulting in reduced displacement of the vessel.

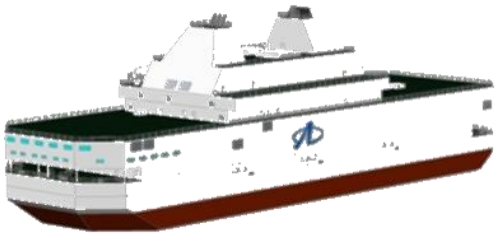

Figure 1 OFPU Design

Today, in order to increase the level of energy security and sustainable development, it is expected to develop utilization of associated petroleum gas, introduce modern innovative technologies and environmentally safe and efficient ways of extracting and producing energy resources. Tighter global fuel regulations are being introduced. The Green Shipping Programme is an example of such regulations to be developed and promoted by 2025, which involves the transition from liquid fuels (diesel, fuel oil) to LNG [3].

In the market of floating power units powered by LNG, the most prominent representative is *Karadeniz Powership* by Turkish *Karadeniz Holding*. In the same niche with the OFPU Karadeniz has a turnkey solution based on floating power ships integrating the whole cycle from the design of floating power plants to the supply of electricity, fully performing all work on the design and construction of the FPU, preparation of the customer's site, and provision of the necessary fuel. *Karadeniz* power unit vessels provide up to 10-25% of the energy mix of several countries in Africa and Asia. A total of 15 power unit vessels have been constructed since 2010 with a total installed capacity of over 2,800 MW [4].

China, Japan, Denmark and a number of other countries are implementing LNG projects or have their own floating power units.

OFPU also has competitors in the domestic market. In 2020, NOVATEK submitted to the Ministry of Energy of the Russian Federation the design of a floating LNG barge with 150 MW of modular regasification equipment [5]. The design of the vessel provides for ice reinforcement as well as tsunami protection. NOVATEK has already implemented a similar LNG barge project in Brazil.

IV. Approaches to the cost-effectiveness analysis and justification of competitive advantages of nuclear power generation and gas power generation

In this article, the competitiveness is placed as a purely economic category. Over the past 15 years, the levelized cost of electricity (LCOE) has found wide application as the main indicator for comparing the competitiveness of projects both abroad and in Russia.

The computational analysis has been performed using the following initial data and assumptions [6]:

- The OFPU operating period is reduced and assumed equal to that of the LNG energy sources namely 40 years;
- Capital costs are evenly distributed over the entire construction period of an energy source, with the costs of design work taken into account in the first year of the energy source construction;
- The discount rate is 7%;
- Absence of equipment downtime during repair activities (availability of a reserve capacity);
- The LNG-fueled power plant construction period is 4 years, while that of the OFPU is 6 years;
- LNG storage self-sufficiency is 30 days;
- Inflation and tax deductions have not been taken into account;

The above assumptions can give a miscalculation up to 25%. However, the dynamics and key trends in the calculation results are considered to be stable.

The calculated analysis of the LCOE sensitivity to changes in the LNG price for a 150 MW energy source was conducted taking into account the assumption of a fixed fuel price for the entire life cycle of the LNG energy source in the calculations of financial and economic models, as well as periodic fluctuations in the world market prices for energy carriers. The price of 1 ton of LNG was assumed to be 16814.7 RUB (at the price of $5 per 1 MMBtu, with US Dollar to Russian Ruble exchange rate of 63 RUB/USD).

These parameters have been recommended by the International Gas Union for use in the aggregated estimates of natural gas consumption. The dependence of LCOE on the fuel price is shown in Figure 2.

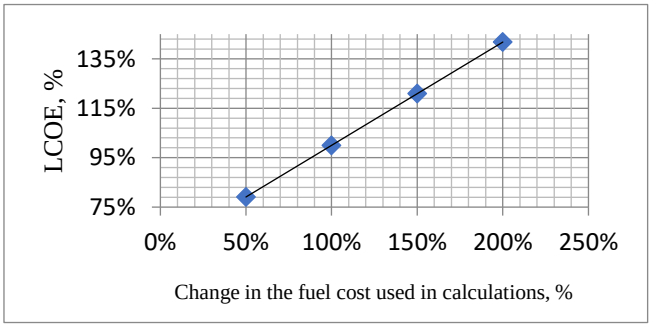

*100% is the point at which the LCOE was calculated based on the basic technical and economic indicators of the project

Figure 2. Sensitivity of the LCOE of a 150 MW LNG-fired energy source to changes in fuel costs

Thus, a 2-fold increase in fuel price results in an LCOE increase of about 40%. It is important to note that fuel (uranium) prices account for less than 20% of the cost of power generation at SNPP, so fuel prices have virtually no effect on LCOE, and thus there is a possibility of fixing tariff indexation approaches over the entire life cycle of OFPU, which is over 60 years. Thus the nuclear generation business is more controllable and predictable.

The operation sites of the facilities are defined conventionally according to the distance to the LNG production/shipment point. The range of distances is taken from 0 to 6000 km. As a result the there is a trend of an increase in the range of fuel transportation that leads to an increase in the LCOE of the project: A 1,000 km step increases the LCOE by up to 5%.

The location of the LNG energy source in close proximity to the energy carrier implies that there is no need for bunkering tankers.

This factor significantly affects the amount of capital costs for the project. For example, accounting for the capital cost spent on construction of an LNG carrier leads to at least 40% increase in CAPEX and a 20% increase in LCOE.

It is significant that a direct comparison of LNG and OFPU projects is incorrect, due to the difference in contracting period and organizational structure of business. In order to compare the economic performance of the LNG-fired power generation designs with that of the OFPU, financial and economic models, which combine LNG-fired energy sources and OFPU, compatible in capacity and service life (40 years) were formed and calculated:

- one first-of-a-kind LNG-fueled energy source and one commercial LNG-fueled energy source of 50 MW each versus a 100 MW OFPU;
- two commercial LNG-fueled energy sources of 150 MW each versus three commercial OFPU of 100 MW each.

A comparative analysis of the LCOE of two 50 MW LNG-fired energy sources and one OFPU showed the greater attractiveness of the OFPU project (LCOE less by 12%).

In a situation comparing two 150 MW LNG-fired energy sources to 3 OFPU, the LCOE of the OFPUs is slightly higher than the LCOE of LNG (by 10%), but this difference can be offset by changes in fuel costs.

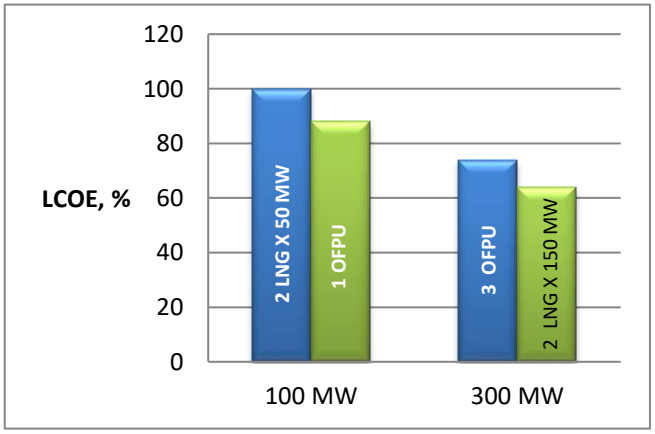

Figure 3. Comparative LCOE analysis of LNG and nuclear generation designs

In its turn, if the comparative analysis of these energy sources assumes an OFPU service life which is 60 years, then the LNG-fueled energy source operation model

includes the operation of 2 energy sources during 40 years with the start of construction of the other two energy sources 5 years prior to the decommissioning of the first two energy sources and subsequent operation of the next two energy sources for 20 years.

The comparative analysis of the LCOE generated by LNG-fueled energy source and OFPU during the life cycle of 60 years showed the greater attractiveness of OFPU (the LCOE is lower by 18%).

V. Analysis results of competitive ability and prospects for further development of the floating power units

The demand for higher living standards, industry promotion, energy supply to particular territories and infrastructure facilities inevitably lead us to floating power unit solutions. But gas or nuclear?

The growing demand for small and medium capacity gas-fired power units is driven by a number of factors. Firstly, the rapid development of the LNG industry. For example, the volume of pipeline supplies of natural gas has increased by 45% over the last 10 years, while the LNG sales have more than doubled.

Secondly, stricter environmental requirements covering an increasing number of countries.

A huge advantage of LNG energy sources is the short construction time, which facilitates quick access to potential electric power customers and enables them to compete with other power suppliers.

For all the advantages of such plants the infrastructure required to accommodate an LNG energy source leads to a strong increase in CAPEX. The unit cost of a 50 MW energy source is relatively small, but the necessary infrastructure solutions (LNG storage facilities, LNG carriers, onshore infrastructure, etc.) increase the CAPEX by a factor of 3. Thus, the sum of capital expenditures for a fleet of two 50 MW LNG-fueled energy sources with infrastructure is comparable with the CAPEX of OFPU with onshore infrastructure.

In its turn, the performance indicators of the LNG project can be significantly improved if the use of infrastructure solutions is optimized, in particular, if a single vessel can be used to transport fuel to provide multiple energy sources within the same region. In addition, it is possible to change the cost structure of the project by chartering or leasing a vessel to transport fuel, which will reduce the CAPEX by increasing the OPEX.

Floating energy sources with nuclear generation of the OFPU type are competitive with gas-fired energy sources in the same capacity range (100-150 MW). At the same time, the business based on nuclear generation is more controllable and predictable, as it is less dependent on fluctuations in the price of fuel, taking into account the refueling interval of up to 10 years.

Gas solutions are sensitive to the price of fuel; its fluctuations cause an increase in LCOE and, consequently, a decrease in profitability. The unstable situation on the global gas market will inevitably affect the implementation of the project to create small-capacity LNG energy sources by increasing the cost and increasing the duration of the project.

VI. Conclusion

Based on all of the above in the short term it seems efficient to deploy LNG-based power supply, while solutions based on nuclear power facilities can be competitive in the long term. New solutions of joint use of LNG and nuclear power generation can at least reduce the volume of budget subsidies.

It is important to realize that the synthesis of nuclear and gas generation pulls with it a significant amount of required investments. In this case it is necessary to analyze the possibility of cooperation with regional partnerships, including industrial enterprises, municipal structures and banking structures.

VII. References

[1] Resolution adopted by the General Assembly on 25 September 2015 A/RES/70/1 *Transforming our world: the 2030 Agenda for Sustainable Development*

[2] N.A. Salnikova, M.K. Roslaya, *Floating solutions for consumer-oriented power supply based on the reactor plants developed by JSC "Afrikantov OKBM"* presented virtually at the INPRO sustainability assessment of SMR, December 8-10, 2020, vol. 16

[3] Green Shipping Concept - URL: https://www.ecomarinepower.com/en/green-shipping (reference date March 20, 2020).

[4] http://www.karpowership.com/en/#home

[5] PAO NOVATEK Letter Reg.No.04-0002 as of January 20, 2020 addressed to the Deputy Ministers in the Ministry of Energy of the Russian Federation P.Yu. Sorokin and Ye.P. Grabchak *On the Construction of the LNG-fueled Energy Generation Source in the Chaunskaya Bay of Chukotka Autonomous Okrug and in the Tauiskaya Bay of the Magadan Region*

[6]N.A. Salnikova, M.K. Roslaya, A.Ye. Arefyev, D.Ye. Ovchinnikov, S.F. Kopeykin, Ya.O. Bykh, Yu.S. Grozdov, R.R. Tangalychev, M.S. Kuznetsova, *Feasibility Study of the Concept Aimed at Developing Small-Power Energy Sources to Supply Heat and Electricity to Consumers on the Northern Sea Route using CNG and LNG Comparative Analysis of Business Development Options on the Basis of Gas-Fired Energy Sources and Nuclear Power Generation*, JSC "Afrikantov OKBM" March 2020, p.64

Proceedings of the European Nuclear Young Generation Forum
ENYGF'21
September 27-30, 2021, Tarragona, Spain

Assessing Advanced Modular Sodium-Cooled Fast Reactors characteristics for fuel cycle closure in a PWR-AMR symbiotic fleet

Tirel, Kévin[1*], Kooyman, Timothée[1], Coquelet-Pascal, Christine[1] and Merle, Elsa[2]

[1] Commissariat à l'Energie Atomique et aux Energies Alternatives (CEA), France; [2] Centre National de la Recherche Scientifique (CNRS), France

*Corresponding author: *kevin.tirel@cea.fr*

I. INTRODUCTION

Closing the fuel cycle is one of the main challenges for nuclear power generation regarding sustainability [1]. In a closed fuel cycle, uranium and plutonium are extracted from irradiated fuels in order to be used in fresh fuels. As a result, the amount of waste to be disposed of is greatly reduced and the consumption of natural resources is minimized.

One essential condition for a nuclear fleet to achieve the fuel cycle closure is to stabilize the plutonium inventory. Indeed, a fleet that consumes more plutonium than it produces will eventually run out of fuel, whereas a fleet that produces more plutonium than it consumes will likely have to get rid of the excess of plutonium by considering it as waste. This would be contradictory with the sustainability goals of closing the fuel cycle and would increase the risk of proliferation. One way to stabilize the plutonium inventory is to build a symbiotic fleet made of breeder reactors that tend to produce more plutonium than they consume and of burner reactors that tend to consume more plutonium than they produce.

Symbiotic fleets composed by fast reactors (FRs) and Pressurized Water Reactors (PWRs) supplied exclusively with MOX fuels have been studied to close the fuel cycle [2]. Thanks to their fast neutron spectrum, FRs are able to provide PWRs with a plutonium of good isotopic composition for two reasons. First, FRs are able to fission even-numbered plutonium isotopes. When only exposed to thermal spectrum, these isotopes tend to accumulate and act like neutron absorbers. Being able to fission them is essential to reuse the plutonium for PWR fresh fuel. Secondly, FRs produce ^{239}Pu in their breeding blankets.

Usually, large FRs are considered for this kind of symbiotic fleet as they can easily reach high breeding ratios. However, it is expected for large FRs to have a higher capital cost than traditional PWR because of their complexity. Moreover, due to their size, these reactors are not versatile. For example, they are not very well suited for scalable electricity needs or industrial applications such as hydrogen production [3].

Advanced Modular Reactors (AMRs) on the other hand are expected to be more flexible regarding their purpose and more economically competitive than large reactors thanks to – among other reasons – their standardized production in factories [4].

The aim of this study is to assess sodium-cooled AMR (AMR-Na) characteristics that would make possible the fuel cycle closure in a symbiotic fleet PWR-MOX - AMR-Na. To do so, flexible SFR models built with artificial neural networks are used and plutonium mass balancing equations are solved.

II. METHODOLOGY

A. Construction of flexible models for AMR-Na

Artificial neural networks (ANNs) have been generated with the statistical platform URANIE [5] in order to build flexible irradiation models of AMR-Na. The definition domain of the flexible models are presented in Table 1. Databases for ANNs training and validation have been generated with the deterministic code ERANOS [6] using 2D-RZ models. The V2B core [7] has been chosen as reference for its simplicity. A simplified representation of the core is available in Figure 1. When shrinking the core volume, the aspect ratio has been maintained constant.

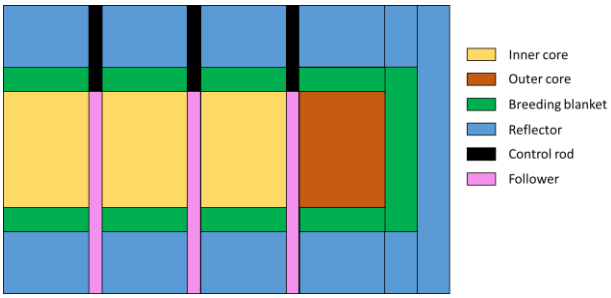

Figure 1. Reference core geometry.

Table 1. Design parameters range of AMR-Na flexible model

	Unit	Min	Max
Power	MWth	100	400
Power density	MWth/m^3	50	350
Fuel fraction	%	35	45
Irradiation time	EFPD	600	2400
Lower breeding blanket thickness	cm	0	30
Upper breeding blanket thickness	cm	0	30
Radial fertile blanket thickness	cm	0	30

B. Symbiotic fleet modelling

As previously stated, a closed fuel cycle is characterized by the fact that plutonium inventory is stabilized. It is possible to describe the stabilization of plutonium inventory in a fleet at steady state with two equations [2]. First, the plutonium production of the fleet has to be equal to the plutonium consumption. This can be written as follows:

$$\sum_{i\in\{reactors\}} x_i(m_e)_i = \sum_{i\in\{reactors\}} x_i(m_s)_i \qquad (1)$$

Where x_i is the fraction of the reactor i, m_e and m_s the annual plutonium mass input and output of a given reactor respectively.

Then, the plutonium isotopic composition has to be stable. A simplified approach of this statement can be made by using the plutonium quality $g = \frac{^{239}Pu + ^{241}Pu}{\sum_{238}^{242} {}^{i}Pu + ^{241}Am}$ instead of the detailed isotopic composition [2]. That way, the stabilization of plutonium quality accounts for the stabilization of the plutonium isotopic composition. The stabilization of plutonium quality is written as follows:

$$g = \frac{\sum_{i\in\{reactors\}} x_i(Gm_s)_i}{\sum_{i\in\{reactors\}} x_i(m_s)_i} \qquad (2)$$

Where G is the quality of the plutonium in the irradiated fuel of a given reactor.

In order to solve these equations, it is necessary to know m_e, m_s and G for the PWR and every AMR-Na. These values are linear functions of the plutonium quality g at first order [2]. PWR data are available in Table 2 and have been calculated with data from [8]. Regarding the AMR-Na, for each design sampled, the expressions of m_e, m_s and G are calculated with the flexible models and put into the system of equations to solve.

Table 2. PWR characteristics

Reactor	Unit	PWR
Fuel type	-	MOX
Thermal Power	MWth	4500
Irradiation time	EFPD	495
Burn up	MWd/t	53.5
Core mass	t	127
Mass of plutonium in fresh fuel	t/year	-11.77 g + 10.00
Mass of plutonium in irradiated fuel	t/year	-10.13 g + 8.24
Plutonium grade after irradiation	-	0.55 g + 0,18

The fleet under study is composed by 100% MOX PWR and AMR-Na. All the irradiated fuels are reprocessed together so that the plutonium coming from PWR and AMR-Na are mixed before being used in fresh fuel. A cooling time of 5 years is considered for the irradiated fuel before it can be reprocessed and a fabrication time of 2 years is taken for the fresh fuel.

The system of equations is solved with the function root of the SciPy package [9] with its defaults settings.

III. RESULTS AND DISCUSSION

A. AMR characteristics to close the fuel cycle

Among the 10,000 AMR-Na designs sampled in the range presented Table 1, only about a hundred lead to a solution. Histograms of their characteristics are available on Figure 2.

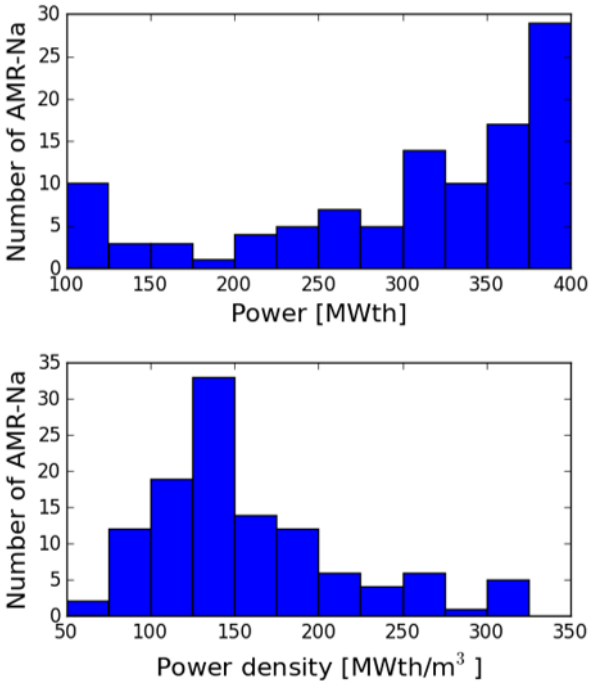

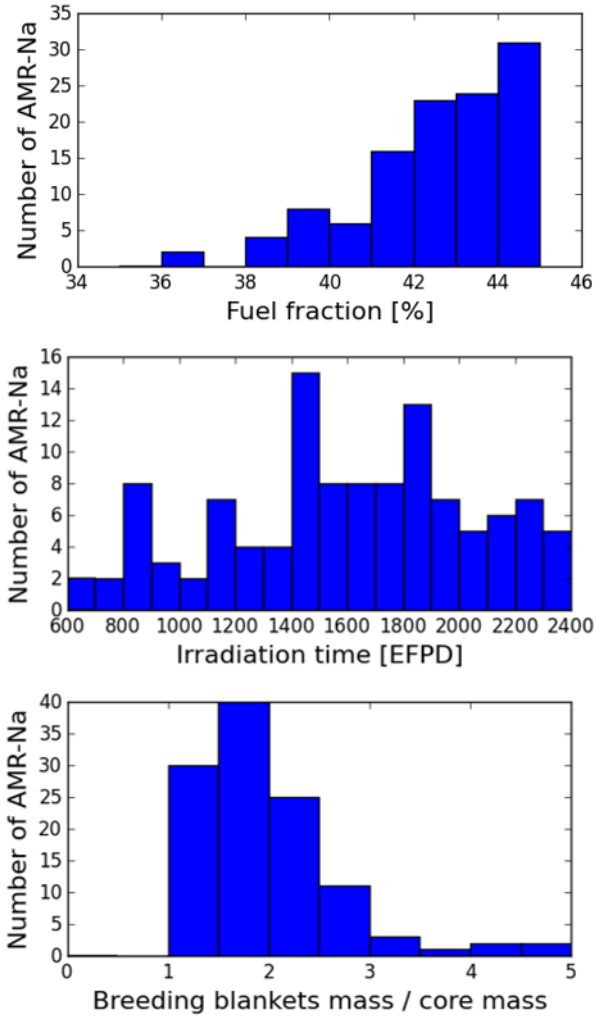

Figure 2. Histograms of AMR-Na core characteristics compatible with fuel cycle closure

It appears that the majority of AMR designs enabling fuel cycle closure has a power higher than 300 MWth, a power density lower than 150 MWth/m^3 and a fuel fraction higher than 42%. The combination of high power and low power density results in cores of high volume, which is consistent with the objective of enhancing the core breeding ratio.

Indeed, the number of neutron leakages decreases when the core volume increases. With less leakage, it is possible to reduce the initial plutonium content leading to an increase in the ^{238}U proportion in the fissile zone and thus to a breeding ratio enhancement. In addition, the high fuel fraction improves the probability for neutrons to interact inside the fuel, which makes the initial plutonium content decrease and then favors the breeding ratio. These results are a proof of the soundness of the methodology used here.

One major result is that the fuel cycle closure seems indeed possible in a symbiotic fleet containing AMR of any thermal power within the range 100 MWth – 400 MWth. This is not intuitive in the sense that small cores tend to have a negative breeding ratio. Although it will always be easier to reach a positive breeding ratio with a large core, this study shows that it is possible to reach positive breeding ratio in small cores by adding enough fertile blankets.

Regarding fertile blankets, an arbitrary threshold value can be derived from this study: the mass of fertile blankets (axial and radial) must be at least equal to the mass of the fissile core. In comparison, the 3600 MWth core used in [2] has a mass of fertile blankets 1.5 times superior to the mass of fissile core, indicating that this threshold does not seem aberrant. Then, the precise value of the ratio fertile blankets mass – fissile zone mass depends on the fissile core volume as shown in Figure 3. Cores with a volume lower than 1 m^3, which correspond to a power lower than 150 MWth, have a ratio included between 2.5 and 5, while the other cores have a ratio that varies between 1 and 3. This confirms the fact that small cores can reach positive breeding ratio through the addition of a large proportion of fertile blankets. However, for the smallest cores, such breeding ratio increase is done at the cost of a noticeable increase of the vessel size.

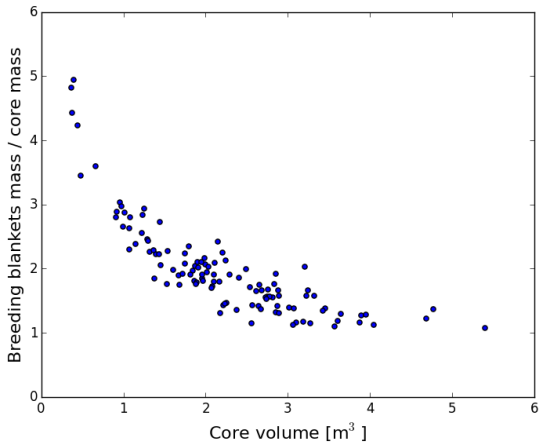

Figure 3. Proportion of breeding blankets in the core vs core volume

Finally, the irradiation time, expressed in equivalent full power day (EFPD), does not seem to have a significant impact. The irradiation time effect is dual. On the one hand, the longer the irradiation time, the higher the initial plutonium content, to maintain the core criticality. As mentioned before, increasing the initial plutonium content is detrimental to the breeding ratio. However, breeding blankets exposed to long irradiation times produce more plutonium. Those antagonist effects explain why there is no clear irradiation time preferred.

B. Discussion

For each AMR-Na design enabling fuel cycle closure, the composition of associated symbiotic fleet is studied. A new estimator is needed in order to make a relevant comparison between the fleets obtained. The plutonium net production is defined as follows:

$$net\ plutonium\ production = Gm_s - gm_e \quad (3)$$

Where g is the plutonium quality at equilibrium, G the quality of the plutonium in AMR-Na irradiated fuel, m_e and m_s the annual plutonium mass input and output respectively. This estimator quantifies the net amount of plutonium fissile isotopes that is produced annually in a reactor.

Figure 4 shows the link between the number of AMR-Na that needs to be built for each PWR in the fleet to ensure the stabilization of plutonium inventory, and thus, fuel closure. It appears that the number of AMR-Na for each PWR is

inversely proportional to the plutonium net production of AMR-Na. When the plutonium net production is lower than 2 kg/year, the AMR-Na breeding ratio is barely positive. As a result, the excess of plutonium is very low and almost no PWRs are needed to stabilize the plutonium inventory.

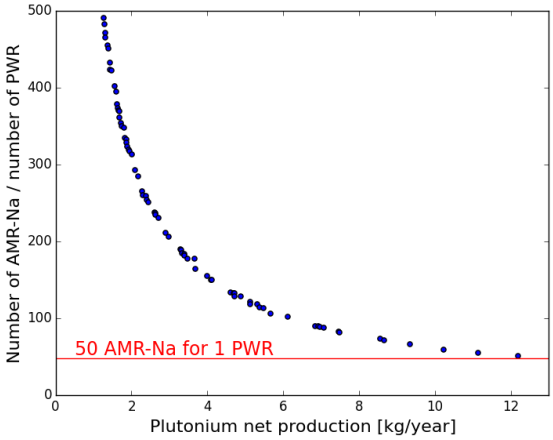

Figure 4. Number of AMR-Na for each PWR in the fleet

On the contrary, when the plutonium net production increases, less AMR-Na are needed to feed the PWRs. Within the domain explored with the flexible models, the maximum plutonium net production achievable is around 12 kg/year. In that case, 50 AMR-Na of 400 MWth are needed for each PWR. In comparison, the fleet in [2] has 3 SFRs of 3600 MWth for each installed PWR, all other assumptions about the fuel cycle being equal. Choosing AMRs-Na over large FRs thus implies having almost 2 times more power generated by fast reactors, which could not be economically advantageous as fast reactors are expected to have high capital cost. However, this cost could be justified by the fact that AMRs-Na should be more suited than large cores for future decentralized needs.

IV. CONCLUSIONS

Flexible irradiation models have been built for a AMR-Na with artificial neural networks on a large definition domain, and then used in a static model of a symbiotic fleet. This model consists in trying to balance plutonium flux in the studied fleet while making sure that the plutonium quality is stable.

After solving the equations with various thousands of designs parameters samplings in the definition domain of the flexible models, only about a hundred designs enables the fuel cycle closure. Among them, the majority presents characteristics that maximize the breeding ratio: high power, low power density and high fuel fraction. Nevertheless, there are designs that enable the fuel cycle closure for any power between 100 MWth and 400 MWth.

The existence of a threshold for the minimum mass of breeding blankets has been highlighted. While cores smaller than 1 m^3 need a mass of breeding blankets 2.5 to 5 times higher than the one of the fissile zone, larger cores need at least a mass of breeding blankets equivalent to the one of the fissile zone.

Finally, it has been shown that the number of AMR-Na installed for each PWR is inversely proportional to an estimator of AMR-Na breeding ratio. Within the definition domain of the flexible models, at least 50 AMR-Na for each PWR are needed in order to close the fuel cycle in a symbiotic fleet, which is almost 2 times more installed power than in the case of 3600 MWth FRs. Although this paper shows that closure of the fuel cycle is possible using AMR-Na, additional considerations such as total fleet size, economic conditions or flexibility requirements are necessary to make a global comparison with large reactors.

V. REFERENCES

[1] F. Gao, W.I. Ko, “Modeling and system analysis of fuel cycles for nuclear power sustainability (I): uranium consumption and waste generation,” Annals of Nuclear Energy vol. 65, pp 10–23, 2014.

[2] G. Martin, C. Coquelet-Pascal, “Symbiotic equilibrium between Sodium Fast Reactors and Pressurized Water Reactors supplied with MOX fuel,” Annals of Nuclear Energy vol. 103, pp 356-362, 2017.

[3] IAEA, “Industrial Applications of Nuclear Energy,” IAEA Nuclear Energy Series, n°NP-T-4.3, 2017.

[4] IAEA, “Advances in Small Modular Reactor Technology Developments,” supplement to IAEA Advanced Reactors Information System (ARIS), 2018.

[5] J-B. Blanchard et al., “The URANIE platform: an open-source software for optimisation, meta-modelling and uncertainty analysis,”EPJ Nuclear Sci. Technol, vol. 5, p.4, 2019.

[6] J. Ruggieri et al., “ERANOS 2.1 : International Code System for GEN IV Fast Reactor,” proceedings of the ICAPP 2006 conference, 2006.

[7] P. Sciora et al., “A break even oxide fuel core for an innovative SFR: CEA neutronic studies,” proceedings of the GLOBAL 2009 congress, 2009.

[8] G. Martin et al., “French transition scenarios toward a symbiotic nuclear fleet”, proceedings of the ICAPP 2016 conference, 2016.

[9] P. Virtanen et al., “SciPy 1.0: Fundamental Algorithms for Scientific Computing in Python,” Nature Methods, vol. 17, pp 261-272, 2020.

Proceedings of the European Nuclear Young Generation Forum
ENYGF'21
September 27-30, 2021, Tarragona, Spain

Applicability of local heat transfer correlations for residual heat removal via loop thermosyphons in Small Modular Reactors (SMRs)

Rincón-Soto, Nelson[1], Ramírez-Carrasco, Fernando[1], Buck, Michael[1] and Starflinger, Jörg[1]

[1] Institute of Nuclear Energy and Energy Systems (IKE), Germany

*Corresponding author: *rincon@ike.uni-stuttgart.de*

I. INTRODUCTION

Interest in Smaller Modular Reactors (SMRs) is gaining momentum over the last decades, as they offer an attractive alternative for a vast range of energy markets due to their flexibility, transportability and simplified manufacturing. SMRs are new generation reactors designed to produce up to 300 MW electric power, introducing advanced reactor technology and safety features [1].

Inherent reactor safety in cahoots with passive residual heat removal systems (PRHRS) are common design features in emerging SMRs. PRHRS are responsible for the removal of residual core-generated heat after plant shutdown [2]. PRHRS rely on naturally-driven forces to transfer the residual heat to an intermediate heat sink, usually a water-filled emergency cooling tank (ECT) with a limited grace period. To avoid ECT-water depletion due to evaporation, the residual heat must be transferred via a secondary loop to an ultimate heat sink (UHS), such as the environment or to an air-cooling tower (ACT). Multiple process schemes and models for indefinite PRHRS-operation in SMRs considering an UHS have been extensively studied [3]. A representative example is shown in figure 1, where the core decay heat is transferred to the secondary loop producing steam, which flows upwards to the ECT via the PRHRS. Then, the surplus heat of the ECT-water is removed by the LTS system and transported to an UHS, in this case an ACT. Loop thermosyphons (LTS) are considered suitable secondary loops for this heat transport purpose [4]. LTS are a type of wickless two-phase operated heat pipes, featuring a closed-loop configuration with an evaporation and a condensation zone connected by two independent flow channels for the gas and liquid phase, respectively. To describe the internal LTS-thermal hydraulic phenomena (THP), local heat transfer coefficients (LHTCs) must be estimated for each section given its geometry and flow regime. LHTCs can be estimated via heat transfer correlations (HTCOs) available in the literature, which must be carefully selected based on the THP present in the system. A critical review of thermosyphon-related HTCOs is available in the literature and the most suitable correlations for LTS were identified [5].

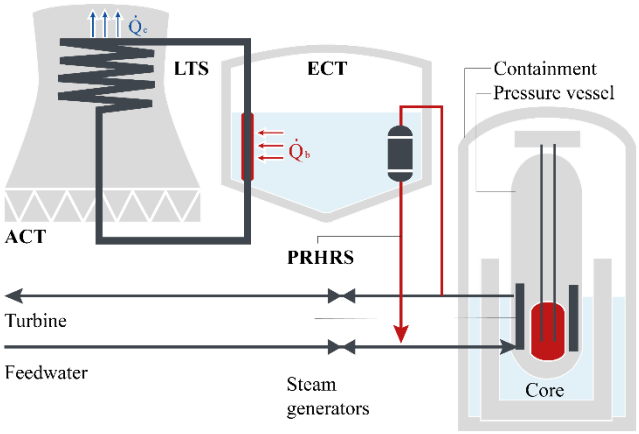

Figure 1. Indefinite PRHRS-operation concept for a pressurized water SMR featuring a LTS-configuration for heat transfer to UHS

In terms of SMR-licensing and design, thermal-hydraulic simulation tools (THS) are widely accepted to evaluate PRHRS under various accident scenarios. An accurate prediction of LHTCs is a decisive factor in assessing the reliability of THS [6]. In the present study, the performance of the system code ATHLET (Analysis of Thermal-Hydraulics of Leaks and Transients) regarding LHTCs-prediction is evaluated and validated against experimental data from a scale-appropriate LTS-experimental facility [7] as well as against LHTCs-values computed from selected HTCOs. The existing experimental results from the LTS-facility, i.e. temperature profiles and heat inputs/outputs, were processed to compute both, overall heat transfer coefficients and LHTCs for further validation purposes. It is expected to identify the most suitable HTCOs which can be integrated in the ATHLET code to accurate assess the efficiency of LTS-configurations in indefinite PRHRS-operation concepts for SMRs.

II. EXPERIMENTAL VALIDATION DATA

The following section briefly describes the LTS-test facility, which experimental data was considered, as well as the corresponding post-processing to compute LHTCs, which will be used for validation.

A. Description of the experimental facility and summary of experiments

The experimental facility developed by Xiong et al. [7] is a 10 m-high closed LTS heated by an external water pool and cooled by a forced-convection air cooling tower. Figure 2 illustrates the main components of the facility. The working fluid (water inside the loop) is heated up in a vertical evaporation section and its temperature (T) and pressure (P) are measured along the height (Points $e_0 - e_8$). A counterflow of hot water in the outer pool is constantly fed to the system at controlled inlet temperature (T_{wi}), mass flow (m) and pressure; its outlet temperature (T_{wo}) is also measured. Due to the selected low operation pressures in the LTS (achieved by action of the vacuum pump), the working fluid starts evaporating in the riser and the density difference facilitates its upward transport to the condensation zone. The condenser is composed by ten inclined pipe-sections placed inside a forced-convection ACT, which inlet air velocity (v_a) and temperature (T_a) are set for every experimental point. Pressure and Temperature in the condenser are also recorded (Points T_{c1} and T_{c2}). Once the working fluid condenses, it flows downwards by gravity back to the starting point. Further details of the test facility can be found in [7].

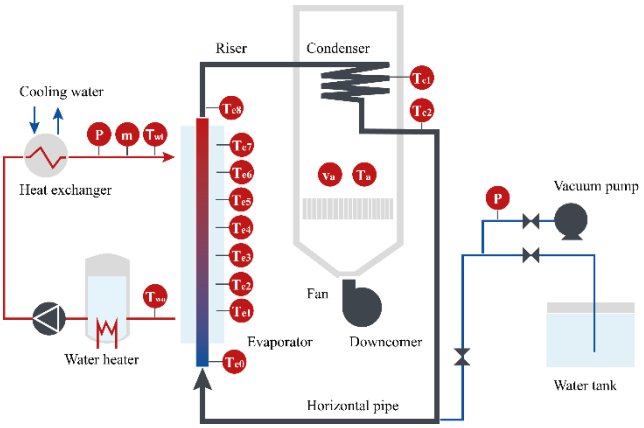

Figure 2. Scheme of the LTS experimental facility. Adapted from [8]

Multiple process parameters, i.e., filling ratio of working fluid (F_R), air velocity and temperature (v_a and T_a), inlet water temperature of pool (T_{wi}) and inlet water velocity (v_w), were studied during the experimental campaigns in the facility. This research tackles experimental points with different values for T_{wi} (50 – 90°C). A summary of the considered stationary state operation points is presented in Table 1.

Table 1. Selected operation points for validation purposes

Operation point (OP)	Process parameters				
	v_a (m/s)	T_a (°C)	F_R (%)	v_w (m/s)	T_{wi} (°C)
1	0.5	28.2	14.7	0.011	50
2	0.5	28.2	14.7	0.011	70
3	0.5	28.2	14.7	0.011	80
4	0.5	28.2	14.7	0.011	90

B. Post-processing of experimental data

To compute the experimental values for LHTCs, the available measured data must be processed for each section of the LTS-facility. The transferred heat rate to the working fluid is computed as:

$$\dot{Q} = \overline{Cp}_w (T_{Wi} - T_{Wo}) \quad (1)$$

Being Cp_w the average water heat capacity in the heating pool. In the case of the evaporator, the overall heat transfer coefficient (k) was calculated based on the logarithmic mean temperature difference (ΔT_m) and with reference to the outer heat transfer area (A_2):

$$k = \dot{Q}/(A_2 \Delta T_m) \quad (2)$$

A thermal resistance analogy allows the estimation of the objective inner-pipe LHTCs (α_i) based on the overall heat transfer coefficient and additional computable LHTCs:

$$\frac{1}{k} = \frac{d_2}{d_1}\frac{1}{\alpha_h} + \frac{1}{\alpha_w} + \frac{1}{\alpha_i} \quad (3)$$

Being d_2 and d_1 the outer and inner pipe diameters, correspondingly, α_h the LHTC of the outer part (water pool, computed with the Dittus Boelter [9] correlation, as in ATHLET), and α_w the LHTC relative to the wall conduction. The corresponding LHTCs were computed analogously for the condensation section.

Table 2 presents the selected HTCOs for nucleate pool boiling and film condensation which will be evaluated within this analysis, as they are common THP in two-phase LTS [8].

Table 2. Selected HTCOs for every LTS-section based on commonly occurring phenomena. Extensive formulae can be found in [5, 8, 9]

Phenomena in two-phase LTS	Selected HTCOs for estimation of inner-pipe LHTCs
Nucleate pool boiling	Rohsenow [5], Kutateladze [5], Imura et al. [5]
Film condensation	Nusselt corrected by Rohsenow [8], Hausen [9] (outer side)

III. ATHLET-MODEL DESCRIPTION

An ATHLET-Model of the LTS-experimental facility was developed and evaluated within this project. The geometry, i.e., dimensions, pipe diameters, inclined sections, elevations, were taken from the test facility directly. The model features three thermo-fluid dynamics (TFD) systems (Main loop, heating pool and the ACT) linked by Heat conduction objects (HCOs), representing the pipe walls. The main loop is composed by three TFD objects (RISER, COND, DOWNDOMER), which are divided into control volumes (CV) as shown in the nodalization depicted in figure 3. The heating pool consists of two TFD objects (WPOOL_1 and TDV_2) and a fill for a constant downwards hot water supply. Finally, the ACT has two TFD objects (ATOWER_1 and TDV_3), which are filled with air. WPOOL_1 is attached to a section of RISER to represent the evaporator. Analogously ATOWER is attached to the inclined pipe sections of COND to represent the condenser section.

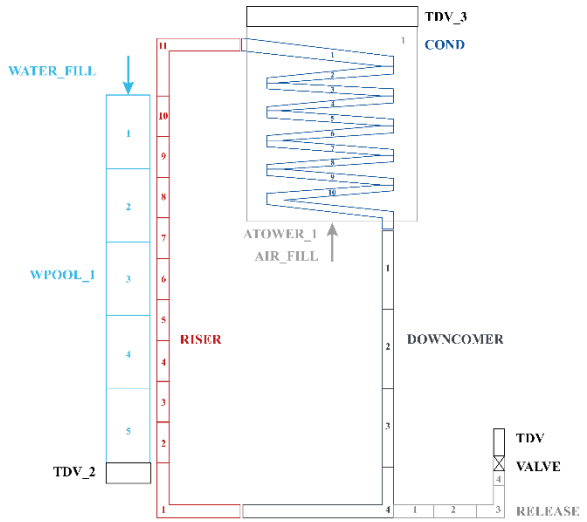

Figure 3. ATHLET Nodalization of the LTS-experimental facility.

As initial conditions, the pressure, mass flow and temperature of the inlet water (T_{wi}) at the heating pool were specified, along with the same parameters for the air in the ACT. The initial working fluid inventory was also specified as 14.7% of the volume of the system. Moreover, an initial guess of the inner-loop pressure was also provided. As boundary conditions, the outlet pressure and enthalpy of the water in the heating pool (Pool outlet) and of the air in the ACT (Surroundings) were considered.

IV. RESULTS AND DISCUSSIONS

This section presents the results of the HTCOs assessment and comparison to the processed experimental data and ATHLET output. Four operation points (OP1 - OP4) were selected to evaluate the LHTCs as shown in table 2. Concerning the evaporator, the experimental data indicate a two-phase flow mainly between the measuring points e_4 to e_8 (see figure 2); hence, LHTCs were evaluated for this segment of the evaporator, corresponding to nodes 7 – 10 of the RISER object. Figure 4 illustrates the results of LHTCs estimation for the selected OP and their corresponding heat input to the evaporator.

A clear overestimation of the ATHLET-computed LHTCs is evidenced for all OP. For the current two-phase heat transfer scenario (heating, transitioning to two phase flow), ATHLET interpolates between the values of the Modified Chen correlation for subcooled and 2-phase heating [9], which might be incurring additional sources of uncertainty. Furthermore, ATHLET-computed LHTCs display a larger spatial variation over the segment (e_4 – e_8) in comparison with the experimental data and HTCOs. On the one hand, some HTCOs seem to underpredict the LHTCs for most OP, such as the case of Imura et al. [5], which although it was developed for thermosyphons, some authors agree that the Rosenhow correlation generally delivers more fitting results for LTS [5]. On the other hand, the correlations by Rosenhow and Kutatelatze [5] seem to reproduce a more accurate representation of the experimental LHTCs and display potential to be implemented in ATHLET.

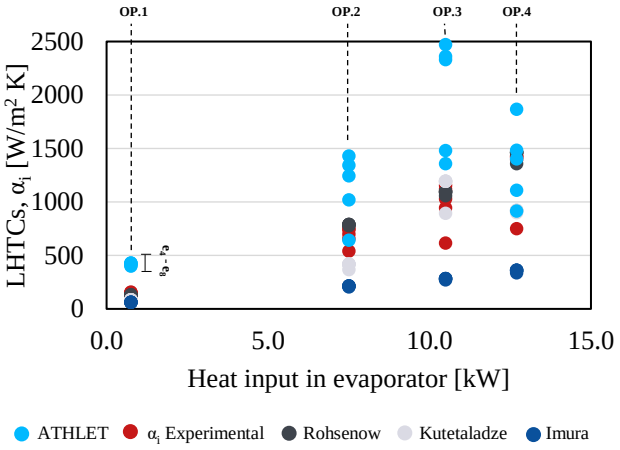

Figure 4. Evaluation of two-phase HTCOs in the evaporator section

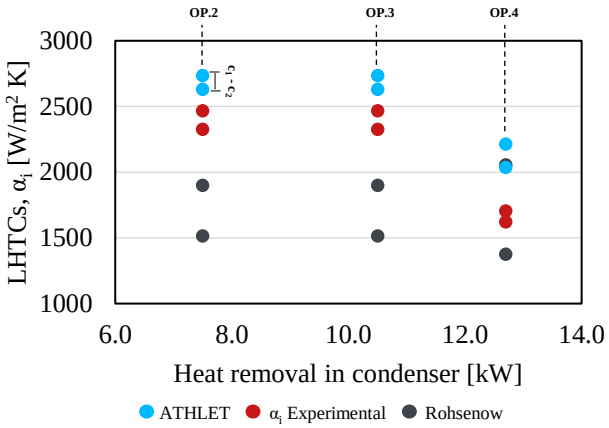

Figure 5. Evaluation of two-phase HTCOs in the condenser section

Regarding the condenser, three OP were selected (OP2 - OP4) for the analysis due to the range of applicability of the studied HTCOs. Based on the available experimental data, LHTCs could be estimated for the initial (From e_8 to c_1, or nodes 1-5 of COND object) and final segment (From c_1 to c_2, or nodes 6-10 of COND object) of the condenser, as c_1 is a measuring point located in the geometric center of the condenser's length. Figure 5 depicts the results in terms of the heat removed from the condenser.

ATHLET-computed LHTCs (with Chato's correlation [9]) also display an overall overestimation in comparison with the experimental data, specially at higher heat flows. On the contrary, the studied Nusselt corrected by Rohsenow correlation seems to offer a more accurate representation for higher heat flows, but felt short in the prediction at lower ones. A spatially even estimation of LHTCs could be evidenced for ATHLET-computed LHTCs, which match the observed experimental data. To get an illuminating insight about the effect of the LHTCs-overestimation on the ATHLET output results, figure 6 displays the thermodynamic states of the working fluid within the LTS once the stationary state is reached in the case of OP 3. Figure 6 also displays the saturation line to facilitate recognizing two-phase flow segments within the LTS. It is clear that for the standard ATHLET HTCOs selection, a sudden rise in the temperature of the two-phase segment

(e_4-e_8) is presented, overheating the working fluid close to the pinch point of the heat exchanger at the saturation pressure predicted by the experiments. On the other hand, for the liquid-two-phase transition segment (e_0-e_3), the LHTCs are calculated with the subcooled nucleate boiling Chen modified correlation, which even though is out of the scope of this research, seems to underpredict the values. In terms of the condenser, the temperature difference between c_1 and c_2 is larger in the model's prediction, pointing out a possible overestimation of the condenser's LHTCs as discussed over figure 5.

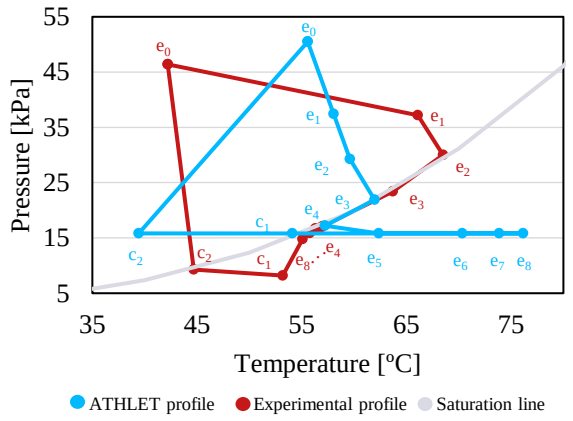

Figure 6. Steady state comparison of LTS working fluid conditions: Standard ATHLET HTCOs selection, OP. 3

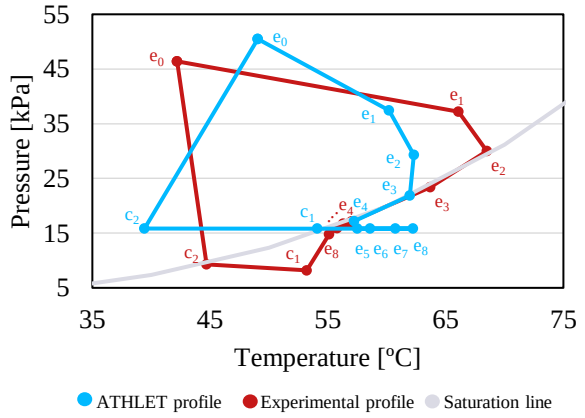

Figure 7. Steady state comparison of LTS working fluid conditions: After integration of simplified HTCOs in ATHLET, OP. 3

After integrating simplified versions of the Rosehnow's correlation in ATHLET for the evaporator section as a function of the wall temperature, a slightly enhanced ATHLET-output was achieved in terms of the thermodynamic states of the working fluid within the LTS once the stationary state is reached (OP 3). Figure 7 illustrates the corresponding outcomes of the HTCOs partial integration. The temperatures over the two-phase section (e_5 – e_8) are still above the experimental measurements, but considerably closer as in comparison to the standard ATHLET- correlations for heating in two-phase flows.A rigorous integration of the Rosehnow's correlation may lead to a better agreement in terms of the maximum local temperature and the values for the two-phase segment, as well as the integration of an inclined-pipe appropriate film condensation correlation.

V. CONCLUSIONS

Due to the increasing interest in PHRS for SMRs, indefinite operating process schemes have been brought to the table and are worth research. A LTS-ATHLET model for a scale appropriate facility was developed with the aim to study the applicability of HTCOs in the two-phase segments of the device. Regarding the evaporation section, the correlations from Rosehnow and Kutetaladze [5] delivered an accurate representation of the experimental LHTCs and can be considered for modelling the heat transfer in the two-phase segments of a LTS, and therefore, integrated in the ATHLET code. Nonetheless, other correlations, such as Imura, felt short at estimating the LHTCs for most studied operation points. In terms of the condensation section, the Nusselt corrected by Rohsenow [6] correlation seems to offer a more precise representation of LHTCs for higher heat flows, but underpredicteds the values at lower ones. ATHLET's existing Chato correlation [9] (for laminar film condensation) seems to represent the phenomena properly. As an outlook, additional HTCOs must be evaluated for the condensation zone, focusing on the effect of inclined pipes, as that group of correlations might deliver a better estimation of film condensation LHTCS.

VI. References

[1] International Atomic Energy Agency – IAEA, "Advances in Small Modular Reactor Technology Developments". Austria, September 2018.

[2] K. H. Bae, H. C. Kim, M. H. Chang, S. K. Sim, "Safety evaluation of the inherent and passive safety features of the smart design". Annals of Nuclear Energy, vol. 28, no. 4, 2001, 333-349.

[3] K. H. Bae, H. C. Kim, M. H. Chang, S. K. Sim, "Indefinite sustainability of passive residual heat removal system of small modular reactor using dry air cooling tower". Nuclear Engineering and Technology, vol. 52, no. 5, 2020, 964-974.

[4] R. Swart, R.T. Dobson, "Thermal-hydraulic simulation and evaluation of a natural circulation thermosyphon loop for a reactor cavity cooling system of a high-temperature reactor". Nuclear Engineering and Technology, vol. 52, no. 2, 2020, 271-278.

[5] V. Guichet, S. Almahmoud, H. Jouhara, "Nucleate pool boiling heat transfer in wickless heat pipes (two-phase closed thermosyphons): A critical review of correlations". Thermal Science and Engineering Progress, vol. 13, 2019, 100384.

[6] L. Ge, Z. Yang, H. Li, J. Shan, "Improvement and validation of the heat transfer model for the containment module in the RCS-containment integral system code". Annals of Nuclear Energy, 2020, vol. 144, 107531.

[7] Z. Xiong, C. Ye, M. Wang, H. Gu, "Experimental study on the sub-atmospheric loop heat pipe passive cooling system for spent fuel pool". Progress in Nuclear Energy, 2015, vol. 79, 40-47.

[8] V. Guichet, H. Jouhara, "Condensation, evaporation and boiling of falling films in wickless heat pipes (two-phase closed thermosyphons): A critical review of correlations". International Journal of Thermofluids, 2020, 100001.

[9] H. Austregesilo, C. Bals, A. Langenfeld, G. Lerchl, P. Schöffel, T. Skorek, D. Von der Cron, F. Weyermann, "ATHLET 3.2. Models and Methods". Gesellschaft für Anlagen-und Reaktorsicherheit (GRS) gGmbH, 2019, Vol. 4 Rev.

Proceedings of the European Nuclear Young Generation Forum

ENYGF'21

September 27-30, 2021, Tarragona, Spain

CASE-STUDY ANALYSIS OF THE POTENTIAL FOR IMPLEMENTATION OF A SMALL MODULAR REACTOR IN SPAIN

González Navarro, Miguel Ángel[1], Martín Huete, Laura[2], Suárez Ortiz, Francisco[3*]

[1] Tecnatom, Spain; [2] IDOM, Spain; [3] ENEN/Tecnatom, Spain

*Corresponding author: *fsuarez@tecnatom.es*

I. INTRODUCTION

Small Modular Reactors (SMRs) are advanced reactors designed to generate power typically up to 300 MWe, whose components can be factory built and transported as modules for installation at the sites where they are needed. In addition to electricity generation, the versatility of SMR designs can cover additional applications such as cogeneration, water desalination and hydrogen production.

This study analyses the potential for an SMR in Spain focusing on a particular case from the several combinations that could hypothetically be explored. The aim has been to consider both practical implementation aspects together with maximizing the usefulness of this technology to cover expected national needs, ultimately identifying a tentative candidate site. Although the current roadmap of Spain's Energy and Climate Integrated National Plan (PNIEC) envisages the gradual phase-out of nuclear, the actual future is yet to be seen.

II. OVERALL POTENTIAL AND OPPORTUNITIES FOR AN SMR IN SPAIN

SMRs could fulfil the need of flexible power generation for a wider range of uses and applications, including replacing aging fossil power plants, providing cogeneration to power a variety of industrial processes (including water desalination and H_2 production), serving small electricity grids and enabling hybrid nuclear/renewables energy systems. All of the previous opportunities could be explored for Spain as it counts with: fossil fuel plants, a wide variety of industrial processes, smaller sized grids in its islands and an expected increase in the share of renewable intermittent electricity generation.

When considering additional applications to couple an SMR to, a crucial factor is the process temperature required. Therefore, the process temperature intrinsically defines the type of SMRs that can serve it, as summarized below:

Table 1. Table of process temperatures associated to the alternative SMR applications on top of electricity generation (adapted from [1]).

Aplication / Process	Process temperature [°C]	Candidate SMR typology as heat input
District heating	80 – 200	LWR, o rejected heat from higher temperature reactors
Seawater desalination		
Oil refineries	250 – 550	LWR, LMR, FHR
Oil sludge processing	300 – 600	LMR, FHR
Syngas production, steam reforming with gas or coal steam	500 – 900	LMR, FHR, HTGR
Hydrogen production (various methods)	800 – 1.000	FHR, HTGR

Higher process temperature applications, such as hydrogen production or synthetic gas production, would require an LMR, FHR or HTGR type of reactor (liquid metal, molten salt of high temperature gas cooled, respectively). Spain's, nuclear fleet, with exception of Vandellós-I, has been composed by light water reactor (LWR) technology with which the industry and the regulator have mature experience.

To converge the scope of this case-study LWR SMRs were considered, as a practical continuity of the current operational plants and national experience (considering synergies with established know-how and infrastructure such as LWR fuel fabrication and a somewhat more similar licensing process). Therefore, on top of considering electricity generation, the additional applications that the case-study SMR could be combined with are: industrial applications (low temperature cogeneration) and water desalination. In the following sub-sections, these possible outcomes that the SMR could serve in Spain are analysed.

A. Industrial Applications

The diversity of industrial facilities spread throughout the national territory made it necessary to identify and evaluate those with more promising future projection or stability - guaranteeing demand- and also being compatible with the requirements of the process temperatures previously depicted. During 2020, several industries made the headlines due to their needs of power and/or heat, such as an Aluminium plant in the north-west (electricity intensive

process) or ceramic production plants in the east Mediterranean (high temperature process with implemented cogeneration), which saw their economic viability compromised. The consideration of an SMR to cover their energetic needs in such cases would either require it to divert its electricity production almost exclusively to the industrial process or to consider non-LWR technologies in order to provide higher temperatures. In line with the previously argued, the potential of the oil refineries in Spain was explored.

Spain has nine refineries, which are located close to the cities of: Coruña, Bilbao, Tarragona, Castellón, Cartagena, Puertollano, Algeciras, Huelva and Tenerife (figure 1). All sites are located in coastal areas except for Puertollano and they usually have cogeneration units that supply them with electricity and steam for their processes. Exploring some of these cogeneration units in further detail allows to evaluate the energetic needs of such facilities. Of course, the size and additional purposes, such as integrated chemical production lines, will require different energetic needs, but the aim is to reach a representative figure. The Bilbao refinery has a capacity of 38 MWe (Unit 1) and 43 MWe (Unit 2), exporting a 30% surplus to the electricity grid. Under normal conditions, unit 1 produces 86 [t/h] of steam at 260ºC [2]. For Puertollano, these figures are 70MWe and 125 [t/h] of steam and for Coruña: 80MWe (data from Repsol websites). Therefore, the energetic needs for these facilities can be considered around ~50 MWe and ~150 [t/h] of steam.

The facility which would be located in the less densely populated area and counts on available space at a reasonable distance would be Puertollano refinery (the smallest of the previous cities and has a pilot plant with a cooling tower close by whose infrastructure could potentially be utilized). It must be noted that, from the SMR point of view, 50 MWe would be derived to power processes and due to the need of steam (~260ºC), that would require extractions from the BOP, the net output of electricity towards the grid would be reduced further. Compatibility would be possible but if additional power is to be delivered to the grid, the bigger (power >100MWe) LWR SMR designs would be required.

B. Desalination

Access to fresh water is included within the Sustainable Development Goals of the United Nations. The climate of Spain is divided into multiple climatic regions and we can find areas with semi-arid climates, mainly in the interior and areas of the Levante coast. These areas highly demand water supply for human, agricultural and industrial consumption. To avoid reaching a competition situation between the previous demand types (if the water resources become too scarce), both natural and non-conventional sources should be considered. Aquifers often suffer from over-exploitation rates and natural contributions in many areas are expected to show a decreasing trend. On the other hand, Spain is among the top 5 countries in desalination capacity globally.

The AGUA plan (2004-2011) had among its objectives the development of desalination infrastructures, supported by the re-allocation of European funds. Installed capacity doubled from 1.5 to 3 Mm^3/day [3] but a rushed implementation of the Plan left some facilities not fully completed and with little or no inter-connection infrastructure. This heritage, together with the operational model which does not seem to ultimately integrate these resources in a continuous fashion, makes the desalination plants find themselves in a utilization range (supplying 537hm^3/yr [4] or 1.47Mm^3/day in 2018) of around 50%. This ratio was of 36% for the year 2015.

In April 2020, the Ecological Transition Ministry announced the intention to interconnect the desalination plants of the Levante region. This would allow correcting the remaining aspects inherited from the AGUA plan (which mainly boosted capacity) allowing for a more integrated system. In parallel, the development of desalination technology has optimized energy requirements from 50 kWh/m^3 in the early designs to around 3-8 kWh/m^3[2]. Although the utilization ratio of desalination production in Spain might suggest there is still room for further contribution of the existing fleet, older and less-efficient plants could need replacing as well as requiring more supply if the system (natural + desalination) becomes indeed integrated. The following figures represent some regional characteristics relative to water use/availability:

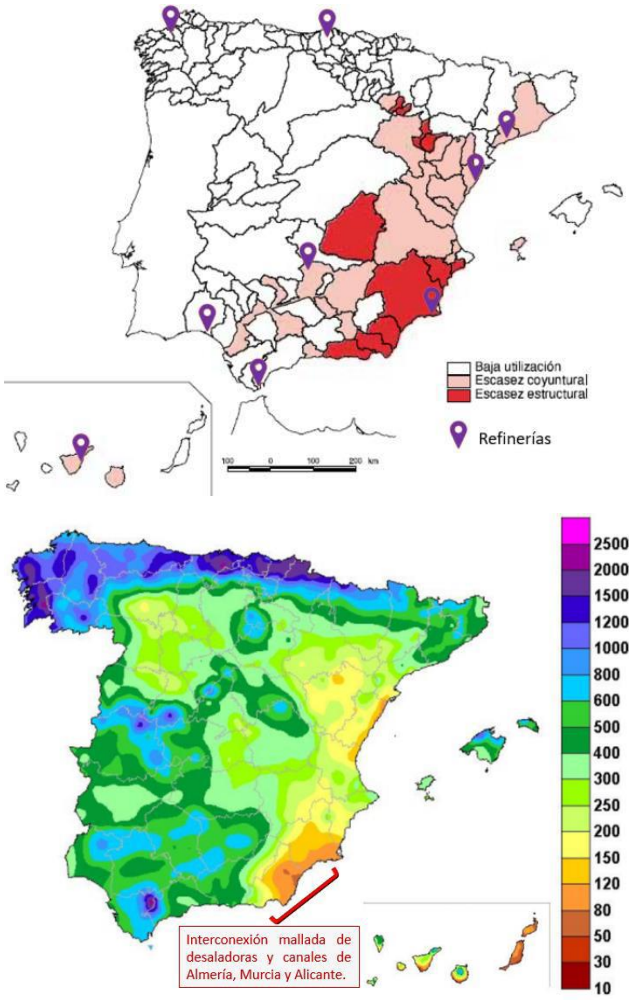

Figure 1. Above: Water exploitation systems with structural deficit *[Ministry of Industry, "White Book of Water", 2000]* and location of the Spanish refineries. Below: Rain accumulation in mm *[Ministry of Agriculture and Environment "National Hydraulic Balance" 2018]*.

As can be depicted from figure 1, the south-east (Levante) region presents a particularly arid climate, with low natural contribution of rain. This region counted on several

desalination plants being installed during the AGUA plan and is where the intention to construct integrating infrastructure would take place.

C. Electricity

The electricity sector is expected to have major changes in the energy transition, both on the supply side (conditioning the mix by climate objectives) and on the consumption side (with new demands arising from general electrification). The roadmap set out in the PNIEC, in principle in the interests of decarbonising the system, dictates the closure of coal plants and expects an ambitious installation of renewable generation. In this regard, the development of solar in particular can be foreseen in the regions with higher solar potential:

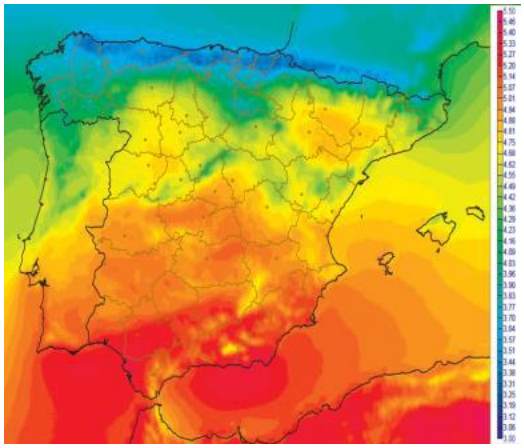

Figure 2. Average solar radiation in kWh/m^2·day ***[AEMET "Atlas de Radiación Solar en España utilizando datos del SAF de Clima de EUMETSAT" 2005].***

For an efficient operation of the electricity grid, it would be optimal to consider areas for the SMR contribution where: generation gaps may arise and/or significant development of renewables is expected without nearby stable generation points. As can be depicted from figure 2, the south-east region, amongst others, shows high potential for the deployment of solar generation. The local particularities of the grid in such area will be addressed later.

At this point, focusing on water desalination as the hybrid application of the case-study SMR was decided instead of cogeneration in refineries (which would require the operator to stop using the already operational cogeneration units. This opportunity cost could be significant).

III. PARTICULAR CASE-STUDY OF AN SMR FOR ELECTRICITY GENERATION AND WATER DESALINATION

Having analysed some opportunities for an SMR nuclear power plant in Spain, a more specific analysis was carried out to select an optimum location. Decreasing long-term expectations of natural water resources highlights the option of combining the facility with a desalination plant. Current technologies are more efficient, and it will be necessary to guarantee the supply of the areas most affected by an arid climate (Almería, Murcia and Alicante).

On the basis of the previous analysis, we decided to focus on a candidate site for an SMR plant with desalination capacity in the south of the Levante region, pursuing the following objectives:

- Be useful in supplying net electricity to the grid, ideally in a place where a certain base load would be beneficial, e.g.: where a large growth of renewables is expected.
- Be useful to contribute to water desalination production.

A. Site selection

The main desirable criteria for the site of the plant are: available cooling source, proximity to high voltage (HV) electrical substation, proximity to water network for desalinated water evacuation (with minimal additional cost of pumping and interconnection), nuclear licensing (geology, meteorology, seismic and climatic characteristics compatible with the requirements for a nuclear power plant), low density of nearby population centres and convenient access for the transport of freights both during the construction and the operation of the plant.

Focusing on the southern part of Levante, 3 possible site candidate sites were identified: Cabo Santa Pola (Alicante), Cabo Cope (Murcia) and Carboneras (Almería).

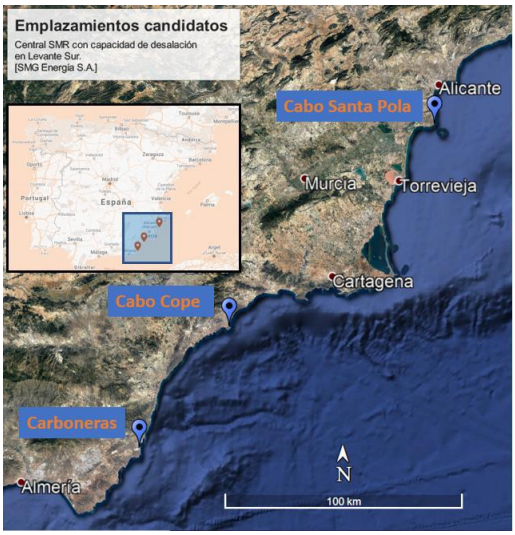

Figure 3. Candidate sites for the case-study SMR.

Cabo Santa Pola: This location has several drawbacks. It is a seismically active zone, being one of the local maximum national areas, which would probably affect the licensing process. In addition, the connection to the electricity grid would need to be at 132kV (4.2km away) if approved by the TSO or construct a line of 40km to reach the 400kV infrastructure. Such long-distance line permits are increasingly difficult to get in addition to the added expense. The closest desalination plant is around 11km away.

Cabo Cope: The licensing process would be easier, as it has already been proposed in the past as a location for a nuclear power plant (by Hidrola in 1973). The location would have the problem of being far from the electricity grid, around 22km from the closest 400kV substation ('Carril', which was newly built to evacuate photovoltaic capacity). It is also some distance from the closest desalination plant (10km).

Carboneras: This identified site complies remarkably well with all the desirable criteria. It is an industrial site with very low population density, a cement plant, a small biodiesel production plant, a desalination plant and a coal power plant (CT Litoral, 1,159MWe). The SMR would take advantage of a lot of infrastructure from the coal plant, such as the substation and the seawater intake and discharge channels, as well as its naval port terminal (module(s) could be shipped directly). It offers advantages over the nuclear licensing process as it is already an industrial site with the same seismic category as Cabo Cope. The permits related to desalination are simplified as the site already has a notable desalination plant, also reasonably guaranteeing that the water network interconnection project would connect there. The evacuation of electrical energy is optimal, with three 400 kV lines connected to its current substation.

Based on this evaluation, the site of Carboneras (Almería) was found to be the best proposal.

B. Desalination technology selection

The main types of desalination technologies were analysed: Multi-stage flash distillation (MSF), Multi-effect distillation (MED) and Reverse Osmosis (RO). The most convenient strategy is to achieve a high production capacity of desalinated water with minimum detriment in the net production of electrical energy of the plant. We used the IAEA tool DE-TOP (*Desalination Thermodynamic Optimization Program*) to perform a series of simulations with different couplings to the BOP, considering a representative SMR plant of 740MWth (~300MWe).

Desalinated water production was set at 60,000 m^3/day, which would expand the capacity of the current desalination plant at Carboneras by 50%. In order to cover all possible technologies, both a conventional reverse osmosis (RO) process and an improved process that incorporates a preheater to improve the efficiency of the membranes (RO + PH) were also considered. Considering these technological alternatives and possible couplings, the reverse osmosis desalination plant with preheater (RO + PH) proved optimal for this case-study as it is the option with lowest opportunity cost (smallest detriment of net electricity production to the grid).

C. Tentative SMR specifications

The coal plant at Carboneras constituted 64% of installed capacity of the Almería region in 2019, making it have a high overall electricity surplus that was evacuated towards Andalucía and Murcia. Murcia, has a high proportion of CCGT (75% in 2017), providing a prominent base-load production source -actually neighbouring the Cartagena refinery- but has also duplicated its photovoltaic capacity since 2017 to 2020. It is expected that both Murcia and Andalucía continue deploying solar, so a baseload point substituting the retiring coal plant could be convenient to smoothen intermittency. From the previous, the tentative specifications for the case-study SMR plant would be:

- Electric power: 100 - 600MWe (up to half of original).
- Desalination capacity: parallel production of 60,000 m^3/day of desalinated water (doubling current capacity).

A simplified financial simulation of tenders was performed, highlighting that low power SMRs could have similar incomes from electricity and water production and the profitability impact of the expected non-linearity of personnel costs to MWe for smaller power plants.

IV. CONCLUSIONS

We have explored the potential for an SMR plant in Spain, focusing specifically on the combination of desalinated water production and electricity production. After analysing different site options, we identified an optimal location in Carboneras (Almería) as very suitable because:

- By replacing a coal plant, it would take advantage of its existing and very convenient infrastructures.
- It would provide stable electricity coverage in an area where significant intermittent solar growth is expected.
- It would contribute to the desalinated water production system, where network integration is expected.
- The particularities of the location would be favourable for the licensing processes.

Having identified a specific site for an SMR to cover two particular demands shows that there is potential for implementation of SMR technology in Spain, in addition to the many other options and combinations that fell out of the scope of this work.

V. AKNOWLEDGEMENTS

The authors wish to thank the Spanish Nuclear Society for the organization of the interesting 2020 talent attraction competition, focused on SMRs, that motivated this work.

VI. REFERENCES

[1] D. T. Ingersoll, "Handbook of Small Modular Nuclear Reactors," *Elsevier,* 2015.

[2] J.M. Montserrat, PETRONOR, "Otros procesos sostenibles de generación de energía: Plantas de Cogeneración," 2011.

[3] E. Cabrera, "Pasado, presente y futuro de la desalación en España," *Ingeniería del Agua,* 2019.

[4] Ministerio para la Transición Ecológica, "Informe de seguimiento de Planes Hidrológicos y Recursos Hídricos en España. Año 2018," 2019.

Proceedings of the European Nuclear Young Generation Forum
ENYGF'21
September 27-30, 2021, Tarragona, Spain

Application of Digital Twin Technology for the Calculation Justification of Small-Sized Nuclear Power

Zotov, Igor[1], Bolnov, Vladimir[1], Zotova, Maria[1*] and Kulikov, Aleksey[1]

[1] JSC "Afrikantov OKBM", Russia

*Corresponding author: *mv.zotova@okbm.nnov.ru*

I. INTRODUCTION

Increased requirements are established for capacity, reliability and assigned lifetime duration of the reactor plants equipment for various purposes, while reducing the mass-and-size characteristics, as well as cost of the generated power. Such tasks require a new approach to designs calculation justification, implementation of modern digitalization tools, integrated systems of computer-aided designing, calculation analysis, and production justification and preparation. The implementation of modern approaches to designs calculation justification is especially relevant in the context of increased requirements for the nuclear facilities safety and high duration of the NPP lifecycle, and it will allow to reduce the number of full-scale tests in the future.

The term "digital twin" came into common use in the 1960s, and for the first time it was used in the aviation industry [1]. Later, this term became widely applicable in engineering, petroleum industry, and medicine. At present, this notion implies that, a computer model of a facility can be created based on its design data and this model can produce a fully-functional digital image. However, digital twins of complicated process facilities are still rather rare.

Application of the digital twin technology for small-sized nuclear power plants is of a special interest. Because this technology will allow to carry out interconnected calculations of neutron-physical and thermal-hydraulic facility parameters distribution, ionization radiation distribution, measurement of parameters and control system response to the change of the facility controlled state, strength and residual lifetime of facility equipment at the stages of designing and carrying out the designs calculation justification, and also can be used to create personnel training tools.

This approach is especially promising to apply for new projects of nuclear power plants, since it allows us to work out all new technical solutions.

II. MODELLING OBJECT

JSC "Afrikantov OKBM" is developing a small-sized nuclear power plant with the RITM-200H reactor plant, which will be an independent power source used, for example, in remote or hard-to-reach areas. The plant is designed to operate in stationary or maneuverable mode, and enables to change the load in the required range.

The small-sized NPP power unit is supposed to include:

– two integral-type reactor units with a thermal capacity of 190 MW each,
– two steam-turbine plants with an electric capacity of 50 MW each.

Below are the distinctive features of the small-sized nuclear power plant with the RITM-200H reactor plant:

– the plant complies with high environmental safety requirements, since the integral layout of the reactor significantly reduces the radiation impact on the environment,
– the small-sized nuclear power plant can be deployed in a wide range of climatic conditions, which significantly increases the opportunities for selecting the plant construction site,
– maximum requirements, stipulated by the modern regulatory framework, are established for external impacts,
– high degree of the reactor plant equipment factory preparedness. The size of the integral-type reactor makes it possible to transport it complete with the equipment components;
– nuclear fuel reloading is performed once in 6...7 years, which constitutes a significant advantage as compared to other sources of power supply;
– the number of personnel at the small-sized nuclear power plant can be significantly reduced as compared to traditional nuclear power plants due to using modern automatic process control system and monitoring and control system, and due to the equipment maintenance performed by the repair personnel.

III. DIGITAL TWIN COMPOSITION

At present, with reference to a reactor plant, a virtual (digital) twin of a facility under study represents a composition of:

– software which is a unified system of calculation codes integrated into a common system environment and providing coordinated calculation of various physical processes and equipment;
– a system of verified input data (design models database) to describe equipment behavior in design and emergency operation modes of the facility;
– hardware equipment enabling to carry out high-performance computing of mathematical models at high level of detalization.

At present JSC "Afrikantov OKBM" is developing a unified system of calculation codes integrated into the common system environment and providing coordinated calculation of various physical processes and equipment. This system incorporates:

– one-dimensional code enabling simulation of transient processes in the reactor plant. This code uses a system of equations describing the reactor kinetics, heat and mass transfer processes, electromechanical processes in an electricity generating plant and algorithms for the control system operation.
– the system of model-based designing of the functional software of automatic control systems where it is possible to create control algorithms, control interfaces and visualization of calculation schemes of mathematical models of various objects under study.
– a CFD code that, coupled with the one-dimensional code, enables users to take into account the slight effects of non-isothermal coolant flows.

Figure 1 provides a flow chart of the unified system of calculation codes integrated into a common system environment and providing coordinated calculation of various physical processes and equipment.

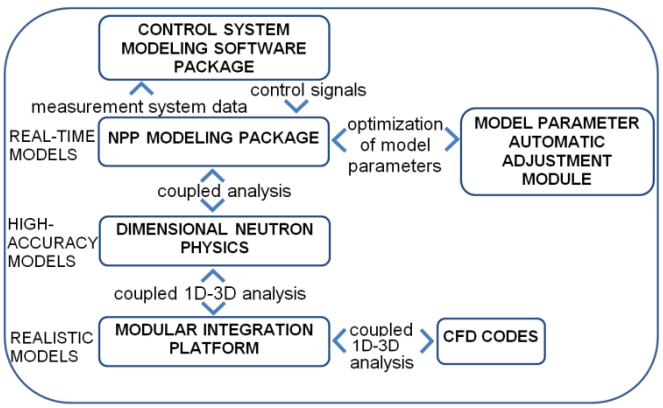

Figure 1. Digital twin development tools.

The system of verified input data includes the database of all Project technical documentation developed from the design to putting into operation and the design models database.

The development of this system includes several stages.

At the first stage design three-dimensional models are developed in CAD-system, the geometry of which fully describes the product being designed without any simplifications and conventions.

The second stage involves the preparation of initial data in 3D format for further calculation justification.This process is based on a list of parameters formed by a specialist that is necessary for the corresponding calculation, for example, the calculation of hydrodynamics. Based on this data, a 3D grid is built for conducting CFD calculations

The third stage is the development of the calculation model on the basis of the initial data in 3D format that were prepared at the previous stage [2].

The hardware of the computational package consists of:

– a tool server for storage of mathematical models and the database under the Project;
– workstations where a mathematical model is being developed, locally debugged and run, and where the calculation process is being controlled;
– a system of interaction with the mathematical model, operating panels and a system of displaying calculation parameters.

IV. APPLICATION OF DIGITAL TWIN AT LIFECYCLE STAGES

At the stage of designing, a small-sized nuclear power plant digital twin or models (which constitute its basis) are required to validate the normal operation modes, determine the requirements for the control algorithms based on the conditions of ensuring the transients required quality, validate the modes with equipment failures, justify the sufficiency of the provided measures aimed at preventing the possibility of an emergency situation due to the actuation of preventive protection, justify the emergency modes by calculations ensuring conservatism of the results in terms of safety criteria or justify the application of statistical methods of realistic analysis with conservative choice of equipment operation conditions.

At the stage of manufacturing and supply of the automatic process control system, the small-sized nuclear power plant digital twin is applied to correct the characteristic drawbacks of the existing process aimed at creating a functional software for the automatic process control system, that can both increase the development and debugging time of the algorithms and reduce the overall quality of the finished system.

At the stage of operation, the small-sized nuclear power plant digital twin is used as the basis for the system of on-line parametric technical diagnostics of the facility overall state and the state of its individual components. The need to use such kind of systems is due to the fact that the technical facilities are becoming more sophisticated, their operating life grows and the automation degree of the control processes increases, resulting in the need to optimally organize the operation of objects under diagnosis.

Here great importance is attached to determining the facilities condition which is being changed due to the impact of internal and external factors in the course of time. The technical diagnostics resolves issues related to determining the condition of technical facilities and pattern of their changes over time, and is aimed at determining the current condition of the facility to be diagnosed. The advanced technical diagnostics systems shall provide not only qualitative but also quantitative assessment of the condition of the facility under diagnostics. This is ensured by the use of the digital twins of the facilities under study. Further on, the obtained data are used for strength analyses, when justifying the residual lifetime and during diagnostics of the actual state of equipment.

V. Conclusion

The use of the digital twin technology for the small-sized nuclear power plant will allow to improve the design quality and safety, reduce the number of costly tests and technological processes refinement attempts, reduce the time and cost of design.

As of today, JSC "Afrikantov OKBM" has developed supercomputing twins for reactor plants of various purposes [3], and the results of using digital twins have shown the prospects for implementing this technology in terms of the design justification. The achieved results have revealed that digital twins can reduce excessive conservatism stipulated during the design, implement new perspective modes of facilities operation, justify the extension of the equipment assigned lifetime, and reduce the commissioning period of the control systems.

VI. References

[1] Luenberger, D.G., 1979. Introduction to Dynamic System Theory, Models and Applications. Springer

[2] V A Bolnov, M A Bolshukhin, A V Budnikov, S M Dmitriev, M V Zotova, I S Zotov, V V Petrunin, D N Sveshnikov, R I Romanov "Developing Supercomputer Twins Of Nuclear Power Plants For Various Applications With The Use Of Russian 3D Numerical Analysis Codes", American Journal of Physics and Applications 2020, p 223-232.

[3] M.A. Bol'shukhin, V.A. Bolnov, A.V. Budnikov, M.N. Ereev, M.V. Zotova, I.S. Zotov, A.N. Lepekhin, V.A. Panov, V.V. Petrunin, S.A. Rogozhkin, R.I. Romanov & V.I. Fomichev Supercomputer Twin of a Nuclear Energy Installation: Developmental Approaches and Application Experience, Atomic Energy, vol 129 No 2, p 74-79

Proceedings of the European Nuclear Young Generation Forum
ENYGF'21
September 27-30, 2021, Tarragona, Spain

Small Modular Reactors

Krapivin Anton, Kukhtevich Daria[1]

[1] JSC ATOMPROEKT, Russian Federation

*Corresponding author: *Anton.krapivin@inbox.ru*

I. INTRODUCTION

The nuclear power industry in our common understanding has been developing already for decades. The trend for the nuclear power industry development has always been the urge to increase the capacity; the half-century history of developing a nucleus fission has always been connected with the consistent increase of capacity from 500 MW to 1500 MW. The small-scaled nuclear power industry solved basically problems that were not related to civilian ones. Warships, nuclear submarines and nuclear icebreakers are all examples of low-power reactor plants.

Thus, the small-scaled nuclear power industry has been poor developed for peaceful purposes, particularly for power generation tasks.

If we consider Russia as the modular electric power consumer, it turns out that power supply to remote and sparsely populated regions is a burning issue. The lack of electricity and power supply hinders the development of these territories. An example of targeting and use of modular reactors is the territory of Siberia, which occupies about 25% of the entire country, yet the population of this vast territory is only about 11% of the country.

Numerous existing low-capacity, outdated diesel and fuel oil power plants and boiler houses are not able to cover the growing load. Under harsh environmental conditions, traditional energy sources based on renewable resources are not able to meet the growing demand for heat and electric power everywhere, while meeting economic and environmental requirements.

A solution to this problem could be a wide introduction of small modular reactors (SMR): floating, mobile and stationary. The most promising in these terms are compact nuclear power units of modular design that are mass-produced, the Units for which are delivered to a location as ready-to-operate, and which operate without core overload for up to 20-30 years, and then are removed. Thus, the main principle and one of the main differences of such plants from high-capacity reactors plants is: Supplier of such plants sells not the plant itself or equipment for it, but the end product - electricity. The Supplier is responsible for delivery, installation and commissioning of the mobile plant at the Customer's site for the entire period of operation. At the end of such operation the Supplier takes all the equipment from the plant for recycling, supplying a new Unit instead. Such solutions cover the main task - ensuring the development of remote deposits and formation of local power hubs. Taking into account the labor-intensive and expensive power supply of remote regions, SMR can become a backbone of the power industry both for industrial development and for maintaining the social aspect.

II. THE POWER UNIT BASED ON KLT-40S

Mobile SMR-type nuclear power plant "Akademik Lomonosov" is currently in operation in Russia. It is a floating Russian nuclear power plant of Project 20870, located in the seaport of the city of Pevek (Chukotka Autonomous Region). It is the world's northernmost nuclear power plant; it consists of a floating power unit, an onshore platform with facilities to provide power to Consumers, and hydraulic engineering structures to ensure that the power unit is safely moored in the water area. The plant was commissioned in 2020. The main objectives of the floating power plant are to supply power to major industrial enterprises, seaports, offshore oil and gas upstream and midstream facilities and to replace the retired capacities of Bilibino NPP. The floating power unit provides in the nominal mode 60MW of electric power to the onshore networks and up to 50 Gcal/h of thermal energy for heating the district heating water.

Given the interest shown in the recent years to low-capacity nuclear power sources and the scale of work being performed to create them, we can assert that we are at the start of a new trend in the development of nuclear industry, namely, widespread application of the SMR. The main advantages associated with the use of small nuclear power industry for development of remote, underdeveloped regions are as follows:

- minimizing the volume and cost of capital construction in the area where nuclear power plants are located. All high-tech, expensive and labor-intensive operations are transferred to specialized workshops of the plants and they are performed by qualified personnel. The consequences of these are minimizing costs for deployment and commissioning of small nuclear power sources.

- a very important advantage is a possibility to transfer the most nuclear and radiation-hazardous operations, associated with repair and refueling from the site to specialized workshops which ensures the high safety level and quality of performed procedures;
- a significant simplification of problems associated with decommissioning of these nuclear power plants upon runout of their service life;
- minimizing environmental consequences;
- and the last but not the least advantage is a possibility to make do with minimum of personnel working on shifts.

The Floating Nuclear Thermoelectric Plant (FNTP) is a new generation power source based on the Russian nuclear shipbuilding technologies and designed for reliable year-round power supply to Arctic and Far East regions of Russia and other isolated fuel-deficient regions of Russia and abroad. The most significant feature of the FNTP is the mobility and ability to be placed practically in any coastal area, including areas with high seismic activity and in the permafrost zone, no need for the developed infrastructure and a large number of personnel.

The main component of the plant is a Floating Power Unit (FPU). It is a non-self-propelled berth-connected vessel, that is constructed at the shipbuilding facility and is delivered fabricated to the location of FNTP by sea. Only auxiliary onshore and hydraulic engineering structures are fabricated at the site of the nuclear power plant to ensure installation of the floating power unit and transfer of heat and electricity to the shore. This technology makes it possible to significantly reduce the construction deadlines, ensure quality control, minimize impact to the environment both during construction and during operation of the plant.

KLT-40S reactors are equipped with state-of-the-art safety systems including those based on passive (i.e. not dependent on human and automatic involvement) actuation principles. Such safety systems based on the undeniable laws of physics (gravitation, nucleus fission and etc.) exclude severe consequences from terrorist and military attacks..

Upon completion of operation the FPU is delivered to the shipyard specializing in repair and scrapping of ships and vessels equipped with nuclear power units. Onshore facilities can be used as part of the FNTP with new power units, converted for other purposes or scrapped to a “greenfield site”.

Depending on the tasks that are supposed to be solved by small-capacity power plants, the variants of floating power plants based on KLT-40S are possible. Below are the parameters of the FPU with one or two reactor plants:

Maximum electric power	2 x 38.5
Maximum heat output, Gcal/h	2 x 73
Coastline area, ha	1.5
Water area, ha	6.0
Number of maintenance personnel, persons	approximately 70
Construction period, years	4

The economic efficiency of the FNTP application in remote areas is primarily due to replacement of expensive long-range organic fuel, reducing the need for transportation vehicles and labor resources to service the supply and storage chain of the organic fuel. Thus, according the calculations, construction of one FNTP with reactor plant KLT-40S allows releasing about 350 000 tons of fuel equivalent annually.

Construction and layout solutions include the following features (the main facilities are demonstrated in Figure 1):

- each power unit includes nuclear, steam-turbine and electric-power plants;
- power generation and output is performed according to the traditional scheme: nuclear plant- turbine-generator- power transmission line;
- in order to release heat, the necessary process engineering equipment and heating networks connected with a consumer are provided.

The possibility to locate the plant in close proximity to the consumers allows using the thermal component of the energy generated at the plant to the maximum extent, firstly in the sphere of heating the population living nearby the plant.

At the nominal heat output of 150 MW, each Unit of the FNTP power plant ensures generation of 240 t/h of steam with temperature of 290 °C for a steam-turbine plant. The steam generated in steam generators and delivered to turbine generators is not radioactive which is ensured by the layout, design and high efficiency of radiation protection.

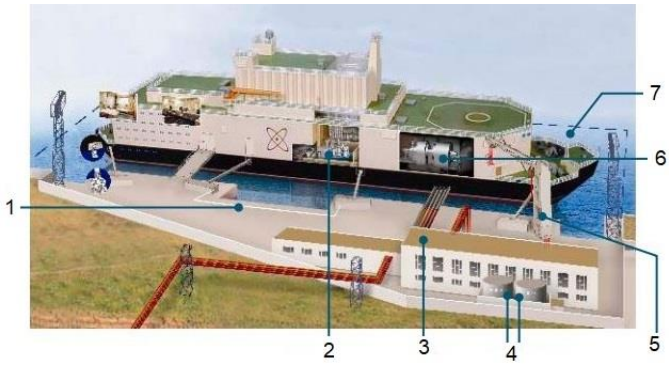

Figure 1 – Overall layout of main facilities

FNTP has the following main facilities:

1. hydraulic facilities;
2. reactor facilities;
3. heat point;
4. hot water tanks;
5. systems for distribution and transmission of the energy to consumers;
6. steam-turbine plants;
7. underwater trench 175×45, depth – 9 m.

In case of failure of the power unit main equipment there are provisions for standby infeed without decrease of power, power decrease at the rate of 5%/s to the permissible level or shutdown of one power unit with reducing the total power output of the FNTP to 50% of the nominal power output for the time of follow-up remedial action.

The layout of the plant ensures the rationality of functional connections and mutual arrangement of the suites, maximum fail safe operation of the reactor plant (RP) and increased reliability of the systems associated with

generation and transmission of electricity to the shore. Maintenance including refueling is performed using equipment arranged at the plant.

The high reliability of RP KLT-40S is achieved by the layout of the main equipment, where the reactor, steam generators and primary circuit pumps are combined into a compact steam generating unit by short heavy-duty branch pipes of “pipe-in-pipe” type, equal in strength with the reactor vessel. The primary circuit pipelines are minimal in the diameter, have an insignificant length and can be disconnected from the Unit. Leaktightness of the primary circuit is ensured by using only welded joints of equipment and pipelines. The layout of main equipment is shown in Figure 2 below.

The containment is a leaktight structure with the reactor, all equipment and pipelines with radioactive coolant inside, designed to resist pressure arising in case of the primary circuit depressurization.

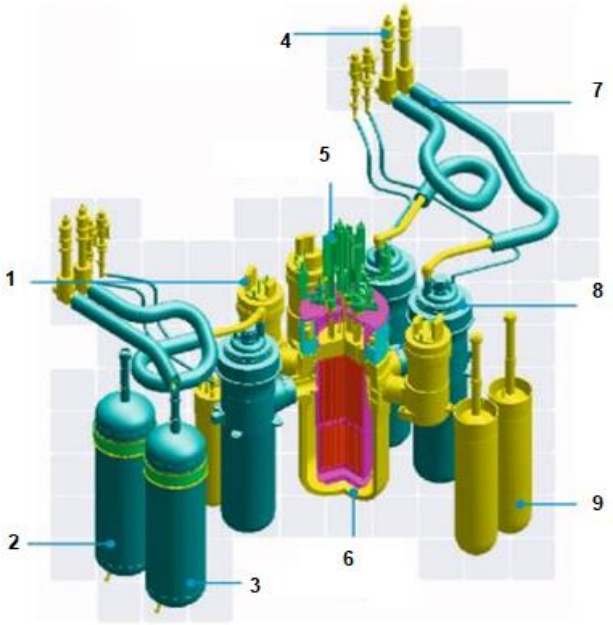

Figure 2 – Layout of RP KLT-40S main equipment

RP KLT-40S has the following main equipment:

1. reactor coolant pumps;
2. hydraulic accumulator;
3. hydraulic accumulator;
4. localization valves;
5. CPS actuators;
6. reactor;
7. steam pipelines;
8. steam generator;
9. pressurizer.

III. GENERAL PROPERTIES AND MAIN EQUIPMENT

The main equipment of the plant:

1) reactor plant KLT-40S is a complex of systems and components, designed to convert nuclear to heating energy, comprising the nuclear reactor and directly related components required for normal operation and safety. The plant consists of two circuits with water-water reactor, which is connected by the “pipe-in-pipe” branch pipe system with the coil-type steam generators (4SG) and reactor coolant pumps (4 RCP);

Technical characteristics of RP KLT-40S:

Thermal power, MW	150
Primary circuit parameters:	
Reactor coolant temperature at reactor inlet, °C	280
Reactor coolant temperature at reactor outlet, °C	316
Pressure, MPa	12.7
Secondary circuit parameters:	
Steam capacity, t/h	240
Steam temperature, C	290
Feedwater temperature, C	170

2) the steam generator (SG) is designed to remove heat from the primary circuit and generation of superheated steam. The steam generator is designed based on commercial steam generator PG-28 for the RP KLT-40 with maintenance and maximum harmonization of the basic solutions and overall dimensions and finalized to state-of-the-art safety requirements. The SG is a coiled type parallel-tube heat exchanger with heat generation inside the tubes. The SG tube system is built of cylindrical spiral coils made of titanium alloy. The SG body is made of low-alloy steel with anticorrosive cladding;
3) the RCP is a leaktight centrifugal single-stage pump with shielded two-speed (two-winded) asynchronous motor. It is designed to initiate circulation of coolant (pumped water) in the primary circuit system under normal and emergency operating conditions. Flow rate is 870 m3/h, head is 0.38 MPa. The body components are made of austenitic stainless steel; electric motor rotor is made of ferrite stainless steel. Lubrication and cooling of bearings as well as cooling of the electric motor rotor and stator is performed by the primary coolant circulating in an autonomous circuit, the heat from which is removed by cooling water;
4) electromechanical reactor emergency shutdown system. The system is designed for emergency shutdown of the reactor and maintaining in subcritical state under any conditions including design and beyond design basis accidents. The system includes CPS actuators comprising: emergency shutdown actuator groups and actuator compensating groups;
5) emergency shutdown actuator group is designed to shutdown the reactor quickly and maintain it in subcritical state under emergency conditions. The emergency shutdown actuator group consists of three emergency shutdown actuator groups. Each of the emergency shutdown actuator groups comprises: two shutdown rods, connecting components and an actuator;
6) the actuator compensating group is designed to compensate for excess reactivity in the startup mode, power operation and reactor shutdown. The actuator compensating group comprises: four peripheral actuator compensating groups, three middle actuator

compensating groups and one central actuator compensating group.

7) the steam turbine plant (STP) is designed to convert the steam heating energy obtained in the RP to the electric and heating energies to heat the water in the intermediate circuit of the heat cogeneration system. There are two steam turbine plants in the FPU. Each of the steam turbine plants is autonomous and is connected to its own RP.

The main nominal characteristics of the STP:

Electric coupling power at generator, MW	38,5
Heating power with output to the heat supply system, Gcal/h	to 73
Steam parameters upstream of the turbine set:	
Steam flowrate per the turbine set in the nominal mode, t/h	240
Pressure, MPa (kgf/cm2)	3.43 (35)
Temperature, °C	285

Heat output to the shore is performed by heating of intermediate circuit water circulating between the FPU and the shore, by the steam from controlled turbine bleed. The intermediate circuit water is heated from 70 ° C to 130 ° C in the heaters located in the turbine hall.

IV. ELECTRICAL POWER SYSTEM

The FPU electrical power system consists of the electrical energy generation system with an output to the shore power grid, the auxiliary power supply system and emergency power supply system.

The main objective to ensure safety during construction and nuclear facility functioning is protection of the environment and public health during the whole NPP operation. At the same time, the admissibility of such a measure as evacuation of population is excluded even in the hypothetically considered accidents with severe damage of the core. The living conditions of the people near the NPP, the radiation conditions shall not affect their health, regardless of the severity of the incidents.

The universal safety approach for the nuclear reactors of any type is to suppress the fission reaction and to remove the heat accumulated by the core. These simple requirements shall be met as simply and reliably, and in passive safety facilities this does not require personnel participation or operation of power supply systems. They are characterized by their ability to maintain a safe condition over a long period of time even in the face of human error or in the face of inactivity.

Due to the hydraulic characteristics and the selected Unit layout, the core cooling never stops under any conditions, since self-circulation of the primary coolant is ensured - the passive heat removal in the emergency modes.

V. CONCLUSION

Currently the FNTP has been commissioned, the first power output from the plant to Pevek was in 2020. It took about 10 years from the moment of the active construction phase to power output to the isolated power grid of the Chukotka Autonomous Region. Such a long period is due to the fact that this is the first project of its kind that has yet to become commercial. According to the preliminary estimates each power unit can be built in two years under the conditions of mass-production. The FNTP based on the FPU with RP KLT-40S, which is an improved analogue of nuclear icebreakers, can be created at minimum costs and in a short time, being a safe and the most acceptable source of electric and thermal energy for the conditions of the North and the remote regions equated to it.

The commercial model of the project implementation for foreign consumers can be carried out according to the scheme “construction-delivery- operation”: the floating power unit remains in the Russian property, shift crew - is Russian, the consumer is sold electricity, heat, fresh water on the basis of the long-term contract. This scheme allows the country where the power unit operates not to create an operational infrastructure, to ensure guarantees of non-proliferation of technologies and nuclear materials, to ensure unhindered return of the floating power unit with spent fuel to Russia and its complete scrapping at the Russian enterprises.

Parts of the work will be carried out in parallel with the construction of the underground laboratory (URL). In addition it URL, a group-based Demonstration and Research Canter will be created, where they will train in working with equipment for radioactive waste management. It is planned it complete the construction of this facility in 2026, then research will continue for several years. If studies show that this method of disposal is not suitable for high-level radioactive waste, then it can be re-profiled for the disposal of less long-lived waste.

VI. REFERENCES

[1] “KLT-40S. A reactor plant for the floating nuclear power plan” OKBM AFRIKANTOV;

[2] “Low-powered Nuclear Power Plants; a new direction of development” NUCLEAR SAFETY INSTITUTE OF THE RUSSIAN ACADEMY OF SCIENCES;

[3] “Floating Power Unit” Bellona Foundation reports;

[4] “Safety guide of nuclear power resources management” to certain draft laws of the Russian Federation from 11.05.2017 № 157.

Proceedings of the European Nuclear Young Generation Forum
ENYGF'21
September 27-30, 2021, Tarragona, Spain

Innovating UK Nuclear to support Net Zero by 2050

Home, Jacob[1] and Ray, Daisy[1]

[1] Department for Business, Energy & Industrial Strategy (BEIS), UK

I. INTRODUCTION

The UK Government's legally binding target to bring all greenhouse gas emissions to "Net Zero" by 2050 will require wide-spread changes to the entire UK economy. The term net zero means that any residual emissions in 2050 will need to be offset by removing an equivalent amount of greenhouse gases from the atmosphere, such as planting trees or using greenhouse gas removal technology like carbon capture and storage. Tackling climate change is a global endeavour and decarbonisation of areas such as electricity production, transport and industrial processes will be needed. How energy is produced and used to support these sectors will be central to achieving Net Zero and will require a decisive shift away from fossil fuels to using clean energy for heat and industrial processes, alongside supporting a demand for electricity that could nearly double by 2050 [1] as more sectors electrify [2]. This presents a real opportunity for nuclear energy, particularly technologies that could support decarbonisation of high-emission sectors alongside electricity production.

II. THE ROAD TO NET ZERO

In Winter 2020, as the world looked to recover from the Coronavirus pandemic, the UK Prime Minister set out a plan to "Build Back Better" and to make the UK a global leader in green technologies. The *Ten-Point Plan for a Green Industrial Revolution* was published and included over £12 billion (€13.8bn) of UK Government investment [3]. Point 3 of the plan is to deliver new and advanced nuclear power, with a commitment to pursue large scale nuclear and support the future of nuclear power in the UK through further investment in Small Modular Reactors (SMRs) and next generation Advanced Modular Reactors (AMRs).

The Ten-Point Plan was followed by the UK Government's *Energy White Paper: Powering our Net Zero Future* [4] which set out a vision and the key actions needed to enable the UK to transition to a clean energy system by 2050. In UK policy, White Papers are Government policy documents that set out proposals for future legislation (in this case for the net zero legislation) [5]. The White Paper included a commitment to establish a £385m Advanced Nuclear Fund to support the development of both SMRs and AMRs. This paper will focus on AMRs where a commitment of £170m was made for an R&D programme to enable delivery of an AMR demonstration by the early 2030s at the latest. The aim is for the AMR demonstration to test the technology which may be used for future commercial reactors.

As we write this, the UK has enshrined a near-term climate change target into law - to reduce emissions by 78% by 2035 compared to 1990 levels [6]. This reduction pathway was recommended by the independent Climate Change Committee [7] and as a result the Sixth Carbon Budget (CB6) will limit greenhouse gas emissions during the 5-year period from 2033 to 2037, bringing the UK closer to carbon neutrality by 2050.

III. DECARBONISING THE UK ECONOMY

Currently over a third (37%) of all greenhouse gas emissions in the UK are associated with heat demand (see Figure 1). Eliminating these emissions will require a greater push than solely using low-carbon sources of electricity as baseload for the electrical grid [8].

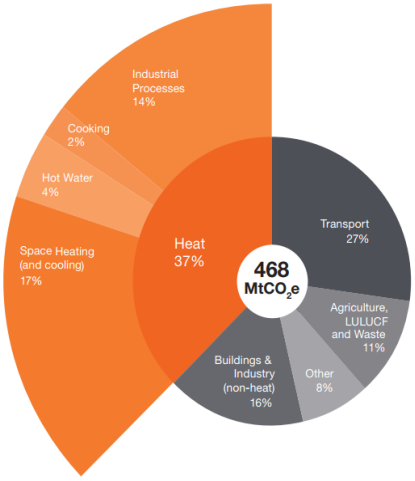

Figure 1: UK emissions associated with heat demand in million tonnes of CO_2 equivalent [8]

To decarbonise industrial processes (which account for 14% of emissions; Figure 1) like steel, glass, paper and cement production, multiple, innovative solutions will be required. In March 2020, the UK Government published its Industrial Decarbonisation Strategy which set out a vision for a

prosperous, low carbon UK industrial sector in 2050 with the aim to provide industry with the long-term certainty to invest in decarbonisation [9].

It is widely thought that some of the emissions associated with heat and transport could be met by Hydrogen as an energy source [10]. The Committee on Climate Change highlighted that the scale of low-carbon hydrogen utilisation will need to be as widespread in 2050 as electricity production is today; with hydrogen being used in shipping and transport fuel in industry and replacing natural gas for heating [7].

New large scale nuclear power stations, like the Hinkley Point C project currently being built in Somerset, England will provide 3.2 GWe of reliable baseload electricity to decarbonise the UK grid. However future nuclear technologies, like AMRs could generate more flexible electricity through utilising thermal storage and co-generation applications including high temperature heat for low-carbon hydrogen production (Royal Society; see Figure 2) which could provide a key role for nuclear alongside renewables in a clean energy system for the future.

IV. ADVANCED MODULAR REACTORS

In the UK Advanced Nuclear Technologies (ANT) are an umbrella term which encompass both near-term Gen III/III+ SMRs and Generation IV AMRs. Most AMRs under development use novel materials and fuels and typically have higher temperature outputs than conventional Light Water Reactors (LWRs), in the range of 500-950°C depending on reactor type (compared to 285°C for LWRs) [11].

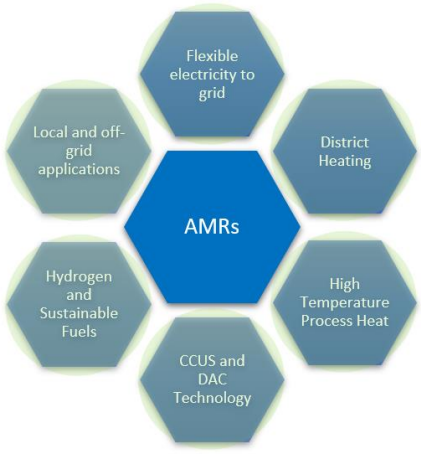

Figure 2: Multiple energy Vectors of AMRs. Informed by [10]

Many industrial processes require high temperature gas or steam to achieve efficient production [10]. If the technology readiness levels of AMRs continue to develop then in the future they may have the potential to support a range of applications (Figure 2).

An energy source with a high temperature output, like AMRs could help unlock more efficient hydrogen production to support a 2050 hydrogen economy [12]. High temperature outputs can also support carbon removal technologies such as Carbon Capture, Usage & Storage (CCUS) and Direct Air Capture (DAC).

V. NUCLEAR INNOVATION PROGRAMME (2016-2021)

As part of the £505m (€580m) Energy Innovation Programme (EIP) BEIS has a specific research and development programme focused on nuclear energy, the *Nuclear Innovation Programme (NIP*). The programme is grouped into six key theme areas (Figure 3) with a broad aim to develop technologies across the fuel cycle, explore future markets whilst securing and developing critical high value skills and jobs [13]. To achieve these goals the NIP includes several sub-programmes such as the Advanced Fuel Cycle Programme (AFCP), Advanced Material and Manufacturing (AMM) and the AMR Feasibility & Development Programme (AMR F&D).

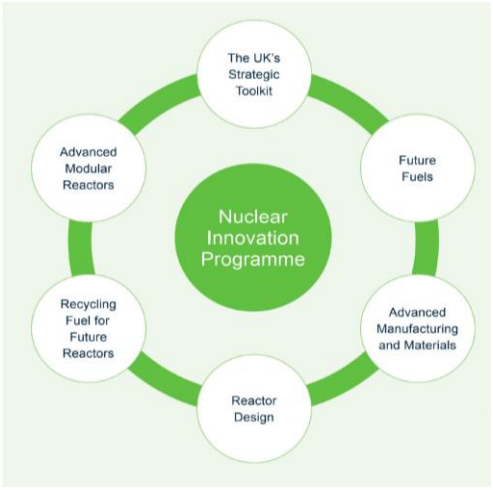

Figure 3: Thematic areas of UK Government's Nuclear Innovation Program (NIP) taken from [14]

VI. ADVANCED FUEL CYCLE & ADVANCED MATERIALS & MANUFACTURING PROGRAMMES

The Advanced Fuel Cycle Programme (AFCP) includes 11 work streams including the development of accident tolerant fuels, coated particle fuels and fast reactor fuels; the development of each of these could be deployed across a range of reactor systems [15]. The AFCP is led in partnership by the National Nuclear Laboratory (NNL) and BEIS and is delivered by over 100 organisations in the UK.

The Advanced Manufacturing and Materials (AMM) Programme is focused on developing and strengthening the UK nuclear supply chain & manufacturing capability through 11 grant funded industrial research projects. The AMM Programme aims to [13]:

- Deploy the UK's AMM research capability to deliver new nuclear technologies;
- Develop and demonstrate a suite of advanced component manufacturing technologies to drive down costs;
- Deliver a suite of modular construction techniques and technologies to enable effective nuclear plant build.

Innovation in this area will allow other aspects of the NIP, including the AMR F&D programme, to be delivered with reduced cost and enhanced safety.

VII. AMR FEASIBILITY & DEVELOPMENT PROGRAMME

The two-stage AMR Feasibility & Development (F&D) Programme was launched in 2018 to enable AMR technology vendors to conduct feasibility studies into their technology as part of Phase 1 and if successful further develop their design via Phase 2. As part of Phase 1 of the programme, over 20 organisations submitted proposals from which eight organisations were selected as recipients of approx. £300k to undertake feasibility assessments [16].

Table 1. AMR F&D Phase 1 successful bidders [16].

Organisation	Reactor	Description
ARC LLC	ARC-100	Sodium Fast Reactor
DBD Ltd	HTR-PM 600	High Temperature Gas Pebble Bed Reactor
LeadCold	Sealer UK	Lead Cooled Reactor
Moltex Energy	SSR-W	Molten Salt Fast Reactor
Tokamak Energy	Fusion Reactor	Fusion Reactor
U-Battery	U-Battery	High Temperature Gas Reactor
USNC	MMR	High Temperature Gas Reactor
Westinghouse	LFR	Lead Cooled Fast Reactor

Based on assessments from Phase 1, Tokomak Energy, U-Battery and Westinghouse Electric Company were selected to receive a further £10m (€11.5m) each to develop their AMR reactor design towards commercialisation through overcoming technical challenges as part of Phase 2 of the programme. This second stage of the programme includes early engagement with the nuclear regulators; the Office for Nuclear Regulation and the Environment Agency.

Importantly, through funding 'real' projects the initiatives within the NIP expect to build commercial capability within the supply chain, gearing it up to support the civil nuclear sector of the future, especially for delivery of new, innovative technologies.

VIII. NET ZERO INNOVATION PORTFOLIO (NZIP) 2021-2025

As part of the 10 Point Plan in 2020 a new R&D programme was launched to support Net Zero by 2050, building on the earlier Energy Innovation Programme (2016-2021). The Net Zero Innovation Portfolio (NZIP) is a £1bn (€1.15bn) fund announced within the 10 Point Plan to accelerate the commercialisation of low-carbon technologies, systems and business models [3]. It was identified that AMRs can play a unique role in meeting the Net Zero commitment and were included as part of the NZIP through the aligned Advanced Nuclear Fund (ANF). Within the ANF £385m has been committed to the development of Small and Advanced Nuclear Reactors. In particular, the ambition is for a £170m R&D programme on AMRs to lead to an AMR Demonstrator by the early 2030s, at the latest. The range of the portfolio reflects that nuclear is one of the technology options that are being progressed to decarbonise our economy and reach net zero.

The UK nuclear sector is well placed to leverage its extensive experience in providing low-carbon electricity to deliver innovative solutions on the road to Net Zero and contribute to the green industrial revolution. In addition, as the UK holds the G7 Presidency in 2021 and will host COP26 in November 2021 the country is in a unique position lead the global fight against climate change.

IX. OBSERVATIONS

There are several key observations that could be taken from the UK's Nuclear Innovation Programme:

- Early engagement between AMR vendors and regulators is valuable in upskilling the regulators on innovative technologies whilst enabling vendors to gain insight into the domestic regulatory regime and potential design challenges;
- Setting clear priorities for an innovation programme can enable focus and provide a 'golden thread' across workstreams. For example, waste management, emissions reduction, materials research, flexible electricity production, enhanced security & safety;
- For innovative technologies, supporting the development of several different designs or fuels early on the in the programme builds breadth of capability;
- Development of the innovation programme has enabled the growth of the UK supply chain building readiness for any future domestic deployment.

X. NEXT STEPS

The ability to produce high quality heat to support a future clean energy system along with technological readiness to deployment to help meet Net Zero could be key factors in informing any future AMR innovation programme. To further build on the domestic capability from the NIP, supporting work could include continued upskilling of the UK regulators to support future regulation and licensing, and research into advanced fuels and advanced manufacturing and construction such as modular build.

XI. REFERENCES

[1] BEIS, UK Government, "Modelling 2050: Electricity System Analysis", December 2020

[2] UK Government, https://www.gov.uk/government/news/uk-enshrines-new-target-in-law-to-slash-emissions-by-78-by-2035, April 2021

[3] BEIS, UK Government, "The Ten Point Plan for a Green Industrial Revolution", November 2020

[4] BEIS, UK Government, "Energy White Paper - Powering our Net Zero Future", December 2020

[5] UK Government, https://www.parliament.uk/site-information/glossary/white-paper/, April 2021
[6] BEIS, UK Government, https://www.gov.uk/government/news/uk-enshrines-new-target-in-law-to-slash-emissions-by-78-by-2035
[7] Climate Change Committee, "Sixth Carbon Budget for the UK", December 2020
[8] BEIS, UK Government, "Clean Heat, Transforming Heating", December 2018
[9] BEIS, UK Government, "Industrial Decarbonisation Strategy", December 2018
[10] The Royal Society, "Nuclear Cogeneration: civil nuclear in a low-carbon future", UK, October 2020
[11] GenIV Reactor Systems, https://www.gen-4.org/gif/jcms/c_9353/systems, April 2021
[12] NIRAB, "Achieving Net Zero: The role of Nuclear Energy in Decarbonisation", December 2020
[13] BEIS, UK Government, "Nuclear innovation programme: advanced manufacturing and materials", July 2020
[14] Clean Energy Ministerial, "Advanced Nuclear Technologies – a UK framework", 2019
[15] Nuclear Future, "Fuelling Net Zero: The UK Advanced Fuel Cycle Programme (AFCP)", January 2021
[16] BEIS F&D Programme Press Release, https://www.gov.uk/government/publications/advanced-modular-reactor-amr-feasibility-and-development-project April 2021

Proceedings of the European Nuclear Young Generation Forum
ENYGF'21
September 27-30, 2021, Tarragona, Spain

Improving the physical characteristics of the fast-neutron SMR by using Radiogenic Lead.

Ildar Sufiyarov [1]

[1] Rosatom Technical Academy (Rosatomtech), Russia

*Corresponding author: *iisufiyarov@rosatomtech.ru*

I. INTRODUCTION

The transformation of the structure of nuclear power, aimed at an integrated approach to the types of reactors (thermal and fast), capacity (small, medium and large), unit sizes, and others has changed the power industry landscape, shaping the opportunities and challenges for the development of small reactors with heavy liquid-metal coolant.

One of the advantages of small reactors is the possibility of their placement to provide electricity and heat to geographically difficult regions.

Improving the physical characteristics of nuclear reactors with a heavy metal coolant by replacing natural lead with radiogenic (lead-208) in the eutectic lead-bismuth alloy, it is advisable to link with the physical and economic features of fast reactor technology.

The theoretical and methodological basis of the study was made up of domestic and foreign developments in the field of fast reactors, heavy metal coolant technology, software and hardware complexes for calculating multiplication coefficients, burnout depth, and campaign time.

The empirical base of the study was the scientific papers and materials of scientific and practical conferences devoted to the problems of lead-bismuth coolant technology development [1].

The directions identified in the work for improving the physical characteristics of nuclear reactors with lead-bismuth coolant by replacing natural lead with radiogenic lead, make it possible to optimize the campaign time and obtain a positive economic effect due to increased power generation

II. THE MONTE CARLO METHOD

The computational and theoretical justification for the modernization of the core and increasing the power, safety and efficiency of lead-bismuth coolant reactors requires the development and implementation of modern approaches, realistic methods, and codes. Currently, companies that traditionally work with reactor subjects are designing, developing and effectively using modern codes and their combined complexes covering neutron-physical, thermal-hydraulic, hydrodynamic, and other necessary aspects of nuclear reactor performance calculations.

Neutron transport can be calculated by analytical or numerical methods. One of these methods is the Monte Carlo Method. Monte Carlo is based on the statistical approach of a given physical problem. Monte Carlo can be judged better than other numerical methods like S_n and P_n methods, which can have a great number of unknowns. Another advantage is not to require discretization in energy or directions, as the aforementioned methods. Monte Carlo method has an uncertainty depending on the number of particles, and being independent on the number of dimensions of the problem. This is an advantage, since all transport methods seek to solve the sevendimensional Boltzmann transport equation.

The essence of the method is to trace each particle leaving the source, from birth to extinction (absorption, leakage, etc.). The playout of events is based on the generation of random numbers. Using transport data, it is possible to determine the location of the particle at each stage of its history.

If there is information about the medium composition and microscopic laws of interaction of neutrons with the substance - it is possible to simulate the process of neutron propagation. This is a random process, as the mentioned microscopic laws are usually of random, rather than deterministic, nature. Interaction of the neutron with the nucleus can go through one of several channels. Based on this information, any reactor parameters can be determined using various calculation methods.

The generally accepted way to describe the energy dependence of cross sections in reactor calculations is the group approach. The region of energies under consideration (usually from 0 to 10 MeV) is divided into a number of intervals (the 26-group and 21-group systems of constants are the most common). It is assumed that within each interval, neither the cross sections nor other parameters characterizing the interaction of neutrons with nuclei

change. It is customary to number the groups from top to bottom: the groups belonging to the fast region first, then to the resonance region, and then to the thermal region last. It is important to choose a library of constants which should provide a high accuracy in solving certain classes of problems [2].

The Monte Carlo method is best suited for solving complex non-stationary problems in three-dimensional space. Since the Monte Carlo method does not resort to phase space cells, there is no need to approximate and average the results by energies, by spatial coordinates and by time.

III. PHYSICAL CHARACTERISTICS OF REACTORS WITH HEAVY METAL COOLANT USING NATURAL AND RADIOGENIC LEAD

A. Construction of the design model of the fast reactor fuel assembly with heavy metal coolant using PSG2 / Serpent

In this study, a model of a reactor cell containing fuel assemblies was used (numerical characteristics are given rounded to integers). The height of the fuel column is 450 mm. There is a 12 mm high spring on top, ending with a 13 mm high nozzle. A detailed diagram of the simulated cassette is shown in Figure 1.

The cassette consists of 198 fuel rods of a triangular grid with spacing of 14 mm. The fuel element contains a fuel pellet with a diameter of 11 mm, surrounded by a shell with a diameter of 12 mm and a wall thickness of 0.45 mm.

Each fuel assembly contains a 57 mm keyed hexagonal caisson tube with a wall thickness of 1 mm, located in the center of the fuel assembly and displacing 19 fuel elements from the regular grid.

Each fuel assembly contains a hexagon-shaped turnkey caisson pipe 57 with a wall thickness of 1 mm, located in the center of the fuel assembly and displacing 19 fuel elements from the regular grid.

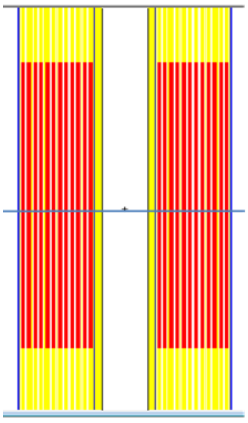

Figure 1 - Schematic diagram of the simulated cassette

Cross sections are shown in Figure 2. The caisson tube is filled with vacuum. The interwell space is filled with lead-bismuth eutectic. Fuel temperature is 800 ºC, and coolant temperature is 450 ºC.

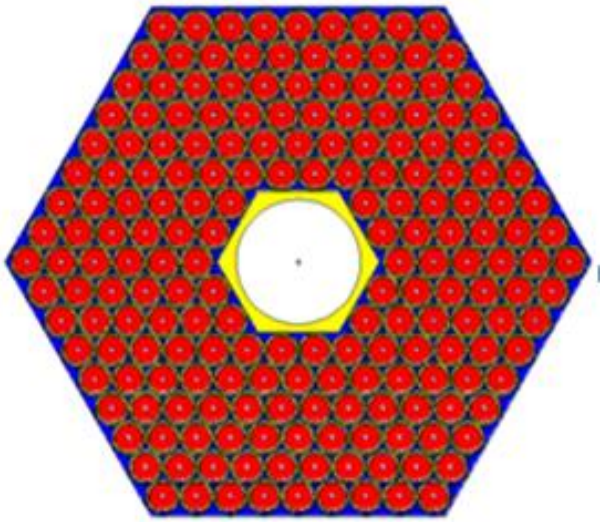

Figure 2 - Cross-sections of the model cassette

Fuel pellets consist of uranium dioxide with a density of 10.6g/cm^3, the enrichment of uranium 235 is 13%.

The geometry was modelled using the PSG2 / Serpent calculation code [3].

B. Coolant - lead-bismuth eutectic

A high coolant boiling point of lead-bismuth eutectic increases the reliability of heat removal from the core. Low pressure in the primary circuit reduces the risk of losing its tightness and allows reducing the thickness of the reactor vessel walls and the limitations imposed on the rate of temperature changes in compliance with thermo-cycling strength conditions.

Lead-bismuth eutectic coolant reacts very slightly with water and air. Progress of the processes caused by loss of primary circuit tightness failure and steam generator inter-circuit leaks occur without hydrogen release and without any exothermic reactions.

Two variants of lead-bismuth coolant are considered:
- Lead-bismuth with lead 45%, bismuth 55% by mass;
- Radiogenic lead-208-bismuth with lead 45%, bismuth 55% by mass. It is characterized by low neutron radiative capture cross-section and highest albedo of thermal neutrons.

Thermophysical properties of lead-bismuth alloy (natural lead) are presented in Table 1. The melting point of the alloy is 124 ºC, the boiling point is 1670 ºC.

Table 1 - Thermophysical properties of the alloy Pb (45%)-Bi (55%)

$t,\cdot K$	ρ, kg/m^3	c_p , J/(g·K)	λ , W/(m·K)	$Pr\times10^{-2}$
423	10 547	0.146	11.2	4.00
523	10 425	0.146	12.2	2.62
623	10 300	0.146	13.1	1.97
723	10 180	0.146	14.2	1.54
823	10 060	0.146	15.2	1.25
973	9 876	0.146	16.7	0.99

C. Physical Characteristics of a Fast Reactor with Lead (Natural) - Bismuth and Lead 208 - Bismuth Eutectic Coolant

Below are various values of neutron multiplication coefficients for the above-described coolant types. Table 2 shows the obtained calculated values of the multiplication factor depending on the two types of coolant

Table 2 - Calculated values of multiplication factor depending on two types of coolant

№	Name	Value of multiplication factor
1	*Pb (natural) - Bi.*	1.0626
2	*Pb radiogenic (208) - Bi*	1.0668

The results of the calculations presented in Table 2 show that the replacement of natural lead by radiogenic lead (isotope 208) in the lead-bismuth alloy leads to an increase in reactivity of 0.39%.

In all cases considered, the statistical error of the calculations did not exceed 0.02%.

D. Calculation of reactor campaign with lead-bismuth coolant

Below are the results of calculating the evolution of the breeding ratio as a function of burnup depth. The reactor power was set at 270 MW(t), the fuel "burned" at a constant 270 MW(t). An irradiation period of 0-2086 days was considered. The calculation was carried out in increments of 10 days by recalculating the spectra and cross sections.

Figure 3 shows the changes of reactivity for two fuel variants depending on the irradiation time.

Based on the calculation, we can conclude about the increase in the campaign time by 75 days due to the replacement of the eutectic lead (natural) - bismuth by lead (radiogenic) - bismuth, which leads to significant economic benefits on the production.

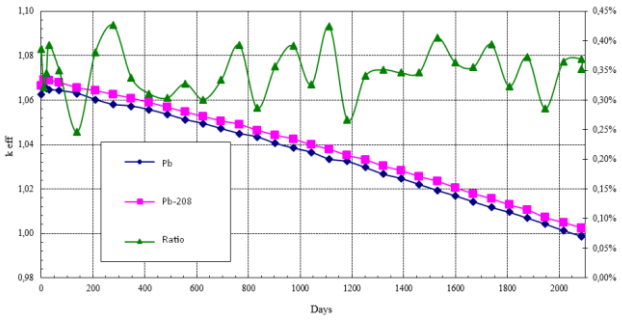

Figure 3 - Variation of multiplication factors for two fuel variants depending on irradiation time

Table 3 shows data on burn-up depending on coolant: eutectics lead (natural) - bismuth and lead (radiogenic) - bismuth.

Table 3 - Burnout depending on the coolant: eutectics lead (natural) - bismuth and lead (radiogenic) – bismuth

Days	Burnup (MWd/m)	K_{eff} (Lead (natural) – bismuth eutectic)	K_{eff} (Lead (radiogenic) – bismuth eutectic)	Ratio (%)
0	0	1.062455	1.066572	0.39%
10	2660	1.0656	1.069048	0.32%
209	55594	1.060185	1.064241	0.38%
695	184870	1.047144	1.050652	0.33%
1251	332766	1.029689	1.033207	0.34%
1807	480662	1.009589	1.012864	0.32%
2086	554610	0.998675	1.002206	0.35%

Table 4 shows the final results of multiplication factor depending on a coolant: eutectics lead (natural) - bismuth and lead (radiogenic) - bismuth at the beginning of irradiation (0 days) and at the end (2086 days).

Table 4 - Effective multiplication factor depending on the coolant: eutectics lead (natural) - bismuth and lead (radiogenic) - bismuth at the beginning of irradiation (0 days) and at the end (2086 days).

Name	0 days	2086 days
Eutectic lead (natural) - bismuth	1.0625	0.9987
Eutectic lead (radiogenic) - bismuth	1.0666	1.0022
Ratio, %	0.39%	0.35%

This change is almost entirely due to an increase in the fission reaction rate of uranium 238, which is known to have a threshold character (E_f>1 MeV), suggesting a significant change in the neutron spectrum when the coolant is replaced.

The obtained values of multiplication factor, burnup depth, and campaign duration have a significant impact on the economic characteristics of the reactor. The calculation of economic indicators, which is not given in this work, showed clear advantages of using radiogenic lead. The economics of the reactor makes the project promising and is one of the priority criteria for the further existence of the technology.

IV. CONCLUSIONS

In the framework of the Generation IV International Forum, a class of lead-bismuth-cooled fast reactors has been chosen as one of six system concepts for further development. Originally, a host of new missions were proposed for Lead Cooled Fast Reactor, made possible by the properties of Lead-Bismuth Eutectic, including hydrogen production, nuclear waste transmutation, and small modular reactors with long-life cores for supplying electricity and heat in remote areas and/or developing economies

This work is an attempt to improve the physical characteristics of reactors with lead-bismuth coolant by replacing natural lead with radiogenic lead.

It was found that the replacement of natural lead with radiogenic lead (isotope 208) in lead-bismuth coolant brings to an increase in the multiplication factor and an increase in burnup time to 2086 days, resulting in improved economic performance.

V. References

[1] Gromov B. F., Orlov Yu. I., Toshinsky G. I., Chekunov V. V. "Nuclear power plants with lead-bismuth coolant", Atomic Energy, Volume 81, Issue 5, November 1996, pp. 340-347.

[2] Zherdev G. M., Kislitsyna T. S., Nikolaev M. N. ROKOKO - a system of constant support for the calculation of reactors by the Monte Carlo method. News of higher educational institutions. Nuclear power engineering. 2018. No. 1. pp. 41-52.

[3] Jaakko Leppänen – PSG2 / Serpent – a Continuous-energy Monte Carlo Reactor Physics Burnup Calculation Code June 18, 2015 Methodology – User's Manua

Proceedings of the European Nuclear Young Generation Forum
ENYGF'21
September 27-30, 2021, Tarragona, Spain

The specific aspects of the New Generation SMLWRs, taking into account EUR requirements

Simonov, Pavel[1*], Chetverikov, Alexander[1] and Soldatov, Alexey[2]

[1] Rosenergoatom, Joint-Stock Company (REA JSC), Russian Federation; [2] WANO Moscow Centre, Russian Federation

*Corresponding author: *simonov-pe@rosenergoatom.ru*

I. INTRODUCTION

This article discusses issues related to the core and fuel for Small Modular Light Water Reactors (hereinafter referred to as SMLWR) in terms of the applicability of the current European Utility Requirements (hereinafter referred to as EUR [1]) and the specifics of these units.

The entry of SMLWRs into the Power Generation Market opens great potentials for further spread of the nuclear power into new sectors of the power generation market.

In order to be competitive on this new market, sectors designers and utilities should work together in development of the SMLWR designs to provide combination of high safety, reliability and performance characteristics.

New materials, new design solutions and new operation strategies should be introduced to achieve these goals.

The EUR Club (hereinafter referred to as the EUR Club) was establish by several European Electricity Producers. The one goal was to write down a common requirement document, called EUR, to control the design of the new LWR nuclear power plants to be built in Europe. It should provide suppliers with a clear vision of the needs of power generating companies, formulated in the form of requirements. The other is to provide new NPPs customers with information received from nuclear power generating companies on the selection of the best projects.

Russian specialists with the EUR Club partners together are carefully studying the requirements set by EUR in order to avoid a situation where the past experience of operating high power NPPs (PWR / BWR) would make the EUR requirements partially unsuitable for SMLWRs. In particular, current requirements may limit the use of new materials in fuel and the use of new fuel cycles that can make innovative SMLWR designs competitive. The object of consideration in the article is the SMLWR of a land-based location less than 300 MW (e).

II. SPECIFICITY OF CORES AND FUELS

There are a number of requirements related to the core as a whole, and a number of requirements concerning fuel use issues in the requirements of the EUR Club [1].

The following features of SMLWR can be distinguished, reflecting the specificity of cores and fuel design:

- smaller size of the core (greater power density gradients and potentially greater neutron leakage)

Below and further in the paragraph, I cite the requirements of the EUR, concerning the corresponding feature of the SMLWRs.

"The core design shall allow the flexibility of various reload fuel management schemes, including low neutron-leakage core configuration."

Figure 1. Requirement 2.2.3.3 A [1]

> For SMLWR the core design shall allow the flexibility of various reload fuel management schemes supporting achievement of safety and competitiveness goals. Low neutron leakage from the core is preferable, but should not override the priority of nuclear safety and competitiveness on the selected market;

- use of the new materials such as accident tolerant fuels of high thermal conductivity fuels

"The core design shall be optimised for UO_2 Fuel Assemblies.
However, provisions shall be made to allow the use of up to 30% standard MOX Fuel Assemblies* in the core, the remainder being UO_2 assemblies."

Figure 2. Requirements 2.2.3.1 A, B [1]

> There are significant expectations regarding the potential implementation of the different innovative fuel designs using advanced fuel and cladding related materials (e.g. in so called accident tolerant fuel (ATF)). Therefore, it should be ensured much higher extent of fuel cycle flexibility for SMLWR, e.g. full content of MOX,

recycled fuel (REMIX), thorium fuel and non-oxide fuels (e.g. metallic);

- use of the different fuel cycle management strategies (for example: full cartridge refueling of the core - with the entire batch of fuel assemblies in the core or removing the entire reactor module for refueling);
- use of the fuel with non-standard enrichment (above 5%) or MOX/REMIX as a major fissile material fuel;
- use of new materials for fuel rod cladding (for example: use of composite materials for fuel rod cladding instead of zirconium ones);
- use of a different geometry of fuel elements or assemblies (for example: fuel rods in the form of plates);
- fuel cycle length: desired fuel cycle length is defined by safety considerations, design specific limitations, local regulations, economic rationale providing competitiveness, and effective fuel use

"The core design shall allow the flexibility of operating on fuel cycles with refuelling intervals from 12 months up to 24 months, assuming Refuelling-only Outage."

Figure 3. Requirement 2.2.3.2 A [1]

- using of "boron free concept": SMLWR designs which do not use boric acid (i.e. so called "boron free concept") should also be covered. In the case that the "boron free concept" is applied the requirements on the assurance of two alternative (diverse) means for reactor shutdown shall be developed

"The capability of operation with low boron concentrations shall be considered in the design process. Appropriate investigations shall be performed and documented."

Figure 4. Requirement 2.2.3.7 [1]

- burnup: burnup requirements equal to the burnup values for large LWRs are practically unattainable. Assuming variety of potential design solutions for future SMLWR, allowable value of fuel assembly average burnup does not solely represent the real effectives of SMLWR fuel use. The vendor should provide the customer with design documentation illustrated that proposed fuel cycle parameters (fuel initial enrichment, discharged fuel burnup), are adequately considered, balanced and optimized to achieve design safety goals and economic competitiveness

"Fuel mechanical endurance

The mechanical design of the Fuel Assembly shall be such that discharged fuel is capable of an average burn-up of at least:

•55 MWd/kg of heavy metals atoms (kgHM) for UO_2 fuel with aMaximum Assembly Burn-up of at least 60 MWd/kgHM; and
•40 MWd/kgHM for MOX fuel, with a Maximum Assembly Burn-up of at least 45 MWd/kgHM.

The target for average burn-up should be:

•65 MWd/kgHM for UO_2 fuel (with a Maximum Assembly Burn-up of at least 70 MWd/kgHM); and
•55 MWd/kgHM for MOX fuel (with a Maximum Assembly Burn-up of at least 60 MWd/kgHM)."

Figure 5. Requirements 2.2.4.1 A, B [1]

These aspects result in the wider envelop of the possible design solutions and introduce new detentions for core design. Specific requirements to SMLWR fuel cycle, fuel system and core design are related to SMLWRs assumed character of operation in future electric systems.

All this, most likely, will require a revision of approaches to the design of the core, ensuring a balanced combination of the efficient use of nuclear materials and improving safety.

As an example, we can consider such a parameter as the fuel burnup (requirements 2.2.4.1 A and 2.2.4.1 B).

For SMLWR, it is impossible to achieve burnup values equal to burnup values for large LWRs for the following reasons:

1. Large neutron leakage from the lateral surface of the core (leakage is inversely proportional to the radius of the core).
2. Maneuverable mode of the reactor operation (estimated daily range of power variation: 20-100-20).

The burnup rate and the requirements for the duration of the company are determined by the underlying design solutions, in particular, by the customer's requirements, namely:

- operating modes of the reactor plant,
- economics of the project,
- the requirements of the power system and the implementation of these requirements in technical decisions concerning:
  - core designs;
  - materials of fuel assemblies and reactor plant;
  - fuel mechanical endurances.

A low value of neutron leakage from the core, as established by the EUR requirements, can be achieved only at large LWRs operating in a stationary mode with partial refueling of the core.

As a feature of SMLWR, one can single out the fact that in the case of a full refuel of the core, the one is refueled as a cartridge and there will be underburning of peripheral fuel assemblies, and the core will have residual criticality.

The features of the land based SMLWR cores are presented in Figure 6 below and scaled one – at the end of the article.

Pos.	Design	Country/Vendor	Fuel burnup (GWd/ton)	Fuel cycle (months)	Fuel enrichment (%)	Fuel type/assembly array
1.	CAREM	Argentina(CNEA)	24	14	3.1	UO2 pellet/hexagonal
2.	ACP100	China (CNNC)	<52	24	<4.95	UO2 pellet/17x17 square
3.	CAP200	China (SNERDI/SNPTC)	37	24	4.2	UO2 pellet/17x17 square
4.	DHR	China (CNNC)	30	10	<5.0	UO2 pellet/17x17 square
5.	IRIS	International Consortium (IRIS) Led by Westinghouse	65 (max)	48 (max)	4.95	UO2/MOX/17x17 square
6.	DMS	Japan (Hitachi-GE Nuclear Energy)	< 60	24	< 5.0	UO2 pellet/10x10 square
7.	IMR	Japan (Mitsubishi Heavy Industries)	40	24	4.8	UO2 pellet/21x21 square
8.	SMART	Republic of Korea (KAER)	< 60	36	< 5.0	UO2 pellet/17x17 square
9.	ELENA	Russian Federation (National Research Centre "Kurchatov Institute")	57.6/27.39	300	15.2	UO2 pellet; MOX is an option
10.	KARAT-45	Russian Federation (NIKIET)	45.9	84	4.5	UO2 pellet/hexagonal
11.	KARAT-100	Russian Federation (NIKIET)	45.9	90	4.0	UO2 pellet/hexagonal
12.	RITM-200	Russian Federation (Afrikantov OKBM)	-	60	<20.0	UO2 pellet/hexagonal
13.	RUTA-70	Russian Federation (NIKIET)	25-30	36	3.0	Cermet (0.6 UO2÷ 0.4 Al alloy) / hexagonal
14.	UNITHERM	Russian Federation (NIKIET)	1.15	200	19.75	UO2 particles in a metallic (silumin or zirconium) matrix, metal-ceramic
15.	VK-300	Russian Federation (NIKIET)	41.4	72	4.0	UO2 pellet/hexahedron
16.	UK SMR	UK (Rolls-Royce and Partners)	55 – 60	18 – 24	< 4.95	UO2 fuel in 17x17 array
17.	mPower	USA (BWX Technologies, Inc.)	< 40	24	< 5	UO2 pellet/17x17 square
18.	NuScale	USA, (NuScale Power Inc.,)	> 30	24	< 4.95	UO2 pellet/17x17 square
19.	SMR-160	USA Holtec International)	45 maximum.	18 – 24	< 4.95	UO2 pellet / square array
20.	Westinghouse SMR	USA (Westinghouse Electric Company LLC)	> 62	24	< 5	UO2 pellet/17x17 square

Figure 6. Cores features. Extract from [2]

Reactor designs that do not satisfy either EUR requirement 2.2.4.1 A, or requirement 2.2.3.2, or the generally accepted limit on the fuel burnup rate of 5%, or requirements 2.2.3.1 A, B, are marked with red.

Reactor designs that declare compliance with EUR requirement 2.2.4.1 A, requirement 2.2.3.2, the generally accepted limit on the fuel burn-up rate of 5%, requirements 2.2.3.1 A, B, are marked with yellow.

If the above requirements (applicable for large LWRs) are applied to SMLWR projects, then we will be faced with a situation where only 1 (out of 20) will meet these requirements.

III. CONCLUSION

As we can see, some of the aspects mentioned in relation to large LWRs have already been considered in the requirements of the EUR Club, however, apparently, the applicability of these requirements to SMLWRs needs to be clarified. And the Figure 6 clearly shows that the situation is ripe when the EUR requirements need to be revised taking into account the specific features of the SMLWRs. Otherwise, a situation may arise that a significant part of SMLWR projects will not receive a EUR Club certificate and will not be able to compete in the European market due to their specificity. The presence of the EUR Club certificate for the project means that the project meets the EUR requirements [1] and the trust of potential SMLWR customers is associated with it.

IV. References

[1] CEZ - EDF - EDF Energy - ENERGOATOM - ENGIE/TRACTEBEL - FORTUM - Gen Energija - HORIZON - IBERDROLA - MVM Paks II - NRG - ROSENERGOATOM - TVO - VGB PowerTech, “European Utility Requirements for LWR Nuclear Power Plants,” Revision E, December, 2016.

[2] IAEA, “Advances in Small Modular Reactor Technology Developments. A Supplement to: IAEA Advanced Reactors Information System (ARIS),” 2018 Edition.

Proceedings of the European Nuclear Young Generation Forum
ENYGF'21
September 27-30, 2021, Tarragona, Spain

Boron dilution sequence analysis in NuScale SMR using TRACE

Sánchez-Torrijos, Jorge[1*] and Queral, César[1]

[1] Universidad Politécnica de Madrid (UPM), Spain

* Corresponding author: *jorge.sanchez.torrijos@alumnos.upm.es*

I. INTRODUCTION

During the last few years, the nuclear industry has demonstrated a growing interest in the Small Modular Reactors (SMRs) throughout the world. In that sense, NuScale is a disruptive SMR design consisting of an integral PWR which relies on the natural circulation phenomenon to establish the RCS flow rate. Another important safety feature of the NuScale design is based on the implementation of only passive safety systems to deal with any accidental situations.

One of the most relevant international projects related to SMR modelling is the "High-Performance Advanced Methods and Experimental Investigations for the Safety Evaluation of Generic Small Modular Reactors" (McSAFER) Horizon 2020 Project launched in 2020. It is coordinated by Karlsruher Institut fuer Technologie (KIT) in which 12 additional partners are participating and the aim of the application of advanced simulation tools such as multiscale or multiphysics approaches to assess the performance of different SMR designs under specific transient scenarios is pursued. Within the framework of the McSAFER project, one task in which the UPM is involved consists of the development of a TRACE-1D model of the NuScale Power Module (NPM). In this study, a similar analysis to the one presented in the NuScale Design Standard Application (DCA) report of the Boron Dilution sequence is performed by means of the simulation of the commented transient with the UPM TRACE-1D model of the NuScale Reactor Coolant System (RCS). Afterwards, the results obtained using the TRACE model are presented and a good agreement is shown with the ones obtained in the DCA report.

II. NuSCALE DESIGN DESCRIPTION

NuScale Power Module ™ (NPM) is an integral concept of Small Modular Pressurized Water Reactor which relies on natural circulation to provide the primary coolant flow, in other words, the Reactor Coolant System (RCS) and the pressurizer (PZR) are integrated within a cylindrical Reactor Pressure Vessel (RPV), [1].

The RCS is composed of a small-sized core which is able to generate 160 MW of thermal power, a central hot riser divided into lower and upper riser regions with a transition region joining them, two independent and intertwined helically coiled steam generators (SGs) surrounding the upper riser, and a cold leg formed by the downcomer and the lower plenum. Furthermore, the RPV is contained within a cylindrical steel Containment Vessel (CNV) which internal pressure is maintained at a vacuum during normal operation. 90% of the CNV height is submerged in the reactor pool which acts as the ultimate heat sink under accidental conditions, [1].

Regarding the flow path within NuScale RPV, the heat generated within the core is transferred to the primary coolant accelerating it upwards from the core region to the riser. Then, the flow reaches the top of the riser where it is radially redirected into the annular region between the riser and the RPV and then, it is forced to flow downwards directly through the outer region of the SG tube bundles so that the heat in the coolant could be removed by the SGs. Within that region, the SGs performance results in an efficient cooling of the primary coolant flow, becoming denser, and it eventually returns to the lower plenum through the downcomer reaching the core inlet again and closing the primary loop, see Figure 1, [1].

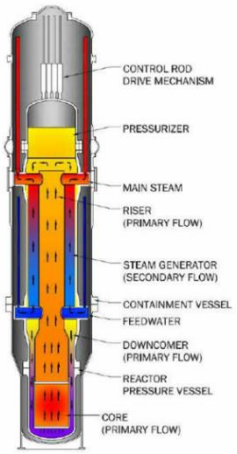

Figure 1. General arrangement and flow paths in an NPM

It is worth noticing that each NPM has an independent steam turbine, a dedicated Chemical and Volume Control System (CVCS), and two passive safety systems such that the

Emergency Core Cooling System (ECCS) and the Decay Heat Removal System (DHRS), [2].

The CVCS is responsible for controlling the Boron concentration in the RCS, the RCS water inventory, the PZR spray for controlling RCS pressure and the extraction of the non-condensable gases accumulated in the PZR steam bubble during normal operation, [3].

Table 1. Overall characteristics of a NPM [1]

Parameter	Value	SI Units
Core thermal power	160	MW
NPM electrical capacity	50	MW
RCS operating pressure	12.755	MPa
Steam generator type	Vertical helical tube	2
Number of fuel assemblies	37	-
Fuel assembly lattice	17x17	Square
Refueling intervals	24	months

III. NuSCALE TRACE MODEL DESCRIPTION

As part of the UPM participation in the McSAFER European Project, [4], a 1D TRACE model of the NPM has been developed. The main aim of this project is based on being able to compare the results obtained by means of the application of the different modelling tools (from the 1D model to the 3D multi-scale and multi-physics approaches) to investigate the impact of the usage of those tools on the results during Main Steam Line Break (MSLB) and Boron Dilution events.

Within that framework, an important effort was made to retrieve all data necessary to develop a TRACE model "from scratch" using only information coming from NuScale public references, see [5] to [11]. Furthermore, it is highly remarkable that TRACE options for modelling special geometry configurations have been used in the model, including certain type of PIPEs like "Tube Bank Crossflow" for modelling the primary side of the helical SGs.

With regard to the Boron Dilution event, the aim pursued by this study is to reproduce the results presented in the NuScale DCA report obtained by means of the analytical expressions of a perfect mixing model or a slug flow model, for further information see [7]. For that reason, the CVCS makeup and letdown flow rates have been explicitly modelled by means of FILLs components connected to the lower cell of the upper riser PIPE and to the cell immediately above of the transition region in the downcomer PIPE, see Figure 2.

Another important aspect to consider is that, similarly to what it is done in the NuScale DCA report, a constant power option with neither credit to the reactor protection system (RPS) nor reactivity feedback are deployed in the model.

Finally, the numerical approaches used in this study are the semi-implicit method for the time integration and the Van Leer modified with flux limiters method for the spatial difference in order to avoid the numerical diffusion phenomenon as much as possible.

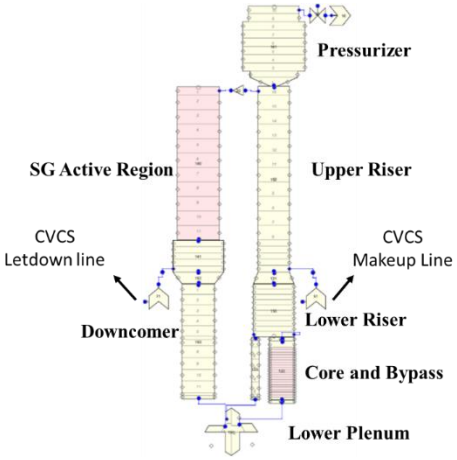

Figure 2. 1D TRACE model of the RCS of the NPM

IV. STEADY-STATE CALCULATION

A steady-state calculation of 5000 s has been performed to reach the correct starting point for the Boron Dilution event described in [6] and [7]. To do so, several assumptions are made and listed below:

- The reactor is initially working at Hot Full Power condition (100% Nominal Power). [9]
- Nominal values are assumed for the RCS parameters except for the mass flow rate which is restrained to its minimum DCA value (535.24 kg/s).
- The letdown flow rate is assumed to be equal to the makeup flow rate which is restrained to its maximum value (3.15 kg/s).
- The makeup temperature is assumed to be equal to the letdown temperature (531.47 K).
- The initial Boron concentration is 1600 ppm.

A comparison between the steady state results obtained by means of the TRACE model and the NuScale DCA report is depicted in the table 2.

Table 2. Steady-State values comparison

Parameter (SI Units)	DCA report	TRACE
RCS Pressure (MPa)	12.755	12.754
Core Inlet Temperature (K)	531.48	531.44
RCS Mass flow rate (kg/s)	535.24	535.15
Core Mass flow rate (kg/s)	496.17	495.93
Bypass Mass flow rate (kg/s)	39.08	39.22
PZR level (%)	60.00	59.99

V. BORON DILUTION EVENT IN NuSCALE

In this section, a brief description of the Boron Dilution event at full power as well as its consequences in the NPM is made. Then, the mixing models applied in the DCA report

to calculate the time to loss the SDM and the Boron concentration at that instant are analysed and, finally, the results obtained in the simulation with the TRACE model are described.

As a reminder, the main aim of this study is to verify that the acceptance criterion for the Boron Dilution transient at full power is met by means of the demonstration of that the available time to loss the minimum Shutdown Margin (SDM, defined as the instantaneous amount of reactivity by which the reactor is subcritical or would be subcritical assuming all full-length control rods cluster assemblies are fully inserted except for the single rod cluster assembly of highest reactivity worth that is assumed to be fully withdrawn) is greater than 15 minutes. To do so, the Boron concentration at the instant in which the SDM results completely lost is calculated simulating the transient with the TRACE model and then, the results are compared against the ones obtained by the different approaches presented in the DCA report.

A. Boron dilution event description

In accordance with [7], the unintentionally addition of unborated water within the RCS could be produced by the malfunction of the CVCS or an operator error in the Boron concentration adjustment operation. In addition, the dilution rate is obviously influenced by the Boron concentration of the water inventory pumped by CVCS into the RCS but also by the actual flow rate provided by the makeup pumps, the actual RCS flow rate, and the RCS loop length.

Once the unborated water starts to be pumped within the RCS by CVCS, it must go through all RCS loop long spreading the reduction in the Boron concentration to all regions in that loop, so it could be understood as a dilution front which is turning around the RCS, see Figure 3. In that sense, the definition of the “transit time” concept becomes mandatory, so it is the time taken by the fluid for passing along the whole RCS one time and, it determines the time intervals within the Boron dilution takes place.

The main consequence of the Boron Dilution event within the RCS consists of a reactivity increase caused by the reduction in the Boron concentration within the core region and, consequently, a reduction of the SDM. Therefore, the core power is increased, the RPS trips the reactor, and the Demineralized Water System isolation signal is triggered, stopping the injection of the unborated water to the RCS.

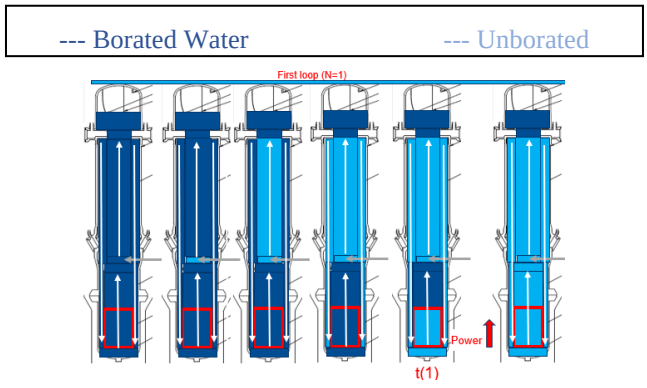

Figure 3. Boron Dilution Front evolution within the RCS

B. Perfect mixing and Slug flow models

Both, the perfect mixing model, and the slug flow model are applied in Chapter 15 of the NuScale DCA Report, for further information about those models see [7]. The **perfect mixing model** assumes that the unborated water injected in the RCS by the CVCS is mixed instantaneously with the whole RCS volume in a homogenous way resulting in a continuous and decreasingly monotonic variation in the Boron concentration of the RCS, as shown in Figure 4.

On the other hand, the **slug flow model** is based on the movement of the dilution front along the RCS. Therefore, the Boron concentration variation within the core is function of the transit time, the number of times that the dilution front had passed through the core and the dilution front Boron concentration itself. In addition, the slug flow model is a discrete one, as it can be seen in Figure 5.

In accordance with the results obtained by means of the perfect mixing model application presented in [7], the reactivity insertion rate is 1.11 pcm/s and the time to loss of SDM is 30.5 min. Similarly, for the slug model case, the initial reactivity insertion rate is 34.35 pcm/s and the time to loss of SDM 31.3 min. Finally, the Boron concentration at the instant in which the SDM is lost is 1388.47 ppm. Then, the objective of the analysis with the NPM TRACE model is to verify in what instant of time this concentration is obtained and that this value is greater than 15 minutes.

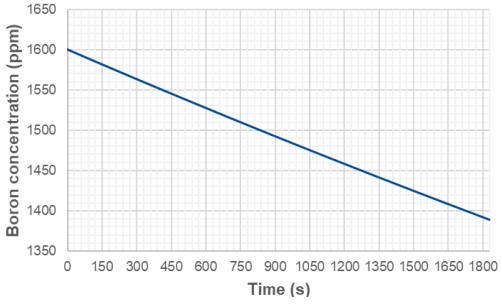

Figure 4. Boron Dilution assuming perfect mixing

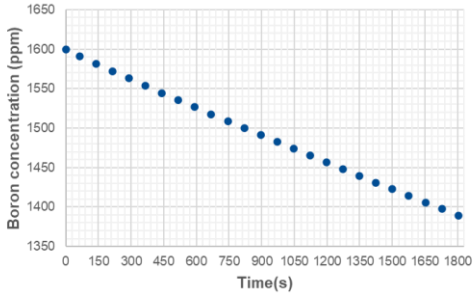

Figure 5. Boron Dilution assuming a dilution front propagation

C. TRACE model: Transient calculation

After 5000 s of steady-state calculation, the Boron concentration of the CVCS makeup flow starts to inject unborated water to the RCS, the Boron concentration in the injection goes from 1600 to 0 ppm and the transient calculation begins.

As it can be seen in Figure 6, the Boron concentration within the core region follows a decreasing stepwise function of time as expected. After 1840 s of transient simulation, the

critical Boron concentration value is reached and the SDM is considered lost and then the acceptance criterion is verified (t > 15 min). Furthermore, it is worth noticing that the fluid needs to turn around the RCS 25 times to eventually diminish the Boron concentration to the critical value.

Finally, a summarizing table with a comparison amongst the results obtained by means of TRACE and the previously commented model used in the DCA is included, see Table 3. These results show a good agreement between the slug flow model from DCA report, and the TRACE model developed by UPM.

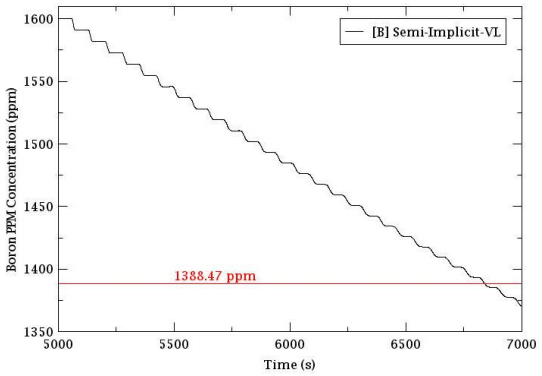

Figure 6. Boron concentration evolution in the core region (TRACE)

Table 3. DCA models and TRACE simulation results

Loss of SDM	Perfect mixing	Slug flow	TRACE-1D
Time to loss of SDM (s)	1830	1879	1840
Times that the wave front passes through the core	-	25	25

VI. CONCLUSIONS AND FUTURE WORKS

The conclusions extracted from this study are listed below:

- The acceptance criterion for the Boron dilution sequence at full power is met in the UPM TRACE-1D model.
- The results obtained using the UPM TRACE-1D model have shown a good agreement with the ones obtained by means of the DCA report models.
- TRACE is able to capture the physics of the Boron dilution transient and it will be applied to future works considering the reactor trip and reactivity feedbacks.
- An unavoidable amount of numerical diffusion is shown in the results. An analysis in depth of this issue is currently in progress.

Regarding the ongoing works, the point kinetics model will be included in the UPM TRACE-1D model to verify the results of the Boron dilution transient by means of a 1D best-estimate model. Later, more detailed 3D models will also be developed allowing us to assess the impact of possible asymmetrical effects in the results and additional transients will be analysed.

VII. ACKNOWLEGMENTS

McSAFER project has received funding from the Euratom research and training programme 2019-2020 under the grant agreement No 945063.

The content of this paper reflects only the authors' views and the European Commission is not responsible for any use that may be made of the information it contains.

The authors would like to thank to NuScale Power, LLC for granting us the permission to use the NuScale figures in this paper.

VIII. REFERENCES

[1] NuScale Power LLC, «NuScale Standard Plant: Design Certification Application: CHAPTER 1: Introduction and General Description of the Plant,» Rev.5, July 2020.

[2] NuScale Power LLC, «NuScale Plant Design Overview,» Rev.2, September 2013.

[3] NuScale Power, LLC, «NuScale Standard Plant: Design Certification Application: CHAPTER 9: Auxiliary Systems,» Rev.5, July 2020.

[4] Karlsruhe Institute of Technology (KIT), "McSAFER Project website," 2020. [Online]. Available: https://mcsafer-h2020.eu/about-mcsafer/.

[5] NuScale Power LLC, «NuScale Standard Plant: Design Certification Application: CHAPTER 3: Design of Structures, Systems, Components and Equipment,» Rev.5, July 2020.

[6] NuScale Power LLC, «NuScale Standard Plant: Design Certification Application: CHAPTER 4: Reactor,» Rev.5, July 2020.

[7] NuScale Power LLC, «NuScale Standard Plant: Design Certification Application: CHAPTER 5: Reactor Coolant System and Connection systems,» Rev.5, July 2020.

[8] NuScale Power LLC, «NuScale Standard Plant: Design Certification Application: CHAPTER 6: Engineered Safety Features,» Rev.5, July 2020.

[9] NuScale Power LLC, «Submittal of "NuFuel-HTP2 Fuel and Control Rod Assembly Designs",» TR-0816-51127, Rev.3, December 2019.

[10] NuScale Power LLC, «Submittal of Technical Report TR-0916-51502, "NuScale Power Module Seismic Analysis",» Rev.2, April 2019.

[11] NuScale Power, LLC, «Nuclear Analysis Codes and Methods Qualification,» Rev.1, November 2018.

[12] NuScale Power, LLC, «NuScale Standard Plant: Design Certification Application: CHAPTER 15: Transient and Accident Analyses,» Rev.5, July 2020.

Proceedings of the European Nuclear Young Generation Forum
ENYGF'21
September 27-30, 2021, Tarragona, Spain

Main Control Room Staffing of Small Modular Reactors: Analysis and Validation

Hervás, Borja[1*]

[1] Tecnatom S.A., Spain

* Corresponding author: *bhervas@tecnatom.es*

I. INTRODUCTION

The Small Modular Reactors (SMRs) constitute a promising way of delivering reliable, carbon-free energy in many applications, such as providing heat and electricity to remote locations. One of the major objectives of the advanced designs is to improve the economics, especially to reduce the operational costs of the plant. The resulting design is expected to be a cost-competitive nuclear facility that will help to meet climate change goals in the new clean-energy economy.

The SMRs are optimized with a fixed number of reactors, up to twelve depending on the design, because it maximizes the capabilities of the shared systems. Human-machine interaction has been simplified from the early conceptual design phases by the massive use of passive safety systems and maximizing automatization of processes. In that way, the initial philosophy of operation oversees one control room governing several reactors and controlled by a reduced crew of licensed operators.

This concept goes beyond the current rules and codes for existing nuclear power plants. In this sense, Human Factors Engineering (HFE) analysis and validation activities are suitable to prove the safe operation of the plant, so that an exemption of the existing regulation can be addressed by the license applicants.

The analysis phase includes new tactics to face the HFE Program of an advance Small Modular Reactor (SMR) compared to a large Light-Water reactor: new plant missions, system functions, operator tasks and jobs, roles, and responsibilities in the operation crews. Later, staggered validations using virtual mock-ups are planned at several steps of the design process. Finally, an integrated system validation will be performed in the plant full scope simulator, which will replicate the operational conditions of the most challenging scenarios from the Human Factors perspective.

II. HUMAN FACTORS ENGINEERING PROGRAM

The HFE Program covers the analysis and validation of the control room staff. In this case, the HFE Program represents a new challenge completely different from a conventional large Nuclear Power Plant staff analysis. Besides designing human-oriented Human-System Interfaces (HSIs) and reducing human error risk to the minimum, the Program's goals target to lower drastically the operations staff.

New plant missions and different critical scenarios due to the advanced technology designs are facts that need to be addressed in the HFE Program.

The guidance to be followed is NUREG-0711 [1]. The Program basically addresses the technical elements described on that document. However, this guidance is complemented with NUREG-1791 [4] requirements, to comply with the challenging plant staffing reduction goals.

Among all the NUREG-0711 [1] technical elements, the following ones are essential to ensure a correct staffing analysis and validation:

- Operating Experience Review (OER)
- Functional Requirements Analysis and Function Allocation (FRA & FA)
- Task Analysis (TA)
- Staffing & Qualifications (S&Q)
- Human Factors Verification & Validation (HF V&V)

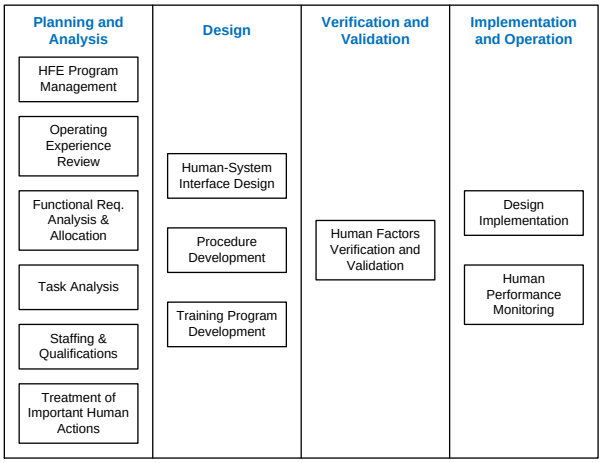

Fig.1. NUREG-0711 [1] technical elements

This paper describes how the control room staffing is determined, evaluated, and tested, from the initial Concept of Operations until the last Integrated System Validation explaining some of the key-aspects from the NUREG-0711 elements listed.

III. CONCEPT OF OPERATIONS

The Concept of Operations introduces the staffing, qualifications and operation assumptions that will be subsequently consolidated, modified or dismissed during the development of the HFE Program.

The SMRs control philosophy relies on a high level of automation and passive phenomena enabling a much-simplified control that significantly reduces the workload of the operator and the control system in normal operation.

The plant control concept facilitates continuous monitoring, plant manoeuvring, and allows the operators to avoid repetitive tasks. This design objective aims to minimize operator human error. In the same way automation performs functions associated with parameter and process monitoring, continuous process control, safety function monitoring, and safety actuations. Operators periodically check process parameters being continuously monitored by automation. For example, plant mode changes are automated in specific designs, so the operator only verifies the automatic action. This represents a big difference in the usual concept of operations from the HFE perspective.

IV. ANALYSIS

The initial iteration of the analysis relies on the assumptions made in the Concept of Operations and provides reasonable inputs to the S&Q evaluation.

A. Operating Experience Review

The starting activity of the analysis is the Operating Experience Review. which should identify two types of experiences: staffing issues to be avoided, and effective staffing practices to be incorporated into the operation environment. Research shall look into similar designs, prototype reactors and recent modular designs. Multi-unit operation experiences can be found in other industries and plants giving valuable insights for the plant operation. For example, remote and multi turbine operation can be found in Combined Cycle power plants. Practices, especially for the maintenance staff, more than the control room can be found into gas and coal units. However, safety culture from nuclear industry shall prevail.

B. Functional Requirements Analysis and Function Allocation.

The second activity of the analysis is the Functional Requirements Analysis and Function Allocation. The first one aims to identify the functions that must be performed to achieve plant goals. The different applications of the plant may add new functions and system functions, such as hydrogen production (specially in those high-temperature advance designs), process heat industrial application or district heating.

The Function Allocation assigns the functions to personnel, system elements, or combination of both. It is expected a massive allocation to system elements due to the high automation of processes and passive features.

C. Task Analysis.

The remaining functions allocated to personnel require actions that are integrated into a hierarchical structure of tasks and activities, which is the subject of the next analysis. The task analysis provides information to identify task timing and workload issues, giving potential information to determine conflicts that would affect the staffing configuration.

The results of these analysis, specially from Task Analysis, are a powerful tool for the subsequent steps. The following activities consistently share the task requirements for different purposes: job definition, staffing & qualifications evaluation, HSI design, and procedures and training programs.

V. EVALUATION

The staffing evaluation shall be done by using the tasks information. At this point, an evaluation is performed by assigning each activity to the adequate operator in several scenarios. In this case, the evaluation focuses in the more challenging scenarios, not typically seen in large nuclear plants analysis.

For example, multi-unit emergencies, online refuelling in pebble bed reactor designs, and critical scenarios identified through the Probabilistic Risk Assessment (PRA) of the plant design.

The staffing evaluation is based in the preliminary sequence and timing of tasks set by subject matter expert, showing the potential limitations of the staff. The conclusions lead to staffing modifications and Human-machine interface design change decisions.

It is worth noting that operators are planned to be multi-skilled and versatile, so extra tasks related to plant maintenance can be assigned also to them. Also, maintenance personnel are going to be instructed in control room tasks, so the entire plant staff would be able to share its functions across the plant in a flexible and efficient way.

This is supported by the previous analysis in which control room tasks have been reduced and allows the operators not only to extent their responsibility to more than one reactor, but also to have the ability to perform local tasks.

The results of the evaluations, after iterations of the analysis if required, confirm the size of the control room shift crew, which might vary from the initial established in the Concept of Operations.

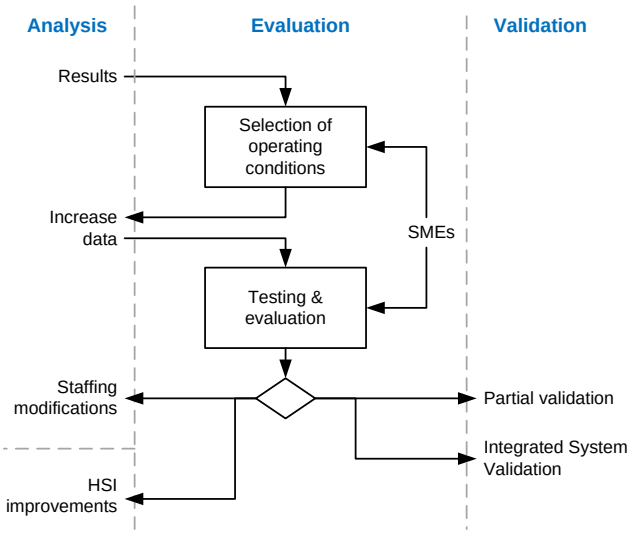

Fig.2. MCR crew evaluation process

VI. VALIDATION

The staffing validation refers to an assessment using performance-based tests to determine whether the staffing plan meets performance requirements and supports a safe operation of the plant.

The validation tests are planned to be performed during several phases of the design. In the beginning, by early partial validations with portions of the HSI design. Finally, when the complete simulation environment is ready, the Integrated System Validation (ISV) is performed. In this way, the HFE Program ensures operator's gradual adaptation to the HSI and control room environment from the beginning of the design until meeting the final one. Tools such as augmented reality, virtual reality and digital twins can be used during partial validations at intermediate design phases.

The validations should demonstrate that the reduced plant shift crew can satisfy the plant and human performance requirements identified in the analysis. Or, if the result is negative, to iterate the previous analysis and design activities.

The fundamentals for conducting a successful validation are:

a. Sampling of Scenarios. The range of operational conditions identified as relevant during the analysis should be part of this sample. As previously commented, multi-unit emergencies and critical sequences from the PRA should be part of the sample.
There are three kind of multiple scenarios to be examined: a. specific design bases accidents of equipment malfunction at the same time in different reactor modules, b. plant events such as fire, flooding or earthquakes that affect shared systems (heat sink, common external grid) and common plant areas and c. accidents during construction or commissioning phase in one reactor unit that affect the rest that are in operation.
The plant simulator shall be capable to simulate such kind of scenarios to conduct a proper validation.

b. Testbed conditions. A description of the validation environment, providing: the scenarios to be tested, a representative number of trained crews and scenario repetition, the state of the simulator and simulation conditions, and the number and duties of the HFE observers.
In the early stages of the validation a wide range of profiles can be selected as operators. People from different fields of engineering and industry might be candidates to receive the training and perform the simulations.

c. Human Performance Measures. Data shall be collected during the tests through observation, questionnaires, plant data extracted from the simulation console, and alternative methods: eye-tracking, health parameters tracking or operators movement tracking.

d. The data should be analysed and processed considering a set of performance measurements that are established prior to the validation:
- time to complete actions, especially those identified as critical
- timeliness of actions
- accuracy and completeness of actions.
- omitted actions
- percentage of automated actions verified by the operators
- workload metrics based in NASA-Task Load Index (NASA-TLX)
- situation awareness metrics based in Behaviourally Anchored Rating Scale (BARS) and
- teamwork metrics based in Situation Awareness Rating Technique (SART).

e. Validation criteria. To determine the acceptability of the results, a set of criteria, related to the performance measures, is identified in advance of the validation. Examples of validation criteria are:
- nominal task performance times have not been exceeded,
- no more than N seconds have been required to begin Task X after Event Y,
- no actions in the procedures have been be omitted,
- critical actions have been performed on time,
- percentage of verified automated actions is above 90%,
- main plant parameters have been kept inside normal operational range,
- the scenario finished with the plant in a safe state, and/or
- plant mode X was reached.

VII. CONCLUSION

The four facts below will ensure the plant success on its staff analysis and validation.

i. To perform a complete Task Analysis, which is key-important to ensure proper correspondence between staffing evaluation and validation, procedures, training program and HSI design. A multi-skilled and versatile operations crew aids to reduce operation and maintenance costs.

ii. To perform a staggered validation through human-in-the-loop simulations from the initial partial validations until the final integrated system validation in order to ensure end-user and human-oriented HSI design. New technologies such as augmented reality, virtual reality and 3D models help to develop these tests without significantly increasing project costs.

iii. To include simultaneous abnormal and emergency events on multiple modules in the control room simulator in the validations. Those scenarios likely produce challenging and high workload conditions which are need-ed to assess the proposed staffing reduction to operate the plant safely.

iv. A wide range of profiles should be selected for the early validations, including technicians, engineers, and experienced operators who will be previously trained in the new technology. This variety of profiles will enhance the quality of the test results.

VIII. ACKNOWLEDGMENTS

To my family and to the Tecnatom team involved in the development of a new era of reactors, for a clean and reliable world's energy future. Special thanks to Héctor Martínez-Pinna for providing some of the figures in this paper and give valuable comments to it.

IX. REFERENCES

[1] M. O'Hara et al., "Human Factors Engineering Program Review Model," NUREG-0711, U.S. Nuclear Regulatory Commission, Washington, United States (2012).

[2] "Design of Reactor Facilities: Nuclear Power Plants," REGDOC-2.5.2, Canadian Nuclear Safety Commission, Ottawa, Canada (2014).

[3] "Human Factors Engineering in the Design of Nuclear Power Plants," SSG-51, International Atomic Energy Agency, Vienna, Austria (2019).

[4] J. Persensky et al., "Guidance for Assessing Exemption Requests from the Nuclear Power Plant Licensed Operator Staffing Requirements Specified in 10 CFR 50.54(m)," NUREG-1791, U.S. Nuclear Regulatory Commission, Washington, United States (2005).

[5] "Human Performance Management: Minimum Staff Complement," REGDOC-2.2.5, Canadian Nuclear Safety Commission, Ottawa, Canada (2019).

[6] J. O'Hara, J. Higgins, and M. Pena, "Human-Performance Issues Related to the Design and Operation of Small Modular Reactors," NUREG/CR-7126, U.S. Nuclear Regulatory Commission, Washington, United States (2012).

[7] J. O'Hara, J. Higgins, and A. D'Agostino, "NRC Reviewer Aid for Evaluating the Human-Performance Aspects Related to the design and Operation of Small Modular Reactors," NUREG/CR-7202, U.S. Nuclear Regulatory Commission, Washington, United States (2015).

Hot Topic 2 - Energy Transition: The Role of Nuclear

Opportunities and challenges for the production of hydrogen using nuclear energy in the UK.
Authors: Simpson, Allan; Veron, Emin; Saleh, Amr

Unique Approaches to Reshaping the Nuclear Narrative.
Authors: Mairinger, Matthew

Nuclear energy: a stumbling-stone on the way to “green” future or a provider of power grids stability.
Authors: Lazareva, Polina

Aging management: the key to long-term operation.
Authors: Martín Huete, Laura; Colomines Martí, Martí; Páez Galice, Andrea; Fole Hernández, Joaquín; Bernad Rodríguez, Maria del Salz; Salvador Fernández, Óscar; Amorós Trias, Xavier

Small Modular Reactors in terms of architectural design and site construction.
Authors: Smakhtina, Anastasia

Nuclear costs and policy.
Authors: Kokurin, Nikita

The role of nuclear energy in electricity power systems with high res share.
Authors: Korolev, Vyacheslav Igorevitch

Developing nuclear technologies as a vital step in the approach to reduce CO2 emissions.
Authors: Talyzina, Olga

Development and implementation of Project Management in Akkuyu Nuclear Power Plant construction and operation project.
Authors: Feoktistov, Anton

A hybrid project management approach in the nuclear industry. Project tracking.
Authors: Malozemov, Sergey

Gender Balance for a Sustainable Energy Transition.
Authors: Emelianova, Anastasiia; Ozerina, Milana; Andriushina, Anastasiia

The assessment of perspective npp implementation for industrial hydrogen production.
Authors: Kolbantcev, Iurii; Seleznev, Nikolai

Key factors affecting public acceptance of nuclear power.
Authors: Okorokova, Margarita

The uranium markets: a way through policies.
Authors: De Maria, Sergio

Automatic control system for NPP participation in electrical current frequency regulation in the power network with thermal energy storage system.
Authors: Shchuklinov, Aleksei

What happens when everything goes wrong: Insurance.
Authors: González Felgueroso, Ana; García García, Pablo

Building an atomic future: The role for nuclear power in addressing major humanitarian challenges in the 21st century.
Authors: Lindberg, John C.H.

Detailed numerical analysis of different energy scenarios and the role of nuclear energy in the decarbonization pathways of the Hungarian electricity system.
Authors: Biró, Bence; Aszódi, Attila

Analysis of some specific uranium and transuranium isotopic mixtures to enhance the mass and radiation barriers of uranium-plutonium compositions against unauthorized proliferation.
Authors: Ozerina, Milana

Proceedings of the European Nuclear Young Generation Forum
ENYGF'21
September 27-30, 2021, Tarragona, Spain

Opportunities and challenges for the production of hydrogen using nuclear energy in the UK

Simpson, Allan*, Veron, Emin and Saleh, Amr

National Nuclear Laboratory, United Kingdom

*Corresponding author: allan.simpson@uknnl.com

I. INTRODUCTION

Achieving worldwide carbon emissions reduction targets will require decarbonisation of both electricity and non-electricity energy vectors. Hydrogen has been suggested as a clean energy carrier for multiple sectors such as transport, industrial applications and heating, therefore the ability to produce hydrogen at scale has been studied by various research projects throughout the nuclear sector.

The UK government's own carbon reduction strategy targets 'net zero' carbon emissions by 2050 [1]. This has highlighted the potential of hydrogen to address this unprecedented decarbonisation challenge in the UK. National Nuclear Laboratory (NNL) has led a research project that helps understand further how the demands of hydrogen generated from nuclear technology are likely to evolve over the coming decades and how these technologies, when paired together could address future demand. It aims to understand:

- the most likely hydrogen production technologies for deployment;
- the required target cost for generating hydrogen these will need to achieve.

Given the large range of technologies proposed for nuclear derived hydrogen production worldwide, an early step in the project was to prioritise the technologies likely to give the most benefit to UK decarbonisation needs. An array of future markets and technology couplings were selected based upon the requirements of the project including current and forecast energy consumption and maturity of the technology or market. This has then been analysed in the context of potential benefits and dis-benefits of each different technology to each market using available literature. An assessment of the integration of a nuclear-hydrogen paired technology in each market is captured in a five-point ranking system and intended to underpin recommendations for further research. These assessments have been made using a supply chain model to understand where nuclear enabled hydrogen may have benefits over non-nuclear competitor solutions.

Based on the outputs of this analysis, further research has been completed to understand the main pain-points associated with deployment of the proposed technologies. This paper summarises the technologies and the high level associated challenges.

II. ANALYSIS

A qualitative method was used to consider the benefits and dis-benefits of hydrogen from nuclear in comparison to other, market appropriate, decarbonization options. This method was based around the hydrogen supply chain (as shown in Figure 1). It is known that the cost of hydrogen to the consumer is influenced by many factors throughout this supply chain such as conversion and storage requirements, which can in turn be influenced by the hydrogen production technologies and fuel forms used.

To make this assessment, future hydrogen markets and coupled systems (a combination of a nuclear technology and a hydrogen production technology) were split out into relevant groups. For each intersection, the available open literature evidence was used to answer a series of questions focused around the market, geography, competitors, technology and the supply chain and in turn generate a ranking on a five point scale that was averaged to create a final rating for that intersection.

Hydrogen production technologies were split into direct electrolysis of water using only electricity, steam electrolysis utilising both heat and electricity for higher efficiency conversion and thermochemical techniques that make use of predominantly reactor to process heat to drive catalytic processes. Table 3 summarises the splitting of the markets selected for analysis.

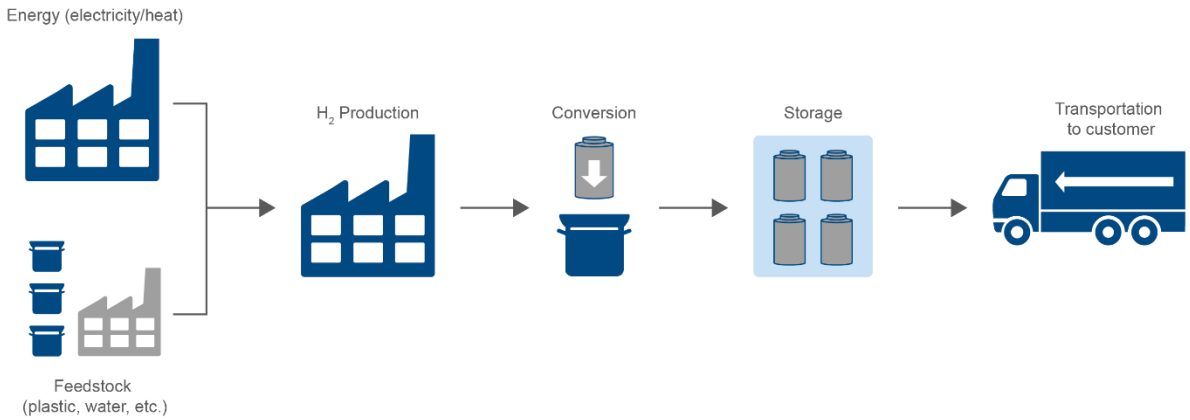

Figure 2: Analysis of market and coupled system intersections was based on the different aspects of a hydrogen supply chain and how nuclear technologies offer benefits over other proposed hydrogen and decarbonization options

Table 1: Summary of the split applied to current and future markets for hydrogen in the UK

Category	Subcategory	Notes
Industrial	Chemicals	Presents a current demand, predominantly in the production of fertilizer
	Refineries	Presents a current demand, noting that hydrogen is also a by-product of refining
Mobility	Large scale land	Defined as uses where a need for long distance or heavy haulage are paramount, such as trains and HGVs
	Small scale land	Covers all other powered land based transportation that often relies on networks of fuel stations
	Air	Covers all types of aviation, although dominated by commercial air traffic
	Sea	Covers all types of shipping, dominated by cargo
	Space	Includes the rising use of commercial space launch, and potential for commercial human flight
Electricity & Storage		Hydrogen as a method for inter-seasonal energy storage or transferring energy to remote communities
Heating	Domestic	Covers space heating where the current process is dominated by local boilers
	Industrial	Includes both space heating and process heat

The analysis showed that the energy consumption in some of these markets is significant and has the potential to support tens if not hundreds of reactors, dependant on the rate of deployment of non-nuclear technologies. Whilst there may be technical limitations on deployment in some markets, capturing a fraction of the market would be a substantial demand for nuclear technology deployment through to 2050 [2].

Table 4 provides the full set of rankings applied for the different technology couplings and markets identified. It was noted through these analyses that several markets have correlations in how they develop and there are strong parallels between some of the technology couplings. As such, groupings of markets and technologies have been selected for further investigation and development:

- Steam electrolysis hydrogen production technology coupled with small modular reactors or advanced modular reactors has potential for aviation, large and small scale land transport markets and domestic heating.
- Thermochemical processes for producing hydrogen coupled with advanced modular reactors has potential for aviation and large scale land transport markets and domestic heating.

It should be noted that the intention of this process was to identify areas where nuclear derived hydrogen production is most likely to offer relative benefits as a prioritisation process as opposed to down selection of options. This has then been used to focus the next stage of research and development on technology challenges.

Table 4: Summary results from the qualitative analysis in each market and technology intersection. Intersections are ranked on a five-point scale of 1 to 5 where 1 corresponds to very poor 5 very good based on a set of qualitative considerations. Five groupings are highlighted which indicate the most promising applications for nuclear generated hydrogen according to this analysis.

	GW scale LWR with direct electrolysis	LWR SMR with direct electrolysis	LWR SMR with low temperature steam electrolysis	HTGR with steam electrolysis	HTGR with thermochemical processes	LMFR with thermochemical processes	LMFR with steam electrolysis
Industrial – Chemicals	3	1	4	2	2	2	2
Industrial – Refineries	2	2	3	1	1	1	1
Mobility – Small scale land	3	4	4	4	4	3	2
Mobility – Large scale land	4	3	5	5	5	3	3
Mobility – Air	3	3	4	5	4	4	4
Mobility – Sea	2	2	3	3	4	4	3
Mobility - Space	2	2	4	4	3	3	4
Electricity & Storage	3	2	3	4	4	4	3
Heating – Domestic	2	3	4	5	4	3	3
Heating – Industrial	3	1	4	4	3	1	3

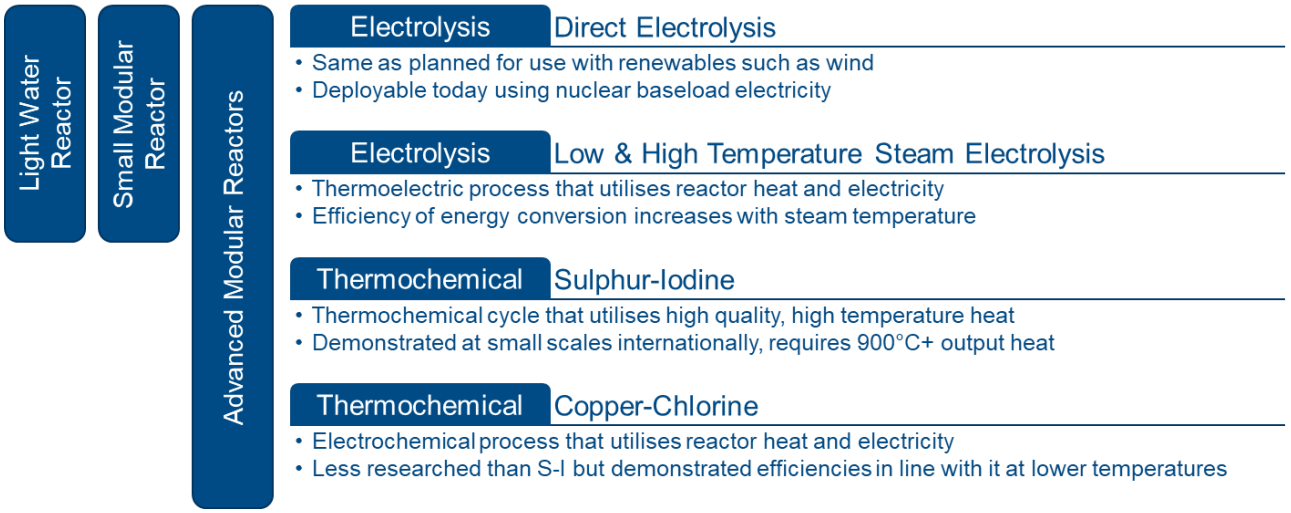

Figure 3: Summary of hydrogen generation technology options and associated reactor technologies that are considered suitable for coupling with them

III. TECHNOLOGY OPTIONS

For industrial large-scale production nuclear power plants could be employed to provide the electricity for direct electrolysis. Electrolysers may be spatially separated from the sources of electricity generation. However, the long-term economics of hydrogen production from direct electrolysis are expected to be challenging [3]. Long term research has demonstrated that hydrogen production processes operating at higher temperatures will be more energy efficient. Such processes may involve energy inputs of both heat and electricity, but the supply of heat at higher temperatures and reduced requirements for electricity offer the potential for better long-term economics for hydrogen production than low temperature electrolysis.

Nuclear heat and nuclear waste heat are significant sources of energy and are yet to be fully exploited commercially in the various opportunities created through the need to move to a global low carbon economy. Most Generation IV reactors produce heat and waste heat at a much higher temperature than light-water Generation II/III reactors, and so potentially make an ideal coupling for thermochemical processes to generate hydrogen which tend to operate in regions of 500-950°C [3].

Hydrogen production technologies identified and considered in the market analysis encompass electrolysis and thermochemical processes. Figure 5 outlines how these technologies could be coupled with reactor technologies.

Research on steam electrolysis, specifically in the form of Solid Oxide Electrolysis Cells (SOECs) has grown in recent years [4]. Research is predominantly focused on optimising new microstructures for the materials of the anode and cathode solid electrolytes to promote the longevity of systems, especially for high temperature regimes. Commercial solid oxide electrolysers are used for splitting CO2 and for Fuel Cell mode operation. SOEs for SOECs have not yet been commercialised [5].

The Cu-Cl process liberates hydrogen from water using a copper and chlorine intermediate species which reacts with water to produce hydrochloric acid. The chlorine is recovered from the acid using a solid copper phase and recycled in the process as $CuCl_2$. There are many different variants of this process, all relying on the use of Cu-Cl intermediate species which are recycled through the process. The lower potential of the electrolysers used within this process help to increase efficiency in comparison with the water electrolysis options previously outlined.

The S-I process is a thermochemical process that runs at high temperatures and is shown to be one of the most promising of the thermochemical cycles in literature. Despite the high visibility and interest in this process, there are numerous technical challenges still to be overcome with this technology. Given the high process temperature input required at points in the cycle, it is often proposed to be paired with HTGR technology [6].

Hydrogen generation plants which use the heat of a nuclear reactor will need intermediate exchangers to transfer the heat from nuclear reactor. It is usual (except in boiling water reactors) for a primary coolant to circulate heat from the core to a secondary coolant via an intermediate heat exchanger. Where there is process heat extraction this is typically from the secondary coolant system or from the power conversion plant. This reduces the number of components and systems on the primary side and eases the management of system transients when electricity generation and heat extraction loads may vary independently. Therefore a combined and variable thermal load will typically be managed through steam generators as the Intermediate Heat Exchangers (IHXs) on the reactor side of the coupling.

Current reactor systems are managed through complex regulation to ensure that reactor operation is ALARP and within the envelope of the safety case. The author notes that for nuclear generated heat to be utilised, this must be addressed within the safety case for reactor operation, or the hydrogen production plant must be decoupled from the nuclear site. Both approaches have potential to impact the economics of hydrogen production using nuclear heat.

IV. CONCLUSION

Analysis of the potential role for nuclear energy to support the clean energy transition through the production of low carbon hydrogen has been explored. Benefits of nuclear energy compared to other decarbonisation options has been analysed and shown that there is potential role in certain future markets for hydrogen. Consideration has also been given to the challenges associated with the development of these technologies, highlighting key considerations such as the maturity of the technology and options for coupling this to the reactor.

V. References

[1] NIRAB, “UK Nuclear Innovation and Research Programme Reccomendations,” NIRO, London, 2015.

[2] Department for Business, Energy & Industrial Strategy, “Digest of United Kingdom Energy Statistics,” National Statistics, London, 2020.

[3] International Atomic Energy Agency, “IAEA-TECDOC-1859: Examining the Technoeconomics of Nuclear Hydrogen Production and Benchmark Analysis of the IAEA HEEP Software,” International Atomic Energy Agency, Vienna, 2018.

[4] M. Laguna-Bercero, “Recent advances in high temperature electrolysis using solid oxide fuel cells: A review,” *Journal of Power Sources,* vol. 203, pp. 4-16, 2012.

[5] A. Caponiti, “Clean Energy Ministerial: Hydrogen Integration with Nuclear Power,” US DoE Office of Nuclear Energy, 2020.

[6] E. Ingersoll and K. Gogan, “Missing Link to a Livable Climate - How Hydrogen-Enabled Synthetic Fuels Can Help Deliver the Paris Goals,” Lucid Catalyst, London, 2020.

Proceedings of the European Nuclear Young Generation Forum
ENYGF'21
September 27-30, 2021, Tarragona, Spain

Unique Approaches to Reshaping the Nuclear Narrative

Mairinger, Matthew[1*]

[1]North America Young Generation in Nuclear, Canada

*Corresponding author: *Canada@naygn.org*

I. INTRODUCTION

Even after declaring a climate emergency some nations are shutting down existing nuclear plants and others still have bans on building nuclear plants. The public remains largely unaware of the benefits of nuclear (medical isotopes, energy density, lifecycle environmental impact and the speed of decarbonisation) partially due to large Hollywood films such as the China Syndrome, HBO Chernobyl miniseries, and others. Advocating and educating for nuclear from a non-profit organization and modifying advocacy strategies represents a key element to ensure that nuclear power is a continued part of the energy sector going forward. These organizations can gain access to non-traditional circles such as other clean energy organizations, climate conferences, schools, and in the media.

II. THE APPROACH

Biases have been consistently shown to be present and firm through various psychology studies and works [1]. In order to influence change when conveying the nuclear narrative the full context of who, what, when, where, why, and how need to be considered if the bias has any chance of being moved.

A. Who

Who is the audience the message is being delivered to and who is the messenger?

In order for the message to be delivered effectively the audience needs to be taken into account. Some questions to consider:

- Composition: is the audience homogeneous or heterogeneous?
- Education: are you saying things they already know (patronizing) or going the opposite direction and providing technical jargon?
- Age
- Sentiment: is the audience for, against, or unaware of the issue being presented?
- Ethos: what are the main core values, beliefs, and/or biases of the audience?
- Genuineness – does the messenger believe in his/her own message?

Based on these factors if the messenger can be selected to match closely with the audience there are a number of benefits. Being born in a different era with different life-shaping circumstances and environments will fundamentally change the perspective of the individual. The benefits of matching the speaker to the audience include that they will be able to relate more with the speaker, the message will come across as more authentic, and the audience is more likely to actively listen to what is being presented.

Based on the age, sentiment and education of the audience the message should be tailored to ensure it is has the right complexity and tone.

B. What

What format are you delivering the message?

- Type: in person, video, audio, printed text
- Formality: is it formal (i.e. speaker at conference, a book) or informal (i.e. casual conversation, Subreddit forum)
- Length – what is the ideal duration to deliver the message to optimize audience engagement?

C. When

When are you delivering the message?

To consider how the audience will react to the message consider:

- Focus: is it early in the morning or late at night? If applicable, when was the last break? Is there a break/lunch coming up which is distracting from your information?
- Mood: are there counter or complimentary messages being delivered before or after your message?
- Recent news: have there been recent events related to your topic? Is there any major topic event which has happened or will happen?

You want your message to make an impression so think about how to shake up the status quo – if the energy/focus is low a key element is remaining engaging and upbeat.

In regards to other messages which have been delivered - if all of the topics are similar try and tie your topic to what has already been presented to make it relevant and really hone your key value statements. If, on the other hand, the messages are counter to what you are presenting try and find common ground and focus on the positives of your message and how it ties into the shared values.

Be aware of recent news in your subject area to either mention this during your delivery or to at least be ready if questions/comments are brought up. Try and incorporate key events or news to your message to provide context and relevance for what you are presenting.

D. Where

Where is the message being delivered?

- Setting: is it informal or formal? Are people standing, seated, or in motion?
- Location: are there any nuclear labs/utilities/waste repositories in the community where the message is being presented?
- History: was there a nuclear incident in the past at this location, what is the indigenous story for the land? What has nuclear done to help this area/region (i.e. medical isotopes)?

E. Why

Why is the message being delivered?

This is an important question that sometimes the individuals conveying the message sometimes fail to fully account for and should be reflected upon. Some key reflection points include:

- Reflection: was I asked to share this message or am I intruding (i.e. at a rally)?
- Cause: what is the main purpose of the conference/rally/webinar? What is the issue?

F. How

How else can you optimize?

- Previous engagements: are there past attempts at the same message, audience, and/or location? What can be learned from these past engagements?
- Previous speakers: ensure you attend previous webinars/panels/speeches/etc. from the event to tie messages to the broader theme and also to know what has been said previously.
- Next steps: how can individuals continue to support your cause (handouts, website links, etc.)?

III. RESHAPING THE NARRATIVE

A. Social Media

Social media opens up the message to a broader audience as the post goes to the entire network of the poster, which may not be aware/for nuclear.

One successful example is #NetZeroNeedsNuclear campaign [2] and the North American Young Generation in Nuclear (NAYGN) Social Media '20 for 20' Chapter Takeover [3]. These campaigns provided pre-made templates so individuals could add their unique message along with their photo in social media using a common hashtag. This allows the individual to have an avenue to express their viewpoint while still being part of something collective. Furthermore, by providing various options (individuals could pose with a sign, could use a still-photo template, or could record a video) the individual has freedom to express their views in the format/way they believe will be most effective. Another benefit to having a post from their account is that it opens the message to a larger network and also opens up different media options (i.e. TikTok, Facebook, Instagram, etc.). It is also helpful to have people tag/nominate others to keep the momentum going. Not every post needs to be serious, Generation Atomic has been very successful with educating and informing using memes on #MondayMeme.

The one pitfall I've seen is that nuclear advocates are pitting nuclear against renewables (i.e. the Facebook Group 'Renewables vs. Nuclear DEBATE'). By positioning nuclear against renewables this is a lose-lose strategy whereas we should be working towards commonalities/shared values to combat climate change and reach the United Nations Sustainable Development Goals.

B. Take Action

A great way to show backing for an idea is to create a petition. A petition exposes a broader audience to a message, gives supporters a concrete way to get involved, and can be used to influence policy makers since it demonstrates their voter base considers the issue important. Some petitions can be created for free and are quite simple to setup. Some countries/regions also have petitions that can be created and if they reach a certain number of supporters they will be read in the legislature. One example is the #NetZeroNeedsNuclear petition [4] which has thousands of signatures and is addressed to key policy makers.

Another way to have individuals get involved is to create a letter template or similar format where they can inform their politician about their views. At NAYGN there is an annual postcard push day [5] where members send postcards to their elected officials advocating for nuclear. There is also some software such as SoftEdge that can allow the organization to track active bills, and legislators past social media posts [6]. This software can help specifically target action for the maximum benefit. To keep the momentum going it helps to have a regular call to action, Generation Atomic uses the Take Action Tuesdays to keep a regular pathway to make a difference.

C. Education

One of the main barriers for nuclear acceptance is education and understanding. Surveys have consistently shown that the more informed the individual is about the nuclear, the more supportive they are [7]. There are some individuals who are strongly opposed, and regardless of their level of outreach this group seems consistently opposed. This is not the audience to focus extensively on – rather there is a "blue ocean" strategy for the large contingent which feel not too informed or not informed at all, specifically those which have no opinion or are somewhat opposed.

Nuclear Science Week [8] is a fantastic initiative to rally around nuclear education for one week during the year. Furthermore, school visits (career days), contests (drawing contest or essay contest [9]), and bringing props (nuclear children's books [9], mock fuel pellets, etc.) are a great way to keep the audience engaged and present material in a novel format.

Infographics are another amazing resource as they can present the material in an easy-to-understand format and are ideal for others to distribute.

D. Conferences

Companies should be looking to send more employees to non-nuclear conferences. Part of the problem with nuclear acceptance is that there are just too many nuclear people going to nuclear conferences… and speaking to nuclear people. Nuclear presence at clean energy, climate change, and/or renewable conferences has been lacking. How can we expect to humanize this industry and also to be recognized as clean energy if we aren't at these important conferences, networking with policy makers and influencers? It is crucial that advocates participate in these non-nuclear events (Clean Energy Ministerial, United Nations Conference of Parties, etc.) and there is a new program being launched by Generation Atomic & Energy Wealth Project to address this very issue.

E. Rallies & Protests

To shift public opinion on nuclear and improve understanding we need boots on the ground interacting with the public. Some advocates for nuclear are more broadly advocates for clean energy and combating climate change – we need to empower these individuals to participate in the various rallies and protests. The nuclear industry has been wary of having employees engage with the public and with the media – this needs to change. Yes, there are risks that individuals may say the wrong things about nuclear. However, the status quo is not working – we need real people sharing their real stories AND their common values to start to change the nuclear narrative. We need to be seen, be heard, and to let it be known that the nuclear sector is helping to solve so many global problems (many of the United Nations Sustainable Development Goals).

In regards to a nuclear specific rally, Stand Up for Nuclear [10] is a great opportunity to have a combined global effort for awareness. This is a proactive, non confrontational opportunity to allow a venue for advocates to share their passion with the public. Engagements in rallies should be a sustainable, ongoing initiative rather than some of the knee-jerk rallies which have occurred AFTER the announcement of a nuclear facility closing down.

IV. CONCLUSION

By modifying traditional techniques to reshape the nuclear narrative there is hope for a future in which nuclear can be a large contributor to increasing the quality of life. Organizations and advocates should take note of the approach strategies mentioned as well as tapping into the existing organizations and initiatives mentioned within this article.

V. References

[1] D. Kahneman, *Thinking Fast and Slow*, New York, NY, USA: Straus and Giroux, 2011.

[2] "Get Involved." Netzeroneedsnuclear.com

https://www.netzeroneedsnuclear.com/get-involved (accessed Apr. 6, 2021).

[3] "Membership Newsletter." Naygn.org

https://naygn.org/membership-newsletter-social-media-takeover-metrics-and-awards/ (accessed Apr. 6, 2021).

[4] "Save Our Climate" change.org

https://www.change.org/p/save-our-climate-we-need-your-signatures-acknowledge-that-net-zero-needs-nuclear-at-cop26 (accessed Apr. 5, 2021).

[5] "Government Outreach." naygn.org

https://naygn.org/committees/public-information/government-outreach/ (accessed Mar. 9, 2021).

[6] "Take Action." naygn.org

https://naygn.org/take-action/#/1 (accessed Mar. 9, 2021).

[7] "Public opinion on nuclear energy: Turning a corner?" ans.org

https://www.ans.org/news/article-314/public-opinion-on-nuclear-energy-turning-a-corner/ (accessed Apr. 1, 2021).

[8] "Nuclear Science Week." Nuclearscienceweek.org

https://www.nuclearscienceweek.org/ (accessed Apr. 1, 2021).

[9] "Student Outreach." Naygn.org

https://naygn.org/committees/public-information/student-outreach/ (accessed Apr. 2, 2021).

[10] "Stand Up for Nuclear." Standupfornuclear.org

https://standupfornuclear.org/schedule (accessed Apr. 1, 2021).

Proceedings of the European Nuclear Young Generation Forum
ENYGF'21
September 27-30, 2021, Tarragona, Spain

Nuclear energy is a stumbling-stone on the way to "green" future or a provider of power grids stability

Lazarena, Polina[1]

[1] JSC Atomenergomash (Rosatom), Russian Foreign Trade Academy, Russia

*Corresponding author: *lazarevapolin88@gmail.com*

I. INTRODUCTION

Several years ago, European countries confidently decided to become carbon-neutral by the middle of the 21st century. It means to produce as much or less greenhouse gases (GHG) than nature and industry absorb on their territory.

This term is called "Energiewende" or "Energy transition".

The main idea of this phenomenon is the possibility of economic growth and sustainable energy supply without the use of oil, gas and nuclear energy, which pollute our planet according to the opinion of some EU countries.

The main drivers of energy transition development are wind turbines, hydroelectric power plants and solar panels, which level of GHG emissions is minimum.

However, more and more countries in the world, incl. some EU countries doubt the success of energy transition without nuclear energy.

They are sure that nuclear energy deserves to be included in the list of renewable energy sources (RES) because the level of GHG emissions of Nuclear Power Plants (NPP) is only 2 points higher than the level of GHG emissions resulting from the use of wind turbines and hydroelectric power plants and amounts about 28 Tonnes CO_2e/GWh.

At the same time it is required to pay more attention to the issue of "safety" as after the accident at the Japanese nuclear power plant Fukushima many countries are afraid of using nuclear energy as RES, specifying that RES amongst other things should be safe.

This question is very controversial and the decision to include nuclear energy in RES is on the agenda nowadays.

II. ENERGY TRANSITION: BENEFITS AND DRAWBACKS

The broad-scale development of the "energy transition" process started from signing the Paris Agreement. According to this agreement, the countries should maintain the rise of global average temperature at a level well below 2˚C above the pre-industrial levels. This shall be done by reducing GHG emissions through the introduction of a plan of mitigation of global warming.

The governments of EU countries have begun massive construction of wind turbines, solar panels and started their move to producing electricity from biofuels. This was facilitated by both the tightening of environmental policy and general guidelines for reducing CO2 emissions into the atmosphere, as well as the need to reduce the dependence of the countries' economy on the import of fossil fuels and agreements signed in the international arena.

The experience of different EU countries is in many ways similar to each other. In Denmark and Sweden, the level of electricity generation from renewable sources is above 50%, in Spain - 40%, in the Netherlands and Italy - about 20%, in Poland - 15%. Even in France, where the share of nuclear power plants in the total generation is about 70%, the share of renewable energy sources is growing.

The best indicator, which shows the current situation in Energy transition, is Energy transition index (ETI). The ETI provides a data-driven framework to foster understanding of the performance and readiness of energy systems across countries for transition.

According to ETI Sweden leads the global rankings, followed by Norway and Denmark. Among the world's 10 largest economies, only the United Kingdom and France feature in the top 10. The top 10 account for only around 3% of energy-related CO2 emissions and around 2% of the global population.

Figure 1.ETI 2021 results table

However, RES have brought with them new problems - higher energy tariffs, the difficulty of utilizing wind blades and solar panels, and the decentralization of power supply.

Exclusion of "nuclear energy" from the list of RES does not satisfy the needs of participants of Agenda for Sustainable Development, such as France, Poland, Slovakia, Czech Republic, Slovenia, Hungary and Romania.

Today they are urging the European Commission to make nuclear energy "green". Otherwise, the funds allocated under the European Green Deal financing program cannot be spent on it. All these countries want to ensure their economic development through the construction of nuclear power plants. They want to use for their position the "non-greenhouse" nuclear energy.

For example, in the author`s opinion for France it is more profitable to spend the green money on upgrading its nuclear potential through orders from its nuclear industry rather than to buy solar panels in China and wind turbines in Germany.

There is also a problem of social acceptability of complete transition to renewable energy sources. It means, among other things, the introduction of "demand flexibility" measures. In the embryonic stage, the Swedes, who closed two nuclear reactors and several coal ones, felt it this winter. Cold weather came, and with it a shortage of electricity. In addition, the government urged citizens not to use household electrical appliances, and it was a reason of people's displeasure.

On the other hand, Belgium is one of the world leaders in the field of offshore wind energy. However, in order to replace the closed nuclear power plant it will build greenhouse gas stations.

Recently in 2019 within the frame of energy transition, the European Commission adopted the European Green Deal. It is a plan to achieve zero net GHG emissions and zero total environmental pollution by switching from the use of fossil fuels to renewable energy and raw materials in the member states of the European Union by 2050.

The European Green Deal is being touted as a role model. Nevertheless, more than one year has passed since its publication, and its main contradictions are far from being resolved. A bitter behind-the-scenes struggle continues over the methods of hydrogen production, and the scope of the new hydrogen revolution is completely unclear. There is a stormy stream of reports of giant projects. The reality may be much more modest. In reality, everything can be limited to pilot plans in the field of decarbonisation of industrial processes.

III. NUCLEAR ENERGY AS ONE OF THE SAFEST WAY FOR ENERGY TRANSITION

In March 2021 a specialized working group of the European Commission came to the conclusion that nuclear energy does not cause significant harm to the environment.

Firstly, in terms of the overall level of environmental impact NPP is better or comparable to RES- hydroelectric power plants, wind turbines and solar panels. During its research this working group assessed the full cycle of nuclear energy production, not only the generation of electricity itself, starting from the extraction and enrichment of nuclear fuel and to the construction, operation and decommissioning of nuclear power plants, as well as waste disposal.

Secondly, at the modern technological level nuclear power plants have either already been created sufficiently environmentally friendly, or can be easily and relatively cheaply modernized so that the harm to the environment becomes insignificant.

A number of inventions for the safe use of nuclear power plants are listed below.

A. NUCLEAR REACTORS GENERATION IV

With the IVth generation of nuclear technology, the term "reactor" is replaced by the more correct term "system", which includes both the reactor installation itself and its nuclear fuel cycle including processing (recycling) of nuclear fuel. Such new systems perform better than previous generations in terms of sustainability, competitiveness, safety and reliability, and proliferation protection. Surely, it makes them a "technological breakthrough".

The 4th generation of nuclear technology ensures the cost-effective and safe use of the natural resources energy potential of, optimal management of nuclear waste, minimal proliferation risks, co-production of heat and electricity required for hydrogen production.

The main characteristics of the fourth generation reactors:

- the continuation of highly safe and economic power generation with the possibility of other applications, such as, for example, desalination of seawater and brines, the production of hydrogen as a basis for synthetic fuels;
- accessibility to as many countries of the world as possible, taking into account the simplification of security systems without compromising its quality, the economic competitiveness of smaller reactors, effective protection against nuclear proliferation and terrorist attacks;
- full-scale use of the huge amount of energy contained in fissile and fertile materials - uranium and thorium;
- production of smaller volumes of long-lived radioactive wastes and the inclusion of actinides in the fuel cycle.

B. ACCIDENT TOLERANT FUEL

Accident-Tolerant Fuel is a nuclear fuel that is resistant to emergencies at nuclear power plants. The term Accident-Tolerant Fuel (ATF) originated after the Fukushima accident. In the formulation of the IAEA, this fuel should be efficient both under normal operating conditions and what is more important under conditions of loss of coolant. The main factor destroying fuel elements is associated with the vapor-zirconium reaction occurring at temperatures above 1200 ° C. Naturally, the ways to solve this problem lie both in the modification or replacement of the zirconium shells, and in the modification or use of a new fuel.

The main concept of tolerant fuel is to exclude the reaction of interaction of superheated steam and zirconium with the

release of explosive hydrogen that occurs in a situation of emergency heating. The solution of this problem could be the use of new fuel materials with a higher thermal conductivity, applying of heat-resistant protective coatings to the zirconium cladding of fuel elements, or the use of new structural materials that do not contain zirconium.

What does the tolerant fuel concept include?

Firstly, this is the development of shells - various steels, including new Fe-Cr-Al, heat-resistant metals (Mo), ceramic SiC shells, Zr alloys, as well as all kinds of protective coatings on Zr shells.

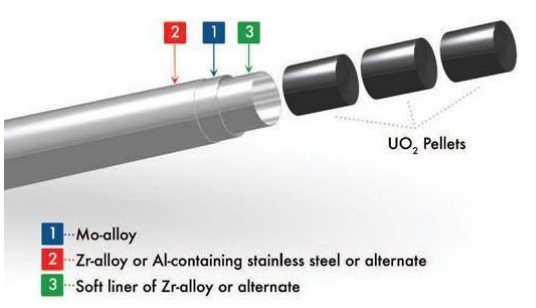

Figure 2. An option of layered shell for a reactor vessel

Secondly, it is the fuel itself, which is total uranium-intensive cold fuel - metal, uranium nitrides and silicide - reducing the amount of stored heat. As a result, the heating time to the critical temperature increases. Uranium capacity is also important for the economy, in order to compensate for the costs both for the development of new types of fuel and for the case of using steel shells with thermal neutron capture, and in order not to exceed the 5% uranium-235 enrichment barrier.

Thirdly, dispersion and microcapsule fuel (a type of fuel for gas reactors), and modification of dioxide fuel for the purpose of better binding of fission products are considered.

The introduction of emergency fuel is of key importance for bringing the systemic safety and reliability of nuclear power to a qualitatively new level.

Rosatom is also working in this sphere. In 2019 Rosatom finished the first phase of reactor tests of tolerant fuel for LWR of Russian and foreign design. In separate water loops of the reactor two experimental fuel assemblies were irradiated. Each consisted of 24 fuel elements with four different combinations of cladding materials and fuel composition. Fuel pellets were made of traditional uranium dioxide and uranium-molybdenum alloy with increased density and thermal conductivity.

C. CORE CATCHER (MELT TRAP)

Water-cooled reactor is the most widespread type of reactor in the world. The greatest danger for such type of reactor pose accidents with the loss of core cooling. As a result of such accident nuclear fuel melts and a large amount of hydrogen forms when water vapour interacts with the melting zirconium cladding of fuel elements. Therefore, new solutions were developed in order to improve the safety of the next-generation NPPs and prevent the occurrence of severe accidents and localizing their consequences.

Melt trap is an optional part of the nuclear reactor containment, a structure used to localize the melt of the core of nuclear reactor in severe accidents with melting of the reactor core and penetration of the melt core through the reactor vessel. It is one of the passive nuclear safety systems, it provides insulation of the foundation from the melt, sub-criticality of the melt and cooling of the melt.

The method for localizing the melt includes capturing, holding and cooling the melt in a tank located under the reactor. Cooling of the melt is carried out by means of heat removal into the atmosphere through a protective screen and through the contact of the melt with cooled walls of the tank. When leaking through the reactor or in the process of filling the tank, the melt is mixed with refractory compounds of heavy elements in particular with oxides of hafnium, tantalum, europium, and gadolinium, that absorb thermal neutrons.

Nevertheless, the main objective of ensuring safety during NPP operation is to follow the norms of “Safety culture”. Safety culture is based on the qualification and psychological preparedness of all personnel. Within the framework of such culture, ensuring the safety of nuclear power plants is a priority goal and an internal need of the personnel, leading to self-awareness of responsibility and self-control when performing all works affecting safety.

IV. ENERGY TRANSITION AND SUSTAINABLE DEVELOPMENT GOALS (EXPERIENCE OF ROSATOM)

While there is a lot of evidence that nuclear energy can be safe, as I mentioned before, nowadays the strategy of energy transition development is built based on the usage of wind turbines, hydroelectric power plants and solar panels as well as the following SDGs.

Sustainable Development Goals (SDGs) are a collection of 17 interlinked global goals designed to be a “blueprint to achieve a better and more sustainable future for all”. Achieving these goals depends both directly and indirectly on ensuring a sustainable energy supply. The issue of including atomic energy in the category of RES is still on the agenda. Despite this fact, Rosatom has now taken a course towards the development of wind energy and other RES, for example, hydrogen energy.

The company NovaWind was founded in 2017 as a part of the Rosatom group of companies, which specializes in wind energy. The total volume of NovaWind's order portfolio now is about 1.2 GW, which corresponds to 35% of the wind energy market in Russia.

Moreover, since 2018, hydrogen energy has been a priority area of scientific and technological development of Rosatom. The Russian nuclear industry has significant technological and research potential for the development of the main methods of hydrogen production - both steam reforming of methane and electrolysis production. One of the priority technological tasks is to ensure the decrease of carbon dioxide emissions from hydrogen production.

More than that Russia and particularly Rosatom aim to follow SDGs and try to implement it in our ordinary work and life.

On July 27, 2020 Rosatom approved the Unified Sectoral Sustainable Development Policy. The main purpose of the document is the structuring and alignment of activities in the field of sustainable development of the nuclear sector.

The document secures the position of the state-owned corporation regarding sustainable development issues, including goals, objectives and main principles of activity in this area. The priority areas include the six of the 17 UN Sustainable Development Goals, including "Available and Cheap Energy", "Climate Action" and "Responsible Consumption and Production".

Figure 4. Contribution in achievement of the UN Sustainable Development Goals in detail

Rosatom activities influence all 17 SDGs. However, given the scale of influence and features of the Corporation's activity, the key goals will be mentioned further.

As for No.7 goal, Rosatom directs towards contribution to carbon-free generation, including the development of solutions in the wind power segment. NPP ensures stable generation of low carbon electricity during 60 years.

According to No.8 goal, construction and operation of two-unit NPPs provide jobs for more than 10,000 people in the area of nuclear infrastructure and create more than 3,000 new jobs to work at NPP. Each US dollar invested in a NPP construction project (recalculated in the local currency) brings, on average, US $4.3 to GDP to the host country and, on average, US $1.4 to the host country's budget as taxes.

As for No. 9 goal, NPP construction and operation provides the development of related infrastructure, basic and applied science and local personnel training system.

No. 12 goal is being implemented through building a "sustainable" chain of supplies. The sector has developed and implemented Rosatom Production System (RPS) related to observance of the lean production culture. The quality management system has been implemented; international standards ISO 9001, ISO 14001, OHSAS 18001 are applied.

Achievement of No.13 goal is to solve the global problem of climate change. Electricity generation at NPPs is one of the sources of low-carbon energy and has substantial environmental effects. All NPPs of Russian design across the world save emissions of about 210 million tons of CO2 per year, including in the territory of Russia of 107 million tons of CO2.

According to No.17 goal, the sustainable development agenda is actively worked out at the related international platforms: the IAEA and World Nuclear Association (WNA) conferences. In addition to traditional nuclear platforms, Rosatom is an active participant of the dialogue on sustainable development at the World Energy Council etc.

V. CONCLUSION

According to the common mind, nuclear energy is very dangerous for people and the planet. Nevertheless, there is a lot of evidence that this opinion is just a myth. Nowadays the processes in the nuclear sphere become safer and safer, nevertheless the main goal for people shall remain following the rules and norms of the "safety culture".

Combination of economic, legal and infrastructure policies as well as fiscal interventions are needed to drive and support behavioural changes and consumption patterns by influencing and incentivising sustainable behaviour. It is clear that countries could not all follow the same path, but it is critical to identify the ways to make changes at the individual level more attractive and accessible.

Certainly, the construction of a nuclear power plant is a long-term project that requires large investments and is critically important for the energy independence of many countries. Therefore, their financing usually either completely or in large part falls on the shoulders of the state. And without a clear classification of energy types according to the level of environmental impact, it is impossible to determine the scope of possible investments in them.

Actions and progress of the current decade will determine if the global ambition to achieve carbon neutrality by 2050 will be realized. And to the author's mind, nuclear energy should help to achieve a low rate of GHG.

Policymakers and private sectors must act and work together now and seize the opportunities to build the foundation for a resilient energy transition—one that not only set us up for a sustainable future but also for long-term inclusive growth and prosperity.

VI. References

[1] European Atomic Energy Community "Technical assessment of nuclear energy with respect to the 'do no significant harm' criteria of Regulation (EU) 2020/852 ('Taxonomy Regulation')", the Netherlands, 19.03.2021,p.35-39.

[2] Rob West, Bassam Fattouh, "The Energy Transition and Oil Companies' Hard Choices", presented at the Energy Insight:50, The Oxford Institute for energy studies, Great Britain, July 2019, p.1-14.

[3] World Economic Forum, "Fostering Effective Energy Transition", presented in Insight report, Geneva, Switzerland, April 2021, p.26-28.

[4] Wei Zhou, Wenzhong Zhou, "Enhanced thermal conductivity accident fuels for improved reactor safety" presented at "Elsevier", Hong Kong, China, 2018, p.68-71, 77-79.

[5] Polina Lion, Marina Loseva, "Nuclear power for sustainable development", 2019, p.5-19.

[6] Nuclear energy agency OECD,"State-of-the-Art Report on Light Water Reactor Accident Tolerant Fuels", 2018, p. 33-34, 67-84, 169-176.

Proceedings of the European Nuclear Young Generation Forum
ENYGF'21
September 27-30, 2021, Tarragona, Spain

Ageing management: the key to long-term operation

Amorós, Xavier[1], Bernad, María del Salz[1], Colomines, Martí[1], Fole, Joaquín[1], Martín, Laura[1*], Páez, Andrea[1] and Salvador, Óscar[1].

[1]IDOM | CONSULTING, ENGINEERING, ARCHITECTURE, Spain

*Corresponding author: *laura.martin@idom.com*

I. INTRODUCTION

The global energy sector is undergoing a profound transition driven by the need to expand energy access to support socioeconomic development, especially in emerging economies, while limiting the impacts of climate change, pollution and other global environmental crisis. This requires a change from the use of polluting energy sources to the use of sustainable alternatives [1].

The Net Zero Emissions scenario 2050 (NZE2050) - which aims to achieve global CO2 neutrality by 2050 - will require an increase in the installed capacity of known clean energy sources, as well as new initiatives, including innovation programs across a wide range of technologies, from electrolysers for hydrogen production to small modular nuclear reactors [2].

In this context, renewables have accounted for almost 90% of the increase in total energy capacity worldwide in the last year [3]. They are capable of supporting a significant part of energy demands, however, they still suffer from a fundamental problem of being dependent on the flow of the energy agent, which is unfeasible in a fluctuating society that demands to be satisfied at every instant and with a constant increase in energy demand.

Otherwise, nuclear power provides a firm and predictable basis for the security of electricity supply. The availability, reliability, stability and predictability it offers, knowing that it operates continuously, under all circumstances and with very high regularity, enables proper management of the electricity system. Moreover, as a CO_2-free source, it can make a significant contribution to achieving sustainability goals and improving energy security [4].

All of the above confirms that nuclear energy is indispensable for achieving global sustainable development and plays a crucial role in the decarbonization of the energy sector and, consequently, it can be affirmed that the continued operation of nuclear reactors is a sound energy strategy, which will also maintain a skilled and technological industry that creates wealth and employment and has great international projection.

At world level, nuclear generation currently represents almost 11%, with 447 reactors in operation in 31 countries and 52 new reactors under construction in 20 countries. Furthermore, the construction of an additional 180 GWe of nuclear power is envisaged over the next decade. [5].

In order to comply with international environmental commitments and in view of the transformation of the electricity sector, with the rapid growth of renewable energies, the energy mix nowadays requires competitive adaptation of nuclear power plants, taking into account that nuclear energy is the ideal support to cover the variability of renewable energies. In addition, an increasing number of countries are opting for the commissioning of new plants, the refurbishment and reactivation of existing plants, or opting for a Long-Term Operation (LTO) strategy.

LTO is intended to continue the operation of an industrial facility beyond its original design life, maintaining or improving safety and reliability levels, while meeting the safety requirements applicable to the facility's Structures, Systems and Components (SSC). Furthermore, according to the report "*Projected Costs of Generating Electricity 2020*", LTO is the most cost-efficient source of clean electricity generation. [6].

There are 147 nuclear reactors in the world that have been granted authorizations by the various regulatory bodies to operate beyond 40 years, adopting different schemes: in some cases, authorizations have been granted for an additional 20 years, in others for a fixed period, and in other cases indefinitely. In the United States, four units have, for the first time in history, been authorized to operate for 80 years [7].

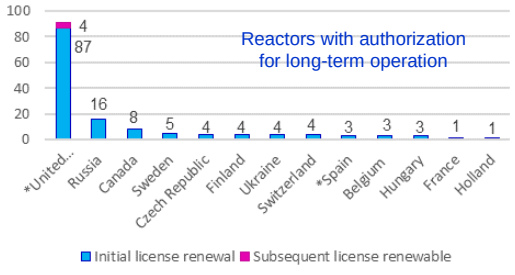

Fig. 1. Representation of the reactors with authorization for long term operation (*update to 2021) [8].

In summary, nuclear power offers high levels of safety, exceptional performance with high availability, as well as reliable, affordable, and low-carbon electricity. In order to achieve a plant operation with these characteristics, it is necessary to carry out a correct strategic maintenance of the plant's SSC, which is based on the performance of activities necessary for ageing management in order to ensure the surveillance, control and mitigation of ageing and degradation mechanisms of safety-related and/or safety-relevant elements, while at the same time reducing maintenance and operation costs.

II. AGEING MANAGEMENT

Ageing management is a systematic approach to reasonably guarantee the functionality of a discrete group of elements throughout the life cycle of a nuclear power plant, exceeding, if possible, its design life.

In order to achieve a safe, economic and reliable operation of a nuclear power plant, it is essential to have a flexible and effective ageing management programme, developed in the preliminary design phases, implemented from the construction phase and during the operation of such plant, determining all its needs and even in the final decommissioning phase.

For the ageing management programme to be effective and useful for the plant, it must be transversally integrated in the main activities that are part of the electricity generation process, having a proactive and multidisciplinary team with resources throughout the development, implementation and monitoring of the programme.

The ageing management programme must have established clear, concise, and quantifiable long-term objectives and expectations, sponsored by the management, and internalized by the execution technicians, determining a defined methodology adequate to the organization’s needs.

Thus, an organization unable to embrace the change in mindset and execution, or in the absence of a support mechanism to incorporate the change permanently, will rarely successfully complete the implementation of an ageing management system.

A. Methodology

There are several standards that define methodologies for ageing management in industry. The following is a description of IDOM's strategy based on these standards and operational experience acquired over years of service through different fields of expertise.

It is worth mentioning that all these methodologies share a common attribute index with the objective of describing and implementing systematic processes to monitor, control and mitigate certain postulated failure modes.

The scope of the programme should be determined to include those SSCs with critical functions. How critical the functions will be lies in the desired outcomes.

The different industry references used for plant life extension have in common safety enhancement terms that define critical functions as important or relevant safety related, safe shutdown, environmental qualification, station blackout, fire protection, ATWS, PTS, among others.

It should be considered that company strategies for LTO and competition from the energy sector may indirectly introduce terms such as production capacity, cost reduction, spare parts optimization, or even other documentary ones.

Regardless of whether an ageing management programme is foreseen for specific SSCs or groupings, or if the characterization of SSCs is considered, it is important to have a good knowledge of their component parts or subcomponents, construction materials, operation modes, service conditions, environmental conditions, other particular conditions of the system, initial operating capacities, expected service life or spare parts, among others.

For the ageing management programme to be efficient, a clear relationship must be established between maintenance tasks and the functions performed by the SSCs included in the study.

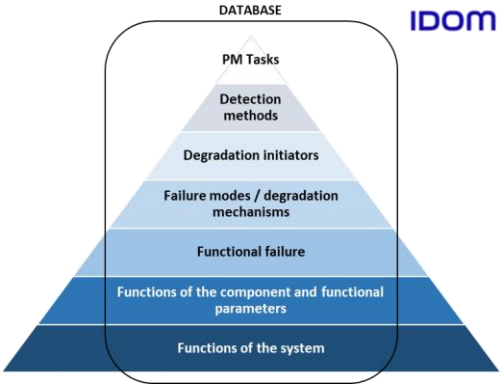

Fig. 2. Descriptive pyramid of the definition of a maintenance plan.

One of the possibilities to establish this relationship can be the development of Failure Mode and Effects Analysis (FMEA) exercises. The FMEA matrix answers questions such as: What is the component or part of the component that we believe could fail? What is the function we are going to analyze? What are the potential failure modes? In what way is it conceived that the SSC could fail? How could the SSC cease to fulfil its assigned functions?

A good practice is to consider the analysis described above in all phases of the SSC life cycle, as well as to incorporate experiences in the industry.

Since this relationship intends to be the basis on which the ageing management programme shall be designed, its analysis and development shall have a direct impact on the efficiency and optimization of the maintenance and operational tasks included in the implementation manuals. Therefore, the depth in which the exercise is carried out must be weighed, as it must be aligned with the objectives and expectations pursued.

In order to mitigate or prevent each postulated failure mode, a series of efficient preventive, predictive or monitoring tasks will be defined. For the purpose of adopting standardized and benchmarked maintenance tasks, failure modes can be grouped in various ways.

If the reference standards allow it, as a means to optimize the frequency of execution of the tasks, the failure modes can be characterized, for example, by criticality, occurrences, etc. Likewise, as mentioned above, depending on the value and weight to be given to the indirect objectives that have an impact on the programme, exercises and technical-economic analyses can be carried out to obtain a compromise between safety, reliability and costs.

The result of this process shall be structured by means of implementation manuals, that shall indicate which maintenance activities and with which requirements shall be performed, and execution procedures.

Any ageing management programme requires a follow-up of each of its manuals. It should verify that effective management is performed and that tasks are correctly executed. It shall also be verified if it is necessary to update it due to the inclusion of new SSCs, new regulations, deficiencies in the implementation, events detected in the plants, etc.

A monitoring of the Key Performance Indicators (KPIs) is carried out to check that the expectations in terms of degradation are met, as well as the results of the tasks, evaluating that they meet the acceptance criteria, developing a history of the status of the SSCs and analyzing recurrences and trends that may lead to a review of the process carried out or the execution of corrective actions.

So, the implemented ageing management programme must be a living process that allows continuous revisions to improve tasks, adjust frequencies and identify alternative strategies.

Consequently, once the design life of the plant is fulfilled, it is possible to propose an adapted management programme for the LTO period that offers guarantees that all the systems continue to fulfil their functions.

B. Benefits of implementing an ageing management programme

Operational experience shows that the analysis of an installation, based on the RCM (Reliability Centered Maintenance) methodology and the practical application of the preventive and mitigating measures that emanate from this rigorous analysis process, has a series of advantages over other ways of approaching the maintenance of an installation and avoiding degradation and its collateral damage. These advantages have much to do with the depth of the analysis and the rigour of its application, and with the fact that it is a maintenance programme that considers not only the equipment, but the plant as a whole that goes beyond a simple sum of equipment. These advantages are cited below:

- **Improvement of safety:** The implementation of a maintenance programme allows the identification and monitoring of the critical function of the SSCs included in the analysis, which is the one that can affect safety. This automatically provides reasonable assurance that ageing effects are managed so that components continue operating without compromising their functions. By consolidating and strengthening the safety of the plant, the collateral benefit of improving the environmental impact is obtained since, by studying the failures with environmental implications, the bases are analyzed and defined to avoid accidents and failures with a negative impact on the environment.
- **Increase of reliability of the installation:** In many companies where reliability is important, it is found that the maintenance carried out is excessive, that is, they are over-maintained. The manufacturers of the equipment and components of the installations propose exaggerated maintenance tasks or that they must be carried out with very high frequencies. For this reason, one of the main benefits of the RCM methodology is to avoid manipulating SSCs, reducing human error (reducing the appearance of faults associated with systematic assembly and disassembly) and the degradation resulting from this manipulation.
- **Reduction of maintenance costs:** An efficient and logical implementation of the maintenance programme and the identification of sufficiently effective conditional maintenance tasks leads to a decrease in maintenance costs, additionally leading to an increase in plant availability and reliability. In addition, applying an effective maintenance strategy automatically increases the efficiency of spare parts and lubricant management and eliminates unnecessary equipment replacements.
- **Reduction of unscheduled shutdowns:** Orienting the maintenance plan strategy of the equipment by addressing specific failure modes according to their relevance to perform their function in the system and through efficient monitoring of the main characteristics of the SSCs, it is possible to detect failures before they occur, ensuring that the equipment fulfils its function reducing unproductive times.
- **Optimization of resources:** The optimization of human and material resources in the maintenance of equipment is closely related to effectiveness and efficiency, as better planning of maintenance tasks will lead to better results or less use of resources to achieve the defined objectives.
- **Increase of knowledge of the installation:** Another of the undoubted advantages of the application of RCM is the improvement in the know-how of the installations. This analysis allows the technicians who must take care of the facility to have a very deep understanding of the equipment, its operation and its relative importance, which helps them in the future to make more convenient and correct decisions in the operation and maintenance of the different parts of the nuclear installation.

Therefore, it is evident that ageing management is the key to the development of the main lines of action that guarantee the efficient and safe long-term operation of nuclear facilities.

III. INNOVATION IN AGEING MANAGEMENT

Industry is evolving towards a trend of automation and interconnection of data in industrial technologies, that is using technology as a connector between machines, operations, equipment and people. This evolution includes the Industrial Internet of Things (IIoT), Additive

Manufacturing, Cloud Computing, Virtual Reality, Connectivity, Cybersecurity, Artificial Intelligence (AI), Robotics, Quantum and Photonics, Simulation and Big Data.

Nuclear industry, regulatory bodies and international organisms related to nuclear energy have realized the multiple benefits that Smart devices can introduce in nuclear installations. For instance, the IAEA (International Atomic Energy Agency) has published a report to establish guidelines on the selection and evaluation of smart devices to be used in systems deemed important for the safety of power plants. In addition, some regulatory bodies, as the National Commission for Nuclear Activities Control (CNCAN) in Romania, are developing their regulatory framework [9] and others, as Nuclear Safety Council (CSN) in Spain, are funding I+D+i projects based on the implementation of new technologies in nuclear power plants [10].

IDOM has experience in sorting databases (Big Data), processing these data and managing them in order to be able to draw results and trends that allow us to obtain decisive conclusions. Moreover, the company has knowledge in the field of AI and Machine Learning, with projects in which, for example, artificial vision is used to control the quality of raw materials in a logistics department.

Regarding the IIoT, in combination with Big Data, the corporation carries out projects with the aim of providing a data network to manage information, such as, for example, the creation and implementation of cameras with processing capacity. This technology project has great applicability in the maintenance sector, as through the analysis of images from this camera, it is possible to detect wear, damage, contamination in nuclear power plant equipment, etc.

These are just a few examples of projects carried out, and although it is only the beginning, the real challenge of this revolution is to discover ways to interconnect existing processes, implement this evolution in the maintenance sector and discover all the benefits it can bring.

Without innovation, the maintenance department loses strength and responsiveness. With the use of sensors, IIoT, Big Data, Artificial Intelligence and other intelligent systems, the door is open to a myriad of applications that could increase the efficiency and effectiveness of maintenance.

Generally, when it is necessary to collect data on the condition of machines, we turn to technicians specialized in this area. With the development of new connected technologies, there are machines that collect and analyze these data on a massive scale, which facilitates decision making and failure predictability, thus tending to maximize component life and avoid failures. With new maintenance technologies, data seek out humans, not the other way around.

Some of the advantages of this new digital era are to accompany the investment and profitability of the equipment, to overcome communication barriers or to boost the organization in the market.

The implementation of new technologies in the nuclear sector has many possible applications and would be of great benefit in many areas. Through the technological components related to maintenance, the possibilities for analysis and monitoring of operating parameters of a nuclear power plant become endless, as do the potential benefits, for example:

- Determine with greater precision the lifetime of equipment, the risk of failure and the respective impact on the system.
- Live monitoring of the main operating parameters of the equipment.
- Automate the control, carry out analyses and foresee a possible failure of a component and thus act in advance to prevent it.
- Achieve exhaustive and continuous control of spare parts, as well as the need to purchase new ones.
- Drastically reduce the presence of personnel in the radiological area, which is beneficial for the health of workers and the safety of the plant.

Industry is evolving and so its maintenance. The nuclear sector must evolve and adapt to new technologies and take advantage of all the benefits of this revolution.

IV. References

[1] UNECE, Aplicación de las clasificación Marco de las Naciones Unidas para los recursos y sistemas de gestión de recursos de las Naciones Unidas., 2020.

[2] Foro Nuclear, «Así crecerá la energía nuclear, según el World Energy Outlook 2020».

[3] Enrique Pérez, «Un año histórico para las energías renovables en Europa: en 2020 por primera vez superaron a los combustibles fósiles,» 2020.

[4] Foro Nuclear, «Valores del sector: Garantia de suministro».

[5] Foro nuclear, Catálogo industria nuclear española, 2020.

[6] IEA, «Projected Costs of Generating Electricity 2020,» 2020.

[7] Foro Nuclear, Energía nuclear en el mundo.

[8] Foro Nuclear, «Resultados nucleares del 2019 y perspectivas de futuro.».

[9] IAEA , «Addressing Safety of Smart Devices for Use in Nuclear Power Plants».

[10] Foro Nuclear, «Investigadores españoles aplican inteligencia artificial a la predicción de daños en las centrales nucleares,» 29 Mayo 2020.

Proceedings of the European Nuclear Young Generation Forum
ENYGF'21
September 27-30, 2021, Tarragona, Spain

Small Modular Reactors in Terms of Architectural Design and Site Construction

Smakhtina, Anastasia[1]*

[1]JSC ATOMPROEKT, Russian Federation

*Corresponding author: *AVSmakhtina@atomproekt.com*

I. INTRODUCTION

In 1965 the USSR government made a decision to start an extensive program of the construction of several nuclear power plants all across the country, including Kursk NPP. Construction of two RBMK-1000 (Figure 1) reactors (high-power channel-type reactors) started in 1971; two more reactors were added between 1983 and 1985 [1]. The technological layout of the NPP equipment affects the layout of the building. The project of Kursk NPP has closed configuration. It means that all equipment is located in one building but divided into areas (e.g. turbine, capacitor, block control panel, air duct room, valve for maintenance of the main circulation pump, etc.) [2].

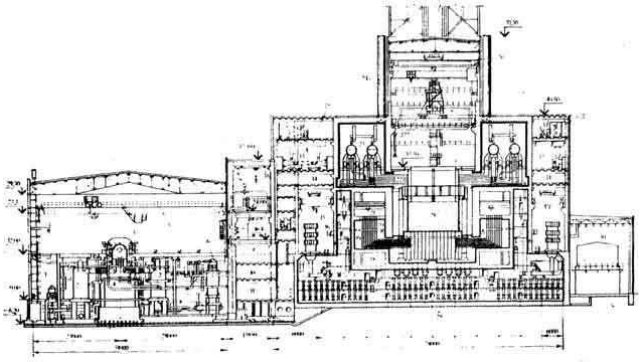

Figure 1. Cross section for NPP with RBMK-1000 [3].

In 2013 it was decided to develop the project of Kursk NPP-2. The purpose of the construction is to replace power units of the Kursk NPP at the end of the working lifespan. Construction of VVER-TOI (Figure 2) (water-water energy reactor; typical, optimized, with enhanced information) started in 2018 [4]. The project of Kursk NPP-2 has open configuration. It means that the open layout, from one hand, increases the overall cubic capacity of the building and has a bigger length of communications. On the other hand, it increases safety and gives more freedom for the construction design and installation works. Particular attention within the VVER-TOI realization is provided to improving the safety of the power unit. The project implements a full range of technical solutions to ensure the safety of nuclear power plant and exclude excessive environmental impact.

Figure 2. NPP with VVER-TOI [5].

The world changes rapidly. Scientists and engineers constantly generate new ideas. One of them is Small Modular Reactors (SMR) – an adjustable, reliable and low-carbon energy source. Nowadays there are around 70 [6] projects and concepts of SMR in the world. The advanced SMRs currently under development represent a variety of sizes, technology options, capabilities, and deployment scenarios.

Figure 3. NuScale, USA [7].

How will they look in terms of architectural design and site construction? Will it be closed configuration like CAREM-25 and Rolls-Royce SMR (Figure 4) or open configuration like NuScale project (Figure 3)?

Figure 3 - UK SMR Aerial View

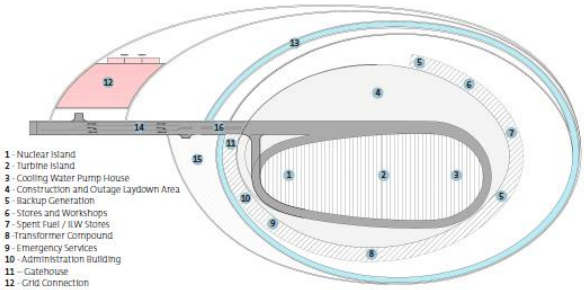

Figure 4 - UK SMR Plan Functional Arrangement

Figure 4. Rolls-Royce SMR, UK [8].

II. SMR LAYOUT OPTIONS

When we talk about nuclear reactors, we refer to a containment building with thick concrete walls, safety measures, and cooling system. Although safety measures are still the main goal of any SMR project, the design can be adjusted according to the need of energy consumption for the specific region, climate, and economic situation and can be developed in a much smaller size compared to an average Nuclear Power Plant. It also means that the parts of SMR can be produced in factories, and then be shipped to the installation site [9]. It gives an opportunity to transfer these modules to any location in the world. Multiple SMRs can be set up at a single nuclear plant to supply a similar level of power, as larger generators, which means a nuclear power plant could be expanded gradually, as demand increases. This new generation of nuclear power reactors, with output of no more than 300 MW(e) per unit, offers the possibility of flexible supply, including in combination with renewables, while being deployable either as single or multi-module plant [10].

A. Construction and Digital Technologies

There's an expectation that the digital revolution will transform the process of information exchange, improve project management and reduce costs for construction. Digital technology is already having an impact on the nuclear industry around the world. Even now engineers and architects perform advanced analysis through 3D building simulation tools to achieve higher efficiencies. They can perform a climate analysis and heating, ventilation, air conditioning simulations to optimize what materials use and how to find the best location for SMR power plants. Not to mention Virtual and Augmented Reality (VR and AR), which allows to see the whole design of nuclear facility before it is built. With AR architects and constructors are able to visualize the designs within the natural topography – it provides them with data about the site that wasn't previously available to them.

The usage of digital technologies throughout the life cycle of a nuclear power plant (including project development, modernization, construction and operation) can help industry to maintain Small Modular Reactor functions and to prevent some potential issues.

B. Small Modular Architecture for Small Modular Reactors

With the maximum use of modular components in the construction and implementation of programs for the integrated construction the final estimation cost of the Nuclear Power Plants can be drastically reduced. Such an integrated approach or serial construction is the most effective method for developing the nuclear power industry, as it reduces the cost of technology as it develops. Usually, it leads to a reduction of construction time and a significant reduction of cost of power units [11]. But what will the standardized project look like in case of SMR architecture?

Small Modular Reactors are called "modular" because they can operate individually, or as part of a larger nuclear complex. In terms of architecture, it means that modular design (Figure 5) and small size lends itself to having multiple units on the same construction site. The compact architecture enables modularity of factory production, which can also lead to the implementation of higher quality standards.

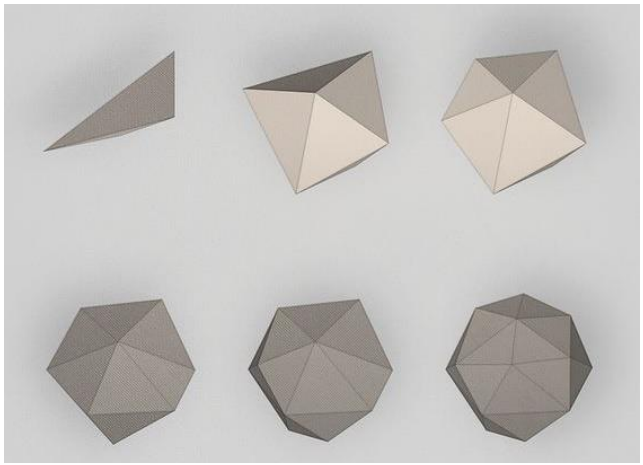

Figure 5. Possible modules of architectural forms [12].

The SMR community (developers, suppliers, and potential customers) have quoted estimates that the plant cost of SMRs (all-in capital costs) would be in the range of $6,000 per kW, comparable to the unit cost of large LWRs (light water reactor) [13].

There's also a common opinion that the reactor unit of SMR has a potential for subgrade location (underwater or underground) to create an additional protection from natural

disasters, man-made hazards and terrorist threats (Figure 6). However, this design reduces risk in some situations (such as earthquakes) and increases it in others (such as flooding). It can also make emergency intervention more difficult [14].

Traditional reactor safety systems are 'active' in the sense that they involve electrical or mechanical operation on command. Some engineered systems operate passively, e.g., pressure relief valves. Both require parallel redundant systems. Inherent or full passive safety depends only on physical phenomena such as convection, gravity or resistance to high temperatures, not on functioning of engineered components. Because small reactors have a higher surface area to volume (and core heat) ratio compared with large units, a lot of the engineering for safety (including heat removal in large reactors) is not needed in the small ones. [15] Small Modular Reactors also require a smaller emergency planning zone.

For even more reducing the large land plot requirements, it can be developed as an architectural design with the closed structure. After all, the SMR module is not a space-consuming system. It's also economically beneficial and can dramatically accelerate the construction process. Closed-structural modular SMR buildings could have a noticeable advantage for the maintenance and supervisory authority.

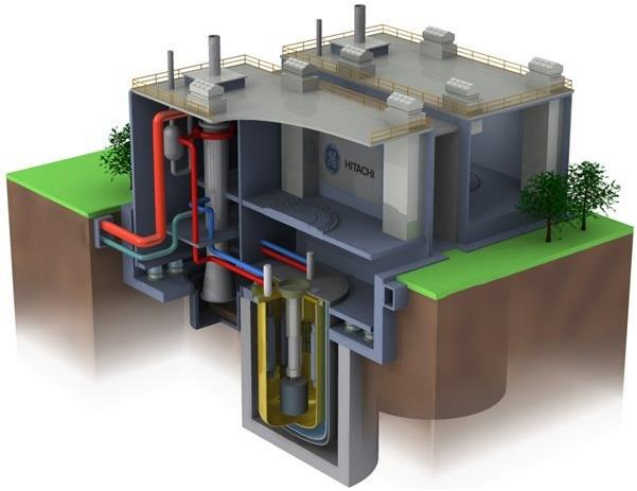

Figure 6. ***PRISM (Hitachi) is partly located underground*** **[16].**

Other simplification opportunities for SMRs may arise at the level of overall plant architecture, ranging from reactor components to regular civil structure, constructability and the use of commercial, off-the-shelf components. Some multi-unit SMR developers are also considering additional simplifications through the development of shared plant infrastructure, such as shared turbine buildings and control rooms. These different simplification approaches could translate into lower construction costs for SMRs, both directly through a reduction in the number and size of components and systems, and indirectly through benefits at the project management level. Design simplification, for instance, could lead to a reduction in the risks associated with rework, as well as a reduction in the delays during construction [17].

And at the end of its lifespan, SMR provides an opportunity to remove reactor modules or/and structure itself without creating additional security measures. Thanks to the technology of installation of SMRs there's a possibility to extract and store an entire module upon decommissioning. This process will reduce a significant part of the energy and material demands of the decommissioning process. The design of micro-reactors that include simplified decommissioning of an entire module has been already proposed by Westinghouse Nuclear and it's called eVinchi™ Microreactor [18].

III. CONCLUSIONS

SMRs could be a stable and low-carbon solution to energy production and consuming problems. Because of its simplicity, low cost and fast construction time SMRs could become a future of nuclear power. Every year science offers us new solutions in terms of engineering and architecture - new concepts, new programs, new materials, new technologies. We can only imagine what the SMR power plants will look like in the future. One thing is for sure – we need to find the best possible solution not only in terms of functionality and design but also in terms of safety and ecology. Together.

IV. References

[1] Wikipedia, "Kursk Nuclear Power Plant", https://en.wikipedia.org/wiki/Kursk_Nuclear_Power_Plant

[2], [3] Ядерные технологии, http://nuclearfactor.ru/energy/aes/62-201.html

[4] Wikipedia, "Курская АЭС-2", https://ru.wikipedia.org/wiki/Курская_АЭС-2

[5] ProAtom, Андрей Кучумов, "Основные проектные и компоновочные решения ВВЭР-ТОИ / Basic design and layout solutions of VVER-TOI", http://www.proatom.ru/modules.php?name=News&file=article&sid=4397, Mar. 20, 2013

[6] Nuclear Technology Development and Economics, "Small Modular Reactors: Challenges and Opportunities", https://www.oecd-nea.org/upload/docs/application/pdf/2021-03/7560_smr_report.pdf, NEA № 7560, 2021, p. 9

[7] NuScale, https://www.nuscalepower.com/projects

[8] Rolls-Royce, https://www.rolls-royce.com/innovation/small-modular-reactors.aspx#/

[9] YouTube, Undecided with Matt Farrell, "Small Modular Reactors Explained – Nuclear Power's Future?", https://www.youtube.com/channel/UCjtUS7-SZTi6pXjUbzGHQCg, Dec., 2020

[10] IAEA, "New Recommendations on Safety of SMRs from the SMR Regulator's Forum", https://www.iaea.org/newscenter/news/new-recommendations-on-safety-of-smrs-from-the-smr-regulators-forum, Apr. 22, 2020

[11] World Energy Council, "Nuclear Scenarios Report 2019", https://www.worldenergy.org/assets/downloads/WEC_Nuclear_Scenarios_Report_2019_RU.pdf, Sep. 11, 2019

[12] Archillect, “Evolution of a Sphere” art, https://archillect.com/

[13] Energy Policy Institute at Chicago The Harris School of Public Policy Studies, Robert Rosner and Stephen Goldberg, “Small Modular Reactors – Key to Future Nuclear Power Generation in the U.S.”, https://www.energy.gov/sites/prod/files/2015/12/f27/ECON-SMRKeytoNuclearPowerDec2011.pdf, Nov., 2011, p. 55

[14] Union of Concerned Scientists, “Small Modular Reactors: Safety, Security and Cost Concerns”, https://www.ucsusa.org/resources/small-modular-reactors, Sep. 23, 2013

[15] World Nuclear Assosiation, “Small Nuclear Power Reactors”, https://www.world-nuclear.org/information-library/nuclear-fuel-cycle/nuclear-power-reactors/small-nuclear-power-reactors.aspx#Notes, Updated Jun., 2021

[16] Ge Hitachi Nuclear Energy, https://nuclear.gepower.com/build-a-plant/products/nuclear-power-plants-overview/prism1

[17] NEA News, “Reducing the construction costs of nuclear power”, https://www.oecd-nea.org/upload/docs/application/pdf/2020-10/7548_web_nea_news_38-1_2020-10-08_11-25-27_180.pdf, NEA № 38.1, 2020, p. 7

[18] Westinghouse Nuclear, eVinchi™ Microreactor, https://www.westinghousenuclear.com/new-plants/evinci-micro-reactor, 2019

Proceedings of the European Nuclear Young Generation Forum
ENYGF'21
September 27-30, 2021, Tarragona, Spain

Nuclear costs and policy

Kokurin Nikita[1]

[1]State Atomic Energy Corporation ROSATOM JSK Atomproekt, Russia

*Corresponding author: NAKokurin@atomproekt.com; *forzajuventus010493@gmail.com*

I. INTRODUCTION

Based on the 2030 Climate and Energy Policy Framework 28/10/2014 - European Council 23/24 October 2014 – Conclusions [1], substantial progress has been made towards the attainment of the European Union (EU) targets for greenhouse gas emission reduction. The main way for achieving emission reduction is the gradual leaving coal energy and transition to renewable sources. The goal is to reduce emissions for at least 40%. That was accepted by EU legislatively in part of 2030 Climate and Energy Policy Framework and current contribution in Paris Agreement. The EU aims to be climate-neutral by 2050 – an economy with net-zero greenhouse gas emissions. This aim is at the heart of European Green Deal [3] and corresponds the EU's commitment to global climate action under the Paris Agreement [2].

Nowadays, green and sustainable development have become the mainstream of the current China as well. In order to achieve development strategic targets of non-fossil energy consumption amount accounted for 15% and 20% of energy consumption in 2020 and 2030 respectively, in 2016, the NDRC (National Development and Reform Commission of the People's Republic of China) issued the "13th Five-Year Plan for Renewable Energy Development" and stipulated that the total amount of renewable energy should reach 7.3 million tce (Ton of Coal Equivalent, 1 ton of coal equivalent = 29,307 gigajoules (GJ)), of which the total amount of commercialized renewable energy should reach 5.8 million tce by 2020, providing guidance for the development of renewable energy in the new period. The development of renewable energy policy in China have begun to stabilize in the new period, and China began to pay more attention to the point of promoting energy transformation by quota mechanism, so as to realize the sustainable green development of country [9].

After a careful process involving analysis and consultation across the United States federal government and with leaders in state, local, and tribal governments, the United States is setting an economy-wide target of reducing its net greenhouse gas emissions by 50-52 percent below 2005 levels in 2030 [14].

Nuclear power provides about 10% of the world's electricity, and 18% of electricity in OECD (Organization for Economic Cooperation and Development) countries, in this way, nuclear energy is able to contribute to mitigation of climate change consequences (In accordance with International Atomic Energy Agency (IAEA) Climate Change and Nuclear Power 2020 [4] ch. 2.3.2). Such contribution is life extension of Nuclear Power Plant.

II. NUCLEAR POWER PLANT (NPP) POLICY

A. NPP Life extension

More than two-thirds of the 442 nuclear power reactors in operation are over 30 years old and approaching or have already reached the end of their originally envisaged operational lifetime of around 40 years. Although NPP's do not have a predetermined lifetime, their components do, but almost all of them can be replaced with new parts to safely extend the plant's operational lifespan. The operators of many of these older reactors have received permits from regulators to continue operations or are planning to apply for such permits, following refurbishments and corresponding safety reviews by authorities.

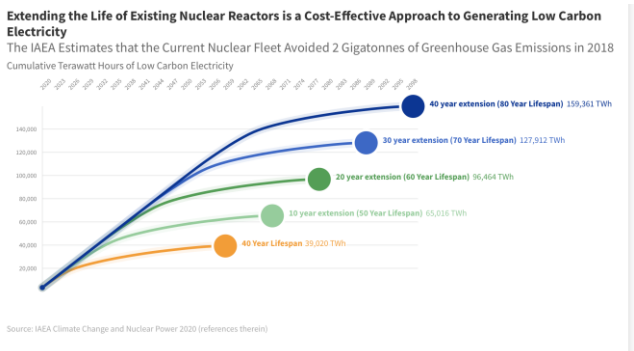

Figure 1. Extending the Life of Existing Nuclear Reactors is a Cost-Effective Approach to Generating Low Carbon Electricity (data: IAEA Climate Change and Nuclear Power [4]).

Figure 1 by IAEA shows that extending the life of existing nuclear power plants significantly increases the availability of reliable low carbon power, helping to meet climate goals and the transition to clean energy by 2050.

The economically reasonable duration of the complementary service life of NPP power units is from 15 to 30 years and is defined by both technical and economic factors in each specific case.

World Nuclear Association has issued the new document "The Enduring Value of Nuclear Energy Assets. Long-term Operation Task Force" [5]. According to the document, in most energy markets, Long-term Operation (LTO) is the lowest-cost option for generating electricity, based on Levelized Cost of Electricity (LCOE) and is expected to stay that way for decades to come, says World Nuclear Association (WNA) (Figure 2). Levelized Cost of Electricity (LCOE) predicted to 2040 in European Union is given in Figure 3 from "Nuclear Power in a Clean Energy System" [8].

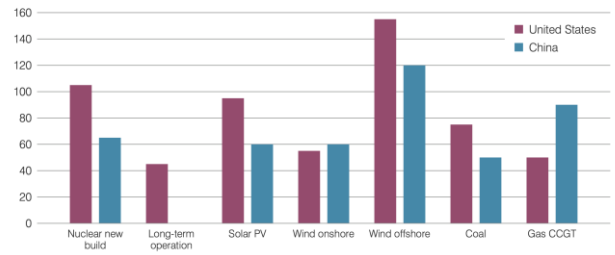

Figure 2. Levelized cost of energy (LCOE) by technology for China and United States (data: World Energy Outlook (WEO) 2019, International Energy Agency (IEA) [13])

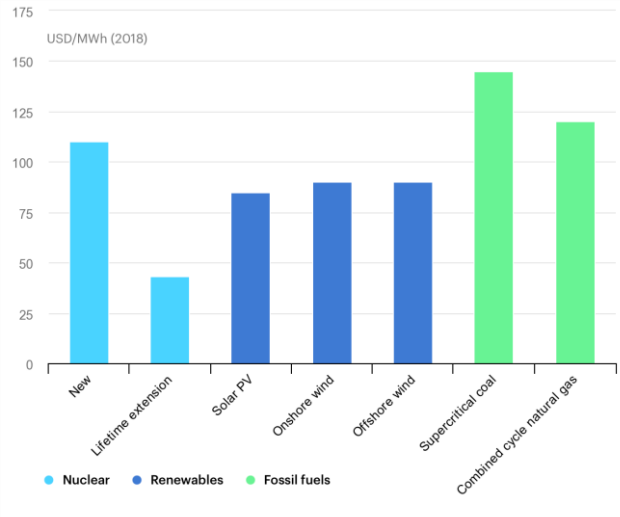

Figure 3. Levelized cost of electricity in the European Union, 2040 (data: Nuclear Power in a Clean Energy System, 2019, IEA [8])

For most reactor technologies, there is no fixed technical lifetime limit. The NPP operation extension has been successfully and repeatedly demonstrated worldwide and is currently standard practice for nuclear power plants with a planned operating life of 60 to 80 years [5].

For companies in the private sector, extending the design lifetime of plants may also allow them to spread decommissioning charges over a longer period than originally planned and further improve profitability. Nevertheless, the substantial capital expenditure associated with longer operational lifetimes may still force closure on some current nuclear plants that cannot justify the upfront costs involved – especially for the smaller, older and inherently less efficient units. But in general, extension of the operational lifetimes of nuclear plants is economically attractive, so long as the political environment is supportive. For example, in Canada, Bruce Power is extending the operational lifetimes of six of its reactors by 30-35 years at a cost of $13 billion, which compares favorably with the cost of alternative generation possibilities [6].

In France, a figure for the 58 nuclear units of up to €10 billion in additional costs has been announced to deploy post-Fukushima modifications and comply with the requirements of the safety authority. Extending the operating lifetimes of the existing reactors has been judged by the national audit body as the most economical way to continue the long history of low power prices in France (ch 2.4 [6]

B. NPP operation and maintenance cost

Nuclear Power Plant economy consists of several aspects:

1. **Capital costs**, which include the cost of site preparation, construction, manufacture, commissioning and financing a nuclear power plant.
2. **Plant operating costs**, which include the costs of fuel, operation and maintenance (O&M), and a provision for funding the costs of decommissioning the plant and treating and disposing of used fuel and wastes.
3. **External costs** to society from the operation, which in the case of nuclear power is usually assumed to be zero, but could include the costs of dealing with a serious accident that are beyond the insurance limit and in practice need to be picked up by the government.
4. **Other costs** such as system costs and nuclear-specific taxes.

More details about operating costs;

Operating costs include the cost of fuel and of O&M. Fuel cost include used fuel management and final waste disposal.

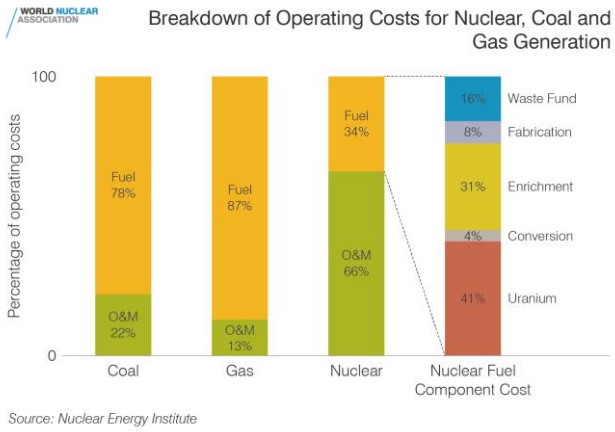

Figure 3. Breakdown of operating costs for nuclear, coal and gas generation (data: Nuclear Energy Institute)

Although there are many country-specific factors, it is possible to make some general statements about the trend of fuel and O&M costs of nuclear plants: nuclear fuel costs have fallen over time due to lower uranium and enrichment prices together with new fuel designs allowing higher burn-ups, while O&M costs tend to be somewhat higher than for other thermal types of generation [6].

O&M costs account for about 66% of the total operating cost (Figure 3). O&M may be divided into 'fixed costs', which are incurred whether or not the plant is generating electricity, and 'variable costs', which vary in relation to the output. Normally these costs are expressed relative to a unit of electricity (for example, cents per kilowatt hour) to allow a consistent comparison with other energy technologies.

Decommissioning costs are about 9-15% of the initial capital cost of a nuclear power plant. But when discounted over the lifetime of the plant, they contribute only a few percent to the investment cost and even less to the generation cost. In the USA they account for 0.1-0.2 cent/kWh, which is no more than 5% of the cost of the electricity produced.

C. Nuclear taxes and subsides

Economy of nuclear power, as well as other energy sectors is associated to taxes and subsidies.

8 of the 14 nuclear energy countries in the EU levy some nuclear tax, which generally do not generate substantial revenues (see table 1). These taxes differ particularly in three dimensions: in their design, particularly with regard to the tax base; in the effective tax burden they create per unit of electricity produced; and to what extent the revenues are earmarked [7].

Table 1 Nuclear power taxes and charges in the EU [7]

Country	Tax design	Tax burden in € per MWh	Tax revenues in Mio. € (in % of GDP)	Introduced in/ Modifications
Abolished nuclear power taxes				
Germany	Nuclear fuel tax; €145 per gram of fissile uranium or plutonium lump-sum payments into decommissioning fund	n.a.	n.a.	
Netherlands	Nuclear fuel tax; Dfl. 31.95 n.a. per gram uranium-235	n.a.	6.8 (0.002%) (1997)	1997/ Abolished in 2000
Existing nuclear power taxes				
Belgium	Lump-sum nuclear plant charge	5 (2014)	200 (0.05%) (2015)	2010/ Initially temporary for the period 2010 to 2014. Increased in 2012. Decreased in 2015, 2016 Increased in 2017.
Bulgaria	Lump-sum nuclear plant charge	5 (2014)	200 (0.05%) (2015)	2010/ Initially temporary for the period 2010 to 2014 Increased in 2012 Decreased in 2015, 2016 Increased in 2017.
Finland	Higher property tax rate for buildings used for nuclear waste management, based on property value lump-sum fee for nuclear waste management fund	0.4 (2012) 1.6 (2012)	n.a.	n.a./ Increased in 2016 1997/ contribution determined yearly
France	Lump-sum nuclear plant tax, multiplied by coefficient depending on type and power of plant 3 additional taxes (research, support and technological transfer tax); lump sum multiplied by coefficients	0.8 (2012) 0.3 (2012)	350 (0.02%)) (2012) n.a.	2000/ Increased in 2006, 2010, 2017 2006
Hungary	Fee for nuclear waste fund	n.a	64 (0.06%) (2012)	1998
Romania	Fee for nuclear waste disposal Fee for decommissioning of nuclear power plants	1.40 0.60	n.a. n.a.	2007 n.a.
Slovakia	Nuclear facility tax and immovable property tax levy of 10% on the wholesale price of electricity for state fund for radioactive waste and decommissioning	0.31 n.a.	n.a.	2004 1995
Spain	Four charges related to nuclear waste management	n.a. 6.60 – 7.80	n.a. n.a.	1997 2012

	Nuclear waste taxes on nuclear waste generation and storage			
Sweden	Capacity tax based on thermal output fee for final storage of spent fuel and decommissioning of nuclear power plants	7.50 4.40	403 (0.09%) (2015) n.a.	2000/ Increased in 2006, 2008, 2015 phased out between 2017 and 2019 1982/ Increased in 2015

Evolution of nuclear power taxes in EU in more detail is given in [7]. Currently (last ten years) the level of taxation of nuclear power in Europe is the lowest in years. In several Member States nuclear energy taxes are reduced or phased out because of the heavy competition from other (renewable) sources for electricity generation. As of 2017, there is no nuclear tax in Germany, the Swedish nuclear tax is in the process of phase out, and the tax burden on nuclear energy produced in Belgium is substantially lower compared to previous years. Those nuclear taxes still in place in EU Member States mainly aim at accruing earmarked revenues to finance the management of radioactive waste and decommissioning [7].

In United States, each year, the average 1,000 megawatt (MW) nuclear plant generates approximately $470 million in electricity sales (economic output) in the local community and more than $40 million in total labor income.

Analyses of 23 U.S. nuclear plants representing 41 units show that every dollar spent by the average unit results in the creation of $1.04 in the local community, $1.18 in the state economy and $1.87 in the U.S. economy.

The average nuclear plant pays about $16 million in state and local taxes annually. These tax dollars benefit schools, roads and other state and local infra- structure. The average nuclear plant also pays federal taxes of $67 million annually [10].

In general, nuclear taxes are a politically very sensitive and debated issue, and tax provisions change rather frequently. One specific characteristic of the nuclear power producing sector legislators are facing when attempting to implement nuclear taxes is that the sector usually consists of only one or very few big electricity producing companies with considerable lobbying power. Therefore, companies negotiating with the government about the tax, as for example in Belgium or Sweden, or even filing lawsuits against it, as for example in Germany, are not unusual [7].

III. CONCLUSIONS

Although nuclear is a proven source of low-carbon, dispatchable electricity giving a high degree of energy security and provides half of the EU's carbon-free electricity, the sector today faces major challenges within the EU. Some member states are strongly anti-nuclear, and electricity markets are often structured in response to populist support for renewables. In the period to 2030, nuclear capacity that will be lost due to the closure of a number of reactors – either because they have reached the end of their operating lifetimes or due to political interference – is expected to outweigh that gained from new reactors. A slight decrease from the current EU nuclear capacity is therefore expected in the near term.

Nuclear plant construction is currently underway in only three EU member states – Finland, France and Slovakia. These construction projects have all experienced cost overruns and delays. Further new units likely to come online before 2030 are outlined in the table below. The long-term future of nuclear power in the EU is likely to depend on the outcome of these projects, which are relatively few in number – in total less than planned in Russia.

The Euratom Treaty (officially, the Treaty establishing the European Atomic Energy Community) requires the European Comission to periodically issue a Nuclear Illustrative Program (PINC) [11], based on data from member states, and the latest of these was a draft in April 2016 (the first since 2007). It forecast a decline in EU nuclear capacity to 2025 and then a levelling out to 2050 at 95 to 105 GWe (the current capacity in the EU is 120 GWe) [12].

The overall picture for current nuclear plants is that they are operating more efficiently than in the past and unit operating costs are low relative to those of alternative generating technologies. More output is being achieved from each reactor through improved performance and capacity uprates. Their operation should continue for many years in the future, supported by the necessary investment in refurbishment. These improvements have now become routine and will be integrated into the construction of new nuclear plants [6].

As far as around two thirds of the world's electricity still coming from burning fossil fuels, reaching these climate goals by 2050 will require at least 80% of electricity to be shifted to low carbon sources, according to the IEA. Nuclear power is the second-largest source of low carbon energy used today to produce electricity, following hydropower. During operation, nuclear power plants produce almost no greenhouse gas emissions. According to the IEA, the use of nuclear power has reduced carbon dioxide emissions by more than 60 gigatonnes over the past 50 years, which is almost two years' worth of global energy-related emissions. So, nuclear power is an essential part of the clean energy transition.

"There is no solution to a sustainable energy future without nuclear energy. All serious scenarios for the future, where the world achieves a clean, reliable, 24/7 electricity supply, demonstrate that nuclear is of key importance" **s**ays Agneta Rising, World Nuclear Association Director general.

IV. References

[1] European Council 23/24 October 2014 – Conclusions;

[2] United Nations, Paris Agreement, 2015

[3] European Commission, The European Green Deal, Brussels, 11.12.2019

[4] IAEA, CLIMATE CHANGE AND NUCLEAR POWER, ch. 2.3.2

[5] WNA, The Enduring Value of Nuclear Energy Assets Long-term Operation Task Force, June 2020

[6] WNA, Nuclear Power Economics and Project Structuring, 2017

[7] F. Dellinger, M. Schratzenstaller, Austrian Institute of Economic Research, Sustainability-oriented Future EU Funding: A European Nuclear Power Tax, may 2017

[8] IEA, Nuclear Power in a Clean Energy System, Fuel report — May 2019

[9] IOP Conference Series: Materials Science and Engineering, The Development of China's Renewable Energy Policy and Implications to Africa

[10] NEI, Nuclear Energy's Economic Benefits — Current and Future, April 2012

[11] European Commission, Nuclear Illustrative Programme, Brussels, 4.4.2016 COM(2016) 177 final

[12] WNA, Nuclear Power in the European Union, February 2021

[13] The United States's Nationally Determined Contribution. Reducing Greenhouse Gases in the United States: A 2030 Emissions Target, 2021

[15] IEA, World Energy Outlook (WEO), 2019

Proceedings of the European Nuclear Young Generation Forum
ENYGF'21
September 27-30, 2021, Tarragona, Spain

The Role Of Nuclear Energy In Electricity Power Systems With High Renewables Share

Korolev, Vyatcheslav[1,2]

[1] JSC "Atomenergoproekt", Russian Federation; [2] National Research University MPEI, Russian Federation;

**vya.korolev@gmail.com*

I. INTRODUCTION

Global warming is a significant problem for the world. Global warming is mainly caused by the greenhouse effect, where greenhouse gases (GHG) absorb and redirect terrestrial radiation as infrared radiation [1]. According to Intergovernmental Panel on Climate Change (IPCC), this causes the net amount of radiation sent to space to decrease, which leads to increasing surface temperatures. The stronger the effect is, the more there are GHG. While other things, such as clouds contribute to global warming, GHG are the main contributors. The main GHG in Earth's atmosphere according to IPCC are water vapor (H2O), carbon dioxide (CO2), Nitrous oxide (N2O), Methane (CH4) and Ozone (O3). CO2 is the principal anthropogenic greenhouse gas. Electricity production is also a significant producer of greenhouse gas emissions in Europe. The electricity sector therefore produces a significant share of emissions each year. In the future, the importance of a carbon-free power sector will become even more relevant, as electrification of the heating and transportation sectors are predicted to increase the electricity demand [1,2,3].

All of the world, nuclear has increasingly been accepted by people because of low resource consumption, low environment pollution and strong supplement, and has been the one of electricity supply paralleling with thermal power and water power. European sector is no exception. The electricity generation sector in Europe has changed dramatically in the almost half-century since the first nuclear reactor started to operate. There is a list of countries (Sweden, Germany, France and et.) that historically selected a nuclear power expansion program as the principal energy source for meeting demand growth. The green-house-gas emissions of electricity and heat production in Europe vary over time during the last three decades. For example, in Sweden, largest amount of greenhouse-gas emissions was 13.5 Mt CO_2 in 1996, and the smallest amount was 6.4 Mt CO_2 in 2015.

The Carbon-Neutral Scenario (CNS) was published by the IEA in 2016, which was aiming a near carbon- neutral energy system in Europe by 2050 [4]. The report concluded that wind could replace both fossil fuels (coal) and nuclear by increasing the wind share from 7% to 30% by 2050 [3]. Nordic countries would then export 53 TWh of electricity to the rest of Europe. Sweden would phase out all nuclear fleets by 2050 while increasing wind capacity up to 31.4 GW by 2050. The results of this report have two serious issues that should be addressed. First, the high penetration of variable renewables, mostly wind, will require technical (e.g., energy storage and backup power) and economic (e.g., demand response and market mechanisms) balancing mechanisms. Second, for the expansion of wind, the interconnection between European countries will require substantial upgrades.

As we can see, there is a trend to replace nuclear power generation with wind and lower-carbon fossil systems in Europe.

The main goal of this thesis is to answer the following questions:

- Is a carbon-free power system technically feasible?
- Is a carbon-free power system economically feasible?

II. MODEL DESCRIPTION AND CASE STUDY

In spite of the thermal power still acting as the important development direction in the future, but developing others, high effective and clear energy source, such as High Renewable Energy Sources (RES), becomes decisive and important object.

The power system plays an integral role in achieving carbon neutrality. This thesis presents analyzation of modelling of a carbon-free European power system, which produces electricity from wind, photovoltaics, hydro and nuclear power. A carbon-free power system is defined, in this thesis, as a system which uses only such generation technologies, which emit neither fossil nor

biogenic CO2-emissions. Therefore, it is essential to phase-out fossil fuels in power generation. That is the reason why one of the main theme for different countries is to achieve carbon neutrality. Different renewable power system models were developed for Europe in 2050, using only solar and wind power as the generating power sources. Additionally, an electricity storage is also the part of the ways. Due to the intermittent nature of certain renewable technologies, such as wind and PV, electricity storage is needed, especially if they constitute a large fraction of the overall power generation. [5]. This is the case in the proposed carbon-free power system for Europe. Therefore, electricity storage is required.

Electrochemical storage options include batteries such as lead-acid batteries, sodium-sulfur batteries, and lithium ion batteries. While these technologies are good for short-term storage, and some of these technologies are already very mature technologies, various problems, such as low cycle life, hazardous materials and especially resource consumption limit the potential of these technologies in large-scale deployment [6].

Flow batteries could be a solution for these problems, however, as they can be scaled for large applications. However, large-scale flow batteries are still in development. A large-scale vanadium redox battery of 3MW / 12 MWh has already been commissioned in China, with even larger 100 MW / 500 MWh being planned in the future [7].

Additionally, fuel cells are also classified as electrochemical storages. Fuel cells can be used to produce hydrogen from electricity, or electricity from hydrogen, and therefore are also an option for long-term storages. However, according to Evans et al. these technologies still suffer from low round-trip efficiencies.

Data for this work is gathered from [8,9], the Fingrid open data and open-power-system-data services during period since 2018 until now. Jupyter notebooks were used as a format that combines script code and documentation in a single file. The notebooks contain the most detailed documentation of the provided data files and enable users to find out how the data was sourced, treated and packaged up to the final product.

The model assigns power generation capacities as variable for wind, PV and SMR nuclear. The generation capacities for hydro, thermal power and nuclear plants are given as inputs to the model.

According to the World Nuclear Industry report in the European Union (EU) [10] (As the U.K. left the EU only on 31 January 2020, the data is taken with the statistics for 2019 for the EU28 including the U.K.), renewables, including hydro, continue to grow and supplied a record 35 percent of the power in 2019, up by 1.8 percent over the previous year. During 2019, the combined outputs from solar and wind at 18 percent were greater than that provided by coal. The other renewables, hydro and biomass provided 10.8 percent and 6.2 percent respectively, while nuclear power provided 25.5 percent. [11]

Overall fossil fuel generation fell by 6 percent, with natural gas increasing by 12 percent, hard coal decreasing by 32 percent—caused by renewables growth and rising CO_2 prices (leading to increased gas generation)—and a fall in lignite-based production of 16 percent. Electricity consumption decreased by 1.7 percent in 2019 (–56TWh), bringing demand back to 2015 levels. Because of all of these changes, CO2 emissions from the power sectors fell by 12 percent.

In 2019, solar installed capacity for the first time exceeded the nuclear one in the EU28 with 130 GW vs. 116 GW. Wind had outpaced nuclear already in the 2014 and has ever since enlarged the gap with a total of 191 GW installed as of the end of 2019. On the electricity generation side, nuclear is still generating more than either wind or solar, but its slow decline continues.

From the other hand, there are studies that say, that new nuclear power can be invested in countries with existing nuclear fleet and the upper limit is the current capacity. Three exceptions are Germany, Switzerland and Belgium; where there are clear policies to phase out nuclear power plants [12, 13]. This means that the maximum potential nuclear energy supply is equivalent to 20% of current European electricity demand if a capacity factor of 80% is applied to nuclear power.

Several studies have investigated the transition towards a non-nuclear electricity system for Sweden [2, 14, 15]. All these studies assessed the requirement of Variable Renewable Energy (VRE) to replace nuclear power, but only Hong et al. [14] singled out the influence of phasing-out nuclear power on the electricity system cost.

There are a handful of studies that have assessed the cost difference of electricity system without nuclear as compared to a system with nuclear for regions other than Sweden [16, 17, 18, 19]. Jaagemann et al. [16] investigated the deep decarbonization for Europe's power sector and found that the cost of decarbonization and electricity system cost together might increase by 11% if nuclear power and Carbon Dioxide Capture and Storage (CCS) were not included in the electricity system. Similarly, Zappa et al. [17] showed a 30% cost increase for the 100% renewable European electricity system if nuclear power and CCS were excluded.

III. RESULTS

The results of research showed that in different countries situation with economic rationality to invest in nuclear power differs. For example, the nodal net average system cost for Sweden is virtually the same, irrespective of whether nuclear power is included in the electricity system or not. From the other hand it can be economically justified because it can enable exporting to the highly renewable European electricity system rather than to satisfy domestic demand.

In general, the established state of affairs has both the lowest annual costs and the leveled cost of electricity compared to alternative cases. The leveled cost of generated electricity in the alternative cases is about twice that of the existing condition case, and up to five times

higher when framed in terms of consumption. Note that the price does not include the additional balancing costs such as transmission costs and flexibility costs that will increase substantially if the intermittent renewable energy share increases [14].

Most of the trends over the past decade show that nuclear power can compete in the decarbonized energy sector with a range of renewables. The market of renewable energy needs to be sufficiently developed. However, to reach this level, colossal costs are required, which may not pay off in the existing releases of Covid19 (when various sectors of the economy may suffer a decline). Thus, nuclear power remains the only economically viable solution.

IV. References

[1] IPCC (2014b)'Glossary', in Intergovernmental Panel on Climate Change (ed.) Climate Change 2013 – The Physical Science Basis. Cambridge: Cambridge University Press, pp. 1447–1466. doi:10.1017/cbo9781107415324.031.

[2] International Energy Agency. Nordic energy technology perspectives 2016. Available from: https://www.nordicenergy.org/wp-content/uploads/2016/04/ Nordic-Energy-Technology-Perspectives-2016.pdf; 2016.

[3] European Commission, "Statement: Europe leads the global clean energy transition: Commission welcomes ambitious agreement on further renewable energy development in the EU." European Commission – Press release, 14-Jun-2018 [Online]. Available: https://ec.europa.eu/commission/presscorner/detail/en/ STATEMENT_18_4155

[4] IEA, 2016a. IEA - Sweden [Online]. URLhttp://www.iea.org

https://iea.blob.core.windows.net/assets/680c05c8-1d6e-42ae-b953-68e0420d46d5/WEO2016.pdf

[5] Evans, A., Strezov, V. and Evans, T. J. (2012) 'Assessment of utility energy storage options for increased renewable energy penetration', Renewable and Susta inable Energy Reviews. Elsevier Ltd, 16(6), pp. 4141–4147. doi:10.1016/j.rser.2012.03.048.

[6] Zhang, C., Wei, Y.-L., Cao, P.-F., & Lin, M.-C. (2018). Energy storage system: Current studies on batteries and power condition system. Renewable and Sustainable Energy Reviews, 82, 3091–3106. doi:10.1016/j.rser.2017.10.030

[7] Giulianini, M., & Dart, M. (2017). Flow battery versatility: Adapting the battery to the specific application. 2017 IEEE International Telecommunications Energy Conference (INTELEC). doi:10.1109/intlec.2017.8214152

[8] Research and data to make progress against the world's largest problems https://ourworldindata.org/

[9] The European Environment Agency https://www.eea.europa.eu/

[10] he world nuclear industry status report 2020, A Mycle Schneider Consulting Project, Paris, September 2020. [Online]. Avaliable: https://www.worldnuclearreport.org/IMG/pdf/wnisr2020-v2_hr.pdf

[11] "The European Power Sector in 2019: Up-to-Date Analysis on the Electricity Transition", February 2020, [Online]. Avaliable https://www.agora-energiewende.de/en/publications/the-european-power-sector-in-2019/

[12] Joskow PL, Parsons JE. The Future of Nuclear Power After Fukushima. Econ Energy Environ Policy 2012; https://www.jstor.org/stable/26189494.

[13] Kunsch PL, Friesewinkel J. Nuclear energy policy in Belgium after Fukushima. Energy Pol 2014;66:462-74. https://doi.org/10.1016/j.enpol.2013.11.035

[14] Hong S, Qvist S, Brook BW. Economic and environmental costs of replacing Nuclear fission with solar and wind energy in Sweden. Energy Pol

[15] Sooder L. Pa vaag mot en elfoorsorjning baserad på enbart foornybar el i Sverige.Available from: https://www.diva-portal.org/smash/get/diva2:727697/FULLTEXT01.pdf ; 2014

[16] Jagemann C, et al. Decarbonizing Europe's power sector by 2050 - Analyzingthe economic implications of alternative decarbonization pathways. Energy Econ 2013;40:622-36. https://doi.org/10.1016/j.eneco.2013.08.019

[17] Zappa W, Junginger M, Van Den Broek M. Is a 100% renewable European power system feasible by 2050? Appl Energy; 2019. p. 1027-50. https://doi.org/10.1016/j.apenergy.2018.08.109. 233-234.

[18] Buongiorno, et al. The future of nuclear energy in a carbon-constrained world 2018. Available from: http://energy.mit.edu/wp-ontent/uploads/2018/09/The-Future-of-Nuclear-Energy-in-a-Carbon-Constrained-world.pdf.

[19] Sepulveda NA, et al. The role of firm low-carbon electricity resources in deep decarbonization of power generation. Joule 2018;2(11):2403-20. https://doi.org/10.1016/j.joule.2018.08.006

Proceedings of the European Nuclear Young Generation Forum

ENYGF'21
September 27-30, 2021, Tarragona, Spain

Developing nuclear technologies as a vital step in the approach to reduce CO2 emissions

Talyzina, Olga[1]

[1]Private Institution "Situation and Crisis Center of Rosatom", Russian Federation

*Corresponding author: *otalyzina11@gmail.com*

I. INTRODUCTION

The issue of climate change has been on the agenda for quite a while. The world community has made numerous joint efforts to reduce CO2 emissions – one of the biggest factors of global warming. So, what can society do?

The most vital goal in this respect is decreasing nations' dependency on fossil fuels as a source of energy, as they are responsible for gas emissions.

Many efforts have already been undertaken in this direction. For example, in 2016 the Paris Agreement came into effect. Out of 195 initial signatories, 191 are currently members of the agreement. It implies that by 2050 the level of CO2 emissions will drop to 0. In order to achieve this goal, many countries are actively working on developing renewable energy sources.

However, this isn't always enough to fully meet energy demand. Moreover, a significant drawback of renewable energy sources is their unreliability due to unstable energy transmission.

In 2018 the EU adopted the "Clean Energy for All Europeans" package, which regulates the countries' policies regarding energy and promotes the introduction and increasing use of "clean energy" and investments in this sphere. The package sets a number of goals to be achieved by 2030. The "Clean Energy for All Europeans" package means that EU-members will lower their dependency on fossil fuel energy. At the moment around 80% of energy in the world comes from fossil fuels. Three decades ago, the numbers were the same.

But if society decides to leave dependence on fossil fuels behind, it is to find a suitable alternative. One of them is nuclear energy.

Many countries have already started to use nuclear energy (France, Korea, Russia, UK, USA, China, etc). Moreover, they are currently focused on developing new technologies, such as small nuclear power plants (SNPPs). And there is currently a lot of focus on developing promising emerging technologies, among which are small modular reactors (SMRs).

II. WHY NUCLEAR ENERGY

Despite the fact that there are many who criticize the idea of seriously considering nuclear power as a viable variant in terms of a nation's energy solution, there are many reasons for it to be the next main energy source.

A. Safety

First of all, given that nuclear power plants (NPPs) are constructed correctly and in accordance with all rules, guidelines and regulations, nuclear power is the safest form of energy in the world. Due to energy being created out of nuclear fission and not due to a chemical reaction, no carbon is emitted into the atmosphere. NPPs are sustainable, they produce no CO2 during operation and the amount of greenhouse gases they produce during their entire lifecycle is incomparable to the amount produced during the use of other energy sources in this respect.

B. Affordability

Secondly, there is the issue of affordability. Constructing NPPs is a long and costly process. The payback period of such projects is also lengthy. Operational costs however remain low and stable, which means that while these power plants are expensive to construct, they are cheap to run. Much cheaper to run, in fact, than almost all fossil fuel alternatives. There are a number of factors that determine the cost of electricity the NPP generates. If we speak about the levelized cost of electricity from an NPP, it is obvious

that such a form of energy is quite economical compared to others.

C. Socio-economic Impact and Issues

The most important socioeconomic aspects of the transition to nuclear energy include the creation of new jobs, workplaces and education facilities. In the long run this can contribute to decreasing unemployment rate. Moreover, the development of nuclear energy will inevitably lead to an advance in various technological spheres, from geological exploration to dealing with depleted uranium.

There are several nations that are sceptic about switching from traditional energy sources (such as oil and gas) to nuclear energy and those that are phasing it out. This is why public acceptance of nuclear energy is another important issue many nations face before they can start implementing nuclear power programmes. The population must be well educated about this form of energy in order to understand all its advantages.

D. New Developments

Currently several nations including Russia, USA, Canada, Great Britain and many others are actively developing technologies used during SMR and advanced reactor construction. SMPPs have a number of advantages compared to traditional NPPs and thus can be seen as a viable alternative both for states where nuclear power isn't yet part of the energy policy, and for developing countries that need to meet growing demand at relatively lower costs.

Among the abovementioned advantages are such factors as:

- a higher level of safety and security due to lower power
- a smaller scale (making it more feasible to construct, using parts made in a factory environment)
- shorter construction span
- less costly and risky to build

Therefore, the SMR market can become one of the most promising areas for the development in the nuclear industry, especially considering the fact that several companies at once are planning to commission the first SMPPs by 2030.

Speaking about other advances in the sphere of nuclear energy, it would be fair to mention that in 2020, Russia began the commercial development of the world's only floating nuclear thermal power plant "Akademik Lomonosov", designed to supply power to the Chukotka Autonomous Region and heat the city of Pevek. The State Atomic Energy Corporation Rosatom is also promoting the land-based SNPP project based on the RITM-200 reactor. Such a plant will be built in the town of Ust-Kuyga (Yakutia) by 2028.

One more point to be raised in this context is the feasibility of introducing hybrid systems, that would merge nuclear energy with renewable energy systems. The most popular argument for undertaking action in this field is the fact that experts believe nuclear power can help improve existing renewable energy systems. At the moment, some nations with a high share of nuclear power have introduced 'flexible operation". France is a good example of this. Now that the use of SMRs is becoming increasingly more popular, the prospects of creating hybrid energy systems using small modular reactors seem highly likely. What is more, this is the case both for power and non-power uses. Currently, only experiments to achieve such systems are underway and these test systems are without a nuclear component.

One more interesting prospect for the use of SMRs is their use in remote locations, where they could be utilized as both a source of electricity and for desalination. Another potential area of SMR use is hydrogen production. Experts predict this to be a very worthwhile cause. This is because many petrol producers, seeing as there is currently a rising popularity of electric ecofriendly vehicles, are eyeing hydrogen as a viable alternative to fossil fuels.

III. CONCLUSION

Global warming and climate change are some of the most acute challenges facing the world community. It has long become evident that unless certain action is undertaken, this may become a much bigger problem than it currently already is.

The biggest issue with global warming is CO2 emission, which harms the ozone layer, leading to what at a first glance may seem an insignificant increase in temperature all around the world.

Most of the CO2 comes from burning fossil fuels, used to generate electricity which is why it is vital to find and introduce a suitable alternative.

Many nations are already taking action and implementing policies that are aimed at reducing their detrimental effect on the environment.

It is safe to say that nuclear energy may be that very alternative. It is affordable, safe, leaves almost no carbon footprint behind, promotes the creation of new jobs and fuels technological development.

IV. References

[1] Rakshay Jain, "Nuclear Power: A Nuclear Solution to CO2 Emissions," SSRN Electronic Journal, 2007.

[2] Richard Rhodes, "Why Nuclear Power Must Be Part of the Energy Solution," Yale Environment 360, 2018.

[3] World Nuclear Performance Report 2020

[4] OECD International Energy Agency, World Energy Outlook 2020

[5] Dan Yurman, "Study Finds Advanced Reactors Will Have Competitive Costs," Neutron Bytes, 2019

Proceedings of the European Nuclear Young Generation Forum
ENYGF'21
September 27-30, 2021, Tarragona, Spain

Development and implementation of Project Management in Akkuyu Nuclear Power Plant construction and operation project

Feoktistov, Anton[1*]

[1] AKKUYU NÜKLEER ANONİM ŞİRKETİ, Turkey

*Corresponding author: *A.Feoktistov@akkuyu.com*

I. INTRODUCTION

On May 12, 2010, the government of the Russian Federation and the government of the Republic of Turkey signed an agreement on cooperation in relation to the construction and operation of Akkuyu Nuclear Power Plant (hereinafter the "Project"), comprised of four power units with VVER-1200 reactors with a total capacity of 4800 MW, on the southern coast of Turkey in Mersin province (Figure 1).

Figure 1. Location of Akkuyu NPP.

Akkuyu NPP is the world's first NPP project implemented according to the BOO (Build – Own – Operate) model.

Akkuyu is also the first NPP construction project in Turkey. It is planned that Akkuyu NPP will generate about 35 billion kWh of electricity per year, providing an estimated 10% of Turkey's electricity needs.

The attainment of this ambitious goal will demonstrate the efficiency of the nuclear energy and the benefits a country, which is implementing a NPP project, will receive, ensuring the achievement of Sustainable Development Goals.

"Project Management" in NPP construction is one of the 19 elements of the Nuclear Infrastructure (Figure 2), which establishes the requirements for legal and governmental responsibilities in respect to the safety of nuclear facilities (in accordance with IAEA [1]).

Turkey has been a member state of IAEA since 1956 and is actively pursuing a nuclear energy program.

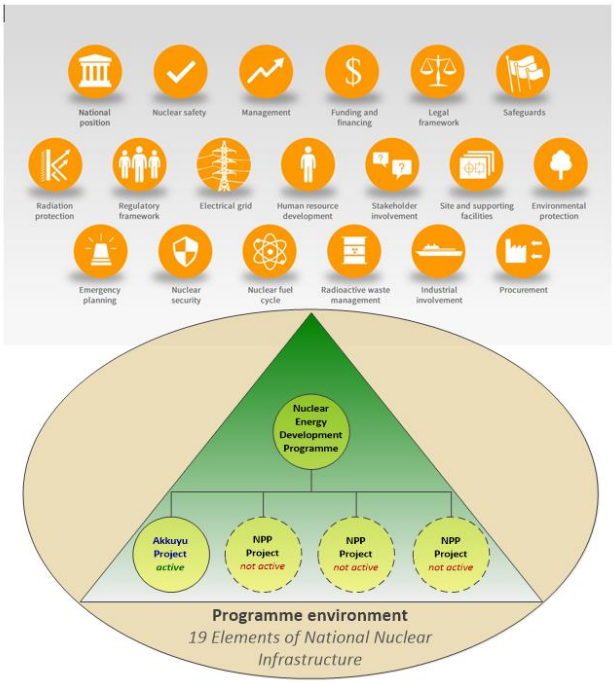

Figure 2. Akkuyu Project in the Turkish Nuclear Energy Program.

Under the terms of the Agreement between the Russian Federation and the Republic of Turkey, on December 13, 2010, the Russian side established a Project Company on the territory of the Republic of Turkey – AKKUYU NUCLEAR JSC (hereinafter the "PC").

PC manages Akkuyu NPP Project and is responsible for:

Build: Permitting, Contracting, Construction & Installation	✓ Ensuring nuclear safety at all stages of NPP life cycle
Own: Owning Akkuyu NPP, Financing the Project	✓ Successful implementation of the Project in accordance with the agreement between Russia and Turkey
Operate: Licensing, Commissioning, Operation & Maintenance, Decommissioning	✓ Coordination & integration of all aspects related with the Project

Based on the BOO model, PC performs the following roles and functions:

- Management of Akkuyu NPP Project,
- Design and construction of Akkuyu NPP,
- Development of the infrastructure for Akkuyu NPP,
- Design, development, production, installation of systems, equipment, components, materials for use in construction and during operation of Akkuyu NPP,
- Quality assurance and control at all stages of the Project,
- Safe and reliable commissioning of Akkuyu NPP,
- Maintenance of Akkuyu NPP,
- Provision of spare parts during entire service life of NPP,
- Training of operating personnel,
- Physical protection of Akkuyu NPP (a joint effort with the government of the Republic of Turkey),
- Ensuring safety and physical protection of the nuclear and radioactive materials,
- Supply of fresh nuclear fuel,
- Decontamination and safe handling of radioactive waste,
- Safe handling and transportation of spent nuclear fuel,
- Planning of emergency response at Akkuyu NPP,
- Decommissioning of Akkuyu NPP.

Thus, for an organization implementing a NPP Project based on the BOO model it is necessary to develop and implement an Integrated Management System (the "IMS"), which is a set of interconnected systems, which:

- ensure achievement of policy & goals of the organization,
- integrate elements of safety, security, environment, health and quality, as well as individual, social, economic factors of management,
- include organizational structure, resources and processes of the organization,
- take into account at all levels of decision-making within the PC the requirements (Figure 3) that are defined in the National Nuclear Program of Turkey (the "Management" element in the top row in Figure 2).

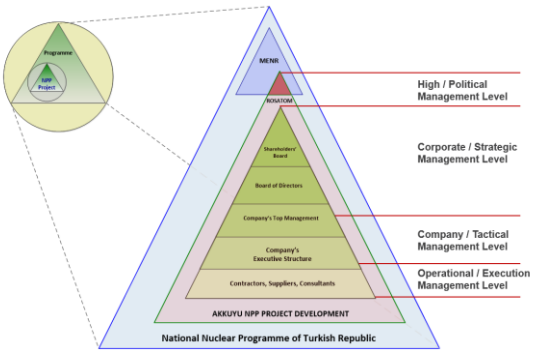

Figure 3. Akkuyu NPP Project management structure.

II. DEVELOPMENT OF IMS

A whole range of requirements of external stakeholders and international standards for Project's IMS was included in the Regulation on Management System in Nuclear Facilities issued by the Nuclear Regulatory Authority of the Republic of Turkey [2] that is based on IAEA GSR Part 2 "Leadership and Management for Safety" [3].

In compliance with the aforementioned Regulation the PC's management system was transitioned from a Quality Management System to an Integrated Management System, integrating safety, security, environmental, health & quality aspects, as well as individual, social and economic factors without compromising safety, in line with corporate safety objectives (Figure 4).

Figure 4. Key requirements included in the IMS.

Activities for implementation of IMS in PC were organized and carried out in accordance with an IMS Implementation Roadmap that was revised and updated in view of granting of the Construction License for Unit No. 1 on April 2, 2018, marking the start of a new phase in the lifecycle of Akkuyu NPP [5].

IMS of the PC was designed and implemented in a way that ensures effective realization of the corporate development strategy, vision and mission, and achievement of corporate objectives at all phases of Akkuyu NPP. Safety is the fundamental objective of PC's IMS [6].

The architecture of PC's IMS is comprised of the following:

- Governing principles of PC: Vision, Mission & Policies,
- Corporate strategies,
- Organizational structure (incl. functions, responsibilities, authority and organizational changes),
- A set of interconnected and managed processes,
- IMS documentation (Management plans etc.),
- Resources.

The underlying principles of PC's IMS are described in IMS Policy, which establishes priority of safety above all other aspects of PC's activities.

IMS is described in the "IMS Manual" [7], which includes information about the following aspects of the IMS:

- Corporate mission, vision and objectives, including the primary safety objective.
- Corporate policies that enable the organization to attain its primary safety objective.
- Organizational structure, distribution of responsibilities and authority.
- Corporate values and behavioral expectations.
- Responsibility of the organization for ensuring safety.
- Leadership role of managers.
- Safety culture.
- Graded approach.
- Corporate process model.
- Interfaces with stakeholders.
- Assessment and improvement of the IMS.

PC's activity is organized into processes, categorized under the following four process groups (Figure 5):

– Management Processes.
– Core Processes.
– Supporting Processes.
– Safety Processes.

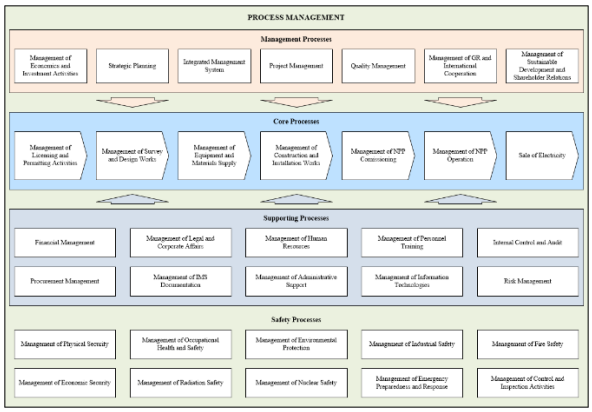

Figure 5. The process model of PC's IMS.

The process model of PC's IMS covers all functional areas of Project Management:

– Integration Management.
– Schedule Management.
– Scope Management.
– Cost Management.
– Quality Management.
– Human Resources Management.
– Communications Management.
– Risk Management.
– Procurement Management.
– Safety Management.

A. Principles of Project Management

The application of project management principles within the framework of IMS made it possible, by means of the Work Breakdown Structure (the "WBS"), to decompose Project's strategy into individual work packages (Figure 6).

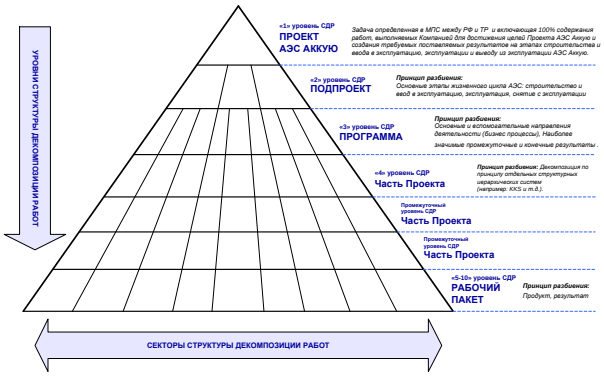

Figure 6. Structure of Akkuyu NPP Project (WBS levels).

At the top of the pyramid resides the Cooperation agreement between the Russian Federation and the Republic of Turkey, constituting 100% of Project scope. Further, down the levels of WBS the Project is divided into components starting with stages of Project's life cycle and down to the work packages specified for individual facilities of Akkuyu NPP.

In the beginning of implementation of IMS the management structure at PC was predominantly function-oriented, which lead to difficulties in flow of information between different levels of management. Therefore, one of the main goals of IMS implementation at PC was to transform the structure of management organization at PC from "function-oriented" to a "project-oriented" one (see Figure 7).

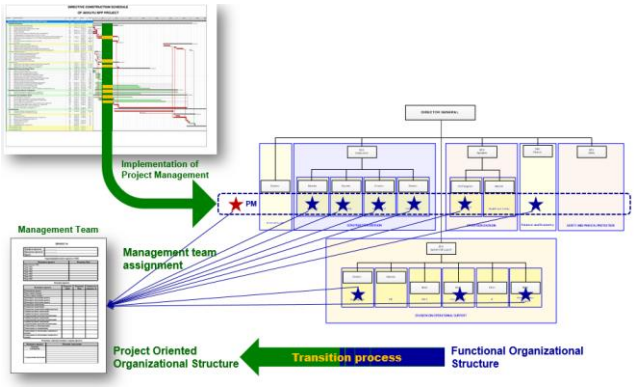

Figure 7. Transition to project-oriented management structure at PC.

B. Approaches for Project Management

During implementation of IMS, the following approaches to management were taken into consideration:

– Process-based approach to management.
– Project-based approach to management.
– Graded approach.

Implementation of aforementioned management approaches is necessitated by the requirements of the Turkish Nuclear Regulatory Authority [2] for the process-based management approach (i.e. IMS), and requirements of IAEA NG-T-1.6 "Management of Nuclear Power Plant Projects" [4] and ROSATOM guidelines on project management. This results in the integration of process-based approach to management with project management (Figure 8).

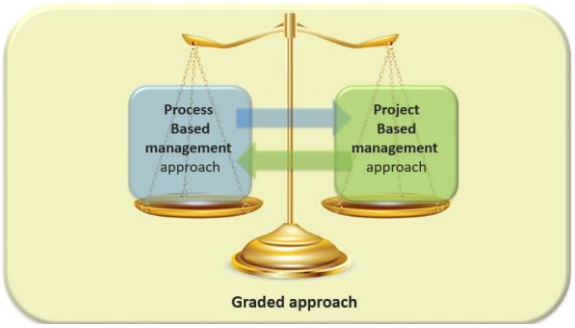

Figure 8. Balance between process and project-based approaches.

Within the IMS, the process and project-based management approaches should be balanced. This balance depends on the stage of NPP Project implementation (see Figure 9).

At the start of a NPP project, the project-based management approach usually prevails (due to the uniqueness of the final product / service).

At the construction stage the project management approach still prevails, however, process-based approach is developed actively due to operational nature of the activity.

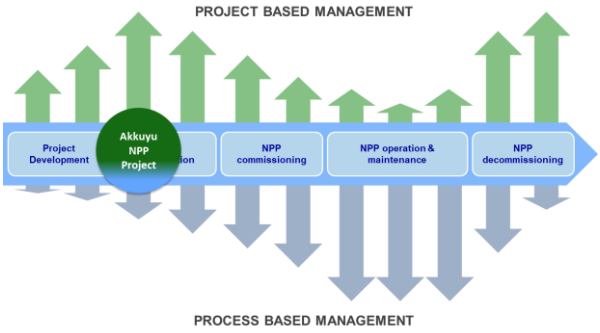

Figure 9. Time variation of intensity of process and project-based management approaches throughout NPP Project's lifecycle.

At NPP commissioning stage the management environment is getting more and more process-oriented, and prevails over project management at the end of the commissioning stage.

During NPP operation stage the process-based management is fully developed and implemented as the primary approach to management, with project management used for specific activities, such as improvements, upgrades, modernization etc.

As NPP nears the end of its operational lifetime, the project-based management approach starts to develop gradually.

During NPP decommissioning stage, after defueling of NPP unit, project management approach once again prevails over the process-based approach.

Important: responsibility for balancing process and project-based approaches resides with the top management.

III. RESULTS

At present stage of IMS implementation at PC, the IMS documentation, which is required by the Turkish Nuclear Regulatory Authority, has been developed (as of 2019).

The transition from a Quality Management System to an Integrated Management System in Akkuyu Nuclear JSC is being realized in accordance with the IMS Implementation Roadmap.

Processes identified in the process model of the IMS and to be defined in the IMS Manual, are being documented.

Akkuyu NPP Project Management System Manual, which defines the approaches and mechanisms for the management of Akkuyu NPP Project, was developed and approved.

Integration of management systems allowed PC to create an effective planning mechanism for Akkuyu NPP Project (a 4-level scheduling & network planning system), develop a strong safety culture, a system for documenting and determining process indicators and risks, a knowledge management system (Project's lessons learned), a system of motivation and development of competencies of the project management personnel, as well as other effective tools for the development of the PC.

IV. CONCLUSIONS

Akkuyu NPP Project complexity has increased dramatically due to changes in regulations and safety requirements, new industrial set up, new technologies, internationalization and tighter financial requirements.

This higher level of complexity requires:

– A well-defined organization with a project-oriented approach to management.
– Clear definition of Project strategy, targets & milestones.
– Effective management of the configuration and changes.
– Risk management system with mitigation action plans.
– Strong management of all Project stakeholders.
– Focus on nuclear safety requirements.

Considering the discussion and results provided above, a strong Integrated Management System, which incorporates process and project-based approaches in a balanced manner, is mandatory for a successful implementation of a NPP Project.

V. REFERENCES

[1] International Atomic Energy Agency, Milestones in the Development of a National Infrastructure for Nuclear Power, Nuclear Energy Series No. NG-G-3.1 (Rev.1), IAEA, Vienna, 2015.

[2] Regulation on Management System in Nuclear Installations, published in Official Gazette No. 30032 dated 08.04.2017.

[3] International Atomic Energy Agency, Leadership and Management for Safety, IAEA Safety Standards Series No. GSR Part 2, IAEA, Vienna, 2016.

[4] International Atomic Energy Agency, Management of Nuclear Power Plant Projects, Nuclear Energy Series No. NG-T-1.6, IAEA, Vienna, 2020.

[5] Akkuyu Nuclear JSC, Directive No. 43-P dated 31.07.2018 on "Approval of Akkuyu Nuclear JSC integrated management system implementation roadmap".

[6] Memorandum No. 309 dated 01.10.2018 of the CEO of Akkuyu Nuclear JSC on "Development of a corporate Management System based on Fundamental Safety Principles of IAEA No. SF-1".

[7] Akkuyu Nuclear JSC, Order No. 120 dated 22.03.2019 on "Approval of Integrated Management System Manual of Akkuyu Nuclear JSC".

Proceedings of the European Nuclear Young Generation Forum
ENYGF'21
September 27-30, 2021, Tarragona, Spain

A hybrid project management approach in the nuclear industry. Project tracking.

Malozemov Sergey

Fuel Company of Rosatom TVEL, Russia

SNiMalozemov@tvel.ru

I. INTRODUCTION

Nowadays project management has become an important part of the management system for most successful companies. According to modern research, the introduction of project management allows organizations to significantly increase customer and customer satisfaction, increase the number of projects implemented on time and with budget savings, and ensure the implementation of the strategy by forming links with projects.

The development and application of many new tools and practices of project management has historically been carried out in large, high-tech companies and in the implementation of Mega-projects.

Significant experience in project management has been accumulated in the nuclear industry. Every year, hundreds of projects of various topics, volume and complexity are implemented in this industry, which contributes to the constant development of the project management system, adaptation and application of modern management approaches.

In accordance with one of the widespread classifications, all methods of project management are divided into classic, Agile and hybrid [1, 2]. Each of the methods has its own advantages and disadvantages, as well as an area of applicability. The nuclear industry has accumulated experience in applying each of these methods.

II. APPLICATION OF CLASSICAL PROJECT MANAGEMENT METHODS

Classical methods, project management, by definition, is a mating and unifying activity, and to describe it, you first need to understand the relevant functions, such as engineering support, quality assurance, logistics and accounting. Classical methods relate to all aspects related to the management of the construction of nuclear power plants, and allow commissioning of nuclear power plants as soon as possible, safely and in accordance with high quality standards [3].

Classical methods include leadership functions related mainly to the organization, coordination and control of important tasks related to human resources, equipment and materials, in order to achieve technical excellence, thanks to work in accordance with high quality standards, optimization of the work schedule, supply chain and lower costs. Project management can reduce costs by using a more efficient work sequence, increasing productivity, shortening the duration of work, and reducing the accumulated backlog during construction. The main aspects of project management during the construction of nuclear power plants will be:

- Design Management
- Contract Management
- Stakeholder Management
- Management of risks
- Security Management
- Construction management
- Licensing management

It is obvious that it is advisable to carry out many types of activities sequentially according to well-developed and approved plans, which is the basis of classical management methods.

III. APPLICATION OF AGILE PROJECT MANAGEMENT METHODS

Consider the use of Agile methods on a real project for optimizing the technical solutions of NPP [4]. This work was attended by technical specialists from various design institutes. To optimize the project was given only three months. Given the extremely tight deadlines, based on the accumulated experience, it was decided for the first time in Russian nuclear industry to use Agile management approaches. In the optimization work package, the following basic and adapted principles of Agile management were applied:

- main focus is optimization;
- generation and development of all hypotheses, technical ideas and optimization options, analysis and prioritization;
- creating in the Scrum-team the roles of the Administrator (Scrum-master), the representative of the customer, the Technical Leader (Product Owner);
- Formation of autonomous groups of specialists in five areas of optimization;
- planning iteration tasks, daily monitoring, conducting demonstration meetings and retrospectives at each sprint (iteration);
- sprint duration - two weeks;
- rapid introduction and prioritization of necessary changes.

As a result of a set of optimization work, the main goal of the project was achieved on time — the volume of buildings on the nuclear island of NPP was reduced by 26%. The number of technological systems and equipment was reduced, the layout of the premises and the general layout structure were optimized, new measures for the physical protection of buildings were proposed. All these results were achieved without compromising the reliability and safety of nuclear power plants.

Among the positive effects of implementing Agile approaches, the following can be noted:

- prompt resolution of any organizational issues;
- joint work of highly qualified experts from various design institutes;
- the possibility of direct interaction with the customer and other stakeholders of the project;
- work of several autonomous teams in one room, high pace of work, team responsibility;
- A disciplining, dynamic workflow structure (sprints, reports, reviews, Scrum tools).

IV. PROJECT TRACKING

In 2020 Fuel Company of Rosatom TVEL applied a hybrid approach "Project tracking" for managing additive technologies projects. How project tracking works, the main roles and tools are shown in Figure 1.

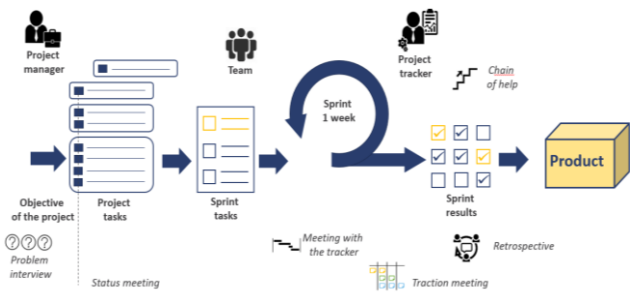

Figure 1. Project Tracking Scheme

The use of project tracking has provided the following positive effects:

- Acceleration of the implementation of project tasks, solution of problematic issues, approval processes.
- improving the quality of communications and the effectiveness of interaction on the project, involving the customer and representatives of functional services in the implementation of project tasks.
- Conducting a quick analysis of alternatives, identifying and managing project risks at early stages, promptly making management decisions on the project.

V. PROSPECTS FOR APPLICATION OF HYBRID PROJECT MANAGEMENT METHODS

Thus, within the framework of various projects of the nuclear industry, it is possible to successfully apply flexible and classical approaches. It is obvious that a combination of these methods can give better results [5]. To form the best combination, you need to think through the project management tools and choose the most appropriate ones. Table 1 provides examples of flexible and classic project management tools.

Table 1. Examples of project management tools

№	*Project management tool*	*Agile*	*Classical*
1.	Integrated schedule		+
2.	Task board	+	
3.	Meeting Schedule		+
4.	Retrospective	+	
5.	Reporting form during the construction of nuclear power plant		+
6.	Methodologist role		+
7.	Work in one room	+	
8.	Scrum-meeting	+	
9.	Reporting forms		+

When choosing tools, it is recommended to form the minimum necessary set of tools in order not to complicate the management process. Tools can be selected depending on the characteristics, project risks, labor and financial costs of using the tools themselves. Thanks to this approach, you can independently assemble your own effective management methodology.

Obviously, with the significant advantages of the hybrid project management method, there are also disadvantages. The main disadvantages of the method include the lack of a scientifically-based mechanism for choosing the most optimal set of tools for the hybrid approach.

VI. CONCLUSION

Hybrid project management methods have already shown their effectiveness in practice within the nuclear industry. But for the systematic application of these methods, a scientific justification for the selection of the most optimal project management tools and the formation of appropriate models are necessary. Further actions to develop the applicability of hybrid approaches to managing projects in the nuclear industry should be the formation of statistical indicators and the use of mathematical optimization methods.

VII. REFERENCES

[1] Agilemanifesto. [Electronic resource]/iso/en/manifesto. URL: https://www.agilemanifesto.org/ (date of access: 08.04.2021).

[2] Binfire. [Electronic resource]/hybrid-project-management-manifesto/introduction URL: https://www.binfire.com (date of access: 08.04.2021).

[3] IAEA.[Electronic resource]/MTCD/Publications/PDF/ Pub1537_web URL: https://www-pub.iaea.org (date of access: 08.04.2021).

[4] Paramonov D.V., Funtov V.N., Malozemov S.N., Prusova Zh.V., "Agile in design: more efficient, cheaper, safer", *Atomic expert, (2017),* Retrieved from http://atomicexpert.com/agile-mathod-v-proectirovaniiL.

[5] PROKACHESTVO. [Electronic resource]/kachestvo-upravleniya/proektnoe-upravlenie/entsiklopediya-gibridnykh-metodov-upravleniya URL: https://www.kachestvo.pro (date of access: 08.04.2021).

Proceedings of the European Nuclear Young Generation Forum
ENYGF'21
September 27-30, 2021, Tarragona, Spain

Gender Balance for a Sustainable Energy Transition

Ozerina, Milana[1,2], Andriushina, Anastasiia[1,2] and Emelianova, Anastasiia[1,2*]

[1]Rosatom Technical Academy (Rosatom Tech), Russia; [2]National Research Nuclear University MEPhI (Moscow Engineering Physics Institute) (MEPhI), Russia

*Corresponding author: *AVEmelianova@rosatomtech.ru*

I. INTRODUCTION

Reaching the climate goals set in the Paris Agreement and Agenda for Sustainable Development 2030 requires shifting around 80% of electricity to low carbon sources [1]. Clean energy transition in line with the meeting of ever-more growing energy needs will require innovative solutions and greater participation from diverse talents – utmost of the world's potential, half of which is represented by women. The gender aspect for the clean energy transition is incorporated into both – Sustainable Development Goal (SDG) 7 "Affordable and Clean Energy" and SDG 5 "Gender Equality". Nuclear energy plays a vital role in combating global warming, providing sustainable energy supply and energy transformation.

Despite the recognition of the increasing demands for cross-nationally and cross-organizationally comparable gender balance statistics, national and organizational data and their application in policymaking generally remain limited [2]. Therefore, it is necessary to attract more women into careers in the nuclear field building up favourable conditions and prospects to support their professional development. Conducting more research on gender balance at various organizational levels and job types in the nuclear sector and implementing international events encouraging women in science, technology, engineering, and mathematics (STEM) are driving forces for reducing the gender gap in moving towards clean energy transition.

The present paper analyses the role of gender balance in the clean energy transition taking as an example the nuclear education and training organizations and provides approaches supporting gender equality in the process of energy transformation. It demonstrates gender statistics of the Rosatom Technical Academy (Rosatom Tech), which has a status of the International Atomic Energy Agency (IAEA) Collaborating Centre; and Institute of International Relations at the National Research Nuclear University MEPhI (Moscow Engineering Physics Institute) (MEPhI), the leading nuclear university in Russia, where students are engaged in training in the field of international relations and scientific, technological and industrial cooperation for obtaining distinctive competences for further work in the Russian nuclear industry and international organizations in the nuclear field.

II. THE ROLE OF GENDER BALANCE IN CLEAN ENERGY TRANSITION

Electricity is a cornerstone to drive the world's economic development. Recent studies show that electricity demand has been growing steadily for the last 100 years and will continue to grow while striving to phase out the use of hydrocarbons [3]. Among clean-energy sources nuclear is the most competitive and reliable with the lowest greenhouse gases emissions, producing only 15 grams CO2-equivalent per kWh, over the entire nuclear power plant's lifecycle [4].

Currently, nuclear energy shares 10% of the global energy mix and is the second-largest source of low-carbon energy, following hydropower. It is also considered to make a great contribution to reach a goal set by Paris Agreement limiting global warming to 1,5°C. Nevertheless, innovations (i.e., new types of reactors, fuel cycle design, etc.) enhancing reliability, efficiency, economics and flexibility are needed. In its turn, innovations require a wide range of diverse competencies and resources.

As far as women represent half of the world's population it means they also represent a half of world's potential. Science and gender equality are vital for achieving all SDGs established by the United Nations. However, women are still under-represented in science: they make up less than 30% of researchers worldwide [5]. At the same time, it is obvious that women and men are completing each other in all social-economic spheres of life. Improving the gender gap has a significant impact on countries' GDP increasing over time due to empowerment of women in STEM education, participation in the labour market, and reducing the gender pay gap.

III. GENDER STATISTICS IN RUSSIA AND ORGANIZATIONS FOR NUCLEAR EDUCATION AND TRAINING

Notwithstanding a growing international interest and research activities in expanding women's role in the clean energy sector, women are still under-represented in political and economic decision-making processes. To support gender parity, in 2017 the Russian Federation adopted the National Action Strategy for Women for 2017-2022, approved by the Government. The strategy promotes the active engagement of women in scientific, political and social activities across all levels. Later in this section, we analyze the Russian Federation progress in closing the gender gap as stated by the World Economic Forum's Global Gender Gap Report 2021 and gender balance statistics in the Russian nuclear education and training organizations.

A. Global Gender Gap Index in Russia

According to the World Economic Forum's Global Gender Gap Report 2021, the Russian Federation ranks 81st out of 156 countries compared by their gender gap index. The Global Gender Gap Index is an index designed to "measure gender-based gaps in access to resources and opportunities in countries rather than the actual levels of the available resources and opportunities in those countries" [6]. The 2021 ranking shows that it is not necessarily that developed countries represent higher-ranking scores. Currently, the Russian Federation closed 70.8% of its overall gender gap, since 2006. The evolution of the Russian gender gap index score and rank is shown in Figure 1.

Figure 1. The evolution of the Russian global gender gap.

According to the World Economic Forum's Global Gender Gap Report 2020 [6], Russian women are more educated than men and live longer but seldom achieve positions of leadership. As many women (64%) as men (66%) holding a PhD. Russian women not only participate in the labour force at high levels (68.9% are in the labour market) but they are employed in skilled jobs to a greater extent than men (62.3% of professional and technical workers are women). Women are still penalized financially: only 71.2% of the wage gap and 57.9% of the income gap have been closed so far. Income disparities are partially explained by the fact the women encounter resistance to access senior or managerial positions: 41.8% of managers and senior officials are women and only 7% of board members are women. Political participation is even more difficult. Not only has there never been a woman as a head of State, but also there are few women among ministers (12.9%) and parliamentarians (15.8%). Table 1 demonstrates the overall global gender gap scores across the four subindexes: economic participation and opportunity, educational attainment, health and survival and political empowerment.

Table 1. Russian overall global gender gap scores across the main subindexes.

Year	Economic participation and opportunity		Educational attainment		Health and survival		Political empowerment	
	Score	Place	Score	Place	Score	Place	Score	Place
2006	0.696	22	0.999	19	0.979	36	0.034	108
2021	0.767	25	1.000	1	0.980	1	0.085	133

Taking into account data analyzed the gradual progress in gender equality issues in Russia is seen clearly. The awareness of society is increasing, more women choose a career in STEM fields, and more women go into politics and reach leadership positions in organizations.

B. Gender equality in nuclear education and training

As for the Russian nuclear sector – 30% of women work at nuclear enterprises in the Russia, which exceeds the average share of 12% in the world. The Russian State Atomic Energy Corporation "Rosatom" (ROSATOM) is encouraging its supporting universities and subsidiary organizations to improve gender balance in the nuclear sector. Figure 2 shows gender statistics of the MEPhI – the leading nuclear university in Russia. 3 out of 10 MEPhI students are female students. Traditionally, more men enter MEPhI than women, especially in STEM specialities. However, every year the number of women who see their future in the nuclear industry is rapidly increasing. Gender balance is maintained in faculties related to economics and management, as well as in the Institute of Biomedicine. The percentage of men and women in technical faculties has remained approximately the same over the years. One of the reasons may be that in society there are certain divisions into "male" and "female" professions.

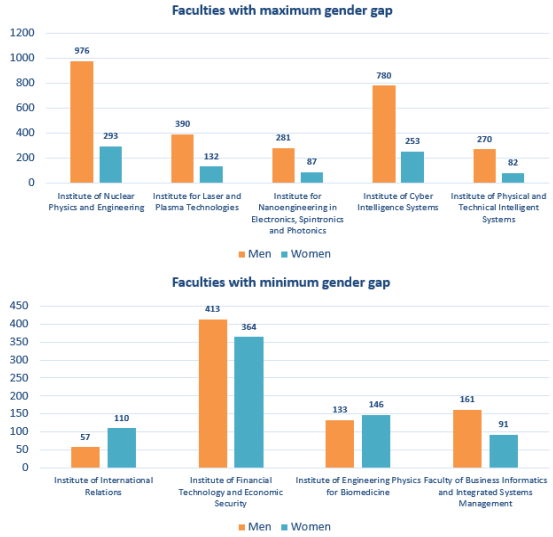

Figure 2. Faculties of the National Research Nuclear University MEPhI with maximum and minimum gender gap.

Another nuclear organization subject to the analysis performed is Rosatom Tech, which is a Centre of Excellence in Russia for building competence in nuclear engineering and IAEA Collaborating Centre in three programmatic areas: nuclear sciences and applications, nuclear security and nuclear energy. Figure 3 demonstrates the gender statistics at Rosatom Tech. In the general case, Rosatom tech is almost balanced employing 49% of women and 51% of men. Regarding professional positions, the situation is close to desired gender balance with 46% of women and 54% of men, but there is an untapped capacity in the management area where women occupy 31% of positions. An opposite case in this regard represents the International Training Centre and its Moscow branch where women occupy more than 50% of professional positions. A unified portrait of the worker shows that Rosatom Tech's personnel is gender-balanced between ages of 29 and 37, after 38 there is a pike of women employment which is gradually decreasing.

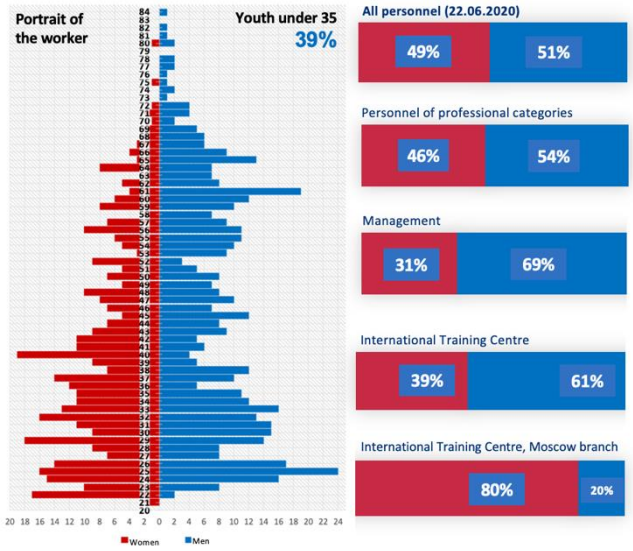

Figure 3. Gender statistics and a portrait of the Rosatom Tech's worker.

According to McKinsey&Company report "Why diversity matters", gender-diverse companies are 15% more likely to outperform [7]. Companies in the top quartile for gender diversity are more likely to have financial returns above their national industry medians. Companies in the bottom quartile are statistically less likely to achieve above-average returns.

In Russia, gender equality situation is changing for the better (awareness of society increasing, more women choose a career in STEM fields), more women go into politics and reach leadership positions in organizations.

IV. INITIATIVES FOR REDUCING THE GENDER GAP IN NUCLEAR SECTOR

International organizations put gender issues on the top of their agenda and implement many programmes aimed at women's encouragement and support. Nuclear organizations provide a number of mentoring programmes and educational networks, for example, Nuclear Energy Agency International Mentoring Workshops, Women in Nuclear Global Network, mentoring programmes at the International Youth Nuclear Congress, IAEA activities on encouraging women and gender balance.

ROSATOM supports the nuclear industry career portal for students, and graduates, where interested students can find all the information about organizations within Rosatom, open internship opportunities, as well as open positions. Moreover, ROSATOM has a career centre and strong mentorship programme, traditionally conducting days of career for undergraduates.

Rosatom Tech implements the target programme for employees of the Russian nuclear industry to strengthen their competencies required to cooperate with and work in the international organizations in the field of nuclear energy. Since 2020, this programme includes a separate session on gender policy to discuss the importance of the topic and to introduce key definitions related to it.

In order to reach the goals set, nuclear organizations at the national and international level should unify their efforts in achieving a gender-balanced work environment and raising awareness of the younger generation and their parents worldwide about opportunities to explore careers in STEM fields. One of the examples of such activities could be the international workshops for sharing the best practices and experience in implementing targeted policies in nuclear organizations towards closing the gender gap.

V. CONCLUSIONS

Gender equality in the energy sector in general and in the nuclear sector, in particular, is not just favourable for women. When more women are involved in leadership and decision-making roles, organizations are more effective and profitable. Diversity and utilization of maximum talented human resource capacity are the key aspects for clean energy transition.

Nuclear and energy sector encounters the lack of women. Legal reform, strengthening gender-responsive social protection and public service delivery, quotas for women's representation, and support for women's movements are all strategies that have made a difference and should be scaled up.

Efforts of international and national organizations in the nuclear sector should be unified by means of workshops, joint research and reports on the best practices in closing the gender gap, sharing gender statistics and implementing targeted policies.

VI. References

[1] International Atomic Energy Agency, "IAEA Bulletin: Nuclear Power and the Clean Energy Transition, Vol. 61-3," IAEA, Vienna, 2020.

[2] The UNESCO Institute for Statistics. "Women in Science, Fact Sheet No. 55", 2019.

[3] OECD, "OECD Green Growth Studies: Energy," 2011.

[4] International Atomic Energy Agency, “Climate Change and Nuclear Power” IAEA, Vienna, 2016.

[5] UNESCO, “Just 30% of the world’s researchers are women. What's the situation in your country?”, [Online]. Available: https://en.unesco.org/news/just-30-world%E2%80%99s-researchers-are-women-whats-situation-your-country. [Accessed 14 April 2021].

[6] World Economic Forum, “Global Gender Gap Report 2021”, 2021.

[7] McKinsey&Company, “Why diversity matters,” Vivian Hunt, Dennis Layton, Sara Prince, 1 January 2015. [Online]. Available: https://www.mckinsey.com/business-functions/organization/our-insights/why-diversity-matters. [Accessed 2020 Septemper 4].

Proceedings of the European Nuclear Young Generation Forum
ENYGF'21
September 27-30, 2021, Tarragona, Spain

The Assessment of Perspective NPP Implementation for Industrial Hydrogen Production

Kolbantcev, Iurii[1*], Seleznev, Nikolai[1]

[1] JSC Atomenergoproekt, Russian Federation

*Corresponding author: *kolbancev.u@gmail.com*

I. INTRODUCTION

To date, humanity is experiencing a problem of lack of energy resources. There are three main reasons for this problem: the limitation of fossil fuels natural reserves; the growth of industry and energy consumption in general; and the pressing need to reduce the negative effects of global industry on the environment.

Hydrogen, which is mainly used in chemical and petroleum industry, metallurgy, etc., is considered as a promising source of clean energy. However, the production of hydrogen is associated with significant greenhouse gas emissions and decreases the environmental efficiency of hydrogen energy industry.

In a normal operation environment nuclear power plants (NPP) do not generate contaminants as thermal power plants and in this way NPP might be concerned as a safe and perspective source of energy for hydrogen production.

II. HYDROGEN CONSUMPTION AND PRODUCTION METHODS OVERVIEW

The total volume of hydrogen produced in the world relative to other industrial gases is small. As already mentioned, according to various estimates, it is about 70 million tons per year [1], mainly for purposes outside the energy industry (the areas of hydrogen consumption are shown in Figure 1).

The largest consumer of hydrogen is considered to be the chemical industry (up to 62% of the volume of consumption), where hydrogen is the main intermediate necessary for the production of widely used ammonia.

The second largest consumer of industrial hydrogen is the oil refining industry (up to 31% of annually hydrogen consumption). In this industry, both high-purity hydrogen (more than 99.99% H_2) and hydrogen-containing gases (up to 75% H_2) are key parts of refining processes.

One of the most common hydrogen-consuming refining processes is hydrotreating, aimed at improving the quality of the feedstock. Another refining process that requires the use of hydrogen is hydrocracking, i.e., catalytic cracking in the presence of hydrogen. Cracking refers to the process of decomposition of heavy hydrocarbon molecules into lighter ones when passing through a catalyst for deeper processing, and as a result, the production of high-octane gasoline.

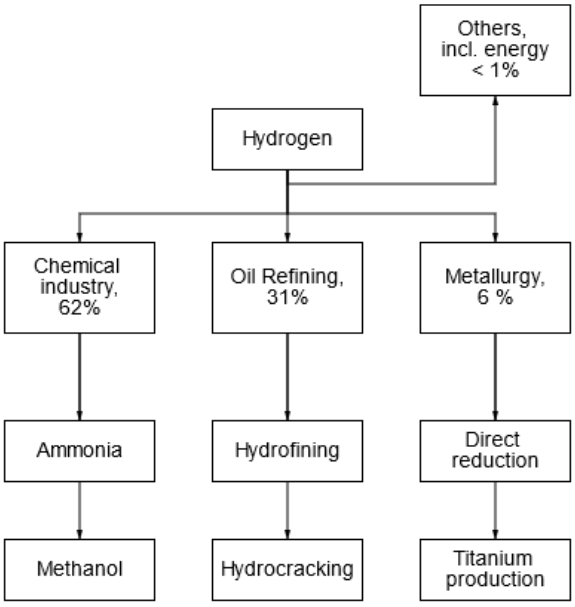

Figure 1. Hydrogen consumption outside the energy industry

Another major area of hydrogen consumption is metallurgy, mainly, as a part of the direct production of raw materials by reduction of iron from the extracted ore.

Therefore, titanium alloys made it possible to develop and apply appropriate hydrogen technological processes that reduce the metal consumption and energy consumption for the production of the product and ensure the reliability of the resulting final product, as well as in some cases allow you to create conditions for obtaining unique properties that are not available by other processing methods.

Just as the areas listed above, hydrogen is also widely used in large energy facilities, thermal power plants and nuclear power plants, mainly for cooling systems of high-power

turbo generators. The most effective method is the direct cooling of the moving part of the turbine generator (rotor) with hydrogen.

In addition to the consumption of hydrogen as a technical gas, in some cases it might be used as a fuel by mixing with natural gas and then burning in the energy cycle.

In recent years, research has been conducted around the world to develop a gas turbine that could run on pure hydrogen. This technology is necessary for the global application of hydrogen in the energy sector of developed countries.

According to Mitsubishi Hitachi Power Systems (MHPS), existing gas turbine plants can increase the proportion of hydrogen to 20% in its mixture with natural gas without significant changes in the design. MHPS has successfully tested a J-series heavy-duty gas turbine in Japan using a fuel mixture of natural gas (70%) and hydrogen (30%). The tests were carried out at the Takasago plant on a combined – cycle gas plant with a capacity of 700 MW (efficiency – 63% with a gas temperature after the combustion chamber of the gas turbine-1600°C).

Other Japanese companies-Kawasaki Heavy Industries and Obayashi-in 2018 brought the share of hydrogen in the fuel balance of a 1 MW gas turbine CHPP in Kobe in Japan to 100% with short tests. In the normal mode, the CHPP operates on a mixture of methane and hydrogen in the proportions of 80:20, respectively" [2].

The most common due to its economic attractiveness is the steam reforming of hydrocarbons [3] (more often natural gas). This method is used to produce either pure hydrogen or hydrogen with an admixture of carbon monoxide. technical hydrogen with a purity of 96-97%. Despite the fact that high-purity hydrogen is formed as a result of steam reforming of hydrocarbons, this process is not environmentally friendly. In addition to carbon monoxide, which is formed directly in the reaction to produce hydrogen, maintaining the reaction requires an external supply of thermal energy due to the exothermic nature of processes. Therefore, the heat supply is provided by the constant burning of fuel in boilers, causing even greater emissions of carbon dioxide.

The most environmentally friendly methods of hydrogen production include [4]: steam reforming at nuclear power plants and the electrolysis of water from electricity generated at power plants.

Electrolysis is the process of decomposition of water under the action of a direct electric current to oxygen and hydrogen.

The method of water electrolysis can be widely used in the energy industry due to the environmental friendliness of the process and the high quality of the resulting product, but for the production of large volumes of the product, large electricity costs are required, which can be provided by nuclear power plants due to the following factors: NPP have the necessary capacities (up to 1.2 GW); the share of nuclear power plants in the UES (United Energy System) of Russia is increasing; the cost of electricity generated at NPP is significantly lower; the technology of using domestic-made electrolysis plants has been tested. To be noted, requirement of using domestic-made technologies in nuclear industry (if there is no possibility of that, it is required to justify the safety of foreign technology) is fixed in the Russian regulatory documentation and federal laws.

Considering as an example, in St. Petersburg, a number of industries that consume hydrogen represents: oil refining, chemical, energy, metallurgical, glass, food, electronics, etc. All enterprises are characterized by the problem of the high cost of the necessary hydrogen.

As a solution, large-scale centralized production of hydrogen at the NPP, and in the case of St. Petersburg – the second Stage of the Leningrad NPP (Units 5 and 6), will allow to supply the city with environmentally friendly technical hydrogen.

It is impossible not to note the potential of hydrogen for the transport networks of St. Petersburg. At the moment, the first tram running on hydrogen has been launched in the Moskovsky district. However, there is a long way to go before the large-scale transition of the transport network from hydrocarbon fuels to hydrogen.

III. ESTIMATION OF NPP RESOURCE COSTS FOR HYDROGEN PRODUCTION BY ELECTROLYSIS METHOD

Let's assume that it is possible to create a nuclear-hydrogen complex for the cogeneration of electricity and hydrogen, which has sufficient capacity to cover the needs of the Russian domestic market of industrial hydrogen exclusively with its own resources. According to various estimates, at the time of 2015-2018, Russia consumes about 2.5 million tons of hydrogen per year.

Based on the study [5], [7] we will consider the FV-500M (Russian manufacture) electrolyzer as a prototype of the electrolysis plant, the maximum possible number of installations N' equals to 50 pcs. Power unit with VVER-1200 is taken as a prototype of energy source according to selection of Leningrad NPP Stage 2 as a reference project.

According to State Atomic Energy Corporation Rosatom [6], in 2016-2017, the utilization rate of the installed capacity of nuclear power plants in Russia was at the level of 83.1 and 83.29%, respectively, and in 2018 it decreased to 79.9%, which is due to the shutdown of power units for modernization and decommissioning. The installed capacity utilization rate (CUR) shows the ratio of the actual duration of power output to the theoretically possible one at the nominal power mode of operation of the power unit for a specified period of time. For the evaluation, we will take one calendar year for a specified period of time, and the CUR as the arithmetic mean for the period under consideration 2016-2018. – 82.1%. Then the number of operating hours of one conventional power unit is T=7191.9 hours/yr.

The results of the calculations based on the methods given in [7] are shown in Table 1.

Table 1. The results of maximum potential hydrogen production

Parameter	Value
The maximum volume of produced hydrogen on one NPP unit, m^3/yr	$1.927 \cdot 10^8$
Coverage of produced hydrogen from annual consumption, %	18.53
Necessary amount of power capacity for produced volume, kW	$1.5 \cdot 10^5$
Necessary amount of cost, mln rubles	$2.055 \cdot 10^3$

IV. CONCLUSIONS

The problem of industrial production of hydrogen on a large scale is one of the most promising for study.

However, the successful solution of technical issues related to the establishment of the technological process and further implementation in the nuclear industry will allow Russia not only to meet the needs of the industry in the domestic market, but also to become one of the first countries to enter the global hydrogen market, and further consolidate its competitiveness.

Based on the results of the potential hydrogen production assessment, we might concider NPP as a perspectiveenergy source that enables the way more environmentally-friendly method of high-quality hydrogen generation. The amount of NPP units in world allows us to assume that global implementation of that cogeneration technology will enable humanity to take step forward to hydrogen revolution.

However, internal fire and explosion hazards place a restriction on the layout of such hydrogen complex and safety assessment of the general design remains questionable. Possibility of hydrogen deflagration near the turbine generator and auxiliary systems of turbine unit is high in case of gas leakage due to huge amount of high-temperature mechanism and mediums in the turbine building. Passive chemical hydrogen recombinators or spray injection of hydrogen deposition solution in nuclear power systems may be used as a proven one. Thus, safety should be justified via calculations before implementing such technology in the realm of atomic energy globally.

V. References

[1]. IAEA Report “The Future of Hydrogen,” pp. 31-32. 2019.

[2]. N. Grib, “Vodorodnaya energetika: mify i real'nost'”. Neftegazovaya vertikal', vol. 19, pp. 61-69, 2019.

[3]. N. Solodova, R. Minugulov, E. Emel'yanycheva, “Vodorod kak perspektivnyi energonositel'. Sovremennye metody polucheniya vodoroda”. Vestnik Kazanskogo tekhnologicheskogo universiteta, vol. 18, № 3, pp. 137-140, 2015.

[4]. S. Kulikov, “Pervyi khochet stat' glavnym”. Ekspert, vol. 48, pp. 46-52, 2019.

[5]. R. Aminov, A. Bairamov, “Otsenka effektivnosti polucheniya vodoroda na baze vnepikovoi elektroenergii AES”. Al'ternativnaya energetika i ekologiya, vol. 05-06, pp. 59-70, 2016.

[6]. Rosenergoatom JSC Annual report – 2018.

[7]. Kolbantcev Yu.A., Konyushin M.V., Kalyutik A.A. The usage of probabilistic assessment for cost calculations of using NPP with hydrogen industrial production. Prower engineering, research, equipment, technology. 2021; 23(2):14-26. (In Russ.) https://doi.org/10.30724/1998-9903-2021-23-2-14-26

Proceedings of the European Nuclear Young Generation Forum
ENYGF'21
September 27-30, 2021, Tarragona, Spain

Key factors affecting public acceptance of nuclear power

Okorokova, Margarita[1*]

[1] Rusatom Service JSC, Russian Federation

*Corresponding author: *MAOkorokova@rusatomservice.ru*

I. INTRODUCTION

Presently, the world energy markets are undergoing significant changes due to general trends in development of the global economy. Thus, the underlying determinants of the current and projected transformation of these markets include the relatively low and heterogeneous growth rates of national economies, increasing geopolitical competition, accelerating scientific and technological progress, and global climate change.

Indeed, over the past decade the global economy has experienced several profound shocks, namely the global financial crisis, the sovereign debt crisis of some EU countries, and price changes in global commodity markets. As a result of a prolonged decline in productivity growth and an increasing demographic burden due to an aging population with insufficient capital investment, the potential for global economic growth is diminishing. The coronavirus pandemic, closure of borders and suspension of entire industries due to measures taken to prevent the spread of the pandemic have also dealt a blow to the global electric power industry.

Secondly, the development of science and technology today is at an all-time high. The main directions are the development of intelligent production, increasing the competitiveness of industry and the creation of environmentally consciously production. Comprehensive modernization and digitalization of various sectors of the economy is carried out through the innovative introduction of robotics, the Internet of Things, cloud computing, big data, nanotechnology, artificial intelligence and smart grids.

Thirdly, the threat of dramatic climate change is becoming more and more serious every year. The negative consequence of the breakthrough development of industry, coupled with an increase in energy consumption with the predominance of traditional energy sources, is enormous carbon dioxide emissions and its further accumulation in the atmosphere. The result is a growing number of natural disasters, which cause significant human losses and major economic damage. However, it is worth noting that global warming is not solely the result of human activity, but is also partly natural. The recovery of the world economy and the increase in GDP growth potentially creates risks of environmental degradation on the planet.

All of the above factors determine a profound transformation of global energy markets and can intensify competition between different types of generation. This transformation is a good opportunity for nuclear power to carve a niche in a climate-neutral world, and success in this is largely determined by positive changes in stakeholders' perceptions of the reliability and attractiveness of nuclear power, including its public acceptance.

This paper contributes to a large number of reviews covering public attitude to nuclear power written over last decades. Indeed, following the increase of public interest in energy issues in the 1970s resulted by OPEC oil supply disruption and subsequent rise in price, public acceptance of nuclear power has become a subject of many long-term scientific studies. For instance, comprehensive reviews were conducted by researchers from South Korea [1], Switzerland [2], the USA [3].

II. FACTORS AFFECTING PUBLIC ACCEPTANCE OF NUCLEAR POWER

Nuclear reactions occurring in the nuclear fuel of reactors offer broad opportunities for energy-technological use: the use of radiation for processing various materials, obtaining useful radioisotopes, and using the heat of the reactor coolant in technological processes occurring in the chemical industry, metal industry, and other industries. In particular, a promising area is the use of atomic energy for seawater desalination on a large scale. In the context of multidisciplinary use (electricity generation, heating, and fresh water production), a number of advantages of nuclear power compared to traditional energy sources should be highlighted. Firstly, the presence of rich reserves of uranium and thorium guarantees a relatively cheap fuel supply for a long period of time. At the moment we are talking about a period of 100-120 years, but successful development of fast neutron reactors will significantly extend the time frame. In addition, one of the most cost-effective options for low-carbon power generation is NPP life extension with its LCOEs ranging from $30 to $50 per megawatt hour, and

small modular reactors offer lower costs and risks through factory construction and higher project availability [4]. Secondly, it is important to note the possibility of creating a multipurpose nuclear complex with a wide power range - from several megawatts to several thousand megawatts. Finally, a nuclear power source has less negative impact on the environment during the design modes of NPP operation than fossil fuel power plants.

The main factors that affect the public acceptance of nuclear energy in a negative way include high capital costs, which today amount to approximately $4,500 per kilowatt, as well as long construction period - it takes up to 10 years to build one power plant. Most importantly, it should not be overlooked that the operation of nuclear power plants is always associated with a high level of potential nuclear and radiation hazards. Indeed, it is in light of this that the world has developed an ambiguous and sometimes prejudiced attitude toward nuclear power, which was exacerbated by the accident at Fukushima, Japan, in March 2011 [4].

In light of the above pros and cons of nuclear power, its public acceptance depends to some extent on understanding what NPPs provide in terms of increases in human well-being. For example, cost-benefit analysis (CBA) and SWOT-analysis can be considered quite efficient analytical tools that can be used to raise public awareness regarding economics of nuclear power and the extent to which they are covering the costs of construction and operation.

A. Public acceptance of nuclear power in Russia

Nuclear power is one of the high-tech industries in which Russian technology has been at the forefront for a long period of time. Russia's nuclear industry in the third millennium is given a strategically important role and close attention. Thus, the first important step was the adoption of The Development Strategy of the Russian Nuclear Power Industry in the First Half of the 21st Century, also known as "Strategy-2000", which defined the main directions of modernization of this industry, including the development of nuclear fuel fabrication at third-generation fuel elements, improvement of safety and extending the service life of nuclear reactors. Strategic importance of nuclear power is also defined in Russian Energy Strategy till 2035, which points out the necessity of further development of the industry to provide energy balance and, mainly, to maintain state technological leadership. At present Russia is one of the six world leaders in production and consumption of nuclear energy. It is predicted that with the implementation of this Strategy the installed capacity of Russian nuclear power plants will increase almost one and a half times by 2035 [5]. In light of the fact that explosive growth of domestic energy consumption is not expected, as well as within the framework of the objectives to increase high-tech exports, both strategies imply an increase in foreign activities and a focus on foreign customers of NPPs.

In order to increase public acceptance of nuclear power in Russia the work is being carried out to form a positive public attitude to the development of the nuclear technologies by increasing information transparency and open interaction with interested parties (including through the functioning of an industry-wide system of public reporting).

The state of public opinion on NPP construction and information on decisions made by the government and regulatory bodies on the curtailment of nuclear power is constantly monitored. There is continuous monitoring and analysis of reports in the national and foreign media, at business meetings, industry conferences and workshops. There is an operative notification of the industry's management of the key events in the information field in Russia and abroad. In case of reasonable changes in the timeline of NPP construction projects in Russia and abroad, decisions are agreed upon with all parties to the projects and are transparently reflected in communications both with partners and other stakeholders (including the public and local communities). Moreover, technical tours and press tours to Russian nuclear facilities are arranged for representatives of foreign media.

The results of the poll on the attitude of Russians to nuclear power held by sociologists of the Levada Center in 2013 shows that the so-called "Fukushima syndrome", which arose in 2011 after the accident at Fukushima NPP, has been overcome (Figure 1) [4].

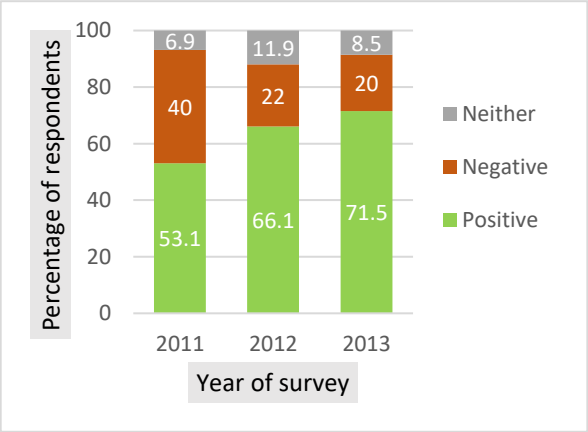

Figure 1. Attitude of Russians to nuclear power.

B. Public acceptance of nuclear power in China

According to forecasts, by 2040 China will become the main consumer in the global energy market. There are several factors that determine the development of the energy sector in China at the present stage.

First, we should note the uneven distribution of energy resources in the country. For example, coal reserves are mainly concentrated in the North and North-West of China, and the provinces in the South-West are rich in hydro-resources. For almost 20 years China has been one of the biggest consumers of energy resources in the world, which is determined by high industrial share in the GDP structure and high energy intensity of production. Hydrocarbons steadily occupy an important place in the structure of Chinese imports. In addition, today there is a significant decrease in the level of oil production in the country. It was predicted that by 2020, the decrease in domestic production of this energy carrier would be 7% compared to 2015, which would entail a 17% increase in oil imports. Indeed, already in 2018, more than 460 million tons were imported, which is almost 10% more than the same figure of the previous year. Thus, due to decline in domestic production, there is a growing dependence on foreign energy resources, so the

need to buy large quantities from other countries is still an important factor in the context of China's economy and foreign policy [5]. To a large extent, this is the reason for China's desire to expand into Africa, Latin America and the Middle East, i.e. countries with significant energy reserves. But the development of this initiative of China's foreign policy is limited by the opposition of the United States, which controls many important sources of energy resources. In 2011, the U.S. began, not without relying on the country's military power, to be actively involved in the Middle East and Central Asia. If necessary, the U.S. Navy can cut off China's transportation of energy resources from the Middle East through the Strait of Malacca. In light of the unfolding trade war, we can expect further tensions in Sino-U.S. relations, so China is extremely interested in finding alternative ways to import energy resources. Therefore, the need to reduce dependence on foreign energy supply is currently the second important determinant of China's energy development.

Thirdly, changes in the country's energy balance are dictated by the transformation of the Chinese leadership's overall vision of domestic economic development priorities. With Xi Jinping coming to power in 2012, China declared that it was entering a new phase of economic growth, dubbed the new normal, which involves the search for new drivers and the transition from actively increasing the rate of economic growth to improving its quality. The transition to qualitative growth is impossible without a global restructuring of the fundamental spheres of the national economy. In this context, Chinese experts consider increasing the share of nuclear power and renewables as one of the measures to ensure the transition to a low-carbon economy, energy efficiency and energy security. By 2040, more than 80% of China's energy consumption growth will come from renewable energy sources, hydropower and nuclear power. In particular, the five-year plans for the development of China's economy specified an increase of nuclear power. For example, the Sixth Five-Year Plan resulted in 0.3 GW of nuclear capacity by 1985, and the Eighth Five-Year Plan (1991-1995) increased the target to 0.6 GW. Since 2001, the government's attention to the sector has increased remarkably: the Tenth Five-Year Plan (2001-05) set a target of 30% annual growth in China's nuclear capacity. This five-year plan also envisioned China's cooperation with relevant foreign corporations, while encouraging the domestic industry to develop its own nuclear technology. The next step (2006-10) was a proposal to build nuclear reactors at four new sites. In 2007, the State Council of the PRC adopted the Nuclear Power Development Plan 2020, which set a target of 40 GW of installed nuclear capacity by 2020. It also called for increasing nuclear capacity by 2 GW each year through 2010 and by 4 GW per year for the remainder of the plan. The current law on foreign investment treats nuclear power as a strategic industry. Particular emphasis is placed on investing in the development of some specific technologies, including the construction of nuclear power plants, the development of radiation protection and more advanced monitoring equipment, and some types of nuclear reactors. Along with wind, solar, and tidal power, nuclear generation is positioned as a form of "clean energy" that should be actively developed.

The Chinese leadership has repeatedly increased the targets. For example, in early 2008 Chinese officials raised the targets for installed nuclear capacity by 2020 to nearly 60 GW and the share of nuclear generation to 5 percent [6]. Setting such an ambitious goal led to China becoming the world's leading designer of nuclear reactors.

III. CONCLUSIONS

Key takeaways show that, in addition to potential nuclear and radiation hazard posed by nuclear power, there are some economic and political factors that have a negative impact on the development of this type of generation and explain the decline in its share in the global energy balance.

The first category includes high capital costs, long payback periods for the construction of nuclear power plants, and significant costs for disposal or reprocessing of spent nuclear fuel that significantly reduces the attractiveness of nuclear energy in comparison with subsidized renewable energy sources. Indeed, if we consider low carbon dioxide emissions as the main advantage of nuclear power, then, at first glance, it seems more rational to invest in development of renewable energy sources, primarily solar and wind energy.

However, a more detailed analysis of the advantages and disadvantages of using certain types of generation, which is not limited only to indicators of greenhouse emissions, shows that nuclear energy has several advantages that are not specific for renewable energy sources: low indicators of the average cost of 1 MWh, the possibility of multi-purpose use (electricity production, district heating and fresh water production), as well as the presence of rich reserves of uranium and thorium, which guarantees the provision of relatively cheap fuel for a long time and regardless of weather conditions.

IV. References

[1] Kim Y., Kim W., Kim M., 2014. "An international comparative analysis of public acceptance of nuclear energy", Energy Policy, vol.66.

[2] Visschers, Vivianne H.M. & Keller, Carmen & Siegrist, Michael, 2011. "Climate change benefits and energy supply benefits as determinants of acceptance of nuclear power stations: Investigating an explanatory model", Energy Policy, Elsevier, vol. 39(6).

[3] Rankin W.L., Melber B.D., Overcast T.D., Nealey S.M., 1981. "Nuclear power and the public: an update of collected survey research on nuclear power".

[4] BP Energy Outlook, 2020.

[5] BP Statistical Review of World Energy, 2018

[6] Rosatom Annual report, 2019

[7] International Energy Agency, World Energy outlook 2017: China

Proceedings of the European Nuclear Young Generation Forum
ENYGF'21
September 27-30, 2021, Tarragona, Spain

The uranium markets: A way through policies

De Maria, Sergio[1*]

[1] ENUSA Industrias Avanzadas S.A S.M.E, Spain;

*Corresponding author: sdm@enusa.es

I. INTRODUCTION

The uranium markets have been marked in recent years by multiple decisions of a political nature. Government policies play a crucial role in the nuclear industry and are the determining factor for the future of the nuclear energy industry and, therefore, the uranium markets.

In this article, we will refer to the markets created in the nuclear front-end part of the cycle: the mining of uranium, conversion and the enrichment, explaining its fundamentals and the issues that arises in each one of them. Each of the different steps shown in Figure 1 is a different industrial process that creates a market that follows different dynamics, although all of them are linked. Later, the enriched uranium is converted into UO_2 powder and introduced in the fuel assemblies that will be burnt in the nuclear reactor.

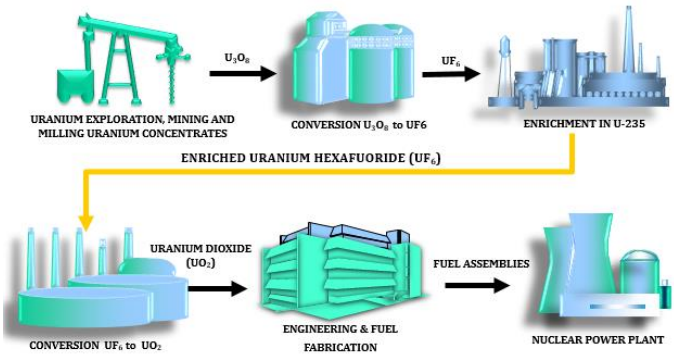

Figure 1. Nuclear Fuel Cycle - Front-End (Source: Own preparation)

The uranium markets are of course, very dependent on the perspectives of the evolution of the nuclear industry. Every policy affecting the nuclear industry has a significant impact on uranium markets. In the coming paragraphs, energy plans in the three main regions with nuclear energy are analysed and the consequences on uranium markets.

A. Joe Biden elected US President

The United States continues to be a key player in the nuclear industry and the uranium markets, not only because it is the largest consumer (as of today, the USA accounts for about a quarter of the total nuclear energy demand) but also because of its geopolitical weight and the relevance of its political decisions. As Joe Biden arrives to Office, he has to take decisions concerning the country's energy and climate policies. The first decision was to re-join the Paris Agreement, committing his country to reduce CO_2 emissions with an increase share of renewables. It is very important to mention that nuclear is specifically included in its energy and climate plans. However, it is not expected big changes from the plans and projects initiated by its predecessors.

The American nuclear power industry has been historically in a position of dominance. There are American reactors all over the world and they are present in all the uranium supply chain. As we will see in the coming sections, their decisions concerning the mining and the conversion industries have shocked the markets in recent years.

However, America has lost its competitive global position as the world leader in nuclear. Their objective is to restore their competiveness by addressing a series of actions in all the fuel cycle industries.

The Nuclear Fuel Working Group (created during the Trump Administration) will execute the policy measures to achieve the new Biden Administrations goals [1].

B. The EU Taxonomy

In Europe, the most important policy decision that might be key for the future of the sector is the inclusion of nuclear energy in the EU Taxonomy Regulation. The EU Joint Research Centre determined last March that nuclear energy meets the "do no significant harm" criteria of the Regulation, for which it was excluded at first place [2]. The final decision of the EU Commission of whether to include nuclear energy in the Taxonomy is expected in the second half of 2021.

The main objective of the Taxonomy is to enable the EU to meet its 2030 climate and energy targets for a carbon-neutral economy. Inclusion of nuclear energy in the Taxonomy should support government financing of new nuclear

projects, unlock the funding potential for advanced nuclear technologies.

However, if nuclear energy were to be excluded, governments might accelerate the nuclear phase out, as no financing might be dedicated to care and maintenance of the current fleet.

This decision might also affect the powerful front-end European nuclear industry. There are also three enrichment facilities (four including the one in the UK) that supplies more than one third of the world's enrichment needs

C. China's 14th Five Year Plan

The five-year plan shows the general direction of the national energy strategy and is a measurement of China's commitment to climate change in the near term. Last December, China announced that it would peak emissions by 2030 and reach carbon neutrality by 2060.

In the five-year- plan, China set a moderate five-year growth target for its nuclear power program with a domestic nuclear capacity reaching 70 GWe gross by the end of 2025.

China is right now the impulse for the nuclear industry in the world. The question is if they would be able to keep the pace of building new reactors. It is already the second largest consumer of uranium, right behind the USA. They have conversion and enrichment facilities to cover some of their domestic needs. Concerning natural uranium, they have kept a strategy of one third of domestic production, another third of foreign production of mines under Chinese property and the rest from the market.

Their presence in the market is very important. They have bought a lot of uranium to build the stocks for the future fleet depending the pace of new builds. China became the main shareholder in Rössing mine, which was having trouble due to low market prices.

The importance of China in the nuclear industry and the uranium markets is unquestionable and we will have a close look at their policies.

II. URANIUM MARKETS

A. Natural Uranium market

The most important policy related issue concerning this market started back in 2018. Two uranium-mining companies requested the DOC to investigate the possible application of section 232 of the Trade Expansion Act to the imports of enriched uranium into the USA, which was already applied to other commodities such as aluminium and steel. Section 232 allows the US President to impose any commercial restriction, advised by the DOC, if it threatens national security.

In 2019, following the resolution of section 232 investigation, former US President Donald Trump decided not to put any commercial restrictions to the imports of uranium and instead created a Working Group to provide recommendations with the objective to boost the domestic fuel cycle and nuclear industry. The most important policy to come out from this Working Group was the creation of a government-funded U.S. Uranium Reserve for purposes of national security and security of supply, but it will help American front-end fuel cycle companies. However, this uranium reserve needs Congress approval every year.

This investigation made the uranium market not very active, with few transactions in those years, for the fear of possible tariffs or quotas for their purchases. Figure 2 shows the historical price evolution for natural uranium, and it can be seen that spot prices were moving around 25$/lb$U_3O_8$, more or less in a two dollar range for the last couple of years.

However, what really shocked the natural uranium market was the coronavirus pandemic. Although this paper deals with policies that affects the uranium markets, it is unquestionable that the COVID19 pandemic has not only affected our lives in all possible aspects, but also the nuclear industry and the uranium markets for both 2020 and the perspectives for 2021. Clearly, the most affected has been the natural uranium market. Conversion and enrichment have been much less affected, as they have managed to operate with minimum personnel in the plants.

In March 2020, at the outbreak of the pandemic, Cameco decided to close the Cigar Lake, one of the biggest mines in the world, for undetermined time. To fulfil their supply contracts, they purchased in the spot market. At the same time, Kazatomprom, the biggest uranium producer in the world, announced that he would cut production in the following months. All this together made the spot price to increase more than 30% (Figure 2).

What will happen in this market for the rest of 2021 will depend on the evolution of the pandemic and the possible reductions of productions, particularly in Kazakhstan and Canada. In addition, the conclusion of the NFWG and the RSA (explained hereafter) has clear the stage for a better perspective on the demand side, which has led in recent months to an increasing volatility in prices.

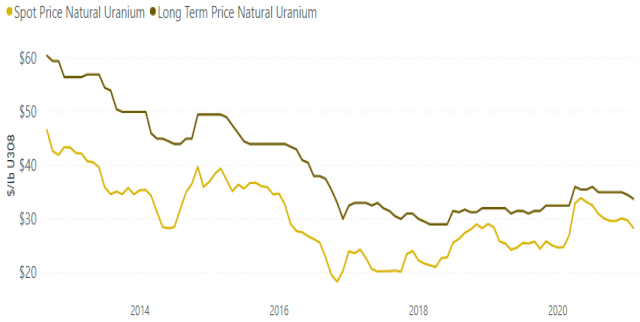

Figure 2. Natural Uranium historical price evolution (Source: Own preparation based on UxC and TradeTech prices)

B. Conversion market

The conversion market has historically remained in a position of oversupply. There are only three western converters, so any problem with any of them might disrupt the market. Due to this situation of oversupply, the American Conversion Plant of Metropolis, operated by ConverDyn, decided to close its production centre in 2018. They went to the spot market to buy UF_6 to fulfil their contracts and that helped the prices to increase but also, this contributed to eliminate the excess of secondary supplies

that have been very important to this market, and have kept prices low. If this situation were to continue in time, secondary supplies will be reduced and the market will come to a more balance market in its fundamentals of supply and demand.

As shown in Figure 3, in 2017, the conversion market was below 5$/kgU($UF_6$) and reached around 22$/kgU(UF_6) at the end 2019, a historical maximum. The price has remained at this maximum for almost all of 2020, with a very slightly decrease.

Another issue that contributed to this situation was the difficult transition from France's Comurhex I conversion plant, operated by Orano that ended operation in 2017, to its new Comurhex II. The plant started operation in 2019 at half of its capacity. It is expected that the new plant will reach full capacity over the next year, but due to the market situation, they might wait a little longer. Therefore, in 2018, the only conversion production came from Russia and Canada.

The evolution of this market depended upon the decision on ConverDyn to restart or not their plant. In March 2021, ConverDyn announced the re-opening of its conversion facility in Metropolis. However, it will take between 18 and 24 months due to requalification processes and training of the personnel.

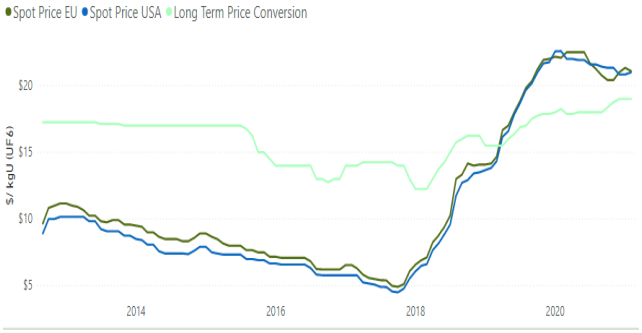

Figure 3. Conversion historical price evolution (Source: Own preparation based on UxC and TradeTech prices)

C. Enrichment market

Since the Fukushima accident in March 2011, the enrichment market has experienced a continuous decline in both demand and price. However, since mid-2018 there has been an increase in activity, placing the contracting of this service well above the levels of the last decade. Figure 4 shows the historical evolution of SWU (Separative Work Unit) prices which has experienced a continuous rise, surpassing the barrier of 50$/UTS. This represents an increase of more than 40% compared to the historical minimum price reached in August 2018.

This increase in demand and consequently in price, has been favoured by the uncertainty that exists around some international trade issues such as the Russian Suspension Agreement and the possible sanctions by the American government to companies that collaborate with the Iranian nuclear program.

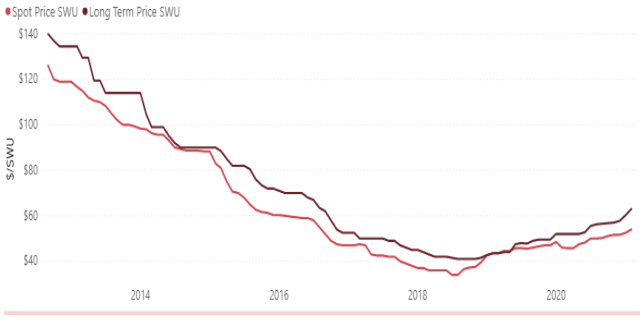

Figure 4. Enrichment historical price evolution (Source: Own preparation based on UxC and TradeTech prices)

The Russian Suspension Agreement (RSA)

The Russian Suspension Agreement (RSA) is an agreement signed between the United States and Rosatom [3] that limits enriched uranium imports from Russia to a 20% quota. The last review of this agreement lasted until the end of 2020, so during this year representatives of both governments will begin the review of the RSA.

The origin of the RSA dates back to 1991, when several representatives of the United States uranium industry requested the DOC to initiate an investigation into possible dumping of Soviet uranium imports, which was damaging the US domestic nuclear industry. After the offset of the Soviet Union, suspension agreements were signed with all the new emerging nations, which suspended anti-dumping investigations and allowed uranium to be imported from these countries on a quota basis. In 2001, all restrictions on the countries of the former Soviet Union were ended, except with Russia. The DOC conducted five-year reviews of this equivalent RSA in the belief that if terminated, a dumping of Russian uranium would reoccur. The last RSA in place, until this year, was signed in 2008.

The new amendment to the RSA was signed late in 2020 and it will extend the RSA until 2040. It drops the quota to an average of 17% and no higher than 15% from 2028. This quotas are based on a tails assay of 0,30% however, if the optimal tails assay remains at current levels of around 0,16%, the effective quota is hence reduced.

This amendment also seeks protection to the US nuclear industry. Centrus, the American enricher gained for the first time a Russian SWU quota amount that they can sell in the US.

It also incorporates new features that were not included in the previous revision of 2008. The agreement will allowed a portion (about 7%, and no higher than 5% from 2028) of the export quota to be used for the natural uranium and conversion from Russia. In addition, the amendment corrects the issue with the returned feed that affects the US uranium miners and the US converter. In the previous amendment, this returned feed could be returned to Russia, enriched in Europe and then exported back into the US outside the quota. Now, this feed is subject to the quota.

Iran sanctions

In 2015, Iran signed a nuclear deal where they promised that the development of its nuclear program would be exclusively for peaceful purposes and would not seek, by no

means, the development of nuclear weapons. This Deal allows foreign companies to get involved in the development of the Iranian Nuclear Program without being sanctioned.

In 2018, the American Administration decided unilaterally to withdraw from this agreement and granted sanction waivers that allowed foreign companies to continue participating in the Iranian nuclear program while circumventing American sanctions. If these waivers were not be renewed, companies that collaborate in Iran's nuclear program will automatically be sanctioned by the United States.

Meanwhile, Russia, which is the most important supplier of the enriched uranium worldwide, is on the one hand (1) committed to Iran's nuclear program and on the other, (2) supplies 20% of the needs of nuclear fuel to American utilities.

There were nine initial sanction waivers for as of today there is only one remaining concerning the Bushehr Nuclear Power Plant. This is trade issue is to be resolved by the incoming Biden's administration.

III. CONCLUSIONS

The year 2020 will always remain in the memory of mankind. And this is also true for the uranium markets, for which the coronavirus pandemic has added more uncertainties to the policy issues that already existed and that have governed the markets over the last years.

However, as it also happens with the pandemic, there is no other option for nuclear industry and the uranium markets than to be optimistic. Moreover, there are reasons for that. Mainly because there is a growing recognition of the role of nuclear power to the decarbonisation of electricity.

China has set a decarbonisation target until 2060 and a clear policy of supporting nuclear that is crucial for the industry. In this sense, it also of great importance that the United States have re-joined the Paris Agreement, and committed themselves to regain the leadership with an ambitious plan set out as part of the Nuclear Fuel Working Group. Now it is time for Europe, which hopefully will follow the steps of other leading countries and, taking into account that the EU has the most ambitious policies against climate change and energy transition, there is hope for nuclear to be included in the EU Taxonomy.

This positive trend will lead to a more balance market in terms of an improved supply and better demand dynamics. The extension of the RSA will set the stage for the years to come and a level playing field for all the participants in the market.

However, several questions remain to be answered, before the policies explained in this paper translate themselves into concrete changes. We will keep a close eye on every aspect, including changing policies to monitor every possible outcome in this thriving uranium market.

IV. REFERENCES

[1] U.S Department of Energy, “Restoring America's Competitive Nuclear Energy Advantage. A strategy to assure U.S national security”, 2020.

[2] Joint Research Center (JRC) , “Technical assessment of nuclear energy with respect to the ‘do no significant harm’ criteria of Regulation (EU) 2020/852 (‘Taxonomy Regulation’), European Atomic Energy Community, 2021.

[3] International Trade Administration, Department of Commerce. "2020 Amendment to the Agreement Suspending the Antidumping Investigation on Uranium From the Russian Federation", 85 FR 64112, October 5, 2020.

Proceedings of the European Nuclear Young Generation Forum
ENYGF'21
September 27-30, 2021, Tarragona, Spain

Automatic control system for NPP participation in electrical current frequency regulation in the power network with thermal energy storage system

Aleksei Shchuklinov[1*]

[1] JSC ATOMPROEKT, Russian Federation

*Corresponding author: *mupol@mail.ru*

I. INTRODUCTION

Increasing the number of NPPs in total electricity production and a large equipment degradation of thermal power plants attracted to work in variable operating modes, raises the question of attraction NPPs for regulation the power and electrical current frequency. Now in Russia NPPs work in stationary base mode (in other words, operated at a constant power).

Currently, according to the legislation of Russian Federation, all generating facilities (except for NPPs with reactors type fast breeder reactor (BN type) and high-power pressure-tube reactor (RBMK type)) shall participate in the regulation of the electrical current frequency in the network [1].

Requirements for the NPPs (with VVER type of reactor) participation in the regulation of the network current frequency, which are shown on Fig. 1, in accordance with [1]:

- NPP unit power change in any direction regardless of the magnitude of this change should be performed during no more than 30 seconds, and 50% of this power change should be performed in the first 10-15 seconds;
- maximum range of NPP unit power - ± 2% (for comparison, for thermal power plants - ± 8%);
- an unlimited number of NPP unit power changes in the case of NPP participation in the current frequency regulation mode.

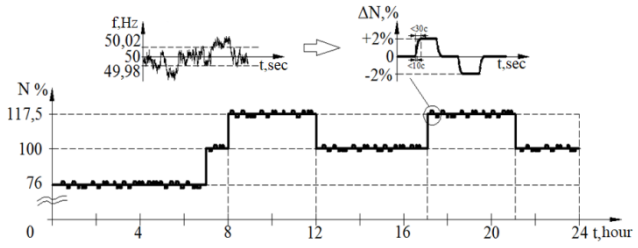

Figure 1. Requirements for the NPPs participation in the regulation of the network current frequency (for example, during participation in the Operations load schedule)

Today technical problem in Russia is the absence of NPP participation in the regulation of electrical current frequency in the power network due to low maneuverable characteristics of the reactor cores.

II. THERMAL ENERGY STORAGE SYSTEM

One of solutions of this problem is achieved by using Thermal Energy Storage System (TESS) at the NPP with reactor type VVER [2].

Today in Russia, TESS is regarded as the most cost-effective option to participate NPPs only in the Operations load schedule without changing of the reactor power [2].

One of the possible variants of the thermal scheme of a nuclear power plant with thermal energy storage system is shown on Fig. 2 (the TESS is inside of the dark frame).

In this variant of the thermal scheme, oil is used as an accumulating substance (oil type is TLV-330). TESS has two modes of operation: charging mode and discharging mode.

Charging mode of the TESS - the heating of the oil is realized by the heat of condensation of fresh steam portion in the special oil charge heat exchanger. The portion of fresh steam is taken from the main stream (from steam generator) at the time of NPP power reduction (for example, at night time). Heated oil is accumulated in the special storage tank.

In the Discharging mode of the TESS, at the time of NPP power increase in day time, heat recovery is realized in the special oil discharge heat exchangers, which connected to the regeneration system of the turbine.

So, the steam from the turbine regenerative bleed-off is partly used for heating of turbine main condensate and feed water, or completely not used. And this steam can be used to increase the turbine power.

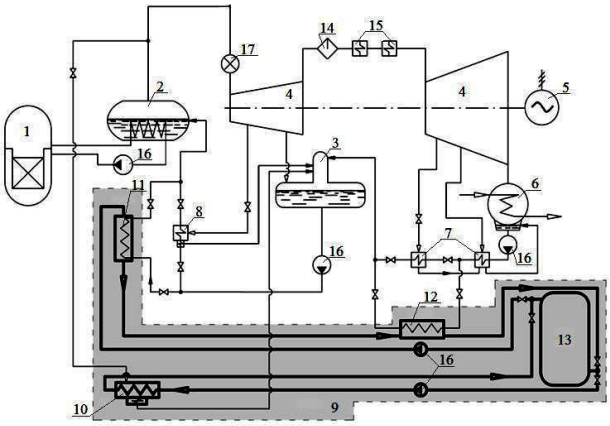

Figure 2. Possible variants of the thermal scheme of a nuclear power plant with thermal energy storage system. In this diagram is indicated: 1 – reactor; 2 – steam generator; 3 – deaerator; 4 – turbine; 5 – electric generator; 6 – main condenser; 7 – low-pressure regenerative heaters; 8 – high-pressure regenerative heaters; 9 – thermal energy storage system; 10 – oil charge heat exchanger; 11 – high-pressure oil discharge heat exchangers; 12 – low-pressure oil discharge heat exchangers; 13 – oil storage tank; 14 – separator; 15 – over heater; 16 – pump; 17 – turbine stop-control valve.

III. AUTOMATIC CONTROL SYSTEM

The proposed system (functional diagram of that is shown on Fig. 3) consists of 2 regulators: the regulator of turbine power changing and regulator of feed water temperature into the steam generator inlet.

This automatic regulation system of electrical current frequency in the power network works this way.

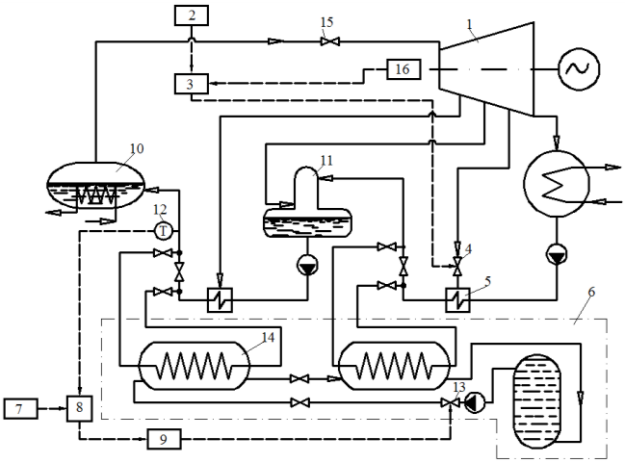

Figure 3. Functional diagram of the proposed automatic control system. In this diagram is indicated: 1– turbine; 2 – group current frequency network controller; 3 –turbine power changing regulator; 4 – control valve for changing turbine power; 5 – low-pressure regenerative heaters; 6 – thermal energy storage system; 7 – feed water temperature setting device; 8 – summator of pre-set and current feed water temperature; 9 – regulator of feed water temperature at the steam generator inlet; 10 – steam generator; 11 – deaerator; 12 – feed water temperature detector; 13 – oil control valve. 14 – oil heat exchanger; 15 – turbine stop-control valve; 16 – current turbo-generator power.

Changing the network power load leads to the changing of electrical current frequency in the power network. The group current frequency network controller (2) distributes the required power changing between all power units, which participate in regulation of electrical current frequency in the power network. The signal of the required power change (ΔN) for our NPP (in the discharging mode of the TESS (6)) is transmitted to the turbine power changing controller (3), which changes the position of the control valve (4), located on the turbine regenerative bleed-off. This leads to changing of the steam flow rate in the turbine regenerative bleed-off, and then to changing of the total steam flow rate through the turbine (1). This leads to the turbine power changing. As the result, proposed system ensures the participation of the NPP in the regulation of electrical current frequency in the power network with the required rate.

At the same time, changing of steam flow rate to the low-pressure regenerative heater (5) leads to water temperature changing from the heater (to the deaerator inlet (11)). Changing of temperature is compensated in the deaerator, where a constant steam pressure is maintained. This means that we have the required feed water temperature at the deaerator outlet.

The summator (8) compares the current feed water temperature at the steam generator inlet (10) and the pre-set (nominal) temperature. In the case of a non-zero signal (ΔT) from the summator (8), the regulator of the feed water temperature (9) changes the position of the control valve (13), located on the oil pipeline of the TESS (6). This leads to the oil flow rate changing through the oil heat exchanger (14), and ensures the constant feed water temperature at the steam generator inlet (10).

Therefore, the change of the reactor power due to the movement of the control rods is eliminated (due to the maintenance of constant steam flow rate and steam pressure in front of the turbine) [3].

IV. CONCLUSIONS

The research is dedicated to the innovative automatic control system in the nuclear power industry, developed for existing NPP's with VVER type of reactor (in case of NPP modernization), and the future NPP projects. The system will provide:

- achievement of the technical efficiency of the NPP units with TESS (in comparison with current NPP units without TESS),
- increase of power productivity, by means of NPP additional participation in the regulation of electrical current frequency in the power network without changing of the reactor power,
- increase of reactor reliability (the reactor works at the constant power all the time) and hence the power unit safety in whole.

V. References

[6] Operational dispatch control. Frequency control and active power flows. Standards and requirements. GOST R 55890-2013. Russia, Moscow, 2014, 31.

[7] V.M. Chakhovskiy, K.I. Soplenkov, Let's save? Energy efficiency of heat accumulation systems in the nuclear power. Rosenergoatom REA №2, Russia, Moscow, 2010, 20-25.

[8] V.V. Bazhanov, I.I. Loshchakov, A.P. Shchuklinov, Research of possiblity of using thermal energy accumulators on the nuclear power plant at regulation of frequency of cirrent in the power network. Izvestiya vuzov. Yadernaya energetika, №4. Russia, Moscow, 2013, 29-36.

Proceedings of the European Nuclear Young Generation Forum
ENYGF'21
September 27-30, 2021, Tarragona, Spain

What happens when everything goes wrong: Insurance

González Felgueroso, Ana[1*], and García García, Pablo[1**]

[1] Aseguradores de Riesgos Nucleares AIE(ARN), Spain

Corresponding authors: *ana.gonzalez@espanuclear.com; ** pablo.garcia@espanuclear.com

I. INTRODUCTION

The Nuclear Energetic Sector, even if it fulfils a great purpose in the energetic mix of many countries and being used as a reliable source for energy, is nothing more than a business, meaning that the final aim of it would be always to make these activities profitable for their final owners.

As in any other course of business, nuclear installations would be the main asset for these enterprises, and the one in charge of generating the energy that later would be sold in the market and therefore generate an income.

But, on the contrary to other fields where enterprises would be only focusing on reducing cost to make that income turn into profit, is well known that nuclear energy comes along with huge repercussions, because not only enterprises must manage financial risks while operating the plants, but also, because of the sensitivity of the field and the potential hazardous situations that could be provoked if not well managed, nuclear companies must fulfil a long list of legal requirements that would focus on both risks and benefits, and would take an impact on their final net profit.

Depending on the State and the nuclear activities that they would sanction – let us not forget that even though nuclear is best known for energetic generation, nuclear technology has also numerous appliances in fields like agriculture or medicine – the exploitation of nuclear technology can involve the application of a wide variety of laws that would cover from environmental protection to administrative procedures, mining, or transport. Also, States are usually not concerned about nuclear principles on their own, having been developed worldwide numerous conventions and treaties that bring together common thoughts on this regard with the sole purpose to cover specific nuclear related subjects. Because of this joint effort, it is common nowadays for the states to just transpose these international codes into national legislation to avoid gaps in regards of their coverage.

In this article, we would focus just on the situation applicable in Spain, knowing that Spain is a Contracting Party to the Paris Convention of July 29, 1960, on third party liability in the field of nuclear energy, as well as the Brussels Supplementary Convention of January 31, 1963, complementary to the previous one, from whose provisions basically the national regulation arises in this matter.

Modifications have been made through the years to these two conventions, being the lasts one the 2004 Protocols, that would be incorporated to our national legislation through Law 12/2011, on third party liability for nuclear damage or damage caused by radioactive materials. Although the law was approved in May 2011, its entry into force is subject to the entry into force of the 2004 Protocols amending the Paris and Brussels Conventions expected to take place in January 2022. Until then, the applicable law would remain being Law 25/1694 of April 29th, on nuclear energy.

II. THE IMPORTANCE OF INSURANCE

Going back to our main issue here, and focusing only on energetic generation, Nuclear Power Plants would be the main asset for making an income, and therefore, it should be protected and taken care off at every single moment. But, as has been proven during the past century, we all know that another concern should always be the possible harm that we could inflict on third parties that, more often than not, could end up representing huge amounts of money in compensations, that could exceed the value of your asset.

This dualism became very handy to identify the two main insurance contracts that every single nuclear installation would always consider as essential, material damage policies (for the installation per se) and Third-Party Liability policies (for possible harms to outsiders).

And because in case of an accident, it is possible (that not probable) that both kind of damages would be triggered, insurance could be the best protection against bankruptcy as it would provide the funds needed for both the reconstruction of the installation and any compensations due to anyone.

It is important to remark that, as everything else in the nuclear sector, insurance policies are tailor made for each and every client, and frequently aggreging on huge amounts, what makes them expensive, but because of the possible scenarios that could face the operator if not having

them that could be far more harmful to their finances, insurance is paid year by year, and as Ms. Leigh Anne Tuohy said, “every housewife knows that the first check you write is for the mortgage, but the second, is for insurance”, meaning for us that the main focus would be having the installations working smoothly, and therefore, where our main resources should be allocated, but we cannot forget that because is the sole asset in this business, risking losing it is not a great idea, turning the insurance as needed as the plant itself.

Concerning the amount, you could insure in the nuclear field, when in relation with nuclear liability the law is very specific with the minimums to fulfil, but when material damage policies are in consideration, everything is valid and is open to negotiation - what is the common one, and what do these policies protect the operators against varies from one to another.

A. Material Damage policies

Insurance of material damage will provide coverage for all the operator’s assets on the nuclear facility. This damage could consist of various types of actual damage caused by different events as well as of future damage or loss of income which results from the actual damage.

Because explaining every single possibility could be an article itself, let us just remark that material damage policies are nothing more than a private contract between two parties, in which one (the contracting one) asks for a series of perils to be covered up to an amount and under certain circumstances, and the other part (the insurer) usually grants them for a year in exchange of a premium.

As in any other industry, machines and equipment suffer from time and usage, making these policies usually face loss ratios between 10% and 19%, meaning this that every year, between 10% and 19% of the subscribed premium in this field is allocated to loss expenses. Anyhow, it is important to punctuate that even though there are losses that compromise the assets, these accidents have not led to nuclear damage to third parties.

B. Third-Party Liability policies

Third-Party liability policies are designed to cover liability claims of members of the public for personal injury and property damage caused by a commercial nuclear power plant accident.

Today, there are three basic international regimes for nuclear third-party liability in force:

- Convention on Third Party Liability in the Field of Nuclear Energy of 29 July1960 (Paris Convention), this coverage is extended by the Supplementary Convention on Third Party Liability in the Field of Nuclear Energy of 31 January 1963 ("the Brussels Supplementary Convention").

- Convention on Civil Liability for Nuclear Damage of 1963(Vienna Convention)

- Convention on Supplementary Compensation for Nuclear Damage of 1997 ("the CSC")

These international regimes have set three basic principles that underlie the special nuclear third-party liability and compensation regimes at both national and international levels:

- Strict and exclusive liability
- Compulsory financial securities
- Liability limits in amount and in time.

The third-party liability of the nuclear operator is strict, which means that the operator is liable regardless his fault or negligence. The damage may have resulted from any kind of guilt that can be found with the nuclear operator but there is no need (in legal sense) to proof that. This base of liability was adopted due to the need to assure a greater protection for the public.

According to the principle of compulsory financial security the nuclear operator is required to secure finances to cover the nuclear liability. Traditionally this is provided by the insurance market, although there are other known financial instruments that can be used to achieve this goal, such as bank guarantees, operators pooling system, or self - insurance.

Regarding the liability amounts and time, the minimum amount of protection required is set by national laws, which often depend on international treaty obligations. Over time the amounts of this mandatory protection had increased, in order to increase the burden of responsibility of nuclear operators. Also, conventions and national laws set the time and procedures to present every type of claim.

If we focus on the start of the nuclear generation period, the international legislation helped encourage public and private investment in commercial nuclear power by placing a cap, or ceiling, on the total amount of liability each nuclear power plant licensee faced in the event of an accident, but, as we just said, over time, this limits of liability for a nuclear accident have been increased. In the particular case of Spain, it has escalated from 150.000.000 pesetas in 1964 (roughly 900.000 euros) to our current 700.000.000 euros, soon to be increased to 1.200.000.000 when the new legislation entries into force.

Table 1. Coverage provided for Third-Party Liability compensations in Spain according to Law 25/1964 on Nuclear Energy

Amount	Responsible
Up to 700 M€	The Operator
From 700 M€ to 1.200 M€	The State
From 1.200M€ to 1.500 M€	All the countries part of the Brussels Convention, taking into consideration the allocation method established in it.
As of 1.500 M€	Possibly the State in accordance with its own criteria, but not granted.

As we can conclude from this information, third-party liability insurance for nuclear power plants, even though has not been used in Spain up to now (being the loss ratio for this segment of operation 0%) is nowadays a requisite

to operate the installation, being therefore mandatory and an expense that operations should face every single year.

III. HOW DO INSURERS PROTECT THEIR INVESTMENT?

As we just explained, operators are sole responsible for any damage occurred by and to their installation, and, in order to protect themselves against possible casualties, insurance would be giving them the financial strength to get over an accident with repercussions.

But do not forget that insurance is a business as well and in the second part of the 20th century, it became clear to insurers that any nuclear accident had catastrophic potential, turning the coverage of nuclear risks unattractive to individual insurers.

The insurance industry was challenged to create structural and legal mechanisms to be able to deal with the new hazard, being the most important mechanism the pooling system, which has contributed to the insurance industry remaining an essential part of the development of the nuclear industry and the nuclear third-party liability regime. Today, the insurance market, through the nuclear insurance pools, is involved in the parallel creation of legislation and insurance policies.

The development of the nuclear industry has been associated with the insurance industry from the start, due to the principle of compulsory financial security that must be provided by the nuclear operator under the international third-party nuclear liability regime.

But nuclear insurance pools do not only contribute while providing the financial securities, also, the pooling of the resources allow this insurance well-oiled machine to survey every installation in which they took part, being this group able to give recommendations to operators for them to keep the installations in their best operating conditions.

Because of the perks that the insurance pooling systems provides to operators - mainly economic as they diversify the risk and the impact of possible losses through a net that extends itself worldwide making it possible to reduce premiums but also because of the know-how associated with the risk management of nuclear installations -, nowadays, this financial solution is used to a greater or lesser extent in 29 different countries, and taking into consideration that there are only 34 countries with nuclear power installations (operating or in construction), this makes it the most used financial security solution.

IV. THEORETICAL EXAMPLE

For the purpose of studying the application of this policies, we would consider an accident with repercussions for both the nuclear facility and to the public through emission of radiation to the outside - what could be consider as a nuclear accident with wider consequences, similar to Chalk River event (INES 5, 1952).

On one side, we would have our harmed installation where the water circuit has been affected, and according to the independent evaluation of the experts, this would represent a loss of 35 M€ and a stop in business for the next 13 weeks because every piece must be manufactured from scratch. Taking into consideration that a nuclear facility can generate an income of 500.000 euros per day, being stopped for 13 weeks would cost them 45,5 M€.

Let us assume that in their material damage policy they have agreed to cover a limit for physical damage up to 1.000 M€ with a deductible of 5 M€ and, they had coverage for business interruption up to 24 months, with a deductible of 8 weeks.

The total loss for this event, in regards of their material damage policy would be 80,5 M€, and the insurance contract would cover a total of 47,5 M€ (30 M€ of the broken piece plus 17,5 M€ of their business interruption).

Now we would consider as well that because something unexpected went wrong, contaminated material was left out in the open, contaminating the near village, where 12.000 people lived. This people are entitled not only to an economic compensation for the harm they could suffer but also the environment should be clean. The judge established compensation in 50.000 € per person in the area, adding a total of 600 M€ plus expenses for this event. Fortunately, third-party liability policies are mandatory in Spain, with a minimum coverage of 700 M€, and being the operator financially responsible of a deductible of 5% of the loss (30M€).

If we consider the effect of one event in both policies, the loss will sum up to 680,5 M€, and because of the insurance policies that the operator has, the insurer will answer of 617,5 M€, leaving the operator to face reputational repercussions and financial obligations of 63 M€.

V. References

[1] Convention on Third Party Liability in the Field of Nuclear Energy of 29th July 1960, as amended by the Additional Protocol of 28th January 1964 and by the Protocol of 16th November 1982, Organisation for Economic Co-operation and Development, Paris (1982)

[2] Convention of 31st January 1963 Supplementary to the Paris Convention of 29th July 1960, as amended by the additional Protocol of 28th January 1964 and by the Protocol of 16th November 1982, Organisation for Economic Co-operation and Development, Paris (1982).

[3] Exposé des Motifs of the Paris Convention, Organisation for Economic Cooperation and Development, Paris (1982).

[4] Convention on Third Party Liability in the Field of Nuclear Energy of 29th July 1960, as amended by the Additional Protocol of 28th January 1964, by the Protocol of 16th November 1982, and by the Protocol of 12 February 2004, Organisation for Economic Co-operation and Development, Paris (1982)

[5] Convention of 31st January 1963 Supplementary to the Paris Convention of 29th July 1960, as amended by the additional Protocol of 28th January 1964, by the Protocol of 16th November 1982, and by the Protocol of 12 February 2004, Organisation for Economic Co-operation and Development, Paris (1982).

[6] BOE núm. 107, de 4 de mayo de 1964, páginas 5688 a 56961964. Ley 25/1964, de 29 de abril, sobre energía nuclear.

[7] BOE núm. 127, de 28 de mayo de 2011, páginas 52951 a 52975 Ley 12/2011, de 27 de mayo, sobre responsabilidad civil por daños nucleares o producidos por materiales radiactivos.

[8] Handbook on nuclear law / C. Stoiber … [et al.], Vienna, International Atomic Energy Agency, 2003

[9] Nuclear power reactors in the world, Vienna, International Atomic Energy Agency, 2020

[10] Balkan Social Science Review, Marija Ampovska, Vol. 9, June 2017, 7-2

Proceedings of the European Nuclear Young Generation Forum
ENYGF'21
September 27-30, 2021, Tarragona, Spain

Building an atomic future: The role for nuclear power in addressing major humanitarian challenges in the 21st century

Lindberg, John C.H. [1,2,3*]

[1] World Nuclear Association, United Kingdom; [2] Department of Geography, King's College London, United Kingdom; [3] Department of Surgery and Cancer, Imperial College London, United Kingdom

*Corresponding author: john.lindberg@world-nuclear.org

I. INTRODUCTION

Ever since modern humans first appeared on Earth, there has been a gradual, but steadfast, transformation of our planet. Arguably, no single species have had as great an impact on life as we know it. Humans domesticated animals for labour and companionship, claimed lordship over arable lands, and slowly – but steadily – started to master the many forces of nature we once worshiped as divine. The face of the Earth itself began to change, increasingly bearing the mark of humans.

Whilst this process had already begun prior to the last ice age, the advent of farming in approximately 9000BC set in motion changes in lifestyles which, eventually, resulted in more time being available to the pursuit of activities not directly related to food acquisition, thus slowly unshackling human ingenuity.

However, humanity's ability to fundamentally alter its surroundings began in earnest with the onset of the first industrial revolution in the 18th century. With the advent of the use of coal, later augmented by oil, in various industrial processes, the stage was set for modernity as we know it. By harnessing the energy stored in fossil fuels, humanity could break the constraints placed upon us by nature, enabling us to change every aspect of life on Earth. This was, however, done in an inherently unsustainable fashion.

With the discovery of radiation in 1895 and the various scientific breakthroughs in the run-up to World War II, the immense energy found at the heart of the atom – previously only metaphorically powering mostly science-fiction novels – became more than just a tantalising daydream. However, the first stage appearance of nuclear energy in terms of a global audience took place in the dying days of the war, with the wholesale destruction of Hiroshima and Nagasaki.

From that day onward, nuclear energy was to have a dual place in the public imagination, especially as the prospects of peaceful nuclear energy entered the conversation in the 1950s. On the one hand, the promise of de facto limitless, affordable and clean electricity, on the other, the promise of fiery destruction in a nuclear war [2]. Whilst initially well separated, concerted efforts saw the discourse merging considerably, facilitated largely by an emerging fear of radiation associated with nuclear energy. Despite this, reactors were constructed at great pace across many parts of the world, providing jobs and clean, abundant and affordable electricity to millions of people.

In many ways, the dawn of nuclear energy promised to represent a shift away from practices of old, whereby humanity would move away from asking future generations to pay for today's prosperity and move towards genuine sustainability. However, the promises of the atomic revolution have yet to be fully realised, having been stymied by factors mostly relating to politicisation, public perception, and public acceptance.

Today, the global community faces many challenges, which are to a large degree the result of the past 250 years of unprecedented growth. Whilst this has led to tremendously positive developments, be it in terms of life expectancy, quality of life, or reducing poverty globally, there is a polluted legacy which requires serious attention. Urgent action on air pollution, environmental degradation and climate change are but some part of this legacy. Additionally, it is crucial that efforts addressing these issues, as well as furthering the Sustainable Development Goals, are done in a way that does not ask future generations to pay for the development of today. Nuclear power has already been an important contributor in these fields but will have to play an even bigger role if we want to address the challenges the global community faces, once and for all.

II. THE CHALLENGES AHEAD, AND THE ROLE FOR NUCLEAR

In many ways, it is the unsustainability of habits past and present which have delivered us to where we find ourselves today. The Secretary-General of the United Nations, alongside with many parliaments, scientists and civil society groups have declared "climate emergencies" [3-5], escalating the discourse to that of an existential threat. But whilst resorting to such an escalation might find favour in some quarters politically, as well as generating dramatic

news headlines, it is most likely a counterproductive strategy, risking disengagement and alienation amongst the public. Equally, whilst climate change is a major challenge which poses considerable risks to humans both alive and future generations, it is important to adopt a broader perspective to gain full appreciation of the interconnectedness of these issues. By failing to do so, it is likely that previous mistakes will be repeated, therefore hampering any efforts towards building a more sustainable tomorrow, with immediate fixes to climate change creating risks elsewhere.

A. Responsibly Addressing Climate Change

Emissions of greenhouse gases have been rising continuously since 1850 [1], with most interruptions in emissions growth being caused by the World Wars, severe financial crises, or global pandemics. Since climate change re-emerged in political discourse in the 1990s (climate change has been central to human society for time immemorial [6], global emissions have continued to rise drastically. This increase is largely driven by the fact more people have access to electricity, transport, etc., and the associated improvements in both lifestyle and life expectancy.

In terms of global emissions, the electricity sector is responsible for the largest individual share, approximately 31% of all emissions. Of all electricity, some 67% comes from the combustion of mostly coal, fossil gas, and oil. The largest low-carbon electricity source is hydropower, followed by nuclear power. There has, however, been no significant shift in the proportion of fossil vis-à-vis low-carbon electricity sources since 1990. When broadening the horizon examining global energy supplies, it becomes evident that almost 85% of all energy consumption is fossil-based. Between 2000 and 2019, the share of fossil fuels fell merely 1.8% (from 86.1% to 84.3%) [7], despite countless trillions of dollars spent on renewable energy sources. With electricity demand likely expanding quickly and significantly as a result of the move to decarbonisation of various sectors, it is clear that a course correction will be required.

Nuclear power's role in combatting climate change is well-recognised [8-10], having amongst the lowest – if not the lowest – greenhouse gas emissions throughout the lifecycle out of all electricity generators. Since the first deployment of nuclear reactors for electricity generation, 64 gigatons of greenhouse gas emissions have been avoided [11]. Nuclear power has also been used to de facto decarbonise electricity systems in advanced economies, whilst still delivering economic growth and increased living standards – with France and Sweden being the clearest examples of this. In fact, Sweden managed to decarbonise its electricity sector in little more than 10 years using nuclear power [12], highlighting that nuclear power can deliver deep decarbonisation within the timeframes identified by *e.g.* the Intergovernmental Panel on Climate Change.

However, for any actions to be meaningful on climate change, it is crucial that everyone gets access to reliable, affordable and sustainable electricity – and at significant quantities. It is estimated that some 770 million people still live without even rudimentary access to electricity [13]. Nuclear reactors are the most reliable electricity generators globally, often at annual capacity factors above 90% (in comparison, offshore wind has an annual capacity factor of between 29-52%, with onshore wind between 23-44%. Solar fares even worse, with an annual capacity factor between 10-21% on average [14]). With climate change, the weather is becoming less predictable, and more extreme, and it would seem counterintuitive to suggest that we should solely build the future energy system based on inherently weather-dependent technologies. Nuclear power, either on its own or as a part of an integrated system with renewables, can provide the reliability required to build a modern society that can be available across the world. This feature, alongside with the sheer quantity of electricity generated, its affordability and low-carbon credentials, makes nuclear energy an inherently crucial tool in addressing climate change in a sustainable and humanitarian fashion.

B. Affordable Water Supplies

Water scarcity is already affecting 1.42 billion people globally who live in areas of high or extremely high water vulnerability [15], and approximately 4 billion people experience severe water scarcity for at least one month every year [16]. Climate change will further exacerbate this problem, resulting in increased water scarcity due to both increasing temperatures, and weather patterns becoming more extreme and less predictable [17].

In order to address the already considerable demand for potable water in certain parts of the world, desalination will likely play a very important role in future water supplies. There are almost 16,000 desalination facilities worldwide, with the majority using electricity to provide potable water by way of the reverse osmosis process. The Middle East is the region with most desalination plants globally, where about 66% of these plants use heat from fossil-fuel cogeneration, with the remaining 33% relying on electricity which, in turn, is heavily dependent on fossil gas [18].

However, desalination remains expensive, with some estimates placing desalinated water at 2 to 3 times more expensive than water from traditional sources [19]. This means that many of the areas which already experience water scarcity in many instances cannot afford it. Nuclear power can play an important role in rectifying this. Desalination using nuclear reactors is by no means a novel application of nuclear power, with more than 200 reactor-years' worth of experience of nuclear desalination [20].

C. Combatting Air Pollution

Air pollution causes considerable harm in terms of public health, and is a major contributor to the development of diseases such as lower respiratory infections, ischaemic heart disease, ischaemic stroke, haemorrhagic stroke, and chronic obstructive pulmonary disease. The Global Burden of Diseases, Injuries, and Risk Factors Study 2015 ranked ambient and indoor air pollution as leading causes of global disease burden [21], and the World Health Organization has identified air pollution as one of the top three global risk factors causing illness and contribution to increase mortality. [22]. The combustion of fossil fuels (especially coal) for electricity generation, cooking, and transport are

significant contributors to particulate air pollution, and it has been estimated that these emissions caused 10.2 million premature deaths in 2012 [23]. At present, more than 2.6 billion people do not have access to clean cooking facilities, which is a major contributor to air pollution and to the premature deaths caused by it [24].

Unlike coal-fired power plants, nuclear power emits virtually no air pollutants during operation [25]. Modelling suggests that the use of nuclear power has prevented approximately 1.84 million premature deaths related to air pollution, by way of displacing mostly coal as an electricity generator, and could - depending on the magnitude of nuclear deployment and the amount of fossil fuels it would replace – prevent further air pollution-related premature deaths by 2050 [11]

III. PUBLIC PERCEPTION: MAIN BARRIER FOR EXPANSION

Following the heydays of nuclear expansion in the period 1960-1975, the nuclear industry has been fighting against firm headwinds in most regions of the world. Whilst there are a multitude of factors that have played a role in causing this change of fortunes, including decreasing electricity demand, the major cause is doubtlessly linked to public perception and public acceptance.

Public perception plays a key role in decision making, especially if proposed siting or construction causes public resistance, which in turn can result in delays or cancellation of entire projects (thus increasing costs), a trend which has been seen historically [27]. The degree to which the public supports projects will in many ways determine not only whether a project can go ahead or not, but also how difficult the process may prove to be [28]. Three basic "conditions" conditions for gaining acceptance of nuclear power to exist have been identified, where the public agrees that [29]:

1. There are benefits to nuclear power.
2. The risks are manageable (and managed).
3. There is a necessity for nuclear power.

Given the current policy environment on both an international and national level, it is questionable whether either of point 1 or 3 has widespread public support. Indeed, for as long as nuclear energy remains politically divisive and associated with long-running opposition, it is highly unlikely that politicians will use their political capital to convince the public of the virtues of nuclear energy [30]. As summarised by Stoutenborough et al. (2013) *"[w]ithout public support, there may be little motivation for policymakers to act on an issue like nuclear power regardless of the scientific support"* [4].

However, the issue of perception and acceptance is by no means new to the nuclear conversation. Alvin Weinberg, a leading pioneer behind many nuclear power designs, reflected on the importance of public perception in 1976, writing *'[a]s I compare the issues we perceived during the infancy of nuclear energy with those that have emerged during its maturity, the public perception and acceptance of nuclear energy appears to be the question that we missed rather badly…This issue has emerged as the most critical question concerning the future of nuclear energy'* [5]. Weinberg concluded that it is easier to "scare" than to "unscare" people, but that, just like with electricity, people would sooner or later shed their apprehension for nuclear energy. It is, however, clear 40+ years after Weinberg's musings that the apprehension towards nuclear energy remains alive and well, and that the "familiarity" argument, which experts assumed would come to pass, has not materialised.

The nuclear industry is largely at fault for this. In most instances, there is a veritable chasm between public and industry views, as far as nuclear is concerned, and this invariably translates into the way the industry communicates with the public. Flynn (2003) summarises this well, writing that there is a clear *"…contrast between the public's stigmatization of nuclear power, a widely held belief that certain nuclear technologies are inherently dangerous, unwise, unnatural, and even immoral, and the position of nuclear proponents who envision nuclear technologies as right, necessary, and inevitable because they are based on deep scientific and natural truths"* [29]. All too often, we encounter the notion amongst pro-nuclear proponents that *"…incorrect information from the media made people afraid of nuclear energy" [3]*. For a considerable part of the history of nuclear energy, the industry's mantra has been based on the notion that *"tell them the facts and they will love nuclear power"* [26]. However, this runs counter to decades' worth of research within realms such as psychology, risk perception, neuroscience, and behavioural science.

In order to regain public acceptance, it is paramount that the nuclear community once and for all abandons its baggage of badging any of its detractors as "irrational", and equally moves beyond its near-obsession with its "facts with save the day" mantra. We must move our communications paradigm away from facts and figures, towards making emotional appeals. The humanitarian aspects of nuclear energy are eminently suitable as a starting point for a communications revolution that is decades overdue, but the lives and prosperity of countless humans lie in the balance.

IV. CONCLUSION

Nuclear power has already played a major role in addressing issues such as particulate air pollution, greenhouse gas emissions, and has been a catalyst for economic development around the world. If global targets for limiting greenhouse gas emissions are to be met, and achieving "Net Zero" by 2050, it is clear that there will have to be a considerable expansion in nuclear energy capacity worldwide. However, there is a moral impetus to ensure that the transition towards a low-carbon future is done in a socio-economically equitable fashion. Access to electricity is crucial as far as poverty alleviation is concerned. With more than 770 million people without access to electricity, and with billions more still unable to enjoy a high-powered lifestyle, it is crucial that any policy initiatives towards achieving "Net Zero" will ensure equitable access to electricity globally.

There are outstanding challenges which will need to be resolved in order to ensure that the humanitarian potential that nuclear power possesses can be maximised. As has been highlighted in this paper, the main challenge is related to

public acceptance and public perception, both of which are well-known issues. Many of the cornerstones in the nuclear policy debates of today – such as the EU Sustainable Taxonomy or financing of projects – are firmly linked, if not directly caused by, issues around public perception. Yet, the approaches historically applied to communication with the public and policymakers is long out of date, harking back to a time before major breakthroughs highlighted that it is emotions and heuristics, not facts, that largely dictate how we all make sense of the world. If nuclear power is to play a major role in the future, we need to find ways to address public perception, and get the public firmly behind nuclear power as a power source for the future.

V. REFERENCES

[1] IPCC, 2014: Climate Change 2014: Synthesis Report. Contribution of Working Groups I, II and III to the Fifth Assessment Report of the Intergovernmental Panel on Climate Change, pp. 3

[2] Hilgarner, S., Bell, R. C. & O'Connor, R., 1982. *Nukespeak: Nuclear Language, Vissions, and Mindset.* San Fransisco: Sierra Club Books.

[3] World Nuclear News, 2019d. New dawn for nuclear if issues are faced, say industry leaders. [Online] Available at: https://www.world-nuclear-news.org/Articles/New-dawn-for-nuclear-if-issues-faced,-say-industry.

[4] Stoutenborough, J. W., Sturgess, S. G. & Vedlitz, A., 2013. Knowledge, risk, and policy support: Public perception of nuclear power. Energy Policy, Volume 62, pp. 176-184.

[5] Weinberg, A., 1976. The Maturity and Future of Nuclear Energy: The most serious question now facing nuclear energy is its acceptance by the public. American Scientist, 64(1), pp. 16-21.

[6] Hulme, M., 2016. *Weathered: cultures of climate*. Sage Publishing.

[7] Ritchie, H., 2020. Energy mix. [Online] Available at: https://ourworldindata.org/energy-mix

[8] Brook, B. W., 2012. Could nuclear fission energy, etc., solve the greenhouse problem? The affirmative case. *Energy Policy,* Volume 42, pp. 4-8.

[9] Liddle, B. & Sadorsky, P., 2017. How much does increasing non-fossil fuels in electricity generation reduce carbon dioxide emissions?. *Applied Energy*, Volume 197, pp. 212-221.

[10] Baek, J. & Pride, D., 2014. On the income–nuclear energy–CO2 emissions nexus revisited. *Energy Economics*, Volume 43, pp. 6-10.

[11] Kharecha, P.A., and J.E. Hansen, 2013: Prevented mortality and greenhouse gas emissions from historical and projected nuclear power. *Environmental Science & Technology*, **47**, 4889-4895.

[12] Lindberg, J. C. H., 2017. Sweden's silent phaseout. *Nuclear Engineering International*, 62(758), pp. 12-14.

[13] IEA, 2020. SDG7: Data and Projections: Access to electricity. [Online] Available at: https://www.iea.org/reports/sdg7-data-and-projections/access-to-electricity

[14] IEA, 2020. Average annual capacity factors by technology, 2018. [Online] Available at: https://www.iea.org/data-and-statistics/charts/average-annual-capacity-factors-by-technology-2018

[15] UNICEF, 2020. Reimagining WASH: Water Security for All. [Online] Available at: https://www.unicef.org/reports/reimagining-wash-water-security-for-all

[16] Mekonnen, M. M., & Hoekstra, A. Y., 2016. Four billion people facing severe water scarcity. *Science advances*, *2*(2), e1500323.

[17] United Nations, 2021. Water and Climate Change. [Online] Available at: https://www.unwater.org/water-facts/climate-change/.

[18] Walton, M., 2019. Desalinated water affects the energy equation in the Middle East. [Online] Available at: https://www.iea.org/commentaries/desalinated-water-affects-the-energy-equation-in-the-middle-east.

[19] Ziolkowska, J. R., 2015. Is desalination affordable?—regional cost and price analysis. *Water Resources Management*, *29*(5), 1385-1397.

[20] IAEA, 2020. "*Nuclear desalination"*. Available at: https://www.iaea.org/topics/non-electric-applications/nuclear-desalination.

[21] Cohen, A. J., et al., 2017. Estimates and 25-year trends of the global burden of disease attributable to ambient air pollution: an analysis of data from the Global Burden of Diseases Study 2015. *Lancet*, **389** (10082), pp. 1907-1918.

[22] WHO (2018). Health, environment and climate change: Road map for an enhanced global response to the adverse health effects of air pollution. Available at: https://apps.who.int/iris/bitstream/handle/10665/276321/A71_10Add1-en.pdf?sequence=1&isAllowed=y.

[23] Vohra, K., 2021. Global mortality from outdoor fine particle pollution generated by fossil fuel combustion: Results from GEOS-Chem. *Environmental Research*, **195**.

[24] IEA, 2020, SDG7: Data and Projections: access to clean cooking. [Online] Available at: https://www.iea.org/reports/sdg7-data-and-projections/access-to-clean-cooking

[25] Severini, E., 2017. Impacts of nuclear plant shutdown on coal-fired power generation and infant health in the Tennessee Valley in the 1980s. *Nature Energy*, **2**.

[26] Coates, R., 2014. Radiation protection: where are we after Fukushima?. Journal of Radiological Protection, Volume 34, pp. E13-E16.

[27] Glaser, A., 2012. From Brokdorf to Fukushima: The long journey to nuclear phase-out. Bulletin of the Atomic Scentists, 68(6), pp. 10-21.

[28] Pidgeon, N. F. & Demski, C. C., 2012. From nuclear to renewable: Energy system transformation and public attitudes. Bulletin of the Atomic Scientists, 68(4), pp. 41-51. [29] Flynn (2003)

[30] van de Graaf, S., 2016. Understanding the nuclear controversy: An application of cultural theory. Energy Policy, Volume 97, pp. 50-59.

Proceedings of the European Nuclear Young Generation Forum
ENYGF'21
September 27-30, 2021, Tarragona, Spain

Detailed numerical analysis of different energy scenarios and the role of nuclear energy in the decarbonization pathways of the Hungarian electricity system

Biró, Bence[1*] and Aszódi, Attila[2]

[1] Budapest University of Technology and Economics, Institute of Nuclear Techniques (BME, NTI), Hungary;
[2] Budapest University of Technology and Economics, Institute of Nuclear Techniques (BME, NTI), Hungary; aszodi@reak.bme.hu.

*Corresponding author: *bencebiiro@gmail.com*

I. INTRODUCTION

Electricity systems in European countries need to begin their path towards carbon neutrality to meet climate targets. Hungary has a target of 90% carbon-free electricity generation by 2030 and 2040. Our work included hourly resolution simulations of the Hungarian electricity system using the International Atomic Energy Agency's (IAEA) Energy Scenarios Simulation Tool (ESST) program. We examined Hungary's ability to meet its commitments and the role that nuclear power plants could play in meeting them. Beside technical feasibility of the investigated power plant fleets and the environmental consequences (including the assumed CO2 emissions) the results also show why it is necessary to describe the electricity systems with – at least – hourly resolution models where weather-dependent renewables have a larger share.

II. HOT TOPICS

We have used IAEA's ESST model [1] for our investigations. ESST is a scenario-based simulations program that models the consumption and also the production side of the electricity system using hourly resolution. To make this feasible, the user must provide data for the 8760 hours of a given year to the model both the consumer side and also the production side. For the consumer side, historical consumption data, for the producer side the specific load factors of weather-dependent primary energy sources are required. It is also required to define technical, economic and environmental parameters in the model (e.g. fuel costs, fixed and variable operating costs, maintenance costs, specific emissions etc.) for power plant technologies using different primary energy sources. In order to collect this data, an extensive literature study collecting and processing data from 36 different international publications and the synthesis of the data has been carried out. In addition to providing the costs, we also defined the dispatch order according to which the power plants using different energy sources participate in the national load balancing.

A. Consumption scenarios

By the estimation of the possible future electricity needs we had to take into consideration the effects of the economic crisis caused by the COVID-19 pandemic. Based on the 2020 consumption, we estimated what Hungary's annual electricity consumption could be in 2030 and 2040. To do this we have defined 4 scenarios, shown in Figure 1 and explained as follows:

A) consumption scenario: In this scenario, we have assumed that the relative electricity consumption growth [2] in the 10 years after the 2008/2009 economic crisis and the coronavirus pandemic crisis will be the same so that Hungary's annual electricity demand will increase by 10.24% both between 2020 and 2030 and between 2030 and 2040.

B) consumption scenario: This consumption scenario is similar to the previous one, but here we went back a bit further in time and looked at the growth of the electricity consumption in the years after the political regime change in Central Europe in 1989 [2] and we assumed that between 2020 and 2030 and between 2030 and 2040 similar growth could be expected like between 1992 and 2002, meaning our country's annual electricity consumption will increase by 14.97% in these periods.

C) consumption scenario: In this scenario, we used the ramp-up presented in the Ministry of Innovation and Technology's (ITM) document titled "National Energy Strategy 2030, with an outlook to 2040" [3], which assumes that Hungary's electricity consumption will grow by 12.86% from 2020 to 2025, by 9.35% from 2025 to 2030, by 9.9% from 2030 to 2035 and by 4.9% from 2035 to 2040.

Z) consumption scenario: We wanted to test whether the future power plants portfolios would be able to meet today's consumption needs, so we also defined a consumption scenario in which the electricity consumption in 2030 and 2040 is the same as the electricity consumption was in 2019. This is not a realistic scenario, taking into account the increase in energy demand as the economy develops, but an analysis of this scenario is useful for assessing the viability of the planned power plant portfolios.

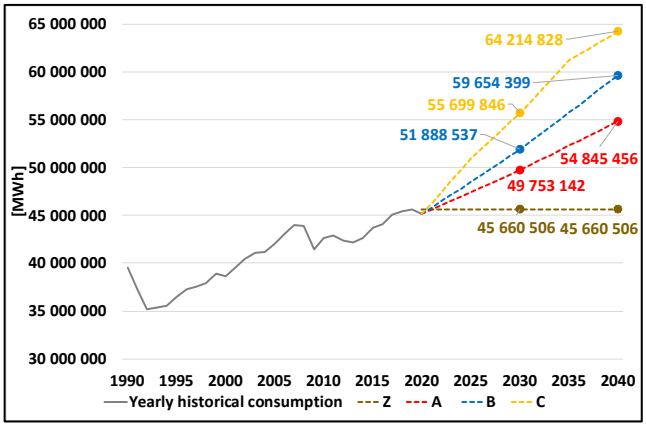

Figure 1. Consumption scenarios (source of the historical data [2], own representation)

B. Power plant portfolios

After defining the consumption scenarios, we defined the production side of the electricity system in order to integrate it into our model built in the ESST simulation environment. For both year 2030 and 2040 several different power plant portfolios have been investigated, two of which are presented here, taking into account the limits of this publication. The power plant portfolios were prepared based on the official document "National Energy Strategy 2030, with an outlook to 2040" [3] published in January 2020 by the Ministry of Innovation and Technology of Hungary, which Ministry is responsible for setting up the Hungarian energy policy. The here presented power plant portfolios are named RES+Gas and RES+Nuc showing the dominant primary energy sources being renewables and natural gas, and renewables and nuclear energy, respectively. The first rectangle in Figure 2 below shows the energy source distribution of Hungary's current power plant system. It shows that, apart from nuclear energy, lignite and natural gas based power plants play a dominant role. Based on the fact that approximately 80% of the natural gas is being imported, any further use of natural gas would mean increased import dependency, and the appearance of LNG based gas could have impact on the market. At the same time significant solar photovoltaic capacities are currently being developed. Currently Hungary has one single nuclear power plant with four operational units. These four existing VVER-440 nuclear power units will reach their 50 years licensed lifetime between 2032 and 2037, which already includes a 20-year extension. Two new VVER-1200 pressurised water reactors are now scheduled to come into operation by 2030 at the same site for which the implementation licensing is underway right now. Accordingly, the RES+Nuc portfolio will have a total of 4400 MW nuclear capacity in 2030, of which 2400 MW will remain in 2040 due to the planned decommissioning of the VVER-440 units. In addition to nuclear power, the RES+Nuc portfolio assumes in the year 2030 2900 MW natural gas based, 6000 MW photovoltaic, 300 MW wind, 800 MW biomass, 150 MW waste firing and 50 MW hydro capacity by 2030. By 2040, these capacities are assumed to be 12000 MW photovoltaic, 350 MW wind, 1150 MW biomass, 150 MW waste firing and 50 MW hydro. The RES+Gas portfolio illustrates what would happen if Hungary would phase out nuclear power: if the current Paks units were to cease operation between 2032 and 2037 and the two new VVER-1200 units were not built to replace them. The Energy Strategy of the Ministry of Innovation and Technology assumes that in this case in year 2030 in addition to 2000 MW nuclear power there will be 3000 MW natural gas based, 4500 MW photovoltaic, 1670 MW wind, 700 MW biomass, 150 MW waste firing and 50 MW hydro capacities in the RES+Gas portfolio. By 2040 these capacities are assumed to be: 2200 MW natural gas based, 8400 MW photovoltaic, 3100 MW wind, 100 MW biomass, 150 MW waste firing and 50 MW hydro capacities with 0 MW of nuclear.

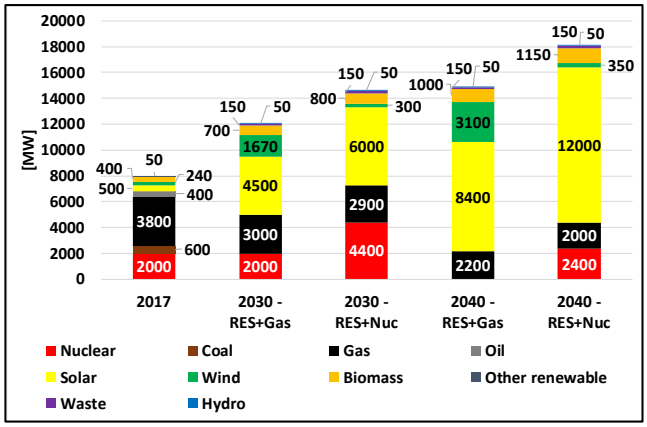

Figure 2. Power plant portfolios

One of the main aims of our below presented analysis is to examine the role of nuclear energy in relation to security of supply and climate objectives. It is worth pointing out that solar capacity is growing rapidly in both here analysed portfolios. It is inline with the developments being currently implemented in Hungary. The annual load factor for each power plant technologies used in the initial calculations for the annual balance estimation is shown in Table 1.

Table 1. Annual load factors for each power plant technologies

Primary energy source	Load factor
Solar energy	Calculated from 8760 hourly specific production data
Wind energy	Calculated from 8760 hourly specific production data
Hydro energy, waste	50 %
Nuclear	90 %
Biomass	75 %
Natural gas	56 %

The order in which the different energy sources take part in the supply of electricity in a given hour has been defined in the following order: 1. solar, 2. wind, 3. hydro, 4. nuclear, 5. waste firing, 6. biomass, 7. natural gas, 8. import. This is called in the ESST model dispatch order, and this will be used throughout all the simulations presented below.

C. Simulation results

After defining the consumer and production side, the simulations were carried out in the IAEA's ESST scenario analysis software. Figure 3 shows the test matrix for the calculations analysed in this paper.

Power plant portfolio \ Consumption scenario	A	B	C	Z
RES+Gas = 1	A1	B1	C1	Z1
RES+Nuc = 2	A2	B2	C2	Z2

Figure 3. Test matrix (The consumption scenarios are described in Section II/A, the power plant portfolios in Section II/B)

Our simulations point out that the emission targets and the security of supply targets cannot be met with all the power plant portfolios proposed. Figure 4 below shows that only 4 of the 16 cases examined in the simulations meet the emission targets of 90% carbon free electricity generation. Some of the cases are further complicated by the fact that the power plant portfolios are not able to meet the domestic demand on its own, thus requiring the use of import electricity sources. With our current knowledge, we don't know on what power plant technologies, and on what fuel base these import sources will generate electricity, and this also carries the uncertainty of operating a foreign power plant using fossil fuels resulting in foreign carbon dioxide emissions. This would actually increase emissions from domestic electricity supply through the so called "carbon leakage". The uncertainty resulted from this phenomenon is indicated by the uncertainty bands in Figure 4, which show that in some cases it could increase the carbon-dioxide emissions of the electricity supply by up to 20-30%. From the results, the RES+Gas portfolio (1Z, 1A, 1B, 1C) data for 2040 is worth highlighting, where it can be concluded that the portfolio cannot replace the four VVER-440 units with domestic sources, thus a significant amount of import will enter the system, reducing the security of supply of the Hungarian electricity system and increasing the likelihood of carbon leakage.

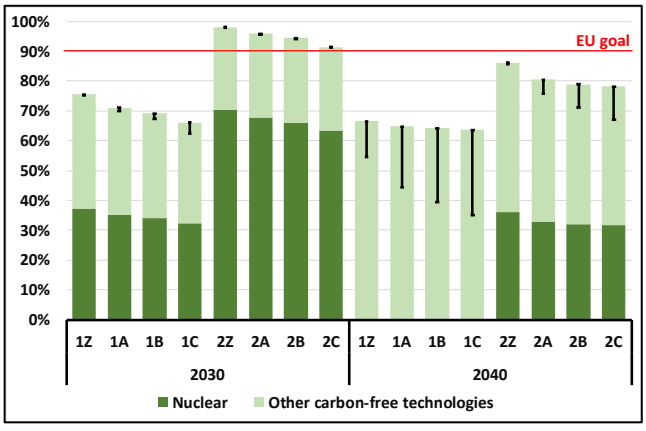

Figure 4. Share of carbon-free electricity generation in each of the studied cases

The continuous variation in electricity demand and the fluctuation of weather-dependent renewable resources requires that individual cases are analysed in highly detailed (at least) hourly resolution simulations in addition to annual energy balance calculations. Figures 5 and 6 compare the operation of the RES+Gas and RES+Nuc power plant portfolios for the consumption scenario B. In these figures we can see the share of the carbon-neutral electricity generation in the following way: the horizontal axis represents one year over the 365 days, while the vertical axis represents the 24 hours of the days, so all 8760 hours of the year are shown in these figures. Figure 5 clearly indicates that for the system states where the solar power plant utilisation factor is low (almost all-day during winter days, and during the evening, night and dawn hours during spring, summer and autumn days), the share of carbon-free generation (shown in green) is significantly reduced and can only be replaced by significant amounts of fossil fuel (shown in red).

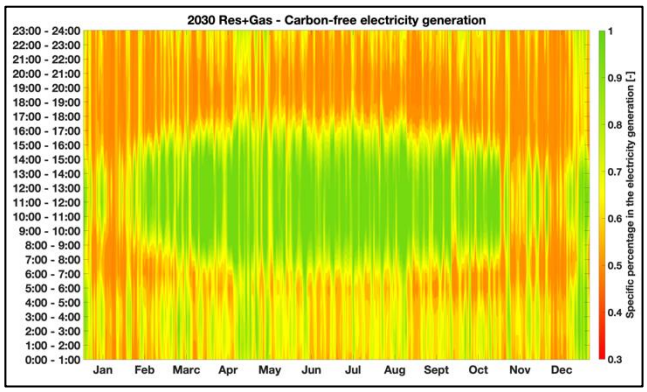

Figure 5. Share of carbon-free electricity generation for the 8760 hours of the year in the RES+Gas portfolio for consumption scenario B (2030 - 1B case)

For the RES+Nuc power plant portfolio, the situation is much more favourable. During the early hours of the morning (0:00 - 6:00), there are hardly any operating conditions where it is necessary to use fossil fuel, as the nuclear units cover the baseload electricity demands. However, during the evening hours, when consumer demand is typically at the highest level, there are several instances where fossil generation is required to meet demand, but to a much lesser extent than in the RES+Gas portfolio.

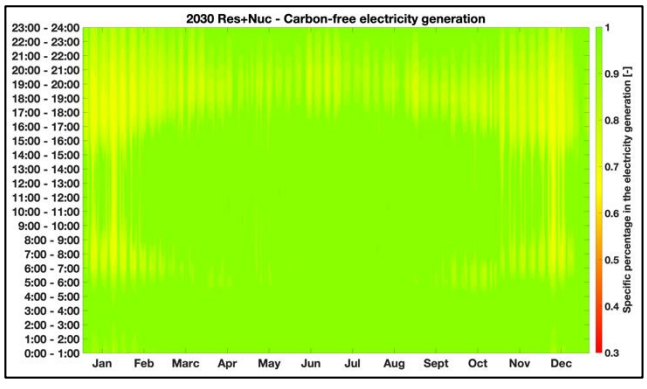

Figure 6. Share of carbon-free electricity generation for the 8760 hours of the year in the RES+Nuc portfolio for consumption scenario B (2030 - 2B case)

In addition to the analyses for 2030, calculations have been made for 2040, too. Figures 7 and 8 show how the RES+Gas and RES+Nuc power plant portfolios operate for the consumption scenario B. In these figures the share of carbon-free electricity generation for each hour of the 365 days of the year is represented. The RES+Gas portfolio no longer includes nuclear capacity in 2040, the unequivocal

impact of which can be clearly observed in Figure 7. Although in this case between 2030 and 2040 the installed capacity of solar and wind increases by 3900 MW and 1430 MW, respectively, the natural characteristics of weather-dependent capacity means that the nuclear capacity lost is replaced by fossil fuels, resulting in a large reduction in the share of carbon-free electricity generation, except for sunny hours. This results in a lot of states indicated by red color in the diagram. These are system states where the share of carbon-free sources is only around 30% or below.

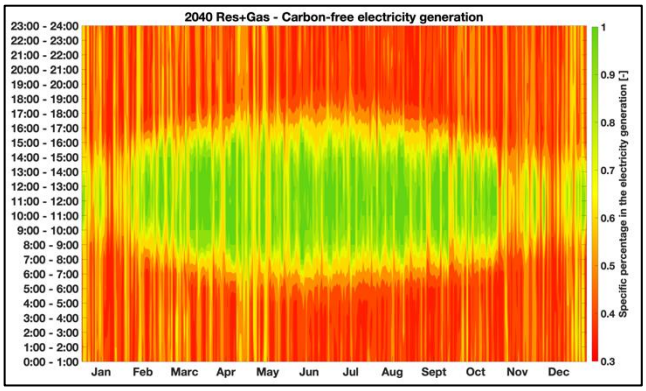

Figure 7. Share of carbon-free electricity generation for the 8760 hours of the year in the RES+Gas portfolio for consumption scenario B (2040 - 1B case)

The situation for year 2040 is clearly better in case of the RES+Nuc portfolio in terms of carbon-free electricity generation, as there are no "red" regions in Figure 8. It is worth noting, however, that with 2000 MW less nuclear capacity defined in the system in this case, there is much more fossil fuel in the grid during the more problematic winter months and during the morning and evening hours.

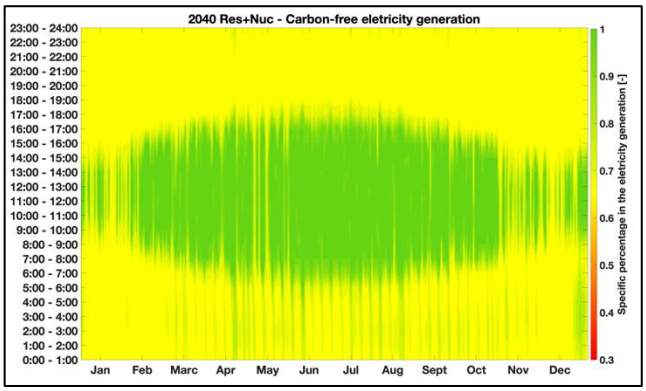

Figure 8. Share of carbon-free electricity generation for the 8760 hours of the year in the RES+Nuc portfolio for consumption scenario B (2040 - 2B case)

By comparing Figure 8 with Figure 6, it is clear that a more carbon intensive electricity system will characterise the country's supply for the year 2040 as a whole. Both the increase in electricity demand and the reduction in nuclear capacity will play a decisive role in this. Based on the analysis of the data, it is clear that the reduction of the nuclear capacity from 4,400 MW to 2,000 MW in 2040 will mean that Hungary will not be able to meet its carbon-free electricity generation commitments for this portfolio in any consumption scenarios, as fossil fuels will have to play too big role in meeting the demand. We must refer back to Figure 4, where, in addition to the 2030 data, we can also see a summary of the 2040 data. It can be clearly seen that, despite the large increase in renewable capacities, carbon-free generation is declining because fluctuating weather-dependent renewable sources cannot ensure continuous supply, so they can neither take play the necessary role in the baseload production nor in the load-following.

Based on the results of our simulations, in 2040, the solar and wind over-generation (the amount of renewable energy that could be produced in principle but exceeds the actual electricity demand for a given hour) ranges between 415 GWh and 2134 GWh for the consumption scenarios B analysed in detail above. This energy could be used by utilizing export-import opportunities or by integrating grid-level electricity storage capacities into the system. Taking these into account in our simulation model requires additional model developments and further studies, which are underway.

D. Summary

In this article, we have used detailed, hourly-resolution simulations to investigate the source structure of electricity generation and the share of carbon-free power generation for 2030 and 2040 for four different electricity consumption scenarios and two different power plant portfolios. For the simulations, we used the International Atomic Energy Agency's ESST program, in which we built 16 different models and we studied how the system operates. Several European countries, including Hungary, are planning to use natural gas-fired power plants to replace the conventional power plants they have today to bridge the periods when the intensively expanding wind and solar energy sources are not available. At the same time, our hourly resolution simulations show that keeping nuclear capacity in the system is necessary for the power sector to meet carbon emission targets while also ensuring that the security of supply targets are met. In case of Hungary, 90% of electricity can only be produced from carbon-free sources in 2030 if the planned new nuclear units start operating together with the existing four nuclear power plant units at Paks NPP. However, if the current Paks units were shut down by 2040, renewables and the two new nuclear generating units of 1200 MW each will not be sufficient to meet the climate protection targets. The operation of additional nuclear generation capacities seems to be necessary. Our simulations also point out that energy scenario analyses which are based on annual energy balances are not detailed enough to provide an accurate picture of the contribution of each different energy source, given the fluctuations of the weather-dependent renewable sources. Therefore, simulations with at least hourly resolution are needed to analyse such future scenarios.

III. References

[1] International Atomic Energy Agency (2020): Energy Scenario Simulation Tool (ESST) User and Methodology Manual – May 2020

[2] https://www.mavir.hu/web/mavir/rendszerterheles

[3] Ministry of Innovation and Technology (2020 January): National Energy Strategy 2030, with an outlook up to 2040

Proceedings of the European Nuclear Young Generation Forum
ENYGF'21
September 27-30, 2021, Tarragona, Spain

Analysis of some specific uranium and transuranium isotopic mixtures to enhance the mass and radiation barriers of uranium-plutonium compositions against unauthorized proliferation

Ozerina, Milana[1,2]

[1]Rosatom Technical Academy (Rosatom Tech), Russia, [2]National Research Nuclear University MEPhI (Moscow Engineering Physics Institute), Russia

*Corresponding author: MAOzerina@rosatomtech.ru

I.INTRODUCTION

The UN's Sustainable Development Goal (SDG) 7 deals with ensuring access to affordable, reliable, sustainable, and modern energy for all. Nuclear power, among other technologies, can provide the energy to ultimately achieve high living standards, good health (SDG3), a sustainable economy (SDG8), and combat climate change caused by an increase in greenhouse gases (SDG13). As well, the pandemic of new COVID-19 infection revealed the strong need for reliable power supply, as affordable and reliable energy is critical for health facilities.

Wide-scale and coming soon rapid deployment of innovative small modular reactors (SMRs) and Generation IV nuclear power systems, is one of the ways to meet these challenges. Their fuel cycles could be significantly different from existing ones thus giving an additional focus on the non-proliferation regime that remains to be an essential factor in the global development of nuclear energy. It is a matter of fact that well-established criteria for proliferation resistance exist only in manageable mass (for uranium) and isotopic composition (for plutonium). Any other mixture of fissionable nuclides for its assessment requires deeper research.

II.CHARACTERISTICS OF NUCLEAR MATERIALS

There are concerns that the widespread expansion of nuclear energy could lead to the theft of fissile materials or to a diversion to the production of nuclear weapons.

According to TOPS (Technological Opportunities to Increase the Proliferation Resistance of Global Civic Nuclear Power Systems), barriers to nuclear proliferation can be:

• Material barriers: isotopic, chemical, radiation, mass and volume, and detection barrier.

• Technical barriers: non-attractiveness of objects, difficult accessibility of objects and significant quantity, detection of diversion, knowledge, skills, expertise, and time.

• External administrative barriers: IAEA safeguards, physical protection, control and accounting of nuclear materials, location.

The critical mass of nuclear material is one of the important properties of the material with regard to its applicability to the manufacture of a nuclear explosive device. By definition, critical mass is the amount of material with a certain concentration of fissile isotopes that is required to maintain a self-sustaining fission chain reaction. In general, the critical mass represents a reasonable estimate of the amount of material required to create a nuclear weapon or explosive device using material of a given isotope composition.

Materials with the lowest isotopic barrier efficiency (especially highly enriched uranium and weapon-grade plutonium (> 90% Pu-239)) are the most attractive for use in the manufacture of nuclear explosive devices [1]. Higher isotopic barrier materials may include a more complex explosive device design, fabrication and processing of the material, and/or isotopic enrichment for use in nuclear weapons. The topic of the discussion of barriers against nuclear proliferation has developed a specialized term - resistance to nuclear proliferation - it describes the degree of obstruction of the diversion or undeclared production of nuclear material or the misuse of technology by States for the acquisition of nuclear weapons or other nuclear explosive devices.

Intrinsic characteristics of resistance to nuclear proliferation can be those related to either the peculiarities

of technological processes, for example, using mixtures of nuclear materials with increased radioactive radiation, or the result of the technical design of nuclear energy systems.

External measures for resilience to nuclear nonproliferation are those arising from the decisions and commitments of States with nuclear-energy programmes [2].

The protective barrier for plutonium is mainly formed by two even isotopes Pu-238 and Pu-240. Pu-238 is characterized by high energy release, which interferes with the manufacture and reliability of explosives, causing degradation or even melting of chemical explosives; and Pu-240 is characterized by a high level of generation of spontaneous fission neutrons, which reduces the power of a nuclear explosion. High heat release of Pu-238 leads to the fact that plutonium with an isotope content of Pu-238 more than 80% is excluded from IAEA safeguards.

There are different opinions on the protection of plutonium with these isotopes. It should be noted that a nuclear explosive device can be created with an increased content of Pu-240. Therefore, the term "weapons-grade plutonium" has rather an economic characteristic (i.e., affects the cost of bomb design, which can be performed at different technological and technical levels) than the characteristic of plutonium, from which it is possible to create an atomic bomb. On the one hand, with an increase in the share of Pu-240, the cost of plutonium material drops, on the other hand, the presence of Pu-240 increases the critical mass, which leads to an increase in the cost of the product. However, it should be borne in mind that the main parameter affecting the risk of nuclear proliferation is not the amount of isotope Pu-240 in the plutonium material, but its content of isotopes Pu-241 and to some extent Pu-238. These isotopes have a short lifetime (the half-life of Pu-241 is about 14.4 years, and Pu-238 - 86.4 years) and, turning by beta- and alpha-decay into other isotopes (Am-241 and U-234, respectively), significantly change the isotopic composition of plutonium and, accordingly, its capabilities for use as weapons. In this context, it is necessary to speak of a significant amount of nuclear material in relation to safeguards.

A separate consideration requires the assertion that reactor plutonium can be used to create a nuclear explosive device whose explosive power cannot be accurately predicted, but whose minimum power is still much higher than that of conventional chemical explosive charges. Due to the presence of spontaneous fission neutrons in plutonium, unlike uranium mixtures, the main principle of plutonium based IVU is the implosion principle, that is, the detonation of external chemical explosives, which creates a shock wave directed to the centre of the plutonium sphere and leads to rapid compression of the spherical plutonium charge. The presence of Pu-238 in the plutonium charge can lead to a decrease in the properties and even a melt of chemical explosives.

III. PROLIFERATION RESISTANT FUEL COMPOSITIONS

To maintain plutonium with the required (proliferation-proof) content of isotope Pu-238, several percent of americium, which is not a special fissile material, must be added to fresh fuel. Reactor-grade americium produced in spent fuel cannot be used for nuclear weapons for the same reasons as reactor-grade plutonium. The isotope Am-241, always present in reactor-grade americium, and generates so much heat as a result of alpha decay that any use of hypothetical nuclear weapons becomes technically impossible [3].

Thus, in the future, the proliferation-proof uranium-plutonium fuel cycle can be used in light water reactors, breeder reactors by forming plutonium compositions with a higher content of isotope Pu-238.

For further use of thorium in the proliferation-proof uranium-thorium fuel cycle, an isotope U-232 can be similarly used.

Similarly, the fuel mixture from the U-233/U-235 for future light water reactors operating in the uranium-thorium fuel cycle can become proliferation resistant in the gas centrifuge cascade, since this fuel causes a certain contamination of U-232 as a result of nuclear reactions of neutrons with Th-232 during its burnout in the reactor core.

IV.GENERATION IV NUCLEAR ENERGY SYSTEMS

The main risk associated with Generation IV nuclear energy systems is associated with the possibility of isotopic enrichment of uranium; or with the possibility of separation of plutonium from the mixture during reprocessing of spent nuclear fuel. However, among nuclear power systems of Generation IV there is no reactor system which would demand use of high-enriched uranium therefore use of the plants on uranium enrichment having constructive restrictions for enrichment on U-235 to 20% will be the reasonable decision. In the nuclear fuel cycle of fast neutron reactors, U-238 and Th-232 are involved (the reserves of these isotopes in nature are much larger than U-235), which eliminates the stage of uranium enrichment.

However, the risk of nuclear proliferation associated with plutonium remains and requires further study.

The so-called two-component system, which involves the involvement of fast reactors in an already existing system based on thermal installations, can contribute to solving this problem by establishing a zero balance between the production of plutonium and its consumption. Fast reactors in such a system will not only generate electricity, but also solve the problems of nuclear energy that are inherent in it today - resource and high-activity waste management. Reactors with sodium coolant fit into this concept. Russia relies on the reactor project BN-1200 with a reproduction coefficient of 1.2 - that is, one such plant will produce fuel for itself and for two VVER reactors. At the same time, the

BN-1200 will operate on MOX fuel, and VVER - on oxide fuel and partially on MOX.

V.CONCLUSIONS

Significant quantities (SQ) of plutonium and other transuranic elements must be determined and considered in addition to certain SQ in the IAEA Charter. This is important for strengthening the international non-proliferation regime and material accounting.

Furthermore, not only Pu-238 but also other plutonium isotopes with even-mass-number have important role for denaturing of plutonium due to their large critical mass and high spontaneous fission neutron generation. With the changes of the minor-actinide doping ratio in U–Pu mix oxide fuel, it is found that the reactor-grade plutonium from conventional light water reactors can be denatured to satisfy the proliferation resistance criterion [4].

VI. REFERENCES

[1] G. Kessler, «Proliferation-Proof Uranium/Plutonium and thorium/Uranium fuel Cycles, safeguards and non-Proliferation,» Karlsruhe: KIT Scientific Publishing, 2017.

[2] International Atomic Energy Agency, «Proliferation Resistance Fundamentals for Future Nuclear Energy Systems,» IAEA, Como, 2002.

[3] M. Saito, V.V. Artisyuk, H. Sagara, A.A.Ezoubtchenko, «Proliferation resistance properties of U and Pu isotopes,» *Progress in Nuclear Energy*, 2005.

[4] H. Sagara, M. Saito , Y. Peryoga , A. Ezoubtchhenko, A. Takivayev, «Denaturing of Plutonium by Transmutation of Minor-Actinides for Enhancement of Proliferation Resistance,» *Journal of Nuclear Science and Technology*, pp. 161-168, 15 February 2012.

Hot Topic 3 - Radioactive Waste: Closing the circle

Measurement of residual stress in spent AGR fuel cladding using incremental center hole drilling.

Authors: van Heule, Xavier (1); Truman, Christopher (1); Coules, Harry (1); Clark, Ronald (2)

Radioactive Byproduct Characterization – Are the Data Good?.

Authors: Hylko, James M.

Study of radium behaviour in contact with cementitious phase CSH.

Authors: Kittnerová, Jana (1); Drtinová, Barbora (1); Štamberg, Karel (1); Evans, Nicholas (2); Deissmann, Guido (3); Lange, Steve (3)

Bottom Drain Melters for Solidifying HLW into Borosilicate Glass.

Authors: Shaydullin, Sergey Minullovich (1,2); Remizov, Mikhail Borisovich (1); Kozlov, Pavel Vasilievich (1); Verbitsky, Kirill Vladimirovich (1); Melentyev, Anatoly Borisovich (1); Bendasov, Danil Igorevich (1); Rebrin, Mikhail Alexeyevich (1)

How should the IAEA Code of Practice on the International Transboundary Movement of Radioactive Wastes 1991 be Interpreted to Ensure that a Best Available Technique (BAT) is Applied to the Waste Hierarchy?

Authors: Clarke Dhadli, Jasvinder James

Effect of pH on the dissolution rate of MoO2(s).

Authors: García-Gómez, Sonia; Rivero, Alejandro; Ribas, Joan de Pablo; Casas, Ignasi

Possibilities and Features of REMIX Technology as an Initial Stage in the Establishing of a Full-Scale Two-Component Nuclear Energy System.

Authors: Sitdikov, Emil; Vasilenko, Alexei; Diachenko, Anton

Technical Considerations for the Geological Disposal of Liquid Nuclear Waste.

Authors: Bychkov, Maksim Anatolyevich; Lvova, Darya Dmitrievna

Engineering of a heating / cooling system for spent fuel pool at Bilibino nuclear power plant in the post-operational period.

Authors: Gavrilova, Anastasia

Development of a gamma irradiation loop to evaluate the performance of a EURO-GANEX process.

Authors: Sánchez García, Iván (1,2); Galán Montano, Hitos (1); Núñez Gómez-Aleixandre, Ana (1); Perlado, Jose Manuel (2); Cobos Sabaté, Joaquin (3)

Development of the first Russian research molten salt nuclear reactor aimed to elaborate the technology of minor actinides recycling and to prepare for construction of the full-scope industrial minor actinides burning reactor.

Authors: Vlasenko, Evgeny

Isolation of solid organic matter from complex clay matrices from the Boom Clay formation.

Authors: Bagaria, Ferran (1); García, David (1); Duro, Lara (1); Brassinnes, Stéphane (2)

Spent fuel alteration model: integrating different time-scale processes.

Authors: Coene, Emilie; Riba, Olga; Silva, Orlando; Duro, Lara

Interaction of low molecular weight organics, cement phases and radionuclides.

Authors: Guidone, Rosa Ester (1,2); Lothenbach, Barbara (1); Gaona, Xavier (2); Tasi, Agost (2); Altmaier, Marcus (2); Geckeis, Horst (2)

Modeling of γ-spectra for characterization of surface and volume activity in deferent geometry metallic waste samples.

Authors: Lagzdina, Elena; Germanas, Darius; Lingis, Danielius; Garankin, Jevgenij; Konstantinova, Marina; Plukienė, Rita; Plukis, Artūras; Remeikis, Vidmantas

Development of a Simplified Preliminary Risk Assessment Model for the Geological Disposal of Radioactive Waste in the United Arab Emirates.

Authors: Al Nuaimi, Abdulla Hashem; Williams, Laurence

Depth profiling of radiologically contaminated concrete, using CT-scan images and Monte Carlo simulations.

Authors: Brabants, Lowie (1); Reniers, Brigitte (1); Paepen, Jan (2); Vandoren, Bram (3); Schroeyers, Wouter

Research on Cement-Organics-Radionuclides-Interactions within the collaborative EURAD project.

Authors: Altmaier, Marcus (1); Blin, Virginie (2); García, David (3); Henocq, Pierre (4); Missana, Tiziana (5); Ricard, Denise (4); Vandeborre, Johan (6)

Development of a gamma irradiation loop to evaluate the performance of the EURO-GANEX process.

Authors: Sánchez García, Iván (1,2); J. Bonales, Laura (3); Galán Montano, Hitos (1); Perlado, Jose Manuel (2); Cobos Sabaté, Joaquin (4)

Dissolution studies at repository conditions of advanced doped UO2 fuel.

Authors: Milena-Pérez, Abel (1); Rodríguez-Villagra, Nieves (1); Fernández-Carretero, Sergio (1); Jiménez-Bonales, Laura (1,2); Núñez, Ana (1); Durán, Sofía (1); Anta, Laureano (1); Gutiérrez-Nebot, Luis (1); Cobos, Joaquín (1,3)

"Creation of the final system for the isolation of radioactive waste in the Russian Federation".

Authors: Igin, Vsevolod

Safety Case for the Disposal of LLW and ILW in the Russian Federation.

Authors: Trofimova, Iuliia

Consumption of hydrogen peroxide in the dissolution of mixed oxide fuels under the anoxic conditions of a geological disposal facility..

Authors: Perry, Emma; Farnan, Ian

Proceedings of the European Nuclear Young Generation Forum
ENYGF'21
September 27-30, 2021, Tarragona, Spain

Measurement of residual stress in spent AGR fuel cladding using Incremental Centre Hole Drilling

van Heule, Xavier[1*], Truman, Christopher[1], Coules, Harry[1] and Clark, Ronald[2]

[1] University of Bristol, UK; [2] National Nuclear Laboratory Ltd, UK

*Corresponding author: *xavier.vanheule@bristol.ac.uk*

I. INTRODUCTION

Following the closing of the Thermal Oxide Reprocessing Plant (THORP) at Sellafield, the Nuclear Decommissioning Authority (NDA) has made the strategic decision to cease the reprocessing of spent Advanced Gas-Cooled Reactor (AGR) fuel [1]. Instead, the spent fuel pins will be kept in long term storage until at least 2075 [1]. In practice, the fuel ponds which are still available at THORP are used for this long term storage. In these ponds, one of the major risks is the release of radioactivity into the water due to cladding failure. As a result, the structural integrity of the AGR fuel cladding must be guaranteed. However, in the past, failure of AGR cladding under identical conditions has already been observed [2], and the main failure mechanism has been identified as Stress Corrosion Cracking (SCC) [3].

One of the requirements for SCC to occur, besides a susceptible material and corrosive environment, is the presence of tensile stresses [4]. In the case of spent AGR fuel cladding, it is suspected that the main contributor to the stress state are the residual stresses present in the cladding. These are mechanical stresses that exist in a material in the absence of an externally applied load, and are the result of internal incompatibilities introduced by, for instance, non-uniform thermal expansion (or contraction), machining operations or plastic deformation [5].

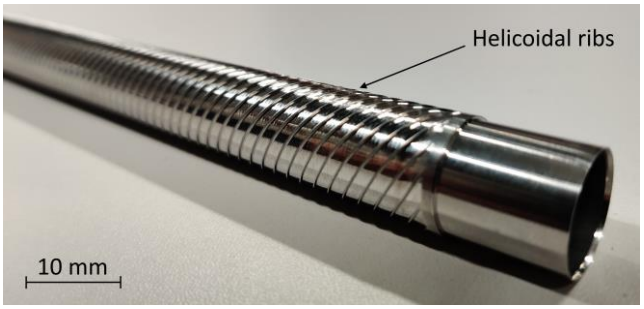

Figure 1. AGR Fuel Cladding (Tube with helicoidal ribs)

The residual stress state in spent AGR fuel cladding is currently unknown, and as a result, its influence on the SCC behaviour is unclear. Furthermore, there is no readily applicable method available to measure mechanical stresses in spent AGR fuel cladding, mainly due to their high radioactivity and complex, helicoidally ribbed geometry (see Figure 1). Therefore, the adaptation for use on AGR fuel cladding, of an existing (residual) stress measurement technique, Incremental Centre Hole Drilling (ICHD), which has been identified as a feasible method, is investigated.

II. INCREMENTAL CENTRE HOLE DRILLING (ICHD)

ICHD is a widely known [6] and standardized [7], method for quantifying macroscopic residual stresses in materials and components. Its parameters and their influence on the uncertainties and errors are well studied and understood [8][9]. It is considered as a semi-destructive method as it only leaves a small (1 - 2 mm), non-penetrating hole, often without impairing the functionality or safety of the component.

The technique consists of incrementally drilling a (relative to the sample) small hole in a specimen suspected of containing residual stresses. As material is removed, residual stress is relaxed, and the material deforms. By measuring these deformations at the surface around the hole, between each increment, the stresses which were present before the hole was drilled can be determined.

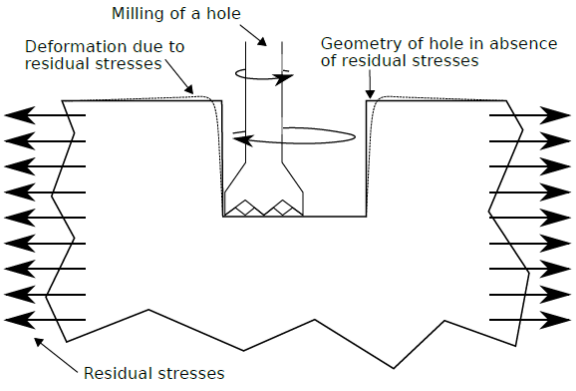

Figure 2. Schematic representation of ICHD

The standard, ASTM E837-13a [7], prescribes a detailed procedure for performing ICHD measurements. This includes the use of strain gauge rosettes (see Figure 3) to measure strains at three points around the hole, as well as calibration data to calculate the stresses from these strains.

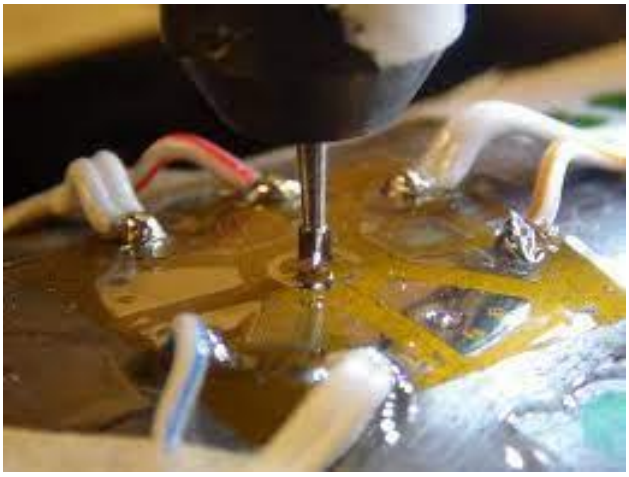

Figure 3. ICHD using a standardized strain gauge rosette [10]

There are however some issues regarding the compatibility of this procedure with application on AGR fuel cladding. Firstly, the calibration factors are only valid for geometries with limited curvature and free from surface features [11], and secondly, the presence of the ribs prevents the application of strain gauge rosettes entirely.

The first issue is resolved by determining bespoke calibration data using a Finite Element (FE) model of the fuel cladding, which is, in literature, considered as good practice for geometries or samples incompatible with the standard [12-14].

The second issue is resolved by using an optical method for measurement of strain or deformation, such as Digital Image Correlation (DIC). Successful application of DIC in ICHD measurements has already been demonstrated the past [15, 16], and is therefore chosen as the reference approach due to its robustness with regards to vibrations and rigid body motion.

III. CALIBRATION DATA

A. Theory

The integral method [17], used for reconstructing non-uniform residual stresses with ICHD using strain gauge rosettes can be expanded and adapted for use with full-field measurements such as DIC. In the classic integral method, only 3 measurement points are used (1 for each strain gauge in the rosette), while for a full-field method, this can be hundreds to thousands of points (one for each pixel in DIC).

In what follows, the following indexations are used:

- index i: hole depth (first depth: $i = 1$, second: $i = 2$, etc.);
- index j: depth increment at current depth ($j \leq i$);
- index k: index indicating the displacement component (hoop or axial) at a certain point;
- index x: indicates the stress tensor component ($x = \theta$ for hoop, $x = a$ for axial, and $x = \tau$ for shear).

A linear expression between the displacements around the hole and the stresses relaxed in the hole exists [18]:

$$u_{ki} = \int_0^{h_i} \sum_x C_{ikx}(z)\sigma_x(z)dz \qquad (1)$$

In which u_{ki} is a displacement component at a point with index k and hole depth i, σ_x is a stress tensor component at depth z and $C_{kix}(z)$ is a kernel function between the stress and displacement for hole depth i.

Eq. 1 describes an inverse problem which does not have a straightforward solution. Therefore, very often the stresses are represented by power series such as unit pulses or Légendre polynomials [18]. For the current purpose, unit pulses of constant stress over each depth increment are chosen for their simplicity:

$$\sigma_x(z) = \sum_{j=1}^{i} \sigma_{jx} U_j(z) \; with \begin{cases} U_j(z) = 1 \; (h_{j-1} \leq z \leq h_j) \\ U_j(z) = 0 \; (elsewhere) \end{cases} \qquad (2)$$

After substitution of Eq. 2, Eq. 1 can be reduced to:

$$u_{ki} = \sum_x \sum_{j=1}^{i} \sigma_{jx} \int_{h_{j-1}}^{h_j} C_{ikx}(z)dz = \sum_x \sum_{j=1}^{i} \sigma_{jx} G_{ij,kx} \qquad (3)$$

The integral in Eq. 3 has a unique, single value for each combination of the indices i, j, k, and x, which will be indicated by $G_{ij,kx}$. These factors quantify the influence of stress component x at increment j of hole depth i on a displacement component at a point k.

In an ICHD experiment, the displacements u_{ki} are measured, but the stresses σ_{jx} are the variable of interest. As a result, the factors $G_{ij,kx}$ in Eq. 3 act as calibration factors to calculate stresses from displacements.

It should also be noted that Eq. 3 forms a system of thousands of equations (one for each pixel in the DIC measurement), but with only a limited number of unknowns (3 times the number of hole depth increments). As a result, Eq. 3 is over-defined, and furthermore, due to noise there will not be an exact solution, and must therefore be solved using a least squares approach. This, however, requires the calibration factors $G_{ij,kx}$ to be known.

B. Calculation of the Calibration Factors $G_{ij,kx}$

As mentioned earlier, it is considered good practice to determine bespoke calibration data for ICHD measurements on samples which are incompatible with the standard ASTM E837-13a.

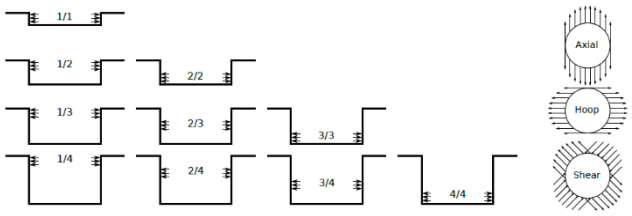

Figure 4. Required combinations of loads and hole depths to determine the ICHD calibration data

In practice, the calibration data are obtained by modelling the sample using FE. This FE model is then used to simulate the ICHD experiment with known residual stresses at every combination of hole depth and increment shown on Figure 4. From each of these simulations, a displacement field

around the hole is obtained from the FE model. With these known stresses and displacements, the calibration factors $G_{ij,kx}$ from Eq. 3 can be determined.

For AGR fuel cladding, advantage is taken from the periodic nature of the geometry to limit the domain to a single repetitive unit cell with adequate periodic boundary conditions, shown in Figure 5. The boundary conditions were validated by comparing FE results for a smooth cylinder with an analytical solution.

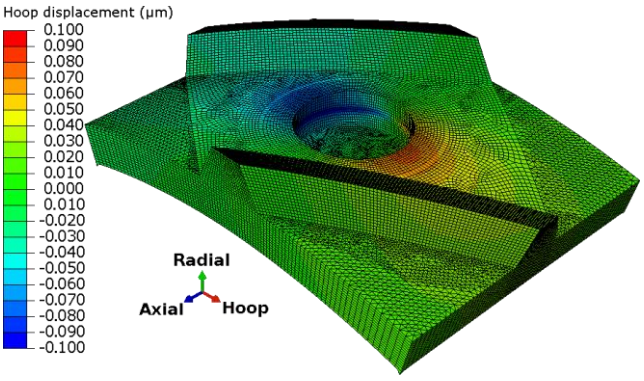

Figure 5. Result of the FE simulation for a hoop load at the 5th increment for the 7th hole depth.

The displacement fields for a theoretical residual stress states were calculated for a hole of 1 mm diameter with 7 increments of 0.05 mm, and compared to a full-field calibration dataset compatible with the standard ASTM E837-13a. Figure 6 shows the large discrepancies resulting from this comparison, demonstrating the need for bespoke calibration data.

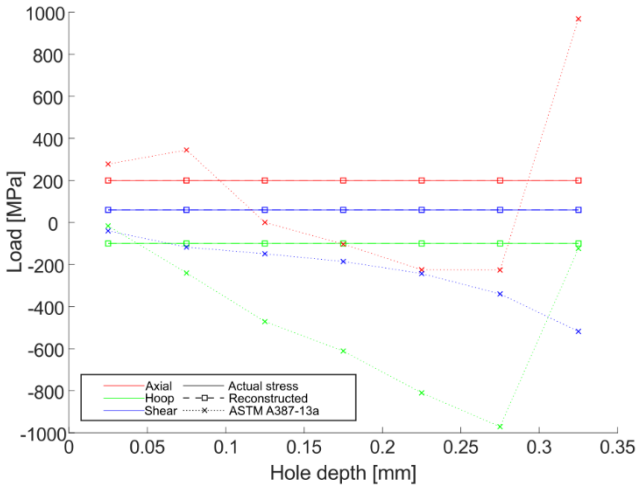

Figure 6. Comparison between stresses reconstructed with custom calibration data and calibration data compatible with ASTM E837-13a. Stresses are reconstructed from a theoretical displacement field, obtained from FE using a known stress state ("Actual Stress" in the legend). This is done using both the bespoke calibration data ("Reconstructed" in the legend) as well as ASTM A387-13a compatible calibration data ("ASTM A387-13a" in the legend).

The FE model also indicates a stress resolution of roughly 0.05 µm / 100 MPa, which would require a DIC noise floor with an upper limit of 0.01 µm [19]. This is considered to be attainable with a camera resolution of 16 megapixels (resulting in 2000 pixels / mm) [20].

IV. EXPERIMENTAL STAGE

Combining ICHD with DIC requires a specific stage to repeatedly position the sample relative to the drill and the camera system between each increment, such that these are always aligned with the hole. An example of the development of such a stage is given in [21], where the camera system and drill are mounted on a translation stage driven by servos. While such a device works well in conventional cases, it is not suitable for remote operation, and furthermore, the electronics would break down under the intense radiation given off by the fuel pins.

Therefore, a new prototype needs to be designed, with the constraints of hot cell operation in mind. Requirements for this prototype include capabilities related to:

- resilience with regards to high radiation doses;
- remote operability in a hot-cell environment using tele-manipulators, this includes introduction and positioning of the sample, drilling of hole increments, and capture of images;
- precise, repeated alignment of the hole between drill and camera system orientations with high repeatability.

To fulfil these requirements, it was decided to eliminate all electronics in favour of manual (for sample orientation) or pneumatic (for drilling) operation, except for the camera system where it is inevitable.

Advantage is taken of the cladding's axial geometry to design self-centring clamps (Figure 7, bottom left). The clamps are supported by bearings, allowing them to rotate together with the sample, and foreseen with cams (Figure 7, bottom right) to limit the rotation to 90°. As the drill (working vertically) and camera system (working horizontally) are oriented perpendicularly with regards to each other, repeated alignment is guaranteed by fully compressing the cams in either orientation.

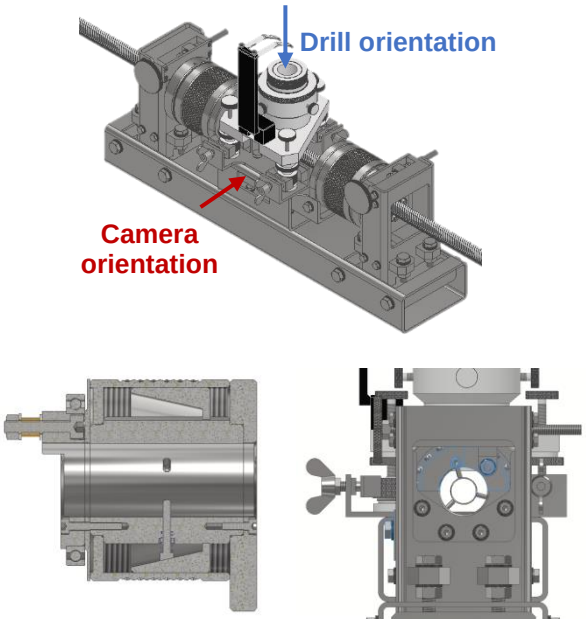

Figure 7. Design of the combined ICHD-DIC stage (top) with details of a centring clamp for cladding (bottom left) and position cam (bottom right)

A picture of the completed stage (without drill or camera) is shown on Figure 8. This stage is not yet compatible with a hot cell environment as it is not possible to operate the clamps and orientation screws with hot-cell tele-manipulators. Furthermore, this stage still makes use of a laboratory based stereo-DIC system.

Nevertheless, this stage will be able to serve as a lab-based prototype to confirm the practical feasibility of combined ICHD and DIC measurements on AGR fuel cladding. A second iteration of the prototype will then address hot-cell requirements such as having a fixed camera system in a shielded box, and remote operation by means of tele-manipulators.

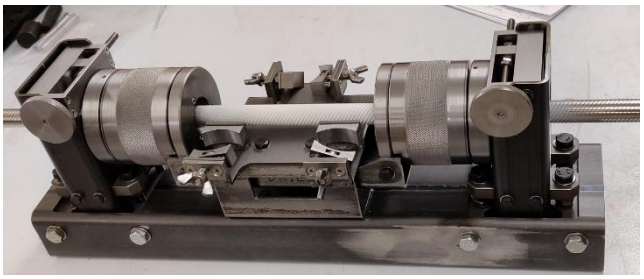

Figure 8. Completed ICHD-DIC prototype for AGR fuel cladding

V. CONCLUSIONS AND NEXT STEPS

Application of the ICHD method for measurement of residual stresses in AGR fuel cladding is investigated. For this purpose:

- DIC is chosen as displacement measurement method;
- a bespoke set of calibration data is required and has been calculated;
- theoretical feasibility of DIC with a 16 megapixel camera has been demonstrated;
- an initial prototype stage for combined ICHD and DIC for AGR fuel pins has been developed.

Future work will focus on hands-on tests on inactive samples to demonstrate the practical feasibility.

Further steps are modification of the prototype for use in a hot cell environment (specifically with regards to the camera system and compatibility with fuel pins exhibiting a certain level of bowing), and remote testing with non-active samples.

VI. REFERENCES

[1] Nuclear Decommissioning Authority, “Oxide fuels: Preferred Option,” Tech. Rep. SMS/TS/C2-OF/001/Preferred Option, 2012.

[2] National Nuclear Laboratory, “Summary of AGR Wet Storage,” Tech. Rep. IP200709-6-10-01, 2009.

[3] National Nuclear Laboratory, “The scope and availability of information characterizing irradiated AGR cladding to support the investigation of AGR cladding sensitisation and corrosion behaviours,” Tech. Rep. NNL(16) 13843, Issue 2, 2016

[4] S. P. Lynch, “Mechanistic and fractographic aspects of stress-corrosion cracking (SCC),” in Stress Corrosion Cracking : Theory and Practice, V. Raja, T. Shoji, Elsevier Science & Technology, Ch. I, pp. 3-89.

[5] P. J. Withers, “Residual stress and its role in failure,” Reports on Progress in Physics, vol. 70, no. 12, pp. 2211–2264, 2007.

[6] G. S. Schajer, “Advances in hole-drilling residual stress measurements,” Exp. Mech, vol. 50, no. 2, pp. 159-168, 2010.

[7] American Society for Testing and Materials, “Test Method for Determining Residual Stresses by the Hole-Drilling Strain-Gage Method,” Standard ASTM E837-13a, 2013.

[8] M. B. Prime, M. R. Hill, “Uncertainty, model error, and order selection for series-expanded, residual-stress inverse solutions,” J. Eng. Mater. Technol., vol. 128, no. 2, pp. 175-185, 2006.

[9] M. Steinzig, D. Upshaw, J. Rasty, “Influence of drilling parameters on the accuracy of hole-drilling residual stress measurements,” J. Eng. Mater. Technol., vol. 54, no. 9, pp. 1537-1543, 2014.

[10] Veqter, “Centre-Hole Drilling Technique”, online: https://www.veqter.co.uk (accessed 06/04/2021).

[11] G. S. Schajer, “Practical Residual Stress Measurement Methods,” John Wiley & Sons, Ch. II, pp. 29-64.

[12] S. Akbari, F. Taheri-Behrooz, M. M. Shokrieh, “Characterization of residual stresses in a thin-walled filament wound epoxy/carbon ring using incremental hole drilling method,” Compos. Sci. and Technol., vol. 94, pp. 8–15, 2014.

[13] A. R. Ghasemi, M. M. Mohammadi, “Residual stress measurement of fiber metal laminates using incremental hole-drilling technique in consideration of the integral method,” Int. J. Mech. Sci., vol. 114, pp. 246–256, 2016.

[14] S. Amir-Ahmadi, A. R. Ghasemi, M. Mohammadi, “Evaluation of thermal residual stresses of thin-walled laminated composite pipes to characterize the effects of mandrel materials and addition MWCNTs,” Mech. Mater., vol. 136, no. 2, pp. 157–163, 2019.

[15] Y. Ma, X. Yao, D. Zhang, “Axially symmetrical stresses measurement in the cylindrical tube using DIC with hole-drilling,” Opt. Lasers Eng., vol. 66, pp. 174-180, 2015.

[16] M. Hagara, F. Trebuna, M. Pastor, R. Hunady, P. Lengvarsky, “Analysis of the aspects of residual stresses quantification performed by 3D DIC combined with standardized hole-drilling method,” Measurement, vol. 137, pp. 238-256, 2019.

[17] G. S. Schajer, “Measurement of non-uniform residual stresses using the hole-drilling method. Part II - practical application of the integral method,” J. Eng. Mater. Technol., vol. 110, no. 4, pp. 344-349, 1988.

[18] G. S. Schajer, “Advances in hole-drilling residual stress measurements,” Exp. Mech., vol. 50, no. 2, pp. 159-168, 2010.

[19] International Digital Image Correlation Society, “A Good Practices Guide for Digital Image Correlation,” 2018.

[20] P. L. Reu, W. Sweatt, T. Miller, D. Fleming, “Camera system resolution and its influence on digital image correlation," Exp. Mech., vol. 55, pp. 9-25, 2015.

[21] M, Pástor, M. Hagara, I. Virgala, A. Kal’avský, A. Sapietová, L. Hagarová, “Design of a Unique Device for Residual Stresses Quantification by the Drilling Method Combining the PhotoStress and Digital Image Correlation,” Materials, vol. 14, no 2, pp. 314, 2021.

Proceedings of the European Nuclear Young Generation Forum
ENYGF'21
September 27-30, 2021, Tarragona, Spain

Radioactive Byproduct Characterization – Are the Data Good?

Hylko, James M.*

JJE, LLC, USA

*Corresponding author: *JHylko1@msn.com*

I. INTRODUCTION

Radioactive byproduct characterization is the quantification of samples comprised of solid, liquid, and gaseous matrices collected from commercial nuclear plants and fuel cycle facilities. Quantification involves measuring and reporting the collected representative sample results in response to a particular metric, such as:

- Monitoring radioactive byproduct concentrations per volume in reactor coolant system samples collected over specified intervals to either confirm steady-state operating conditions or to ascertain suspect perturbations.
- Substantiating container-waste matrix stability and radioactive byproduct concentrations per weight or volume that are suitable for final disposal in an engineered surface or below-grade landfill-type facility.

Verification and validation, consisting of quality assurance objectives (e.g., precision, accuracy, representativeness, completeness, comparability) and measurement quality objectives specific to the measurement method (e.g., radioactive byproduct quantification in the presence of interferences, method uncertainty) contribute to robustness in the numbers themselves. This information can then reliably be used to authenticate the characterization data package [1] [2] [3].

Depending on interim or final container-matrix disposition, the verified and validated concentrations and external radiological survey results are compared against transportation limits, interim storage facility license requirements (if permanent disposal is not immediately available), and disposal site waste acceptance criteria (WAC) "endpoints" [4]. Using the characterization data package to assign the correct waste classification is a common container-matrix "endpoint" [5]. Additional regulatory compliance "endpoints" at the receiving facility can consist of securing container lids with tamper-proof seals; setting and hardening of a solidification agent to prevent radioactive byproduct migration and ground surface collapse; and preserving the container-matrix in a stable, safe, and secured configuration - possibly for decades - prior to final disposal.

"Endpoint" confirmation before site departure is absolutely necessary to prevent transportation disruptions and container-matrix rejection upon arrival, that can also lead to schedule delays and costly regulatory fines. "Endpoint" confirmation begins with defining WAC requirements, then navigating in reverse to representative sample collection (e.g., matrices, amounts, volumes, preservation) that is in concert with your characterization program (e.g., radioactive byproduct measurement and interference resolution capabilities, verification and validation processes, application of scaling factors, reporting results and uncertainties).

Characterization guidance has been published for distinguishing building surface areas and soil measurements near background levels [6]. However, conditions to acquire a representative sample collected from an operating nuclear plant sample panel or radioactive byproduct collection system can vary significantly [7]. Also, data generated at any interim stage without proper context can disqualify confidence in the entire characterization process [8].

II. THE DATA QUALITY OBJECTIVES (DQO) PROCESS

Providing context to achieve matrix characterization regulatory compliance "endpoint" confirmation is demonstrated using the generic Data Quality Objectives (DQO) process [9]. In this paper, two prevalent commercial nuclear plant waste stream profiles are presented that demonstrate how to customize the DQO process by using the represented iterative steps to capture evidence and substantiate sampling and data quality requirements:

A. Decision Inputs
B. Physical Boundaries
C. Characterization Method, Performance and Acceptance Criteria
D. Uncertainties and Interferences
E. Decision Statement
F. Continuous Improvement

Outputs from one step may lead to re-examining prior steps, with the intention of answering the question, "Are the data

good?" The two prevalent commercial nuclear plant waste stream profiles follow:

Profile A: Contaminated protective clothing (CPC) - low activity, low external survey dose rates, fixed and removable contamination. Source term concentrations, volumes, and weights can vary depending on routine (e.g., general housekeeping) vs. scheduled outage activities (e.g., replacing reactor coolant pump seals). Doffing station collection containers are processed daily. The CPC can either be sent to a licensed laundry facility for washing then reused, or disposed if unsalvageable for repair.

Profile B: Spent ion-exchange resins - high activity, high external survey dose rates, hot particles, removable contamination. Source term concentrations and tank volumes are constant. Spent resins are replaced during scheduled plant outages.

A. Decision Inputs

State the Problem: What is the required information necessary to achieve regulatory compliance "endpoints" combining transportation, facility receipt and disposal requirements?

State the Goal: The matrix is stable (√), waste container is accepted for transportation and disposal (√), verified and validated characterization data package (√), securely containerized matrix ready for off-site shipment (√), complies with applicable transportation regulations (√), facility license receipt requirements (√), and disposal site WAC (√).

Operational history shows that **Profile A**, when shipped for disposal, has been classified as either very-low-level radioactive waste or low-level radioactive waste. Instead of disposal, the CPC will be shipped using industrial packaging to a licensed CPC laundry facility for cleaning, and then returned to the nuclear plant for reuse. The laundry facility possesses a "maximum amount of radioactive byproducts all at any one time" facility license.

Profile B is being shipped using a high integrity container for below-grade disposal and has been previously classified as either low-level radioactive waste or intermediate-level radioactive waste according to the disposal site WAC. Additional considerations include waste matrix stability and packaging requirements. While DQOs consider a combination of parallel factors influencing characterization, such as matrix stability affecting attenuation, high-activity source terms can impact employee safety when optimizing sample sizes and counting times to reduce uncertainties.

B. Physical Boundaries

Profile A: Radtech employees are trained, qualified and authorized using procedures and calibrated equipment to survey 208-litre (L) collection containers (e.g., exterior dose rates, removable contamination), and can visually screen containers on a routine schedule to prevent spill over. Two-person teams and carts contribute to reducing ergonomic injuries from excessive bending and when lifting heavy containers. Collection container contents are screened in a dedicated sorting area equipped with high-efficiency particulate air (HEPA) filtered ventilation to prevent airborne dispersion of removable radioactive byproduct contamination and then repackaged. Also, the sorting process eliminates matrix non-uniformity, and reduces costs from inadvertently shipping unauthorized and unsalvageable items to the laundry facility. Container lids are secured with tamper-proof seals and surveyed for release. Fully-loaded containers are then staged and secured on a placarded truck for off-site shipment.

Profile B: Radwaste engineers are trained, qualified and authorized using procedures to remotely operate the liquid waste management system that filters activation, corrosion and fission products through ion-exchange resins. The system is checked and maintained using a preventive maintenance schedule. The media at the top (inlet side) of the resin bed concentrates radioactive byproducts and particulate material compared to the tank bottom. Spent resins are transferred to a holdup tank, allowing for a 30-day decay of short-lived radioactive byproducts. Mixing during transfer eliminates layering, hot spots, and channelling to produce a uniform, homogeneous matrix. The spent resin is sampled for analysis with collection sizes varying up to 200 grams for low-activity resins, and 1 gram for high-activity resins. Chain-of-custody protocols are being followed. Also, very high gamma-ray emission rates may saturate the detector analytical capability, and even mask the presence of radioactive byproducts required to be reported on the disposal manifest.

C. Characterization Method, Performance and Acceptance Criteria

For Profiles A and B, characterization methods can range from simple hand-held instrumentation to sophisticated non-invasive screening systems using manufacturer's specifications and standard operating procedures. Performance and acceptance criteria include, but is not limited to, detecting and identifying radioactive byproducts of interest; consistent geometries (e.g., distance, spacing); and factor-of-10 lower detection limits compared to regulatory action limits [10].

Profile A: The collection containers are emptied, and the CPC is sorted to remove unauthorized items, then repackaged into 208-L industrial packaging containers authorized for shipment and disposal. The repackaged containers are analyzed non-intrusively using a camera-based radioscopic/tomographic system producing internal 2-D or 3-D images that qualitatively confirm uniform distribution. A known radioactive transmission source corrects for matrix attenuation. Performance Demonstration Programs place traceable standards at different positions inside equivalent-matrix-type packages declaring results are within precision and accuracy requirements. These features can be universally applied to other containerized waste profiles destined for shipment and disposal.

Profile B: A resin sample is analyzed using an in-house gamma-ray detector system. Considerations are made to minimize detector dead time and spectral interferences for high-activity resins.

Following gamma-ray analysis, scaling factors are applied correlating KEY (i.e., easy-to-measure) gamma-emitting radioactive byproducts, such as Co-60 or Cs-137/Ba-137m with difficult-to-measure (DTM) low-energy, alpha- and beta-emitting radioactive byproducts.

Both profile data packages are independently reviewed, organized and formatted for reporting results and uncertainties for a particular sample, waste package geometry, and/or matrix to achieve quality assurance objectives (QAOs) - accuracy, precision, bias; and measurement quality objectives (MQO) - calibration, method uncertainty, and radioactive byproduct detection capability to support DQOs. Control charts, for example, are used to monitor method stability and identify adverse trends requiring corrective action.

D. Uncertainties and Interferences

Profile A: The CPC is sorted and uniformly distributed in the container as part of the characterization and repackaging process to remove unauthorized items. Resampling is not required since the container contents are verified visually from repackaging and 2-D imaging. Recharacterization is not required derived from instrumentation control chart parameter stability.

Profile B: Transferring spent resins to the holdup tank for sampling eliminates layering, hot spots, and channelling producing a uniform, homogeneous matrix. Once the shipment schedule is confirmed, the resins are transferred into a high integrity container and mixed with a solidification agent to comply with disposal site WAC stability criteria. Survey readings from multiple exterior container locations are consistent indicating a uniform matrix distribution. Therefore, resampling and recharacterization are not required. After the matrix cures into a solidified monolith, a bridge crane transfers the container from a shielded interim storage area to a shielded cask anchored to a placarded flatbed trailer stationed in the truck bay for offsite shipment. During this transfer, reactor control room radiological area monitors are reporting expected results. Contamination and dose rate surveys in the truck bay are conducted routinely in preparation for off-site shipment and to confirm the absence of any detectable removable contamination.

Since each profile had an operational history of having two distinct waste classifications, consider corrective actions in advance of discovering an off-normal event yielding a profile misclassification that exceeds transportation, facility license limits, and disposal site WAC (e.g., detector deterioration, fuel cladding failure, CRUD burst – [Chalk River Unidentified Deposits consisting of corrosion products transported to the reactor core region, activated by neutron capture, and adhering to surfaces. A "CRUD burst" is a relatively large, rapid re-suspension of CRUD into the reactor coolant by chemical shock, thermal shock or mechanical shock [11]).

E. Decision Statement

IF the characterization DQOs are met, **THEN** the characterization process is considered complete.

IF the characterization DQOs are not met, **THEN** the deficiencies are tracked and resolved according to the corrective action processes.

For these two scenarios, the characterization DQOs are met granting authorization to proceed with transportation; facility receipt; and disposal site WAC acceptance.

F. Continuous Improvement

Because of limited in-house capability, a screened and approved offsite laboratory conducts destructive analysis quantifying KEY and DTM radioactive byproduct scaling factors, and independently verifies and validates the on-site characterization measurement program. Verifying offsite laboratory accreditation to analyze specific samples, and adding to the Approved Suppliers List is performed in cooperation with the Quality Assurance and Procurement Departments. Operational history is continuously recorded for both profiles to reveal adverse trends and significant changes. Scaling factors are updated every plant outage.

III. CONCLUSION

Two nuclear plant waste profiles, **Profile A** consisting of CPC and **Profile B** comprised of spent resins, were evaluated for compliance with transportation regulations, facility license receipt requirements, and disposal site WAC "endpoints" using the DQO process. The information was evaluated and reported with proper context to achieve our decision statement (DQOs are met), and conclude with confidence, "The data are good!"

IV. REFERENCES

[1] Determination and Use of Scaling Factors for Waste Characterization in Nuclear Power Plants, International Atomic Energy Agency, Vienna, Austria, IAEA Nuclear Energy Series, No. NW-T-1.18, 2009.

[2] Strategy and Methodology for Radioactive Waste Characterization, International Atomic Energy Agency, Vienna, Austria, IAEA-TECDOC-1537, 2007.

[3] Multi-Agency Radiological Laboratory Analytical Protocols Manual (MARLAP), U.S. Environmental Protection Agency, et al., NUREG-1576, EPA-402-B-04-00lA, NTIS-PB2004-105421, July 2004.

[4] The IAEA Online Information Resource for Radioactive Waste Management, newmdb.iaea.org. [Accessed April 3, 2021].

[5] Classification of Radioactive Waste, International Atomic Energy Agency, Vienna, Austria, IAEA Safety Standards Series No. GSG-1, 2009.

[6] Multi-Agency Radiation Survey and Site Investigation Manual (MARSSIM), U.S. Nuclear Regulatory

Commission, Rockville, Maryland, NUREG-1575, Revision 1, August 2000.

[7] C.C. Lin, *Radiochemical Technology in Nuclear Power Plants*, American Nuclear Society, La Grange Park, Illinois. 2013.

[8] T. Kalinowski, D.W. James, "Building Context for Radioactive Waste Characterization," Paper 14040 in *Waste Management Symposia 2014 Conference Proceedings, WM2014, Phoenix, AZ, USA, March 2-6, 2014*, wmsym.org. [Accessed April 3, 2021].

[9] Guidance for the Data Quality Objective Process, U.S. Environmental Protection Agency, Washington, DC, EPA-QA/G-4, August 2000.

[10] S.H. Fong, J.L. Alvarez, "When is a Lower Limit of Detection Low Enough?", Health Phys., 72(2), pp. 282-285, February 1997.

[11] *Radioactive Waste Management Technology*, Chapter 3: LWR Chemistry, U.S. U.S. Nuclear Regulatory Commission, Rockville, Maryland. www.nrc.gov/docs/ML1215/ML12151A436.pdf. [Accessed June 11, 2021].

Proceedings of the European Nuclear Young Generation Forum
ENYGF'21
September 27-30, 2021, Tarragona, Spain

Study of radium behaviour in contact with the cementitious phase CSH

Kittnerová, Jana[1*], Drtinová, Barbora[1], Štamberg, Karel[1], Evans, Nicholas[2], Deissmann, Guido[3] and Lange, Steve[3]

[1] Czech Technical University in Prague, Czech Republic; [2] Centre for Environment Fisheries and Aquaculture Science, United Kingdom; [3]Forschungszentrum Jülich, Germany

*Corresponding author: *Jana.Kittnerova@fjfi.cvut.cz*

I. Introduction

Cementitious materials are important barriers in repositories for low and intermediate level radioactive wastes, where ^{226}Ra can be one of the contaminants of concern. Moreover, they are intended also for use as structural support and plugs, or in some cases also as backfill material and buffer, in deep geological repositories for high-level radioactive waste and spent nuclear fuel. Regarding spent nuclear fuel, ^{226}Ra will possibly be a one of the most important contributors to dose in the long term due to the large amount of ^{238}U present. [1]–[3]

For the assessment of the long-term safety of a repository, the retardation mechanisms of radionuclides on cementitious materials within the engineered barriers need to be understood. Thus, the sorption behaviour of Ra, Ba and Sr on *calcium silicate hydrates* (CSH), which form the predominant hydration product in hardened cement pastes (HCP) besides portlandite ($Ca(OH)_2$), AFm (aluminate ferrite monosulphate) or ettringite (AFt), was investigated. In addition to research on HCP and concrete made from commercial cements, studies on individual hydration phases can provide further insights into the radionuclide retention mechanisms. [4], [5]

Studies on Ra sorption on cementitious materials are quite rare. Due to the facilitation by working with (inactive) Sr and Ba, which are considered as chemical analogues of Ra, ([6], [7]), these are more often used in sorption studies. Ra and Sr (and probably also Ba) sorption on CSH phases, and accordingly on HCP, is probably governed by cation exchange of e.g., Ra^{2+} vs. Ca^{2+} on edge and planar silanol groups of the CSH phases ([8], [9]). These groups are deprotonated under the alkaline conditions in cementitious systems and their negative charge neutralized e.g. by Ca. The exchange proceeds as described for Ra in Eq. (1)

$$\text{Ca-CSH} + Ra^{2+} \Longleftrightarrow \text{Ra-CSH} + Ca^{2+} \quad (1)$$

Distribution ratios for alkaline earths elements on pure CSH phases are higher compared to commercial cementitious materials. The range of distribution ratios of Ra for pure CSH phases was determined to be in the order of 10^2-10^4 L kg^{-1} depending on the C/S (Ca/Si) ratios of CSH, with higher R_d values at lower C/S ([4], [8]). R_d's of ^{226}Ra for CSH with C/S ratios of 1.4 and 0.9 are in the order of 10^3 and 10^4 L kg^{-1}, respectively. R_d values of Sr for CSH were determined in several studies ([7], [10]). Here, the R_d values were also dependent on the C/S ratios and significantly lower than those for Ra – R_d values for C/S 1.4 are about 100 L kg^{-1} and for C/S 0.9 up to 10^3 L kg^{-1}. Ba sorption on CSH is reported in [11], where the R_d's are in the range of 10^3-10^4 L kg^{-1} for C/S ratios of about 0.9, the R_d for higher C/S ratios can be expected to be lower.

In addition to obtaining values of R_d under various conditions, the aim of the work is to evaluate the effect of temperature on the sorption of Ra on CSH and to estimate the related equilibrium, kinetic and thermodynamic quantities.

II. Materials and methods

A. CSH

Synthetic CSH phases with different C/S ratios (i.e. 0.9, 1 and 1.4) were prepared following the procedure of [12] as described in detail in [4], i.e. synthesized from CaO (produced from ignited $CaCO_3$), amorphous fumed SiO_2 and deionized H_2O in inert gas atmosphere.

B. Radionuclides

The isotopes of interest, i.e., ^{226}Ra, ^{90}Sr and ^{133}Ba were studied to compare their sorption isotherms on CSH. ^{223}Ra was used as substitute for ^{226}Ra in the experiments to investigate the temperature dependency of Ra sorption. ^{223}Ra is predominantly an α-emitter (half-life = 11.43 days) that decays to ^{219}Rn with a final decay product of ^{207}Pb. The radon isotope ^{219}Rn has a half-life of only 4 seconds. The advantage of the much shorter half-life of ^{219}Rn compared to ^{222}Rn is that it is safer to work with. The isotope ^{223}Ra (commonly used in radiotherapy) was obtained from a ^{227}Ac/^{223}Ra generator consisting of a glass column filled with Dowex-1 × 8 resin. Elution of ^{223}Ra was carried out with 0.7 mol L^{-1} nitric acid in 80% methanol.

The eluate was evaporated to dryness in a vacuum evaporator and then dissolved in 1 mol L^{-1} nitric acid [13].

C. Methods

All sorption experiments were of batch type and carried out in plastic ampoules under inert gas atmosphere in a glove-box, as CSH is sensitive to CO_2. After the required reaction time and centrifugation, samples of the liquid phase were taken and analysed for the radionuclide activity.

For the temperature study, sorption experiments were carried out at 22, 50 and 80 °C in saturated CSH solution (pH ~ 11) for 4 days, using liquid to solid (L/S) ratios of 100-1000 L kg^{-1} and ^{223}Ra concentrations of approx. $2.5 \cdot 10^{-12}$ mol L^{-1}. The kinetic experiments (L/S 250 and 500 L kg^{-1}) confirmed that the duration was appropriate to achieve close-to-equilibrium state (i.e. virtually zero concentration changes). Due to the relatively short half-life of ^{223}Ra, the observed decrease of radioactivity in the liquid phase caused by the Ra uptake on the solid cementitious material had to be decay corrected. Furthermore, the sorption on the walls of the experimental vials was determined across all conditions and included during evaluation of the experiments, the value is 10 %.

The comparison of the sorption of Ra (^{226}Ra), Sr (^{90}Sr) and Ba (^{133}Ba) was performed using an L/S ratio of 200 L kg^{-1} with radionuclide concentrations in the range of $4 \cdot 10^{-10}$-$8 \cdot 10^{-7}$ mol L^{-1}, which were achieved in the cases of Sr and Ba by the addition of a carrier ($Sr(OH)_2$ and $Ba(OH)_2$, respectively). These sorption studies were performed at room temperature and lasted for three weeks (approx. 500 hours).

D. Detection

Ra and Ba isotopes in the liquid phase were measured by gamma spectroscopy mostly with HPGe detectors (^{226}Ra: HPGe detector system, type: EGC 35-195-R, EurisysMesures, spectrometer system obtained from EG & G Ortec, GammaVision® Modell A66-B32 software version 5.20, ^{223}Ra: HPGe detector system, type GEM40P4 with Ortec DSPEC jr 2.0, Maestro software version 7.0, or NaI(Tl) well type detector; ^{133}Ba: HPGe detector, PGC 2018, DSC: detector system GmbH, Gamma-W for Windows version 2.55); for ^{90}Sr liquid scintillation counting (LSC) was used (1220l Quantulus, Perkin Elmer, Winq software version 1.2).

E. Assessment

The uptake of the radionuclides by CSH is characterized here in terms of the distribution ratio, R_d, between liquid and solid phases and calculated according to Eq. (2)

$$R_d = \frac{A_{init} - A_t}{A_t} \cdot \frac{V}{m}, \qquad (2)$$

where A_{init} is the initial activity concentration of the radionuclide in solution, and A_t corresponds to the activity concentration at time t, respectively, both in the unit of activity (Bq), V is the volume of the liquid phase (L), and m (kg) the mass of solid phase used in the experiment.

Beside the R_d value the Langmuir isotherm (Eq. (3)) was used for the description of the sorption at equilibrium state

$$q = \frac{K_L \cdot c \cdot q_{max}}{1 + K_L \cdot c}, \qquad (3)$$

where q is the equilibrium concentration in the solid phase (mol kg^{-1}) (q_{max} – maximum achievable concentration), c is equilibrium concentration in the liquid phase (mol L^{-1}) and K_L is the equilibrium addition reaction constant (L mol^{-1}).

The influence of the temperature on sorption is described using the apparent activation energy E_A (J mol^{-1}) and changes in enthalpy ΔH (J mol^{-1}) and entropy ΔS (J mol^{-1} K^{-1}). Enthalpy and entropy are obtained from the linear dependence of $\ln R_d$ as a function of $1/T$ – Eq. (4)

$$\ln R_d = -\left(\Delta H / R\right) \cdot 1/T + \Delta S / R, \qquad (4)$$

where R is the gas constant (8.314 J mol^{-1} K^{-1}) and T is temperature (K). Equation (4) is derived for low concentrations of a given component in the liquid phase, if the quantity R_d can be considered constant in time for one L/S (thermodynamic relations for the change of free Gibbs energy were used to derive the equation) [14].

Apparent activation energies were derived via the Arrhenius equation by plotting $\ln k$ as a function of $1/T$ – Eq. (5)

$$\ln k = \ln A - E_A / RT, \qquad (5)$$

where k is a kinetic coefficient (s^{-1}) and A is the frequency factor (L mol^{-1} s^{-1}). The kinetic coefficients were determined in the course of the evaluation of kinetic experiments with one of the following models of possible rate-controlling processes: mass transfer (DM), film diffusion (FD), diffusion in inert layer (ID) and chemical reaction (CR). A detailed derivation of the models can be found in [15] and [16], respectively; all models are described in detail also in [17].

III. Results and discussion

A. Temperature

The effect of temperature on radium (^{223}Ra) sorption on CSH C/S 1 was studied and described in the terms of sorption isotherm and estimated values of activation energy, enthalpy and entropy.

Distribution ratio and Langmuir isotherm of Ra sorption on CSH

The R_d values for the sorption of ^{223}Ra on CSH are affected with a considerable error due to the low concentration of Ra in solution (cf. Figure 1, top). Nevertheless, the R_d values determined at 22 °C in the range of 35,000 to 60,600 L kg^{-1}, slightly increasing with L/S ratio, with an average value of $R_{d(22\,°C)}$ = 44,838 ±4,605 L kg^{-1}, are comparable to published data ([4], [8], [18]). Moreover, the significant change in the shape of the ^{223}Ra isotherm with temperature from 22 to 80 °C from convex to concave (cf. Figure 1, bottom) corresponds to the previously determined behaviour of sorption of Ra on real cementitious materials [17].

Activation energy, Enthalpy and Entropy

The entropy and enthalpy of sorption of ^{223}Ra on CSH was determined for L/S ratios within the range of 250-1000 L kg^{-1} using data obtained for 2 or 3 temperatures as shown in Table 1 and Figure 2.

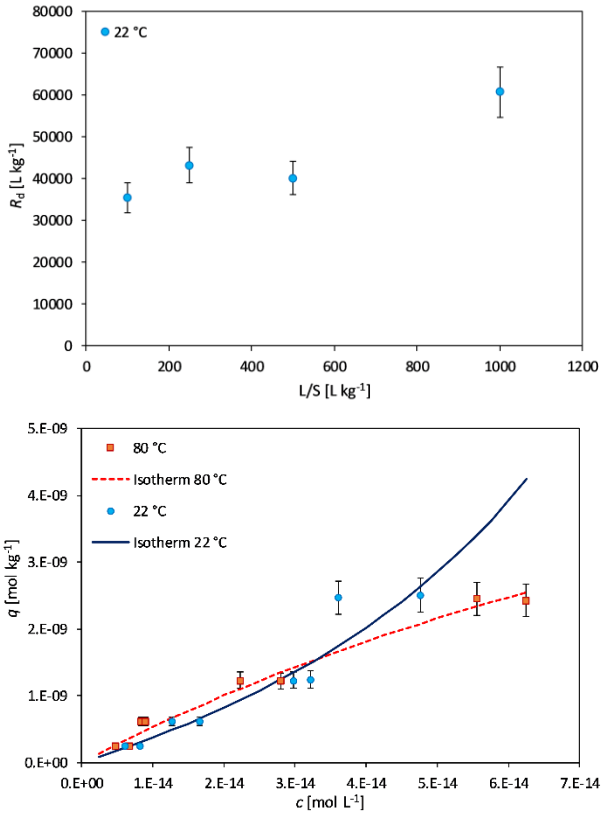

Figure 1. Distribution ratios of ^{223}Ra sorption on CSH (C/S 1) as function of L/S ratio (top) and evaluation of Langmuir sorption isotherm for 22 and 80 °C (bottom). The data points presented in Figure 1 (bottom) are shown here for two parallel determinations to demonstrate the uncertainty more clearly.

Table 1. Entropy and enthalpy of sorption of ^{223}Ra on CSH (C/S 1) at different L/S ratios.

L/S (L kg^{-1})	Temp. used (°C)	ΔH (kJ mol^{-1})	ΔS (J mol^{-1} K^{-1})
250	22, 50, 80	-9.5 ±2	48.5 ±7
500	22, 50, 80	-1.7 ±1	82.6 ±2
1000	22, 80	-5.6 ±2	72.4 ±7

The negative values of ΔH and positive values of ΔS confirmed that Ra sorption on CSH is an exothermic and spontaneous process, respectively.

Activation energies were determined for L/S 250 and 500 L kg^{-1} as described in Eq. (5) and shown in Figure 2. The experimentally measured decreasing concentrations in the liquid phase, $-dc/dt$, were compared to the concentrations computed by the individual kinetic models. The model describing diffusion in an inert layer (ID) was determined as the most convenient based on the value of goodness-of-fit. Kinetic coefficients obtained from this model were used for the evaluation of the apparent activation energy. Values of apparent activation energy were determined as $E_{A(L/S\ 250)}$ = 24.5 ±3 kJ mol^{-1} and $E_{A(L/S\ 500)}$ = 67.6 ±9 kJ mol^{-1}. These values suggest both diffusion (lower E_A) and chemical reaction (higher E_A) as rate controlling, but the boundary between the processes in terms of E_A values is not exactly clear, thus the rate controlling process has not been convincingly determined in this case and has to be further explored.

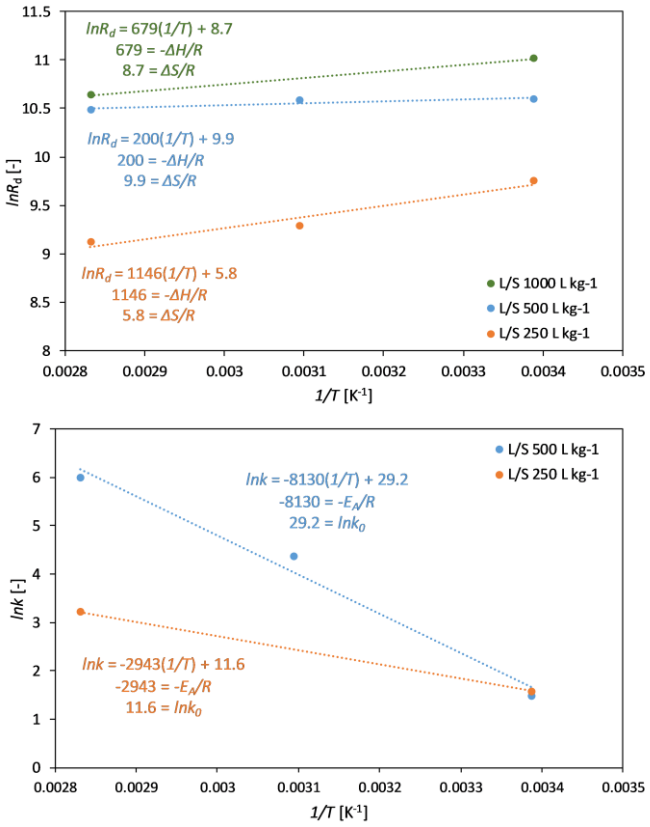

Figure 2. Plots used for the determination of enthalpy, entropy (top) and activation energy (bottom) for sorption of ^{223}Ra on CSH (C/S 1) for L/S 250, 500 and 1000 L kg^{-1}. (Error bars are omitted for the sake of clarity.)

B. Comparison of Ra, Ba, and Sr sorption on CSH

In Figure 3, R_d values for the uptake of ^{226}Ra, ^{133}Ba and ^{90}Sr on CSH (C/S ratios 0.9 and 1.4) are compared (some of the data – ^{226}Ra and ^{90}Sr on CSH C/S 1.4 – has already been published in our previous work [17]).

The comparison confirms 1) Ra sorption as the strongest in the R_d range of thousands L kg^{-1} (average $R_{d(C/S\ 0.9)}$ = 19,374 ±3,750 L kg^{-1}, $R_{d(C/S\ 1.4)}$ = 1,981 ±383 L kg^{-1}) and Sr sorption as the weakest at about 10^2 L kg^{-1} ($R_{d(C/S\ 0.9)}$ = 293 ±18 L kg^{-1}, $R_{d(C/S\ 1.4)}$ = 108 ±7 L kg^{-1}), while distribution ratios for Ba show intermediate values in the range from hundreds to thousands L kg^{-1} ($R_{d(C/S\ 0.9)}$ = 4,919 ±751 L kg^{-1}, $R_{d(C/S\ 1.4)}$ = 636 ±97 L kg^{-1}); and 2) higher R_d values for the CSH with lower C/S ratio. All data obtained are in good agreement with the literature mentioned above (for Ra e.g. [4], [8], for Ba [11] and for Sr [7]). In the investigated concentration range, the sorption isotherms of all elements reveal a Langmuir sorption isotherm approaching a linear shape (it is neither clearly convex nor concave) in the log-log plot in Figure 3. However, though the sorption behaviour of the elements is

similar in principle, the use of Ba or Sr to estimate R_d values of Ra, e.g., for safety assessments, does not seem appropriate.

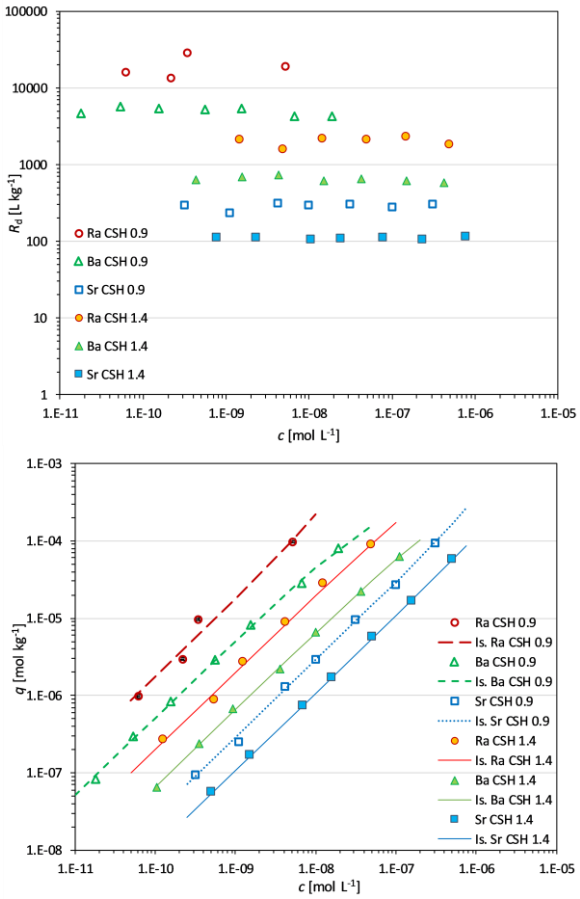

Figure 3. Comparison of sorption of ^{226}Ra, ^{133}Ba and ^{90}Sr on CSH with C/S 0.9 and 1.4 in form of the R_d and Langmuir isotherms. (Error bars are omitted for the sake of clarity because of the logarithmic scale.)

IV. Conclusions

The radium sorption experiments performed at different temperatures showed slight changes in the shape of the isotherm from convex to concave with an increase of temperature from 22 to 80 °C for very low Ra concentrations. An estimate of activation energy, enthalpy and entropy of Ra sorption was made. Sorption of Ra on CSH has the character of an exothermic and spontaneous reaction taking place in the transition region controlled very likely by diffusion and/or a chemical process. The comparison of the sorption of Ra and 2 other alkaline earths elements on CSH confirmed 1) the significant difference between the uptake of Ra, Ba and Sr, with the R_d values decreasing by about an order of magnitude each from Ra via Ba to Sr, but with similar shaped sorption isotherms in the given concentration range; 2) the influence of C/S ratios in CSH on sorption, where lower C/S means higher cation sorption, as expected.

V. References

[1] C. Jantzen, A. Johnson, D. Read, and J. A. Stegemann, 'Cement in waste management', *Adv. Cem. Res.*, vol. 22, pp. 225–231, 2010.

[2] B. Lagerblad, 'Leaching performance of concrete based on studies of samples from old concrete constructions', *SKB TR-01-27.*, p. 85 pp, 2001.

[3] SKB, 'Long-term safety for the final repository for spent nuclear fuel at Forsmark. Main report of the SR-Site project.', *SKB TR-11-01.*, no. March, p. 271 pp, 2011.

[4] S. Lange *et al.*, 'Uptake of 226Ra in cementitious systems: A complementary solution chemistry and atomistic simulation study', *Appl. Geochemistry*, vol. 96, no. March, pp. 204–216, 2018.

[5] M. Atkins and F. P. Glasser, 'Application of Portland cement-based materials to radioactive waste immobilization', *Waste Manag.*, vol. 12, pp. 105–131, 1992.

[6] U. Berner, 'Project Opalinus Clay: Radionuclide concentration limits in the cementitious near-field of an ILW repository', *PSI Bericht Nr. 02-26. 62 pp*, 2003.

[7] J. Tits, E. Wieland, C. J. Müller, C. Landesman, and M. H. Bradbury, 'Strontium binding by calcium silicate hydrates', *J. Colloid Interface Sci.*, vol. 300, pp. 78–87, 2006.

[8] J. Tits, K. Iijima, E. Wieland, and G. Kamei, 'The uptake of radium by calcium silicate hydrates and hardened cement paste', *Radiochim. Acta*, vol. 94, pp. 637–643, 2006.

[9] E. Wieland, J. Tits, D. Kunz, and R. Dähn, 'Strontium uptake by cementitious materials', *Environ. Sci. Technol.*, vol. 42, pp. 403–409, 2008.

[10] T. Iwaida, S. Nagasaki, and S. Tanaka, 'Sorption study of strontium onto hydrated cement phases using a sequential desorption method', *Radiochim. Acta*, vol. 88, pp. 463–486, 2000.

[11] T. Missana, M. García-Gutiérrez, M. Mingarro, and U. Alonso, 'Analysis of barium retention mechanisms on calcium silicate hydrate phases', *Cem. Concr. Res.*, vol. 93, pp. 8–16, 2017.

[12] M. Atkins, F. P. Glasser, and A. Kindness, 'Cement hydrate phases: Solubility at 25 °C', *Cem. Concr. Res.*, vol. 22, pp. 241–246, 1992.

[13] J. Kozempel *et al.*, 'Prospective carriers of 223Ra for targeted alpha particle therapy', *J. Radioanal. Nucl. Chem.*, vol. 304, pp. 443–447, 2015.

[14] P. Distler, K. Stamberg, J. John, L. M. Harwood, and F. W. Lewis, 'Thermodynamic parameters of Am(III), Cm(III) and Eu(III) extraction by CyMe4-BTPhen in cyclohexanone from HNO3 solutions', *J. Chem. Thermodyn.*, vol. 141, 2020.

[15] K. Štamberg and J. Cabicar, 'Models of sorption kinetics in liquid-solid phase systems (in Czech)', *Acta Polytech. - Tech. Univ. Prague*, vol. 8, pp. 107–130, 1980.

[16] R. E. Treybal, *Mass Transfer Operations*. McGraw-Hill, Book Company, New York, 1956.

[17] J. Kittnerová *et al.*, 'Comparative study of radium and strontium behaviour in contact with cementitious materials', *Appl. Geochemistry*, vol. 122, p. 104713, 2020.

[18] J. Olmeda *et al.*, 'Radium retention by blended cement pastes and pure phases (C-S-H and C-A-S-H gels): Experimental assessment and modelling exercises', *Appl. Geochemistry*, vol. 105, pp. 45–54, 2019.

Proceedings of the European Nuclear Young Generation Forum
ENYGF'21
September 27-30, 2021, Tarragona, Spain

Bottom Drain Melters for Solidifying HLW into Borosilicate Glass

Shaydullin S.M.[1*], Remizov M.B.[1], Kozlov P.V.[1], Melentyev A.B.[1], Verbitskiy K.V.[1], Bendasov D.I.[1], Rebrin M.A.[1]

[1] FSUE Mayak Production Association (FSUE Mayak PA), Russia

*Corresponding author: *cpl@po-mayak.ru*

I. INTRODUCTION

One of the most difficult and challenging problems related to development of nuclear power engineering is isolation from the biosphere of a large amount of radionuclides generated as a result of fission of uranium nuclei. Suffice it to say that, already by the end of the 1990s, only in Russia radioactive waste with a total activity of about $1.5 \cdot 10^9$ Ci had been accumulated. More than 90 % of this accumulated activity resulted from production of weapons-grade plutonium. About 15,000 t of SNF from nuclear power plants and naval propulsion reactors accumulated by 2004 should be regarded as another potential source of radioactive waste. This waste is currently held at interim storage facilities and subject to reprocessing [1].

It is known that more than 99 % of the total activity of generated fission products is concentrated in liquid HLW. According to the IAEA regulations, liquid HLW is to be solidified [2]. The primary goal is to reduce the HLW volume as much as possible and to carry out the HLW conditioning, i.e. conversion of radioactive waste into a chemically stable and radiation-resistant form maintaining its stability throughout the entire storage period.

Two process technologies for immobilization of HLW in glass matrices have been implemented by now. Facilities for immobilization of HLW in borosilicate glass are operated in France and the Great Britain [3]. In Russia the Mayak PA has introduced a technology of immobilization of HLW in aluminophosphate glass [4].

A new vitrification complex is planned to be constructed at the Mayak PA in 2028 that will be versatile in terms of composition of liquid HLW intended for solidification. For example, small-size borosilicate glass melters with direct electrical heating are assumed to be used for solidification of liquid HLW generated as a result of reprocessing of SNF from power reactors (VVER-440, VVER-1000, BN-600, BN-800) [5]. Borosilicate glasses demonstrate a unique combination of characteristics that makes them almost ideal for fulfilling the above mentioned purpose. Borosilicate glasses containing nuclear waste are as durable as basalts, which are millions years old, and, therefore, are expected to be long-lived themselves. These glasses display a capacity for dissolving a full range of nuclear waste. At that, they can do this task at temperatures which are hundreds degrees lower than those required for producing similar silicate glasses without boron. For example, a glass melt temperature will be maintained at 1,150 °C in case of borosilicate glasses, whereas basalt glasses (similar glasses without boron) would require a melting temperature of about 1,350 °C. At such a high temperature, none of the volatile radionuclides (such as Cs and Ru) will be retained in the glass [6].

The design-basis procedure of dismantling, disassembling and removing is to be developed for these melters to ensure compliance with the environmental regulations and to provide cost saving by construction of new facilities due to reuse of a considerable part of the infrastructure [5].

Solidification of other types of liquid HLW is planned through the development of aluminophosphate glass EP melters, the design of which will provide for an inherent procedure of dismantling upon completion of the service life.

Thus, in the coming decade the main method for HLW solidification in Russia will be based on the technology of radiactive waste vitrification in melters with direct electric heating. At that, a range of glasses applied for vitrification and characteristics of waste intended for solidification will be expanded.

II. APPROACHES FOR VITRIFICATION OF HLW AT THE MAYAK PA

The paper describes the current state of the HLW vitrification technology implemented at the Radiochemical Plant of the Mayak PA. Conceptual and technical approaches are considered to developing the technology for vitrification of different types of liquid HLW at the Mayak PA. Main technical differences are given that distinguish the promising removable small-size melter from facilities used at the enterprise earlier. Main results of the prototype melter testing as well as prospects for continuation of work in this area are presented.

III. RESULTS AND DISCUSSION

Vitrification of liquid HLW has been carried out at the Mayak PA on the industrial scale from 1987. Immobilization of liquid HLW of the Radiochemical Plant in stable matrix materials is implemented using nonremovable melters with direct electric heating of the EP-500 type. Over the past period of time, four such melters have reached the end of their design service life and have been decommissioned. The fifth EP-500/5 melter was stopped in 2020. As a result of operation of melters of this type, over a period of 20 years (efficient time of the equipment operation), 35,000 m^3 of LRW was solidified; more than 8,000 t was produced of highly active aluminophosphate glass containing radionuclides, total activity of which, at the moment of vitrification, was more than 800 million Ci (Figure 1) [7].

Figure 1. Results of operation of HLW vitrification melters at the Mayak PA.

The sixth industrial-scale electric melter EP-500/6 is scheduled for commissioning for 2023. Its design service life is 6 years; glass throughput capacity is up to 720 t/year (100 kg/h); solution throughput capacity is 350 L/h, its weight is 130 t; fluxing additives are to be introduced in liquid form.

The electric furnace EP-500/6 is the last nonremovable melter of this type. Next generation of electric melters should have the design-basis procedure of dismantling, disassembling and removal to ensure compliance with the environmental regulations and to provide cost saving by construction of new facilities due to reuse of a considerable part of the infrastructure.

And yet, at the Radiochemical Plant, the following issues related to development of the vitrification technology stay relevant and require solutions:

1. To enable immobilization of all types of produced liquid HLW.

2. To introduce a technology ensuring return of vitrified HLW generated during reprocessing of foreign SNF to the country of its origin.

3. To switch from nonremovable melters to small-size removable facilities.

The above mentioned tasks are to be addressed in the course of construction of a new vitrification complex commissioning of which is tentatively scheduled for 2028. According to the developed concept of the new vitrification complex, it is planned to use a removable small-size melter with direct electric heating with a throughout capacity in terms of evaporated solution of about 20 L/h.

The melter is designed for melting borosilicate glass which has the following advantages over aluminophosphate glass: significantly higher capacity of incorporation of fission products, chemical stability, radiation resistance, and resistance to decrystallization [8]. At the same time, borosilicate glass has a higher melting temperature (ranging from 1,100 °C to 1,200 °C).

The melter under discussion is a small-size vitrification furnace of direct electric heating with a capacity of 250 kW. The melter design provides for its removal into a container (transport package) upon completion of its service life. The melter is fitted with an outer stainless steel shell and corrosion-resistant nickel-chromium alloy electrodes. The electrodes and melter bottom are cooled with dehydrated compressed air.

The melter has a funnel-shaped melting pool made of refractory ceramic blocks with additional thermal insulation (Figure 2).

Figure 2. Melter pool made of refractory ceramic blocks.

The melter is equipped with a bottom drain valve with an inductively heated outlet channel (Figure 4).

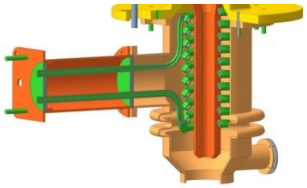

Figure 3. Bottom drain system equipped with an inductively heated outlet channel.

The cooling system of the induction heater uses water and contains two circuits. Vitrification is carried out as glass frit melts and mixes with the HLW solution. Discharge of molten glass into a canister is ensured by heating the drain valve outlet channel. The canister is pressed against the bellows expansion joint to avoid contamination of the melter chamber. Glass discharge is stopped by a simultaneous shutdown of the induction heater and closure of cooling air supply to the specially designed cavities of the facility.

Design work on this melter began in 2015. Two full size prototypes have been already developed and tested by now to optimize the main design solutions.

In 2018-2019, the first prototype of the removable small-size melter was tested. In the course of its operation, a considerable data set was obtained concerning electrical and thermal parameters of the melter. Optimal electrical and time parameters of the electric melter control system were

found. Preliminary (start-up) heating of the melter process zone loaded with glass frit was worked out using silicon-carbide heaters. Process of glass melting by means of air-cooled nickel-chromium electrodes was studied including loading of frit and measuring the glass melt level. Performance of all the electrodes was verified. Different interconnections of the electrodes were tested. Operation of the first prototype lasted for 120 days.

Based on data obtained in 2019-2020, the second melter prototype was updated and tested. All primary and auxiliary systems of the melter pilot unit were checked. Procedures of the melter brickwork drying and glass frit loading, heating and melting were carried out.

Maximum water evaporation efficiency of the melter was determined to be 25 dm^3/h. In the course of dosing procedure, temperature parameters of the melter and temperature of the gas mixture were monitored, surface of the glass melt was visually observed via an auxiliary port in the melter cover. Each dosing stage lasted for 12 hours to ensure stabilization of temperature parameters. Efficiency of the evaporation process was determined based on the melter temperature parameters (temperature of the glass melt and temperature of the gas phase) as well as on area of a cooled glass spot on the glass melt surface.

Throughput capacity in terms of initial solution containing fluxing additives (sodium carbonate and borax) was determined at simultaneous dosing of dry glass frit to the melter. Throughput capacity at simultaneous dosing of salt solution (containing 144 g/dm^3 of sodium carbonate and 36 g/dm^3 of borax) and glass frit was 15 dm^3/h and 10.5 kg/h, correspondingly.

Optimum conditions for discharge of molten glass and for stop of the glass discharge were identified as applied to the second melter prototype.

Performance capacity of the system for dosing dry reagents and glass frit was evaluated. The system provides for dosing of specified weighed portions of reagents at given time intervals.

A set of three discharge procedures was carried out with a stepwise increase in viscosity and melting temperature of the glass melt due to dosing of the glass frit without fluxing solution added. It was noted that start-up of glass discharge took more time, and that molten glass flow rate from the drain valve outlet channel decreased significantly.

Two experiments were conducted on sedimentation and discharge of the powder simulating the disperse phase of noble metals that are contained in HLW resulted from SNF reprocessing. It was determined that during discharge the fine-dispersed powder was distributed in the glass melt rather uniformly, and that deposition and sedimentation of the powder particles in the melter lasted for less than four hours. The bottom drain valve design ensures efficient removal of metal particles from the melter with the glass melt flow.

Stop of the discharge flow took from 2 to 10 minutes. Temperature of the glass melt, glass viscosity and cooling air flow rate supplied to blow off the drain valve outlet channel are the main factors that have impact on speed of the discharge halt.

Table 1 presents the composition of glass frit used during tests (this is a new formula that is different from the one used with the old melters).

Table 1. Composition of glass frit used in tests.

Mass concentration of the element oxide, wt %					
SiO_2	B_2O_3	Al_2O_3	CaO	Na_2O	MgO
44.53	21.36	3.90	4.53	25.12	0.56

Transition of the substance to a glassy state requires, first, melting of the substance and then, by supercooling of the obtained glass melt, producing hard glass. Variation of glass melt viscosity within the glass-transition range is of great importance here. Viscosity of the glass melt considerably determines the rate of glass melting. Rate of dissolution and chemical interaction of components in the melt and rate of diffusion processes increase as glass melt viscosity decreases. Figure 4 shows dependence of borosilicate glass viscosity (described in Table 1) on temperature.

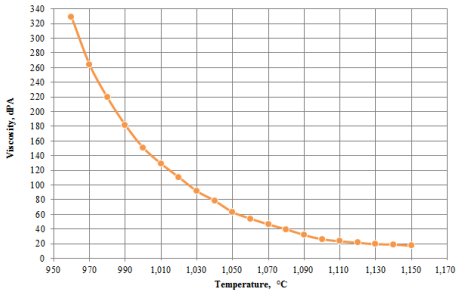

Figure 4. Temperature dependence of viscosity.

As viscosity of silicate glasses depends on strength of chemical ionic bonds and degree of connectivity of the silicon-oxygen structure [9], oxides of alkali metals and metals of group II (of alkaline earth MgO, CaO, SrO, BaO and of auxiliary subgroup: ZnO, CdO) decreases viscosity. At that, impact of Zn, Cd and Pb oxides is stronger as compared to that of alkaline earth ones, however, in the region of low temperatures, their effect is rather ambiguous. Introduction of refractory oxides $A1_2O_3$, SiO_2 and ZrO_2 results in increased viscosity [10]. According to [7], glass melt viscosity in the working range of glass production from 900 °C to 1,100 °C should be less than 100 dPa to ensure controlled discharge, and at the same time there should not be any sharp increases in viscosity within the given range.

In compliance with State Standard GOST R 52126-2003 [11], chemical stability of the applied glass was studied to evaluate rate of radionuclide leaching from specimens which were in prolonged contact with water. The contact solution was changed in 1, 3, 7, 10, 15, 21, 28, 35, 56 and 90 day(s) counting from the beginning of the experiment. Upon completion of the specified period, the solution was decanted and analyzed in terms of content of the elements by the ICP-MS method.

Figures 5 and 6 show time dependence of rate and degree of leaching of macrocomponents (Na, B) from the glass.

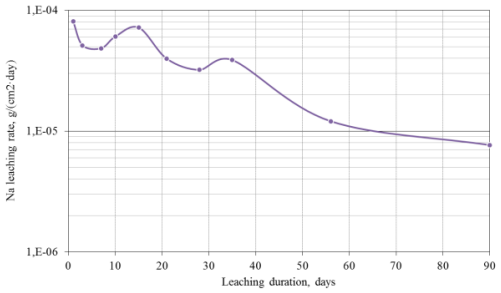

Figure 5. Time dependence of sodium leaching rate.

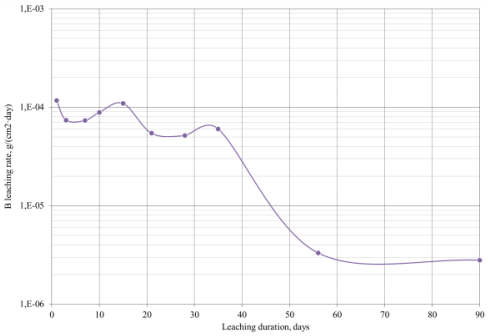

Figure 6. Time dependence of boron leaching rate.

Results of leaching were analyzed based on the following assumptions. As regulatory requirements [12] impose limitations only on individual radionuclides (^{137}Cs, ^{90}Sr and ^{239}Pu), when leaching of stable elements was evaluated, they were grouped in terms of similarity of their chemical properties with those of the mentioned radionuclides, for example, based on the type and characteristics of bonds with other components in the glass structure. In this context, it follows that sodium is close to cesium, while magnesium is close to strontium.

The provided data demonstrate that increased mass fraction of sodium oxide in borosilicate glasses is accompanied by decreased chemical stability of these glasses.

Rate of sodium and boron leaching was lower than the regulatory value already on the 21 day. It was noted that boron behavior at leaching was identical to that of sodium.

IV. CONCLUSIONS

A test bench was commissioned to verify the melter design and validate the glass melting technology. Thermal and physical characteristics of the melter brickwork were obtained. Electrical parameters of the melter operation were studies. Process monitoring and control systems were worked through as well as systems of cooling of the melter structural components, glass frit feed, solution feed and molten glass discharge.

It was found that viscosity of the examined glass composition varied from 25 dPa to 100 dPa in the temperature range from 1,030 °C to 1,100 °C. It follows that the glass under consideration does not have appropriate chemical stability.

Development of an industrial-scale prototype is underway in which results of the undertaken tests are taken into account. The changes were introduced concerning the design and refractory materials of brickwork of the melter, assemblies of feeding of glass frit and solutions, individual elements of the cooling system, bottom drain system as well as systems for monitoring glass melt level and temperature. Testing of the new small-size melter prototype is scheduled for 2022. Work on the composition of glass matrix with a decreased melting temperature will be further continued to ensure matrix chemical stability and compliance with the regulatory requirements.

V. REFERENCES

[1] M. I. Solonin, “Current state and development trends of nuclear fuel cycle in Russian and world’s energy sector”, in *Nuclear Energy*, vol. 90, iss. 6, pp. 448 – 459, 2005.

[2] *Underground Disposal of Radioactive Waste: Basic Guidanc*e. Vienna: IAEA, 1981.

[3] J. L. Crandall, H. Krause, C. Sombert, K. Uematsu, “High level waste reprocessing and disposal”, in *Trans. Amer. Nucl. Soc*., vol. 48, pp. 106-117, 1985.

[4] Yu. V. Glagolenko, Ye. G. Dzekun, Ye. G. Drozhko, G. M. Medvedev, S. I. Rovniy, A. P. Suslov, “Strategy of radioactive waste management at the Mayak Production Association”, in *Radiation Safety Problems*, no.2, p.3, 1996.

[5] S. M. Shaydullin, P. V. Kozlov, M. B. Remizov, K. V. Verbitskiy, A. B. Melentyev, D. I. Bendasov, “Melter equipped with the bottom drain system for solidification of HLW in borosilicate glass”, in *Current Challenges of Innovation Development of Nuclear Technologies*: *Proceedings of the Conference in the framework of the NRNU MEPhI Scientific Session*, Seversk, April 8-12, 2019. Seversk: STI NRNU MEPhI, 2019, p. 47.

[6] T. Advocat, J.-M. Delayve, S. Peuget, O. Pinet, X. Deschanels, “Nuclear glass formulation, structure and properties”, in *Nuclear Waste Conditioning*, J.-F. Parisot, Ed. Paris: CEA Saclay and Group Moniteur, 2009, pp. 33-49.

[7] P. V. Kozlov, M. B. Remizov, Ye. A. Belanova, N. V. Vlasova, V. A. Orlova, K. V. Martynov, “Modification of composition of aluminophosphate glasses containing HLW simulators to increase their stability. 1. Impact of modificators on viscosity and crystallization capacity of glass melts”, in *Radiation Safety Problems*, no.1, pp. 3-15, 2019.

[8] A. S. Aloy, A. V. Trofimenko, T. I. Koltsova, M. V. Nikandrova, “Physical and chemical characteristics of vitrified simulated HLW from the Pilot Demonstration Center of the Siberian Chemical Combine”, in *Radioactive Waste*, no. 4 (5), pp. 67-75, 2018.

[9] I. A. Sobolev, M. I. Ozhovan, et al., *Glasses for Radioactive Waste.* Moscow: Energoatomizdat, 1999.

[10] S. A. Dmitriyev, S. V. Stefanovskiy, *Radioactive Waste Management: Study Guide*, Mendeleyev University of Chemical Technology of Russia, Moscow, 2000.

[11] *Radioactive Waste. Determination of Chemical Stability of Solidified High Level Waste by the Method of Long-Term Leaching*, State Standard GOST R 52126-2003. Moscow: Gosstandart Rossii: Izdatelstvo standartov, 2003.

[12] *Collection, Reprocessing, Storage and Conditioning of Liquid Radioactive Waste. Safety Requirements (text)*, Federal Rules and Regulations NP-019-15, entered into force June 25, 2016. Moscow: Rosteckhnadzor Rossii, 2015.

European Nuclear Young Generation Forum
ENYGF'21
September 27-30, 2021, Tarragona, Spain

How should the IAEA Code of Practice on the International Transboundary Movement of Radioactive Wastes, 1991, be Interpreted to Ensure that a Best Available Technique (BAT) is Applied to the Waste Hierarchy?

Clarke Dhadli, Jasvinder[1*]

[1] Frazer-Nash Consultancy, United Kingdom

*Corresponding author: *J.ClarkeDhadli@fnc.co.uk*

I. INTRODUCTION

Sixty one percent (61%) of people surveyed by the European Commission stated that "unsafe disposal of radioactive wastes" was their largest concern with the nuclear industry [1].

The proper disposal of nuclear waste relies on many factors, one of which is local geology. Unlocking the ability to move nuclear waste to a site best suited for its disposal, regardless of international borders, would help open the possibility for more countries to utilise nuclear power. It enables states to become global industry experts in the handling and disposal of radioactive wastes, and profit from this expertise.

In 1989 the Basel Convention on the Control of Transboundary Movements of Hazardous Wastes and their Disposal (henceforth referred to as the Basel Convention) was adopted. It is the most comprehensive global environmental agreement on hazardous wastes and other wastes, but not radioactive wastes. The Convention allows for the transboundary movement of hazardous wastes for disposal under strict regulations [2].

Table 1. Acronyms.

Acronyms	
BAT	Best Available Technique
GDF	Geological Disposal Facility
HLW	High Level Waste
IAEA	International Atomic Energy Agency
ILW	Intermediate Level Waste
LLW	Low Level Waste
NDA	Nuclear Decommissioning Authority
OECD	Organisation for Economic Co-operation and Development
RAG	Red-Amber-Green
SQEP	Suitably Qualified and Experienced Personnel
VLLW	Very Low Level Waste

In 1991 the IAEA Code of Practice on the International Transboundary Movement of Radioactive Wastes (henceforth referred to as IAEA Code of Practice or CoP) was enacted [3]. The text in the CoP is similar to that of the Basel Convention, yet the interpretation is that transboundary movement of radioactive wastes for disposal should be prohibited (except when wastes are being returned following reprocessing procedures such as that previously run by Sellafield Ltd), whereas hazardous wastes can move across borders provided they are handled appropriately. Even though both codes are similar the way they are used is different.

The management and disposal of radioactive wastes is a global issue. The technical solutions for dealing with radioactive waste disposal exist but have often not been accepted by the public. **Table 2** outlines the global radioactive waste inventory as estimated by the IAEA. It shows a large proportion of nuclear waste yet to be disposed of including 100% of HLW. Policies are being introduced by individual states to legislate the disposal of radioactive wastes, one such policy being the construction of GDF's. These policies combat the issue on a state-by-state basis whereas it could be BAT to consider this as a global concern.

Table 2. Nuclear waste inventory (IAEA estimates 2018) [6].

	Solid radioactive waste in storage (m^3)	Solid radioactive waste in disposal (m^3)	Proportion of waste in disposal (%)
VLLW	2,356,000	7,906,000	77
LLW	3,479,000	20,451,000	85
ILW	460,000	107,000	19
HLW	22,000	0	0

This paper will propose that the IAEA Code of Practice is interpreted in the same way as the Basel Convention, to allow for the transboundary movement of waste.

II. REVIEW

The IAEA Code of Practice dictates that radioactive wastes can only be disposed of within the country they are produced. As a result, the current practices of the global community are constrained by the CoP and limited by state borders. As seen in **Table 2** most wastes still require disposal and many nations plan to use geological disposal for this. This approach thus relies on each country constructing their own GDF, which subsequently limits the build-up of expertise. It is considered best practice to construct a GDF in a stable geological formation [4], this could be problematic as this is not possible for all waste producers. **Figure *1*** shows the limitations to the current methodology. Each individual nation needs to have the motivation, local geology, time and finances to construct a suitable disposal facility and this cannot be guaranteed.

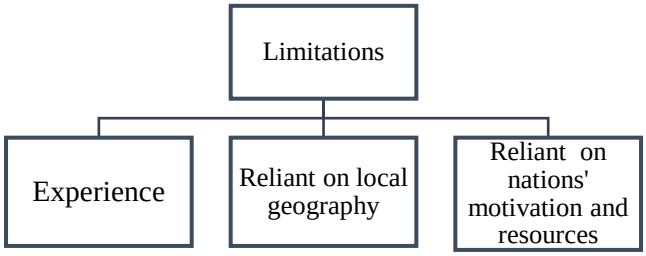

Figure 1. Limitations of the current interpretation and implementation of the IAEA Code of Practice on the International Transboundary Movement of Radioactive Wastes.

A. Proposed changes to the IAEA Code of Practice on the International Transboundary Movement of Radioactive Wastes, 1991

To evaluate the impact of changes to the CoP on the global management of radioactive wastes, it is necessary to identify what the proposed changes are and where they will take place. This is summarised in **Table 3.**

Table 3. IAEA Code of Practice, 1991 and the proposed changes in interpretations of its policies (it can be assumed policies not shown will remain unchanged).

IAEA Code of Practice on the International Transboundary Movement of Radioactive Wastes, 1991 [3]	Suggested changes to interpretation
Every state should take the appropriate steps necessary to ensure that radioactive waste within its territory, or under its jurisdiction or control is safely managed and disposed of, to ensure the protection of human health and the environment.	Ensuring radioactive waste within a states' territory is safely managed and disposed of, could include safe disposal abroad and potentially increase the likelihood of safe disposal for states where they have nuclear, but not the infrastructure for radioactive waste disposal.
Every state should take the appropriate steps necessary to minimize the amount of radioactive waste, taking into account social, environmental, technological and economic considerations.	Encouraging international cooperation enables sharing of information and technology to reduce waste.
Every state should take the appropriate steps necessary to ensure that, subject to the relevant norms of international law, the international transboundary movement of radioactive waste takes place only with the prior notification and consent of the sending, receiving and transit states in accordance with their respective laws and regulations.	This must be maintained, however whilst wastes are considered national issues, this area remains unutilised.
No receiving state should permit the receipt of radioactive waste for management or disposal unless it has the administrative and technical capacity and regulatory structure to manage and dispose of such waste in a manner consistent with international safety standards. The sending state should satisfy itself in accordance with the receiving state's consent that the above requirement is met prior to the international transboundary movement of radioactive waste.	No country that cannot safely treat and dispose of radioactive wastes would receive wastes as part of the change in interpretation.
Every state should take the appropriate steps to introduce into its national laws and regulations relevant provisions as necessary for liability, compensation or other remedies for damage that could arise from the international transboundary movement of radioactive waste.	A more cohesive approach to responsibility and liability in the management of radioactive wastes.
Every state should take the appropriate steps necessary, including the adoption of laws and regulations, to ensure that the international transboundary movement of radioactive waste is carried out in accordance with this Code.	Interpreted that in accordance with this Code that transboundary movement can occur.
The sending state should take the appropriate steps necessary to permit readmission into its territory of any radioactive waste previously transferred from its territory if such transfer is not or cannot be completed in conformity with this Code, unless an alternative safe arrangement can be made.	Can now be utilised.

B. Risks for implementation of proposed changes

When evaluating the suggested changes referenced in **Table 3**, it is necessary to consider the risks that might arise alongside the opportunities that might be fostered. In the UK, the NDA Value Framework [5] has been developed to guide the evaluation of policy changes against set values; this paper will use the NDA Framework when considering the risks arising from the proposed changes. This paper will

consider the Tier 1 Values only, as seen in the **Table 5** sub-headings.

Table 5 demonstrates a significant number of risks that must be considered if the changes in **Table 3** were to be implemented. These risks were generated using the NDA Value Framework to identify areas of importance. Most of the risks are relatively benign as they are unlikely to occur or will have minimal impact, there are two risks which are deemed to be likely and impactful should they occur. Both risks are due to nations changing their priorities, which would lead to issues with the transport and management of waste following agreed deals. **Table 4** demonstrates the scoring system, green shows a suitably mitigated risk and has low impact and low likelihood. Amber implies that either the likelihood or the impact of the risk occurring needs to be reduced. Red implies that this is a serious risk, and must be managed accordingly.

Table 4. RAG matrix.

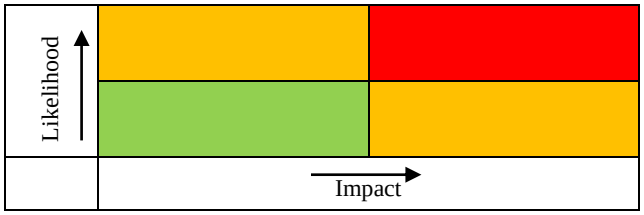

Table 5. Risk matrix outlining potential risks arising from changes to IAEA Code of Practice.

Risk	Mitigation	Rating After Mitigation (RAG)
Health and Safety		
Danger to workers	Set radiation standards for signatories and ensure all staff are SQEP	
Danger to the public	Set radiation standards for signatories and ensure all staff are SQEP	
Security		
Increased transport of radioactive wastes increases opportunities for organised crime or terrorists to target it	All participating nations must sign up to agreed protection protocols	
Increased transport of radioactive wastes increases opportunities for states utilising wastes in proliferation efforts	All participating nations must sign up to agreed anti-proliferation protocols	
Environment		
Contamination to non-nuclear nations	All participating nations must sign up to agreed environmental standards	
Increased transport of radioactive wastes increases chance of accidents leading to contamination of environment	All participating nations must sign up to agreed environmental standards	
Risk/hazard reduction		
Inability to ensure SQEP staff	All participating nations must agree to certain level of training for all necessary staff	
Inability to access necessary equipment	Trade deals set up to support nations managing radioactive wastes	
Socio-economic impacts		
Social pressures of people not wanting radioactive wastes being transported around the world	Participating nations to sign up to a communications plan promoting sharing of information	
Non-OECD countries coerced to take wastes in exchange of short-term economic gain	Only financially capable parties can receive radioactive wastes for management &/or disposal	
Finance		
Greater expense for managing radioactive wastes globally	Increase in transport costs, but a decrease in disposal facilities	
Greater expense for managing radioactive wastes for states disposing of more waste than they have produced	Opportunities for states to generate funds on the receival of radioactive wastes thus offsetting operational costs	
Enabling the Mission		
States less likely to share technology and information relating to managing rad wastes as it would impede on profits.	Trade deals set up to support nations managing radioactive wastes	
Not enough countries sign up	Nations can sign up to increase in the share of technology and ideas, even if they refuse to accept or distribute their wastes.	
Implementability		
Elections leading to changes in policy direction in states disrupting the global transport, management and disposal of radioactive wastes	Introduce a divorce settlement process into any withdrawals from the CoP	
Transport risks i.e. ship crashes at sea, who's legal responsibility	All participating nations must sign up to agreed environmental standards	

Transport incident leading to contamination, who's responsibility	All participating nations must sign up to agreed environmental standards	
A nation who has agreed to receive wastes has a change in circumstances and no longer wishes to take the agreed waste	Introduce a divorce settlement process into any withdrawals from the CoP	
Wastes delivered are not at appropriate standards	All participants agree to a 'return policy' or sanctions	

C. Opportunities for implementation of proposed changes

These changes there will have benefits and opportunities for global radioactive waste management processes.

1. Enabling countries to become experts in geological disposal and to profit from the practice increases the likelihood of processes being improved through experience.
2. Increased expertise and experience.
3. Opportunity for nations to generate income through the management of radioactive wastes.
4. Increases likelihood of wastes entering final disposal sooner.
5. BAT can be applied to the GDF siting process with regards to optimum geology.
6. Enables countries without nuclear waste disposal routes to make use of nuclear power and reduce carbon emissions.

These opportunities will have significant impacts in dealing with the global radioactive waste issue. All benefits outlined above are to create an environment where the management and disposal of radioactive wastes is done in as safe and secure manner as possible. All policy changes therefore need to be considered and developed with the aim of ensuring BAT is applied to each waste stream and final disposal is as safe as possible.

III. CONCLUSION

As outlined throughout this paper, there are serious limitations with regards to the current implementation of the IAEA Code of Practice. The management of radioactive wastes is overly reliant on individual nations having the motivation, resources, and geological capability of disposing radioactive wastes. In an era of globalisation, which has fostered both increased international cooperation and the sharing of information, it is inconceivable that an issue which affects 30 countries with nuclear power is not an issue shared and tackled cooperatively by the global community. This issue not only impacts nuclear states but also every country with waste from other sources such as hospitals, research facilities and uranium mining operations.

The current interpretation of the CoP prevents some countries managing radioactive wastes effectively due to resources, geology, and experience. There are many nations who have the geology and space to build a GDF (such as Australia who also have relevant experience in mining uranium) but do not produce significant radioactive waste and therefore it is currently not a viable option. This could be seen as a "wasted opportunity" to assist countries with large volumes of radioactive waste who are limited by some of the areas mentioned in **Figure *1***. The proposed changes to allow for the transboundary movement of radioactive wastes (with strict guidelines in place ensuring important values such as those in the NDA Value Framework are prioritised), encourage the formation of a holistic global strategy. The proposed changes will provide several benefits including:

- Increased expertise and experience.
- Chance for nations to generate profits from providing services.
- More wastes to enter final disposal sooner.
- BAT can be applied to the GDF siting process.

Large scale changes, such as those recommended in this paper, would be challenging to implement, requiring active participation from all relevant nations. In order for the change in CoP to be successful, disposal sites will need to be built, regulatory processes implemented and national legislation written. However, these steps will no longer be taken alone and can instead occur with the support of the global network working together to tackle the global radioactive waste issue.

IV. REFERENCES

[1]. European Commission, "Europeans and Nuclear Safety," Special EUROBAROMETER 271, February, 2007.

[2]. United Nations Environment Programme, "Basel Convention on the Control of Transboundary Movements of Hazardous Wastes and their disposal," Basel Convention, Basel, Switzerland, 22nd March 1989.

[3]. International Atomic Energy Agency, "Code of Practice on the International Transboundary Movement of Radioactive Waste," presented at the General Conference, Vienna, Austria, 21st September, 1991.

[4]. World Nuclear Association, "Storage and Disposal of Radioactive Waste," March, 2022. Accessed on: 1st April 2021. [Online]. Available: https://www.world-nuclear.org/information-library/nuclear-fuel-cycle/nuclear-waste/storage-and-disposal-of-radioactive-waste.aspx

[5]. Nuclear Decommissioning Authority, "NDA Value Framework," January, 2016, Version 1.

[6]. World Nuclear Association, "Radioactive Waste Management," February, 2020. Accessed on: 1st April 2021. [Online]. Available: Radioactive Waste Management | Nuclear Waste Disposal - World Nuclear Association (world-nuclear.org)

Proceedings of the European Nuclear Young Generation Forum
ENYGF'21
September 27-30, 2021, Tarragona, Spain

Effect of pH on the dissolution rate of MoO_2(s)

García-Gómez, Sonia[1,2*], Rivero, Alejandro[1,2], de Pablo, Joan[1,2] and Casas, Ignasi[1,2]

[1] Department of Chemical Engineering, UPC (Barcelona-Tech), Spain; [2] Barcelona Research Centre for Multiscale Science and Engineering, UPC (Barcelona-Tech), Spain

*Corresponding author: *sonia.garcia.gomez@upc.edu*

I. INTRODUCTION

To assess the performance of a geological disposal, the interaction between spent nuclear fuel and groundwater must be studied, since uranium and other radionuclides may be released into the surrounding environment.

The design of high-level nuclear waste repositories include materials based on cement due to their structural properties and their capacity to retard radionuclide release. However, the interaction of cement materials with groundwater produces significant alterations on the groundwater composition such as high alkalinity and high silicate and calcium concentrations [1]. In light of this, the influence of high pH conditions within the repository on the spent nuclear fuel dissolution rate must be considered.

Most of the fission products generated during fuel irradiation are kept inside of the UO_2 matrix, and therefore will be released only as a function of the matrix dissolution/alteration. However, some of the fission products are partialy segregated from the matrix and diffuse in the void spaces such as the gap, cracks, bubbles and grain boundaries, hence, a fraction of them will not be released congruently with the matrix. Depending on their chemical state, distribution and solubility, a fraction of the segregated fission products are dissolved faster than the matrix. This group is known as Instant Release Fraction (IRF) and is considered one of the main sources of radiological hazard in a geological disposal [2]. Because of this, the release of radionuclides from spent nuclear fuel (SNF) has been the subject of numerous studies.

Among all the fission products formed in UO_2 fuel, molybdenum is one of the most abundant due to its high fission yield [3]. Since the oxygen potential of Mo/MoO_2 is very similar to the fuel, the excess oxygen created during fission is neutralized by the oxidation of metallic Mo to Mo(IV), buffering the oxidation of uranium dioxide [3]. Therefore, dissolution/migration of Mo could mean an increase of the spent fuel matrix alteration.

Mo is known to be present both in solid solution in UO_2 matrix and forming precipitates [3][4]. The fraction of molybdenum segregated from the matrix of SNF is found to be either as metallic molybdenum or as molybdenum dioxide [5].

Several studies have performed experiments to calculate the dissolution rate of some radionuclides, including molybdenum. Rollin et al. studied their dissolution rates under oxidizing, anoxic and reducing conditions in the pH range 3-9.3 by using flow-through experiments [6]. They determined that the dissolution rate of molybdenum under reducing conditions dropped by up to four orders of magnitude when compared to oxidizing conditions. Cui et al. studied the leaching of an alloy made by Mo-Ru-Pd and Rh, under reducing and oxidizing conditions by inmersion in a synthetic groundwater at pH 8.2 [7]. They concluded that under both conditions, Mo is dissolved at a rate several thousand times faster than the rest of the metals from the alloy.

Iglesias et al. recently studied the dissolution of SNF under hyperalkaline conditions in batch experiments [8]. The results showed an unexpected increase of molybdenum release, as well as technetium, as compared with previous results obtained at slightly alkaline bicarbonate conditions. Although the first hypothesis was based on a kinetic effect, we could not find in the literature data to corroborate this assumption. Whereas molybdenum seems not to be part of the IRF under slightly alkaline conditions, these new data implies that at higher alkaline conditions molybdenum could clearly form part of the IRF.

The aim of this work is to determine the effect of pH on the dissolution rate of MoO_2(s) under oxidizing conditions by using a thin-film continuous flow through reactor.

II. EXPERIMENTAL

A. Solid sample

MoO_2(s) provided by Sigma-Aldrich was ground using a mortar and a pestle. The powder was sieved and the particles with a size between 20 and 50 µm were collected. The characterization of the powder was performed by using Phenom XL Scanning Electron Microscopy with Energy

Dispersive X-ray Spectroscopy (SEM-EDS). The specific surface area of the solid, a key parameter in dissolution studies, was determined by the Brunauer, Emmett, Teller (BET) method (Micromeritics ASAP 2020 Surface area and porosity analyzer) based on adsorption/desorption isotherms of nitrogen at room temperature.

B. Leaching solution

All the solutions contained 5.10^{-3} M of $NaHCO_3$ (Sigma Aldrich) to approach the composition of a groundwater in a granitic environment. The range of pH studied was from 8 to 13.5. The desired value of pH in the test solution for each experiment was adjusted by adding NaOH (supplied by Sigma Aldrich). The pH was measured with a pH meter from Orion, model 720A and was daily calibrated with three pH (7, 9 and 13) standard buffer solutions from Panreac. The ionic strength of each solution was maintained constant and equal to 0.1 M (with the exception of pH 13.5) by using the required amount of sodium perchlorate (Sigma Aldrich). The test solution was continuously bubbled with N_2 to prevent CO_2 intrusion. All the experiments were performed at room temperature.

C. Experimental set-up

The continuous flow-through thin solid layer reactor used in this work for kinetic determinations is described in detail in [9].

0.090g of MoO_2 solid was enclosed in a reactor (Swinnex filter holder 13mm), between two millipore filters (PTFE membrane filters from Osmonics, resistant at a pH range of 1-14, with a diameter of 13 mm and a pore size of 0.22µm). The use of such filters ensure that only the concentration of dissolved molybdenum is measured. By using a thin layer of solid phase, the contact between solid and liquid phase is optimal, therefore the diffusion effect is minimized and mass-transport influence is avoided.

A feed tank, with two liters capacity, contained the leaching solution. By means of a peristaltic pump (Ismatec reglo) the dissolution was circulated through the botton of the reactor containing MoO_2(s) to prevent unfilled spaces (bubbles of air) in the reactor.

At the outlet of the reactor, aliquots were collected periodically for subsequent analysis of the molybdenum concentration. To determine the exact flow rate, both the weight and the collection time of every sample was measured. The samples were then acidified with HNO_3 (Sigma-Aldrich, 69%) for analysis of molybdenum in solution by ICP-MS 7800 from Agilent Technologies. The ICP-MS was calibrated before the analysis by using a set of molybdenum standards (from Inorganic Ventures) ranging from 1 ppb to 2000 ppb. Samples were analyzed within a week of their collection.

When steady state was reached, only the test solution concentration was changed and a new experiment was started.

D. Determination of steady state conditions and dissolution rate

To guarantee that the molybdenum concentration measured is at steady state, rather than at solubility equilibrium, the concentration should be proportional to the residence time of the test solution in the reactor. Residence time can be expressed by:

$$t = \frac{V}{Q} \quad (1)$$

where V is the volume of solution in contact with the solid phase and Q is the flow rate.

Considering that the volume is constant, the concentration must be inversely proportional to Q when steady state is reached. For this reason, the effect of flow rate on the molybdenum concentration in the output was first studied. Once a flow rate range at which this ideal behaviour was found, a flow rate within this range was selected and kept constant for the rest of the experiments.

If no secondary solid phases are formed and both the surface area and flow rate remain constant, the dissolution rate can be calculated by multiplying the flow rate by the concentration in the output solution. Finally, the dissolution rate was normalized to the total exposed surface area of the solid:

$$r_{diss}(mol \cdot m^{-2} \cdot s^{-1}) = \frac{Q(mL \cdot s^{-1}) \cdot [Mo](mol \cdot mL^{-1})}{SA(m^2 \cdot g^{-1}) \cdot m(g)} \quad (2)$$

where Q is the flow rate, [Mo] is the molybdenum concentration of the effluent once steady state is reached, SA is the surface area of the solid and m is the mass of the solid enclosed in the reactor.

III. RESULTS AND DISCUSSION

The specific surface area determined by BET method was 0.1105 ± 0.0017 $m^2.g^{-1}$. Surface examination of the MoO_2 powders by SEM verified the absence of any alteration of the powder after testing. Figure 1 shows the appearance of the sample pre and after testing. Small fines were present attached to the MoO_2 powder after sieving prior to testing.

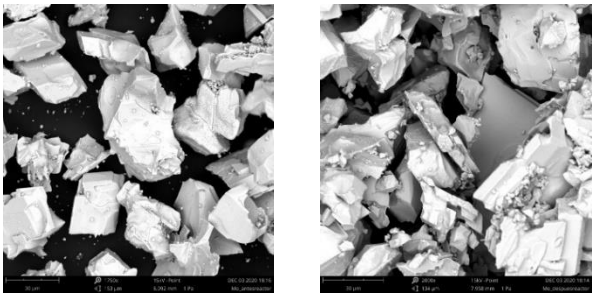

Figure 1. SEM of the solid sample before (left) and after (right) leaching.

The concentration of the output was plotted as a function of time as shown in Figure 2. The high initial concentrations of Mo over the first few hours were probably due to the dissolution of the more soluble fines present on the surface of the particles as already corroborated by SEM (Figure 1), which is very common in flow experiments [6]. However,

its dissolution was relatively fast, since a steady state was reached in less than one day.

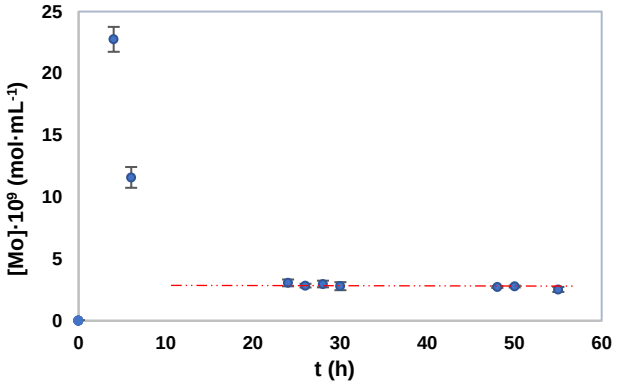

Figure 2. Concentration of Mo as a function of the duration time for the dynamic experiment with MoO_2 in contact with the leaching solution at pH 13 and a flow rate of 0.2 mL·min^{-1}. The average concentration at steady state is represented by a red dashed line.

To confirm that a steady state was effectively reached under working conditions, different flow rates were examined with the same leaching solution. In Figure 3 the molybdenum concentration is plotted versus the reciprocal of flow rate. In the flow rate range between 0.1 and 0.5 mL·min^{-1}, the average concentration in the steady state is inversely proportional to the reciprocal of the flow rate used. This behaviour shows that these concentrations obtained correspond to a steady state rather than a solubility equilibrium. The results were fitted to the following equation (R^2=0.997):

$$[Mo]\ 10^9 \cdot (mol \cdot mL^{-1}) = 0.67(\pm 0.02)(mol.min^{-1}) \cdot Q^{-1}(min \cdot mL^{-1}) \quad (3)$$

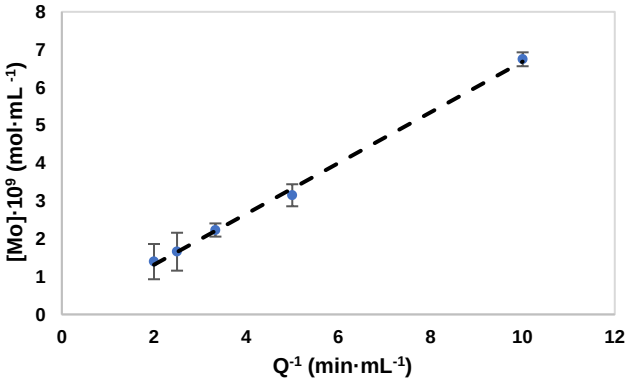

Figure 3. Molybdenum concentration vs reciprocal of flow rate at pH 13.

Taking this into account, a flow rate of 0.2 mL·min^{-1} was fixed for the subsequent experiments performed to study the effect of pH on the dissolution kinetics of MoO_2.

In order to conduct another experiment, only the composition of the leaching test was changed once steady state is reached. By means of the averaged concentration in the steady state, the normalized dissolution rate was calculated by Equation 2. The dissolution rate of all experiments performed was tabulated in Table 1.

Table 1. Experimental dissolution rates calculated for MoO_2 at different pH under steady-state conditions.

pH	$r_{diss} \cdot 10^{10}$ (mol·m^{-2}·s^{-1})
8.0±0.3	3.93±0.06
9.0±0.2	4.22±1.08
10.0±0.1	4.64±0.76
11.0±0.1	4.96±1.19
12.0±0.1	8.51±0.75
12.5±0.1	22.98±3.54
13.0±0.1	33.68±6.12
13.5±0.1	104±6.24

Based on these experimental observations, a clear change in behaviour was observed at pH 11. At hyperalkaline pH values (from pH 12 to 13.5) the dissolution rate increased drastically. In Figure 4 the values of log r_{diss} are plotted versus pH.

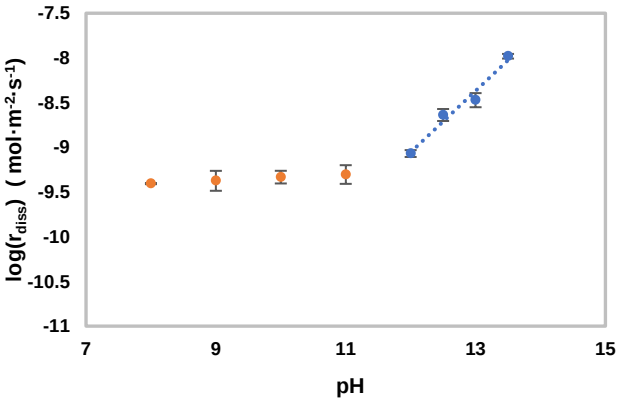

Figure 4. Logarithm of the normalized dissolution rates of molybdenum as a function of pH. Q= 0.2 mL·min^{-1}.

The dissolution rate in the hyperalkaline region (12≤pH≤13.5) can be fitted according to the following equation:

$$r_{diss}(mol \cdot m^{-2} \cdot s^{-1}) = 10^{-17.29(\pm 1.09)} \cdot [H^+]^{-0.69(\pm 0.09)} \quad (4)$$

The trend shown in Figure 4 provides evidence that [OH$^-$] concentration influences the dissolution rate of MoO_2 for pH>11. The dependence of r_{diss} for MoO_2 on [H$^+$] can be explained by the following terms: (i) The negative dependence evidence that the dissolution rate is promoted by the presence of OH$^-$ ions in the solution. (ii) As stated by Stumm [10] fractional order dependence on protons is commonly seen in surface complexation promoted reactions for minerals dissolution, including oxides.

Consequently, this behaviour could be explained by the effect of a hydroxyl promoted dissolution, whereas the

fractional rate order was a clear indication of a surface complexation promoted dissolution mechanism.

This dependence observed at hyperalkaline conditions supports the results presented by Iglesias et al. [8]. In batch experiments they determined that the release of molybdenum from spent nuclear fuel increased at pH 13.5 compared to previous results using the same type of sample but a lower pH of the leaching test (pH 7). As seen in the present work, this effect can be clearly attributed to an increase of the rate reaction.

Regarding the pH range between 8 and 11, minimal effect of proton concentration on the dissolution rate was observed. These data are similar to the results obtained by Rollin et al. [6]. Experiments performed in flow-through experiments with 10 mM $NaHCO_3$ under oxidizing conditions determined a dissolution rate around 3.10^{-10} $mol \cdot m^{-2} \cdot s^{-1}$ for ^{100}Mo, which is a value comparable to the one obtained in this work under the same pH values (pH 9 from Table 1).

IV. CONCLUSIONS

In this work, the rate of MoO_2(s) dissolution as a function of pH at room temperature has been investigated under oxidizing conditions. The experiments were conducted in unsaturated solutions far from equilibrium using a thin-film continuous flow through reactor. Steady-state conditions were found in the flow rate range 0.1-0.5 $mL.min^{-1}$.

The dependence observed at hyperalkaline values can be explained by the effect of a hydroxyl promoted dissolution, and the fractional rate order is an indication of a surface reaction controlled dissolution mechanism. These results are congruent with the increase of molybdenum release obtained at high pH from the SNF experiments performed by Iglesias et al. [8]. On the contrary, no significant difference was observed in the dissolution rate of MoO_2 between pH 8 and 11.

Acknowledgements: This work has been financially supported by Ministerio de Economía y Competitividad (Spain) with the project ENE2017-83048-R and ENRESA. S. García-Gómez wants to acknowledge the fellowship with reference code PRE2018-085618.

V. References

[1] T. Heath, J. Schofield, and A. Shelton, "Understanding cementitious backfill interactions with groundwater components," Appl. Geochemistry, vol. 113, pp. 1-11, 2020.

[2] A. Martínez-Torrents, D. Serrano-Purroy, R. Sureda, I. Casas, and J. de Pablo, "Instant release fraction corrosion studies of commercial UO2 BWR spent nuclear fuel," J. Nucl. Mater., vol. 488, pp. 302–313, 2017.

[3] Y. K. Ha, J. G. Kim, Y. S. Park, S. D. Park, and K. Song, "Behaviors of molybdenum in UO2 fuel matrix," Nucl. Eng. Technol., vol. 43, pp. 309–316, 2011.

[4] L. Desgranges, B. Pasquet, and M. Fraczkiewicz, "Interpretation of the molybdenum behaviour in irradiated UO2 using a point defect approach," Nucl. Instruments Methods Phys. Res. Sect. B Beam Interact. with Mater. Atoms, vol. 266, pp. 3018–3022, 2008.

[5] H. Kleykamp, "The chemical state of the fission products in oxide fuels," J. Nucl. Mater., vol. 131, pp. 221–246, 1984.

[6] S. Röllin, K. Spahiu, and U. B. Eklund, "Determination of dissolution rates of spent fuel in carbonate solutions under different redox conditions with a flow-through experiment," J. Nucl. Mater., vol. 297, pp. 231–243, 2001.

[7] D. Cui, T. Eriksen and U. B. Erklund, "On Metal Aggregates in Spent Fuel, Synthesis and Leaching of Mo-Ru-Pd-Rh Alloy," Mat. Res. Soc. Symp. Proc., vol. 663, 2001.

[8] L. Iglesias, D. Serrano-Purroy, A. Martinez-Torrens, F. Clarens, J. de Pablo, and I. Casas, "High-burnup spent nuclear fuel dissolution under highly alkaline conditions," DISCO 1st Annu. Meet. Proc., pp. 33–36, 2018.

[9] J. Bruno, I. Casas, and I. Puigdomènech, "The kinetics of dissolution of UO2 under reducing conditions and the influence of an oxidized surface layer (UO2+x): Application of a continuous flow-through reactor," Geochim. Cosmochim. Acta, vol. 55, pp. 647–658, 1991.

[10] W. Stumm and R. Wollast, "COORDINATION CHEMISTRY OF WEATHERING: Kinetics of the Surface-Controlled Dissolution of Oxide Minerals," Rev. Geophys., vol. 28, pp. 53–69, 1990.

Proceedings of the European Nuclear Young Generation Forum
ENYGF'21
September 27-30, 2021, Tarragona, Spain

Technical Considerations for the Geological Disposal of Liquid Nuclear Waste

Bychkov Maksim and Lvova Darya

Kalinin Nuclear Power Plant, Russia

**Corresponding author: m.bychkov37@mail*

I. WHAT IS IT ALL ABOUT?

Preventing harmful effects of nuclear waste on humans is an urgent issue, attracting wide public attention Nowadays there are the following ways of disposing nuclear waste:

- Shallow ground disposal (nuclear wastes with half-lives of less than 30 years);
- Direct pumping-in (liquid nuclear waste);
- Sea disposal or seabed disposal (These methods can't be used now, because there is a high chance of causing unexpected negative effect);
- Space disposal (high cost);
- Deep geological repository;
- Rock burial.

Nuclear Waste is divided along its specific activity, half-lives and change of state (there can be solid, liquid and gaseous waste). Liquid nuclear waste generated in large quantity is particularly alarming. They are solutions containing radioactive nuclides, which, because of some technical and economical parameters or for other reasons can't be used for manufacture or for other management objectives. Liquid nuclear waste is characterized by a great variety of compositions, chemical and physical properties, depending on place and conditions of their generation and the way they are treated before being disposed.

The main idea of liquid nuclear waste disposal is using porous geological horizons similar to ones that are used for containing oil and gas. These horizons contain saline water, which is of no practical use, above and below and are isolated with impenetrable (waterproof) horizons. Subsoils have the unique ability to contain and hold a certain amount of various substances no matter solid or liquid. These soils are characterized by the stability of their structure over a long period of time. All above-mentioned is possible under favourable geological conditions.

Preferably there should be stable tectonic conditions to provide long-term sustainability of an underground structure (for at least 10^4 years) and integrity of a whole waste storage system in relatively short-term.

Tectonic conditions should be stable to exclude the posibility of strong earthquakes and subductions in the near or/and distant future. In stable zones there is less chance of volcanism, that's why the tectonic settings of potential disposal site must be evaluated on seismic risk, recent fault activity, signs of contemporary or new volcanism and speed of downward or upward vertical movements of earth masses.

Stable tectonic conditions are usually characterized by little tension of tectonic zone and low natural temperatures. A broad parameter, characterizing tectonic activity of structural elements is often used to evaluate a disposal site. This parameter has different names, for example, "tectonic element" and is a criterion of tectonic suitability.

II. A GENERAL DESCRIPTION OF THE DISPOSAL. TECHNIQUES AND METHODS OF SAFE OPERATION.

The disposal (burial) of industrial liquid waste started in the 20-ies of the XX century and hasn't always been successful as the result of the absence of preliminary examination of disposal sites and the lack of attention to the possible implications

There are several factories in Russia, that use this technology nowadays, for example: Federal State Unitary Enterprise (FSUE) "Siberian Chemical Combine" (Seversk), FSUE "Mining and Chemical Combine" (Zheleznogorsk), FSUE State Research Center "the Research Institute of Atomic Reactors" (Dimitrovgrad) – these factories has over half a century of experience of safe operation of deep geological disposal sites.

A. A general description of the process and the proper site for a disposal

The industrial waste disposal is carried out by pumping it through boreholes into deep strata of a porous horizon (waste-holding layer), usually lying in depths below 1 km. After being pumped through boreholes the waste fills the porous space of a waste-holding layer, displaces groundwater and mixes with it partially. As the result, a waste deposit appears in the strata. The place there waste mixes with groundwater is called a transition zone and is located on the periphery of a waste deposit. The upper area

is an area of an active water exchange, it contains freshwater. The lower area is an area of a slow water exchange, it contains saline water. Surface and upper water is hardly connected with water from the lower area. The area of stagnant water is isolated from upper horizons with layers of impenetrable (waterproof) rocks, such as clay, plaster, anhydrite, etc. In natural conditions the insulation properties of the waterproof systems help to separate various hydrodynamic areas and aquifers different in their water pressure and chemical quality of groundwater. There are intermediate areas between the upper and the lower areas. They are characterized by the increase of mineralization of groundwater by the increase of depth. Waste-holding layers located in the lower area are mainly used for waste disposal. These layers contain saline water.

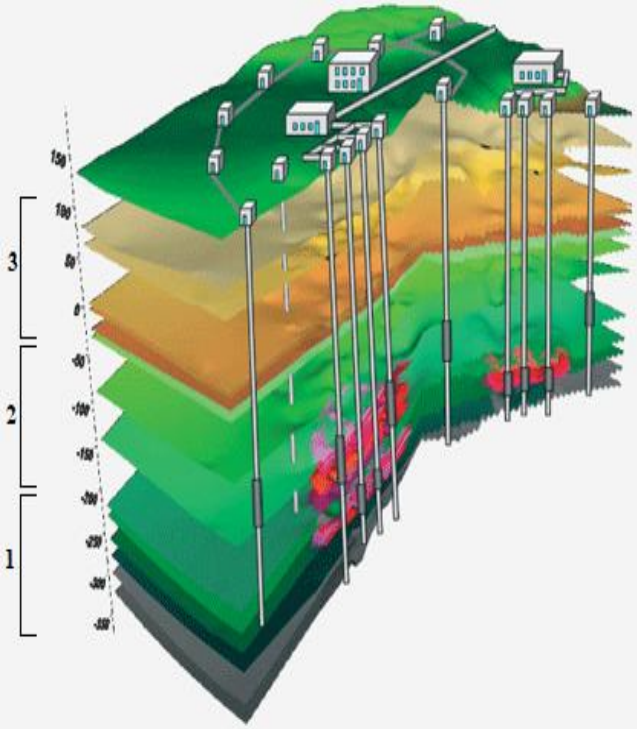

Figure 1. A scheme of layers required for safe liquid nuclear waste disposal; (1) Waste-holding layers, (2) Waterproof layer, (3) Buffer layer

Liquid waste disposal is preceded by a preparation, implemented in the main proceedings factories and disposal facilities. Liquid nuclear waste has high temperature, due to radioactive decay. For example, when high level nuclear waste is buried, its temperature can cause dislocation of rocks, accompanied by growth of thermoelastic tension. It can lead to swelling of subsoils, which, in turn, can lead to instability of underground structure and, as a result, to leaking of nuclear waste.

The possibility of overhearing the environment and accidental leakage of radionuclides is defined by thermal properties of hosting rocks, the waste density and natural temperature at the disposal site. That means that liquid nuclear waste, that is going to be buried, should meet certain requirements, providing continuous work of injection wells in a given time frame. Physico-chemical interaction between waste and rocks of waste-holding layers should not lead to destruction of the latter.

The main requirements for a liquid nuclear waste disposal site were provided on the basis of laboratory testing and experimental-industrial work:

- Regulation of the content of suspended solids, depending on characteristics of a waste-holding layer;
- Regulation of the composition of wastes to prevent sediment and formation and gas generation in a filer zone;
- Establishing threshold concentration of waste components, which are harmful to rocks of waste-holding layers;
- Restricting the content of long-lived and most energy-efficient nuclides, taking into account the possible heating of a waste-holding layer.

The technology of preparation of liquid nuclear waste for burial was developed to meet these requirements. This preparation includes particulate disengagement by means of sedimentation and filtering, adjusting pH, chemical preprocessing of waste and preprocessing of filter zone of an injection well.

One more way of safe disposal of liquid nuclear waste should be added to the above listed. It is solidification of wastes, which means the transition of nuclear waste from liquid to solid state, used to decrease the chance of migration or spreading of radionuclides. There are several ways of transition from liquid nuclear waste to immobilized solid substance:

- Bituminization;
- Cementation;
- Vitrification;
- Enclosing in ceramic.

The technology of waste preparation was developed by IPCE RAS (Frumkin Institute of Physical chemistry and Electrochemistry Russian academy of sciences). The processed waste is sent through pipeline to a pumping station, located on the territory of a disposal area. Then this waste goes to through high pressure pipeline to injection wells.

Figure 2. An indicative plan of liquid nuclear waste disposal; (1) A waste generator, (2) Low pressure pipeline, (3) A waste processing unit, (4) Relift station, (5) Injection station, (6) Force mains, (7) Maintenance building, (8) Injection wells, (9) An absorbing layer, (10) Observation wells, (11) A waste-holding layer filled with waste, (12) Isolating impenetrable (waterproof) layers, (13) A buffer layer

B. The list of requirements for a disposal site

It should be admitted that the occurrence depth of liquid nuclear waste is essential, because some characteristics of rocks change at different depths. For example pressure and temperature go up by the increase of depth, while porosity and permeability go down.

As stated above the idea liquid nuclear waste disposal is based on using geological environments that can provide containment of waste in the place of burial, despite of presence of mostly saline groundwater, natural movement of which is moderate. That groundwater plays a large part in liquid nuclear waste disposal, because the burial is closely connected with the interaction between wastes and water, as it is carried out in natural interstices. The speed of natural movement of groundwater is usually measured in centimetres per year and there is no water exchange between surface, upper and ground water.

The most favorable depth of disposal is more that 1000 m, as it's the depth of groundwater. However the depth of burial can negatively affect some rocks. For example, insulation properties of clay are reduced by the increase of depth (in the area of stagnant water), because of the loss of plasticity as some cracks appear. Then it's more preferable to use upper and middle zone for disposal.

Waste-holding layers used for disposal should meet certain requirements and the characteristic values of rocks should lie within appropriate limits. This requirements and limits depend on geological conditions of the site of burial and on the composition and structure of porous space of waste-holding layers in particular.

In general the requirements are the following:

- The occurrence depth of waste-holding layers should be more than 1000m. Though in some cases it can be less than that if all the following requirements are met (for example, (FSUE) "Siberian Chemical Combine", city Seversk in accordance to Federal rules and regulations 055-14 and Federal Law № 2395-1;
- The water contained in waste-holding layers should be of no interest to be used as a source of water supply; this water is mostly the water with high salt content;
- A waste-holding layer should be isolated from upper soil horizons with layers of impenetrable (waterproof) rocks, preventing vertical filtering of waste effectively, the minimum thickness shouldn't be less than 50 m;
- There should not be any disjunctive dislocations, which can lead to one horizon interfering in another;
- Above a waste-holding layer should be a buffer layer, which contains water not suitable for practical use. This horizon should also be isolated with layers of impenetrable (waterproof) rocks;
- Storage capacities of a waste-holding layer are a specific capacity understood as the amount of waste, which is stored on $1m^2$ of a layer. It is supposed to provide waste disposal within the borders of an allotment – a circle with a radius of several kilometres.

It follows from the above that due to the great occurrence depth of a waste-holding layer, containing saline water and due to waste being isolated reliably in a waste-holding layer, the potential risk of radioactive waste is dramatically decreased. And the geological conditions of the disposal area of Kalinin Nuclear Power Plant meet all the listed requirements.

Basically a waste-holding layer lies in of the disposal area at a depth of 1285 ÷ 1349 m in the area of slow water exchange, which contains highly mineralized water not suitable for practical use and containing no favourable components in industrial concentration. Therefore, industrial or liquid nuclear waste disposal in Tiskresky horizon provides safety and security conditions.

C. ABOUT THE OPPORTUNITIES FOR IMPLEMENTATION

The preliminary studies of compositions of liquid nuclear waste and its compatibility with industrial waste and rocks of waste-holding layers, the development of technological schemes of preparing wastes, transferring them to injection wells and disposing of them in waste-holding layer, the prediction of the consequences of burial showed the opportunity of potential usage of this technology and its efficiency. It requires significantly lower cost, provided that the necessary security is ensured.

Based on the above, it is possible to implement liquid nuclear waste disposal in existing industrial waste storage, separating nuclear and saline industrial waste. Nuclear waste can be transferred through separate pipeline to specifically earmarked injection wells. Under this scheme saline waste (chemical water treatment system, condensate purification plant) can be disposed of as a single flow. It will be joined by washing water of heat-exchange equipment and steam generators as it accumulates, water freed from radionuclide by water purification and boron concentrates. Nuclear waste will be held in drain water tanks and after mechanical purification goes to holding tanks, located on the territory of the special building (there are three tanks $160m^3$ each). Nuclear waste disposal on industrial waste disposal site is feasible if it's done periodically through a separate line to a specifically earmarked injection well with subsequent displacement of nuclear waste from the well by industrial waste. According to the data of Kalinin Nuclear Power Plant the total volume of liquid nuclear waste, which can be sent for disposal will not exceed 50 m^3 per day (~2000 m^3/per year). It is only 5% of regulated volume of injection.

This system of nuclear waste disposal will eliminate evaporation of drain water and accumulation of waste bottoms in tanks and storage facilities. Moreover, the accumulation of tritium water, which occurs while the evaporation will be eliminated as well. Some units of water purification will also be removed, which will lead to reduction of the amount of solid nuclear waste – exhaust sorbents. In this way the system of nuclear waste disposal will be significantly simplified. According to the researches of IPCE RAS, the disposal of liquid nuclear waste won't lead to the instability of a waste-holding layer, which gives grounds to recommend disposing of them on industrial waste disposal site of Kalinin Nuclear Power Plant.

IV. CONCLUSION

The document prepared by State Atomic Energy Corporation "Rosatom" in June 2008 suggested the following wording: "the alternative way to dispose of liquid nuclear waste is deep geological disposal" The peer review suggests that even with the cost of development of special transport equipment and its certification, cost of transportation of waste to the disposal area and cost of disposal itself, this approach may have significant positive economic impacts within Rosatom. Therefore, liquid nuclear waste disposal using wells is considered to be an acceptable technology in future.

The implementation of liquid nuclear waste disposal on Kalinin Nuclear Power Plant will help to implement this technology on the other Nuclear Power Plants, both functioning and being built, the sites of which can provide favourable geological conditions for these purposes.

V. REFERENCES

[1] Materials of the justification of the license for the operation of the existing PGZ LRO (landfill "Sites 18, 18A") of the Seversky branch of the FSUE "NO RAO", Seversk, Tomsk region, Russia, 2018, Volume 1;

[2] Materials of the justification of the license for the operation of the existing PGZ-landfill Severny of the branch "Zheleznogorsk" of the FSUE "NO RAO", Zheleznogorsk, Krasnoyarsk region, Russia, 2018, Volume 1;

[3] Materials of the justification of the license for the operation of the existing PGZ LRO "Experimental-industrial landfill" of the branch "Dimitrovgradsky" of FSUE "NO RAO", Dimitrovgrad, Ulyanovsk region, Russia, 2018, Volume 1;

[4] Federal norms and rules in the field of the use of atomic energy "Disposal of radioactive waste. Principles, criteria and basic requirements" - NP-055-114;

[5] Law of the Russian Federation "On Subsoil" of 21.02.1192 No. 2395-1;

[6] Rybalchenko A.I., "Deep disposal of liquid radioactive waste" Moscow: IzdAT, 1994. 256 p.;

[7] Kochkin B.,"The choice of geological conditions for the disposal of highly radioactive waste", Graduation qualification thesis, Moscow, Russia, 2002, 211 p.;

[8] Semak E., "Perspective methods of disposal of long-lived radioactive waste", VIII All-Russian Conference "Youth and Science", Krasnoyarsk, Siberian Federal District, Russia, 2012;

[9] Order of July 10, 1996 N 321 on approval of the conclusion of the expert commission on the project "Landfill of underground disposal of waste water of the Kalinin NPP";

[10] E. V. Evstratov, "Problems of nuclear heritage and ways to solve them" Volume 1, Moscow, Russia, 2012, 356 p.;

[11] Melnikov N. N., Konukhin V. P., Komlev V. N. "Underground disposal of radioactive waste" - Apatity: Publishing House of the KSC RAS, 1994.;

[12] Komkov I.,"Deep burial of liquid radioactive waste", Graduation qualification thesis, Ivanovo, Ivanovo region, Russia, 2020, 118 p.

Proceedings of the European Nuclear Young Generation Forum
ENYGF'21
September 27-30, 2021, Tarragona, Spain

Possibilities and Features of REMIX Technology as an Initial Stage in the Establishing of a Full-Scale Two-Component Nuclear Energy System

Sitdikov, Emil*, Vasilenko, Alexey and Diachenko, Anton

Rosatom Technical Academy, Russian Federation

*Corresponding author: *emilsitdikov@gmail.com*

I. INTRODUCTION

To achieve the sustainability of nuclear power industry it necessary to solve issues dealing with the spent nuclear fuel (SNF) management and expansion of fuel resource base. Despite the fact that once-through nuclear fuel cycle presently seems to be more economically attractive it leads to accumulation of tremendous amount of SNF and consumes plenty of exhaustible natural uranium. To solve these issues and according to the Energy Strategy of Russia for the period up to 2035, the key challenges facing ROSATOM State Atomic Energy Corporation are to form a new technological platform for nuclear power with nuclear power plants (NPPs) on improved water-cooled and fast neutron reactors operating in a closed nuclear fuel cycle, and to increase the export potential of Russian nuclear technologies, as well as the further development of the export of NPPs, nuclear fuel and electricity [1].

In support of the development of a full-scale two-component nuclear power program, Rosenergoatom JSC is currently implementing a project focused on optimizing a two-component NES based on the use of VVER (Russian design pressurized water reactor) and BN reactor (Russian design sodium cooled fast neutron reactor) together. The key feature of this project is a two-stage programme for development of a two-component nuclear energy system (NES) [2].

The first stage of development of a two-component NES is related to the setting up the pilot-industrial power complexes with BN and VVER reactors, that involves R&D on all parts of a two-component NES, including development of plutonium-based fuel and obtaining a license to operate MOX fuel (Mixed Oxide Fuel - nuclear fuel made from reprocessed plutonium and uranium) in VVER reactors. In support of this stage, a pilot line for the production of MOX fuel for the BN-800 reactor has been set up, and the first batch of 18 fuel assemblies with MOX fuel has been delivered and loaded to Beloyarsk NPP [3]. Along with this, the Mining and Chemical Combine has already manufactured 169 MOX fuel assemblies with for the BN-800 reactor (2020) [4].

At the same time, it should be noted that in parallel since 2016 State Scientific Center – Research Institute of Atomic Reactors (SSC RIAR) has been conducting research on an innovative REMIX fuel (Regenerated Mixture fuel - mixture of reprocessed uranium and plutonium, extracted from spent nuclear fuel) based on the concept of multiple recycling of reprocessed uranium and plutonium [5], and tests of REMIX fuel in the third fuel cycle at the Balakovo NPP are continuing [6].

Further development of the national two-component NES (the second stage) is associated with the solution of such issues as:

- development of facilities and achievement of industrial scale for closed nuclear fuel cycle, and serial operation of BN reactors,
- increasing the level of safety, economics of a two-component NES,
- development of new generation reactors,
- solving the issues of spent nuclear fuel accumulation and radioactive waste management.

At the same time, according to the Energy Strategy of Russia for the period up to 2035, the commissioning of new generating capacities based on fast reactors with a sodium coolant is postponed at least until 2035. This may be one of the key constraints to the establishing of a full-scale two-component NES. Thus, under current conditions, considering the ongoing tests of REMIX fuel in the VVER reactor, and the needs of foreign recipient countries of Russian energy technologies in resolving the issue of spent nuclear fuel management and taking into account the Energy Strategy in terms of commissioning new units with fast neutron reactors, REMIX fuel may have a number of preferences at the initial stage of the formation of a two-component NES [7].

II. MODELING OF THE ISOTOPIC COMPOSITION OF SPENT FUEL

One of the necessary stages of this study was to analyze the change in the isotopic composition of plutonium during multiple recycling of plutonium-based fuels in order to identify the features of their use in the establishing of a two-

component NES based on the joint use of pressurized water reactors and fast reactors with sodium coolant.

A. Recycling strategies

Table 1 specifies the sequence of recycling plutonium-based fuels considered in this study in VVER-1200 and BN-800 reactor facilities, where:

- "MOX" - recycling of MOX fuel,
- "MOX-WG" - recycling of MOX fuel with the involvement of ex-weapons-grade plutonium,
- "REMIX 1" - recycling of REMIX fuel,
- "REMIX 2" - recycling of REMX fuel with "purification" of plutonium fraction in a fast reactor.

At each recycle after spent nuclear fuel reprocessing, actinides are sent for long-term storage, and in the MOX fuel recycling sequence, reprocessed uranium is also sent for storage. Enriched natural uranium with a ^{235}U isotope content of 16% is used as the feed material for the formation of REMIX fuel of equivalent enrichment.

Table 1. The sequence of fuel recycling in different types of reactors.

No. of recycle	"MOX"	"MOX – WG"	"REMIX 1"	"REMIX 2"
1	VVER (UOX fuel)	VVER (MOX with ex-weapon-grade Pu)	VVER (UOX fuel)	VVER (UOX fuel)
2	BN	BN	VVER	VVER
3	VVER	VVER	VVER	BN
4	BN	BN	VVER	VVER
5	VVER	VVER	VVER	BN
6	-	-	-	VVER

Table 2. Unit cells characteristics of VVER-1200 and BN-800 reactor facilities.

Characteristics, measure unit	VVER-1200	BN-800
Fuel cladding external diameter, mm	9,1	6,9
Fuel cladding material	Alloy E-110 (Zr + 1% Nb)	ChS-68HD
Fuel pin external diameter, mm	7,6	6,1
Fuel pin central hole diameter, mm	1,2	-
Fuel rod pitch, mm	12,75	7,95
Fuel enrichment, %	4,95	20
Fuel density, g/cm^3	10,5	10,5
Power density, kW/kg	36,8	107,2
Estimated burnup range, MWd/kg	55	66
Coolant density, g/cm^3	0,7278	0,84

In the present study, the analysis of the neutron multiplication properties of the fuel as well as the characteristics of the isotopic composition of the spent fuel were carried out in the unit cell approximation using the SERPENT 1.1.7 code, which implements the Monte Carlo method. This software package is developed by VTT (Technical Research Centre of Finland) Technical Research Center of Finland and is used in more than 100 universities and research organizations around the world [8].

The SERPENT code is a certified software tool, and it has a certificate issued by the SEC NRS (Scientific and Engineering Centre for Nuclear and Radiation Safety) valid until 16.12.2025, which means the possibility of using for calculating K_{inf} of the systems with nuclear fuel and nuclear fissile materials [9].

Table 2 indicates the characteristics of the fuel cells used in the estimations. The characteristics of the unit cells of the fuel assemblies of VVER-1200 and BN-800 are selected as the reference data.

B. K_{inf} behaviour during multiple sequential fuel recycling

Figures 1-2 show the dependence of the infinite neutron multiplication factor of the VVER-1200 cell lattice for different strategies of MOX and REMIX fuel recycling (table 1) depending on the burnup.

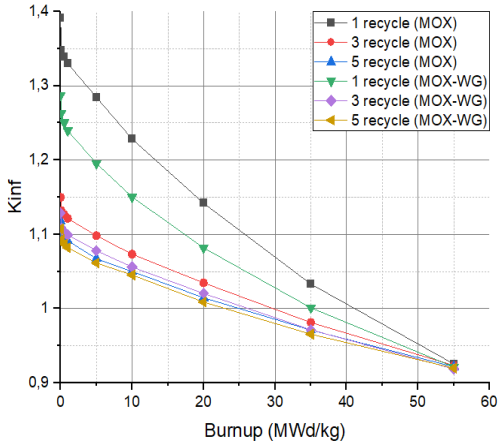

Figure 1. K_{inf} behavior in VVER-1200 with "MOX" and "MOX-WG" recycling strategies.

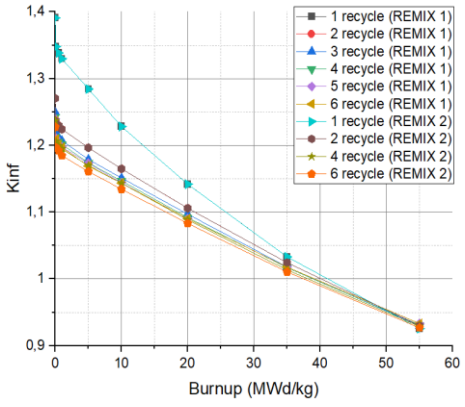

Figure 2. K_{inf} behavior in VVER-1200 with "REMIX 1" and "REMIX 2" recycling strategies.

As the result of the accumulation of non-fissile isotopes of uranium and plutonium the condition of equivalent enrichment must be met during the arrangement of fuel load

for each subsequent cycle, i.e. the fuel should have multiplying characteristics similar to fresh uranium oxide fuel.

During sequential recycling of MOX and REMIX fuel, the value of the neutron multiplication factor decreases depending on the recycle number, which is due to the involvement in the fuel cycle of plutonium isotopes with large neutron-absorption cross sections in comparison with uranium isotopes. In the case of recycling MOX fuel with the involvement of ex-weapon-grade plutonium, the effect is higher than in the case of recycling MOX fuel based on reactor plutonium. For the case of recycling REMIX fuel, it was shown that each subsequent recycle makes a smaller contribution to the decrease in K_{inf}.

In all the considered recycling strategies, the calculated isotopic composition of the fuel makes it possible to achieve the required burnup, i.e. the condition of equivalent enrichment is satisfied. Equivalent characteristics of MOX fuel were achieved by trial and error method of the required fractions of plutonium and depleted uranium. The formation of the equivalent characteristics of REMIX fuel was carried out using the equation given in [10].

C. Evolution of plutonium fraction isotopic vector

Figures 3 and 4 show the evolution of the plutonium fraction isotopic vector in different fuel recycling sequences, which is expressed as a change in the ratio of the fractions of odd plutonium isotopes (^{239}Pu, ^{241}Pu) to the total plutonium concentration in the discharged fuel.

The results presented in figure 4 indicate that the change in the isotopic composition of plutonium in the process of multiple recycling of REMIX fuel in VVER-1200 compared to MOX fuel stabilizes after the second recycle and there is no significant degradation in terms of energy potential for thermal reactors. Also, it should be noted that the involvement of the BN-800 reactor in the recycling sequence has a positive effect on the fissile properties of the fuel.

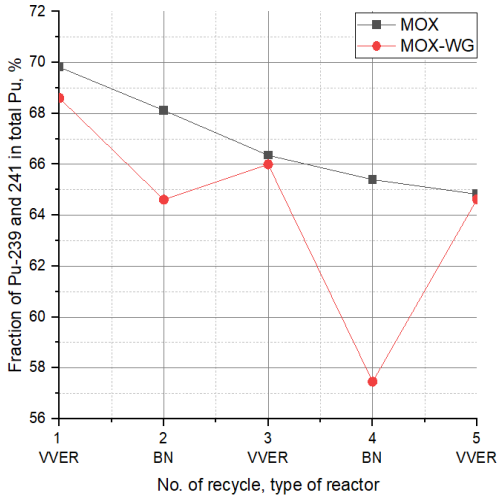

Figure 3. Change in the total fraction of odd plutonium isotopes in MOX fuel at the end of the cycle.

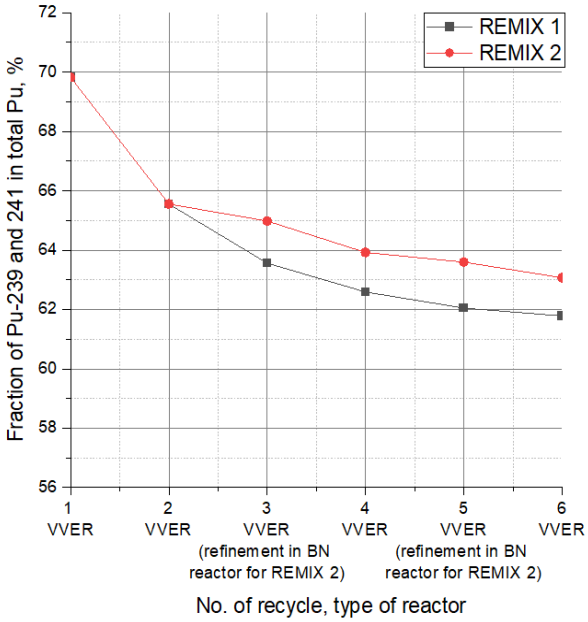

Figure 4. Change in the total fraction of odd plutonium isotopes in REMIX fuel at the end of the cycle.

The opposite effect is observed when ex-weapon-grade plutonium is included in the MOX fuel cycle - the change in the fraction of fissile plutonium isotopes occurs abruptly, which indicates a high degree of degradation of the plutonium fraction isotopic composition.

In addition to considering the change in the fraction of ^{239}Pu and ^{241}Pu, it is especially important to take into account the effect of ^{238}Pu accumulation, since an increase in the fraction of this isotope leads to an increased heat release of the fuel.

When recycling MOX fuel using the “MOX” sequence, the ^{238}Pu accumulation is stabilized at the range of 2-3% of the total plutonium fraction (figure 5). Also, it should be noted that by the 5th recycle the composition of MOX fuel according to the “MOX-WG” sequence with the involvement of ex-weapon-grade plutonium is close to the composition of traditional MOX fuel (based on reactor-grade plutonium) and the accumulation of ^{238}Pu is about the same level.

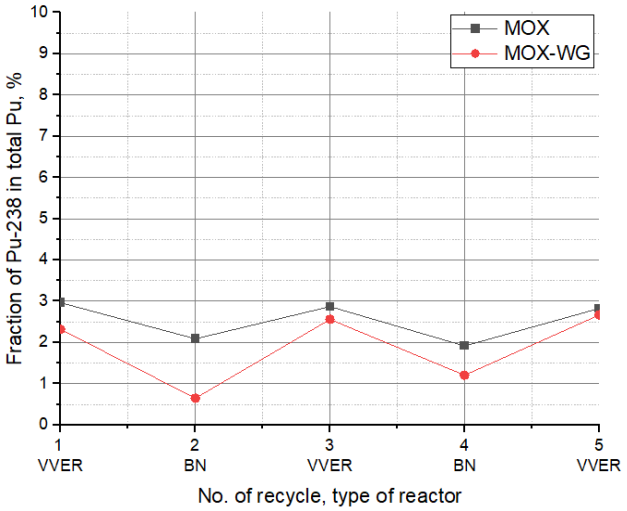

Figure 5. Change in the fraction of ^{238}Pu in the Pu composition of the MOX fuel at the end of the cycle.

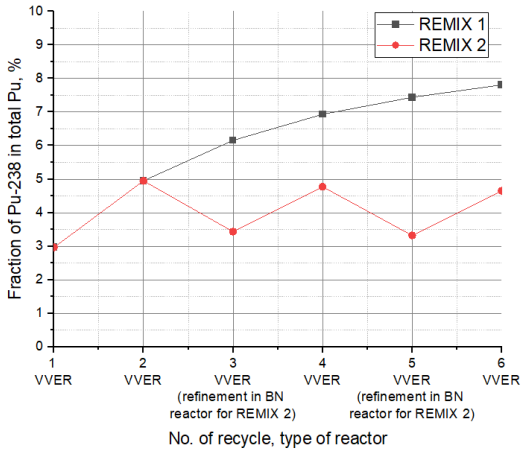

Figure 6. Change in the fraction of ^{238}Pu in the Pu composition of the REMIX fuel at the end of the cycle.

In the case of recycling REMIX fuel according to the "REMIX 1" sequence, the fraction of ^{238}Pu increases with each subsequent recycling, which will bring difficulties in handling the fuel (figure 6). The inclusion of the BN-800 reactor in the "REMIX 2" sequence makes it possible to reduce the ^{238}Pu fraction by 1.7 times (at the 6th recycle) and stabilize it at the range of 3-5%, thus positively affecting on the fissile properties of the REMIX fuel in thermal reactors.

III. NUCLEAR FUEL CONSUMPTION IN NPPS IN A TWO-COMPONENT NES

The results presented above show that considering less degree of reduction in the multiplication properties and less accumulation of ^{238}Pu the most acceptable options are the "MOX" fuel recycling sequence using traditional MOX fuel and the "REMIX 2" sequence using REMIX fuel with intermediate "purification" of plutonium fraction in BN reactor (table 1).

In order to assess the plutonium consumption in thermal and fast reactors, the analysis of plutonium loading and discharging in the "MOX" and "REMIX 2" sequences was carried out. The results are shown in figures 7 and 8.

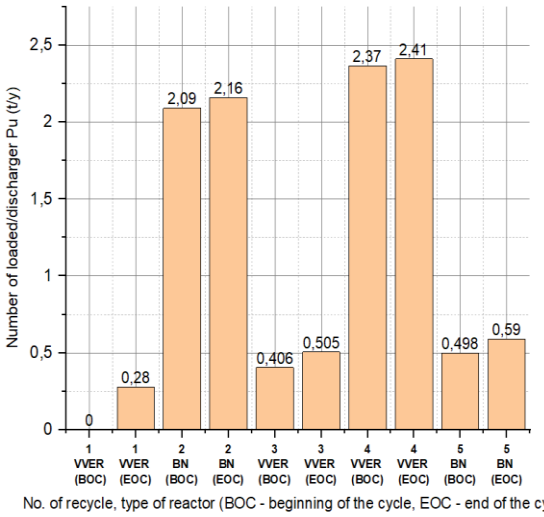

Figure 7. Change in Pu consumption according to the "MOX" recycling sequence.

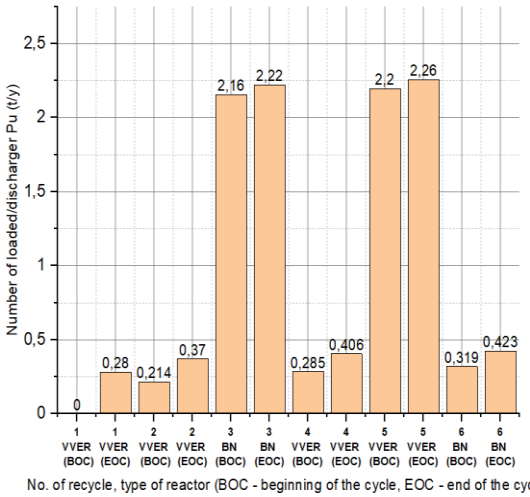

Figure 8. Change in Pu consumption according to the "REMIX 2" recycling sequence.

Based on the analysis of the plutonium consumption in VVER-1200 and BN-800 reactors, several specific features can be identified. When the VVER-1200 reactor is refueled (figure 7), up to ~ 0.28 t/year of plutonium can be discharged, while to load BN-800 reactor with fuel based on MOX (cycle No. 2) ~ 2.09 t/year of plutonium is required. To ensure the subsequent recycling (No. 3) in the VVER-1200 reactor MOX fuel with a quality corresponding to that discharged from the BN-800 reactor (~ 2.16 t/year after cycle No. 2) ~ 0.406 t/year of plutonium is required. Accordingly, to form a full load of the BN-800 reactor based on MOX fuel, the required amount of plutonium can be discharged from 7 VVER-1200 reactors, and the amount of plutonium discharged from the BN-800 reactor can provide up to 5 VVER-1200 reactors, i.e. in a nuclear power plant with a MOX fuel recycling sequence, up to 12 VVER-1200 units can be involved for each BN-800 unit in operation at the initial stages of fuel recycling (figure 9).

In turn, in the "REMIX 2" recycling sequence the fuel is subsequently irradiated in a VVER-1200 reactor. At the same time, according to the results obtained and shown in figure 8 the amount of discharged plutonium is about ~0.28 t/year, which is sufficient to form the next VVER-1200 load with REMIX fuel (~ 0.214 t/year at the beginning of cycle No. 2). The next stage is the "purification" of the fuel in the BN-800 reactor, i.e. improvement of the plutonium isotopic vector in terms of its energy potential in thermal reactors. To ensure the full load (No. 3) of the BN-800 reactor, ~ 2.16 t/year of plutonium is required. The fissile properties of discharged plutonium (~ 2.22 t/year after cycle No. 3) are sufficient to form a load with REMIX fuel in VVER-1200 with a demand of ~ 0.285 t/year.

Accordingly, to form a full load of BN-800 in the "REMIX 2" sequence, it is necessary to discharge and reprocess fuel from 6 VVER-1200 reactors (from cycle No. 2). Fuel "purified" in BN-800 reactor (cycle No. 3) can provide up to 8 VVER-1200 units (cycle No. 4) in the next cycle.

Thus, in a NES with a REMIX fuel recycling sequence with intermediate "purification" in BN-800 reactor, up to 20 VVER-1200 units can be involved for each BN-800 unit in operation at the initial stages of fuel recycling (figure 10).

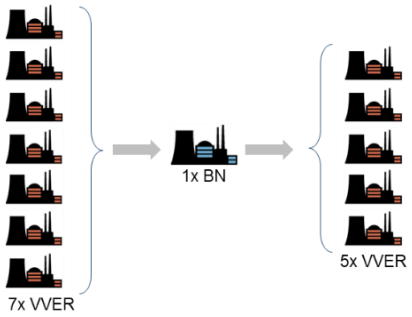

Figure 9. Involvement of thermal reactors in a two-component NES for each operating fast reactor in case of using MOX fuel.

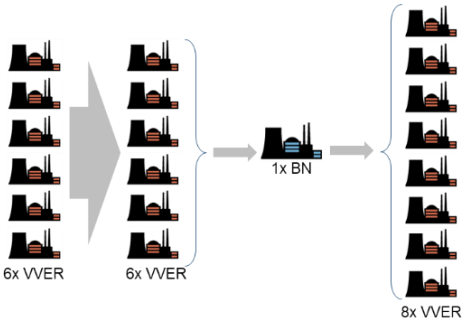

Figure 10. Involvement of thermal reactors in a two-component NES for each operating fast reactor in case of using REMIX fuel.

IV. CONCLUSION

Analysis of the change in the plutonium fraction isotopic vector in the process of multiple recycling of REMIX fuel in VVER-1200 compared to MOX fuel indicates that the composition of plutonium stabilizes after the second recycle and there is no significant degradation in terms of the energy potential for thermal reactors.

An assessment of plutonium consumption in thermal and fast reactors with recycling strategies using traditional MOX fuel and REMIX fuel with intermediate "purification" in the BN reactor showed that the use of REMIX fuel at the initial stage of the transition to a two-component NES can allow a larger number of VVER reactors to be involved in the cycle for each BN reactor operated, which is an advantage in conditions of the high cost of BN technology.

One of the possible option to settle the issue related to ^{238}Pu accumulation could be the inclusion of fast reactors in the recycling sequence, and the "purification" of the plutonium fraction in the fast BN spectrum, similar to the MOX fuel recycling sequence.

The use of ex-weapon-grade plutonium for the fabrication of MOX fuel at the moment seems inappropriate due to the degradation of the plutonium isotope vector in MOX fuel cycles. It is more expedient to analyze the option of using ex-weapon-grade plutonium as a feed material for the formation of fuel.

V. REFERENCES

[1] Government of the Russian Federation, "Energy Strategy of Russia for the period up to 2035". Available: https://minenergo.gov.ru/node/1026. [Online]. Accessed 21.06.2021.

[2] A. Petrov, A. Shutikov, N. Ponomarev-Stepnoi, V. Bezzubtsev, M. Bakanov, V. Troyanov. "Prospects of Creation of the Dual Component Nuclear Energy System", Izvestiya vuzov. Yadernaya Energetika, vol. 2, 2019, pp. 5-15.

[3] ROSATOM, "The first serial batch of MOX fuel loaded into BN-800 fast reactor at Beloyarsk NPP", 2020. Available: https://www.rosatom.ru/en/press-centre/news/the-first-serial-batch-of-mox-fuel-loaded. [Online]. Accessed 21.06.2021.

[4] ROSATOM, "ROSATOM manufactures the first full refueling batch of MOX fuel for BN-800 fast reactor", 2020. Available: https://rosatom.ru/en/press-centre/news/rosatom-manufactures-the-first-full-refueling-batch-of-mox-fuel-for-bn-800-fast-reactor/. [Online]. Accessed 21.06.2021.

[5] SSC RIAR, "Reactor research of REMIX fuel began at SSC RIAR", 2016. Available:http://www.niiar.ru/node/4427. [Online]. Accessed 21.06.2021.

[6] ROSATOM, "Balakovo NPP has completed scheduled maintenance on unit №3", 2020. Available: https://www.rosatom.ru/journalist/news/na-balakovskoy-aes-zavershilsya-planovo-predupreditelnyy-remont-energobloka-3/. [Online]. Accessed 21.06.2021.

[7] Yu. Fedorov, O. Kryukov, A. Khaperskaya, "Multiple Recycle of Remix Fuel Based on Reprocessed Uranium and Plutonium Mixture in Thermal Reactors", International Conference on Spent Fuel Management, 15 – 19 June 2015 in Vienna, Austria. Available: https://www-pub.iaea.org/iaeameetings/cn226p/Session6/ID106Fedorov.pdf. [Online]. Accessed 21.06.2021.

[8] J. Leppänen, et al., "The Serpent Monte Carlo code: Status, development and applications in 2013", Ann. Nucl. Energy 82, 2015, pp. 142-150.

[9] SEC NRS, "List of valid attestation certificates of software tools", 2020, p. 14. Available: http://www.secnrs.ru/expertise/software-review. [Online]. Accessed 21.06.2021.

[10] S. Solovyev, A. Dyachenko, M. Fedorov, R. Efremov, V. Artisyuk, "Analysis of VVER-1000 nuclear fuel cycle based on REMIX fuel against proliferation of fissile materials" Izvestiya vuzov. Yadernaya Energetika, vol. 4, 2018, pp. 62-70.

Proceedings of the European Nuclear Young Generation Forum
ENYGF'21
September 27-30, 2021, Tarragona, Spain

Engineering of a heating / cooling system for spent fuel pool at Bilibino nuclear power plant in the post-operational period.

Gavrilova Anastasia

Moscow Polytechnic University, Russia

anastasia_gav@mail.ru

I. INTRODUCTION

Today, there are many operating nuclear power plants (NPP) in the world, that generate electric and/or thermal energy. In addition to them, there are also many nuclear power plants (and/or power units operating nuclear power plants) that are at the stage of design, installation and commissioning.

For operating stations at all stages of NPP operation, designers, specialists who carry out installation and operational personnel of the stations carry out a lot of work on modernization of existing station systems, elimination of problems of certain existing station systems, perform measures for starting operations of power units and common-station systems of NPP, shutdown for carrying out scheduled preventive repairs and thus have extensive experience in the procedures specified in the above procedures.

Despite this, there is an important stage in the life cycle of the NPP, which requires special measures, namely, the decommissioning stage.

Unfortunately, due to the small number of NPP shutdown and decommissioning, this stage raises a large number of questions.

As well as design, installation and commissioning, decommissioning requires an individual approach to each specific site, but in addition, the following must be taken into account when decommissioning:

- State of existing station systems;

- The entire scope of measures for modernization, dismantling, repair of existing station systems for the entire life of the facility;

- Experience of NPP operating personnel operation for the whole NPP operation period.

This report will be devoted to the problem of decommissioning of the NPP facility and will describe one important system at the entire stage of the NPP life cycle - both during operation and in the post-operation period.

II. SUBJECT MATTER OF REVIEW

The object of consideration is the Bilibino Nuclear Power Plant (hereinafter referred to as the BIL NPP). The location of the nuclear power plant is the Chukotka Autonomous Okrug near the city of Bilibino in Russia. The BIL NPP includes four power units of the same type and auxiliary common-station buildings/structures and systems.

Each of the BIL NPP power units includes the following elements:

- Reactor plant;
- Heating plant;
- Auxiliary process systems;
- Auxiliary systems for electrical power output to the network;
- Auxiliary systems for thermal power output to the heating system;
- Security systems.

The installed electric capacity of the nuclear power plant is 48 MW. The maximum heat output (for heat supply) from the nuclear power plant was 116 MW (with a decrease in electric power to 40 MW). To date, two power units of the nuclear power plant are in operation - power unit No. 3 and power unit No. 4. Power units No. 1 and No. 2 are stopped.

III. OBJECTIVES

Due to the fact that the operating units of the nuclear power plant are required to be stopped in the foreseeable future, a number of measures are required to ensure the reliable and safe decommissioning of the nuclear power plant.

The present report will consider only part of the necessary activities, namely, activities to ensure the required temperature conditions of water in the fuel basins - 3 and 4 (hereinafter referred to as BV-3, BV-4) at all stages of the post-operational period, excluding accidents taking into account the characteristics of the climate and the existing state of station systems.

In accordance with federal norms and rules in the field of nuclear energy, the concept of "NPP accident" implies the

following definition - violation of NPP normal operation, in which radioactive substances and (or) ionizing radiation have escaped beyond the limits stipulated by the NPP design documentation for normal operation in quantities exceeding the established limits of safe operation; the accident is characterized by the initial event, the ways and the consequences (NP-001-15 "General provisions for the provision of nuclear power plants").

Spent fuel pool - a special structure inside the reactor shop, which is used as a temporary storage of spent nuclear fuel discharged from the reactor.

Spent nuclear fuel enters the fuel pool using a specially designed lifting mechanism, which installs the fuel unit in a special bottle, which is part of the pool structure.

Due to the residual heat generation of fuel cells installed in the fuel pools, as well as due to the need to protect maintenance personnel, the fuel pool is filled with water.

Each fuel pool is equipped with the following auxiliary systems:

- Fuel pool water circulation system;
- Fuel pool water cooling system;
- Fuel pool makeup system.

Fuel pool water circulation system provides working medium movement and together with cooling system provides residual heat removal from fuel cells.

Fuel pool makeup system provides compensation of working medium lost during evaporation.

Schematic diagram of circulation system and cooling system is given in Figure 1.

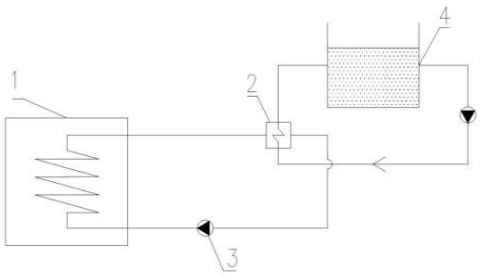

Fig. 1. Diagram of circulation system and cooling system. 1 - cooling tower, 2 - heat exchange apparatus, 3 - water circulation pump unit, 4 – spent fuel pool.

Spent nuclear fuel will be located in the fuel pool until residual heat release is reduced to values that allow for safe refueling of fuel and implementation of measures for fuel removal to special storage facilities.

IV. DESCRIPTION OF EXISTING SYSTEMS

In connection with the need for decommissioning of the nuclear power plant, training will be required, namely:

- dismantle existing NPP systems and components that will not be required in the post-operation period;
- modernize existing NPP systems and components that will be required in the post-operational period;
- develop and install new NPP systems and components that will be required in the post-operation period.

In this article, the systems described above are as follows:
- System requiring dismantling - cooling system and cooling tower.
- System requiring modernization - existing fuel pool cooling system;
- System requiring new development - heating system (to be described in the next section).

The existing cooling system consists of two coolant circuits, namely:
- Fuel pool water circuit;
- cooling water circuit that circulates through cooling tower heat exchange surfaces.

Circuits are separated from each other by surface-type heat exchange apparatus. The proposed dismantling of the cooling system is related to the dilapidated structure of the cooling tower.

V. RELEVANCE

Spent nuclear fuel (SNF) storage is one of the final stages of the nuclear power plant fuel cycle. The spent nuclear fuel unloaded from the reactor is initially sent for storage to the spent fuel pool (SPF) to reduce the residual heat release, and then transferred to dry storage. The complexity of SNF handling problems is associated with its high activity, the presence of a large amount of fissile substances in the composition, and significant heat release after unloading from the reactor.

SNF storage should ensure the removal of residual heat release from spent fuel assemblies (SFAs), protection of personnel and the environment from ionizing radiation and release of radioactive substances into the environment, and physical protection of spent fuel.

These requirements are fully met by storing spent nuclear fuel in an aquatic environment ("wet" storage method), in which there is a decrease in residual heat generation and decay of the most active short-lived radionuclides, such as iodine-131, xenon-133, etc. The time required for this is 1–3 years, depending on the type of nuclear fuel. Long-term experience of “wet” SNF storage has proved its reliability and convenience, especially for reducing the level of radiation loads and heat release of spent fuel immediately after unloading from the reactor.

During the accident at the Fukushima NPP, the spent fuel pool (SF) turned out to be a weak point of the NPP, since the overwhelming majority of new fuel assemblies (FAs) were located in the SF, and not in the reactor itself. As a result of water leakage and boiling away in the BV, the fuel assemblies became bare and began to melt. Undoubtedly, SFAs emit less heat than new assemblies, but nevertheless it is enough to lead, under conditions of ineffective cooling in SFA, to heating of the zirconium shells of the rods and, accordingly, to the possible destruction of their integrity.

In this case, as a result of excess pressure from under the cladding of the fuel assembly, radioactive gases (for example, iodine-131 vapors), accumulated in the rods during their stay in the reactor, begin to escape.

In connection with the above, the justification of the safety of "wet" storage of spent nuclear fuel is associated with the introduction of reliable methods for calculating their thermal parameters into the practice of analyzing the

efficiency of SF cooling systems. And, in particular, in emergency situations with a possible partial or complete shutdown of forced circulation in the cooling circuit.

VI. MAIN TASKS

Taking into account the current state of existing station systems, experience of operation of nuclear power plants and climatic features, it is required to modernize the cooling system and provide a new cooling source for it.

In addition, taking into account that during the storage of spent fuel in the fuel pool in the post-operation period, residual heat emissions will decrease with time, the fall of internal heat emissions of the main body (in connection with the shutdown of reactor plants), taking into account the dilapidated thermal insulation structures of the main body and taking into account the climatic features of the location of the nuclear power plant, there is a risk of falling water temperature in the pool to 0 °C.

Extreme design outside air temperature is minus 60 °C. Thus, the developed system for maintaining the water temperature of the fuel pools should carry out the following operation modes:

- Fuel pool water cooling mode - when the temperature of water in the fuel pool is higher than necessary;
- Fuel pool water heating mode - when the temperature of the water in the fuel pool is below the required one;
- Standby mode - when the water temperature in the fuel pool is within the permissible limits.

The system for maintaining the temperature of the water in the fuel pool should be developed taking into account that the remaining pools (BV-3, BV-4) have different volumes and, accordingly, the need for cooling will be different.

Also, due to different volume and loading time, residual total heat emissions from fuel will also be different and the possibility of the following operating modes of the temperature maintenance system should be taken into account in the calculation:

- Provision of cooling of both basins;
- Provision of heat supply to both basins;
- Providing one of the basins with heat supply/cooling, and the other does not need heat supply/cooling;
- Providing one of the pools with heat supply and the other with cooling.

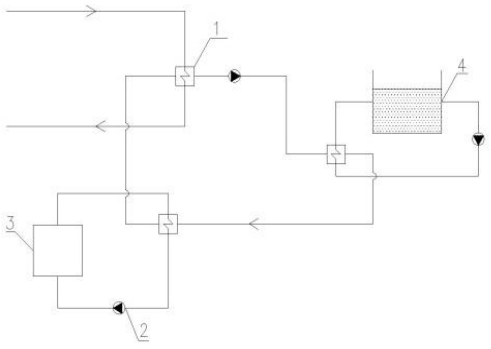

Fig. 2. Heating and cooling circuit diagram

1 - heat exchange apparatus, 2 - water circulation pump unit, 3 - electric boiler, 4 - spent fuel pool.

For cooling, technical water is used - "raw water" It cools the intermediate circuit with demineralized water, which in turn cools the fuel pool. The heating circuit heats the intermediate circuit, which in turn heats the fuel pool circuit. The heating circuit is also filled with demineralized water. Depending on the water temperature in the fuel pool, a particular circuit is switched on based on commands from the automation system.

To ensure safety, in order to avoid the ingress of radioactive working medium (water from the fuel pool) into the intermediate circuit, a "pressure barrier" is provided, namely, the pressure in the intermediate circuit is higher than possible in the water circuit for the fuel pool. Also on the intermediate circuit there are devices for control of medium activity.

VII. CONCLUSIONS

The developed water temperature maintenance system in the fuel pool shall meet the following conditions:

1.1 Based on the conditions of post-operation modes and volumes of refuelling fuel, two fuel pools BV-3, BV-4 will be in operation. The system for maintaining the water temperature of the fuel pools is the same for both pools.

1.2 Considering the difficulties in cleaning the heat exchangers of the existing fuel pool cooling system (pos. 3 in Fig. 1) in connection with radiation, in order to avoid possible contamination of the heat exchange surface, it is planned to use chemically demineralized water (CDW) in a closed circuit.

1.3 To avoid accident of heat exchangers (Fig. 1) it is assumed to keep constant monitoring of CDW activity by measuring instruments. If the activity value exceeds the permissible limits, the temperature maintenance system shall be stopped.

1.4 From the reliability conditions, all key elements of the temperature maintenance system shall be redundant.

1.5 Based on the conditions for ensuring the temperature of the fuel pool water in all operating modes, the newly developed system should be able to repair the key components of the system without stopping it.

1.6 Due to the fact that the volume and existing fuel pools BV-3 and BV-4 are different, and heat release from fuel cells in different post-operational periods, the newly developed system should be able to simultaneously operate different pools in different modes, for example, providing water heating of one of the pools and cooling of the water of the other pool.

1.7 The newly developed system shall be equipped with a sufficient number of process controls and automation controls that ensure reliable and safe operation.

1.8 In addition to the material barrier, a pressure barrier shall be provided between the contours of the fuel and cold water basins.

All of the above conditions can be realized by providing the system with a source of cooling and heating water.

As a cooling source, it is planned to use the existing service water system, which will cool the CDW closed loop through the heat exchanger. As a source of heating, electric heating plants are supposed to be used.

VIII. REFERENCES

1. Технологический процесс перевода ОЯТ РБМК-1000 с «мокрого» на «сухое» хранение / В. И. Калинкин [и др.]. – СПб.: ОАО «Головной институт «ВНИПИЭТ», 2010. – С. 107./ SNF transfer technological process RBMK-1000 from "wet" to "dry" storage / V. I. Kalinkin [and others]. - SPb .: JSC "Golovnoy Institute "VNIPIET", 2010. - P. 107.

2. Хранение отработавшего ядерного топлива энергетических реакторов / В. И. Калинкин [и др.]. – СПб.: ОАО «Головной институт «ВНИПИЭТ», 2009. – С. 107./ Storage of spent nuclear fuel of power reactors / V. I. Kalinkin [et al.]. - SPb .: JSC "Head Institute "VNIPIET", 2009. - P. 107.

Proceedings of the European Nuclear Young Generation Forum
ENYGF'21
September 27-30, 2021, Tarragona, Spain

Development of a gamma irradiation loop to evaluate the performance of the EURO-GANEX process

Sánchez-García, Iván[1,2*], Galán Montano, Hitos[1], Núñez Gómez-Aleixandre, Ana[1], Perlado Martín, Jose Manuel[2] and Cobos Sabaté, Joaquín[3]

[1] CIEMAT, Spain; [2] UPM, IFN, Spain; [3] EBD-CSIC, Spain.

*Corresponding author: *ivan.sanchez@ciemat.es*

I. INTRODUCTION

The reprocessing of nuclear fuel is currently moving towards advanced cycles that contemplate the recycling of minor actinides (MAs: Am, Cm, Np) as a strategy to minimise the radiotoxicity of the waste that must be stored [1, 2]. To validate a new separation process for this purpose, solvents are not only tested concerning the extraction efficiency but also their resistance against radiolysis and hydrolysis effects. This is because extracting systems will be in contact with a highly radioactive field and high nitric acid concentration, producing its degradation and undesirables effects such as decrease of selectivity, third phase formation, etc., and the consequent increase of secondary waste and process costs [3, 4]. Hence, the development of a successful industrial process demands an approach of the stability problems, from the initial design of the extractant to a hot test in a pilot plant. The initial irradiation studies of individual solvents involving isolated molecules, in batch and static conditions, allow the fundamental comprehension of the degradation pathways and an easy way to compare the robustness of different extractants. However, to predict the long-term behaviour during the operation, a more realistic assessment of the process conditions must be considered. Although batch irradiation experiments can be designed to cover many scenarios, dynamic experiments simulating counter-current processes, as lifelike as possible, are always needed. Nowadays, it exists an important gap between fundamental irradiation experiments and advanced test in pilot plants, which require sophisticated dynamic irradiation platforms (irradiation loops) where the settings are not normally easily modifiable. CEA Marcel-Proust loop (Commissariat à l'énergie atomique et aux énergies alternatives) in France and the Idaho National Laboratory (INL) loop in United States are two of the most successful irradiation loops developed for these kind of tests until now.

In this work, an irradiation test loop has been designed and implemented in the Náyade facility at CIEMAT, where some of the most relevant process conditions can be studied with the possibility to perform easily modifiable experiments. Moreover, this design allows the irradiation of two phases in contact, its configuration step by step improves the simulation of the doses expected for each phase, but also permits a straightforward modification of the experiment settings and has a low volume of solvent requirement compared to the other mentioned loops.

As part of a homogeneous actinides recycling strategy, Grouped Actinide Extraction (GANEX) concept was found which consists of two cycles: the first one for the bulk recovering of uranium (U) and the second one aiming for the separation of all transuranic elements (TRU: Pu, Np, Am, Cm) together [5]. The EURO-GANEX process is one of the most promising options for GANEX second cycle, which is based on the complementary selectivity of extractants used in its organic and aqueous phases [5]. It comprises two steps, the co-extraction of Actinides (An) and Lanthanides (Ln) and the TRU stripping [6]. In the An and Ln co-extraction, a solvent consisting in TODGA (*N,N,N',N'*-tetraoctyl diglycolamide) and DMDOHEMA (*N,N'*-dimethyl-*N,N'*-dioctylhexylethoxymalonamide) in Exxsol D80 (a kerosene diluent) is blended with the feed from the GANEX first cycle raffinate and CDTA (trans-1,2-cyclohexanediaminetetraacetic acid), which prevents the co-extraction of Pd(II) and Zr(IV) along with An and Ln [7]. TODGA is used to co-extract An and Ln and DMDOHEMA is employed to prevent the third phase formation increasing the Pu loading capacity of the organic phase [6]. After the co-extraction step, a scrubbing is needed to remove the elements co-extracted as Sr, Fe, Mo, Ru and Tc among others [6]. Then, TRU elements are selectively recovered into the aqueous phase in the TRU stripping step by using a combination of two water-soluble complexants in a lower nitric acid concentration: a sulphonated bis-triazinyl pyridine (2,6-bis(5,6-di-(sulfophenyl)-1,2,4-triazin-3-yl)-pyridine (SO_3-Ph-BTP) and acetohydroxamic acid (AHA) [6]. SO_3-Ph-BTP is used to strip Am(III) and Cm(III) selectively from Ln [6], while AHA is added to strip Pu and Np [6, 8].

The new irradiation loop has been adapted to assess the performance of the EURO-GANEX process [5, 6]. In order to simulate the most relevant aspects of these processes, the design of the loop should involve the irradiation of two phases in contact and take into account its composition, the nitric acid concentration, the renewal of oxygen content and the dose

expected for each phase. With this purpose, phases will be mixed under an open atmosphere outside the Náyade pool and irradiated together when they are passing thought the coil in the CIEMAT irradiation loop (Figure 1).

II. EXPERIMENTAL

A. Materials

The extractants used in the organic phase were TODGA and DMDOHEMA, and the diluent was odourless kerosene (OK). TODGA was synthesized at CIEMAT and the purity was determined by HPLC-MS as 98 %. DMDOHEMA with a purity of 99 % by HPLC-MS was purchased from Technocomm Ltd (United Kingdom). The reagents in the aqueous phase were the water-soluble BTP (SO_3-Ph-BTP) and CDTA, using nitric acid (HNO_3) as diluent. The reagents were used without further purification except HNO_3. The radioactive tracer solutions of ^{241}Am(III) and ^{152}Eu(III), and Highly Active Raffinate (HAR) solution were used to simulate the high-level waste stream after reprocessing typical spent fuels [9].

B. Irradiation test loop

Gamma irradiation experiments of the extraction systems involved in the different steps of the loop were performed at the Náyade facility (CIEMAT). Solvents to be irradiated were mixed outside of the pool, at 1:1 ratio and opened atmosphere, and pumped by peristaltic pumps through the tubing to a 316 stainless steel coil designed and manufactured at CIEMAT (10 mm outside and 8 mm inner diameters and 110 mm length) for the irradiation (Figure 1). The stainless steel coil was introduced in the hermetic irradiation device located at the bottom of the Náyade pool. ISO-Versinic (Viton) tubing employed has passed all resistance test done up to 1000 kGy in contact with nitric acid. The connections between the Viton (6 mm outside and 4 mm inner diameters) tubing and the stainless steel coil are composed of an outlet valve with a screw cap of stainless steel. To know the effective dose rate provided by ^{60}Co sources in static conditions, a Fricke dosimetry using a shielding of stainless steel with the same thickness that coil reactor was carried out. As the residence time of solvent within the irradiator coil is only a fraction of the total, the effective dose rate applied over the coil was determined by taking into account the coil volume, phases residence time and the effective dose through the steel, giving a result of 2.89 kGy/h.

C. Solvent extraction performance

The behaviour of EURO-GANEX process after the two different steps mentioned before was assessed with spiked samples (^{241}Am and ^{152}Eu) and the phases composition shown in Table 1. Samples of the organic phase taken at 200 and 500 kGy after the first irradiation (An+Ln co-

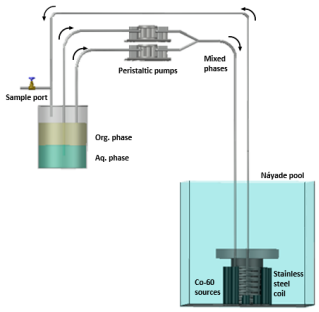

Figure 4. Schematic diagram of the irradiation test loop.

extraction), were put in contact with a fresh aqueous phase consisting of 10 $\%_{vol}$ of a simulated HAR solution and 0.055 mol/L CDTA in 5 mol/L HNO_3 and spiked with 10 µL of ^{241}Am and ^{152}Eu (100 kBq/ml each). Between both irradiations steps, a scrubbing step with diluted nitric acid was introduced to simulate EURO-GANEX conditions for adjusting the acidity of the following step and removing Fission products (FP) and corrosion products (CP) co-extracted into the organic phase. Therefore, the loaded organic phase was put twice in contact with the same volume of fresh 0.5 mol/L HNO_3 for 5 minutes. After the second step of irradiation (TRU stripping step), the behaviour of the system was assessed by using samples taken from both irradiated phases (Table 1): TODGA and DMDOHEMA (up to 540 kGy) and 0.018 mol/L SO_3-Ph-BTP in 0.5 mol/L HNO_3 (from 10 to 40 kGy) and then spiked with 10 µL of ^{241}Am and ^{152}Eu (100 kBq/ml each). AHA is not included in the extraction experiments because neither Pu and Np were used in the current tests.

All extraction experiments were performed by mixing 500 µL of both, aqueous and organic phases, for 30 min at room temperature (22 ± 2 ºC). Then, the phases were separated by centrifugation (5 min at 5000 rpm) and aliquots of each one were taken for analysis. For ^{241}Am and ^{152}Eu analysis, gamma spectrometry was employed and the concentration of the elements presented in the HAR solution as well as those coming from the stainless steel CP (Fe, Cr, Ni and Mo) were determined by ICP-MS. All extraction results are reported as distribution ratio D ($D_M = [M^{3+}]_{org} / [M^{3+}]_{aq}$), and D_M between 0.01 and 100 exhibit a maximum error of ± 5 %.

D. Solvent composition analysis

The chemical composition of the irradiated organic and aqueous samples was determined by HPLC-MS and Raman spectroscopy, respectively. HPLC-MS measurements were performed by using an HPLC-MS Bruker EVOQTM (Triple Quadrupole detector) with a ACE 3 C18-PFP column (50mm × 2.1mm) at 40°C, using a gradient of mobile phase [(A: 0.1% HCOOH in H_2O), (B: 0.1% HCOOH in CH_3CN)]. $APCI^+$ ionization mode was used for TODGA and DMDOHEMA quantification, meanwhile ESI^+ mode was used for TODGA degradation compounds (DCs) quantification. The concentration of SO_3-Ph-BTP was measured by Quantitative Raman Spectroscopy (QRS). Raman spectra of samples were acquired by using a B&W Tek i-Raman™, model BWS415-785S. A red laser of HeNe with a wavelength of 785 nm and an operation power of 300 mW was employed. The spectral range available to this spectrometer is from 175 to 3200 cm^{-1}, with a spectral resolution about 5 cm^{-1}.

Table 2. Composition of the organic and aqueous phases in the different steps of the irradiation test loop and the following extraction experiments.

Experiments		Solvent formulation	
		Organic phase	Aqueous phase
An+Ln co-extraction Step	a) Irradiation	Fresh EURO-GANEX solvent 0.2 mol/L TODGA + 0.5 mol/L DMDOHEMA in OK	Fresh 5 mol/L HNO_3
	b) Extraction after the 1st irradiation	Irradiated EURO-GANEX solvent 200 and 500 kGy TODGA +DMDOHEMA in OK	Fresh 0.055 mol/L CDTA + 10 $\%_{vol}$ HAR in 5 mol/L HNO_3
Scrubbing Step	Intermediate step between irradiations	Irradiated EURO-GANEX solvent from the previous step (500 kGy) TODGA +DMDOHEMA in OK	Fresh in 0.5 mol/L HNO_3
TRU stripping Step	a) Irradiation	Irradiated EURO-GANEX solvent from the previous step (500 kGy) + scrubbing TODGA +DMDOHEMA in OK	Fresh 0.018 mol/L SO_3-Ph-BTP in 0.5 mol/L HNO_3
	b) Extraction after the 2nd irradiation	Irradiated EURO-GANEX solvent from the second step (540 kGy) TODGA +DMDOHEMA in OK	Irradiated Aq. phase (10, 20, 30 and 40 kGy) 0.018 mol/L SO_3-Ph-BTP in 0.5 mol/L HNO_3

III. RESULTS AND DISCUSSION

The An+Ln co-extraction system (0.2 mol/L TODGA + 0.5 mol/L DMDOHEMA in OK in contact with 5 mol/L HNO_3) was irradiated at 200 and 500 kGy, simulating an accumulative absorbed dose of the recycled organic phase. During the irradiation process, a colour change of the organic phase from slightly yellow to dark yellow was found, but not third phase formation, precipitate, or other physical changes. After that, the 5 mol/L HNO_3 aqueous phase was replaced by a fresh solution containing CDTA, HAR solution in 5 mol/L HNO_3 and spiked with ^{241}Am and ^{152}Eu. A normal phase separation behaviour was also obtained without any precipitates or third phase formation. The variation of $D_{Am(III)}$ and $D_{Eu(III)}$ as a function of absorbed dose is shown in Figure 2. As expected from the previous studies [6], both metals are well extracted into the organic phase even after a 500 kGy (D > 100), although a slight decrease in the D values is always observed for both elements. Therefore, under the irradiation loop condition applied, the system can still extract An and Ln even after 500 kGy of absorbed dose.

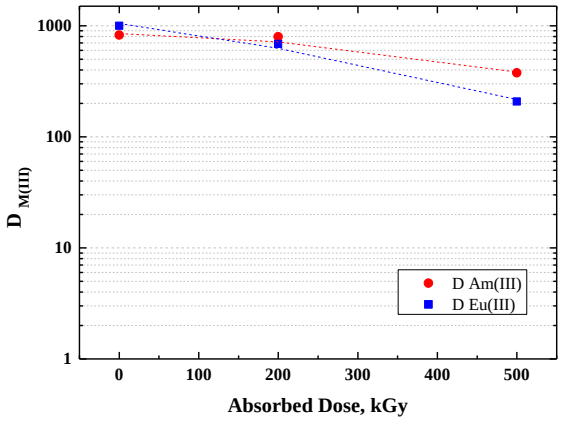

Figure 5. Distribution ratios of Am(III) and Eu(III) as a function of absorbed dose after the first step of the irradiation loop test (An+Ln co-extraction, see Figure 2).

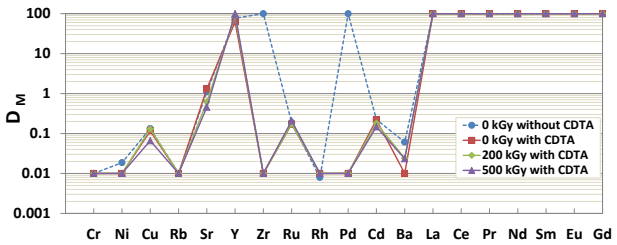

Figure 6. Ln and FP extraction by fresh and irradiated Euro-GANEX solvent (0.2 mol/L TODGA + 0.5 mol/L DMDOHEMA in OK) at 200 and 500 kGy from a fresh aqueous phase consisting of 5 mol/L HNO_3 with and without 0.055 mol/L CDTA.

FP and Ln elements concentrations were measured in both phases by ICP-MS, and the distribution ratios obtained for these elements are represented as a function of absorbed dose in Figure 3. As can be observed, the extraction behaviour for most of these elements kept unchanged when the irradiated and non-irradiated samples are compared, showing Y and Ln high D values in all cases (D > 100). The influence of the CDTA presence on the extraction of Zr and Pd is clearly observed in a significant decrease of the D_{Pd} and D_{Zr} reaching values of D < 0.01, in agreement with previous studies [6, 7].

As the reactor coil employed in the irradiation loop is made of 316 stainless steel, the possible corrosion products as a consequence of the contact with nitric acid and radiation, and the acidity have been studied for all process, concluding that Fe, Cr, Ni and Mo are the most relevant stainless steel corrosion products.

After simulating a long-term spent organic phase (after 500 kGy), and the corresponding scrubbing step, the organic phase was again irradiated in contact with a new aqueous phase, consisting in 0.018 mol/L SO_3-Ph-BTP in 0.5 mol/L HNO_3, to simulate the possible effects over the global performance during the TRU stripping (see Table 1). This system was irradiated up to 10, 20, 30 and 40 additional kGy. Over the course of the second irradiation step, the aqueous phase containing the SO_3-Ph-BTP darkened considerably, from the green of the unirradiated samples to opaque black of the irradiated samples, which has been widely related to its radiolytic degradation [10]. The $D_{Am(III)}$ and $D_{Eu(III)}$ values determined at the corresponding doses selected along the irradiation of the TRU stripping step are presented in Figure 4. An unexpected high $D_{Am(III)}$ values was observed from the beginning of the experiment, letting an ineffective separation between An and Ln. This phenomenon could be attributed to three possibilities: the metals corrosion presence, the variation of pH or the ligand degradation.

Additional extraction experiments with EURO-GANEX solvent to check the TRU stripping as function of the Fe, Cr and Ni concentrations have been carried out. As the concentration of Fe, Cr and Ni increases (Exp. 2-5, Table 2), the $D_{Am(III)}$ values also increase. These results point out that the presence of these metals in the aqueous phase effectively influences the extraction capacity of the system modifying the distribution ratios, and therefore, the system performance. However, an acidity rise (from 0.50 mol/L to 0.84 mol/L for all absorbed dose studied) has also been observed in this step, which can not be either ignored due to it is well-known the relation between the pH and the extraction capacity of the solvents.

Table 3. Distribution ratios of An(III) and Ln(III) by fresh EURO-GANEX solvent from the fresh aqueous phase varying Fe(III), Cr(III) and Ni(II) concentrations.

Exp.	Samples composition					Distribution ratios	
	Org. phase	Aq. phase	Fe(III), mmol/L	Cr(III), mmol/L	Ni (III), mmol/L	$D_{Am(III)}$	$D_{Eu(III)}$
1	0.2 mol/L TODGA + 0.5 mol/L DMDOHEMA in OK	0.018 mol/L SO_3-Ph-BTP in 0.5 mol/L HNO_3	-	-	-	0.09	22.5
2			-	0.02	0.02	0.18	35.4
3			-	0.10	0.09	0.21	55.4
4			0.02	0.02	0.02	0.30	65.9
5			0.36	0.10	0.09	0.31	41.0

The degradation of the extractants and the subsequent DCs formation affect the extraction capacity due to the DCs formed could have different extraction properties which could interfere in the correct process performance. Therefore, the effect over the main extractants in the organic phase was analysed. As expected, the extractants concentrations diminish as a function of dose, reaching a decrease of 32 % for TODGA and 33 % for DMDOHEMA in agreement with the literature [10, 11, 12]. In parallel to the main extractants, also TODGA and DMDOHEMA DCs were identified. Eight of the main typical TODGA DCs [3, 11] and six of the DMDOHEMA DCs [12] could be identified. Moreover, three new signals have been identified as possible undescribed DCs, probably as a consequence of the irradiation in dynamic conditions, which is in concordance with our recent works [10]. Additionally, the radiolytic degradation of SO_3-Ph-BTP was analysed by QRS. In the conditions of this work, the SO_3-Ph-BTP concentration decrease as a function of absorbed dose, i.e., approx. 65 % is lost after 40 kGy, showing that this compound is very susceptible to degradation under the studied radiation conditions, which also agrees with the studies found in the literature [10].

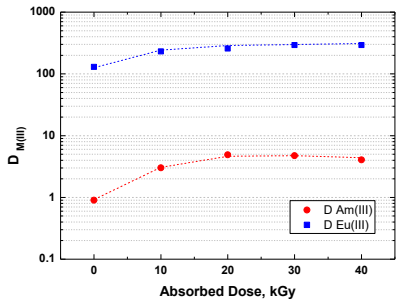

Figure 7. Distribution ratios of Am(III) and Eu(III) as a function of dose for the second irradiation step (TRU stripping, see Figure 2).

IV. CONCLUSIONS

In this work, an irradiation test loop that combines the advantages of simple statics irradiation experiments with those of sophisticated irradiation dynamic plants has been developed for the first time. The configuration let an easy modification of settings with a really low volume requirement. This new design allows simulating relevant process conditions such as the composition and contact between phases involved, the oxygen content and the dose expected for each of them. This new irradiation loop implemented at the Náyade irradiation facility at CIEMAT has been initially developed for assessing the performance of the two main steps of the EURO-GANEX process (An+Ln co-extraction and TRU stripping), under the most relevant and realistic experimental conditions in an easy and adaptable way. EURO-GANEX is a promising process to achieve the recovery of the transuranic elements in the same process, reducing the necessary steps and consecutive processes.

The An and Ln co-extraction step shows an excellent extraction performance for An and Ln. The monitoring of the different effects over the system (stainless steel corrosion, acidity, ligand concentration and presence of degradation compounds) in this step still revealed a situation under control. Fortunately, the scrubbing section introduced between the first and second irradiation steps of the loop was effective in reducing the proton concentration and removing some of the corrosion metals. However, an unexpected high $D_{Am(III)}$ values were observed from the beginning of the experiment during the TRU stripping, letting an ineffective separation between An and Ln. It could be said that the unexpected $D_{Am(III)}$ values are the result of a mixture of factors that can not be isolated. The metal corrosion presence has demonstrated the correlation between the metals concentrations and the $D_{Am(III)}$. The variation of the pH is an important factor that could modify the performance of the process. And the ligand degradation together the DCs formation, is crucial to understand the long-term process. All results obtained evidence the importance of developing realistic irradiation experiments where different factors affecting the performance should be studied.

V. ACKNOWLEDGMENT

This work has been developed under the framework of the European H2020 GENIORS Project, CIEMAT-ENRESA collaboration agreement (SOPSEP project) and Spanish SYTRAD II project.

VI. REFERENCES

[1] E. Collins, G. DelCul, B. Spencer, R. Jubin, C. Maher and I.-T. Kim, "State-of-the-Art Report on the Progress of Nuclear Fuel Cycle Chemistry," Organisation for Economic Co-Operation and Development 2018.

[2] Spent Fuel Reprocessing Options. Vienna: INTERNATIONAL ATOMIC ENERGY AGENCY, IAEA 2009.

[3] H. Galán, A. Núñez, A. G. Espartero, R. Sedano, A. Durana, and J. de Mendoza, "Radiolytic stability of TODGA: characterization of degraded samples under different experimental conditions," Procedia Chemistry, vol. 7, pp. 195-201, 2012.

[4] A. Nunez, H. Galan, and J. Cobos, "TODGA degradation compounds: properties and effects on extraction systems-5400," in GLOBAL 2015 Proceedings, ed, 2015.

[5] J.-M. Adnet, M. Miguirditchian, C. Hill, X. Heres, M. Lecomte, and M. Masson, "Development of new hydrometallurgical processes for actinide recovery: GANEX concept," in Proceedings of GLOBAL, 2005.

[6] R. Malmbeck, D. Magnusson, S. Bourg, M. Carrott, A. Geist, and X. Hérès, "Homogenous recycling of transuranium elements from irradiated fast reactor fuel by the EURO-GANEX solvent extraction process," Radiochimica Acta, vol. 107, pp. 917-929, 2019.

[7] M. Sypula, A. Wilden, C. Schreinemachers, R. Malmbeck, A. Geist, and R. Taylor, "Use of polyaminocarboxylic acids as hydrophilic masking agents for fission products in actinide partitioning processes," Solvent Extraction and Ion Exchange, vol. 30, pp. 748-764, 2012.

[8] R. Taylor, I. May, A. Wallwork, I. Denniss, N. Hill, and B. Y. Galkin, "The applications of formo-and aceto-hydroxamic acids in nuclear fuel reprocessing," Journal of Alloys and Compounds, vol. 271, pp. 534-537, 1998.

[9] Modolo, G., Asp, H., Schreinemachers, C., and Vijgen, H. “Development of a TODGA based process for partitioning of actinides from a PUREX raffinate Part I: Batch extraction optimization studies and stability tests.” Solvent Extraction and Ion Exchange, vol. 25, no 6, p. 703-721, 2007.

[10] I. Sánchez-García, H. Galán, J. M. Perlado, and J. Cobos, "Development of experimental irradiation strategies to evaluate the robustness of TODGA and water-soluble BTP extraction systems for advanced nuclear fuel recycling," Radiation Physics and Chemistry, vol. 177, p. 109094., 2020.

[11] Y. Sugo, Y. Sasaki, and S. Tachimori, "Studies on hydrolysis and radiolysis of N, N, N′, N′-tetraoctyl-3-oxapentane-1, 5-diamide," Radiochimica Acta, vol. 90, pp. 161-165, 2002.

[12] L. Berthon, J. Morel, N. Zorz, C. Nicol, H. Virelizier, and C. Madic, "DIAMEX process for minor actinide partitioning: hydrolytic and radiolytic degradations of malonamide extractants," Separation Science and Technology, vol. 36, pp. 709-728, 2001.

Proceedings of the European Nuclear Young Generation Forum
ENYGF'21
September 27-30, 2021, Tarragona, Spain

Development of the first Russian research molten salt nuclear reactor aimed to elaborate the technology of minor actinides recycling and to prepare for construction of the full-scope industrial minor actinides burning reactor

Vlasenko Evgeny[1*]

[1] Federal State Unitary Enterprise "Mining and Chemical Combine" (FSUE "MCC"), Russia

*Corresponding author: *vlasenko_zhene@mail.ru*

I. INTRODUCTION

The State Corporation for Atomic Energy "Rosatom" and, particularly, its subsidiary company "Mining and Chemical Combine" (MCC) is actively engaged in the nuclear back-end: the construction of the spent nuclear fuel recycling center has been completed, and the MOX-fuel for fast reactor plant has been operating successfully.

The important part of the nuclear back-end is closure is minor actinides afterburning aimed to decrease the capacity and radiotoxicity of highly radioactive wastes of spent nuclear fuel recycling subject to final isolation. Finding the solution for this problem will improve ecological characteristics of atomic energy generation. A research molten salt nuclear reactor integrated with the module for fuel salt recycling is being developed as the first step for generating the new technology of minor actinides burning.

II. TECHNICAL FEATURES

The main technical specifications of the research molten salt nuclear reactor according to the technical design report [1] are presented in the table.

Table 1. Research reactor technical specifications.

Parameter	Value
Thermal power, MWt	10
Reactor type	Homogenous
Nuclear fuel	PuF3+AnFn
Heat removal scheme	Three-circuit
Reactor core volume, m^3	1
Specified lifetime, years	10

Let's look at technical features in more detail.

A. Consumption of minor actinides

It is assumed that a part of the spent nuclear fuel (about 10%) should be replaced with the fresh fuel annually. That is why fuel composition should guarantee reactivity margin which is enough to work for a whole year without refueling. According to this, starting fuel composition should contain about 0.78% (molar) of PuF3. Minor actinides are to be added when refueling. A fresh fuel should contain about 4% (molar) of PuF3+AnFn. The ratio of Pu to minor actinides is 80/20%.

The research molten salt nuclear reactor is aimed to elaborate the technology of minor actinides burning. That is why optimum Pu and minor actinides concentrations are a subject of scientific work of future periods as well as an option of "online" fuel salt recycling.

B. Fuel circuit configurations

Three main variants of fuel circuit configuration are being considered: loop configuration inside the "cold" box, loop configuration inside the "hot" box, and, finally, integrated configuration. All the variants include systems to pre-heat reactor vessel and devices inside the vessel with hot noble gas.

Loop configuration inside the "cold" box means that pipelines and fuel circuit devices are placed in safety cases. Electric heaters and thermal insulation encircle the cases. The inner space between safety cases and pipelines or devices is divided into sections. Every section is being ventilated with noble gas. The leakage detectors are installed in every section.

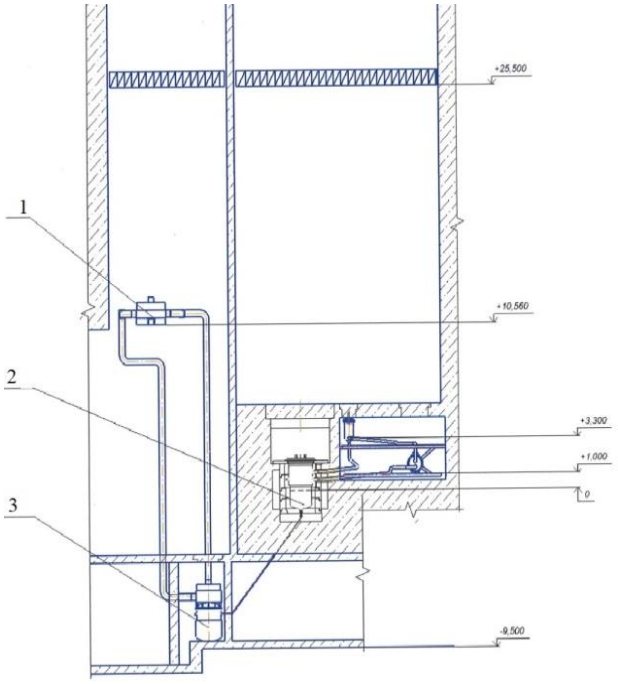

Figure 1. Loop configuration inside the "cold" box (1 – emergency heat exchanger, 2 – reactor vessel, 3 – vessels of the system for passive fuel salt drainage)

Loop configuration inside the "hot" box means that pipelines, fuel circuit devices and reactor vessel are placed inside hermetical "hot" (heated) box. The inner space of the box is filled with noble gas. The temperature inside the box is about 600℃. The box is surrounded with thermal insulation.

Finally, integrated configuration means that all the fuel circle including intermediate heat exchanger and main circulation pump are placed inside the reactor vessel.

Fuel circuit configurations described above have their advantages and disadvantages. For instance, loop configuration inside the "cold" box makes it possible to place drive mechanisms of pumps and check valves as well as process control instruments in normal working conditions. Another benefit is that fuel salt leakage can be isolated within a safety case.

In contrast to loop configuration inside the "cold" box, loop configuration inside the "hot" box allows to simplify design of fuel circuit devices and pipelines. However, it's more diffucult to perform maintenance and repair operations inside hermetical "hot" (heated) box. For instance, in case of leakage it's necessary to decontaminate the whole box volume after repair.

A mixture of plutonium fluorides and minor acitinides fluorides dissolved in molten salt was chosen as a nuclear fuel. Molten salt fuel composition circulates through a cavity-type core. Thus, the heat is transferred to a molten salt reactor coolant that circulates within the intermediate circuit.

It's assumed that a part of spent nuclear fuel should be replaced with the fresh fuel containing minor actinides fluorides on an annual basis.

Table 2. Circuits technical specifications.

Parameter	Value
Fuel circuit	
Molar composition	73LiF-27BeF2
Input salt temperature	650℃
Output salt temperature	700℃
Intermediate circuit	
Molar composition	66LiF-34BeF2
Input salt temperature	550℃
Output salt temperature	600℃
Final heat utilization circuit	
Input air temperature	30℃
Output air temperature	275℃

Looking ahead, another type of fuel salt (LiF-NaF-KF) may be used if durable structural materials for the fuel circuit are found and justified, and if effective methods for dissolved elements disposal are developed.

Final heat utilization could be performed at air heat exchangers or at steam heating systems.

Emergency heat utilization system is a passive circulation system designed to cooldown vessels of the system for passive fuel salt drainage. The heat transfer agent is noble gas (argon).

C. Structural materials

A highly-nickel alloy is to be used as a structural material for the fuel circuit containing FLiBe salt. The alloy is resistant to surface embrittlement in mechanical tension and irradiation conditions. The material is corrosion-resistant in molten fluoride salts and mechanically stable in a long term period when irradiated in high temperature conditions. Taking into account the MSRE nuclear reactor operational experience in the USA, special attention is focused on resistance to tellurium intercrystalline corrosion and selective chromium corrosion within alloy modification development and review process [2].

D. Fuel salt composition modification and reprocessing

The fuel salt composition is to be modified within the nuclear reactor operation. The modification should involve constant gaseous fission products disposal, introducing trans-uranium elements fluorides to compensate fission material burnout, elimination of soluble and slightly soluble (both noble and semi-noble) fission products along with the corrosion products of structural materials.

In order to capture slightly soluble elements, a filter section system with a big nickel-based surface is going to be used in a bypass of the reaction circle. The technology for dissolved elements disposal may be based upon the extraction to the liquid bismuth. The development of structural materials for the fuel salt recycling module is an important complicated task. Graphite and molybdenum are being considered as the candidate structural materials for the parts of the module that contain bismuth.

III. CONCLUSION

By 2024 the necessary justifying R&D are to be completed, as well as the nuclear reactor technical project. According to preliminary estimates, the physical start-up of the research reactor is 2032. Technologies and the results of material science and other types of experiments will be used as a basis for construction of the full-scope industrial minor actinides burning reactor.

IV. REFERENCES

[1] A.V. Kaplienko “Technical design report and technical task for draft proposal. Accomplishment of scientific works in justification of research nuclear molten salt reactor. 2020 phase”, JSC “NIKIET”, Moscow, Russia. Sci. Rep. NIOKTR AAAA-A20-120101690017-2, Nov. 2020.

[1] H.E. McCoy, Jr. “Status of materials development for molten salt reactors”, Oak Ridge National Laboratory, Oak Ridge Tennessee, USA, Rep. ORNL/TM-5920, Jan. 1978.

Proceedings of the European Nuclear Young Generation Forum
ENYGF'21
September 27-30, 2021, Tarragona, Spain

Isolation of solid organic matter from complex clay matrices

Ferran Bagaria[1,*], David García[1], Lara Duro[1], Stéphane Brassinnes[2]

[1]Amphos 21 Consulting SL, Carrer Veneçuela 103, 08019, Barcelona, Spain; [2]Belgian Agency for Radioactive Waste and Enriched Fissile materials (ONDRAF/NIRAS), Belgium

**corresponding author: ferran.bagaria@amphos21.com*

I. INTRODUCTION

Boom Clay (BC) formation is widely studied due to its consideration as a Geological Disposal Facility (GDF) of high-level nuclear waste [1]. BC is enriched in immature organic matter [2], this type of organic matter is highly reactive and expected to affect radionuclide (RN) transport of strongly hydrolysing RN. In conditions of thermal stress, immature organic matter is able to generate CO_2 and soluble oxygen-containing components that could affect the chemistry of the clay interstitial water and change the confinement properties of the clay barrier.

Solid Organic Matter (SOM) is common in reducing clay rocks, with contents of total organic carbon (TOC) up to 5% (of the total rock) in the case of Boom Clay formation [3]. SOM can be divided into water-soluble solid organic matter (e.g., humic and fulvic acids), SOM water-insoluble but soluble in organic solvents (i.e. bitumen), and totally insoluble solid organic matter (i.e. kerogen).

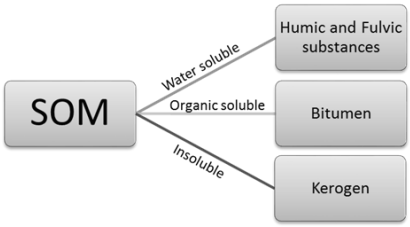

Figure 1. Different fractions of SOM in BC.

Water-soluble OM is the fraction of SOM more suitable for being isolated. The contact of the water with the BC is sufficient to dissolve and allow the analysis of this type of SOM. In the literature, several works have been investigating OM within the BC formation. Studies of OM are done through water leaching experiments, or directly analysing the porewater from the BC formation [4].

Bitumen extraction is mainly linked to the use of a soxhlet device, which allows the contact between the BC sample and a solvent that recirculates in a closed system. Different solvents are used to extract bitumen, such as chloroform, toluene, and dichloromethane. Sometimes, the solvent is not a pure phase and is mixed with 2 or 3 organic compounds [5].

To isolate kerogen, the most common method is the acid treatment, with HCl and HF, followed by a drying process [6]. This method is based on the palynological treatment for the study of pollen. Other methods such as thermals or physicals are also used [7], but, if the objective is to preserve the SOM sample as much as possible, the thermal method is not an option. Hétenyi &Varsáni [7] do a comparative study between physical methods (flotation) and acid treatment, concluding that acid treatment presents higher recovery levels than physical methods. Otherwise, also in Hétenyi &Varsáni [7] proves that chemical treatments can affect the chemical structure of kerogen.

The experiences presented in this contribution are focused on the reproduction of extraction methods used in the literature for the different SOM fractions and its characterization, in an attempt to facilitate the interpretation of the results obtained.

This work aims to optimize the extraction methods to isolate this SOM, preserving its initial structure and maximising the purity of the product obtained.

The production of an accurate protocol and an evaluation of the influence of these extraction methods on SOM will increase the confidence in future works related to the organic matter present in BC formation.

II. METHODOLOGY

A. Boom Clay samples

Two samples from different members of the BC formation were selected: Putte member (ON Mol 2D core 74.1 as reference code) with higher TOC content [3], and the Boeretang member (ON Mol 2D core 23.2 as reference code). The stratigraphic position of the samples is indicated in Figure 2.

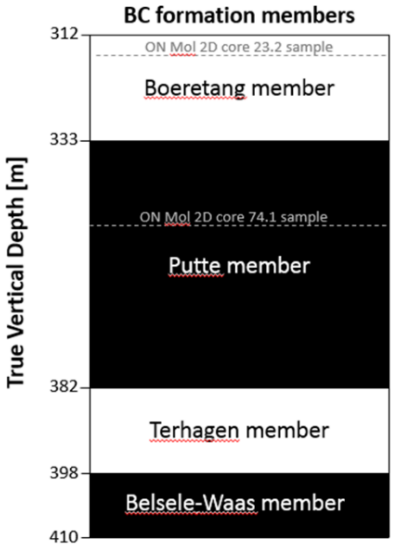

Figure 2. Stratigraphic location of BC samples and clay members of the BC formation.

B. Dissolved organic matter (DOM) extraction: Leaching experiments

Batch sequential extraction experiments were done by contacting the BC samples with carbonated water (

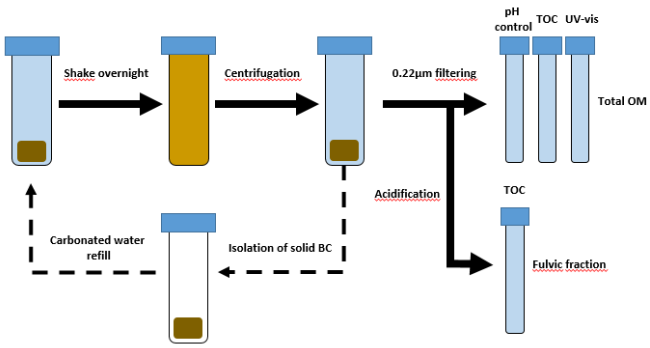

Figure *8*). Sequential extractions allow the study of the different type of released organic material with the contact time.

For these tests, 2 duplicate experiments with 4.5g of BC and 45mL of carbonated water (deionized water + $NaHCO_3$ 15 mM) were prepared. The experiments were under continuous stirring for 1 day. Presence of oxygen could affect the composition of OM, to avoid the sample oxidation, the samples were preserved with Parafilm®.

Removal of supernatant was carried out every day. After removal, the sample was filtered (0.45µm nylon filters). One aliquot was used to measure pH and the TOC content (Shimadzu 5050); another aliquot was acidified (pH<2) to precipitate the humic fraction. Non precipitated OM was assumed to be the fulvic fraction.

The evolution of the type of organic matter dissolved was studied by UV-vis analyses.

TOC measurements of non-acidified (Total OM) solution and acidified solution (Fulvic fraction) were used to calculate the amount of extracted humic acids.

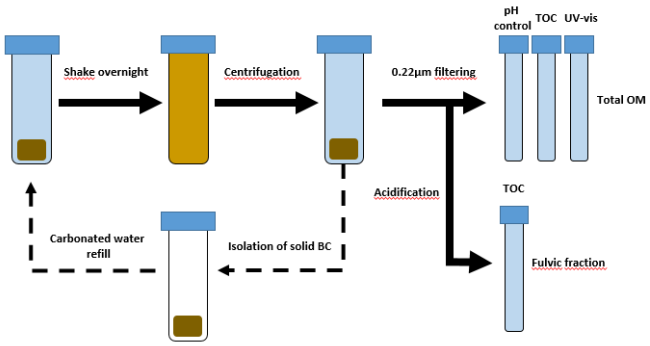

Figure 8. Experimental procedure to characterize the organic matter released from BC.

C. Bitumen extraction: Soxhlet device

Extraction of bitumen was carried out using the soxhlet extraction method (Figure 4). The organic matter was dissolved in dichloromethane. Following the EPA guidelines [8], a solid to liquid ratio of 100 g/L was used.

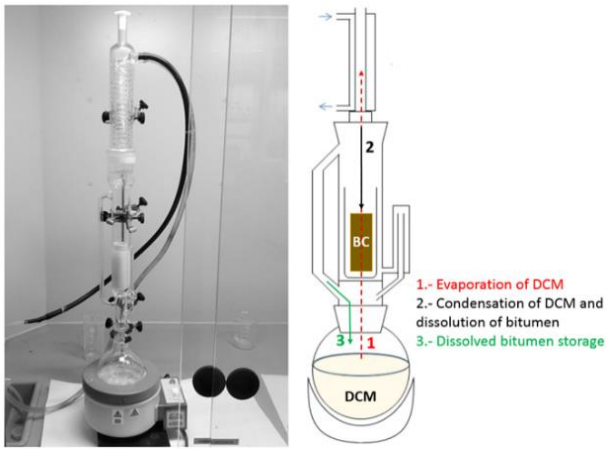

Figure 4. Soxhlet device used to extract bitumen with DCM.

The soxhlet extraction was continuously run for times over 72 hours.

Once the bitumen was extracted with DCM, FTIR (Perkin Elmer Spectrum Two) and GC-MS (Agilent® 6890) analysis of the extracted organic components were performed.

D. Kerogen extraction: Acid treatment

Prior to the isolation of the insoluble organic matter, an acid treatment was used to dissolve the minerals present in the sample. The procedure used for this process (Table 1) was based on the acid treatment proposed by Durand [6]. After treatment with concentrated HCl and HF, pyrite is the only mineral expected to remain in the solid. The acid treatment lasted 3 days, during day 1, HCl was added to the solid to dissolve all the carbonates. On day 2, after washing the sample with water to extract all the residual acid, a solution of HCl + HF was introduced to dissolve the remaining minerals. Finally, on day 3 the sample was washed again with HCl to dissolve possible secondary fluoride minerals that could have appeared in HCl-HF treatment on the second day.

Table 1. Demineralization process used to isolate kerogen. Based on [6].

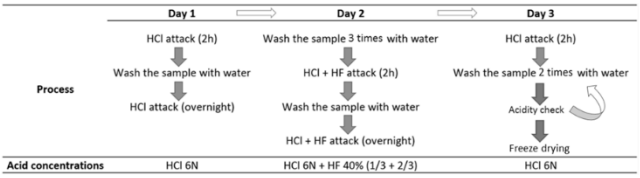

Once finished the demineralization process, the sample was washed with water until reaching neutral pH and freeze-dried.

After the isolation of kerogen, it was analysed by FTIR (Perkin Elmer Spectrum Two), EA (EA 1108 Thermo Fisher Scientific), and SEM (FE-SEM - ZEISS Ultraplus).

III. RESULTS AND DISCUSSION

A. Dissolved Organic Matter

Leaching of OM in experiments carried out with Putte and Boeretang BC samples has similar behaviour. After 50 days, an accumulated amount of 325-350 mg/L of OM is dissolved (Figure 5), out of which more than a 85% in weight are fulvic components.

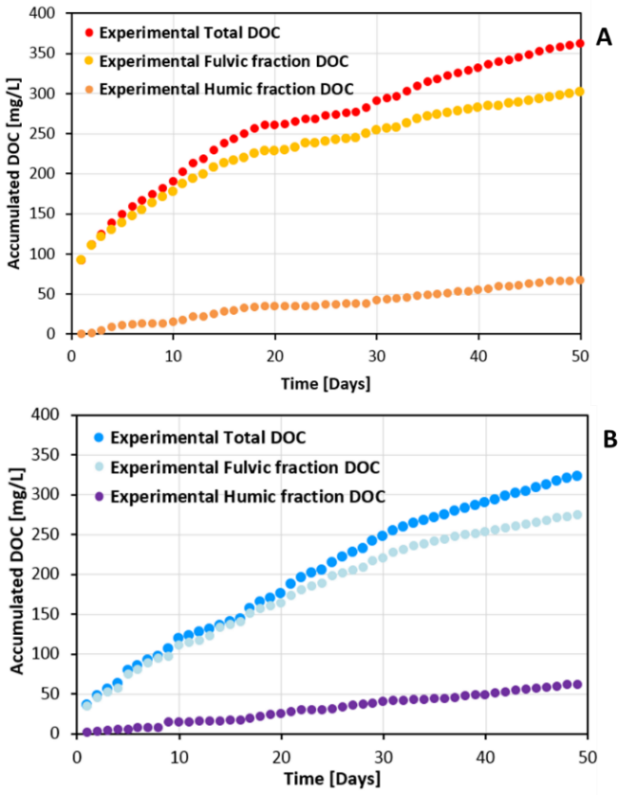

Figure 5. Accumulated concentration of OM released in water leaching experiments. Total OM, humic acids and fulvic acids are represented. (A) figure was carried out with BC from Putte member, and (B) with Boeretang member BC.

Using experimental data from the leaching experiments and considering that the release of OM can be adjusted to a logarithmic function [9], is possible to make an approximation to the final leached amount of OM, as well as the total time that the experiment should be in operation to achieve the dissolution of all the available organic matter. The results are presented in Table 2.

Table 2. Calculated values of final concentration (C_f) and time (t_f) from the leaching experiments.

	Putte member		Boeretang member	
	C_f [mg/L]	t_f [days]	C_f [mg/L]	t_f [days]
Humic acids	200	671	160	507
Fulvic fraction	350	187	310	134
Total DOM	550	376	470	270

B. Bitumen

The two IR spectra of BC samples are represented in Figure 6. There are important differences between the two different bitumen samples. In the Boeretang bitumen, the peaks of C-H stretch (around 2900 cm^{-1}) are less important than the C=O and C=C moieties (1700 and 1600 cm-1 approximately). In the case of Putte bitumen, the IR spectra is nearly the inverse of the Boereteng bitumen, with a marked aliphatic character (C-H stretch), and some double bonds stretch.

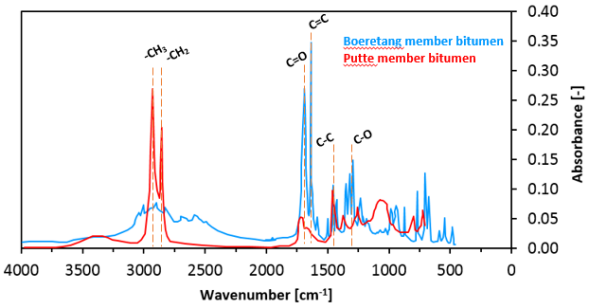

Figure 6. Comparison of IR spectra from different organic matter and bitumen. Putte and Boeretang samples are from ON-Mol-2D borehole.

Comparing the studied bitumen samples with other natural bitumen FTIR spectra from the literature [10], it can be seen that the Putte member sample presented similarities with bitumen, with a marked aliphatic character, while Boeretang bitumen spectra composition does not match with previous literature values. This fact could be attributed to the different origins of the organic matter within the different BC formations.

GC-MS is used to quantify aromatic and aliphatic molecules; a summary of the results is presented in Table 3. In Putte and Boeretang bitumen, the presence of aliphatic molecules is higher than the aromatic molecules. No polycyclic aromatic hydrocarbons are detected.

Table 3 Summarized GC-MS results of bitumen samples from Boeretang and Putte BC members.

	Aliphatic molecules		Aromatic molecules		Polycyclic aromatic	
Boom Clay member	%w from Bitumen	Main molecule	%w from Bitumen	Main molecule	%w from Bitumen	Main molecule
Boeretang member	93.63	29 C	6.37	21-35 C	0	-
Putte member	96.80	14 C	3.20	21-35 C	0	-

The distribution between aliphatic and aromatic molecules from Putte and Boeretang members may seem similar, but there are remarkable differences, as the concentration distribution of the different lengths of aliphatic molecules. In the Boeretang bitumen the most abundant molecule is 29C while in the case of bitumen from Putte it is the 14C molecule. This difference in abundance between the different molecule lengths is clearly visible in Figure 7.

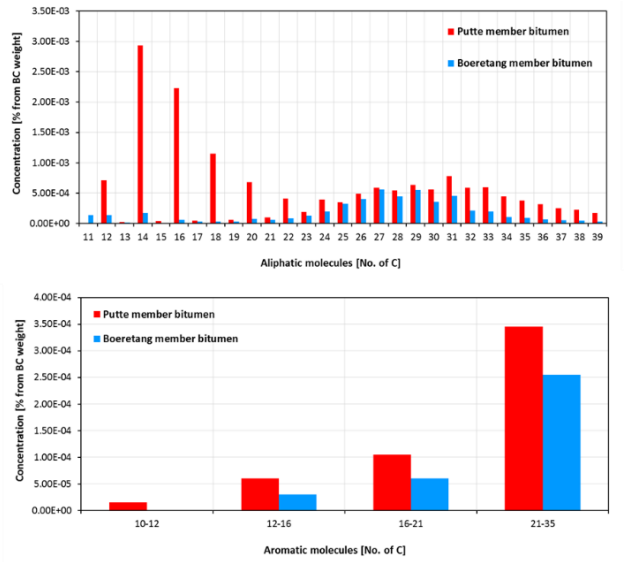

Figure 7. Concentration of aliphatic and aromatic molecules per number of C in bitumen from Boeretang and Putte BC members.

In the case of the bitumen from Putte, the molecules with higher concentration have less than 20C, while in Boeretang bitumen samples, the highest concentrations are around 26 and 31C. There is no significant difference in the abundance distribution of aromatics between the Boeretang and Putte bitumen, although aromatics are much more abundant in the Boeretang than in the Putte member.

C. Kerogen

In the FTIR analysis, shown in Figure 8, there are no clear differences between Putte and Boeretang kerogens. In both cases, the presence of moieties with a double bond is more important than the simple bond moieties (–CH_3 and –CH_2).

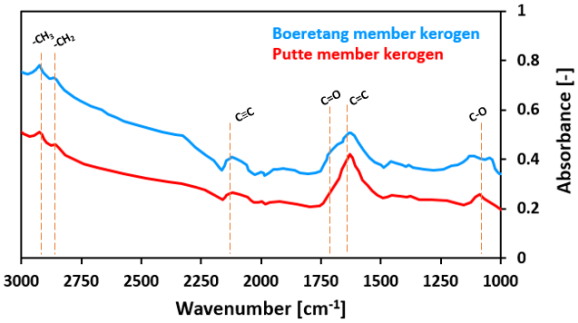

Figure 8. FTIR analysis of two different isolated kerogens by acid demineralization, blue line for Boeretang member kerogen and red line for Putte member kerogen.

Kerogen spectra have significant differences with the FTIR from the bitumen fraction of the same analysed samples (Figure 6). The kerogen has an important decrease of the aliphatic character (more evidenced in the case of Putte), compared with the respective bitumen, since C-H moieties seem much less predominant than in the case of bitumen.

IV. CONCLUSIONS

In this study, the extraction and characterization of SOM fractions from two members of BC formation, Putte and Boeretang are assessed.

The analysed samples from Boeretang and Putte members present a similar abundance of OM in clay, with close DOC values.

The analysis of extracted bitumen from the Organic Matter (OM) contained in Putte and Boeretang members present different composition. Differences in composition are consistent with a possible different origin of the OM.

There are no differences in kerogen composition from Putte and Boeretang members. Compared with bitumen, C-H moieties are less important in kerogen samples, in agreement with the degree of maturation of each OM fraction.

After analysing the different results of SOM in BC, is clear that the origin of OM could result in important compositional differences between BC members.

V. REFERENCES

[1] ONDRAF/NIRAS Research, "Development and Demonstration (RD&D) Plan for the geological disposal of high-level and/or long-lived radioactive waste including irradiated fuel if considered as waste", ONDRAF/NIRAS, report NIROND-TR 2013-12 E, 2013, December 2012.

[2] J. Decleer, W. Viane, N. Vandenberghe, "Relationships between chemical, physical and mineralogical characteristics of the Rupelian Boom clay, Belgium", Clay Minerals, vol. 18, pp. 1-10, 1983.

[3] B. Laenen, "The geochemical signature of relative sea-level cycles recognised in the Boom Clay", Aardkundige Mededelingen, University Press Leuven, vol. 9, pp. 61-82, 1998.

[4] M. De Craen, L. Wang, M. Van Geet, H. Hoors, "Geochemistry of Boom Clay pore water at the Mol site", Scientific report. SCK·CEN-BLG-990, 2004.

[5] P. Rahimi, T. Gentzis, "The Chemistry of Bitumen and Heavy Oil Processing", Practical Advances in Petroleum Processing; Springer: Canada, pp. 597–634, 2006.

[6] B. Durand, "Kerogen: insoluble organic matter from sedimentary rocks", Editions Technip, 519p, 1980.

[7] M. Hetényi, I. Varsányi, "Contributions to the isolation of the kerogen in Hungarian oil shales", Acta Mineralogica-Petrographica, Szeged, vol. XXII/2, pp. 231-239, 1976.

[8] EPA method 3540C, "Soxhlet extraction part of Test methods for Evaluating Solid Waste, Physical/Chemical Methods". CD-ROM 3540C, Revision 3, December 1996.

[9] A. Büyükkılıç, A. Mermut, I. Halil, A. Cano, I. Yanardağ, M. Garrido, "Organic carbon fluxes using column leaching experiments in soil treated with pig slurry in SE Spain", Arid Land Research and Management, vol. 34:2, pp. 136-151, 2019.

[10] B. Hofko, L. Porot, A. Falchetto-Cannone, L. Poulikakos, L. Huber, X. Lu, K. Mollenhauer, H. Grothe, "FTIR spectral analysis of bituminous binders: reproducibility and impact of ageing temperature", Materials and Structures, vol. 51(2), 2018.

Proceedings of the European Nuclear Young Generation Forum
ENYGF'21
September 27-30, 2021, Tarragona, Spain

Spent Fuel Alteration Model: Integrating Different Time-scale Processes

Coene, Emilie[1*], Riba, Olga[1], Silva, Orlando[1] and Duro, Lara[1]

[1] Amphos 21 Consulting S.L., Spain

*Corresponding author: *emilie.coene@amphos21.com*

I. INTRODUCTION AND OBJECTIVES

The safety assessment of deep geological repositories of spent nuclear fuel (SF) requires a fundamental understanding of the processes controlling fuel alteration and the release of radionuclides into the geosphere.

In a deep geological repository, groundwater will eventually reach the SF due to container corrosion and failure. Due to the corrosion of steel and cast iron of the canisters, this groundwater is expected to have low oxygen concentrations and high H_2 and Fe(II) contents. At the same time, water radiolysis by the effect of alpha radiation emitted by the SF surface will generate oxidizing and reducing species in solution. Note that emitting gamma fission products are expected to be decayed at the time of container failure. This radiolysis can potentially lead to relatively fast oxidative dissolution despite the bulk reducing environment, mainly due to the slow activation kinetics of H_2. However, in the last decades, several studies have shown that the catalytic effect of epsilon particles (Rh, Pd, Ru) on H_2 activation, can suppress the oxidation of UO_2 even at low H_2 concentrations [1, 2, 3].

In the framework of the EURATOM Project "DisCo" (modern spent fuel Dissolution and chemistry in failed Container conditions), Amphos 21 has developed a 1D reactive transport model of SF dissolution.

Spent fuel dissolution is a very complex system controlled by different interrelated processes. Previous modelling efforts implemented in COMSOL [4, 5], MATLAB [6], and HYTEC [7] were able to include the most relevant processes of the system but required some simplifications in the chemistry or the radiolytic scheme. The model that is outlined here, on the other hand, solves the challenge of coupling the complete water radiolysis system with chemical complexation and dissolution/precipitation reactions.

II. CONCEPTUAL MODEL

The conceptual model presented here is based on the matrix alteration model (MAM), initially developed in the Spent Fuel Stability project [8] and implemented in ChemSimul [9] as a set of kinetic processes. This model was improved afterwards in the MICADO project [10] and in several projects in collaboration with ENRESA with the implementation of H_2 activation by epsilon particles and the reducing effect of the activated H_2 on the oxidized matrix surface [11, 12].

In this work, radiolysis and the kinetic processes have been coupled with aqueous chemistry and solute transport with the reactive transport code iCP [13]. The integration of the different physico-chemical processes is achieved by a two-way coupling approach, as shown in Figure 1.

This modelling setup allowed to couple radiolysis with chemical complexation and dissolution/precipitation processes which occur at very different time scales (more than 6 orders of magnitude) and to integrate the complex chemistries of uranium and iron.

The coupled processes included in the model are described below:

Generation of oxidants and reductants by water radiolysis

Water radiolysis by alpha and beta radiation is considered according to the treatment performed in [14] and involves the following species: H^+, OH^-, O_2, H_2O_2, H_2, HO_2^-, $HO_2\cdot$, $O\cdot$, O^-, O_2^-, $H\cdot$ and $\cdot OH$. All the radiolytic kinetic reactions of the water scheme from [15] and the yields of primary products from [15] and [16] are considered here.

The model also accounts for the generation of $\cdot OH$ by H_2O_2 decomposition on the UO_2(am, hyd) surface and the generation of $H\cdot$ by activation of H_2 on the Pd surface. The kinetic constants used for these two processes correspond to the values reported in [17] and [18], respectively.

The generation of the products described above has been implemented in COMSOL with a set of ordinary differential equations (ODE) and was coupled with the solute transport equation through a source term.

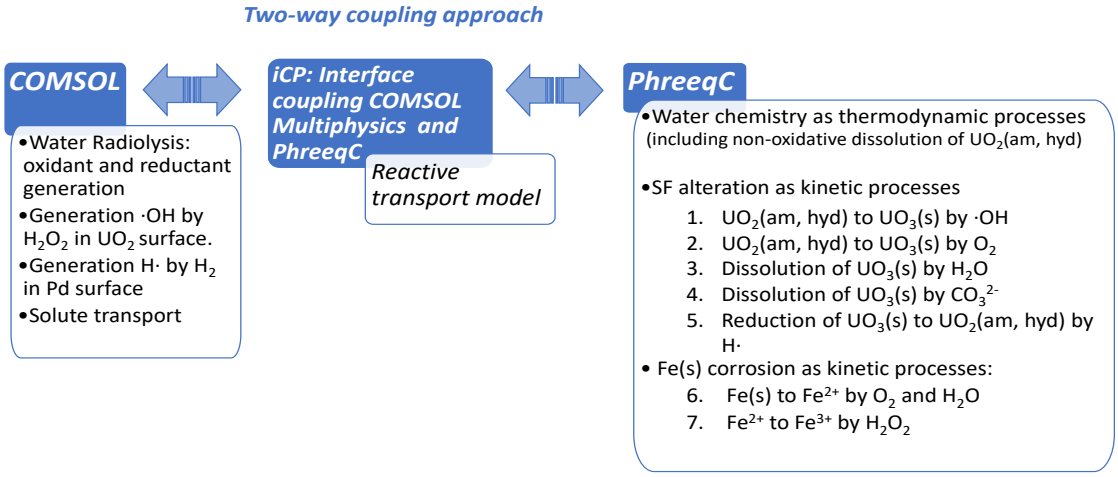

Figure 1: Integration in iCP of the different processes involved in Spent Fuel alteration.

Chemical reactions

The SF matrix is modelled as amorphous UO_2 with a homogeneous 1 atom % distribution of Pd, as representative element of the epsilon particles. The following kinetic reactions related to SF alteration have been implemented in PhreeqC:

1. Oxidation of UO_2(am, hyd) to UO_3(s) by ·OH
2. Oxidation of UO_2(am, hyd) to UO_3(s) by O_2
3. Dissolution of UO_3(s) by H_2O
4. Dissolution of UO_3(s) by CO_3^{2-}
5. Reduction of UO_3(s) to UO_2(am, hyd) by H·

The oxidation of metallic Fe(s), on the other hand, has been accounted for with the following kinetic processes:

6. Corrosion of Fe(s) to Fe^{2+} by O_2 and H_2O
7. Oxidation of Fe^{2+} to Fe^{3+} by H_2O_2

The kinetic constants of reactions 1-7 have been calibrated with experimental data reported in the scientific literature [19].

Aqueous speciation reactions have been included according to the ThermoChimie version 9b0 thermodynamic database [20]. The precipitation of secondary solid phases of iron is allowed to occur when thermodynamically supersaturated in solution.

Solute Transport

The present model considers a SF canister saturated with water where solute transport is governed by Fickian diffusion. The governing equation for solute transport in saturated porous media is the following:

$$\phi \frac{\partial c_i}{\partial t} + \nabla(-D_e \nabla c_i) = S_i + \sum_j R_{ij} \quad (1)$$

where ϕ [-] is the porosity, c_i [mol/kg$_w$] the aqueous concentration of species i, D_e [m^2/s] the effective diffusion coefficient, S_i [mol/kg$_w$·s] the source term of species i and R_{ij} the reactive term between species i and j.

The effective diffusion coefficient is a function of porosity and is described by Millington and Quirk tortuosity model [21]:

$$D_e = \phi^{4/3} D_F \quad (2)$$

where $D_F = 10^{-9}$ m^2/s is the fluid diffusion coefficient.

III. MODEL SETUP

The SF alteration model has been implemented with a 1D geometry representative of the gap between SF and the cast iron insert of the canister used for final disposal in the repository [22]. The dimensions considered in this setup are presented in Figure 2, where the left boundary represents the center of a SF pellet and the right boundary a point of the insert in contact with external porewater.

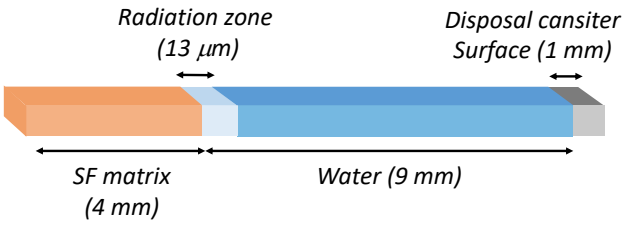

Figure 2. Geometry (not to scale) of the Spent Fuel alteration 1D model.

The solid phase considered as SF matrix is a homogeneous chemical composition of UO_2, with the formulation: UO_2(am, hyd), containing 1 atom % of Pd, as representative element of the epsilon particles.

The porosity of the SF matrix was estimated with a dry density of 8.93 g/cm^3 [23] and a grain density of 10.52 g/cm^3 [24], yielding a value of 0.15.

A uniform alpha dose rate of $2.86 \cdot 10^{-2}$ Gy·s^{-1} was applied inside of the SF matrix and in the first 13 μm of water adjacent to it. This uniform alpha dose rate is equivalent to a non-uniform exponential dose rate distribution affecting 35 μm of water, in the sense that both produce the same total dose rate [4].

The initial aqueous solution contains 10^{-10} M of NaCl, 10^{-8} M of Fe and has a pH of 9. The left boundary is a no flux boundary, whereas the right boundary allows for out-diffusion with a prescribed concentration for all solutes equal to the initial concentration.

IV. RESULTS

The model described above has been used to simulate SF alteration for 36 days.

Figure 3 displays how steel corrosion causes a decrease of Eh to -0.47 V in the whole model in less than 1 day. Interestingly, at the interval from 20 to 30 days the Eh in the pellet centre increases reaching -0.16 V, and this value is maintained until the end of the simulation.

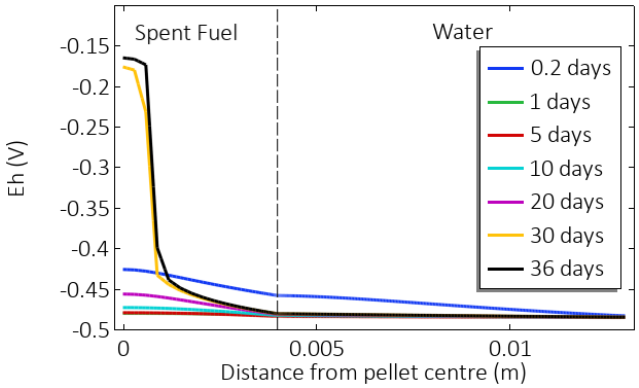

Figure 3. Evolution of Eh (V) in the modelled domain obtained with the SF alteration model.

Figure 4 shows the concentrations of aqueous U that result from UO_2(am,hyd) alteration and dissolution. The non-oxidative dissolution of UO_2(am,hyd) leads to aqueous U(IV) concentrations of $3 \cdot 10^{-9}$ M inside the SF pellet, in thermodynamic equilibrium with UO_2(am,hyd), which diffuses out towards the right boundary of the model.

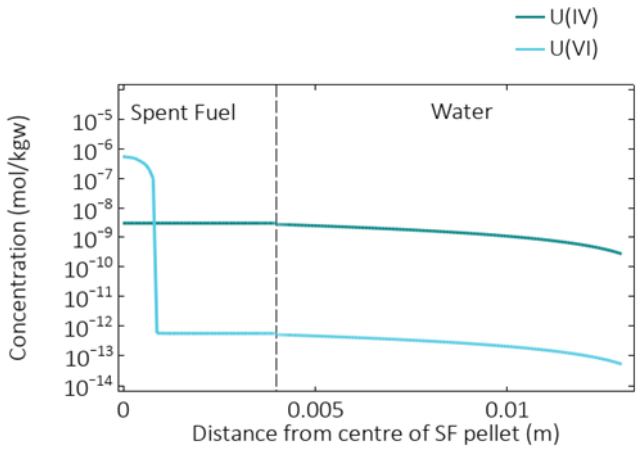

Figure 4. Concentration of aqueous U(IV) and U(VI) obtained with the SF alteration model after 36 days.

At the center of the pellet, the relatively oxidizing conditions promoted by the radiolysis of water result in [U(VI)] of $5 \cdot 10^{-7}$ M, limited by the precipitation of schoepite ($UO_2(OH)_2$). The behaviour of the [U(VI)] is in agreement with the Eh pattern shown in the different domains in Figure 3. At the outer part of the pellet, U(VI) concentrations are much lower (10^{-12} M) and most of the aqueous uranium is present as U(IV). The total aqueous U diffusing out from the SF is in its reduced form, as U(IV).

The overall UO_2(am,hyd) alteration predicted by the model is displayed in Figure 5. After 36 days a fraction of $2 \cdot 10^{-8}$ has been altered, with a decreasing alteration rate in time: Initially it is $7 \cdot 10^{-7}$ y^{-1} and it decreases to $3 \cdot 10^{-8}$ y^{-1}. These values are in the range of the values considered in safety assessments (10^{-7} y^{-1}, with maximum = 10^{-6} y^{-1} and minimum = 10^{-8} y^{-1}) when the inhibiting (protecting) effect of H_2 on the long-term dissolution of SF matrix is considered (Martínez Esparza, 2005; SKB, 2010; POSIVA, 2013; Johnson, 2014; NWMO, 2015; JAEA, 2015).

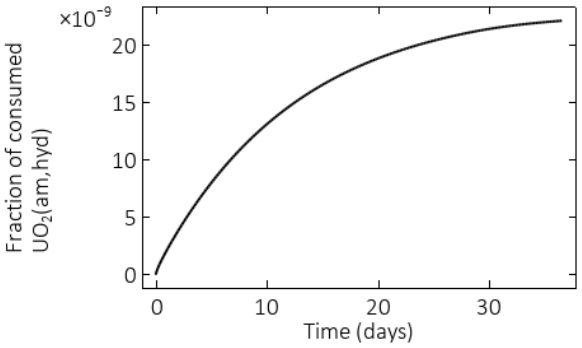

Figure 5. Evolution of the fraction of total UO2(am,hyd) that is altered as a function of time.

V. CONCLUSIONS

This work describes the development of a spent fuel alteration model that includes and couples the following processes: water radiolysis, kinetic reactions at the spent fuel surface, aqueous speciation (including U and Fe) and solute transport.

The model was used to simulate spent fuel alteration under repository conditions, predicting low U(VI) concentrations at the outer part of the pellet and an alteration rate decreasing from $7 \cdot 10^{-7}$ y^{-1} to $3 \cdot 10^{-8}$ y^{-1} in 36 days.

The present model was developed to simulate standard UOx spent fuel but can be applied to simulate "modern" type fuels with Cr/Al doping. As such, this modelling work can be a useful tool to assess the fuel dissolution and U release of different fuel types under different repository conditions.

The modelling work carried out here could be further improved by extending the geometry of the system to 2D or 3D (e.g., by adding part of the outside of the fuel rod) and simulating more realistic geochemical conditions (porewater compositions).

VI. ACKNOWLEDGEMENTS

The research leading to these results has received funding from the European Commission Horizon 2020 Research and Training Programme of the European Atomic Energy Community (EURATOM) (H2020-NFRP-2016-2017-1) under grant agreement n° 755443 (DisCo project).

VII. REFERENCES

[1] P. Carbol, P. Fors, T. Gouder, K. Spahiu, "Hydrogen suppresses UO2 corrosion", Geochimica et Cosmochimica Acta, vol 73, 2009, 4366–4375.

[2] M. Trummer, M. Jonsson, "Resolving the H2 effect on radiation induced dissolution of UO2-based spent nuclear fuel", Nucl. Mater., vol 396, 2010, 163–169.

[3] K. Ollila K, “Influence of Radiolysis on UO2 Fuel Matrix Dissolution Under Disposal Conditions - Literature Study”, Posiva Working Report 2011-27, 2011, 64.

[4] L. Wu, Y. Beauregard, Z. Qin, S. Rohani, D.W. Shoesmith, “A model for the influence of steel corrosion products on nuclear fuel corrosion under permanent disposal conditions”, Corrosion Science, vol 61, 2012, 83-91.

[5] L. Wu, N. Liu, Z. Qin, D.W. Shoesmith, “Modeling the radiolytic corrosion of fractured nuclear fuel under permanent disposal conditions” Journal of The Electrochemical Society, vol 161(8), 2014, E3259-E3266.

[6] J. L. Jerden, K. Frey, W. Ebert, “A multiphase interfacial model for the dissolution of spent nuclear fuel”, Journal of Nuclear Materials, vol 462, 2015, 135-146.

[7] M. Odorowski, “Etude de l'altération de la matrice (U,Pu)O2 du combustible irradié en conditions de stockage géologique: Approche expérimentale et modélisation géochimique”, Doctoral Thesis, 2015.

[8] C. Poinssot, M. Cowper, B. Grambow, J.M. Cavedon, T. McMenamin, EURADWASTE ‘04, 29–31 March 2004, Luxembourg.

[9] P. Kirkegaard, E. Bjergbakke, “CHEMSIMUL: a simulator for chemical kinetics” Riso-R-1085(EN), 2002.

[10] B. Grambow, J. Bruno, L. Duro, J. Merino, A. Tamayo, C. Martin, G. Pepin, S. Schumacher, O. Smidt, C. Ferry, C. Jegou, J. Quiñones, E. Iglesias, N.R. Villagra, J.M. Nieto, A. Martínez-Esparza, A. Loida, V. Metz, B. Kienzler, G. Bracke, D. Pellegrini, G. Mathieu, V. Wasselin-Trupin, C. Serres, D. Wegen, M. Jonsson, L. Johnson, K. Lemmens, J. Liu, K. Spahiu, E. Ekeroth, I. Casas, J. de Pablo, C. Watson, P. Robinson, D. Hodgkinson, “MICADO: Model uncertainty for the mechanism of dissolution of spent fuel in nuclear waste repository”, Final report, 2010.

[11] L. Duro, A. Tamayo, J. Bruno, A. Martínez-Esparza, “Integration of the H2 inhibition effect of UO2 matrix dissolution into radiolytic models”, Proceedings of the ICEM 2009-16239.

[12] L. Duro, O. Riba, A. Martínez-Esparza, J. Bruno, “Modelling the activation of H2 on spent fuel surface and inhibiting effect of UO2 dissolution”. MRS Proceedings 1518, 2013, 133.

[13] A. Nardi, A. Idiart, P. Trinchero, L.M. de Vries, J. Molinero, “Interface COMSOL-PHREEQC (iCP), an efficient numerical framework for the solution of coupled multiphysics and geochemistry”, Computers & Geosciences, vol 69, 2014, 10-21.

[14] E. Cera, J. Bruno, L. Duro, T. Eriksen, “Experimental determination and chemical modelling of radiolytic processes at the spent fuel/water interface”, SKB Report TR 06-07, 2006.

[15] M. Kelm, E. Bohnert, “A kinetic model for the radiolysis of chloride brine, its sensitivity against model parameters and a comparison with experiments”, Forschungszentreum Karlsruhe, FZKA 6977, 2004.

[16] T. E. Eriksen, M. Jonsson, J. Merino, “Modelling of time resolved and long contact time dissolution studies of spent nuclear fuel in 10 mM carbonate solution–a comparison between two different models and experimental data”, Journal of Nuclear Materials, vol 375(3), 2008, 331-339.

[17] J. Merino, E. Cera, J. Bruno, J. Quiñones, I. Casas, F. Clarens, J. Giménez, J. de Pablo, M. Rovira, A. Martínez-Esparza, “Radiolytic modelling of spent fuel oxidative dissolution mechanism. Calibration against UO2 dynamic leaching experiments”, Journal of nuclear materials, vol 346(1), 2005, 40-47.

[18] M. Trummer, S. Nilsson, M. Jonsson, “On the effects of fission product noble metal inclusions on the kinetics of radiation induced dissolution of spent nuclear fuel” Journal of Nuclear Materials, vol 378(1), 2008, 55-59.

[19] O. Riba, E. Coene, O. Silva, L. Duro, “Spent fuel alteration model integrating processes of different time-scales” MRS Advances, vol 5(3), 2020, 159-166.

[20] E. Giffaut, M. Grivé, P. Blanc, P. Vieillard, E. Colàs, H. Gailhanou, S. Gaboreau, N. Marty, B. Madé, L. Duro, “Andra thermodynamic database for performance assessment: ThermoChimie”, Applied Geochemistry, vol 49, 2014, 225-236.

[21] R.J. Millington, J.M. Quirk, “Permeability of Porous Solids”, Trans. Faraday Soc., vol. 57, 1961, 1200–1207.

[22] H. Raiko, “Canister design 2012”, Posiva Report 2012-13, 2012.

[23] J. Cobos, N. Rodríguez-Villagra, S. Fernández, L. Gutierrez, L.J. Bonales, S. Durán, L. Anta, “Ongoing CIEMAT activities on fabrication and stability studies of doped UO2 in the fame of the DisCo project: sample characterization, experimental set-up and first results”, 2nd Annual Meeting Proceedings DisCo project, 2019.

[24] J. Arborelius, K. Backman, L. Hallstadius, M. Limbäck, J. Nilsson, B. Rebensdorff, G. Zhou, K. Kitano, R. Löfström, G. Rönnberg, “Advanced doped UO2 pellets in LWR applications”, J. Nucl. Sci. Techn., vol 43, 2012, 967-976.

Proceedings of the European Nuclear Young Generation Forum
ENYGF'21
September 27-30, 2021, Tarragona, Spain

Interaction of low molecular weight organics, cement phases and radionuclides

Guidone, Rosa Ester[1,2*], Lothenbach, Barbara[1], Gaona, Xavier[2], Tasi Agost[2], Altmaier, Marcus[2] and Geckeis, Horst[2]

[1] Empa (Swiss Federal Laboratories for Materials Science and Technology), Überlandstrasse 129, 8600 Dübendorf, Switzerland; [2] KIT-INE (Karlsruhe Institute of Technology, Institute for Nuclear Waste Disposal), Hermann-von-Helmholtz-Platz 1, 76344 Eggenstein-Leopoldshafen, Germany

*Corresponding author: *rosa.guidone@empa.ch*

I. INTRODUCTION

The internationally favoured option for the disposal of high-level waste (HLW), long-lived intermediate waste (ILW), and for low- and intermediate-level waste (L/ILW) is the deep geological repository. The safety concept in such repositories relies in a multi-barrier system preventing the release of radionuclides into the biosphere. Depending on the repository concept and waste type, the waste can be solidified in a cementitious matrix, emplaced in concrete disposal containers, or stacked in disposal caverns, where special cement-based materials are used as backfill. As a part of the multi-barrier system, cementitious materials are expected to contribute to the confinement of radionuclides and the retardation of their migration into the biosphere.

The main hydrates formed during the hydration of Portland cement (PC) include calcium silicate hydrates (C-S-H) phases, portlandite, ettringite and so-called AFm-phases [1]. AFm phases are layered calcium aluminate-ferrite double hydroxides (LDH). The AFm structure consists of sheets of $Ca(OH)_6$ in which one-third of Ca^{2+} sites are replaced by Al^{3+} (and/or Fe^{3+}) generating a positive net charge compensated by interlayer anions. Common interlayer anions in cement environments are CO_3^{2-}, OH^-, SO_4^{2-}, resulting in monocarboaluminate (Mc), hemicarboaluminate (Hc) and monosulfoaluminate (Ms), respectively. The type of interlayer anion and the amount of interlayer water determine the layer thickness [2] visible by XRD. The structure of ettringite crystals (AFt) is based on positively charged columns $\{Ca_3[Al(OH)_6]^{3-}\cdot 12\ H_2O\}^{3+}$ and SO_4^{2-} tetrahedra and H_2O in the channels in between.

Low molecular weight (LMW) organics are present in repository system as (i) component of conditioned waste (medicine and industry wastes), (ii) due to the decomposition of different organic components [3], and (iii) as additives (e.g. superplasticizer, set accelerator [4-5]) used in cement mixtures to improve their workability. Although the sorption of organics on cement hydrates is expected to be weak, the organics-cement interactions can alter surface properties of cement minerals. Furthermore, organics can interact with radionuclides disposed of in the repository, eventually affecting their solubility and sorption properties [6].

Thus organic compounds are expected to have an impact on the long-term safety and performance of the repository system. Despite the importance in the safety case, the information on LMW organics speciation and on their potential retention by cement in deep geologic repository is very limited.

The present work aims to quantify the uptake of LMW organics (formate, $HCOO^-$, citrate $C_6H_5O_7^{3-}$, and gluconate $C_6H_{11}O_7^-$) and understand the occurring binding mechanism. These ligands are considered representative of degradation products, chelating agents expected in the waste or cement additives. Sorption experiments were carried out to study the partitioning of soluble organic compounds between the cement phases (AFm phases, ettringite) and solution.

II. MATERIALS AND METHODS

A. AFm phases and ettringite synthesis

All sample manipulations were performed in a N_2 filled glove box. Solutions were prepared using high-purity deionized water (resistivity = 18.2 MΩ cm) generated by a Milli-Q Gradient A10 System and the different organics Na salts (Na-formate, Fluka Analytical, Buchs, Switzerland; Na_3-citrate, and Na-gluconate, Sigma-Aldrich, St. Louis, Missouri, USA).

AFm-phases were synthesized by mixing stoichiometric amounts of tricalcium aluminate ($Ca_3Al_2O_6$), with $CaSO_4$ in the case of monosulfoaluminate, Ms: $Ca_4Al_2O_6SO_4\cdot 12\text{-}14H_2O$ (solid to liquid ratio: S/L = 55 $g\cdot L^{-1}$) with $CaCO_3$ for monocarboaluminate, Mc: $Ca_4Al_2O_6CO_3\cdot 11H_2O$ (S/L = 46 $g\cdot L^{-1}$) and with $CaCO_3$ and CaO for hemicarboaluminate, Hc: $Ca_4Al_2O_6(CO_3)_{0.5}(OH)\cdot 11.5H_2O$ (S/L = 44 $g\cdot L^{-1}$). Tricalcium aluminate was prepared by mixing $CaCO_3$ and Al_2O_3 in a molar ratio of 3:1 and by heating the mixing according to the following procedure: at 800 °C for 1 h, at 1000 °C for another 4 h and at 1425 °C for 24 h.

Ettringite was synthesized by mixing stoichiometric amounts of CaO and $Al_2SO_4 \cdot 18\ H_2O$ at an S/L equal of 42 $g \cdot L^{-1}$. CaO was prepared by heating $CaCO_3$ at 900 °C for 12 h, to minimize the CO_2 content in CaO.

The samples were equilibrated for two months in closed PE bottles at 20 °C on horizontal shakers (100 rpm).

B. Sorption experiments

Sorption experiments were performed on the pre-synthesized hydrate phases adding different volumes of Na-formate, Na_3-citrate and Na-gluconate and NaOH solutions resulting in a total Na concentration of 0.2 M (pH ~ 13) and in an organic concentration ranging from 10^{-4} M to 0.1 M. The specimens were equilibrated for 7 days at 20 °C on horizontal shakers (100 rpm). After equilibration, the solid and the liquid phases were separated by filtration using 0.45 µm nylon filters. The solid phases were dried in a desiccator over saturated $CaCl_2$ solution (~35% relative humidity) at room temperature for two to four weeks under vacuum.

Kinetic experiments were performed adding the highest concentration used in sorption experiments (0.2 M of citrate and formate and 0.12 M of gluconate). The samples were equilibrated for 1, 2, 4, 7 and 14 days and then filtered as described above.

In the present study, the term "sorption" is used in a general sense, indicating both the uptake on the surface of hydrate phases or in the interlayer (e.g. for AFm-phases).

The partitioning of organic compounds (formate, citrate, and gluconate) between the solid and the liquid phase was determined in terms of distribution coefficient R_d:

$$R_d = \frac{C_{i,eq} - C_{i,0}}{C_{i,0}} \cdot \frac{V}{m} \quad [m^3 kg^{-1}] \ .$$

where $C_{i,eq}$ denotes the concentration [mol L^{-1}] of the organic species at equilibrium; $C_{i,0}$ is the initial concentration [mol L^{-1}] of the organic compound; m is the mass [kg] of sorbent (cement phase) and V is the volume [m^3] of solution.

C. Solid phase characterization

After drying, the samples were characterized by X-ray powder diffraction (XRPD) and thermogravimetric analysis (TGA).

XRPD analyses were performed on a Panalytical X'Pert Pro MPD diffractometer with geometry θ-θ, using CuKα radiation (λ= 1.54184 Å) equipped with a solid X-Celerator detector. XRPD patterns were recorded at room temperature in the interval 5°<2θ<70° with a step size of 0.017° (2θ) and a total counting time of ~2s or each step.

TGA was carried out on a Mettler Toledo TGA/SDTA 851 instrument (Mettler Toledo, Switzerland) on ~30 mg of sample using a heating rate of 20 °C/min and a temperature range between 30 °C and 980 °C under N_2.

D. Liquid phase characterization

The pH values of solution at equilibrium were measured on an aliquot of the solution using a Knick pH-meter with a SE 100 pH/Pt 1000 electrode at room temperature. The instrument was calibrated with NaOH solution of known concentrations to minimize the alkali error.

The total concentration Al, Ca, Na, Si and S were measured on Agilent 5110 ICP-OES equipped with an Agilent SPS 4 autosampler using Argon. The samples were diluted by a factor of 10, 100 and 1000 with 2 wt.% HNO_3 to prevent precipitation of any solids.

The total organic concentration was measured using a Sievers 5310 C TOC analyser. The samples were diluted at least by a factor of 5 (at low organic concentrations) with 0.01 M and 0.1 M HCl.

III. RESULT AND DISCUSSION

A. Sorption experiments with cement phases

Due to their positively charged main layer AFm phases can efficiently sorb mono- and bivalent species, while ettringite preferentially bind bivalent oxyanions such as sulfate species in their channels. The present work aims to identify the difference in the uptake of formate, citrate and gluconate by diverse AFm phases (Ms, Mc, Hc) and ettringite.

Kinetic experiments (data not shown) indicated that no further changes in the uptake of the anions were observed after 4 days, and that an equilibration time of 7 days was sufficient in all cases to reach equilibrium conditions. No significant sorption of formate ($HCOO^-$) was observed as visible from the comparison of the total initial concentration and the formate concentrations measured after 7 days as shown in Figure 1. Only in the case of Ms, some sorption occurred at very low organic concentrations (1-5 mM). Although no R_d value was determined, Wieland and co-workers [7] estimated formate sorption occurs with $R_d \leq 10^{-2}$ $m^3 \cdot kg^{-1}$ on AFm phases and ettringite. This finding agrees with Matsumoto and co-workers' result [8], who observed that the electrostatic interaction of the carboxylate group of formate ($HCOO^-$) with the positively charged site of cement phases is very weak.

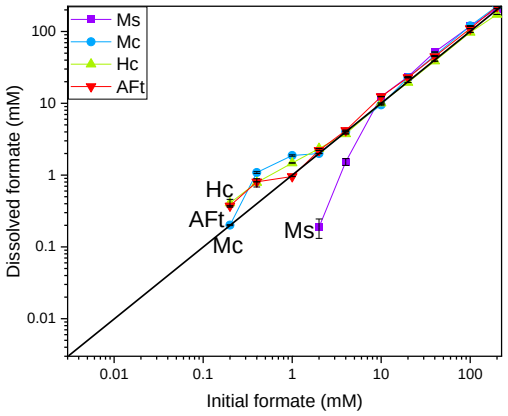

Figure 1. Dissolved concentration of formate as a function of the initial formate concentration. No strong uptake was observed by AFm-phases and ettringite.

Citrate ($C_6H_5O_7^{3-}$) uptake was observed on all hydrates investigated in this study (Figure 2). Considering the average value of R_d, (Table 1), the uptake decreases in the following order: Hc > Ms > Mc > AFt.

Table 1. R_d average values determined for citrate and gluconate uptake by Ms, Mc, Hc and AFt

Cement phase	Distribution coefficient R_d value ($m^3 \cdot kg^{-1}$) Citrate	Distribution coefficient R_d value ($m^3 \cdot kg^{-1}$) Gluconate
Hc	0.29±0.03	0.36±0.03
Ms	0.17±0.02	0.15±0.02
Mc	0.13±0.01	0.019±0.002
AFt	0.080±0.003	0.19±0.01

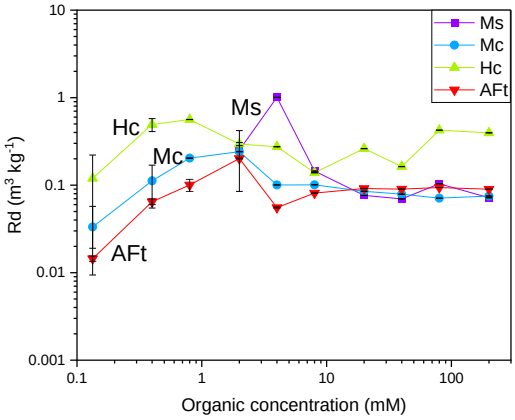

Figure 2. Citrate uptake on AFm phases (Ms, Mc and Hc) and ettringite (AFt).

A higher citrate uptake was observed on the AFm phases than on ettringite. The highest uptake was observed for Hc, which contains a single charged OH^- and half a double charged carbonate in its interlayer per formula unit, while the uptake on monocarboaluminate and monosulfoaluminate, which contain bivalent CO_3^{-2} and SO_4^{-2} in its interlayer, is weaker. Such an effect of the interlayer anion on the sorption on AFm phases has been observed previously and has been assigned to ion-exchange reaction with the interlayer ions [9, 10]. In the case of Hc, citrate uptake could occur by the exchange $3OH^-/C_6H_5O_7^{3-}$ or $1.5CO_3^{2-}/C_6H_5O_7^{3-}$. The occurrence of an anion exchange in the interlayer is confirmed by the shift of peak position of the basal spacing of AFm phases detected by XRD. The AFm phases Ms and Hc show an increase of the basal spacing with increasing citrate concentration, while no significant change was observed for Mc as shown in Fig. 3, in agreement with the very limited uptake observed for Mc.

Also for ettringite low uptake and no significant changes were observed as shown by the constant position of peak related to the a-axis of ettringite in Fig. 3. This low uptake could be related to the larger size of citrate compared to SO_4^{2-} and H_2O resulting in a steric hindrance of citrate to enter the channels of the ettringite structures.

As for citrate, significant sorption of gluconate ($HOCH_2(CHOH)_4COO^-$) is observed for all AFm phases and ettringite. The R_d values shown in Fig. 4 and Table 1, indicate the same order for gluconate uptake on AFm phases: Hc > Ms > Mc, but a higher uptake on ettringite, comparable to monosulfoaluminate. The absence of any clear changes in the basal spacing (Figure 5), may suggest a preferential sorption on the outer surface of AFm phases and ettringite (AFt) [4, 11] or alternatively that the incorporation of limited amounts of gluconate has no effect on the d-spacing (a-axis). This will be further investigated by FTIR and other spectroscopic techniques.

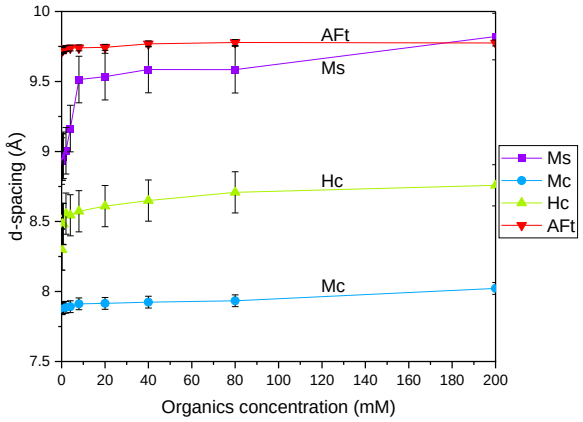

Figure 3. Structure phase changing by citrate sorption. d-spacing (c-axis for AFm-phases) increases with organic concentration.

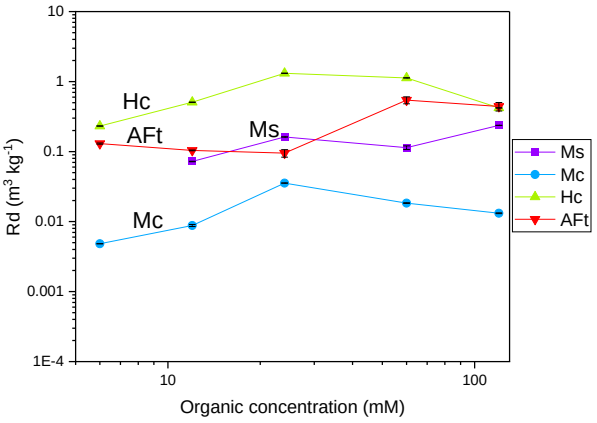

Figure 4. Gluconate uptake on AFm phases (Ms, Mc and Hc) and ettringite (AFt).

The higher uptake of citrate than of formate could be related to the chemical structure of citrate: the presence of three negatively charged carboxylate groups (≡COO^-) compared to the one of formate ($HCOO^-$) indicates a higher probability of citrate interacting with positively charged sites present at the surface and the interlayer of AFm phases. The alcohol group of citrate plays also a key role in the interaction of this ligand with metal cations in alkaline systems, and this might also be the case when interacting with cement surfaces.

The R_d values could also be related to the acid-base properties of molecules or more specifically to their acidity constant (pK_a) as suggested tentatively by Wieland and co-workers [7]. They have observed a correlation of pK_a (as an indicator of the polarizability of functional groups) and R_d, with a higher sorption for those organics with a lower pK_a.

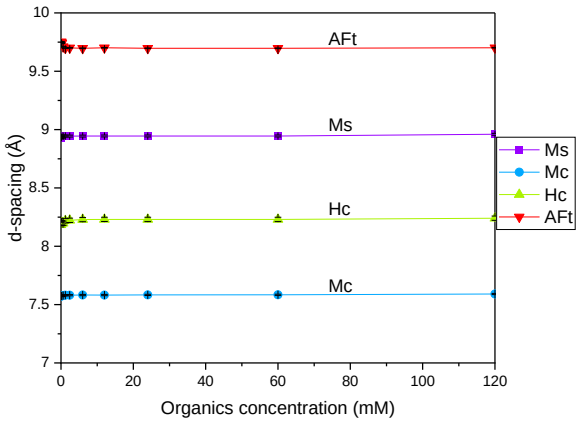

Figure 5. Structure phase changing by gluconate sorption. d-spacing (c-axis for AFm-phases and a-axis for AFt) doesn't change with organic concentration.

This correlation is shown in Fig. 6 for R_d values determined in this work for formate, citrate and gluconate uptake on monosulfate (Ms). From the figure, it appears evident that for organic ligands other than monocarboxylates (e.g. polycarboxylic or polyhydroxocarboxylic acids) other parameters need to be taken into account, e.g. overall charge, type and number of functional groups.

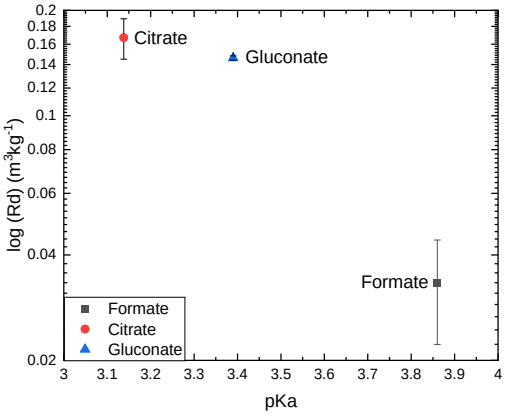

Figure 6. R_d values for formate (black), citrate (red) and gluconate (blue) uptake by Ms as a function of pK_a.

IV. CONCLUSIONS AND OUTLOOK

In the present study, the uptake of formate, citrate and gluconate by cement hydrates (AFm phases, ettringite) was investigated. Despite its small size, formate sorbs very weakly on AFm phases and ettringite. In contrast, citrate and gluconate uptake occur on AFm and ettringite. In both cases, hemicarboaluminate shows higher sorption for citrate (R_d=0.29 m^3kg^{-1}) and gluconate (R_d=0.36 m^3kg^{-1}) than monosulfoaluminate or monocarboaluminate. In a second stage of this project, the impact of these organic ligands on the uptake of An(III)/Ln(III) (^{243}Am, ^{152}Eu) and An(IV) (^{242}Pu, ^{238}Pu) by cement and individual cement phases will be also investigated.

V. ACKNOWLEDGEMENTS

The research leading to this results is has received funding from the European Union's Horizon 2020 research and innovation programme under grant agreement n° 847593 (EURAD).

VI. REFERENCES

[1] B. Lothenbach, F. Winnefeld, "Thermodynamic modelling of the hydration of Portland cement", Cem. Concr. Res., vol. 36, no. 2, pp. 209-226, Feb., 2006.

[2] H. F. Taylor, "Cement chemistry", Thomas Telford Publishing, London, New England, 1997.

[3] E. Wieland, W. Hummel, "Formation and stability of carbon-14 containing organic compounds in alkaline iron-water-systems: preliminary assessment based on literature survey and thermodynamic modelling", Mineral. Mag., vol. 79, no. 6, pp. 1275-1286, Jan., 2015.

[4] V. S. Ramachandran, "Concrete Admixtures Handbook, 2nd Ed.: Properties, Science and Technology", NP Noyes Publications Park Ridge, New Jersey, USA, 1995.

[5] G. Möschner, B. Lothenbach, R. Figi, R. Kretzschmar "Influence of citric acid on the hydration of Portland cement", Cem. Concr. Res., vol. 39, no. 4, pp. 275-282, Apr., 2009.

[6] I. Androniuk, C. Landesman, P. Henocq, A.G. Kalinichev, "Adsorption of gluconate and uranyl on CSH phases: Combination of wet chemistry experiments and molecular dynamics simulations for the binary systems", Phys. Chem. Earth, vol. 99, pp. 194-203, Jun., 2017.

[7] E. Wieland, A. Jacob, J. Tits, B. Lothenbach, D. Kunz, "Sorption and diffusion studies with low molecular weight organic compounds in cementitious systems", App. Geoc., vol. 67, pp. 101-117, Feb., 2016.

[8] J. Matsumoto, T. Banba, S. Muraoka, "Adsorption of carbon-14 on mortar", Mater. Res. Soc. Symp. Proc., vol. 353, no. 2, pp. 1029-1035, Oct., 1995.

[9] H. Pöllman, "Carboxylic acid anions: the reaction mechanism and products with the aluminate phase of cement", presented at: Proceedings of 9th Int. Cong. Chem Cem. (ICCC), New Delhi, India, 1992.

[10] L. Nedyalkova, B. Lothenbach, G. Geng, U. Mäder, J. Tits, "Uptake of iodide by calcium aluminate phases (AFm phases)", App. Geoc., vol. 116, May, 2020.

[11] S. Ma, W. Li, S. Zhang, D. Ge, J. Yu, X. Shen, "Influence of sodium gluconate on the performance and hydration of Portland cement", Cons. Buil. Mat., vol. 91, pp. 138-144, Aug., 2015.

Proceedings of the European Nuclear Young Generation Forum
ENYGF'21
September 27-30, 2021, Tarragona, Spain

Modeling of γ-spectra for characterization of surface and volume activity in different geometry metallic waste samples

Lagzdina, Elena[1*], Germanas, Darius[1], Lingis, Danielius[1], Garankin, Jevgenij[1], Konstantinova, Marina[1], Plukienė, Rita[1], Plukis, Artūras[1] and Remeikis, Vidmantas[1]

[1] Center for Physical Sciences and Technology (CPST), Lithuania

*Corresponding author: *elena.lagzdina@ftmc.lt*

I. INTRODUCTION

One of important tasks for smooth and successful nuclear power plant (NPP) decommissioning process is optimization of nuclear facility metallic radioactive waste (MRW) management by applying grouping and separation of MRW. During the construction of nuclear reactor metal structures from various grades of steel and other metal alloys are used. The choice of a specific type of material depends on the conditions in which the reactor will operate. The materials used in the construction of the reactor become radioactive during neutron activation and also can be contaminated. The contamination with radioactive elements occurs due to radiation leakage during normal reactor operation or incident events.

Decommissioning of RBMK-1500 reactors operating in Ignalina Nuclear Power Plant (INPP) started in 2004 when the first unit was shut down, while the second one was shut down in 2009. Like in other nuclear reactors, the RBMK-1500 reactor core is the main source of radionuclides generated in a INPP [1]. For structural elements of RBMK-type reactors, the following metal materials are used: steel 20 (support blocks and shielding plates), steel 10KhN1M (support structures, upper and lower parts of biological shield), steel 08Kh18N10T (parts of pipes of technological channels, channel paths), steel 10KhSND (metallic construction of biological shielding material), zirconium-niobium alloy E125 (parts of pipes of technological channels located in the reactor core), etc. [2][3].

Development of the deep geological repository (DGR) in Lithuania is in its early stages and the repository concept as well as final conditioning of the waste has not been selected yet. Concrete containers that are considered for disposal of short-lived low and intermediate level waste from the INPP in the near surface repository are not the best solution due to low loading efficiency. The radionuclides in metallic waste can be present as surface contamination or can be distributed in the metal matrix. The nature of the contamination determines the release mechanism: radionuclides from the surface can be easily leached as groundwater reaches the waste while radionuclides from the bulk activated metal are released congruent with corrosion. Experience from other countries suggests that metallic waste could be disposed of in stainless steel containers, but before making the final decision on what containers should be used, different options have to be analyzed.

The main radionuclides (especially with long decay times) associated with the activity of metal structures of a reactor facility are the long-lived isotopes of nickel and niobium (in case of technological channels). The list of radionuclides related to contamination contains isotopes of Cs, Eu, actinides and others.

Metal waste from decommissioning may corrode and form hydrogen. A small surface/volume ratio will help to minimize this risk. Molten ingots produced from the metal resulting from decommissioning will not only reduce the waste volume but also provide a minimized surface/volume ratio. Surface contaminated metals can be decontaminated using dry processes (e.g. blasting) or wet processes (e.g. electrochemical). After decontamination, measurement of activity will inform the decision on further management, i.e. free release and introduction to conventional residue material management or classification as waste according to the national regulations. However, in the case of induced radioactivity, melting fails to clean metal waste, hence it should be compacted and sent away for storage in order to wait for ^{60}Co to decay [4].

For efficient characterization of very low level metallic waste the determination of surface contamination part is needed by simple nondestructive γ-spectrometry measurement or combination of dose rate/γ-spectrometry measurement application. The aim of this work is to investigate the spectra of main activation (^{60}Co) and surface contamination (^{137}Cs) sources in different metal shields environment and to find out parameters which could be used for surface and volume activity discrimination by non-destructive gamma measurement.

The preliminary experiments using MCNP6 modelling and HPGe semiconductor detector measurements of known-home-made different geometry metallic waste samples with ^{60}Co and ^{137}Cs sources have been performed. Modelling, inter-comparison of γ-spectra and analysis of the nuclides peaks and Compton scattering edges for samples with sources of ^{60}Co and ^{137}Cs in different iron shielding conditions is presented below.

II. MATERIALS AND METHODS

Usually both computer modelling and spectrometric measurement methods are used for assessing the activity of reactor activated structures. Modelling tools (MCNP6, SCALE6.2) are used for obtaining activation of materials in the reactor core for characterization and separation of waste streams of highly activated zones, zone of intermediate and low activation metal waste and also non-activated materials for which only surface contamination is relevant [5]. Control of ^{137}Cs isotope activity in radioactive waste is important due to high mobility of the Cs which appears due damage of cladding of fuel elements in the core. Gamma spectrometry is very important for characterization and monitoring of different activity level radioactive waste. For many radionuclides, γ-spectrometry is a precise and often the only possible method of measurement.

A. γ-spectrometry

Interacting with matter gamma rays can collide with an electron and bounce off it (Compton scatter) or it can push an electron to a higher energy level (photoelectric ejection). Also part of this energy can be transformed into matter directly by creating an electron and a positron (pair production). These interactions create an electric current in the detector, which are amplified and measured to estimate the energy and direction of the original γ-ray.

Gamma-ray spectrometric measurements of the known-home-made different geometry metallic waste samples with different radioactive sources were carried out using HPGe detector coupled to the MCA Canberra DSA1000 with Genie-2000 gamma ray spectroscopy analysis software (*Canberra Industries, USA*). The HPGe detector of GC2520 series by Canberra, USA, with relative efficiency of 25%, and energy resolution of 1.1 keV at 121.78 keV (^{152}Eu) and at 2.0 keV at 1332.5 keV (^{60}Co) was used. Detector has been efficiency-calibrated for the standard geometry of the measurement. For the efficiency calibration the reference standards with ^{137}Cs, ^{60}Co and ^{152}Eu were used. The energy calibration curve was produced for 122 – 1408 keV energy range.

^{137}Cs and ^{60}Co point sources were measured, which were placed on several steel plates 1 cm thick above the detector and covered on top with few steel plates of the same thickness (see Table 1 and Figure 1 for details). There were plates of two sizes: 50x71x10 mm and 75x79x11 mm. If the source was between the plates, it was placed inside an Al disk with an inner diameter of 26 mm, an outer diameter of 75 mm, and a thickness of 3 mm.

Table.1 Radioactive decay energies and transition probabilities of usually detectable metallic waste gamma sources

Gamma ray transition	E, keV	Probability, %
^{137}Cs (β-) γ→^{137}Ba	661.657	85
^{60}Co (β-) γ→^{60}Ni	1332.492	100
^{60}Co (β-) γ→^{60}Ni	1173.228	100

B. MCNP modelling

In order to understand the gamma detector response in the different contamination - radioactive source - geometry and background conditions, for gamma radiation assessment we have used MCNP6 code and ENDF-VII cross-section libraries [6], [7]. Monte Carlo particle transport is based on the explicit tracking of particles. Probability distributions are randomly sampled using transport data. In calculations these distributions are used to determine the type of interaction, energy of particles if it scatters and leakage. In our case MCNP6 has been used for gamma rays interaction calculation with radioactive source shielding materials, detectors materials and Fe-Pb protective shields of the detector (see Figure 1) in different source cases: point source, volume source and planar source. This was accomplished by using the F8 tally (pulse height distribution in cell) from MCNP6. The modelling of efficiency calibration of particular HPGe detector using Monte Carlo simulations including coincidence-summing corrections for two peaks was done in [8].

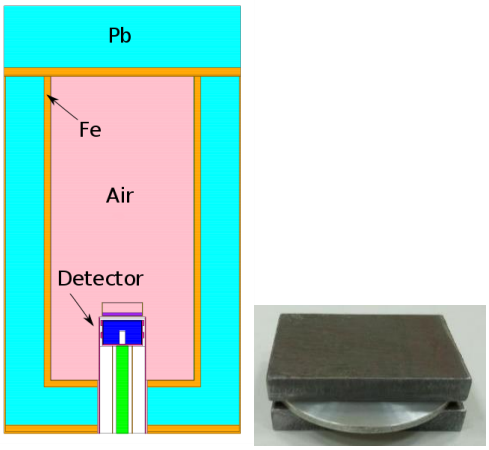

Figure 1. Scheme of the simulated HPGe detector with iron-lead shield and sample with radioactive source between 1 cm iron plates.

III. RESULTS AND DISCUSSION

Analysis of experimental measurement and modelling of the different geometry metallic waste samples was performed for ^{60}Co and ^{137}Cs point sources shielded by different thickness of iron plates. In Figure 2 comparison of measured and modelled γ-spectra of point sources shielded by 1cm thickness iron shields is presented. One can notice, what a good consistency of experimental and modelled results have been obtained and this allows investigating of γ-spectra of surface contaminated and volume activated metallic waste samples of various shapes.

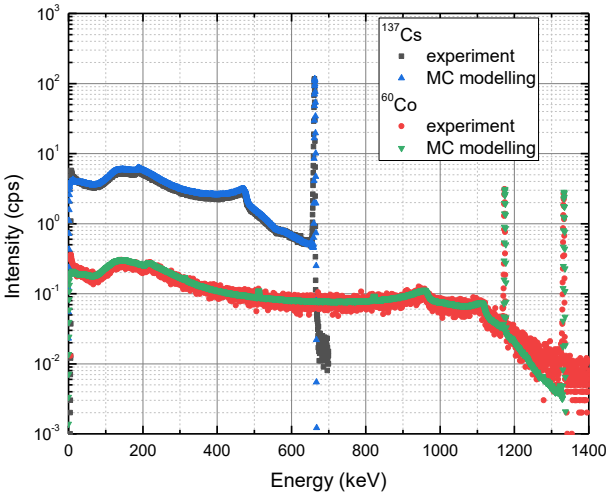

Figure 2. Inter-comparison of measured and modeled γ-spectra of ^{60}Co and ^{137}Cs point sources shielded by 1cm thickness iron shields.

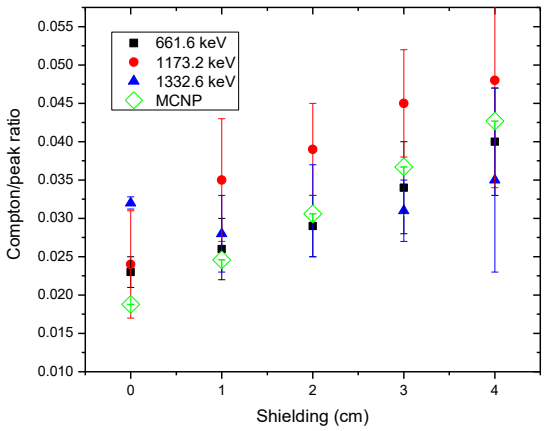

Figure 3. Experimental Compton/peak ratio for different ^{60}Co and ^{137}Cs point sources shielding geometries.

The dependence of Compton/peak ratio values for different thickness of shielding metal plates (at bottom and on top) of the ^{60}Co and ^{137}Cs point sources is presented in Figure 3. The preliminary analysis shows, that one can clearly distinguish between non shielded source and source shielded with different thickness of iron. The strongest dependence has been obtained for bottom shielding case (this would represent the inner surface of half cut pipe in the reality) – comparing with surface source: 0.023±0.002 unshielded case with 0.04±0.007 for 4 cm shielding case for ^{137}Cs. The similar result was obtained also in case of ^{60}Co source 0.024±0.001 comparing with 0.048±0.014 for 4 cm shielding case. The good agreement (up to 8%) have been obtained between ^{137}Cs modeling and experimental cases with shielding, the higher discrepancies (about 23%) occurred in non-shielded case due to point source activity and measurement dead time (see Figure 4 for details).

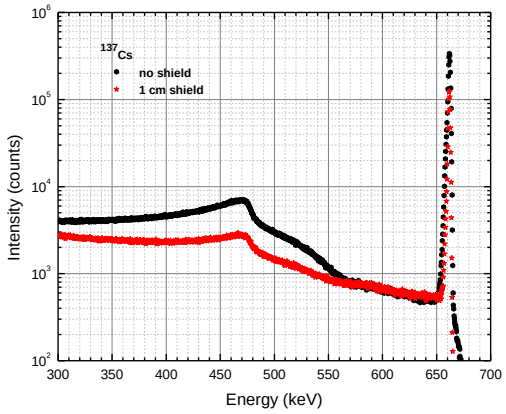

Figure 4. ^{137}Cs γ-spectra in case of non-shielded source and shielded with 1cm of iron plate.

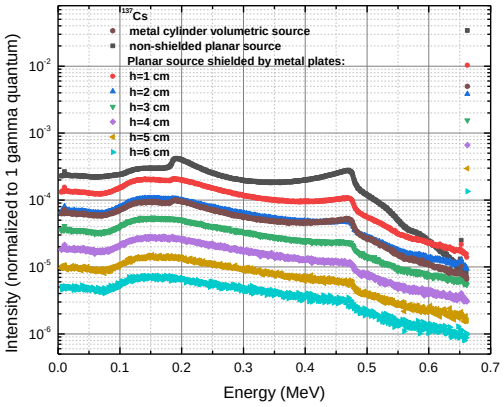

Figure 5. Comparison of modeled ^{137}Cs γ-spectra for different source cases: volumetric source (homogeneously distributed in the h=6cm r=3.36 cm metal cylinder) and planar source shielded with metal plates of different thickness.

The modeling shows that planar surface contaminated ^{137}Cs source could be distinguished from shielded or volumetric source by the shape/intensity of photo peak and Compton/peak ratio of γ-spectra as it is presented in Figure 5. The intensity of photo peak decreases with shielding material thickness from 3 to 250 times comparing 1 cm – to 6 cm shielding plates, the Compton/peak ratio changes from 0.021±0.0001 and 0.06±0.009 for non-shielded source and shielded by 6 cm metal plate source respectively. We should note, that h=6 cm metal cylinder ^{137}Cs volumetric source γ-spectrum looks quite similar with planar source shielded by 2 cm metal plate: the photo peak intensity ratio is 0.8, but Compton/peak ratio stands out better 0.033±0.0002 and 0.027±0.001 for 2 cm shielded planar source and volumetric source respectively.

IV. CONCLUSIONS

A good consistency of experimental and modelled results have been obtained during comparison of measured and modeled γ-spectra of ^{60}Co and ^{137}Cs point sources shielded by different thickness of iron. This allows investigating of γ-spectra of surface contaminated and volume activated different geometry metallic waste samples.

Analysis of experimental measurement and modelling of the ^{60}Co and ^{137}Cs point source samples have shown, that there is peak/Compton ratio dependence for different thickness iron shield environment of ^{60}Co and ^{137}Cs point sources. The possibility to use this type of analysis could be useful for real radioactive metallic waste samples surface activation identification (both on the surface and on the inner surface of the tube).

MCNP modeling of different source cases: planar source shielded with different metal plates and volume source have revealed, that surface contamination ^{137}Cs source can be distinguished if compared with reference source case by using modeling and measurement techniques from the shape/intensity and peak/Compton ratio of γ-spectra analysis.

Acknowledgements

This research is part of a project that has received funding from the EU HORIZON 2020 Euratom research and training programme PREDIS under grant agreement No. 945098.

V. REFERENCES

[1] R. Plukienė, A. Plukis, A. Puzas, V. Remeikis, G. Duškesas, and D. Germanas, "Modelling of Impurity Activation in the RBMK Reactor Graphite Using MCNPX," *Prog. Nucl. Sci. Technol.*, vol. 2, no. 0, pp. 421–426, 2011.

[2] B. K. Bylkin *et al.*, "Induced radioactivity and waste classification of reactor zone components of the chernobyl nuclear power plant unit 1 after final shutdown," *Nucl. Technol.*, vol. 136, no. 1, pp. 76–88, 2001.

[3] E. Narkūnas, "Reaktoriaus RBMK-1500 konstrukcinių elementų nuklidinės sudėties kitimo tyrimai." Doctoral dissertation, 2009.

[4] "Methodology to Manage Material and Waste from Nuclear Decommissioning Waste Management & Decommissioning Working Group, World Nuclear Association," *World Nucl. Assoc.*, vol. Report, no. 2019/001, 2019.

[5] V. Remeikis *et al.*, "Characterisation of RBMK-1500 graphite: A method to identify the neutron activation and surface contamination terms," *Nucl. Eng. Des.*, vol. 361, 2020.

[6] M. B. Chadwick *et al.*, "ENDF/B-VII.0 : Next Generation Evaluated Nuclear Data Library for Nuclear Science and Technology," vol. 107, pp. 2931–3060, 2006.

[7] B. Colling, I. Kodeli, S. Lilley, and L. W. Packer, "Benchmarking comparison and validation of MCNP photon," vol. 06024, 2017.

[8] M. Konstantinova, D. Germanas, A. Gudelis, and A. Plukis, "Efficiency Calibration of High-Purity Germanium Detector Using Monte Carlo Simulations Including Coincidence-Summing Corrections : Volume Source Case," vol. 61, no. 1, pp. 66–73, 2021.

Proceedings of the European Nuclear Young Generation Forum
ENYGF'21
September 27-30, 2021, Tarragona, Spain

Development of a Simplified Preliminary Risk Assessment Model for the Geological Disposal of Radioactive Waste in the United Arab Emirates.

Abdulla H. Al Nuaimi, Laurence G. Williams

Imperial College of London, United Kingdom

*Corresponding author: *a.alnuaimi19@imperial.ac.uk*

I. INTRODUCTION

The United Arab Emirates has embarked on nuclear power in 2009 and has just recently started commercial operations of the first out of four Advanced Power Reactors (APR-1400) with an individual electrical power capacity of 1,400 MWe, and a collective electric capacity of 5,600MWe [1].

The UAE is committed to the peaceful use of nuclear energy and it has made it a priority to assert that radioactive waste related activities are managed and monitored closely in accordance with the highest standards. Being in its early operational stages, the Barakah Nuclear Power Plant (BNPP) facility, located in the Western Region of the UAE, has yet to produce any significant volumes of radioactive waste. However, the wise decision of UAE leadership is reflected in the 2009 approved UAE Nuclear Law, where Chapter 8, Articles "41 "and "42", mandate the development of a radioactive waste management facility capable of effectively and efficiently managing the disposal of radioactive waste and SNF in accordance with the highest of safety standards [2].

The IAEA has set a fundamental safety objective for geological disposal, which focuses on providing necessary means to protect people and the environment from the harmful effects of ionizing radiation [3]. The Radioactive Waste Management Organisation (RWMO) under the Emirates Nuclear Energy Corporation (ENEC) is responsible for the safe and effective implementation of the UAE's policy towards the long-term management of higher activity radioactive wastes. Chapter 5, Article 6, Clause 8 of the Federal Authority of Nuclear Regulation's (FANR) regulatory document REG-27 titled "Regulation on Disposal of Spent Fuel and Radioactive Waste" identifies features with regards to an expected UAE Geological Disposal Facility (GDF), such that "features shall aim to provide isolation for at least several thousands of years for intermediate (ILW) and high-level (HLW) Radioactive Waste". HLW is currently a characterisation that is only given to Spent Nuclear Fuel (SNF) by the RWMO [4]. In order to provide evidence that can satisfy this requirement, the RWMO would need to scientifically confirm, with a certain accuracy, that during the period specified by FANR, radiological risks and hazards relating to the presence of the GDF at a selected location in the UAE is within acceptable limits.

The IAEA suggests that performing safety analyses facilitates scientific and methodical arguments, aiding and contributing to a better safety assessment in which radiological hazards are analytically assessed and compared with potential radiation dose and other risk criteria. Safety analysis is an important part of a GDF safety case. Switzerland's Nagra define a safety case as a "set of arguments and analyses used to justify the conclusion that a specific repository system will be safe", providing the basis on which GDF safety capabilities can be demonstrated to interested parties, facilitating transparency and dialog [5]. Safety analyses and other related assessments generally evolve over time as GDF design concepts develop further with more detail.

This paper describes the development of a simplified model to assess the risks to people from the disposal of HLW in a GDF.

II. DEVELOPMENT OF THE GENERIC GDF MODEL FOR HARD ROCK GEOLOGY

The conceptual disposal system design considered for the development of the Simplified Geological Disposal (SGD) model is illustrated in Figure 1, where it is assumed that SNF canisters are to be emplaced vertically in boreholes, with a distance of 6m between each canister in the emplacement tunnel, and a separation distance of 20m between each emplacement tunnel. Assemblies of SNF are packaged into copper canisters and in accordance with the SKB waste canister design as illustrated by Figure 2 [6].

The GoldSim's Contaminant Transport code was used to develop the SGD model to evaluate the dispersion of radioactivity released from a hypothetical GDF located in the UAE following the breakdown of the GDF's engineered barriers. The SGD model is also capable of evaluating radiological risks to people living in the biosphere. The SGD model enabled the simulation of the transport of radionuclides through the engineered barrier

systems (EBS) of the facility, to the surrounding geosphere until it reaches a reference receptor via ingestion (from well drinking water, consumption of livestock etc.) and inhalation through atmospheric dispersion.

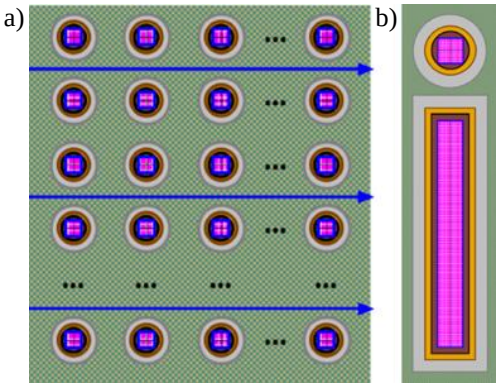

Figure 1: a) Plan View of SGD model Conceptual Disposal System, b) Waste Canister Emplacement in SGD Model with a Bentonite Buffer Surrounding Copper Canister

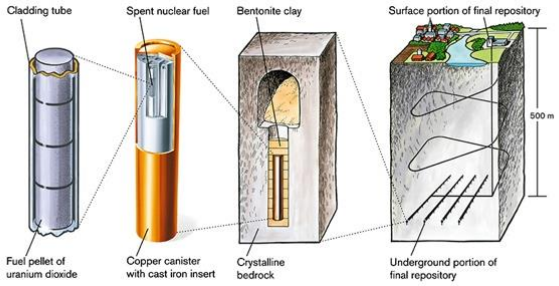

Figure 2: SKB Disposal Concept in Hard Rock [6].

The developed SGD model is comprised of four major components, the source term, the near-field surrounding the SNF package, the far-field (geosphere) and the biosphere. The source term was an input to the model calculations. The near-field component of the SGD model includes a bentonite buffer encompassing the SNF canister, with diffusion as the only mechanism of transport through it. The conceptual layout of the GDF and the configuration of waste canisters is addressed in the near-field region. The far-field component of the SGD model is divided into two parts, the vertical far-field consisting of the geological layers above the GDF to simulate the transport of radionuclides in the vertical direction, and the lateral far-field consisting of geological layers. Together, the evaluation of the near and far-field components allows for the demonstration of capability in the presented simplified indicative performance assessment model. An overview of the structure of the SGD model is illustrated by Figure 3.

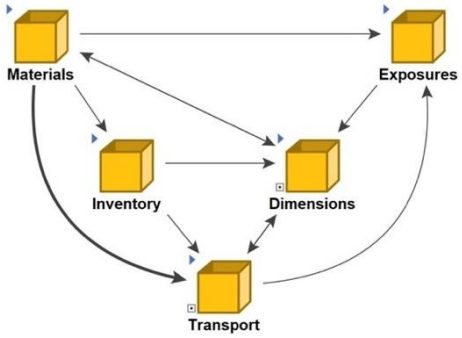

Figure 3: Overview of SGD model Structure

The SGD model's transport container defines pathways considered for the transport of radionuclide species released from the waste canisters through the near and far-fields, to a receptor as illustrated by Figure 4.

Two pathways, in the lateral and vertical directions were incorporated into the SGD model. In the case of a GDF located in hard rock, the most dominant pathway in which radionuclides are transported to the biosphere is through the lateral pathways, in the direction of flowing groundwater as illustrated in Figure 5.

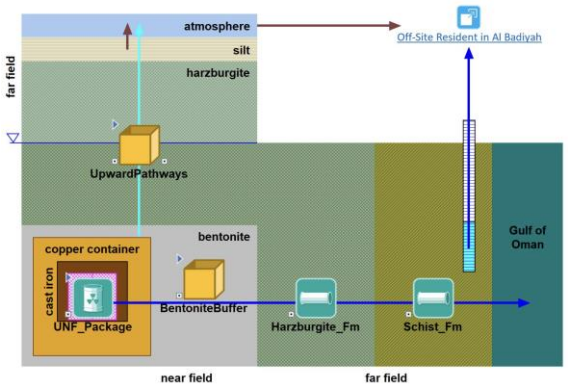

Figure 4: SGD Model Radionuclide Transport Pathways

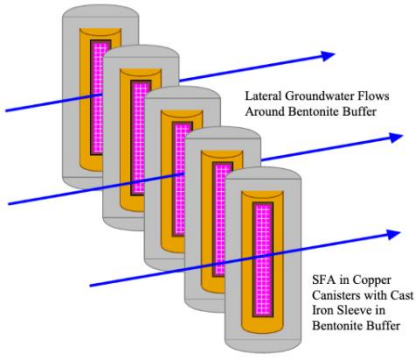

Figure 5: Lateral Groundwater Flow Through GDF.

In the near-field, degradation only starts when the cast iron insert has failed due to corrosion. The cast iron, in turn, does not start corroding until the surrounding copper canister has corroded. Once all barriers are breached, UO_2 fuel pellets start degrading, releasing radionuclides to the surrounding bentonite. Groundwater does not flow through the bentonite layer, preferring to flow around as illustrated in Figure 5. However, the bentonite buffer becomes saturated, and permits diffusion of radionuclides released from the UNF degradation. Once at the outer zone of the bentonite, radionuclides both diffuse upward to the ground surface and are entrained in lateral groundwater advective flow, entering the far field.

Once at the surface, gaseous radionuclides diffuse into the atmosphere and particulates enter via resuspension. Atmospheric dispersion carries radionuclides to the receptor. The entire lateral transport model is situated in the saturated zone. The flow path in groundwater is mostly around the bentonite buffer and copper containers, but some water enters the containers once they are breached by corrosion. The SNF is modelled as a matrix source that degrades in its own time, once introduced to water through the breached container. As the SNF matrix degrades, radionuclides are released to the bentonite buffer and

partition onto the clay. Some are entrained in the attenuated groundwater flow field within the bentonite buffer, and others diffuse upward towards the ground surface. Flowing laterally through the buffer, they are diluted into the natural flow field through the fractured hard rock. A water supply well extracts water downstream. This water is used in human exposure assessment calculations.

The exposure container, as seen in Figure 3, holds values and calculations for the assessment of exposures to a reference receptor. Human health effects evaluated in the SGD model include radiological effects related to ionizing radiation to a reference receptor that is defined as "a resident who grows some of their own food, including chickens (and their eggs), and fruits and vegetables".

The nearest user of groundwater is assumed to have a residence and grows crops. This receptor is assumed to use the groundwater for domestic purposes (including drinking water) and agriculture. The following exposure pathways were implemented:

- Ingestion of well water for drinking;
- Ingestion of plants from a small garden watered with well water;
- Ingestion of livestock (e.g. chickens) that spend time in the garden;
- Inadvertent ingestion of soil; and,
- Inhalation of ambient air that contains dust and gases transported from the site via atmospheric dispersion.

In order to quantify dose received via ingestion by a reference receptor, conversion factors were used to convert radionuclide concentrations in the water supply well to dose. These include pathway-specific dose conversion factors (DCFs), transfer factors (TFs) for food animals, and plat/soil concentration ratios (CRs) for food plants. DCF values that are used can be found from the US's DOE report, DOE-STD-1196-2011 [7].

To quantify dose received via inhalation by a reference receptor, conversion factors were used to convert radionuclide concentrations in air at the reference location. The receptor will be immersed in a plume of airborne radioactivity released from the upwards pathway adopted in the SGD model, resulting in the inhalation of some of the radioactivity from the plum.

III. VALIDATION OF THE MODEL

Data from the US's Granite General Disposal System (GGDS) model was used to validate the accuracy of the SGD model. The GGDS model was developed using the FEHM computer code alongside the GoldSim code, unlike the SGD model, which utilised an updated and more robust version of the GoldSim code. The source term and the geological parameters used in the DoE study were fed into the SGD model and the results were compared with those produced by the US's DoE's GGDS model. As results presented in the DoE GGDS model only consider dose from I^{129}, only the inventory of I^{129} was considered in the comparison exercise.

The input parameters considered for the validation exercise are available in Tables 4.6 and E-3 in the DoE's "Generic Deep Geologic Disposal Safety Case" [8]. For this comparison exercise, the SGD model is referred to as the "SGD (DoE) model" to reflect the DoE input parameters in the model. A summary of key input parameters used in the SGD (DoE) model to be compared with the DoE GGDS model result are presented in Table 1.

Table 1: Summary of SGD (DoE) Input Parameters

Parameters	DoE GGDS Model
Inventory	10 SNF Assemblies/Canister, I^{129} = 2462 g / Canister, # Assemblies = 366,840
Hard Rock Porosity	0.018
Water Velocity	9.6E-03 mm/yr
Canister Failure Time	50,000 years
UNF Waste-Form Degradation rate	2 x10^{-5} /yr
Distance to Receptor	5000 m

For this comparison exercise, as the DoE GGDS model does not consider an upwards pathway for radionuclide release, the SGD (DoE) model was changed to only present the lateral transport of radionuclides. Figure 6 illustrates a comparison between results from the DoE GGDS model and results obtained from the SGD (DoE) model.

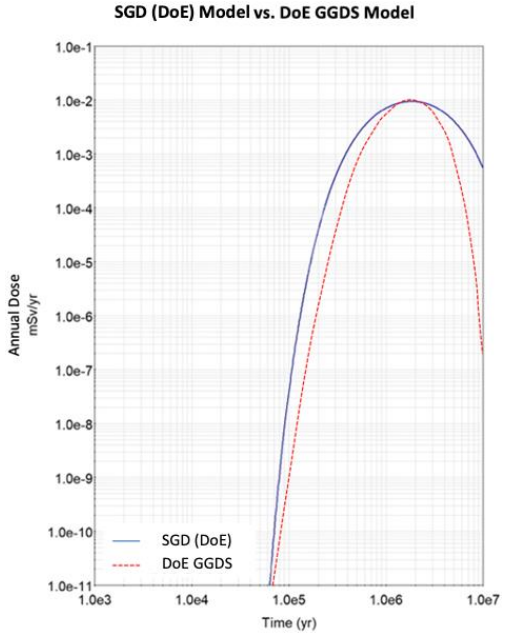

Figure 6: SGD (DoE) Model Results vs. DoE GGDS Model Results

The profile illustrated by the DoE GGDS model has a slight discrepancy in time, showing a more delayed release of I^{129} into the biosphere. This difference may be attributed to differences in some release mechanisms considered for I^{129} which may contribute to lower dose rates. Results generated from the SGD (DoE) model considers disposed I^{129} inventory coming from a single source, being from the SNF waste packages that are disposed in a "as is" condition without further reprocessing activities. Although most of the I^{129} inventory considered by the DoE in the GGDS model come from unconditioned Commercial Used Nuclear Fuel (CUNF), or SNF from the once-through fuel, another form of SNF I^{129} source was also incorporated into the GGDS model in small quantities. I^{129} from SNF immobilised in borosilicate glass characterised by the DoE as Commercial High-Level Waste (CHLW) is another source considered by the GGDS model and not by the SGD (DoE) model. Reprocessed SNF was not considered in the original SGD model to reflect the UAE's strict opposition towards domestic reprocessing of SNF as dictated by Article "41.3" of the UAE Nuclear Law [2], hence it was also not considered by the SGD (DoE) model for the

validation exercise. Therefore, it is expected that the delay in release when comparing the plot from the SGD (DoE) model and the actual plot from the DoE GGDS model is due to CHLW inventories of I^{129}, where transport through borosilicate glass is extremely limited [8].

Overall, the trend illustrated by both plots are very similar in terms of the time of initial registration of dose. Similarly, annual peak dose from the SGD model with the same input values to the DoE GGDS is registered at $8.8x10^{-3}$mSv/yr at a time of 1,700,000 years, which is close to DoE's reported value of $9.5x10^{-3}$mSv/yr at 1,730,000 years. This comparison provides confidence in the use of the SGD model for evaluating the performance of a GDF in UAE geological settings.

IV. APPLICATION OF THE MODEL TO UAE GEOLOGY

The UAE has yet to identify or decide on a disposal site or a disposal concept, and geological data specific to the characterisation of GDF host rock is not detailed enough or is not available in the public domain. However, initial screenings of geological environments in the UAE gave an indication of potentially suitable host rock formations. The Khor Fakkan (KF) block, located in the Northern Emirates, is a Higher Strength Rock (HSR) in the form of Harzburgite igneous rock, and preliminary investigations suggest that the location and geological environment might be suitable to host a UAE GDF.

The KF locations is set to the east coast of the UAE, on the Gulf of Oman. The topographic nature of the region is mountainous as can be seen from the satellite image in Figure 7[9].

Figure 7: Satellite image of Khorr Fakkan Area [9].

The SGD model has been used to evaluate risks associated with the location of a GDF for the disposal of the UAE's SNF and other HAW using geological data made available by the Environmental Agency of Abu Dhabi (EAD) and the UAE's Ministry of Energy and Infrastructure (MoEI). The results of this work are under review and will be published shortly.

V. CONCLUSIONS

A simplified model has been developed to evaluate the risks from the disposal of the UAE's HAW in a deep underground GDF. This paper has described the model and how it has been validated against the US's DoE modelling data.

The close comparison of the results from the SGD model predictions and those from the published DoE data suggests that the SGD model can be used with confidence when evaluating the risks to people from a GDF located in the UAE's geological settings.

The SGD model presented in this paper is generic and not site specific and hence can be used in different geological settings. The model can be used to undertake preliminary analyses of locations to determine if the location is appropriate to perform more comprehensive siting evaluation before any decision is made.

The developed SGD model presented in this paper can be used by the UAE's RWMO as a foundation for the development of a more robust, accurate and site-specific performance assessment model. Additionally, the developed model can be altered to also provide an indicative performance assessment of a Near Surface Disposal Facility (NSDF).

The SGD model has been used to evaluate the risks associated with the location of a GDF for the disposal of the UAE's SNF and other HAW at two specific locations in the UAE. The results of this work is expected to be published in the near future.

VI. REFERENCES

[1] KEPCO/KHNP. APR1400-K-X-ER-14002-NP, Revision 0, " APR1400: DESIGN CONTROL DOCUMENT TIER 2 - CHAPTER 4 REACTOR."

[2] UAE. Federal Law by Decree No.6 of 2009 Concerning the Peaceful Uses of Nuclear Energy. [Online] 2009. https://www.fanr.gov.ae/en/Lists/LawOfNuclear/Attachments/1/20101024_nuclear-law-scan-eng.pdf. [Accessed 26 Aug. 2020]

[3] IAEA (2006): Fundamental Safety Principles, IAEA Safety Standards Series No. SF-1, International Atomic Energy Agency, Vienna, Austria.

[4] UAE. (Draft) UAE National Policy regarding the Long-Term Management and Disposal of Spent Nuclear Fuel and Radioactive Waste. Abu Dhabi. UAE. 2017.

[5] Nagra, National Cooperative for the Disposal of Radioactive Waste (2002a): Project Opalinus Clay, Safety Report, Demonstration of Disposal Feasibility for Spent Fuel, Vitrified High-Level Waste and Long-Lived Intermediate-Level Waste (Entsorgungsnachweis), Nagra Technical Report NTB 02-05, Nagra, Wettingen, Switzerland.

[6] SKB. 2011. Long-term Safety for the Final Repository for Spent Nuclear Fuel at Forsmark: Main Report of the SR-Site Project. Technical Report TR-11-01 (3 volumes). Stockholm, Sweden: SKB. www.skb.se

[7] DOE-STD-1196-2011, Derived Concentration Technical Standard.

[8] G. Freeze, M. Voegele, P. Vaughn, J. Prouty, W.M. Nutt, E. Hardin, S.D. Sevougian. 2013. Generic Disposal System Modelling — Fiscal Year 2013 Progress Report. FCRD-UFD-2012-000146 SAND2013-0974P Albuquerque, NM: Sandia National Laboratories.

[9] Google. (n.d.). *Khorr Fakkan Block*. Retrieved from https://www.google.com/maps/@25.3832772,56.1970106,31184m/data=!3m1!1e3

Proceedings of the European Nuclear Young Generation Forum
ENYGF'21
September 27-30, 2021, Tarragona, Spain

Depth profiling of radiologically contaminated concrete using computed tomography images and Monte Carlo simulations

Brabants, Lowie[1*], Simons Mattias[1], Reniers, Brigitte[1], Paepen, Jan[2], Vandoren, Bram[3] and Schroeyers, Wouter[1]

[1] Hasselt University, NuTeC, CMK, Nuclear Technology - Faculty of Engineering Technology, Agoralaan building H, B-3590 Diepenbeek, Belgium; [2] European Commission, Joint Research Centre, Retieseweg 111, B-2440 Geel, Belgium; [3] Hasselt University, CERG, Faculty of Engineering Technology, Agoralaan building H, B-3590 Diepenbeek, Belgium

*Corresponding author: *lowie.brabants@uhasselt.be*

I. INTRODUCTION

Due to the ageing of the nuclear power plants (NPPs) in Europe, it is expected that during next decade more and more reactors will have to be decommissioned and dismantled [1]. This ageing trend can also be observed for the 7 operational reactors in Belgium. Three of the reactors finished construction in 1975. The other four reactors were commissioned between 1982 and 1985 which leads to an average age that exceeds 40 years. All of the reactors are planned to be closed by 2025, opening up the Belgian nuclear decommissioning market. For the decommissioning of these reactors, a "back to greenfield" strategy will be applied, meaning that the site of the NPPs will be brought back to the initial situation before the power plants were built [2].

For the decommissioning, an important factor that determines the total cost is the amount of generated radioactive waste. The approach will be to minimize the fraction of radioactive waste, by accurately performing radiological characterizations of the waste streams to separate non-radioactive waste streams from radioactive waste and by (where possible) decontamination of waste [3].

A frequently encountered waste stream is concrete as it is one of the most common material used in the construction of a NPP. Most concrete waste can be classified as conventional waste, but for concrete used in the containment building, radiological contamination is frequently encountered. To determine a correct decontamination strategy for this concrete, the first step is to perform radiological characterisations to quantify the nature of the contamination and its depth [4].

These characterisations can be destructive (by taking core drilling samples), but can also be performed by non-destructive in-situ measurements (see Figure 1). Core drilling samples are frequently used to determine the contamination depth. Concrete cores are extracted from structures, segmented, pulverized and characterized. Although this technique is accurate, it only provides information on the contamination depth at a very local level. The sample might not be representative for the surrounding material and as a result, a gross over or underestimation of the contamination depth may be present. Moreover, this technique is labour intensive (and thus costly) and may also lead to the spreading of contaminated dust [5], [6].

Figure 1. destructive core drilling procedure (left)[7]**, non-destructive radiological characterisation with handheld scintillator detector (right)**[8]

An alternative to destructive sampling are in-situ measurements. The most basic approach to determine contamination non-destructively is by using handheld equipment such as scintillator detectors. However, this technique is not only time consuming as scanning is performed manually, but the depth information is also limited to the superficial activity. As a result, multiple cycles of measurements and decontaminations are often performed before the desired residual activity levels are achieved [5], [9].

A more advanced non-destructive technique can be performed using the spectral information acquired with high-purity germanium (HPGe) detectors and to determine contamination characteristics such as activity levels, radionuclide inventory and contamination depths.

The depth profiling technique that is considered in this research is the relative linear attenuation (RLA) model. This method is applied to the relative intensities of the X-ray and gamma emissions of key radionuclide ^{137}Cs [10]. The model assumes an exponential decrease of the contamination as a

function of depth. Such profile has been frequently reported for contaminations in both an environmental and decommissioning context. The RLA model can be applied to determine the total activity of ^{137}Cs and the relaxation length RL (which is an important depth parameter) of the exponential contamination profile [7], [8], [12]. After determining these quantities, the decontamination plan, indicating the locations and depths of concrete to be removed, can be constructed.

Although the RLA technique has already been applied in a decommissioning context, this method still has its shortcomings as it assumes a perfect exponential function and a perfect homogeneous base material. Both of these assumptions are not completely applicable for concrete. Concrete is far from homogeneous as it consists out of a mixture of mortar, aggregates and voids. Furthermore, the contamination is observed to be more pronounced in the porous mortar phase of the concrete than in the aggregates [13], [14].

As the performance of a depth profiling technique directly influences the total amount of radioactive waste being generated, it is important to further optimize the existing techniques and quantify operational limits and error sources. In other words, having correct radiological information of the installation, even before the start of the decontamination process, is an upstream tool to directly limit the amount of radioactive waste being generated in a decommissioning project.

To study the performance of the RLA technique, a Monte Carlo (MC) model was constructed in this research consisting of a HPGe detector setup with contaminated concrete samples. A MC model is a computational method to study interactions of ionizing radiation with matter. The complexity of the concrete was incorporated into the model by making Computed Tomography (CT) images of the concrete in order to visualize the aggregates, mortar and voids. Different exponential profiles were then applied to the concrete model to quantify the error on the contamination activity (determined by the full-energy peak efficiency), and on the depth estimation (determined by the relaxation length) resulting from the RLA model.

II. HPGE MODEL

An extended-range coaxial p-type HPGe detector (type GX9023 from Mirion) was modelled and the performance of the resulting MC model was validated by comparing the full-energy peak (FEP) efficiency of the MC model to the experimentally determined FEP efficiency. The FEP efficiency is an important factor that links the area of a spectral peak directly to the activity of the source.

These measurements were performed with a variety of reference sources, measured at different source-to-endcap distances. The sources contained multiple radionuclides to validate the detector model over a broad energy range. The following sources were used:

- Point sources: ^{137}Cs, ^{134}Cs, ^{60}Co, ^{152}Eu and ^{241}Am;
- Volumetric water sources: ^{60}Co, ^{137}Cs, ^{134}Cs, ^{133}Ba and ^{152}Eu;
- Volumetric silicone-based sources: ^{139}Ce, ^{60}Co, ^{137}Cs, ^{113}Sn, ^{85}Sr, ^{57}Co, ^{51}Cr, ^{88}Y, ^{133}Ba, ^{109}Cd, ^{241}Am and ^{210}Pb.

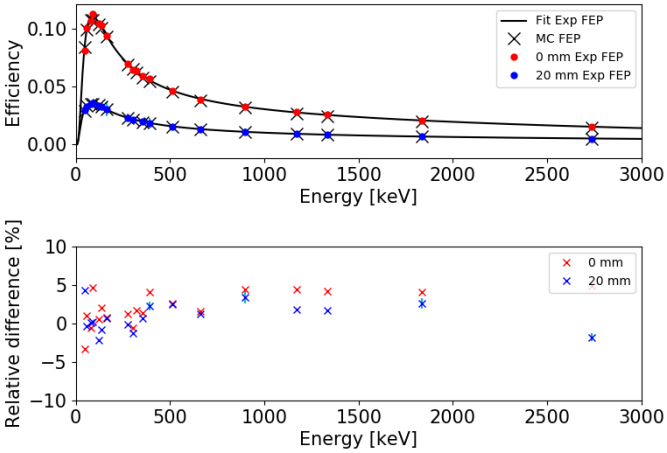

Figure 2. Experimental and MC calculated detector efficiencies for measurements of the volumetric silicone source at 0 mm and 40 mm from the detector endcap (top). The relative difference between the experimental and MC detector efficiencies (bottom) [15].

The MC model was considered to be validated when the relative difference of the model to the experimental data was in agreement considering an imposed criterion of 5% relative difference for gamma rays with an energy between 100 keV and 2000 keV and 10% relative difference for gamma or x-rays with energies lower than 100 keV or higher than 2000 keV. For each source, the model performed within these tolerance limits. Figure 2 shows the results of the MC model for the volumetric silicone source which was measured at 0 and 20 mm distance from the detector endcap [15].

III. CONCRETE MODEL

Different concrete samples containing limestone aggregates were made and used as the basis for the contamination measurements. After demoulding, the samples were cured for 21 days. In the next step, the samples were scanned with a CT-scanner (Philips Brilliance CT Big Bore). These CT images are then converted to a MC model to study the impact of the inhomogeneity of the concrete samples on the performance of the RLA model. As this model is based on the assumption of a completely homogeneous base material, it is expected that errors in depth estimations will be made when the method is applied to the complex matrix of concrete which consists of higher density aggregates, surrounded by mortar in which air cavities are also present (so-called voids).

As the casted concrete samples were not spiked with any radioactive ^{137}Cs, the contamination was simulated by incorporating multiple contamination profiles in the MC model. Different exponential equations are simulated on different concrete samples according to equation 1:

$$A(x) = A(0)e^{-x/RL} \quad (1)$$

Where A is the activity level [Bq] at the surface or at depth x [mm] and RL stands for the relaxation length [mm] which describes the slope of the activity decrease with depth. Simulated 1/RL values varied from 0 (representing a

completely uniform profile) to 1 (representing a steep exponentially decreasing contamination profile) [12].

Adding to this contamination profile, activity has also been shown to be more present in the porous mortar phase of the concrete rather than in the aggregates themselves [13], [14]. This aspect of selectivity of the contamination is also incorporated in the MC model, as no particles are generated within the volume occupied by the aggregates. Figure 3 represents the different steps that were performed to construct the MC model.

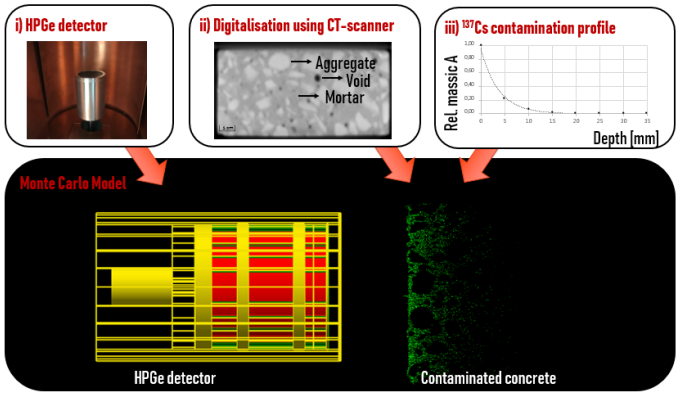

Figure 3. Illustration of the different steps that were performed to create the MC model; i) creating a model of the HPGe detector, ii) making CT scans of the concrete samples, iii) applying different contamination profiles with varying relaxation lengths

IV. RESULTS AND DISCUSSION

Concrete samples were modelled to contain different contamination profiles of ^{137}Cs. In total, ten different concrete samples were scanned. Although all the samples were made with the same mixing recipe, the internal composition per sample is different, as the internal arrangement of voids and aggregates is unique for each sample. The effect of the internal composition on the RLA model is studied by looking at the effect on the FEP efficiency (which is used to calculate the contamination activity) and on the relaxation length (which describes the decrease of contamination with depth).

A. Fluctuations on the FEP efficiency

When applying a contamination profile with a 1/RL value of 0.2 to the different samples, the spectral counts at an energy of 661 keV show deviations that can directly be related to the internal structure. Samples that have more aggregates near the surface of the concrete samples tend to have fewer counts in the peak area, whereas samples that have more mortar (or voids) at the surface lead to more registered counts. This effect is illustrated in Figure 4, where the FEP efficiency at 661 keV of the 10 different spectra are compared to a benchmark situation where a completely homogeneous concrete sample is simulated.

Relative deviations to the FEP efficiency are observed varying from 4% to 9%. For each of the 10 samples, a systematic underestimation of the efficiency would be made when the FEP of the benchmark would be applied. For the X-rays of ^{137}Cs, the relative deviation is even more pronounced as the lower energetic photons are more sensitive to small deviations in the sample density.

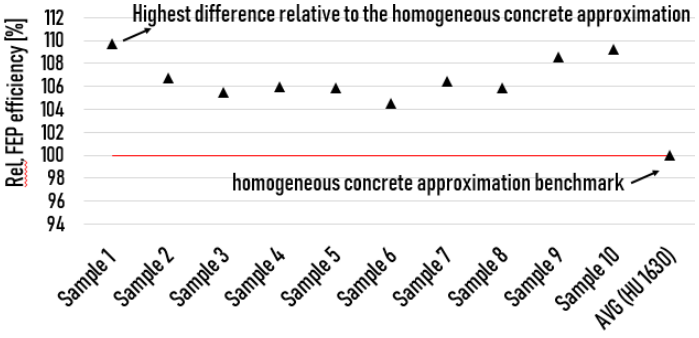

Figure 4. fluctuations of the FEP efficiency of the detector model at 661 keV for 10 different concrete samples. The last data point represents the FEP efficiency of a completely homogeneous concrete sample.

As the FEP efficiency is directly used to calculate the total activity of the contamination, this underestimation would also lead to an erroneous overestimation of the total activity of the contamination. The systematic deviation of the FEP compared to the benchmark can be explained by the density of the concrete near the surface. The top layer of concrete consists of fewer aggregates than the composition of the concrete deeper inside of the samples, leading to an overestimation of the density at the surface.

B. Fluctuations of the relaxation length

Next to the deviations observed for the FEP efficiency (which is used to calculate the source activity), the internal structure will also influence the performance of the RLA model and the corresponding estimation of the relaxation length.

Figure 5 shows the application of the RLA model for 2 extreme situations where i) a concrete sample containing only mortar is simulated and ii) a concrete sample having a density of pure limestone aggregate is simulated for different RL's. These two situations are considered extreme because the densities are respectively the lowest and highest. As a result, the corresponding X-ray to gamma ratio's (which represents the peak area registered in the X-ray peak compared to the peak area of the 661 keV peak) will also represent the boundaries for encountered ratios of more realistic concrete samples as their respective densities lie within the interval constrained by the boundary conditions.

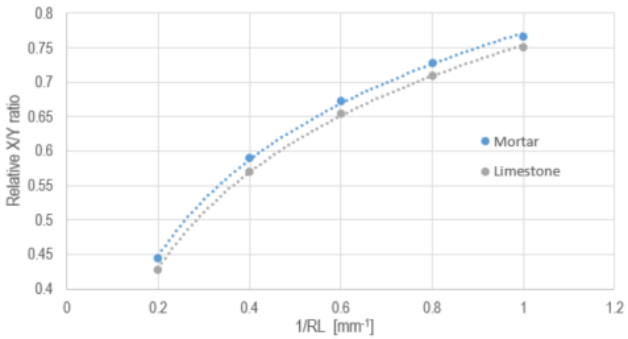

Figure 5. X-ray to gamma intensities for contamination profiles with different RL's relative to a completely planar contamination profile.

The X-ray to gamma ratios are expressed relative to the X-ray to gamma ratios of a completely planar contamination distribution (corresponding to a surface contamination). The ratio increases with increasing 1/RL values. Bigger 1/RL values mean the activity is more concentrated on the surface. In this case, the contamination profile shows a steep decreasing activity with depth and thus resembles pure planar contamination. For 1/RL $\rightarrow$ 0 the relative X-ray to gamma intensity of the contamination profile will match that of a uniform distribution.

As pure limestone is the densest boundary condition, the X-ray to gamma ratio is always lower compared to the ratio of a mortar sample. This is a result of the lower energetic X-rays whose self-attenuation is considerably more sensitive to small changes in density compared to the higher energetic gamma rays.

Figure 5 can be used to determine the maximum error when the density of the concrete sample does not exactly match that of the boundary situations. For example, when an X-ray to gamma ratio of 0.5 is observed (compared to the ratio for a planar source), the matching 1/RL value of the boundary conditions would be 0.258 and 0.284 for respectively mortar and limestone. As a result, the maximum error between both estimations of 1/RL would be approximately 9%. This error can then be used in combination with the error on the FEP efficiency to fully determine the error on the contamination profile and, subsequently, be used to create a decontamination plan.

V. CONCLUSIONS

CT scanning of concrete samples provides valuable insights into the internal structure of concrete. It was demonstrated that CT images can successfully be incorporated into a MC model to study the effects of the internal structure on the RLA model.

By incorporating the internal structure of the 10 concrete samples in the MC model, deviations of up to 9% in the FEP efficiency were observed which are directly linked to the internal structure. The results show that estimations of the FEP efficiency based on a homogeneous concrete sample systematically underestimate the actual FEP efficiency leading to an overestimation of the contamination activity.

For estimating the error on the 1/RL values, an interval described by the boundary conditions defined by pure mortar and limestone samples was determined. The relations between the ratio and the 1/RL can subsequently be used to estimate errors on the 1/RL value when actual concrete samples, consisting of a mixture of mortar and aggregates are measured.

Having quantified the errors on the FEP efficiency and the errors on the determination of 1/RL, a better estimation of the total amount of 'to be removed concrete' material can be made.

VI. REFERENCES

[1] R. Volk, F. Hübner, T. Hünlich, and F. Schultmann, "The future of nuclear decommissioning – A worldwide market potential study," *Energy Policy*, vol. 124, no. August 2018, pp. 226–261, 2019.

[2] Federaal Agenschap voor Nucleaire Controle (FANC), "Kerncentrales in België." [Online]. Available: https://fanc.fgov.be/nl/dossiers/kerncentrales-belgie.

[3] M. Felipe-Sotelo, J. Hinchliff, D. Drury, N. D. M. Evans, S. Williams, and D. Read, "Radial diffusion of radiocaesium and radioiodide through cementitious backfill," *Phys. Chem. Earth*, vol. 70–71, pp. 60–70, 2014.

[4] OECD & NEA, "R&D and Innovation Needs for Decommissioning Nuclear Facilities," 2014.

[5] S. Boden, B. Rogiers, and D. Jacques, "Determination of 137Cs contamination depth distribution in building structures using geostatistical modeling of ISOCS measurements," *Appl. Radiat. Isot.*, vol. 79, pp. 25–36, 2013.

[6] D. Gurau, S. Boden, O. Sima, and D. Stanga, "Determination of the neutron activation profile of core drill samples by gamma-ray spectrometry," *Appl. Radiat. Isot.*, vol. 134, pp. 194–199, Apr. 2018.

[7] SCKCEN, "Customized training courses in decommissioning and decontamination." [Online]. Available: https://www.sckcen.be/en/academy/training-courses/personalized-training-courses/customized-training-courses-decommissioning-and-decontamination.

[8] M. J. Joyce, J. C. Adams, J. A. Heathcote, and M. Mellor, "Finding the depth of radioactivity in construction materials," *Proc. Inst. Civ. Eng. Energy*, vol. 166, no. 2, pp. 67–73, 2013.

[9] International Atomic Energy Agency, "Managing Low Radioactivity Material from the Decommissioning of Nuclear Facilities," 2008.

[10] K. Rybacek, P. Jacob, and R. Meckbach, "In Situ Determination of Deposited Radionuclide Activities : Improved Method Measured Photon Spectra," no. January, 1992.

[11] A. Shippen and M. J. Joyce, "Profiling the depth of caesium-137 contamination in concrete via a relative linear attenuation model," *Appl. Radiat. Isot.*, vol. 68, no. 4–5, pp. 631–634, 2010.

[12] K. M. Miller, P. Shebell, and G. A. Klemic, "In situ gamma-ray spectrometry for the measurement of uranium in surface soils," *Health Phys.*, vol. 67, no. 2, pp. 140–150, 1994.

[13] I. Sato, K. Maeda, M. Suto, M. Osaka, T. Usuki, and S. I. Koyama, "Penetration behavior of water solution containing radioactive species into dried concrete/mortar and epoxy resin materials," *J. Nucl. Sci. Technol.*, vol. 52, no. 4, pp. 580–587, 2015.

[14] K. Maeda *et al.*, "Distribution of radioactive nuclides of boring core samples extracted from concrete structures of reactor buildings in the Fukushima Daiichi Nuclear Power Plant," *J. Nucl. Sci. Technol.*, vol. 51, no. 7–8, pp. 1006–1023, 2014.

[15] L. Brabants, G. Lutter, J. Paepen, B. Vandoren, B. Reniers, and M. Carlo, "Validation of TOPAS MC for modelling the efficiency of an extended-range coaxial p-type HPGe detector," *Appl. Radiat. Isot.*, vol. 173, no. November 2020, 2021.

Proceedings of the European Nuclear Young Generation Forum
ENYGF'21
September 27-30, 2021, Tarragona, Spain

Research on Cement-Organics-Radionuclides-Interactions within the collaborative EURAD project

Altmaier, Marcus[1], Blin, Virginie[2], García, David[3*], Henocq, Pierre[4], Missana, Tiziana[5], Ricard, Denise[4] and Vandeborre, Johan[6], Macé, Nathalie[2]

[1] Karlsruhe Institute of Technology, Institute for Nuclear Waste Disposal (KIT-INE), Karlsruhe – Germany; [2] Commissariat à l'énergie atomique, DEN, CEA, Université Paris-Saclay, Gif-sur-Yvette – France; [3] Amphos 21 Consulting S.L., Barcelona – Spain; [4] Agence Nationale pour la gestion des Déchets Radioactifs (Andra), Châtenay-Malabry cedex – France; [5] CIEMAT, Madrid – Spain; [6] SUBATECH, UMR 6457, Institut Mines-Télécom Atlantique, CNRS/IN2P3, Université de Nantes, Nantes – France

*Corresponding author: *david.garcia@amphos21.com*

I. INTRODUCTION

The CORI (Cement-Organics-Radionuclides-Interactions) Workpackage in EURAD [1] aims to improve the knowledge on the organic release issues which can accelerate the radionuclide migration in the context of the post closure phase of geological repositories for ILW and LLW/VLLW including surface/shallow disposal. The R&D in CORI is expected to extend the current state-of-the-art, contribute to optimize disposal solutions and consider questions of regulatory concern. CORI will help member states to further develop their national R&D programs and support programs at an early implementation stage.

CORI objectives are addressing topics in the context of cement-organics-radionuclides-interactions. Organic materials are present in some nuclear waste and as admixtures in cement-based materials and can potentially influence the performance of a geological disposal system, especially in the context of low and intermediate level waste disposal. The potential effect of organic molecules is related to the formation of complexes in solution with some radionuclides of interest (actinides and lanthanides) which can (i) increase the radionuclide solubility and (ii) decrease the radionuclide sorption. Organic substances require increased attention since a significant quantity exists in the waste and in the cementitious materials, with a large degree of chemical diversity. Cement-based materials will be degraded with time, leading to specific alkaline pH conditions under which the organics can degrade, thus increasing their impact on repository performance.

II. CORI STRUCTURE

The CORI project is formed by 24 partners from 10 different European Countries (Figure 1). The project coordinator is KIT-INE from Germany (CORI contact: marcus.altmaier@kit.edu)

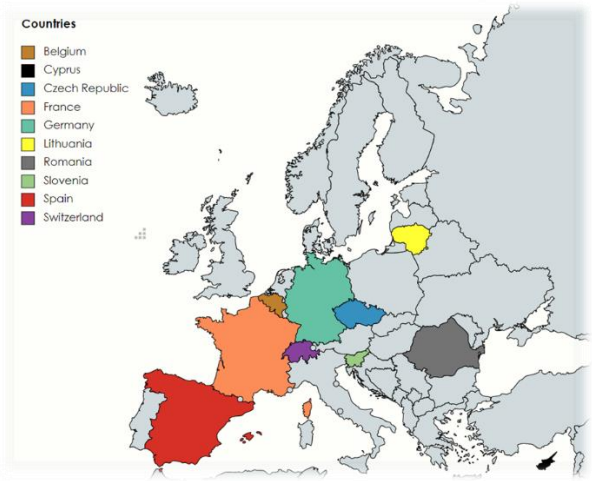

Figure 1. Countries involved in CORI.

The project is structured in four different tasks:

- T1. Coordination, State-of-the-art and training material
- T2. Organic Degradation
- T3. Organic-Cement-Interactions
- T4. Radionuclide-Organic-Cement-Interactions

Among these tasks three of them are focused on R&D scientific topics:

- T2 Organics Degradation. Focus is on the characterization of soluble organic species generated by radiolytic and hydrolytic degradation of selected organics (PVC, cellulose, resins, superplasticizers). Studies also include the analysis of degradation/stability of small organic molecules such as carboxylic acids and determination of degradation rates.
- T3 Organics-Cement-Interactions. Studies focus on investigating the mobility of selected organic molecules in cement-based materials. Mobility of

organic molecules includes sorption and transport properties. Organics will also include small ^{14}C bearing molecules as identified in the EC EURATOM project CAST [2]. Both retention on individual cement phases and actual cementitious systems are investigated.

- T4 Radionuclides-Organics-Cement-Interactions. Consistent with the set of organics, individual cement phases and materials identified in the above two Tasks, radionuclide migration processes are studied in the ternary system. The role of organic molecules on the transfer properties of radionuclides are investigated through sorption and transport experiments. Selected radionuclides cover a range of chemical characteristics and redox states relevant for the expected conditions in L/ILW disposal.

III. EXPECTED IMPACTS

Predicting and assessing radionuclide transport is a key topic in nuclear waste disposal. Improved quantification of radionuclide solubility and sorption phenomena in cementitious environments can provide important input into predicting radionuclide transport. CORI is expected to provide new scientific information in this context and generate specific impact regarding implementation needs and safety. A preliminary State of the Art (SOTA) document on key topics addressed in CORI has been already prepared (https://www.ejp-eurad.eu/publications/eurad-deliverable-31-cori-sota-cement-organic-radionuclide-interactions-content-lilw) and will be updated at the end of the project with the results generated by the different partners.

An important objective in CORI is enhancing cooperation between the different participating beneficiaries and countries. Knowledge transfer and training of young researchers in view of future demands for qualified staff is likewise a key aspect of CORI. CORI is fully integrated into EURAD, working both in exchange with other RD&D WPs and the Networking and Knowledge Management activities.

Issues of interest at the repository scale are identified as follows:

- Improved scientific basis for the Safety Case for L/ILW waste repositories featuring high organic content.
- Co-storage of waste: support decisions regarding the question whether or not a mix of various wastes (organics, soluble salts, exothermic waste) can be foreseen.
- Optimization of vault design: limitations of interactions between the vaults regarding their content. CORI will provide information on the organic plume by characterizing the transfer behaviour in cement-based materials.
- Optimization of concrete formulations as regards the potential effect of superplasticizers on radionuclide transfer properties.

The CORI WP is linked to the EURAD [1] Roadmap Theme 3 (EBS properties, function and long-term performance) phases 2 -4 and Theme 4 (Geoscience to understand rock properties, radionuclide transport and long-term geological evolution) phases 1 and 2.

Regarding safety, characterizing the effect of the organic plume on the behaviour of radionuclides in terms of:

- Solubility (limitation of solubility increase)
- Sorption (limitation of retention decrease) in terms of K_d values.
- The retention of potentially ^{14}C-bearing organic molecules (determined in CAST project [2]) in cementitious environments in the case of specific waste.

The overall project aims are twofold:

- Reduce the uncertainties on the current knowledge, which is mainly based on K_d values,
- Improve the knowledge on the known organic molecules present in degradation solutions (not considered so far) with their complexing properties: better definition of the organic inventory regarding the waste and the concrete vault (geological and surface repositories).

IV. REFERENCES

[1] M. Garcia, T. Beattie, & S. Schumacher. EURAD− the European Joint Programme for research on radioactive waste management between EU members states national programmes. EPJ Nuclear Sciences & Technologies, 6, 21. 2020.

[2] S. Norris & M. Capouet. Overview of CAST project. Radiocarbon, 60(6), 1649-1656. 2018.

Proceedings of the European Nuclear Young Generation Forum
ENYGF'21
September 27-30, 2021, Tarragona, Spain

Development of a gamma irradiation loop to evaluate the performance of the EURO-GANEX process

Sánchez-García, Iván[1,2*], Galán Montano, Hitos[1], Núñez Gómez-Aleixandre, Ana[1], Perlado Martín, Jose Manuel[2] and Cobos Sabaté, Joaquín[3]

[1] CIEMAT, Spain; [2] UPM, IFN, Spain; [3] EBD-CSIC, Spain.

*Corresponding author: *ivan.sanchez@ciemat.es*

I. INTRODUCTION

The reprocessing of nuclear fuel is currently moving towards advanced cycles that contemplate the recycling of minor actinides (MAs: Am, Cm, Np) as a strategy to minimise the radiotoxicity of the waste that must be stored [1, 2]. To validate a new separation process for this purpose, solvents are not only tested concerning the extraction efficiency but also their resistance against radiolysis and hydrolysis effects. This is because extracting systems will be in contact with a highly radioactive field and high nitric acid concentration, producing its degradation and undesirables effects such as decrease of selectivity, third phase formation, etc., and the consequent increase of secondary waste and process costs [3, 4]. Hence, the development of a successful industrial process demands an approach of the stability problems, from the initial design of the extractant to a hot test in a pilot plant. The initial irradiation studies of individual solvents involving isolated molecules, in batch and static conditions, allow the fundamental comprehension of the degradation pathways and an easy way to compare the robustness of different extractants. However, to predict the long-term behaviour during the operation, a more realistic assessment of the process conditions must be considered. Although batch irradiation experiments can be designed to cover many scenarios, dynamic experiments simulating counter-current processes, as lifelike as possible, are always needed. Nowadays, it exists an important gap between fundamental irradiation experiments and advanced test in pilot plants, which require sophisticated dynamic irradiation platforms (irradiation loops) where the settings are not normally easily modifiable. CEA Marcel-Proust loop (Commissariat à l'énergie atomique et aux énergies alternatives) in France and the Idaho National Laboratory (INL) loop in United States are two of the most successful irradiation loops developed for these kind of tests until now.

In this work, an irradiation test loop has been designed and implemented in the Náyade facility at CIEMAT, where some of the most relevant process conditions can be studied with the possibility to perform easily modifiable experiments. Moreover, this design allows the irradiation of two phases in contact, its configuration step by step improves the simulation of the doses expected for each phase, but also permits a straightforward modification of the experiment settings and has a low volume of solvent requirement compared to the other mentioned loops.

As part of a homogeneous actinides recycling strategy, Grouped Actinide Extraction (GANEX) concept was found which consists of two cycles: the first one for the bulk recovering of uranium (U) and the second one aiming for the separation of all transuranic elements (TRU: Pu, Np, Am, Cm) together [5]. The EURO-GANEX process is one of the most promising options for GANEX second cycle, which is based on the complementary selectivity of extractants used in its organic and aqueous phases [5]. It comprises two steps, the co-extraction of Actinides (An) and Lanthanides (Ln) and the TRU stripping [6]. In the An and Ln co-extraction, a solvent consisting in TODGA (*N,N,N',N'*-tetraoctyl diglycolamide) and DMDOHEMA (*N,N'*-dimethyl-*N,N'*-dioctylhexylethoxymalonamide) in Exxsol D80 (a kerosene diluent) is blended with the feed from the GANEX first cycle raffinate and CDTA (trans-1,2-cyclohexanediaminetetraacetic acid), which prevents the co-extraction of Pd(II) and Zr(IV) along with An and Ln [7]. TODGA is used to co-extract An and Ln and DMDOHEMA is employed to prevent the third phase formation increasing the Pu loading capacity of the organic phase [6]. After the co-extraction step, a scrubbing is needed to remove the elements co-extracted as Sr, Fe, Mo, Ru and Tc among others [6]. Then, TRU elements are selectively recovered into the aqueous phase in the TRU stripping step by using a combination of two water-soluble complexants in a lower nitric acid concentration: a sulphonated bis-triazinyl pyridine (2,6-bis(5,6-di-(sulfophenyl)-1,2,4-triazin-3-yl)-pyridine (SO_3-Ph-BTP) and acetohydroxamic acid (AHA) [6]. SO_3-Ph-BTP is used to strip Am(III) and Cm(III) selectively from Ln [6], while AHA is added to strip Pu and Np [6, 8].

The new irradiation loop has been adapted to assess the performance of the EURO-GANEX process [5, 6]. In order

to simulate the most relevant aspects of these processes, the design of the loop should involve the irradiation of two phases in contact and take into account its composition, the nitric acid concentration, the renewal of oxygen content and the dose expected for each phase. With this purpose, phases will be mixed under an open atmosphere outside the Náyade pool and irradiated together when they are passing thought the coil in the CIEMAT irradiation loop (Figure 1).

II. EXPERIMENTAL

A. Materials

The extractants used in the organic phase were TODGA and DMDOHEMA, and the diluent was odourless kerosene (OK). TODGA was synthesized at CIEMAT and the purity was determined by HPLC-MS as 98 %. DMDOHEMA with a purity of 99 % by HPLC-MS was purchased from Technocomm Ltd (United Kingdom). The reagents in the aqueous phase were the water-soluble BTP (SO_3-Ph-BTP) and CDTA, using nitric acid (HNO_3) as diluent. The reagents were used without further purification except HNO_3. The radioactive tracer solutions of ^{241}Am(III) and ^{152}Eu(III), and Highly Active Raffinate (HAR) solution were used to simulate the high-level waste stream after reprocessing typical spent fuels [9].

B. Irradiation test loop

Gamma irradiation experiments of the extraction systems involved in the different steps of the loop were performed at the Náyade facility (CIEMAT). Solvents to be irradiated were mixed outside of the pool, at 1:1 ratio and opened atmosphere, and pumped by peristaltic pumps through the tubing to a 316 stainless steel coil designed and manufactured at CIEMAT (10 mm outside and 8 mm inner diameters and 110 mm length) for the irradiation (Figure 1). The stainless steel coil was introduced in the hermetic irradiation device located at the bottom of the Náyade pool. ISO-Versinic (Viton) tubing employed has passed all resistance test done up to 1000 kGy in contact with nitric acid. The connections between the Viton (6 mm outside and 4 mm inner diameters) tubing and the stainless steel coil are composed of an outlet valve with a screw cap of stainless steel. To know the effective dose rate provided by ^{60}Co sources in static conditions, a Fricke dosimetry using a shielding of stainless steel with the same thickness that coil reactor was carried out. As the residence time of solvent within the irradiator coil is only a fraction of the total, the effective dose rate applied over the coil was determined by taking into account the coil volume, phases residence time and the effective dose through the steel, giving a result of 2.89 kGy/h.

C. Solvent extraction performance

The behaviour of EURO-GANEX process after the two different steps mentioned before was assessed with spiked samples (^{241}Am and ^{152}Eu) and the phases composition shown in Table 1. Samples of the organic phase taken at 200 and 500 kGy after the first irradiation (An+Ln co-extraction), were put in contact with a fresh aqueous phase consisting of 10 $\%_{vol}$ of a simulated HAR solution and

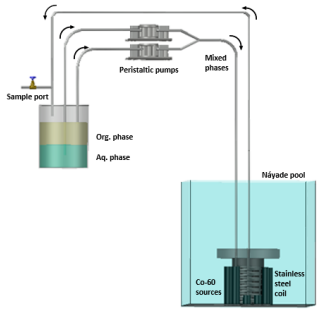

Figure 9. Schematic diagram of the irradiation test loop.

0.055 mol/L CDTA in 5 mol/L HNO_3 and spiked with 10 µL of ^{241}Am and ^{152}Eu (100 kBq/ml each). Between both irradiations steps, a scrubbing step with diluted nitric acid was introduced to simulate EURO-GANEX conditions for adjusting the acidity of the following step and removing Fission products (FP) and corrosion products (CP) co-extracted into the organic phase. Therefore, the loaded organic phase was put twice in contact with the same volume of fresh 0.5 mol/L HNO_3 for 5 minutes. After the second step of irradiation (TRU stripping step), the behaviour of the system was assessed by using samples taken from both irradiated phases (Table 1): TODGA and DMDOHEMA (up to 540 kGy) and 0.018 mol/L SO_3-Ph-BTP in 0.5 mol/L HNO_3 (from 10 to 40 kGy) and then spiked with 10 µL of ^{241}Am and ^{152}Eu (100 kBq/ml each). AHA is not included in the extraction experiments because neither Pu and Np were used in the current tests.

All extraction experiments were performed by mixing 500 µL of both, aqueous and organic phases, for 30 min at room temperature (22 ± 2 ºC). Then, the phases were separated by centrifugation (5 min at 5000 rpm) and aliquots of each one were taken for analysis. For ^{241}Am and ^{152}Eu analysis, gamma spectrometry was employed and the concentration of the elements presented in the HAR solution as well as those coming from the stainless steel CP (Fe, Cr, Ni and Mo) were determined by ICP-MS. All extraction results are reported as distribution ratio D ($D_M = [M^{3+}]_{org} / [M^{3+}]_{aq}$), and D_M between 0.01 and 100 exhibit a maximum error of ± 5 %.

D. Solvent composition analysis

The chemical composition of the irradiated organic and aqueous samples was determined by HPLC-MS and Raman spectroscopy, respectively. HPLC-MS measurements were performed by using an HPLC-MS Bruker EVOQTM (Triple Quadrupole detector) with a ACE 3 C18-PFP column (50mm × 2.1mm) at 40°C, using a gradient of mobile phase [(A: 0.1% HCOOH in H_2O), (B: 0.1% HCOOH in CH_3CN)]. $APCI^+$ ionization mode was used for TODGA and DMDOHEMA quantification, meanwhile ESI^+ mode was used for TODGA degradation compounds (DCs) quantification. The concentration of SO_3-Ph-BTP was measured by Quantitative Raman Spectroscopy (QRS). Raman spectra of samples were acquired by using a B&W Tek i-Raman™, model BWS415-785S. A red laser of HeNe with a wavelength of 785 nm and an operation power of 300

mW was employed. The spectral range available to this spectrometer is from 175 to 3200 cm^{-1}, with a spectral resolution about 5 cm^{-1}.

Table 4. Composition of the organic and aqueous phases in the different steps of the irradiation test loop and the following extraction experiments.

Experiments		Solvent formulation	
		Organic phase	Aqueous phase
An+Ln co-extraction Step	a) Irradiation	Fresh EURO-GANEX solvent 0.2 mol/L TODGA + 0.5 mol/L DMDOHEMA in OK	Fresh 5 mol/L HNO_3
	b) Extraction after the 1st irradiation	Irradiated EURO-GANEX solvent 200 and 500 kGy TODGA +DMDOHEMA in OK	Fresh 0.055 mol/L CDTA + 10 $\%_{vol}$ HAR in 5 mol/L HNO_3
Scrubbing Step	Intermediate step between irradiations	Irradiated EURO-GANEX solvent from the previous step (500 kGy) TODGA +DMDOHEMA in OK	Fresh in 0.5 mol/L HNO_3
TRU stripping Step	a) Irradiation	Irradiated EURO-GANEX solvent from the previous step (500 kGy) + scrubbing TODGA +DMDOHEMA in OK	Fresh 0.018 mol/L SO_3-Ph-BTP in 0.5 mol/L HNO_3
	b) Extraction after the 2nd irradiation	Irradiated EURO-GANEX solvent from the second step (540 kGy) TODGA +DMDOHEMA in OK	Irradiated Aq. phase (10, 20, 30 and 40 kGy) 0.018 mol/L SO_3-Ph-BTP in 0.5 mol/L HNO_3

III. RESULTS AND DISCUSSION

The An+Ln co-extraction system (0.2 mol/L TODGA + 0.5 mol/L DMDOHEMA in OK in contact with 5 mol/L HNO_3) was irradiated at 200 and 500 kGy, simulating an accumulative absorbed dose of the recycled organic phase. During the irradiation process, a colour change of the organic phase from slightly yellow to dark yellow was found, but not third phase formation, precipitate, or other physical changes. After that, the 5 mol/L HNO_3 aqueous phase was replaced by a fresh solution containing CDTA, HAR solution in 5 mol/L HNO_3 and spiked with ^{241}Am and ^{152}Eu. A normal phase separation behaviour was also obtained without any precipitates or third phase formation. The variation of $D_{Am(III)}$ and $D_{Eu(III)}$ as a function of absorbed dose is shown in Figure 2. As expected from the previous studies [6], both metals are well extracted into the organic phase even after a 500 kGy (D > 100), although a slight decrease in the D values is always observed for both elements. Therefore, under the irradiation loop condition applied, the system can still extract An and Ln even after 500 kGy of absorbed dose.

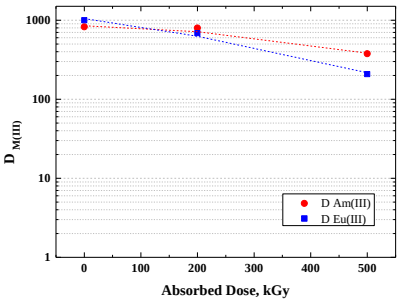

Figure 10. Distribution ratios of Am(III) and Eu(III) as a function of absorbed dose after the first step of the irradiation loop test (An+Ln co-extraction, see Figure 2).

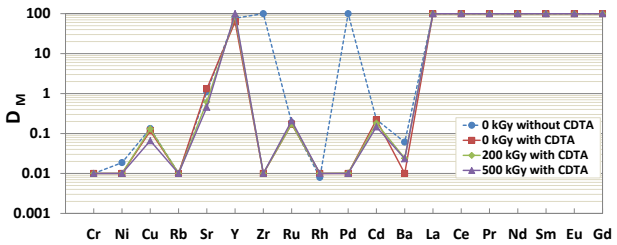

Figure 11. Ln and FP extraction by fresh and irradiated Euro-GANEX solvent (0.2 mol/L TODGA + 0.5 mol/L DMDOHEMA in OK) at 200 and 500 kGy from a fresh aqueous phase consisting of 5 mol/L HNO_3 with and without 0.055 mol/L CDTA.

FP and Ln elements concentrations were measured in both phases by ICP-MS, and the distribution ratios obtained for these elements are represented as a function of absorbed dose in Figure 3. As can be observed, the extraction behaviour for most of these elements kept unchanged when the irradiated and non-irradiated samples are compared, showing Y and Ln high D values in all cases (D > 100). The influence of the CDTA presence on the extraction of Zr and Pd is clearly observed in a significant decrease of the D_{Pd} and D_{Zr} reaching values of D < 0.01, in agreement with previous studies [6, 7].

As the reactor coil employed in the irradiation loop is made of 316 stainless steel, the possible corrosion products as a consequence of the contact with nitric acid and radiation, and the acidity have been studied for all process, concluding that Fe, Cr, Ni and Mo are the most relevant stainless steel corrosion products.

After simulating a long-term spent organic phase (after 500 kGy), and the corresponding scrubbing step, the organic phase was again irradiated in contact with a new aqueous phase, consisting in 0.018 mol/L SO_3-Ph-BTP in 0.5 mol/L HNO_3, to simulate the possible effects over the global performance during the TRU stripping (see Table 1). This system was irradiated up to 10, 20, 30 and 40 additional kGy. Over the course of the second irradiation step, the aqueous phase containing the SO_3-Ph-BTP darkened considerably, from the green of the unirradiated samples to opaque black of the irradiated samples, which has been widely related to its radiolytic degradation [10]. The $D_{Am(III)}$ and $D_{Eu(III)}$ values determined at the corresponding doses selected along the irradiation of the TRU stripping step are presented in Figure 4. An unexpected high $D_{Am(III)}$ values was observed from the beginning of the experiment, letting an ineffective separation between An and Ln. This phenomenon could be attributed to three possibilities: the metals corrosion presence, the variation of pH or the ligand degradation.

Additional extraction experiments with EURO-GANEX solvent to check the TRU stripping as function of the Fe, Cr and Ni concentrations have been carried out. As the concentration of Fe, Cr and Ni increases (Exp. 2-5, Table 2), the $D_{Am(III)}$ values also increase. These results point out that the presence of these metals in the aqueous phase effectively influences the extraction capacity of the system modifying the distribution ratios, and therefore, the system performance. However, an acidity rise (from 0.50 mol/L to 0.84 mol/L for all absorbed dose studied) has also been observed in this step, which can not be either ignored due to

it is well-known the relation between the pH and the extraction capacity of the solvents.

Table 5. Distribution ratios of An(III) and Ln(III) by fresh EURO-GANEX solvent from the fresh aqueous phase varying Fe(III), Cr(III) and Ni(II) concentrations.

Exp.	Samples composition					Distribution ratios	
	Org. phase	Aq. phase	Fe(III), mmol/L	Cr(III), mmol/L	Ni (III), mmol/L	$D_{Am(III)}$	$D_{Eu(III)}$
1	0.2 mol/L TODGA + 0.5 mol/L DMDOHEMA in OK	0.018 mol/L SO_3-Ph-BTP in 0.5 mol/L HNO_3	-	-	-	0.09	22.5
2			-	0.02	0.02	0.18	35.4
3			-	0.10	0.09	0.21	55.4
4			0.02	0.02	0.02	0.30	65.9
5			0.36	0.10	0.09	0.31	41.0

The degradation of the extractants and the subsequent DCs formation affect the extraction capacity due to the DCs formed could have different extraction properties which could interfere in the correct process performance. Therefore, the effect over the main extractants in the organic phase was analysed. As expected, the extractants concentrations diminish as a function of dose, reaching a decrease of 32 % for TODGA and 33 % for DMDOHEMA in agreement with the literature [10, 11, 12]. In parallel to the main extractants, also TODGA and DMDOHEMA DCs were identified. Eight of the main typical TODGA DCs [3, 11] and six of the DMDOHEMA DCs [12] could be identified. Moreover, three new signals have been identified as possible undescribed DCs, probably as a consequence of the irradiation in dynamic conditions, which is in concordance with our recent works [10]. Additionally, the radiolytic degradation of SO_3-Ph-BTP was analysed by QRS. In the conditions of this work, the SO_3-Ph-BTP concentration decrease as a function of absorbed dose, i.e., approx. 65 % is lost after 40 kGy, showing that this compound is very susceptible to degradation under the studied radiation conditions, which also agrees with the studies found in the literature [10].

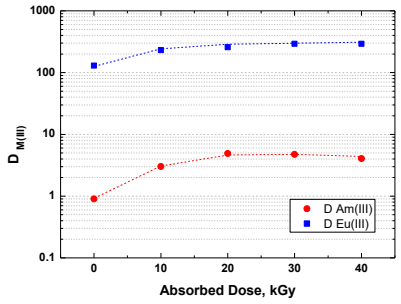

Figure 12. Distribution ratios of Am(III) and Eu(III) as a function of dose for the second irradiation step (TRU stripping, see Figure 2).

IV. CONCLUSIONS

In this work, an irradiation test loop that combines the advantages of simple statics irradiation experiments with those of sophisticated irradiation dynamic plants has been developed for the first time. The configuration let an easy modification of settings with a really low volume requirement. This new design allows simulating relevant process conditions such as the composition and contact between phases involved, the oxygen content and the dose expected for each of them. This new irradiation loop implemented at the Náyade irradiation facility at CIEMAT has been initially developed for assessing the performance of the two main steps of the EURO-GANEX process (An+Ln co-extraction and TRU stripping), under the most relevant and realistic experimental conditions in an easy and adaptable way. EURO-GANEX is a promising process to achieve the recovery of the transuranic elements in the same process, reducing the necessary steps and consecutive processes.

The An and Ln co-extraction step shows an excellent extraction performance for An and Ln. The monitoring of the different effects over the system (stainless steel corrosion, acidity, ligand concentration and presence of degradation compounds) in this step still revealed a situation under control. Fortunately, the scrubbing section introduced between the first and second irradiation steps of the loop was effective in reducing the proton concentration and removing some of the corrosion metals. However, an unexpected high $D_{Am(III)}$ values were observed from the beginning of the experiment during the TRU stripping, letting an ineffective separation between An and Ln. It could be said that the unexpected $D_{Am(III)}$ values are the result of a mixture of factors that can not be isolated. The metal corrosion presence has demonstrated the correlation between the metals concentrations and the $D_{Am(III)}$. The variation of the pH is an important factor that could modify the performance of the process. And the ligand degradation together the DCs formation, is crucial to understand the long-term process. All results obtained evidence the importance of developing realistic irradiation experiments where different factors affecting the performance should be studied.

V. Acknowledgment

This work has been developed under the framework of the European H2020 GENIORS Project, CIEMAT-ENRESA collaboration agreement (SOPSEP project) and Spanish SYTRAD II project.

VI. References

[1] E. Collins, G. DelCul, B. Spencer, R. Jubin, C. Maher and I.-T. Kim, "State-of-the-Art Report on the Progress of Nuclear Fuel Cycle Chemistry," Organisation for Economic Co-Operation and Development 2018.

[2] Spent Fuel Reprocessing Options. Vienna: INTERNATIONAL ATOMIC ENERGY AGENCY, IAEA 2009.

[3] H. Galán, A. Núñez, A. G. Espartero, R. Sedano, A. Durana, and J. de Mendoza, "Radiolytic stability of TODGA: characterization of degraded samples under different experimental conditions," Procedia Chemistry, vol. 7, pp. 195-201, 2012.

[4] A. Nunez, H. Galan, and J. Cobos, "TODGA degradation compounds: properties and effects on extraction systems-5400," in GLOBAL 2015 Proceedings, ed, 2015.

[5] J.-M. Adnet, M. Miguirditchian, C. Hill, X. Heres, M. Lecomte, and M. Masson, "Development of new hydrometallurgical processes for actinide recovery: GANEX concept," in Proceedings of GLOBAL, 2005.

[6] R. Malmbeck, D. Magnusson, S. Bourg, M. Carrott, A. Geist, and X. Hérès, "Homogenous recycling of transuranium elements from irradiated fast reactor fuel by the EURO-GANEX solvent extraction process," Radiochimica Acta, vol. 107, pp. 917-929, 2019.

[7] M. Sypula, A. Wilden, C. Schreinemachers, R. Malmbeck, A. Geist, and R. Taylor, "Use of polyaminocarboxylic acids as hydrophilic masking agents for fission products in actinide partitioning processes," Solvent Extraction and Ion Exchange, vol. 30, pp. 748-764, 2012.

[8] R. Taylor, I. May, A. Wallwork, I. Denniss, N. Hill, and B. Y. Galkin, "The applications of formo-and aceto-hydroxamic acids in nuclear fuel reprocessing," Journal of Alloys and Compounds, vol. 271, pp. 534-537, 1998.

[9] Modolo, G., Asp, H., Schreinemachers, C., and Vijgen, H. “Development of a TODGA based process for partitioning of actinides from a PUREX raffinate Part I: Batch extraction optimization studies and stability tests.” Solvent Extraction and Ion Exchange, vol. 25, no 6, p. 703-721, 2007.

[10] I. Sánchez-García, H. Galán, J. M. Perlado, and J. Cobos, "Development of experimental irradiation strategies to evaluate the robustness of TODGA and water-soluble BTP extraction systems for advanced nuclear fuel recycling," Radiation Physics and Chemistry, vol. 177, p. 109094., 2020.

[11] Y. Sugo, Y. Sasaki, and S. Tachimori, "Studies on hydrolysis and radiolysis of N, N, N′, N′-tetraoctyl-3-oxapentane-1, 5-diamide," Radiochimica Acta, vol. 90, pp. 161-165, 2002.

[12] L. Berthon, J. Morel, N. Zorz, C. Nicol, H. Virelizier, and C. Madic, "DIAMEX process for minor actinide partitioning: hydrolytic and radiolytic degradations of malonamide extractants," Separation Science and Technology, vol. 36, pp. 709-728, 2001.

Proceedings of the European Nuclear Young Generation Forum
ENYGF'21
September 27-30, 2021, Tarragona, Spain

Dissolution studies at repository conditions of advanced doped UO_2 fuel

Rodríguez-Villagra, Nieves [1*], Milena-Pérez, Abel[1], Fernández-Carretero, Sergio[1], J. Bonales, Laura[1,2], Durán, Sofía[1], Anta, Laureano[1], Gutiérrez, Luis[1], and Cobos, Joaquín[1,3]

[1] Centro de Investigaciones Energética, Medioambientales y Tecnológicas (CIEMAT), Spain; [2] Centro de Astrobiología (CSIC-INTA), Spain; [3] Estación Biológica de Doñana (EBD-CSIC), Spain

*Corresponding author: *nieves.rodriguez@ciemat.es*

I. INTRODUCTION

Extensive work has been devoted to conventional UO_2 fuel stability under representative conditions of a Deep Geological Repository (DGR). Additions of other elements in UO_2 fuel, such as chromium or aluminium, are expected to improve its performance during operation, by improving the mechanical properties of fuel matrices.

A number of comprehensive experiments have been previously carried out to study the oxidative dissolution of the UO_2 nuclear fuel in a long-term safety assessment. However, new developments like UO_2-based model materials must be considered, presently an option for current LWR, as it would feed Spent Nuclear Fuel inventories in a DGR. The addition of certain amount of selected dopants, such as Cr_2O_3 or Cr_2O_3/Al_2O_3 to UO_2 fuel varies the microstructure through the formation of larger grains during sintering of the UO_2 pellets, so that, a higher amount of fission gases can be retained during fission. This reduces the pellet-cladding interaction of the fuel rods, allowing achieving higher power rates and higher burnups than conventional UO_2 fuel. Focused on the spent fuel alteration process, there are a few basic parameters that control the kinetics of the UO_2 dissolution, some of them are associated to spent fuel characteristics (*e.g.* final composition, burnup and microstructure, temperature, radiation fields, initial oxidation state of the matrix, etc.) and other are environmentally dependant, such us hydrogen partial pressure or groundwater chemical composition. Previous studies suggest that trivalent rare-earth dopants (RE^{III}) play an important role on UO_2 oxidation [1], preventing the complete oxidation to U_3O_8 [2, 3], so in order to better understand the effect of RE^{III} dopants, a set of dissolution experiments has been performed. The dissolved bicarbonate is a common groundwater constituent and one of the main complexing agents. The HCO_3^- anion enhances the dissolution of UO_2^{2+}, facilitated by the formation of soluble complexes, and thus avoids secondary phase precipitation [4]. Simultaneously, the groundwater-radiation interaction is of interest in DGR conditions because it affects the redox system through several chemical species formation by water radiolysis, including H_2O_2 and H_2 [5].

This research about fuel stability under relevant repository conditions is targeted on new promising candidates: Chromia-doped UO_2 and Chromia/Alumina-doped UO_2. Both types of fuels are already licensed in some light water reactors in order to maximize the energy production and their use is foreseen to be grown. However, the lack of data with respect to the impact of oxide fuels containing additives on the long-term behaviour becomes an important issue to obtain dissolution data on these fuels and to correlate to that of conventional UO_2 fuels under geological storage conditions.

Therefore, this work aims to expand the database on fuel dissolution and the effects of dopants under expected chemical conditions inside a failed waste container in a deep geological repository environment. Here, it is presented the impact of Cr and Cr/Al combined with effect of leachant composition on UO_2 matrix stability, in order to acquire further knowledge regarding disposal conditions, within the frame of EC DISCO Project. Dissolution experiments of freshly prepared 0.06wt%Cr_2O_3-UO_2 and 0.05wt%Cr_2O_3-0.02wt%Al_2O_3-UO_2 disks were conducted in synthetic groundwater solutions without and with HCO_3^-. The results will be the basis for studying more complex systems as irradiated doped fuels.

II. SAMPLE PREPARATION

The methodology applied for disks fabrication was classical powder pressing and sintering. UO_2 (provided by ENUSA, the Spanish producer of nuclear fuel) was thermally annealed in a 4.7% H_2–N_2 atmosphere at 1100°C to attain stoichiometric $UO_{2.00}$. UO_2 was mixed with weighted amounts of Cr_2O_3 (Alfa Aesar), or Cr_2O_3/Al_2O_3 (Alfa Aesar) together with 1wt% of EBS (Ethyl Bis Stearamide, $C_{38}H_{76}N_2O_2$, supplied by Tokyo Chemical Industry) as binder and lubricant, using low-energy ball milling. This fabrication process has been previously described in [6]. As a result, a series of UO_2-0.06wt%Cr_2O_3 and UO_2-0.05wt%Cr_2O_3-0.02wt%Al_2O_3 solid solutions were obtained. Prior to the sintering of the samples, raw powders have been characterized in terms of the lattice parameter

(XRD; Philips PANalytical X'Pert MPD diffractometer using Cu Kα radiation and a Bragg– Brentano configuration), Specific Surface Area (SSA) by BET with N_2 adsorption (ASAP 2020 Micromeritics) and the mean particle size by Laser Diffraction (Malvern, Series 2600). The results of this characterization can be seen in Table 1. Once the powders were mixed in the desired proportions, the monoliths obtained by pressing and sintering were characterized. This characterization is shown in Table 2.

Table 1. Raw material characterization.

Sample	Lattice parameter / nm	SSA (BET) / $m^2 \cdot g^{-1}$	D(v,0.5) / µm	TD / $g \cdot cm^{-3}$
UO_2	a=b=c=0.546920(4)	0.95±0.02	19.6±0.69	10.97
Al_2O_3	a=0.7944(6); b=0.7980(4); c=1.1722(6)	37.6±0.4	23.5±0.87	3.95
Cr_2O_3	a=b=0.49586(7); c=1.3592(2)	3.47±0.02	2.09±0.34	5.22

Table 2. Summary of the results obtained from the analysis of the doped UO_2 pellets.

Sample / %wt	Lattice parameter / nm	SSA (BET) / $m^2 \cdot g^{-1}$	SSA (GEOM) / $m^2 \cdot g^{-1}$	Density / $g \cdot cm^{-3}$
UO_2-0.06 Cr_2O_3	a= 0.547113(7)	0.63±0.02	0.0002±0.0001	9.83±0.07
UO_2-0.05Cr_2O_3 - 0.02Al_2O_3	a= 0.547198(5)	0.25±0.01	0.0002±0.0001	9.80±0.43

III. AUTOCLAVE DISSOLUTION EXPERIMENTS SET-UP

In order to understand the matrix dissolution of modern LWR fuels and in particular the effect of Cr and Cr/Al on the dissolution rate of the spent fuel, sintered pellets have been exposed to three reference waters for more than one year: inert system (0.02M $NaClO_4$) at pH 7.2 (PC), bicarbonate water (0.019M $NaHCO_3$+0.001M NaCl) at pH 8.9 (BC) and young cementitious water at pH 13.5 (YCW) relevant for geological disposal. Further details about the simulated water compositions can be found in [7]. The PC system is used as a blank test (without carbonate), to investigate low ionic strength with a non-complexing agent in order to be compared with BC and YCW systems.

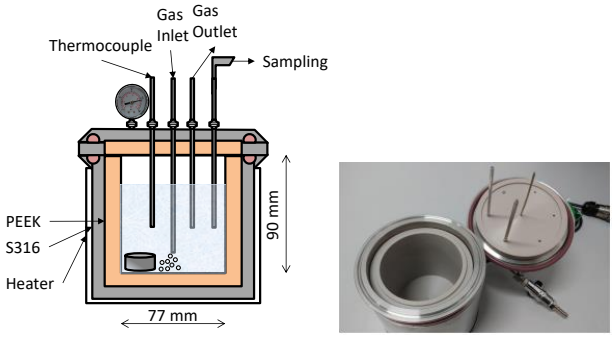

Figure 1. Images of PEEK-lined stainless steel autoclaves at CIEMAT radioactive facilities.

Static dissolution experiments were performed in autoclaves under 7-8 bar 4.7% H_2/N_2 (PC system without Pt wire and BC and YCW systems with a Pt wire, in which the sample disk was suspended) inside an Ar glove box at room temperature (Figure 1). Aliquots of aqueous phase were collected through a sampling valve without opening the reactor. Then, autoclaves were refilled with 4.7%H_2/N_2 up to 8 bar. Filtered (GHP Acrodisc, PALL, 0.2 µm) samples were measured by ICP-MS (Thermo Fischer Sci ICAP-Qc model with collision cell (QCell) and KED mode (He-Kinetic Energy Discrimination)) to quantify dissolved U concentrations.

IV. URANIUMN RELEASE FROM DOPED-UO_2 PELLETS AT DIFFERENT pH

Figure 2 illustrates uranium concentration versus time for dissolution of a) UO_2-0.06wt%Cr_2O_3, and b) UO_2-0.05wt%Cr_2O_3-0.02wt%Al_2O_3, respectively. Based on the first series of tests, H_2 atmosphere (pH_2 = 0.37±1bar) was not capable to keep the system under reducing conditions, as it is suggested from concentration results. The U concentration in the solutions reach plateau levels in PC and YCW for both materials, whereas this effect is hardly observed in BC.

At pH = 7.2 (PC) the filtered U concentration remains close to 10^{-9} M for the two doped UO_2 samples over the whole test duration (~140 d), close to the solubility limit of 10^{-8}-10^{-9}M [8] in absence of complexing agents.

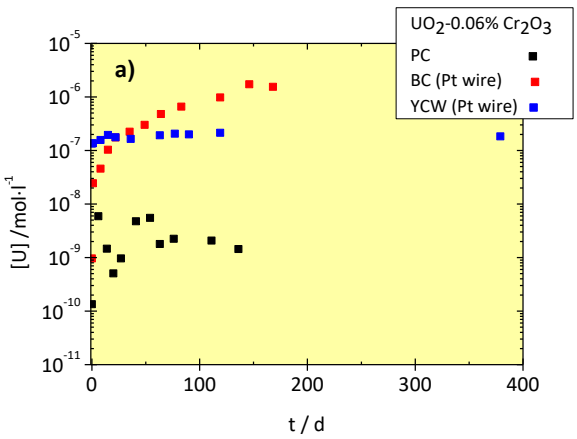

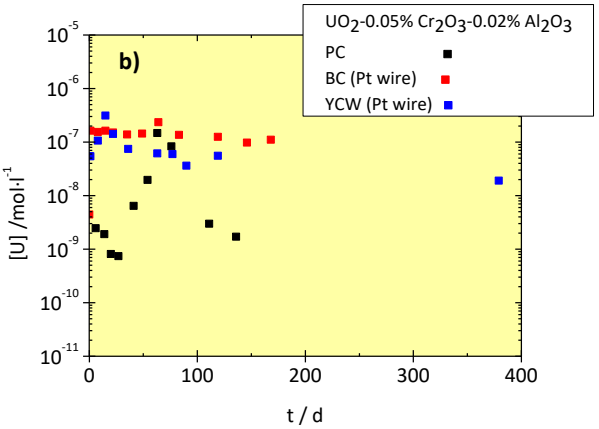

Figure 2. Concentration of U as a function of leaching time of a) UO_2-0.06wt%Cr_2O_3 and b) UO_2-0.05wt%Cr_2O_3-0.02wt%Al_2O_3 of dissolution experiments.

At pH = 8.9 (BC), higher final U concentrations are quantified when compared to those at 7.2 (~10^{-6}M for Cr-doped UO_2 and ~10^{-7}M for Cr/Al-doped UO_2). The trend of U concentration in solution shows that there is a slight increase in dissolution with time for the Cr-doped UO_2 in BC with no plateau when compared with PC or YCW media. The presence of H_2 was expected to provide reducing conditions and to decrease the obtained uranium concentrations (unless two orders of magnitude than in oxidizing). High concentration values are close to that found under oxidizing environment, so it could be caused by slight oxidation/dissolution of U^{IV} to U^{VI} on the pellet surface presumably caused by some remaining traces of oxygen (in the glove-box or dissolved in the solution), and promoted by the presence of complexing agent (HCO_3^-). Under this assumption, the aqueous species of uranium in hexavalent state would occur as carbonate complexes more dominantly than hydroxy-complexes. Nevertheless, as it was suggested by Bosbach et al. in [9], more analysis for longer time periods are required.

At pH = 13.5 (YCW), U concentrations are similar to those in the tests in BC, despite the highest CO_3^{2-} concentration expected in YCW. At that conditions of pH higher than 8, the $UO_2(CO_3)_3^{4-}$ complex ion predominates in the solution, and at pH >12 aqueous U^{VI} occurs in the solution exclusively in the form of polynuclear hydroxo- complexes with the general form $(UO_2)_m(OH)_n^{2m-n}$. Ollila [10] pointed out that strongly alkaline pH like the cement pore water conditions, and with medium/low carbonate content, the solubility remains lower than in groundwater with a high carbonate content. Results suggest that the measured Eh (YCW) in these experiments, in the range of -9 to -40 mV, could be enough to increase the U concentrations over expected values (~10^{-9}M) [11] while in BC the Eh has been found to be higher (70 – 138 mV). The normalised dissolution rates of U (R_L(U) in g·(m^2d)$^{-1}$) as a function of time were calculated from the concentrations of dissolved U, the geometric specific surface area (SSA), the U mass fraction in the solid sample (f_U) and the time (t).

$$R_L(U)\left(g\cdot(m^2\cdot d)^{-1}\right) = \frac{[U](mol\cdot l^{-1})}{f_U\cdot\left(\frac{SSA_{geom}(m^2)}{V_t(l)}\right)\cdot t(d)}$$

Generally, the normalized dissolution rate profile decreased vs time, as shown in Figure 3.

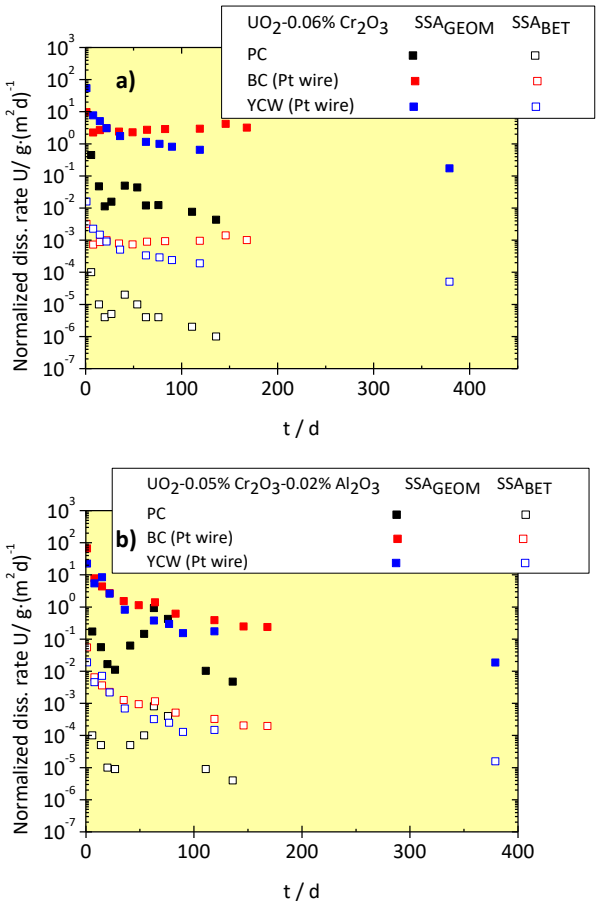

Figure 3. Calculated R_L(U) for the first test series of a) UO_2-0.06wt%Cr_2O_3, and b) UO_2-0.05wt%Cr_2O_3-0.02wt%Al_2O_3. Filled symbols represent filtered (or not-filtered) and empty symbols are ultrafiltered.

In PC solution (pH=7.2), the initial/final dissolution rates were found to be 0.4 to 4·10^{-3} g·(m^2d)$^{-1}$ for Cr-doped UO_2 pellet, and 0.2 to 5·10^{-3} g·(m^2d)$^{-1}$ for the Cr/Al-doped UO_2. Taking into account the low geometric surface area, the final U dissolution rates for the studied pellets are quite similar; showing that dopants (Cr and Cr/Al) have no significant effect on the dissolution rates of these UO_2-based materials in a neutral pH medium.

In BC solution (pH=8.9), normalised dissolution rates were noticeably higher, as a consequence of the bicarbonate. In this media the dissolution rates were found to be 9.7 to 3.2 g·(m^2d)$^{-1}$ for Cr-doped UO_2 pellet, and 66.2 to 0.2 g·(m^2d)$^{-1}$ for the Cr/Al-doped UO_2. The obtained data are far from those obtained in [12] for unirradiated UO_2 in flow through reactors using [HCO_3^-] 10^{-3}M. The mentioned authors reported a dissolution rate of U of 2·10^{-3} g·(m^2d)$^{-1}$. According to Ollila, at 10^{-3} M of free HCO_3^-, the major complex formation with carbonate would be the $UO_2(CO_3)_3^{4-}$ [11]. Nguyen et al. [13] report rates results from flow-through dissolution tests of UO_2 pellets (calculated using geometric surface area and roughness factor of 3) in solutions of 20 mM HCO_3^- (pH=11) with fixed partial pressure of oxygen (0.02 atm) of around 4·10^{-3} g·(m^2d)$^{-1}$.

In YCW solution (pH=13.5), normalised dissolution rates were close to those calculated in BC, even though the bicarbonate concentration was higher than other values used in literature. In this media the initial/final dissolution rates were found to be $5 \cdot 10^{1}$ to $2 \cdot 10^{-1}$ $g \cdot (m^2 d)^{-1}$ for Cr-doped UO_2 pellet, and $2 \cdot 10^{1}$ to $2 \cdot 10^{-2}$ $g \cdot (m^2 d)^{-1}$ for the Cr/Al-doped UO_2.

In general, the results obtained from these static dissolution tests for the three media considered are far from those expected in reducing systems. Actually, they are not in accordance with literature data, when dissolution rates were calculated using geometric SSA with no roughness factor, which consider grain boundary accessibility, thus the geometric choice underestimates real surface area. Taking into account the aforementioned discussion, dissolution rates are overestimated in 3 orders of magnitude. It is well known that the SSA of the matrix will play a critical role on the final reaction rates [14]. By calculating R_L from BET values (Figure 3), values are, theoretically, underestimated (empty symbols). Using BET surface area method, the calculated rates in PC are in the same range than Casas et al. [15] from 100-1100 um (BET = 0.0113-0.0016 $m^2 \cdot g^{-1}$) on unirradiated fuel pellets and crushed material from pellets using 0.01 $mol \cdot L^{-1}$ PC at pH = 8 with an atmosphere of 5% O_2 in N_2, around 10^{-4} – 10^{-7} $g \cdot (m^2 d)^{-1}$. In BC and YCW, values are also in consonance with those obtained by Bruno et al. [16] from 100-300 μm SIMFUEL powder (BET=0.0113 $m^2 \cdot g^{-1}$) in 10mM HCO_3^- and presumably oxic conditions, around 10^{-3}–10^{-4} $g \cdot (m^2 d)^{-1}$. They are also comparable with static experiments, under similar test conditions, conducted by same authors with UO_2 pellets (BET = 0.00019 $m^2 \cdot g^{-1}$) in 10mM HCO_3^- of $(2.41\text{-}1.27) \cdot 10^{-3}$ $g \cdot (m^2 d)^{-1}$. This indicates that dissolution rates are largely dependent on assuming geometric surface area for the pellet, or based on BET surface area, varying on several orders of magnitude. These exposed uncertainties in surface area selections are decisive for the conversion between leach data for unirradiated UO_2 to spent fuel [14]. Anyhow, from values revised in literature, it is reasonable to think that dissolutions rates in this work are closer to oxic conditions, $(10^{-5} – 10^{-2})$ $g \cdot (m^2 d)^{-1}$, than under reducing conditions, 10^{-7} $g \cdot (m^2 d)^{-1}$ [14]. SEM, XRD and Raman measurements on pellets after the dissolution experiments are in progress and will complement the picture of data obtained. More studies of the dissolution as a function of dopant concentration are essential to predict this effect at the long-term.

V. CONCLUSIONS

The effects of additives (Cr and Cr/Al) on dissolution behaviour of UO_2 has been investigated through experiments using fresh nuclear fuel and synthetic groundwaters. A comparison between Cr-doped UO_2 and Al-Cr-doped UO_2 dissolution behaviour showed almost negligible differences in U released over the whole test duration (more than 140 d) for each media considered. The data shown indicates that leachants composition and pH have a higher influence on the uranium dissolution than dopants (Cr or Cr/Al) embedded in UO_2 matrix. The normalized dissolution rates of these fuel matrixes depend, as expected, on the SSA. Uncertainties in surface area are very large, and consequently up to 3 orders of magnitude for surface area normalized dissolution rates were found depending on the approach considered (geometric without correction for surface roughness or BET method).

The lowest dissolution rates found for unirradiated Cr- and Cr/Al-doped UO_2 were those for dissolution in PC, even considering the presence of oxygen in the system. These rates (calculated using BET values) are in close agreement within the literature range of 10^{-4}–10^{-7} $g \cdot (m^2 d)^{-1}$ for UO_2. In contrast to this, changing the leachant from a synthetic groundwater with about $2 \cdot 10^{-3}$M bicarbonate concentration to a YCW with 0.45M of $NaHCO_3$ produce a rather unforeseen similarity in dissolution rate results. Apparently, the total doping effect on the leaching behaviour seems to be minimal, since there are not great differences in U released between the two doped fresh fuels, except in bicarbonate water. In bicarbonate system, complexing agents could enhance the dissolution of U^{VI} formed in the surface.

VI. ACKNOWLEDGEMENTS

Authors want to thank the funding for this research from the European Commission Horizon 2020 Research and Training Programme DisCo (grant agreement 755443).

VII. REFERENCES

[1] E. Curti, "Development and application of a solid solution model for Cr doped UO_2 fuel," in 2nd Annual Workshop Proceedings, H2020-project DisCo. D1.15, 131-141, 2019.

[2] J.-G. Kim, Y.-K. Ha, S.-D. Park, K.-Y. Jee, and W.-H. Kim, "Effect of a trivalent dopant, Gd^{3+}, on the oxidation of uranium dioxide," J. Nucl. Mater., vol. 297, pp. 327-331, 2001.

[3] A. Travis, "Oxidation and anion lattice defect signatures of hypostoichiometric lanthanide-doped UO_2," J. Nucl. Mater., vol. 530, p. 151959, 2020.

[4] M. M. Hossain, E. Ekeroth, and M. Jonsson, "Effects of on the kinetics of UO_2 oxidation by H_2O_2," J. Nucl. Mater., vol. 358, pp. 202-208, 2006.

[5] M. E. Dzaugis, A. J. Spivack, and S. D'Hondt, "A quantitative model of water radiolysis and chemical production rates near radionuclide-containing solids," Radiat. Phys. Chem., vol. 115, pp. 127-134, 2015.

[6] A. Milena-Pérez, L. J. Bonales, N. Rodríguez-Villagra, S. Fernández, V. G. Baonza, and J. Cobos, "Raman spectroscopy coupled to principal component analysis for studying UO_2 nuclear fuels with different grain sizes due to the chromia addition," J. Nucl. Mater., vol. 543, p. 152581, 2021.

[7] N. Rodríguez-Villagra, S. Fernández, L. J. Bonales, L. Gutiérrez, J. M. Elorrieta, and J. Cobos, "Annual report of the Modern Spent Fuel Dissolution and Chemistry in Failed Container Conditions project (DISCO) “Manufacture and characterization of CIEMAT fuel samples used for leaching tests in DISCO project”," CIEMAT, Madrid, Spain, 2018.

[8] T. Yajima, Kawamura, Y., Ueta, S., "Uranium(IV) solubility and hydrolysis constants under reduced conditions," Mat. Res. Soc. Symp. Proc, vol. 353, p. 1137, 1995.

[9] D. Bosbach, C. Christelle, E. Myllykylä, C. Jegout, J. Cobos, I. Farnan, *et al.*, "Model materials experiments: First dissolution results. H2020-project DisCo," Deliverable 4.1, 2019.

[10] K. Ollila, "Solubility of UO_2 in the high pH range in 0.01 to 0.1 M NaCl solution under reducing conditions," POSIVA report, 2008.

[11] K. Ollila and L. Ahonen, "Solubilities of uranium for HLA-99," POSIVA report 98-13, 1998.

[12] J. Giménez, F. Clarens, I. Casas, M. Rovira, J. de Pablo, and J. Bruno, "Oxidation and dissolution of UO_2 in bicarbonate media: Implications for the spent nuclear fuel oxidative dissolution mechanism," J. Nucl. Mater., vol. 345, pp. 232-238, 2005.

[13] S. N. Nguyen, H. C. Weed, H. R. Leider, and R. B. Stout, "Dissolution kinetics of UO_2. I. Flow-through tests on $UO_{2.00}$ pellets and polycrystalline schoepite samples in oxygenated, carbonate/bicarbonate buffer solutions at 25°C," MRS Proceedings, vol. 257, p. 339, 2011.

[14] B. Grambow, J. Bruno, L. Duro, J. Merino, A. Tamayo, C. Martin, *et al.*, "Project MICADO Model for Uncertainty for the mechanism of dissolution of spent fuel in nuclear waste repository," Final Activity Report, 2010.

[15] I. Casas, J. Gimenez, V. Marti, M. E. Torrero, and J. De Pabloc, "Kinetically controlled dissolution of UO_2(s) under oxidizing conditions. A combined dissolution-oxidation model," MRS Proceedings, vol. 294, p. 61, 1992.

[16] J. Bruno, I. Casas, E. Cera, J. de Pablo, J. Giménez, and M. E. Torrero, "Uranium (IV) dioxide and Simfuel as chemical analogues of nuclear spent fuel matrix dissolution. A comparison of dissolution results in a standard $NaCl/NaHCO_3$ solution," MRS Proceedings, vol. 353, p. 601, 1994.

Proceedings of the European Nuclear Young Generation Forum
ENYGF'21
September 27-30, 2021, Tarragona, Spain

Creation of system of final isolation (disposal) of radioactive waste in the Russian Federation

Vsevolod Igin[1]*

[1] The Federal State Unitary Enterprise «National Operator For Radioactive Waste Management» (NORWM), Russian Federation

*Corresponding author: *vsevolodig@gmail.com*

I. INTRODUCTION

First issues on radioactive waste disposal have been raised in Soviet Union at the beginning of 1960s. Since then, step-by-step studies aiming reasonable choice of site for the deep geological repository have been carried out for more than 60 years in full accordance with international recommendations.

The modern history of radioactive waste disposal in the Russian Federation starts with the adoption of the Federal Law No. 139-FL on November 4, 2005 "On ratification of the Joint Convention on the Safety of Spent Fuel Management and on the Safety of Radioactive Waste Management" (the Convention) [1]. After the adoption of the named law [2] the provisions of the Convention became mandatory for all executive authorities and organizations, including those directly related to radioactive waste management. The Convention serves as the basis for further improvement of the Russian regulatory system of radioactive waste management and disposal in accordance with international obligations of the Russian Federation.

Together with the Convention, two federal laws: FL-170 "On the Use of Atomic Energy" [3] and FL-190 "On the management of radioactive waste and the introduction of amendments to certain legislative acts of the Russian Federation" [4] create three pillars of the Russian regulatory system on the management and final disposal of radioactive waste.

II. LEGAL AND REGULATORY FRAMEWORK OF RADWASTE DISPOSAL IN RUSSIA

FL-190 not only regulates Radwaste management, but also identifies the National Operator for radioactive waste management as the only organization responsible for the disposal of all classes of Radwaste in the Russian Federation.

FL-190 has also identified the key element of the state policy in the field of radioactive waste management: shift from the previous practice of accumulation and controlled storage of radioactive waste to the practice of disposal of all classes of Radwaste.

In 2012 the Federal State Unitary Enterprise "The National Operator for Radioactive Waste Management" (FSUE "NO RWM") has been created with the main goal of creating the system of disposal facilities intended for the final disposal of all classes of radioactive waste in the Russian Federation.

The National Operator has following main obligations (as per Federal Law-190):

- Receive Radwaste, which meets waste acceptance criteria from the its producers;
- Serve as customer for the design and construction of Radwaste disposal facilities;
- Act as an operator and responsible organization for safe final disposal of Radwaste.

According to FL-190, the Radwaste management cycle consists of the formation of Radwaste carried out by the Manufacturer of Radwaste, Radwaste collection, sorting, processing, conditioning and storage carried out by a specialized organization and, finally, disposal of Radwaste carried out by the National Operator (Figure 1).

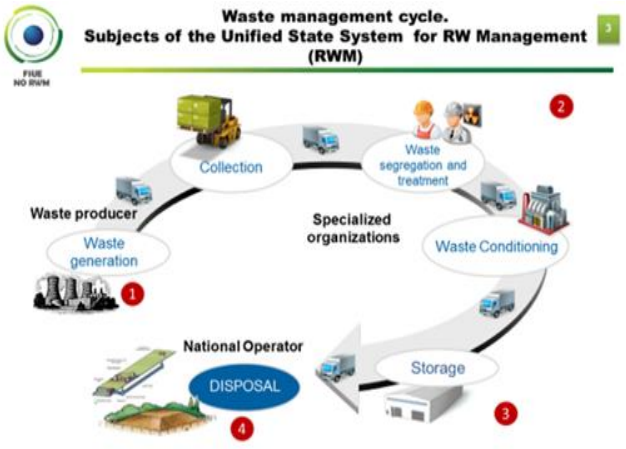

Figure 1. Waste management cycle [4].

FSUE “NO RWM” is under direct supervision of the State Atomic Energy Corporation “Rosatom” and the Government of the Russian Federation. It’s needless to say, that the National Operator is also under regulatory control of several organizations, full list of which is presented below:

- Federal Service for Supervision of Natural Resources (ROSPRIRODNADZOR);
- Federal Service for Environmental, Technological and Nuclear Supervision (ROSTEKHNADZOR);
- Federal Medical and Biological Agency (FMBA);
- Federal Agency for Subsoil Use (ROSNEDRA);
- Ministry of Natural Resources of the Russian Federation.

III. THE RUSSIAN NATIONAL OPERATOR

The main mission of FSUE "NO RWM" is the creation of **the Unified State System for the radioactive waste management (USS RWM)**. FSUE "NO RWM" should also provide safe and economically efficient management and final disposal of Radwaste as part of USS RWM.

By the Decree of the Government of the Russian Federation dated 19.11.2012 No. 1185 [5] “On the determination of the procedure and terms for the creation of the Unified State System for the radioactive waste management three stages of the system’s creation have been identified:

- Development of legal and regulatory framework;
- Development of disposal system for low and intermediate Radwaste;
- Development of disposal system for High-Level Radwaste.

Implementation of the first stage (2011 - 2014) of the USS RWM included three main steps:

- creation of the National Operator for Radioactive Waste Management (FSUE “NO RWM”);
- formation of a reserve fund for the final disposal of Radwaste;
- signing Declarations of Intent for siting and construction of Radwaste disposal facilities by FSUE “NO RWM” and governments of several regions of Russia.

Within the implementation of the second stage (2015 - 2018) of the USS RWM the licenses for construction and operation of waste disposal facility for low and intermediate level radioactive waste (classes 3&4) in Sverdlovsk Region have been obtained in 2015 from the Regulatory Authority (ROSTECHNADZOR). In 2016 the first near surface disposal facility has been commissioned.

Following activities have been also performed during the second stage:

- Start of the construction of the second stage of facility in Sverdlovsk Region in 2017;
- Investigation and site-selection for other low and intermediate level radioactive waste;
- As a part of the implementation of the second stage of USS RWM the construction of the Underground Research Laboratory (URL) in Nizhne-Kanskiy rock massif (Krasnoyarsk region of Russia) has started in 2018.

The main goal of the URL is to explore the host rock mass characteristics and confirm (under natural conditions) the rock mass suitability for safe deep geological disposal of long-lived conditioned radioactive waste.

Under stage three (2019-2024) of the USS following milestones are planned:

- Obtaining permit for operation in 2021 of the second stage of near surface disposal facility (Sverdlovsk region) after it was commissioned is 2020;
- Beginning of tunneling excavations in 2022 for the Underground Research Laboratory in Nizhnekanskiy rock massif;
- end of construction, licensing and commissioning of disposal facilities in Chelyabinsk and Tomsk regions in 2024.

The third stage of USS RWM has also included adoption of the following documents: The “Strategy for the development of Geological Disposal Facility” and the “Strategic Master Plan for Researches”.

IV. NEW RADWASTE CLASSIFICATION

FL-190 has introduced the concept of “disposable” Radwaste and “special” Radwaste.

The new radioactive waste classification introduced by the law considered waste characteristics, but is mainly based on waste disposal feasibility.

Federal Law of 11.07.2011 N 190- "On the management of radioactive waste and on amendments to certain legislative acts of the Russian Federation" (as amended and further effective as of July 16, 2013) has given following definition to the special Radwaste:

“Special radioactive waste includes radioactive waste generated as a result of: as a result of the state armament program and state defense order;

- as a result of using nuclear charges for peaceful purposes or as a result of a nuclear and (or) radiation accident at an atomic energy facility;
- liquid Radwaste placed in surface water bodies - radioactive waste storage facilities with a total volume of over 25 000 cubic meters, commissioned before the Federal Law № 190 of July 11, 2011 came into force.

As for disposable Radwaste, its classification has been later extended by the Decree of the Government of the Russian Federation of 10.19.2012 № 1069 (as amended on 02/04/2015) "On the criteria for classifying solid, liquid and gaseous waste as radioactive waste, the criteria for classifying radioactive waste as special radioactive waste and for disposable radioactive waste and the classification criteria for disposable radioactive waste" [6].

Under the named Decree disposable radioactive waste is divided into 6 classes (Figure 2):

- 1 and 2 classes. Solid HLW and long-lived ILW. Disposal in deep disposal facility;
- 3 and 4 classes. Solid ILW and long-lived LLW. Disposal in near-surface disposal facility;
- 5 class liquid RW (LLW and ILW). Disposal in existing deep well injection disposal facility;
- 6 class Radwaste, resulting from the extraction and processing of uranium ores and mineral and organic materials with a high content of natural radionuclides. Disposal in near-surface disposal facility.

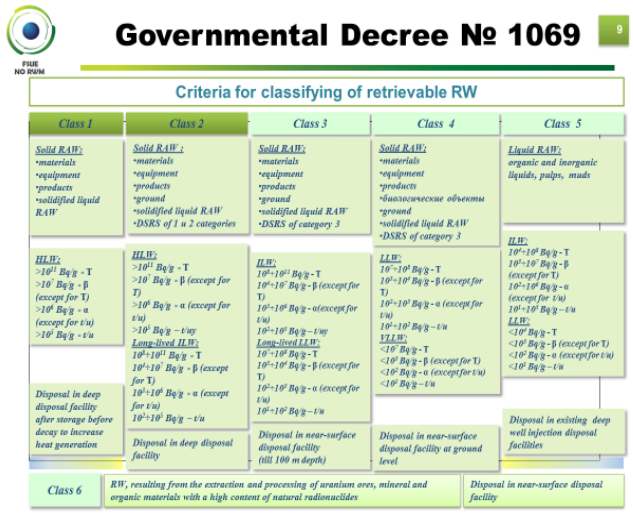

Figure 2. Radwaste classification [6].

Currently, FSUE "NO RWM" is planning to construct and operate several near-surface disposal facilities for low and intermediate level waste (LLW and ILW), with total capacity up to 550 000 cubic meters (including existing one in Sverdlovsk Region).

V. PLANS FOR HIGH LEVEL RADWASTE DISPOSAL [7]

As it was mentioned at the beginning of the article, exploration works for site selection for the underground research laboratory and justification of the suitability of the site for disposal of long-lived Radwaste (high-level Radwaste) has been carried out in Russia for more than 60 years. In 70s and 80s, vast explorations were held at Novaya Zemlya, the Kola Peninsula, Kalmykia and Chelyabinsk region. After assessment of enlarged data, it was considered that there were no sites in the European part of Russia suitable for disposal of long-lived radioactive waste.

At the beginning of the 90s, the decision was made to create storage facility for Spent Nuclear Fuel for reprocessing plant at the site of Mining and Chemical Combine (MCC). This decision has shifted exploration focus for deep geological repository to Krasnoyarsk region. Thus, since 1992, within the range of 100 km from MCC, 20 potential sites have been identified on the basis of available data.

After significant number of exploration activities two most promising sites - "Verkhneitatskiy" and "Yeniseyskiy have been identified. Complex surface and well surveys were carried out in 1996-1999 at the Verkhneitatskiy site, and in 2002-2008 - at the Yeniseyskiy site.

Since 2008, comprehensive detailed studies have been carried out at the Yeniseisky site to confirm its suitability for disposal of long-lived Radwaste. As a result of comprehensive geological studies and mathematical modeling conducted within 2008-2015 the Yeniseyskiy site has been selected for the construction of the Underground Research Laboratory (URL).

A. URL CHARACTERISTICS:

- Three vertical shafts: depth of 525 m, diameter 6.0 – 6,5 m;
- Surface infrastructure, including auxiliary buildings and engineering communications;
- 1 Horizontal capital mining gallery [8].

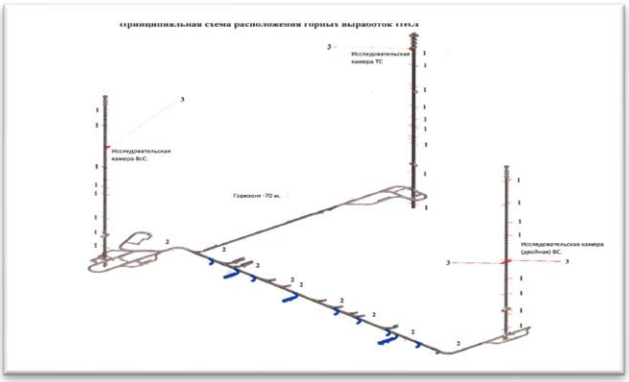

Figure 3. Scheme of the Underground Research laboratory, Nizhnekanskiy rock massif [8].

The host rocks are represented in varying degrees by metasomatically altered gneisses of different composition and dolerite dikes. The host rocks have favorable physical and mechanical properties, homogeneous structure and low fracturing [9].

B. URL GOALS:

The URL is being created for the following purposes:

- Refined research of the host rock mass characteristics and confirmation (under natural conditions) of the rock mass suitability for safe deep geological disposal of long-lived conditioned radioactive waste;
- Research and justification of the isolating properties of engineering barriers;
- Testing of technical solutions for the construction of the object, including engineering barriers, on-site logistic operations, final placement of waste packages and closure of disposal units;
- Testing of logistics and technological schemes for the construction and operation of radioactive waste disposal facility, testing and development of non-standard equipment;
- Staff training on on-site operations;
- Raising public awareness and expert community confidence in long-term operational safety of the possible deep geological repository [10].

It is anticipated that research works in more than 150 areas will be performed at the URL. It is also planned to create a Ground Demonstration Research Center to carry out comprehensive research of the rock massif, test radioactive waste management operations and optimize engineering barriers as well as demonstrate operational safety.

VI. CONCLUSIONS

After receiving sufficient amount of data at the underground research laboratory, its analysis and interpretation three scenarios will be possible:

1. Validation of design solutions, simulation of results and long-term safety assessments resulting in application for the deep geological disposal facility construction license;

2. The conclusion that there is insufficient operational and/or long-term safety provided by current design of engineering barriers resulting in change of the composition, geometry or technology of engineering barriers construction;

3. The conclusion that there is insufficient long-term safety of the facility provided by primary safety barrier - geological environment, resulting in refusal from the decision to place the facility of any type at this site or change of waste class, appropriate for disposal at this site.

The decision, based on the mentioned three scenarios should be done after 2031.

The URL project will also involve international cooperation and vast public communication. International cooperation will include work with International Atomic Energy Agency (IAEA) and Nuclear Energy Agency (NEA) of The Organization for Economic Co-operation and Development (OECD) and involvement of expert community from national operators on Radwaste management and final disposal of third States.

Cooperation with the public will include raising public awareness (public hearings, provision of detailed answers to public inquiries, etc.), cooperation with local authorities and establishment of information centres in the immediate vicinity of disposal facilities.

VII. REFERENCES

[1] Joint Convention on the Safety of Spent Fuel Management and on the Safety of Radioactive Waste Management, INFCIRC/546 of 24 December 1997.

[2] Federal Law of 04.11.2005 N 139-FL"On ratification of the Joint Convention on the Safety of Spent Fuel Management and on the Safety of Radioactive Waste Management", published on the 9.11.2005 in the “Russian Gazette”;

[3] Federal Law of 11.21.1995 N 170-FL (as amended on 30.04.2021) "On the use of atomic energy", published on the 5.05.2021 in the “Russian Gazette”;

[4] Federal Law of 11.07.2011 N 190- "On the management of radioactive waste and on amendments to certain legislative acts of the Russian Federation" (as amended and further effective as of July 16, 2013);

[5] Resolution of the Government of the Russian Federation of November 19, 2012 N 1185 (as amended on September 13, 2017) “On the determination of the procedure and terms for creating a unified state system for the management of radioactive waste” (together with the "Regulation on the determination of the procedure and terms for creating a unified state system for the management of radioactive waste");

[6] Resolution of the Government of the Russian Federation of 10.19.2012 N 1069 (as amended on 02/04/2015) "On the criteria for classifying solid, liquid and gaseous waste as radioactive waste, the criteria for classifying radioactive waste as special radioactive waste and for disposable radioactive waste and the classification criteria for disposable radioactive waste";

[7] V.P. Beygul “Stages of Researches, Pre-project and Project Works for Creation of NKM Underground Laboratory”, presented at the 3rd Crystalline Club meeting in Krasnoyarsk, Russian Federation, 25-27 June 2019 (unpublished);

[8] Igin V.I. “Creating system of final isolation (disposal) of radioactive waste in the Russian Federation” Technical Meeting on Global Progress in Developing Geological Disposal Solutions within the Underground Research Facilities Network, IAEA virtual meeting 22 February - 4 March 2022 (unpublished);

[9] Gupalo V S, Kazakov K S: “The Study of the State of Rock Mass During Construction of Underground Research” Laboratory as a Stage of Obtaining Initial Data for the Safety Assessments of Deep Geological Disposal Radioactive Waste - Radioactive waste journal, 2019, no 1 (6), pp 90—99 (In Russian).

[10] URL official web-source: http://nkmlab.ru/ **(**Accessed on: 18th June 2021).

Proceedings of the European Nuclear Young Generation Forum
ENYGF'21
September 27-30, 2021, Tarragona, Spain

Safety Case for the Disposal of LLW and ILW in the Russian Federation

Iuliia Trofimova [1]

[1] Federal State Unitary Enterprise «National operator for radioactive waste management» (FSUE NORWM), the Russian Federation

yvtrofimova@norao.ru

I. INTRODUCTION

The disposal of radioactive waste in the Russian Federation is carried out on the basis of Federal Law No. 190 "On the management of radioactive waste..." [4]. According to the terminology of the Joint Convention [1] and the national legislation, waste disposal refers to the activity of placing waste at a disposal site without the intention of retrieving it. The creation of a system for the disposal of low-and medium-level radioactive waste is one of the main activities within the framework of establishing the Unified State System for the Radioactive Waste Management (USS RWM).

The classification of radioactive waste in the Russian Federation is established in a special Government Decree [5]. Medium-level waste (or the 3rd waste class according to the national classification) and low-level waste (or the 4th waste class) are subject to disposal in near-surface disposal facilities (hereinafter – NSDF), which are placed at the same level with the surface or at a depth of up to one hundred meters from the ground level. Joint disposal of the specified waste is allowed, but if placing Class 3 RW below ground level.

The safety of NSDF should be ensured at all stages of its life cycle during the entire period of potential hazard of the RW disposed [7].

The safety justification of the NSDF is based on the results of the NSDF safety assessment, which includes an NSDF safety analysis during its operation and closure stage, and a forecast assessment of the long-term safety of the RW disposal system after the NSDF closure.

In accordance with national requirements, the safety justification must be presented in the safety justification report.

II. SAFETY REQUIREMENTS FOR THE NSDF

Near-surface RW disposal facilities are constructions whose structures, as well as the composition and properties of safety barriers, are determined and justified depending on the characteristics of RW (RW class, radionuclide composition, volume activity, period of potential hazard, physical and chemical properties) and their volume, taking into account the natural conditions of the NSDF location [7].

RW, meeting the disposal acceptance criteria, which are established in accordance with the requirements of the federal norms and regulations in the field of nuclear energy use, are subject to near-surface disposal [8].

Areas that are favorable for the NSDF placement are determined by conditions restricting the possibility of radionuclides escaping from the NSDF and its distribution in the environment. When choosing the NSDF location, geological and hydrogeological, hydrographic, engineering-geological, seismic, tectonic, climatic and demographic conditions are investigated. The final selection of the NSDF site and the fulfillment of the established requirements for external impacts on the NSDF are confirmed by the results of surveys and studies in the area of the proposed NSDF site, as well as the results of the NSDF safety assessment.

At the design stage, a system of technical and organizational measures to ensure the NSDF safety for the entire period of potential hazard of disposed RW is justified, taking into account possible external influences and factors of natural and man-made origin in the NSDF area, and physical and chemical processes occurring in the NSDF using computational modeling methods.

Due to the fact that the NSDF should have a system of safety barriers (engineering and natural) that prevent the spread of ionizing radiation and radioactive substances into the environment [7], the justification of the system of engineering safety barriers of the NSDF is an important activity implemented during the design.

A. Operational safety

The concept of ensuring radiation safety and protection of personnel, the population and the environment is based on the implementation of the basic principles of ensuring radiation safety under normal operating conditions of RW disposal facilities [9] and the principles of ensuring safety in the disposal of RW [6].

NSDF radiation safety is ensured through the consistent implementation of the deep-layered protection concept,

based on the use of a system of physical barriers to restrict the spread of ionizing radiation, radioactive substances into the environment, a system of technical and organizational measures to protect physical barriers and preserve their effectiveness, as well as to protect workers, the population and the environment.

The main purpose of the operational safety assessment for waste management is to assess the hazards and radioactive effects on workers, the population and the environment.

Safety assessment during the operational period is performed for normal operation, design and beyond-design accidents.

As a safety criterion, the individual dose rate is used that amounts to 20 mSv/year for a worker, and 1 mSv/year – for the population [9]. The concentrations of air, water and soil (for accidents and incidents) are generally used as a safety criterion for the environment.

To confirm the safety of RW disposal during operation, the RW disposal system is monitored [2, 4], including monitoring the state of engineering and natural barriers, ensuring timely detection of violations of the engineering barriers integrity, and monitoring the potential migration of radionuclides into the environment.

B. Long-term safety

The purpose of the long-term safety assessment is to confirm the absence of negative impact of the NSDF on the environment and people and to justify the compliance with the established sanitary standards established for the impact on people after the NSDF closure under condition of design solutions implementation [10, 11]. As a rule, the results of the forecast calculations include the activity of radionuclides in the water of aquifers, the dose received by the critical population group, and the generalized risk (if necessary).

The long-term safety assessment is performed for the period of potential RW hazard, which is understood as the beginning of a decrease in activity at the control points of the calculation after reaching the peak values.

In accordance with the requirements of the regulatory framework of the Russian Federation, radiation control and monitoring should be carried out for the entire period of potential hazard of disposed RW during the period after the closure of the NSDF.

The results of radiation control and monitoring should confirm the results of the long-term safety assessment.

A comprehensive approach to the assessment of the NSDF safety, including operational and long-term safety, is implemented to establish acceptance criteria of RW meant for disposal at each specific NSDF, as well as to justify technological solutions for disposal; limits and conditions for safe operation and closure of the disposal site, etc.

III. NEAR-SURFACE DISPOSAL IN THE RUSSIAN FEDERATION

The Russian Federation currently operates the first near-surface disposal facility for low- and medium-level waste, which was put into operation in 2016.

In the Russian Federation, the only organization authorized to dispose of radioactive waste is the Federal State Unitary Enterprise "National Operator for the Management of Radioactive Waste" – FSUE "NORWM".

The NSDF is located in the Sverdlovsk region. The NSDF site is confined to the zone of metamorphic rocks development represented by quartz-chlorite shale of Early Silurian age and gabbro-diorite. The underground water level was uncovered at depths of more than 16 m.

The disposal facility of the first stage is a monolithic reinforced concrete construction fully deepened in the ground.

In accordance with the requirements of Federal Law No. 190-FZ of 11.07.2011 "On the management of radioactive waste..." [4], RW accepted for disposal meets the acceptance criteria meaning the requirements for the physical and chemical properties of RW and RW packages established for the purpose of safe disposal. The acceptance criteria are mandatory for fulfillment.

In accordance with the NSDF status defined in the project, the final conditioned forms of 3rd and 4th classes RW according to the national classification [5] are accepted for disposal.

Containers with SRW are placed in the cells of the work card in an orderly vertical position in a stack with layer-by-layer filling using a gantry crane.

As the compartment is filled with RW packages, in order to ensure the spatial stability of the containers and long-term isolation of RW from the external environment, they are stabilized (primary preservation) by filling free space between the RW packages with buffer material.

The stabilization of RW packages in the facility compartment consists in a stepwise, layer-by-layer filling of the free space (voids) between the walls of the compartment and the packages, and between the packages with an buffer material – a material based on a mixture of natural kaolin and bentonite clays.

The second stage of this NSDF is at the stage of obtaining an operational license.

The second stage includes three constructions for the disposal of 3rd and 4th classes RW. Figure 1 shows an illustration of one of the constructed maps.

Figure 1. RW disposal [12]

The disposal facility of the second stage are monolithic reinforced concrete constructions, partially buried in the ground (maximum depth is up to -9.5 m).

The design of the facilities for the disposal of radioactive waste ensures the disposal of class 3 radioactive waste below the surface, class 4, in accordance with the legislation, can be located including on the surface.

In order to avoid the ingress of natural waters into the underground part of the NSDF along the contour and under the base, a clay barrier was created from compacted clay. The walls and the basement were additionally waterproofed with bentonite mats.

At the same time, the creation of the clay barrier was also aimed at reducing the permeability (clogging) of the boundary zone of the enclosing rocks, which could potentially be disturbed during the construction of the facility. The conducted hydrodynamic studies and measurements of the groundwater level at the site do not indicate the creation of a zone of increased fracturing during the construction process, which could reduce the insulating properties of the natural safety barrier.

As in the first stage of the NSDF, after placing the RW packages in the compartment, the free space is filled layer by layer with the buffer material.

Upon completion of operation, after filling in all NSDF cards, a covering screen (embankment) is created.

The covering screen should have a layered structure (bottom-up):

- a waterproofing layer to prevent the infiltration of atmospheric precipitation into the NSDF (clay with Kf - no more than 10^{-5} m / day, thickness – 1 m);

- a drainage layer (on top of the clay) of a gravel-sand mixture to remove atmospheric precipitation from the surface (thickness – 0,5 m);

- a protective layer of crushed stone with a size of 15-20 cm, (thickness – 0,5 m) to protect against mechanical destruction of the waterproofing layer of clay as a result of the penetration of plants, animals and as a result of inadvertent human intrusion (its presence in the future should warn a population about the existence of some the old engineering system and, therefore, reduce the likelihood of unintentional penetration or the severity of the radiation consequences of such penetration), (thickness – 0,5 m);

- a protective layer of loam with a soil and vegetation cover to maintain the moisture content in the underlying layers at a level necessary to prevent the clay screen from losing its waterproofing properties due to drying out and the appearance of fractures, (thickness – 1 m).

The slope angles of the future covering screen provide natural drainage of atmospheric precipitation from the NSDF site.

The service life of each of the materials used is justified in the RWDF project.

Long-term safety assessment has been carried out in accordance with the recommendations of the current Safety Guide RB-117-16 “Long-term safety assessment of near-surface disposal facilities for radioactive waste” [11].

The normal evolution scenario (NEA) and three alternative scenarios were considered: the “groundwater level rise” (AS1) scenario, the “volley release” scenario (AS2) and the “premature loss of filtration properties by engineering safety barriers” (AS3) scenario. Scenarios of inadvertent human intrusion (IHI) were also considered.

The following general conceptual assumptions and provisions were adopted when performing the safety assessment of NSDF:

- NSDF was constructed, put into operation and closed as planned in the project;

- for the zero time of calculations of the long-term safety assessment, the time for closing the NSDF is set;

- the period of active administrative (departmental) control is the first 100 years after closure. During this period, preservation of the structural integrity of the NSDF disposal system is ensured;

- during the period of passive administrative control (the first 300 years after the closure), the territory of the NSDF placement cannot be used by people for living and agricultural work, while a person can settle near the NSDF site after the end of this period of time;

- service life of engineering safety barriers corresponds to the design one. Upon reaching the design date, it is assumed that the filtration properties will decrease and lose, but the physicochemical ("sorption") will be preserved;

- calculations were carried out for the time of preservation of the potential hazard of radioactive waste. In accordance with national recommendations, the calculation period of the long-term safety assessment of the NSDF may be limited to the period for which the results of the calculations show that the level of radiation impact of NSDF on the population and the environment reaches a maximum value and cannot longer increase.

The results of forecast calculations for all scenarios are presented in the Table 1.

Table 1. Safety Assessment Results

Scenario	Parameter	Value
NEA	D_{max}[1], μSv / year	0,6
	t_{max}[2], year	6100
AS1	D_{max}, μSv / year	0,6
	t_{max}, year	5900
AS2	D_{max}, μSv / year	6,5
	t_{max}, year	5100
AS3	D_{max}, μSv / year	6,6
	t_{max}, year	3650
IHI[3]	Workers, μSv / year	3,8
	Population, μSv / year	3,2

Note: 1 – D_{max}, μSv / year – effective dose for the population from the critical group; 2 – t_{max}, year – time of reaching the peak values of activities; 3 – in the worst-case scenario of IHI.

Also as an example the structure of the potential exposure of the population along all routes of exposure under the most negative alternative scenario of evolution (AS3) is shown in figure 2.

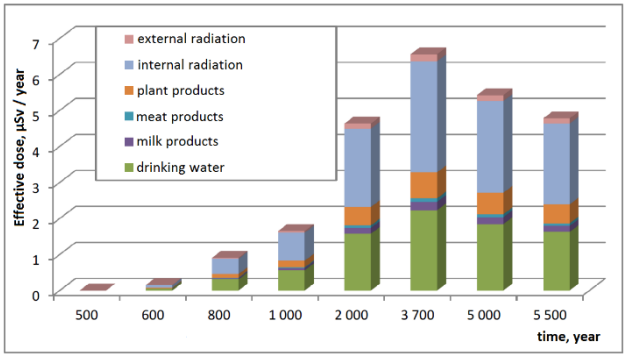

Figure 2. The structure of the potential exposure of the population in the scenario AS3

Thus, the results of the long-term safety assessment show that the total potential individual dose impact on the population along all possible radiation routes, including in case of an inadvertent intrusion, does not exceed the established limit of 10 μSv / year for the critical group of the population.

Justification of the safety of the created facility for the disposal of low-level and intermediate-level radioactive waste at all stages of its life cycle during the entire period of potential hazard of the disposed RW is confirmed by a safety expertise of the atomic regulator

FSUE "NO RWM" is also working on the creation of NSDF for 3rd and 4th classes RW in Chelyabinsk and Tomsk regions.

IV. CONCLUSION

The system of disposal of low-level and medium-level radioactive waste in the Russian Federation is in the process of formation and development. The phased establishment of disposal sites meets the needs of the state and industry in the safe final disposal of RW generated in the process of development of nuclear energy and related fields (medicine, science). Ensuring the basic safety principles at all stages of the NSDF life cycle is a priority in the field of RW management.

V. REFERENCES

[1] Joint Convention on the Safety of Spent Fuel Management and on the Safety of Radioactive Waste Management, IAEA, 1997.

[2] The IAEA Safety Standards for the Protection of People and the Environment “Disposal of Radioactive Waste”, IAEA, Specific Safety requirements № SSR-5, 2011.

[3] On the Use of Atomic Energy, Federal Law of the Russian Federation, No. 170-FZ, 1995.

[4] On the Management of Radioactive Waste and on Amendments to Certain Legislative Acts of the Russian Federation, Federal Law of the Russian Federation, No. 190-FZ., 2011.

[5] Criteria for classifying solid, liquid and gaseous waste as radioactive waste, criteria for classifying radioactive waste as special radioactive waste and as disposed radioactive waste, and criteria for classifying disposed radioactive waste, Decree of the Government of the Russian Federation, No 1069, 2012

[6] Federal norms and rules in the field of the use of atomic energy “Disposal of Radioactive Waste. Principles, Criteria and Basic Safety Requirements”, Rostechnadzor, NP-055-14, 2014.

[7] Federal norms and rules in the field of the use of atomic energy “Near-surface Disposal of Radioactive Waste. Safety Requirements”, Rostechnadzor, NP-069-14, 2014.

[8] Federal norms and rules in the field of the use of atomic energy “Acceptance Criteria of Radioactive Waste for disposal”, Rostechnadzor, NP-093-14, 2014.

[9] Radiation safety norms. Sanitary regulations SanPiN 2.6.1.2523-09, NRB-99/2009, 2009.

[10] The IAEA Safety Standards for the Protection of People and the Environment “Safety Case and Safety Assessment for the Disposal of Radioactive Waste”, IAEA, Special Safety Guide № SSG-23, 2012.

[11] Safety guidelines for the use of nuclear energy “Assessment of the Long-term Safety of Near-Surface Disposal Sites for Radioactive Waste”, Rostechnadzor, RB-117-16, 2016.

[12] The Official Website of FSUE “NO RWM”; www.norao.ru.

Proceedings of the European Nuclear Young Generation Forum
ENYGF'21
September 27-30, 2021, Tarragona, Spain

Consumption of hydrogen peroxide in the dissolution of mixed oxide fuels under the anoxic conditions of a geological disposal facility.

Perry, Emma[1*], Popel, Aleksej[1] and Farnan, Ian[1]

[1]University of Cambridge, Department of Earth Sciences

*Corresponding author: *etp22@cam.ac.uk*

I. INTRODUCTION

A primary pathway of radioactive release from spent nuclear fuel in a geological disposal facility is the dissolution of the uranium dioxide matrix in groundwater. U(VI) is significantly more soluble than U(IV) so understanding processes that lead to oxidation of the fuel are of paramount importance to the safety case.

On the one hand, disposal sites are chosen or designed to include organic-rich layers and reducing minerals, to make the groundwater anoxic [1]. On the other hand, radiation emitted by the spent nuclear fuel causes the radiolysis of water molecules. Radiolytic oxidants produced near the surface of the fuel can oxidise U(IV) to U(VI). Among the radiolytic oxidants, hydrogen peroxide and oxygen are the most long-lived oxidants and hydrogen peroxide is considered as the dominant oxidant [2].

The hydrogen peroxide concentration is determined by:

1. Production. H_2O_2 is formed in solution near the surface of the fuel at a rate dependant on the energy and activity of alpha decay and surface area of the spent nuclear fuel [3].

2. **Oxidative dissolution**. H_2O_2 is consumed when it oxidises uranium. Uranium in solution and in precipitated secondary phases can indicate the amount of H_2O_2 consumed during the oxidative dissolution process. Dissolution yield is a way to compare the percentage of consumed H_2O_2 that leads to dissolution of uranium, independent of surface area.

3. Disproportionation. Although it is considered as a long-lived radiolytic oxidant, H_2O_2 readily decomposes. This paper considers:
   a. **Catalytic decomposition** [4,5]. Not all interactions between a metal oxide and H_2O_2 lead to dissolution but H_2O_2 is still consumed. The rate of the catalytic decomposition depends on the number of reactive sites [5]. Pellet samples have more catalytic decomposition than powders [8]. Doped UO_2 has a more catalytic decomposition than undoped [8].
   b. **Background disproportionation**. In experiments, vessel surfaces can accelerate disproportionation. Polyethylene containers lead to an increased disproportionation of H_2O_2 compared to glass [6]. Disproportionation is accelerated by increasing pH from neutral to alkali and by raising the temperature [6, 7].

Uranium dioxide is the most common nuclear fuel but 10% of reactors worldwide use mixed oxide (MOx) fuels, made of uranium and plutonium dioxide. The addition of plutonium allows the fuel to be used in reactors for longer and is a way to use up a plutonium stockpile. Disposal of MOx fuel requires some extra consideration. On the one hand plutonium is less soluble than uranium and a plutonium rich layer could protect the MOx fuel from dissolution. On the other hand, plutonium is much more radioactive than uranium so there would be an increase in H_2O_2 production to increase dissolution [3].

Leaching studies of homogenous $(U,Pu)O_2$ pellets in 10 mM $NaHCO_3$ solution in titanium dioxide vessels under Argon atmosphere, have had some surprising results, as presented in Table 1 [9, 3]. Firstly, the concentrations of H_2O_2 were lower than expected. So the production was less than calculated and/or consumption was higher. Secondly, in the long-term dissolution the dissolution yield dropped to less than 1%, but no passivating plutonium phase was observed at the surface.

Table 1. H_2O_2 consumption rate per volumetric surface area in the presence of actinide oxides, the oxidative dissolution rate and resultant dissolution yield.

	H_2O_2 consumption $mol.m^{-2}.day^{-1}$	Oxidative dissolution $mol.m^{-2}.day^{-1}$	Dissolution yield
Heterogenous MIMAS $(U,Pu)O_2$ MOx [9]	$3.4 \cdot 10^{-3}$	$9.4 \cdot 10^{-4}$	28 %
Homogeneous $(U,Pu)O_2$ [3]	$9.5 \cdot 10^{-4}$	$1.2 \cdot 10^{-4}$	12.5 %

To underpin the mechanism of mixed uranium plutonium dioxide it is useful to study an analogue material. Studying the dissolution of (U,Th)O_2 allows observation of the effect of a different actinide in the UO_2 matrix with a reduced radioactivity compared to (U, Pu)O_2 in order to elucidate the H_2O_2 consumption mechanisms:

1. The **production** term of H_2O_2 by water radiolysis is removed. Instead a known amount of H_2O_2 is added to the solution and its consumption is followed.

2. The **oxidative dissolution** can be followed by the normalised uranium mass loss, $NL(U)$ over time,
$$NL(U) = \frac{m_U}{x_{solid} \times S}$$
x_{solid} is the fraction of this element in the material, m_U is the mass of uranium in solution and S is the area of the pellets (m^2) [3].

3. **Background disproportionation** occurring on the surfaces of the vessels and by interaction with ions in solution can be studied in experiments without pellets. By comparison, the **catalytic decomposition** of H_2O_2 on the surface of (U,Th)O_2 can be considered.

This paper presents preliminary results on hydrogen peroxide decomposition during the dissolution of (U, Th)O_2 in hydrogen peroxide doped ground water solutions in polypropylene vessels.

In contrast to the synthetic COx groundwater solutions used here, previous (U, Pu)O_2 leaching experiments presented in Table 1 have been performed in 10 mM $NaHCO_3$ [3, 9]. Additional blank experiments are presented to compare disproportionation in solutions without the groundwater ions and with increased HCO_3^- concentrations.

(Blank space required before a new

II. EXPERIMENTAL METHODOLOGY

All experiments were conducted under argon atmosphere.

A. Solutions preparation

Sodium bicarbonate ($NaHCO_3$) solutions of varying concentrations for blank experiments and prerinse solutions were made with deionised (DI) water.

Synthetic Callovian Oxfordian groundwater (COx), solution characteristic of the French disposal site at Bure, made as listed in Table 2 in DI water.

Table 2. Synthetic Callovian Oxfordian groundwater composition at 25 ºC[2]

	Na^+	K^+	Ca^{2+}	Mg^{2+}	Sr^{2+}	Cl^-	SO^{2-}	HCO_3^-	Si
$g.L^{-1}$	1.0	0.04	0.36	0.13	0.02	1.4	1.5	0.15	1.4
$mmol.L^{-1}$	44	1.0	8.5	5.5	0.21	41	16	2.4	0.2

All solutions were deaerated by bubbling with 5% H_2/N_2 gas for 30 minutes per 100 ml before use.

B. Pellet preparation

(U,Th)O_2 powders were produced from uranium nitrate hexahydrate and thorium nitrate hexahydrate by oxalic coprecipitation and thermal decomposition at 800 ºC. Powders were pressed under 150 MPa and sintered at 1600 ºC under argon for five hours to produce 4 mm diameter, 1 mm thick pellets. Two pellets were used in this leaching study.

Using back scattered electron (BSE) images and averaging along several lines in ImageJ the 2.1 ± 0.4 µm average grain size was determined. Porosity was calculated, using particle analysis in Image J, to be 5 % porosity. A 146 % developed interfacial ratio (SDR) (i.e. the additional surface area added by the texture) was calculated using secondary electron (SE) images in MountainsLab presented in Figure 1 [11].

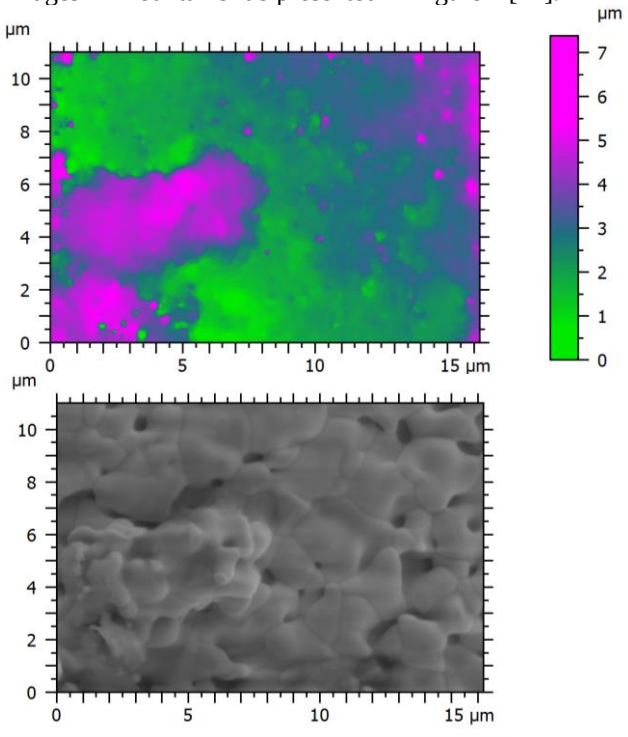

Figure 1. Top: Height map produced using MountainsLab software for an unleached (U, Th)O_2 pellet. Bottom: SE image taken at 22,000 times magnification.

Reitveld refinement carried out by Topas V6, of a molybdenum sourced X-ray diffraction spectrum, found a face centred cubic lattice parameter of 5.502 Å. Using Vegard's law [12-14] along with a UO_2 lattice parameter of 5.471 Å [14] and 5.598 Å [12] for ThO_2, the average composition was found to be $U_{0.75}Th_{0.25}O_2$. EDS has qualitatively shown the actinide composition to be quite uniform, with no thorium rich regions.

C. Leaching experiments

Naglene 125 ml polypropelene (PP) vessels were cleaned by filling and shaking with 10 ml of DI water three times.

Prior to leaching there were four 1 hour, one 16 hour and five 1 hour prerinse cycles with 50 ml of 1 mM $NaHCO_3$ solution. This procedure is intended to remove peroxidised phases at the surface of the pellet.

Leaching experiments of $(U,Th)O_2$ in COx solution doped with 1.3×10^{-4} M H_2O_2 were performed in duplicate. Blanks of COx solution with 1.3×10^{-4} M H_2O_2 in triplicate. Aliquots were sampled throughout the study and analysed by ultraviolet-visible spectrophotometry and pH determination immediately. ICP-MS samples were acidified to 0.2 M HNO_3 and reserved for batch analysis at the end of the experiment.

D. Blank experiments

To observe the dissolution over time, aliquots were sampled throughout the study and analysed by ultraviolet-visible spectrophotometry and pH determination.

One set of experiments considered H_2O_2 disproportionation due to the ions in solution by comparing consumption rate in DI and COx solution, with 1.2×10^{-4} M H_2O_2 initially. Another set considered H_2O_2 disproportionation due to bicarbonate ions using 3 mM and 10 mM $NaHCO_3$ solutions with 2.3×10^{-4} M H_2O_2 initially. These experiments were in Naglene 125 ml low density polyethelene (LDPE) vessels.

The difference in pH between these experiments is very small and not expected to be significant [5,7].

E. Ultraviolet-visible spectrophotometry

The Ghormley method has been used to track H_2O_2 concentrations [10]. H_2O_2 oxidises iodine to form a triiodide ion that absorbs 350 nm light. This absorbance is converted to a concentration by a calibration curve produced in house using H_2O_2 additions to DI water under an air atmosphere.

III. RESULTS AND DISCUSSION

A. Leaching experiments

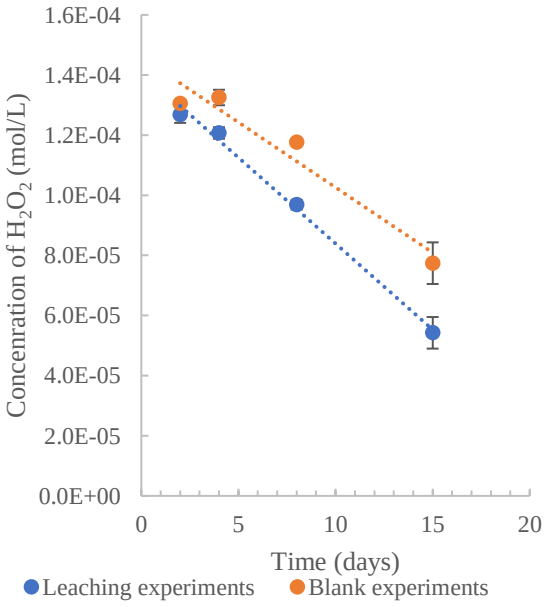

Figure 2. H_2O_2 concentrations over time in COx solutions with and without $(U,Th)O_2$ pellets under Ar at ambient temperature in PP vessels. Error bars from standard deviation of from? the mean. Dotted linear fits used to determine H_2O_2 consumption rate.

Table 3. H_2O_2 consumption rate per volumetric surface area (accounting for interfacial ratio calculated from Figure 1) in the presence of $(U,Th)O_2$ pellets broken down into separate mechanisms.

	H_2O_2 consumption $mol.m^{-2}.day^{-1}$	Catalytic decomposition $mol.m^{-2}.day^{-1}$	Oxidative dissolution $mol.m^{-2}.day^{-1}$	Dissolution yield
$(U,Th)O_2$ (incl. SDR)	$1.5 \cdot 10^{-2}$ ($1.0 \cdot 10^{-2}$)	$6.8 \cdot 10^{-3}$ ($4.6 \cdot 10^{-3}$)	$3.1 \cdot 10^{-4}$ ($2.1 \cdot 10^{-4}$)	2.1 %

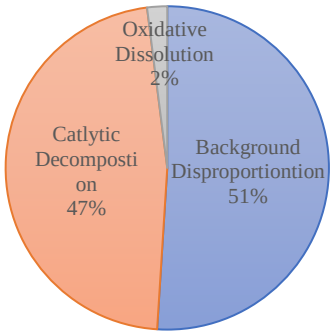

Figure 3: Percentage contributions of H_2O_2 consumption mechanisms in leaching experiments of $(U,Th)O_2$ pellets.

As evident in Figure 2, H_2O_2 consumption is accelerated by the presence of $(U,Th)O_2$ pellets. Uranium ICP-MS has been used to determine a normalised uranium mass loss, listed as the oxidative dissolution rate in Table 3. 2.1 % of the H_2O_2 consumption is due to oxidative dissolution. By comparison to blank experiments, the remaining 97.9 % of the H_2O_2 consumption is split between catalytic decomposition on the surface of the pellet and background disproportionation, as presented in Figure 3.

Compared to Table 1, the dissolution yield in these $(U,Th)O_2$ experiments is much lower than in the literature for $(U,Pu)O_2$ [3,8]. The oxidative dissolution rate was similar but the overall H_2O_2 consumption was much higher. Use of percentages should cancel out the effect of different reactive surface areas so the difference could be due to:

1. **Production**: the difference between initially adding H_2O_2 to the solutions and producing it in situ.
3. a) **Catalytic decomposition**: differing catalytic abilities of thorium and plutonium.
   b) **Background disproportionation**: this could be quite different in an experiment in 10 mM $NaHCO_3$ solution in a titanium dioxide vessel as compared to in COx solution in a PP vessel.

The latter reasoning is investigated in the next section.

B. Blank experiments

Figure 4 presents the results of two separate studies and whilst they had different initial concentrations of H_2O_2, linear trend lines were used to extract a consumption rate for comparison in Table 4. In DI solutions the H_2O_2 concentrations were stable throughout. Increaseing the bicarbonate concentration increased the H_2O_2 consumtpion rate. In COx solutions in LDPE vessels, there was a period of stability before the H_2O_2 concentrations began to drop. This 15 day stability has been verified in 3 repeat

experiments and is not present in any of the $NaHCO_3$ experiments. So the groundwater ions must facilitate the stable period. Interestingly this stable period was not observed in the blank experiments in polypropene vessels presented in Figure 2.

Nevertheless, more background disproportionation would be expected in 10 mM $NaHCO_3$ than in COx solution.

Table 4. H_2O_2 consumption rate in solutions with different carbonate concentrations at ambient temperature in LDPEvessels.

	pH	Consumption rate ($mol.L^{-1}.day^{-1}$)
a) 3 mM $NaHCO_3$	10.8	$3.5 \cdot 10^{-6}$
b) 10 mM $NaHCO_3$	11.1	$7.7 \cdot 10^{-6}$
c) DI water		$-1.1 \cdot 10^{-7}$
COx (2.4 mM $NaHCO_3$)	8.3	
d) Overall		$3.1 \cdot 10^{-6}$
e) After stable period		$6.7 \cdot 10^{-6}$
In PP vessels (Figure 2)		$4.3 \cdot 10^{-6}$

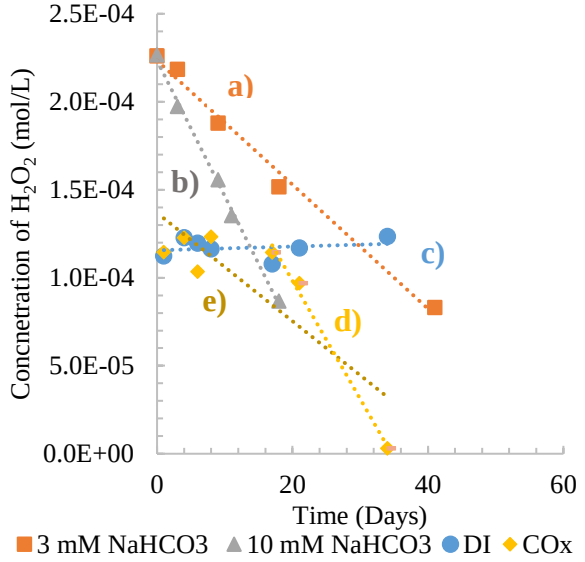

Figure 4. Concentrations of H_2O_2 in COx solutions and deionized water, 10 mM and 3 mM $NaHCO_3$ solution under Ar at ambient temperature in LDPE vessels. Dotted linear fits used to determine H_2O_2 consumption rate.

IV. CONCLUSIONS

The oxidative dissolution rate of (U, Th)O_2 in synthetic COx groundwater solution, initially with 1.3×10^{-4} M H_2O_2 was similar to (U,Pu)O_2 in 10 mM $NaHCO_3$. However, the overall H_2O_2 consumption was an order of magnitude higher in the (U,Th)O_2 synthetic COx groundwater solution experiment which is surprising as background disproportionation in 10 mM $NaHCO_3$ was found to be higher than in synthetic COx groundwater solution.

Further work will include:

Production: exploring the difference between initially adding H_2O_2 to the solutions and producing it in situ by continuously delivering H_2O_2 at the production rate quoted for homogenous (U,Pu)O_2 with a syringe pump [3].

a) **Catalytic decomposition:** repeat experiments with UO_2 and ThO_2.

b) **Background decomposition**: COx solution blank experiment in LDPE vessel with 2.3×10^{-4} M H_2O_2 initially. Leaching experiment of (U,Th)O_2 in 10 mM $NaHCO_3$ with 1.3×10^{-4} M H_2O_2.

V. REFERENCES

[1] É. C. Gaucher *et al.*, "Modelling the porewater chemistry of the Callovian-Oxfordian formation at a regional scale," *Comptes Rendus - Geosci.*, vol. 338, no. 12–13, pp. 917–930, 2006.

[2] D. W. Shoesmith, "Fuel corrosion processes under waste disposal conditions," *J. Nucl. Mater.*, vol. 282, no. 1, pp. 1–31, 2000.

[3] V. Kerleguer *et al.*, "The mechanisms of alteration of a homogeneous $U_{0.73}$ $Pu_{0.27}$ O_2 MOx fuel under alpha radiolysis of water," *J. Nucl. Mater.*, vol. 529, 151920, 2020.

[4] C. M. Lousada, A. J. Johansson, T. Brinck, and M. Jonsson, "Mechanism of H_2O_2 decomposition on transition metal oxide surfaces," *J. Phys. Chem. C*, vol. 116, no. 17, pp. 9533–9543, 2012.

[5] A. Hiroki and J. A. LaVerne, "Decomposition of hydrogen peroxide at water-ceramic oxide interfaces," *J. Phys. Chem. B*, vol. 109, no. 8, pp. 3364–3370, 2005.

[6] M. Amme, J. Švedkauskaite, W. Bors, M. Murray, and J. Merino, "A kinetic study of UO2 dissolution and H2O 2 stability in the presence of groundwater ions," *Radiochim. Acta*, vol. 95, no. 12, pp. 683–692, 2007.

[7] H. Deveci and E. Y. Yazici, "Factors Affecting Decomposition of Hydrogen Peroxide," in *Proceedings of the XIIIth interanltional mineral processing symposium.*, 2010.

[8] A. Barreiro Fidalgo, Y. Kumagai, and M. Jonsson, "The role of surface-bound hydroxyl radicals in the reaction between H 2 O 2 and UO 2," *J. Coord. Chem.*, vol. 71, no. 11–13, pp. 1799–1807, 2018.

[9] M. Odorowski *et al.*, "Oxidative dissolution of unirradiated Mimas MOX fuel (U/Pu oxides) in carbonated water under oxic and anoxic conditions," *J. Nucl. Mater.*, vol. 468, pp. 17–25, 2016.

[10] J. A. Ghormley and A. C. Stewart, "Effects of γ-Radiation on Ice," *J. Am. Chem. Soc.*, vol. 78, no. 13, pp. 2934–2939, 1956.

[11] R. Podor *et al.*, "3D-SEM height maps series to monitor materials corrosion and dissolution," *Mater. Charact.*, vol. 150, no. December 2018, pp. 220–228, 2019.

[12] S. Hubert, J. Purans, G. Heisbourg, P. Moisy, and N. Dacheux, "Local structure of actinide dioxide solid solutions Th_{1-x} U_x O_2 and Th_{1-x} Pu_xO_2," *Inorg. Chem.*, vol. 45, no. 10, pp. 3887–3894, 2006.

[13] M. Kanno, S. Kokubo, and H. Furuya, "Preparation of Thorium-Uranium Mixed Oxide Pellets," *J. Nucl. Sci. Technol.*, vol. 19, no. 11, pp. 956–958, 1982.

[14] G. Leinders, T. Cardinaels, K. Binnemans, and M. Verwerft, "Accurate lattice parameter measurements of stoichiometric uranium dioxide," *J. Nucl. Mater.*, vol. 459, pp. 135–142, 2015.

Acknowledgement: ETP thanks the UK EPSRC for a PhD studentship administered through the Imperial Cambridge Open (ICO) Centre for Doctoral Training and IF, AP and ETP acknowledge the support of the Horizon 2020 Atomic Energy Community Research and Training Programme of the European Commission (EURATOM) (H2020-NFRP-2016-2017-1) under grant agreement n° 755443 (DisCo).

Hot Topic 4 - Breakthroughs in Nuclear Fuel & Materials

Structural materials for Gen-IV reactors.

Authors: Rostova, Hanna; Voyevodin, Victor; Galina, Tolstolutskaya; Alexander, Kalchenko; Mikhail, Tikhonovsky

Advanced Nuclear Fuel Cladding Materials for Light Water Reactors.

Authors: Sevecek, Martin (1,2); Krejci, Jakub (3); Chalupova, Adela (1,3); Cvrček, Ladislav (1)

Fabrication and Development of Self-glowing Crystals for Safe Actinide Handling.

Authors: Ipatova, Iuliia

Quantifying the benefits of the reduced oxidation kinetics in chromium-coated cladding: a parametric study.

Authors: Cozzo, Cedric (1); Lind, Terttaliisa (1); Bertsch, Johannes (2); Nichenko, Sergii (3); Girardin, Gaëtan

International Research Centre MBIR.

Authors: Solntseva, Ekaterina; Alexander, Zagornov

Application of Raman spectroscopy to the characterization of new Cr-UO2 nuclear fuels.

Authors: Milena-Pérez, Abel (1); Jiménez-Bonales, Laura (1,2); Rodríguez-Villagra, Nieves (1); Fernández-Carretero, Sergio (1); García-Baonza, Valentín (3); Cobos, Joaquín (1,4)

Response of Accident Tolerant Fuel Cladding Concepts to LOCA Burst Testing.

Authors: Kane, Kenneth; Bell, Sam; Massey, Caleb; Pint, Bruce

FeCrAl Accident Tolerant Fuel Cladding: Insights from a Decade of Development

Authors: Massey, Caleb P. (1); Edmondson, Philip D. (1); Gussev, Maxim N. ; Yamamoto, Yukinori (1); Pint, Bruce A. (1); Field, Kevin G. (2); Terrani, Kurt A. (1,3)

Poolside Inspection of EnCore Fuel Lead Test Rods at Exelon Byron Unit 2.

Authors: Walters, Jorie L.

Methodology and preliminary results of an experimental and numerical study to determine the toughness of fuel rod cladding during Delayed Hydride Cracking (DHC).

Authors: Francois, Pierrick; Petit, Tom; Auzoux, Quentin; Salliot, Freddy; Besson, Jacques

Porous Crystal Plasticity-based Ductile Fracture assessment for FCC Nuclear materials.

Authors: Sénac, Cédric; Hure, Jeremy; Scherer, Jean-Michel; Helfer, Thomas; Tanguy, Benoît

Impact of dopants on diffusion in crystalline and amorphous zirconia.

Authors: Owen, Megan W. (1); Rushton, Michael J. D. (1); Evitts, Lee J. (1); Claisse, Antoine J. (2); Puide, Mattias (2); Lee, William E. (1); Middleburgh, Simon C. (1)

Modern status of materials for nuclear technologies in ukraine.

Authors: Voyevodin, Victor; Tolstolutskaya, Galina

Proceedings of the European Nuclear Young Generation Forum
ENYGF'21
September 27-30, 2021, Tarragona, Spain

Structural materials for Gen-IV reactors

Voyevodin, Victor[1,2], Rostova, Hanna[1*], Tolstolutskaya, Galina[1] , Kalchenko, Alexander[1] and Tikhonovsky, Mikhail[1]

[1]National Science CenterKharkov Institute of Physics and Technology (NSC KIPT), Ukraine

[2]V. N. Karazin Kharkiv National University, Ukraine

*Corresponding author: *rostova@kipt.kharkov.ua*

I. INTRODUCTION

The creation of the future generation nuclear reactors (GEN IV, BN-800, BN-1200, Terra Power Wave reactor etc.) poses new problems in materials science in terms of higher operating temperatures, increased neutron doses, as well as ensuring the safe and efficient operation of reactors. Various nuclear concepts require low void swelling of structural materials at very high exposures (>200 dpa).

9-12% Cr ferritic-martensitic (F/M) steels (such as T91, HT-9, Eurofer 97, EP-450, EK-181, etc.) can serve as candidates to reach high fuel burn-up levels for many types of reactors [1]. Thermomechanical treatment (TMT) is one of the most effective ways to improve the mechanical properties, structure, and radiation tolerance of these steels. TMT allows to create a nanostructured state of steel with uniformly distributed precipitates and permits producing of increased number of sinks of point radiation defects that lead to a significant suppressing of the of material's swelling and radiation embrittlement.

One of the most effective methods of the grain size refinement in alloys is the severe plastic deformation (SPD), which allows producing ultrafine grain or nanostructured state in steels; this induces the increase of strength characteristics and radiation resistance of steels [2]. There are different methods of SPD, one of them is multiple "upsetting-extrusion" (**MUE**) developed in NSC KIPT [3]. This method proved to be effective for production of ultrafine-grained materials both in laboratory and industrial conditions.

Another perspective class of new metallic materials is so called high entropy alloys (HEAs) [4]. HEAs are defined as alloys consisting of 5 or more principal elements with nearly equiatomic fractions in range 5-35 at.%. Unlike traditional alloy designs, in which one major element is selected as the solvent and several dilute solute elements are added, all elements in HEAs are major.

Several compositions of HEAs or multicomponent alloys have been found to form ductile solid solution structures involving face centered cubic (FCC) or body centered cubic (BCC) phases or mixtures of the two, instead of brittle intermetallic compounds. In addition, their attractive physical and mechanical properties such as high strength, ductility, wear resistance, high temperature softening resistance and corrosion resistance make HEAs potential candidates for high temperature fission or fusion structural applications. Their extraordinary mechanical properties have led to intensive interest in investigating their potential for practical applications, including nuclear and thermonuclear powers [5].

The key objective of this study is to investigate the effect of MUE and subsequent heat treatment on grain size, parameters of secondary phases precipitations, mechanical properties and hardening/embrittlement phenomenon and the level of swelling under irradiation. Other objects of research were high-entropy alloys of the Cr-Fe-Mn-Ni system and oxide dispersion strengthened version one of the alloys (ODS HEA).

II. MATERIALS AND METHODS

The chemical composition of T91 steel is (in wt.%): Cr – 8.76, Mo – 0.862, Mn – 0.597, Si – 0.317, V – 0.186, Ni – 0.099, Nb – 0.073, C – 0.088, N – 0.003, P – 0.019. The heat treatment as-received steel includes normalization at 1040 °C for 30 minutes, followed by air cooling and then tempering at 730 °C for 60 minutes with air cooling to room temperature (the so-called N&T state). The specimen of steel was extruded at T=875ºC from diameter 40mm to diameter 20 mm. Obtained specimens with diameter 20 mm and height 60 mm were subjected to five or three cycles of upsetting-extrusion (MUE) from 20 mm to 30 mm and vice versa. MUE was carried out in two temperature regions: A – five cycles in the region of ferrite stability with a gradual decrease in temperature from 750ºC in the first cycle to 575ºC in the fifth cycle (samples' code MUE –F); B – three cycles in the two-phase region ferrite-austenite at a temperature of 875ºC (samples' code MUE –FA). Total real (logarithmic) deformation during five upsetting-extrusion cycles was e = 8.

HEAs with the compositions (in at. %) of 18Cr-40Fe-28Mn-14Ni (code E30-2), 18Cr-28Fe-27Mn-28Ni (code E31-2), and 20Cr-40Fe-20Mn-20Ni (code E32-2) were produced by arc melting in a high-purity argon in a water-cooled copper

mould. The purity of initial components was not less than 99.9%. To ensure homogeneity ingots were remelted at least 5 times. Powders of HEA were obtained by mechanical grinding using abrasives, and then powders were sieved into fractions. Powders with close to equiaxial shape and less than 300 μm in size were used forfurther operations. Oxide dispersion strengthening was carried out by mechanical alloying. 0.5 wt.% of pre-synthesized nanopowders composition of 80%Y_2O_3+20%ZrO_2 (mol.%) were used as alloying components. The synthesized powders had cubic structure with lattice parameter a = 10.2 Å, average size was about 17 nm. The process of obtaining ODS HEA is described in more detail in [6].

Microstructure was studied by metallographic and electron microscopic methods. Phase composition and structural characteristics was examined by X-ray diffraction study. More information about methods of irradiation and nanoindentation is described in [7, 8].

III. RESULTS AND DISCUSSION

A. T91 steel

As-received samples. Microstructure of as-received steel T91 is typical for tempered martensite and is characterized by the presence of prior austenite grain boundaries and subgrains that are well seen in optical and transmission electron microscopes (Fig. 1). These boundaries are decorated by precipitates of $M_{23}C_6$-type carbides that are always present in steel T91. The average sizes of prior austenite grains, subgrains and $M_{23}C_6$ precipitates are around 20 μm, 5 μm and 125 nm, respectively. Within prior austenitic grains martensitic laths with transverse dimension around 0.25-0.5 μm are observed. At high magnification, except rather large $M_{23}C_6$ precipitates, considerable number of fine precipitates with a diameter ≤50 nm is spotted which are always classified as phases of MX type [9].

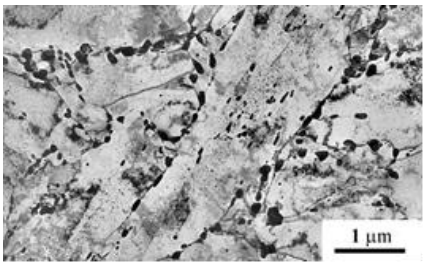

Figure 1. Microstructure of as-received steel T91.

MUE –F samples. The multiple "upsetting-extrusion" method in ferrite region allowed to obtain mean size of ferritic grains of 145 nm. Two types of precipitates are observed – $M_{23}C_6$ (where M=Cr, Fe, Mo, Mn) and MX (where M=Nb, V; X=C, N). It is determined that increase in number of upsetting-extrusion cycles and decrease in deformation temperature induces not only decrease in grain size and increase in dislocation density but also increase in lattice parameter of ferritic phase. Increase in lattice parameter occurs due to the increase of carbon concentration in ferrite lattice as the result of so-called "deformation dissolution" of carbide precipitates. The consequence of such structural changes is the increase of steel microhardness to 2855 MPa, which is 375 MPa higher than that in as-received steel (state of tempered martensite). The results of the microhardness measuring of the samples after heat treatment in the temperature range of 550 - 750 °C for 1-50 hours showed that highmechanical characteristics are maintained during exposure at the temperature of 550 °C. (Fig. 2).

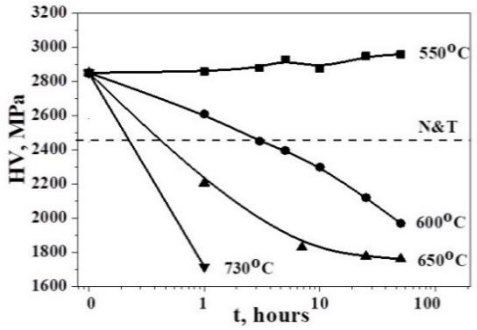

Figure 2. Dependence of microhardness of specimens subjected to 5 cycles of upsetting-extrusion on time of TT at different temperatures. Dashed line defines the level of microhardness in as-received state (tempered martensite).

It was found, that, the temperature of 550 °C is the optimal regime for tempering, which allow to stabilize the structure, since at higher temperatures there is recrystallization and, as a result, a decrease in hardness. Therefore, for further studies, a sample that underwent heat treatment for 25 hours at a temperature of 550 °C was selected. The average grain size for sample with a ferritic structure was 210 nm. The microstructure of the sample is shown in Fig. 3.

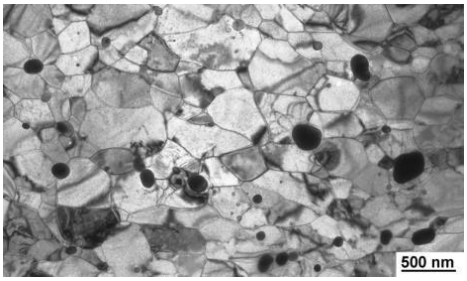

Figure 3. The microstructure of the sample MUE –F after subsequent heat treatment at 550°C for 25 h.

To determine the level of swelling samples of steel T91 in the initial state (martensitic structure) and after severe plastic deformation (ferritic structure) were irradiated with argon ions with energy 1.4 MeV to a dose 120 displacements per atom (dpa) at a temperature 460 °C - the peak of temperature swelling for steel T91 (Fig. 4).

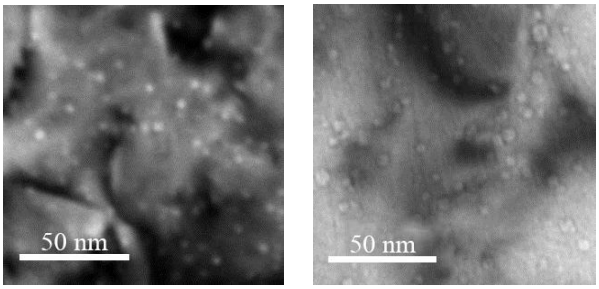

a b

Figure 4. The microstructure of steel T91 for samples with martensitic (a) and ferritic (b) structures, irradiated to a dose 120 dpa (E = 1,4 MeV Ar^+) at 460°C.

A comparison of the initial steel with a martensitic structure and a sample with a ferritic structure (Fig. 4 a, b) showed that the level of swelling of the sample in the martensitic state is 2.5 times lower than in the ferritic state and was 0.26 % and 0.65 %, respectively.

MUE –FA samples. After MUE at 875 ºC samples have microstructure of "broken martensite" with the grain size of 100 nm and their microhardness is 3960 MPa. The heat treatment at 600 °C for 25 h leads to the formation of a ferrite-martensitic microstructure with a grain size of 210 nm and microhardness of samples decrease to 2780 MPa (Fig. 5). The average size and density of $M_{23}C_6$ precipitates is 120 nm, and 4.2×10^{19} m^{-3}, respectively. Carbides of the MX type having the size of ≤ 24 nm and density of 2.6×10^{20} m^{-3} are more evenly distributed in the grains.

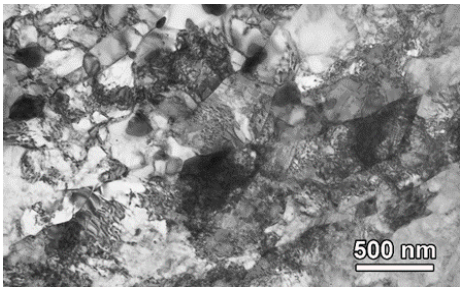

Figure 5. Microstructure of MUE –FA samples.

Ferritic-martensitic steel with such modified ultrafine-grained microstructure was irradiated with 1.4 MeV Ar^+ ions to doses from 10 to 45 dpa at room temperature and 460 °C. The radiation microstructure and hardening of this steel were studied. The hardening of the irradiated steel gradually increases with an increase in the irradiation dose up to 45 dpa due to the formation of dislocation loops and nano-sized Ar-associated bubbles.

Comparison of the radiation-induced hardening (ΔH, the difference of hardness values of irradiated and unirradiated materials) of ferritic-martensitic steels obtained by different authors [10, 11] (Fig. 6) shows some differences in the data, which is probably due, first of all, to the difference in the irradiation temperature.

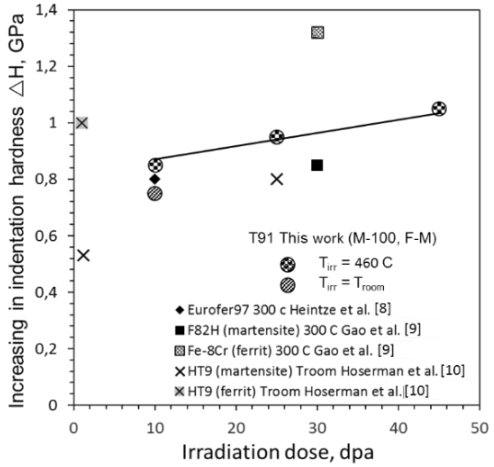

Figure 6. Relative radiation-induced hardening of ferritic-martensitic steels.

Additionally, a noticeable difference in data is observed for materials with different microstructure. For instance, a clear discrepancy can be seen by comparing alloys with ferrite (ΔH = 0.95 GPa) and tempered martensite (ΔH = 0.58 GPa) structures at low doses of 2…3 dpa. At a dose of 30 dpa these values are estimated as 1.32 and 0.85 GPa, respectively.

The fine microstructure of tempered martensite has a significant effect on the decrease in hardening under irradiation. The ultrafine-grained microstructure of T91 steel, in turn, has a high density of distribution boundaries, which act as absorbers of radiation defects. For this reason, the formation of obstacles to the movement of dislocations is expected to be impeded in ferritic-martensitic steel with a high density of initial traps/sinks for radiation defects. And, thus, ferritic-martensitic steels are less susceptible to radiation hardening/embrittlement compared to materials with a purely ferritic microstructure (see Fig. 6).

B. Cr-Fe-Ni-Mn high-entropy alloys

High entropy alloys are a new effort in materials science and engineering. In this study the alloys with the compositions (in at. %) of 18Cr-40Fe-28Mn-14Ni (E30-2), 18Cr-28Fe-27Mn-28Ni (E31-2), 20Cr-40Fe-20Mn-20Ni (E32-2) and it's strengthened with yttrium and zirconium oxides versions were studied.

According to X-ray analysis all as-cast alloys are single-phase and have FCC crystal lattice. After TMT and final heat treatment at 1050 °C all samples contain only FCC phase.

Alloys with different composition were irradiated with 1.4 MeV Ar ions at room temperatures and midrange doses from 0.3 to 5 dpa and nanoindentation was used to measure the ion irradiation effect on hardening of these high-entropy alloys.

There is essential scatter in nanoindentation data, especially for E30-2 alloy. The minimum scatter is observed for E32-2 sample (Fig. 7). As a trend, we can state that in the initial samples the hardness is 1.75…2.5 GPa, while in irradiated ones it grows to 3.5 GPa. The hardening of irradiated E32-2 alloy increases with dose increasing and is 26% for 0.3 dpa, 30% for 1 dpa, and 45% for 5 dpa.

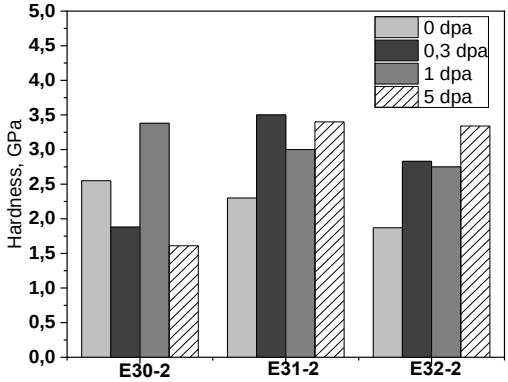

Figure 7. Nanohardness before and after irradiation for E30-2, E31-2 and E32-2 alloys.

Comparison of the nanohardness increments, ΔH, defined by the difference between the irradiated and unirradiated samples, $\Delta H = H_0^{irr} - H_0^{as\text{-}received}$ of high entropy alloy 20Cr-40Fe-20Mn-20Ni (HEA) and it's strengthened with yttrium and zirconium oxides version (ODS-HEA) is graphed in Fig. 8.

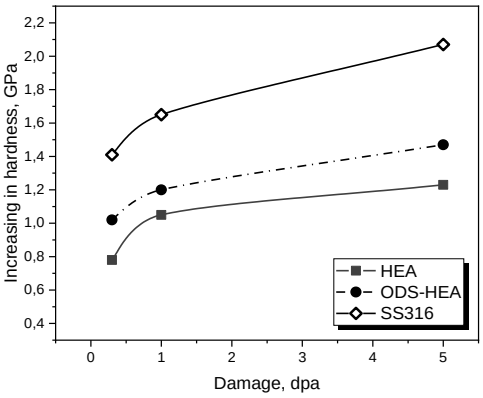

Figure 8. Nanohardness increments of the irradiated HEA, ODS-HEA alloys and SS316.

Irradiated HEA has minimum nanohardness increments, while ΔH of ODS-HEA is 15-25% higher than the HEA. Taking into account that the yield stress of materials is proportional to the hardness and hardening $\Delta\sigma y = K\Delta H$ [12], it can be deduced that hardening increase with irradiation dose, and the largest hardening is detected in SS316.

Irradiated samples showed significant changes in the microstructure relatively the unirradiated sample – the very small-sized black dots and dislocation loops were observed and it is an important factor for irradiation hardening.

An increase in radiation-induced hardening of ODS-HEA is higher than the HEA in the entire range of doses studied, despite the fact that the density of visible dislocation loops is lower in ODS-HEA. It can be assumed that in this case, in addition to the pinning effect of dislocation loops, oxides also have an effect. Future work on the irradiation effects on ODS-HEA should focus on establishing the causes of this phenomenon.

Nevertheless, these results indicate that the processes of hardening/embrittlement will develop in HEAs and ODS-HEAs much slower than conventional Fe-Cr-Ni austenitic alloys.

IV. CONCLUSIONS

A new approach to thermo-mechanical treatment of steel T91 by multiple upsetting-extrusion is proposed. Comparison of obtained results with literature data for steel T91 subjected to SPD by torsion under high pressure and equal-channel angular pressing shows that our method of multiple "upsetting-extrusion" allows grain refining and mechanical characteristics improving. Advantage of this method consists in possibility to refine microstructure of billet of industrial size as well as in the simplicity of the mechanical processing.

Significant increase (1.3 times) in the hardness of unirradiated samples T91- MUE–FA is due to grain refinement, crushing of lamellae, a decrease in the size of carbides of the MX type and their more uniform distribution.

Ferritic-martensitic steel with a certain density of initial traps for radiation defects create fewer obstacles to the movement of dislocations, and thus are less susceptible to radiation hardening/embrittlement compared to materials with a purely ferritic microstructure.

High-entropy alloys must lose less plasticity in comparison with traditional materials of nuclear power – austenitic steels X18H10T and SS316 – for which hardening after identical irradiation almost one and a half times.

ACKNOWLEDGEMENT

This work was prepared within the project № 2020.02/0327 "Fundamental aspects of the new materials creation with unique physical, mechanical and radiation properties based on the concentrated multicomponent alloys", implemented with the financial support of the National Research Foundation of Ukraine.

V. REFERENCES

[1] R.L. Klueh and A.T. Nelson, "Ferritic/martensitic steels for next-generation reactors," J. Nucl. Mat., vol. 371, pp. 37-52, 2007.

[2] Z.Q. Fan, T. Hao, S.X. Zhao, G.N. Luo, C.S. Liuand and Q.F. Fang, "The microstructure and mechanical properties of T91 steel processed by ECAP at room temperature," J. Nucl. Mater., vol. 434, pp. 417–421, 2013.

[3] I.I. Papirov and G.F. Tikhinskiy, "Structure and mechanical properties of fine-grained deformed beryllium," Physics of metals and metal science, vol. 29(5), pp. 1057-1060, 1970. (in Russian)

[4] J.W. Yeh, Y.L. Chen, S.J. Lin and S.K. Chen, "High-entropy alloys – a new era of exploitation," Materials Science Forum, vol. 560, pp. 1-9, 2007.

[5] E. J. Pickering, A. W. Carruthers, P. J. Barron, S. C. Middleburgh, D. E. J. Armstrong and A. S. Gandy, "High-Entropy Alloys for Advanced Nuclear Applications," Entropy, vol. 23, no. 1, p. 98, 2021.

[6] I.V. Kolodiy, O.M. Velikodnyi, M.A. Tikhonovsky and et al., "Microstructure and mechanical properties of oxide dispersion strengthened high-entropy alloys CoCrFeMnNi and $CrFe_2MnNi$," PAST, № 2(132), pp. 87-94, 2021.

[7] G.D. Tolstolutskaya, V.V. Ruzhytskiy, I.E. Kopanetz, V.N. Voyevodin, A.V. Nikitin, S.A. Karpov, A.A. Makienko and T.M. Slusarenko, "Accelerating complex for study of helium and hydrogen behavior in conditions of radiation defects generation," PAST, vol.1(65), pp. 135-140, 2010.

[8] G.N. Tolmachova, G.D. Tolstolutskaya, S.A. Karpov, B.S. Sungurov and R.L. Vasilenko, "Application of nanoindentation for investigation of radiation damage in SS316 stainless steel," PAST, vol.5(99), pp. 168-173, 2015.

[9] F. Abe, S. Nakazawa, H. Araki and T. Noda, "The role of microstructural instability on creep behaviour of a low radioactivation martensitic 9Cr-2 W steel," Metal. Trans., vol. 23, A, pp. 469-477, 1992.

[10] J. Gao, K. Yabuuchi and A. Kimura, "Ion-irradiation hardening and microstructural evolution in F82H and ferritic alloys," J. Nucl. Mater., vol. 515, pp. 294-302, 2019.

[11] C. Heintze, C. Recknagel, F. Bergner, M. Hernandez-Mayoral and A. Kolitsch, "Ion irradiation-induced damage of steels characterized by means of nanoindentation," Nucl. Instrum. Methods in Phys. Res. B., vol. 267, pp. 1505-1508, 2009.

[12] J.T. Busby, M.C. Hash and G.S. Was, "The relationship between hardness and yield stress in irradiated austenitic and ferritic steels," J. Nucl. Mater., vol. 336, pp. 267-278, 2005.

Proceedings of the European Nuclear Young Generation Forum
ENYGF'21
September 27-30, 2021, Tarragona, Spain

Advanced Nuclear Fuel Cladding Materials for Light Water Reactors

Sevecek, Martin[1,3*], Krejci, Jakub[2], Chalupova, Adela[1] and Cvrcek, Ladislav[1]

[1] Czech Technical University in Prague, Czech Republic; [2] UJP Praha, Czech Republic; [3] ALVEL, Czech Republic

*Corresponding author: *martin.sevecek@fjfi.cvut.cz*

I. INTRODUCTION

The traditional nuclear fuel system of basically all Light Water Reactors operated in the world is based on the combination of ceramic uranium oxide pellets slightly enriched with ^{235}U enclosed in a cladding made of a Zr-based alloy [1]–[3]. This traditional fuel system proved its extraordinary operational performance during the last decades with incremental improvements related to limitations of fuel failures, improved corrosion, higher burnups, longer fuel cycles, etc. [4], [5]

However, there are many open challenges and issues linked to the traditional fuel system. The main disadvantage linked to high-temperature reaction with steam negatively affected the progression of the events at Fukushima Daiichi or Three Mile Island [6]–[8]. When exposed to a high-temperature oxidizing environment, Zr-based alloys undergo a rapid exothermal reaction, producing additional heat and releasing hydrogen. The heat produced by the oxidation reaction is during some stages of the transient higher than the residual heat produced by the fuel. This leads to rapid acceleration of high-temperature reactor accidents and accelerated core degradation.

On the other hand, the reactor operators, e.g., in the USA, face significant economical challenges mainly due to competition with very cheap natural gas. This forces operators to improve the economy of operation by uprating the power of units, increasing fuel cycle length and fuel burnups. Additionally, nuclear power reactors need to operate in load-follow conditions for extended time periods due to the increasing share of renewable sources in the energy mix around the world. All these requirements further challenge the fuel systems that have their inherent limits given by material properties and performance.

As a result of these needs, the US Department of Energy initiated projects related to the further enhancement of nuclear fuel safety. These fuels are called Accident Tolerant Fuels, and their goal is to improve the fuel behavior during potential severe accidents and thus provide the operators more time to handle the accident before complete fuel degradation [3], [9]. Later, the operators emphasized also the need to resolve their operational challenges. Therefore, a group of innovative fuel types called "Advanced Technology Fuels" has been included in the development plans. Both advanced fuel types are referred to as ATFs, however, the objectives of the first group are mainly related to severe accident scenarios, whereas the second mainly considers costs and benefits on the level of nominal operation.

There were many ATF concepts proposed around the world and new types are still under investigation. Generally, these types can be divided into three groups – cladding materials, fuels, and non-fuel components (Figure 1).

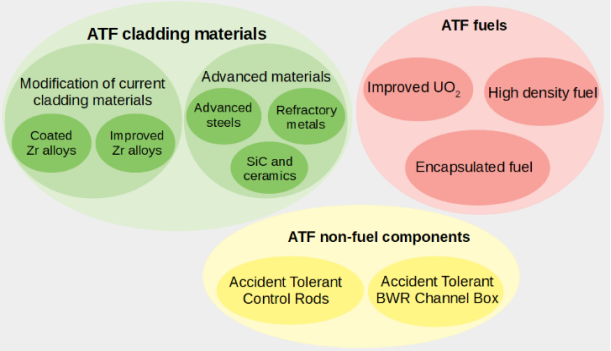

Figure 1. Three types of ATF materials that are under investigation around the world

As shown in the figure, the three main groups can be further divided depending on the chosen approach from the improvement of traditional fuels (coated/improved Zr, doped UO_2, etc.) over complete replacement with new materials (advanced steels – FeCrAl, SiC/SiC, U-Mo, USi, etc.) to change of fuel design and other core components (ATCR – accident tolerant control rods) [10], [11].

II. FUEL CLADDING MATERIALS

Czech Technical University in Prague together with its partners has been researching, testing, developing, and qualifying several types of advanced fuel cladding materials [12]–[15].

C. Modifications of current cladding materials

To produce, characterize, and test the coated cladding concept, several types of commercial Zr-based alloys were used as a substrate (E110, Zircaloy-4, Zircaloy-2, Opt. ZIRLO™, HiFi). Four deposition methods were chosen and tested. The Zr alloys should not degrade during the deposition of the coatings, therefore temperature and time limits were defined to avoid reannealing occurring at temperatures around 450°C. Moreover, the deposition technique should be able to produce a high-quality coating with the required thickness of protective material. Based on an evaluation, four methods were chosen (Figure 2):

- Cold-spray process
- Unbalanced magnetron sputtering (UMS)
- Ionized jet deposition
- Cathodic arc deposition

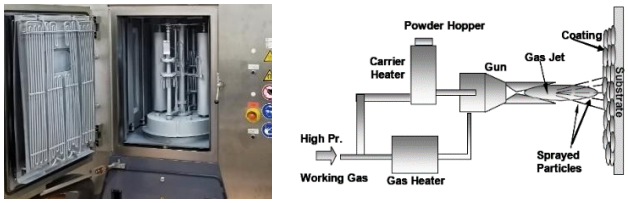

Figure 2. Picture of UMS deposition chamber and schematic of a cold spray deposition process

The deposited and studied coatings are – Cr, CrN, Cr_xN_y, ZrSi-Cr, MAX phases, TiN, CrAl, FeCrAl low alloy, FeCrAl high alloy, Mo, Mo+FeCrAl, Cr+CrN, and their combinations. The coatings were chosen based on evaluation metrics that take into account neutronics, physical and chemical compatibility, corrosion/oxidation performance, melting point, etc. The micrographs shown in Figure 3 illustrate several types of Zr-coated cladding materials in as-deposited and oxidized states.

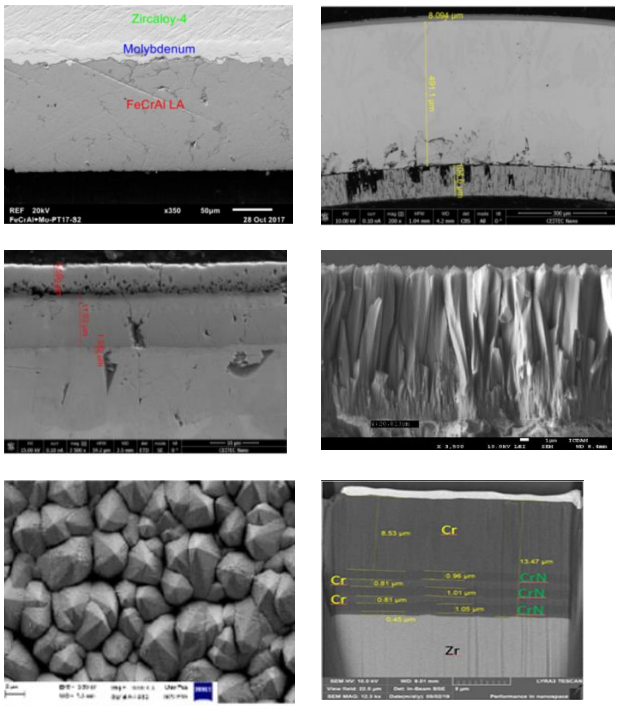

Figure 3. Micrographs of coated Zr using different coating materials and deposition techniques

D. Advanced materials

The second group of studied ATF cladding materials is based on a complete replacement of Zirconium-based tubes. Three concepts were studied – FeCrAl (B136Y type), SiC, 42XHM [16], and AISI 348 [17]. These concepts were produced by partners outside of CTU. The pictures in Figure 4 show the appearance and micrographs of these cladding concepts before and after testing.

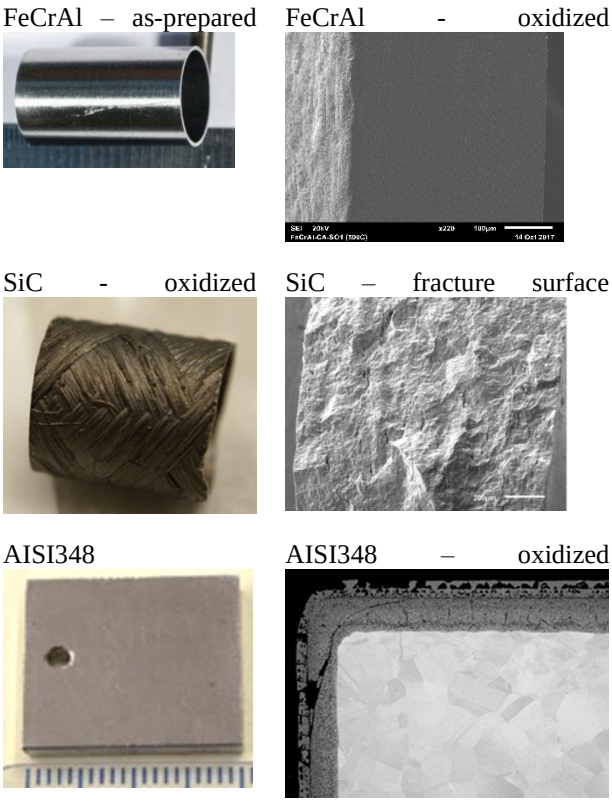

Figure 4. As-prepared and oxidized advanced cladding materials

III. RESULTS

Extensive experimental testing followed by modeling and simulation was performed. The chapter summarizes the main findings relevant to both normal operation and accidental scenarios.

A. Corrosion testing (Nominal operation)

Materials that form stable and protective oxides at LWR operating conditions proved to significantly reduce corrosion kinetics, e.g., chromia forming materials such as FeCrAl or Cr coatings. On the other hand, materials containing elements that are unstable in the LWRs conditions such as Al or Si do not form stable protective oxides in LWR chemistry (e.g. Ti), This leads to dissolution of the coatings, complete oxidation, or spallation [18]. Corrosion kinetics in VVER chemistry is shown in Figure 5.

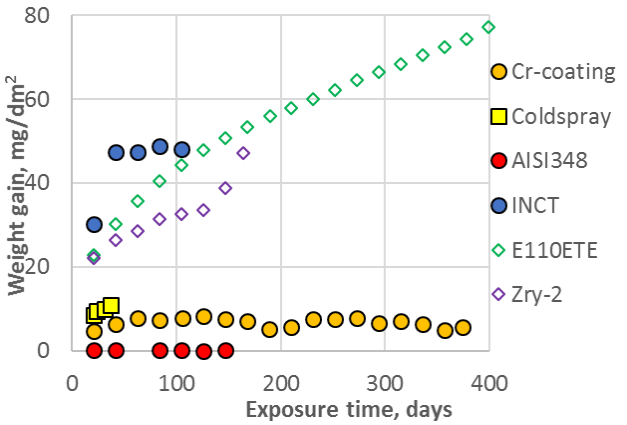

Figure 5. Corrosion kinetics of ATF materials in simulated VVER environment for different ATF candidate materials

Interestingly, corrosion of Zr-based alloys is also indirectly responsible for hydrogen pickup. A certain fraction of hydrogen released during the corrosion reaction is absorbed by Zr. This effect is affected by applied coatings and, for example, in the case of ZrSi-Cr coatings, the hydrogen pickup increases by an order of magnitude.

B. Creep

Creep of all materials is different compared to Zr. Even thin several micron thick coatings affect creep rates both at operating and accidental temperatures. For nominal operation, the slower creep rate might affect the fuel rod design due to different times of pellet/cladding gap closure. At accidental conditions, the reduced creep rate is beneficial in reducing the risk of fuel dispersion or limiting inner oxidation after cladding burst. A comparison of uncoated and Cr cold spray coated Opt. ZIRLO™ after high-temperature creep tests is shown in Figure 6. [19], [20]

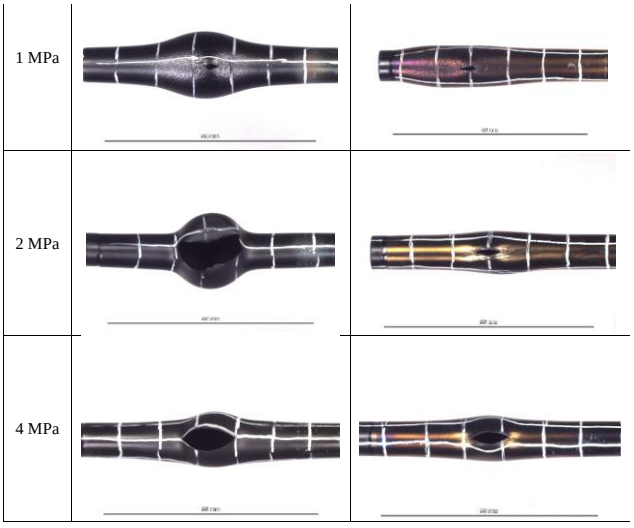

Figure 6. Visual analysis of Cr cold spray coated Opt. ZIRLO™ after high-temperature creep test and bursts. Reduction of deformation of the coated samples is clearly visible.

C. Material interaction

New materials introduced in a reactor core might lead to new material interactions. For example, iron forms low-temperature eutectics with Zirconium, which accelerates melting and degradation.

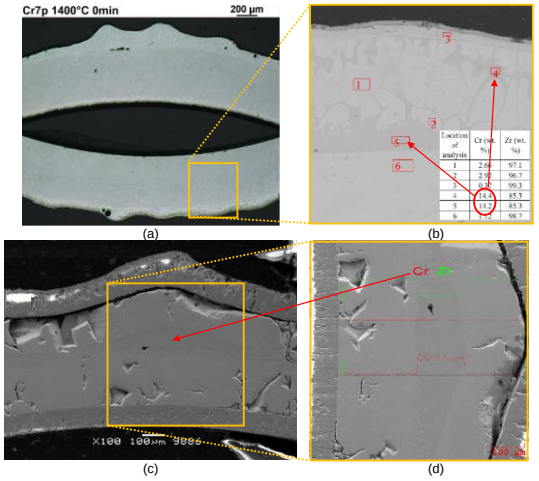

Figure 7. Post-test appearance showing Cr-Zr interactions above 1330°C with accelerated degradation

As the most promising concept, Cr coated Zr was studied in detail and it was found that the interaction between Cr and Zr leads to additional embrittlement of Zr due to Cr interdiffusion and precipitation. Additionally, at around 1330°C the eutectic forms and initiates melting and accelerated degradation of the cladding concept. The post-tech characterization of Cr-coated cladding after a test at 1400°C is shown in Figure 7.

D. High-temperature oxidation (Accidental conditions)

High-temperature oxidation resistance is crucial for cladding performance in postulated and severe accidents. For that reason, it has been extensively studied by many groups. It was found that weight gain should not be used as a sole parameter for oxidation resistance evaluation and needs to be combined with other measurements such as H-release or mechanical tests. [19], [21]

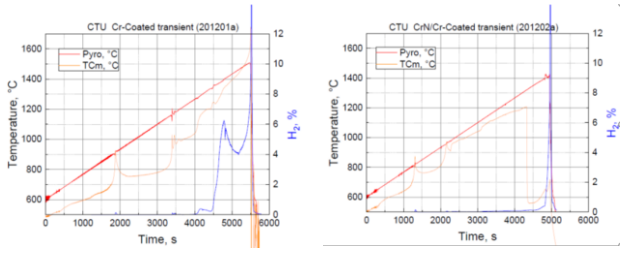

Figure 8. High-temperature oxidation ramp test from 600°C to 1450°C showing the benefits of the double Cr/CrN coating layer due to delay in the eutectic formation.

To confirm the fuel rod response in hypothetical accidental scenarios, single rod ramp tests were done confirming negligible oxidation kinetics until temperatures around 1300°C which is beneficial compared to reference uncoated Zirconium-based alloys. Figure 8 shows the results of the single rod tests with delayed material interaction due to the application of the CrN interlayer.

IV. DISSCUSION AND CONCLUSIONS

ATF materials are subject to active investigation around the world with substantial funding and interests of utilities,

international agencies, and industry. Industrial users focus on ATF features that are linked to potential improvements in economic performance, whereas other institutes might be interested mainly in improved accidental tolerance.

Several ATF concepts have been studied at CTU as a part of development or qualification. The main high-level conclusions from the extensive experimental testing are:

- It is difficult to find a material combination that would perform better in all required conditions. Some concepts bring significant benefits in accidental scenarios but might open new serious issues in nominal operating conditions, e.g., SiC/SiC.
- There are clear benefits proven by some of the advanced concepts, e.g., Cr coated Zr and FeCrAl, such as improved creep behavior, corrosion kinetics, and high-temperature oxidation. On the other hand, their implementation brings new challenges such as material interactions, higher neutron absorption, lower melting point, or tritium release.
- There are new failure mechanisms and phenomena such as embrittlement mechanisms, hydrogen pickup mechanism, and radiation damage that are not addressed in the current safety evaluation approach and by current safety criteria and needs to be resolved.

Irradiation testing in commercial reactors of several advanced cladding concepts started in 2019 in commercial reactors around the world, with dozens of concepts being still studied.

V. References

[1] K. A. Terrani, "Accident tolerant fuel cladding development: Promise, status, and challenges," *J. Nucl. Mater.*, vol. 501, pp. 13–30, Apr. 2018, doi: 10.1016/j.jnucmat.2017.12.043.

[2] S. Bragg-Sitton, "Development of advanced accident-tolerant fuels for commercial LWRs," *Nucl. News*, vol. 57, no. 3, p. 83, 2014.

[3] OECD/NEA, *State-of-the-Art Report on Light Water Reactor Accident-Tolerant Fuels*, vol. 2018. Organisation for Economic Co-Operation and Development.

[4] R. B. Adamson, Ed., *Zirconium Production and Technology: The Kroll Medal Papers 1975–2010*. 100 Barr Harbor Drive, PO Box C700, West Conshohocken, PA 19428-2959: ASTM International, 2010.

[5] B. R. Frost, *Nuclear Fuel Elements: design, fabrication and performance*. Elsevier, 2013.

[6] N. P. Neureiter *et al.*, "Lessons learned from the Fukushima nuclear accident for improving the safety of US nuclear plants," *Natl. Acad. Sci.*, 2014.

[7] F. Tanabe, "Analyses of core melt and re-melt in the Fukushima Daiichi nuclear reactors," *J. Nucl. Sci. Technol.*, vol. 49, no. 1, pp. 18–36, Jan. 2012, doi: 10.1080/18811248.2011.636537.

[8] S. J. Zinkle, K. A. Terrani, J. C. Gehin, L. J. Ott, and L. L. Snead, "Accident tolerant fuels for LWRs: A perspective," *J. Nucl. Mater.*, vol. 448, no. 1–3, pp. 374–379, May 2014, doi: 10.1016/j.jnucmat.2013.12.005.

[9] J. Carmack, F. Goldner, S. M. Bragg-Sitton, and L. L. Snead, "Overview of the U.S. DOE Accident Tolerant Fuel Development Program," Idaho National Laboratory (INL), INL/CON-13-29288, Sep. 2013. Accessed: Apr. 06, 2018. [Online]. Available: https://www.osti.gov/biblio/1130553.

[10] M. Sevecek and M. Valach, "Evaluation Metrics Applied to Accident Tolerant Fuel Cladding Concepts for VVER Recators," *Acta Polytech. CTU Proc.*, no. 4, pp. 89–96, 2016.

[11] S. Bragg-Sitton, "Advanced LWR Nuclear Fuel Cladding System Development Technical Program Plan," *Light Water React. Sustain. Program US Dep. Energy Ida. Falls ID Ida. Natl. Lab.*, 2012.

[12] J. Krejčí *et al.*, "EXPERIMENTAL BEHAVIOR OF CHROMIUM-BASED COATINGS," *Top Fuel 2018 - React. Fuel Perform.*, vol. 2018, p. 13, 9. - 4.10 2018.

[13] J. Krejčí, M. Ševeček, L. Cvrcek, J. Kabátová, and F. Manoch, "Chromium and Chromium Nitride Coated Cladding for Nuclear Reactor Fuel," presented at the EUROCORR 2017, Prague, Czech Republic, 2017.

[14] J. Krejčí *et al.*, "Development and testing of multicomponent fuel cladding with enhanced accidental performance," *Nucl. Eng. Technol.*, vol. 52, no. 3, pp. 597–609, 2020.

[15] M. Ševeček *et al.*, "Development of Cr cold spray–coated fuel cladding with enhanced accident tolerance," *Nucl. Eng. Technol.*, vol. 50, no. 2, pp. 229–236, Mar. 2018, doi: 10.1016/j.net.2017.12.011.

[16] A. Chalupová, M. Steinbrück, M. Grosse, J. Krejčí, and M. Ševeček, "HIGH-TEMPERATURE OXIDATION OF CHROME-NICKEL ALLOY," *Acta Polytech. CTU Proc.*, vol. 28, pp. 8–14, Dec. 2020, doi: 10.14311/APP.2020.28.0008.

[17] *Analysis of options and experimental examination of fuels for water cooled reactors with increased accident tolerance (ACTOF)*. Vienna: INTERNATIONAL ATOMIC ENERGY AGENCY, 2020.

[18] M. Ševeček *et al.*, "Round Robin Exercise of the Candidate ATF Cladding Materials Within the ACTOF Project [in press]," in *Top Fuel 2019, American Nuclear Society, Seattle, WA, September, 22-26*, 2019, pp. 283–290.

[19] A. Chalupová *et al.*, "COATED CLADDING BEHAVIOR DURING HIGH-TEMPERATURE TRANSIENTS," *Acta Polytech. CTU Proc.*, vol. 24, Dec. 2019, doi: 10.14311/APP.2019.24.0009.

[20] M. Ševeček, K. Shirvan, and R. G. Ballinger, "STUDY OF THERMAL CREEP OF COATED CLADDING MATERIALS," *Acta Polytech. CTU Proc.*, vol. 19, no. 0, pp. 22–29, Dec. 2018, doi: 10.14311/APP.2018.19.0022.

[21] G. Bourdon, M. Ševecek, J. Krejčí, and L. Cvrček, "HIGH-TEMPERATURE STEAM AND AIR OXIDATION OF CHROMIUM-COATED OPTIMIZED ZIRLO™," *Acta Polytech. CTU Proc.*, vol. 24, Dec. 2019, doi: 10.14311/APP.2019.24.0001.

Proceedings of the European Nuclear Young Generation Forum
ENYGF'21
September 27-30, 2021, Tarragona, Spain

Fabrication and Development of Self-glowing Crystals for Safe Actinide Handling

Ipatova, Iuliia[1*], Burakov, Boris[2]

[1] School of Metallurgy and Materials, University of Birmingham, United Kingdom, [2] V.G. Khlopin Radium Institute, Russia

*Corresponding author: i.ipatova@bangor.ac.uk; i.ipatova@bham.ac.uk

I. INTRODUCTION

The idea to convert the energy released as a result of radioactive decay into electricity, heat, or optical radiation is very feasible. Solid radioactive crystals doped with actinides have been a subject of the current research. Crystalline materials, such as zircon, with high chemical resistance, mechanical durability, and stability under self-irradiation are considered for the development of a new generation of radio-luminescence emitters [1-3]. To form environmentally friendly long-served light-emitters we have suggested incorporating the actinides and non-radioactive luminescence ions in the common durable crystalline matrix in the form of a solid solution. These crystals were reported to have specific intensive glow in the dark which can be used as advanced materials for their applications in robotic systems, medicine as well as advantageously, the intensive radio-luminescence can be converted into electric current.

This may foster development of reliable "nuclear" batteries for long-term use in the cosmogenic environment. The advantages of the proposed battery concepts are a result of the consistent power generation, not the efficiency of conversion, which allows their use in sensor system developed specifically for extreme environments and/or in space microelectronics. The power of the nuclear battery is expected to reach a few to several hundred milliwatts. Higher power can be achieved via connecting several batteries in a parallel chain.

The current research summarizes results on synthesis and study of various single zircon crystals doped with different concentrations of the actinides (^{238}Pu, ^{241}Am, ^{237}Np) and non-radioactive luminescence ions (Tb and/or Eu). The ^{238}Pu content was 0.02 wt.% and the Tb/Eu concentration varied between 0.2 and 0.3 wt.%.

II. EXPERIMENTAL

Zircon is known as a particularly resistant material, unique in its properties, such as high chemical, mechanical and radiation resistance in combination with a large capacity of the crystal structure to the introduction of actinides. The single zircon crystals were synthesized by the flux method [4] at temperature 1070°C in Pt-crucibles using a starting precursor that is based on MoO_3. The flux method has the advantage of allowing the rapid synthesis of zircon crystals of ~1 mm in size. Some crystals were selected from each batch, mounted in epoxy resin, polished and coated with carbon for electron microprobe analysis (EMPA) and Cathodoluminescence investigations (CL). CL method allows for the identification of the optimal amount and type of luminescence ion(s) embedded in any non-radioactive crystals.

Table 1. Principal features of self-glowing zircon crystals

Simplified zircon formula	Average content of luminescence ion, wt. %	Content of actinide, wt. %	Relative intensity of self-glowing
$(Zr,Tb,Pu)(Si,P)O_4$	Tb – 0.2-0.3 (optimal content confirmed by CL method)	^{238}Pu – 0.02	very high
$(Zr,Eu,Pu)(Si,P)O_4$	Eu – 0.1	^{238}Pu – 0.02	weak
	Eu – 0.1	^{238}Pu – 0.01	weak
	Eu – 0.3 (optimal content confirmed by CL method)	^{238}Pu – 0.01	high
$(Zr,Eu,Pu)(Si,P)O_4$	Eu – 0.1	^{238}Pu – 0.01	weak
$(Zr,Am,Np)SiO_4$	no	^{237}Np – 0.35; ^{241}Am – 0.01	weak
$(Zr,Np)SiO_4$	no	^{237}Np – 1.9	no
$(Zr,Tb,Eu,Am)(Si,P)O_4$	Tb – 0.2-0.3 Eu – less 0.1	^{241}Am – 0.002	weak

The key idea is to incorporate non-radioactive luminescence ions and a selected radionuclide as an impurity within a radiation-tolerant zircon crystal lattice. As the crystal doped with luminescence ions has already luminescent properties, the radiation emitted by the addition of alpha radionuclide causes the crystal to 'self-glow'. The light that is emitted by the self-glowing crystal can be converted into an electric current by the means of a photoelectric converter (e.g., a photodiode operating in photovoltaic mode) and can be used to measure the intensity of the emitting radiation.

Radioluminescence can be excited by different types of ionizing radiation, but for our purposes the use of alpha radiation is preferable due to the smallest alpha decay energy loss. The penetration depth of alpha particles with energy about 5 MeV in solids does not exceed the first dozens of microns. The energy of alpha radiation is preserved mainly inside the crystal matrix. Alpha particles with energy 5.59 and 5.5MeV are released during the decay of ^{238}Pu and ^{241}Am, respectively [5]. Due to elastic and inelastic collisions with atoms of the matrix alpha particles lose their energy, forming radiation defects (displacement of the matrix atoms), exciting electronic system, and generating heat (phonon formation).

Past experimental experience has allowed to establish that the highest degree of self-glowing from zircon crystals occurred when doped with a ^{238}Pu admixture not exceeding 0.02wt% [1]. Excessive radionuclide concentrations in solid solution suppress luminescence, lead to the destruction of the crystal structure and reduce environmental safety of the self-glowing material. Non-optimal concentrations (excess and insufficient) of a luminescent ion will not allow the achievement of intense self-luminescence. At present this concentration (or that of the sensitization pair) remains unclear. A key aim of the work is to identify the optimal balance between concentrations of luminescent species and a radionuclide.

A. Non-radioactive crystals

The non-radioactive crystals with an optimal addition of luminescence ions can be used as starting precursors for the synthesis of self-glowing crystals containing actinides. The luminescence ions were added into the flux in a form of oxides (Tb_4O_7, Eu_2O_3).

The basic features of the luminescence of various ions (Tb^{3+}, Eu^{3+}, Ce^{3+}, etc.) in solid crystalline materials and glasses have been broadly studied in the past. Also sensitized luminescence was studied via luminescence enhancement in pairs of the type Eu^{3+}+Tb^{3+} or Ce^{3+}+Eu^{3+}. The luminescence of the same luminescent ions is different depending on the host material. The goal of the proposal is to use the well-known luminescent ions and their sensitization pairs based on the fundamental understanding of the luminescence mechanisms and to find the optimal concentration providing the maximum luminescence of zircon.

The first task was to select the most promising activators - luminescence centers via synthesis of concentration series of scintillator crystals, determining the optimal concentrations of activators. **Figure 1** shows the optical microscope images of the synthesized crystals with the highest intensity of the luminescence in UV.

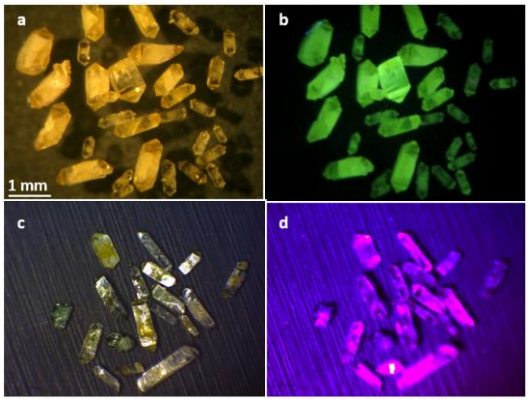

Fig.1 Zircon crystals Zr,TbSiO$_4$ and Zr,EuSiO$_4$: a, c – in normal light; b, d – in UV showing intense green and pink luminescence respectively

The CL images were obtained to understand the correlation between chemical composition and the CL intensity even in heterogeneous zoned crystals (**Fig. 2**).

It is very difficult to incorporate essential amount of Tb into zircon crystal structure substituting Zr. Also, Tb incorporated into zircon can be in two valence states: (3+) and (4+) but only trivalent Tb^{3+} are luminescence ions. Admixture of phosphor (P) may support incorporation of trivalent lanthanides into zircon structure due to charge compensation.

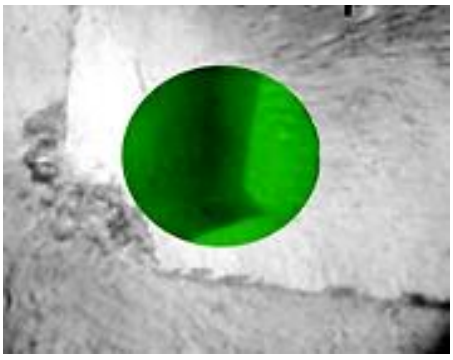

Fig.2 Cathodoluminescence image of valence – zoned non-radioactive zircon crystal doped with Tb (Zr,TbSiO$_4$) *(diameter of electron beam 100 μm)*

B. Actinide-doped crystals

Actinide contents in the crystals were measured by precise gamma-spectroscopy using a Ge detector with Schlumberger EGP 20P11A. The relative self-glowing intensity of the different radioactive samples was evaluated visually (**Fig. 3, 4**). The principal features of synthesized crystals are summarised in Table I.

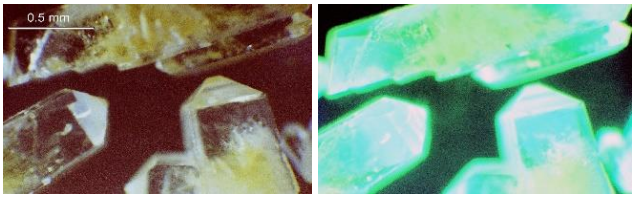

Fig. 3 Self-glowing crystals of zircon, (Zr,Tb,Pu)SiO$_4$, doped with 0.2-0.3 wt. % Tb and 0.02 wt. % ^{238}Pu, under binocular a) in the light and b) glowing in the dark

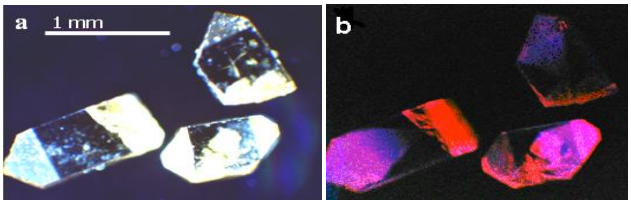

Fig. 4 Crystals of zircon (Zr,Pu,Eu)(Si,P)O_4, doped with 0.3 wt. % Eu and 0.01 wt. % ^{238}Pu, under binocular: a) in the light and b) self-glowing in the dark

This research confirmed that actinide-doped zircon, is prospective materials not only for ceramic waste forms but also for the development of durable and safe radioactive light-emitters used in nuclear batteries which can be used for a very long time (several decades as a minimum) before their final disposal in the initial form (without reprocessing).

III. CONCLUSION

The study is a steppingstone in the understanding of selected host-phase resistance to self-irradiation damage and chemical alteration processes over long periods of time which is in paramount importance during immobilisation of actinide-bearing wastes of complex chemical composition.

The following results were obtained:

1. Intensively glowing crystals of zircon were successfully obtained. Contents of ^{238}Pu or ^{241}Am didn't exceed 0.1wt.%.
2. The most durable and intensively self-glowing actinide-doped crystals of zircon, (Zr,Tb,Pu)(Si,P)O_4, were successfully synthesized by the flux method. Contents of ^{238}Pu, Tb, and P were (in wt.%): 0.02; 0.2 to 0.3; 0.2 to 0.3, respectively.
3. A small addition of Zr-phosphate to the flux supports Tb incorporation into zircon lattice and stabilizes preferably Tb3+.
4. Crystals doped with ^{237}Np or ^{239}Pu were not characterized by a self-glowing effect.

IV. REFERENCES

[1] B.E. Burakov, Y.V. Domracheva, M.V. Zamoryanskaya, et al. J. Nucl. Mater., 2009, 385.

[2] B.E. Burakov, M.V. Zamoryanskaya, Y.V. Domracheva, Mat. Res. Soc. Symp. Proc. *Scientific Basis for Nuclear Waste Management XXXIII*, 2009, 1193.

[3] B.E. Burakov, M.I. Ojovan, W.E. Lee, Crystalline materials fo actinide immobilization. Imperial College Press, Materials for Engineering, 2010, Vol.1.

[4] J.M. Hanchar, B.E. Burakov, E.B. Anderson, M.V. Zamoryanskaya, Mat. Res. Soc. Symp. Proc. *Scientific Basis for Nuclear Waste Management XXVI*, 2003, 757.

[5] Audi, G., Wapstra, A. H., &Thibault, C. 2003. *The AME2003 atomic mass evaluation:(II). Tables, graphs and references.* Nuclear physics A, 729(1), 337-676

Proceedings of the European Nuclear Young Generation Forum
ENYGF'21
September 27-30, 2021, Tarragona, Spain

Quantifying the benefits of the reduced oxidation kinetics in chromium-coated cladding: a parametric study

Cozzo, Cedric[1*], Lind, Terttaliisa[1], Bertsch, Johannes[2], Nichenko, Sergii[3], Girardin, Gaëtan[4]

[1]Paul Scherrer Institut (PSI), Laboratory for Reactor Physics and Thermal-Hydraulics, Forschungsstrasse 111, 5232 Villigen, Switzerland,
[2]Paul Scherrer Institut (PSI), Laboratory for Nuclear Materials, Forschungsstrasse 111, 5232 Villigen, Switzerland
[3]Paul Scherrer Institut (PSI), Laboratory for Scientific Computing and modelling, Forschungsstrasse 111, 5232 Villigen, Switzerland
[4]Kernkraftwerk Goesgen-Daeniken AG, CH-4658 Daeniken, Switzerland

*Corresponding author: cedric.cozzo@psi.ch

I. INTRODUCTION

Zircaloy cladding can be coated in order to increase the performance of the material in normal and accidental conditions. This results in a high reduction of the corrosion kinetics not only in operating conditions but also in higher temperatures such as during a loss of coolant accident (LOCA). This accident tolerant fuel (ATF) has already reached a high technology readiness level [1] and is considered as one of the near-term ATF candidates by several fuel vendors [2]–[4]. In particular, coating the cladding substrate with the less reactive chromium metal is supported by the industry and research institutions in many countries, and samples, lead-test rods as well as lead-tests assemblies have been or are being irradiated [5]–[7]. Based on corrosion experimental data, ATF claddings oxidation behaviour of ATF rods has been simulated during a LOCA transient with a fuel performance code. The performance of the ATF is compared to that of zircaloy-4 (Zr4).

II. LITERATURE SURVEY

Several documents have reviewed the expected benefits of ATF and provided a list of already published results as well as past and ongoing irradiation programmes. One can cite Terrani's paper [8], the NEA EGATFL reports [1] or the more recent reports from the IAEA [9] and the NEA [10]. Other publications have a stronger focus on chromium-coated zirconium alloys, e.g. Geelhood's report [11], as well as the articles by Chen, Tang or Lee [12]–[14]. Regarding the performance of the coated cladding, the fabrication process and consumption rate are of paramount importance.

A. Fabrication

The fabrication process of the cladding is important as the coating should be dense and adhering well to the substrate. Indeed, cracks could nullify the corrosion benefit of the cladding. A decohesion between the coating layer and the substrate could cause a drop in the effective thermal conductivity of the cladding and lead to delamination in particular. According to several studies, the coating processes used in the last five years resulted in a good bonding of the chromium on the zirconium alloy substrate [15], [16].

In this paper, results for Physical Vapour Deposition (PVD) and Cold Spray (CS) are considered. While PVD allows for deposition of thin films (10-15 µm), CS allows for higher manufacturing rates. The thicker films obtained with CS are later reduced (down to 50 µm) by polishing.

B. Corrosion protection and consumption rate

The presence of a thin layer (about 15 µm) of protective metal drastically reduces the oxidation rate of the cladding in operating and accident conditions (up to approx. 1583 K).

Weight gain and oxidation in steam at low temperature (415-500 °C), representative of operating conditions (i.e. pressurized water at operating temperatures), have been published by e.g. Ševeček [15] and Brachet [16]. The reported weight gain is between approx. 6 and 50 times lower than that of Zr4. These values have been used for calibration of the low-oxidation kinetics.

In the high temperature regime, the consumption rate by oxidation in high temperature steam is based on the published results by Yeom [17] and Brachet [18] for CS and PVD coated samples, respectively. The derived constants A and B of the oxidation rate, based on the published data, are shown in Table 1, where K_p is the parabolic rate constant in $\mu m^2 \cdot s^{-1}$ and the oxide layer thickness X_{oxide} in µm can be calculated with the following equations:

$$K_p = A \cdot exp\left(-B \cdot \frac{10^4}{T}\right)$$

$$X_{oxide} = \left(K_p \cdot t\right)^{1/2}$$

The transition temperature between low and high temperature chromium oxidation mechanisms is set to 623 K, based on Hope's study [19]. The continuity at the transition temperature of the two proposed extrapolated high-temperature oxidation rates with the lower oxidation model used for the study (EPRI/SLI) has been verified.

Volatilization of Cr can be neglected according to [18]. Based on observations by Brachet for tests at 1200 °C, an equal amount of coating is consumed by diffusion into the substrate and by outer chromia scale formation [16], therefore the consumption of Cr by diffusion is set equal to that of oxide scale formation.

Table 1. Oxidation rate constants A and B for Cr-coated claddings in high temperature regimes derived from published data.

Source	Temperature range [K]	A	B
Yeom [17]	1403-1583	268.94	1.499
Brachet [18]	1273-1473	168797	2.321

C. Other properties

Given the relatively low thickness of the coating, the mechanical properties of the coated cladding can be considered unchanged from those of the bulk material considering, when applicable, a reduction of the bulk wall thickness. Besides its highly superior oxidation properties, studies show that coating the cladding can bestow it with superior behaviour, such as wear [20] or wettability [21].

Thin coatings have been proven not to notably modify the core physics in LWRs [22]. However, new phenomena have to be considered before the ATF produced can be licensed [10]. These include for example the hydrogen behaviour, nitridation and interdiffusion.

III. SIMULATION

A. Fuel performance code

The thermo-mechanical simulation of the PWR fuel rod is performed with the EPRI fuel performance code Falcon [23]. The code version is a development version based on Falcon 1.5.

Falcon is a state-of-the-art analysis code designed to calculate behavior of a single LWR fuel rod under normal operation, operational power manoeuvres, and transients/postulated accidents. The code is built on a 2-dimensional finite element formulation of fully coupled time dependent thermal and mechanical modules. Full-length fuel rod analyses are performed using an axisymmetric R-Z (radial-axial) representation. The modelled fuel rod consists of two plugs at top and bottom locations, upper- and lower- gas plenums, fuel stack, gap elements and cladding element separating the fuel from the coolant. The rod was divided axially into 32 fuel elements, plus 1 upper- and 1 lower- plenum and plugs. Radially, the rod was modelled with 5 fuel element columns, 1 gap element and 5 cladding element columns.

As far as ATF is concerned, the release version of Falcon offers several models related to SiC, which have been extended by research developments at PSI [24] along with a U_3Si_2 fuel section [25]. Since PSI is part of the Falcon development team, the code has been modified in order to allow a reduced oxidation rate offered by the coating on the zirconium alloy. The results obtained with the ATF concepts are then compared against those obtained with the reference cladding Zr4. The reference Zr4 oxidation model used in Falcon for PWR rods is the EPRI/SLI model.

B. Base irradiation and LOCA transient

Two rods have been considered for the base irradiation (BI): a one-cycle rod and a five-cycle rod have been studied to account for the oxide layer thickness built during the BI. A power shape and linear heat generation rate representative of a Swiss Pressurised Water Reactor (PWR) rod have been used.

A hypothetical and conservative Large Break LOCA (LB-LOCA) is simulated in this study. The boundary conditions used for the simulation are the inlet pressure and the cladding outer surface temperature of the hottest rod. The inlet pressure and peak cladding temperature (PCT) are plotted in Figure 1.

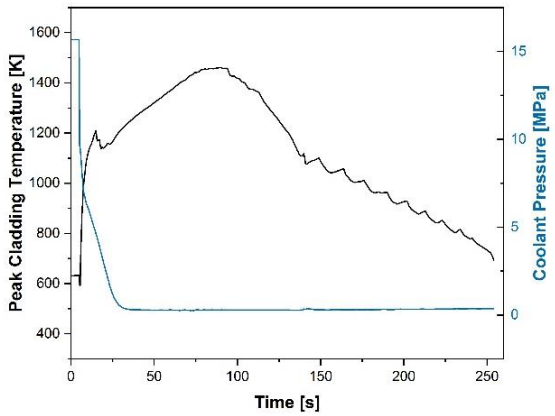

Figure 1. PCT and core pressure during the transient.

C. Failure criteria

A Zr-Cr eutectic reaction occurs at 1606 K. Since this temperature is lower than the Cr melting point, reaching this eutectic is therefore considered as a cladding failure. As far as the conventional Zr4 is concerned, the failure criteria of the NRC guide [26] are used, i.e. the hydride-dependent equivalent cladding reacted (ECR) and the maximum Zr4 peak cladding temperature (PCT) is set to 1477 K.

The consumption of the coating material also needs to be taken into account, in particular at high temperatures, i.e. beyond the transition temperature up to eutectic point. A full consumption by oxidation (or dissolution, wearing) of the coating would expose the substrate to the corrosive environment. Efficient corrosion protection is assumed for

coating thicknesses down to 5 μm [11], this value is therefore defined as a failure criterion. This value is also used to account for the intermetallic layer that is a couple of microns thick. This is conservative since the bulk still needs to undergo oxidation before the cladding actually fails.

IV. RESULTS

A. Base irradiation

The maximum calculated oxide layer thickness for Zr4 rods at the end of the base irradiation is shown in Table 2. As expected, the corrosion is greatly reduced with chromium. The H-pickup in Table 2 is calculated with the NRC model (15.3% for Zr4 [27]), which has been validated against numerous irradiated Zr4 claddings. Concerning Cr-coated claddings, corrosion experiments representative of nominal PWR conditions [9] concluded in similar H-contents for Zr4 and Cr-coated Zr4.

Table 2. Oxidation layer thickness and corresponding H-content at end of BI.

Burnup [MWd/kg$_U$]	Data used for oxidation kinetics [-]	Oxide layer thickness [μm]	H-content [wppm]
14.4	Falcon (Zr4)	5.4	36
	[15] (ATF)	2.8	18
	[16] (ATF)	0.7	5
59.5	Falcon (Zr4)	74.7	564
	[15] (ATF)	12.1	82
	[16] (ATF)	1.5	10

B. LOCA transient

In the selected scenario, the maximum PCT reached is approx. 1460 K, which is below both failure criteria of the Zr4 and the ATF claddings. However, the temperature margin to failure is extended from 17 to 146 K for the Zr4 and the Cr-coated cladding, respectively.

Table 3. Oxidation layer thickness and corresponding H-content at end of BI. The two oxidation kinetics correspond to the low and high temperature models.

Burnup [MWd/kg$_U$]	Data used for oxidation kinetics [-]	Post-transient oxide layer thickness / ECR [μm / %]	H-content [wppm]
14.4	EPRI/SLI-Cathcart	22.2 / 3.1	154
	[15]-[17] (ATF)	2.9 / 0.4	19
	[16]- [18] (ATF)	1.2 / 0.2	8
59.5	EPRI/SLI-Cathcart	77.7 / 10.7	590
	[15]-[17] (ATF)	12.1 / 1.7	82
	[16]- [18] (ATF)	1.8 / 0.2	12

The final calculated maximum oxide layer thickness, the ECR and the H-content for each case is reported in Table 3. Considering the current coating thicknesses of commercial Cr-coated Zr4 (between 50 and 10 μm for CS and PVD, respectively), the remaining chromium layer remains above 5 μm and is therefore assumed protective. This means that none of the considered ATF concepts simulated here would fail due to chromium consumption. As far as the one-cycle rod is concerned, the oxide layer thickness of the Zr4 cladding has increased by more than 22 μm during the LOCA compared to a few microns for the ATF claddings. However, the rod is expected to survive the transient with all types of cladding. Regarding the high exposure rod, the Zr4 cladding has reached an ECR of 10.7 %. Combined with the hydrogen value of 590 wppm, this rod does not fulfil the NRC criterion. On the other hand, the low oxide layer thickness calculated with the ATF claddings would allow it to survive the transient. This would also be the case even if the H-content of the ATF claddings was assumed similar to that of the Zr4 cladding (i.e. 590 wppm).

V. CONCLUSIONS

In this paper, a literature survey of Cr-coated cladding has been carried out. The latest ATF-related developments of the fuel performance code Falcon have been presented.

A methodology has been presented which includes several failure criteria such as: Zr-Cr eutectic temperature, coating consumption and embrittlement of the cladding bulk by H-ingress. While the transient was not severe enough to quantify an increase in coping time, i.e. no ATF failure, the ATF claddings (manufactured by CS or PVD) have demonstrated a superior behaviour for the considered criteria. In operating conditions, the consumption of cladding material is greatly reduced by a protective chromium coating. This has a direct consequence in the proposed LB-LOCA scenario where a high exposure ATF cladding survives the transient unlike Zr4. The margin to maximum temperature is also increased by more than 100 K.

However, it should be mentioned that the oxidation models have been used down to 623 K, which is much lower than the experimental range. The completeness of the models depends on the availability of experimental data in the 750-1100 K range. The implementation of the energy release by Cr oxidation (instead of Zr) in Falcon is foreseen.

VI. ACKNOWLEDGMENTS

This work has been financed by the swissnuclear/PSI project ‘MOCH-ATF’.

VII. References

[1] K. Pasamehmetoglu *et al.*, ‘State-of-the-Art Report on Light Water Reactor Accident-Tolerant Fuels’, OECD/NEA, 7317, 2018. Accessed: Dec. 11, 2018. [Online]. Available: https://www.oecd-nea.org/science/pubs/2018/7317-accident-tolerant-fuels-2018.pdf.

[2] J. Bischoff *et al.*, 'AREVA NP's enhanced accident-tolerant fuel developments: Focus on Cr-coated M5 cladding', *Nucl. Eng. Technol.*, vol. 50, no. 2, pp. 223–228, Mar. 2018, doi: 10.1016/j.net.2017.12.004.

[3] Y. P. Lin and R. M. Fawcett, 'Path towards industrialization of accident tolerant fuel', presented at the Top Fuel 2018, Prag, Czech Republic, Sep. 2018, [Online]. Available: https://www.euronuclear.org/archiv/topfuel2018/fullpapers/TopFuel2018-A0141-fullpaper.pdf.

[4] H. Shah *et al.*, 'Westinghouse-Exelon EnCore® Fuel Lead Test Rod (LTR) Program including Coated cladding Development and Advanced Pellets', presented at the Top Fuel 2018, Prag, Czech Republic, 2018, [Online]. Available: https://www.euronuclear.org/archiv/topfuel2018/fullpapers/TopFuel2018-A0145-fullpaper.pdf.

[5] J. Bischoff *et al.*, 'PROtect: Accelerated Implementation of Framatome's Evolutionary eATF Solution', in *Top Fuel 2019*, Seattle, WA, USA, p. 109.

[6] R. L. Oelrich *et al.*, 'Overview of Westinghouse Lead EnCore® Accident Tolerant Fuel Program', presented at the Top Fuel 2019, Seattle, WA, USA, Sep. 2019, [Online]. Available: file://afs/psi.ch/project/stars/archive/EXT/PROC/SB-PROC-DAT-007-19/proc_v_n_pp192-196.pdf.

[7] G. Girardin, R. Meier, F. Jatuff, J. Bischoff, C. Delafoy, and E. Schweitzer, 'Inspection Capabilities and In-Pile Experience With Innovative and Enhanced Accident Tolerant Fuel Materials at KKG', presented at the Top Fuel 2018, Prag, Czech Republic.

[8] K. A. Terrani, 'Accident tolerant fuel cladding development: Promise, status, and challenges', *J. Nucl. Mater.*, vol. 501, pp. 13–30, Apr. 2018, doi: 10.1016/j.jnucmat.2017.12.043.

[9] 'Analysis of Options and Experimental Examination of Fuels for Water Cooled Reactors with Increased Accident Tolerance (ACTOF)', Jul. 15, 2020. https://www.iaea.org/publications/14691/analysis-of-options-and-experimental-examination-of-fuels-for-water-cooled-reactors-with-increased-accident-tolerance-actof (accessed Feb. 03, 2021).

[10] 'Applicability of Nuclear Fuel Safety Criteria to Accident Tolerant Fuel Designs (TOPATF report)', OECD/NEA, CSNI Technical Opinion Papers in revision-version v6, Oct. 2020.

[11] K. G. Geelhood and W. G. Luscher, 'Degradation and Failure Phenomena of Accident Tolerant Fuel Concepts; Chromium Coated Zirconium Alloy.', Pacific Northwest National Laboratory, PNNL-28437, Jan. 2019. Accessed: Mar. 13, 2019. [Online]. Available: https://www.nrc.gov/docs/ML1903/ML19036A716.pdf.

[12] H. Chen, X. Wang, and R. Zhang, 'Application and Development Progress of Cr-Based Surface Coatings in Nuclear Fuel Element: I. Selection, Preparation, and Characteristics of Coating Materials', *Coatings*, vol. 10, no. 9, Art. no. 9, Sep. 2020, doi: 10.3390/coatings10090808.

[13] C. Tang, M. Stueber, H. J. Seifert, and M. Steinbrueck, 'Protective coatings on zirconium-based alloys as accident-tolerant fuel (ATF) claddings', *Corros. Rev.*, vol. 35, no. 3, pp. 141–165, 2017, doi: 10.1515/corrrev-2017-0010.

[14] Y. Lee, J. I. Lee, and H. C. No, 'Mechanical analysis of surface-coated zircaloy cladding', *Nucl. Eng. Technol.*, vol. 49, no. 5, pp. 1031–1043, Aug. 2017, doi: 10.1016/j.net.2017.03.012.

[15] M. Ševeček *et al.*, 'Development of Cr cold spray–coated fuel cladding with enhanced accident tolerance', *Nucl. Eng. Technol.*, vol. 50, no. 2, pp. 229–236, Mar. 2018, doi: 10.1016/j.net.2017.12.011.

[16] J.-C. Brachet *et al.*, 'Early studies on Cr-Coated Zircaloy-4 as enhanced accident tolerant nuclear fuel claddings for light water reactors', *J. Nucl. Mater.*, vol. 517, pp. 268–285, Apr. 2019, doi: 10.1016/j.jnucmat.2019.02.018.

[17] H. Yeom, B. Maier, G. Johnson, T. Dabney, M. Lenling, and K. Sridharan, 'High temperature oxidation and microstructural evolution of cold spray chromium coatings on Zircaloy-4 in steam environments', *J. Nucl. Mater.*, vol. 526, p. 151737, Dec. 2019, doi: 10.1016/j.jnucmat.2019.151737.

[18] J.-C. Brachet *et al.*, 'High temperature steam oxidation of chromium-coated zirconium-based alloys: Kinetics and process', *Corros. Sci.*, vol. 167, p. 108537, May 2020, doi: 10.1016/j.corsci.2020.108537.

[19] G. A. Hope and I. M. Ritchie, 'Mechanism of chromium oxidation', *J. Chem. Soc. Faraday Trans. 1 Phys. Chem. Condens. Phases*, vol. 77, no. 11, pp. 2621–2631, Jan. 1981, doi: 10.1039/F19817702621.

[20] Ch. Delafoy, J. Bischoff, J. Larocque, P. Attal, L. Gerken, and K. Nimishakavi, 'Benefits of Framatome's E-ATF evolutionary solution: Cr-coated cladding with Cr2O3-Doped fuel', presented at the Top Fuel 2018, Prag, Czech Republic, Oct. 2018, [Online]. Available: https://www.euronuclear.org/archiv/topfuel2018/fullpapers/TopFuel2018-A0149-fullpaper.pdf.

[21] R. V. Umretiya, S. Vargas, D. Galeano, R. Mohammadi, C. E. Castano, and J. V. Rojas, 'Effect of surface characteristics and environmental aging on wetting of Cr-coated Zircaloy-4 accident tolerant fuel cladding material', *J. Nucl. Mater.*, vol. 535, p. 152163, Jul. 2020, doi: 10.1016/j.jnucmat.2020.152163.

[22] I. Younker and M. Fratoni, 'Neutronic evaluation of coating and cladding materials for accident tolerant fuels', *Prog. Nucl. Energy*, vol. 88, pp. 10–18, Apr. 2016, doi: 10.1016/j.pnucene.2015.11.006.

[23] EPRI, 'Fuel Analysis and Licensing Code: FALCON MOD01: Volume 1: Theoretical and Numerical Bases', EPRI, 2004. Accessed: May 18, 2020. [Online]. Available: https://www.epri.com/research/products/000000000001011307.

[24] C. Cozzo and S. Rahman, 'SiC cladding thermal conductivity requirements for normal operation and LOCA conditions', *Prog. Nucl. Energy*, vol. 106, pp. 278–283, Jul. 2018, doi: 10.1016/j.pnucene.2018.03.016.

[25] C. Cozzo, R. Ngayam-Happy, J.-C. Chen, M. Pecchia, and G. Girardin, 'Modeling of the U3Si2/SiC fuel system behaviour for a RIA scenario', presented at the Top Fuel 2019, Seattle, WA, USA, Sep. 2019.

[26] M. Bales, 'Establishing Analytical Limits for Zirconium-alloy Cladding Material', U.S. N.R.C. Regulatory Guide - Preliminary Draft DG-1263, Mar. 2014. [Online]. Available: https://www.nrc.gov/docs/ML1528/ML15281A192.pdf.

[27] P. M. Clifford, 'Acceptable Fuel Cladding Hydrogen Uptake Models', May 13, 2015.

Proceedings of the European Nuclear Young Generation Forum
ENYGF'21
September 27-30, 2021, Tarragona, Spain

International Research Centre MBIR

Solntseva, Ekaterina [1*], Alexander, Zagornov[2]

[1] Science and Innovation, Rosatom, Russian Federation; [2] Rosatom, Russia

**EkSeSolntseva@rosatom.ru*

I. RESEARCH REACTORS IN THE WORLD

Nuclear research reactors have contributed substantially to safety, innovation and increase in efficiency of the commercial nuclear power plants. They serve as centres for research, training and development of nuclear science and technologies and ensure the competitiveness of nuclear energy vs other energy sources.

The advanced reactor systems SMRs, Generation 4 reactor technologies require modern, powerful research infrastructure, based on high flux reactors with well-equipped laboratories for post-irradiation experiments and extended research options. Currently the world reactor fleet is inevitably aging. There are less than 250 operating research reactors in the world. The vast majority of them are approaching their decommissioning within the next couple of decades.

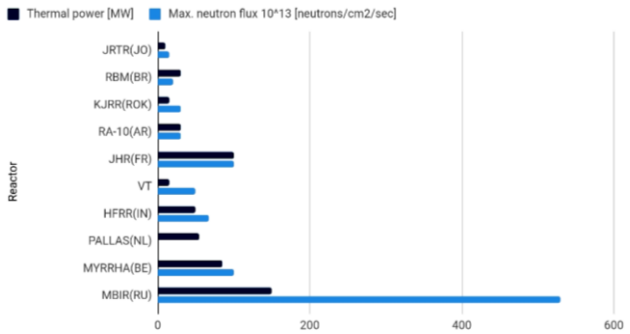

Figure 1. Characteristics of current research reactor projects

In the last decade's research reactors park is shrinking. The situation with fast neutron research reactors even worse: today there are only the Russian BOR-60 (60 MW), which is similar to the Chinese CEFR and the Indian FBTR (40 MW) operated.

There are only two modern reactors with high-flux and power over 100 MW under construction (JHR – thermal neutrons, MBIR – fast neutrons). Although it is possible to conduct certain experiments in the demonstrator reactors (such as BN-600), they are not suitable for a large number of research activities. Therefore, without new high flux research reactors within a decade nuclear science and material testing may face a stagnation period.

II. MBIR IS A UNIQUE MULTI-PURPOSE RESEARCH FACILITY

Figure 2. MBIR appearance

Today Rosatom is constructing the most powerful world-class nuclear facility Multi-Purpose Fast Research Reactor (MBIR) at the Research Institute of Atomic Reactors site in Dimitrovgrad, where five (5) other research reactors are in operation and all the necessary research infrastructure is in place to carry out irradiation of materials and fuels and conduct post-irradiation studies. The MBIR is a multipurpose sodium-cooled fast-neutron nuclear research facility with 150 MW thermal power, designed for a broad range of reactor research activities and post-irradiation examination.

The MBIR will become a platform for performing large-scale tests, research and development of innovative nuclear energy technologies that can supply the world with abundant carbon-free energy, developing new technologies for radioisotopes and modified materials production.

MBIR's unique technical characteristics meet various research requirements allowing to conduct research on advanced nuclear fuel and absorber materials under transient and abnormal conditions, studies into the problems of closed fuel cycle, radiation tests of advanced structural materials, study of new and modified liquid-metal coolants, validation of new equipment, production of radioisotopes, and use of neutron beams for medical applications and silicon doping.

Once commissioned MBIR will be equipped with a wide range of experimental devices providing various research options and will allow conducting a number of scientific research activities in the key areas:

- study of advanced nuclear fuel and absorbing materials;
- structural materials testing;
- study of different coolants performance (lead, sodium, gas or molten), means of their control and quality management;
- testing of different types of fuel rods and assemblies in transient, cyclic and emergency modes of operation;
- simulation, study and design of closed fuel cycle, actinide utilization, long-living fission products handling.

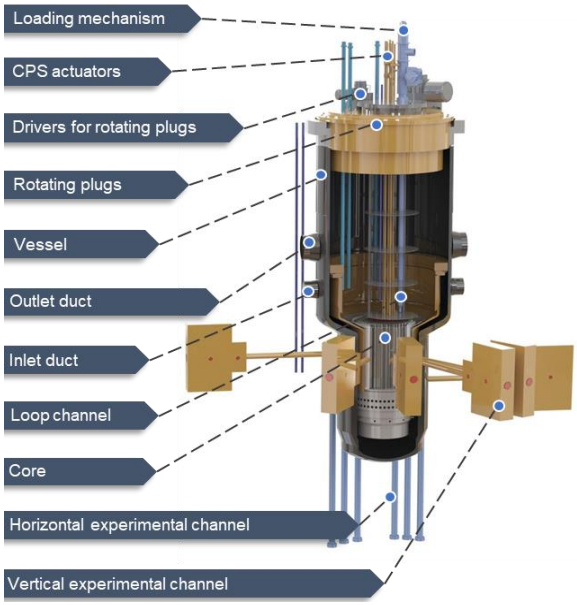

Figure 2. MBIR Reactor design features

A. MBIR's experimental capabilities

The MBIR includes a number of experimental devices to be accommodated within the core. There will be 3 independent loop channels, 3 instrumented experimental channels and more than 10 material testing and isotope production assemblies. In addition, there will be 6 vertical and 8 horizontal experimental channels outside the reactor vessel.

The following experimental devises are provided, placed in the MBIR vessel:

- loops for simulating the operational conditions in the reactor core cores for various coolants;
- independent loops for various coolants;
- specialized assemblies for testing different absorbing and structural materials;
- ordinary fuel elements to produce target isotopes;
- isolated loop to sustain the required thermodynamic parameters in the coolant by natural and forced circulation, organized within the channel.

B. Characteristics of MBIR reactor

Unique physical and technical characteristics of the MBIR are best suited for material science experiments (e.g. testing innovative fuel and new coolants) and allow solving a wide range of scientific problems to justify new competitive and safe nuclear power installations, including fast reactors and technologies required to close the nuclear fuel cycle. Due to high fluence, the required test time will be reduced at least in half compared to the existing research reactors.

Table 2. Characteristics of MBIR reactor

PARAMETER	VALUE
Nominal thermal power, MW	150
Nominal electric power, MW	55
Max / average neutron flux density in the core, $sm^{-2}s^{-1}$	5.3×10^{15} / 3.1x 10^{15}
Fuel	MOX
Reactor fuel campaigns, not less than, days	100
Safety systems	Active/Hybrid
Number of safety systems	2
Reactor configuration	Loop-type
Number of loops for heat transfer	2
Number of heat removal circuits	3
Coolant Flow	Bottom – up
Coolant: I and II circuits / III circuit	Sodium / Water-steam
Pressure in the I circuit, MPa	до 0.6
Coolant temperature of the I circuit, °C	330-512
Capacity utilization coefficient	0.65
Design lifetime, years	50
Commissioning, year	2028
Unique design features	Combination of the internal and external experimental facilities

MBIR will have a design life of 50 years and use vibro-packed MOX fuel. The commissioning of the reactor for research operation is scheduled for 2028.

III. POLYFUNCTIONAL RADIOCHEMICAL COMPLEX (R&D COMPLEX) - NEXT GENERATION NUCLEAR LAB

Multi-functional radio-chemistry research facility (R&D complex) is intended to provide support in the following areas:

- Testing of the innovative technological schemes of fast reactors spent nuclear fuel management in order to issue the input data for the establishment of the full-scale reprocessing production, which will allow to prepare the industrial implementation of the closed nuclear fuel cycle technologies;
- Testing and justification of the closed nuclear fuel cycle at the reactor and technological levels (the minor actinides level);
- Optimization of the handling scheme for RAW management in order to provide transition of long-lived radionuclides into compact and safe forms for storage and/or deposition of high activity RAW;

- Testing of the perspective equipment in order to receive engineering and technical data to establish the cost-effective reprocessing production;
- International cooperation activities and creation of the International centre for management of the fast reactors spent nuclear fuel based on RIAR R&D complex.

Within the framework of the R&D complex, the following activities are on the way: development, creation of prototypes and testing of equipment elements for reprocessing of SNF with pyro-chemical and hydro-metallurgic methods.

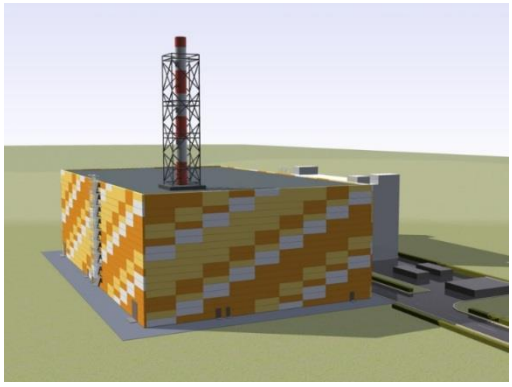

Figure 3. R&D complex

IV. INTERNATIONAL RESEARCH CENTRE BASED ON MBIR REACTOR (IRC MBIR)

MBIR is a key element of the International Research Centre, which is being set up in the form of Consortium agreement.

Therefore, international partners can access the MBIR research capabilities by joining International Research Center based on MBIR Consortium.

Foreign collaboration is also possible in connection with the International Atomic Energy Agency's International Project on Innovative Nuclear Reactors and Fuel Cycles.

Rosatom calls for international research partnerships based on the MBIR reactor. One of the main advantage to participate in the Consortium is the cost reduction. The user may buy the flux share required to execute its research program. The acquired flux share can be freely sold to other parties or submitted to the multilateral research programs.

All the research activities and coordination is executed at the Consortium level. The MBIR reactor complex owned by the Russian Federation and managed by the authorized Russian organization RIAR. RIAR will be bearing direct responsibility for liabilities, operation, and maintenance and the research program's execution. RIAR can also perform the post irradiation studies at additional cost.

ROSATOM has set up the special purpose company – Leader of IRC MBIR Consortium, LLC, which will manage the Consortium, including the budgeting process. Early bird participation in the Consortium allows receiving the best price for the reactor resource, choosing the testing channels in the core and influencing the equipment of the reactor complex with the research equipment.

Share in IRC MBIR Consortium will provide a pro-rata share of the reactor neutron flux.

The flux-sharing concept ultimate goal is to set up a system where the title for the flux share can become a marketable product applicable within not only the IRC MBIR community but also allowing the cross-reactor resource exchange.

The flux share is «transferable» and may be used not only for the shareholder's own research but:

- sub-leased (without change of the ownership) to other members or third parties at a market price;
- merged with other members for joint research or assigned in exchange for the research results;
- swapped for a certain time, which may be of interest to members with small shares.

Today Rosatom has started discussions with the international partners on their participation in the Consortium, which will allow them to develop fast reactor technologies, test new fuels, license new generation codes, as well as develop technologies for the treatment of SNF and MA.

V. REFERENCES

[1] http:/www.mbir-rosatom.ru/en/.

[2] http://www.niiar.ru/eng/.

Proceedings of the European Nuclear Young Generation Forum
ENYGF'21
September 27-30, 2021, Tarragona, Spain

Application of Raman spectroscopy to the oxidation behaviour of new Cr-UO_2 nuclear fuels

Milena-Pérez, Abel[1*], J. Bonales, Laura[1,2], Rodríguez-Villagra, Nieves[1] , Fernández-Carretero, Sergio[1], García-Baonza, Valentín[3] and Cobos, Joaquín[1,4]

[1] Centro de Investigaciones Energética, Medioambientales y Tecnológicas (CIEMAT), Spain; [2] Centro de Astrobiología (CSIC-INTA), Spain; [3] MALTA-Consolider Team (CSIC-UCM), Spain; [4] Estación Biológica de Doñana (EBD-CSIC), Spain

*Corresponding author: *abel.milena@ciemat.es*

I. INTRODUCTION

Existing requirements of energy production in nuclear power plants have led to increasing the burnup in operating reactors, with the main goal to improve the performance of the fuel power in those UO_2-based fuels. In fact, present Light Water Reactors (LWR) are typically designed to operate with burnups about 50 GWd/tU, but with newer fuel technology (*i.e.* doped fuels), these same reactors are able to reach burnups up to 60 or even 70 GWd/tU with the present enrichment limit (between 3-5% ^{235}U) [1, 2]. However, this increased burnup comes along with several undesirable processes that must be taken into account and could be significant in accident scenarios. Especially important are the fission gas release and the pellet-cladding interaction, whose main effect is to decrease the capability of the reactor to operate at high burnups maintaining the established security requirements [3, 4].

In this context, and taking into account that existing fuel designs are vulnerable to severe accident conditions, there is a growing interest in obtaining improved fuel designs with higher resistance against failure. One of the most accepted concepts developed as a consequence of this interest are the so-called Accident-Tolerant Fuels (ATFs) [4-6]. ATF comprises a variety of improvements in current fuel and cladding designs. These challenging advanced fuels could significantly reduce the consequences of potential future severe accidents while covering current high burnups needs.

In particular, the addition of dopants to UO_2-based nuclear fuel is the shortest-term ATF concept. The purpose of additives in doped pellets is to increase the fuel resistance and plasticity by increasing the average grain size in the pellet surface. It is known that this change in grain size alters the diffusion phenomena inside the pellet, and as a consequence, enhanced retention of gaseous products inside the ceramic is obtained [3]. Among the dopants that have been studied through the years, chromia (Cr_2O_3) has turned out to be especially effective in the grain growth process during sintering [7], acting as a grain growth promoter, in particular when the amount of Cr_2O_3 added is close to the solubility limit [8].

The analysis of these Cr-doped UO_2 fuels has been traditionally performed by using techniques such as XRD, SEM or XPS. However, there is a lack of studies regarding the use of Raman spectroscopy with this purpose, in spite of have been widely used in the characterization of other UO_2-doped fuels [9]. This technique meets two relevant features: it provides a spectral fingerprint to distinguish between chemically similar compounds and, more important, it allows the possibility to perform *in-situ* measurements with the aim to track different processes that may occur to the samples, such as oxidation, thermal decomposition, hydrolysis reactions, etc., in controlled conditions of temperature and gaseous atmosphere. This property allows studying different materials in their original conditions, due to the existence of portable Raman instruments; i.e. real Cr-doped fuel could be studied in quality control and its performance could be tested. But first, measurement protocols must be developed and optimized, so they can be later applied.

Furthermore, the back-end cycle of this novel ATFs needs to be properly assessed (either at dry storage or at long-term waste disposal). One of the main problems to deal with at dry storage conditions is the potential oxidation of the fuel, in case of cladding failure. It is accepted that, when UO_2 (cubic) incorporates certain trivalent cation dopants, the oxidation behaviour is slower than pure UO_2, due to the stabilization of cubic U_4O_9 or UO_{2+x} phase [10]. The reason is that the arrangement of oxygen vacancies in clusters is stabilized by trivalent dopants. In order to study the effect of delayed oxidations, Cr-doped UO_2 pellets were exposed to oxidizing environment (air) using thermogravimetric analyses in combination with XRD and Raman spectroscopy. These results have direct application in safety terms, and as far as our knowledge, no previous investigations of Cr-doped UO_2 fuel oxidation have been carried out.

Thus, in this work we use the samples prepared and characterized in a recently published paper [11], consisting of a series of UO_2 and $(U,Cr)O_2$ pellets covering possible scenarios concerning the solubility of Cr in the UO_2 matrix, to study the influence of Cr addition in the oxidation behaviour of these new fuels. Measurement protocols for Raman spectroscopy that were optimized in [11] will be used here, together with SEM and XRD, in order to obtain a complete picture of ATF oxidation.

II. SYNTHESIS AND CHARACTERISATION OF Cr-DOPED UO_2

UO_2 and Cr_2O_3 powders were provided by ENUSA and Alfa Aesar, respectively, and both were mixed in weighted amounts. Then, following a conventional metallurgical procedure, the mixtures obtained were subjected to a fabrication process described previously tested in our laboratory [11]. In these sintering conditions, this solubility value is found to be around 1000 ppm [3, 8]. An undoped UO_2 sample was also prepared following the same procedure.

Raman spectra were acquired by using a Horiba LabRam HR evolution spectrometer (Jobin Yvon Technology) equipped with an Olympus BX41 microscope and using a He-Ne laser with a wavelength equal to 632.8 nm. XRD characterization was performed by means of a Bruker D8 Advance Eco diffractometer using Cu Kα radiation (λ=1.54056 Å) and operating at 40 kV and 25 mA. Sample surface morphology has been visualized by means of a TM4000 Plus SEM (HITACHI). The grain size of the samples was estimated by the linear intercept method. Finally, oxidation experiments were carried out by means of a TA Instruments Q50 thermobalance under a constant synthetic airflow (60 $mL \cdot min^{-1}$) using 10ºC/min heating rate up to 700°C. The O/(U+M) atomic ratios of the final samples were then calculated by assuming completely oxidation to U_3O_8. Samples were afterwards identified by SEM, XRD and Raman spectroscopy. Firstly, pure materials were tested in powder form, and after, sintered UO_2 and Cr-doped UO_2 pellets were oxidized at the same conditions.

By means of the combination of the mentioned analytical techniques, pre-oxidized pellets have been characterized in terms of:

a) Refining lattice parameters (by XRD), observing a linear trend (Vegard´s like behaviour) in the range below the solubility limit. This fact has allowed us to estimate a solubility limit of (1094±23) ppm of Cr_2O_3.
b) Calculating average grain sizes in order to confirm the effect of the dopant (by SEM), obtaining the highest value in the sample doped with the amount of Cr_2O_3 closest to the solubility limit.
c) Using Raman spectroscopy as a sensitive technique for distinguishing between UO_2-based fuels with different grain sizes. This distinction has been possible thanks to the distortion in the lattice caused by the entry of Cr, which provokes a change in the intensity of the Raman band associated with defects (see section IV for further details).

All of these results are presented in Table 1 and will be the basis to perfectly define the system that will be oxidized.

Table 1. Main characterization results of the prepared samples. See the text for details.

Cr_2O_3 / ppm	Lattice parameter / nm	Grain size / µm	$A_{LO}/A_{T_{2g}}$
0	a=0.54726(9)	6.55±1.03	0.0584±0.0192
200	a=0.54719(8)	6.30±1.17	0.0715±0.0176
600	a=0.54712(8)	12.92±1.12	0.1442±0.0275
1000	a=0.54706(7)	16.74±1.43	0.2280±0.0600
6000	a=0.54703(8)	10.91±0.87	0.3282±0.0473

III. OXIDATION BEHAVIOUR OF ATF

The oxidation characteristics of pure UO_2 and Cr_2O_3 powders, as well as UO_2 and Cr-doped UO_2 pellets, were measured under a continuous clean air flow by the TGA up to 700°C.

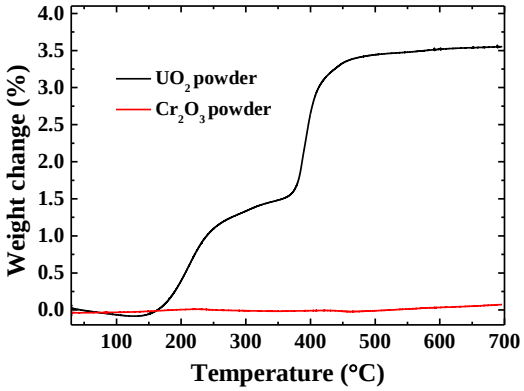

Figure 1. Weight gain curves of starting UO_2 (black) and Cr_2O_3 (red) powders.

Regarding the oxidation behaviour of raw materials, the weight gain curves of starting powders are plotted in Figure 1 as a function of temperature. As can be seen in the Figure, fresh UO_2 powder oxidizes via a two-step reaction $UO_2 \rightarrow U_4O_9/U_3O_7 \rightarrow U_3O_8$, according to the mechanism of oxygen diffusion for the first stage of the oxidation and nucleation and growth for the second [12]. This is an oxygen diffusion-controlled process proportional to powder surface area. No significant mass change has been observed for Cr_2O_3 powder, given its thermodynamic stability [13].

On the other hand, a macroscopic image of the physical changes that the pellet undergoes during the complete oxidation is shown in Figure 2, and the oxidation behaviour of undoped UO_2 and Cr-doped UO_2 pellets is shown in Figure 3. The main characteristic of this reaction is the pulverization of the sample, which transforms from a sintered pellet to powder.

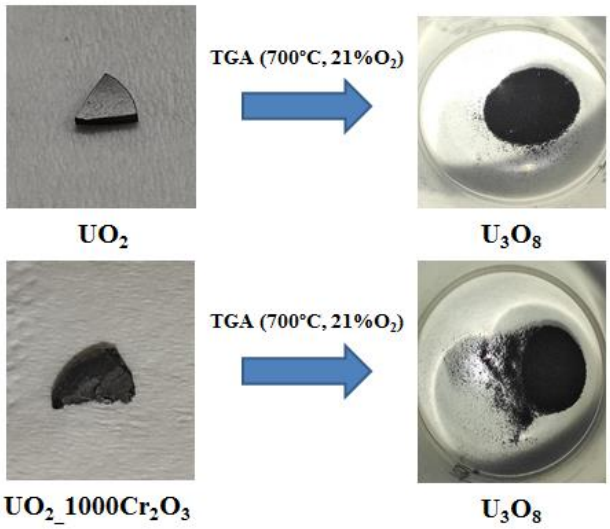

Figure 2. Pulverization of the UO_2 and UO_2_1000Cr_2O_3 pellets after complete oxidation to U_3O_8 in air at 700°C.

For the purpose of this work, the pellet doped with the optimal Cr_2O_3 concentration (1000 ppm [11]) has been selected to be oxidized, in order to make a comparison with pure UO_2 pellet. It is observed that no significant changes can be appreciated until temperatures are high enough to observe U_3O_8. In sintered materials, the formation of U_3O_8 (with subsequent integrity loss) occurs simultaneously with U_4O_9 and U_3O_7 formation, while oxygen diffuses into the lattice [12]. The reason relies on the oxidation mechanism itself, as surface reaction rates are proportional to the exposed surface area, and because during the first step of the oxidation, sintered pellets oxidize by a surface reaction along grain boundaries. Furthermore, boundary diffusion of oxygen becomes more difficult with larger grains (highest density), such as in Cr-doped UO_2. In fact, for Cr-doped UO_2 samples, the slowdown in the reaction kinetics is noticeable as a result of both, the higher grain size and the partial substitution of U^{4+} by Cr^{3+} ions. No reference data on oxidation behaviour of these ATF samples exist in literature. In order to cover all scenarios concerning the solubility of Cr in the UO_2 matrix and its effect on the oxidation, further work on obtaining the weight gain curves for the UO_2 samples shown in Table 1 with different chromium content are presently in progress.

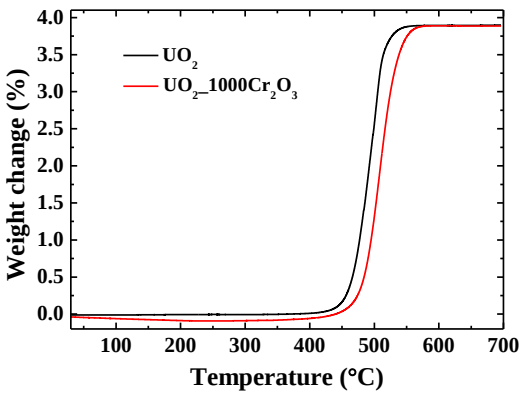

Figure 3. Weight gain curves of studied pellets.

Morphologically, the thermal oxidation of the studied pellets comes along with the pulverization of the samples. This known effect in the formation of U_3O_8 is especially relevant in safety terms, as it could induce the release of radioactive material to the environment, when oxidation of irradiated fuel occurred. The characteristic pop-corn like shape on the U_3O_8 has been clearly observed in the samples by taking SEM images of the pre-oxidized pellets and post-oxidized powdered samples. Two representative images of this process are shown in Figure 4.

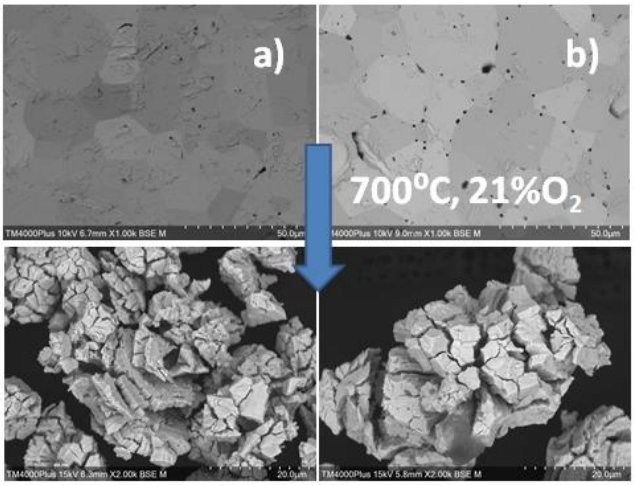

Figure 4. Representative SEM images of a) UO_2 pellet (grain size 6.55 µm) and b) UO_2_1000Cr_2O_3 pellet (16.74 µm). Blue arrow indicates the oxidation of samples, from sintered material to U_3O_8 powder.

At the top of Figure 3, SEM images are taken from the surface of the pellets, showing the grain boundaries where oxygen will diffuse during oxidation. The effect of Cr increasing the average grain size in the doped sample is also observed [11]. On the other hand, at the bottom of Figure 4, U_3O_8 spalled particles are observed, with the typical "pop-corn" morphology [14] and plate-like parallel cracks developed on the surface. Both U_3O_8 powders formed showed similar morphology.

IV. RAMAN SPECTROSCOPY TO STUDY ATF OXIDATION

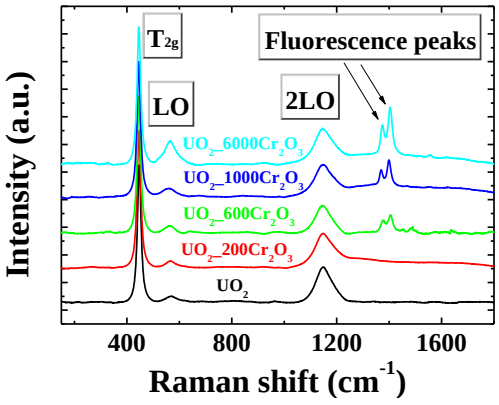

Figure 5. Raman spectra of pre-oxidized Cr_2O_3 – doped UO_2 pellets.

Raman spectroscopy has been used in order to fully-characterize Cr-doped UO_2, using it as an analytical technique that is able to distinguish between UO_2 fuels with different doping levels [11] and to calculate the oxidation degree of oxidized samples in both undoped and doped UO_2-based fuels [10, 15]. In Figure 5, Raman spectra of the pre-oxidized pellets are shown. The known Raman features of an undistorted, face-centered cubic structure like

undoped UO_2 [10] are seen in the Figure. In addition, in some of the Raman spectra, an intense doublet around 1380 cm^{-1} and 1410 cm^{-1} has been found (Figure 5) that has been associated with fluorescence of Cr_2O_3 [16]. The presence of these peaks is a consequence of a Cr_2O_3-enriched region where the Raman laser spot has acquired the spectrum, thus there is chromium present at the surface of the pellet and it has not entered in the UO_2 matrix.

Also in Figure 5, a marked increase in the intensity of the band centred at around 570 cm^{-1} is observed. This band has been ascribed to a first-order LO phonon [10], and its observation is related to lattice distortions, causing a breakdown in the selection rules. The systematic study of this band remarks the applicability of Raman spectroscopy as an analytical technique, which is sensitive to dopant concentration [11].

After oxidation, Raman spectroscopy has been used to confirm the complete oxidation of the pellets to U_3O_8. In the same way that pre-oxidized samples, Raman spectra have been acquired in different zones of the samples, where typical Raman features of U_3O_8 are shown in Figure 6. The wide different spectroscopic profiles obtained from U_3O_8 with respect to those from UO_2 are a consequence of the aforementioned change in the structure from fluorite to orthorhombic. The marked numbers that appear in Figure 6 correspond to Raman shifts at which found bands are centred. They have been previously described [17, 18]. While the band centred at 239 cm^{-1} has an uncertain origin, the rest of features have been assigned to: A_{1g} U-O stretching (345 and 417 cm^{-1}), E_g U-O stretching (483 cm^{-1}) and combination of the two A_{1g} stretching modes (752 cm^{-1}). It is also a remarkable fact that Cr fluorescence bands remains similar for the oxidized sample than the pre-oxidized pellet, as can be seen in Figure 6.

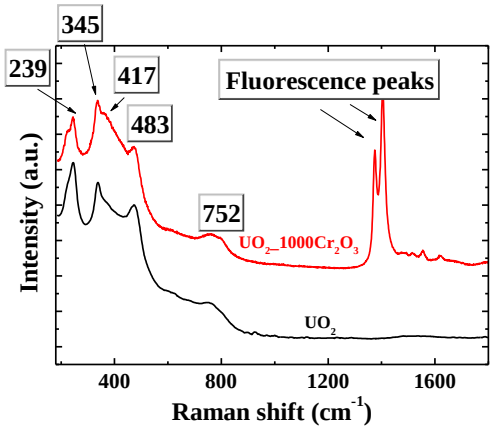

Figure 6. Raman spectra of post-oxidized Cr_2O_3 – doped UO_2 pellets.

V. CONCLUSIONS

This work focuses on ATFs as a new material to cover the current needs of nuclear plants, but also puts the light on the necessity of studying its behaviour under storage conditions that are foreseen after irradiation of these fuels, mainly in an eventual cladding failure scenario that could induce an oxygen contact with the fuel, and therefore produce the oxidation of UO_2 up to U_3O_8. Under this assumption, this work will be the basis in the study of the oxidation of new fuels, in order to completely characterize its behaviour in storage conditions after irradiation.

Regarding this potential oxidation, significant differences found between sintered and powder materials are explained as the oxygen diffusion dependence. Concerning the oxidation of pellets, a delaying effect due to the effect of Cr has been observed in the weight gain curves, due to the larger grains of doped samples. Thermal oxidation behaviour of Cr-doped UO_2 pellets has been addressed for the first time. Further studies on Cr-doped UO_2 fuel oxidation will provide with the complete picture of the oxidation of ATFs in all the solubility scenarios.

VI. ACKNOWLEDGEMENTS

We wish to acknowledge funding for this research from the European Commission Horizon 2020 Euratom projects DISCO (grant agreement 755443).

VII. REFERENCES

[1] J. Arborelius, K. Backman, L. Hallstadius, M. Limbäck, J. Nilsson, B. Rebensdorff, et al., “Advanced doped UO_2 pellets in LWR applications,” vol. 43, 2006.

[2] IAEA, Accident Tolerant Fuel Concepts for Light Water Reactors. Vienna: International Atomic Energy Agency, 2016.

[3] A. Leenaers, L. de Tollenaere, C. Delafoy, and S. Van den Berghe, "On the solubility of chromium sesquioxide in uranium dioxide fuel," Journal of Nuclear Materials, vol. 317, pp. 62-68, 2003.

[4] S. Bragg-Sitton, "Development of Advanced accident-tolerant fuels for commercial LWRs," Nuclear News, vol. 57, pp. 83-91, 2014.

[5] NEA, State-of-the-Art Report on Light Water Reactor Accident-Tolerant Fuels, 2018.

[6] K. A. Gamble, G. Pastore, D. Andersson, and M. W. D. Cooper, "ATF material model development and validation for priority fuel concepts," United States 2019.

[7] L. Bourgeois, P. Dehaudt, C. Lemaignan, and A. Hammou, "Factors governing microstructure development of Cr_2O_3-doped UO_2 during sintering," Journal of Nuclear Materials, vol. 297, pp. 313-326, 2001.

[8] T. Cardinaels, K. Govers, B. Vos, S. Van den Berghe, M. Verwerft, L. de Tollenaere, et al., "Chromia doped UO_2 fuel: Investigation of the lattice parameter," Journal of Nuclear Materials, vol. 424, pp. 252-260, 2012.

[9] M. Razdan and D. Shoesmith, "Influence of trivalent-dopants on the structural and electrochemical properties of uranium dioxide (UO_2)," Journal of the Electrochemical Society, vol. 161, H105, 2013.

[10] J. M. Elorrieta, L. J. Bonales, N. Rodriguez-Villagra, V. G. Baonza, and J. Cobos, "A detailed Raman and X-ray study of UO_{2+x} oxides and related structure transitions," Physical Chemistry Chemical Physics, vol. 18, pp. 28209-28216, 2016.

[11] A. Milena-Pérez, L. J. Bonales, N. Rodríguez-Villagra, S. Fernández, V. G. Baonza, and J. Cobos, "Raman spectroscopy coupled to principal component analysis for studying UO_2 nuclear fuels with different grain sizes due to the chromia addition," Journal of Nuclear Materials, vol. 543, p. 152581, 2021.

[12] T. A. Olds, S. E. Karcher, K. W. Kriegsman, X. Guo, and J. S. McCloy, "Oxidation and anion lattice defect signatures of hypostoichiometric lanthanide-doped UO_2," Journal of Nuclear Materials, vol. 530, p. 151959, 2020.

[13] E. Povoden, A. Nicholas Grundy, and L. J. Gauckler, "Thermodynamic reassessment of the Cr−O system in the framework of solid oxide fuel cell (SOFC) research," Journal of Phase Equilibria and Diffusion, vol. 27, pp. 353-362, 2006.

[14] K. W. Kang, J. H. Yang, J. H. Kim, Y. W. Rhee, D. J. Kim, K. S. Kim, et al., "Improvement of UO_2 pellet properties by controlling the powder morphology of recycled U_3O_8 powder," Journal of Nuclear Science and Technology, vol. 45, pp. 1150-1154, 2008.

[15] J.M. Elorrieta, S. Fernández, N. Rodríguez-Villagra, L. Gutiérrez-Nebot, V.G. Baonza, J. Cobos, "Pre-and post-oxidation Raman analysis of (U, Ce)O_2 oxides," Journal of Nuclear Materials, vol. 508, pp. 116-122, 2018.

[16] F. Adara, Raman Spectra of Metal Oxides. Spectroscopy. Solutions for Materials Analysis 29(10), 14-24, 2014.

[17] D. Manara and B. Renker, "Raman spectra of stoichiometric and hyperstoichiometric uranium dioxide," Journal of Nuclear Materials, vol. 321, pp. 233-237, 2003.

[18] I. S. Butler, G. C. Allen, and N. A. Tuan, "Micro-Raman spectrum of triuranium octoxide, U_3O_8," Applied Spectroscopy, vol. 42, pp. 901-902, 1988.

Proceedings of the European Nuclear Young Generation Forum
ENYGF'21
September 27-30, 2021, Tarragona, Spain

Response of Accident Tolerant Fuel Cladding concepts to LOCA Burst Testing

Ken Kane[1*], Sam Bell[2], Caleb Massey[3], Adele Evans[4], Peter Kelly[4], Bruce A. Pint[1]

[1] Materials Science and Technology Division, Oak Ridge National Laboratory, USA; [2] Department of Materials Science and Engineering, University of Tennessee-Knoxville, USA; [3] Nuclear Energy and Fuel Cycle Division, Oak Ridge National Laboratory, USA; [4]Advanced Materials and Surface Engineering Research Centre, Manchester Metropolitan University

*Corresponding author: *kaneka@ornl.gov*

I. INTRODUCTION

Since the Fukushima Daiichi station blackout in 2011, the nuclear community has sought to increase safety margins during design basis and beyond design basis accidents. Zr alloys have been used historically as fuel cladding for many reasons but Zr oxidizes rapidly in high temperature steam environments in a highly exothermic manner, potentially generating large volumes of H_2 and driving up core temperatures during a loss-of-coolant accident (LOCA) [1]. Furthermore, the rapid thermal transient can cause the Zr-based claddings to balloon and possibly burst, exposing the fuel and potentially blocking coolant pathways in the assembly. Accident tolerant fuel (ATF) cladding concepts aim to increase the ability of the fuel system to cope during accident scenarios. Compared to Zr alloys, ATF cladding materials will have reduced steam oxidation kinetics and improved mechanical response in terms of strength, deformation, and post-failure fuel retention capabilities during accident scenarios. In the present study, the response of two candidate ATF cladding concepts, a Cr coated Zr cladding and C26M, a second generation FeCrAl alloy, were compared to uncoated Zr cladding in a simulated LOCA burst test. Specifically, the temperatures and hoop stresses at burst, burst openings, and estimated H_2 generation during steam oxidation were compared.

II. EXPERIMENTAL DETAILS

Burst testing was conducted on non-irradiated cladding utilizing the Severe Accident Test Station [1] (SATS) at ORNL. Briefly, ~30 cm long cladding tubes were internally pressurized with Ar to designated overpressures, heated from 300°-1200°C at 5°C/s, then held at 1200°C for 5 min. Burst occurred during the temperature ramp. A quartz reaction tube was used with steam flowing at ~200 ml/h. A more detailed description of the test is available elsewhere [2], [3] .

Burst temperature and pressure are signalled by the sudden loss of internal pressure, and the perforation hoop stress was calculated by a thin wall approximation:

$$\sigma_H = \frac{PR}{h} \quad (1)$$

where σ_H is the burst hoop stress, P is the burst internal overpressure, R is the pre-transient mean radius, and h is the initial thickness of the cladding wall. Zirlo (Zr-1.1Sn-1.1Fe-1.1Nb) cladding dimensions were 9.49 mm outer diameter (OD) and 0.61 mm wall thickness (*h)*. For the Cr coated Zirlo system, an approximately ~6 µm Cr coating was deposited with high power impulse magnetron sputtering onto the Zirlo OD. C26M (Fe-12Cr-6Al-2Mo-0.2Si-0.04Y) cladding dimensions were 10.3 mm OD and 0.38 mm *h*. Due to neutronic penalties, the FeCrAl fuel claddings were thinner than Zr-based claddings.

III. RESULTS AND DISCUSSION

The relationship between perforation hoop stress and burst temperature of Zirlo, Cr coated Zirlo, and C26M is shown in Figure 1(a). For comparative purposes, burst data from T35Y2 (Fe-13Cr-5Al-Y), a first generation FeCrAl [3], and Zircaloy-2 are also shown. Qualitatively, there was no difference between the Zirlo, Zr-2, or Cr coated Zirlo. Conversely, C26M, a second generation FeCrAl, consistently withstood ~200°-250°C greater temperatures than Zr-based claddings and ~100°C than T35Y2 at all hoop stresses, indicating superior high temperature strength. The relationship between burst temperature and internal cladding pressure at burst is shown in Figure 1(b). With this consideration, C26M still withstands significantly higher temperatures than the other claddings. The improved

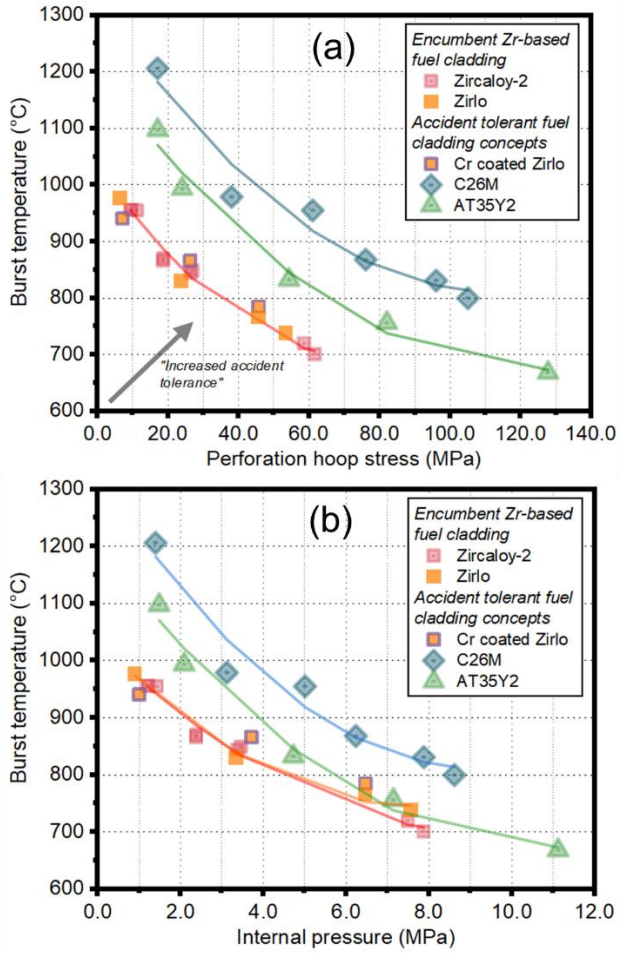

Figure 1 (a) Relationship between burst temperature and hoop stress for Zr-based nuclear grade alloys and accident tolerant fuel cladding concepts. (b) Similar diagram but showing relationship between burst temperature and internal cladding pressure.

mechanical response presently reported agrees with previous findings that C26M exhibited superior resistance to failure compared to Zr-2 during simulated cyclic dryout conditions [4].

Light optical images of the burst regions of Zirlo and Cr coated Zirlo (both burst at 46 MPa), and C26M burst at 79 MPa are shown in Figures 2(a)-2(c), respectively. Although the 46 MPa images suggest that the Cr coating reduced the burst opening area of Zirlo, this effect was not observed at other stresses. However, macroscopically visible cracking in the axial direction was generally observed to be more prominent on the Cr coated Zirlo at all hoop stresses, suggesting some form of embrittlement, but more work is necessary to confirm. Comparatively, burst openings of C26M were significantly smaller than all other claddings, and remained relatively consistent up to ~100 MPa. After which, opening size transitioned to larger openings that were consistent with the other cladding materials that burst at lower temperatures.

The majority of cladding oxidation happens during the 5 min 1200°C isothermal hold under steam, after the temperature ramp during which burst occurs. Due to cladding deformation in the outward radial direction, the temperature at the burst tips is not confidently known.

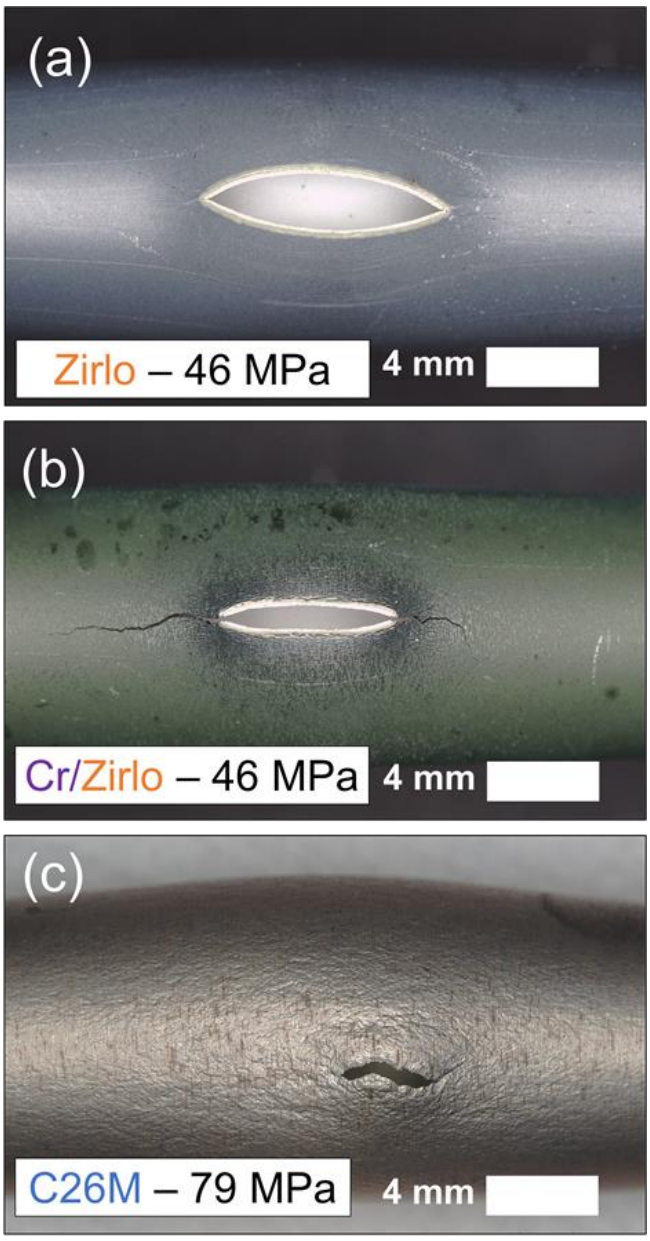

Figure 2 Light optical macrographs of burst region of (a) Zirlo burst at 46 MPa, (b) Cr coated Zirlo burst at 46 MPa, and (c) C26M (FeCrAl) burst at 79 MPa hoop stress

Therefore, to examine oxidation resistance, optical microscopy was conducted, on cross sections taken from the burst regions, on the mount side opposite of burst. A light optical micrograph taken from bare Zirlo is shown in Figure 3(a). Extensive zirconia formation occurred on both the OD and ID, where in the latter case, cladding burst during testing exposes the ID to high temperature steam. An approximately 42 ± 5 µm scale formed on the Zirlo OD. In stark contrast, the Cr coating suppressed all zirconia formation on the OD, seen in Figure 3(b). Not visible in the micrograph, the Cr coating oxidized to form a ~1.7 µm Cr_2O_3 scale and thin interdiffusion layer, consistent with the findings of Ma *et al.* [5]. For C26M, Figure 3(c), a < 1 µm alumina scale formed on both the ID and OD, consistent with the excellent steam oxidation resistance of nuclear grade FeCrAl alloys [6], [7].

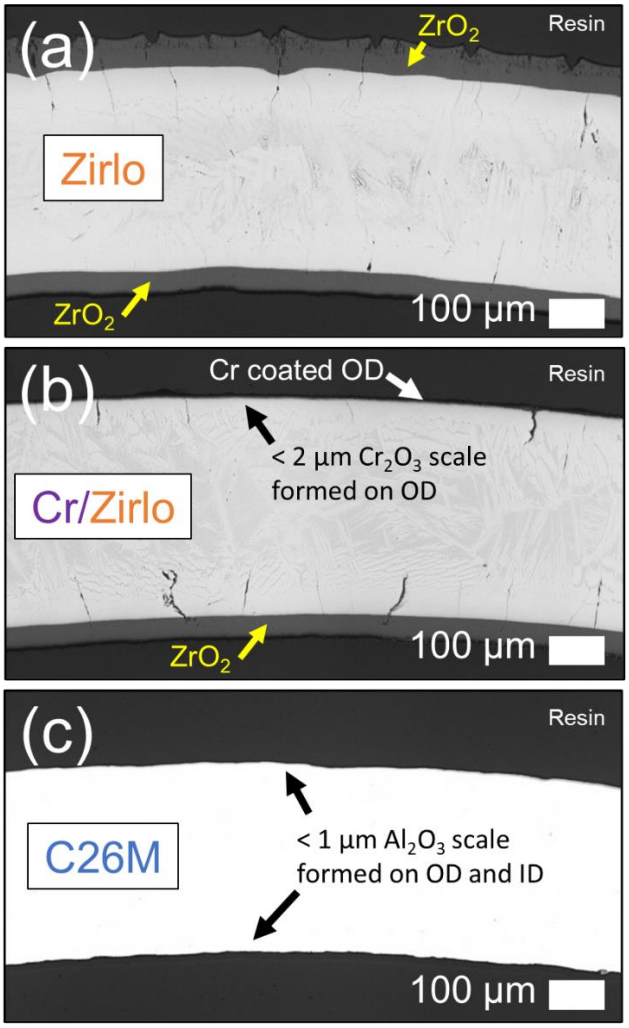

Figure 3 Representative light optical micrographs of (a) Zirlo, (b) Cr coated Zirlo, and (c) C26M (FeCrAl) on regions opposite burst showing scale formation on cladding on ID and OD.

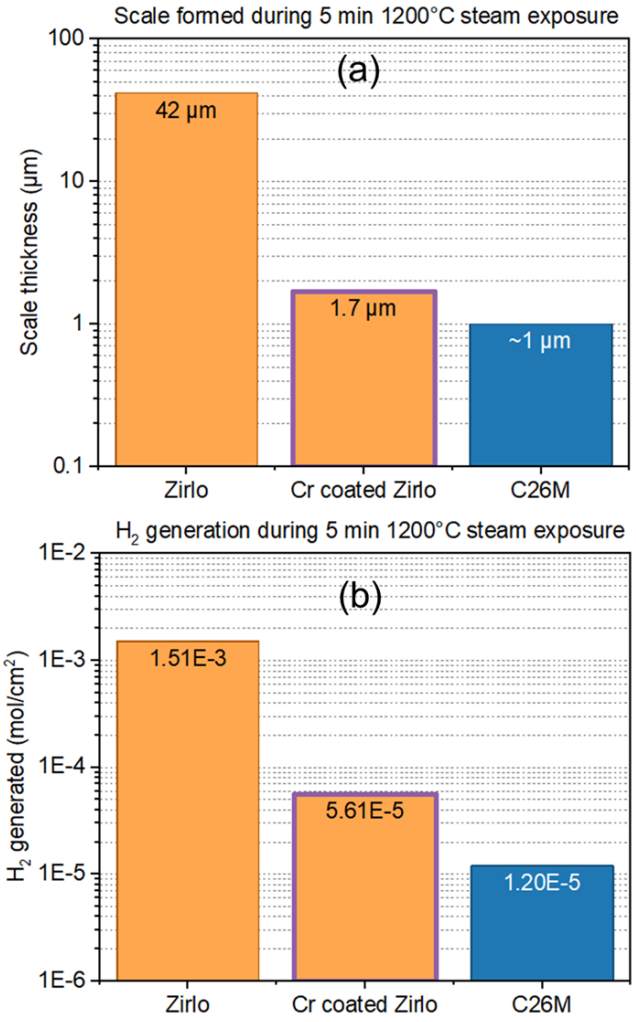

Figure 4 (a) Scale thickness formed during LOCA burst testing and (b) estimated H_2 generation due to steam oxidation.

Scale thicknesses representative of the three claddings are reported in Figure 4(a). The oxidation reactions of the above cladding materials are:

$$Zr + 2\ H_2O\ (g) \rightarrow ZrO_2 + 2\ H_2\ (g)$$

$$2\ Cr + 3\ H_2O\ (g) \rightarrow Cr_2O_3 + 2\ H_2\ (g)$$

$$2\ Al + 3\ H_2O\ (g) \rightarrow Al_2O_3 + 2\ H_2\ (g).$$

Assuming stoichiometric oxidation, and using zirconia, chromia, and alumina densities of 5.68, 5.22, and 3.95 g/cm^3, respectively, the amount of H_2 generation per cm^2 during the 5 min 1200°C isothermal hold was calculated and is reported in Figure 4(b). Application of the Cr coating reduced estimated H_2 generation by over an order of magnitude on the OD compared to bare Zirlo, while C26M reduced H_2 generation by an estimated two orders of magnitude, in agreement with previous calculations comparing Cr coated SiC, Zr4, and APMT (FeCrAl) during 4h of 1200°C isothermal steam exposure [8].

A cross section taken in the burst vicinity of a Cr coated Zirlo cladding burst at 7 MPa hoop stress is shown in Figure 5. On the majority of the coated Zirlo cladding, the Cr coating mitigated zirconia formation entirely. However, in the burst vicinity, where cladding deformation and strain was largest, zirconia formation was observed. From the burst tip on the OD, the microstructure was composed of an outer chromia layer, an intermediate un-oxidized Cr layer, and underlying zirconia. Moving in the direction opposite of the burst tip, the microstructure gradually transitioned to a solely Cr_2O_3 oxide scale where zirconia formation was mitigated entirely. Close examination of the regions where both chromia and zirconia formation occurred indicated that the Cr coating may have cracked during the burst event, providing direct pathways for oxidant diffusion to underlying Zr. It's postulated that, due to poor Cr ductility, the coating shears rather than elongates during the burst event, rendering the coating non-protective in some regions. In most regions, it appeared to remain protective. Thicker Cr coatings may respond differently than the current ~6 µm coatings. A primary benefit of Cr coatings is reducing cladding heating rates during a LOCA scenario, thereby extending coping time [10]. This factor is not reflected in the current LOCA test characterization, where only the post-1200°C exposure specimen was examined.

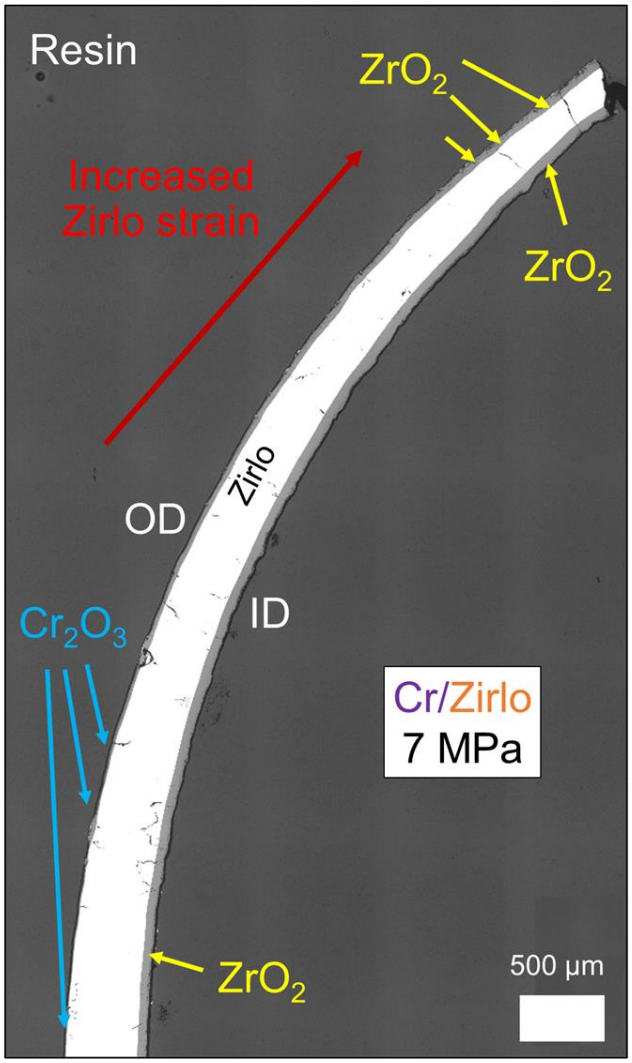

Figure 5 Light optical micrograph taken from the burst region of Cr coated Zirlo burst at 7 MPa hoop stress

IV. CONCLUSIONS

LOCA burst testing was conducted on non-irradiated Zirlo, Cr coated Zirlo, and C26M cladding. The Cr coating was not found to increase burst temperatures of Zirlo, and both bare Zirlo and Cr coated Zirlo burst at similar temperatures and hoop stresses as Zircaloy-2. C26M cladding burst at higher temperatures and hoop stresses than Zr-based claddings and first generation FeCrAl cladding. Of all the claddings, C26M exhibited the smallest burst openings. Both Cr coated Zirlo and C26M formed significantly thinner oxide scales than Zirlo and were estimated to reduce H_2 generation during the present LOCA testing by over an order of magnitude. However, the Cr coating was found to be less protective in the burst vicinity where substrate deformation and strain was largest.

V. ACKNOWLEDGMENTS

This work was funded by the Advanced Fuels Campaign, Office of Nuclear Energy, Department of Energy. The authors would like to thank Ben Garrison and Tim Graening for their technical review of this document, and Victoria Cox and Tom Geer for their incredible aid in metallography.

VI. REFERENCES

[1] S. J. Zinkle, K. A. Terrani, J. C. Gehin, L. J. Ott, and L. L. Snead, "Accident tolerant fuels for LWRs: A perspective," *J. Nucl. Mater.*, vol. 448, no. 1–3, pp. 374–379, 2014.

[2] M. Snead, Y. Yan, M. Howell, J. Keiser, and K. Terrani, "Severe Accident Test Station Design Document," *ORNL/TM-2015/556, Oak Ridge Natl. Lab.*, 2015.

[3] C. P. Massey, K. A. Terrani, S. N. Dryepondt, and B. A. Pint, "Cladding burst behavior of Fe-based alloys under LOCA," *J. Nucl. Mater.*, vol. 470, pp. 128–138, 2016.

[4] K. A. Kane, S. K. Lee, S. B. Bell, N. R. Brown, and B. A. Pint, "Burst behavior of nuclear grade FeCrAl and Zircaloy-2 fuel cladding under simulated cyclic dryout conditions," *J. Nucl. Mater.*, vol. 539, p. 152256, 2020.

[5] H.-B. Ma *et al.*, "Oxidation behavior of Cr-coated zirconium alloy cladding in high-temperature steam above 1200 °C," *npj Mater. Degrad.*, vol. 5, no. 1, pp. 1–11, 2021.

[6] B. A. Pint, K. A. Terrani, M. P. Brady, T. Cheng, and J. R. Keiser, "High temperature oxidation of fuel cladding candidate materials in steam-hydrogen environments," *J. Nucl. Mater.*, vol. 440, no. 1–3, pp. 420–427, 2013.

[7] B. A. Pint, K. A. Terrani, Y. Yamamoto, and L. L. Snead, "Material Selection for Accident Tolerant Fuel Cladding," *Metall. Mater. Trans. E*, vol. 2, no. 3, pp. 190–196, 2015.

[8] K. A. Kane, P. I. M. Stack, P. A. Mouche, R. R. Pillai, and B. A. Pint, "Steam oxidation of chromium corrosion barrier coatings for sic-based accident tolerant fuel cladding," *J. Nucl. Mater.*, vol. 543, 2021.

[9] K. A. Terrani, "Accident tolerant fuel cladding development: Promise, status, and challenges," *J. Nucl. Mater.*, vol. 501, 2018.

[10] T. Feng *et al.*, "Quantification of the effect of Cr-coated-Zircaloy cladding during a short term station black out," *Nucl. Eng. Des.*, vol. 363, no. April, p. 110678, 2020.

Notice: This manuscript has been authored by UT-Battelle, LLC, under Contract No. DE-AC0500OR22725 with the U.S. Department of Energy. The United States Government retains and the publisher, by accepting the article for publication, acknowledges that the United States Government retains a non-exclusive, paid-up, irrevocable, world-wide license to publish or reproduce the published form of this manuscript, or allow others to do so, for the United States Government purposes. The Department of Energy will provide public access to these results of federally sponsored research in accordance with the DOE Public Access Plan (http://energy.gov/downloads/doe- public- access- plan).

Proceedings of the European Nuclear Young Generation Forum
ENYGF'21
September 27-30, 2021, Tarragona, Spain

FeCrAl Accident-Tolerant Fuel Cladding: Insights from a Decade of Development

Caleb P. Massey[1,*], Philip D. Edmondson[1], Maxim N. Gussev[1], Yukinori Yamamoto[1], Kenneth A. Kane[1], Bruce A. Pint[1], Kevin G. Field[2], Raul B. Rebak[3], Kurt A. Terrani[1,4]

[1] Oak Ridge National Laboratory, Oak Ridge, Tennessee, USA, [2] University of Michigan, Ann Arbor, Michigan, USA, [3] General Electric Global Research, Schenectady, New York, USA, [4] Ultra Safe Nuclear Corporation, Knoxville, Tennessee, USA

*Corresponding author: *masseycp@ornl.gov*

I. INTRODUCTION

Following the Fukushima Daiichi nuclear accident in March 2011, research institutions across the world began an initiative to develop accident-tolerant fuel (ATF) cladding concepts to further enhance nuclear safety. Additionally, the potential adoption of one of the various ATF concepts would provide a strong argument for the extension of existing reactor operating licenses and lifetimes. Life extension in the United States is important because many existing light water reactors in the country have licenses that are set to expire before 2050. The most widely adopted near-term ATF cladding solution is the potential to use Cr coatings on currently existing Zr alloys, but longer term solutions, such as using SiC or FeCrAl claddings, could provide even greater safety benefits.

Oak Ridge National Laboratory (ORNL) played a significant role in leading the research for SiC and FeCrAl development efforts. From an engineering position, many of the same pilgering and high-precision tube rolling techniques that are currently used for Zr-based alloys could also be adapted for FeCrAl alloy tubes, which made the FeCrAl development effort one that focused more on material science and irradiation effects rather than the development of new manufacturing processes. Therefore, this work summarizes some of ORNL's contributions over the last decade to the increasing world interest in the FeCrAl ATF concept.

II. DISCUSSION

In 2012, ORNL initiated a technology maturation plan that comprised three phases: (1) feasibility, (2) development and qualification, and (3) commercialization. Phase one comprised understanding the role of the main alloying elements on materials performance, namely the effect of Cr and Al on weldability, tube fabrication, steam oxidation resistance, and unirradiated and irradiated mechanical properties. The first-generation FeCrAl alloys from this phase were quickly established to have superior high-temperature oxidation resistance compared with conventional Zr-based alloys when the composition contained at least 10 wt% Cr and 5 wt% Al [1]. Additionally, the first-generation FeCrAl alloys were found to also exhibited beneficial tube burst properties, illustrating higher burst temperatures and lower post-burst oxidation than Zr alloys [2, 3]. Following the initial optimization of welding techniques [4], ORNL initiated ion and neutron irradiation campaigns to obtain preliminary information concerning irradiation effects (Figure 1). In the first FCAY irradiation campaign, postirradiation examination (PIE) provided some of the first evidence for the destabilization of irradiation-enhanced Cr precipitates with increasing Al addition, although significant irradiation hardening still existed at lower irradiation temperatures and high starting Cr alloy contents [5, 6].

The second phase of the FeCrAl maturation plan focused on optimizing minor alloying elements, such as Mo and Nb. These second-generation FeCrAl alloys are differentiated from first-generation alloys with a sample name prefix of "C" instead of "B." The second-generation alloys targeted a much narrower compositional range informed by prior studies on the alloys [7, 8]. Fracture toughness, Charpy impact, and post-weld investigations have shown that with increasing Al addition, the added solid solution strengthening component also increases the difficulty of fabricability and increases susceptibility to crack propagation through the material. Therefore, although increasing Al contents are desired for high-temperature

(>1,000°C) oxidation [9, 10], the second-generation Cr and Al compositions range from 10 to 13 wt% and 5 to 7 wt%, respectively (Figure 2). Based on the combination of corrosion [11–15], oxidation [1, 16, 17], PIE, and fabricability [7, 8, 18–20], the second-generation alloy C26M (Fe-12Cr-6Al-2Mo-0.2Si-0.04Y, wt%) continues to perform as the leading FeCrAl alloy for potential deployment.

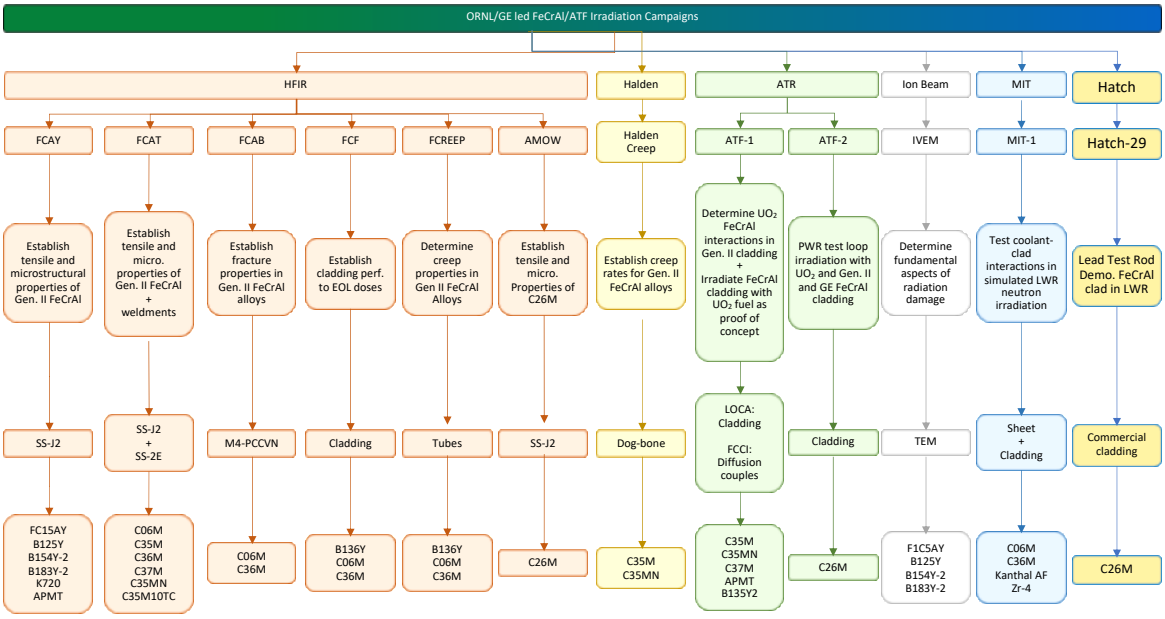

Figure 1: List of ORNL-led and/or main participant irradiation campaigns for FeCrAl alloy qualification.

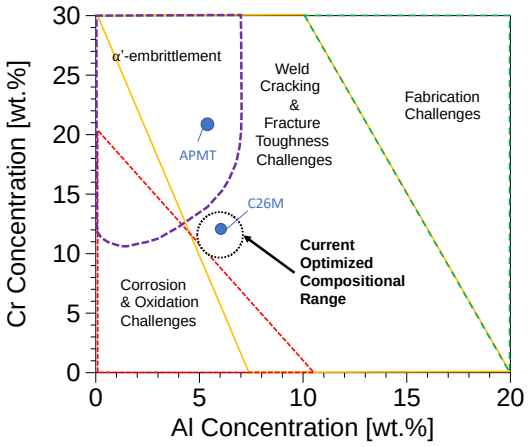

Figure 2: Design space for modern FeCrAl alloys for nuclear applications.

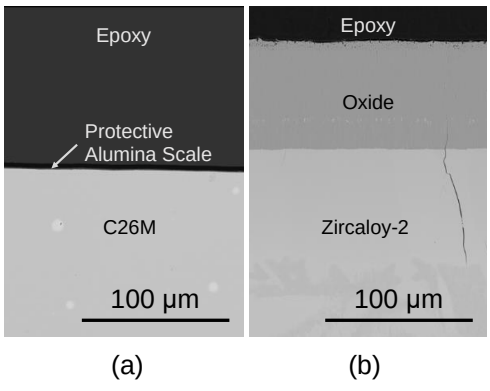

Figure 3: Post loss-of-coolant accident burst test oxidation comparison for (a) a model FeCrAl alloy C26M comparison with (b) a conventional Zircaloy-2. The alumina oxide scale on C26M is too small to see at this magnification compared with the substantial zirconia oxide scale on Zircaloy-2.

An example of the benefits that an optimized FeCrAl alloy can provide during a nuclear accident scenario is shown in Figure 3. Using ORNL's severe accident test station, pressurized tubes can be rapidly heated in a flowing steam environment to temperatures as high as 1,200°C. This allows for the burst of prototypic tube geometries to assess their burst behavior and their post-burst oxidation. For Zr-based alloys, the exothermic oxidation reaction of Zr with steam generates heat and hydrogen gas as byproducts. After a 5°C/s ramp to 1,200°C followed by a 5 min hold and a subsequent quench to room temperature, the oxide scale on Zircaloy-2 is almost 0.1 mm thick, whereas the oxide on an identically tested tube of C26M shows an almost irresolvable oxide scale on the order of a few microns. This oxidation resistance is supplemented by an over 100°C increase in burst temperature for an identical tube internal pressure (Figure 4).

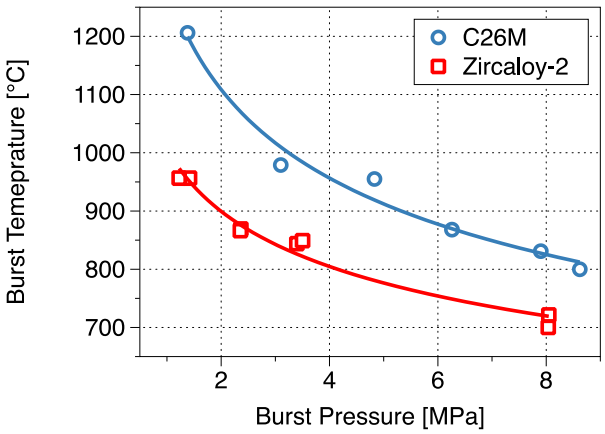

Figure 4: Loss-of-coolant accident burst temperature as a function of tube internal burst pressure for C25M and Zircaloy-2 tubes of relevant boiling water reactor geometry.

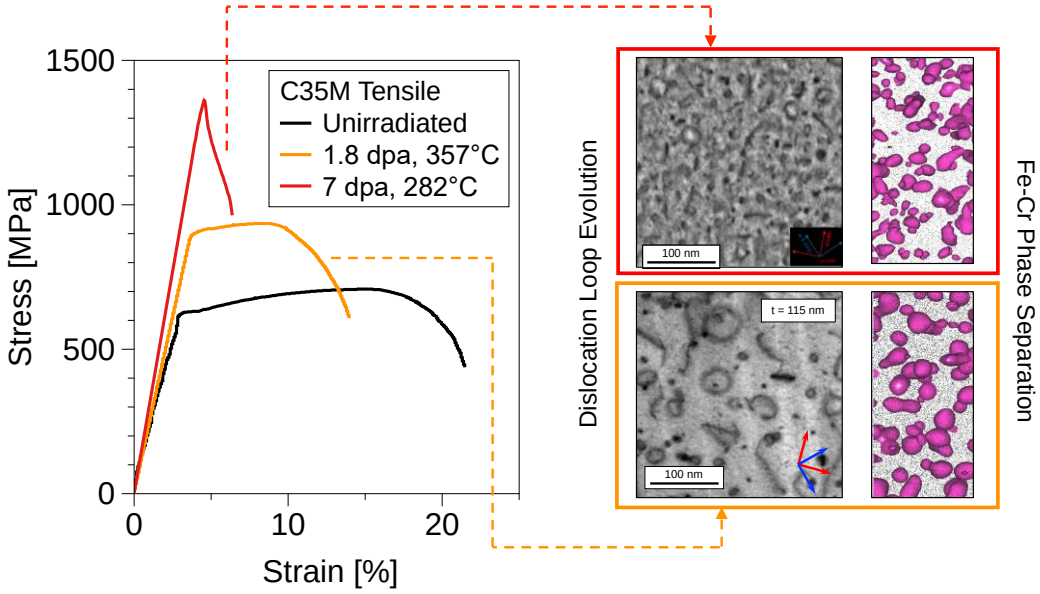

Figure 5: The irradiation hardening in model FeCrAl alloy C35M is highlighted through stress-strain curves of unirradiated and neutron-irradiated conditions. The microstructural features responsible for these macroscale material property changes, notably dislocation loops and Cr-rich precipitates, are highlighted by using scanning transmission electron microscopy micrographs and atom probe tomography, respectively. Magenta iso-concentration surfaces represent regions in which at least 20% of the atoms in those volumes are Cr and comprise a total volume rendered of 25 × 25 × 50 nm, respectively.

Although the maturation and deployment plan has now transitioned into the final commercialization stage, there are still some challenges and opportunities for alloy development and materials science understanding. For example, irradiation hardening in the second-generation model FeCrAl alloys can still be severe, depending on irradiation temperature and dose. Although it was previously postulated that the irradiation hardening should saturate by around 7 dpa, as shown from hardness data following ion irradiation [21], the loss of ductility and increase in hardening even at 7 dpa can be appreciable because of the nucleation of significant dislocation loops and Fe-Cr phase separation. As illustrated in Figure 5, scanning transmission electron microscope micrographs show the presence of many dislocation loops within the FeCrAl microstructure for a neutron-irradiated alloy C35M. These loops are smaller and higher in density for the higher irradiation dose case, although the refined size is also partly due to the somewhat lower irradiation temperature experienced by the higher dose sample. In both irradiated cases, which are shown in red and orange in Figure 5, the atom probe tomography reconstructions shown on the right highlight magenta iso-concentration surfaces enriched in Cr. These Cr clusters nucleate as a result of the aforementioned Fe-Cr phase separation phenomena, which is accelerated under irradiation.

These engineering stress-strain curves were performed at room temperature, and the material response changes at higher temperatures. Additionally, similar loss of ductility is experienced in Zr-based alloys after irradiation because of a combination of dislocation loop nucleation and hydride embrittlement. Thus, irradiation hardening and embrittlement is not an insurmountable obstacle for cladding candidate materials for nuclear reactors; however, it is one of many factors that requires careful consideration when performing compositional optimization for the FeCrAl alloy system. Future optimization efforts could involve a cost-benefit analysis of Cr content because corrosion resistance is balanced along with the propensity for Fe-Cr phase separation under normal operating conditions.

III. CONCLUSIONS

Although work continues to improve understanding of the irradiation response of FeCrAl cladding, such as the ongoing PIE of the recently irradiated C26M Lead Test Assembly in the Hatch Reactor (2018–2020) and upcoming PIE on fueled rodlets of C26M from the Advanced Test Reactor ATF-2 irradiation, the FeCrAl ATF initiative has rapidly expanded interest in and scientific understanding of pertinent aspects of this prospective accident-tolerant cladding system. Although many references are provided here, this four-page summary only scratches the surface of the numerous completed and ongoing projects associated with this work, so the reader is referred elsewhere for a current summary of published work on the matter [21, 22].

IV. ACKNOWLEDGMENTS

The work in this paper was supported by the Advanced Fuels Campaign of the Fuel Cycle R&D program in the US Department of Energy's (DOE's) Office of Nuclear Energy under contract DE-AC05-00OR22725 with DOE. A portion of this research was conducted at ORNL's Center for Nanophase Materials Sciences, which is a DOE Office of Science User Facility. A portion of this research used resources at the High Flux Isotope Reactor, a DOE Office of Science User Facility operated by ORNL. A portion of this work was funded by a Nuclear Science User Facilities Rapid Turnaround Experiment and was conducted at the Center for Advanced Energy Studies–Microscopy and Characterization Suite. The authors would like to thank Tim Graening and Nathan Capps for their technical review of this work.

V. REFERENCES

[1] B.A. Pint, K.A. Terrani, M.P. Brady, T. Cheng, J.R. Keiser, High temperature oxidation of fuel cladding candidate materials in steam–hydrogen environments, Journal of Nuclear Materials 440(1-3) (2013) 420-427.

[2] M.N. Gussev, T.S. Byun, Y. Yamamoto, S.A. Maloy, K.A. Terrani, In-situ tube burst testing and high-temperature deformation behavior of candidate materials for accident tolerant fuel cladding, Journal of Nuclear Materials 466 (2015) 417-425.

[3] C.P. Massey, K.A. Terrani, S.N. Dryepondt, B.A. Pint, Cladding burst behavior of Fe-based alloys under LOCA, Journal of Nuclear Materials 470 (2016) 128-138.

[4] J. Gan, E. Perez, D. Haggard, C. Nichol, N. Jered, Report on the Development of Weld Techniques for Thin Walled Tubing Fuel Cycle Research & Development Advanced Fuels Campaign, Inl/Ltd-15-34684 (2015).

[5] K.G. Field, X. Hu, K.C. Littrell, Y. Yamamoto, L.L. Snead, Radiation tolerance of neutron-irradiated model Fe–Cr–Al alloys, Journal of Nuclear Materials 465 (2015) 746-755.

[6] P.D. Edmondson, S.A. Briggs, Y.Yamamoto, R.H. Howard, K. Sridharan, K.A. Terrani, K.G. Field, Irradiation-enhanced α ′ precipitation in model FeCrAl alloys, Scripta Materialia 116 (2016) 112-116.

[7] M.N. Gussev, K.G. Field, Y. Yamamoto, Design, properties, and weldability of advanced oxidation-resistant FeCrAl alloys, Materials & Design 129 (2017) 227-238.

[8] S.S. Raiman, K.G. Field, R. Rebak, Y. Yamamoto, K. Terrani, Hydrothermal Corrosion of Second Generation FeCrAl Alloys in Boiling Water Reactor Conditions, Journal of Nuclear Materials 536 (2020) 152221.

[9] K.A. Terrani, B.A. Pint, Y.J. Kim, K.A. Unocic, Y. Yang, C.M. Silva, H.M. Meyer, R.B. Rebak, Uniform corrosion of FeCrAl alloys in LWR coolant environments, Journal of Nuclear Materials 479 (2016) 36-47.

[10] R.B. Rebak, Y.-J. Kim, Hydrogen diffusion in FeCrAl alloys for light water reactors cladding applications, Pressure Vessels and Piping Conference, American Society of Mechanical Engineers, 2016, p. V06BT06A010.

[11] B.A. Pint, K.A. Terrani, Y. Yamamoto, L.L. Snead, Material selection for accident tolerant fuel cladding, Metallurgical and Materials Transactions E 2(3) (2015) 190-196.

[12] Y.-H. Lee, T.S. Byun, A comparative study on the wear behaviors of cladding candidates for accident-tolerant fuel, Journal of Nuclear Materials 465 (2015) 857-865.

[13] Y. Yamamoto, Development and quality assessments of commercial heat production of ATF FeCrAl tubes, ORNL/TM-2015/478, Oak Ridge National Laboratory, Oak Ridge, TN, United States, 2016.

[14] Y. Yamamoto, B.A. Pint, K.A. Terrani, K.G. Field, Y. Yang, L.L. Snead, Development and property evaluation of nuclear grade wrought FeCrAl fuel cladding for light water reactors, Journal of Nuclear Materials 467 (2015) 703-716.

[15] Y. Yamamoto, Z. Sun, B.A. Pint, K.A. Terrani, Optimized Gen-II FeCrAl cladding production in large quantity for campaign testing, Oak Ridge National Laboratory, Oak Ridge, TN, United States, 2016.

[16] K.G. Field, M.A. Snead, Y. Yamamoto, K.A. Terrani, Handbook on the Material Properties of FeCrAl Alloys for Nuclear Power Production Applications, ORNL/SPR-2020/1617, 2020.

[17] K.G. Field, S.A. Briggs, Radiation Effects in FeCrAl Alloys for Nuclear Power Applications, Comprehensive Nuclear Materials, 2020.

Proceedings of the European Nuclear Young Generation Forum
ENYGF'21
September 27-30, 2021, Tarragona, Spain

Poolside Inspection of EnCore® Fuel Lead Test Rods at Exelon Byron Unit 2

Walters, Jorie[1*], Nilsson, Jonathan[1], Lazeski, Shawn[1], Haselden, Charles[1], Smith, Jason[1], Gassmann, William[2] and Nanovsky, Iordanka[2]

[1] Westinghouse Electric Company, USA; [2] Exelon Nuclear, USA

*Corresponding author: *walte2jl@westinghouse.com*

I. INTRODUCTION

Following the event at Fukushima Daiichi nuclear power plant in Japan after the 2011 earthquake and subsequent tsunami, the United States Department of Energy (DOE) initiated a program to develop nuclear fuel, called accident tolerant fuel (ATF), that could enhance performance in accident conditions and extend operator reaction time in the event of an accident [1]. The multi-phase program prompted fuel vendors to collaborate with universities and national laboratories to develop new fuel materials. From this, Westinghouse developed EnCore® fuel to improve fuel performance in normal operating conditions as well as in transient and accident scenarios. Near-term technologies include Cr coated cladding and ADOPT™ fuel pellets which add dopants to standard UO_2 pellets for property enhancement. Long-term technologies include revolutionizing standard zirconium-based fuel cladding to a silicon carbide (SiC) cladding and advanced fuel pellets with increased uranium loading and high thermal conductivity such as UN or U_3Si_2.

A nominal 25 µm Cr coating thickness was applied to the outer diameter of standard Optimized ZIRLO™ cladding using the cold spray process. The primary purpose of the Cr coating is to reduce the corrosion rate in normal operating conditions and to reduce cladding oxidation at high temperatures in steam. Additional benefits arise to reduce ballooning and burst during a loss of coolant accident (LOCA) scenario and to reduce cladding wear.

Westinghouse ADOPT fuel has been in use as a commercial product for the European market since 1999 [2]. ADOPT is a modified UO_2 pellet with dopant additions of chromia (Cr_2O_3) and alumina (Al_2O_3) to facilitate greater densification and diffusion during sintering processes which result in a higher density and an enlarged grain size compared to standard undoped UO_2.

This paper presents the operating experience and post-irradiation inspections of Cr coated cladding with UO_2 and ADOPT fuel pellets.

II. BYRON LTR PROGRAM

To gain operating experience of ATF technologies, Westinghouse partnered with Exelon Nuclear to insert the first ATF technologies in lead test rods (LTRs) into nuclear power plant Byron Unit 2 for Region 24 in spring 2019 [3]. The program included a total of twenty (20) LTRs in two (2) fuel assemblies of the 17x17 OFA (Optimized Fuel Assembly) fuel design. A Cr coating was applied to the outer diameter of sixteen (16) LTRs, each fueled with standard UO_2 fuel except four (4) rods which contained ADOPT pellets. The remaining four (4) LTRs inserted during the program were fueled with uranium silicide (U_3Si_2) pellets in short 30.5 cm long segments.

All LTRs were located on the periphery of the fuel assemblies to enable ease of visual inspections after each cycle of irradiation. The first fuel assembly (FA-1) contained a total of twelve (12) LTRs: eight (8) Cr coated Optimized ZIRLO rods with standard UO_2 pellets and four (4) Cr coated Optimized ZIRLO rods containing ADOPT fuel pellets. The remaining fuel rods in the assembly were standard Optimized ZIRLO cladding with UO_2 pellets. The second fuel assembly (FA-2) consisted of a total of eight (8) LTRs: four (4) Cr coated Optimized ZIRLO rods with standard UO_2 pellets and four (4) segmented rods containing U_3Si_2 advanced fuel pellets. Like FA-1, the remainder of FA-2 consisted of the standard refuel design with Optimized ZIRLO cladding and UO_2 pellets.

The two fuel assemblies were located near the center of the core. As a result, two (2) cycles of irradiation are planned, with the assemblies containing LTRs located in high duty locations to maximize burnup exposures.

III. POOLSIDE INSPECTIONS

One full cycle of irradiation was completed for the ATF LTRs in Byron Unit 2 in fall 2020. In order to evaluate the performance of the Cr coated cladding, poolside inspections

were conducted, and several rods were selected for extraction from the fuel assemblies for future shipment to hot cell. Poolside inspections conducted during the refueling outage (the period between core offload and core reload) included fuel assembly visual inspections, fuel rod removal, and subsequent fiberscope visual inspection of grid cells of the extracted rod. Stainless steel pins were loaded into cells where LTRs were removed per standard procedure. Off critical path of outage work (after core reload was complete), additional inspections of extracted rods were conducted including fuel rod visual inspections, fuel rod length measurements, eddy current testing, fuel rod profilometry measurements, and eddy current lift-off measurements to detect coating thickness.

The following subsections present collected data during the outage and post-outage evaluations. Table 1 details the extracted rods and level of burnup following one cycle of irradiation. Only visual inspections were conducted on the extracted segmented rod with U_3Si_2 pellets (from fuel assembly 2) with no abnormal visual indications and no further discussion is included here.

Table 1. Details of extracted chromium (Cr) coated LTRs after one cycle of irradiation for further poolside inspections and eventual hot cell testing.

Fuel Assembly	Cell Location	Pellet Type	Average Burnup (MWd/MTU)
1	I1	ADOPT	30856
1	N1	UO_2	30856
1	Q4	UO_2	30856
2	N17	UO_2	30990

A. Fuel Assembly and Rod Visual Inspection

Full-face and half-face visual inspections were performed on both assemblies using a Westinghouse BlueRad™ camera. The fuel assemblies were lowered and raised in front of the camera and video of all four assembly faces was recorded. Visual inspections were completed to identify any anomalous conditions of the LTRs with respect to surrounding standard fuel rod designs. Specifically, the Cr coated rods should not exhibit signs of cracking, blistering, or peeling. Figure 1 shows that there is no evidence of coating damage nor excessive oxidation of coated rods following one cycle of irradiation. Visual inspections confirmed the mechanical condition of both fuel assemblies to be satisfactory with no damage or debris noted.

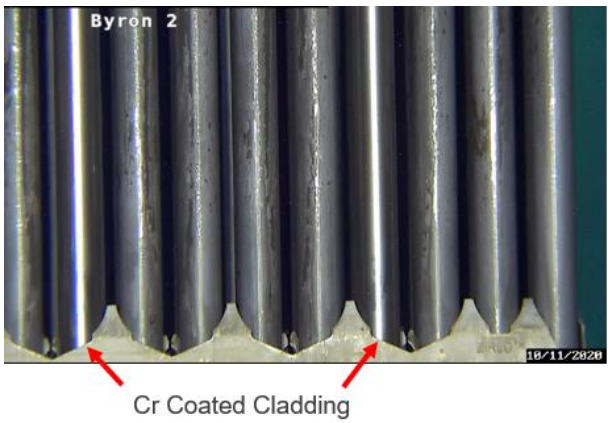

Figure 1. Half-face visual of Fuel Assembly 1 containing Cr coated rods.

Post-outage imaging of extracted fuel rods was conducted both before and after brushing with abrasive pads to remove any crud from the fuel rod surface. The camera provided an approximately 120º view of the rod circumference, so three passes were conducted to obtain views of the entire fuel rod surface. Visual examinations showed a layer of crud that was more loosely adhered to the Cr coated cladding compared to adjacent uncoated rods. All Cr coated rods exhibited this light crud layer with crud peeling in numerous locations and the crud was subsequently removed with a single brushing pass (Figure 2), leaving behind a lustrous Cr coating surface. None of the rods exhibited indications of grid-to-rod fretting damage and the Cr coating appeared to be fully intact with no evidence of Cr spallation or excessive oxidation.

In each cell where a Cr coated LTR was removed, a fiberscope visual inspection of the grid cells was performed to evaluate wear of the springs and dimples supporting the fuel rod. This is particularly important for cells containing Cr coated rods, as Cr is a harder material than zirconium-based alloys and could lead to excessive wear of grid supports. Examinations revealed no excessive wear or damage to grid springs and dimples.

The fact that the thin crud layers were not as adherent to the Cr coated rods compared to uncoated rods could be an unanticipated benefit of the coated cladding. Crud can have operational impacts in some plants and can lead to shifts in power or localized corrosion which could impact the ability to effectively remove heat from the fuel rod. Reduction of crud adherence to the rods could also eliminate the need for costly and time-consuming fuel cleaning procedures.

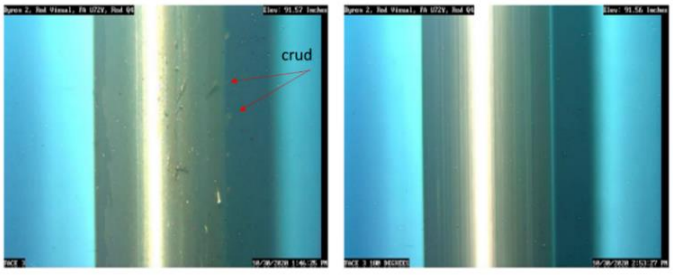

Figure 2. Example of Cr coated rod visuals before (left) and after (right) brushing to remove crud.

B. Fuel Rod Length and Profilometry Measurements

Fuel rod length measurements were performed on extracted coated cladding LTRs after the outage work using visual software to determine rod growth after a single cycle of irradiation. The Cr coated LTR measurements with UO_2 pellets were compared to average uncoated Optimized ZIRLO rod growth at approximately the same burnup levels [4] and the respective ratios are presented in Table 2. Coated cladding rods with UO_2 had less growth after one cycle of irradiation than typical uncoated rods. The single coated rod containing ADOPT pellets had a noticeably higher rod growth of approximately 0.24% compared to less than 0.10% in coated rods containing UO_2 pellets. The additional growth is likely due to ADOPT pellets experiencing a lower percentage of fuel densification during operation, which produces earlier pellet to cladding contact, resulting in a higher axial growth. No comparisons were made in Table 2 for the coated rod containing ADOPT pellets because no reference data for single rod growth of Optimized ZIRLO cladding with ADOPT pellets in pressurized water reactor (PWR) operating conditions was available. The increased growth is bounded by existing fuel rod design models and is unlikely to pose an operational challenge.

Table 2. Ratio of Cr coated to average uncoated Optimized ZIRLO single rod growth measurements at approximately equivalent levels of burnup. Comparisons are for rods containing UO_2 pellets

Fuel Assembly	Cell Location	Pellet Type	Single Rod Growth Ratio (Coated/Uncoated)
1	N1	UO_2	0.55
1	Q4	UO_2	0.68
2	N17	UO_2	0.41

Additionally, fuel rod profilometry was conducted to detect any diametral changes due to irradiation, to determine cladding ovality, and to aid in the understanding of in-reactor creep of the coated rods. The equipment was calibrated to within ±12.7 µm and rod diameters (Optimized ZIRLO cladding plus Cr coating) were measured at 0º, 45º, 90º, and 135º circumferential positions. Measurements were within the expected range for Cr coated fuel rods given as-fabricated dimensional measurements and estimated coating thickness. Coated rods containing UO_2 pellets experienced negligible creep down, while the rod containing ADOPT pellets experienced a measurable amount of creep down. It is noted that these results represent a single data point, and though a large operating database is available for ADOPT pellets in Boiling Water Reactors (BWR) [2], these results constitute some of the first data points for ADOPT behavior in PWR conditions. Additional poolside data for LTRs in this program and in future programs will be valuable in fully understanding the in-reactor rod growth and creep behavior of rods containing ADOPT pellets.

C. Eddy Current and Coating Thickness Measurements

Fuel rods were passed through an encircling eddy current coil to identify any cladding flaws or changes to the Cr coating following one cycle of irradiation. None of the extracted rods that were inspected exhibited any detectable flaws.

On typical zirconium-based fuel rods, measurements may be taken to estimate the thickness of the oxide that is formed during irradiation. The presence of the Cr layer complicates measurements since Cr is more conductive than the zirconium-based cladding, so the impedance response is reduced with increasing Cr layer thicknesses. Additionally, the oxide thickness on the coated rods is expected to be negligible and either at or below the minimum equipment detection limits based on testing to date [5]. Similar measurements to standard oxide measurements were conducted on the Cr coated LTRs and were used to detect Cr layer thickness following one cycle of irradiation. Prior to poolside measurements, unirradiated Cr coated cladding pieces were used to create a new calibration curve. Each rod was brushed prior to eddy current measurements.

Based on the corrosion measurements that indicated Cr layer thickness in this case, the coating was between 28-31 µm, comparable to the as-fabricated coating thickness, and consistent along the fuel rod length. This supports the assertion that there is negligible oxidation and indicates that the Cr coating is still present following one cycle of irradiation.

IV. FUTURE INSPECTIONS

Similar poolside inspections are planned following end of cycle two for fuel assembly 1. FA-1 was reinserted for a second cycle of irradiation, and FA-2 was kept in the spent fuel pool due to scheduling constraints during the outage and may be considered for future irradiation cycles.

Select Cr coated rods that were extracted from the fuel assemblies were loaded into casks for shipment to hot cell for further non-destructive and destructive examinations estimated to begin in 2021. Testing will aim to further confirm the coating integrity following one cycle of operation in a commercial reactor.

V. CONCLUSIONS

The Cr coated ATF LTRs performed as intended during one full cycle of irradiation in Exelon Byron Unit 2 nuclear power plant. There was no observed evidence of damage to the Cr coated rods nor to the grid support features when evaluated with fiberscope inspections. Crud was observed to adhere more loosely to Cr coated rods compared to adjacent uncoated rods and was easily removed during fuel rod brushing. Coated rods containing standard UO_2 pellets did not exhibit appreciable cladding creep nor single rod growth following one cycle of operation. A measurable increase in cladding creep and growth was observed in coated rods with ADOPT pellets; however, this observation was based on a single data point and additional measurements of rods containing ADOPT pellets should be evaluated in the future.

Another LTR program including Westinghouse Cr coated cladding rods is currently underway at Doel Unit 4 power

plant with end of cycle one planned for fall 2021. Future irradiation programs including EnCore fuel are planned. Results from the poolside inspections of ATF technologies after commercial irradiation are paramount to building industry experience at various burnup levels and eventual hot cell examinations will further confirm ATF material performance.

VI. ACKNOWLEDGMENTS

The authors would like to thank those from both Westinghouse and Exelon who supported the outage and reload activities.

Research on chromium coatings was enabled by funding from the U.S. Department of Energy under Award Number DE-NE0008222 and DE-NE0008824. This report was prepared as an account of work sponsored by an agency of the United States Government. Neither the United States Government nor any agency thereof, nor any of their employees, makes any warranty, express or implied, or assumes any legal liability or responsibility for the accuracy, completeness, or usefulness of any information, apparatus, product, or process disclosed, or represents that its use would not infringe privately owned rights. Reference herein to any specific commercial product, process, or service by trade name, trademark, manufacturer, or otherwise does not necessarily constitute or imply its endorsement, recommendation, or favoring by the United States Government or any agency thereof. The views and opinions of authors expressed herein do not necessarily state or reflect those of the United States Government or any agency thereof.

VII. REFERENCES

[1] J. Carmack, F. Goldner, S.M. Bragg-Sitton, L.L. Snead, "Overview of the U.S. DOE Accident Tolerant Fuel Development Program," presented at the TopFuel 2013 Conference, Charlotte, NC, USA, September 2013, INL/CON-13-29288.

[2] J. Wright, C. Anghel, S. Middleburgh, M. Limbäck, "Fuel Hardware Considerations for BWR PCI Mitigation," presented at the TopFuel 2016 Conference, Boise, ID, USA, September 2016.

[3] H. Shah, J. Romero, P. Xu, R. Oelrich, J. Walters, W. Gassmann, "Westinghouse-Exelon EnCore® Fuel Lead Test Rod (LTR) Program Including Coated Cladding Development and Advanced Pellets," presented at the TopFuel 2018 Conference, Prague, Czech Republic, October 2018.

[4] J. Romero, L. Hallstadius, M. Owaki, G. Pan, K. Kakiuchi, R.J.Comstock, J. Partezana, A. Mueller, M. Dahlbäck, A. Garde, A. Atwood, M. Åslund, "Evolution of Westinghouse Fuel Cladding," presented at the TopFuel 2014 Conference, Sendai, Japan, September 2014.

[5] J.L. Lyons, J. Partezana, W.A. Byers, G. Wang, A. Parsi, J.L. Walters, J. Romero, A.J. Mueller, H. Shah, R. Oelrich, "Westinghouse Chromium-Coated Zirconium Alloy Cladding Development and Testing," presented at the TopFuel 2019

Proceedings of the European Nuclear Young Generation Forum
ENYGF'21
September 27-30, 2021, Tarragona, Spain

Methodology and preliminary results of an experimental and numerical study to determine the toughness of fuel rod cladding during Delayed Hydride Cracking (DHC)

Pierrick, Francois[1,3,*], Tom, Petit[1], Quentin, Auzoux[2], Freddy, Salliot[1] and Jacques, Besson[3]

[1] Université Paris-Saclay, CEA, DES – Service d'Etude des Matériaux Irradiés, 91191, Gif-sur-Yvette France; [2] Université Paris-Saclay, CEA, Service de la Corrosion et du Comportement des Matériaux dans leur Environnement, 91191, Gif-sur-Yvette France; [3] MINES ParisTech, PSL Research University, Centre des matériaux, CNRS UMR 7633, France

*Corresponding author: pierrick.francois@cea.fr

I. INTRODUCTION

Fuel rod claddings constitute the first safety barrier of nuclear pressurized water reactors (PWRs): they are used to confine the fission reaction and to avoid contamination of the environment. Therefore, their integrity must be checked in various situations. One of them concerns the study of claddings mechanical behaviour during dry storage. In fact, fuel rod claddings are made of zirconium alloys and their mechanical behaviour is well known. However, during their life inside the reactor fuel rod claddings absorb hydrogen due to a corrosion reaction with the water of the primary circuit. This absorption is not without consequences: the presence of hydrogen in the claddings can lead to a phenomenon referred to as Delayed Hydride Cracking (DHC). DHC risks was first evaluated in 1970 by Simpson and Ells on Zr-2.5%Nb pressure tubes used in CANDU reactors [1]. Since, the hydrogen-induced embrittlement of zirconium alloys was studied in the literature. These studies have raised a possible risk during dry storage because of the combination of stress (caused by the internal pressure of the fuel rod) and hydrogen [2], [3].

The present study concerns the risk assessment of the occurrence of this phenomenon in the PWRs fuel claddings: the objective is to develop a multiscale approach to determine the DHC fracture toughness and the DHC velocity, as a function of thermomechanical and irradiation history by developing a quantitative cracking model that will be based on specifically developed experiments.

II. INDUSTRIAL CONTEXT

A. Presentation of French nuclear assemblies

In 2021 in France, 67.1% of the electricity was produced by 56 nuclear PWRs. For a 900 MW reactor, the core consists of fuel rods gathered in 157 fuel assemblies. One fuel assembly corresponds to 265 fuel rods. Claddings are 4 m-long tubes, with an outer diameter of 9.5 mm and a thickness of 0.57 mm. Two principal zirconium alloys are used in the French nuclear plants: Zirlo and $M5_{Framatome}$.

Inside the claddings, the fuel pellets consist of UO_2 (uranium dioxide) or MOX (mixed uranium and plutonium oxide) and each fuel assembly is used 3 to 4 years in reactor. During operation in reactor, the reaction between the cladding and the water forms a layer of zirconium oxide that is limited to a thickness of 100 µm [4]. Meanwhile, the cladding absorbs a fraction of hydrogen generated during the reaction and hydrogen diffuses in zirconium alloys (discussed in part III). At discharge, fuel assemblies are cooled for a few year in spent fuel ponds. They are then shipped to an interim wet storage in France before reprocessing. Dry storage is explored as an alternative storage solution.

B. Fuel assembly storage before reprocessing

The residual thermal power, due to the presence of radioelements is initially too high for the assemblies to be transported and reprocessed. In France fuel assemblies are stored in a pond associated with each reactor until the assembly power is less than 6 kW [5]. This can take about half a year to 3 years depending on the fuel. Fuel assemblies are then transported to the reprocessing plant and stored there a few years before their reprocessing.

In France, the current storage solution is wet storage. Dry storage could be an alternative solution (used for example in UK, Canada, USA or Hungary) and is studied as such. Fuel assemblies are placed in a closed container filled with an inert gas. Temperatures are higher than in wet storage and decrease for years according to residual power decreases.

The temperature evolution during dry storage depends on fuel enrichment, burnup and cooling performance of the cask. It lies in the range [20°C, 400°C]. The existence of a

sufficiently large defect could lead to DHC, as it is explained in the next part.

III. SCIENTIFIC CONTEXT

A. Chemical description of DHC

Delayed Hydride Cracking is a cyclic and quasi-static phenomenon divided into four steps: dissolution, diffusion, precipitation and incremental brittle fracture.

After dissolution, the diffusion of hydrogen is the consequence of three driving forces: concentration gradient, stress gradient and thermal gradient. Indeed, hydrogen in solid solution in zirconium moves where concentration and temperature are the lowest, and tensile stress is the highest. In this study, the focus is on the stress gradient. The flux of hydrogen is described with the expression below [6]:

$$J_H = -D_H\left(+\nabla C_{ss} + \frac{C_{ss}Q^*}{RT^2}\nabla T - \frac{C_{ss}\bar{V}_H}{RT}\nabla p_h\right)$$

where D_H is the hydrogen diffusion coefficient, C_{ss} the hydrogen concentration in solid solution, Q^* the heat of transport, R the ideal gas constant, $\bar{V}_H$ the partial molar volume of hydrogen in zirconium alloys and p_h the applied hydrostatic stress (mean stress).

Then, the hydrogen in solid solution precipitates into hydrides. The concentration of hydrogen in solid solution increases near by the crack tip, until it reaches a limit and precipitates into hydrides. For a given temperature, this limit is slightly higher than the terminal solid solubility during dissolution [6], [7].

Finally brittle fracture of the hydrided zone ahead of the crack tip occurs. Hydrogen in solid solution continues to diffuse at the crack tip and to precipitate into hydrides: the size of hydride ahead the crack tip increases until its brittle fracture. The hydride's size before fracture depends on the stress in the structure. It is important to notice that over 300°C the fracture of hydrides is ductile: a part of the temperature range of dry storage corresponds to the brittle fracture temperature of hydrides [8], [9].

B. Mechanical description of DHC

Mechanically speaking, the crack propagation can be defined by three conditions.

First, a stress intensity factor value K_{1H} has to be reached before cracking starts. This value allows to evaluate DHC by calculating the critical hydride's length [8]. According to part A, an incubation time is needed before the onset of hydride's growth.

Secondly, after the threshold intensity factor has been reached, the crack propagates at a constant velocity. The crack velocity has little or no dependence on stress intensity factor, whereas it has strong and complex dependence on temperature. It is a complex dependence because hydride's brittleness decreases, whereas hydrogen diffusion rate increases when the temperature increases [3], [10], [11].

Finally, if a critical stress intensity factor K_{1C} is reached, the crack propagates in an unstable and fast way.

IV. PROCEDURE

A. Experimental procedure

The goal of the experimental procedure is to propagate and to control a crack in the thickness of fuel claddings. This procedure is divided into 5 steps.

The first step is the design and the manufacture of a new test specimen. The innovative design is called Notched C-Ring and is presented in Figure 1. The notch allows to create a favourable zone for diffusion and precipitation of hydrogen and the C shape allows to load the specimen using a tensile machine and to limit friction during the test, as compared to standard ring tests. EDM is used to manufacture the notch with a $\emptyset 70\mu m$ wire. The notch is then characterised using an optical microscope, an electronic scanning microscope and a profilometer to observe the notch's shape, dimensions and uniformity along the length of the specimen. The average depth and width of the notch are respectively 100 and 80µm.

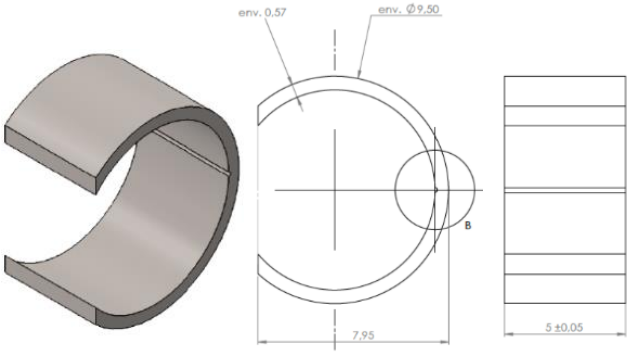

Figure 1. Design of the Notched C-Ring specimen.

The second step is the design and manufacture of a specimen holder (Figure 2): longs rods are used to fit inside an oven, and the use of slotted swings limits friction.

The third step concerns hydrogen charging of the specimens. Several 20 cm tube sections were charged using a gaseous method from 100 up to 800 wt. ppm.

The fourth step consists in the testing of specimens. According to the part III and literature's results [10], [12], the specimen charged at 100 wt. ppm may be tested at 250°C after a peak of temperature at 320°C in order to obtain the maximum hydrogen concentration in solid solution and to favour DHC.

This test enables the study of the following parameters influence on DHC: hydrogen concentration, temperature, applied mechanical load and duration.

The last step consists in analysing with an electronic scanning microscope the specimen's microstructure after the test in order to characterise the DHC's mechanism.

B. Numerical procedure

The aim of the numerical model is to support the understanding and the exploitation of the experimental results, in order to give a relevant toughness value in function of initial parameters, such as irradiation, hydrogen concentration and temperature. The FEM model is developed using the finite element code Cast3M solver [13] and the Mfront code generator [14].

Figure 2. Photograph of the assembly on a tensile test machine (left) and of a C-Ring into the swings (right)

Mechanical behaviour is modelled using constitutive equations described in the literature [15]: isotropic elasticity, anisotropic viscoplastic described by a Hill's quadratic yield criterion, and taking into account thermal and irradiation creep.

In addition, the hydrogen diffusion model presented in part III is used, together with a precipitation kinetics model.

The dependence of diffusion on mechanical constitutive models on the hydride content is also accounted for. Furthermore, hydrogen in solid solution and hydrides produce an increase of the volume, therefore an additional strain is taken into account in the description of the mechanical behaviour of the material. The kinetics of hydride dissolution and hydrogen precipitation is described by the model of Passelaigue et al. [16], based on Marino's and Kammenzind's models [17], [18]. Concerning the new expression of flux and mechanical strain, the Jernkvist et Massih [19] and Xia et al. [20] models are used. Until now, those models were not combined: models are simplified by ignoring stress effect or by not taking into account the latest understanding of hydrogen precipitation and hydride dissolution hysteresis. Finally, one of the scientific challenges of this study is to calculate the stress intensity factor using this new specimen shape by developing a standard method.

V. RESULTS

The qualification of the experiment begins with tests on unhydrided C-ring without notch. Results are shown in Figure 3 and compared with numerical results: results show a good correlation between experiments and simulations at 20 and 250°C. Parameters of the model are based on experimental tests performed above 350°C: they could be modified to obtain a better fit.

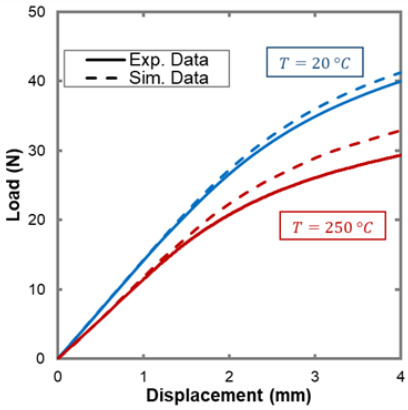

Figure 3. Comparison of load/displacement curve between experiment and numerical tensile test results on C-Ring without notch at 20 and 250°C.

On the numerical side, the coupling of hydrogen diffusion with mechanical model was implemented. Figure 4 shows the result for a simulation with the following parameters: initial hydrogen concentration of 92 wt. ppm (0.6 kg/m^3), temperature of 250°C and an imposed displacement of 1 mm. The influence of hydrogen in solid solution and of hydrides on the mechanical behaviour are not included for the moment.

It shows the opening stress (SMYY, left) and hydrogen concentration (right) profiles after 10 and 50 minutes. The load was applied very rapidly.

The evolutions of SMYY and hydrogen concentration along the ligament are similar: they reach a peak at 0.02 mm from the notch root and decrease towards the end of the ligament. This result was expected because of the stress driven diffusion (the maximum hydrogen concentration is at the maximum of stress), and validates the correct implementation of this part in the numerical model.

Figure 4. Evolution of principal stress in the loading direction SMYY

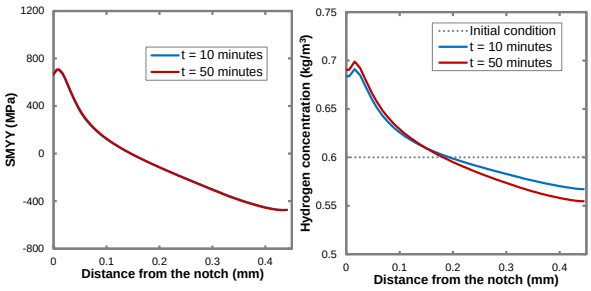

(left) and of hydrogen concentration (right) along the ligament of Notched C-Ring at 250°C.

Figure 5 shows the stress in the loading direction (SMYY) on the deformed mesh. In this case, the simulation was done for an imposed displacement of 4 mm at 250°C. It shows different features: (i) the tensile to compression transition is located at the middle of the thickness (ii) the maximal stress zone is located ahead of the notch root at about 20 µm.

Finally, qualification of the Notched C-Ring test is under progress. Implementation of the kinetic model discussed in part IV is to be done in the next months. A cohesive model will then be used to simulate crack propagation. The methodology to calculate the threshold stress intensity factor from finite elements analysis is developed in parallel.

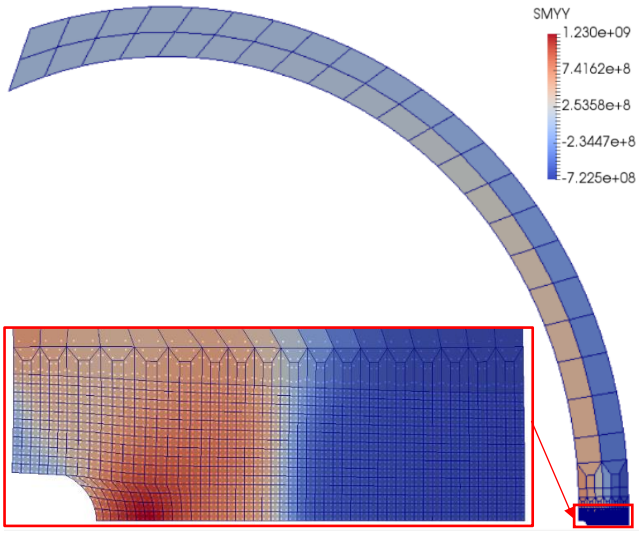

Figure 5. Numerical post-treatment on Paraview: visualization of SMYY (in Pa) values in elements and Gaussian points on deformed mesh at 250°C.

VI. CONCLUSION

DHC is a multiscale and multi-physics phenomenon coupling chemistry (diffusion and precipitation of hydrogen) and thermo-mechanics (fracture of hydrides). An original coupled experimental and simulation procedure is currently developed to evaluate the risk of DHC in cladding tubes. This procedure will be used to determine the material toughness during DHC. Preliminary results show a good agreement between experimental and numerical mechanical behaviour of the specimen under applied load. In addition, a coupled hydrogen diffusion/mechanical behaviour model was implemented in Cast3M.

VII. Acknowledgements

The authors would like to thank the project Transport & Entreposage of the French *Institut Tripartite CEA-EDF-Framatome* for supporting this study.

VIII. References

[1] C. J. Simpson and C. E. Ells, "Delayed hydrogen embrittlement in Zr-2.5 wt % Nb," *J. Nucl. Mater.*, vol. 52, no. 2, pp. 289–295, Oct. 1974, doi: 10.1016/0022-3115(74)90174-3.

[2] IAEA Report, "Delayed Hydride Cracking in Zirconium Alloys in Pressure Tube Nuclear Reactors," TECDOC-1410, 2004.

[3] J.-D. Hong, H.-C. Kim, J.-S. Kim, Y.-S. Yang, and D.-H. Kook, "Delayed hydride cracking assessment of PWR spent fuel during dry storage," *Nucl. Eng. Des.*, vol. 322, pp. 324–330, Oct. 2017, doi: 10.1016/j.nucengdes.2017.07.015.

[4] K. W. Lee and S. I. Hong, "Zirconium hydrides and their effect on the circumferential mechanical properties of Zr–Sn–Fe–Nb tubes," *J. Alloys Compd.*, vol. 346, no. 1–2, pp. 302–307, Nov. 2002, doi: 10.1016/S0925-8388(02)00527-3.

[5] IRSN Report, "Entreposage du combustible nucléaire usé : Concepts et enjeux de sûreté," 2018–3, Aug. 2018.

[6] M. P. Puls, *The Effect of Hydrogen and Hydrides on the Integrity of Zirconium Alloy Components*. London: Springer London, 2012. [Online]. Available: http://link.springer.com/10.1007/978-1-4471-4195-2

[7] O. Zanellato, M. Preuss, J.-Y. Buffiere, F. Ribeiro, A. Steuwer, and B. Krebs, "Synchrotron diffraction study of dissolution and precipitation kinetics of hydrides in Zircaloy-4," *J. Nucl. Mater.*, vol. 420, no. 1–3, pp. 537–547, Jan. 2012, doi: 10.1016/j.jnucmat.2011.11.009.

[8] S.-Q. Shi and M. P. Puls, "Criteria for fracture initiation at hydrides in zirconium alloys I. Sharp crack tip," *J. Nucl. Mater.*, vol. 208, no. 3, pp. 232–242, Feb. 1994, doi: 10.1016/0022-3115(94)90332-8.

[9] T. Kubo, Y. Kobayashi, and H. Uchikoshi, "Determination of fracture strength of δ-zirconium hydrides embedded in zirconium matrix at high temperatures," *J. Nucl. Mater.*, vol. 435, no. 1–3, pp. 222–230, Apr. 2013, doi: 10.1016/j.jnucmat.2012.12.045.

[10] Y. S. Kim, S. S. Park, and S. I. Kwun, "Threshold stress intensity factor, KIH for delayed hydride cracking of a Zr-2.5Nb tube with loading mode," *J. Alloys Compd.*, vol. 462, no. 1–2, pp. 367–375, Aug. 2008, doi: 10.1016/j.jallcom.2007.08.045.

[11] G. A. McRae, C. E. Coleman, and B. W. Leitch, "The first step for delayed hydride cracking in zirconium alloys," *J. Nucl. Mater.*, vol. 396, no. 1, pp. 130–143, Jan. 2010, doi: 10.1016/j.jnucmat.2009.08.019.

[12] M. T. Jovanovic´, G. K. Shek, H. Seahra, and R. L. Eadie, "Metallographic and Fractographic Observations of Hydrides during Delayed Hydride Cracking in Zr-2.5% Nb Alloy," *Mater. Charact.*, vol. 40, no. 1, pp. 15–25, Jan. 1998, doi: 10.1016/S1044-5803(97)00091-0.

[13] "Cast3M website." Available: http://www-cast3m.cea.fr/

[14] T. Helfer, B. Michel, J.-M. Proix, M. Salvo, J. Sercombe, and M. Casella, "Introducing the open-source mfront code generator: Application to mechanical behaviours and material knowledge management within the PLEIADES fuel element modelling platform," *Comput. Math. Appl.*, vol. 70, no. 5, pp. 994–1023, Sep. 2015, doi: 10.1016/j.camwa.2015.06.027.

[15] M. Le Saux, J. Besson, S. Carassou, C. Poussard, and X. Averty, "A model to describe the anisotropic viscoplastic mechanical behavior of fresh and irradiated Zircaloy-4 fuel claddings under RIA loading conditions," *J. Nucl. Mater.*, vol. 378, no. 1, pp. 60–69, Aug. 2008, doi: 10.1016/j.jnucmat.2008.04.017.

[16] F. Passelaigue, E. Lacroix, G. Pastore, and A. T. Motta, "Implementation and Validation of the Hydride Nucleation-Growth-Dissolution (HNGD) model in BISON," *J. Nucl. Mater.*, vol. 544, p. 152683, Feb. 2021, doi: 10.1016/j.jnucmat.2020.152683.

[17] G. P. Marino, "Hydrogen supercharging in Zircaloy," *Mater. Sci. Eng.*, vol. 7, no. 6, pp. 335–341, Jun. 1971, doi: 10.1016/0025-5416(71)90016-4.

[18] B. Kammenzind, D. Franklin, H. Peters, and W. Duffin, "Hydrogen Pickup and Redistribution in Alpha-Annealed Zircaloy-4," in *Zirconium in the Nuclear Industry: Eleventh International Symposium*, E. Bradley and G. Sabol, Eds. 100 Barr Harbor Drive, PO Box C700, West Conshohocken, PA 19428-2959: ASTM International, 1996, pp. 338-338–33. Accessed: Mar. 24, 2021. [Online]. Available: http://www.astm.org/doiLink.cgi?STP16180S

[19] L. O. Jernkvist and A. R. Massih, "Multi-field modelling of hydride forming metals. Part I: Model formulation and validation," *Comput. Mater. Sci.*, vol. 85, pp. 363–382, Apr. 2014, doi: 10.1016/j.commatsci.2013.11.034.

[20] Z. Xia, J. Zhang, Q. Tong, and S. Ding, "Multi-physics modeling of delayed hydride cracking in zirconium alloys," *J. Mech. Phys. Solids*, vol. 132, p. 103677, Nov. 2019, doi: 10.1016/j.jmps.2019.07.020.

Proceedings of the European Nuclear Young Generation Forum
ENYGF'21
September 27-30, 2021, Tarragona, Spain

Porous Crystal Plasticity-based Ductile Fracture assessment for FCC Nuclear materials

Sénac, Cédric[1*], Hure, Jérémy[1], Scherer, Jean-Michel[1, 2, 3], Helfer, Thomas[4] and Tanguy, Benoît[1]

[1] Université Paris-Saclay, CEA, France; [2] Laboratoire Navier, France; [3] Laboratoire de Mécanique des Solides (LMS), France; [4] CEA-Cadarache, France.

*Corresponding author: *cedric.senac@cea.fr*

I. INTRODUCTION

Several nuclear reactor components are made of austenitic stainless steels, owing to their resistance to corrosion and their excellent mechanical properties: ductility – strain upon fracture – and fracture toughness – resistance to crack propagation. For instance, in Light Water Reactors (LWRs), austenitic steels are used for core internal components such as baffle bolts, guide tubes, core plates and support columns, the two main grades being Solution-Annealed (SA) 304L and Cold-Worked (CW) 316L. Austenitic steels are also considered for fuel claddings and reactor vessels of Generation IV sodium-cooled fast reactors.

Safety and security being major concerns in the nuclear field, austenitic stainless steels mechanical properties have been widely studied and their main failure mode happens to be ductile fracture. Simulation of ductile fracture is therefore very important to strengthen structural integrity assessment under standard and accidental conditions, plan inspection activities and develop steels with better mechanical properties. Furthermore, reactor vessel internals are subjected to neutron irradiation, which is known to affect material properties and fracture behavior. Understanding the fracture behavior of irradiated LWR internals thus comes among the challenges of nuclear reactor lifetime extension.

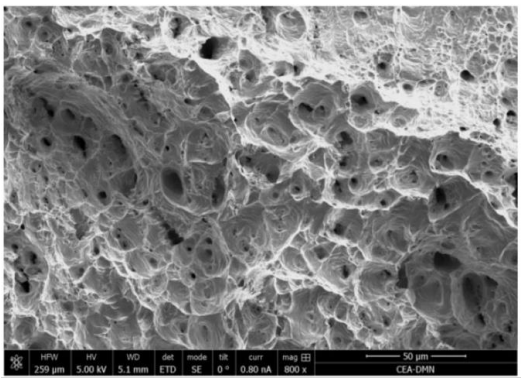

Figure 1. Scanning Electron Microscopy (SEM) observation of the fracture surface of a 304L austenitic stainless steel mechanically loaded at 300°C [1].

II. DUCTILE FRACTURE MECHANISMS

The main ductile fracture mode identified in austenitic stainless steels involves growth and coalescence of internal cavities, as evidenced on fracture surfaces (Fig. 1). Indeed, the dimples are the traces of cavities that have coalesced under mechanical loading. Fig. 2 presents the stages of void growth to coalescence fracture mode [2]: a) voids nucleate by particle decohesion, precipitate cracking or irradiation; b) voids grow without interaction; c) void coalescence occurs when cavities interact with each other until fracture (d).

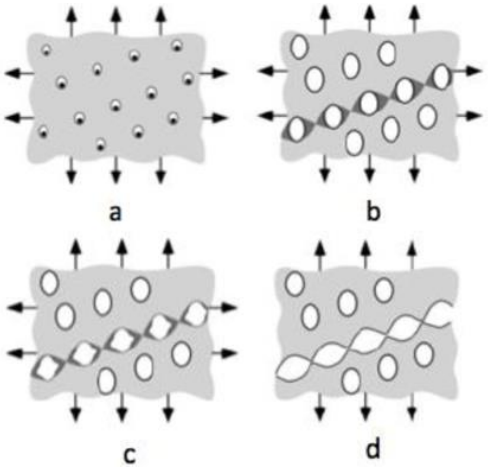

Figure 2. Stages of ductile fracture by growth and coalescence of internal voids [2].

Under high neutron doses, microstructural observations have shown the formation of irradiation-induced nano-sized voids in some particular conditions [4], which may enhance ductile fracture by growth and coalescence of voids [5].

III. HOMOGENIZATION OF POROUS MATERIALS

Austenitic steels have a polycrystalline Face-Centered Cubic (FCC) structure, as shown on Fig. 3 in which each color stands for a different crystallographic orientation.

Since austenitic steels often display grain sizes of micrometric scale and cavities are generally sub-micrometrical, voids - either coming from inclusions or induced by radiation - are located inside grains or at grain boundaries.

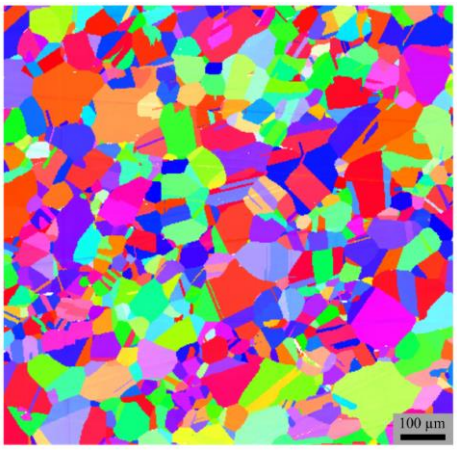

Figure 3. Electron Back-Scatter Diffraction (EBSD) mapping of an austenitic steel (courtesy of A. Courcelle) revealing the crystallographic orientations.

Homogenization of porous solids consists in accounting for the presence of voids on mechanical properties. Therefore, a certain number of internal variables are needed to represent the material microstructure. Classical parameters include porosity f defined as the void volume fraction, void aspect ratio W, ligament size ratio χ describing the distance between voids, etc.

Due to the void size being inferior to the grain size, porous mechanical models developed through homogenization of an isotropic matrix containing voids, such as Gurson-Tvergaard-Needleman (GTN) model or Thomason model ([5], [6]) can be insufficient to describe the mechanisms at the grain scale. Indeed, FCC crystals have strongly anisotropic behaviors [7], which suggests that homogenization should be performed one scale below: at the grain - single crystal - level. This procedure is depicted in Fig. 4.

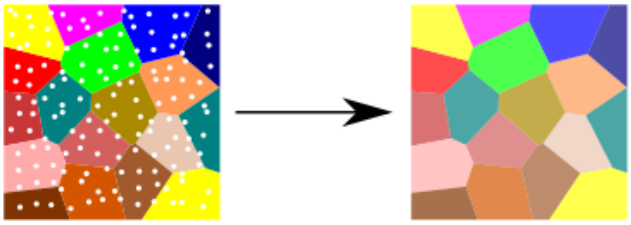

Figure 4. Homogenization of a porous polycrystalline aggregate with a void size inferior to the grain size.

Several plastic yield criteria - describing plastic flow - relevant for the homogenization shown in Fig. 4 are available in the literature; a single-crystal homogenized model is therefore constructed and described in section IV. Finally, in section V, this model is used to simulate the ductile tearing of single crystals and polycrystalline specimens and to underline the influence of crystal anisotropy on the fracture characteristics, thus justifying the interest of the present work when it comes to predict the failure of FCC nuclear materials.

IV. MODEL DESCRIPTION

Homogenization considers simplified void distributions - usually spheroidal voids in cubic unit cells - as shown on Fig. 5. Axisymmetric loading conditions are applied to the unit cells, such as the stress is equal to $\underline{\underline{\Sigma}} = \begin{pmatrix} \Sigma_{11} & 0 & 0 \\ 0 & \alpha\Sigma_{11} & 0 \\ 0 & 0 & \alpha\Sigma_{11} \end{pmatrix}$. The key parameter is known as stress triaxiality, defined as $T = \frac{1+2\alpha}{3-3\alpha}$.

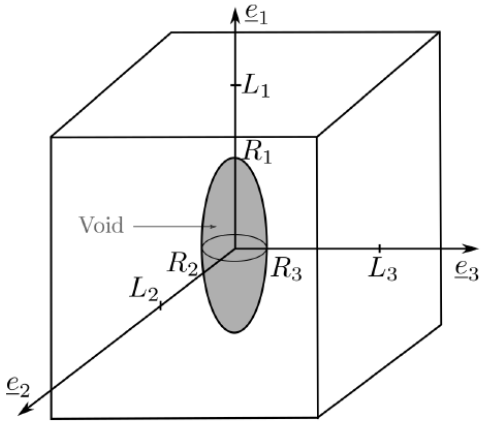

Figure 5. Geometry of the unit cell on which the homogenized model is developed.

According to the homogenization method described in section III, the matrix surrounding the void is a FCC single crystal of a given crystallographic orientation. Using this simplified geometry and loading, the homogenized model is developed to reproduce the results that could be obtained by an explicit Finite Element Modeling performed on the aforementioned unit cell. Under the assumption that the homogenized model is still valid under more complex loadings, it can then be used in macroscopic Finite Element simulations to capture the mechanical behavior of porous single crystals and polycrystalline specimens.

This homogenized model can be summarized under the form of a function G defining the temporal evolution of the studied material under a loading defined by strain increments $d\underline{\underline{\varepsilon}}$:

$$\left\{\underline{\underline{\Sigma}}, f, W, \chi, \lambda\right\}(t+dt) = G\left[d\underline{\underline{\varepsilon}}, \left\{\underline{\underline{\Sigma}}, f, W, \chi, \lambda\right\}(t)\right]$$

where $\underline{\underline{\varepsilon}}$ is the strain, $\underline{\underline{\Sigma}}$ is the stress and f, W, χ, λ are the internal variables described in section III. The main components of function G are briefly described in the rest of the section.

In Fig. 5, the geometrical definition of homogenization internal variables is quite straightforward. For instance, porosity f is defined as follows:

$$f = \frac{V_{cav}}{V_{tot}} = \frac{4\pi}{3}\frac{R_1 R_2 R_2}{L_1 L_2 L_3}$$

Each microstructural variable is controlled by an evolution law depending on stress, strain increments and other microstructural variables. For instance, the evolution of porosity f follows an equation deduced from the plastic incompressibility of the matrix [6]. However, the key

ingredients of the homogenized model are the porous yield criteria that are chosen to account for void growth and void coalescence. These criteria predict the onset of plasticity and have related plastic flow rules that control the evolution of plastic strain, *e.g.* just as the von Mises criterion does for non-porous isotropic materials.

The growth criterion chosen below is the one presented in [8]. Derived for porous crystals, it accounts for the shear stress on each slip system through a regularization function and has demonstrated good accuracy in FCC crystals [9]:

$$\left(\frac{\left(\sum_{k=1}^{K}\left|\underline{\underline{\mu_k}}:\underline{\underline{\Sigma}}\right|^n\right)^{\frac{1}{n}}}{\tau_0}\right)^2 + 2qf\cosh\left(\kappa\frac{\mathrm{tr}\left(\underline{\underline{\Sigma}}\right)}{3\tau_0}\right) - 1 - (qf)^2 = 0$$

The coalescence criterion used below is taken from [10]. It displays uniaxial strain controlled by two crystallographic parameters M_1 and M_2:

$$\frac{\Sigma_I}{\tau_0} - \frac{0.9}{\sqrt{3}}\left(2 - \sqrt{1+3\chi^4} + \ln\left(\frac{1+\sqrt{1+3\chi^4}}{3\chi^2}\right)\right)M_1 - \left(\frac{(12.9\chi - 0.84)W}{1+(12.9\chi-0.84)W}\right)\left(\frac{\chi^3 - 3\chi + 2}{3\sqrt{3}W\chi}\right)M_2 = 0$$

In Fig. 6, comparisons between the predictions of the homogenized model and numerical simulations accounting explicitly for the presence of voids as presented in Fig. 5 are shown for different stress triaxialities T and crystallographic orientations o. It can be seen that prediction of the onset of coalescence – corresponding to the sudden decrease of stress - is very important for the quality of the model: for instance, for orientation n°2, this prediction is better than for orientation n°5. The overall agreement of loading curves is relatively good since the model can predict yield stresses and stress softening, reproduce crystallographic anisotropy (which is strong at low stress triaxialities) and be coupled to different strain hardening laws. The law $2b$ used in Fig. 6 is Peirce-Asaro-Needleman hardening law [11] which exhibits a saturation behavior and is well homogenized by the model.

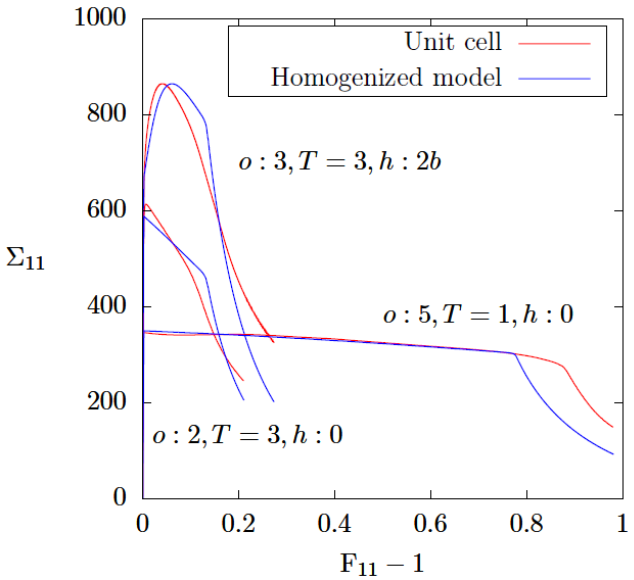

Figure 6. Comparisons of stress-strain curves predicted by the homogenized model to the numerical unit cell simulations accounting explicitly for the presence of voids.

V. DUCTILE TEARING SIMULATIONS

The homogenized model can predict loading curves in good agreement with explicit computations on simple loadings such as axisymmetric ones; it can then be used to study the tearing of notched porous polycrystalline specimens subjected to various boundary conditions. Two of the meshes used are shown in Fig. 7, along with the corresponding displacement boundary conditions. Plane strain conditions are applied to the meshes. The tensile mesh holds 3420 quadratic elements with reduced integration while the bending mesh contains 10469 elements. Since both monocrystalline and polycrystalline specimens are considered, the shape and position of grains are specified on Fig. 6 in the polycrystalline case.

The computations are performed using the finite-element solver Cast3M coupled with the MFront code generator [13], both developed at CEA. Since the material law implicit integration is quite complex, a mixed Newton-Raphson / fixed point algorithm was developed to alleviate numerical difficulties.

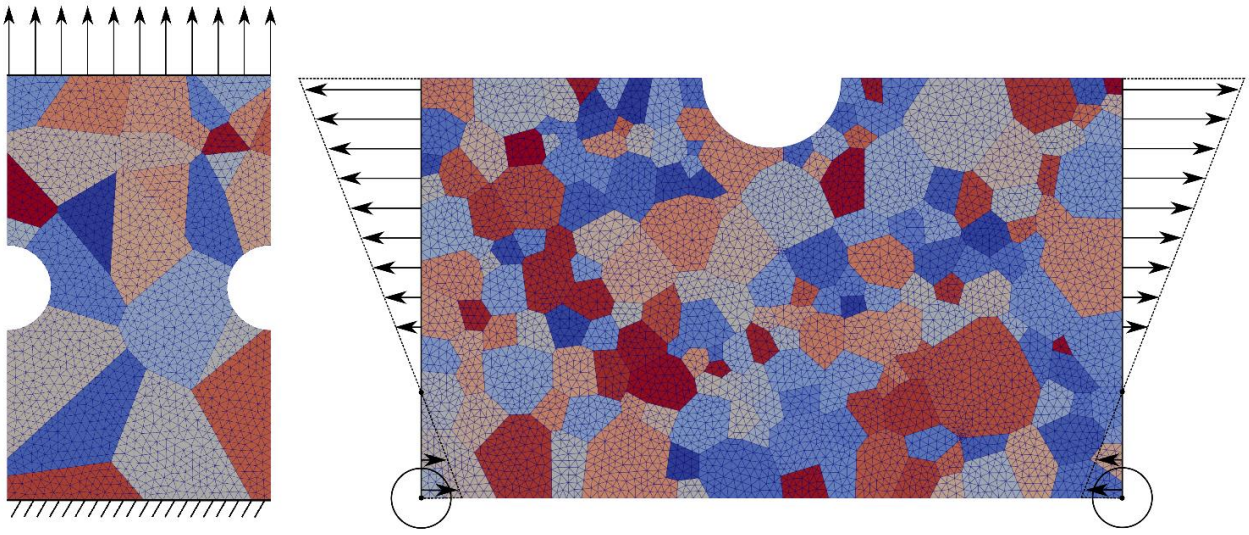

Figure 7. Meshes and boundary conditions used for the finite-element computations: a tensile test and a bending test. In the case of polycrystalline specimens, the grain positions are shown with different colours.

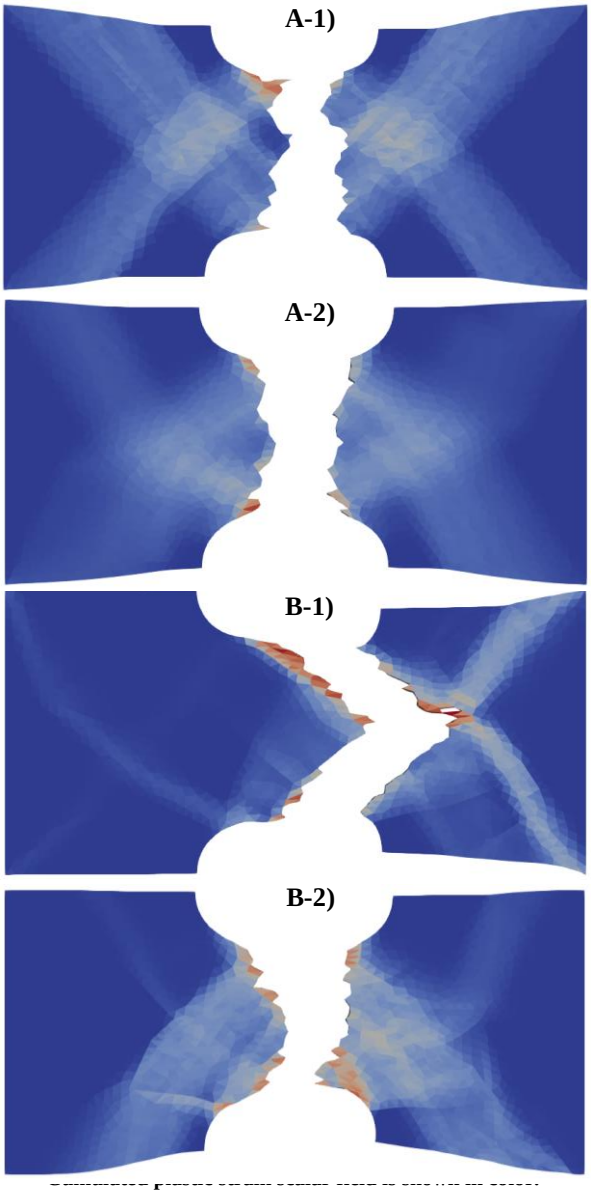

Fig. 8 shows the crack paths for different tensile specimens. Specimen A-1) and A-2) are single crystals; it can be seen that plasticity is localized in four bands because they are not impeded by grain boundaries, as opposed to polycrystalline specimens B-1) and B-2) which display plasticity that is less regular in nature.

From specimens B-1) and B-2), it is clear that crystallographic orientations have an important influence on the ductile fracture path: for various sets of random orientation, the crack path is quite different as some grains are softer. This finding on a tensile specimen with 27 grains is confirmed by the fracture paths obtained on bending specimens with 195 grains. These first simulations prove the feasibility of coupling crystal yield criteria accounting for growth and coalescence to study ductile fracture at polycrystalline scales. As demonstrated in [14], computations using a unique crystalline growth criterion are feasible on larger scales (with over a hundred thousand elements), a feature that seems also possible for the model presented here.

VI. CONCLUSION

In conclusion, models such as the one described here above bridge a gap in multiscale ductile fracture simulations. On the one hand, they can be used to compare simulations accounting for grain anisotropy to isotropic porous models to assess the error that is made by neglecting microstructure; on the other hand, they can as well be directly employed to compute the mechanical behavior and ductile fracture of medium-scale three-dimensional specimens. This opens up a way of improving the understanding of nuclear reactor internal components fracture behavior under mechanical loading and can be a useful tool to support experimental campaigns to extend nuclear reactor lifetime.

VII. References

[1] P.O. Barrioz, “Rupture ductile des matériaux CFC irradiés,” Université Paris Saclay, 2019.

[2] T. L. Anderson, “Fracture Mechanics: Fundamentals and Applications,” CRC Press, 2005.

[3] A. A. Benzerga, J.-B. Leblond, “Ductile fracture by void growth to coalescence,” Adv. Applied Mech., vol. 44, pp. 169–305, dec. 2010.

[4] F.A. Garner, “4.02 - Radiation Damage in Austenitic Steels,” Comp. Nucl. Mater., vol. 4, pp. 33-95, 2012.

[5] P.O. Barrioz, J. Hure, B. Tanguy, “Void growth and coalescence in irradiated copper under deformation,” J. Nucl. Mater., vol. 502, no. 15, pp. 121-131, apr. 2018.

[6] J. Besson, “Continuum models of ductile fracture: a review,” Int. J. Dam. Mech., vol. 19, no. 1, pp. 3–52, jan. 2010.

[7] P.O. Barrioz, J. Hure, B. Tanguy, “Effect of dislocation channelling on void growth to coalescence in FCC crystals,” Mater. Sci. Eng. A , vol. 749, pp. 255–270, 2019.

[8] J. Paux, L. Morin, R. Brenner, D. Kondo, “An approximate yield criterion for porous single crystals,” Eur. J. Mech. A/Solids, vol. 51, pp. 1–10, may-july 2015.

[9] J. Paux, R. Brenner, D. Kondo, “Plastic yield criterion and hardening of porous single crystals,” Int. J. Solids Struct., vol. 132–133, pp. 80-95, 2018.

[10] J. Hure, “A coalescence criterion for porous single crystals,” J. Mech. Phys. Sol., vol. 124, pp. 505–525, mar. 2019.

[11] D. Peirce, R. J. Asaro, A. Needleman, “Material rate dependence and localized deformation in crystalline solids,” Acta Metall., vol. 31, no. 12, pp. 1951–1976, dec. 1983.

[12] P. Franciosi, A. Zaoui, “Multislip in fcc crystals: a theoretical approach compared with experimental data,” Acta Metall., vol. 30, no. 8, pp. 1627–1637, aug. 1982.

[13] T. Helfer, B. Michel, J. Proix, M. Salvo, J. Sercombe, M. Casella, “Introducing the open-source mfront code generator: Application to mechanical behaviours and material knowledge management within the pleiades fuel element modelling platform,” Comput. Math. with Appl., vol. 70, no. 5, sept. 2015.

[14] M. Khadyko, B. H. Frodal, O. S. Hopperstad, “Finite element simulation of ductile fracture in polycrystalline materials using a regularized porous crystal plasticity model,” Int. J. Fract., vol. 228, pp. 15–31, feb. 20

Proceedings of the European Nuclear Young Generation Forum
ENYGF'21
September 27-30, 2021, Tarragona, Spain

Impact of dopants on diffusion in crystalline and amorphous zirconia.

Owen, Megan W. [1*], Rushton, Michael J. D.[1], Evitts, Lee J.[1], Claisse, Antoine J. [1,2], Puide, Mattias [1,2], Lee, William E. [1], and Middleburgh, Simon C. [1**]

[1] Nuclear Futures Institute, Bangor University, United Kingdom; [2] Westinghouse Electric Sweden AB, Sweden;

*Corresponding author: * megan.owen@bangor.ac.uk **s.middleburgh@bangor.ac.uk*

I. INTRODUCTION

Zirconium alloys are used in boiling and pressurised water reactors as fuel cladding surrounding the nuclear fuel pellet. Coolant water causes the formation of a passivation layer (ZrO_2) on the outer side of the cladding, beneficial in hindering oxygen migration and reducing the rate of corrosion. However, ZrO_2 does not act to completely prevent corrosion as oxygen migration is still observed through this layer, impacting operational lifetime [1].

Doping zirconia with aliovalent substitutional ions in place of Zr has been observed for solid oxide fuel cells (SOFC), increasing oxygen diffusivity due to the generation of oxygen vacancies for charge balancing purposes. Common materials include yttria stabilised zirconia (YSZ), with reports of activation energies for oxygen diffusion ranging between 0.20 eV to 0.89 eV, differing due to dopant concentration [2]–[4]. This range is much lower than those reported for undoped, crystalline zirconia, which has been reported as 1.40 eV and 2 eV in tetragonal and monoclinic polymorphs, respectively [5], [6].

Mechanisms of diffusion in bulk ZrO_2 are fairly well understood, however, diffusion along grain boundaries is far less so [1]. Experimental work conducted by Chokshi found diffusion of Zr and O along grain boundaries in 3 mol. % yttria stabilised tetragonal zirconia (3YTZ) and 8 mol. % yttria stabilised cubic zirconia (8YCZ) was much greater than that measured in the bulk [7]. In previous work by Rabkin *et al.*, [8], grain boundaries in CaO and MgO stabilised ZrO_2 (i.e. aliovalent cations), have been identified as "glassy", eluding that they have a heterogeneous and disordered nature, and may be potential high diffusion pathways.

This work is focused on modelling amorphous systems of undoped and trivalent lanthanide doped ZrO_2. Diffusion in both systems has been analysed, and comparisons have been made with corresponding crystalline systems. A range of trivalent lanthanides have been considered (Yb, Dy, Gd, Nd, and La), to model diffusivity as a function of ionic radius to analyse the effects of differing dopant radius. Diffusion coefficients, pre-exponential factors, and activation energies have been calculated to further analyse diffusion properties.

II. METHOD

A. Amorphous Structure Generation

Molecular dynamics (MD) simulations have been used to generate amorphous undoped and trivalent lanthanide doped ZrO_2 systems, using a melt-quench procedure [9], [10]. The MD simulation package used was the Large-scale Atomic/Molecular Massively Parallel Simulator, LAMMPS (version 7 Aug 2019), with a simulation timestep of 1 fs, and use of periodic boundary conditions throughout [11]. The pair potential model developed by Cooper *et al.* [12], [13] has been used for this work to describe the forces acting between atoms. This model describes many-body effects due to the use of the embedded atom model. Dopant interactions in the systems were described using pairwise interactions, developed by Rushton and Chroneos in [14]. Pure pairwise interactions were employed here, due to their effectiveness in modelling low concentrations of dopants in these systems.

An initial fluorite structure was used for all systems, equivalent to an 8×8×8 supercell of the cubic polymorph of ZrO_2 unit cell, consisting of a total of 6144 atoms. Choice of polymorph for the melt-quench method is insignificant, as the system is melted, losing its initial structure regardless. For the trivalent doped systems, Zr ions were randomly substituted with trivalent dopants to achieve the two concentrations of dopant analysed, 5.3 at. % and 11.0 at. %. Charge balancing was preserved through generating an oxygen vacancy for every two dopant ions substituted. The lanthanide dopants considered included Yb, Dy, Gd, Nd, and La. Once the crystalline structures were generated successfully, the melt-quench procedure was conducted to generate amorphous supercells. The systems were heated from 300 K to 5000 K over 920 ps, in 100 K increments using an isothermal-isobaric (NPT) thermodynamic ensemble. A Nosé-Hoover thermostat and barostat were used for the NPT calculations, with relaxation parameters set to 1 ps [15]. At each temperature increment, the system

was equilibrated at temperature for 10 ps, before continued heating. Upon reaching 5000 K the system was held for a further 10 ps, before being quenched to 300 K in 100 ps. At 300 K, the system was held for 60 ps for equilibration purposes. Equilibration at 300 K for a further 60 ps was conducted when calculating the radial distribution function of the systems.

B. Diffusion Calculations

Diffusivities of constituent species were calculated from the mean squared displacements (MSD) using the Einstein equation [16]. MSD calculations were conducted between 500 K and 900 K, in 100 K increments, using the same temperature ramp as described in section A. The MSD calculations were conducted over 20 ns.

Five different amorphous structures were generated via five different melt-quench simulations for both undoped and doped ZrO_2 systems. Averages across the five systems for both undoped and doped ZrO_2 were used for diffusivity data, reducing stochastic spread.

The diffusion coefficients (D) and activation energies (Q_d) for migration were calculated assuming Arrhenius like behaviour. A least squares fit between the logarithm of the MD derived diffusivities and the reciprocal of simulation temperature was conducted as shown by Equation 1.

$$D = D_o \exp\left(\frac{-Q_d}{RT}\right) \quad (1)$$

III. RESULTS

Amorphous undoped zirconia has been generated successfully using the melt-quench method, and the radial distribution function (RDF) for the system is shown in Figure 1a). The two peaks occur at 2.1 Å and 2.7 Å, respectively, before the RDF oscillates at a value of g(r) = 1, characteristic of that of an amorphous system. The partial RDF, shown in Figure 1b), describes the Zr-O, O-O, and Zr-Zr pairs in the system. The first peak for each pair occurs at 2.1 Å, 2.7 Å, and 3.5 Å, respectively, consistent with previous literature, as reported distances for Zr-O, O-O, and Zr-Zr are 2.1 Å, 2.7 Å, and 3.5 Å, respectively [10], [17].

Doped amorphous ZrO_2 systems were generated successfully, with the two prominent peaks of the RDF located at the same position to that of the undoped system. With an increasing concentration of dopant, the prevalence of the second peak begins to diminish. The partial RDFs were also compared, showing a dependence of the M-O (where M is the lanthanide dopant) first peak on ionic radius. The Zr-O distance is effectively unchanged, comparing well with work conducted by Dong et al. in crystalline yttria stabilised zirconia, concluding that the Y-O pair had a larger separation distance than the Zr-O pair [18]. In Figure 2b) an intermediate peak is observed at 2.4 Å, between the first (2.1 Å) and second (2.7 Å) peak in the 11.0 at. % La-doped system. No other systems show this intermediate peak, and when considering the partial RDF, the intermediate peak can be attributed to the La-O pair, as the first peak for this pair occurs at 2.4 Å. The M-O peak in the other doped systems overlaps with the Zr-O peak, indicating it is partially hidden by the larger peak. However, the La result shows the system is preserving the native oxide bond distances observed in the crystalline binary systems.

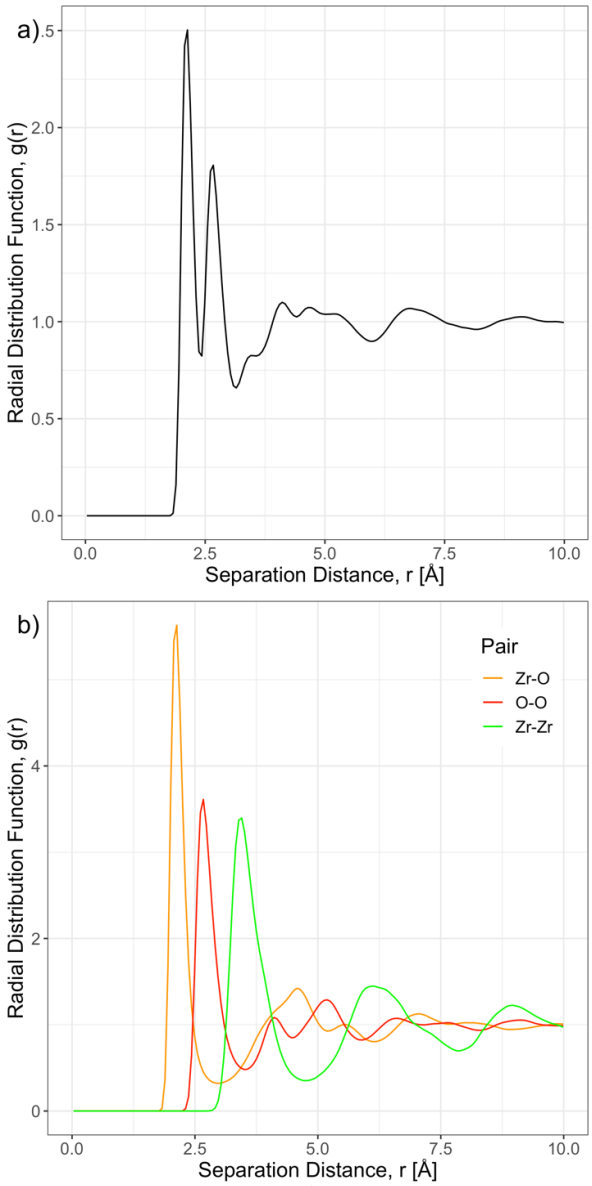

Figure 1. a) Radial distribution function and b) partial radial distribution function for amorphous undoped ZrO_2.

Diffusivity of the undoped and doped amorphous systems was analysed using MSD calculations. Different systems have been analysed in terms of the networks formed, to deduce the impact on diffusion as a function of concentration and dopant radius. Oxygen was the most diffusive species in all systems, whilst zirconium and the lanthanides were effectively immobile in comparison. The immobility of Zr and M compared to O was expected, as the diffusion of anions is much faster in the crystalline oxide systems.

Figure 3 shows an Arrhenius plot of oxygen diffusion in the undoped and doped systems, confirming that the systems behave in an Arrhenius manner. As the temperature is increased from 500 K to 900 K, the diffusion coefficient and pre-exponential factor of oxygen in all systems increases as expected. No observations of cluster or nucleus formation

was observed as this was not specified in the MD code. Values of activation energy calculated for oxygen diffusion in both undoped and doped systems ranges between 0.17 to 0.40 eV, largely independent of dopant radius. A dependence on dopant radius has been observed in corresponding crystalline systems i.e., ZrO_2-Ln_2O_3, where increasing dopant radius caused ionic conductivity to decrease [19]. This dependence is not observed in the amorphous systems, for either concentration analysed, as diffusion is similar in both doped and undoped cases.

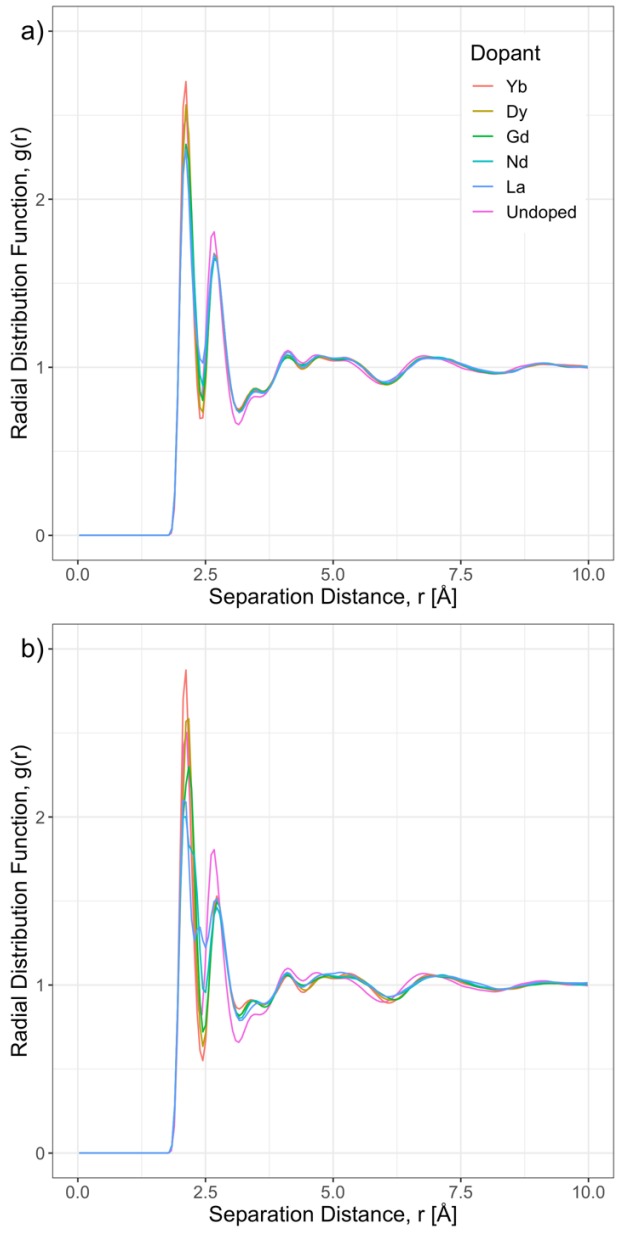

Figure 2. Radial distribution function for a) 5.3 at. % and b) 11.0 at. % lanthanide doped amorphous ZrO_2.

Hafnia (HfO_2) is similar to ZrO_2 in terms of its chemical and physical properties, and as they both exhibit the same tetragonal, monoclinic, and cubic polymorphs [20], [21]. Amorphous hafnia has been analysed in [16], with a low activation energy of 0.29 eV reported for oxygen diffusion. Activation energies for oxygen diffusion in crystalline, monoclinic ZrO_2 for vacancy and interstitial diffusion mechanisms has been reported as approximately 2 eV. Activation energies vary as a function of oxygen partial pressure, changing the dominant diffusion mechanism, from vacancy-assisted at low oxygen partial pressure, to interstitial-dominated at higher oxygen partial pressures [6]. For tetragonal ZrO_2, oxygen diffusion is believed to be mediated by oxygen vacancies associated with +2 and neutral charges, with activation energies reported as 1.40 eV [5]. Both activation energies for monoclinic and tetragonal ZrO_2 are much higher than those derived in this work, indicating increased diffusion in amorphous systems.

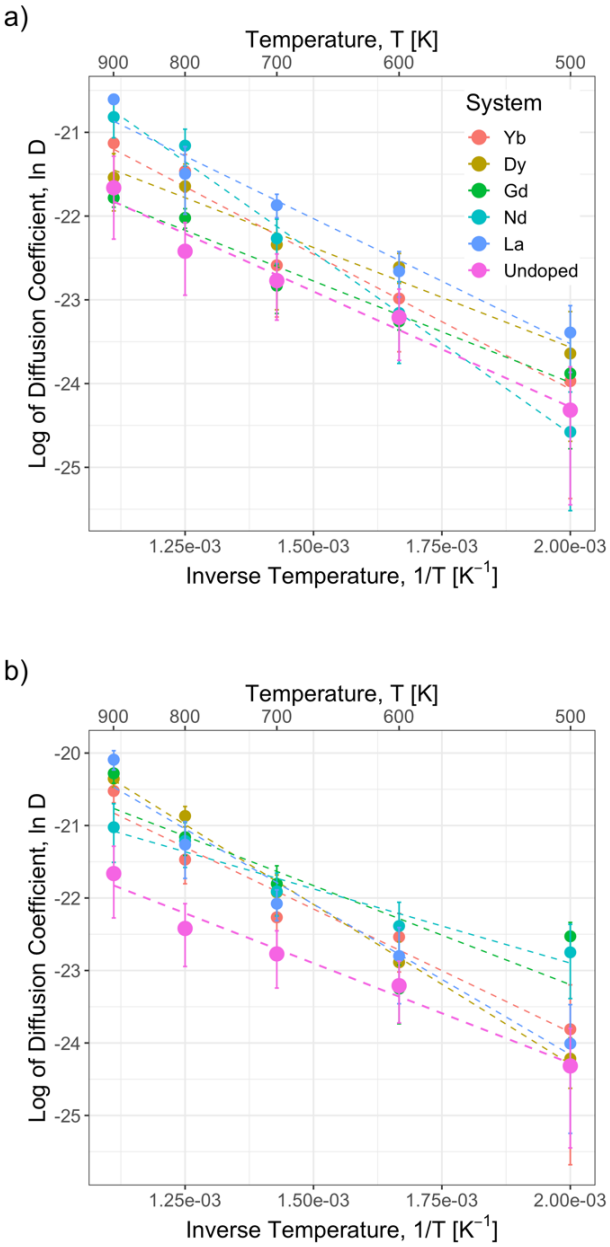

Figure 3. Arrhenius plot of oxygen diffusion in a) 5.3 at. % and b) 11.0 at. % lanthanide doped amorphous ZrO_2.

IV. CONCLUSION

Undoped and trivalent lanthanide doped amorphous zirconia has been analysed using molecular dynamics, exploring diffusion as a function of trivalent lanthanide dopant ionic radius. Oxygen diffusion in amorphous zirconia is much faster than that observed in crystalline

zirconia, for both undoped and doped systems. Trivalent lanthanide dopants do not have a significant impact on oxygen diffusivity, and ionic radius dependence is not observed in the amorphous systems.

The amorphous network is modified upon introducing +3 lanthanides due to the different ionic radii and lanthanides are acting as network modifiers forming dopant channels.

This work provides the basis for further investigation into complex grain boundary phase formation in nuclear fuel cladding. Amorphous grain boundaries may act as high diffusion pathways for corrosion species when compared to the bulk, dictating the pace of oxidation. The formation and favourability of these amorphous grain boundaries will be analysed in future work. Dopants do not have a great impact on the rate of oxygen diffusion; however, they may have other roles such as stabilising the amorphous structure or altering the electro-chemical behaviour.

V. REFERENCES

[1] A. T. Motta, A. Couet, and R. J. Comstock, "Corrosion of Zirconium Alloys Used for Nuclear Fuel Cladding," *Annu. Rev. Mater. Res.*, vol. 45, no. 1, pp. 311–343, Jul. 2015, doi: 10.1146/annurev-matsci-070214-020951.

[2] M. Kilo, C. Argirusis, G. Borchardt, and R. A. Jackson, "Oxygen diffusion in yttria stabilised zirconia - Experimental results and molecular dynamics calculations," *Phys. Chem. Chem. Phys.*, vol. 5, no. 11, pp. 2219–2224, 2003, doi: 10.1039/b300151m.

[3] R. L. González-Romero, J. J. Meléndez, D. Gómez-García, F. L. Cumbrera, A. Domínguez-Rodríguez, and F. Wakai, "Cation diffusion in yttria-zirconia by molecular dynamics," *Solid State Ionics*, vol. 204–205, no. 1, pp. 1–6, 2011, doi: 10.1016/j.ssi.2011.10.006.

[4] A. Tarancón, A. Morata, F. Peiró, and G. Dezanneau, "A molecular dynamics study on the oxygen diffusion in doped fluorites: The effect of the dopant distribution," *Fuel Cells*, vol. 11, no. 1, pp. 26–37, 2011, doi: 10.1002/fuce.201000065.

[5] M. Youssef and B. Yildiz, "Intrinsic point-defect equilibria in tetragonal ZrO 2: Density functional theory analysis with finite-temperature effects," *Phys. Rev. B - Condens. Matter Mater. Phys.*, vol. 86, no. 14, pp. 1–14, 2012, doi: 10.1103/PhysRevB.86.144109.

[6] J. Yang, M. Youssef, and B. Yildiz, "Oxygen self-diffusion mechanisms in monoclinic Zr O2 revealed and quantified by density functional theory, random walk analysis, and kinetic Monte Carlo calculations," *Phys. Rev. B*, vol. 97, no. 2, pp. 1–7, 2018, doi: 10.1103/PhysRevB.97.024114.

[7] A. H. Chokshi, "Diffusion, diffusion creep and grain growth characteristics of nanocrystalline and fine-grained monoclinic, tetragonal and cubic zirconia," *Scr. Mater.*, vol. 48, no. 6, pp. 791–796, 2003, doi: 10.1016/S1359-6462(02)00519-5.

[8] E. Rabkin, C. Y. Ma, and W. Gust, "Diffusion-induced grain boundary phenomena in metals and oxide ceramics," *Mater. Sci. Monogr.*, vol. 81, no. C, pp. 353–369, 1995, doi: 10.1016/S0166-6010(06)80013-5.

[9] S. C. Middleburgh, W. E. Lee, and M. J. D. Rushton, "Structure and properties of amorphous uranium dioxide," *Acta Mater.*, vol. 202, pp. 366–375, 2021, doi: 10.1016/j.actamat.2020.10.069.

[10] M. J. D. Rushton, I. Ipatova, L. J. Evitts, W. E. Lee, and S. C. Middleburgh, "Stoichiometry deviation in amorphous zirconium dioxide," *RSC Adv.*, vol. 9, no. 29, pp. 16320–16327, 2019, doi: 10.1039/c9ra01865d.

[11] S. Plimpton, "Fast parallel algorithms for short-range molecular dynamics," *Journal of Computational Physics*, vol. 117, no. 1. pp. 1–19, 1995, doi: 10.1006/jcph.1995.1039.

[12] M. W. D. Cooper, M. J. D. Rushton, and R. W. Grimes, "A many-body potential approach to modelling the thermomechanical properties of actinide oxides," *J. Phys. Condens. Matter*, vol. 26, no. 10, 2014, doi: 10.1088/0953-8984/26/10/105401.

[13] X. Y. Liu *et al.*, "Molecular Dynamics Simulation of Thermal Transport in UO2 Containing Uranium, Oxygen, and Fission-product Defects," *Phys. Rev. Appl.*, vol. 6, no. 4, pp. 1–19, 2016, doi: 10.1103/PhysRevApplied.6.044015.

[14] M. J. D. Rushton and A. Chroneos, "Impact of uniaxial strain and doping on oxygen diffusion in CeO2," *Sci. Rep.*, vol. 4, pp. 2–7, 2014, doi: 10.1038/srep06068.

[15] D. J. Evans and B. L. Holian, "The Nose-Hoover thermostat," *J. Chem. Phys.*, vol. 83, no. 8, pp. 4069–4074, 1985, doi: 10.1063/1.449071.

[16] M. Schie, M. P. Müller, M. Salinga, R. Waser, and R. A. De Souza, "Ion migration in crystalline and amorphous HfOX," *J. Chem. Phys.*, vol. 146, no. 9, 2017, doi: 10.1063/1.4977453.

[17] M. Durandurdu, "Amorphous zirconia: ab initio molecular dynamics simulations," *Philos. Mag.*, vol. 97, no. 16, pp. 1334–1345, 2017, doi: 10.1080/14786435.2017.1296201.

[18] Y. Dong, L. Qi, J. Li, and I. Chen, "A Computational Study of Yttria-Stabilized Zirconia," *Mater. Acta*, pp. 1–47, 2017, doi: 10.1016/j.actamat.2017.01.006 A.

[19] A. J. Jacobson, "Materials for solid oxide fuel cells," *Chem. Mater.*, vol. 22, no. 3, pp. 660–674, 2010, doi: 10.1021/cm902640j.

[20] J. D. Smith and W. G. Fahrenholtz, "Refractory oxides," *Ceram. Glas. Mater. Struct. Prop. Process.*, pp. 87–110, 2008, doi: 10.1007/978-0-387-73362-3_6.

[21] J. Drennan and B. C. H. Steele, "Zirconia and Hafnia," *Concise Encycl. Adv. Ceram. Mater.*, pp. 525–528, 1991, doi: 10.1016/b978-0-08-034720-2.50146-5.

Proceedings of the European Nuclear Young Generation Forum
ENYGF'21
September 27-30, 2021, Tarragona, Spain

Modern status of materials for nuclear technologies in Ukraine

Voyevodin, Victor[1,2*], Tolstolutskaya, Galina[1]

[1] National Science Center Kharkov Institute of Physics and Technology (NSC KIPT), Ukraine, [2] V. N. Karazin Kharkov National University, Ukraine

*Corresponding author: *voyev@kipt.kharkov.ua*

I. INTRODUCTION

Nuclear power in Ukraine now serves as warrant of energetic independence – 15 working Nuclear Power Plant (NPP) in 2019 supplied more than 50% of total production of electricity. Beside it, performing of Ukrainian obligations with the adoption of the Paris Climate Agreement in 2015, is possible only under stable functioning of Joining Energetic System, which is supported by nuclear power.

Materials in nuclear power engineering play extremely important role. The key problem in material science provision of modern nuclear power and power of the future is the study of mechanisms and influence of degradation of initial physical-mechanical characteristics of materials during operation and dimensional stability. Radiation damages are initiated by creation and interaction of point defects on the nano level (10^{-9} м), but macroscopic effects, which have determinant influence on reactor's safety, created due to co-evolution of all component of the microstructure, and their roles in the macroscopic response in terms of radiation induced phenomena – swelling, anisotropic growth, irradiation creep, radiation induced phase transformations etc.

The development of radiation tolerant materials is the important part of modern nuclear energetics and very big scientific/technical goal that is specific to the success of sustainable nuclear energy. Radiation tolerance and high burn-up are science challenges with very strong technological implications.

The presented paper shortly summarizes the results of investigations performed in the field of radiation material science by Ukrainian scientists.

II. REACTORS ON THERMAL NEUTRONS

The basis of world nuclear power now presented mainly by thermal reactors with pressurized water cooling (PWR) or cooled by boiling water (BWR).

First of all, the main problems of safety for the units of NPP concern the vessel of nuclear reactor because only the vessel can`t be replaced in the case of its not permissible damage or degradation of material properties, that's why service life of reactor vessel (RV) mainly determines the limit of service life of modern NPP unit.

Now three basic micro mechanisms defining the variation of microstructure of pressure vessel steels under an irradiation are considered [1]:

1) damage in matrix due to the formation of radiation – induced clusters and dislocation loops;
2) radiation-accelerated formation of fine-dispersed precipitates – both copper-enriched precipitates and carbonitrides;
3) radiation-induced/accelerated segregation on grain boundaries and on interfaces of such elements as phosphorus, sulphur and arsenic.

Dependence of embrittlement coefficient A_F for vessels (welds metal) of Ukrainian NPPs versus nickel content shown that up to Ni content near1.6 %, influence of nickel on level of radiation embrittlement is negligible [2]. At nickel value close to 1.7 wt. % the significant change in the A_F level is fixed – from the lowest (A_F ~ 10 °C) to the highest (A_F ~ 23 °C), which exceeded the normative value by 20 °C. It is shown that at 1.88 wt. % nickel (weld metal of the reactor vessel, unit No. 1 of Khmelnitsky NPP) the highest degree of embrittlement (A_F = 25 °C) take place.

Analysis and generalization of high quantity of data on effect of impurities on radiation brittleness allowed to put forward the requirement about decrease of phosphorus and copper content to 0.006 and 0.06% respectively, also as decrease of general content of antimony, tin and arsenic (total <0.015%). It is supposed that optimal alloying by nickel 0.6-0.8% and correction of chromium (<3% mass) and molybdenum content (0.5-0.8% mass) will provide thermal and radiation stability of steels and extend the life of pressure vessel not less than 60 years with possibility of extension to 80-100 years.

A. Materials of pressure vessel internals (PVI)

The problem of lifetime extension of Eastern pressurized water reactors up to 60 years is primarily connected with the life time connection of irreplaceable equipment-reactor pressure vessel and reactor vessel internals (RVI).

The evolution of porosity in 18Cr–10Ni–Ti stainless steel shows that the production of damage and the simultaneous implantation of inert gas and deuterium causes increased of

material swelling. Using heavy-ion irradiation and coupling the results to available neutron data a swelling equation has been developed. Next stage in NSC KIPT swelling by cross-section of baffle ring materials for reactor WWER-1000 (WWER - water water energy reactor) was calculated during long-term operation of 30-60 years [3] with the using of neutron-physical calculations of temperature and dose field in central cross-section of reactor that were carried out by SCB "Gidropress" together with NIIAR. Dynamics of swelling development in the baffle ring is shown in Fig. 1.

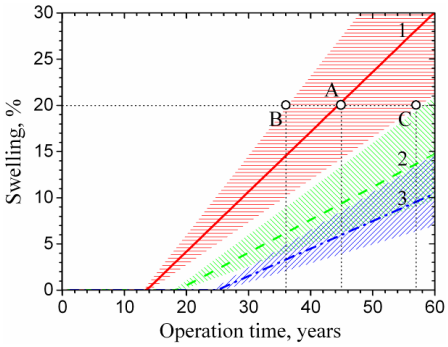

Figure 1. Dependence of swelling on operational time of steel 08Cr18Ni10Ti which shows the areas of highest swelling on the baffle ring [3].

Point A on the curve of Fig. 1 answers to the loss of ductility by the material. Points B and C indicate the lower and upper boundaries of critical time of operation, respectively [3]. As it is known for steel 08Cr18Ni10Ti the swelling of 20% and higher induces the decrease of ductility [4]. Drawing the horizontal line on level of 20% on Fig. 1 one may forecast the operation life of the baffle ring which doesn't exceed the critical level of swelling. It is seen that only curve 1 in point A will exceed the dangerous 20% swelling for 45 years of operation.

The upper boundary of swelling is very pessimistic and indicates on important limitation of service life extension. And lower boundary of swelling is rather optimistic and testifies to potential possibility of life extension. It is seen on Fig. 1 that dangerous 20% swelling is situated into the range of 36-57 years (points B and C, respectively).

Substantiation of the service life of PVI and supporting elements of reactor WWER-1000 and also providing of strength and service life of pressure vessels of reactor WWER on life extension up to 60 years and more requires the development of methods and recommendations on choice of starting data (swelling, change of mechanical properties and others).

B. Zirconium base alloy

In the nearest 50-60 years thermal reactors will dominate in park of commercial nuclear power units which produce electric energy. The main material of the core of these reactors is structural materials on the base of zirconium. Due to the optimal concentration of nuclear (particularly of so called "neutron penetrability"), corrosion, mechanical, thermal and other physical-mechanical properties zirconium alloys were non-alternative structural materials for nuclear power, especially, for complete set of the cores of light-water reactors with operation temperature of coolant 350-400 °C [5]. Zirconium alloys alloyed by Nb (E110, E125) or Sn, Fe, Cr, Ni (E635, Zirlo, ZrY-2, ZrY-4) are widely used in core of water-cooled nuclear reactors.

To guarantee burn-up to 80-100 MWt day/kg of uranium with operation period to 7-10 years at temperature of coolant >385 °C maneuvering by power and reaching of neutron fluence $(4\text{-}5)\cdot10^{26}$ n/m^2, E>0.1 MeV the alloys are needed with increased level of characteristics which will provide their competitiveness on world market.

To attain the appointed goal the following tasks must be resolved:

- modernize the alloy E110 with regard to increasing of forming resistance of fuel elements claddings (is inferior of M5 in PWR);
- increase reliability of fuel elements (FE) of new generation (zirconium sponge, thinning of the wall (from 0.65 to 0.57 mm);
- guarantee the competitiveness (corrosion and forming resistance).

On solving the above-mentioned tasks, it is necessary to consider the following phenomena which cause the degradation of characteristic of zirconium alloys: hydrogenation, oxidation, radiation-thermal creep, radiation growth, change of mechanical properties, microstructure changes.

In NSC KIPT phenomenological mechanisms of the phenomenon of radiation growth is proposed [6]. Thermal mechanical treatment used on production of tubes for fuel elements produces the anisotropic orientation of zirconium grains. Radial oriented grains dominate into texture of FE, that is, the direction of axe **c** is chiefly radial (in certain range of angles; this is named the structure scattering), and direction **a** is chiefly tangent**.** Such texture of FE claddings is the reason of that during radiation growth the increase of the length of FE occurs with simultaneous contraction. With the increase of irradiation dose, the density of dislocation loops of **c**-type increases because the vacancies are directed on base of pyramidal planes and interstitials stabilize **a**-loops in prismatic planes (Fig. 2).

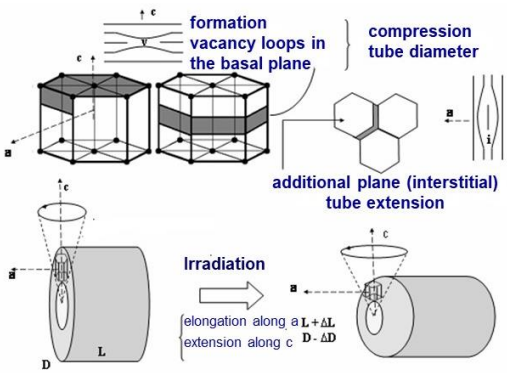

Figure 2. Diagram of the effect of distribution of interstitial and vacancy loops on radiation growth of cladding tube [6].

Oxygen which is contained in zirconium alloys dissolves in α-zirconium in rather high quantity. In low quantity (900-1400 mass ppm) oxygen doesn't influence on corrosion of zirconium but hardened it considerably. Mechanism of hardening is that the region around dislocations represents the sink for vacancies and interstitials. For instance, at temperature 300 °C atoms of oxygen in zirconium interact with dislocations and harden considerably unirradiated

material. High quantities of oxygen are not used due to its embrittling effect on zirconium alloys [7].

C. Modern state of development into the field of production of nuclear fuel resistant to accidental condition for water- cooled reactors

The main problems of existing zirconium alloys are: decrease of corrosion resistance at temperatures of coolant above 400 °C, intensive oxidation with the release of high quantity of hydrogen in accident with the coolant loss (LOCA), fretting-wear, accumulation of high quantity of hydrogen and embrittlement with fuel burn-up more than 50 GWD/MTU (gigawatt day for metric ton of uranium). Now round the world exist two main approaches in development of new fuel claddings resistant to accidental conditions (*ATFC – accident-tolerant fuel claddings*): revolutionary one and evolutionary.

In NSC KIPT during last 5 years vacuum-arc protective nanostructured (multilayers) coatings with thickness 10-20 μm on Zr1Nb alloy claddings are successfully developed. This chromium-based coating can effectively protect Zr-alloy claddings in the case of accident with the loss of coolant (LOCA) not less than 1 hour (which is sufficient for accept of correct solving by station operator) and increase their operational possibilities in conditions of normal operation of reactor. The high resistance to oxidation of the developed coatings is determined by the formation of a dense chromium-oxide layer on their surfaces [8].

The NSC KIPT scientists are involved in the development of SiC-based materials using method of high-speed hot pressing (HSHP), and also, in the studies into the influence of alloying additives on the mechanical characteristics of the SiC [9] and its corrosion resistance under hydrothermal conditions. The best corrosion resistance under hydrothermal test conditions was shown by the SiC ceramics with Cr additions.

Many types of potential accident-tolerant fuel-cladding systems were discussed and three concepts under active development: Cr-coated Zr-based cladding, FeCrAl and SiC/SiC cladding. It is expected that one or more of the discussed systems will be implemented in commercial reactors. However, intensive research is needed not only on the properties of various new materials and coatings, but also on improving the technologies for their creation.

III. MATERIALS FOR REACTORS OF GENERATION IV

Three systems which are working on neutrons of fast spectrum (SFR, GFR, LFR, one – on thermal neutrons (SCWR) and two systems (MSR, VHTR), which allowed to work as at fast, and thermal spectrum were selected by world nuclear community as the main objective of Generation IV (GEN IV) reactors – producing an abundant, reliable, proliferation resistant, safe and of course competitive energy.

Current efforts on R&D of materials for future nuclear technologies are concentrated principally on two directions: improvement of existing materials (mainly austenitic and ferritic-martensitic steels) and creation of innovative materials – oxide dispersion strengthened (ODS) steels and high entropy alloys that will be able to meet the different challenges for the new generations of nuclear reactors.

The influence of alloying and treatment on radiation resistance of austenitic stainless steels consists in following:

- production of more stable dislocation structure (conservation of low mobile Frank loops) and increase of the recombination level TD. It may be reached due to the solution treatment or by the processes of segregation of alloying elements on dislocation components that decreases their mobility;
- saving of fine carbides precipitates (TiC) and phosphides (Fe_2P) up to higher damage doses;
- delay of formation of G-phase and η-carbides will keep in the solid solution the sufficient quantity of such elements as Ni, Si and P which strongly influence on nucleation and growth of voids.

It was established that BCC-iron and ferritic alloys on its base have immunity to high rate of swelling. But the question remains: if always α-alloys will have low rate of swelling and if can swelling of these alloys under high dose of irradiation (more than 100 displacement per atom (dpa)) reach the value of several tens of percent? The effect of high-dose irradiation on swelling of ferritic alloys has been identified in [10] (Fig. 3). After long-term incubation stage ~150 dpa the transition is observed to steady state stage of swelling with the rate 0,14%/dpa and swelling of steel with BCC lattice may reach the value more than 20%.

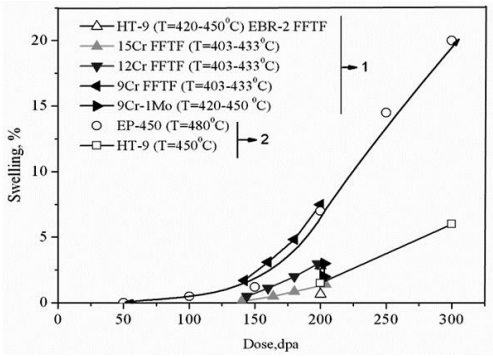

Figure 3. Dose dependence of swelling for Fe-Cr binary alloys and F/M steels [10].

One more promising line for solving the problem of production of radiation resistant and high-temperature strengthened steels consists now into the use of new class of ferritic-martensitic radiation resistant steels strengthened by particles of oxides of nanometer size (ODS).

Ukrainian scientists took part in investigation of radiation tolerance of different kind of ODS ferritic steels after very high damage doses.

Steel 14YWT represents formation of stable elements of microstructure highly resistant to swelling. Super fine grain and high concentration of oxide nanoparticles will produce all conditions for suppression of swelling up to super high doses of damaging irradiation due to increasing of recombination of point defects. The size of grain also influences on swelling of 14YWT [11]. Large coarse grains in 14YWT swell much more than fine grains (Fig. 4).

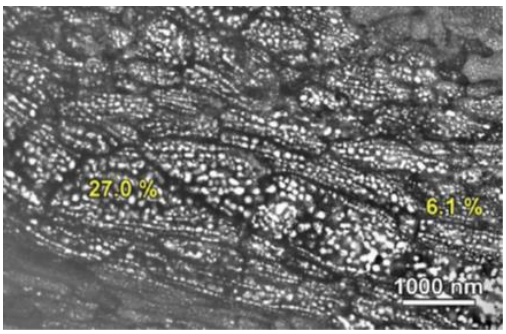

Figure 4. Microstructure of 14YWT steel after irradiation at 450ºC to 500 dpa [11].

In NSC KIPT the experimental technology of fabrication of austenitic ODS steel 18Cr10NiTi is developed. ODS steel after final thermal treatment have grain size 1.2-2 μm and the density of precipitates of complex nanooxides changes in the range $(1.7…7.3)\cdot10^{15}cm^{-3}$ at mean size near 10 nm. Investigation of swelling features in oxide dispersion strengthened (ODS) austenitic stainless steel 18Cr10NiTi $+Y_2O_3$ after irradiation at accelerator of heavy ions showed, that level of swelling at determined swelling maximum was 5 time less relatively base steel [12].

High entropy alloys (HEAs) are principally novel effort in R&D of materials science and engineering. The cobalt free 20Cr-40Fe-20Mn-20Ni (wt. %) high entropy alloy and it's strengthened with yttrium and zirconium oxides version have been investigated in relation to the development of hardening phenomenon under the irradiation [13]. The main irradiation defects observed were defect clusters at low doses and dislocation loops at higher doses. These observations suggest that high entropy alloys must lose less plasticity in comparison with conventional austenitic steels of nuclear power.

Moreover, there were only few publications and communications regarding HEA corrosion behavior exposed to the fluids foreseen in advanced nuclear reactors Gen IV. Scientists from NSC "KIPT" (Kharkiv) and Karpenko Physical-Mechanical Institute (Lviv) have been performed evaluation of the high-entropy Cr-Fe-Mn-Ni alloys compatibility with a liquid lead coolant [14]. Conducted research showed that HEAs can be served as promising structural materials for Gen-IV reactors.

IV. CONCLUSIONS

Nuclear power meets the best the principles of sustainable development; the main requirement of such development is the presence of sufficient fuel-energetic resources on their stable consumption in long-term prospects.

Materials in nuclear power play extremely important role. Radiation material science which studies the influence of irradiation by high energy particles of different origin and energy on properties of materials and operational characteristics of nuclear plants makes its important contribution into the solving of these tasks because only on the base of modern scientific ideas about the role of microstructural processes in degradation of base physical-mechanical characteristics the posed goals may be realized.

The further development of fundamental and applied researches in the field of radiation material science, radiation technologies and new nuclear-power sources are needed for increasing the role of nuclear energetics as a main source of low carbon electricity in the world.

V. ACKNOWLEDGEMENT

This work was prepared within the project № 2020.02/0327 "Fundamental aspects of the new materials creation with unique physical, mechanical and radiation properties based on the concentrated multicomponent alloys", implemented with the financial support of the National Research Foundation of Ukraine.

VI. REFERENCES

[1] E.U. Grinik et al., "Analysis of the influence of nickel on the radiation embrittlement of the metal of the seams of the WWER-1000 reactor vessels of the Ukrainian NPP", "Problems of resource and safety of operation of structures and machines", Kyiv, 709 p., 2009.

[2] S. Kotrechko, "Embrittlement of RPV metal under long-term irradiation: State of-the-art and challenges", Procedia Structural Integrity, vol. 13, pp. 11–21, 2018.

[3] A.S. Kalchenko et al., "Prediction of void swelling in the baffle ring of WWER-1000 reactors for service life of 30-60 years", J. Nucl. Mater., vol. 437, pp. 415–423, 2013.

[4] V.S. Neustroev, V.N. Golovanov, V.N. Shamardin, "Radiation embrittlement of materials irradiated at temperature interval of maximum swelling", At. Energiya, vol. 69(4), pp.223–226, 1990.

[5] V.N. Voyevodin, "Structural materials of nuclear power – challenge to 21 centuries", Problems of Atomic Science and Technology, vol. 2, pp. 10–22, 2007 (in Russian).

[6] V.V. Novikov et al., "Investigation of the microstructure of zirconium alloys irradiated with zirconium ions on an accelerator", At. Energiya, vol. 11, pp. 255-260, 2013.

[7] O.V. Borodin et al., "Influence of oxygen content on evolution of the structure of alloy Zr1%Nb under ion irradiation", PAST, vol. 2, pp. 53–61, 2008 (in Russian).

[8] A.S. Kuprin et al., "Vacuum arc chromium-based coatings for protection of zirconium alloys from the high-temperature oxidation in air", J. Nucl. Mater., vol. 465, pp. 400-406, 2015.

[9] K. Lobach et al., "Optimization of properties of silicon carbide ceramics with the use of different additives", Functional Materials, vol. 25 (3), pp. 496–504, 2018.

[10] O.V. Borodin et al., "Radiation swelling of ferritic-martensitic steels EP-450 and HT-9 under irradiation by metallic ions to super high doses", PAST, vol. 2(72), pp. 256–258, 2008.

[11] M.B. Tolochko et al., "Ion-induced swelling of ODS ferritic alloy MA957 tubing to 500 dpa", J. Nucl. Mater., vol. 453, pp. 323–333, 2014.

[12] S.V. Starostenko et al., "Influence of irradiation by heavy ions Cr^{3+} on microstructure of steel 08X18H10T ODS, mechanically alloyed by nanopowder of system Y_2O_3-ZrO_2", PAST, vol. 4 (104), pp. 3–8, 2016.

[13] V.N. Voyevodin et al., "Effect of irradiation on microstructure and hardening of Cr-Fe-Ni-Mn high-entropy alloy and its strengthened version", Phil. Mag., vol. 100, pp. 822–836, 2020.

[14] V.M. Fedirko et.al., "Influence of the Dispersion Hardening with Nanooxides on the Corrosion Resistance of High-Entropy Alloys of the Cr–Fe–Mn–Ni System in Lead Melts", Mat. Sc., vol. 55, pp. 529–535, 2020.

Technical Track 1 – Reactor physics, Thermal-hydraulics and Simulation

Core Power Distribution Reconstruction by Radial Basis Function Method for WWER Reactors.

Authors: Krempaský, Robin

Application of Artificial Neural Network and Particle Swarm Optimization in determining selected parameters of the nuclear reactor core.

Authors: Kubinski, Wojciech (1); Bojarski, Patryk (1); Darnowski, Piotr (2)

Modelization of the EPR coolant system with MELCOR 2.2.

Authors: Fallot, Lucile; Larriba, Samantha; Jiménez, Gonzalo

Model for premixed layer formation in stratified fuel-coolant configuration and its application.

Authors: Kokalj, Janez (1,2); Uršič, Mitja (1); Leskovar, Matjaž (1)

Study of discharges in stagnant water using spargers in an experimental facility.

Authors: Blanco de las Muelas, David; Córdova Chávez, Yaisel; Berna Escriche, César; Muñoz-Cobo Gonzalez, José Luis; Escrivá Castells, Facundo Alberto

Validation of Serpent-SUBCHANFLOW-TRANSURANUS pin-by-pin depletion for PWR and VVER reactors

Authors: García, Manuel

Preventive methodology: geometric simplifications a priori for containment models optimization with the GOTHIC code.

Authors: Arfinengo-del-Carpio, Sofía; Vázquez-Rodríguez, Carlos; Jiménez, Gonzalo

SIMMER-V validation against thermohydraulic instabilities in GENESIS facility.

Authors: Kedzierska, Barbara; Gubernatis, Pierre

Experience Simulating of ATF on a 3-loop PWR using SEANAP System.

Authors: Muñoz Garcia, Miguel; Cabellos de Francisco, Oscar Luis

Comparative Analysis of Mo-99 Production in the Jules Horowitz Reactor and in the SHINE® System.

Authors: Ratero Talavera, Cristina; Serna Moñino, Pablo; García-Herranz, Nuria

Thermo-hydraulic calculation of the can with tellurium dioxide target material during irradiation process.

Authors: Talarowska, Anna; Prokopowicz, Rafał

Nuclear data sensitivity and uncertainty analysis for reactor physics parameters of the European Sodium Fast Reactor.

Authors: Jiménez-Carrascosa, Antonio; García-Herranz, Nuria; Cabellos, Oscar

One-dimensional investigation of turbulent heat transfer along coroded rod in vertical channels at supercritical pressure.

Authors: Wiltschko, Fabian; Otic, Ivan; Cheng, Xu

Thermal-hydraulic analysis of a VVER-1000/V-320 reactor with TRACE5P5 code.

Authors: Redondo-Valero, Elena (1); Sanchez-Espinoza, Victor (2); Queral, Cesar (1)

Sensitivity and uncertainty analysis of hydrogen generation in a BWR during a severe accident using MAAP5 and AZTUSIA.

Authors: Sánchez-Mora, Heriberto (1); Melisa Reyes-Fuentes, Melisa Reyes-Fuentes (1); Ortiz-Villafuerte, Javier (2); del-Valle-Gallegos, Edmundo (1); Queral, César (3)

Implementation of dynamic nuclear fuel thermo-mechanics in transient simulation of lead-cooled reactors.

Authors: Aragón Grabiel, Pau; Wallenius, Janne

Cloud computing CFD analysis assessment of an ITER Vacuum Vessel Component.

Authors: Catalán, David; Bernad, Andreu; Alberto, Patricio; Fradera, Jorge

Development of a Code for the Thermal-Hydraulic Simulation of the Canadian Supercritical-Water-Cooled Reactor Using Improved Nuclear Fuels.

Authors: Ramos, Daniel; Morales, Jaime B.

Spent fuel criticality assessment comparison between Keno and OpenMC.

Authors: Castro, Emilio (1); Garcia-Herranz, Nuria (2)

Development of a detailed 3D CAD model of a generic PWR-KWU containment as a basis for thermal-hydraulic analysis.

Authors: Serra, Luis (1); Domínguez-Bugarín, Araceli (1); Estévez-Albuja, Samanta (1); Vázquez-Rodríguez, Carlos (1); Jiménez, Gonzalo (1); Kelm, Stephan (2); Herranz, Luis E. (3)

Optimisation of the I-131 production from enriched and natural tellurium dioxide in MARIA research reactor.

Authors: Madejowski, Gaweł

Software and hardware complex “Virtual NPP” as an instrument for scientific and technological assistance of nuclear operating company.

Authors: Druzhaev, Andrey; Chernakov, Victor

Spent Nuclear Fuel Cask Partial Loading Pattern Analyses Applied to ENUN 52B Casks for Santa María de Garoña Nuclear Power Plant.

Authors: Saiz de Omeñaca Tijero, Jesús

Proceedings of the European Nuclear Young Generation Forum
ENYGF'21
September 27-30, 2021, Tarragona, Spain

Core Power Distribution Reconstruction by Radial Basis Function Method for WWER Reactors

Krempaský, Robin*

[1] Department of Nuclear Reactors, Faculty of Nuclear Sciences and Physical Engineering, Czech Technical University in Prague, Czech Republic

*Corresponding author: *kremprob@fjfi.cvut.cz*

I. INTRODUCTION

Reactor core power distribution is a key attribute to be determined by core monitoring system during reactor operation. Two fundamental approaches for core power distribution determination can be identified. The first approach lies in in-core measurement which is in WWER (water-water energetic reactor) provided by self-powered neutron detectors or by thermocouples. The second approach lies in on-line core power distribution calculation provided by computer codes referred to as core simulators.

Despite the qualities of in-core instrumentation and core simulators both ways can lead to slightly different results in determination of core power distribution. Thus, core power distribution reconstruction represents way to combine results of both approaches.

In order to perform core power reconstruction, scattered data interpolation or approximation problem has to be solved. Unlike currently used interpolation approach described in [1], this paper introduces possibility of approximation approach with in-core instrumentation measurement uncertainty inclusion.

For analysis in this paper, core power distribution data set used for core power distribution reconstruction methods development was provided by ÚJV Řež, a.s. (previously NRI – Nuclear Research Institute Řež). The data set contains data for Dukovany Nuclear Power Plant equiped with reactor units WWER440 type 213.

The core of WWER440 contains 349 fuel assemblies in hexagonal geometry of which 210 are equiped with thermocouples to measure fuel assembly coolant outlet temperature. Owing to WWER440 fuel assemblies are equipped with fuel assembly shroud, fuel assembly outlet temperature information (together with fuel assembly inlet temperature information) allows to determine power developed by each of 210 instrumented fuel assemblies.

Thus, this paper is focused on 2D radial core power distribution reconstruction based on thermocouples measurement.

II. CORE POWER DISTRIBUTION RECONSTRUCTION

Core power distribution reconstruction can be defined as a mathematical process used to determine core power distribution which is based on measured and predicted power distribution data.

To perform core power distribution reconstruction, it is assumed that predicted power distribution $P_P(\boldsymbol{x})$ (i.e. power distribution determined by core simulator) is known for all points $\boldsymbol{x} = (x, y) \in \mathbb{R}^2$ in reactor core and measured power distribution $P_M(\boldsymbol{x_i})$ is known for all points $\boldsymbol{x_i} = (x_i, y_i) \in \mathbb{R}^2$ where measured power distribution data are available from thermocouple measurement. It is also assumed that each thermocouple is characterized by measurement uncertainty σ_i.

Based on predicted and measured power distribution data, predicted-measured ratios w_i are evaluated for thermocouples positions $\boldsymbol{x}_i$:

$$w_i = \frac{P_M(\boldsymbol{x_i}) - P_P(\boldsymbol{x_i})}{P_M(\boldsymbol{x_i})}. \quad (1)$$

These predicted-measured ratio values represent scattered data values at points $\boldsymbol{x_i}$ in core where thermocouple measurement is available. Then interpolation factor $W(\boldsymbol{x})$ is calculated by scattered data approximation:

$$W(\boldsymbol{x}) = \overline{[\boldsymbol{w}]}, \quad (2)$$

where $\boldsymbol{w} = (\boldsymbol{w_1}, \boldsymbol{w_2}, \ldots, \boldsymbol{w_N})$ for N measured positions, and $\overline{[\,]}$ denotes approximation process of scattered data.

Then assembly wise reconstructed power distribution is obtained for all 349 fuel assembly centres as:

$$P_{rec}(\boldsymbol{x}) = \frac{P_P(\boldsymbol{x})}{1 - W(\boldsymbol{x})}. \quad (3)$$

An influence of interpolation factor on reconstructed power distribution follows from equation (3). If interpolation factor is a zero function, i.e. $W(\boldsymbol{x}) = 0$ then from equation (3) follows that reconstructed power distribution is equal to

predicted power distribution. Furthermore, if interpolation factor equals predicted-measured ratio values w_i at measurement points $\boldsymbol{x_i}$, i.e. $W(\boldsymbol{x_i}) = w_i$ then reconstructed power distribution equals measured power distribution.

Therefore, it is desirable to implement approximation method which can consider measurement uncertainty of each thermocouple. Approximation method requirements can be written as

$$\sigma_i \to 0 \Rightarrow W(x_i) \to w_i \tag{4}$$

and

$$\sigma_i \to +\infty \Rightarrow W(x_i) \to 0. \tag{5}$$

III. RADIAL BASIS FUNCTION APPROXIMATION

For radial basis function (RBF) approximation general form for the interpolation factor is [1]:

$$W(\boldsymbol{x}) = b_0 + b_1 x + b_2 y + \sum_{j=1}^{N} c_j \phi\left(|\boldsymbol{x} - \boldsymbol{x_j}|\right) \tag{6}$$

where b_0, b_1, b_2 are coefficients of polynomial, c_j for $j = 1, \dots N$ are RBF coefficients, $\phi(|\boldsymbol{x} - \boldsymbol{x_i}|)$ is radial basis function (see Table 1) and $|\cdot|$ denotes Euclidean norm.

In general, different polynomials in Equation (6) can be used instead of $b_0 + b_1 x + b_2 y$ (e.g. zero function or constant b_0).

Table 1. RBF types considered in numerical tests, *C* is arbitrary constant

Function Name	Function Form
Linear	$\phi(\lvert\boldsymbol{x} - \boldsymbol{x_i}\rvert) = \lvert\boldsymbol{x} - \boldsymbol{x_i}\rvert$
Cubic	$\phi(\lvert\boldsymbol{x} - \boldsymbol{x_i}\rvert) = \lvert\boldsymbol{x} - \boldsymbol{x_i}\rvert^3$
Gaussian	$\phi(\lvert\boldsymbol{x} - \boldsymbol{x_i}\rvert) = e^{-\frac{\lvert\boldsymbol{x}-\boldsymbol{x_i}\rvert^2}{2C^2}}$
Multiquadric	$\phi(\lvert\boldsymbol{x} - \boldsymbol{x_i}\rvert) = \sqrt{1 + \frac{\lvert\boldsymbol{x} - \boldsymbol{x_i}\rvert^2}{C^2}}$
Inverse multiquadric	$\phi(\lvert\boldsymbol{x} - \boldsymbol{x_i}\rvert) = \frac{1}{\sqrt{1 + \frac{\lvert\boldsymbol{x} - \boldsymbol{x_i}\rvert^2}{C^2}}}$
Thinplate	$\phi(\lvert\boldsymbol{x} - \boldsymbol{x_i}\rvert) = \lvert\boldsymbol{x} - \boldsymbol{x_i}\rvert^2 ln(\lvert\boldsymbol{x} - \boldsymbol{x_i}\rvert + 1)$

To determine specific form of the interpolation factor, interpolation conditions for function (6) follow that

$$W(\boldsymbol{x_i}) = b_0 + b_1 x_i + b_2 y_i + \sum_{j=1}^{N} c_j \phi\left(|\boldsymbol{x_i} - \boldsymbol{x_j}|\right) = w_i. \tag{7}$$

Furthermore, side conditions imposed on the coefficients are:

$$\sum_{i}^{N} c_i = \sum_{i}^{N} c_i x_i = \sum_{i}^{N} c_i y_i = 0. \tag{8}$$

All the conditions lead to system of linear equations in matrix form:

$$\begin{bmatrix} \boldsymbol{\Phi} & \boldsymbol{P} \\ \boldsymbol{P^T} & \boldsymbol{0} \end{bmatrix} \begin{bmatrix} \boldsymbol{c} \\ \boldsymbol{b} \end{bmatrix} = \begin{bmatrix} \boldsymbol{w} \\ \boldsymbol{0} \end{bmatrix}, \tag{9}$$

Where matrices elements are $\boldsymbol{\Phi_{i,j}} = \phi(|\boldsymbol{x_i} - \boldsymbol{x_j}|)$ for $i, j = 1, \dots N$ and $\boldsymbol{P} = (1, x_i, y_i)$ for $i = 1, \dots N$.

In addition to interpolation approach in [1] which lies in interpolation using function (6), in-core measurement uncertainty can be considered by including tolerance factor vector $\boldsymbol{T} = (\boldsymbol{T_1}, \dots \boldsymbol{T_N})$ into interpolation conditions (7). The tolerance factor inclusion is based on noisy data approximation approach in [2]. With tolerance factor inclusion interpolation conditions in (7) become:

$$W(\boldsymbol{x_i}) = b_0 + b_1 x_i + b_2 y_i + \sum_{j=1}^{N} c_j \phi\left(|\boldsymbol{x_i} - \boldsymbol{x_j}|\right) \pm c_i T_i = w_i, \tag{10}$$

which leads to system of equations

$$\begin{bmatrix} \boldsymbol{\Phi} \pm diag(\boldsymbol{T}) & \boldsymbol{P} \\ \boldsymbol{P^T} & \boldsymbol{0} \end{bmatrix} \begin{bmatrix} \boldsymbol{c} \\ \boldsymbol{b} \end{bmatrix} = \boldsymbol{A} \begin{bmatrix} \boldsymbol{c} \\ \boldsymbol{b} \end{bmatrix} = \begin{bmatrix} \boldsymbol{w} \\ \boldsymbol{0} \end{bmatrix}, \tag{11}$$

where $diag(\boldsymbol{T})$ is diagonal matrix with vector $\boldsymbol{T}$ on its diagonal. Sign of tolerance factor in Equation (10) and Equation (11) is further analysed in Section IV. The meaning of the tolerance factor lies in measurement uncertainty inclusion into approximation method for each thermocouple. Thus, tolerance factor i-th component is chosen as function of i-th thermocouple measurement uncertainty:

$$T_i = f(\sigma_i) \sim \sigma_i. \tag{12}$$

IV. NUMERICAL TESTS

A. Tolerance factor effect

To analyse tolerance factor effect on interpolation factor, RBF approximations were performed for different tolerance factor values – see Figure 1 and Figure 2.

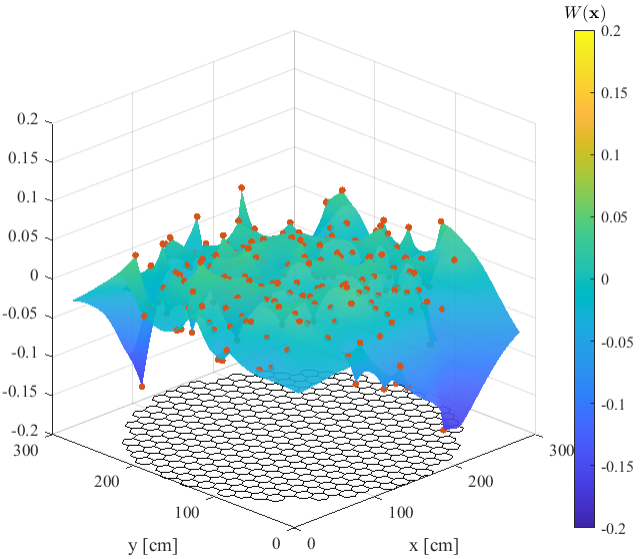

Figure 1. Interpolation factor for $T_i = 0$ for $i = 1, \dots N$ and linear RBF – the surface is the interpolation factor $W(x)$, red points denote predicted-measured ratios and bottom plane illustrates WWER440 core geometry

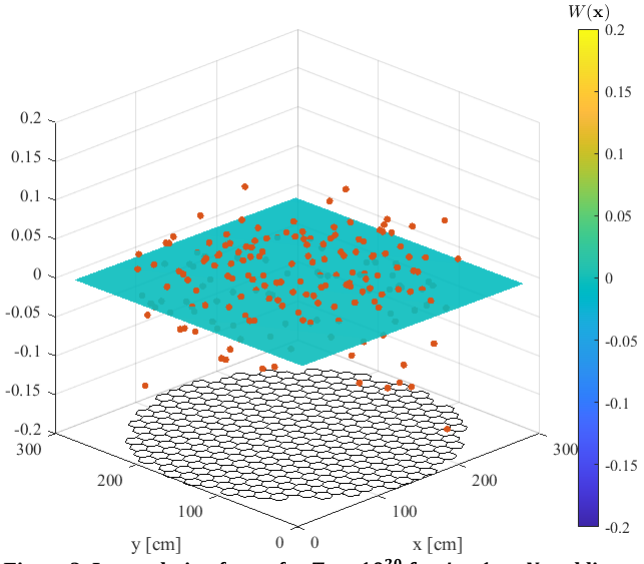

Figure 2. Interpolation factor for $T_i = 10^{20}$ for $i = 1,\dots N$ and linear RBF – the surface is the interpolation factor $W(x)$, red points denote predicted-measured ratios and bottom plane illustrates WWER440 core geometry

From approximation examples in Figure 1 and Figure 2 it follows that RBF approximation method with tolerance factor inclusion can meet the requirements proposed in Equation (4) and Equation (5). Same results were obtained for all radial basis function types considered in analysis (see Table 1). It should be noted that to achieve same level of smoothness for different types of RBF different tolerance factor value is necessary.

In Figure 1 and Figure 2 tolerance factor was applied as same value for all positions. It can be shown that tolerance factor smoothing effect on interpolation factor is observable even if it is applied locally (as an example see Figure 3).

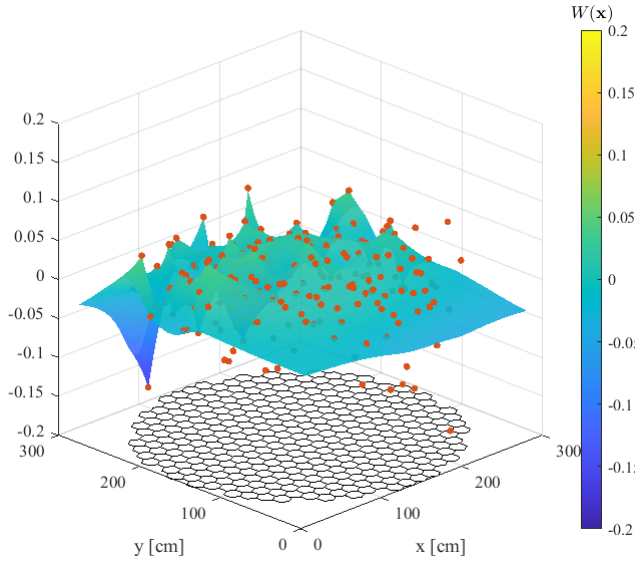

Figure 3. Interpolation factor for $T_i = 500$ for $i = 1,\dots 100$ and $T_i = 0$ for $i = 100,\dots N$ and linear RBF – the surface is the interpolation factor $W(x)$, red points denote predicted-measured ratios and bottom plane illustrates WWER440 core geometry

B. Numerical stability and credibility

To ensure numerical stability of RBF approximation method approximations for wide range of RBF method were performed. To measure method credibility and stability, following metrics were introduced.

Sum of squared residuals defined as:

$$R^2 = \frac{1}{N}\sum_{i=1}^{N}(W(\boldsymbol{x}_i) - w_i)^2 \qquad (13)$$

which meaning is to measure distance between predicted-measured ratio values and interpolation factor values at measurement points.

A second metric used was condition number of RBF method matrix (see Equation (11)) which has form:

$$\kappa(\boldsymbol{A}) = \frac{\lambda_{max}(\boldsymbol{A})}{\lambda_{min}(\boldsymbol{A})}, \qquad (14)$$

where $\lambda_{max}(\boldsymbol{A})$ and $\lambda_{min}(\boldsymbol{A})$ are maximal and minimal eigenvalues of $\boldsymbol{A}$ respectively. The condition number measures the matrix stability – the higher it gets the more ill-conditioned the matrix is.

During numerical tests it was found that stability and credibility of the method strongly depends on combination of RBF type and sign of tolerance factor in RBF approximation matrix (see Equation (11)).

For some combinations of RBF parameters approximation becomes strongly unstable. The instability can be observed by plotting the interpolation factor (see Figure 4).

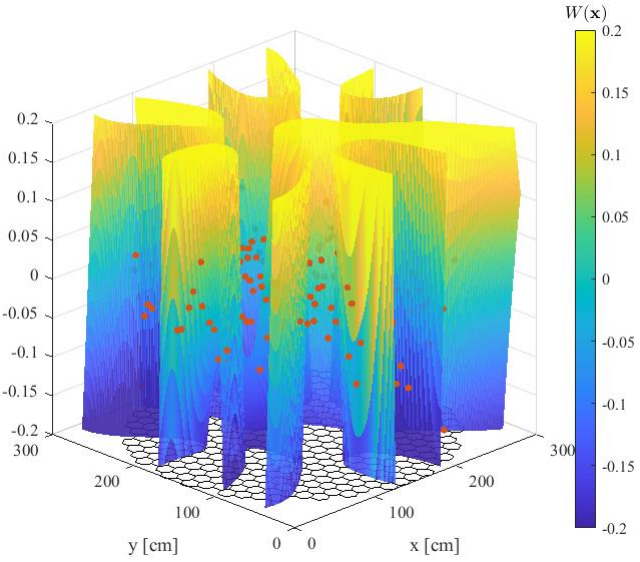

Figure 4. Interpolation factor for linear RBF, plus sign of tolerance factor in RBF approximation matrix, $T_i = 100$ for $i = 1,\dots N$ – an example of instable approximation, the surface is the interpolation factor $W(x)$, red points denote predicted-measured ratios and bottom plane illustrates WWER440 core geometry

To study stability of RBF approximations, a method based on metrices R^2 and κ was introduced. RBF approximations were performed for wide range of tolerance factor values and both signs of tolerance factor in RBF method matrix. For each approximation R^2 and κ values were calculated. As a result, these metrices were plotted together as functions of T_i for $\forall i$ (see Figure 5 for minus sign of tolerance factor and Figure 6 for plus sign of tolerance factor in RBF matrix for linear RBF).

In Figure 5, both R^2 and κ are smooth and monotonous functions of tolerance factor value. For tolerance factor

value about 10^3 tolerance factor smoothness effect, measured by R^2, gets saturated. In Figure 6 both metrics oscillate and reach higher values compared to Figure 5 which indicates instable approximation which can be seen in Figure 4.

Using methods described above, it was found that to ensure RBF approximation stability certain combinations of RBFs and tolerance factor sign in RBF matrix have to be used. The combinations of RBFs and tolerance factor signs for which stability was observed are stated in Table 2.

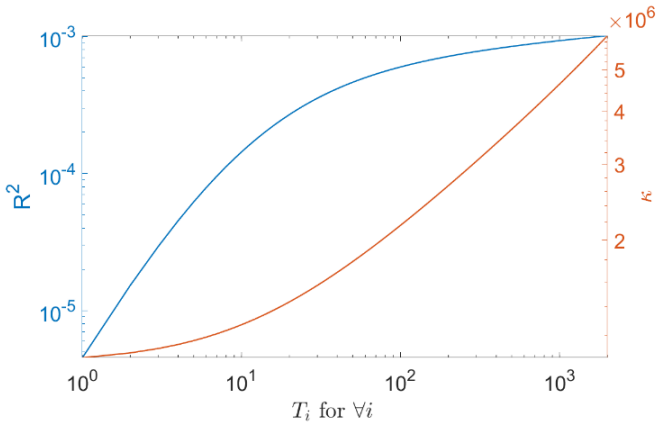

Figure 5. Metrics R^2 and κ as functions of tolerance factor value for linear RBF and minus tolerance factor sign

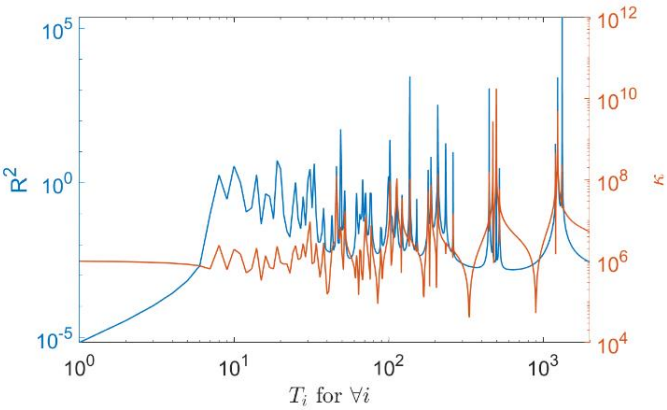

Figure 6. Metrics R^2 and κ as functions of tolerance factor value for linear RBF and plus tolerance factor sign

Table 2. Combinations of radial basis function types and tolerance factor signs in RBF matrix for which stability was observed

Function Name	Tolerance Factor Sign
Linear	-
Cubic	+
Gaussian	+
Multiquadric	-
Inverse multiquadric	+
Thinplate	+

V. CONCLUSION

This paper presents application of scattered data approximation by RBF method for reactor core power distribution reconstruction. Approximation approach is introduced by application of tolerance factor in RBF method matrix. RBF matrix stability problem is investigated for different RBFs. Approximation stability criteria were set for further analysis of the method.

VI. REFERENCES

[1] X. Peng, Q. Wu, Y. Cai, L. Lou, Y. Yu, Q. Li, "The application of radial basis function interpolation in reactor core power distribution on-line monitoring," *Annals of Nuclear Energy*, vol. 132, pp. 752–762, Oct. 2019, doi: 10.1016/j.anucene.2019.06.059.

[2] J. C. Carr, W. R. Fright, and R. K. Beatson, "Surface interpolation with radial basis functions for medical imaging," *IEEE Transactions on Medical Imaging*, vol. 16, no. 1, pp. 96–107, Feb. 1997, doi: 10.1109/42.552059.

[3] W. Li, P. Ding, C. Duan, R. Qiu, J. Lin, and X. Shi, "Comparison of spatial interpolation approaches for in-core power distribution reconstruction," *Nuclear Engineering and Design*, vol. 337, pp. 66–73, Oct. 2018, doi: 10.1016/j.nucengdes.2018.06.016.

[4] W. du Toit, "Radial basis function interpolation," Master thesis, University of Stellenbosch, 2008.

Proceedings of the European Nuclear Young Generation Forum
ENYGF'21
September 27-30, 2021, Tarragona, Spain

Application of Artificial Neural Network and Particle Swarm Optimization in determining selected parameters of the nuclear reactor core

Kubiński Wojciech[1*], Bojarski Patryk[1] and Darnowski Piotr[2]

[1] Warsaw University of Technology, Faculty of Physics, Poland

[2] Warsaw University of Technology, Institute of Heat Engineering, Poland

*Corresponding author: *wojciech.kubinski@pw.edu.pl*

I. INTRODUCTION

Reactivity of a nuclear reactor core (ρ) determines rate of change of the neutron population in the chain reaction. This value is the basic parameter of safety and operation of every nuclear reactor core and is defined as the relative deviation of the effective neutron multiplication factor (k_{eff}) from critical state of k_{eff}=1:

$$\rho = \frac{k_{eff} - 1}{k_{eff}} \quad (1)$$

Where k_{eff} , in the simplest definition, can be defined as the ratio of neutron population in a given generation (t+1) to the number of neutrons in the previous one (t):

$$k_{eff} = \frac{n_{t+1}}{n_t} \quad (2)$$

When k_{eff}<1, the core is in the subcritical state (the chain reaction will be suppressed), when k_{eff}>1, the core is in the supercritical state (more and more neutrons will be produced in the chain reaction). When k_{eff}=1, the core is in the critical state and the average number of neutrons does not change in time (the number of neutrons produced in the core is equal to losses mainly due to the escape of neutrons and their absorption by the atoms of the medium) [1].

In practice k_{eff} (or ρ) is a parameter measured or simulated in the analysis of each system containing fissile material. Specialized computation codes (deterministic or Monte Carlo) are often used for this purpose. However, depending on the complexity of the problem and the method chosen, these calculations can be time consuming. One solution to obtain an approximate result in a much shorter time can be the use of an artificial neural network (ANN) [2].

In previous studies, ANN have been successfully used to predict core parameters such as boron concentration, power peaking factor (with an accuracy in the range of 1-10%) [3], neutron flux mapping (< 5%) [4] control rod levels (~5%) and length of the cycle (up to 20%) [2]. As the increasing resources of computing power enable more and more complex calculations, it is important to develop the topic of the use of ANN in nuclear engineering as a fast and flexible tool supporting the analysis and design of nuclear installations.

II. BEAVRS CORE MODEL

The model of the core considered in this project is described in the BEAVRS benchmark (*Benchmark for Evaluation And Validation of Reactor Simulations*), published by the MIT Computational Reactor Physics Group [5]. It describes one of the Pressurized Water Reactors (PWR), with a thermal power of 3411 MW, produced by the Westinghouse company.

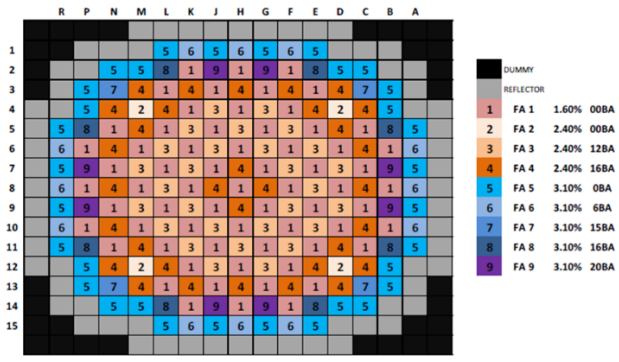

Figure 1. BEAVRS core configuration [5].

The BEAVRS core (Fig 1.) consists of 9 types of fuel assemblies (FA) that differ in enrichment (1.6%, 2.4% and 3.1% U-235) and the number of rods filled with burnable absorber (0, 6, 12, 15, 16 or 20 rods). The entire core consists of 193 assemblies in total. The value of the effective neutron multiplication factor for the original arrangement of the core at the beginning of the cycle is equal to k_{eff}=1.080 (ρ=0.074) and it was calculated using the PARCS 3.2 deterministic core simulator [6].

III. ANALYSED DATA

The purpose of this project was to use ANN to replace PARCS core simulator in the determination of core reactivity for a given configuration of the fuel assemblies. To do so, 7,000 patterns were generated, including a learning set of 5,000 patterns, a validation set of 1,000 patterns and the test of 1,000 patterns. Each of the pattern contained randomly generated fuel configuration. Using PARCS code, the reactivity of each configuration was determined, creating a set of inputs and outputs for the ANN. In order to reduce the amount of input and simplify the problem, it was decided to limit the considered configurations only to those that had 1/4th of the symmetry. Thus, only 1/4th of the configuration was generated, and then symmetrically mirrored to build up the whole core. This assumption reduced the size of input layer from 192 to 56. The input was therefore a set of 56 different types of fuel assemblies (numbers from 1 to 9), while the output was the value of the core reactivity (Fig. 2).

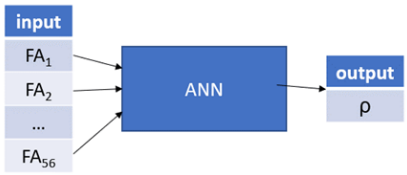

Figure 2. General scheme of the artificial neural network.

IV. PARTICLE SWARM OPTIMIZATION

There are many biologically inspired algorithms in the literature that have been successfully used for optimization in nuclear engineering problems (e.g. genetic algorithms [7], bee colony, simulated annealing [8]). Particle Swarm Optimization (PSO) is one of them and it is a method of searching for a global extremum with the use of a swarm of agents (particles) distributed over a multidimensional space of solutions. One type of PSO method is the firefly algorithm, which involves the use of particles with characteristics and principles of operation inspired by the behavior of fireflies. In this method, each of the particles (initially randomly placed in the space of solutions) is characterized by a certain brightness (analogically to its biological equivalent). This brightness is proportional to the quality of the solution that characterizes the given particle (its position). There are many possible variants of this algorithm, but in the simplest version, each of the particles moves towards the brightest particle in its neighborhood. It moves at a certain speed (and inertia) through the solution space, and at the same time, it can find a better position and become the brightest particle. In this way, particles search the solutions space, potentially approaching the global optimum [8], [9].

When we consider the *k*-dimensional solution space, each of the particles can be described as a vector:

$$\hat{x} = [x_1, x_2, \dots, x_k] \tag{3}$$

Then the distance between particles *i* and *j* can be defined as the cartesian distance between two points:

$$r_{ij} = \sqrt{\sum_{m=1}^{k} (x_{j,m} - x_{i,m})^2} \tag{4}$$

Assuming that the position of particle *i* at time *t* is $\hat{x}_i^{\,t}$, and particle *j* is the brightest one in its neighborhood, the position of particle *i* at time *t + 1* will change as follows [8]:

$$\hat{x}_i^{\,t+1} = \hat{x}_i^{\,t} + \beta_0 \cdot e^{(-\gamma \cdot r_{ij})}\left(\hat{x}_j^{\,t} - \hat{x}_j^{\,t}\right) + \alpha\varepsilon_i^t \tag{5}$$

Where α, β_0 and γ are the parameters of the algorithm, ε_i is the random factor (inertia) of the particle, and r_{ij} is the distance between the particle *i* and the brightest particle *j*.

V. NEURAL NETWORK PARAMETERS

A multi-layer perceptron was selected as the primary ANN architecture for the simulations (Fig. 2). It was implemented using Python 3.8 language. First of all, it was necessary to define its structure, i.e. to choose the number of hidden layers, the number of neurons in each of them, the value of the training parameter, batch size and the number of epochs. These parameters can be searched for by trial and error method, however, in the case of this study, it was decided to automate this process and use the PSO algorithm. Each of the particles was therefore coded as a set of parameters to be optimized, i.e.:

$$\hat{x} = [n_1, n_2, \dots, n_m, \eta, B, N] \tag{6}$$

Where: $n_1, n_2, \dots, n_m$ are numbers of neurons in *m* hidden layers, η is the learning parameter, *B* is the batch size and *N* is the number of epochs. All of these parameters (including *m*) were optimized using the PSO method.

In order to determine the quality of the network's operation and calculate brightness of each particle, the average relative error was calculated on a case-by-case basis:

$$ERR = \frac{1}{N}\sum_{i=1}^{N} \frac{|\rho_{ANN\,i} - \rho_{PARCS\,i}|}{\rho_{PARCS\,i}} \tag{7}$$

Then the brightness of the *i* particle was equal to the inverse value of *ERR*:

$$f(\hat{x}_i) = 1/ERR \tag{8}$$

VI. INPUT DATA ADJUSTMENT

After determining the parameters of the neural network (Fig. 3), it was decided to perform full learning. Initially, the network input was the set of the number between 1 and 9 that corresponded to a given configuration of the fuel. However, this approach led to the relative error of around 15%. In order to improve the operation of the network and speed up the learning process, it was decided to use as the input, not the numbers corresponding to the types of fuel assemblies but a pre-determined reactivity of an infinite lattice of given assembly type (ρ_∞). In practice, ρ_∞ (or k_∞) is calculated by defining a single assembly and setting the

periodic boundary conditions. A similar procedure was carried out in [10].

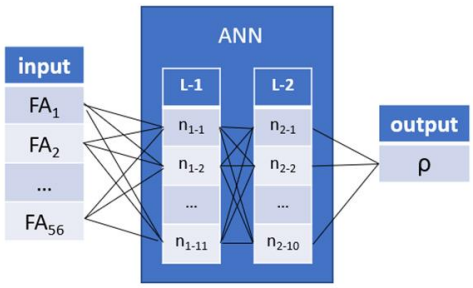

Figure 3. ANN architecture.

Table 1. k_∞ and ρ_∞ of the fuel assemblies.

FA	k_∞	ρ_∞
1	1.0934	0.0854
2	1.2212	0.1811
3	1.0721	0.0672
4	1.0266	0.0259
5	1.2917	0.2258
6	1.2247	0.1835
7	1.1260	0.1119
8	1.1087	0.0981
9	1.0673	0.0631

VII. RESULTS

After the input data was adjusted (see Table 1), the network learning was carried out, and mean relative error was calculated. Table 2 shows several examples of reactivity calculated by the ANN, compared to the values determined by PARCS.

Table 2. Comparison of reactivity calculated by ANN and PARCS code.

ρ_{ANN}:	ρ_{PARCS}:	Relative error:
0.0539	0.0549	-2%
0.0752	0.0786	-5%
0.0730	0.0770	-5%
0.0776	0.0801	-3%
0.0757	0.0673	11%
0.0735	0.0662	10%
0.0812	0.0771	5%

The mean error determined according to equation (7) was *ERR*=7.67% (or 0.0059) (mean relative deviation from the expected value) while the standard deviation of the error value was σ≈9.30%. The mean value including the sign of the error was equal to approximately 1.14% (or 0.0009).

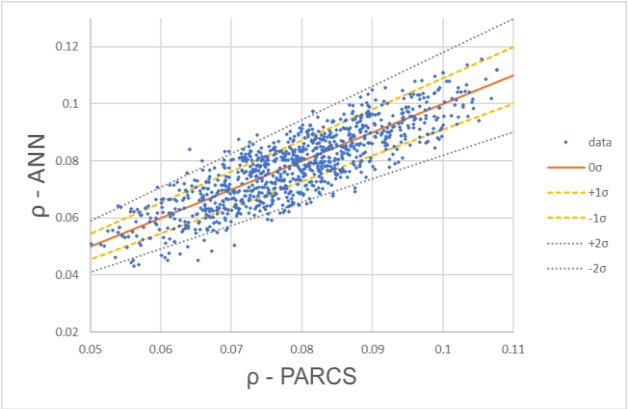

Figure 4. ρ-ANN as a function of ρ-PARCS.

The calculations were performed on a 12-thread core. Generating the data took about 2 hours, while training the network with the PSO method about 1 hour. As a result, determining the reactivity for the selected configuration was much below 1s.

For additional visualization of the network's operation, Figure 4 shows reactivity calculated by ANN (ρ_{ANN}) as a function of reactivity calculated by PARCS (ρ_{PARCS}). Ideally, the points should form a straight line with a slope angle of 45^0. However, the graph shows a certain dispersion of points. Orange dashed lines represent ρ_{PARCS} values with a margin of 1σ (9.30%) and grey lines show a margin of 2σ (18.60%). One can see that the vast majority of the points are within the range of 2σ.

VIII. SUMMARY AND CONCLUSIONS

In the frame the study, an artificial neural network was implemented, and its operating parameters were determined by the PSO algorithm. Then, the ANN was taught to determine the reactivity of a given configuration of the fuel assemblies in the PWR core model. The simulations showed that the PSO method can be used to find optimized parameters of the ANN whereas the network itself can predict the reactivity with a relative accuracy of about 9% (for 1σ). It should be noted, however, that the neural network was solving a multidimensional, complex problem with 56 input parameters with 9 possible values ($9^{56}\approx10^{53}$ possible configurations). In the literature, similar problems of approximation of the parameters of the full reactor core using the neural network are solved with an accuracy of up to 20% [2], hence it can be concluded that the obtained result does not deviate from the norm and the network works properly. The ANN can therefore replace the operation of the core simulator when a less accurate but instant determination of the desired parameters is needed (e.g. in the follow-up calculations of a nuclear power plant or in the first approximations of the tested systems).

In future research, it is possible to increase the accuracy of calculations by reducing the number of assemblies, i.e. consider similar assemblies (with the same enrichment but a slight difference in the number of burnable absorber rods as one type of assembly and/or assume further symmetry (1/8) and thus limit the amount of data input for the ANN. Additionally, it is possible to generate more patterns for the

training set and perform more epochs. Unfortunately, due to computational reasons, these modifications were beyond the scope of this project.

IX. REFERENCES

[1] Lewis, E. E., *Fundamentals of Nuclear Reactor Physics*, AcademicPress, 2008, https://doi.org/10.1016/B978-0-12-370631-7.X0001-0

[2] R. A. Saleema, M. I. Radaidehb, T. Kozlowski, *Application of deep neural networks for high-dimensional large BWR core neutronics*, Nuclear Engineering and Technology (52), 2020 https://doi.org/10.1016/j.net.2020.05.010

[3] L. P. Filho, K. C. Souto , M. D. Machado, *Using Neural Networks for Prediction of Nuclear Parameters*, International Nuclear Atlantic Conference, Recife, Brazil , 2013

[4] S. K. Bahuguna , S. Mukhopadhyay, and A. P. Tiwari, *Compressed Sensing Artificial Neural Network for Reactor Core Flux Mapping*, Transactions on Nuclear Science, 2018

[5] MIT CRPG, *BEAVRS - Benchmark for Evaluation Reactor Validation of And Simulations Rev. 2.0.2*, 2018, https://crpg.mit.edu/sites/default/files/css_injector_images_image/BEAVRS_2.0.2_spec.pdf

[6] P. Darnowski , M. Pawluczyk, *Analysis of the BEAVRS PWR benchmark using SCALE and PARCS*, Nukleonika, 2019, DOI:10.2478/nuka-2019-0011

[7] W. Kubinski, P. Darnowski, K. Chec, *The development of a novel adaptive genetic algorithm for the optimization of fuel cycle length*, ANE 155(2021):108153, 2021, DOI: 10.1016/j.anucene.2021.108153

[8] M. Louzazni, A. Khouya, K. Amechnoue et al., *Metaheuristic Algorithm for Photovoltaic Parameters: Comparative Study and Prediction with a Firefly Algorithm*, Applied Sciences, February 2018, https://doi.org/10.3390/app8030339

[9] A. Tjahjono, D. O. Anggriawan, A. K. Faizin et al., *Optimal Coordination of Overcurrent Relays in Radial System with Distributed Generation Using Modified Firefly Algorithm*, IJEEI vol 7, no 4, December 2015

[10] Jiang, S., Pain, C.C., et al. *Nuclear Reactor Reactivity Prediction Using Feed Forward Artificial Neural Networks*, Advances in Neural Networks ,2008, https://doi.org/10.1007/978-3-540-87732-5_45

Proceedings of the European Nuclear Young Generation Forum
ENYGF'21
September 27-30, 2021, Tarragona, Spain

Modelization of the European Pressurized Reactor coolant system with MELCOR 2.2

Fallot, Lucile[1*], Larriba, Samantha[1] and Jiménez, Gonzalo[1]

[1] Universidad Politécnica de Madrid – Escuela Técnica Superior de Ingenieros Industriales (UPM – ETSII), Spain

*Corresponding author: lcjf@enusa.es

I. INTRODUCTION

At the end of the 80s', Framatome and Siemens, with the collaboration of Electricité de France (EDF) and a group of major German Utilities, decided to cooperate for creating a new nuclear reactor design: the European Pressurized Reactor (EPR). The main objectives were the creation of a nuclear reactor which would be competitive economically, whose design would take into account severe accidents and their consequences. Moreover, the EPR would be designed on the basis of deterministic and probabilistic safety analyses [1]. Nowadays, two EPR plants are operating in China and other units are in construction in several countries.

The EPR is an evolutive reactor, corresponding to the combination of the French N4 and REP2000 reactor designs and the German KONVOI design [2]. It generates a 1600 MWe electric power (4500 MWth) from the heat produced by the core which is composed by 241 fuel assemblies (UO2 or Mixed Oxides (MOx)) and cooled by pressurized light water circulating in 4 loops [2]. This reactor has some innovative systems that allow achieving a low risk level regarding core melt situations and large radioactive product releases, such as the concrete doble-wall containment which can resist against internal and external hazards (fire, flooding, earthquakes, aircraft crash, etc.) and the core catcher which is an ex-vessel system for core melt retention and stabilization in case of low-pressure break of the reactor vessel [3].

This paper presents the creation of the EPR coolant system model, developed with MELCOR 2.2 computer code, in order to study the behaviour of this system in normal operating conditions.

II. DESCRIPTION OF THE MODELS

Before the creation of the EPR coolant system model with MELCOR 2.2 computer code, a complete research of geometric and thermohydraulic characteristics of all the components of the reactor was done. To obtain the geometric data needed for modelling the steam generators, a geometric 3D-model of one of them was created with AutoCAD.

A. Steam generator AutoCAD model

AutoCAD is a commercial computer-aided design (CAD) and drafting software application. It was used for designing a 3D-model of one of the EPR steam generators, in order to calculate the volume available for hydrodynamic materials within the primary and secondary systems of the steam generators. The data were obtained from a public drawing [4]. Firstly, the shell of the system, the partition plate and the tubesheet were created (see Figure 1). Instead of modelling each one of the 5980 U-tubes, the enveloping volume was represented along with one of the tubes, whose characteristics correspond to the average dimensions of all the U-tubes. To design the swirl vane separator and the dryer, the enveloping volumes were built, in the absence of more detailed data. These geometric data were used later for modelling the steam generators of the EPR with MELCOR.

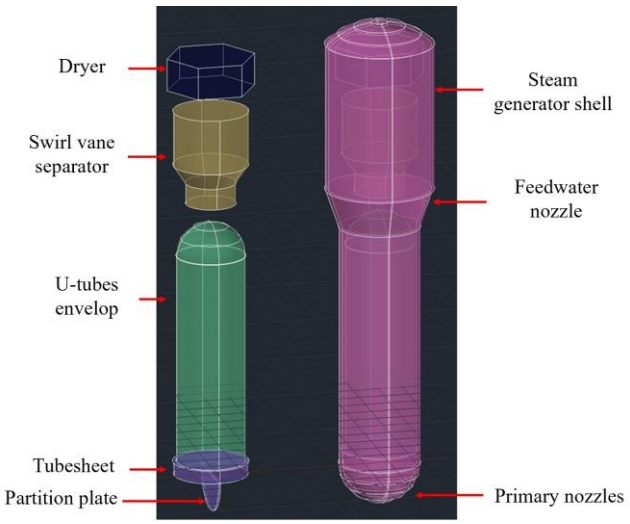

Figure 1. Steam generator AutoCAD model

B. EPR Coolant System MELCOR 2.2 model

MELCOR 2.2 is a fully integrated, engineering-level computer code that models the progression of severe accidents in light water reactors and calculates an estimation of fission product source terms [5]. It is composed of an executive driver and several calculating modules (called "packages") that model the main systems of a reactor plant and their coupled interactions. The thermal-hydraulic behaviour of coolant liquids and gases is modelled by the Control Volume Hydrodynamics (CVH) and Flow Path (FL) packages. These two packages provide boundary conditions to other phenomenological packages, such as the Heat Structures (HS) and COR packages, which calculate sources and sinks of mass and energy and also the volumes available to hydrodynamic materials for CVH. One control volume represents one calculation node, and the connections that allow transfer of hydrodynamic material between two control volumes are modelled by flow paths. The EPR coolant system model also includes heat structures for calculating heat conduction within the intact solid structures and energy transfer across its boundary surfaces into control volumes, and Control Functions (CF), which define functions of variables in the MELCOR database and make the values of these functions available to other packages in MELCOR. To simulate the thermal power generated by the core and the phenomena that occur in it, the COR package is used. The COR package also models the relocation of core and lower plenum structural materials during melting, slumping and formation of molten pool and debris.

MELCOR code was already used for simulating accident scenarios and analysing the response of the EPR reactor in case of total loss of AC power [6] and a large break loss of coolant without safety injection [7], among others. In both papers, the reactor cooling system consisting of four loops is divided into two model loops. First loop is called "broken" loop and corresponds to the loop with the connection to the pressurizer, whose geometry is equivalent to the dimensions of one of the EPR loop. The other three loops are merged into one, the "intact" loop, with a properly rescaled geometry. In the present paper, each one of the four loops was modelling.

The EPR coolant system model developed with MELCOR (see Figure 2) is composed by 176 control volumes, 249 flow paths and 120 heat structures, distributed into the reactor vessel, the 4 steam generators, the pipes of each one of the 4 loops, the configuration of the pumps and the pressurizer.

The model of each one of the 4 steam generators is composed by the primary system and the secondary system models, and both were divided into several nodes (9 for the primary system and 19 for the secondary systems per steam generator). Moreover, there is a correspondence in height between the primary and secondary system nodes, in order to achieve a better simulation of the heat transfer between both circuits.

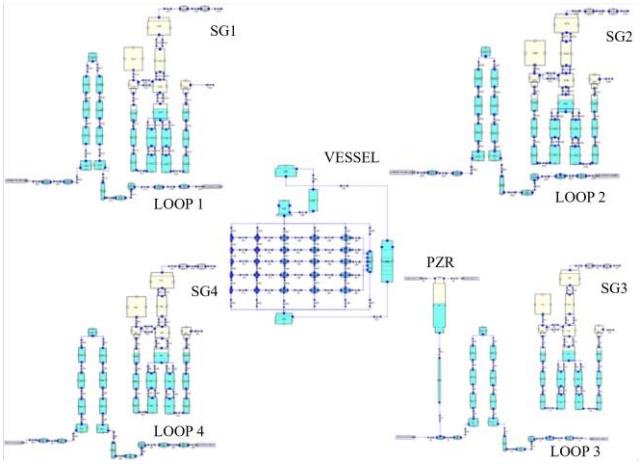

Figure 2. EPR Coolant System model built with MELCOR 2.2 (visualization with SNAP graphic interface)

The reactor vessel is composed by several control volumes corresponding to the active core length (25 control volumes), the core bypass flow (water inside guide thimbles and around the core, 1 control volume), the downcomer (1 control volume), the lower plenum (1 control volume), the upper plenum (1 control volume), the upper head (1 control volume) and the water volume inside the control rod guide tubes (1 control volume) [8][9]. When setting the COR package components, the core is divided into 6 cylindric radial levels (rings) and 13 axial levels (see Figure 3). The radial nodalization was determined from the nodalization of the Surry NPP core described in [10] and adapted to the EPR core which is composed by 241 fuel assemblies. The lower plenum is represented by the two lower axial levels. Within the second axial level are also included the bottom nozzles of the fuel assemblies and the lower core plate. The core active length is modelled by the intersection between the 10 intermediate axial levels and the inner 5 rings (in blue on Figure 3). The fuel assembly top nozzles are modelled by the nodes of the five inner nodes of the upper axial level. The downcomer is represented by the 6th ring, from the 2nd to the 13th axial level. Each node is associated to one control volume. Then, the initial temperatures, masses and geometric data for all the components in the core are set.

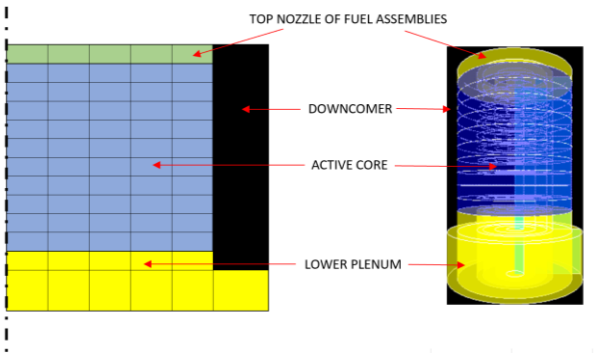

Figure 3. Nodalization of the core

Each loop of the EPR coolant primary system includes a hot leg between the reactor vessel and the steam generator inlet, a crossover leg between the steam generator outlet and the pump, and a cold leg between the pump and the vessel downcomer [4]. Each leg is modelled by two control volumes and the corresponding flow paths.

For modelling each one of the primary pumps, one control volume represents the water volume which passes by the pump and the pump curve is implemented within a flow path [4]. Since no data about the characteristic curve of the primary pumps were available, the pumps were defined by a control function similar to the one described in the MELCOR user's guide [11].

The pressurizer is modelled by one control volume filled with steam in the upper part, and water in the lower part. It is connected to the hot leg of the third loop through the surge line, which was modelled by another control volume [4]. In order to control the primary system pressure, sprays and heaters were implemented through control functions. When the pressure increases and reaches the top threshold value, the spraying system turns on and water is injected into the pressurizer to decrease the pressure. Afterwards, the heaters get activated in order to retrieve the equilibrium state within the pressurizer that has been disrupted due to the activation of the spraying systems. Indeed, the heaters turn on when the pressurization of the system is needed.

The containment building is modelled by only one control volume, which is used as a boundary condition for the primary system [12].

III. RESULTS

To validate the model in normal operating conditions, the simulation results were compared to reference values, which correspond to the design values of each system parameter of interest, obtained from references [4][13][14][15]. Since the magnitudes oscillate (see Figure 4 and Figure 5), the "nominal operation value" obtained from the simulation, presented in Table 1, corresponds to the value averaged on the total duration of the simulation, 15 000 s (4 hours approximately). Most of the analysed magnitudes (pressures, temperatures and flows in primary and secondary systems) show values close to the reference ones, despite the oscillations, as it can be seen on Figure 4 and Figure 5, that respectively present the evolution of the pressure in the pressurizer and the core inlet and outlet temperatures. The difference between the reference value and the simulation results is considered acceptable for most of the magnitudes. However, the simulated recirculation ratio in the steam generators, which is equal to the downcomer mass flow divided by the steam mass flow leaving the boiler, is significantly inferior to the reference value. Modifications will be necessary for improving the steam generator model to achieve a more realistic simulation of this system.

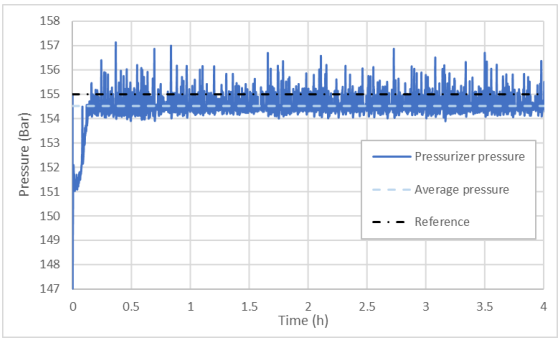

Figure 4. Pressurizer pressure

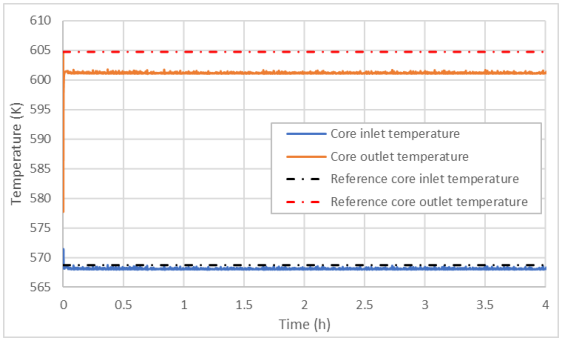

Figure 5. Core inlet and outlet temperature

Table 1. Comparison of simulated results with bibliography data

	Nominal operation value – Reference data	**Nominal operation value – MELCOR results**	**Difference [%]**
Thermal power generated in the core [MWth]	4500	4500	0
Primary system pressure in the pressurizer [bar]	155.00	154.44	0.36
Vessel inlet flow [kg/s]	23140.00	23191.40	-0.22
Core inlet temperature [K]	568.75	568.11	0.11
Core outlet temperature [K]	604.75	601.17	0.59
Steam generator inlet temperature (primary water) [K]	602.05	601.03	0.16
Steam Generator outlet temperature (primary water) [K]	568.85	567.87	0.61
Steam pressure in the steam line [bar]	78.00	78.58	-0.74
Steam temperature in the steam line [K]	566.15	568.29	-0.38
Steam mass flow rate in the steam line [kg/s]	2552.40	2531.35	0.82
Steam generator recirculation ratio	3.60	1.25	65

IV. CONCLUSIONS

The EPR coolant system model presented in this paper was created with MELCOR 2.2 computer code, from public information and geometric data obtained from the 3D-model of a steam generator made with AutoCAD. It allowed studying the reactor behaviour in normal operating conditions. The comparison between the steady state simulation results and the reference data led to the verification of the model, despite the absence of some data.

This work is a first step towards the simulation of accident scenarios in the EPR with MELCOR 2.2. For a realistic analyse of the response of the EPR reactor during accident conditions, the following modifications are necessary: enhancing the configuration of the primary pumps, improving the control of the pressurizer, implementing the safety systems, improving the containment building modelization and achieving a more realistic steam generator recirculation ratio.

V. AKNOWLEDGEMENTS

This work was partly granted by the the "Cátedra Federico Goded" of the UPM-E.T.S. Ingenieros Industriales, financed by the Consejo de Seguridad Nuclear Español.

VI. REFERENCES

[1] U. Fischer, "The European Pressurized water Reactor. Result of the French-German cooperation of experienced NPP suppliers and operators", Nuclear Engineering and Design, Vol. 187, Jan. 1999.

[2] G. Martin, "The Pre-Construction Safety Report, Sub-chapter 1.3 – Comparison with reactors of similar design", UK EPR, Oct. 2012.

[3] F. Bouteille et al., "The EPR overall approach for severe accident mitigation", Nuclear Engineering and Design, Vol. 236, Aug. 2006.

[4] F. Ghestemme, "The Pre-Construction Safety Report, Sub-chapter 5.4 – Components and Systems sizing", UK EPR, Oct. 2012.

[5] "MELCOR Computer Code Manuals. Vol. 2: Reference Manual", 2017.

[6] P. Darnowski et al., "Total loss of AC power analysis for EPR reactor", Nuclear Engineering and Design, Vol. 289, Mar. 2015.

[7] P. Darnowski et al., "Simulations of Large Break Loss of Coolant Accident without Safety Injection for EPR Reactor using MELCOR Computer Code", ERMSAR-2015, Mar. 2015.

[8] F. Ghestemme, "The Pre-Construction Safety Report, Sub-chapter 3.4 – Mechanical systems and components", UK EPR, Oct. 2012.

[9] F. Ghestemme "The Pre-Construction Safety Report, Sub-chapter 5.3 – Reactor Vessel", UK EPR, Nov. 2012.

[10] "State-of-the-Art Reactor Consequence Analyses Project. Volume 2: Surry Integrated Analysis", NUREG/CR-7110, Vol. 2, Jan. 2012.

[11] "MELCOR Computer Code Manuals. Vol. 1: Primer and User's guide", 2017.

[12] M. Lachaise, "The Pre-Construction Safety Report, Sub-chapter 6.2 – Containment systems", UK EPR, Oct. 2012.

[13] "Nuclear Power Plant Unit Olkiluoto 3", Teollisuuden Voima Oyj, Oct. 2010.

[14] D. Page Blair, "The Pre-Construction Safety Report, Sub-chapter 4.1 – Summary Description", UK EPR, Jul. 2012.

[15] D. Page Pair, "The Pre-Construction Safety Report, Sub-chapter 4.4. – Thermal and hydraulic design", UK EPR, Jul. 2012.

Proceedings of the European Nuclear Young Generation Forum
ENYGF'21
September 27-30, 2021, Tarragona, Spain

Model for premixed layer formation in stratified fuel-coolant configuration and its application

Kokalj, Janez[1,2*], Uršič, Mitja[1] and Leskovar, Matjaž[1]

[1] Jožef Stefan Institute (JSI), Slovenia; [2] University of Ljubljana (UNI LJ), Slovenia

*Corresponding author: *janez.kokalj@ijs.si*

I. INTRODUCTION

A hypothetical severe accident in a nuclear power plant can lead to significant core damage, including melting of the core [1]. The hot melt in contact with the coolant water can result in a vapour explosion. Similar explosion phenomenon can be a threat also in some industrial processes, such as foundries and liquefied natural gas operations or in certain volcanic activity where water is present. In analyses of severe accidents in nuclear power plants, a fuel-coolant interaction was mostly addressed in a geometry of a melt jet poured into a coolant pool. Based on some experimental and analytical work from the past a geometry with a continuous layer of melt under a layer of water, called stratified configuration, was believed to be incapable of producing energetic fuel-coolant interaction [2]. However, the results from recent experiments performed at the PULiMS and SES facilities (KTH, Sweden) with corium simulants materials contradict this hypothesis [3, 4]. In some of the tests, a premixed layer of ejected melt drops in water was clearly visible and was followed by strong spontaneous vapour explosions.

The purpose of our research was to improve the knowledge, understanding and modelling of the fuel-coolant interaction phenomena in the stratified configuration. In the paper, a model for the premixed layer formation [5], developed based on the visual observations and some available mechanisms from the literature, is presented. The developed model was implemented into the MC3D code (IRSN, France) as a patch and validated against the experimental results. The presented analyses demonstrate the model capability to describe the premixed layer formation in agreement with the experimental data.

II. MODEL FOR PREMIXED LAYER FORMATION

Different experiments in stratified configuration with observed premixed layer and/or vapour explosion were studied [5]. It can be observed, that one of the most common plausible mechanisms for the premixed layer formation seems to be the formation, growth and collapse of vapour bubbles. The melt is usually hot enough for initiating the boiling of the coolant and if the coolant is subcooled and the coolant layer high enough, the bubbles collapse. The bubble formation, growth and collapse were observed also by the KTH [3] in the SES and PULiMS experiments and thus our developed model for the premixed layer formation in the stratified melt-coolant configuration is based on this mechanism.

Due to the instabilities, the bubbles arise from the vapour film. In subcooled water, bubbles condense and collapse. During the bubble collapse, water at the bubble interface accelerates towards the melt surface, creating a so-called coolant micro-jet. The coolant micro-jet impacts on the melt surface and can produce the melt surface instabilities and fragmentation of the melt.

Our model describes the premixed layer formation with three key characteristics, i.e. size of ejected melt drops, their initial velocity and the fragmentation rate of the continuous melt phase.

The modelling values depend on the scale of the instabilities, given by the value of the most dangerous wavelength on the surface, for which the instability growth rate is the highest – in our case this is the distance between the formed bubbles [6]:

$$\Lambda = 2\pi \sqrt{\frac{3\sigma_L}{g(\rho_L - \rho_G)}}, \qquad (1)$$

where σ_L is the liquid coolant surface tension, g the gravity acceleration and ρ_L and ρ_G density of liquid and gaseous phase of the coolant, respectively.

The melt surface instabilities can result in fragmentation of the melt. The size of the ejected melt drops in our model is related to the instability wavelength. The hypothesis by Leclerc and Berthoud [7] for the thermal fragmentation of single melt drop is adopted. The melt drop diameter is defined as one quarter of the instability wavelength. Due to the uncertainties, it is multiplied with the factor C_d:

$$d = C_d \cdot 0.25 \cdot \Lambda\,. \qquad (2)$$

The fragmentation rate of the melt layer can be established from the size of the ejected melt drops and the frequency of their ejections per melt area. The size of the melt drop is defined in Eq. 2. The single melt drop ejects from the surface area that is defined with the wavelength as given in Eq. 1. It should be emphasized that in this area we have node and antinode, therefore the effective surface area is $\frac{1}{2}\Lambda^2$. Due to the uncertainties, the fragmentation rate is multiplied with the factor C_f:

$$\Gamma = C_f \cdot \frac{\pi d^3 F}{3\Lambda^2}, \qquad (3)$$

The frequency of the melt ejections F is proportional to the frequency of the bubble formations and collapses. It can be derived from the relation by Berenson [6] for the bubble detachments for a horizontal surface film-boiling heat transfer, considering the Rayleigh-Taylor instabilities. With some simplifications due to the large differences in the liquid and vapour density, the following equation is obtained:

$$F = \frac{1}{2\pi}\sqrt{\frac{\rho_G v_{vf}^2 n}{\rho_L a} + gn - \frac{\sigma_L n^3}{\rho_L}} \qquad (4)$$

where n is wavenumber and v_{vf} and a vapour velocity and vapour film thickness:

$$v_{vf} = 0.45\frac{\lambda_{vf}\Delta T}{\rho_{vf}\Delta H a^2 n}, \qquad (5)$$

$$a = 2.35 \cdot \frac{\sigma_L^{\frac{1}{8}}}{(g\rho_L)^{\frac{3}{8}}} \cdot \left(\frac{\mu_{vf}\lambda_{vf}\Delta T}{\Delta H \rho_{vf}}\right)^{\frac{1}{4}}. \qquad (6)$$

where index vf stands for the vapour film, ΔT is temperature difference between the melt and the coolant and ΔH is average enthalpy difference between vapour and liquid coolant.

The initial velocity of the ejected melt drops is calculated from the available energy. As shown in experiments by Caldarola and Kastenberg [8], the available energy (and consequently velocity) lies between the transmitted (energy due to the shock wave from a hemispherical source to the surrounding medium) and the acoustic (energy of the elastic wave traveling in the fuel) energy limits. Thus, the velocity as calculated from the acoustic energy (lower limit) is in our model multiplied with a free factor C_v:

$$v = C_v\sqrt{C_{v1} \cdot C_{v2} \cdot \frac{(p_{max} - p_0)^2 \Delta T_{sub}^2}{\Lambda^{0.8}\sqrt{\Delta p}}}. \qquad (7)$$

where p_0 is the ambient pressure, p_{max} is the pressure of coolant micro jets acting on the melt, ΔT_{sub} is the water subcooling, Δp is the pressure difference between inside and outside of the bubble, C_{v1} is a constant, related to the dimension of the formed coolant micro-jet generated after the bubble collapse and its value is around 0.01. C_{v2} is related to the material properties:

$$C_{v2} = \frac{(\rho_M - \rho_L)\rho_L^{1.9}}{(\rho_M + \rho_L)\rho_M^2\rho_G^2} \cdot \frac{\lambda_L^{\frac{4}{3}} c_p^{\frac{2}{3}}}{c g^{0.2} L^2 \sigma_L^{0.2} \mu_L^{\frac{8}{15}}}. \qquad (8)$$

where index M stands for melt, λ is thermal conductivity, c_p is specific heat, c is sound velocity, L is latent heat and μ is dynamic viscosity.

Our model, reduced to the three equations for the melt drops diameter (Eq. 2), fragmentation rate (Eq. 3) and ejected melt drop initial velocity (Eq. 7), can be implemented into the fuel-coolant interaction codes to mathematically describe the phenomenon of the premixed layer formation in stratified configuration.

III. APPLICATION TO EXPERIMENTS

The developed model was implemented as a patch in the computational fluid dynamic MC3D code V3.9.0.p1, which is being developed at IRSN (France) with fuel-coolant interactions in mind [9, 10]. MC3D is one of the leading codes in the field of fuel-coolant interactions. It covers both the premixing phase and the explosion phase of the fuel-coolant interaction. The premixing phase module deals with the initial mixing of the melt and the coolant. In case a vapour explosion occurs, the results from the premixing phase module serve as an input for the explosion phase module. The explosion phase module concerns the fine fragmentation of the melt during the explosion and the heat transfer between the created fine fragments and the coolant.

The complex phenomena of premixed layer formation as described by our model was assessed on the experimental results by simulating the SES S1 and PULiMS E6 experimental tests. On these tests, some previous simulation analysis were performed, but without modelling the premixed layer formation [11].

A. SES S1 experimental test

The SES experiments were performed at KTH (Sweden). The test section consisted of a square tank of the size of 1 m^2, filled with water to the height of 25 cm. The melt was released in the water through the funnel, which ended in the water, 25 mm above the melt spreading surface. The initial melt temperature was 1303 K, which corresponds to 160 K of superheating. Water was at 348 K. During the release of the melt under water, a spontaneous vapour explosion occurred after 0.6 s. A more detailed description is given in [12].

The 3D calculation domain contains half of the experimental tank applying symmetry boundary conditions at the symmetry plane. The melt pouring and spreading is not modelled. Therefore, initially all the continuous melt is described as a 5 mm high melt pool with diameter of around 25 cm. The analyses are based on the best case, determined on the best values to fit the existing data [5]. Used parameters C_v, C_d and C_f are 6, 1.25 and 0.5.

Firstly, the premixed layer formation phase was simulated. After the initial transient of first melt drops being ejected, quasi-stationary conditions are developed. The melt drops are constantly being ejected from the continuous melt and coalescing back. In Figure 1, the formed premixed layer is shown. The melt drop volume fraction increases towards the top of the premixed layer because the velocity of the melt drops decreases. The phenomenon of the premixed layer formation is not completely homogeneous, which indicates the complexity of the feedback loops. Namely, heating of the coolant water, vaporization and flow currents of the vapour, water and melt affect the height of the premixed layer and the melt fraction distribution. Nevertheless, the simulation results where the maximum reached height of melt drops is around 10 cm seem to be close to the experimental observation.

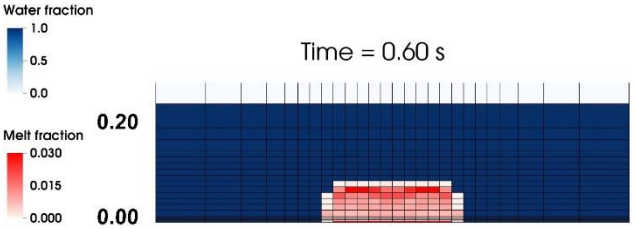

Figure 1: Simulated premixed layer for the SES S1 experimental test after 0.6 s.

Because of the lack of more detailed experimental data regarding the premixed layer, further analyses and comparison are made regarding the explosion phase, as seen in Figure 2. The force signal on the bottom of the test section and the total gained impulse are compared. The total gained impulse is in the simulation around 20 % lower, compared to the experimental one. Initially, the simulation's impulse is almost identical to the experimental one. The difference is made in the second half of the explosion, when the explosion in the simulation decays earlier.

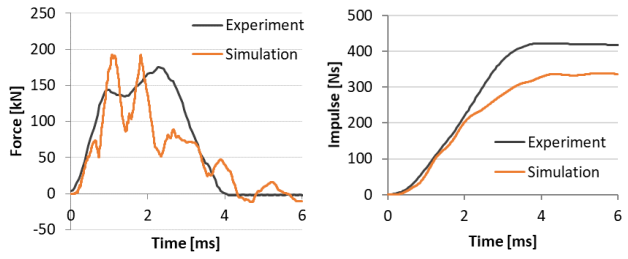

Figure 2: Comparison of the force and total gained impulse on the bottom plate for SES S1 simulation and experiment.

For the simulation case, the force signal is more fluctuating compared to the experimental one, although in the experimental results two force peaks can be also observed. In the simulation, the pressure shock waves are reflected and when meeting, a maximum in the force signal can be observed. The force signal in the simulation decreases more gradually compared to the experiment.

The simulation results for the SES S1 experimental test seem to be, considering the uncertainty in simulating the vapour explosions, in relatively good agreement with the experimental findings. The height of the developed premixed layer seems to be similar to the experimental one and the total impulse of simulation is around 80% of the experimental one.

B. PULiMS E6 experimental test

The PULiMS experiment was simulated in addition. The PULiMS experiment was performed at KTH (Sweden). Main experimental conditions and results are summarized here, while more detailed description is given in [4, 13]. The test section consisted of a rectangular tank of the size of 2 m × 1 m, filled with water to the height of 20 cm. The melt was released through the funnel, which ended 20 cm above the water surface. The initial melt temperature was 1322 K, which corresponds to 179 K of superheating. Water was at 348 K. During the release of the melt, a spontaneous vapour explosion occurred after around 7 s.

The 3D calculation domain contains half of the experimental tank applying symmetry boundary conditions at the symmetry plane. The continuous melt is described as a 25 mm high melt pool with diameter of around 40 cm. The analyses are based on the best case [5] with the same parameters as in the SES case - C_v, C_d and C_f being 6, 1.25 and 0.5.

For the PULiMS E6 case, the simulated premixed layer also seems to be close to the experimental observations. However, the explosion for the PULiMS E6 case is underpredicted to around one third of the experimental impulse in the simulation analysis (Figure 3). Although the impulse of the explosion is underpredicted in the simulations, the force signal is initially almost identical to the experimental one, indicating similar initial development of the explosion. Overall, it seems the simulation does not describe the explosion phenomena as good as for the SES S1 case.

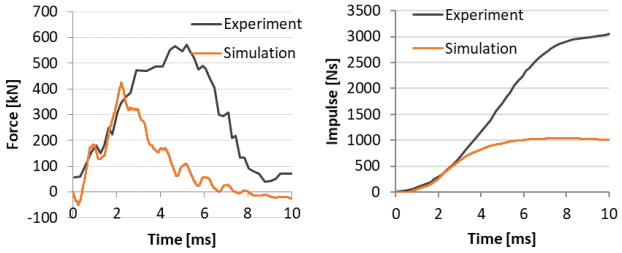

Figure 3: Comparison of the force and total gained impulse on the bottom plate for PULiMS E6 simulation and experiment.

IV. CONCLUSIONS WITH DISCUSSION

The recent experimental results from the PULiMS and SES (KTH, Sweden) experimental facilities with spontaneous vapour explosions again raised interest in vapour explosions in the stratified configuration. During the experiments, an extensive premixed layer was observed prior to the explosion. From the perspective of nuclear safety studies, it is important to be able to simulate potential energetic fuel-coolant interactions in stratified configurations with the preceded premixed layer of ejected melt drops in the coolant layer.

Developed model for the premixed layer formation, based on the bubble formation and collapse mechanism is presented in the paper. The model was implemented into the Eulerian fuel-coolant interaction code MC3D (IRSN, France) and validated against the SES S1 and the PULiMS E6 experimental results. The simulation results are in

agreement with the experimental results regarding the expected premixed layer. For the explosion phase, it seems that the simulations very accurately describe the initial phase of the vapour explosion in both aspects – force and impulse, but underestimate the explosion strength of the second part. The discrepancy is larger for the PULiMS E6 case, while it is around 20% for the SES S1 case.

The observed underestimation of the explosion strength in simulations might indicate possible additional contributions from the other mechanisms related to the melt-coolant mixing, premixed layer formation and vapour explosion. Some amount of mixing between the melt and the coolant could be a consequence of the melt jet breakup, especially in the PULiMS case, where in the experiment the melt jet falls through 20 cm of water. Additional contribution to the amount of melt, participating in the explosion, can be a consequence of mixing during the explosion itself.

In favour of this assessment, the simulation results with our model, considering only the bubble formation, growth and collapse mechanism, underestimate the experimental results. This indicates some other plausible contributions, for research of which the future experimental and analytical work would be of great help. With improved experimental observations, more detailed comparison of the premixed layer characteristic would also be possible.

Overall, the proposed premixed layer formation model enables more reliable assessment of the stratified vapour explosions risk in nuclear power plants and in other industries.

V. Acknowledgments

The authors acknowledge the financial support of the Slovenian Research Agency within the research program Reactor engineering (P2-0026) and the projects Understanding stratified steam explosions in reactor conditions (L2-1828).

The authors acknowledge the IRSN, France, and the MC3D development team, specifically Renaud Meignen, Stephane Picchi and Alejandro Villarreal Larrauri.

VI. References

[1] B. R. Seghal, Ed. *Nuclear Safety in Light Water Reactors: Severe Accident Phenomenology*. Elsevier Inc, 2012.

[2] G. Berthoud, "Vapor explosions," *Annual Review of Fluid Mechanics*, vol. 32, no. 1, pp. 573-611, 2000.

[3] D. Grishchenko, A. Konovalenko, A. Karbojian, V. Kudinova, S. Bechta, and P. Kudinov, "Insight into steam explosion in stratified melt-coolant configuration," in *15th International Topical Meeting on Nuclear Reactor Thermal Hydraulics*, Pisa, Italy, 2013, p. 19.

[4] P. Kudinov, D. Grishchenko, A. Konovalenko, and A. Karbojian, "Premixing and steam explosion phenomena in the tests with stratified melt-coolant configuration and binary oxidic melt simulant materials," *Nuclear Engineering and Design*, vol. 314, pp. 182-197, 4/1/ 2017.

[5] J. Kokalj, M. Uršič, and M. Leskovar, "Modelling of premixed layer formation in stratified fuel-coolant configuration," *Under review in Nuclear Engineering and Design*, 2021.

[6] P. J. Berenson, "Film-boiling heat transfer from a horizontal surface," *Journal of Heat Transfer*, vol. 83, no. 3, pp. 351-356, 1961.

[7] E. Leclerc and G. J. Berthoud, "Modeling of Melt Droplet Fragmentation Following Vapor Film Destabilization by a Trigger Pulse," *Nuclear Technology*, vol. 144, no. 2, pp. 158-174, 2003/11/01 2003.

[8] L. Caldarola and W. E. Kastenberg, "Mechanism of fragmentation during molten fuel/coolant thermal interactions," presented at the Fast reactor safety meeting, Beverly Hills, California, USA, 1974.

[9] R. Meignen, S. Picchi, J. Lamome, B. Raverdy, S. C. Escobar, and G. Nicaise, "The challenge of modeling fuel–coolant interaction: Part I – Premixing," *Nuclear Engineering and Design*, vol. 280, pp. 511-527, 12// 2014.

[10] R. Meignen, B. Raverdy, S. Picchi, and J. Lamome, "The challenge of modeling fuel–coolant interaction: Part II – Steam explosion," *Nuclear Engineering and Design*, vol. 280, pp. 528-541, 2014/12/01/ 2014.

[11] M. Leskovar, V. Centrih, M. Uršič, and J. Kokalj, "Investigation of steam explosion duration in stratified configuration," *Nuclear Engineering and Design*, vol. 353, p. 110233, 2019.

[12] E. De Malmazet *et al.*, "Stratified Steam Explosion Phenomena: SAFEST SES-S1 test results and preliminary analysis," in *The 8th European Review Meeting on Severe Accident Research, ERMSAR, Warsaw, Poland*, 2017, no. 203.

[13] A. Konovalenko, A. Karbojian, and P. Kudinov, "Experimental results on pouring and underwater liquid melt spreading and energetic melt-coolant interaction," in *The 9th International Topical Meeting on Nuclear Thermal-Hydraulics, Operation and Safety*, Kaohsiung, Taiwan, 2012, p. 11: American Nuclear Society.

Proceedings of the European Nuclear Young Generation Forum
ENYGF'21
September 27-30, 2021, Tarragona, Spain

Study of discharges in stagnant water using spargers in an experimental facility

Blanco, David[1*], Córdova, Yaisel[1], Berna, César[1], Muñoz-Cobo, José Luis[1] and Escrivá, Alberto[1]

[1]Universitat Politècnica de València - Institute for Energy Engineering, Spain

*Corresponding author: *dablade@upv.es*

I. INTRODUCTION

The discharge of jets in pools has been used in different industrial branches due to its wide applications. It is a phenomenon of great interest for nuclear power plants and other industries, being a process that offers high heat transfer and mass exchange capacity, without forgetting that it is one of the most efficient forms of steam condensation. This type of discharges often uses complex configurations such as spargers.

The characterization of these phenomena has been studied by means of the development of a large number of experiments, providing information of interest to this field. Since it is important to work towards a larger database, in order to increase the number of variables and parameters studied. This allows for more accurate correlations that can cover a wider range and more diverse scenarios. Usually, almost all studies focus on the behavior of isolated jets. Then, it would be very important to analyze the interference between jets, this weakness has been covered in the current study. In particular, within the nuclear field, it is necessary to study the behavior that takes place in a sparger, analyzing the influence that neighboring orifices can exert on the nature of the discharge.

Several types of light water reactors adopt the concept of steam discharge into a subcooled water pool as a safety system. In this case, steam is discharged from a reactor coolant system or from a compartment of a containment system, these discharges can be pure steam or mixtures of steam and non-condensable gases [1]. Examples where this phenomenon can be observed are the depressurization systems of today's nuclear power plants, specifically in the BWR suppression pool. In the first case, there is direct contact condensation which allows rapid condensation of the steam by providing a large interfacial area and high turbulence [2].

A facility has been developed to carry out different studies of discharges in a pool in which a wide variety of situations can be simulated, allowing the study of discharges of different gases, combining different pressures, temperatures, flow rates, among other variables of interest. Through the results obtained by processing the images captured with a high-speed camera, it is possible to characterize the discharge by means of different correlations. These correlations use the properties that define the experimental conditions, such as pressure, flow rate, etc., by means of dimensionless numbers such as Reynolds and Froude to predict the lengths that characterize the nature of the discharge [3] - [5].

The current study consists of air discharges in which two jets interfere in the vertical plane. Many authors [6] - [12] have developed correlations for the dimensionless penetration length based on the dimensionless numerical terms. Some authors have also contemplated the study of the interference produced by solid elements positioned in the discharge path, but the studies about the influence of flow currents produced by other jets are scarce. This study is carried out with the intention of assessing the most influential and determining variables of this particular type of discharge. In addition, it is intended to apply the knowledge gained in this research to starting point of future works, possibly focused on steam discharges.

II. EXPERIMENTAL FACILITY

The experimental facility has been designed to study air jet discharges into a pool of stagnant subcooled water. The discharge takes a place in a glass tank, which allows the observation of the phenomenon. Through a sparger, air is injected into the pool with the required conditions of each test. A schematic view of the facility can be seen in Figure 1.

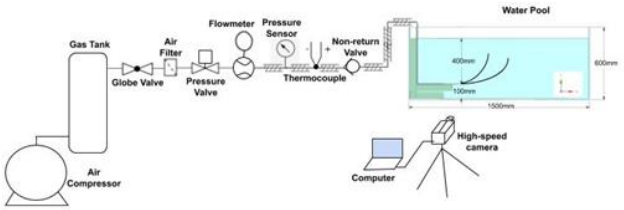

Figure 1. Experimental facility.

The air line is fed by a compressor with the capacity, in terms of flow rate and pressure, to perform the planned experiments. The air flow passes through several valves and an air reservoir, so that air flow is stabilized and adjusted to the conditions required in each experiment. This entire line

contains the necessary instrumentation to measure pressure, flow and temperature conditions.

The submerged injection is carried out by means of a sparger configuration provided with two orifices. A jet will be produced in each of them, so that there will be an interference that may modify the nature of their trajectory. The effect of varying the exit velocity, orifice size or pitch (distance between holes) between the two injections will be studied.

The pressure, temperature and flow sensors are connected to a data acquisition system controlled by Labview software. Post-processing of the results will characterize the conditions of each test.

For image capture, a LED illumination panel is located at the rear of the pool to provide the necessary light to the high-speed camera for the short exposure times of each photograph.

In order to create a discharge to study the interference between two jets, a simple element with two orifices has been configured. This study focuses in the analysis of two jet interactions in the vertical plane through the variation of the diameter and distance between orifices. The distance between orifices (pitch) are 20, 30 and 40 mm, while the orifice diameter are 2, 3 and 4 mm. Figure 2 shows the appearance of this element.

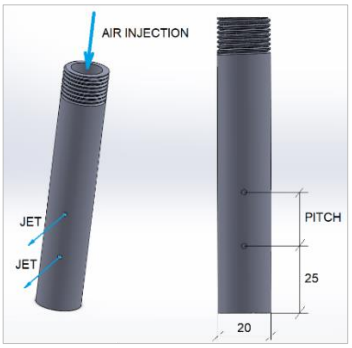

Figure 2. Spargers configuration (dimensions in mm).

III. IMAGE ANALYSIS

The penetration length and the interface between gas and liquid were measured with a direct visualization technique using a high-speed camera. Through a multi-step process programmed in MATLAB, the original grayscale image is binarized by determining a threshold value that can delimit the liquid zone and the gas zone. Then, a median filter is applied depending on the value of the neighborhood of each pixel to subsequently fill the gaps that may exist in the jet zone. Finally, an adjustment operation is applied to eliminate small bubbles in the binary image and a perimeter corresponding to the silhouette is established.

To obtain correlations and dimension the jet profile it is necessary to define regions and delimit the magnitudes to be worked with. It is also necessary to establish the parameters on which the calculations will be based according to the conditions of the experiments. In addition, it is important to non-dimensionalize and normalize data with the intention of obtaining equations that can be extrapolated to other experiments or installations.

The study focuses on the characterization of two lengths. First the jet region, in which the gas motion is governed by the momentum. Second, the rising plume region, in which the buoyancy forces dominates the jet behaviour. The momentum length (L_m) is defined by a horizontal line bounded between the nozzle, just where the jet starts, and the intersection point between this line and the gas-liquid boundary. On the other hand, the buoyancy length (L_b) is delimited from the point where the momentum length ends to the maximum distance where the jet arrives. This length is also a parameter included in the direction of the horizontal axis. Then, the variation of these two variables are evaluated for the different orifice diameters and pitch distances. Additionally, the point at which the two jets join (merge point) has been also characterized for the different experimental conditions. Figure 3 represents these parameters in a schematic way.

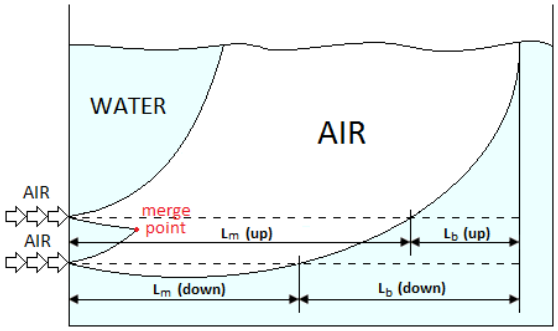

Figure 3. Characterization of the jet.

All the characterized lengths are calculated by measuring a sequence of continuous images and taking an arithmetic mean value. While the dispersion of all these experimental variables is characterized by their standard deviation (s).

IV. EXPERIMENTAL RESULTS

The range covered by the different variables analyzed in the current experiments is shown in Table 1. The flow rate ranges depend on the size of the sparger orifice, being narrower for those with smaller cross-section. The aim is to cover the widest possible velocity spectrum in order to appreciate the effect of pitch and to achieve a knowledge base for future experiments, in which it is intended to concentrate the study in a particular range or to focus the test on a particular event.

Table 1. Range of test performed.

Diameter [mm]	Pitch [mm]	Volumetric Flow Rate [l/min]
1,	20, 30, 40	100-200
2	20, 30, 40	150-500
3	20, 30, 40	200-450
4	20, 30, 40	200-500

The influence of the upper jet on the lower jet has a relevance that is directly dependent on the pitch. To illustrate this effect, Figure 4, Figure 5 and Figure 6 are included. All the points presented maintain the discharge

velocity at 530 m/s, however the behavior is different even for spargers with the same orifice size.

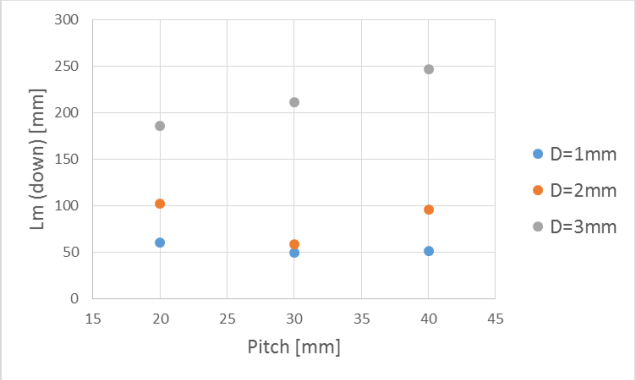

Figure 4. Pitch and orifice diameter influence on momentum length for discharges at 530m/s velocity.

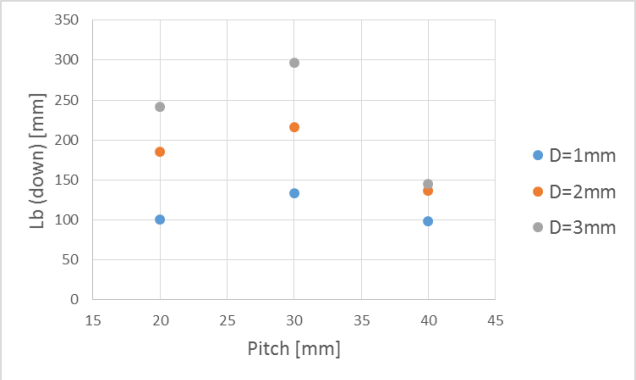

Figure 5. Pitch and orifice diameter influence on buoyancy length for discharges at 530m/s velocity.

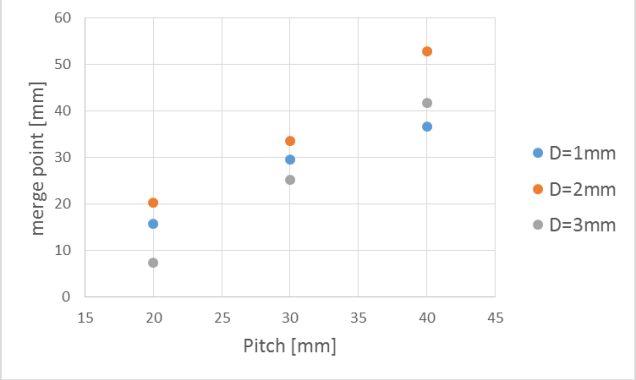

Figure 6. Pitch and orifice diameter influence on merge point position for discharges at 530m/s velocity.

It can be seen that there is a direct trend between some of the parameters shown and the pitch, but it can also be seen that there are situations in which it is necessary to consider more factors. For instance, the merge point and the buoyancy length have a quite clear direct trend with the pitch and orifice diameter. But, on the other hand, the momentum length has not that so clear tendency for the two smaller orifice diameters, while this tendency is so clear for the bigger orifice diameters

Another important aspect is to characterize the effect of the air flow rate and the pitch distance in the different analyzed lengths for an orifice diameter. In this case, the output velocities and the influence of pitch will determine the evolution of these lengths. Figure 7, Figure 8 and Figure 9 show some of the results obtained for the 2 mm hole spargers.

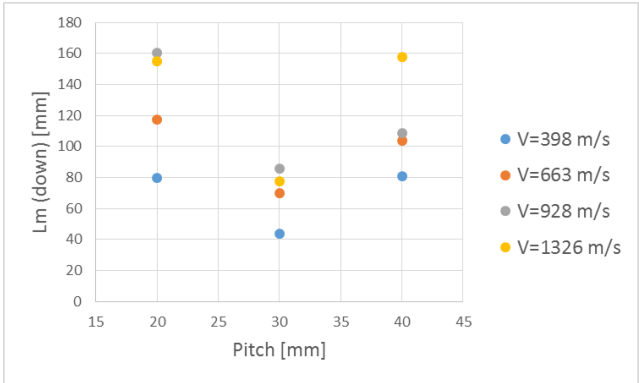

Figure 7. Pitch and velocity influence on momentum length for discharges at in sparger with 2mm orifice.

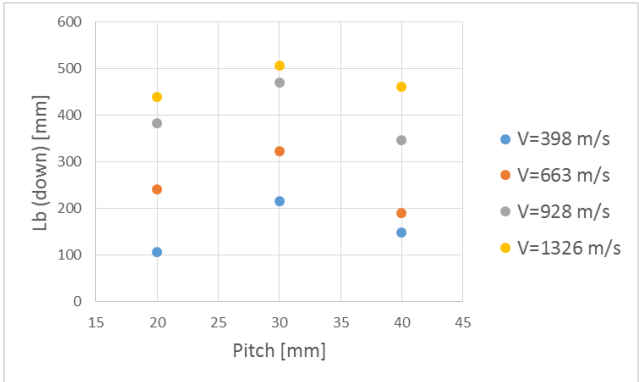

Figure 8. Pitch and velocity influence on buoyancy length for discharges at in sparger with 2mm orifice.

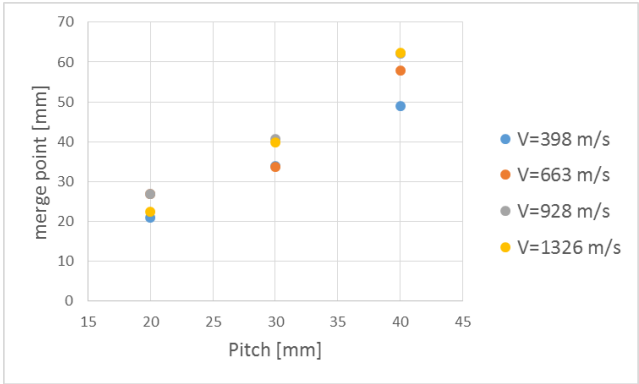

Figure 9. Pitch and velocity influence on merge point position for discharges at in sparger with 2mm orifice.

It can be seen that the influence of velocity has a direct relationship with the lengths presented. Apparently, an increase in gas exit velocity leads to an increase in momentum lengths, buoyancy length and merge point position. The pitch increase moves the position away from the merge point, but the momentum and buoyancy lengths go up and down, having an obvious but not proportional relationship.

Given the influence found, it is important the development of new tools that would allow the analytical calculation of these parameters. Seeing the dependence of the merge point on the mentioned parameters, a new correlation has been obtained, this expression estimates the merge point position in terms of the Froude number and a dimensionless length

parameter (ratio of the pitch distance and the sparger orifice size).

In order to have a dimensionless pitch value, an equivalent diameter will be defined, which would represent the diameter of the hole whose area is the total area of the sparger holes:

$$D_{eq} = 2 \cdot \sqrt{\frac{Area_{all\ orifices}}{\pi}}$$

To obtain this correlation, the Froude number is also calculated:

$$Fr = \frac{u}{\sqrt{\frac{\rho_a - \rho_g}{\rho_g} \cdot g \cdot D}}$$

Where u is the fluid velocity, ρ_a is the density of the water in the discharge tank, ρ_g is the density of the injected gas, g is the acceleration of gravity and D is the diameter of an orifice.

Finally, the correlation obtained is the following:

$$\frac{merge\ point}{D_{eq}} = 0.0614 \cdot \left({}^{Pitch}/_{D_{eq}}\right)^{1.4968} \cdot Fr^{0.2841}$$

With this equation, a correlation coefficient of 0.95 is obtained for the data measured in the presented experiment. The predictions obtained with the correlation with respect to the experimental measurements are presented in Figure 10.

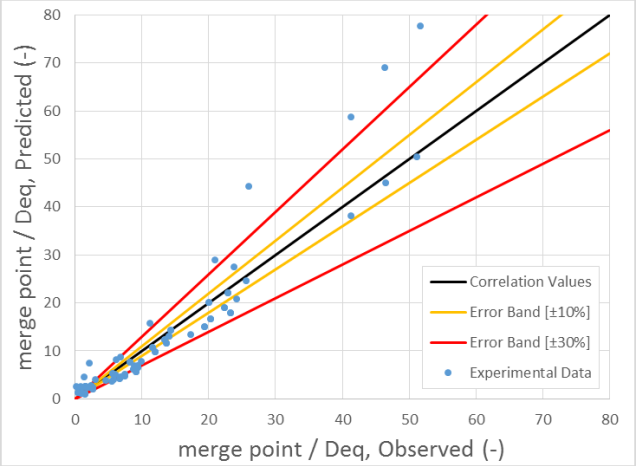

Figure 10. Merge point position prediction.

V. CONCLUSIONS

A study of air discharges in subcooled pools using spargers has been presented, analyzing the influence of several variables in the interaction between jets, in particular, orifice diameter, pitch distance and flow rate have been studied.

The influence of pitch has an important bearing on the characteristics of such a discharge. It determines, together with the fluid properties, the magnitudes of the characteristic lengths of the discharge, such as the momentum length, the buoyancy length and the position of the merge point.

In addition, a correlation has been obtained for the calculation of the position of the merge point that can be a useful tool to evaluate the conditions of a discharge.

This study is a support for future works focused on the characterization of complex jets, being able to advance in different directions and enabling more particular approaches.

VI. References

[1] D. E. Bessette, "Thermal-Hydraulic Evaluation of Pressurized Thermal Shock," NUREG, vol. 1809, p. 333, 2005.

[2] D. Heinze, T. Schulenberg, and L. Behnke, "A physically based, one-dimensional three-fluid model for direct contact condensation of steam jets in flowing water," Int. J. Heat Mass Transf., vol. 106, pp. 1041–1050, Mar. 2017, doi: 10.1016/j.ijheatmasstransfer.2016.10.076.

[3] P. J. Kerney, G. M. Faeth, and D. R. Olson, "Penetration characteristics of a submerged steam jet," AIChE J., vol. 18, no. 3, pp. 548–553, May 1972, doi: 10.1002/aic.690180314.

[4] H. Y. Kim, Y. Y. Bae, C. H. Song, J. K. Park, and S. M. Choi, "Experimental study on stable steam condensation in a quenching tank," Int. J. Energy Res., vol. 25, no. 3, pp. 239–252, Mar. 2001, doi: 10.1002/er.675.

[5] D. Chong, Q. Zhao, F. Yuan, W. Wang, W. Chen, and J. Yan, "Research on the steam jet length with different nozzle structures," Exp. Therm. Fluid Sci., vol. 64, pp. 134–141, 2015, doi: 10.1016/j.expthermflusci.2015.02.015.

[6] K. Harby, S. Chiva, and J. L. Muñoz-Cobo, "An experimental investigation on the characteristics of submerged horizontal gas jets in liquid ambient," Exp. Therm. Fluid Sci., vol. 53, pp. 26–39, Feb. 2014, doi: 10.1016/J.EXPTHERMFLUSCI.2013.10.009.

[7] K. Harby, S. Chiva, and J. L. Muñoz-Cobo, "Modelling and experimental investigation of horizontal buoyant gas jets injected into stagnant uniform ambient liquid," Int. J. Multiph. Flow, vol. 93, pp. 33–47, Jul. 2017, doi: 10.1016/j.ijmultiphaseflow.2017.03.008.

[8] S. Rassame, T. Hibiki, and M. Ishii, "Void penetration length from air injection through a downward large diameter submerged pipe in water pool," Ann. Nucl. Energy, vol. 94, pp. 832–840, 2015, doi: 10.1016/j.anucene.2016.04.046.

[9] B. U. N. Igwe, S. Ramachandran, and J. C. Fulton, "Jet penetration and liquid splash in submerged gas injection," Metall. Trans., vol. 4, no. 8, pp. 1887–1894, 1973, doi: 10.1007/BF02665417.

[10] E. O. Hoefele and J. K. Brimacombe, "Flow regimes in submerged gas injection," Metall. Trans. B, vol. 10, no. 4, pp. 631–648, 1979, doi: 10.1007/BF02662566.

[11] A. Emani and C. Briens, "Study of Downward Gas Jets into a Liquid," AlChe J., vol. 54, no. 9, pp. 2269–2280, 2008, doi: 10.1002/aic.

[12] J. L. Carreau, F. Roger, L. Loukarfi, L. Gbahoue, and P. Hobbes, "Penetration of a horizontal gas jet sumerged in a liquid," in Proceedings of the Intersociety Energy Conversion Engineering Conference, 1986, pp. 315–319.

Proceedings of the European Nuclear Young Generation Forum
ENYGF'21
September 27-30, 2021, Tarragona, Spain

Validation of Serpent-SUBCHANFLOW-TRANSURANUS pin-by-pin depletion for PWR and VVER reactors

García, Manuel[1*]

[1] Karlsruhe Institute of Technology (KIT), Institute of Neutron Physics and Reactor Technology (INR), Hermann-von-Helmholtz-Platz 1, 76344 Eggenstein-Leopoldshafen, Germany

*Corresponding author: manuel.garcia@kit.edu

I. INTRODUCTION

Driven by the growing interest in the nuclear industry in high-fidelity simulations for design and safety analysis, the EU Horizon 2020 McSAFE project was set to tackle the implementation of multiphysics tools based on the continuous-energy Monte Carlo particle transport method. During the development phase of McSAFE, a coupling scheme for Serpent 2, SUBCHANFLOW (SCF) and TRANSURANUS (TU) has been implemented [1]. The objective of this three-code system is the simulation of large-scale pin-by-pin depletion problems with a fully coupled burnup methodology. Furthermore, to manage the massive memory demand involved in pin-level depletion, a Collision-based Domain Decomposition (CDD) scheme has been implemented in Serpent 2 [2].

The objective of this work is to summarize the validation of Serpent-SCF-TU with CDD using experimental data from two nuclear power plants: a German Pre-Konvoi PWR [3] and the Temelín II VVER-1000 reactor [4]. The numerical results for two burnup calculations are compared against pin-level neutron flux data from Self Powered Neutron Detector (SPND) and aeroball readings, as well as critical boron concentration measurements.

II. SERPENT-SCF-TU DEPLETION

Figure 1 shows the calculation and feedback scheme used for Serpent-SCF-TU coupled depletion for a step from time t_n to t_{n+1} [1]. A semi-implicit algorithm is used, i.e. code-to-code feedback is done using the fields at the end of the step (EOS) and convergence at EOS is achieved iterating each burnup step. This improves the stability of the coupled solution relative to an explicit method and provides a converged state across physics for each burnup step.

For each iteration, a SCF steady-state calculation is performed first to obtain the cooling conditions for the Serpent power distribution at EOS. Second, TU solves a burnup step from t_n to t_{n+1} using the SCF solution as boundary condition and the Serpent power as heat source, both at EOS. For the first iteration in each burnup step, when the Serpent solution at EOS has not yet been calculated, the power at the beginning of the step (BOS) is used in SCF and TU. Third, Serpent carries out a burnup iteration using the Stochastic Implicit Euler (SIE) method, with the thermalhydraulic conditions at EOS. The rationale for this code order is that (a) SCF calculates the boundary conditions for TU and receives no feedback from it and (b) the Serpent calculation is the most expensive step, and therefore should be performed with the latest thermalhydraulic data. It is important to note here that Serpent and TU perform independent burnup calculations, Serpent with the full set of Bateman equations and TU with a reduced one suitable for fuel-performance analysis.

As an alternative to this three-code coupling, the traditional neutronic-thermalhydraulic scheme can be used without TU. In this case, the fuel calculation is handled by SCF, which includes a simplified fuel-performance model based on fuel-cladding-gap evolution and irradiation-driven thermal-conductivity degradation.

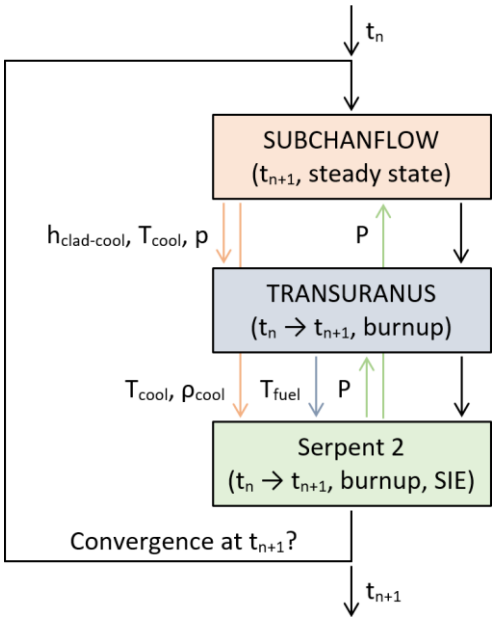

Figure 1. Depletion scheme [1].

Full-core pin-by-pin depletion problems in Serpent 2 can take several TB of RAM memory, mainly in order to store the compositions, reaction rates and additional data for burnable materials. This exceeds the memory available in each single node for any High Performance Computing (HPC) architecture. To solve this issue, a domain decomposition scheme has been implemented in Serpent 2 [2]. The idea of the method is to define domains containing only a subset of the burnable materials, while all other model data, such as geometry, non-burnable materials and spatial tallies, is replicated in all domains. Figure 2 shows the material decomposition for an xy-slice of the VVER problem considered in this work [4]. The tracking algorithm is modified to account for neutrons flying across domains when they have collisions in non-local materials, but the method does not rely in any numerical or physical approximations and hence the results are equivalent to the traditional Monte Carlo approach, within their statistical uncertainty.

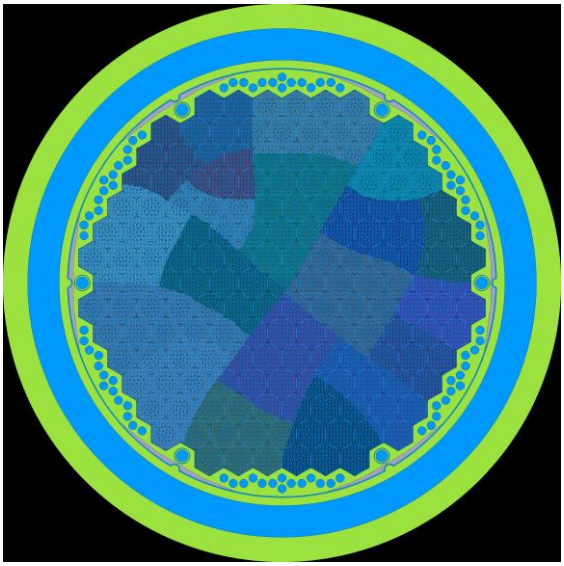

Figure 2. Material division for CDD [4].

III. SELECTED RESULTS

This section presents selected results for the validation calculations using experimental data from a German Pre-Konvoi PWR [3] and the Temelín II VVER-1000 reactor [4]. The simulations correspond to full-core pin-by-pin depletion using Serpent-SCF with and without TU for the fuel thermomechanics calculation. Using the CDD feature developed for Serpent, the massive memory footprint of the problem is distributed across 64 computing nodes with 20 cores each, where the simulations take about 7 days.

A. Pre-Konvoi PWR power plant

The calculated and measured critical boron concentration for the PWR case is shown in Figure 3. The results correspond to the beginning of the first operating cycle of the reactor. The Root Mean Square (RMS) difference between the results and the experimental data is 3.5 and 4.8 ppm for Serpent-SCF and Serpent-SCF-TU respectively. The deviations with the measurements are well below the acceptability criterion for this type of calculation, which is usually between 50 and 100 ppm, and within the typical uncertainties due to specifications and nuclear data. The differences between results with and without TU, which are lower than 4 ppm for the whole range, are not significant.

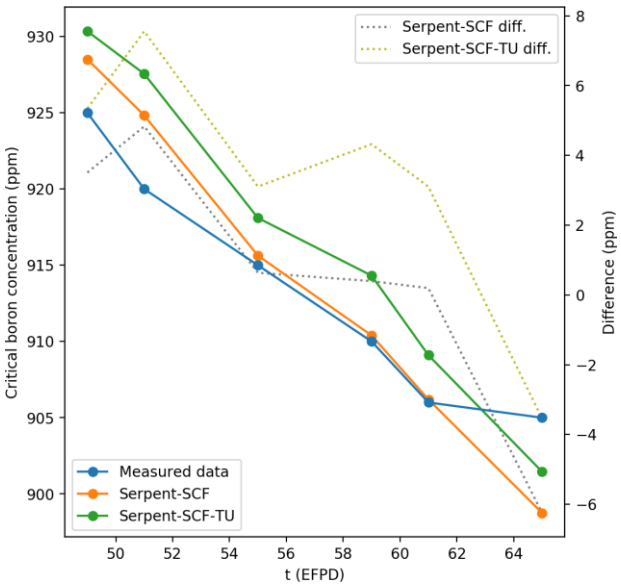

Figure 3. Critical boron for the PWR case [3].

Figure 4 shows the neutron flux for one of the 28 locations with aeroball detectors. The aeroballs are inserted in the instrumentation tubes and consist of a stack of 32 aeroballs at equidistant positions. The error bars correspond to three standard deviations σ for each axial location, and the relative differences are taken between the calculated and measured neutron fluxes normalized with the average value for each aeroball. The experimental data falls within the statistical range of the results, and no significant differences are observed between the calculations with and without TU. Larger RMS deviations can be observed in fuel assemblies in the core periphery where the statistical uncertainty is larger due to a lower number of particles. This behaviour can always be improved increasing the amount of histories, at the expense of a higher computing cost.

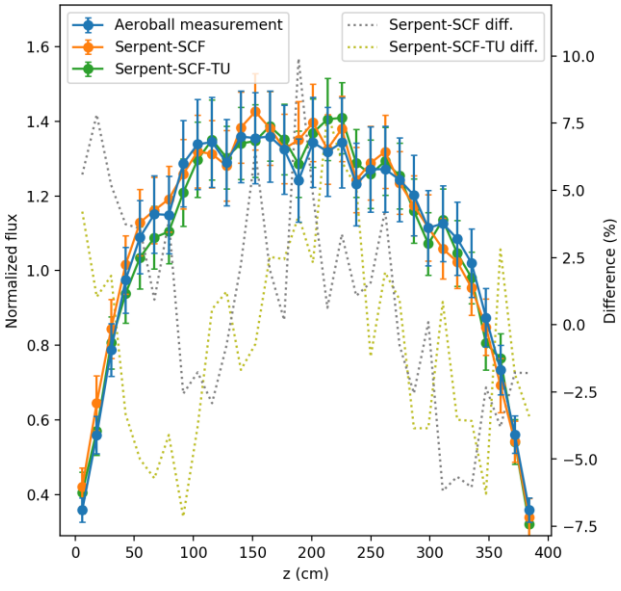

Figure 4. Neutron flux (aeroball) for the PWR case [3].

B. Temelín II VVER-1000 power plant

The calculated and measured critical boron concentration is shown in Figure 5. The results correspond to the ninth operating cycle of the reactor, which starts from a fresh core with TVSA fuel. The RMS difference between the results and the experimental data is 33.8 and 31.5 ppm for Serpent-SCF and Serpent-SCF-TU respectively. In this case the deviations with the measurements are around the acceptability criterion and the differences between results with and without TU are not significant.

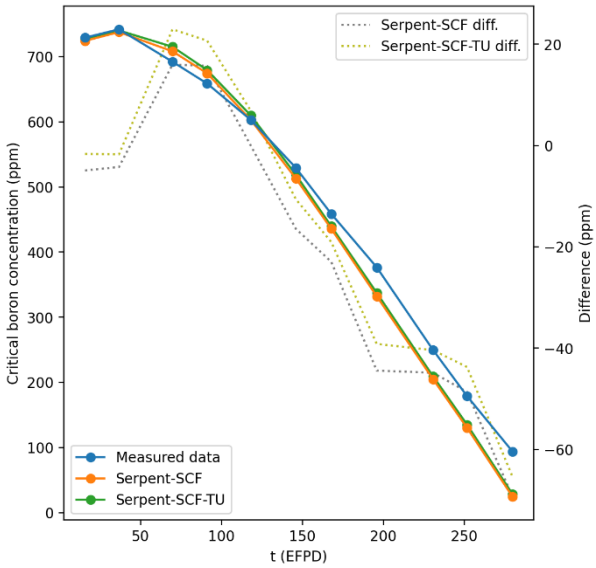

Figure 5. Critical boron for the VVER case [4].

Figures 6 and 7 show the neutron flux for one of the 64 locations with SPNDs at Beginning of Cycle (BOC) and End of Cycle (EOC), respectively. The SPNDs are inserted in the central instrumentation tubes and consist of a string of 7 SPNDs separated by about 50 cm, with the lowest position approximately 30 cm above the bottom of the fuel stack. A good agreement between the results and the measurements is found here as well.

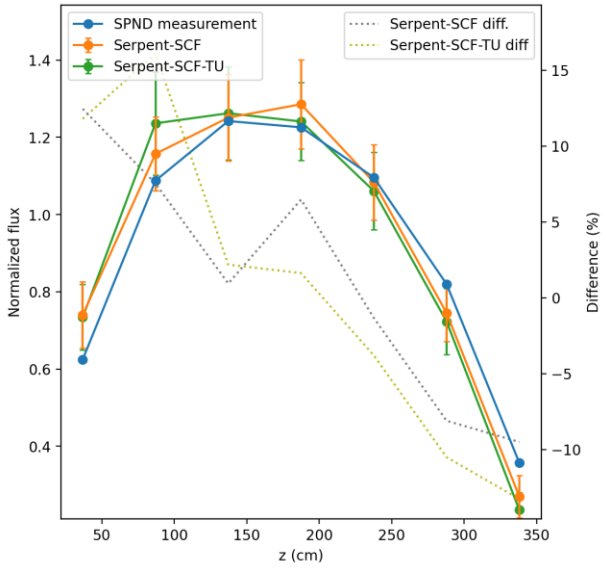

Figure 6. Neutron flux (SPND) for the VVER case (BOC) [4].

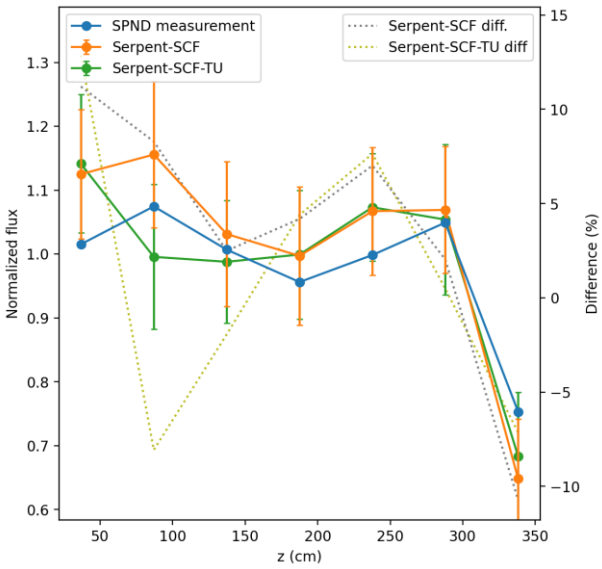

Figure 7. Neutron flux (SPND) for the VVER case (EOC) [4].

C. Pin-level results

As shown in the previous sections, the impact of including fuel-performance capabilities in the calculation system does not influence the neutronic results in a significant way, at least not for the burnup calculations considered here. This is in line with previous investigations dealing with smaller-scale problems [1]. However, the main advantage of the three-code approach used in this work is the ability to model the neutronic, thermalhydraulic and thermomechanic behaviour of the core with a fully coupled high-fidelity scheme. In particular, the fuel-performance calculation is done within the burnup simulation, obtaining a fuel solution with full detail for consistent core states. Figures 8 and 9 show pin-level power and fuel-cladding gap size results.

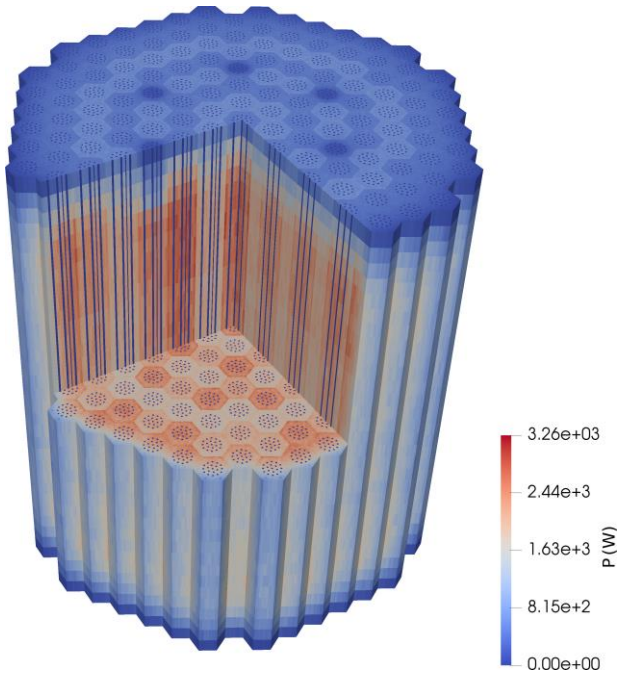

Figure 8. Power distribution for the VVER case [4].

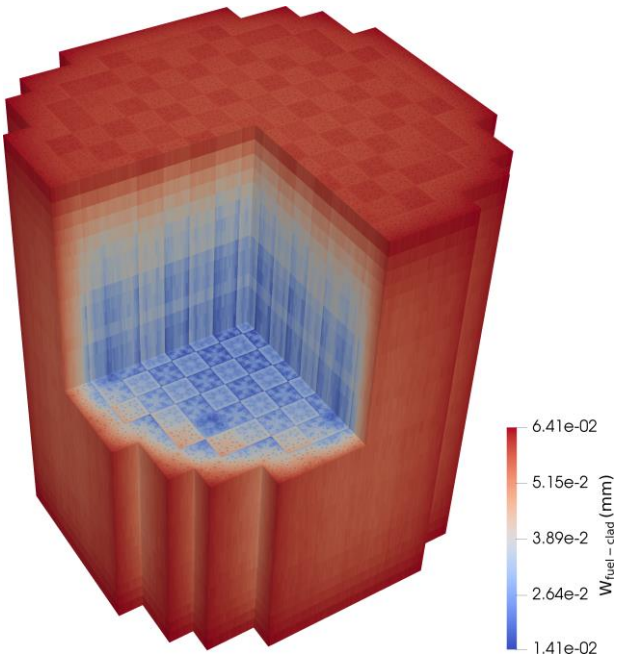

Figure 9. Fuel-cladding gap size for the PWR case [3].

IV. SUMMARY AND ADDITIONAL REMARKS

Overall, the results obtained with Serpent-SCF with and without TU are in quite good agreement with the experimental data for the two reactors considered. The deviations between the calculated and measured critical boron concentrations are within the typical acceptability criterion for criticality calculations. The pin-level neutron flux profiles obtained with Serpent are consistent with the aeroball and SPND measurements within their statistical uncertainty in most cases. These results demonstrate the accuracy of the simulation tool, both in terms of global behaviour and of local pin-level parameters.

A. Neutronic feedback to TU

While the coupling scheme used in this work captures the main interaction mechanisms in the system, the neutronic feedback to TU could in principle be refined. On the one hand, radial power profiles could be tallied by Serpent and used directly in the thermomechanic simulation instead of calculating them in TU from the total pin power. However, doing this would dramatically increase the number of particles needed to obtain statistically meaningful values for the radial power profiles for each rod and axial level, which is not feasible in full-core pin-by-pin calculations. On the other hand, the burnup calculation could be performed only in Serpent and the isotope concentrations transferred to TU. The drawback of this approach is that it involves massive amounts of feedback data, considering the radial dependence of material compositions. Moreover, the multiphysics interface in Serpent, which is extremely convenient to exchange power, density and temperature distributions, is not suitable for obtaining material data. For this reasons, the internal TU neutronic model is used in the current implementation, although this issue merits further investigation.

B. Impact of including fuel-performance analysis

The results presented in this work show that using a fuel-performance code to improve the fuel modelling does not seem to have a significant impact on the neutronic solution during burnup, for which a standard subchannel code like SCF is quite adequate. This might not be true for transient calculations where fuel parameters such as gap width and conductance play a major role.

C. High-fidelity calculation method

The calculation system used in this work provides significant capabilities for high-fidelity core analysis. On the one hand, the ability to handle full-core pin-by-pin burnup problems in Serpent, which is enabled by the newly implemented CDD scheme, is a key feature. In this way, depletion calculations can be performed directly using continuous-energy nuclear data and an extremely detailed geometrical representation, which provides a high-fidelity alternative to the traditional multistep approach based on lattice- and core-level computations. On the other hand, the three-code coupling combining Monte Carlo neutron transport, subchannel thermalhydraulics and fuel-performance analysis provides a very valuable framework to perform a thorough analysis of the core for realistic conditions. Even if the impact of the thermomechanic solution on the neutronics is not significant, a complete fuel-performance analysis of the core is carried out as part of the burnup calculation. As a result, most parameters of interest for both design and safety analysis can be obtained directly from a single simulation.

V. References

[1] M. García, R. Tuominen, A. Gommlich, et al. “A Serpent2-SUBCHANFLOW-TRANSURANUS coupling for pin-by-pin depletion calculations in Light Water Reactors”. Annals of Nuclear Energy 139 (2020). doi: 10.1016/j.anucene.2019.107213.

[2] M. García, J. Leppänen, and V. Sanchez-Espinoza. “A Collision-based Domain Decomposition scheme for large-scale depletion with the Serpent 2 Monte Carlo code”. Annals of Nuclear Energy 152 (2021). doi: 10.1016/j.anucene.2020.108026.

[3] M. García, Y. Bilodid, J. Basualdo Perello, et al. “Validation of Serpent-SUBCHANFLOW-TRANSURANUS pin-by-pin burnup calculations using experimental data from a Pre-Konvoi PWR reactor”. Nuclear Engineering and Design 379 (2021). doi: 10.1016/j.nucengdes.2021.111173.

[4] M. García, R. Vočka, R. Tuominen, et al. “Validation of Serpent-SUBCHANFLOW-TRANSURANUS pin-by-pin burnup calculations using experimental data from the Temelín II VVER-1000 reactor”. Nuclear Engineering and Technology (2021), in press. doi: 10.1016/j.net.2021.04.023.

Proceedings of the European Nuclear Young Generation Forum
ENYGF'21
September 27-30, 2021, Tarragona, Spain

Preventive methodology: geometric simplifications a priori for containment models optimization with the GOTHIC code

Arfinengo-del-Carpio, Sofía[1*], Vázquez-Rodríguez, Carlos[1] and Jiménez, Gonzalo[1]

[1] Universidad Politécnica de Madrid, Avda. de Ramiro de Maeztu, 7, 28040 Madrid, Spain

*Corresponding author: *s.arfinengo@alumnos.upm.es*

I. INTRODUCTION

Computational codes have been an essential tool for fulfilling the nuclear power plants design and regulatory needs since the first nuclear reactors were designed [1]. The large and complex geometry of the containment building, along with a wide spectrum of phenomena, creates a demanding scenario for thermal-hydraulics numerical analysis, which were traditionally accomplished through the Lumped Parameters (LP) approximation.

The LP codes have proved to accurately represent average pressure and temperature values, but their inherent approximations incur in the impossibility of simulating certain phenomena precisely, such as hydrogen distribution in a severe accident scenario [2].

However, containment codes such as GOTHIC have undergone significant progress in their capacity to simulate three-dimensional geometries in the last years [2]. Besides providing new information related to the containment thermal hydraulics, three-dimensional models overcome the aforementioned issues related to the LP approach.

Nevertheless, whereas 3D models entail many benefits regarding containment analysis, they also imply a worth-mentioning drawback: they require a high level of geometric detail. To cope with this issue, the Universidad Politécnica de Madrid (UPM) has developed a series of modelling methodologies using the GOTHIC computational code, based on the creation of a detailed 3D CAD model [3]–[5]. In these processes, the CAD environment becomes the main workspace, both for model development and diverse result postprocessing phases.

The main objective of the previous methodologies was to comply with the GOTHIC geometry modelling and domain discretization particularities. In detail, GOTHIC is a thermal hydraulic code with 3D capabilities, which uses a Cartesian mesh and formulates the conservation equations using the porous media approach. By using this approach, the geometry is constructed by defining simple solid shapes (wedges, cylinders, caps, etc.) in the fluid domain. The solid shapes, also known as blockages, partially or completely occupy the cell volume and cell faces, meaning that the liquid and solid phases are allowed to coexist inside the same cell, unlike commercial CFD codes.

Whereas in [3] the aim was to represent the containment geometry with the highest level of accuracy allowed by the code, in [4], [5] a few geometric simplifications were adopted to reduce the number of cells needed to model the geometry of the containment properly. Hence, the models developed in [4], [5] have provided new model optimization possibilities since the small modifications of the geometry do not have a strong impact on the thermal-hydraulic results. However, these models still allow some problematic configurations of the geometry to appear, which will be assessed afterwards as it causes an important increase of the computational costs [6].

With the aim of solving this issue, a new model creation methodology has been developed, where the geometric simplifications not only consider the GOTHIC modelling particularities, but also intend to prevent the problematic cells to appear by means of slightly modifying the original containment geometry. The porous media approach allows these minor modifications, as they do not significantly affect the model thermal hydraulics.

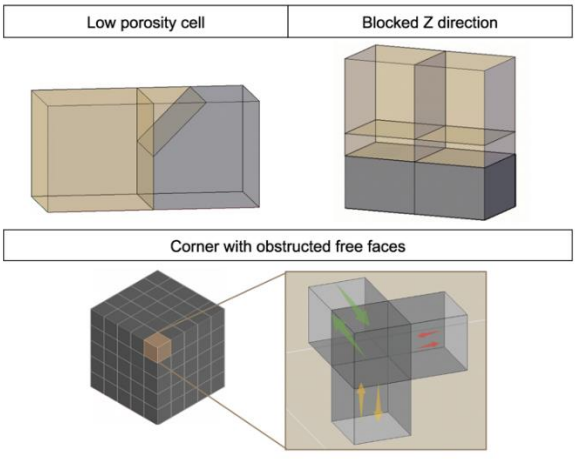

Figure 1. Problematic cells configurations.

II. METHODOLOGY

Before developing the methodology, the different geometric configurations that would lead to problematic cells were recognized and classified. For this purpose, a long identification process was performed, using a model of an isolated steam generator (SG) compartment to have a reduced study domain. This compartment was extracted from a multizone model, developed previously [3]. The 3D control volume of the compartment was connected to a LP control volume, representing the free volume of all other spaces of the containment, and the simulated transient was a double-ended guillotine break LOCA (Loss Of Coolant Accident).

As a result of this process, three main types of problematic cells were identified: low porosity cells, partial blockages in the Z direction, and corners whose free faces are partially or totally obstructed. Examples of these three configurations are depicted in Figure 1.

The first two types of problematic cells become an issue due to the fact that connecting a cell with a large free volume to a cell having a significantly smaller free volume (i. e., low porosity) causes numerical instabilities.

Regarding the third type of problematic cells, the "corners" of the domain have at least three of its six cell faces completely blocked. Any additional solids hindering the possible paths for mass transport in the corners, tend to "accumulate" the fluid and to cause convergence issues, eventually provoking an interruption of the simulation.

This identification process was a common task for models previously published [3]–[5]. However, it had been done to solve the numerical problems which the models usually showed when simulating transients with abrupt mass and energy releases, not as a comprehensive process to avoid the appearance of these problematic cells.

This process, which has been called "corrective methodology", was applied to the SG compartment model, achieving an 80% reduction of the computational time. To identify the problematic configurations took tens of iterations and was a time-consuming manual process.

To overcome this issue, a "preventive methodology" is developed. This methodology is aimed to define a generic model construction process using the GOTHIC code, where the appearance of the problematic cells is avoided from the definition of the model geometry. This methodology allows to obtain more efficient models without the long iterative process of the "corrective methodology".

The lessons learned in [3]–[5], as it was aforementioned, imply that the model geometry can be slightly modified, as far as the free volume of each compartment and of the containment is maintained. The geometric simplifications are enabled by using the built-in 1D correlations which GOTHIC uses to calculate wall friction and wall heat transfer. The boundary layer is modelled instead of being resolved in GOTHIC, and thus the adaptation of curved surfaces to the Cartesian mesh does not introduce relevant changes to the calculated velocity field.

The basis of the methodology consists of adapting the geometry to the GOTHIC Cartesian mesh. This can be achieved by slightly displacing the compartments walls to fit within the mesh, considering that the free volume modifications must be compensated afterwards. In addition, the equipment, such as SGs, pumps or pipes, should be represented using cuboids, as it is the best fit for the Cartesian mesh.

Having defined those guidelines, the methodology is applied to the same 3D SG compartment model in which the "corrective" methodology was applied. The first step is to define the Cartesian mesh, accounting that the compartment will later be connected to a three-dimensional control volume representing the containment, which will replace the current LP control volume. The mesh size is selected as the largest thickness able to correctly separate all de containment hydraulic independent zones. After setting that value, it is divided by four in order to use a fine mesh inside the compartment.

Once the mesh is defined, the compartment walls are adapted to the mesh (Figure 2) and the equipment is represented with cuboids (Figure 3), considering that the compartment free volume has to be maintained. That adaptation process is carried out by using the 3D CAD environment, as it is an easier way of proceeding, rather than doing that directly with the GOTHIC pre-processor.

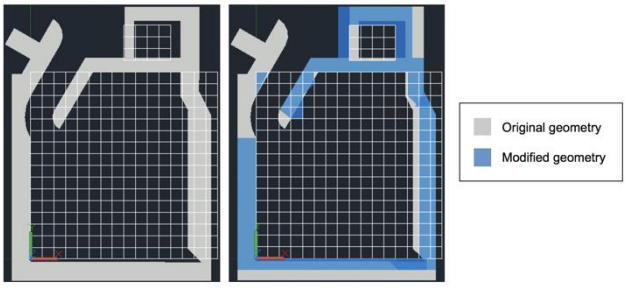

Figure 2. Adaptation of the compartment geometry to the Cartesian mesh.

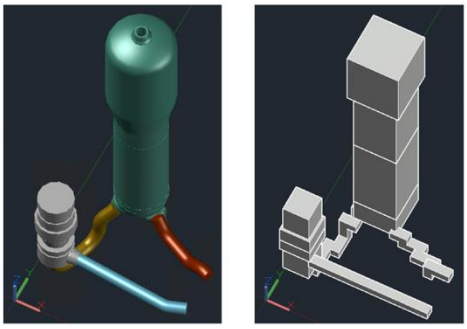

Figure 3. Equipment construction using the GOTHIC "block" geometric shape.

Once the modified geometry is defined, it is represented using the GOTHIC "wedge" blockages, as it is the one that most easily adapts to each geometric configuration.

The thermal conductors, which GOTHIC uses to model the solid-to-fluid heat transfer, are represented in the 3D CAD model to measure their specific location within the 3D compartment and heat transfer surface. Finally, the coordinates of both the wedges and the thermal conductors are extracted and stored in an Excel file, ready to be input in the GOTHIC model, and allowing to trace the source of all data employed for the model development.

III. RESULTS

A. Computational time optimization

By applying the preventive methodology, a very significative reduction of the computational time is achieved. Table 1 gathers the computational times for three different cases. The displayed times correspond to a 100 seconds transient, simulated on a 3.20 GHz core.

The first case is a model where no methodology is applied. The second one consists of an intermediate step before reaching the final model. It has the modified geometry implemented, according to the preventive methodology guidelines, but the equipment and the thermal conductors are not modelled yet, with the aim of having a simpler model to identify eventual geometric issues. The third case has the benefits of the preventive methodology, where both the equipment and the thermal conductors are implemented.

Therefore, by applying the preventive methodology, a 90% reduction of the computational time is directly obtained, because the appearance of the problematic cells is avoided through the definition of the model geometry.

Table 1. Comparison of different computational times.

Case	Computational time
Case without any methodology applied.	78 hours.
Case applying the preventive methodology, without adding the equipment.	10 hours.
Final case (applying the preventive methodology, adding equipment).	8 hours.

B. Full 3D vs 3D - LP models

As it was aforementioned, the SG compartment control volume, which was initially connected to a LP containment, is now connected to a three-dimensional control volume representing the containment to assess the differences between both approaches. The 3D model of the containment comes from [3] and it is included in the model without applying the preventive methodology on it.

The mesh size used for the SG compartment control volume is 0.625 meters in X, Y and Z, whereas for the containment the cell size is 2.5 meters. As both values are submultiples, the control volumes can be connected by using 3D connectors, a component of GOTHIC which allows to connect several cells of different control volumes straightforwardly. The Diffusion Layer Model with Film roughening and Mist formation (DLM-FM) model is used for wall condensation and the Drop Breakup Model (DBM) is selected for the liquid flashing. Both are best estimate semiempirical models [6]. The flux variables are calculated upstream with a space-differencing scheme of first order. Regarding specific parameters of the 3D model, the turbulence model used is the k-ε standard, which is a semiempirical model based on the modelling of two transport equations for turbulent kinetic energy, k, and its dissipation rate, ε [7]. The molecular diffusion is enabled.

To provide an overview of both models phenomenology, their containment pressures are displayed in Figure 4. As it can be seen, both pressure values are very similar, with a 2.4% relative difference. There is no pressure decrease since most of the concrete walls of the containment control volume are not included in the model.

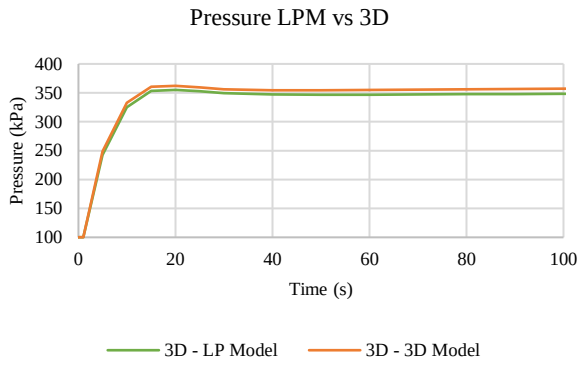

Figure 4. Containment pressure for both models.

The other aspect of the models that is studied is the gases (steam + air) flow rate through all hydraulic connections, which are represented in Figure 5.

There are four connections between the SG compartment and the containment control volume: an upper one and three sideways ones. Additionally, there is a connection between the compartment and an adjacent vertical corridor, which has been called “chimney” because the fluid moves through it, and another connection between that corridor and the containment.

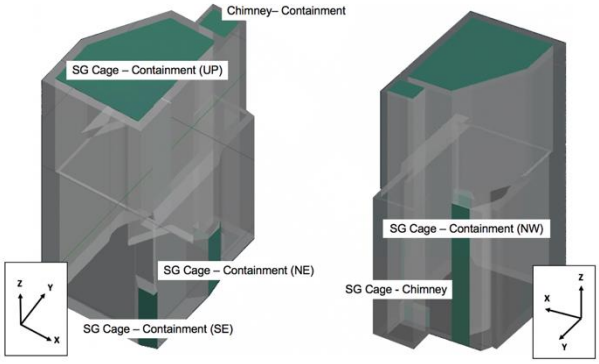

Figure 5. Hydraulic connections scheme.

Analysing the gas flow rate transported through the different hydraulic connections, it is found that both behaviours are very different. To give a simple evidence of the differences, the sum of the flow rates for the different connections is shown in Figure 6.

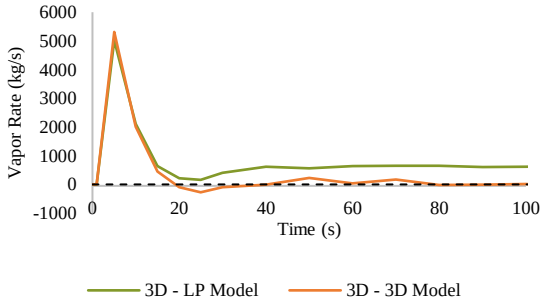

Figure 6. Total vapor rate through the hydraulic connections.

In order to understand the reason for these differences, the vapor rate through each cell of the top compartment-containment hydraulic connection is studied, as represented in Figure 7. As the figure shows, in the case where the containment is modelled using three-dimensional control volume, the vapor enters the compartment for the majority of the cells. On the contrary, for the model where the containment is represented by a LP volume, the vapor phase leaves the compartment to reach the containment volume for all cells.

The first of these behaviors could be caused due to the steam jet that leaves the compartment following the break might hit the containment dome and recirculate to enter the compartment again. These flow patterns cannot be simulated through a LP volume, and this is the reason why the second model would be showing a different behavior.

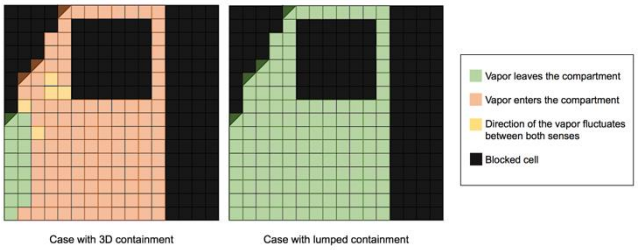

Figure 7. Top compartment-containment hydraulic connection.

To verify the hypothesis, the velocity fields at the dome predicted by the three-dimensional model are represented using the ParaView software, Figure 8. As it is shown in the figure, for the first five seconds after the break, the steam jet leaves the compartment, but for the rest of the transient, the vapor recirculation in the dome leads the flow back to the containment.

Therefore, it has been demonstrated that the case where the rest of the containment (excluding the SG compartment) is modeled as a LP model is not able to accurately represent the model thermal hydraulics. Hence, it is recommended to connect the compartment to a three-dimensional control volume if the detailed analysis of the containment phenomenology is the objective of the study.

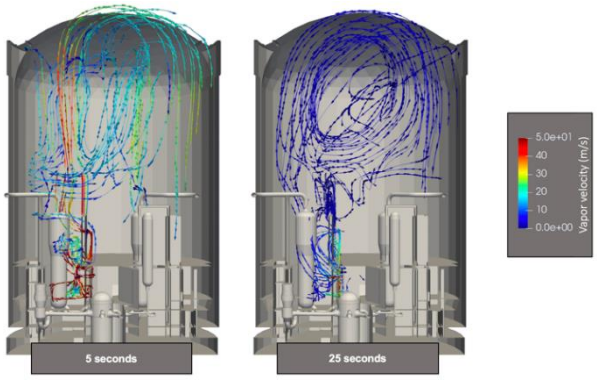

Figure 8. Vapor flow patterns inside the 3D containment for t = 5 s and t = 25 s.

IV. CONCLUSION

The preventive methodology has proved to be an efficient way of optimizing the computational cost of 3D containment models without compromising the geometrical detail. The reduction of computational effort demonstrated for the presented application of the methodology for a 3D SG compartment has been more than 90%.

In addition, it was found that the way of discretizing the model control volumes (3D vs LP) significantly affects the containment gases distribution and, therefore, the compartment phenomenology, which could have an important impact on the severe accident analysis. This issue needs to be deeply studied for future analysis, as this result suggests that to perform a detailed analysis of a specific compartment requires a 3D model as a boundary condition.

The presented preventive methodology is going to be the starting point for the development of new more efficient containment models, and for an exhaustive optimization of the balance between resolution and computational cost in 3D containment analysis. Furthermore, the promising results regarding computational time optimization have led the UPM to apply the preventive methodology to the project AMHYCO 3D containment models development using the GOTHIC code, as mentioned in [8], which is also presented in this conference.

V. REFERENCES

[1] E. Merzari, '40th Anniversary of the first international topical meeting on nuclear reactor thermal-hydraulics: Highlights of thermal-hydraulics research in the past four decades', *Nuclear Engineering and Design*, p. 16, 2021.

[2] OECD/NEA, 'Status Report on Hydrogen Management and Related Computer Codes', p. 211, 2014.

[3] R. Bocanegra, G. Jimenez, and M. K. Fernández-Cosials, 'Development of a PWR-W GOTHIC 3D model for containment accident analysis', *Annals of Nuclear Energy*, vol. 87, pp. 547–560, Jan. 2016, doi: 10.1016/j.anucene.2015.10.022.

[4] K. Fernández-Cosials *et al.*, '3D containment modeling of PWR-KWU Trillo NPP with the GOTHIC code', *Annals of Nuclear Energy*, vol. 133, pp. 387–399, Nov. 2019, doi: 10.1016/j.anucene.2019.05.041.

[5] C. Vázquez-Rodríguez *et al.*, 'Toward Conservatism in Containment Design Basis Accident Analyses. Lumped parameters and 3D Approaches.', *ICAPP'19 : 2009 International Congress on Advances in Nuclear Power Plants*, 2019.

[6] EPRI, 'GOTHIC Thermal Hydraulic Analysis Package, Version 8.2(QA). EPRI Palo Alto, CA.' 2016.

[7] J. M. Fernández Oro, *Técnicas numéricas en ingeniería de fluidos: Introducción a la dinámica de fluidos computacional (CFD) por el método de volúmenes finitos*. Editorial Reverté, 2011.

[8] Development of a detailed 3D CAD model of a generic PWR-KWU containment as a basis for a better assessment of H2/CO combustion risk. Serra, Luis; Domínguez-Bugarín, Araceli; Estévez-Albuja, Samanta; Vázquez-Rodríguez, Carlos; Jiménez, Gonzalo; Kelm, Stephan and Herranz, Luis E

Proceedings of the European Nuclear Young Generation Forum
ENYGF'21
September 27-30, 2021, Tarragona, Spain

SIMMER-V validation against thermohydraulic instabilities in GENESIS facility

Kędzierska, Barbara[1*], Gubernatis, Pierre[1] and Medale, Marc[2]

[1] CEA, DES, IRESNE, DTN, SMTA, Severe Accident Modeling Laboratory, France

[2] Aix-Marseille University, CNRS, IUSTI, France

*Corresponding author: *barbara.kedzierska@cea.fr*

I. INTRODUCTION

Sodium-cooled fast reactor (SFR) has been chosen as one of the six designs to be developed in the framework of the Generation IV nuclear reactors forum [1]. Although application of sodium as a coolant is not a novelty in nuclear technology and it has been practiced since 40s, the 21st century brought its renaissance by the fast reactor technology development.

The SFR technology allows achieving higher temperatures than in light water reactors, without pressurizing the system. High power densities due to the excellent thermal conductivity, intrinsic safety and breeding possibility are the main advantages, while the design is challenged by a risk of positive reactivity coefficient. Thus, the safety assessment needs to be conducted even with more attention than in light water reactors.

In all the reactor types, the safety assessment contains numerical analyses of postulated accidents. One of the most studied severe accident in SFR is an unprotected loss-of-flow accident (ULOF), typically with boiling initialization when the power drops to 1/4 to 1/3 of its nominal value [2]. It is known that it is possible to stabilize the sodium boiling during ULOF [2], even though only few analytical criteria have been found. Experimental and numerical studies have shown that during the loss of flow, the feedback loops in SFR allow to gain a grace period to shut down the reactor [3].

Relying on natural circulation, at least a small coolant flow is ensured during the accident sequence. The lack of a pump which forces the flow, results in changes in mass flow rate. The natural circulation drives the liquid coolant upward the core. The liquid, normally slightly subcooled at the core inlet, is heated and reaches the saturation temperature. It causes small bubbles formation, which in sodium grow very rapidly, due to the large heat conductance and the surface tension twice as big as in water. A large slug causes a decrease in the core pressure drop, which in turn chokes the flow.

The problem of stability is addressed for all types of the nuclear reactors. It has been studied since the 1970s, when the first instability events occurred in existing facilities. The first widely known instability event happened in Italy in Caorso plant in 1982 [4], [5], followed by a one Spanish and several Finnish incidents at TVO General Electric power plants [6]. One of the most famous incidents related to this phenomenon happened in LaSalle reactor in 1988 [7] and was an impulse to start a NRC program investigating the BWR stability issues, although similar events had happened in Europe before.

II. GENESIS EXPERIMENT SIMULATION

The GENESIS facility is a prototypic Economic Simplified Boiling Water Reactor (ESBWR) which has been constructed at the Delft University of Technology [8]. Next to other Delft experimental loops, like DESIRE, CIRCUS [9] and DeLight [10], GENESIS was designed to study the safety aspects of the natural circulation loops. It has been constructed in collaboration with General Electric and the experiments have been run between 2004 and 2006.

Designing of a prototype facility has been performed based on dimensionless analysis, with a starting point at the density number equality. It allowed to decrease the ESBWR pressure by a factor 0.16. The next step comprised geometric scaling: radial and afterwards, axial. The Eotvos (Bond) number equality resulted in a radial scaling factor 0.46, which due to the geometry number constraint, must be the same for the axial scaling. The whole procedure is described by Marcel [11].

A. Context of instabilities

The experiment aims at verifying a range of operational conditions to predict the stability boundary in terms of Type-I [12] and Type-II [13] oscillation regions. This method is widely used for reactor stability assessment and comparison [14].

Table 1. Nomenclature.

Symbol	Meaning	Unit
$\dot{Q}$	Core power	kW
$\dot{m}$	Mass flow rate	kg/s
h_{in}	Specific enthalpy at the inlet	kJ/kg
h_{sat}	Specific enthalpy at saturation	kJ/kg
ρ_l	Liquid density	kg/m^3
ρ_g	Vapor density	kg/m^3
ΔH_{fg}	Latent heat	kJ/kg
A_{core}	Core flow cross-section	m^2
N_{sub}	Subcooling number	-
N_{Zu}	Zuber number	-

These regions are defined based on dimensionless numbers, a subcooling and a Zuber number, respectively:

$$N_{sub} = \frac{h_{sat} - h_{in}}{\Delta H_{fg}} \frac{\rho_l - \rho_g}{\rho_g}$$

$$N_{Zu} = \frac{\dot{Q}}{\dot{m}_{\text{core}} \Delta H_{fg}} \frac{\rho_l - \rho_g}{\rho_g}$$

The GENESIS experiment covered a range of conditions of two-phase R-134a (CH_2FCF_3) flow. The map of tests is shown in the figure 1. The operational regime is on the two-phase flow region, i.e. where $N_{Zu} > N_{sub}$. Several points lie close enough to saturated liquid (x=1) line, meaning that they enter the Type-I instabilities region. The ESBWR nominal operation point is $(N_{sub}, N_{Zu}) = (0.9, 5.5)$, and was maintained as a privileged property during the facility scaling.

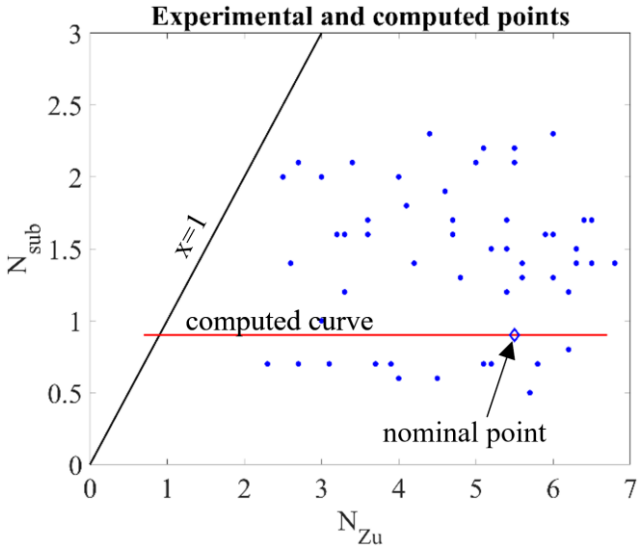

Figure 1. Map of points of the GENESIS transients series presented on a dimensionless map. Computed flow rate/power curve.

B. Fluid implementation in SIMMER-V: R-134a

SIMMER-V is a compressible-fluid code created mainly for SFR calculations. However, the code contains coefficients of a state equation for a few more fluids, like lead and water. Nevertheless, the GENESIS computation imposed the choice between sodium and R-134a [15], [16]. Any change of the working fluid imposes discussion on dimensionless analysis. Firstly, privileged processes have to be identified, secondly one has to face the problem of the choice between them, if keeping several criterions is rapidly impossible from the mathematical point of view. Thus, the authors decided to implement the new fluid to avoid uncertainty from one more facility scaling.

The method of the equation-of-state definition in SIMMER-V is based on the approach used by Morita and Fischer [17]. Fitting functions have been designed primarily for sodium, but here the fitting is extrapolated for R-134a. The general approach, however, did not allow us to correctly represent the derivative of liquid energy on a saturation line $\left(\frac{de_L}{dT}\right)_{sat}$. Thus, a simplified method was used to obtain the rest of derivatives, as proposed by Morita [18]. The direct translation of methodology was not sufficient for R-134a, whose density changes significantly in the liquid range. The difficulty was solved by artificial specific volume adjustment to fit the curve in the expected range of temperature.

C. GENESIS facility model

The GENESIS facility was constructed to reflect most important features of an ESBWR geometry. The downscaling was accompanied by construction simplification, for example by removing a complex steam separator and replacing fuel rods by electrically heated rods. In the basic GENESIS construction no neutronic feedback is present. It has been added by a digital controller in later phase of the experimental series. In this paper, only pure thermohydraulic effects are compared.

Table 2. Facility dimensions and properties.

Property	Differences		
	ESBWR	GENESIS	Unit
Heated length	3.0	1.41	m
Chimney + steam separator length	8.61 + 4.2	4.05 + 1.97	m
Downcomer length	16.4	7.71	m
Number of rods	92x1132 bundles	25	-
Pressure	71	11.4	bar
Core mass flow rate	10003	0.5148	kg/s
Core mass flux	993	1040	kg/m^2/s
Bypass area	0.0009	-	m^2

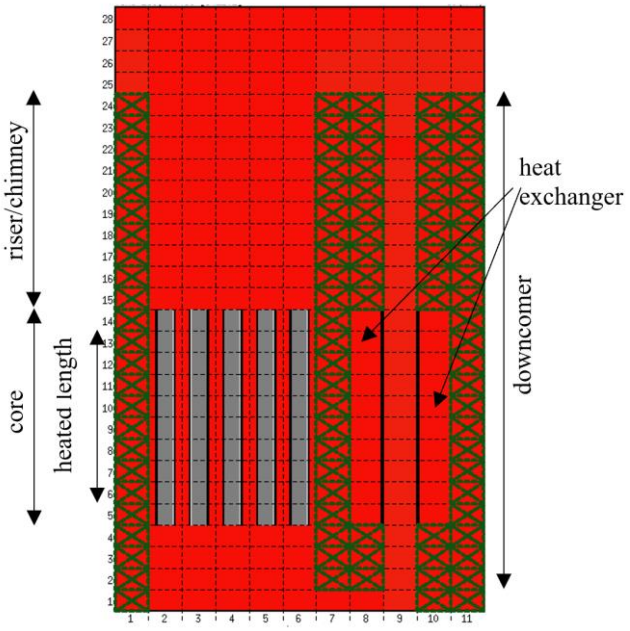

Figure 2. Simplified GENESIS geometry as represented in SIMMER-V. Cross section through the system.

Specificities of SIMMER-V impose a need for a few system simplifications (table 3). It is known that the uncertainties in the analysis can bring their effects on the final results. However, two of them have been encountered by Rohde et al. [19] in his ATHLET simulations. In this paper, one new uncertainty is introduced, which is the usage of SIMMER-V itself as it has never been used for R-134a simulations.

Table 3. Sources of uncertainties in SIMMER-V modelling of GENESIS facility.

Issue	Description
Heating rods	SIMMER-V does not allow application of electrically heated rods. Real fuel rods (consisting of a pellet, a gap and a cladding) had to be designed to keep appropriate heat transfer resistance.
Water supply	The GENESIS facility is supplied partly by a fresh coolant, while the model is a completely closed loop. It may result in different mechanisms driving slight changes of the coolant inlet temperature.
Operating fluid	R-134a is a fluid newly implemented in SIMMER-V. In spite of its validation, it might be a matter of lack of experience or method incoherence between sodium and R-134a.

III. RESULTS AND DISCUSSION

The simulations have been conducted in SIMMER-V code, modified to represent R-134a coolant.

A. GENESIS operating curve

Results obtained from the computations were postprocessed to obtain the operational curve of the GENESIS facility. Similarly to Marcel et al. [20], the authors performed calculations to verify the correctness of the model. Results obtained by SIMMER-V are compared to experimental values. In case of oscillating mass flow rates, the points represent an averaged value (figure 3).

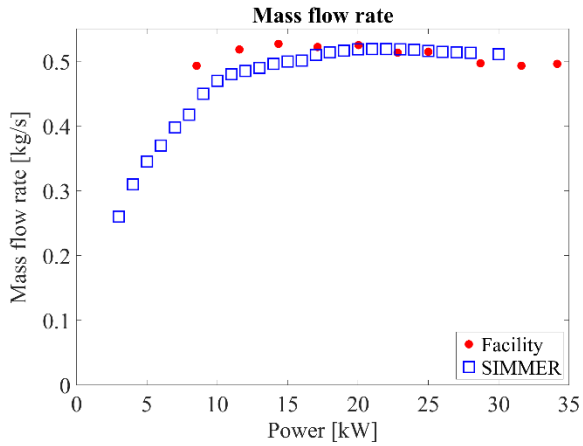

Figure 3. The flow rate/power curve: GENESIS experiment vs. SIMMER-V computations.

The calculated values match very well to the experimental ones, what allows us to say that the model represents the real facility in a way which makes further calculations reliable.

B. Stability analysis based on decay ratio method

The system stability was examined based on the decay ratio method, proposed for the GENESIS stability analysis by Marcel [11], Marcel et al. [20], followed by Rohde et al. [19] and Spoelstra [21]. To find a decay ratio of a real system, this method requires the noised signal analysis. The procedure [11] consists of the following steps: signal detrending, signal normalization and fitting the third order model to reproduce the signal response. The fitted curve is described by the function:

$$y = b_1 e^{b_4 t}\cos(b_5 t) + b_2 e^{b_4 t}\sin(b_5 t) + b_3 e^{b_6 t}$$

And the decay ratio and resonance frequency are, respectively, found from:

$$DR = e^{2\pi b_4/abs(b_5)}, f = 2\pi/abs(b_5)$$

Similarly to GENESIS designers, the authors chose the flow signal at the core inlet. Finding a decay ratio of a SIMMER-V system at a given power is straightforward: it requires a perturbation input on a power signal.

The results (table 4) correspond well to the experimental values. The difference appears in the resonance frequency and increases for lower power. The decay ratio, which is the determinant of the system stability, remains close to the expected value.

Table 4. Calculated stability parameters.

Point	Decay ratio		Resonance frequency [Hz]	
	Facility	SIMMER	Facility	SIMMER
25 kW	0.12	0.13	0.11	0.12
20 kW	0.11	0.13	0.09	0.13
15 kW	0.11	0.12	0.09	0.15

IV. CONCLUSIONS

The obtained flow rate/power curve proves that the SIMMER-V system has been properly designed. It ensures that the nominal point corresponds to the same conditions in the simulation and in the GENESIS facility (in ESBWR as well). The curve computed for $N_{sub} = 0.9$ corresponds to the same subcooling in a simulation as in the facility.

The decay ratios obtained for simulated systems are very close to the experimental ones. For the nominal point, the value can be compared with M. Rohde et al. [19], who in ATHLET obtained a $DR = 0.11$, slightly below the experimental value. SIMMER-V overestimated the value, which may result in finding a narrower stability boundary for Type-II instabilities.

The operating curve can be considered validated correctly against GENESIS experiments. The next step of the validation process may be a benchmark of SIMMER-V against the stability boundary obtained in ATHLET [19].

V. Acknowledgments

This study has been realised with the SIMMER-V code, property of JAEA and co-developed with CEA. The experimental data from GENESIS has been obtained through the courtesy of the General Electric. We would like to thank Dr Martin Rohde and Dick de Haas from Delft University of Technology for help, sharing the experience and making it possible to conduct this research.

VI. References

[1] *Charter of the Generation IV International Forum*. 2006.

[2] J. M. Seiler, D. Juhel, and Ph. Dufour, "Sodium boiling stabilisation in a fast breeder subassembly during an unprotected loss of flow accident," *Nucl. Eng. Des.*, vol. 240, no. 10, pp. 3329–3335, Oct. 2010, doi: 10.1016/j.nucengdes.2010.07.001.

[3] N. Alpy *et al.*, "Phenomenological investigation of sodium boiling in a SFR core during a postulated ULOF transient with CATHARE 2 system code: a stabilized boiling case," *J. Nucl. Sci. Technol.*, vol. 53, no. 5, pp. 692–697, May 2016, doi: 10.1080/00223131.2015.1111778.

[4] E. Gialdi, S. Grifoni, C. Parmeggiani, and C. Tricoli, "Core stability in operating BWR: operational experience," *Prog. Nucl. Energy*, vol. 15, pp. 447–459, Jan. 1985, doi: 10.1016/0149-1970(85)90070-8.

[5] E. Lorenzini, C. Crescentini, and M. Spiga, "Two-phase flow instability in channels with sinusoidal heat supply," *Nucl. Eng. Des.*, vol. 74, no. 1, pp. 133–137, Jan. 1983, doi: 10.1016/0029-5493(83)90146-2.

[6] K. Valtonen, "BWR stability analysis," Finnish Centre for Radiation and Nuclear Safety (STUK), Helsinki, Finland, STUK-A88, Jan. 1990.

[7] J. March-Leuba and J. M. Rey, "Coupled thermohydraulic-neutronic instabilities in boiling water nuclear reactors: a review of the state of the art," *Nucl. Eng. Des.*, vol. 145, no. 1, pp. 97–111, Nov. 1993, doi: 10.1016/0029-5493(93)90061-D.

[8] C. P. Marcel, M. Rohde, and T. H. J. J. Van Der Hagen, "An experimental parametric study on natural circulation BWRs stability," *Nucl. Eng. Des.*, vol. 318, pp. 135–146, Jul. 2017, doi: 10.1016/j.nucengdes.2017.04.020.

[9] W. J. M. de Kruijf, T. H. J. J. van der Haden, R. Zboray, A. Manera, and R. F. Mudde, "CIRCUS and DESIRE: Experimental facilities for research on natural-circulation-cooled boiling water reactors," International Atomic Energy Agency (IAEA), 1011–4289, 2002.

[10] C. T'Joen and M. Rohde, "Experimental study of the coupled thermo-hydraulic–neutronic stability of a natural circulation HPLWR," *Nucl. Eng. Des.*, vol. 242, pp. 221–232, Jan. 2012, doi: 10.1016/j.nucengdes.2011.10.055.

[11] C. P. Marcel, "Experimental and numerical stability investigations on natural circulation boiling water reactors," PhD thesis, Delft University of Technology, Delft, 2007.

[12] M. Aritomi, J. H. Chiang, T. Nakahashi, M. Wataru, and M. MORI, "Fundamental Study on Thermo-Hydraulics during Start-Up in Natural Circulation Boiling Water Reactors, (I)," *J. Nucl. Sci. Technol.*, vol. 29, no. 7, pp. 631–641, Jul. 1992, doi: 10.1080/18811248.1992.9731576.

[13] Y. F. Rao, K. Fukuda, and R. Kaneshima, "Analytical study of coupled neutronic and thermodynamic instabilities in a boiling channel," *Nucl. Eng. Des.*, vol. 154, no. 2, pp. 133–144, Mar. 1995, doi: 10.1016/0029-5493(94)00911-H.

[14] T. H. J. J. van der Hagen, A. J. C. Stekelenburg, and D. D. B. van Bragt, "Reactor experiments on type-I and type-II BWR stability," *Nucl. Eng. Des.*, vol. 200, no. 1, pp. 177–185, Aug. 2000, doi: 10.1016/S0029-5493(99)00337-4.

[15] F. Huber, A. Kaiser, K. Mattes, and W. Peppler, "Steady state and transient sodium boiling experiments in a 37-pin bundle," *Nucl. Eng. Des.*, vol. 100, no. 3, pp. 377–386, Mar. 1987, doi: 10.1016/0029-5493(87)90087-2.

[16] "Thermophysical Properties of Fluid Systems," *NIST Chemistry WebBook*. https://webbook.nist.gov/chemistry/fluid/ (accessed Apr. 30, 2021).

[17] K. Morita and E. A. Fischer, "Thermodynamic properties and equations of state for fast reactor safety analysis: Part I: Analytic equation-of-state model," *Nucl. Eng. Des.*, vol. 183, no. 3, pp. 177–191, Jul. 1998, doi: 10.1016/S0029-5493(98)00175-7.

[18] K. Morita and E. A. Fischer, "Simplified Analytical Equation-of-State Model for SIMMER-III ver. 2. A," Oarai Engineering Center, Ibaraki, Japan, Jun. 1996.

[19] M. Rohde, C. P. Marcel, A. Manera, T. H. J. J. Van der Hagen, and B. Shiralkar, "Investigating the ESBWR stability with experimental and numerical tools: A comparative study," *Nucl. Eng. Des.*, vol. 240, no. 2, pp. 375–384, Feb. 2010, doi: 10.1016/j.nucengdes.2008.01.016.

[20] C. P. Marcel, M. Rohde, and T. H. J. J. V. der Hagen, "Experimental Investigations on the ESBWR Stability Performance," *Nucl. Technol.*, vol. 164, no. 2, pp. 232–244, Nov. 2008, doi: 10.13182/NT08-A4022.

[21] J. Spoelstra, "Numerical stability analysis of natural circulation driven supercritical water reactors," M.Sc. Thesis, Delft University of Technology, 2012.

Proceedings of the European Nuclear Young Generation Forum
ENYGF'21
September 27-30, 2021, Tarragona, Spain

Experience Simulating ATF on a 3 loop PWR using SEANAP System.

M. Muñoz*, V. Casas, J. Santamaría, I. Sánchez, J. Bonilla, A. Ramos, J. Esteban, A. Cacheiro, C. Martin, L. Martin, J. Marín, J. Sierra, G. Pérez, D. Rodríguez, L. Martín, G. Piedra, I. Senet and Prof. O. Cabellos*

*Corresponding author: *mgmiguel21@outlook.com; oscar.cabellos@upm.es*

I. INTRODUCTION

Following Fukushima-Daiichi accident, Accident Tolerant Fuel (ATF) concepts have been under research and development to enhance safety while providing better performance during normal operation, including manoeuvring and transient conditions, and hypothetical accident scenarios. The main ATF technologies can be classified as follows: cladding technologies (e.g., coated claddings, selected steels and SiC) and fuel technologies (e.g., U_3Si_2, dopped fuels and TRISO).

All these ATF simulations have been the core of a UPM (Polytechnical University of Madrid) course during 2019-2020. In this paper it is described the experience of simulation of different ATFs on a 3-loop PWR using the SEANAP system. Additionally, different nuclear data libraries (JEF-2.2, JEFF-3.1, JEFF-3.3, ENDF/B-VII.1 and ENDF/B-VIII.0) were tested to assess the importance of the nuclear data in the simulation of ATFs.

This course is called INGENIA and takes place every year at ETSII in UPM. The complete name of the course is INGENIA-PWR Simulation & Design (12 ECTS), and it is based on the CDIO training and education approach (Conceive, Design, Implement and Operate).

The objective of this study is both to analyse the performance of different ATF technologies in LWRs and validate the SEANAP system for simulating other types of fuels

II. Methodology

First, an in-depth bibliographic study of ATFs is performed to obtain main neutronic parameters to run simulations in PWR properly. These studied parameters have been: technological data, temperatures profile, isotopic concentration, etc. A summary of them can be found in sections II.B and II.C.

Next, a reference PWR based on a typical UO2-Zircaloy reloading pattern is defined to test the different ATF technologies. This reference case is a real operational cycle of a 100MWe PWR-Westinghouse. Thus, the typical configuration and loading scheme are known.

Once the reference case is defined, simulations with different ATFs are performed. A total of 48 fresh fuel assemblies (FAs) are loaded in the core based on different types of ATF concepts. The aim is to match an equivalent cycle length to the typical UO2-Zircaloy reloading pattern. For the reference case, 0 ppm of boron concentration was reached at 11.08 GWd/MTU. So, simulated ATF technologies should reach 0 ppm of boron at 11.08 GWd/MTU (same cycle length) too to be considered as a valid choice.

Additionally, operational manoeuvres are simulated to give a global scope about transient behaviours of these ATFs. A summary of manoeuvres in PWRs is presented in II.D.

A. Reference Case

As mentioned before, reference case was based on a PWR (Westinghouse type) with 3 loops. The reactor thermal power is 2775 MWTh. Figure 1 shows the core which contains 157 Fuel Assemblies (FA) using UO_2 – Zircaloy as fuel with a lattice of 17x17-264 fuel rods and an active length of 365.76 cm. A total of 48 fresh fuels were loaded in this reference cycle. Fresh fuel assemblies are enriched at 3.6%wo with different number of burnable absorbers: Eight fresh fuel assemblies has been loaded with 0 wet annular burnable absorbers (8FA[0]), sixteen with four wet annular burnable absorbers (16FA[4]). The remaining ones were loaded as 8FA[12] 16FA[8].

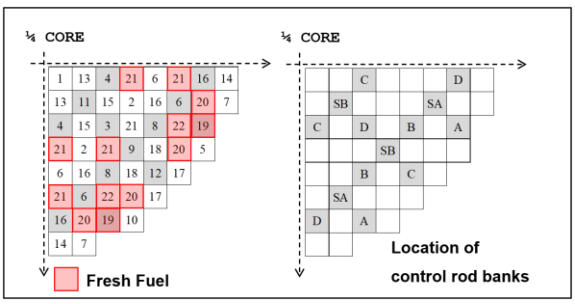

Figure 1. Core of base-case PWR.

For the reference case, the cycle length is calculated with SEANAP [1] code which gives a cycle length of 11.08 GWd/MTU.

To assess the neutronic impact of new ATFs in the core, the 48 UO2(3.6%wo)-Zircaloy fresh fuels are substituted by ATFs. Then, SEANAP code is used to predict the new cycle length with the new reloading pattern of ATFs.

The enrichment of the ATFs is calculated to match the same cycle length of the reference case. Results are shown in Section III.

The following ATF technologies have been selected based on the reactivity effect and implementation feasibility on LWRs.

B. Cladding Technologies

As mentioned, different cladding technologies were tested: FeCrAl Steel, Coated-Cr, Coated-Ti_2AlC and SiC.

Coatings: the coatings are destinated to overcome classical Zr problems such as hydrogen generation and embrittlement. They offer a realistic alternative due to its minimal changes which leads to several advantages when simulating and licensing. Studied coating are:

Cr: 20 μm coating [2]; ρ_{cr} =1.75 g/cm^3 [3].

Ti2AlC: 30 μm coating [4] ; ρ_{Ti2AlC} =1.75 g/cm3 [5]

In the simulation, both cladding and coating are assumed to be one single homogeneous material, instead of two different ones.

FeCrAl Clad: Steel properties are low absorption cross-section, low cost, no concentration of Co (which may be activated), low thermal expansion coefficient and great thermal conductivity as main characteristics. Composition: Fe 80.08 wt%, Cr 13wt%, Al 6.20 wt% [6] Thickness: 300 μm

SiC Clad: SiC is intended to be a substitution of traditional Zr claddings due to its radiation and oxidation resistance, a better thermal conductivity, great mechanical properties (almost temperature independent during transient) and great safety margins: up to 3 days at 1600ºC and/or several hours at 1700ºC-1800ºC in a vapor flow several hours at 1700ºC-1800ºC in a vapor flow regime. [7] Density: ρ_{SiC} = 2.71 g/cm^3 [8]. Clad thickness: 0.78 mm

C. Fuel Technologies

Figure 2 shows an example of different ATF fuel technologies.

Uranium Silicide

This compound replaces traditional UO_2. With a bigger thermal conductivity (12.3-20.9 W/mK) than UO_2 (2-5 W/mK) which leads to lower temperatures, high density, melting temperature of 1665ºC. [9]

Dopped Fuels

In this work, a mix of beryllium oxide is used along with U-235/U-238 mix. Pa

Table 1. Temperature per part for simulation.

Part	Temperature	Part	Temperature
Fuel	900 K	Fuel	900 K
Cladding	600 K	Cladding	600 K

Boron Concentration: 630 ppm

Borated Water Density: 0.711 g/cm^3

UO_2 density: 10.47 g/cm^3 [10]

Main characteristics: enhancement of thermal conductivity, decrease of temperature gradient along the pellet. When using BeO, reactivity is decreased, there are less space left for UO_2, thus moderator effect hardens, which eventually leads to an increase of reactivity. Both effects are opposed

TRISO

TRISO consists in micro-pebbles inserted in a SiC matrix for conductivity enhancement. These micro-pebbles are made of UO_2 (in this study case) at 5 wt% and covered by several layers as shown. In this case, two variables are sought: enrichment (some authors propose going up to 19%) and volumetric fraction (how many micro-pebbles are inserted within a fuel matrix).

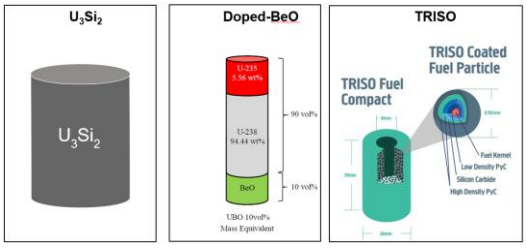

Figure 2. Simulated ATFs Fuel Technologies. Composition and geometry differ from actual simulated cases.

Due to its great thermal conductivity, a temperature drop is observed, additionally, this technology withstands higher temperatures during transients (it is intended to be HTGR fuel). Its layers are buffers where fission products (especially gaseous ones) are trapped in. However, less amount of U is present on the fuel.

The current SEANAP code cannot handle doble-heterogeneous geometries, such as TRISO fuel. To solve this problem methodology based on Reactivity-Equivalent Physical Transformation (RPT) has been implemented in SEANAP system. RPT model creates a single-heterogeneous problem out of double-heterogenous one (see Figure 3).

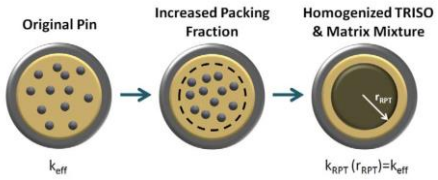

Figure 3. Example of RPT methodology [11].

To obtain the proper radius, which is the radius that makes single-heterogeneous problem as reactive as the double-heterogeneous problem, it is necessary to simulate the original case in advance in KENO. And then, iterating, radii are tested until the equivalent radius is found.

In addition, new effective temperature correlations for the TRISO fuel have been implemented in SEANAP based on empirical data.

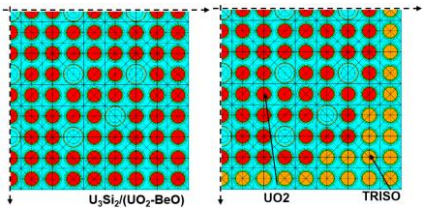

Figure 4. Fuel assemblies for U_3Si and Dopped Fuel and for TRISO.

As shown in Figure 4, two fuel assembly configurations are implemented. For U3Si2 and dopped fuels a full lattice is implemented, whereas for TRISO a CORAIL-type fuel assembly is proposed. The reason why is because screening effects take place, which leads to higher enrichments. [12]

Finally, main studied variables are, equivalent enrichment, axial offset, peaking factors, axial power distribution, reactivity coefficients and the impact of nuclear data.

D. Manoeuvres

Different power manoeuvres can be simulated with SEANAP code. In this work, the return to power after a short (9 hours) shutdown at BOC and EOC is presented. Among main studied variables: Xenon level evolution, boron concentration evolution, control rod position versus relative power, axial flux difference ($AO \cdot P_{rel}$) versus relative power and $P \cdot F_Q$ versus time.

Control Rods are uniformly located in the core and divided in clusters (RCCSAs), A+B+C+D+SA+SB. Control Rods are divided into banks to avoid the effect on power distribution and large reactivity change in control insertion. Control rod limit (D+C) for the operation will allow to reduce the decrement of reactivity worth, limit $F_{\Delta H} \cdot P$ and secure the shutdown margin.

Additionally, Axial Flux Difference (AFD) Limits are defined, see Figure 5. They establish how Flux Difference (ΔI) can evolve with relative power, otherwise penalties are applied. An ideal ΔI target is defined to follow it during operational manoeuvres. It is the Control Axial Offset Constant (CAOC) mode.

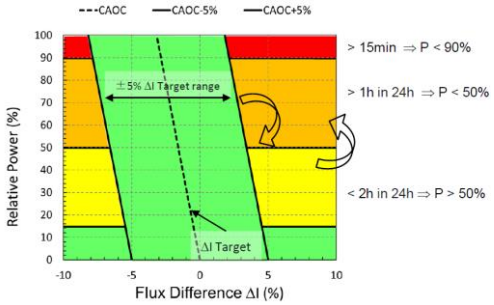

Figure 5. Axial Flux Difference (AFD) Limits as a function of rated thermal power.

III. Results

In this section the following results are shown, equivalent enrichment for ATFs, the impact of nuclear data evaluation and manoeuvres.

A. Equivalent enrichments

Tables 1 and 2 show the change in the enrichment for the different ATF concepts to achieve the same cycle length of the reference case. Figures 6 and 7 show the boron let-down curve for these cases.

Table 2. Equivalent enrichments for Cladding/Coating technologies to match the same cycle length.

Fuel Type/Eq Enrichment	Cladding/Coating
UO_2 3.6%wo (#0)	Zr – 0.5715 mm
UO_2 3.86%wo (#1)	SiC – 0.82 mm.
UO_2 3.99%wo (#2)	FeCrAl – 0.30 mm
UO_2 3.75%wo (#3)	Zr – 05715 mm + Ti_2Al – 30 µm
UO_2 3.71%wo (#4)	Zr – 0.5715 mm + Cr – 20 µm

Table 3. Equivalent enrichments for Fuel technologies to match same cycle length.

Fuel Type/Eq Enrichment	Cladding/Coating
UO_2 3.6%wo (#0)	Zr – 0.5715 mm
U_3Si_2 3.747%wo (#5)	FeCrAl – 0.3 mm
95% UO2 3.439%wo + 5% Be (#6)	Zr – 0.5715 mm
90% UO2 3.403%wo + 10% Be (#7)	Zr – 05715 mm
84 FCM TRISO 5%w - 80 % VF + 180 UO2 3.4%wo (#8)	Zr – 0.5715 mm

B. Main variables

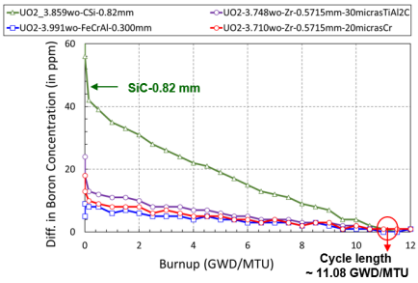

Figure 6. Difference in Boron concentration (ppm) for Cladding/Coatings.

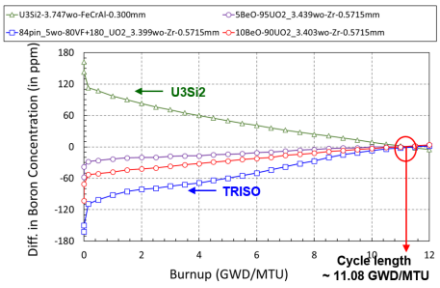

Figure 7. Difference in Boron concentration (ppm) for ATF Fuel.

As expected, larger differences are given by most "unconventional" technologies like TRISO or SiC.

Table 4 shows the **Axial Offset** at Beginning of Cycle (BOC)/Hot ZeroPower (HZP). No large differences are found from reference case during cycle operation.

Table 4. Axial Offset at BOC/HZP per case.

Case	A.O (%) BOC/HZP	Case	A.O (%) BOC/HZP
(#0)	33.9	(#5)	29.2
(#1)	31.6	(#6)	36.2
(#2)	33.5	(#7)	37.8
(#3)	33.1	(#8)	40.0
(#4)	33.3		

Case (#5), corresponding with U_3Si_2 is negative from BOC.

For **peaking Factors**, heat flux hot channel factor (F_Q) and enthalpy peaking factor ($P_{\Delta H}$) were studied. Design limit were stablished at 2.4 and 1.6, respectively. For F_Q, biggest differences were found for ATF fuel but below design limit. Figure 8 shows $F_{\Delta H}$ along burnup, no large differences were found for cladding, but for fuels. TRISO is above design limits, so this solution must be reviewed in the future.

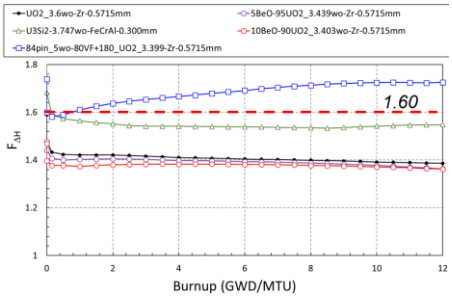

Figure 8. $F_{\Delta H}$ evolution per fuel case. TRISO out of limits.

Finally, **reactivity coefficients** were studied: Boron Worth, Moderator Temperature Coefficient (MTC), Fuel Temperature coefficient, power coefficient of reactivity (only Doppler) and power coefficient temperature. All of them are negative (more negative for claddings, not for fuels). TRISO aroused a MTC of -1.0, very close to be positive.

C. Impact of nuclear data evaluation

No significant deviations were observed for cladding/coating technologies at evaluating equivalent enrichment for different libraries. However, a maximum deviation of 0.08% in enrichment was observed in the case of dopped fuels for the JEFF-2.2 library. This might be due to the difference observed in JEFF-2.2 for elastic cross section associated to Be. However, further review should be done. This review was not done because it was out of the scope of the project.

D. Manoeuvres

Xenon level at 100% power and ΔBoron (ppm) were studied, while constraints were given by ΔI(%) and banks position. Figure 9 is an example of the manoeuvre of return to power after a short (9 hours) shutdown at EOC, changes in Power level(%) and ΔI(%) are simulated. In this case. For EOC manoeuvres, there were penalties for all cases (including reference UO2) except for TRISO and U_3Si_2.

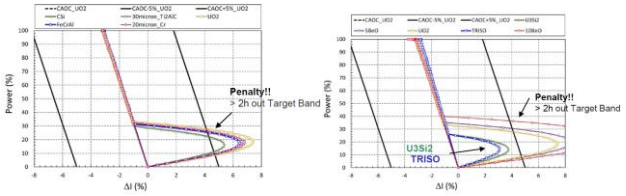

Figure 9. ΔI (%) evolution for EOC manoeuvre, of cladding (left side) and fuel (right side) cases

As it is shown in Figure 9, only dopped fuels give a worst scenario for control manoeuvrers within Technical Specifications Requirements.

IV. Conclusions

The SEANAP system has been implemented with new capabilities to simulate ATFs. The prediction of equivalent cycle length shows that slightly higher enrichments are needed for ATFs except for the dopped fuels. Thus, a balance between licencing and operational costs and a relevant improve in safety must be found.

Referring to claddings: a great overall performance is observed for both a cycle with and without manoeuvres. TRISO and dopped fuels may be out of the design's limits during normal operation and manoeuvres, so further study is needed.

Finally impact of nuclear data is not that relevant as initially expected.

V. References

[1] C. Anhert, J. Aragonés, Ó. Cabellos, and N. Garcia-Herranz, "Continuous Validation and Development for Extender Appliactions of the SEANAP Integrated 3D PWR Core Analysis System," *Mathematics and Computation, Reactor Physiscs and Enviromental Analysis in Nuclear Applications*, vol. 1, pp. 710-719, 1999.

[2] K. Geelhood and W. Luscher, "Degradation and Failure Phenomena of Accident Tolerant Fuel Concepts," Pacific Northwest National Laboratory, Richland, 2019.

[3] J. Lab, "The Element Chromium," DOE, [Online]. Available: https://education.jlab.org/itselemental/ele024.html.

[4] F. Boylan and e. al, "Evaluation of Coatings for Nuclear Fuel Rods for Improved Accident Tolerance.," 2015.

[5] I. M. Younker, "Neutronic and economic evaluation of accident tolerant fuel concepts for light water reactors," 2015.

[6] T. e. a. Fejt, "Study on neutronicsof VVER-1200 with accident tolerant fuel cladding," *Annals of Nuclear Energy*, vol. 124, pp. 579-591, 2019.

[7] T. Koyanagi and e. al, "Mechanical properties of SiC composites netron irradiated under light water reactor relevant temperature and dose conditions," *Journal of Nuclear Materials*, vol. 494, pp. 46-54, 2017.

[8] T. Koyanagi and e. al, "Handbook of LWR SiC/SiC Cladding properties - Revision 1," 2018.

[9] A. G. Padilla and e. al, "Core Performance Improvement Using U3Si2-Al Fuel in the RP-10 Modelization," Santiago de Chile, 2019.

[10]K. Mccoy and C. Mays, “Enhanced thermal conductivity oxide nuclear fuels by co-sintering with BeO: II. Fuel Performance and neutronics,” *Journal of Nuclear Materials,* vol. 375, pp. 157-167, 2008.
[11]S. T. Lyncg, “Reactivity-Equivalent Physical Transformation Model for Pin Cell Arrays,” 2010.
[12]C. A. Gentry, “An investigation of the use of Ceramic Microencapsulated Fuel for Transuranic Waste Recycling in PWRs,” 2012.

Proceedings of the European Nuclear Young Generation Forum
ENYGF'21
September 27-30, 2021, Tarragona, Spain

Comparative Analysis of Mo-99 Production in the Jules Horowitz Reactor and in the SHINE® System

Ratero-Talavera, Cristina[1], Serna-Moñino, Pablo[1] and García-Herranz, Nuria[1]

[1] Department of Energy Engineering, Universidad Politécnica de Madrid (UPM), Spain

*Corresponding author: *cristina.rtalavera@alumnos.upm.es*

I. INTRODUCTION

The production of medical radioisotopes is essential for the diagnosis and treatment of multiple diseases in the field of nuclear medicine. By far, the most widely used medical radioisotope is Tc-99m, which is used in diagnostic imaging in more than 40 million medical procedures every year worldwide [1]. Due to its short half-life of 6 hours, it is not practical to transport it to medical centers, so it is produced from the parent isotope Mo-99, which has a half-life of about 67 hours. Currently, Mo-99 is obtained mainly as a fission product of U-235 in Material Testing Reactors (MTR) [2]. The global demand of Mo-99 in 2019 was about 10000 6-day Ci each week (defined in section III) and a further growth is expected in the coming years [1].

However, despite its importance, its global supply has been threatened by the age of the MTR. Table 1 shows the planned shutdown dates of the various MTR around the world.

Table 1. Situation of main MTR in the world [3].

Name of Reactor	Situation of main MTR in the world			
	Location	Target	Starting date	Closing date
OSIRIS	France	LEU	1966	2015
NRU	Canada	HEU	1957	2018
HFR	Netherlands	HEU	1961	2024
BR2	Belgium	HEU	1961	2026
SAFARI-1	South Africa	LEU	1965	2030

In addition, the closures and shutdowns of some of this MTR led to a shortage of medical radioisotopes during 2017 and 2018 [1]. This has prompted the need to look for new emerging technologies to complement existing ones in order to strengthen the supply chain. One of these technologies is SHINE, whose production proposal is based on the use of a neutron generator coupled to a subcritical system. Furthermore, the Jules Horowitz Reactor (JHR), a critical MTR for large-scale Mo-99 production and a variety of research uses, is under construction in southern France.

In this work, the Mo-99 production rate will be evaluated in both scenarios, characterized by a very different neutron flux and available mass of U-235 (target).

First, a brief explanation of the two systems analyzed will be given: SHINE and JHR. Then, the methodology followed, the results and finally the conclusions will be presented.

II. DESCRIPTION OF THE SHINE SYSTEM AND THE JULES-HOROWITZ REACTOR

A. SHINE system

SHINE is a technology based on a neutron generator coupled to a subcritical system, shown in Figure 1. The neutron generator consists of a deuteron accelerator that impacts on a tritium target, producing high-energy neutrons (14 MeV) by D-T fusion reactions. These neutrons will be supplied to the subcritical system so that it can operate at steady state. In the subcritical system, more specifically in the Target Solution Vessel (TSV), there is a liquid uranium solution in which the fission reactions of U-235 take place, resulting in Mo-99 among other fission products [4].

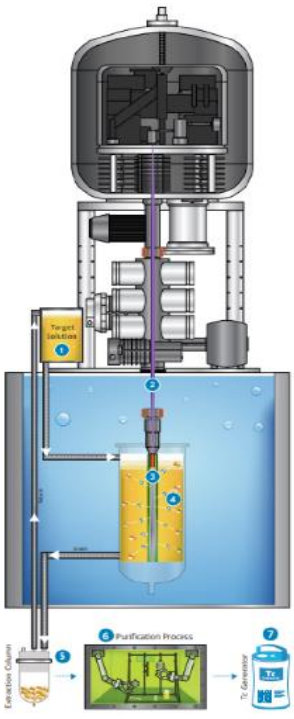

Figure 1. SHINE Subcritical Assembly [4].

The solution is uranyl sulfate hydrate with 19.75% low enriched uranium (LEU). LEU helps to prevent the proliferation of nuclear weapons; on the other hand, the liquid solution allows that, after irradiation, it can be conditioned for reuse as fuel.

A SHINE facility consists of 8 irradiation units as described in Figure 1.

Under normal operating conditions, the solution is irradiated for 5.5 days, after which the Mo stream is transferred and extracted, and then subjected to a purification and filtration process to ensure that the purity of the Mo-99 obtained in SHINE is comparable to that obtained in conventional critical reactors.

B. Jules- Horowitz Reactor

The Jules Horowitz Reactor is a 100 MWth MTR being built by CEA in Cadarache (France) with international participation. The construction began in 2007 and is expected to be completed by 2027. Inside the reactor, two main areas can be distinguished, the core and the beryllium reflector as presented in Figure 2. In the core, up to 34 fuel assemblies can be accommodated and an intense fast flux is achieved, which allows the irradiation of different experimental devices for evaluation. In the beryllium reflector, thanks to its high moderating power, an intense thermal flux is achieved, which is used, among other applications, for the irradiation of uranium targets to obtain Mo-99 as a fission product of U-235. The targets are introduced by a mobile system into the so-called Moly devices.

Up to 4 Moly devices with 12 targets each can be accommodated in the reflector. Once placed in the reactor, they are irradiated for 7 days and then transported to hot cells for conditioning and processing. For the evaluation of Mo^{99} production, U-Al alloy targets with LEU of conventional and high density were chosen [5]. The use of high-density LEU (HDLEU) yields a Mo-99 production similar to the one obtained with the standard used high enriched uranium (HEU) (~94% U-235) targets while respecting the international non-proliferation policies.

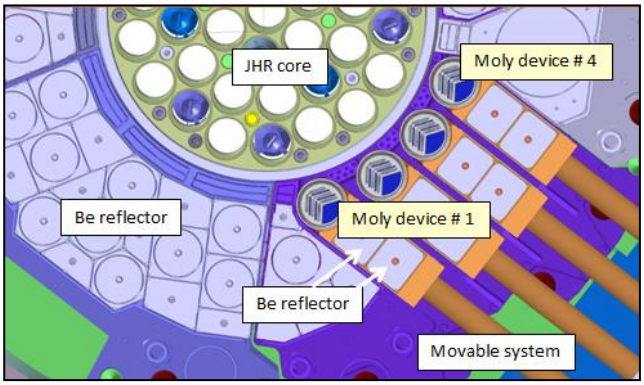

Figure 2. Jules Horowitz Reactor: Core and Be Reflector [6].

III. METHODOLOGY

In order to obtain the evolution of the mass, activity and related responses, the Bateman equations have to be solved. The ORIGEN code of the SCALE 6.2.3 system [7] has been used for that purpose. As shown in Figure 3, it is necessary to provide a problem-dependent effective nuclear data library (.f33), which is obtained by means of the COUPLE module of SCALE. With this module, the JEFF-3.0/A cross-section activation library in 252 energy groups, the ENDF/B-VII.1 decay library and the ENDF/B-VII.0 fission yields library have been combined with the 252-group energy flux spectrum characteristic of the problem. This spectrum has been obtained with the transport code MCNP 6.1 [8] and the ENDF/B-VII.0 library.

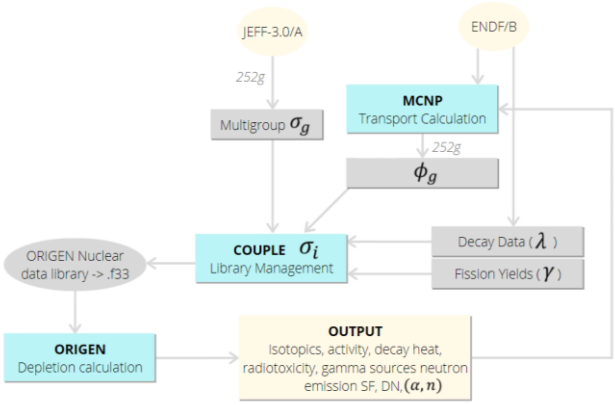

Figure 3. Methodology based on ORIGEN, COUPLE and MCNP.

It was decided to compare 8 SHINE Irradiation Units, equivalent to 23.7 m^3 of uranyl sulphate in aqueous solution, and 4 Moly devices, equivalent to 48 LEU targets for a total of 436.8 cm^3.

Table 2 shows the compositions and irradiation conditions used in the calculation. It is important to mention that all values corresponding to SHINE (except the enrichment) have been estimated from publicly available data, as they are proprietary information. Concerning JHR, both LEU and HDLEU targets only differ in uranium density. As for the flux intensity, it has been taken from [9].

Table 2. Composition and irradiation conditions.

	U Density (g/cm^3)	Target composition (weight%)	U^{235} Enrichment (weight%)	Flux Intensity n/cm^2s
SHINE	0.069	88.58% H_2O 11.42% $UO_2(SO_4)$	19.75	1.31E+11
JHR	2.6 (LEU) 6.5 (HDLEU)	61.8% Al 38.2% U	20	6.00E+14

IV. RESULTS

A. MCNP

Using the MCNP code, the neutron spectrum in the fuel and reflector of the JHR and in the TSV of the SHINE system, as well as other data, have been obtained.

Regarding SHINE, two types of MCNP calculations were performed: i) criticality calculations to estimate the fissile material composition, ensuring subcriticality condition; ii) fixed-source calculations to estimate the flux intensity and spectrum in the solution vessel. Using the heating tally (F6MESH), the energy deposition in the solution vessel was calculated. Then, using the reported thermal fission power (100 kW), the neutron source strength was computed and used to calculate the flux intensity.

Regarding the JHR, a MCNP model with a simplified homogenized reflector was employed to get the flux spectrum.

Figure 4 shows the different neutron spectra of JHR and SHINE. The neutron spectrum in the JHR reflector is much more thermal than in the fuel, which favors the production of Mo-99 by increasing the probability of fission. It is very similar to that of the TSV in SHINE, with the difference that in the latter a peak can be observed at energies of 14 MeV corresponding to the neutrons born from D-T fusion reaction.

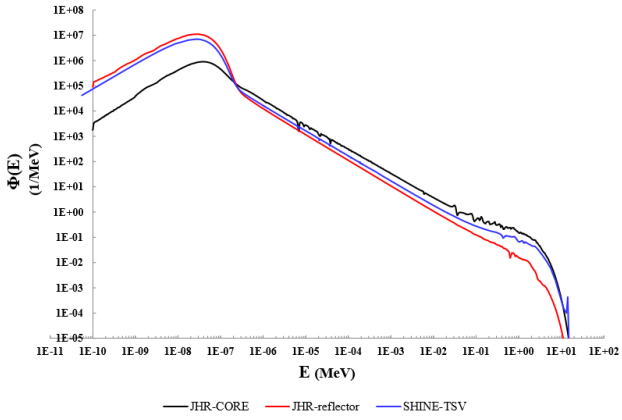

Figure 4. Neutron spectra in JHR and SHINE.

B. ORIGEN

Starting from the flux-dependent cross-section and fission yield library collected in the .f33 file, different results corresponding to each stage of the Mo^{99} production process have been obtained. Figure 5 shows the different time intervals to be simulated and their duration: 7 days of irradiation, 0.5 days of decay, 0.5 days of processing from "Begin Of Processing" (BOP) and 6 days of post-processing from "End Of Processing" (EOP).

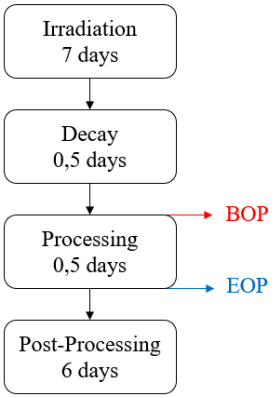

Figure 5. Stages of Mo-99 production simulation in SHINE and JHR.

In addition to the mass and activity, the decay heat and the intensity and spectrum of the emitted particles have also been determined, due to their importance before and during the chemical processing of targets (although not illustrated in this paper).

In the following, the Mo-99 production in both systems will be quantified from the unit of measurement called "6-days Ci after EOP", defined as the activity after 6 days from the end of the processing. This unit has been used as it is the most commonly used to analyze radioisotope production as well as demand trends.

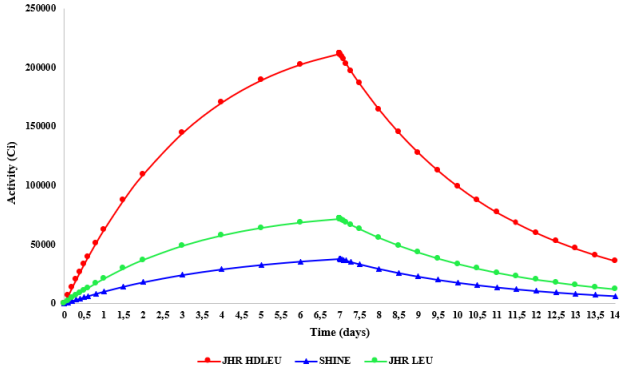

Figure 6. Evolution of Mo^{99} activity in JHR and in SHINE.

Figure 6 shows the evolution of Mo-99 activity in both systems from the beginning of irradiation until 6 days after EOP, and Table 3 shows the 6-day Ci Mo-99 activity values produced in both systems. The activity values for an irradiation of 5.5 days at SHINE have also been added in order to compare the real production of this system with that of JHR under normal operating conditions. It should be added that a processing efficiency of 85% has been established to study a more realistic case.

Table 3. Simulation results in JHR and SHINE with a processing yield of 85%.

			6-days Ci of Mo^{99} after EOP	
	Mass of U (g)	**Irradiation Time (days)**	**Mo-99 Activity (Ci)**	**Mo-99 Activity per gU (Ci/gU)**
SHINE	$1{,}657 \cdot 10^{6}$	5,5	4257	$2{,}56 \cdot 10^{-3}$
JHR (HDLEU)	3009	7	30820	10,24
JHR(LEU)	1202	7	12315	10,24

From Table 3 it can be seen that, with the data used in the study, SHINE can produce around 4257 Mo-99 6-days Ci per week irradiating the fuel for 5.5 days and using its 8 irradiation units. This value is in agreement with the 4000 6-days Ci reported by SHINE developers [10]. That means 34.5% of the maximum JHR production operating at full capacity with the 4 Moly devices completely filled and using LEU targets of conventional density without taking into account the outage reserve capacity that CEA reports [6]. The use of HDLEU targets would increase the production by 150% with respect to low density targets, reaching 30820 Mo-99 6-days Ci.

In addition, Table 3 shows a comparison of Mo-99 activity per initial mass of U in both systems, SHINE and JHR, in order to compare the "efficiency" in terms of how much of the uranium is effectively converted into usable Mo-99. It can be seen that, from one gram of uranium, the activity obtained in SHINE is about ten thousand times lower than in the case of JHR, reflecting the high efficiency of JHR.

V. CONCLUSIONS

The methodology based on the use of the transport code MCNP and the inventory code ORIGEN was shown to be a valid approach to characterize the production of Mo-99 and inventory-related quantities in the JHR and the SHINE system. Even if a variety of assumptions was adopted, results are realistic and allow the comparison of the efficiency of different production strategies.

Regarding the Mo-99 production methods, results show that the Mo-99 production rate depends on the flux intensity, the spectrum (since the fission cross sections of U-235 are larger the more thermal the flux) and the mass of fissile material. The higher production rate in the JHR is due to the intense thermal flux achieved in the beryllium reflector, together with the higher density of U-235, which increases significantly when using high density alloy targets. In the SHINE system, the spectrum is similar, but there is a lower flux (around 103 times lower than in the JHR), and a lower fuel density as it is in solution form, which results in a lower production of the medical isotope.

However, the size of the installation, the financial investment and the construction time of the SHINE system are much smaller than those required for the construction of a large-scale nuclear reactor such as the Jules Horowitz Reactor. This may make the implementation of more compact systems like SHINE worthwhile especially in hard-to-reach or resource-poor locations.

Nevertheless, MTR such as the JHR are intended to operate up to 50 years or longer, which gives a return on investment, and their applications are not limited to the production of radioisotopes.

Comparing the production of Mo-99 in SHINE and in the JHR with the global demand, it is found that SHINE is capable of producing a third of the world demand of Mo-99.

On the other hand, the number of devices and targets used for the production levels in JHR reported by the CEA is not known. Therefore, since 4 Moly devices completely filled have been used for simulation, the results show a higher production than the reported by the CEA.

The future of a large part of nuclear medicine depends on the construction of new MTR such as the Jules Horowitz reactor to replace the old ones or the development of new technologies such as the SHINE system, which combined will ensure the continuous and stable production of radioisotopes such as Tc-99m, which is so necessary for the current demand of more than 40 million patients per year.

VI. References

[1] OECD/NEA, The Supply of Medical Radioisotopes, 2019 Medical Isotope Demand and Capacity Projection for the 2019-2024 Period, NEA/SEN/HLGMR(2019)1, 2019

[2] C. Steven van der Marck & J. Arjan Koning & E. Kevin Charlton, Eur J Nucl Med Mol Imaging, "The Options for the Future Production of the Medical Isotope Mo99" (2010) 37:1817–1820. DOI 10.1007/s00259-010-1500-7

[3] M. Capogni; A. Pietropaolo; L. Quintieri; A. Fazio; M. Pillon; P. De Felice; A. Pizzuto(2018). "14 MeV neutrons for medical application: a scientific case for 99Mo/99Tcm production". Journal of Physics: Conference Series. 1021: 012038.

[4] SHINE Medical Technologies

[5] H.J. Ryu et al., "Development of high-density U-Al dispersion plates for Mo-99 production using atomized uranium powder", Nucl. Eng. Tech., 45, pp. 979-986 (2013).

[6] M.Antony, J.-P. Coulon, S. Gay, F. Bourrelly, D. Tarabelli, D. Drapeau, C. Chapuis, F. Derasse, N. Aymard, R. Mallet, "Moly production in the Jules Horowitz Reactor: Capacity and Status of the Development", CEA.

[7] Rearden, B.T., Jessee, M.A., 2016. "SCALE Code System," Ornl/Tm-2005/39, (6.2.3), pp. 2747.

[8] MCNP6 Version 1.0, Los Alamos National Laboratory report LA-UR-13-22934

[9] Joint Meeting of the National Organization of Test, Research, and Training Reactors and the International Group on Research Reactors, Gaithersburg, September 12-16, 2005

[10] T. Gregoire, "Meeting the Molly-99 Challenge", Jun 2018

[11] C. Ratero, "Analysis of the Accelerator-driven Subcritical System Shine for Medical Radioisotope Production", BSc thesis, Technical University of Madrid, Feb 2021

[12] P. Serna "Evaluation of the Production of the Medical Radioisotope Mo99 in the Moly Devices of the Jules Horowitz Reactor", BSc thesis, Technical University of Madrid, Feb 2021

Proceedings of the European Nuclear Young Generation Forum
ENYGF'21
September 27-30, 2021, Tarragona, Spain

Thermo-hydraulic calculation of the can with tellurium dioxide target material during the irradiation process.

Talarowska, Anna[1*], Rafał Prokopowicz[1]

[1] National Centre for Nuclear Research (NCBJ), Poland

*anna.talarowska@ncbj.gov.pl

I. INTRODUCTION –

Tellurium dioxide is widely used as a target material for iodine-131 production. Iodine-131 is used for cancer treatment and medical diagnostics. The production process starts with irradiation of containers with natural tellurium dioxide in the MARIA Research Reactor. The containers are placed in vertical irradiation channels. The neutrons from reactor core are absorbed by the tellurium-130 istope and as a result, the excited state of tellurium-131 is achieved. Due to the beta decay reaction – the iodine-131 is produced. Significant heat generation accompanies the neutron absorption reaction. As a result, there is a possibility of reaching the melting point temperature of the compound, which is objectionable and raises safety concerns. A relatively simple heat transfer calculation shown that the melting point can be easily reached [1]. The scope of presented work is development of the best estimate thermo-hydraulic model of the irradiated can with target material. The simple can model [1] was recreated and upbuilt gradually, so it was possible to determine the impact on the accuracy of each step of model development and indicate the most critical aspect with regards to the possibility of melting. Firstly, the boundary condition applied on the can wall was discussed, then the water flow in the cooling channels was added. The heat transfer calculations were performed by modern CFD code ANSYS Fluent 2020 R1[6]. The process of the model development is described in the section II of the article where the following subsections correspond to each added detail to the model.

A. Hydraulic characteristics of the vertical channel

Multiple cans with natural tellurium dioxide are placed in numerous vertical channels of the MARIA Research. Vertical orifices through beryllium block with aluminium tube create irradiation channels in different reactor core locations (Figure 1). The irradiation technology assumes placing the cans inside the tube in the reactor core. Therefore, the target material is separated from coolant by can and two annular cooling gaps. The can and the tube define the inner gap, and the outer cooling gap is constrained by tube and beryllium block. The hydraulic diameters of inner and outer cooling annular gaps equal 3 mm and 2 mm, respectively. The downward flow in the gaps is forced by the reactor pool cooling pumps, while water acts as a coolant. The pressure drop on the reactor core was measured experimentally and equalled 14.7±0.1 kPa. To estimate the water velocity in each gap, the Darcy-Weisbach equation (1) was used; where Δp is pressure drop, L is the streamwise length of the gap, ρ – fluid density, D – hydraulic diameter, and f_D is Darcy friction factor calculated with Cheng correlation [2].

$$\frac{\Delta p}{L} = f_D \cdot \frac{\rho}{2} \cdot \frac{< v >^2}{D} \quad (1)$$

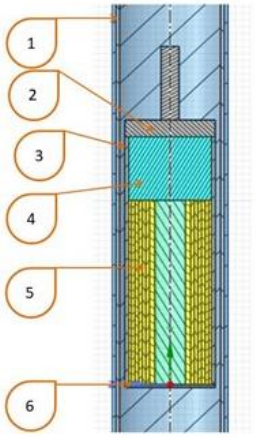

Figure 1: The cross-section view of the irradiation channel with inserted can. The numbers show the following elements: 1-aluminium tube, 2-lid with handle, 3 -can wall,4-air plenum, 5- target material (TeO2), 6-can bottom.

The Cheng correlation was picked for friction factor computation because it covers the entire flow regime from laminar to turbulent one, which is the crux of the MARIA reactor core issue. The calculated coolant velocity in the inner gap ranges from 1.21 to 1.30 m/s and from 1.14 to 1.22 m/s for the outer gap. Then, the Nusselt Number from Gnielinski formula [3] is determined. Finally, wall heat transfer coefficient is calculated and equals 8509.5

W/(m^2·°C) for the slowest coolant velocity and 9122 W/(m^2·°C) for fastest coolant flow in the inner gap. The estimated values were applied as one of the boundary conditions for temperature field estimation described in the section II.B.

B. Material properties

Bykowski [1] and Fllaoui [4] addressed the heat generation problem in the tellurium dioxide target; in both studies, the constant thermal properties were considered. Furthermore, the properties applied are valid for the crystalline tellurium dioxide for, while the target is in amorphous form due to melting and solidification occurring during the can preparation process. As a result, the material's density decreases by about 17% to 4.82 g/cm^3, which affects the heat generation estimation. Due to the amorphous form with significant pores, thermal properties had to be measured experimentally, namely the thermal conductivity and specific heat. In this paper, the thermal conductivity characteristic will be discussed only, while the constant value of specific heat, 0.346 kJ/(kg·°C), is applied for all case. The thermal conductivity was assumed to be constant (0.75 W/(m·°C)) in the first part of the study: sections II.B and II.C, while its decrease with temperature (Figure 2) was discussed in paragraph II.D. The characteristic was prepared based on thermal diffusivity measurements performed by the Microelectronics and Photonics Institute [5].

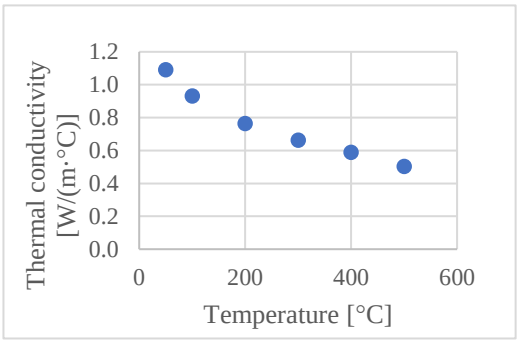

Figure 2: Thermal conductivity of the tellurium dioxide in the amorphous form.

The density, specific heat, and thermal conductivity of aluminium were constant since the aluminium temperature gradient can be less than 10°C. Similarly, water density, thermal conductivity, specific heat, and viscosity remained constant due to the heat up of the coolant of 4°C. The thermal conductivity of air increases with temperature rise, and the air density inside the can decrease with an increase of temperature resulting in pressure rise inside the can, which was taken into account in the presented analysis.

II. Numerical modelling

The finite volume method calculation was performed with ANSYS Fluent 2020 R1 [6]. The SST k-ω turbulence [7] model was used, this is a two-equation model which use a k-ϵ formulation in the free stream and k-ω one in the vicinity on the wall. The boundary conditions for flow were applied as a velocity-inlet and outflow. Three asymmetrical models were prepared to assess the influence of the given boundary conditions on the temperature field in the can with the target material and determine the temperature field under conditions possibly corresponding to the irradiation conditions. The first geometrical model was the same geometry presented in the internal IEA study in 1997. In the second attempt, the aluminium tube and both cooling gaps were added. Finally, the entire can geometry (3rd and final geometry) with air plenum, can bottom and lid with simplified handle was introduced, as presented in figure 3.

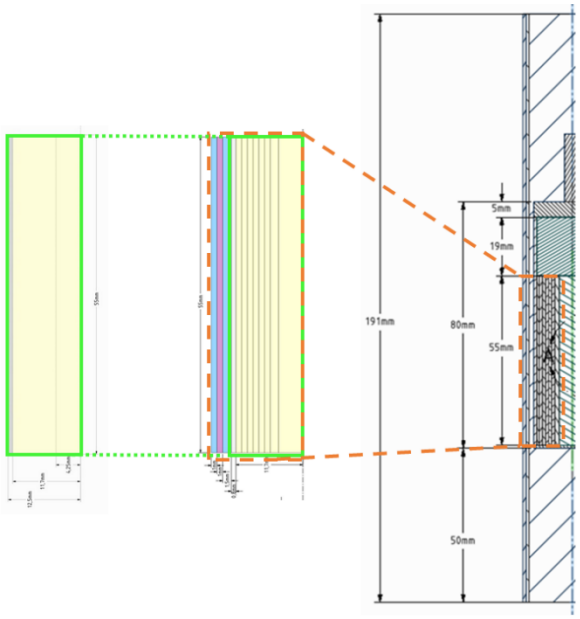

Figure 3: Model evolution overview. Left is so-called 1st geometry, middle – 2nd, right – 3rd.

A. Heat generation within the target material

The heat generation within the target material is considered constant, equal to 5W/g, which is a significant simplification. The neutron absorption rate decreases with the depth of the target material. As a result, the heat generated in the layers located closer to the can axis is significantly lower than in the layer located near the can wall, where the neutron flux is the greatest, disregarding the exact location in the reactor core. This issue is going to be addressed in the future publication of the author.

B. Boundary conditions variants

For the first geometry, five variants of boundary conditions were applied to study their impact on the target's temperature profile.

In Table 1, the calculation variants were presented. It is worth to notice that V1, V2, V3 differ from one another with density and thermal conductivity, while the Dirichlet boundary condition, constant wall temperature equal to 80°C, was identical as in [1]. In case V2 all conditions are the same as in [1], however the latest measurements shown that the thermal conductivity is higher, so the 0.75 W/(m·°C)] was assumed. In the subsequent variants (V4 -V8) the Neuman boundary condition was applied. The heat source was defined as a constant volumetric heat source equal to 5W/g multiplied by the target density. The top and bottom of the target material and aluminium can be considered adiabatic.

Table 1. Boundary condition and thermal properties of target material applied to the 1st geometry model.

Variant number	TeO_2 Density [g/cm^3]	TeO_2 thermal conductivity [W/(m·°C)]	Boundary condition on the can wall Temperature [°C] HTC [W/(m^2·°C)]
V1	4.82	0.75	$T_{w,const\ t}$=80
V2	5.67	0.65	$T_{w,const}$ =80
V3	5.67	0.75	$T_{w,const}$=80
V4	4.82	0.75	HTC=8500 T_{bulk}=50
V5	4.82	0.75	HTC=9122 T_{bulk}=50

The influence of density on the radial temperature distribution in the sample is much smaller than the influence of thermal conductivity, shown in Figure 4. Cases V1 and V3 differ in the adopted material density, which influence the volumetric heat source in the material. For a higher density (V2), the temperature in the can axis is 7 ° C higher. The influence of the adopted boundary condition on the wall is also visible - forcing a constant wall temperature results in significantly higher temperatures of the irradiated material (V1, V2, V3). Both conditions in the form of the heat transfer coefficient and coolant temperature give a similar temperature distribution in the vicinity of the can axis; near the can wall this difference is negligible. The second geometry enabled water flow modelling and analysis of the inlet coolant temperature impact. Three coolant temperatures were considered 50°C (V8), 40°C (V7) and 23°C (V6), the values correspond to the maximum inlet temperature in reactor pool cooling system, frequent inlet temperature in the summer, the frequent cooling temperature in winter respectively. As the temperature of the cooling water increases (Figure 5), the temperature of the irradiated material increases accordingly - an increase in water temperature by 10 ° C causes the temperature of the material to increase by approx. 10 ° C.

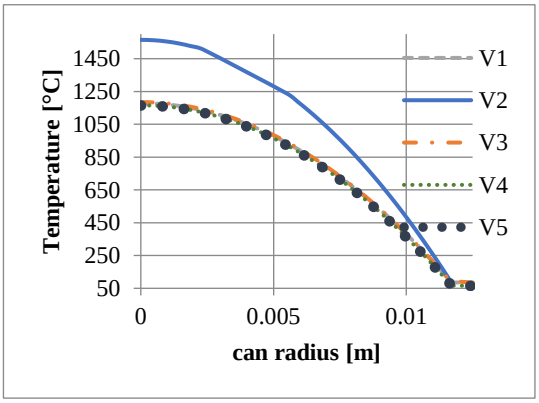

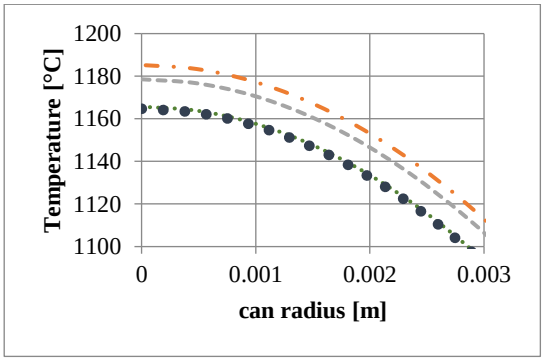

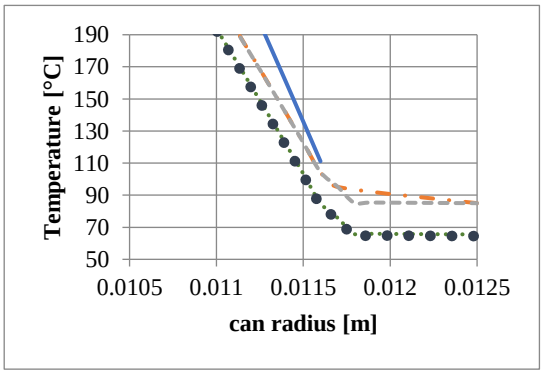

Figure 4: Temperature profile for first geometry depending on the variants presented in Table 1. Top: Overview, middle – can axis zoom, bottom-can wall zoom.

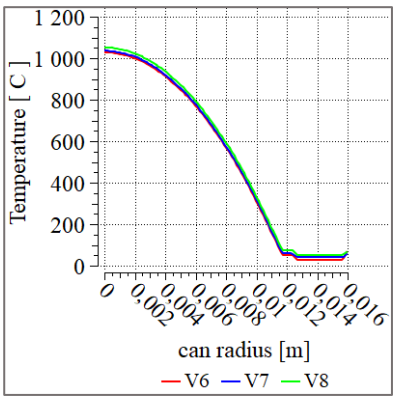

Figure 5: Temperature profile in the domain depending on the coolant temperature.

C. Impact of air

The third version of the geometric model included an irradiation channel with one irradiation can. In this case, the influence of the air in the can was considered. The grid consists of 414,733 elements and includes 423,548 compute nodes. Compared to previously discussed variants, it is an order of magnitude increase in both elements and computing nodes. The model covers the energy equation and the Navier-Stokes equations for fluids, i.e. cooling water and air. Due to the natural convection occurring in the can, it was necessary to consider the gravity defined along the can axis. The model does not consider heat transfer by radiation. The cooling water inlet condition was set as before by forcing the inlet velocity (equal to 0.25 m / s) so that in the gap between the can and the tube, a velocity of 1.20 m / s was obtained. The inlet condition for the outer gap remains the same, i.e., forcing the inlet speed to be 1.14 m / s. The temperature on the outer wall of the outer gap is 70 °C.

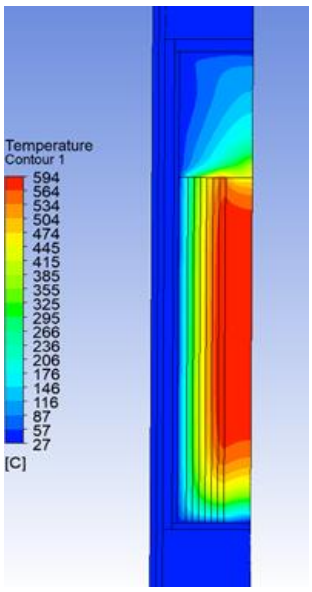

Figure 6: Temperature field in the domain.

The heat generation is significantly lower due to the 4 mm radius cylindrical orifice filled with air. The impact of free convection is visible in Figure 6, which depicts the temperature contour map on the can with target material and air plenum immersed in the water flowing in two annular gaps. The free convection influence is observable in the bottom part of the container and at the interface of the target material and air plenum in the upper part of the container. In contrast to the adiabatic boundary conditions in previous geometrical variants, the realistic model of the top and bottom of the can show the places where there is a possibility of melting may occur. It is essential to determine the temperature distribution in the whole can since the discussed previously simplified variants lead to significant maximum temperatures overestimation.

D. Thermal conductivity dependence on temperature

In Figure 7, the temperature profile of the same 3rd geometry and boundary conditions applied to the model were defined. The heat source is lower than in the previous section and equal to 3 W/g. The cases differed with the tellurium dioxide thermal conductivity definition. The blue curve represents the profile for constant thermal conductivity of the target, while the red one represents the profile for thermal conductivity decrease with temperature. Surprisingly, the maximum temperature is lower for the red curve even though the thermal conductivity is lower for higher temperatures. This observation can be explained by the difference between measured and assumed constant value. The measured values in room temperature are significantly higher than the assumed constant value. The tellurium dioxide layers closest to the aluminium can wall have the bigger thermal conductivity so that they can transfer more energy than in the constant thermal conductivity case. Furthermore, the greater thermal conductivity of the outer layers compensates for its lower value in the inner layers. It is worth noticing that the constant value was 0.75 W/(m·°C), which occurs at 300°C in the characteristic.

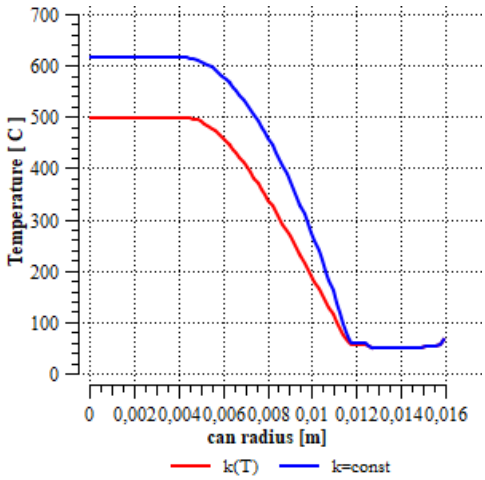

Figure 7: Temperature profile in the half-height of the target material with constant thermal conductivity assumption (k=const) and with thermal conductivity characteristic introduced (k(T)).

III. Conclusions

In this paper, the domain and boundary conditions definition influence on the temperature field in the target was discussed. The temperature profile previous IEA [1] analysis was successfully obtained, then the details were gradually added to the primary model. The prepared model enables the best estimate analysis of the target material and its surroundings temperature field. The tellurium dioxide thermal conductivity plays a vital role in the results, so it has to be defined with the greatest care. The measurements performed on the minuscule samples were required to obtain accurate results. The experiment, which aims to define the substitutive thermal conductivity of aluminium with tellurium dioxide, shall give relevant data for future analysis. Moreover, the impact of neutron absorption attenuation with target depth shall be applied to the existing model to obtain best estimate of heat sources.

IV. References

[1] W. Bykowski, “Analiza cieplna zasobnika z dwutlenkiem telluru jako materialem tarczowym w trakcie napromieniania.”,IEA internal report, Otwock, 1997.

[2] N.-S. Cheng, “Formulas for Friction Factor in Transitional Regimes,” *Journal of Hydraulic Engineering*, vol. 134, no. 9, pp. 1357–1362, Sep. 2008, DOI: 10.1061/(ASCE)0733-9429(2008)134:9(1357).

[3] Y. A. Cengel, “Heat Transfer a Practical Approach,” *MacGraw-Hill*, vol. 4, no. 9, p. 874, 2004, [Online]. Available: http://dx.doi.org/10.1007/978-3-642-20279-7_5.

[4] A. Fllaoui *et al.*, “Validation of a New Design of Tellurium Dioxide-Irradiated Target,” *Nuclear Engineering and Technology*, vol. 48, no. 5, pp. 1273–1279, Oct. 2016, DOI: 10.1016/j.net.2016.05.004.

[5] M. Chmielewski, “Thermal diffusivity measurements report”, Microelectronics and Photonics Institute, Warsaw, 2020

[6] ANSYS Inc, Fluent User Guide. Release 2020 R1, 2020

[7] F.R. Mentner, “Zonal Two Equation k-w Turbulence Models For Aerodynamic Flows “, Procedings of 23rd Fluid Dynamics, Plasmadynamics, and Lasers Conference, 1993, DOI: 10.2514/6.1993-2906

Proceedings of the European Nuclear Young Generation Forum
ENYGF'21
September 27-30, 2021, Tarragona, Spain

Nuclear data sensitivity and uncertainty analysis for reactor physics parameters of the European Sodium Fast Reactor

Jiménez-Carrascosa, Antonio[1*], García-Herranz, Nuria[1,2] and Cabellos, Oscar[1,2]

[1]Department of Energy Engineering/Division of Nuclear Engineering, Universidad Politécnica de Madrid (UPM), Spain;

[2]Instituto de Fusión Nuclear – "Guillermo Velarde", Universidad Politécnica de Madrid (UPM), Spain

*Corresponding author: antonio.jcarrascosa@upm.es

I. INTRODUCTION

Sodium-cooled Fast Reactors (SFR) have been identified as the most promising technology among the Generation-IV nuclear systems. With the aim of further enhancing the safety level of the commercial-size European Sodium Fast Reactor (ESFR), the Horizon 2020 ESFR-SMART project (European Sodium Fast Reactor – Safety Measures Assessment and Research Tools) was launched in 2017 [1].

The most recent ESFR core, proposed within the ESFR-SMART project, exhibits multiple improvements from the core physics perspective. The core has been optimised in order to reduce the overall positive reactivity feedback as a result of sodium boiling. The introduction of a sodium plenum above the fuel assemblies leads to the well-known low-void reactor concept [2]. It enhances the neutron leakage component in case of sodium boiling transient leading to an overall zero reactivity effect. Then, it is mandatory to properly characterise the main reactor physics parameters, which are subsequently used by the transient codes. Research has been already undertaken to provide high-fidelity sodium void reactivity feedback depending on the sodium boiling pattern [3]. Nonetheless, those realistic parameters should be provided along with a sensitivity and uncertainty (S/U) analysis which is essential for the safe design of this type of systems.

The most limiting ESFR End-of-Equilibrium-Cycle (EOEC) has been in-depth characterised and selected for further transient and safety analyses [4]. Then, S/U analyses are performed for the main reactor physics parameters of the EOEC core. In this work, the impact of nuclear data uncertainties is evaluated for the multiplication factor, spatial-dependent sodium-voiding reactivity coefficients, Doppler coefficient and control rod worth. Since the ESFR core presents a very high heterogeneity, a simplified modelling strategy has been selected and verified in terms of sensitivity coefficients. Nuclear data sensitivity calculations have been conducted using the state-of-the-art TSUNAMI-3D continuous energy (CE) approach which is described in Section II. Uncertainty propagation has been performed using different modern covariance matrices, namely JEFF-3.3, ENDF/B-VIII.0 and SCALE-6.2 (Section IV). This study reveals main nuclear data needs for fast spectrum sodium-cooled reactors in different covariance evaluations for a wide range of core physics parameters.

II. COMPUTATIONAL TOOLS

In this work, sensitivity analyses and uncertainty propagation have been performed using the SCALE6.2 system [5] and, specifically, the 6.2.3 version. Hereafter, the SCALE-based computational tools devoted to each step are summarised.

TSUNAMI-3D is the reference SCALE module for performing S/U analyses. TSUNAMI-3D relies on first-order perturbation theory and provides eigenvalue sensitivity to nuclear data. These coefficients ($S_{k,\alpha}$) depict the fractional change of the eigenvalue as a result of a perturbation in a particular nuclide-reaction cross-section α and it can be expressed as:

$$S_{k,\alpha} = \frac{\alpha}{k_{eff}} \frac{\delta k_{eff}}{\delta \alpha} \quad (1)$$

TSUNAMI-3D can be employed both in multigroup (MG) and continuous-energy (CE) approaches. The conventional MG TSUNAMI-3D has been successfully applied for fast spectrum reactor analyses [6]. In this work, the CE TSUNAMI-3D, specifically the most recent Contribution-Linked eigenvalue sensitivity/Uncertainty estimation via Track length importance Characterisation (CLUTCH) approach, has been used to perform the sensitivity analyses [7]. The CLUTCH method allows to compute sensitivity coefficients in a single Monte Carlo neutron transport calculation for eigenvalue responses. It relies on quantifying the importance of interactions during particle's lifetime via the number of fission neutrons generated by the particle of interest after the interaction occurs. This method presents an outstanding computational performance, both in memory and runtime, compared to the CE TSUNAMI-3D Iteration Fission Probability (IFP) method. In this paper, CE

TSUNAMI-3D CLUTCH method is applied to the ESFR S/U analyses and validated against the direct perturbation method. On the other hand, for reactivity coefficients ($\Delta\rho$), sensitivity coefficients are obtained as a variation of reactivity of the nominal state ($S_{k,\alpha}$) and the perturbed state ($S_{k_p,\alpha}$). The SCALE module TSAR allows to combine those sensitivity coefficients to compute the relative sensitivity for $\Delta\rho$ to variations of parameter α:

$$S_{\Delta\rho,\alpha} = \frac{\delta(\Delta\rho)/|\Delta\rho|}{\delta\alpha/\alpha} = \frac{\frac{S_{k_p,\alpha}}{k_p} - \frac{S_{k,\alpha}}{k}}{|\Delta\rho|} \quad (2)$$

Finally, the uncertainty quantification (σ_x) is carried out through the classical "sandwich" rule formula, where $COV_{\alpha,\alpha}$ is the covariance matrix:

$$\sigma_x = \sqrt{S_{x,\alpha}^T \cdot COV_{\alpha,\alpha} \cdot S_{x,\alpha}} \quad (3)$$

As aforementioned, three different covariance evaluations are applied in this paper, JEFF-3.3, ENDF/B-VIII.0 and SCALE6.2, which is mainly based on ENDF/B-VII.1 data. In addition, it is worth mentioning that the Nuclear Data Sensitivity Tool (NDaST) [8], developed by Nuclear Energy Agency (NEA), has been used for the uncertainty propagation based on both JEFF-3.3 and ENDF/B-VIII.0 covariance evaluations. Both covariance matrices have been processed with NJOY [9] on a 238-energy group structure by using a flat weighting function and 1MeV as incident particle energy for the secondary particle energy distribution covariances.

III. ESFR CORE MODELLING APPROACHES

The latest design on the ESFR core has been proposed within the ESFR-SMART project. The ESFR 3D (see Figure 1) core is a highly heterogeneous model including six batches -or loading patterns- for both the inner and outer fuel zones. The inner zone consists of 216 MOX-fueled hexagonal assemblies while the outer zone contains 288 assemblies. Moreover, the active part of the core is divided into several axial regions to account for exposure to different neutron fluxes. This leads to a very high heterogeneity which makes the simulation of the full core impractical. Then, in order to simplify the systematic sensitivity calculations, a R-Z model (Figure 2) has been developed. This model consists of equivalent concentric cylinders with radius determined to preserve the total mass of each material in the different core regions. In the homogenisation process, several materials of the heterogeneous model at different temperatures have been merged into one single mixture at one single temperature, corresponding to the value weighted by the mass of each involved material.

The R-Z model is firstly evaluated in terms of multiplication factor against the heterogeneous 3D core, which was characterised using KENO-VI in previous works [4]. It should be noted that calculations have been performed using the JEFF-3.1 nuclear data evaluation. As it can be seen in Table 1, the use of a simplified R-Z model does not introduce a dramatic variation in the k_{eff}, showing an effect of 300 pcm between both models.

It is important to note that the R-Z model is not conceived as surrogate model for calculating integral parameters such as multiplication factor or reactivity coefficients. In this work, the R-Z model is evaluated as a simplification for sensitivity calculations with respect to the reference model.

Table 1. Comparison of k_{eff} results for the different modelling approaches.

Model	Multiplication factor
Heterogeneous 3-D	$1.00420 \pm 5 \cdot 10^{-5}$
R-Z model	$1.00126 \pm 5 \cdot 10^{-5}$

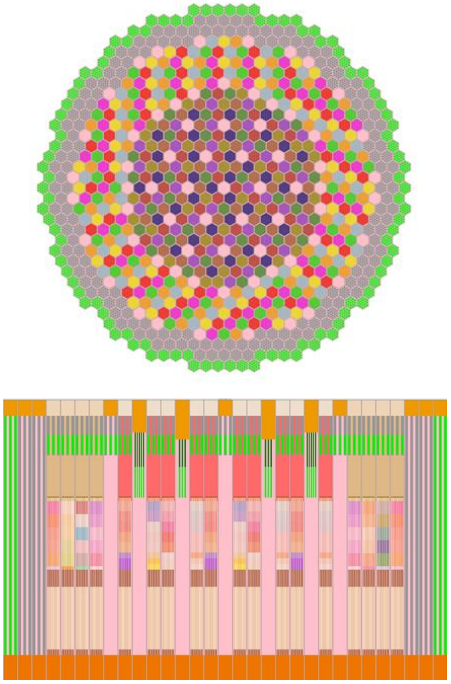

Figure 1. Radial and axial core layout of the ESFR EOEC core.

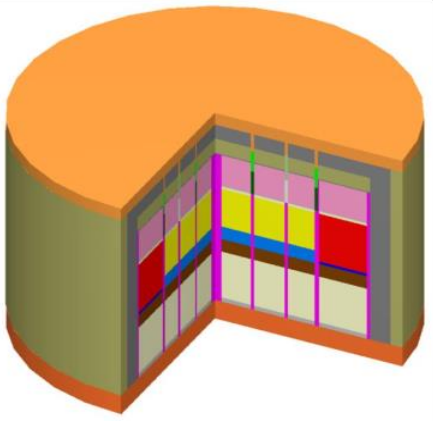

Figure 2. ESFR R-Z simplified model.

Before comparing the sensitivities computed for the different models, sensitivities provided by CE TSUNAMI-3D module for the heterogeneous 3-D core are compared to Direct Perturbation (DP) results and then the applied options for the CLUTCH method validated. Table 2 includes the sensitivities of k-eff to the nuclide concentration of the most important isotopes at specific regions: Fe-56 in cladding,

Na-23 in the coolant of the inner fuel zone and U-238 and Pu-239 in the most sensitive burnable region. It can be seen that CE TSUNAMI-3D total sensitivity coefficients are consistent with DP, with differences lower than 5% for all the nuclides.

Table 2. Integrated sensitivity coefficients for the heterogenous 3-D ESFR core.

Nuclide	Direct Perturbation	CE TSUNAMI-3D
Fe-56	$-1.7 \cdot 10^{-2} \pm 1 \cdot 10^{-4}$	$-1.7 \cdot 10^{-2} \pm 7 \cdot 10^{-4}$
Pu-239	$-1.0 \cdot 10^{-2} \pm 7 \cdot 10^{-5}$	$-1.1 \cdot 10^{-2} \pm 3 \cdot 10^{-5}$
Na-23	$-7.9 \cdot 10^{-3} \pm 5 \cdot 10^{-5}$	$-7.7 \cdot 10^{-3} \pm 3 \cdot 10^{-4}$
U-238	$-4.6 \cdot 10^{-3} \pm 3 \cdot 10^{-4}$	$-4.6 \cdot 10^{-3} \pm 1 \cdot 10^{-4}$

CE TSUNAMI-3D is properly verified against DP and then Integrated Sensitivity Coefficients (ISC) are compared for the heterogeneous and R-Z models. Figure 3 shows the major contributors to the k_{eff} and it can be observed that relative deviations are lower than 3% for all the nuclide-reactions except for Fe-56 inelastic and Na-23 inelastic, where the differences increased up to 7%.

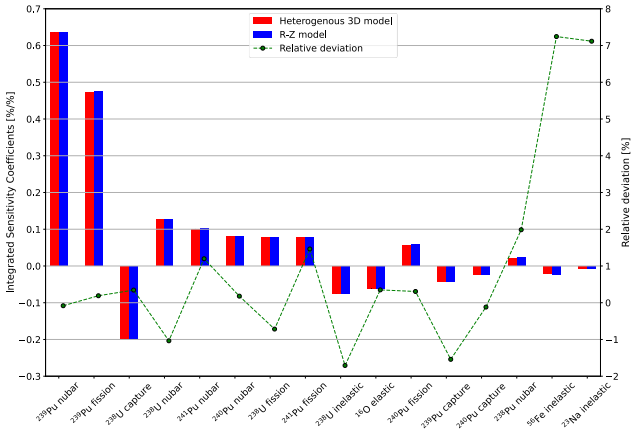

Figure 3. Comparison of Integrated Sensitivity Coefficients for the 3-D and the R-Z ESFR core (nubar refers to $\bar{\nu}$ or average number of neutrons born per fission event).

In general, the simplified R-Z is able to capture the physical behaviour which is in agreement with previous works [10]. Then, this R-Z is selected for systematic S/U calculations.

IV. SENSITIVITY AND UNCERTAINTY ANALYSIS

In this Section, the R-Z model is employed for evaluating nuclear data uncertainties for the multiplication factor and main reactivity coefficients.

A. S/U analysis in k_{eff}

The most important ISC have been shown in Figure 3 but are in-depth discussed in this subsection. It can be seen that k_{eff} is particularly sensitive to the Pu-239 ν and fission and U-238 capture cross-sections. These results are consistent with sensitivity analysis results for other SFRs such as ASTRID [6].

Uncertainties in multiplication factor based on different covariance libraries are shown in Table 3. The use of SCALE6.2 covariance data leads to a higher overall uncertainty compared to JEFF-3.3 evaluation, of about 320 pcm higher. A detailed analysis provides insight into these differences.

Table 3. Uncertainties in nominal k_{eff} for the R-Z model based on different covariance evaluations ($\Delta k/k$ in pcm).

SCALE6.2-56g	JEFF-3.3	ENDF/B-VIII.0
1346	1045	803

Table 4 and Table 5 show the major nuclide-reactions contributing to the uncertainty in k_{eff} using SCALE6.2 and JEFF-3.3. covariance data respectively. A very significant discrepancy between both evaluations can be observed for U-238 inelastic. When working with SCALE6.2 covariances, the uncertainty contribution is 1.174% while with JEFF-3.3 matrix, this contribution reduces to 0.48%. This is due to the fact that for neutron energies higher than 1 MeV, the uncertainty reported in SCALE-6.2 evaluation rises above 20%. In contrast, this uncertainty is lower than 10% in JEFF-3.3 leading to the obtained differences.

On the other hand, the main contributor when applying JEFF-3.3 data is Pu-240 fission whose contribution is close to 0.6%. This is in very good agreement with ENDF/B-VIII.0 (Table 6) but using the SCALE6.2 matrix, this value is lower than 0.1%. It is possible now to identify the main nuclear data needs in each evaluation for fast spectrum systems. In general, the reduction of uncertainty in U-238 inelastic scattering appears to be mandatory in future evaluations.

Table 4. Major nuclide-reactions contributing to the uncertainty in k_{eff} using SCALE6.2-56 covariance data.

Quantity	$\Delta k/k$ (%)
U-238 inelastic	1.174
U-238 capture	0.255
Pu-239 capture	0.218
Pu-239 χ	0.200
U-238 inelastic-elastic	0.196

Nonetheless, ENDF/B-VIII.0 already includes several improvements compared to SCALE6.2, which is mainly based on ENDF/B-VII.1. The overall uncertainty in k_{eff} is reduced by 550 pcm mostly due to the reduction of uncertainty in U-238 inelastic scattering.

Table 5. Major nuclide-reactions contributing to the uncertainty in k_{eff} using JEFF-3.3 covariance data.

Quantity	$\Delta k/k$ (%)
Pu-240 fission	0.594
U-238 inelastic	0.480
Pu-239 χ	0.453
Pu-240 fission-capture	-0.417
U-238 inelastic-fission	-0.349

It is also important to note that target accuracies for fast reactors are exceeded in k_{eff} since the overall uncertainty is recommended to be lower than 300 pcm [11]. Then, efforts in nuclear data mining and evaluation are still to be addressed for the design and licensing of advanced reactors.

Table 6. Major nuclide-reactions contributing to the uncertainty in k_{eff} using ENDF/B-VIII.0 covariance data.

Quantity	$\Delta k/k$ (%)
Pu-239 fission	0.554
U-238 capture	0.253
U-238 inelastic	0.240
Pu-239 χ	0.207
Pu-239 capture	0.203

B. S/U analysis in main reactivity coefficients

A S/U analysis has been carried out for the following reactivity responses: five spatial-dependent sodium void scenarios (Figure 4), Doppler coefficient (+300K in the inner core fuel) and control rod worth.

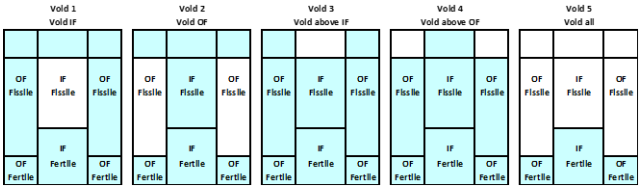

Figure 4. Zone-wise sodium void scenarios.

Table 7 shows the void reactivity worth for the five considered scenarios and the total propagated uncertainty provided by each covariance matrix. Uncertainties estimated with JEFF-3.3 are lower than those obtained with SCALE6.2 and ENDF/B-VIII.0. Pu-239 fission is the most important contributor to the overall uncertainty predicted by JEFF-3.3. On the other hand, uncertainties provided by both SCALE6.2 and ENDF/B-VIII.0 are mainly driven by Na-23 elastic and inelastic scattering.

Table 7. Total propagated uncertainties for all the sodium void scenarios based on different covariance evaluations.

Void case	Void worth (pcm)	Nuclear data uncertainty (pcm)		
		SCALE6.2	JEFF-3.3	ENDF/B-VIII.0
1	1116	58 (5%)	44 (4%)	60 (5%)
2	1013	69 (7%)	51 (5%)	71 (7%)
3	-445	19 (4%)	15 (3%)	12 (3%)
4	-427	17 (4%)	15 (3%)	11 (3%)
5	989	114 (12%)	84 (9%)	111 (11%)

For sodium void uncertainties, elastic and inelastic scattering of structural and coolant materials become more important compared to the multiplication factor uncertainty breakdown. In scenarios 3 and 4, where only the sodium plenum is voided, Fe-56 elastic scattering is the most important contributor to the overall uncertainty. However, uncertainties are especially large for the scenario 5, where both the active fissile core and the sodium plenum are voided. In this case, Pu-239 fission is again the most important contributor in JEFF-3.3 and Na-23 scattering reactions are the key quantities in both SCALE6.2 and ENDF/B-VIII.0 data.

Regarding Doppler coefficient, Table 8 shows the overall uncertainty obtained using different covariance data. In general, uncertainty is very low for this parameter compared to the sodium void scenarios since overall uncertainty is lower than 6% in all cases. Uncertainty is mostly driven by structural nuclides such as Fe-56 and Cr-52.

Table 8. Total propagated uncertainty for Doppler coefficient based on different covariance evaluations.

Temp. coeff. (pcm)	Nuclear data uncertainty (pcm)		
	SCALE6.2	JEFF-3.3	ENDF/B-VIII.0
-148	9 (6%)	6 (4%)	5 (4%)

Finally, control rod worth propagated uncertainty is shown in Table 9. As it can be seen, this parameter does not present large overall uncertainty values since they are around 2% with respect to the control rod reactivity feedback. U-238 inelastic scattering is again the main contributor when using SCALE6.2 covariance matrix. For JEFF-3.3, Pu-240 fission is the most important quantity while Pu-239 fission and Na-23 elastic scattering are the key pairs in ENDF/B-VIII.0.

Table 9. Total propagated uncertainty for control rod worth based on different covariance evaluations.

CR. worth (pcm)	Nuclear data uncertainty (pcm)		
	SCALE6.2	JEFF-3.3	ENDF/B-VIII.0
-5419	128 (2%)	101 (2%)	72 (1%)

V. CONCLUSIONS

A detailed S/U analysis has been performed for the ESFR core at its EOEC state. Main reactor physics parameters have been analysed in order to further use them for the safety analysis of the ESFR core. It was observed that the high level of heterogeneity that presents the core makes almost impractical its use for systematic S/U analyses. Then, a simplified R-Z model has been developed and validated with respect to the reference one. Sensitivity coefficients illustrated that the simplified model is able to capture the physical behaviour of the heterogeneous core. Then, CE TSUNAMI-3D has been used for this study along with different covariance evaluations: SCALE6.2, JEFF-3.3 and ENDF/B-VIII.0. As a result, the most critical nuclear data have been identified for each covariance matrix. In JEFF-3.3, the main contributors to the uncertainty of the evaluated parameters are U-238 inelastic scattering and capture, Pu-240 fission, Pu-239 fission, capture and χ, Na-23 elastic scattering and capture and Fe-56 elastic scattering. On the other hand, in ENDF/B-VIII.0, Na-23 inelastic scattering plays a very relevant role along with those contributors already identified JEFF-3.3.

ACKNOWLEDGMENTS

The research leading to these results has received funding from the Euratom research and training programme 2014-2018 under Grant Agreement Number 754501 (ESFR-SMART Project) and the Grant Agreement Number 847552 (SANDA Project).

VI. References

[1] K. Mikityuk et al., "ESFR-SMART: new H2020 project on SFR safety," in Int. Conf. on Fast Reactors (FR17), Yekaterinburg, Russia, 2017.

[2] J. Guidez et al., "New safety measures proposed for ESFR in H2020 ESFR-SMART project," in GIF Symposium, Paris, France, 2018.

[3] A. Jiménez-Carrascosa, N. García-Herranz, "Use of similarity indexes to identify spatial correlations of sodium void reactivity coefficients," Nuclear Engineering and Technology, vol. 52, no. 11, 2020.

[4] U. Baker et al., "Evaluation of the ESFR End of Equilibrium Cycle State: Spatial Distribution of Reactivity Coefficients", Nuclear Engineering and Radiation Science, submitted, 2021.

[5] B. Rearden, M. Jesse, "SCALE Code System: ver. 6.2," 2016.

[6] N. García-Herranz et al., "Nuclear data sensitivity and uncertainty assessment of sodium voiding reactivity coefficients of an ASTRID-like sodium fast reactor," EPJ Web Conf. 146, 2017.

[7] C. Perfetti et al., "SCALE continuous-energy eigenvalue sensitivity coefficient calculations," Nuclear Science and Engineering, vol. 182, 2016.

[8] J. Dyrda et al., "The new OECD-NEA Nuclear Data and Sensitivity Tool (NDaST)," in ANS Winter Meeting, Washington DC, USA, 2015.

[9] D.W. Muir et al., "The NJOY Nuclear Data Processing System, version 2016," Los Alamos National Laboratory, 2016.

[10] G. Aliberti et al., "Impact on sensitivity coefficients of typical approximations used in scoping sensitivity analyses," in Int. Conf. M&C2011, Rio de Janeiro, Brazil, 2011.

[11] M. Salvatores, R. Jacqmin, OECD/NEA WPEC-SG26, 2008.

Proceedings of the European Nuclear Young Generation Forum
ENYGF'21
September 27-30, 2021, Tarragona, Spain

One-dimensional investigation of turbulent heat transfer along corroded rod in vertical channels at supercritical pressure conditions

Wiltschko, Fabian[1*], Otic, Ivan[1] and Vit, Jan[2]

[1] Karlsruhe Institute for Technology (KIT), Germany, 2 Centrum Výzkumu Řež (CVŘ), Czech Republic

*Corresponding author: *Fabian.Wiltshko@kit.edu*

I. INTRODUCTION

For an engineering design of nuclear reactors, one dimensional analysis of the heat transfer from the fuel rods to the coolant flow can provide important first assessments of the cladding temperatures. In super-critical water reactors (SCWR), high demands on the thermal stability of the materials used in such a reactor, require a precise modelling of the cladding temperatures of the fuel rods. Applications of suitable Nusselt correlations in thermal hydraulic codes is very important to propose a new reactor design. There are numerous Nusselt correlations available in the literature. Most are developed for single phase flow at subcritical pressure conditions, like e.g. the Dittus Boelter correlation [1] but there exist correlations for supercritical pressure fluids as well, see e.g., Jackson [2], Cheng [3], Gnielinski [4] and Krasnoschekov and Protopopov [5], to mention a few.

The fuel rods in SCWRs are exposed to a highly corrosive environment. In the small modular supercritical water reactor (SM-SCWR) proposed by Schulenberg and Otic [6], which serves as a reference for the present investigation, a minimum refuelling cycle of 2 years is aimed to be achieved. Within this time, the outer surface of the fuel rods will be damaged by corrosion and overdrawn by an oxide layer. Both of those effects will result in surface roughness of the fuel rod walls, which can have an influence on the heat transfer to the coolant flow. In this work the effect of surface roughness on the heat transfer to supercritical fluid shall be investigated by one-dimensional analysis, using typical values for the roughness of cladding materials in SCWRs, provided by Penttilä [7].

Furthermore, profilometry measurements of surface roughness at Centrum Výzkumu Rež (CVŘ) has been performed on specimen previously exposed to supercritical water (SCW) conditions corresponding to SM-SCWR proposal (austenitic steel, 600°C). Profilometer Bruker Stylus DektakXT [8] was used and evaluation was done with cut-off value 0.8 mm. However, this specimen was intended for microstructure evaluation on scanning electron microscope (SEM) and therefore its surface was fine grinded before exposition, therefore this type of surface is an ideal state for fuel cladding.

II. CORRELATIONS

The heat transfer coefficient α, which is required for the calculation of wall temperatures T_w, is calculated using the Nusselt number Nu, the hydraulic diameter d and the thermal conductivity of the fluid κ. Following, the wall temperature T_w can be calculated, from the bulk temperature T_b, the applied heat flux q and the heat transfer coefficient α.

$$\alpha = \frac{Nu \cdot d}{\kappa} \tag{1}$$

$$T_w = T_b + \frac{q}{\alpha} \tag{2}$$

Generally, the Nusselt number depends on the Reynolds number Re and the Prandtl number Pr of the fluid and can be expressed by the commonly used equation of Dittus and Boelter [1]:

$$Nu_b = 0.023 Re_b^{0.8} Pr_b^{0.4} \tag{3}$$

The subscript b denotes values for the bulk flow. However, this equation is developed for fluids at subcritical pressure conditions in simple tubes. The Nusselt correlation proposed by Jackson et al. [2] is developed for supercritical pressure fluids:

$$Nu = 0.021 Re_b^{0.8} Pr_b^{0.4} \left(\frac{\rho_w}{\rho_b}\right)^{0.3} \left(\frac{\overline{c_p}}{c_{pb}}\right)^n \tag{4}$$

$$n = \begin{cases} 0.4 \;\; if \; T_b < T_w < T_{pc} \;\; or \; 1.2T_{pc} < T_b < T_w \\ n_1 = 0.4 + 0.2\left(\frac{T_w}{T_{pc}} - 1\right) \;\; if \;\; T_b < T_{pc} < T_w \\ n_1\left[1 - 5\left(\frac{T_b}{T_{pc}} - 1\right)\right] \; if \; T_{pc} < T_b < 1.2T_{pc} \; and \; T_b < T_w \end{cases}$$

The subscripts w and b denote the values at wall and bulk temperature, respectively. The subscript pc denotes the pseudo critical point, ρ is the density and c_p is the specific isobaric heat capacity of the fluid. The average specific heat $\overline{c_p} = (h_w - h_b)/(T_w - T_b)$ is calculated from the specific

enthalpy at wall- and bulk temperature. The correlation of Cheng et al. [3] is also developed for application to supercritical fluids. In comparison to the Jackson correlation [2], in the correlation proposed by Cheng et al. [3], a dimensionless parameter, the acceleration number π_A is used to correct the deviation in heat transfer from sub-critical pressure fluids to super-critical pressure fluids:

$$\pi_A = \frac{\beta}{c_p}\frac{q}{G} \tag{5}$$

$$Nu = 0.023 Re_b^{0.8} Pr_b^{1/3} F \tag{6}$$

$$F = \min(F_1, F_2) \tag{7}$$

$$F_1 = 0.85 + 0.776(\pi_A * 1000)^{2.4} \tag{8}$$

$$F_2 = \frac{0.48}{(\pi_{A,pc}*1000)^{1.55}} + 1.21\left(1 - \frac{\pi_A}{\pi_{A,pc}}\right) \tag{9}$$

The acceleration number π_A is calculated from the relation of the thermal expansion coefficient β and the specific heat capacity c_p and the relation of the heat flux q and the mass flux G. However, those correlations do not consider the effect of the surface roughness on the heat transfer. Therefore, the correlation of Gnielisnki [4], which is dependent on the friction factor f, is applied in this investigation:

$$Nu_b = \frac{\left(\frac{f}{8}\right)(Re_b - 1000)Pr_b}{1+12.7\left(\frac{f}{8}\right)^{1/2}\left(Pr_b^{2/3}-1\right)}\left(\frac{Pr_b}{Pr_w}\right)^{0.11}\left(1+\left(\frac{d}{z}\right)^{2/3}\right) \tag{10}$$

The correlation is developed for sub-critical conditions, but for $T_b > T_{pc}$, the term $\left(\frac{Pr_b}{Pr_w}\right)^{0.11}$ is replaced by $\left(\frac{T_b}{T_w}\right)^{0.45}$, to make the correlation applicable to super-critical conditions. Here, z is the length coordinate. Furthermore, the correlation of Krasnoschekov and Protopapov [5], which is also dependent on the friction factor f, which was developed for supercritical heat transfer (SCHT) to CO_2 with high temperature drops, is applied in this work.

$$Nu_b = \frac{\left(\frac{f}{8}\right)Re_b Pr_b}{12.7\left(\frac{f}{8}\right)^{1/2}\left(Pr_b^{2/3}-1\right)+1.07}\left(\frac{\rho_w}{\rho_b}\right)^{0.3}\left(\frac{\overline{c_p}}{c_{pb}}\right)^{n} \tag{11}$$

$$n = \begin{cases} 0.4 \quad if\ \frac{T_w}{T_{pc}} \le 1\ or\ \frac{T_b}{T_{pc}} \ge 1.2 \\ n_1 = 0.22 + 0.18\frac{T_w}{T_{pc}} \quad if \quad 1 \le \frac{T_w}{T_{pc}} \le 2.5 \\ n_1 + (5n_1 - 2)\left(1 - \frac{T_b}{T_{pc}}\right)\ if\ 1 \le \frac{T_b}{T_{pc}} \le 1.2 \end{cases}$$

The Gnielinski [4] as well as the Krasnoschekov [5] correlation were developed using the friction factor proposed by Filanenko [9]:

$$f = 1/(1.82 log(Re_b) - 1.64)^2 \tag{12}$$

Here, the friction factor only depends on the bulk Reynolds number. However, there exist correlations for the friction factor, which consider the surface roughness ε. Pandey and Laurien [10] suggested the friction factor correlation developed by Swamee and Jain [11] for the application to supercritical pressure fluids, which can be applied for $5000 < Re < 10^8$ and $10^{-7} < \frac{\varepsilon}{d} < 0.05$:

$$f = 0.25\left[log_{10}\left(\left(\left(\frac{\varepsilon}{d}\right)/3.7\right) + \left(\frac{5.74}{Re_b^{0.9}}\right)\right)\right]^{-2} \tag{13}$$

In the present investigation, the friction factor proposed by Filanenko, as well as the friction factor proposed by Swamee and Jain are applied to the Nusselt correlations of Gnielinski [4] and Krasnoschekov [5] and the results are compared.

III. Results

a. Correlation assessment

Heat transfer correlations are first evaluated against existing data [12, 13, 14] applying Swamee and Jain [11] friction factor to the Nusselt correlations of Gnielinski [4] and Krasnoschekov [5]. The Gnielinski [4] and the Krasnoschekov [5] correlation is first used in the standard form, with the friction factor correlation of Filanenko [9] applied to it, and second with the friction factor correlation of Swamee and Jain [11]. Since in the test data [12, 13, 14] provides no information on the surface roughness of the tubes, the roughness is estimated according to the work of and Fang et al. [15], as a roughness height of $\varepsilon = 0.5\ \mu m$ for the calculation of the Swamee and Jain [11] friction factor.

Table 1. Averaged errors and standard deviation of the calculated wall temperatures in comparison to the experimentally obtained wall temperatures from the water and the CO_2 database, including percentages of datapoints in the error ranges of 5%, 10%, 15%, 20% and >20%.

Correlation	Water database							CO_2 database						
	e_{avg}	σ	e_5	e_{10}	e_{15}	e_{20}	$e_{>20}$	e_{avg}	σ	e_5	e_{10}	e_{15}	e_{20}	$e_{>20}$
Cheng	2,6	2,6	85,9	98,0	99,2	99,5	0,5	3,8	9,9	38,4	71,5	86,3	92,6	7,4
Jackson	2,4	2,4	91,7	96,5	100	100	0,0	3,8	11,7	42,3	70,1	83,5	88,0	12,0
Krasnoschekov	2,9	2,9	81,6	95,2	99,7	100	0,0	3,4	9,1	34,5	72,5	86,6	93,0	7,0
Krasnoschekov and Swamee	3,0	3,0	79,3	95,7	99,5	100	0,0	3,7	9,4	25,4	67,6	83,5	92,3	7,8
Gnielinski	12,0	24,9	55,9	75,1	90,1	92,3	7,6	10,9	29,2	0,4	16,9	40,5	59,2	40,8
Gnielinski and Swamee	12,0	24,9	52,6	74,2	90,1	92,3	7,6	11,0	29,2	0,4	16,9	38,0	58,8	41,2

Furthermore, for comparison, the Jackson [2] and the Cheng [3] correlations are applied and evaluated against the data [12, 13, 14]. The data of Razumovskiy et al. [12] consists of supercritical water in a heated tube, with an inner diameter d_i of 6.28 mm, 6.25 mm, and 9.5 mm, with inlet temperatures ranging from 307.8 °C to 395.5 °C, and heat fluxes in a range from 104 kW/m² to 2660.7 kW/m². The pressure is 23.5 MPa and the mass flux is 2193 kg/m²s in all the investigated cases. Furthermore, data of supercritical pressure CO_2, in heated tubes by Kurganov et al. [13, 14] is also considered. The calculation setup for the one-dimensional approach is as follows: Inner diameter of 22.7 mm, with inlet temperatures in the range of 18 °C to 44 °C, heat fluxes ranging from 40.596 kW/m² to 430.5 kW/m², and mass fluxes in the range of 248 kg/m²s to 2140 kg/m²s at pressure of 9 MPa. To assess the performance of the correlations for the heat transfer, the calculated and the experimentally measured wall temperatures are compared. The data [12, 13, 14] includes bulk enthalpy values, for which thermophysical properties are calculated by the NIST REFPROP [16] programme. The Nusselt number is calculated for each correlation mentioned above. Using this, the wall temperatures are calculated using equations (1) and (2). Then, the relative error in percent between the measured and the calculated wall temperature is calculated:

$$e = 100\,\frac{|T_{w,calc} - T_{w,exp}|}{T_{w,exp}} \tag{18}$$

In Table 1, the averaged error e_{avg}, standard deviation σ, as well as the percentages of datapoints within an error range of 5% (e_5), 10% (e_{10}), 15% (e_{15}), 20% (e_{20}), and >20% ($e_{>20}$), are shown for the water database and the CO_2 database, respectively.

Generally, the Jackson [2], Cheng [3] and Krasnoschekov [5] correlations perform good on the selected test data, as can be seen in Table 1. Also, for the Kransoschekov [5] and the Gnielinski [4] correlation, the results are similar, if the Filanenko [9] or the Swamee [11] friction factor is applied. In the investigation of Kirillov et al. [17], the surface roughness of the investigated 4 m long vertical heated pipe is given with 0.63 – 0.8 µm (see Figure 1).

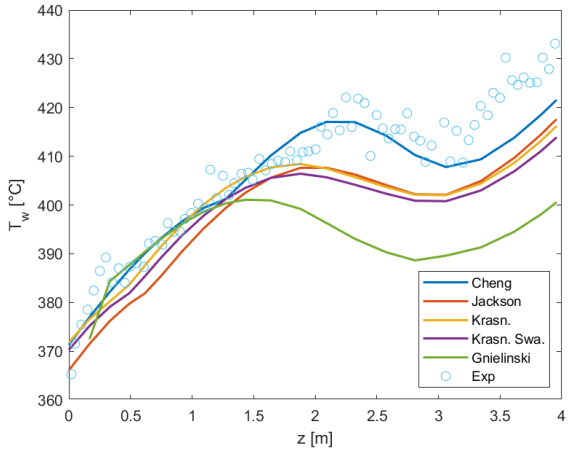

Figure 1. Wall temperatures in test case of Kirillov et al. [17].

Therefore, the correlations are applied to the test case of Kirillov, using water with mass flux 1500 kg/m²s, heat flux 874 kW/m², pressure 24.0 MPa and inlet temperature of 325 °C. The surface roughness used in the Swamee friction factor correlation [11] is chosen to be 0.715 µm, which is the arithmetic average in the given range. In this case, the combination of Krasnoscheko [5] and Swamee [11] correlation indicates that there is only a small difference in the results of the standard Krasnoschekov correlation and the combination of Krasnoschekov with Swamee friction factor, see Figure 1. This shows that the application of the Swamee friction factor [11] and Krasnoschekov [5] may provide good results. Since the performance against the selected test data [12, 13, 14] of the Krasnoschekov correlation [5] is better in comparison to the Gnielinski correlation [4], in the following hypothetical test, the Krasnoschekov correlation [5], with the Swamee friction factor [11] applied to it is used.

b. Application to SCWR design conditions

The investigation of turbulent heat transfer from a corroded rod to water at super-critical pressure is based on the proposed reactor design of Schulenberg and Otic [6]. One dimensional heat transfer approach for SCWR conditions is implemented to commercial software MATLAB [18]. The analysis considers a single fuel rod in an annular channel, which has the same hydraulic diameter $d_h = 4.61mm$ as one subchannel in the proposed reactors fuel assembly. The diameter of the fuel rod is $d = 8mm$, where the outer diameter of the annulus is chosen to be $D = 12.61mm$. The heated length of the fuel rod is, according to the proposed design, chosen to be $L_{heat} = 1680mm$. The proposed reactor consists of 7 heat up stages. Since the transition region from liquid like to gas like fluid is the most interesting, the second heat up stage is chosen for this investigation.

The inlet temperature in the second heat-up stage is $T_{in} = 360°C$. The mass flux is $G = 2042\ kg/s$, which results in an inlet Reynolds number of 138.000. The operating pressure is $p = 25MPa$. The power distribution along the rod is described by:

$$q(x) = q_{max} * sin\left(\pi \frac{x + x_R}{L_{heat} + 2x_R}\right) \tag{19}$$

The peak heat flux is $q_{max} = 1550\ kW/m^2$, the reflector saving is $x_R = 200\ mm$ in the proposed design [6]. According to investigations of Penttilä [7], who tested several typical materials for the cladding, the roughness height of the cladding material will be in the range of $\varepsilon = 2 \ldots 100\mu m$, after exposition to the conditions inside an SM-SCWR, when an exposure time of up to 3000 hours is considered. Therefore, roughness heights of 0.5 µm as a reference, 2 µm, 5 µm, 20 µm, 50 µm and 100 µm are investigated for the case of a single rod inside a circular tube. Furthermore, the experimentally obtained roughness data from CVŘ is used in this investigation. Initially, the surface roughness was 52.5 nm, after the exposition in supercritical water (SCW) at 600°C for 800 hours, the roughness increased to 343.7 nm.

The required fluid properties are calculated from the bulk enthalpy, using the NIST REFOPROP [16] programme. The annulus is divided into 168 sections with a length of 1 cm and the bulk enthalpy is calculated for each section, using the mass flow rate $\dot{m}$ and the heat $\dot{Q}$, as:

$$h_{n+1} = h_n + \frac{\dot{Q}_n}{\dot{m}} \quad (20)$$

Then, using equations (1) and (2), wall temperatures are calculated using the Nusselt correlations of Jackson [2] and Cheng [3], as well as using the Nusselt correlation of Krasnoschekov [5], to which the different friction factors, calculated depending on ε, using the correlation of Swamee [10] are applied. Figure 2 shows the wall temperatures calculated by the selected correlations for the considered roughness heights according to Penttilä [7]. With increasing roughness height, the wall temperature calculated using the Krasnoschekov correlation [5] decreases. Furthermore, the influence of roughness weakens with increasing roughness, if the difference between the wall temperature corresponding to a roughness height of 2 µm and 5 µm is compared to the difference between the temperature courses of 50 µm and 100 µm, see Figure 2.

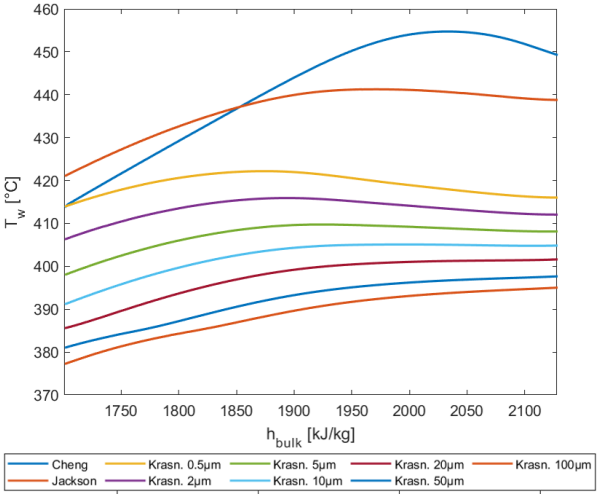

Figure 2. Wall temperatures for different surface roughness of the fuel rod with inlet temperature of 360°C

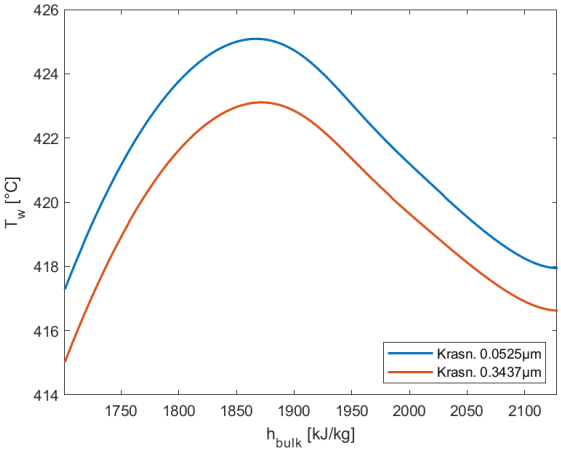

Figure 3. Wall temperatures for different surface roughness obtained from CVR experiment

IV. CONCLUSION

In this work, one dimensional approach is implemented in MATLAB [18]. First, several heat transfer and friction factor correlations proposed in the literature are tested against existing experimental data for SCW conditions [11, 12, 13, 16]. Then, the best performing combination of Nusselt- and friction factor correlations has been chosen to investigate the influence of surface on heat transfer. Typical surface roughness of common cladding materials, exposed to the conditions inside an SCWR for up to 3000 hours was used in the one-dimensional analysis of heat transfer along a corroded rod. As expected, the roughness of the fuel rod increases the heat transfer and therefore results in lower wall temperatures. Furthermore, surface roughness is determined experimentally for a specimen with polished surface, before and after exposition to SCW. In a next step, specimen with a realistic initial roughness will be investigated. Additionally, within the ECC-SMART project, the presented results will be verified by an experimental investigation of the heat transfer along a corroded rod and a non-corroded rod.

Funding

This work has been founded by the European Commission as part of their project ECC-SMART, grant agreement ID: 945234, 2020.

V. References

[1] F. Dittus, L. Boelter, “Heat transfer in automobile radiators of the tubular type”, Univ. Calif. Publ. Eng., vol. 2, no 13, 1930, pp 443-461.

[2] J. Jackson, “Validation of extended heat transfer equation for fluids at supercritical pressure”, ISSCWR-4, Berlin, Germany, Mar. 8-11, paper no. 24.

[3] X. Cheng, Y. H. Yang, S. F. Huang, “A simplified method for heat transfer prediction of supercritical fluids in circular tubes”, Ann. Nucl. Energy, vol. 36, no. 1, 2009, pp. 1120-1128.

[4] V. Gnielinski, “New equations for heat and mass transfer in turbulent pipe and channel flow”, Int. Chem. Eng., vol. 16, no. 2, 1946, pp. 359-368.

[5] E. Krasnoschekov, V. Protopopov, “Experimental study of heat exchange in carbon dioxide in the supercritical range at high temperature drops”, High Temp., vol. 4, no. 3, 1966, pp. 375-382.

[6] T. Schulenberg, I. Otic, “Suggestions for design of a small modular reactor”, ISSCWR-10, Prague, Czech Republic, Mar. 15-19, 2021.

[7] S. Penttilä, “Structure materials corrosion testing and modelling assessment in supercritical water”, PhD dissertation, Dpt. of Chem. and Metall. Engin., Aalto Univ., 2020, Finland.

[8] Bruker Corporation, “DektakXT stylus profilometer”, Billerica; MA, USA.

[9] G. Filanenko, “Gydravlicheskoye soprotivlenyie v trubakh, Teploenergetica”, vol. 1, no. 4, 1954, pp. 40-44 (Russian).

[10] S. Pandey, E. Laurien, “Heat transfer analysis at supercritical pressure using two layer theory”, J. Supercit. Fluids, 2016, pp. 80-86.

[11] P. Swamee, A. Jain, “Explicit equations for pipe flow problems”, J. Hydraulics Div., vol. 102, no. 5, 1976, pp.657-664.

[12] V. G. Razumovskiy, E. N. Pis’mennyi, K. Sidawi, I. L. Pioro, A. E. Koloskov, “Experimental heat transfer in annular channel and 3-rod bundle cooled with upward flow of supercritical water”, JNERS, vol. 2, no. 1, 2016, pp 1-8.

[13] V. A. Kurganov, A. G. Kaptilnyi, “Flow structure and turbulent transport of a supercritical pressure fluid in a vertical tube under the conditions of mixed convection. Experimental data”, Int. J. Heat Mass Transfer, vol 36, no. 1, 1993, pp. 3383-3392.

[14] V. A. Kurganov, A. G. Kaptilnyi, “Velocity and enthalpy fields and eddy diffusivities in a heated supercritical fluid flow”, Exp. Therm. Fluid Sci., vol 5, no. 1, 1992, pp 465-178

[15] X. Fang, Y. Xu, X. Su, R. Shi, “Pressure drop and friction factor correlations of supercritical flow”, Nucl. Eng. Des., vol. 242, no. 1, 2012, pp. 323-330.

[16] E. W. Lemmon, “NIST Standard Reference Database 23: Reference Fluid Thermodynamic and Transport Properties – REFPROP”, Version 10.0, NIST, 2018.

[17] P. Kirillov R. Pometko, A. Smirnov, V. Grabezahnaia, I. Pioro, R. Duffey, H. Khartabil, “Experimental study on heat transfer to supercritical water flowing in 1- and 4-m-long vertical tubes”, GLOBAL 2005, Tsukuba, Japan, Oct 9-13, 2005, paper no. 518.

[18] MATLAB, 2018. 9.7.0.1190202 (R2019b), Natick, MA, USA, The MathWorks Inc.

Proceedings of the European Nuclear Young Generation Forum
ENYGF'21
September 27-30, 2021, Tarragona, Spain

Thermal-hydraulic analysis of a VVER-1000/V-320 reactor with TRACE5p5 code.

Redondo-Valero, Elena[1*], Queral, Cesar[1] and Sanchez-Espinoza, Victor[2]

[1] Universidad Politécnica de Madrid (UPM), Spain; [2] Karlsruhe Institute of Technology (KIT), Germany

*Corresponding author: elena.redondo.valero@alumnos.upm.es

I. INTRODUCTION

VVER reactors are the most common reactor type in the world. Moreover, much of the Gen-III reactors that are being built or have recently come into operation are advanced VVER-1000 and VVER-1200. Therefore, there is a growing interest in studying their behaviour under both anticipated and accidental transients. A peculiarity of the VVER-reactors is the hexagonal fuel assembly design and the horizontal steam generators with a larger amount of coolant inventory compared to the Western-type PWR.

This work is being carried out within the ISASMORE project, aiming to analyse the thermal-hydraulic behaviour of different designs e.g. the VVER-1000, and the advanced VVER-1200 reactor design. In [3] the coolant transient in a VVER-1000 reactor was investigated with RELAP/PARCS. Later in [2] and [1] a 3D model of the Reactor Pressure Vessel (RPV) and the core of the VVER-1000 reactor was developed for TRACE-Version4.

The paper describes the joint effort of the Universidad Politécnica de Madrid (UPM) and the Karlsruhe Institute of Technology (KIT), embedded in a research cooperation, in order to develop integral plant models of the VVER-1000/V-320 reactor for the system thermal-hydraulic code TRACE5p5 that pave the way for the follow-up simulation of the plant response during transients and accidents.

II. SHORT DESCRIPTION OF THE VVER-1000/V-320

VVER-1000/V-320, is the most common Russian design Pressurizer Water Reactor. It is a 4-loops reactor with a thermal power of 3000 MW, and an electric output of 1000 MW [4]. The Reactor Coolant System (RCS) consists of four loops, where each one consists of with a main circulation pump and a horizontal steam generator. The hot leg is connected to the RPV at the same angular position as the cold leg. The four loops connections are not-symmetric in azimuthal direction, but loops 1 and 4 are separated with an azimuthal angle of 55º each other. The total primary side water volume is 337 m^3 [5].

The core consists of 163 hexagonal fuel assemblies (61 of which contain control rods), each comprises 312 fuel rods that are arranged in a triangular grid [4] and made of Zr1%Nb alloy.

III. THERMAL-HYDRAULIC MODEL

The TRACE thermal-hydraulic model for the primary and secondary side including the safety and some control systems is built from the VVER-1000/V-320 RELAP5 model used in [3]. This model is then integrated with the 3D RPV of TRACE developed in [1]. The resulting integral plant model consists of following elements:

- Primary loops: cold legs, hot legs and Reactor Coolant Pumps (RCP).
- Pressurizer (PZR): connected to the hot leg 4 by the surge line. It contains Spray lines, attached to the cold leg 1, three safety valves and four groups of heaters.
- RPV: it has been modelled by a 3D VESSEL component which is divided into 50 axial nodes, 6 azimuthal sectors and 6 radial sectors. In the core region, the three internal rings model the core whereas the fourth rings model the bypass. The core barrel is model by the fifth ring and the downcomer by the sixth ring. The VESSEL also contains the lower and the upper grid plate as well as the upper head.
- Steam Generators (primary side): consists of tubes modelled by three horizontal PIPESs and collectors modelled by three PIPESs each.
- Steam Generators (secondary side): contains three levels where heat transfer occurs, corresponding with the three U-shape tubes PIPEs of the primary side. In the upper part is placed the liquid/steam separator.
- Steam lines: including one BRU-A, two safety valves, one main isolation valve and a check valve in each steam line.
- Steam header: containing the steam dump valves to the condenser BRU-K and the turbine connection.

The Emergency Core Cooling Systems (ECCS) is represented by four hydro-accumulators, two of them are connected to the reactor upper plenum and two others are connected to the downcomer, three Low Pressure Injection System (LPIS) trains and three High Pressure Injection System (HPIS) trains. The model also includes the Emergency Boron Injection System and the Make-up and Let-down mass flows of the Control Volume and Chemical System (CVCS). The Main Feed Water (MFW) and the Emergency Feed water (EFW) are also included in the model as boundary conditions.

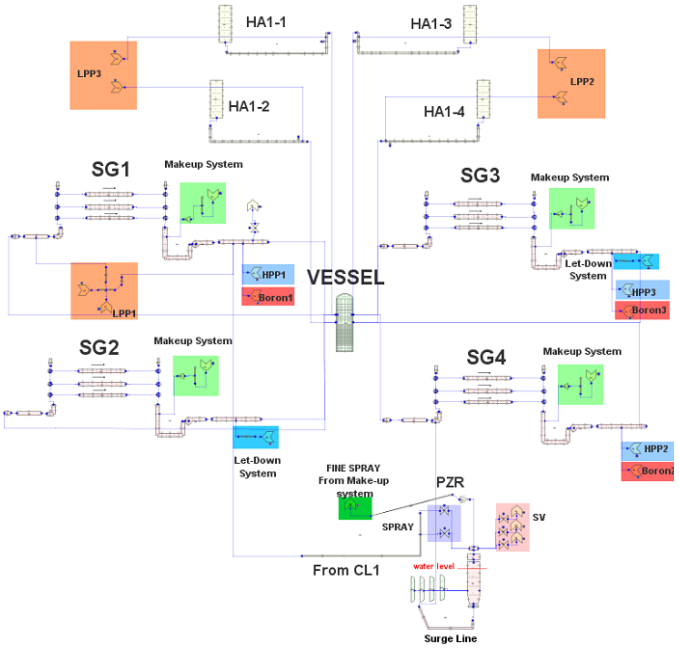

Figure 1. VVER-1000/V-320 RCS model.

IV. STEADY STATE

A steady-state of 2000 s has been simulated in order to obtain the start point of the transients to be analysed. The following assumptions have been made:

- Reactor is working at nominal power level.
- Make-up and Let-down systems are working with a mass flow rate of 8.19 kg/s.
- MFW temperature is 493 K.

A comparison between the steady state results obtained by means of the TRACE5p5 model and the plant values are shown in Table 1.

Table 1. Steady-State values comparison.

Parameter	Measured	TRACE5p5
Core Power	3010	3000
Lower plenum pressure (MPa)	15.84	15.86
Pressure above the core (MPa)	15.7	15.74
PZR level (m)	8.7	8.71
Cold Legs temperature (K)	560.85	560.96
Hot Legs temperature (K)	591.55	591.13
Average loop mass flow (kg/s)	4456	4457.21
SGs outlet pressure (MPa)	6.27	6.27
Feed Water mass flow (kg/s)	409	408.09
SGs level (m)	2.5	2.5

V. SELECTED TRANSIENTS

In order to verify the thermal-hydraulic model and that all safety systems signal and models have been correctly implemented, two transients have been performed: a reactor SCRAM and a simultaneous RCPs Trip.

A. Reactor SCRAM sequence.

The SCRAM signal occurs at 2000s (time user value). Due to the delay time, the control rods start inserting 0.3 seconds later and take 4 seconds to be fully inserted into the core. In primary side the SCRAM causes pressure to decrease to 13.30 MPa in the first 35 seconds and the PZR level to drop to 5.38 m, Figure 4. Subsequently, the pressure starts to increase until it reaches the PZR Spray set-point, which cycle three times until close definitely, Figure 2. Because there is no RCPs Trip, the forced circulation continues, so the hot leg temperature is similar to the cold leg temperature, Figure 3.

In the secondary side, the pressure follows the RCS pressure decrease until the Turbine Trip actuates. Subsequently, the pressure increases until the shutdown of the MFW pumps and the starts of the EFW pumps occurs. Finally, the pressure on the secondary begins to cycle as a result of the opening/closure set-points of the steam dump valves to the condenser BRU-K, Figure 5. The sequence of the SCRAM transient is shown in Table 2.

Table 2. SCRAM sequence

Time	Event	Response
2000	User time-value	SCRAM signal
2000.3	SCRAM signal + delay	SCRAM actuation
2004.3	Control rods fully inserted	-
2005	Hot Legs P < 14.71 MPa	Turbine and MFW/EFW Trip signal
2005	Top RPV P < 15.6 MPa	PZR heaters 2, 3 and 4 on (3 times cycling)
2020	Turbine Trip signal + delay	Turbine Trip actuation
2045	MFW/EFW Trip signal + delay	MFW off and EFW on
2060	PZR level = 5.38 m (minimum)	-
2401	Top PZR P > 16.27	PZR Spray on (3 times cycling)

2571	Top PZR P < 15.97	PZR Spray off
2916	Steam Header P > 6.667 MPa	BRU-K valves open
4588	Top RPV P > 15.5 MPa	PZR heaters 3 and 4 off
4763	Top RPV P > 15.78 MPa	PZR heater 2 off

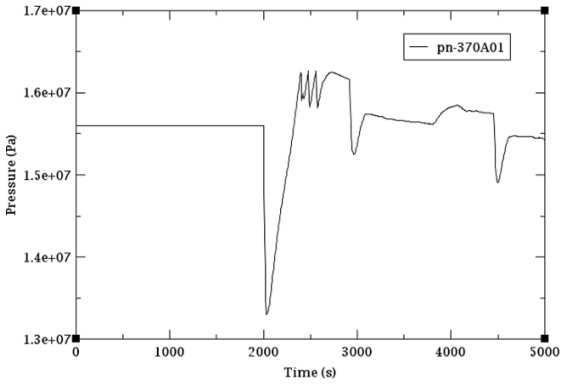

Figure 2. RCS (SCRAM sequence).

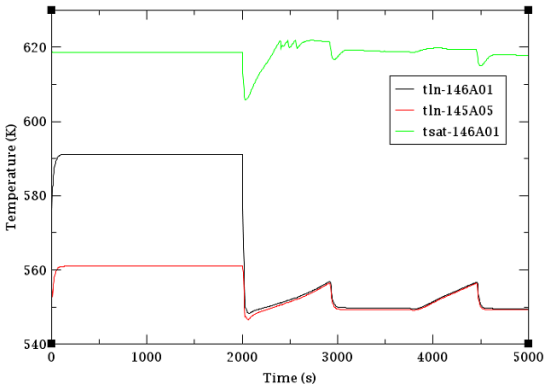

Figure 3. HL/CL and sat. temperature (SCRAM sequence).

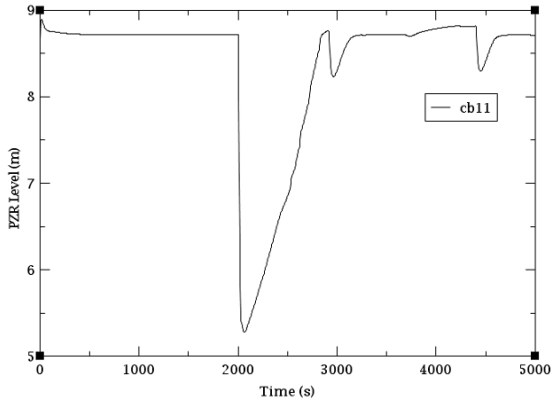

Figure 4. PZR level (SCRAM sequence).

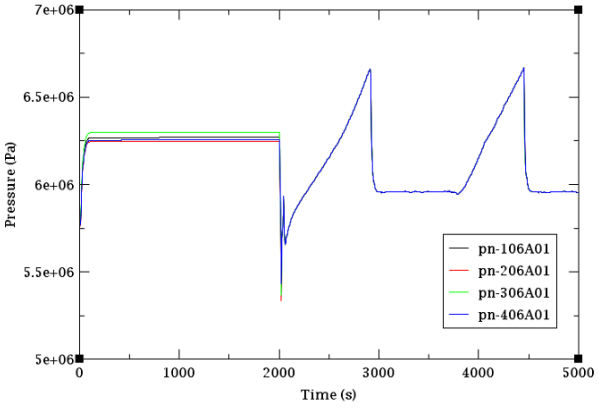

Figure 5. Secondary side pressure (SCRAM sequence).

B. RCPs Trip Sequence.

The transient starts at 2000 seconds, when a simultaneous RCPs Trip. The SCRAM immediately occurs, because more than two RCPs have started the cost-down with the reactor power level above 75%.

In the primary side, pressure decreases to 13.39 MPa in the first 39 seconds. Then, it starts to rise until it reaches the set-point of the PZR Spray, so the pressure starts to decrease again, Figure 6. Due to there is RCPs trip, the temperature difference between the hot legs and the cold legs increases sharply after RCPs cost-down, Figure 7.

In the secondary side, the pressure follows the RCS pressure decrease until the Turbine Trip actuates. Subsequently, the pressure increases until the MFW pumps trip and the start-up of the EFW pumps occurs. Finally, the pressure on the secondary begins to cycle as a result of the opening/closure set-points of the BRU-K valves, Figure 8. The sequence of the RCPs Trip transient is shown in Table 3.

Table 3. RCPs Trip sequence.

Time	Event	Response
2000	User time-value	RCPs Cost-down starts
2000	Two (or more) RCPs Cost-down	SCRAM Signal
2000.3	SCRAM signal + delay	SCRAM actuation
2003	Top RPV P < 15.6 MPa	PZR heaters on
2004.3	Control rods fully inserted	-
2007	Hot Legs P < 14.71 MPa	Turbine and MFW/EFW Trip signal
2021	Turbine Trip signal + delay	Turbine Trip actuation
2047	MFW/EFW Trip signal + delay	MFW trip and EFW start-up
2047	PZR level = 5.59 m (minimum)	
2232	RCPs angular velocity = 0 rad/s	-

2243	Top VESSEL P > 15.5 MPa	PZR heaters and off
2319	Top PZR P > 16.27 MPa	PZR Spray on
4445	Top PZR P < 16.17 MPa	PZR Spray off
2927	Steam Header P > 6.667 MPa	BRU-K valves open

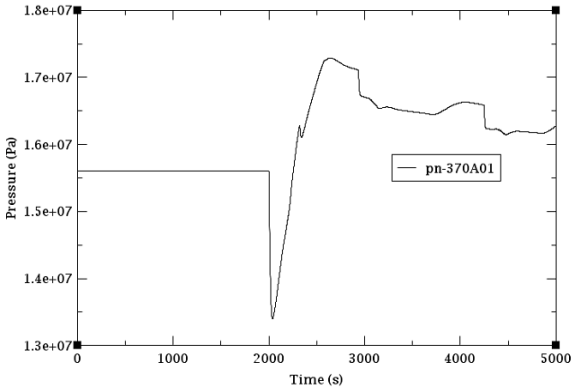

Figure 6. RCS pressure (RCPs Trip sequence).

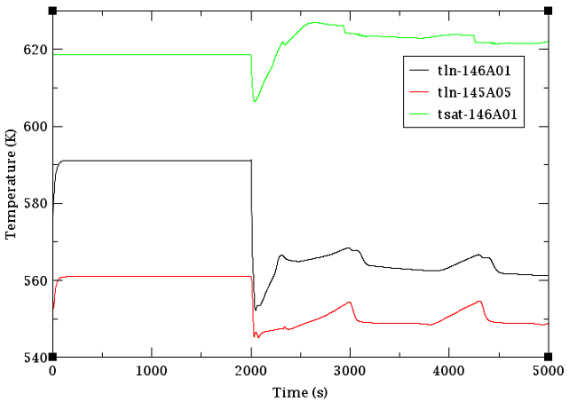

Figure 7. HL/CL and sat. temperature (RCPs Trip sequence).

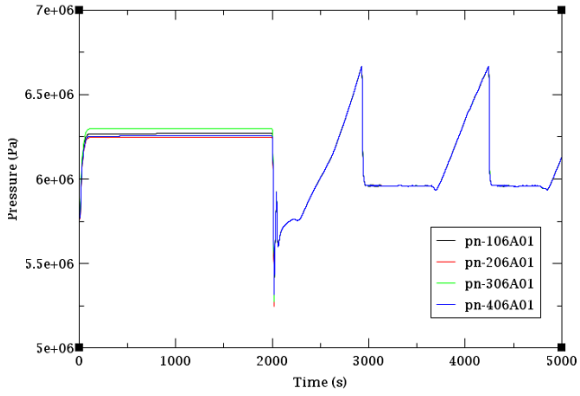

Figure 8. Secondary side pressure (RCPs Trip sequence).

VI. CONCLUSIONS AND FUTURE WORKS

Based on the presented work, the conclusions can be drawn:

- An integral thermal-hydraulic model of a VVER-1000/V-320 reactor has been developed for the TRACE5p5 code.
- The comparison of the predicted stationary plant conditions with the reference plant data confirms the appropriateness of the developed plant model.
- Two transients, a reactor SCRAM and a simultaneous RCPs Trip, have been carried out to verify the correctness of the VVER-1000/V-320 thermal-hydraulic model.
- The results obtained are satisfactory as it shows a behaviour very similar to the expected one.

The next steps are focus on the analysis of transients and accidents such as the Loss of Coolant Accidents, Station Black-Out sequences.

V. II ACKNOWLEDGMENTS

The authors gratefully acknowledge the financial support of the Spanish Ministry of Science and Innovation within ISASMORE project: PID2019-108755RB-I00

V. III REFERENCES

[1] W. Jäger, V. Sanchez-Espinoza & a. W. Lischke, «Safety related Investigations of the VVER-1000 Reactor Type by the coupled code system TRACE/PARCS,» *Journal of Power and Energy Systems*, vol. 2, nº 2, 2008.

[2] V. Sánchez, W. Jäger & T. Kozlowski, «Qualification of the 3D Thermal-Hydraulics Model of the Code System TRACE Based on plant dat,» de *ICAPP 2007: 2007 International Congress on Advanced in Nuclear Power Plants. May 13-18*, Nice, France, 2007.

[3] V. Sanchez-Espinoza & M. Böttcher, «Investigations of the VVER-1000 coolant transient benchmark phase - with the coupled system code RELAP5/PARCS,» *Progress in Nuclear Energy 48 (2006)*, vol. 48, 2006.

[4] S. Iegan, A. Mazur, Y. Vorobyov, O. Zhabin & S. Yanovskuy, «TRACE VVER-1000/V320 Model Validation.,» NUREG/IA-0490, 2018.

[5] N. Müllner, «Simulation of beyond design basis accidents – a contribution to risk analysis of nuclear power plants,» PhD Thesis. Universitat Wien, 2010.

[6] N. Kolev, N. Petrov, J. Donov, D. Angelova, S. Aniel, . E. Royer, K. Ivanov, E. Lukanov, Y. Dinkov, D. Popov & S. Nikonov, « VVER-1000 Coolant Transient Benchmark – Phase 2 (V1000CT-2). Vol. ll: MSLB Problem – Final Specifications.,» NEA/NSC/DOC(2006)6, April, 2006.

[7] P. Tusheva, «Modelling and analysis of severe accidents for VVER-1000 reactors. PhD Thesis. Technische Universität Dresden,» Technical Report HZDR-025. Technische Universität Dresden, Fakultät Maschinenwesen., 2012.

Proceedings of the European Nuclear Young Generation Forum
ENYGF'21
September 27-30, 2021, Tarragona, Spain

Sensitivity and uncertainty analysis of hydrogen generation in a BWR during a severe accident using MAAP5 and AZTUSIA

Sánchez-Mora, Heriberto[1], Reyes-Fuentes, Melisa[1*], Ortiz-Villafuerte, Javier[2], del-Valle-Gallegos, Edmundo[1] and Queral, César[3]

[1] Instituto Politécnico Nacional, Mexico; [2] Instituto Nacional de Investigaciones Nucleares, Mexico;

[3] Universidad Politécnica de Madrid, Spain

*Corresponding author: *rf.melisa@gmail.com*

I. INTRODUCTION

In light water reactors (LWRs), hydrogen generation due to the reaction of steam with zirconium (Zr) during the progression of a severe accident is one of the important phenomena that accelerate core degradation process. This reaction is an exothermic oxidation reaction that increases proportionally to the temperature, releasing ΔH = -6.84 MJ for each kg of zirconium [1]. Such energy release is as important as the decay heat generated after SCRAM.

As mentioned, oxidation of the zirconium contained in the cladding of the fuel rods depends on the temperature, having different regimes according to the temperature ranges. For example, above 1773 K oxidation is an accelerated reaction in a phenomenon called breakaway oxidation [2]. As core degradation takes place, different eutectic mixtures are generated, such as Fe/Zr and Ni/Zr around 1200 K and B_4C/Fe at 1430 K, which lead to a reduction of the melting temperature of metals. On the other hand, during the zirconium melting, which is about at 2033 K, UO_2 might dissolve and liquefy due to the interaction with the cladding, forming U-Zr-O [3], causing the relocation of corium to the bottom of the reactor vessel before the UO_2 reaches its melting temperature.

To analyze the progression of a severe accident and the possible actions to mitigate it, it has been necessary to develop computer codes such as RELAP/SCDAPSIM [4], MELCOR [5], and MAAP [6], to name a few, that consider the degradation of the core. However, the codes have some shortcomings when trying to predict the amount of hydrogen generated once the reactor core loses its geometry. Leyse [7] points out, according to the Oak Ridge National Laboratory [8] report of the BWR CORA-28 and 33 tests, that about 25% of the amount of hydrogen is generated when the fuel rods are intact; while the remaining 75% is generated in the melting process of the components. Currently, hydrogen generation models show an adequate result when the fuel cladding remains intact, but for the core degradation process, those models are not as accurate.

In this work, a sensitivity and uncertainty analysis is performed for hydrogen generation in a BWR during a Short-Term Station Blackout (STSBO), through a statistical evaluation of uncertain parameters, and using MAAP5 and AZTUSIA [9]. The Monte Carlo sampling method and an analysis by means of Pearson's Chi-squared test [10] are applied for the importance of models for the prediction of the hydrogen generation rate in the core, until the moment of the vessel failure, in order to determine the most important parameters that have impact on hydrogen generation.

II. Base Scenario: Short-Term Station Blackout (STSBO)

As the starting event for the severe accident progression, a Station Blackout is considered to occur in a BWR nuclear power plant. In this scenario, there is a loss of offsite power with failure of the emergency diesel generators, which causes a loss of coolant flow to reactor core because of the loss of the Feedwater system and the trip of the recirculation pumps. Consecutively to the loss of core cooling, the reactor is shut down by scram. However, due to the decay of fission products, heat generation continues by decay heat, therefore, this residual heat must be removed by emergency systems. In this hypothetical scenario, no heat removal system acts (RCIC failure) causing the accident progression to accelerate, leading to a severe accident and rapid core degradation. This scenario is called "Short-Term Station Blackout".

For the base case simulation of the scenario, the default MAAP values for this type of reactor were used, in order to compare results of hydrogen generation with the values obtained by the Monte Carlo sampling once applied to the parameters taken as uncertain. Figure 1 shows the coolant level in the reactor, indicating the Top of Active Fuel (TAF) and the Bottom of Active Fuel (BAF) marks, the hydrogen generation and the maximum temperature in the core. In this figure, the red stripe represents the region of time when the

vessel has failed. In this figure it is also possible to observe the increase and decrease of the coolant level, this is attributed to the condensation of the steam generated caused by the change in pressure in the vessel when opening and closing the relief valves. On one hand, core temperature drops rapidly at the start of the simulation, driven by the shutdown through the SCRAM manoeuvring, and eventually increases once the coolant level is at TAF and the oxidation reaction occurs, motivating an accelerated rate around 1600 K, which is near to the breakaway oxidation temperature. On the other hand, the figure also shows that 88% of 309 kg of the hydrogen generated occurs during the core heating process, in the time range 3000-5000 s, obtaining the rest from the melting process. Table I shows the timing of accident progression.

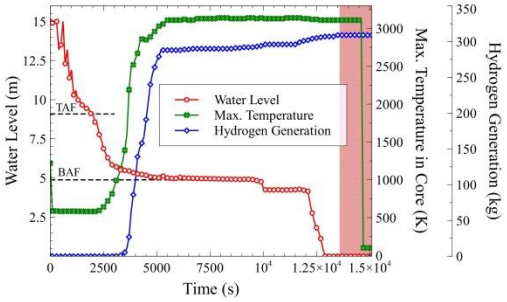

Figure 1. Water level, maximum temperature in the core and the hydrogen generation during the STSBO, base case.

Table 1. Timing of accident progression.

Event	Time (s)
Loss of AC power	0.
SCRAM	0.05
Coolant level at TAF	1,948.0
Hydrogen generation begins	3,002.2
Breakaway oxidation	3,580.0
Coolant level at BAF	5,210.0
Vessel failure	13,360.2

III. Parameter Selection

For the selection of uncertain parameters related with hydrogen generation during a severe accident simulated in MAAP5, variables described by the literature as important and others in the opinion of the authors were taken into account. A previous analysis by Roberts and Sanders [11] demonstrated that parameters such as the heat transfer coefficient between the fuel and the cladding, and the oxidation surface area, are parameters with great impact on the generation of hydrogen in MAAP4. In another STSBO uncertainty analysis performed by Wang and Lee [12], it was concluded that the failure temperature of the fuel cladding under the criterion of the Larson-Miller approximation it is strongly linked with the generation of hydrogen when high temperatures are taken, around 2700 K. However, in none of the aforementioned studies was considered the oxidation of the eutectic mixture of U-Zr-O. In this work, it is taken into account by the authors as an important factor for hydrogen production and that MAAP 5.0.3 is able to simulate.

Table 2 shows the uncertain parameters selected in MAAP5 and the probability density function (PDF) for the statistical analysis carried out, under literature reviewed and the judgment of the authors. It is relevant to mention that 8 out of 10 of the selected variables are quantitative variables, however, IUZROXID and IOXIDE are qualitative variables, where one of them allows activating or deactivating the oxidation of U-Zr-O during the simulation and the other admits the choice of four Zr oxidation models that are described in [12].

Table 2. Selected uncertain parameters for the hydrogen generation analysis.

MAAP5 Parameter	Description	Default value and PDF	Min.	Max.
HTCONC	Heat transfer coefficient between fuel and cladding for covered nodes.	5000 $W\ m^{-2}K^{-1}$ Uniform	-20%	+20%
HTCONR	Heat transfer coefficient between fuel and cladding for uncovered nodes.	750 $W\ m^{-2}K^{-1}$ Uniform	-20%	+20%
FAOX	Multiplication factor for the oxidation surface area.	1 Uniform	1	2
FZORUP	Minimal fraction of oxidized Zr to keep the cladding intact.	0.7 Normal	0.6	0.8
TCLMAX	Temperature for the time of failure of the cladding by means of the Larson-Miller approximation.	2500.0 K Uniform	2000 K	2700 K
IUZROXID	Option to consider or not the oxidation of U-Zr-O (2 options).	0 Uniform	0 = off	1 = on
IOXIDE	Option for Zr oxidation model (4 options).	0 Uniform	0	3
FACT	Multiplier for flow area reduction when nodes collapse..	0.3 Triangular	0.1	1.0
TCLRUP	Cladding failure temperature.	1000 K Triangular	1000 K	1500 K
VFCRCO	Porosity of the collapsed core region.	0.35 Normal	-2σ =20%	$+2\sigma$ =20%

IV. Sensitivity and Uncertainty Analysis: MAAP5 and AZTUSIA

Initially, a sensitivity analysis is performed to establish the statistical dependence of the selected uncertain variables and thus detect the variables with the greatest impact on hydrogen generation during an STSBO consideringuniform PDF for all uncertain parameters considered in the study. Uniform PDFs are selected in order to ensure that all domain percentiles of uncertain variables are adequately sampled, later, in the uncertainty analysis, the PDFs in Table 2 are considered. The sampling is carried out using the AZTUSIA code, which has been modified to adapt it to MAAP5. The amount of samples is created by the Monte Carlo method and depends on the Wilks' formula [13] for 95%/95 % confidence and two-sided tolerance limits. Such value is calculated automatically by AZTUSIA, resulting in 93 simulations. However, for practical terms, this value is rounded to 100 due to the possibility of failure of some simulations.

A. Sensitivity Analysis: Chi-Square Test

Due to the variables IUZROXID and IOXIDE are qualitative variables, a sensitivity analysis is necessary considering their possible combinations and determining the combinations that are statistically dependent and those that are not. This is done by preserving the same sampling of all the quantitative variables selected for each combination, that is, 100 simulations were performed for each combination of the IUZROXID and IOXIDE variables, where the minimum and maximum values of hydrogen generation were 234 kg and 549.1 kg, respectively.

Table 3 shows the number of results divided into percentiles of the amount of hydrogen generated during the STSBO simulation based on the combination of the IUZROXID and IOXIDE parameters. Low, medium and high hydrogen generation cases are considered those values within the percentiles 0-25%, 25-75% and 75-100%, respectively. The combinations of parameters are organized by cases, where, for cases 1 and 2, 2 simulations failed, and for cases 4 and 7, only 1 simulation failed. In this table, it is consistent that the results, with a few simulations in the 0-25 percentile, are those that consider the oxidation of U-Zr-O. To determine the importance of each combination, the chi-square test [10] was applied with the following criterion of statistical dependence,

$$\chi^2_{exp} > \chi^2_{p,fr} \quad (1)$$

where χ^2_{exp} is the experimental chi, $\chi^2_{p,fr}$ is the expected chi, p is the p-value and fr are the degrees of freedom. In this analysis is considered p=0.05.

The chi-square test was performed in an iterative process to identify the combinations that do not have statistical dependency between them, taking Table 3 as the contingency table. Table 4 shows the result of the process showing that the combinations of cases 1 and 2 have null dependency, as do cases 5 and 6. This means, at the end of the day, the analysis might be collapse only in 6 cases. The combinations with the greatest impact on hydrogen generation were cases 3 and 8, for the minimum and maximum values, respectively, obtaining from them the mayor contribution in the chi-square test. Figure 2 shows a scatter plot where is possible to notice the hydrogen generation behaviour in cases 3 and 8.

Table 3. Number of simulations per hydrogen generation percentile.

Case	Parameter		Simulations per Percentile		
	IUZROXID	IOXIDE	0-25	25-75	75-100
1	0	0	49	48	1
2	0	1	37	55	6
3	0	2	65	35	0
4	0	3	30	50	19
5	1	0	0	61	39
6	1	1	0	61	39
7	1	2	8	71	20
8	1	3	0	25	75

Table 4. Statistical dependency base on chi-square test.

Cases	χ^2_{exp}	$\chi^2_{0.05,fr}$	Statistical dependency
1,2,3,4,5,6,7,8	401.03	23.66	Yes
1,2,4,5,6,7	173.16	18.31	Yes
1,2,4,7	57.87	12.59	Yes
1,2	5.72	5.99	Null
5,6	0	5.99	Null

Once the important combinations of the qualitative parameters were spotted, AZTUSIA code calculated the Pearson Simple Correlation Coefficient (PSCC), for the quantitative parameters in cases 3 and 8. Figure 3 shows a histogram for this outcome and, regarding this, TCLMAX and VFCRCO are the parameters with the highest positive correlation. This is attributed to TCLMAX keeps the surface area to the oxidation processes for more time and VFCRCO allows more steam penetration to the collapsed core region and this enables more oxidation.

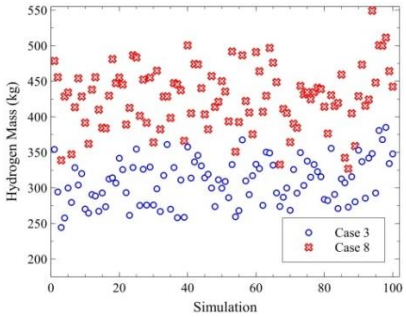

Figure 2. Scatter plot of hydrogen generation for the cases 3 and 8.

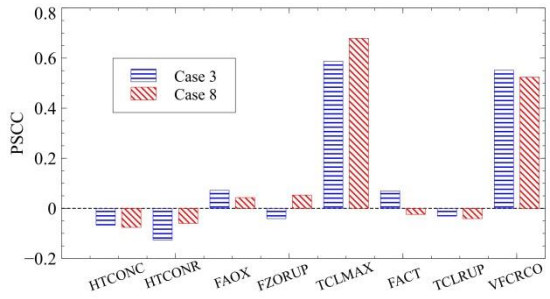

Figure 3. PSCC for the cases 3 and 8.

B. Uncertainty Analysis

Selecting the cases 3 and 8, which correspond to the lower and higher amounts of hydrogen generation, the hydrogen generation was evaluated with a sample of 100 simulations for each case, considering the PDFs of Table 2. Figure 4 shows the hydrogen generation distribution of the simulations, as well as the normal distribution fitted to each case. For cases 3 and 8, the mean hydrogen generation was 306.8 kg and 426.6 kg, and with a standard deviation of 33.36 kg and 47.02 kg, respectively. The p-values of the PDFs of cases 3 and 8 were 0.612 and 0.98, respectively, showing that the normal distribution is acceptable and has a better fit in case 8.

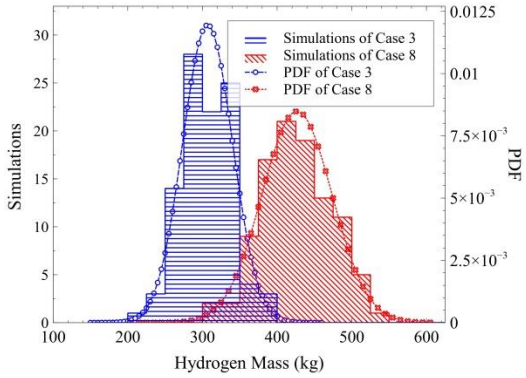

Figure 4. Simulation distribution around the hydrogen generation and PDF with a normal distribution.

With respect to the base case, the hydrogen generation had a value quite close to the mean result of case 3, with only 0.2 kg of difference. However, the difference between the hydrogen generation of the base case and the average value of case 8 was 119.6 kg, which corresponds to 38.95% of the amount of hydrogen in the base case.

V. Conclusion

In this work, a sensitivity and uncertainty analysis for the hydrogen generation was performed for a BWR plant, during a severe accident initiated with a STSBO. A list of uncertain input parameters for the code MAAP5 was generated according to engineering judgment and literature review. In the sensitivity analysis, chi-square test was used to detect the importance from qualitative parameters, and the outcome was that IUZROXID = 0 and IOXIDE = 2 (Urbanic-Heidrick Zr oxidation model) gave that the lowest amount of hydrogen generation and, IUZROXID = 1 and IOXIDE = 3 (Cathcart Zr oxidation model) gave the highest values, using the same sample for the qualitative parameters. In the same way, AZTUSIA code calculated the PSCC of quantitative parameters where TCLMAX and VFRCO were the most important for the hydrogen generation with a PSCC>0.5. Uncertainty analysis showed that the hydrogen production in the base case was too close to the mean value in case 3, with a difference of 0.2 kg.

VI. References

[1] C. Robert and Weast, CRC handbook of Chemistry and Physics, 52nd Edition. Cleveland, OH: Chemical Rubber Publishing CO, 1971.

[2] D. Jacquemain, G. Cenerino, and F. Corenwinder, Nuclear power reactor core melt accidents Current State of Knowledge. France: EDP Sciences, 2015.

[3] P. Hofmann, 'Current knowledge on Core Degradation Phenomena, a Review', Journal of Nucl. Mat., vol. 270, no. 1, Elsevier Science Publishers B.V., pp. 194–211, 01-Apr-1999.

[4] L. J. Siefken, E. W. Coryell, E. A. Harvego, and J. K. Hohorst, 'SCDAP/RELAP5/MOD 3.3 Code Manual, Code Architecture and Interface of Thermal-Hydraulic and Core Behavior Models', NUREG/CR-6150, Rev. 2, INEL-96/0422. Idaho Natl. Eng. Environ Lab., vol. 1, 2001.

[5] R. O. Gauntt et al., 'NUREG/CR-6119, Rev. 2, MELCOR Computer Code Manuals Primer and User's Guide, Version 1.8.5', Prep. by Sandia Natl. Lab. U.S. Nucl. Regul. Comm. Off. Nucl. Regul. Res., vol. 1, 2000.

[6] MAAP4, 'MAAP4: Modular Accident Analysis Program for LWR Plants, Code Manual', Prep. by Fauske Assoc. Inc, Burr Ridge, IL, USA EPRI, Palo Alto, CA, USA., vol. 1–4, 1994.

[7] L. Mark, 'Preventing Hydrogen Explosions in Severe Nuclear Accidents: Unresolved Safety Issues Involving Hydrogen Generation and Mitigation', 2014.

[8] L. J. Ott, 'Advanced BWR Core Component Designs and the Implications for SFD Analysis', Washington, DC (United States), 1997.

[9] M. Reyes-Fuentes, E. del-Valle-Gallegos, J. Duran-Gonzalez, J. Ortíz-Villafuerte, R. Castillo-Durán, A. Gómez-Torres, C. Queral, 'AZTUSIA: A new application software for uncertainty and sensitivity analysis for nuclear reactors', Reliab. Eng. Syst. Saf., vol. 209, p. 107441, 2021.

[10] R. Bermard, Fundamentals of Biostatistics, 8th Edition. Boston, USA: Cengace Learning, 2015.

[11] K. Roberts and R. Sanders, 'Application of uncertainty analysis to maap4 analyses for level 2 PRA parameter importance determination', Nucl. Eng. Technol., vol. 45, no. 6, pp. 767–790, 2013.

[12] T. -C. Wang and M. Lee, 'Uncertainty Quantification Using the MAAP5 Code of In-Vessel Hydrogen Generation in a Severe Accident at an Advanced Boiling Water Reactor', Nucl. Technol., vol. 206, no. 3, pp. 414–427, 2020.

[13] S.S. Wilks, 'Determination of Sample for Setting Tolerance Limits', Ann. Math. Stat., vol. 13, pp. 91-96, 1941.

Proceedings of the European Nuclear Young Generation Forum
ENYGF'21
September 27-30, 2021, Tarragona, Spain

Implementation of dynamic nuclear fuel thermo-mechanics in transient simulation of lead-cooled reactors

Aragón, Pau[1*] and Wallenius, Janne[2]

[1] Centro de Investigaciones Energéticas, Medioambientales y Tecnológicas (CIEMAT), Spain; [2] KTH Royal Institute of Technology (KTH), Sweden

*Corresponding author: *janwal@kth.se*

I. INTRODUCTION

The nuclear industry must address the issues faced by the current new-build nuclear power plants (NPPs) in the western world if it is to remain cost-competitive with other forms of electricity generation. Over the last decade, Member States of the International Atomic Energy Agency (IAEA) have made an ongoing effort to research, develop and deploy small modular reactors (SMRs), recognizing their potential as a viable solution to provide reliable, emission-free power generation to the future energy mix.

The IAEA defines SMRs as advanced nuclear reactors with a power output typically below 300 MWe per module. Most importantly, however, a common feature in any SMR design is the high degree of modularity, i.e., the reliance on serial, factory-based production of stand-alone reactor modules. The driving forces in the commercialization of SMRs are mainly two: reducing the capital cost and thereby the investment risk associated with a conventional large NPP; and providing power to small electricity grids.

In this context enters SEALER, a very small lead-cooled fast reactor (LFR) designed by LeadCold for commercial power production in off-grid areas. Its compactness enables the implementation of unique passive safety features, namely decay heat removal by natural convection and thermal radiation from the primary vessel to the environment. Moreover, LeadCold aims to reduce operating expenses and eliminate proliferation concerns through a long-life core design (30 years), thus avoiding on-site refuelling operations during the whole life of the plant [1].

The dynamic behaviour of a nuclear reactor is intrinsically difficult to model due to the large number of parameters involved and their intricate dependencies. Human reasoning and simple theoretical models are simply not capable of untangling the outcome of the system in response to a perturbation. For this reason, system codes play a critical role in the design and safety analysis of nuclear reactors. Several system codes have been developed for LFR transient analysis. However, complexity and relatively restricted access to the source code for modifying built-in models and correlations make their use for safety-informed reactor design rather cumbersome. In this light, LeadCold and KTH Royal Institute of Technology are developing BELLA, a simple, easily modifiable, yet adequate computer tool intended for the safety-informed design of LFRs [2].

II. MODELLING APPROACH IN BELLA

Simulations of the dynamic behaviour of LFRs under accident conditions are based on a lumped-parameter approach for the time-dependent coupling between thermal-hydraulics and neutron kinetics. BELLA models the primary system as a collection of single points comprised of the reactor core, steam generator, hot leg, cold leg, and cold pool, featuring average and boundary temperatures (Figure 1). The equations governing the kinetic behaviour of the reactor core are derived using the one-group point kinetics approximation with eight delayed neutron precursor groups. Neutronic parameters must be manually introduced through the input file. With regard to thermal-hydraulics, balance equations of energy, momentum, and mass are applied to all primary components, resulting in another set of coupled differential equations. Moreover, a rough estimation of the heat source introduced by the decay of fission products from ^{235}U is provided. Current simulation capabilities of BELLA include several limiting transients identified as unprotected transient over-power (UTOP), loss of flow (ULOF), and loss of heat sink (ULOHS), in addition to reactor SCRAM.

Under transient conditions, the coupling between thermal-hydraulics and neutron kinetics entails a continuous reactivity feedback due to fuel and coolant temperature variations. In the case of LFRs, the main contributions come from the Doppler broadening in the fuel, the axial expansion of the fuel, changes in coolant density, and the radial expansion of the fuel assembly foot diagrid.

Heat transfer between reactor core components is modelled by applying energy balances to the fuel pellet, cladding, and coolant. To that end, the radial mesh structure adopted in BELLA consists of three nodes in the fuel pellet, three more in the cladding, and one in the coolant. Regarding the axial

mesh structure, the whole active height of the core is represented by a single node, thus not considering the temperature distribution along the axial direction.

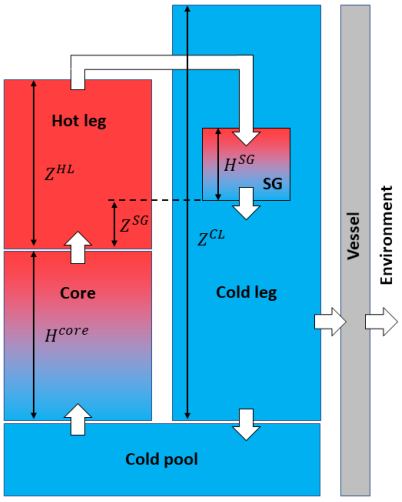

Figure 1. Primary system nodalization.

Despite the fact that BELLA cannot perform a detailed thermal-hydraulic calculation of the steam/water secondary circuit, it provides two different approaches to modelling heat transfer from the primary to the secondary side of the steam generator. These consist of imposing any user-defined function for either power removal or temperature drop between the inlet and outlet of the steam generator.

III. NEW THERMO-MECHANICAL MODEL

BELLA does not consider the thermo-mechanical evolution of the fuel pellet and the cladding. In this section, the most relevant mechanisms having an impact on fuel performance and their implementation in the original code are presented.

A. Thermal expansion

Following the onset of a power transient, the temperature of the fuel pellet increases rapidly. Among the effects resulting solely from temperature, thermal expansion is known to be a limiting factor for the lifetime of the fuel in the reactor. Despite the cladding material having a larger coefficient of thermal expansion as compared to the oxide pellet, the expansion of the latter is always greater in absolute terms due to exposure to much higher temperatures throughout the transient. Altogether this leads to a net reduction of the gap thickness, thereby enhancing pellet-cladding mechanical interaction (PCMI).

The new thermo-mechanical model recalculates the fuel pellet diameter, cladding inner diameter, and cladding outer diameter at every simulation time step. Axial thermal expansion is not currently implemented. It is important to highlight that the dimensional change in the fuel pellet diameter is estimated from its average temperature, meaning that the differential thermal expansion caused by the radial temperature gradient is not considered.

B. Thermal conductivity

Thermal conductivity is one of the most important design parameters of a nuclear fuel rod as it directly determines the temperature gradient between the surface and the centreline of the pellet. In the original BELLA code, the correlation used to calculate the thermal conductivity of the oxide fuel depends solely on temperature, thus does not account for the effects of porosity, burnup (dissolved and precipitated solid fission products), and radiation damage. To improve the accuracy of the code, the new thermo-mechanical model includes a comprehensive approach to modelling the thermal conductivity of irradiated oxide fuel based on the work of Lucuta et al. [3]. Each individual effect envisaged in the model can be considered as a correction factor applied to the expression describing the thermal conductivity of unirradiated, 100% dense oxide fuel (Figure 2).

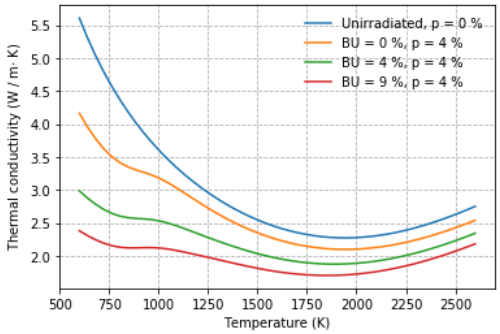

Figure 2. Thermal conductivity of UO_2 as a function of temperature. BU and p refer to burnup in units of atomic percent and as-fabricated porosity, respectively.

C. Fission gas release

The release of gaseous fission products (primarily xenon and krypton) into the void volume of the fuel rod leads to a decrease of the conductive heat transfer through the gas-filled gap. This is due to the significantly lower thermal conductivity of these gases in comparison with helium. Poorer heat conduction from the fuel pellet to the cladding yields higher temperatures in the former, which further enhance fission gas release, thereby giving rise to a positive feedback. At the same time, the accumulation of fission gases in the fuel rod plenum prompts a continuous pressure build-up that may eventually compromise the integrity of the fuel rod.

Observation on the microstructure of oxide fuel pellets irradiated at high burnup suggests the existence of a temperature threshold that determines the onset of a nearly total fission gas release [4]. Its parametrization as a function of burnup is known as the Vitanza threshold [5] (Figure 3). The sudden nature of this phenomenon can be explained as follows. From the very beginning of irradiation, gas atoms with intrinsically low solubility are introduced into the oxide lattice due to fission reactions. Intragranular bubbles migrate to the grain boundaries either in a stochastic manner or under the effect of the thermal gradient, increasing their size as they coalesce with others. Consequently, gas bubbles accumulate along grain boundaries. As burnup advances, the interconnection of several intergranular bubbles leads to the formation of grain edge tunnels, i.e., microstructures resembling a tunnel network that allow for rapid transport

of gaseous fission products. Eventually, grain edge tunnels grow large enough to reach a free surface, thus releasing the accumulated intergranular gas into the fuel rod void volume.

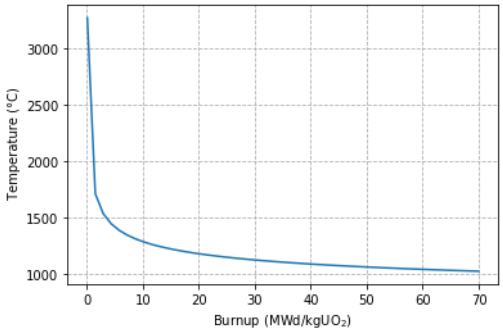

Figure 3. Vitanza threshold for the onset of total fission gas release.

Within the new thermo-mechanical model, fission gas release is limited to xenon and implemented separately for each radial zone in the fuel pellet. The Vitanza threshold is calculated from the user-specified burnup during the initialization phase of the simulation. On the other hand, the number of xenon atoms born from the start-up of the reactor to any time in the transient (t) is computed as

$$B_{\mathrm{Xe}}(t) = \frac{Y_{\mathrm{Xe}}}{\varepsilon}\left(m_0 \mathrm{BU} + \int_0^t \dot{Q}(t')dt'\right),$$

where Y_{Xe} is the xenon fission yield, ε is the energy released per fission event, m_0 is the initial mass of fuel, BU is the user-specified burnup, and $\dot{Q}$ is the reactor power level. At every simulation time step, fuel temperatures – central, middle, and outer – are compared to the Vitanza threshold. The outcome of each comparison determines whether the fission gas release from a particular radial zone is total or partial, in which case the release fraction is set to 1% [6].

D. Fuel swelling

Fuel swelling is defined as the positive change in fuel volume induced by the accumulation of fission products during irradiation. It is driven mainly by gaseous fission products coalescing into bubbles and diffusing along grain boundaries. Measurements carried out on oxide fuel after irradiation in a fast reactor reveal that the pellet density can be described by a linear function of burnup with a constant swelling rate of 0.62% per at. % [7].

The implementation of fuel swelling in BELLA consists of redefining the fuel pellet diameter during the initialization phase of the simulation from its value at beginning-of-life (BOL) and its burnup-dependent density.

The radius of the fuel pellet increases as burnup advances towards end-of-life (EOL), whereas the inner radius of the cladding – only affected by thermal expansion – remains approximately constant. As a result, the gap shrinks and eventually disappears, leading to PCMI. Having a null gap thickness utterly invalidates the heat transfer model implemented in the original BELLA code. In this light, a solid-to-solid heat transfer coefficient based on the work of Lassmann and Pazdera [8] is formulated into the new thermo-mechanical model, thus providing the capability to adequately simulate gap closure.

IV. TRANSIENT SIMULATION OF SEALER

The performance of SEALER during UTOP was simulated using BELLA. The focus of this section is on discussing the differences introduced by the new thermo-mechanical model relative to the results obtained with the original code. Under UTOP conditions, all shut-down assemblies fail to insert, meaning that SEALER relies entirely on reactivity feedbacks to achieve sub-criticality. Heat transfer from the primary to the secondary system is modelled by imposing a constant temperature drop over the steam generator. It is important to mention that simulations performed at different burnup steps used the same neutronic parameters.

The UTOP was simulated for an external reactivity insertion of 0.5 \$, equivalent to the effect caused by the spurious withdrawal of a single control assembly at BOL, over a time interval of one second at $t = 100$ s. Prior to the onset of the transient, the reactor operates under nominal conditions. Immediately following the reactivity insertion, the reactor moves towards super-criticality, and the power level increases rapidly. Then, once the negative reactivity feedbacks introduced by fuel and coolant balance out the initial insertion, the power level reaches a maximum and subsequently decreases.

The evolution over time of the fuel centreline temperature is plotted for the peak assembly in Figure 4. The results show that the curve obtained using the original BELLA code (labelled as 'Reference') lies below the rest. Nevertheless, the maximum fuel temperature is 1660 °C, thus the margin to fuel melting (2847 °C) is still significant. Moreover, both steady-state and transient temperatures reach higher values as burnup advances towards EOL. This can be justified as follows. Regarding the central region of the fuel, the most relevant feature introduced by the new thermo-mechanical model is the improved approach to modelling its thermal conductivity, which includes the detrimental effects of porosity, dissolved fission products, and radiation damage. Because porosity is approximated by as-fabricated porosity, its impact on thermal conductivity can be described by a constant factor (< 1.0) regardless of burnup. However, the continuous dissolution of solid fission products in the matrix entails a progressive reduction of the heat transfer rate from the central to the middle region of the fuel. As higher temperatures are reached, the effect of radiation damage further aggravates this trend. Consequently, fuel centreline temperatures increase as the reactor moves towards EOL. The original BELLA code does not take into account any of the aforementioned effects and therefore yields the highest thermal conductivity, i.e., the lowest centreline temperature.

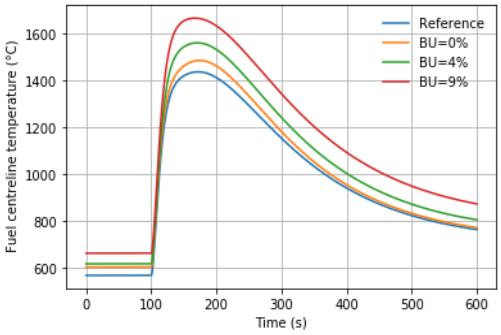

Figure 4. Fuel centreline temperature (peak assembly).

Fuel outer temperatures for the average assembly are plotted in Figure 5. Discrepancies with the original BELLA code are motivated by several phenomena. Following the onset of the UTOP, the thermal expansion of the fuel pellet leads to a reduction in the gap thickness at an early stage of the transient (Figure 6). This translates into a more efficient heat transfer from pellet to cladding, thereby a lower fuel outer temperature and a higher cladding temperature. Due to this reason, the results provided by the new thermo-mechanical model at BOL lie below the original curve.

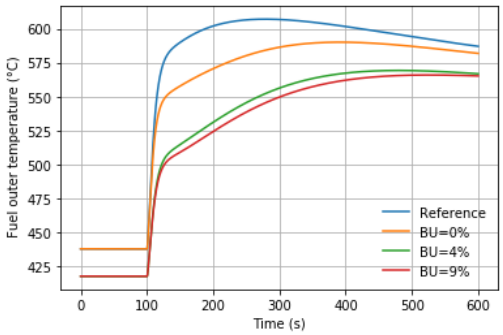

Figure 5. Fuel outer temperature (average assembly).

Given the design parameters of SEALER, the approach to modelling fuel swelling included in the new thermo-mechanical model predicts gap closure to occur around 3% burnup. Note that gap closure might happen at even lower burnups if the contribution from thermal expansion is taken into account. The solid-to-solid heat transfer coefficient is several orders of magnitude larger as compared to that of a gas-filled gap. Therefore, the rate of heat flow from the outer surface of the fuel to the cladding increases dramatically when in contact. The results indicate that from that moment, the outer region of the fuel follows the same temperature evolution as the inner region of the cladding. Hence, the significantly lower values of the simulations performed at 4% and 9% burnup relative to the original BELLA curve.

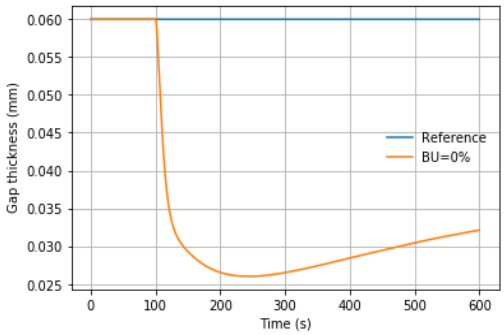

Figure 6. Fuel-cladding gap thickness under BOL conditions.

Figure 5 shows yet another interesting feature. Once gap closure has occurred, fuel outer temperatures reach lower values throughout the transient with increasing burnup. To understand the underlying reason, one must examine the variables that influence the solid-to-solid heat transfer coefficient. For that matter, the time evolution of the pellet-cladding interface pressure, which is approximated by the pressure of the gas mixture in the gap, is plotted in Figure 7.

The steep jump of nearly 10 bar within the first 25 seconds of transient indicates that at least one region of the fuel reached the Vitanza threshold, presumably the central region as it is exposed to the highest temperatures, releasing its xenon content. Fission gas release into the void volume of the fuel rod and subsequent pressure build-up yields a higher pellet-cladding interfacial pressure, thus a more efficient solid-to-solid heat transfer. This explains why the fuel outer temperatures are higher at 4% than at 9% burnup.

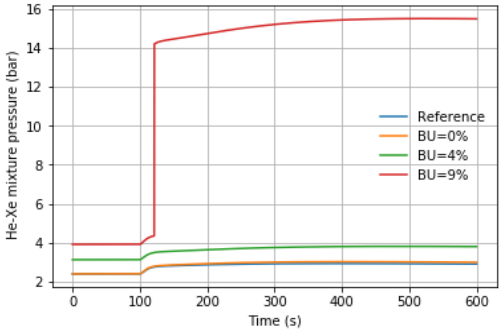

Figure 7. Helium-Xenon mixture pressure in the gap.

V. CONCLUSIONS

The most important physical processes affecting fuel properties and behaviour are modelled and integrated into the BELLA code, enabling a more accurate description of the thermo-mechanical evolution of the fuel and cladding under steady-state and transient conditions.

The performance of SEALER under UTOP conditions is examined using BELLA with and without the new fuel thermo-mechanical model. The maximum fuel centreline temperature is used as the safety criterion for UTOP safety analysis. The results indicate that the fuel centreline temperature is underestimated by the original BELLA code. However, the margin to fuel melting is significant since it does not exceed 40% of the melting point. Conversely, the fuel outer temperature is overestimated.

This work demonstrates the importance of adequately capturing the heat transfer mechanisms through one of the main thermal resistances in this context, namely the gap. The fact that gap closing is predicted at such a low burnup was unexpected and might motivate a future revision of the fuel rod design. Future work includes a benchmark analysis of the new thermo-mechanical model with respect to a qualified system code and a more detailed assessment of the internal stresses arising in the fuel pellet and at the pellet-cladding interface.

VI. References

[1] J. Wallenius et al., “Design of SEALER, a very small lead-cooled reactor for commercial power production in off-grid applications,” Nuclear Engineering and Design, vol. 338, Nov-2018.

[2] S. Bortot, E. Suvdantsetseg, and J. Wallenius, “BELLA: a multi-point dynamics code for safety-informed design of fast reactors,” Annals of Nuclear Energy, vol. 85, Nov-2015.

[3] P. G. Lucuta, H. Matzke, and I. J. Hastings, “A pragmatic approach to modelling thermal conductivity of irradiated UO2 fuel: Review and recommendations,” Journal of Nuclear Materials, vol. 232, Sep-1996.

[4] M. Tourasse, M. Boidron, and B. Pasquet, “Fission product behaviour in PHENIX fuel pins at high burnup,” Journal of Nuclear Materials, vol. 188, Jun-1992.

[5] C. Vitanza, U. Graziani, N.T. Fordestrommen, and K. O. Vilpponen, “Fission gas release from in-pile measurements,” Report HPR-221.10, OECD Halden Reactor Project, 1978.

[6] Institute for Transuranium Elements (Joint Research Centre), and P. Van Uffelen, “Modelling of nuclear fuel behaviour,” Publications Office of the European Union, Feb-2007.

[7] R. Pascard, “Les combustibles nucléaires céramiques,” Annales de Chimie Françaises, vol. 10, 1985.

[8] K. Lassmann, and F. Pazdera, “URGAP: A gap conductance model for transient conditions,” Specialists’ meeting on fuel element performance computer modelling (IWGFPT--13), International Atomic Energy Agency, Mar-1982.

Proceedings of the European Nuclear Young Generation Forum
ENYGF'21
September 27-30, 2021, Tarragona, Spain

Cloud computing CFD analysis assessment of an ITER Vacuum Vessel Component

Catalán, David*[1], Bernad, Andreu[1], Alberto, Patricio[1], Fradera, Jorge[1]

[1] IDOM, Bilbao, Av. de Zarandoa 23, Spain

*Corresponding author: david.catalan@idom.com

I. INTRODUCTION

Modelling and simulation tools have been traditionally used for nuclear reactor safety applications. Such applications are usually addressed by means of simplified and very conservative models which require extensive experimental data. These models are encapsulated in well-known system codes that serve greatly the purpose for which they were built, yet lacking the flexibility needed to tackle new coming applications.

With the evolution in nuclear science and related disciplines, new multiscale/multiphysics tools are allowing to the industry and research to boost nuclear systems applications in ways which are not thinkable with traditional approaches alone. This allows to gain flexibility, increase the range of applicability, and reduce the amount of data needed. One remarkable example of these tools are the Computational Fluid Dynamics (CFD) codes. As the use of the CFD technology evolved from detailed component level studies to more complex system levels, the intricacy and the size of the simulations have increased continuously. In consequence, CFD codes are constantly being updated with the most recent numerical models and techniques; being a key enabler for carrying out more precise and representative high-fidelity simulations. This is leading to larger and more complex geometries used for advanced simulation and modelling [1], which must ensure the reliability and accuracy of the results, demonstrating significant advantages in terms of safety, general understanding, and an overall decrease on cost for engineering organisations.

In this study, IDOM presents with the support of Ansys® a new assessment on the use of Ansys® Fluent® in HPCC already available for the resolution of complex commercial CFD models, aiming to evaluate and optimize more advanced simulations in terms of efficiency and scalability.

The generated outcome provides a valuable insight on the Thermalhydraulic (TH) analysis of components for nuclear technology, especially for fusion, and a decided step towards a wider use of CFD codes for nuclear applications.

E. ITER

ITER (from International Thermonuclear Experimental Reactor) is a large-scale scientific testing site intended to prove the viability of producing and maintaining fusion as an energy source for long periods of time, and to gather the necessary data for the design and later operation of the first electricity-generating commercial fusion power plant. This fusion reaction is housed in a vacuum vessel (VV) Which apart from providing a high-vacuum environment for the plasma, enhances the radiation shielding acting as the primary confinement barrier for radioactivity, and helps with the plasma stability. The vessel itself is composed of 9 sectors (See Figure 1**Figure**) where the volume between the external and internal shells of each sector is designed to be actively cooled by means of a single cooled loop of treated water delivered by the VV Primary Heat Transfer System (VV PHTS) extracting the heat generated during operation. The thermal-hydraulic behaviour of the VV, given its one-of-a-kind nature, is well suited for a single phase CFD simulation. In that regard, several VV sectors have been analysed and studied with the aim to provide a valuable insight on the (TH) analysis of components for fusion technology applications.

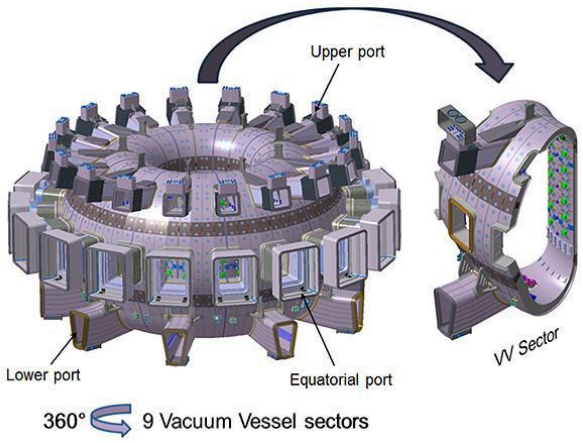

Figure 1. CAD assembly of ITER's Vacuum Vessel. Source: [2]

F. ANSYS CLOUD

Ansys Cloud® [3] has been developed to mitigate the mentioned constraints for simulations regarding computing resources availability, providing a substantial increase on computational power and accelerated results. This service offers access from any location or device to run simulations on-demand, with cloud-based computing resources, including both interactive workstations and HPC clusters, for faster, high-fidelity results offering greater performance insight being a scalable and cost-effective approach to HPC and removing the hardware barrier.

Once subscribed to the service, each server available has an associated hardware consumption rate depending on their specifications or which region of the world the user is accessing from. Similarly, there are software associated costs, depending on the kind of Ansys package or solver it is being used. Once a job is created, the Cloud tool automatically calculates the consumption rate in accordance to the hardware used, software and total spent time. The analyst can access to the web portal to monitor running jobs, view resource usage, visualize results and access files.

A cooperation between Ansys® and IDOM has been established to test and give feedback of this service, giving guidance and advising through the whole course of the preparation of this publication.

This also serves as well as an opportunity, not only for IDOM but for the industry, to assess the likelihood to use this kind of toolboxes for large-sized simulations or during peak workloads.

II. BACKGROUND

IDOM carried out in the past a CFD Benchmark [4] on the TH performance of ITER's Vacuum Vessel. The geometry was selected to be of one of the 4 Poloidal Segments (PS), the PS#01, of a Regular Sector (RS), RS#05, which has been found to be representative, both in terms of size and phenomenology to a whole sector of the VV. Several commercial and Open-Source CFD codes were compared, and the results highlighted the special features and capabilities that the specific codes have and how much of an improvement was using their best practices, workflow, and expertise. The mentioned Benchmark was an additional step to disclose CFD capabilities in favour of safety, showing the effectiveness of resolving with enough accuracy the physics behind conjugate heat transfer simulations.

That study was presented on the last CFD4NRS OECD/NEA forum [5], where numerical analysts and experimentalists exchanged information and new insights on the application of CFD to nuclear power plants safety and design issues.

The results emphasised among other aspects the importance of modelling with proper detail regions where key parameters must be studied. This accentuated the requirement of increasing the size and complexity of future studies, bringing the necessity as well of using more computational resources and running longer simulations, aspect which might not always be covered in the industry due to tight deadlines or important workload.

III. METHODOLOGY

As the current study aims to evaluate and optimize more advanced simulations in terms of efficiency and scalability by using HPC online tools, a clear and stepped methodology is followed.

The geometry, mesh, regions, and properties used were generated during the mentioned Benchmark and they are kept as baseline data for all the current studies. Therefore, meshing performance or turbulence models influence are not checked, only focusing on solver times and Cloud usability, obtaining the strong scaling parameters for the present analysis. The current case is based on a PolyHexCore mesh, representing the boundary layer of the fluid region. A coupled pseudotransient approach is selected with the intention of stabilizing the case giving a faster converge. The final grid size is around 25M cells, giving extra detail to the fluid region. (See Figure 2)

Figure 2. PS#01 meshed geometry.

The list of cases to run is shown in Table 1. Three different servers are used, HBv2 and HC pertaining to Ansys and GD pertaining to IDOM, this last to compare the improvement with respect to inhouse resources. Their characteristics are shown in Table 2

All cases are set-up and run by IDOM analysts with the assistance of Ansys® analysts for the possible needed supervision of the systems.

Table 1. Simulation Matrix.

Server	Hardware Resources		
	Nodes	Cores/Node	Total cores
GD	1	12	12
	1	18	18
	1	24	24
HBv2	1	44	44
	1	60	60
	1	120	120
HC	1	44	44
	2	44	88
	4	44	176

Table 2. Computational Specs.

Server	Processor	RAM/node
GD	Intel(R) Xeon(R) Platinum 6252 CPU @ 2.10GHz	192 GB
HBv2	AMD EPYC 7V12 CPU @ 2.30GHz	480 GB
HC	Intel(R) Xeon(R) Platinum 8168 CPU @ 2.70GHz	352 GB

The next step is to set up the case and initialize it. A custom User Defined Function (UDF) must be loaded, compiled and interpolated to implement the source term in the case, accounting for the Nuclear Heat Deposition (NHD) deposited in the solid external shell.

To reduce the uncertainty related to the analyst or the time needed to perform this operation, the task is performed in advance and saved as initial state of the oncoming simulations. Therefore, each case is simply loaded automatically with Ansys Cloud Agent® and run 200 iterations, then brought back to the personal computer for the required postprocessing.

Finally, the total wall-clock time given by Fluent® is compared, i.e., the time the solver has been running to finish the 200 iterations. The additional time used to upload the case into the Cloud Portal is not considered since it mostly depends on the Internet bandwidth from where the case is being updated and to better compare it with the cases run on the IDOM's calculation server.

IV. RESULTS AND DISCUSSION

Simulations are performed for 200 iterations as commented. The performance is measured based on the average wall clock time, and the strong scaling speedup and efficiency are calculated as defined in (1) and (2).

$$S_p = \frac{t_1}{t_p} \quad (1)$$

$$\varepsilon = \frac{t_1}{p \cdot t_p} \quad (2)$$

Where t_1 and t_p is the time spent to perform the iterations for the baseline case and for the parallelized case respectively, and p the number of cores. The strong speedup measures the relative acceleration achieved increasing the computational resources, and the efficiency or load balance assess the load distribution among the computing resources [6].

Table 3 shows the elapsed time to complete the analysis for each case and Figure 3 shows the evolution of one parameter (Solid domain maximum temperature) versus time and iteration number.

Table 3. Execution times.

Server	Total cores	Elapsed time [s]
GD	12	9532,19
	18	8650,32
	24	4979,14
HBv2	44	3698,58
	60	2929,26
	120	2842,29
HC	44	3515,35
	88	2755,49
	176	2534,20

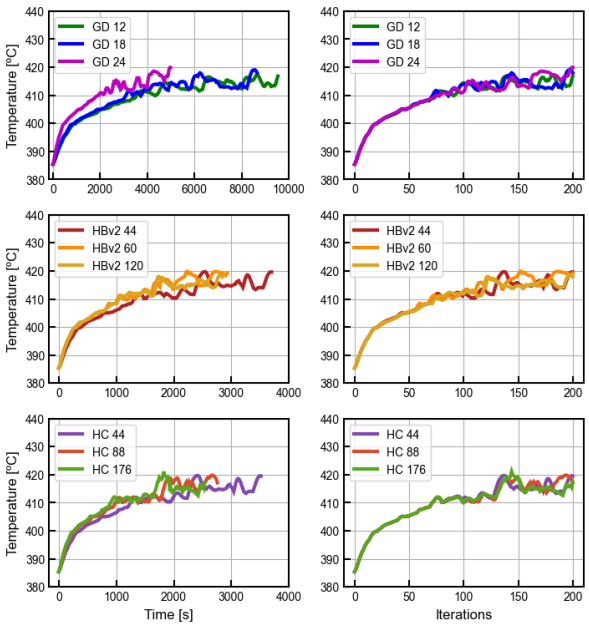

Figure 3. Maximum solid temperature vs. time and iteration.

As observed in Figure 3 the calculation time for the baseline is clearly superior to the rest (note the x axis from the upper left plot), showing an increase on performance when running the simulation in parallel mode as expected.

The plot on the right of Figure 3 show as well anticipated results, observing similar temperature evolution in the first iterations but different as the simulation progresses. Nevertheless, the differences are within an acceptable margin and explained by the interconnection between processors, round-off errors and evolution of turbulent structures solved iteratively [7].

Speedup and efficiency values are presented in Table 4**Table**, note that these parameters are compared to the baseline case from the GD server and not from each individually.

Table 4. Speedup and Efficiency parameters.

Server	Total cores	Speedup	Efficiency
GD	12	1,00	100%
	18	1,10	73%
	24	1,91	96%
HBv2	44	2,58	70%
	60	3,25	65%
	120	3,35	34%
HC	44	2,71	74%
	88	3,46	47%
	176	3,76	26%

Results show how the speedup follows Amdahl's law [8], that gives the maximum theoretical value and efficiency decreases with the number of cores. In comparison with other literature scalability studies, the simulation of complex meshes induces a more important load imbalance, where some specific regions may lead to an increase of the computational time required to solve the equations. This decrease of performance for a very large number of PUs underlines a physical limit often encountered on massively

parallel applications, where some of the processors may be unused for long periods of time causing overhead.

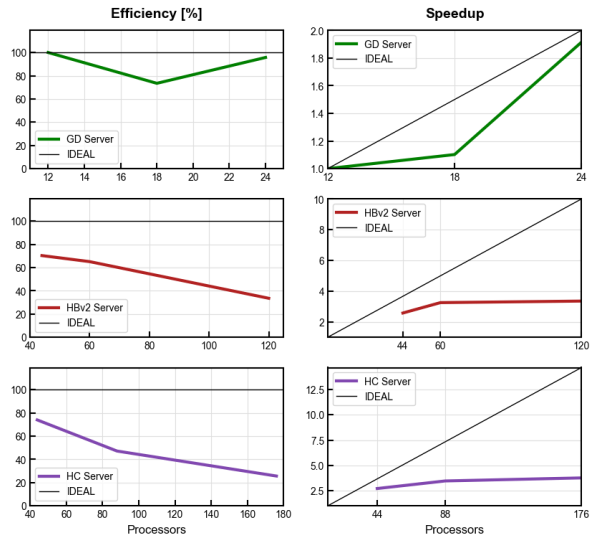

Figure 4. Efficiency and speedup parameters.

Figure 4 represents the calculated parameters for each server compared to the base case. It can be clearly observed together with the elapsed times from Table 3 how the Cloud servers have still a considerable increase of performance between the first two simulations, but the ones with a larger amount of cores are already limited by the parallelization.

Another interesting aspect to observe, this time related with the inhouse IDOM server, are the unconventional results obtained, where there's the expected decrease between the first scaling but an important increase of performance in the 24-core simulation. This may be explained by the processor configuration, where the partitioning of threads is done automatically by Fluent and may not be evenly distributed in those cases where some computational capacity is not assigned. Manually partitioning and assigning processors can mitigate this underperformance and it is being studied to address this finding for future studies.

V. CONCLUSIONS

The present work shows the impact of parallelization aspects of HPC on CFD codes for industrial application dealing with large and complex geometries. The approach needed to carry out these numerical simulations on a series of different servers is presented, showing the strong scaling parameters calculated for a series of parallelized CFD Conjugate Heat Transfer (CHT) calculations with a complex geometry and large meshes.

The results show an expected behaviour in terms of scalability for the presented cases, where the elapsed time to perform a fixed number of iterations decrease with the number of cores increases. Parallel computing limitations are clearly observed, showing that a given job is restricted in terms of scalability and no increase of performance is expected beyond a given number of processor units.

One of the outcomes of this study has been the decision to keep putting efforts into testing the capabilities of the Ansys Cloud® services to benefit from this tool when high workloads or intricate cases are considered.

Another important aspect extracted from the study is the impact of the architecture on the performance as seen in the inhouse servers when it comes to large calculations; some configurations can be clearly advantageous compared to others. Extensive testing for each configuration is, therefore, needed, to achieve optimal performance.

VI. References

[1] F4E Online Webinar. "F4E Technology Transfer Activities: Webinar on Advanced Simulation and Modelling".

[2] IDOM, "ITER VV PS#01 TH Benchmark. Baseline Data and Hypotheses.", 2018

[3] Ansys Cloud, www.ansys.com/products/platform/ansys-cloud.

[4] D. Catalán, A. Bernad, P. Alberto, J. Fradera, "Thermal Hydraulic code analysis Benchmark of ITER Vacuum Vessel components by use of different CFD codes.", CFD4NRS-8, 2020.

[5] Computational Fluid Dynamics for Nuclear Reactor Safety - OECD/NEA Workshop. https://cfd4nrs-8.sciencesconf.org/

[6] Houzeaux, G, "High-Performance Computing: Dos and Don'ts", 2018

[7] N. Gourdain, "High Performance Parallel Computing of Flows in Complex Geometries", 2011

[8] Knight, K., Berkoe, J., "High Performance Computing CFRD Final Technical Report", INL, 2003

Proceedings of the European Nuclear Young Generation Forum
ENYGF'21
September 27-30, 2021, Tarragona, Spain

Development of a Code for the Thermal-Hydraulic Simulation of the Canadian Supercritical-Water-Cooled Reactor Using Improved Nuclear Fuels

Ramos, Daniel* and Morales, Jaime B.

[1] Universidad Nacional Autónoma de México (UNAM), México

Corresponding author: igraveda@comunidad.unam.mx(Ramos, Daniel), jaime.morales@ingenieria.unam.edu (Morales, Jaime B.)*

I. INTRODUCTION

Among the generation IV reactors, the surface water reactor is the only one that is cooled with light water. In the case of Canada, knowledge about light water heat transfer within PHWR pressure channels is the basis to develop the Canadian SCWR. Under supercritical pressure, water will not experience phase change, however, a pseudo-critical point exists around which the water properties such as density and specific heat undergo drastic changes similar to the boiling process under subcritical pressure.

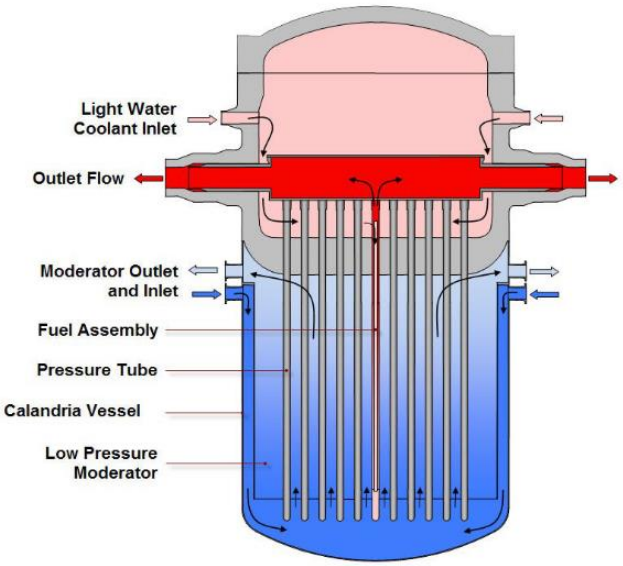

Figure 1. Schematic view of the Canadian SCWR core concept. [1]

A schematic of the reactor core is shown in Figure 1. The reactor core consists of a pressurized inlet plenum, a low pressure calandria vessel containing the heavy water moderator, and pressurized fuel tubes. A 2-step countercurrent fuel assembly is inserted into the fuel channel and is removed or rearranged at each refueling. The concept incorporates a fuel free center flow tube and a 2 ring fuel assembly, Figure 2. The inlet and outlet pipes are positioned above the reactor core so that a complete break in either will not result in an immediate loss of coolant in the reactor core. Figure 3 shows the details of the flow into the fuel assembly and the change in flow direction at the bottom of the assembly.

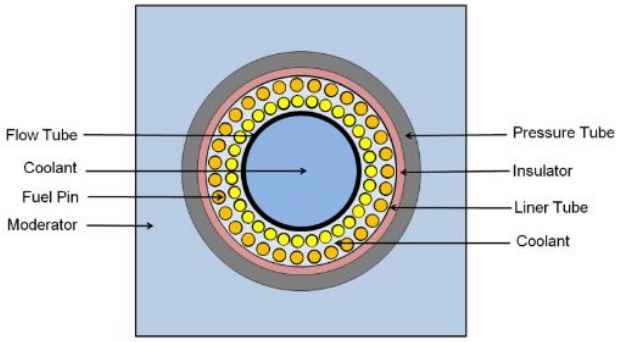

Figure 2. Canadian SCWR Fuel Bundle Cross Section. [1]

Several studies show that at high neutron fluxes the heat transfer coefficient is less than that predicted by the Dittus-Boelter equation, which leads to a high wall temperature [2]. This phenomenon is called heat transfer deterioration (HTD). The use of improved fuels, doped with some materials, can help improve thermal conductivity and prevent HTD.

The thermal conductivity of UO2 is improved with graphene doping for proportions of 1, 5 and 10% by volume, the improvement is 3.02%, 15.76% and 33.26% respectively [3]. That improvement occurs in 74% and 162% for pellets of sintered fuel with a load of 1wt.% and 5wt.% of graphene nanoplates respectively [4]. The fuel composed of UO2-10 vol% SiC exhibits a 62% increase in thermal conductivity [5]. The thermal conductivity of UO2-1.2% BeO at 1,100 K is greater than that of UO2 by approximately a range of 10-25% [6].

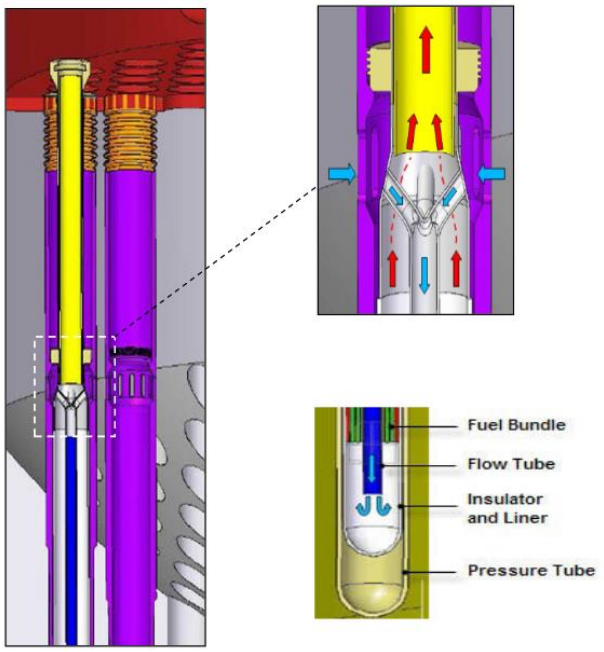

Figure 3. Canadian SCWR Fuel ChannelSchematicand Flow Streams. [1]

II. METHODOLOGY

The thermodynamic cycle is simulated in steady state using free software. OfficeLibreCalc is used as a control sheet, while the calculation of the water properties is programmed in Octave.

To obtain the thermodynamic properties of water under subcritical conditions, the XSteam.m program based on IAPWS IF-97 standard and developed by Magnus Holmgren is used and the NIST data were used for the supercritical region (T >373 °C and P >22 MPa), due to the discontinuities that XSteam.m presents in this area.

To obtain the radial profile of the fuel rod, the method described by Lahey [8] is followed. Figure 4 shows the radial division of a fuel element. The fuel element is divided into m-1 nodes, node m corresponds to the inner radius of the cladding and node n to the outer radius. The conduction equation (equation 1) is solved for a cylindrical geometry and implemented to solve the heat transfer equations in the fuel pellet, gap and cladding.

$$\rho c_p \frac{\partial T}{\partial t} = \frac{1}{r}\frac{\partial}{\partial r}\left(rk\frac{\partial T}{\partial r}\right) + q''' \qquad (1)$$

The model of six different types of nodes (central node, nodes inside the pellet, node at the radius of the pellet, node at the inner radius of the cladding, nodes in the cladding and node at the outer radius of the pellet) is obtained by representing the temperatures in the nodes of the modeled region, for the case of the steady state it results in ordinary differential equations with terms of net heat. Said equations are programmed in Octave and they are solved with the ODE45 function. Radial profiles are obtained for the case of conventional UO2 and for doping with graphene and BeO.

The fuel rod is divided into 7 radial nodes, where node 1 is the center of the pellet, node 4 its surface, node 5 the inner radius of the clad and node 7 the outer radius. The program that contains this algorithm is called Pastilla.m, where the contribution of materials that improve fuel is placed.

With these tools it is possible to simulate the dynamics of the Canadian SCWR following the algorithm described in references [2] and [7]. The transitory modeling also includes the analysis of supercritical water reactors during startup.

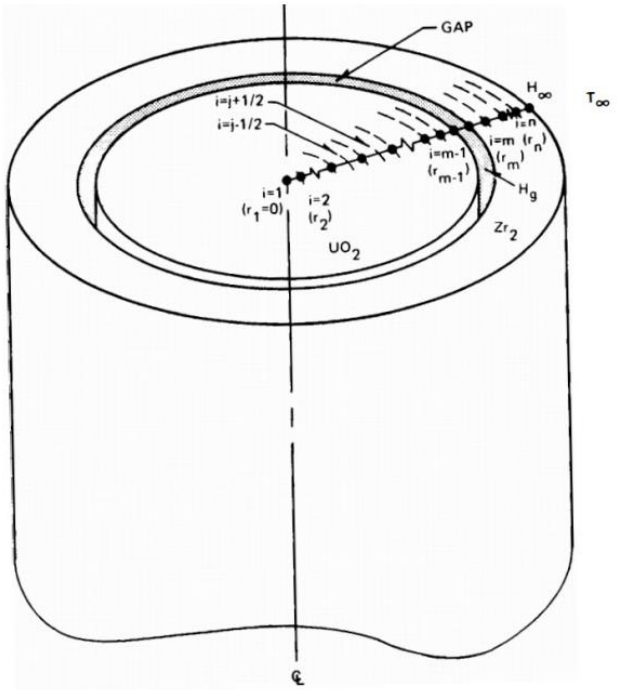

Figure 4. Radial division for the analysis of thermal conduction of a fuel element. [8]

III. RESULTS AND DISCUSSION

Figure 7. shows the control panel for the SCWR, the colored boxes contain the properties obtained for each stage of the cycle for the steady state. The thermodynamic cycle is shown at the bottom. Each of the stages of the cycle has its own subroutine programmed in Octave that uses the program developed XSteam_MX.m to obtain the thermodynamic properties of water.

Once the reactor is modeled in steady state and transient, it will be added to this worksheet. Plant efficiency can also be calculated. In this way it models the dynamics of the entire plant. The T-s diagram at the bottom of the spreadsheet shows that the steady-state parameters were calculated correctly.

The temperatures of the different nodes that are obtained in the convergence with the Pastilla.m program are presented in Figure 5, for different levels of doping of UO2 with graphene. A decrease in temperature can be seen in the four corresponding nodes of the pellet, mainly in the center.

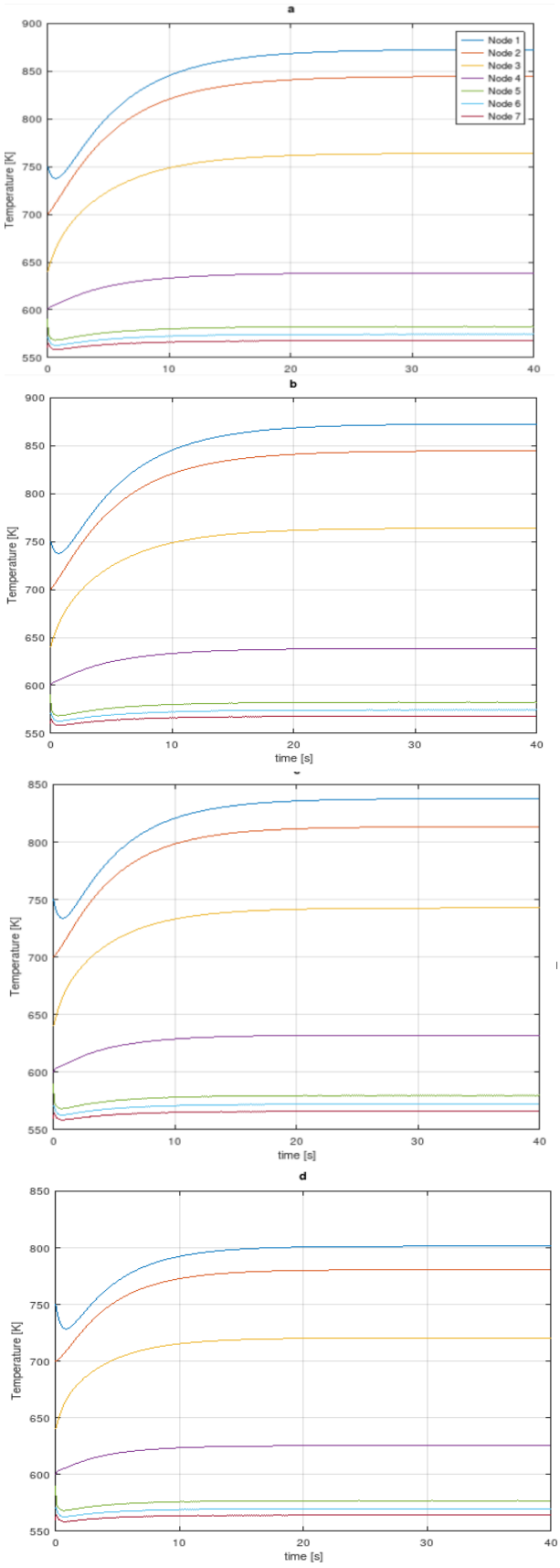

Figure 5. Temperature values for the seven nodes of the fuel road with a. UO2; b. UO2-graphene 1% v/v; c. UO2-graphene 5 % v/v; c. UO2-graphene 10 % v/v.

Decreasing heat flow can prevent HTD, even though the clad temperature remains similar. Figure 6 shows the temperatures of the seven nodes for various BeO ratios. Similar to graphene, the temperature drop for the center of the pellet is about 150 ° C between pure UO2 and doped with 10% v/v BeO, while for clad it is just 10 degrees .

The next step is to nodalize the coolant channel, the use of the Pastilla.m program will allow to calculate the temperature distribution on the fuel rod and with the XSteam_MX.m program the properties of the coolant along the channel.

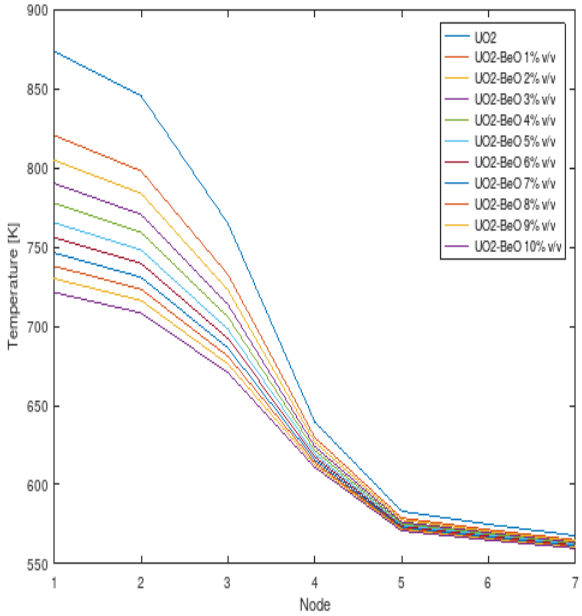

Figure 6. Temperatures of the seven nodes for various BeO ratios

IV. CONCLUSIONS

I. It is possible to use free software (Octave and LibreOffice Calc) to create a control sheet for a nuclear power plant.

II. The use of improved fuels lowers the temperature of the fuel pellet while maintaining the temperature of the clad.

III. The XSteam_MX.m program correctly obtains the thermodynamic properties of water under subcritical and supercritical conditions.

V. References

[1] M. Yetisir, M. Gaudet, D. Rhodes, "Development and integration of canadian SCWR concept with counter-flow fuel assembly," in The 6th International Symposium on Supercritical Water-Cooled Reactors, March 03-07 2013, 2013.

[2] M.M. Rahman, J. Dongxu, M.S. Beni, H.C. Hei, W. He, J. Zhao,"Supercritical water heat transfer for nuclear reactor applications: A review," Annals of Nuclear Energy, vol. 97, pp.53-65, 2016.

[3] S.W. Lee, H. T. Kim, I. C. Bang, “Performance evaluation of UO2/graphene composite fuel and SiC cladding during LBLOCA using MARS-KS,” Nuclear Engineering and Design, vol. 257, pp 139–145, 2013.

[4] T. Yao, G. Xin, S.M. Scott, B. Gong and J. Lian, “Thermally-Conductive and Mechanically-Robust Graphene Nanoplatelet Reinforced UO2 Composite Nuclear Fuels,” SCIENTIFIC REPORTS, 2018.

[5] S. Yeo, E. Mckenna, R. Baney, G. Subhash and J. Tulenko, “Enhanced thermal conductivity of uranium dioxide–silicon carbide composite fuel pellets prepared by Spark Plasma Sintering (SPS),” Journal of Nuclear Materials, vol. 433, pp 66–73, 2013.

[6] S. Ishimoto , M. Hirai , K. Ito and Yoshiaki Korei, “Thermal Conductivity of UO2-BeO Pellet,” Journal of Nuclear Science and Technology, vol. 33, no. 2, pp. 134-140, 1996.

[7] L. Wang, Ph.d, Y. Yuan, Ph.d, J. Shan, Ph.d and X. Zhang, “Study on thermal hydraulic characteristics under startup of SCWR,” Progress in Nuclear Energy, vol. 122, 2020.ial media platforms,” PLoS One, vol. 11, no. 5, pp. 1–22, 2016.

[8] R.T. Lahey, F.J. Moody, “The Thermal-Hydraulics of a Boiling Water Nuclear Reactor,” Second Edition, La Grange Park, 1993, pp. 291-324.

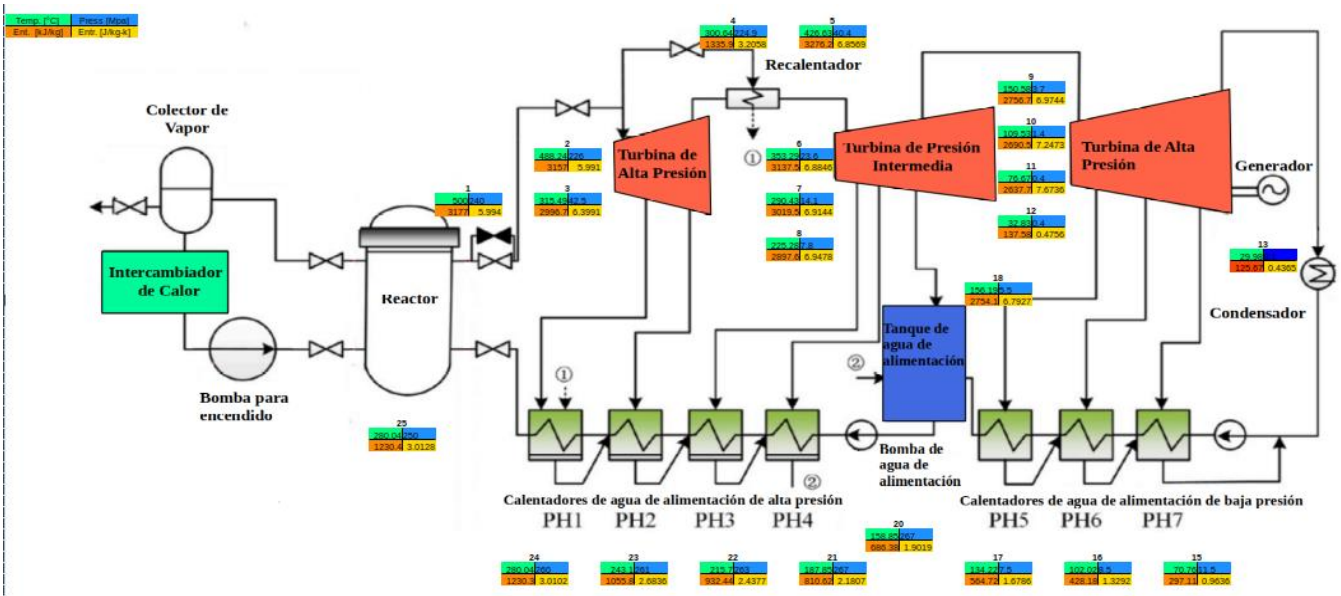

Etapa	Localización	Temperatura °C	Presión Bar	Entalpía kJ/kg	Entropía kJ/kg
1	Salida del Reactor	500	240	3177	5.994
2	Turbina de Alta Presión. Primera Etapa	488.24	226	3157	5.991
3	Turbina de Alta Presión. Segunda Etapa	315.49	42.5	2996.66	6.399109
5	Salida del Recalentador	426.63	40.4	3276.207	6.856923
6	Turbina de Presión Intermedia. Primera Etapa	353.29	23.6	3137.469	6.884566
7	Turbina de Presión Intermedia. Segunda Etapa	290.43	14.1	3019.508	6.914364
8	Turbina de Presión Intermedia. Tercera Etapa	225.28	7.8	2897.551	6.947839
9	Turbina de Baja Presión. Primera Etapa	150.58	3.7	2756.659	6.974399
10	Turbina de Baja Presión. Segunda Etapa	109.53	1.4	2690.494	7.247333
11	Turbina de Baja Presión. Tercera Etapa	76.67	0.4	2637.677	7.673623
12	Turbina de Baja Presión. Cuarta Etapa	32.83	0.1	137.5795	0.4756308
13	Salida del Condensador	29.98	0.1	125.6668	0.4365154
14	Salida de la Bomba del Condensador	29.98	13.5	126.8886	0.4361075
15	HP7 Salida	70.76	11.5	297.1142	0.9635858
16	HP6 Salida	102.02	8.5	428.1782	1.329191
17	HP5 Salida	134.22	7.5	564.7225	1.678605
19	Salida de la Bomba de Alimentación	157.19	267	679.3214	1.885527
20	Entrada de la Bomba de Alimentación	158.85	267	686.3769	1.90189
21	HP4 Salida	187.85	265	810.6157	2.180704
22	HP3 Salida	215.7	263	932.4447	2.437749
23	HP2 Salida	243.1	261	1055.755	2.683611
24	HP1 Salida	280.04	260	1230.273	3.01022
25	Entrada del Núcleo	280.04	250	1230.437	3.012842
1	Salida del Reactor	500	240	3177	5.994
18	Salida del Tanque de Agua de Alimentación	156.19	5.5	2754.109	6.792657
4	Recalentador. Salida del lado secundario	300.64	224.9	1335.878	3.205817

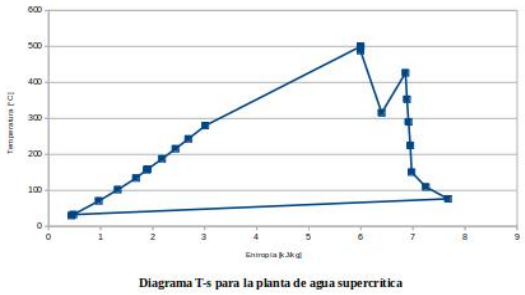

Figure 7. Control Panel of the SCWR.

Proceedings of the European Nuclear Young Generation Forum
ENYGF'21
September 27-30, 2021, Tarragona, Spain

Spent fuel criticality assessment comparison between Keno and OpenMC

Castro, Emilio[1*] and García-Herranz, Nuria[2]

[1] Grupo NFQ, Spain; [2] Universidad Politécnica de Madrid (UPM), Spain

*Corresponding author: *emilio.castro@nfq.es*

I. INTRODUCTION

Spent fuel storage safety assessments must guarantee the fulfilment of three main objectives: subcriticality, heat dissipation and radiation shielding [1]. Each of these objectives requires a specific set of calculations and there are several state-of-the-art computer codes available to address each aspect. This work focuses on criticality safety calculations.

Traditionally, two well-known codes for this kind of simulation have been Keno from SCALE package [2] and MCNP [3], both based on a Monte Carlo approach with proven accuracy and performance over the years. Currently, there is a new alternative to those codes named OpenMC [4]. OpenMC is also a Monte Carlo transport code but it has one unique feature: it is open-source, with freedom to use, distribute and modify the code, and free of cost. Therefore, despite not having so much tradition as other tools, it is a very attractive one, which can play an important role in the criticality safety and reactor physics communities.

The objective of this work is to compare criticality calculations of Keno and OpenMC over decay time using a spent fuel cask based on publicly accessible information. On the one hand, the same nuclear data libraries are used to eliminate a possible source of discrepancies, thus the observed differences would only be attributable to the Monte Carlo codes themselves and possibly to the employed nuclear data processing code (which will differ). On the other hand, the impact of using different nuclear data libraries is also assessed.

II. PROBLEM DEFINITION

This work is based on data from the "OECD/NEA Burn-up Credit Criticality Safety Benchmark Phase VII" [5]. The objective of this exercise was to compare the ability of existing computer codes and nuclear data libraries to predict spent nuclear fuel isotopic composition and criticality over time. For this purpose, a generic fuel cask configuration was defined.

The fuel cask is loaded with 21 fuel assemblies with 17x17 rods submerged in water to consider possible off-normal and accident conditions that could flood the cask with water [6]. All dimensions and geometric details are fully described in the benchmark specifications. Figure 1 represents a radial cut and a vertical cut of the fuel cask at its middle positions.

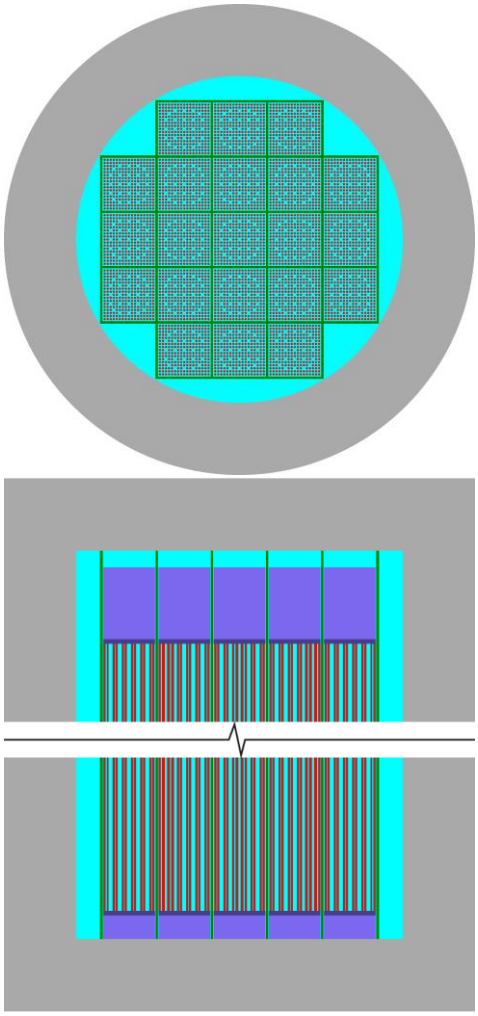

Figure 1. Cask model geometry

The benchmark specifications provide the discharged fuel composition. Using these nuclides densities, the first step is the isotopic characterization of the fuel over decay time. Then, the second step is the criticality calculation, using two nuclide sets, the first one considering only actinides and the second one considering actinides and long-lived fission products. Those subsets are related to the different levels of burnup credit allowed by the regulators in different

countries [7]. On the one hand, if actinide-only burnup credit level is applied, credit is taken only for the net fissile content of the fuel and the absorption effect of the actinides. On the other hand, if the actinide and fission product burnup credit level is implemented, credit is also taken for the neutron absorption in the major fission products. Table 1 shows the isotopes that compose each set.

Table 1. Nuclide sets to use in each scenario of the benchmark for the criticality calculations.

Set	Isotopes
Set 1 Actinides Only	^{233}U, ^{234}U, ^{235}U, ^{236}U, ^{238}U, ^{238}Pu, ^{239}Pu, ^{240}Pu, ^{241}Pu, ^{242}Pu, ^{241}Am
Set 2 Actinides and Fission Products	^{233}U, ^{234}U, ^{235}U, ^{236}U, ^{238}U, ^{237}Np, ^{238}Pu, ^{239}Pu, ^{240}Pu, ^{241}Pu, ^{242}Pu, ^{241}Am, ^{242m}Am, ^{243}Am, ^{95}Mo, ^{99}Tc, ^{101}Ru, ^{103}Rh, ^{109}Ag, ^{133}Cs, ^{143}Nd, ^{145}Nd, ^{147}Sm, ^{149}Sm, ^{150}Sm, ^{151}Sm, ^{152}Sm ^{151}Eu, ^{153}Eu, ^{155}Gd

Keno from SCALE 6.2.4 and OpenMC 0.12 are used in this work. Keno uses 100000 neutrons per generation and runs a large number of generations (ranging from 737 to 1261 depending on the case) until the k_{eff} standard deviation reaches 0.0001, with 200 inactive generations. OpenMC uses 100000 neutrons per generation and runs 1000 generations with 200 inactive generations so that the standard deviation of k_{eff} is approximately 0.0001.

III. RESULTS

A. Comparison of Keno and OpenMC

First, Keno and OpenMC are compared to verify the equivalence of the models and options in both codes. In order to eliminate possible sources of errors, the same nuclear data library (ENDF/B-VII.1 [8]) is used in both codes, using the files officially provided with each code in its distribution.

Figure 2 represents k_{eff} over decay time for the actinide-only set of nuclides, and Figure 3 represents k_{eff} over decay time for the actinide and fission product set. In both figures, the results using SCALE and OpenMC are plotted along with the results of the benchmark participants. The fuel cask neutron multiplication factor k_{eff} is below 0.96 for all calculated decay times, meaning that the fuel cask is far from criticality. After fuel discharge k_{eff} decreases until approximately 100 years because of the decay of ^{241}Pu to ^{241}Am which acts as a neutron absorber. Then k_{eff} increases because of the decay of neutron absorber nuclides (^{238}Pu, ^{240}Pu, ^{241}Am and ^{243}Am).

Using the second set of nuclides, the predicted k_{eff} values are lower than those obtained using the first set, because some of the isotopes are neutron absorbers.

Figures 4 represents the differences in pcm of the calculated k_{eff} between SCALE and OpenMC with both sets of nuclides. There is a very good agreement with a nearly constant difference below 100 pcm, with OpenMC slightly overestimating the k_{eff} value with respect to SCALE. It can be concluded that: *i*) models and methodologies relevant for criticality calculation and decay isotopic prediction used in both codes are equivalent; *ii*) the nuclear data processing systems used for both codes to produce the final application nuclear data files are also equivalent.

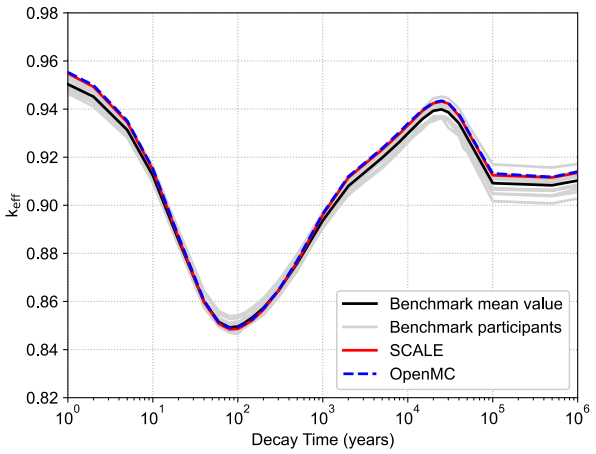

Figure 2. k_{eff} over decay time using SCALE and OpenMC with ENDF/B-VII.1. Actinide-only set.

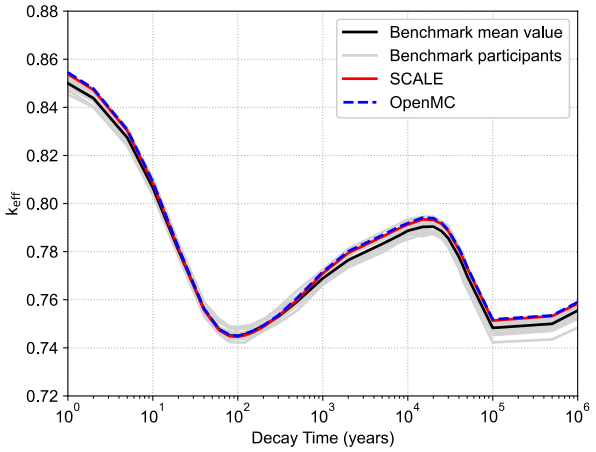

Figure 3. k_{eff} over decay time using SCALE and OpenMC with ENDF/B-VII.1. Actinide and fission product set.

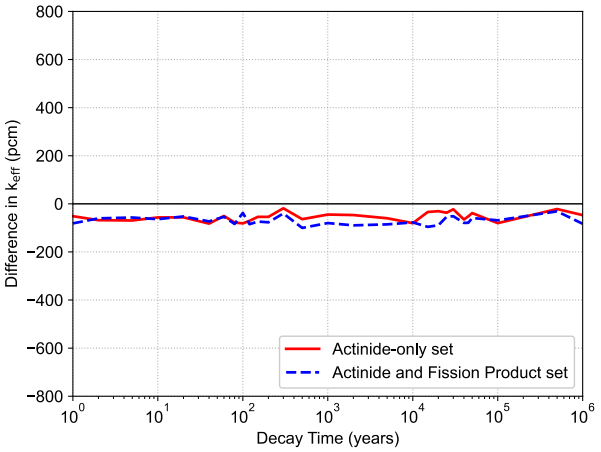

Figure 4. Differences in k_{eff} over decay time between SCALE and OpenMC with ENDF/B-VII.1.

B. Comparison of ENDF/B-VII.1 and JEFF-3.3

It is also interesting to check the impact of different nuclear data libraries on the spent fuel isotopic compositions and associated k_{eff} values over time. In this section, only OpenMC is used to compare the impact of using ENDF/B-VII.1 or JEFF-3.3 [9] nuclear data libraries, both of them officially provided with the software package.

The results are compared in Figures 6 and 7 for the actinide-only and the actinide and fission product sets respectively. A very good agreement between ENDF/B-VII.1 and JEFF-3.3 values can be seen except for decay times around 100 years where the difference is over 600 pcm, with JEFF-3.3 underpredicting the k_{eff} value.

An analysis of the nuclide concentrations showed that ^{241}Am density has a maximum value around 100 years being one of the most relevant isotopes at that decay time. Thus, to highlight the source of discrepancies, an additional OpenMC calculation was performed using JEFF-3.3 library for all isotopes except for ^{241}Am, whose information was taken from ENDF/B-VII.1. Results are included in Figures 6 and 7 where it can be seen that the differences around 100 years vanish, meaning that the information for ^{241}Am from ENDF/B-VII.1 and from JEFF-3.3 differs significantly (excluding an effect on the nuclear data processing code).

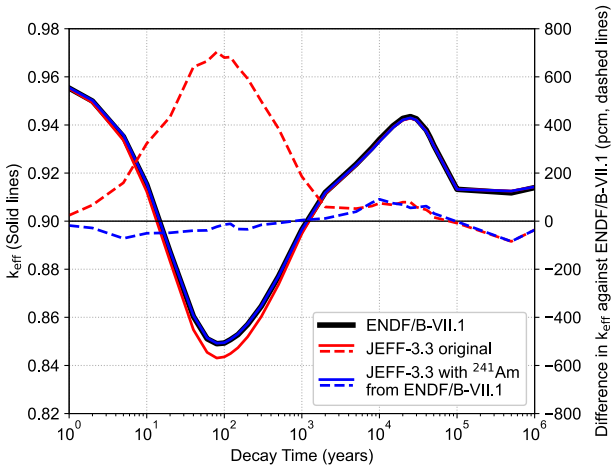

Figure 6. Differences in k_{eff} over decay time using OpenMC between ENDF/B-VII.1 and JEFF-3.3. Actinide-only set.

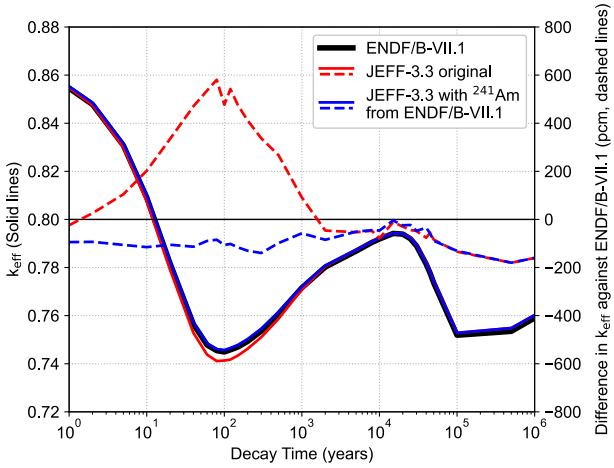

Figure 7. Differences in k_{eff} over decay time using OpenMC between ENDF/B-VII.1 and JEFF-3.3. Actinide and fission product set.

A similar behaviour was also identified in reference [10] using MCNP code with JEFF-3.3 and ENDF/B-VIII-b4 [11] nuclear data libraries.

IV. CONCLUSIONS

Criticality safety calculations are an important part of spent fuel management in order to guarantee that the storage configuration remains in a subcritical state at all times. In this work, SCALE/Keno and OpenMC have been compared using a generic spent fuel cask from the OECD/NEA burnup credit benchmark Phase-VII.

In the first step, the codes have been compared using the same nuclear data library. Predicted values of k_{eff} are in very good agreement with differences below 100 pcm in k_{eff} over all decay times. The fact that the same nuclear data libraries have been used means that not only the theory, implementation and models of both codes are equivalent, but also that the associated nuclear data processing systems are consistent.

In a second step, two nuclear data files are compared using OpenMC: ENDF/B-VII.1 and JEFF-3.3. Differences over 600 pcm in the predicted k_{eff} appear around 100 years, which are caused by differences in the ^{241}Am cross section files in both libraries. As future work, a deeper analysis will be carried out in order to identify which reactions or energy ranges of ^{241}Am cross section files are causing those discrepancies between ENDF/B-VII.1 and JEFF-3.3.

V. References

[1] "Spent fuel performance assessment and research," International Atomic Energy Agency, March, 2003.

[2] W. A. Wieselquist, R. A. Lefebvre and M. A. Jessee, "SCALE Code System," ORNL/TM-2005/39, Version 6.2.4, Oak Ridge National Laboratory, 2020.

[3] T. Goorley et al., "Initial MCNP6 Release Overview," Nuclear Technology, vol. 180, pp. 298-315, December, 2012.

[4] P. K. Romano, N. E. Horelik, B. R. Herman, A. G. Nelson, B. Forget and K. Smith, , "OpenMC: A State-of-the-Art Monte Carlo Code for Research and Development," Annals of Nuclear Energy, vol. 82, pp. 90-97, August, 2015.

[5] "Burn-up Credit Criticality Safety Benchmark Phase VII. UO2 Fuel: Study of Spent Fuel Compositions for Long-term Disposal," OECD/Nuclear Energy Agency, 2012.

[6] W. Lake, "Burnup credit activities being conducted in the United States", in Implementation of burnup credit in spent fuel management systems, International Atomic Energy Agency, April, 1998.

[7] "Practices and developments in spent fuel burnup credit applications", International Atomic Energy Agency, October, 2003.

[8] M. B. Chadwick et al., "ENDF/B-VII.1 Nuclear Data for Science and Technology: Cross Sections, Covariances, Fission Product Yields and Decay Data," Nuclear Data Sheets, vol. 112, issue 12, pp. 2887-2996, December, 2011.

[9] A. J. M. Plompen at al., "The joint evaluated fission and fusion nuclear data library, JEFF-3.3," Eur. Phys. J. A, vol. 56, no. 181, July, 2020.

[10] O. Cabellos, "Testing JEFF-3.3T3 in the Computational PHASE-VII Benchmark," in JEFF Processing & Verification, Benchmarking & Validation Meeting, April, 2017.

[11] D. A. Brown et al., “ENDF/B-VIII.0: The 8th Major Release of the Nuclear Reaction Data Library with CIELO-project Cross Sections, New Standards and Thermal Scattering Data,” Nuclear Data Sheets, vol. 148, pp. 1-142, February, 2018.

Proceedings of the European Nuclear Young Generation Forum
ENYGF'21
September 27-30, 2021, Tarragona, Spain

Development of a detailed 3D CAD model of a generic PWR-KWU containment as a basis for a better assessment of H2/CO combustion risk

Serra, Luis[1*]; Domínguez-Bugarín, Araceli[1]; Estévez-Albuja, Samanta[1]; Vázquez-Rodríguez, Carlos[1]; Jiménez, Gonzalo[1]; Kelm, Stephan[2] and Herranz, Luis E.[3]

[1] Universidad Politécnica de Madrid, Spain; [2] Forschungszentrum Jülich (FZJ), Germany; [3] CIEMAT, Spain

*Corresponding author: *luis.slopez@alumnos.upm.es*

I. INTRODUCTION

In case of a Severe Accident (SA), the Nuclear Power Plant (NPP) reactor containment fulfils an important role acting as the final physical barrier against a release of radioactive material into the environment. Consequently, assuring the integrity of the containment building is a key element of the accident management. Furthermore, the containment geometry and its compartmentalization play an important role in the combustible gas distribution and combustion as it influences notably the thermohydraulic behavior of the gases through the containment. Thus, a comprehensive model of the containment's geometry is the basis of every 3D containment analysis. For this matter, the use of Computational Aided Design (CAD) software as a cornerstone of the modelling process serves as a bridge between the containment layouts and the thermal-hydraulic models [1, 2].

The use of detailed 3D CAD models allows a thorough evaluation of free volumes, flow paths, areas and locations, and wall surfaces. It can be also used as a pre-processing tool to build different nodalization strategies, while storing all the data in the same file, making these models a user-friendly tool to enhance the thermal-hydraulic simulations [3].

This work is being developed under the framework of the AMHYCO project (Euratom 2014-2018, GA No 945057). Its main objective is to improve experimental knowledge and simulation capabilities for the H_2/CO combustion risk management in SAs. The aim is to enhance the accident management strategies; particularly, those related to the mitigation of combustion of heterogeneous gas mixtures. During this project, several models of PWR containments, using different modelling approaches, will be used to simulate the complex scenarios related to SA sequences. Every PWR containment design will have its 3D CAD model, which main application will be to facilitate all the information needed for the creation of all computational models. In this way, the partners of the project using Lumped Parameter (LP), 3D (such as GOTHIC), and Computational Fluid Dynamics (CFD) simulation approaches will build the models on the same basis.

This article is focused on the development of a detailed 3D CAD model for a German PWR-KWU, one of the designs included in AMHYCO, using AutoCAD Autodesk 2021®. Firstly, a description of the methodology which will be used for the PWR-KWU and the other containment designs is given. Then, a process of identification of flow paths and nodalization strategies will be explained, followed by a brief description of the strategy that will be used for modelling the containment geometry into the 3D GOTHIC environment.

II. 3D CAD MODEL METHODOLOGY

The development of the 3D CAD model follows a series of steps: 1. Creation of a fully detailed CAD model, 2. Extraction of relevant information for the creation of lumped models, 3. Extraction of relevant information for the creation of 3D models, 4. Creation of a database with all the relevant information. As stated before, this database will serve as a cornerstone for the development of all numerical models.

This paper will focus on points 1 to 3 for the PWR-KWU. The primary information source this containment model is based on is publicly available in [4]. All floor and elevation layouts have been imported, sized, digitalized, and extruded in the CAD software. The built of the model has been made from bottom to top, using the different plan views as reference for each level construction. Moreover, it has been used to connect concrete and steel structures, accounting for any possible flow paths and junctions within the interior parts of the buildings.

The PWR-KWU containment building is divided into two regions, the spherical inner containment (named UJA) and the outer surrounding region, the annulus (named UJB). The inner region, UJA, contains a missile shield cylinder which allocates the nuclear steam supply systems and the spent fuel pool. The second region, UJB, is enclosed by a thick reinforced concrete wall and protects the inner containment pressure tight steel shell. Furthermore, it houses the

emergency cooling and safety injection systems. During the modelling process, this region will be envisaged as a thermal boundary condition for the scenarios addressed in AMHYCO, and the accuracy in its modelling will not be considered as important as the inner compartments.

The different levels of the buildings are mainly built by extrusion (e.g., inner walls or components). This is an advantageous method of 3D construction in a highly compartmentalized containment as the KWU one. The whole containment building, comprised of UJA and UJB regions, has been enclosed by the dome and a horizontal concrete slab (which serves as ground floor at the lowest point). Other structures, e.g., the concrete lower cap that holds the spherical liner, have instead been built by adding and subtracting curved volumes, something either way impracticable with only a vertical snap method [1], as the extrusion one. Moreover, these curved surfaces are important for CFD studies and justify in a way the detail imposed to the construction.

The construction has mainly relied upon five top views at different elevations and two front sections. Elevation 0.0 m corresponds to the bottom of the Reactor Pressure Vessel. Whenever the public information of a certain elevation was incomplete, or detailed geometrical aspects were not available, certain modelling hypotheses were necessary. As an instance, only one of four symmetrical annular rooms stairwells was depicted in the public layouts. Therefore, the building of the other staircases was made using an analogous geometry. Similar hypotheses were needed to model gratings, walking grids, doors, and the nuclear steam supply system.

All these hypotheses have been done maintaining the structural coherence and the isolation of spaces of the two-room containment. An iterative process, supported by several partners of AMHYCO, helped to refine the geometrical details all along the containment to obtain a reliable 3D model of a generic PWR-KWU containment.

Figure 1 shows a sectional cut and an elevation cut of the public available layouts of the PWR-KWU containment from which the CAD model has been built. Figure 2 shows an intermediate stage in the construction of the full model. Walls and floors in a lighter colour belong to the outer containment building (UJB), while the darker ones belong to the inner containment (UJA). The RCS circuit is embedded to show its location.

III. NODALIZATION AND IDENTIFICATION OF JUNCTIONS AND FLOW PATHS

To exemplify one of the applications of the 3D CAD model, this section shows the main steps to define a nodalization for a LP thermal-hydraulic model of the PWR-KWU. The basis for the nodalization of the containment comes from the framework of the Generic Containment (GC) benchmark, which was initially developed within the European NoE SARNET-2 [5] and continued within the framework of the NUGENIA SAMHYCO-NET project, led by IRSN. Taking into consideration the primary containment building, and assuming that the auxiliary building works as boundary conditions in the LP codes, the proposed nodalization is divided in 11 Control Volumes (CV), presented in Figure 3.

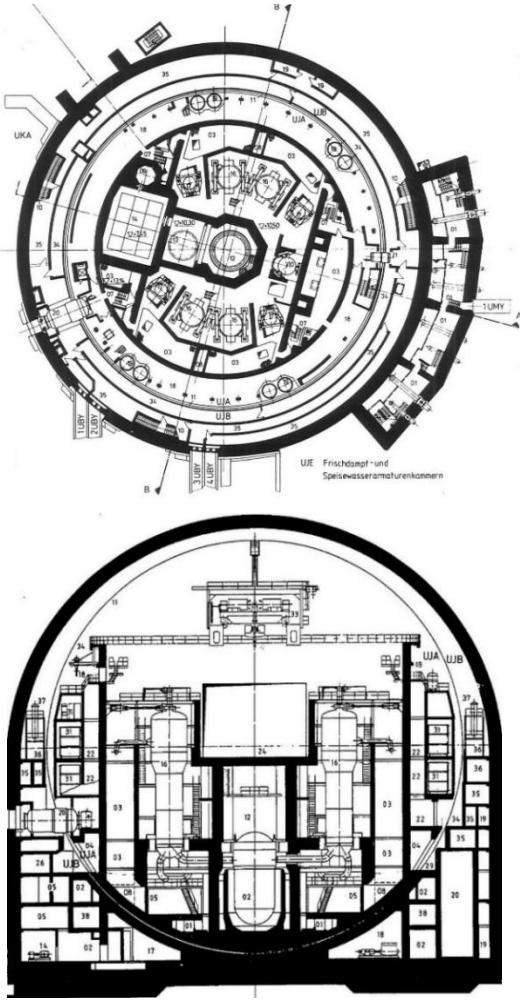

Figure 1. +12 m elevation cut (up) and sectional cut (down) from the public layouts of the PWR-KWU containment. Ref: [4]

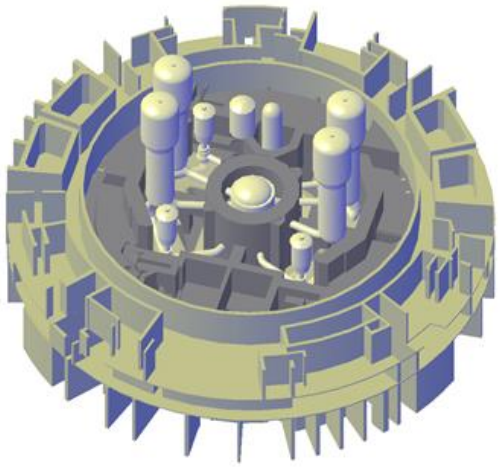

Figure 2. Aerial view of level +6 meters of the KWU 3D containment model with the primary circuit embedded.

The vessel cavity and the SGs compartments have their own CVs in order to study the behavior of gaseous mixtures in detail in postulated transients. Another CV was placed below the SG CVs and surrounding the cavity, which aim to represent the containment sump.

At each side of the SGs, there are two CVs with annular shape. The regions coloured in green, and pink are not

directly connected to the open space where the SGs (yellow and red) are located, and thus pressure and temperature differences may be expected in these zones. Equally, the inner cylinder of the containment isolates these zones located inside it (green and pink) from those locate outside (dark blue and purple), precluding the gas flow between them. Thus, those annular spaces should have individual CVs to allow the LP codes to predict certain heterogeneity in these regions. Finally, the last CVs defined are the reactor room, the spent fuel pool (SFP), and the dome. The basic information to model these spaces in LP codes are free volumes and elevations. The free volume values (see Table 1) are easier to obtain from plan layouts thanks to the CAD capabilities.

Table 1. Nodalization CVs with their free volume and elevations.

Zones	Free Volume (m^3)	Base Elev. (m)	Top Elev. (m)
CAVITY	250.31	-1.9	10.55
SUMP	5635.9	-1.9	10.1
DUCT	2698.17	6.2	11.7
SG-N	4371.98	10.1	29.3
SG-S	4311.97	10.1	29.3
ANN-E-int	1709.24	1.84	21.2
ANN-W-int	1206.29	0.35	21.2
ANN-N-ext	4124.09	12	21.2
ANN-S-ext	4178.99	12	21.2
SFP	1326.85	7.45	21.5
R-ROOM	1115.62	10.3	21.2
DOME	43166.59	21.2	50.85

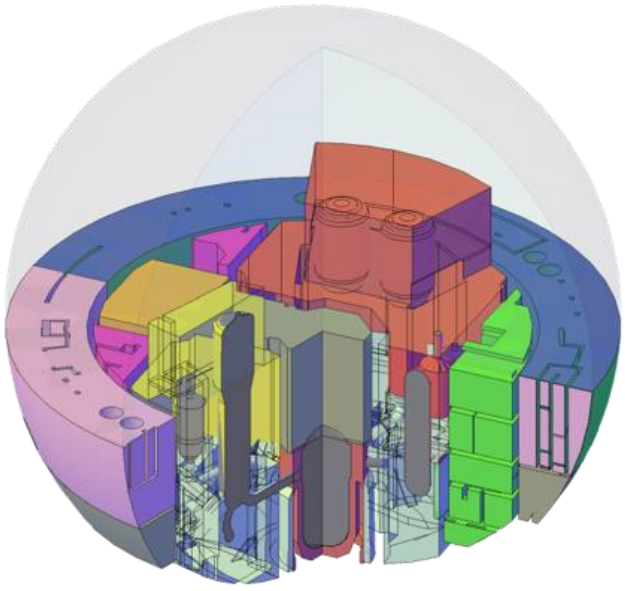

Figure 3. Nodalization of the PWR-KWU Generic Containment

Furthermore, the simulation of the thermal-hydraulic behavior of gaseous mixtures inside the containment requires to define the possible flow paths between the different zones. These connections join CVs of the lumped nodalization and determine the fluid transport between them.

The junctions are defined through an effective area that represent the opening areas between CVs, and other additional variables to approximate friction and form losses. These areas are obtained from the detailed 3D CAD model and are shown in Figure 4, where all identified junctions are displayed under a colored scheme that matches the nodalization representation of Figure 3. Important junctions range from stairwell landings, walking grids, burst foils or open geometrical connections.

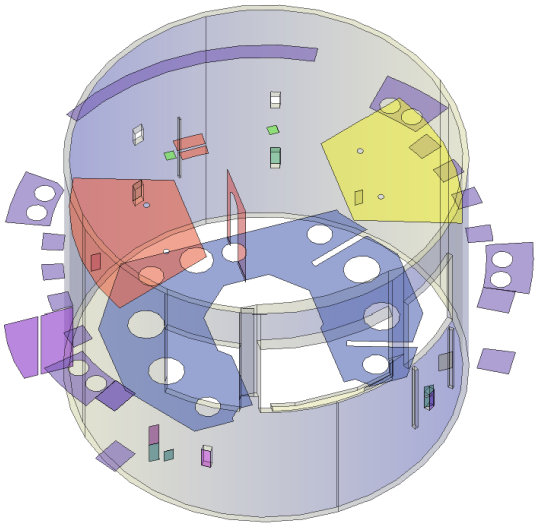

Figure 4. LP junctions between CVs

IV. CREATION OF A SIMPLIFIED MODEL

Some 3D thermal-hydraulic analysis tools, e.g., GOTHIC [6], can import a 3D geometry from external sources. To exploit this capability, the methodology developed at the UPM is based on three stages. The first one is the already depicted creation of a detailed CAD model where all the geometrical relevant data is stored, considerably reducing the required GOTHIC pre-processing time (insight on this matter can be found in [2]). The intermediate stage is the creation of a simplified CAD model which serves as a bridge between the CAD tool and GOTHIC, where the last step, the in-code pre-processing effort, is undertaken.

The simplified CAD model accounts for the geometrical limitations inherent to the analysis code. GOTHIC uses an orthogonal mesh to subdivide volumes into multi-dimensional grids. Also, GOTHIC 3D representation of structures and components relies upon the definition of specific blocks, namely wedges, caps, cones, and cylinders, and on the other hand, in the definition of openings to account for geometrical open connections, flow pathways and 3D local phenomena. To this effect, in the same fashion as the lumped identification of junctions between CVs (see Figure 4), 3D connections are identified by an effective area, e.g., doors, windows, gratings, trapdoors, etc., Thus, the detailed 3D PWR-KWU CAD model needs to be simplified in a further step, by the reconstruction and displacement of walls, floors, openings, etc., to match an adequate and

traceable simplified configuration. To this aim, a recently developed methodology is employed [7], which is based on the identification of problematic couplings between the actual geometry and the meshes utilized for the simulations. The implementation of the simplified geometry adapted to the mesh decreases the computational cost up to a 90%. For this reason, it will be used in all AMHYCO GOTHIC models. Figure 5 shows an example of the adaptation of a SG compartment, as part of the preventive simplification basis for pre-processing in the GOTHIC code.

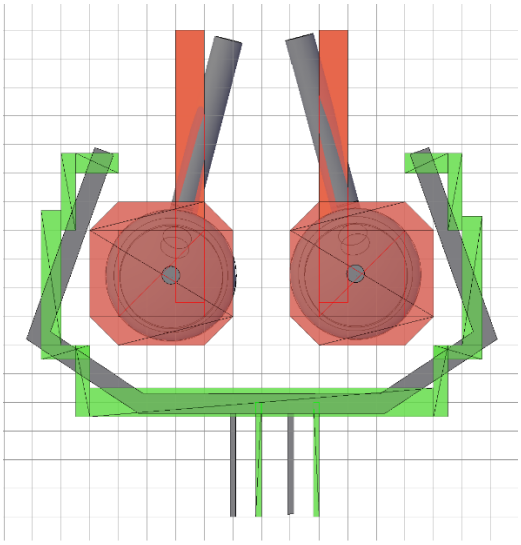

Figure 5. Simplification of KWU SG and its cage and adaptation to a 1x1m mesh

V. CONCLUSIONS

A detailed 3D CAD model of a Generic PWR-KWU containment has been built from publicly available layouts of a 1300 MWe NPP. The model, which can be exported for its use in LP, 3D and CFD codes (under the required adaptations and simplifications) will be used to perform thermal-hydraulic analysis in the AMHYCO project to study the H2/CO combustion risk in the late phases of SAs. The methodology proposed aims to be a cornerstone for the development of other generic PWR 3D detailed models, namely for PWR-W and PWR-VVER containments. Furthermore, to have those generic containments built from the same methodological basis will minimize input data and user effect uncertainties [8] in the various simulations performed by the AMHYCO partners.

The process of 3D modelling a highly compartmentalized containment with CAD tools has brought light to some advantages of the construction methodology presented. The CAD environment is a user-friendly interface where specific data can be traced for further post-processing, e.g., the location of each wall, flow path, thermal surface, etc. Different nodalization strategies can be explored and their free volumes extracted to compare the benefits of each approach or to identify possibly omitted junctions between relevant areas of the containment. Moreover, the CAD model can be simplified to be exported with a geometry usable by thermal-hydraulic analysis codes. This potential is revealed in this case of study in the bridge built between the CAD model and the GOTHIC pre-processing tools. Moreover, the detailed methodology of construction will improve the thermal-hydraulic analysis in both LP code simulations (with accuracy in the definition of free volumes and connections) and 3D containment codes (with the possibility to account for three-dimensional flow paths and sub-compartment interactions) using the CAD as basis for different post-processing tools, such as Paraview.

Acknowledgements

This project has received funding from the Euratom research and training programme 2019-2020 under Grant Agreement n°945057. The content of this paper reflects only the author's view. The European Commission is not responsible for any use that may be made of the information it contains.

References

[1] R. Bocanegra, G. Jiménez and M. K. Fernández-Cosials, "Development of a PWR-W GOTHIC 3D model for containment accident analysis," Annals of Nuclear Energy, vol. 87, 2016.

[2] K. Fernández-Cosials, S. Estévez-Albuja, G. Jiménez, R. Bocanegra and C. Vázquez-Rodríguez, "3D containment modelling of PWR-KWU Trillo NPP with the GOTHIC code," Annals of Nuclear Energy, vol. 133, 2019.

[3] C. Vázquez-Rodríguez, G. Jiménez, S. Estévez-Albuja and C. Queral, "Nodalization Sensitivity Analysis of the AP1000 Containment with MELCOR 2.1," in ICAPP 2019, Juan-les-pins, France, 2019.

[4] SIEMENS, "Dokumentationen SIEMENS / KWU Sicherheitsbericht für die KKW Stendal GmbH 1990," [Online]. Available: http://www.ycdt.de/kkw-stendal/siemens-reaktor-stendal.htm.

[5] S. Kelm, M. Klauck and S. Beck et. al., "Generic Containment: Detailed comparison of containment simulations," Annals of Nuclear Energy, vol. 74, 2014.

[6] EPRI, GOTHIC Thermal Hydraulic Analysis Package, Version 8.3(QA), Palo Alto, CA, 2018.

[7] S. Arfinengo-del-Carpio, C. Vázquez-Rodríguez and G. Jiménez, "Preventive methodology: beforehand geometric simplifications a priori for containment models optimization with the GOTHIC code," in ENYGF 2021, Tarragona, Spain, 2021.

[8] M. Povilaitis, S. Kelm and E. Urbonavicius, "The Generic Containment SB-LOCA accident simulation: comparison of the parameter uncertainties and the user-effect," Annals of Nuclear Energy, no. 106, 2017.

Proceedings of the European Nuclear Young Generation Forum
ENYGF'21
September 27-30, 2021, Tarragona, Spain

Optimisation of the I-131 production from enriched and natural tellurium dioxide in MARIA research reactor

Madejowski, Gaweł[1]

[1] National Centre for Nuclear Research (NCBJ), Poland

*Corresponding author: *gawel.madejowski@ncbj.gov.pl*

I. INTRODUCTION

The aim of this paper is to present a study which was conducted in order to choose the best strategy for the production of radioactive I-131 in MARIA research reactor by the bulk irradiations of tellurium dioxide. The I-131 is one of the most important radionuclides commercially available at the market. It is widely used as a tissue-killing agent in the thyroid cancer treatment, as well as for the medical imaging or as an industrial tracer. The market demand for iodine-131 exceeds its current production capability. Moreover, it is prone to shortages arising from a number of issues affecting continuity of service of the research reactors. The MARIA nuclear research reactor, operating in Świerk, Poland is a channel, beryllium and water moderated reactor. Its thermal power reaches 30 MW and its spacious and versatile core allows it to be one of the major I-131 producing facilities worldwide. Its weekly production serves for half a million patients worldwide for therapeutic and diagnostic purposes [1] The production is based on the activation technique for tellurium irradiation. The study investigates the production volume as well as the reactivity effect and other reactor-specific technical requirements in relation to the possible changes in irradiation positions and the type of irradiation targets (natural tellurium oxide or enriched with tellurium-130).

II. TECHNICAL ASPECTS OF IODINE-131 PRODUCTION

There are two major ways of producing iodine-131: extraction form fission products and an activation of tellurium with neutrons. Both may be conducted on the industrial scale using nuclear reactors. The principle of the activation technique is to use the neutron capture reaction of tellurium-130: Te-130(n;γ)Te-131g and Te-130(n;γ)Te-131m. Both tellurium-131 and tellurium-131m undergo a β^- decay to iodine-131 (with the half-life of 25 minutes and 33.25 hours respectively), however a fraction (25.9%) of tellurium-131m deexcitate reaching the tellurium-131 ground state and finally becoming a iodine-131. Nevertheless, tellurium-130 is the only tellurium isotope useful for iodine-131 production. It is the most abundant among eight stable tellurium isotopes, yet sharing only 34.08% of the mix.

All the remaining natural tellurium nuclides undergo a neutron capture reactions in the nuclear reactor conditions. Figure 1presents a microscopic cross-section for the (n;γ) reactions of all natural tellurium isotopes as a function of incident neutron energy.

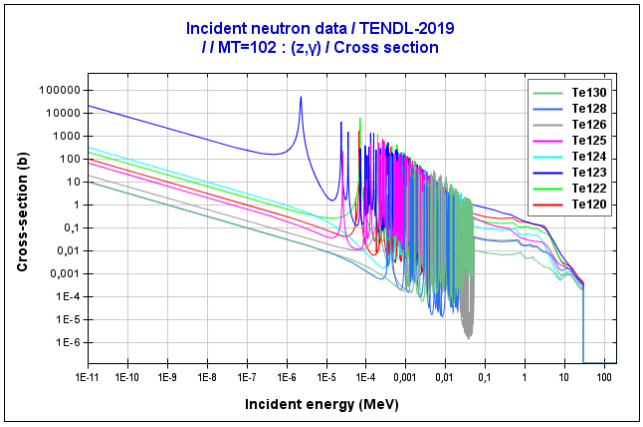

Figure 1. A microscopic cross-section for the (n;γ) reactions of natural tellurium isotopes as a function of incident neutron energy.

As it is shown, the cross-sections for the parasitic reactions are orders of magnitude higher than the desired one (0.1862 barns for 0.0253 eV neutrons and 0.252 barns of resonance integral). In particular, cross-section for neutron capture by tellurium-123 reaches 418.4 barns for 0.0253 eV neutrons and 5649 barns of resonance integral, what makes this reaction dominating despite of the lower abundance of this nuclide (0.89%). The parasitic reactions generate a vast majority of heat produced during the irradiation of natural tellurium oxide target, as well as give the unwanted negative reactivity effect and cause self-shielding effect. Moreover, tellurium-127, which is a product of tellurium-126 activation is an unstable nuclide and undergo a β^- decay producing stable iodine-127. This stable nuclide hence contaminates the final product [2]. That is why using enriched tellurium compound (typically 95% of Te-130) allows not only for simple increasing of target nuclei

concentration and thus total production volume, but also brings another benefits from the technical point of view.

MARIA is a high flux reactor in which thermal neutron density exceeds $1 \cdot 10^{14}$ $n \cdot cm^{-2} \cdot s^{-1}$ in beryllium matrix. During TeO_2 irradation such a high neutron flux density causes issues with target overheating. The current TeO_2 irradation technology bases in the use of standardized alluminum cans of 25 mm diameter, in which tellurium dioxide is casted directly. The casted TeO_2 deposit is then drilled along its axis, what turns it into an annulus of 8 mm inner diameter. The purpose of this procedure is to limit the temperature in the central part of the cast, because it would exceed melting point of the tellurium oxide [3], which is 733 degrees Celsius. Melting the target material and moving the melted part towards the wall could damage the aluminium can by overheating or exothermic oxidation of aluminium [4]. Moreover, it could cause releasing volatile iodine from the target material, generating production loses and unnecessary radioactive releases during further reprocessing. In general, the less temperature of the TeO_2 target, the less iodine releases, thus limiting the nuclear heating is beneficial from the safety, environmental and economical point of view. The separate study is needed to evaluate the need of the axial hole in the case of using enriched tellurium dioxide as well as to determine the target material temperature distribution in that case.

III. RATIONALE FOR CONDUCTING AN OPTIMIZATION STUDY

So far, in the production process in the MARIA reactor natural tellurium dioxide was arranged in two beryllium blocks containing six irradiation channels each. In order to ensure an increase in supply of iodine-131, enriched tellurium as a target nuclide was proposed.

The increase in production efficiency, associated with the use of enriched tellurium would make it possible to reduce not only the target material, but also the number of channels needed for the process, which in turn would enable the replacement of blocks from six-channel to two-channel.

Preliminary estimations were consistent with the assumptions and indicated a potential significant increase in production. Due to that fact it was proposed to reduce the number of irradiation channels to increase the beryllium content in the irradiation area and scatter target materials to prevent the depression of the neutron flux density in their area.

Six-channel beryllium blocks enable for large loading capacity, however they pose certain exploitation issues. Firstly, they are relatively fragile and susceptible to fracture. Secondly, their production is expensive, so the exploitation costs are high. Thirdly, they may cause a large loss of reactivity, as for technical reasons, in MARIA reactor the channels cannot be filled with beryllium plugs when the target materials are not loaded into the core. Thus, they must be filled with water. This considerable drawback could be avoided by substituting them by two-channel blocks.

IV. RESEARCH DESIGN

In order to determine the iodine-131 production volume, heat generation and reactivity effect the neutronic calculations have been conducted using MCNP6 neutronic transport computational code.

Two factors were taken into consideration: target arrangement (by beryllium block type) and enrichment (natural tellurium or enriched). The four variants of the targets arrangement, analysed in the study, are displayed in Table 1.

Table 1. Variants of targets arrangement.

Variant	Configuration
A	Natural tellurium dioxide irradiated in two beryllium blocks with six irradiation channels each
B	Enriched tellurium dioxide (95% Te-130) irradiated in two beryllium blocks with six irradiation channels each
C	Enriched tellurium dioxide (95% Te-130) irradiated in two beryllium blocks with two irradiation channels each
D	Natural tellurium dioxide irradiated in two beryllium blocks with two irradiation channels each

V. COMPUTATIONAL MODEL

A detailed geometric model of the representative arrangement of MARIA reactor core during normal operation cycle had to be designed and implemented in MCNP code to serve as a basis for the mentioned arrangement variants.

Each tellurium dioxide can was modelled individually. What is more, the model includes the shape of the tellurium layer inside the can to account for the self-shielding effect, which cannot be neglected in the thick layer of strong neutron absorber. Nuclear heating rate values in the tellurium layer were calculated using native functions of the code named Tallies F6, configured in that model for recording nuclear heating coming from neutrons and photons.

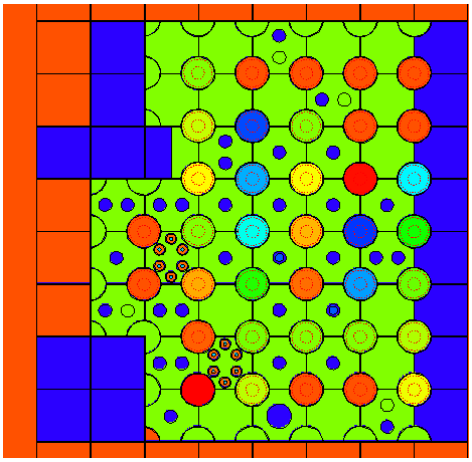

Figure 2. The horizontal cross-section of the core with two six-channelled blocks (variants A and B).

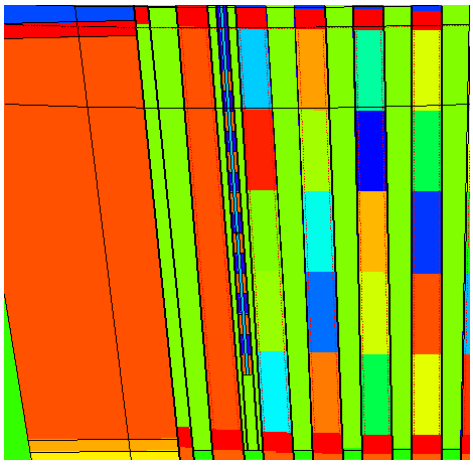

Figure 3. The vertical cross-section of the core with two six-channelled blocks (variants A and B).

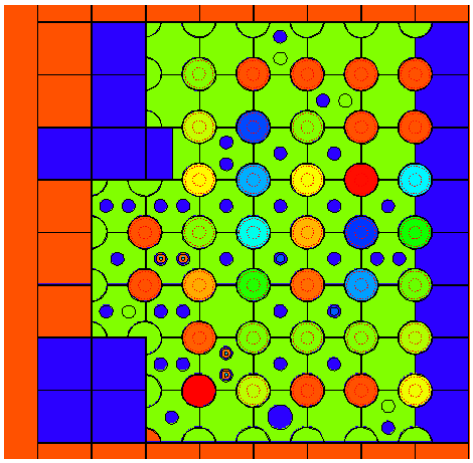

Figure 4. The horizontal cross-section of the core with two two-channelled blocks (variants C and D).

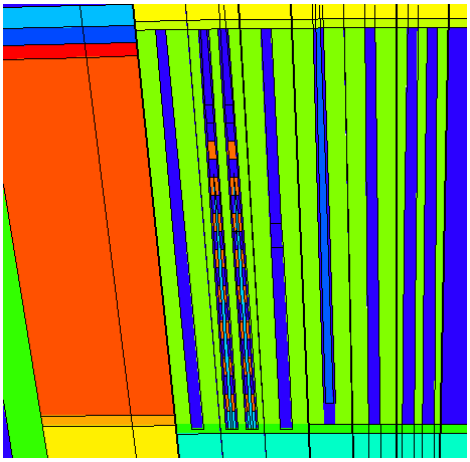

Figure 5. The horizontal cross-section of the core with two two-channelled blocks (variants C and D).

The Te-130(n;γ)Te-131 reaction intensity, which is a measure of the production volume, has been calculated numerically by modifying the native function designed for measuring neutron flux density (Tallie F4) by the DE-DF option in that way, that it multiplies the neutron flux density estimators by the active cross-section for this reaction, therefore to effectively integrate numerically the product of both quantities over neutron energy.

The calculations were carried out in the k-eff mode in order to determine the multiplication factor for each of the considered configuration variant. Due to the fact that the relative change in reactivity was a sought value, the results were normalized to the basic configuration (Variant A), assuming that in the present state of the reactor operation, the k-effective value would be equal to 1.

VI. RESULTS AND ITS INTERPRETATION

The results of the calculations seem to be consistent with predictions. The volume of production calculated for the considered variants is displayed in the Table 2. The calculated total (neutron + gamma) nuclear heating rate for the most thermally loaded can is displayed in the Table 3. Table 4 shows the multiplication factor and reactivity change in relation to the present variant (A).

Table 2. Calculated volume of iodine-131 production.

Variant	Production rate in total (and per one can) [nuclei/s]		Production rate in total in relation to the present techn.
A	2.0E+14	(2.0E+12)	100%
B	7.6E+14	(8.0E+12)	391%
C	2.8E+14	(8.7E+12)	142%
D	8.0E+13	(2.5E+12)	41%

Table 3. Calculated maximum total nuclear heating rate in the target.

Variant	Sum of neutron and gamma heating rate [W/g]
A	6.8
B	2.9
C	3.0
D	8.0

Table 4. Calculated reactivity loss or gain in relation to the present technology.

Variant	Multiplication factor (normalized)	Relative excess reactivity change [$]
A	1	0
B	1.0105	+1.50
C	1.0150	+2.14
D	1.0107	+1.53

The result show that chosing enriched tellurium dioxide would increase the total production four times, improve the neutronic economy of the core (giving back 1.5 $ of reactivity) and decrease the nuclear heating rate in the loading over two times. Probably the nuclear heating would be small enough to allow to increase the loading volume in each can. It is worth to be noted than the production volume gain caused by using enriched tellurium (3.91 for the present configuration) is considerably higher than a simple ratio of the tellurium-130 content in the enriched and natural tellurium target materials (2.79). This clearly shows that this kind of change would improve the economy of utilisation both target material and neutrons in the reactor core.

The data show that using enriched tellurium dioxide with limiting loading capacity, by replacing two beryllium blocks would still increase production capacity (by 42%) and improve the core economy. It is worth to notice, that blocks replacement would improve the efficiency of target material utilization, improving I-131 yield per each can (or per gram of target material). This could be particularly beneficial when the enriched target is used, as the price of the enriched tellurium dioxide is high and therfefore replacing the blocks (switching from variant B to C) would spare over 8% of it.

The calculated nuclear heating rate may suffer from its underestimation originated in the modelling limitations. The MCNP code, in its criticality mode, allows for exact modelling of the fission-origineted particles (neutrons and gamma photons) and their interactions with the matter up to the certain level of complexity. It does not calculate, however, the background of gamma radiation coming from fission products and activated materials, which would require constructing custom-tailored correcting computational schemes. This gamma radiation contributes to the nuclear heating rate in the real reactor, but not in the presented model. This bias may be, however, neglected in conducted calculations as all considered targets are strong neutron absorbers.

VII. CONCLUSIONS

This study proves that using enriched instead of natural tellurium dioxide may significantly improve iodine-131 production capabilities of nuclear reactor as well as resolve some technical problems of medical iodine production. It would significantly lower the heat generation inside the target. From the technical point of view, the recommended variant for MARIA reactor would involve using the enriched target and replacing the six-channelled beryllium blocks with the two-channelled, giving over 40% rise of production capacity, improving the neutron economy of the core and allowing for the better utilization of target material. The detailed determination of expected financial costs and benefits of each variant is assumptions-sensitive and is not covered by the scope of this study. A research reactor is a specific type of device, which usually aims to meet not only the needs of commercial production, but also the requirements of scientific purposes. From that reason treating financial profits as a goal function might raise doubts.

VIII. REFERENCES

[1] Anonymous, “Iodine from Świerk for half a million patients a week”, National Centre for Nuclear Research official website, https://www.ncbj.gov.pl/en/aktualnosci/iodine-swierk-half-million-patients-week (accessed Jun. 1, 2021),

[2] “Manual for reactor produced radioisotopes”, IAEA, Vienna, 2003, ISBN 92–0–101103–2,

[3] W. Bykowski, „Analiza cieplna zasobnika z dwutlenkiem telluru jako materiałem tarczowym w trakcie napromieniania”, Raport B IEA Nr: 29/97, Otwock-Świerk 1997,

[4] A. Fllaoui, Y. Ghamad, B. Zoubir, Z. Ayaz, A. El Morabiti, H. Amayoud, C. El Mahjoub, “Validation of a New Design of Tellurium Dioxide-Irradiated Target”, Nuclear Engineering and Technology, Volume 48, Issue 5, 2016, pp. 1273-1279, ISSN 1738-5733.

Proceedings of the European Nuclear Young Generation Forum
ENYGF'21
September 27-30, 2021, Tarragona, Spain

Software and hardware complex "Virtual NPP" as an instrument for scientific and technological assistance of nuclear operating company

Druzhaev Andrey[1*] and Chernakov Victor[1]

[1] JSK "All-Russian Research Institute for Nuclear Power Plants Operation", Russian Federation

*Corresponding author: *aadruzhaev@vniiaes.ru*

I. INTRODUCTION

Currently, the state-of-the-art mathematical simulation methods and deep understanding of the physics of phenomena occurring in the equipment, as well as capabilities of modern computing systems allow to provide full-scope multiphysics simulation of processes occurring in the NPP power unit. The range of reproducible modes of the power unit may be very wide – from normal operation to severe accidents.

In order to develop mathematical models of power units that are capable, on the one hand, of high-fidelity simulation of physical processes in the widest range of possible operation modes, and, on the other hand, taking into account simultaneous operation of a large number of technological process systems and auxiliary systems, including a detailed I&C model, it is necessary to develop a modern system of calculation codes (or to adapt the existing ones), which are based on the possibility of parallel calculations on a distributed computing platform consisting of computing servers of different types (including super-computers).

An adequate modern system of calculation codes for simulation of various processes and phenomena occurring in the equipment of VVER power units, adapted for high-performance computing, was developed along with the hardware and software complex "Virtual NPP" (hereinafter – H&SC VNPP).

The closest analogue of H&SC VNPP is the system of calculation codes developed within the CASL project [1]. Unlike this system, H&SC VNPP is focused on simulation of severe accident processes, and provides full-scope simulation of the power unit with a detailed account of the operation of the turbine equipment, electrical equipment and automation systems.

For the assessment of qualitative and quantitative characteristics of the developed system of calculation codes within H&SC VNPP, a full-scope model of Novovoronezh NPP Unit 6 was developed. This model was used to reproduce a large number of modes occurring on a real power unit at the test stage, and for further comparison of the simulation results with the operational archives of the power unit. The comparison showed a high level of adequacy of the VNPP-based model, which allows describing various modes of power unit operation with high-fidelity.

II. STRUCTURE OF THE HARDWARE AND SOFTWARE COMPLEX "VIRTUAL NPP"

H&SC VNPP is a universal platform for the simulation of VVER-based power units. H&CS VNPP may serve as a basis to build mathematical models of power units, which allow multiphysics simulation the following processes and phenomena:

- neutronic processes in the core;
- thermohydraulic processes in the equipment of the reactor and turbine islands;
- electromechanical processes in the electric equipment of the power unit;
- operation of power unit I&C;
- processes associated with the accumulation and propagation of fission products in the power unit and throughout the adjacent territory in emergency conditions, including fuel rod cladding leakage, the behaviour of fission products in the gas and aerosol phases in the coolant circuits and in the containment;
- processes occurring in the reactor plant during a severe accident (core destruction, melt behaviour on the vessel bottom, corium melt-through, melt behaviour in the core catcher or on the surface of the concrete shaft of the reactor).

Figure 1 shows the scheme of calculation codes included in the H&SC VNPP [2].

The calculation basis of the H&SC VNPP are Russian-made computer codes, which are further development of the calculation base currently used to build NPP unit simulators and to assess the safety of reactors.

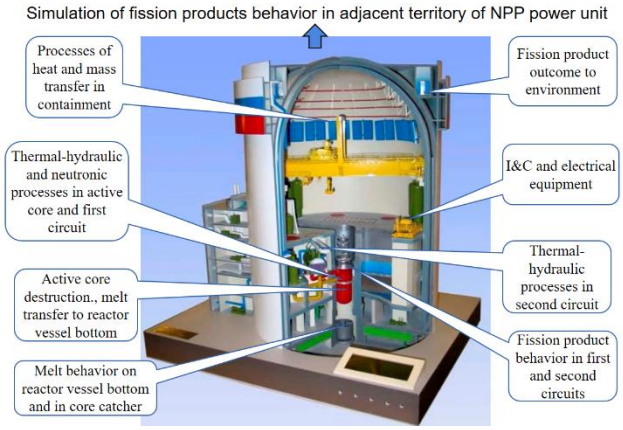

Figure 1. Scheme of calculation codes in H&S VNPP

H&SC VNPP contains calculation codes of different levels of complexity and speed:

- the high-speed level allows building full-scope power unit models that can perform real-time calculations or even faster;
- the high-fidelity level is based on the application of more detailed approximations compared to the high-speed level; this level considers a wider range of processes and phenomena covering the field of severe accident regimes;
- the precision level allows to provide simulation the state of individual equipment by using a detailed partition of the computational domain (up to a billion of individual control volumes).

On the basis of H&SC VNPP, it is possible to build integrated models that combine the capabilities of different levels of modeling.

Neutronic models used at the high-speed level and high-fidelity level are based on the application of the three-dimensional multigroup diffusion approximation with the possibility of modeling spatial kinetics (two energy groups are usually used for neutronic simulation of VVER unit, but higher number of groups can be considered if necessary). At the precision level, the transport approximation solved by the Monte Carlo method is applied.

The thermal-hydraulic models used at the high-speed and high-precision level are based on the application of one-dimensional channel approximation.

At the high-precision level, thermal-hydraulic modeling of the core is possible with use of three-dimensional approximations (porous body model).

At the precision level, the CFD modeling approach is applied.

Electromechanical models allow to provide simulation the main equipment of the power unit as electricity consumer. It is possible to simulate short circuits on consumer sections and in separate cable lines, partial or full blackouts, disturbances in the external network.

The automation system is emulated at the level of application software, which is used in the automation equipment at a real power unit. This approach allows keeping track of the work of automation systems without any simplifications to their real logic of operation.

The fission products propagation processes are modeled in view of possible propagation of fission products in the gas and aerosol phases, and as impurities in the coolant. When modeling fission products in the aerosol phase, processes such as condensation, deposition, coagulation, and nucleation are considered.

Severe accident processes are modeled in a two-dimensional cylindrical approximation based on the solution of the heat and mass transfer problem [3]. When modeling a severe accident, the processes of fission products release from the melt, as well as the processes of hydrogen generation are considered. Radiation doses to the operation staff in various premises are estimated, and also the probability of detonation of the hydrogen gas mix within the containment is calculated.

All of the above processes are simulated in multiphysics way, considering the simultaneous operation of a large amount of equipment.

Seamless simulation of the emergency is possible, starting with the initial effects (failures) in normal operation up to the late stages of severe accidents.

VNPP-based mathematical models of power units may function on a distributed computing environment within H&SC VNPP, which can significantly reduce the time of simulation of complex processes.

An additional feature of H&SC VNPP is the ability to image the calculated information on many different visualization tools (see Figure 2), which not only facilitates the process of analyzing simulation results, but provides additional functionality (e.g., verification of the human-machine interface of the main control room).

III. PRACTICAL APPLICATION FIELDS OF THE HARDWARE AND SOFTWARE COMPLEX "VIRTUAL NPP"

H&SC VNPP was developed for scientific and engineering support of nuclear operators, which implies solving the following important practical problems:

- computational verification of power unit designs (both new ones and those to be modernized); it is expected that changeover from the expert analysis of design documentation to analysis with use of mathematical models of power units will reduce the number of inconsistencies in the design at its early stages and, as a consequence, reduce the timing of commissioning and increase the level of efficiency and safety of industrial operation of power units.
- development of new-generation educational aids; improved fidelity and expanded range of reproducible modes covering severe accidents will improve the quality of training of operation staff, and increase the level of involvement of experts from emergency response centers into the educational and training process;
- design verification and optimization of emergency response instructions will confirm the adequacy of the developed instructions for power unit operation in

Figure 2. General view of the H&SC "Virtual NPP"

emergency situations and, if necessary, make reasonable changes based on calculations, thus implementing better emergency management.

It is worth noting that H&SC VNPP may serve as the basis for the development of full-scope mathematical models of power units, which are essentially digital twins of power units. Such models may be of interest not only in the context of the problems listed above, but also may be considered as an independent supplement to the design documentation of the power unit.

At the time of this writing, underway are the initial stages of the pilot projects of H&SC VNPP application for the verification of design solutions in the I&C part of the power unit, as well as its application for the development of a mathematical model of the unit to be integrated in the full-scope simulator and analytical simulator of the prototype power unit.

IV. EXAMPLE OF PRACTICAL APPLICATION OF THE HARDWARE AND SOFTWARE COMPLEX "VIRTUAL NPP"

In the first half of 2021, H&SC VNPP was used for preparation of an emergency training technological scenario for unit № 6 of the Novovoronezh NPP. The crisis centre of the operating company set the task of developing the emergency scenario with step by step implementation of failures.

Several dozens of different failure combinations were considered using H&SC VNPP. The combination which requires maximum active participation of operating staff was selected. The sequence of the main events of the scenario is the next:

- T_0 + 20 min - earthquake leading to activation of the safety trip procedure, to loss of external power supply and to connection of emergency power supplies (diesel generators);
- T_0 + 200 min. – the appearance of a crack in the connection pipeline between one channel of the passive core flooding system and the reactor vessel leading to formation of a small leak in the primary circuit;
- T_0 + 230 min. – complete rupture of the connection pipeline, in which a crack previously was formed (large leak), and hidden failure (blocking in a closed state) of the back flow valve on the connection pipeline of another channel of the passive core flooding system;
- T_0 + 290 min. – disconnection of emergency power supplies due to a short circuit (complete blackout of the power unit with a large leak from the primary circuit).

Graphs of main power unit parameters are represented below:

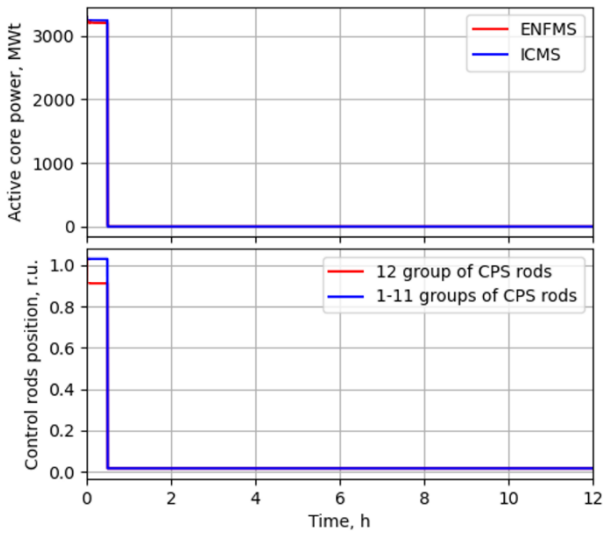

Figure 3. In-Core Monitoring System (ICMS) power, ENFMS (ENFMS) power and power control rods positions

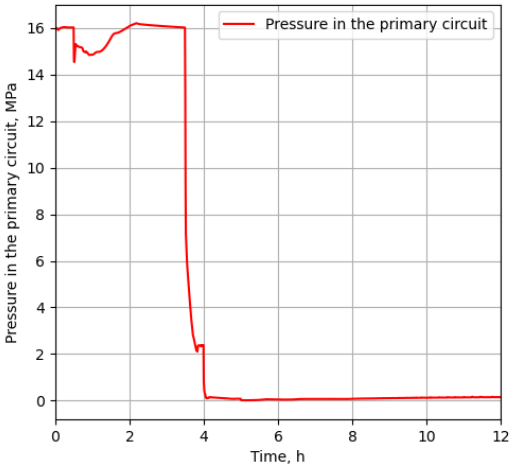

Figure 4. Pressure in the primary circuit

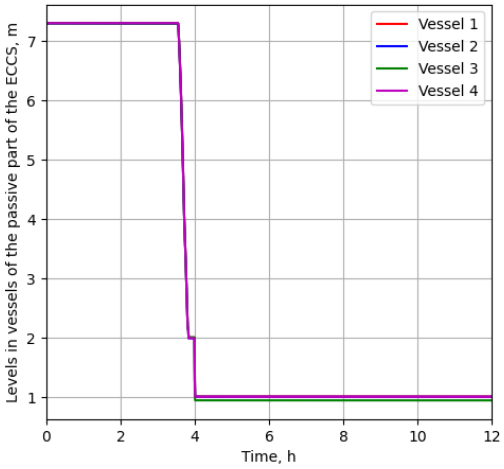

Figure 5. Coolant levels in vessels of the passive part of the emergency core cooling system (ECCS)

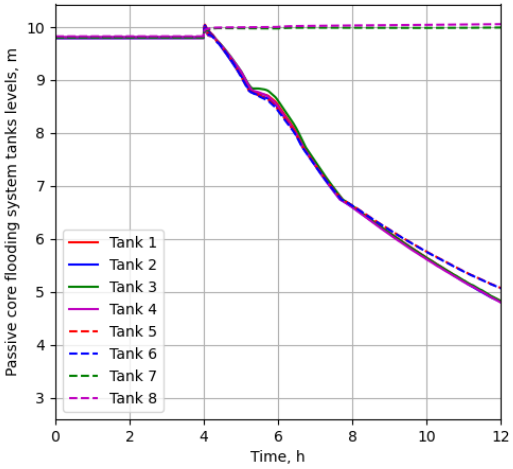

Figure 6. Coolant levels in tanks of the passive core flooding system

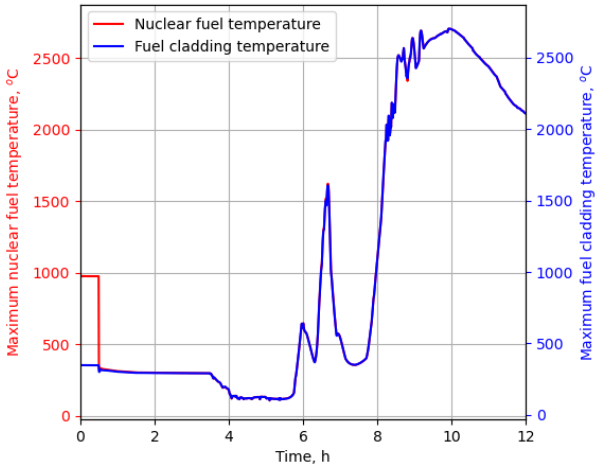

Figure 7. Fuel and cladding maximum temperatures

As it can be seen from above graphs, the considered set of failures leads to a critical increase of fuel temperature in 10 hours after the start of the accident, if the operating staff cannot find appropriate solution (for instance, by connecting additional portable pumps and power sources).

On basis of the solution of this task, which is represented in this section, application of H&SC VNPP for solution of important scientific and engineering problems of the operating company has been practically confirmed.

V. CONCLUSION

The hardware and software complex "Virtual VVER-based NPP" is a modern tool for full-scope simulation of the VVER-based power unit. Moreover, the composition of the model allows it to adequately reproduce a wide range of possible operating modes of a real power unit, from normal operation up to late stages of severe accidents.

H&SC VNPP is considered as an effective tool for scientific and engineering support to nuclear operators and is coming into use for the development of educational aids for the operation staff of new-generation nuclear power units, as well as for the purposes of computational verification of power unit I&C designs.

VI. REFERENCES

[1] Lu, R., et al. «CASL Virtual Reactor Predictive Simulation: Grid-to-rod Fretting Wear», J. of the Minerals Metals and Materials Society. – 2011. – Vol. 63, № 8.

[2] A. Druzhaev, V. Chernakov et al «Application of "Virtual NPP with VVER" for NPP operation safety», Global scientific and practice conference "Safety, effectiveness, resource". – Sevastopol, SevSU, 2017

[3] A. Trunov, V. Zaukova. Researching of LWR active core severe accidents, Atomic technology in foreign countries – Vol. 1 – 1990

Proceedings of the European Nuclear Young Generation Forum
ENYGF'21
September 27-30, 2021, Tarragona, Spain

Spent Nuclear Fuel Cask Partial Loading Pattern Analyses Applied to ENUN 52B Casks for Santa María de Garoña Nuclear Power Plant

Saiz de Omeñaca Tijero, Jesús[1*]

[1] Equipos Nucleares S.A. S.M.E. (ENSA), Spain

*Corresponding author: *saizdeomenaca.jesus@ensa.es*

I. INTRODUCTION

Equipos Nucleares S.A., S.M.E. (ENSA) is a manufacturer and designer of nuclear equipment, including steam generators, reactor vessels, and casks for Spent Nuclear Fuel (SNF) among other large components and services for the nuclear industry. This article will focus on the ENUN 52B, a cask specifically designed by ENSA for Boiling Water Reactor (BWR) SNF, that will be used to unload the SNF pool of Santa María de Garoña nuclear power plant to initiate its decommissioning activities.

Each ENUN 52B cask is equipped with a basket featuring 52 positions for the storage and transportation of BWR SNF, as well as upper and lower impact limiters. See Figure 1 for a conceptual overview of the cask design.

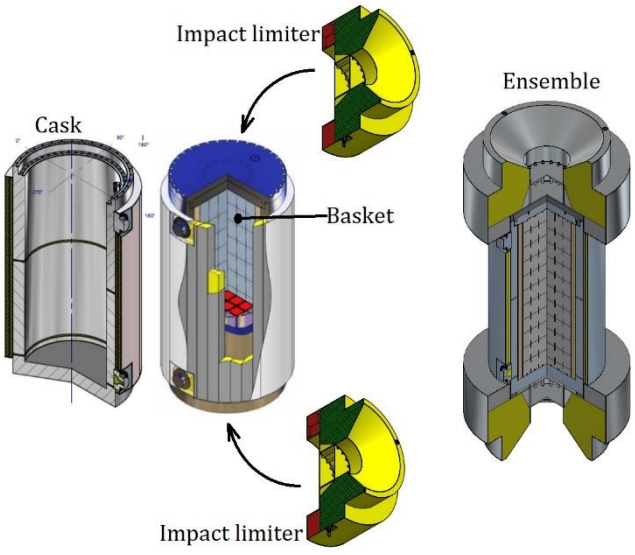

Figure 1. ENUN 52B cask conceptual design.

These casks are required to ensure several safety functions, such as: structural integrity, heat dissipation, subcriticality, dose rate compliance with radiological limits, etc. These safety functions have been analysed for fully loaded casks i.e.: for ENUN 52B loaded with 52 BWR Fuel Assemblies, (FAs). However, the Santa María de Garoña project requires unloading the entire SNF pool into these casks, where the number of FAs in the pool is not a multiple of 52. This means that at least one of the casks will not be fully loaded.

The objective of this article is twofold: (1) to present radiological analyses of partially-loaded ENUN 52B casks; (2) to define a suitable approach to load one of such casks with less than 52 FAs, from a radiological point of view.

II. METHODOLOGY

Dose rates around the ENUN 52B cask (up to two meters away from it) were calculated using nuclear code SCALE/MAVRIC (neutron code developed and maintained by Oak Ridge National Laboratory [1]), version 6.1 with ENDF-B/VII cross section library [3] and the ANSI/ANS-6.1.1-1977 neutron and gamma flux-to-dose conversion factors [2]. Two scenarios were considered:

- ENUN 52B cask fully loaded (52 FAs), which is the reference scenario.
- ENUN 52B cask loaded with 51 FAs (partial load).

For the second scenario, several possibilities were analysed, depending on the location of the free position. See Figure 2.

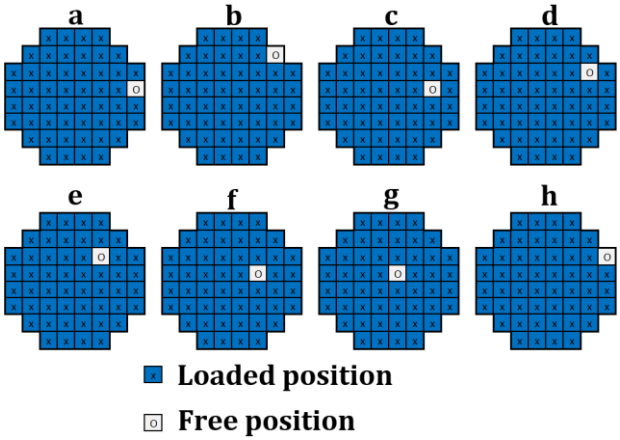

Figure 2. Possible ENUN 52B cask partial loading patterns (51 FAs being loaded into the 52-position basket).

Taking into account the cask radial symmetries, cases “a” to “g” of Figure 2 were considered. Other empty position possibilities were either symmetric to these ones or considered uninteresting/redundant (e.g.: case “h” of Figure 2 is uninteresting, after calculating “a*’* and “b”).

For convenience, the ENUN 52B cask positions are classified into: inner, outer and intermediate, as depicted in Figure 3. Qualitatively, the inner region is loaded with short-cooling-time FAs, the outer one with long-cooling-time FAs and the intermediate region with something in-between.

In this analysis, FAs with the same characteristics were used for each scenario (identical neutron and gamma spectra and intensities, same bundle design, etc.), thereby focusing the study on the differences produced just by loading patterns.

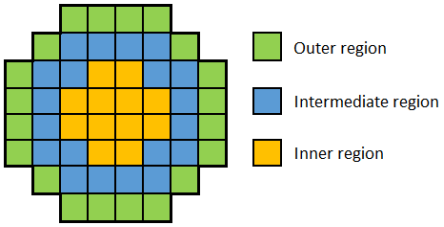

Figure 3. ENUN 52B regions for loading FAs.

III. RESULTS AND DISCUSSION

A. Reference scenario: Fully loaded case

The results of the calculations for the reference scenario are shown in Figure 4 through Figure 6.

In Figure 4 and Figure 5, the four left frames show (from left to right, and from top to bottom) dose rates from neutrons, from secondary gamma, from hardware activation gamma and from fuel gamma, respectively. The right panel of each figure shows the total dose rate map.

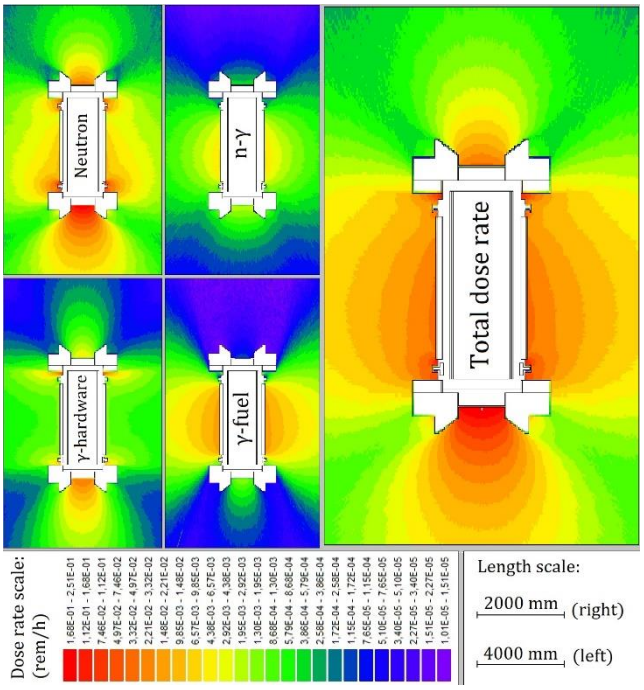

Figure 4. Dose rates around the fully loaded ENUN 52B cask (reference scenario). Vertical section. Colour scale in rem/h.

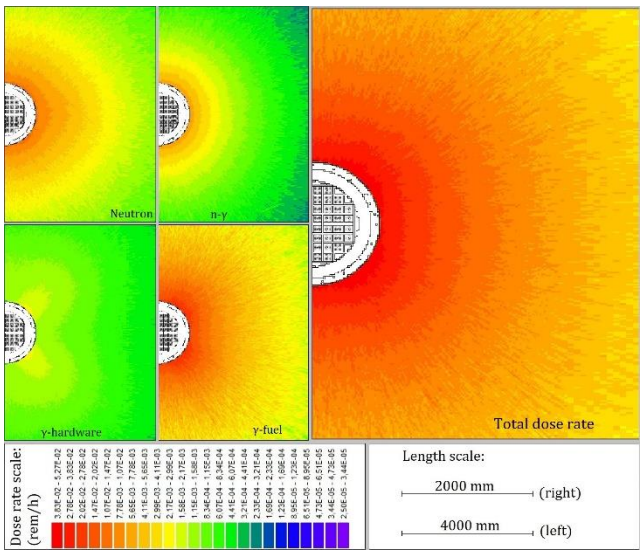

Figure 5. Dose rates around the fully loaded ENUN 52B cask (reference scenario). Horizontal section at 1/3-of-FA-active-length height, where lateral dose rates are representative. Scale in rem/h.

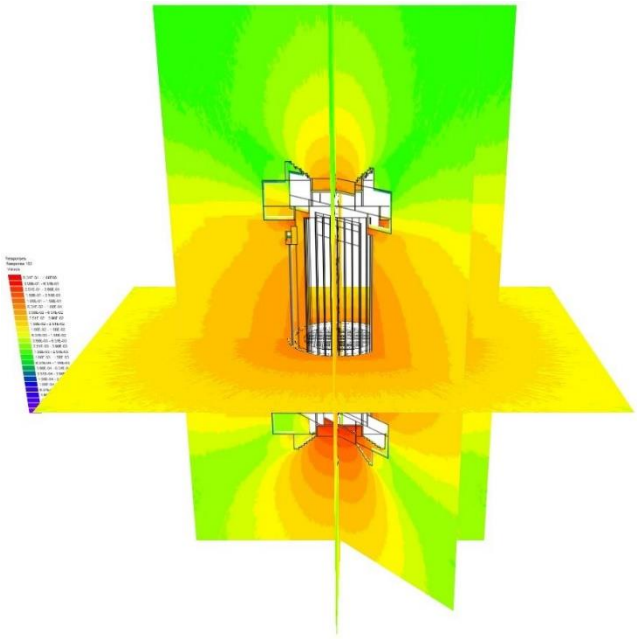

Figure 6. Dose rates around the fully loaded ENUN 52B cask (reference scenario). 3D view. Figures in rem/h (same colour scale as in Figure 4).

B. Partial load: Empty position in the outer region of the cask

Identical maps may be computed for each case of the “partial load” scenario. These maps are not shown in this article for brevity. Instead of a lengthy list of figures showing dose rate maps for each case of the partial load scenario and for each term (neutron, gamma, etc.), only the most significant dose rate maps are included in this article. In particular, the difference (with respect to the reference scenario) of total dose rate is presented for the most meaningful cases. Such as case “b” of Figure 2 (whose free position is in the outer region of the cask). The difference of total dose rates of this case with respect to the reference scenario is shown in Figure 7. (NB: a similar map is

produced by case “a” of Figure 2). These differences are mainly due to hardware-γ and fuel-γ terms.

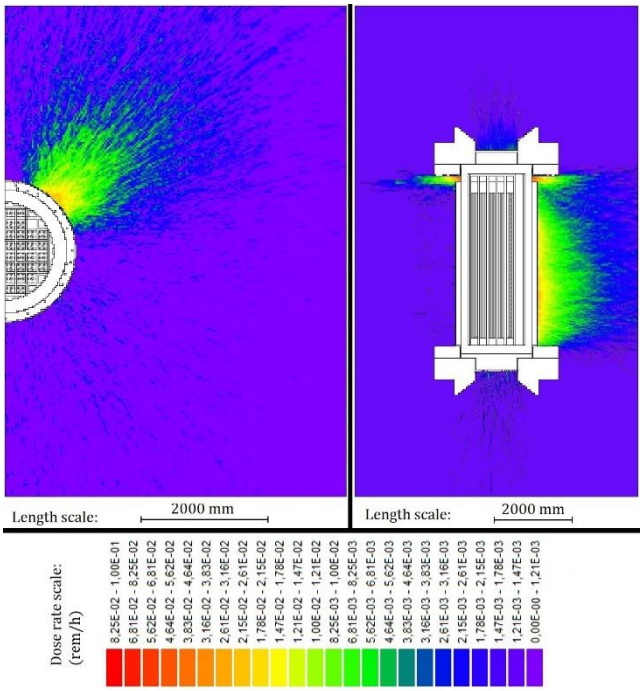

Figure 7. Δ(Total dose rate): unoccupied cell in outer region (case *b*) vs. reference. Horizontal (at 1/3-of-active-length height) and vertical (through centre and empty position) sections. Scales in Δ(rem/h).

Figure 7 shows that dose rates at the lateral side of the cask (in contact, next to the empty position of the cask) are greater than the reference scenario by up to nearly 0.21 mSv/h, hence implying a 50% increase in dose rates in the most critical angular direction. Dose rates 2 m away from the cask in the same direction increase by about 5%.

These values imply that, from an ALARA point of view, the solution is not optimal. This is true for cases “a” and “b” of Figure 2 and may be extrapolated to case “h”.

C. Partial load: Empty position in the intermediate region of the cask

In the cases in which the free position is in the intermediate region of the cask (cases “c”, “d” or “e” of Figure 2), the difference of total dose rates with respect to the reference scenario is as shown in Figure 8 (which is for case “e” specifically. Vertical plane map only. The horizontal map is not shown as differences are negligible).

Figure 8 shows that dose rates around the cask may be considered statistically indistinguishable from the reference scenario (i.e.: calculation uncertainties are about the same or greater than absolute differences between this partial load and the reference scenario, almost all around the cask).

Most of the coloured spots in Figure 8 are not relevant; this was confirmed by additional point-detector calculations around the cask that provided better statistical results. Only the dose rates at the top and bottom in contact with the cask were appreciably greater than the reference scenario, by up to 2%, due to radiation streaming through the empty position of the basket. Differences at the lateral side and 2 m away from the cask in any direction are negligible.

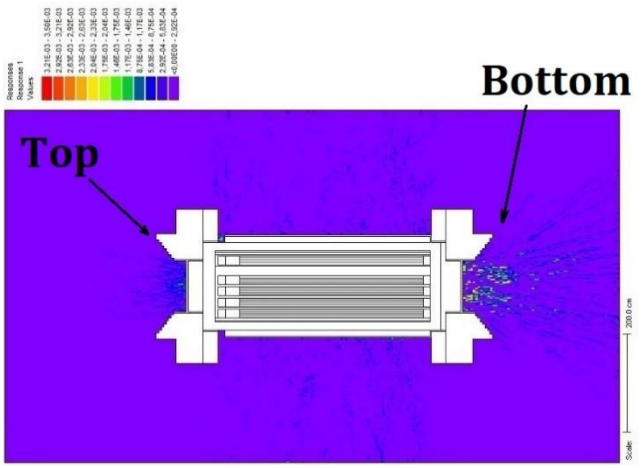

Figure 8. Δ(Total dose rate): unoccupied cell in intermediate region (case *e*) vs. reference. Vertical section. Scale in Δ(rem/h).

D. Partial load: Empty position in the inner region of the cask

When the empty position is in the inner region of the cask (cases “f” and “g” of Figure 2), the difference of total dose rates with respect to the reference scenario is like the example given in Figure 9 (case “g”, vertical plane. The horizontal plane is not shown because there are no noticeable differences).

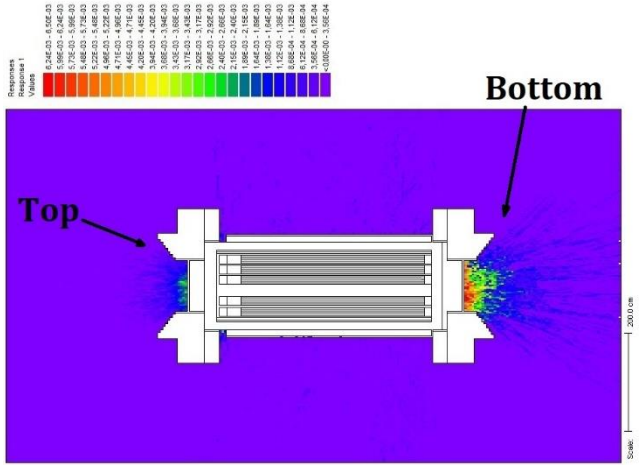

Figure 9. Δ(Total dose rate): unoccupied cell in inner region (case *g*) vs. reference – Vertical section. Scale in Δ(rem/h).

Figure 9 shows that the difference of dose rates around the lateral side of the cask are negligible (i.e.: smaller than the calculation uncertainties). However, dose rates at the top and bottom of the cask increase by up to +5% (in contact) or +2% (2 m from the bottom of the cask) with respect to the reference scenario. The later (2 m from the bottom of the bulk) is a very critical location—from the cask design point of view—to comply with the Spanish and European regulations on transportation of hazardous materials [4], [5].

This implies that, not only cases “f” and “g” of Figure 2 are not ALARA, but they also may potentially yield dose rates above the allowed regulatory thresholds while the reference scenario (with 52 FAs) did not.

IV. UNCERTAINTIES

Total dose rate maps were computed by summing up the neutron, secondary gamma, fuel gamma and hardware gamma terms. Both, for the reference scenario and for each of the analysed loading patterns. Then, "Δ(dose rate) maps" were generated by subtraction: each loading-pattern-dose-rate map minus the reference-scenario-dose-rate map. In each of these operations, the associated uncertainties were propagated using the statistical variance formulae.

Because several binary operations are required to produce each map shown in this paper, uncertainties associated with the original SCALE/MAVRIC calculations had to be particularly small (<1%) to avoid "blurring out" (thus invalidating) the final maps due to large uncertainties; especially when small differences are analysed—e.g.: cases "c", "d" and "e" of Figure 2. Uncertainties of the presented maps (figures 4 through 9) are between about 1% and 10%.

V. FURTHER ANALYSES

Further analyses were carried out for partial loads with 2 and with 4 empty positions, but not all of the possibilities were analysed, as there are 1326 combinations for the ENUN 52B cask with 2 voids (of which 1161 are symmetric and 22 "uninteresting") and 270725 possibilities if 4 voids are left in the cask (with around 240000 symmetric/uninteresting combinations). The computed 2- and 4-void dose rate maps are not shown here for brevity, but Figure 10 summarizes the loading patterns that yielded acceptable dose rates when comparing them with the reference scenario, following the same procedure as for the 1-void cases. Note that all of them feature empty positions in the intermediate region of the cask (region defined in Figure 3).

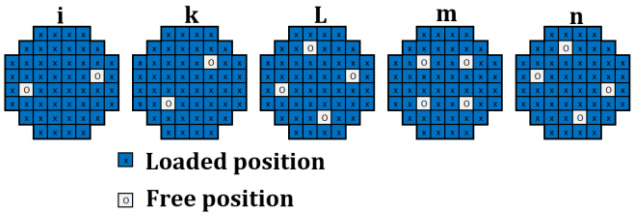

Figure 10. Acceptable ENUN 52B cask partial loading patterns from a radiological point of view (with 2 and with 4 empty positions).

VI. CONCLUSIONS

Results presented and discussed in Section III show that in the analysed cask design (the ENUN 52B):

- When the cask is fully loaded, shielding between FAs contributes to reduce dose rates outside the cask.
- When the cask is partially loaded (less than 52 FAs), radiation streaming effects may arise if an inappropriate loading pattern is used.

An adequate loading pattern shall be applied so as not to increase dose rates around the cask with respect to the reference scenario. This aims to comply with radiological regulation and the ALARA principle.

Essentially, loading patterns "a", "b" "f", "g" and "h" of Figure 2 shall be particularly avoided as they produce greater dose rates (around the cask) than the fully-loaded scenario; even if the number of FAs loaded in the cask (and consequently the overall source term) is lower in the partial-loading case.

Conversely, loading patterns "c" and "e" of Figure 2 are notably beneficial, as dose rates are either smaller or unaffected (in critical locations around the cask) or do not significantly increase (around +2% in non-critical locations around the cask) with respect to the reference scenario.

Loading patterns different of what is shown in Figure 2 for 51-FA loads were not evaluated as they were either symmetric to the analysed cases or unnecessary for the purposes of the project.

Additionally, some analyses were performed for 2-void and 4-void loading cases. These analyses confirm that leaving empty positions in the intermediate region of the cask (region defined in Figure 3) is generally acceptable from a radiological point of view, as dose rates around the cask are either lower than the reference scenario or unaffected.

VII. ACKNOWLEDGEMENTS

The author wants to express thankfulness and appreciation to the always-supportive "Design and Analysis" team in ENSA. Without their help this research would not have been possible. In particular to Alejandro Palacio Alonso and Jesús Fernández García who proofread the manuscript before being considered for ENYGF2021.

VIII. References

[1] Oak Ridge National Laboratory, "ORNL/TM-2005/39, Version 6.1, SCALE: A Comprehensive Modeling and Simulation Suite for Nuclear Safety Analysis and Design", ORNL, TN, US, June 2011.

[2] American National Standards Institute/American Nuclear Society "ANSI/ANS-6.1.1-1977, Neutron and Gamma-Ray Flux-Dose-Rate Factors", US, 1977.

[3] M.B. Chadwick, P. Obložinský, M. Herman, N.M. Greene, R.D. McKnight, D.L. Smith, P.G. Young, R.E. MacFarlane, G.M. Hale, S.C. Frankle, A.C. Kahler, T. Kawano, R.C. Little, D.G. Madland, P. Moller, R.D. Mosteller, P.R. Page, P. Talou, H. Trellue, M.C. White, W.B. Wilson, R. Arcilla, C.L. Dunford, S.F. Mughabghab, B. Pritychenko, D. Rochman, A.A. Sonzogni, C.R. Lubitz, T.H. Trumbull, J.P. Weinman, D.A. Brown, D.E. Cullen, D.P. Heinrichs, D.P. McNabb, H. Derrien, M.E. Dunn, N.M. Larson, L.C. Leal, A.D. Carlson, R.C. Block, J.B. Briggs, E.T. Cheng, H.C. Huria, M.L. Zerkle, K.S. Kozier, A. Courcelle, V. Pronyaev, S.C. van der Marck, "ENDF/B-VII.0: Next generation evaluated nuclear data library for nuclear science and technology", Nuclear Data Sheets , vol. 107, no. 12, 2006, pages 2931-3060.

[4] Ministerio de Transportes, Movilidad y Agenda Urbana, "Acuerdo Europeo sobre el Transporte Internacional de Mercancías Peligrosas por Carretera", Spain, 2019.

[5] United Nations Economic Commission for Europe (UNECE), "European Agreement concerning the International Carriage of Dangerous Goods by Road: ADR applicable as from 1 January 2017", New York and Geneva, US and Switzerland, 2017

Technical Track 2 – Nuclear Safety and Security

Oxidation at liquid state of iron and zirconium under Severe Accident conditions.
Authors: Thilliez, Sarah (1); Piluso, Pascal (1); Delacroix, Jules (1); de Bilbao, Emmanuel (2); Poirier, Jacques

Analysis of the Thermal-Hydraulic Parameters of VVER-1200 due to Fuel Failure at Power Concurrent with Loss of Offsite Power.
Authors: Thulu, Fabiano Gibson (1,2); Tenthani, Chifundo (1); Katengeza, Estiner (1)

Very high temperatures (1500-2500 °C) measurements using the pyroreflectometry technique for nuclear applications.
Authors: Turquais, Benjamin (1,2); Davoust, Laurent (2); Sans, Jean-Louis (3); Delacroix, Jules (1); Journeau, Christophe (1); Piluso, Pascal (1); Chikhi, Nourdine (4)

The necessity and benefits of PSA application in NPP design.
Authors: Makukhin, Sergey

The stress test approach for safety assessment.
Authors: Korolev, Viktor

Numerical modeling of thermo-kinetic processes in the trap of corium melt during severe accidents at NPPs.
Authors: Kovalenko, Anatoliy (2); Shchuklinov, Aleksei (1); Koptyukhov, Artem (3); Meshcheryakov, Dmitriy

ASVAD: A new safety element to keep Nitrogen-Free Reactors.
Authors: Laborda, Arnaldo

The potential effect of radiolyzed superplasticizers contained in cement-based materials on europium uptake.
Authors: Legand, Solene; Mace, Nathalie; Muzeau, Benoist; Le Tutour, Philippe; Therias, Sandrine; Reiller, Pascal

Analysis of venting strategies and hydrogen concentration evolution during a Station Blackout in a BWR-6 containment using GOTHIC 8.3.
Authors: Diez, Maria del Pino; Estévez-Albuja, Samanta; Jimenez, Gonzalo; Gavilán, Carlos

Trillo NPP full scope PRA.
Authors: Calvo, David; Osorio, Franciso

Emergency preparedness and response in Build-Own-Operate projects on the based on Akkuyu NPP.
Authors: Aslankan, Serkan

Feasibility of the last reactor core discharge of a PWR with three years cooling after shutdown.
Authors: Sanchez Fernandez, Rafael; Gonzalez Candal, Rosa

Proceedings of the European Nuclear Young Generation Forum
ENYGF'21
September 27-30, 2021, Tarragona, Spain

Oxidation at liquid state of iron and zirconium under Severe Accident conditions.

Sarah, Thilliez[1*], Pascal, Piluso[1], Jules, Delacroix[1], Emmanuel, De Bilbao[2] and Jacques, Poirier[2]

[1] CEA, DES, IRESNE, DTN, SMTA, LEAG, Cadarache F-13108 Saint-Paul-Lez-Durance, France, [2] CNRS, CEMHTI UPR3079, Univ. Orléans, F-45071 Orléans, France.

*Corresponding author: *sarah.thilliez@cea.fr*

I. INTRODUCTION

In case of nuclear severe accident with a core melt down, a mixture called corium, can be formed at very high temperature (T > 2800 K). Due to the existence of a decay heat, the nuclear fuel UO_2 can interact strongly with the Zircaloy claddings and the stainless steel of the surrounding structures to form corium in a steam atmosphere. The interaction between steam and corium melt including zirconium will produce high exothermic reaction and a release of hydrogen. This kind of oxidation reaction at high temperature will have an impact on severe accident propagation especially hydrogen kinetic production and corium behaviour [1]. Severe accident codes need robust corium kinetic oxidation laws in order to be better predictable whereas they are still a lack of knowledge in this topic.

In this paper, a short review of the main oxidation process will be firstly presented. Then, the VITI facility of the PLINIUS platform devoted to oxidation studies will be described. In order to study the key mechanisms and kinetics of corium oxidation by oxygen, two individual key elements of the corium at liquid state –iron and zirconium- have been chosen and the first results will be presented and discussed.

II. STATE OF THE ART ON OXIDATION MECHANISMS

Currently, the available literature on corium oxidation at liquid state is often based on integral experiments that represents specific scenario. Sulatsky et al. [1] [2] have studied the influence of corium oxidation on the pool structure at high temperature. However, the experimental configuration performed under "oxidant starvation" condition do not allow to identify completely the key mechanisms of oxidation process. The "oxidant starvation" means that the oxidant species are the limiting reactants of the oxidation reaction. In this condition, corium oxidation is controlled by the oxidant species mass transfer at the surface of the molten corium pool and not by the inherent ability of the melt to react in bulk with oxygen [3].

Sarrazin et al. [4] has proposed the following approach to describe oxidation kinetics: a physical parameter -such as mass gain or oxide layer thickness or oxygen consumption- can be chosen and its evolution versus time recorded. The determination of the oxidation kinetic allows the identification of the oxidation key mechanism(s). Khawam et al. [5] have summarized the principal reaction kinetic laws at solid state and their modelling to obtain accurate representation of these mechanisms. According to the authors, the oxidation kinetic of a metal (pure element or alloy) is mainly controlled by diffusion solid-state mechanisms [5].

Metal oxidation process (with a protective compact oxide layer) can be described by a parabolic kinetic law as:

$$W^2 = k_p t \quad (1)$$

where, W is the physical parameter, k_p is the parabolic rate constant and t the time, *i.e* W^2 *in* $g^2.cm^{-4}$, k_p *in* $g^2.cm^{-4}s^{-1}$ *and time in s in the case of thermogravimetric analysis.* .

The rate of the species diffusion decreases proportionally to the thickness of the oxide layer. In this case, the determination of the parabolic rate constant k_p allow the estimation of diffusion coefficient D of the specie that diffuse in the oxide layer : oxygen anion or metallic cation, it depends of the studied metallic system..

Other metal oxidation process (with non-protective oxide layer *i.e. cracks, porosity*) can be described by a linear kinetic law as:

$$W = k_l t \quad (2)$$

where k_l is the linear rate constant, *i.e. W in* $g.cm^{-2}$, k_l *in* $g.cm^{-2}s^{-1}$ *and time in s in the case of thermogravimetric analysis*.

The linear kinetics indicates that the oxidation process is controlled by reactions at the interface gas/metal and the

growth of a non-protective oxide layer. The linear law can also characterize the failure of a protective oxide layer.

To our knowledge, they are no available experimental data on oxidation by oxygen of pure iron and zirconium at liquid state. Khawam approach seems to be the most appropriate methodology to model oxidation process at liquid state.

III. EXPERIMENTAL PROCEDURE

A. VITOX set-up

The iron and zirconium oxidation experiments at liquid state have been carried out in the VITI facility located in the PLINIUS Severe Accident Platform at CEA Cadarache. The VITI facility is a furnace with an induction heating system that allows experiment at high temperature (T > 3000 K). The VITOX (VITI-Oxidation) configuration will be used to conduct analytical oxidation experiments on iron and zirconium at liquid state (Figure 1). The elements 1, 2, 3 and 4 represented on Figure 1 are ceramic materials such as alumina (Al_2O_3), stabilized zirconia (ZrO_2) or stabilized hafnia (HfO_2). The VITOX configuration is equipped with two flow-meters connected to an oxygen and an argon tank in order to supply an oxidant gaseous mixture into the separating tube. An "on-line" oxygen gas analyser at the exit of the VITOX set-up allows monitoring of the oxygen consumption by the sample during the oxidation experiments. The oxidation tests are performed at high temperature by induction heating and coupling to a susceptor in tungsten. Two bichromatic pyrometers video 1 and 2 measure respectively the temperature of the surface sample and the susceptor temperature during the experiment. After the experiments, each samples are analysed with Scanning Electron Microscope (SEM) equipped with an Energy Dispersion (EDX) spectrometer in order to analyse locally elements.

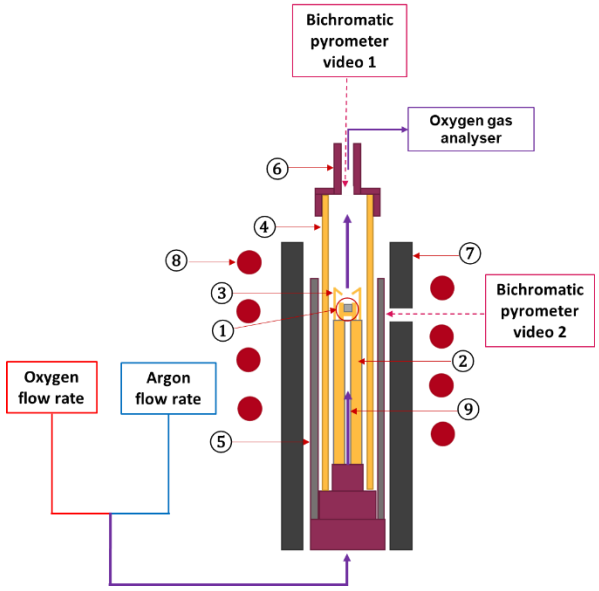

Figure 1: VITOX set-up : ① the crucible and the sample, ② the support, ③ crucible lid, ④ separating tube, ⑤ susceptor, ⑥ tube lid, ⑦ thermal shield, ⑧ inductor and ⑨ oxidant gas flow.

During a VITOX experiment, the increase in temperature is under argon atmosphere to avoid the formation of an oxide layer. When the experimental temperature is reached and a thermal stationary regime is obtained, an oxidant atmosphere is supplied during a given time. At the end of the time, the injection of the oxidant gaseous mixture is stopped and the cooling down is carried out under argon atmosphere. Before and after the experiments the samples are weighted.

B. Materials and experimental procedure

The iron sample are 99.99% pure and the zirconium samples have a purity above 99% with traces of hafnium. The specimens are cylinders of 5 mm of diameter and 5 mm of height. In order to remove a potential very thin surface oxide layer, the samples are mechanically grounding with 120-grit SiC paper. Then, the samples are preserved in acetone to prevent the formation of a new oxide layer. The oxidation experiments are carried out with gaseous mixture composed by 5%mol.O_2-95%mol.Ar. The experiments on liquid iron are conducted at 1893 K. Three duration have been chosen for iron: 10, 20 and 30 minutes. The oxidation experiments on the liquid zirconium are carried out at 2173K. Three duration have been chosen for zirconium 1, 10 and 20 minutes.

IV. RESULTS AND FIRST INTERPRETATIONS

A. Fe-O system

The Figure 2 presents the results of the 20 minutes oxidation experiment of liquid iron.

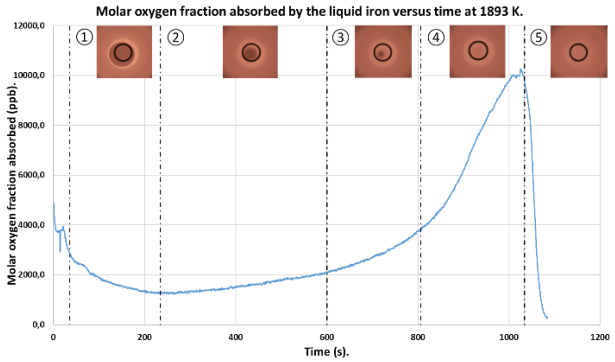

Figure 2: Oxygen consumption by the liquid iron during 20 minutes.

At the beginning of the oxygen supply, measurement of oxygen consumption is unstable. In the part ① of the Figure 2, the oxygen consumption decreases. Then, the oxygen consumption is low and slowly increases (② Figure 2). In part ③ et ④ (Figure 2), the oxygen consumption strongly increases. After 1020s, there is a strong decrease of oxygen consumption. All along the experiments the sample surface is observed by the pyrometer-video 1 (Figure 1) and the surface seems to be liquid. It should be noted that the oxygen consumption evolution is similar to those measured during the experiments of 10 and 30 minutes.

The metallographic observation with SEM-EDX of the oxidized sample during 20 minutes (Figure 3) shows the formation of an oxide phase $Fe_{0.95}O$ (so-called,*wüstite*) and a spinel phase $FeAl_2O_4$ (so-called *hercynite*). The $FeAl_2O_4$ formation reveals an interaction between the liquid wüstite and the alumina from the crucible [6]. The observed phases are located in the sample bulk. However, the presence of

hercynite in the bulk sample seems indicate that oxygen is present in the sample volume.

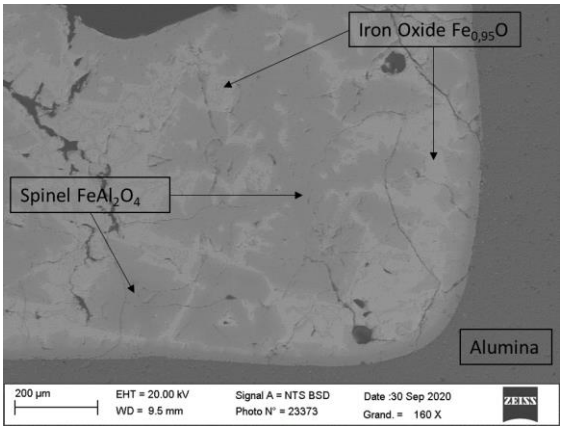

Figure 3: SEM-EDX observation of the left bottom of the iron sample oxidized during 20 minutes.

It is important to precise that metallographic analyses have also be carried out on the iron sample oxidized during 10 and 30 minutes. For the 10 minutes case, there is locally three different phases: an iron metallic phase topped by a thin oxide layer $Fe_{0.95}O$ with aluminium traces and spinel phase $FeAl_2O_4$ located at the crucible interfaces. The 30 minutes oxidized sample is composed only by the spinel phase $FeAl_2O_4$.

To explain the final solid state, the following mechanism can be proposed: a thin liquid *"protective"* iron oxide layer $Fe_{0.95}O$ (melting temperature about 1650 K) is initially formed at the surface of the melt and would blocked the oxidation process. Then, the alumina of the crucible and the liquid iron oxide would interact and a solid spinel layer $FeAl_2O_4$ (melting temperature about 2050 K) is formed. The liquid oxide layer at the sample surface would lose it "*protective properties*" because of the solid spinel phase formation and the oxygen will interact with the liquid iron. Further explanations would explain the formation of a "*non-protective*" spinel layer at the surface of the sample. The presence of macroscopic defaults as cracks or porosities in the solid spinel layer would create preferential diffusion paths for oxygen but, none of these macroscopic defaults are observed during the metallographic observations. It should noted that the formation of "*non protective*" spinel phase $(Fe,Cr)_3O_4$ also occurs during the oxidation of solid stainless steel [8] [9] and causes an increasing of the oxidation rate. In the case of liquid iron oxidation, the same phenomenon will explain the increasing of oxygen consumption during the VITOX experiment. After the formation of the "*non-protective*" $FeAl_2O_4$ phase, the oxygen would diffuse into the sample bulk and the liquid oxide phase $Fe_{0.95}O$ should be formed then the solid spinel phase $FeAl_2O_4$. The oxygen diffusion can be the main mechanism of liquid iron oxidation as in solid state. Iron oxidation process at solid state is controlled according to a parabolic law [7] [8] [9] [10] (Eq.1) and should be represented by a strong oxygen consumption at the beginning of the VITOX experiment and a low oxygen consumption at the end of the interaction which is not the case during the oxidation of liquid iron (Figure 2).

B. Zr-O system

The Figure 4 presents the results of the 10 minutes oxidation experiment of liquid zirconium.

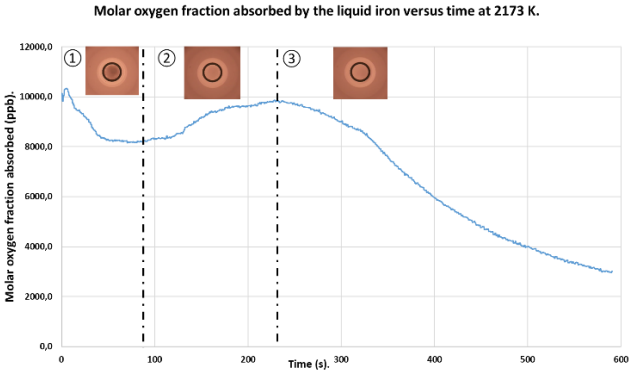

Figure 4: Oxygen consumption by the liquid zirconium during VITOX-Zr-10 as time function.

During the first part of the interaction (① Figure 4) there is a decrease of the oxygen consumption then an increase of the consumption (② Figure 4). At the end of the experiment, the oxygen consumption by the sample decreases again. During the injection of oxygen, it seems to be a formation of solid crust at the sample surface. The oxygen consumption measured during the oxidation experiment of 1 and 10 minutes follow the same evolution.

The post-mortem analysis (Figure 5) revealed the formation of ZrO_2 and a solid solution of zirconium with a mean value of 30%at.of oxygen ("$ZrO_{0.3}$"). The ZrO_2 phase is located at the free interface in contact with gaseous atmosphere whereas the solid solution of zirconium ("$ZrO_{0.3}$") is located in the bulk.

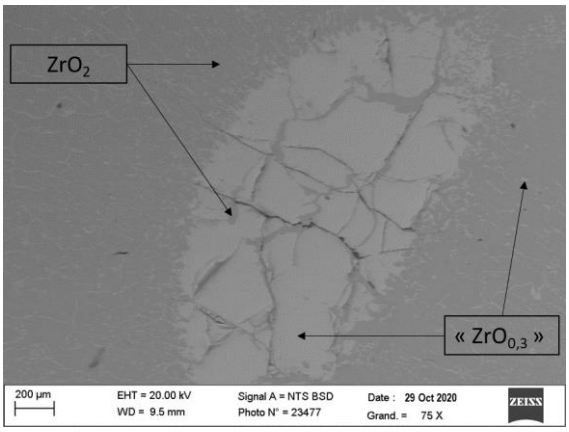

Figure 5: SEM-EDX observation of the bulk of the oxidized zirconium sample during 10 minutes.

The formation of ZrO_2 phase indicates that the sample surface was solid during the experiment because the ZrO_2 melting temperature (about 2988 K) is higher than the temperature of the experiment. Indeed, the melting temperature of the zirconia is higher than the experiment temperature. One possible oxidation process of liquid zirconium could be controlled by the diffusion of the oxygen in the thin solid layer of ZrO_2 phase [4] [11] [12]. In a first time, a solid solution composed by zirconium and oxygen is formed then zirconia. The diffusion of the oxygen through the thin oxide layer should controlled the growth of the zirconia and so the oxidation process.

V. CONCLUSION

Oxidation tests have been carried out in VITOX facility on iron at 1893 K and zirconium at 2173K to insure liquid state. When stationary thermal regime has been reached, oxygen (5%mol.O_2-95%mol.Ar) has been injected in order to study oxidation mechanisms at liquid state of individual element belonging to corium.

The oxidation of liquid iron, at the beginning of the interaction, is slow with the formation of a *"protective*" oxide layer at the sample surface. Then, the oxidation process continues with a strong and quick oxygen consumption. This oxygen consumption change can suggest that the protective oxide layer failed because of the formation of a "*non-protective*" spinel phase $FeAl_2O_4$. Further experiments in the same conditions are planned to be able to propose a modelling of oxidation mechanisms of the liquid iron. The experiments data will be use to determine the oxidation kinetic laws in order to propose a modelling of the oxidation process of liquid iron.

The oxidation experiments on liquid zirconium have shown that the oxygen consumption increases in a first time then decreases. This evolution can indicate that a solid ZrO_2 phase layer is formed at the beginning of the interaction and this oxide layer slows strongly the oxidation process of liquid zirconium. One possible oxidation mechanism of the liquid zirconium could be the diffusion of the oxygen through the oxide layer formed as in solid state. Complementary tests are planned to confirm this possible mechanism and to propose a full modelling of oxidation process.

REFERENCES

[1] B. Sehgal, Nuclear Safety in Light Water Reactors : Severe Accident Phenomenology, Elsevier Science Publishing Co. Inc., 2012.

[2] A. Sulatsky, V. Almjashev, V. Granovsky, V. Khabensky, E. Krushinov, S. Vitol, V. Gusarov, F. Fichot, L. Carenini, M. Bénédicte, P. Piluso, R. Le Tellier, C. Le Guennic, N. Bakouta, T. Keim et M. Lecomte, «Experimental study of oxidic-metallic melt oxidation,» *Nuclear Engineering and Design*, vol. 363, pp. 1-27, 2020.

[3] A. Sulatsky, S. Smirnov, V. Granovsky, V. Khabensky, E. Krushinov, S. Vitol, S. Kotova, M. Fischer, S. Hellman, W. Tromm, A. Miassoedov, D. Bottomley, P. Piluso et M. Barrachin, «Oxidation kinetics of corium pool,» *Nuclear Engineering and Design*, pp. 168-179, 2013.

[4] M. Zancanaro, N. Bertrand et F. Rebillat, «Definition of Optimized Conditions to Extract Accurate Kinetic Laws from TGA Experiments : Modeling and Validation,» *Oxidation of Metals*, vol. 87, pp. 393-402, 2016.

[5] P. Sarrazin, A. Galerie et J. Fouletier, Les mécanismes de la corrosion sèche : une approche cinétique, 2000.

[6] A. Khawam et D. Flanagan, «Solid-State Kinetic Models : Basics and Mathematical Fundamentals.» *The Journal of Physical Chemistry B*, vol. 110, n°135, pp. 17315-17328, 2006.

[7] T. Emi, W. Boorstein et R. Pehlke, «Absorption of Gaseous Oxygen by Liquid Iron.» *Metallurgical Transaction*, vol. 5, 1974-1961.

[8] S.-Y. Cheng, S.-L. Kuan et W.-T. Tsai, «Effect of water vapor on annealingscale formation on 316 SS.» *Corrosion Science*, vol. 48, pp. 634-649, 2006.

[9] E. Essuman, G. Meier, J. Zurek, M. Hänsel, L. Singheiser et W. Quadakkers, «Enhanced internal oxidation as trigger for breakaway oxidation of Fe-Cr alloys in gases containing water vapor,» *Scripta Materialia*, vol. 57, pp. 845-848, 2007.

[10] N. Bertrand, N. Desgranges, C. Poquillon et M.-C. Lafont, «Iron oxidation at low temperature (260-500°C) in air and the effect of water vapor.» *Oxidation of Metals*, vol. 73, n°11-2, pp. 139-162, 2009.

[11] D. Caplan, M.-J. Graham et M. Cohen, «Effect of oxygen pressure and experimental method on the hogh temperature oxidation of pure Fe.» *Corrosion Science*, vol. 10, pp. 1-8, 1970.

[12] R. Hussey, G. Sproule, D. Caplan et M. Graham, «The growth and structure of oxide films formed on Fe in O2 and CO2 at 550°C.» *Oxidation of Metals*, vol. 11, n°12, pp. 65-79, 1977.

[13] L. Jansson et N.-G. Vannerberg, «The effect of the oxygen pressure and the growth of whiskers on the oxidation of pure Fe.» *Oxidation of Metals*, vol. 3, n°15, pp. 453-461, 1971.

[14] N. Lakshmi, H.-I. Yoo et M. Martin, «Oxidation Kinetics of Zirconium Examined by In Situ X-Ray Diffraction.» *Journal of The Electrochemical Society*, vol. 3, n°1160, pp. 136-141, 2013.

[15] H.-I. Yoo, B.-J. Koo, J.-O. Hong, I.-S. Hwang et Y.-H. Jeong, «A working hypothesis on oxidation kinetics of Zircaloy.» *Journal of Nuclear Materials*, vol. 299, pp. 235-241, 2001.

Proceedings of the European Nuclear Young Generation Forum
ENYGF'21
September 27-30, 2021, Tarragona, Spain

Analysis of the Thermal-Hydraulic Parameters of VVER-1200 due to Fuel Failure at Power Concurrent with Loss of Offsite Power

Thulu, Fabiano[1&2*], Ayah, Elshahat[2], Tenthani, Chifundo[1], Katengeza, Estiner[1] and Caroline C.S., Bwanali[1]

[1] Physics and Biochemical Sciences Department, The Polytechnic, University of Malawi, P/Bag 303, Chichiri, Blantyre 3, Malawi.
[2] Nuclear and Radiation Engineering Department, Faculty of Engineering, Alexandria University, 21544 Alexandria, Egypt;

*Corresponding author: *fthulu@poly.ac.mw*

I. INTRODUCTION

Safety analysis of Nuclear Power Plants (NPPs) is of prime importance due to severe detrimental side effects of nuclear radiation. The development and popularization of the nuclear energy, reactor safety has attracted great public attention. The inevitable radioactivity of reactor fuel poses both risks and challenges to the development of the nuclear industry. Research into nuclear safety technology, prevention measures and mitigation of reactor accidents is, therefore, vital to the optimization of safety systems and evaluation of operational, under construction and designs of NPPs [1].

The water-water energetic reactor 1200 (VVER-1200) is a superior performer in comparison to 6 loop- VVER-440 Model V230 and a modified version of VVER-440, Model V213. It is, therefore, crucial that the VVER-1200's reliability and levels of safety are heightened for its commercial operation [2]. Thus, confirmation of the VVER-1200 safety under all the anticipated transients and accidents by designers, operators and regulators will be unequivocal. Safety analysis thermal hydraulic codes such as Personal Transient Computer Analyser (PCTRAN) thermal-hydraulic program have a pivotal role in enforcing such thermal hydraulic safety hence its use in this research [3].

Reactor fuel failure at full power may lead to core heat up, and propagate to Beyond Design Basis Accident (BDBA) or Severe Accident (SA). Accordingly, appropriate steps to avert these situations should be taken [4]. Analysis of thermal-hydraulic parameters in case of fuel failure at full power has become an integral part of NPPs especially after Chernobyl and Fukushima nuclear accidents where core melting could have occurred [5] [6]. It is against this backdrop that the research focused on analysis of reactor changes caused by fuel failure at full power followed by loss of offsite power in VVER-1200 (or AES-2006). Responses of monitored plant parameters; timing of the loss of critical safety functions and operational actions - to avoid the loss of critical safety functions- and heat removal capability; cladding failure and core damage; and radiation contamination were investigated. The analyses could contribute towards making informed decision on occupational, public and environmental radiation exposure that may arise. They may also serve as a guide in future modifications of core and reactor safety systems.

The research used PCTRAN for VVER-1200, a transient accident simulator program developed by Micro Simulation Technology (MST) [7]. It has different versions for PWR, BWR, advanced AREVA EPR, Westinghouse AP1000, GE ABWR and other reactors. It is also used to evaluate off-site dose distributions for various malfunctions of NPP and also as a successful IAEA training platform for probabilistic safety assessment and emergency exercises [8].

II. VVER 1200 REACTOR CORE AND FUEL DESIGN

The core thermal power and operation pressure are slightly higher [9]. The reactor core of VVER-1200 comprises 163 hexagonal design fuel assemblies (FAs). The FAs are designed for heat generation and its transfer from the fuel rod surface to the coolant during the service life without exceeding the permissible design limits of fuel rod damage [10]. The FAs are 4570 mm high (nominal value). When the reactor is in the hot state the height of the power generating part of the fuel rod is 3750 mm (Fig 1). Each FA contains 312 fuel rods. The FA skeleton is assembled of 18 guide channels, 13 spacer grids welded to them, an instrumentation channel and a support grid [11]. The fuel rod cladding is a zirconium alloy tube. Sintered UO_2 pellets with a 5% (4.95±0.05) maximum enrichment are stacked inside the cladding. The average linear heat rate of a fuel rod is 167.8 W/cm. The maximum effective time of FA operation between refuelling for a 12-month fuel cycle is 8400 effective hours. The average burn-up of unloaded fuel is up to 60 MWD/kg U. Annually, 42 fresh FAs are loaded into the core for the basic fuel cycle [12].

Reactor output is controlled using the 121 rod cluster control assemblies (RCCAs) of the control and protection system by burnable neutron absorber in the fuel rods and change of boric acid concentration in the primary circuit water. The

RCCAs are designed for quick chain reaction suppression, power sustenance at assigned level and its level-to-level transition, axial power field levelling and xenon oscillation suppression. Pitch electromagnet drives with pitch position indicators are used for RCCAs drive mechanisms. The drives are installed on the reactor top head [13].

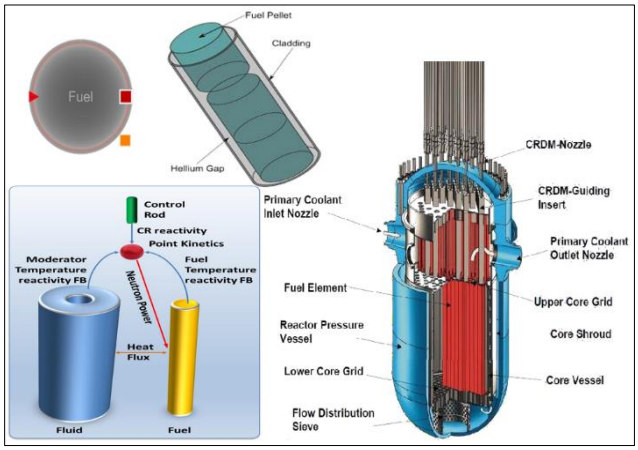

Figure 1. Fuel rods and Fuel assembly

III. PCTRAN VVER 1200

PCTRAN VVER-1200 Visualized Modularization program is recognized as one of the best estimate transient simulation programs for Light Water Reactors, in combination with new options for improved modelling methods, advanced programming, computational simulation techniques, and integrated graphics displays. It has a visual simulation interface. The platform can achieve two modelling objectives. These are:

- The actual component-based modular modelling method comprising the reactor, the steam generator, the pressurizer, the main pump, steam turbine and heat exchanger, and other real components; and
- The simplified block diagram representation of the system components in the form of 'control volume' as the basic unit of division and modelling and, for some special components, the direct application of the 'special model' of the system, such as the main pump and valves.

The Preliminary Safety Analysis Safety Report (PSAR) of model 392M at the Novovoronezh NPP-II was used for developing and benchmarking of the PCTRAN VVER 1200 program [7]. Substantive changes were made to the thermal hydraulic program to render it more realistic and user friendly, with large range of analytics. Challenges related to PCTRAN VVER-1200, include but not limited to:

- Too many components make it hard and complex for beginners to understand and use; and
- There is no input editing option, which makes it impossible to modify and seek specific parameters [8].

IV. STUDY SIMULATION

A. Validation of PCTRAN Simulator Program

Validation of NPPs safety analysis codes is a crucial requirement [14]. This research, therefore, applied the same to ensure completeness and correctness of simulator used . In this case, a systematic representation of PCTRAN Simulator was assumed validated after it had a functional fidelity that represented the VVER-12000 reactor's designs. The reproduction of a nominal measured steady-state condition of the reactor system was necessary. Equally important, was the demonstration of an acceptable condition for time dependent scenarios.

B. Program Qualification

A key feature of NPP safety technology is constituted by the necessity to exhibit the qualification level of each computational tool adopted within an assigned process of each step of the concerned process [15]. PCTRAN thermal-hydraulic program had the capability to: Predict relevant phenomena occurring for the selected spectrum of accidents; reproduce the peculiarities of the reference VVER-1200 plant; and produce suitable results for comparison with the acceptable criteria of the VVER-1200. It was also available to qualified users of this study.

PCTRAN utilises developed and validated thermal hydraulic systems, fuel behaviour, and severe accident models of NPPs commonly used by researchers worldwide. This is in combination with a flexible building block approach to model thermal hydraulic and reactor systems. It uses a building block approach and user defined graphics screens in combination with the ability to interactively control the PCTRAN simulation. These available requisites in PCTRAN thermal-hydraulic program, made it qualify for this study.

C. Research Accident Modelling

In this study, the possible reactor transients and malfunctions were considered and simulated for fuel failure at full power followed by loss of offsite power. The simulations of the transient situations were performed using the PCTRAN VVER-1200 thermal hydraulic program.

D. Initial and Boundary Conditions of VVER-1200 in PCTRAN

After setting up the initial and boundary conditions, the necessary parameters were measured to analyse the reactor performance. The appropriate malfunction number on the PCTRAN program was used for the activation of the fuel failure at full power while the reactor was operating at 100%, followed by loss of offsite power.

E. Simulations

The default conditions of PCTRAN thermal hydraulic program were satisfied, then fuel failure was induced and the parameters used for the moderator dilution were: delay time of 20 seconds, ramp time of 20 seconds and failure fraction of 50%. While the parameters used for the loss of offsite power were: delay time of 70 seconds, ramp time of 30 seconds. The total simulation time was 5500 seconds.

There was no interaction of the operator involved during the accident.

V. Results and Discussion

A. Results of the Steady State Simulation

It was necessary that the commencement and boundary conditions had to be as close to the conditions of the real VVER-1200 plant as possible before simulating the behaviour of the accident. This facilitated the attainment of credible calculated results from the simulation program [16]. A preliminary calculation called steady state calculation was done in order to attain all these conditions.

Thereafter, the PCTRAN ran for a while until the values of the main variables were stabilized around their nominal values. In the simulation the stationary calculation lasted for 20 sec. The results have been compared with the design specifications of the VVER-1200. The calculated results and actual VVER-1200 design data were equal or closer. The comparison showed that the results were within acceptable limits. Therefore, it was convincing to carry out accident analyses using on the built VVER-1200 PCTRAN thermal hydraulic program. Steady state results have been showed in Table 1.

Table 1. The Initial and Steady State Conditions

	Dimension	Design value	Steady State Value
Reactor Power	MWth	3200	3200
RC Pressure	MPa	16.2	16.2
Core Average Temp	ºC	306.9	306.8
SG Pressure	MPa	6.8	6.9
Coolant Temp at reactor inlet	ºC	298.2	298.1
Coolant Temp at reactor outlet	ºC	298.9	298.7
Coolant flow rate through the reactor	Kg/s	23888	23889

B. Analysis of the PCTRAN Results for Failure at Power Concurrent with Loss of Offsite Power

It was observed from the simulation that reactor scram occurred at 23.5 seconds. Following the reactor scram, core thermal power dropped to below 200MWth in 90 sec (Fig 2) and nuclear flux dropped to 5% after 60 seconds (Fig 3). When loss of power occurred, the primary coolant system (PCS) increased to maximum to 174 bars in 10 sec. Thereafter, it dropped below 130 bars in about 100 sec. The RCS pressure continuously and slowly dropped until end of simulation. The steam generator (SG) pressures increased and peaked at 79 bars for SG-A at 151 seconds and 93 bars for SG-B at 105 sec. Then, both pressures dropped below 80 bars. No significant change in reactor building pressure was observed during simulation period (Fig 4).

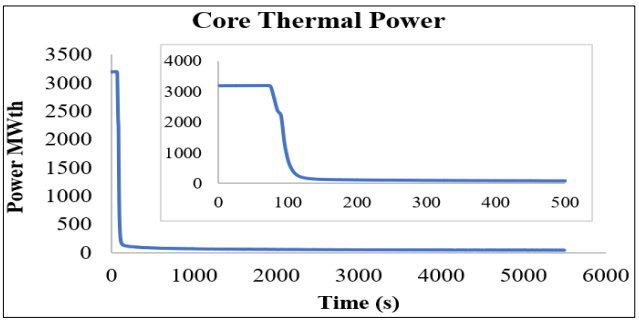

Figure 2. Core Thermal Power

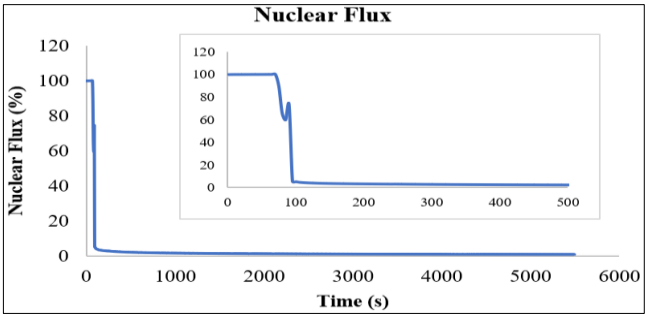

Figure 3. Nuclear Flux

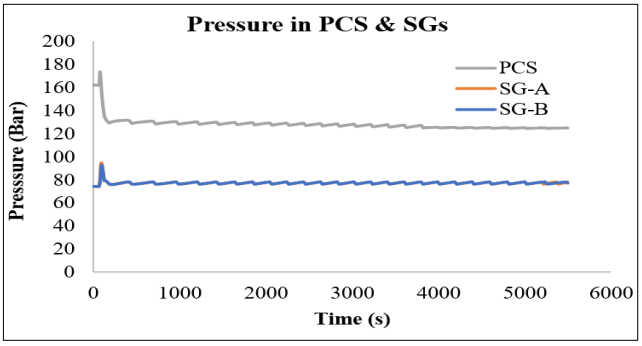

Figure 4. RCS, SG-A and SG-B Pressure

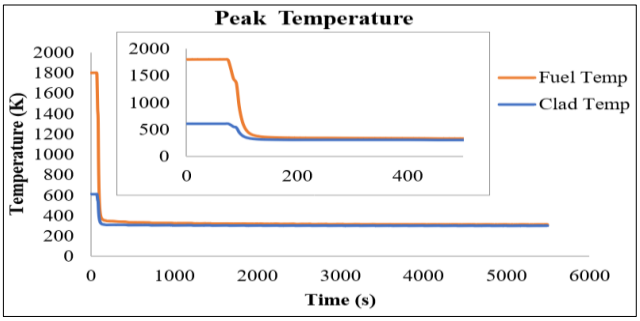

Figure 5. Fuel and Cladding Temperature

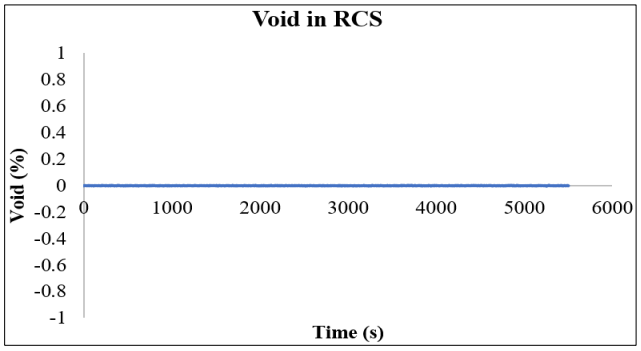

Figure 6. Reactor Void in RCS

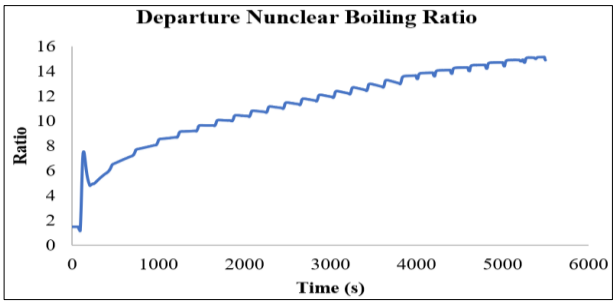

Figure 7. Departure from Nuclear Boiling Ratio

Fig. 5 illustrates that the peak fuel and clad temperature dropped to 350 ^{0}K from 1800 ^{0}K after 130 sec and to 310 ^{0}K from 610 ^{0}K for the transient respectively. The Reactor void changed from zero to a peak of 0.005% at 60 sec after the malfunction (Fig 6). Then, the void fraction of RCS reduced to zero in 150 sec. Availability of primary coolant in the core played a significant role in keeping the situation under control. The boiling departure ratio suddenly increased from 1.5 to 7 in 150 sec of simulation, followed by a sharp decrease to 4.9 in 250 sec. Thereafter, it gradually increased until the end of simulation. Lastly, there was no injection of ECCSs and HA, no corium was formed and no significant radiation traces were observed during simulation time.

VI. Conclusions

Thermal Hydraulic parameters in case of Fuel Failure at Power followed by offsite power of VVER- 1200 were analysed in this research. The fuel rod cladding temperature was below 350 K; much lower from the prescribed value for DBA (1200 ^{0}K). The pressure of RCS did not exceed the prescribed value. This ensured the structural integrity of the rest of the system. It is observed from the simulation that the percentage of clad failure is 0%, which indicated no oxidation of the clad and no change in core geometry.

The conclusion, therefore, is that the VVER-1200 has sufficient arrangement to mitigate the consequences of a fuel failure at power followed by loss of offsite power accident without any interaction of the operator. Data found from the simulation corresponds well with IAEA Safety Report Series [17].

The results confirm high standard engineering design of the core and safety systems and can be used to create positive awareness for the general public especially for those in or around prospective sites.

Funding: This study received no external funding.

Data Availability Statement: All data are available in publicly accessible repositories.

Acknowledgments:

The authors would like to thank IAEA-AFRA and Nuclear and Radiation Department of Alexandria University for support rendered towards the study. The authors also thank Micro-Simulation Technology for letting them use PCTRAN VVER-1200.

Conflicts of Interest: The authors declare no conflict of interest.

VII. References

[1] Y. A. Kurakov, Y. G. Dragunov, N. S. Fil, V. N. Krushelnttsky, V. M. Berkovich, and R. Federation, "Improvement of operational performance and increase of safety of wwer-1000/v-392," no. July 1998, pp. 143–154, 2010.

[2] Gidropress, "Status report 108 - VVER-1200 (V-491)," vol. 1200, 2011.

[3] S. Lee, K. S. Ha, H. Y. Kim, and S. J. Kim, "Validation of RCS depressurization strategy and core coolability for independent scenarios of SBLOCA, SBO, and TLOFW," *J. Nucl. Sci. Technol.*, vol. 51, no. 2, pp. 181–195, 2014. https://doi.org/10.1080/00223131.2014.854713

[4] W. European, "Safety Objectives for New Power Reactors," no. December, 2009.

[5] Nuclear Regulatory Commission, "Report on the Accident at the Chernobyl Nuclear Power Station (NUREG-1250)," p. 135, 1987.

[6] E. K. Puska, "Nuclear reactor core modelling in multifunctional simulators," *VTT Publ.*, no. 376, pp. 1–67, 1999.

[7] A. H. Khan, A. K. Ghosh, M. S. Rahman, S. M. T. Ahmed, and C. L. Karmakar, "An Investigation on the Possible Radioactive Contamination of Environment during a Steam-Line Break Accident in a VVER-1200 Nuclear Power Plant," *Curr. World Environ.*, vol. 14, no. 2, pp. 299–311, 2019. https://doi.org/10.12944/CWE.14.2.14

[8] W. R. Simulator and E. Handbook, "PCTRAN Generic Pressurized Water Reactor Simulator Exercise Handbook," 2019.

[9] M. S. Dwiddar, A. A. Badawi, H. H. Abou-Gabal, and I. A. El-Osery, "From Vver-1000 To Vver-1200: Investigation of the Effect of the Changes in Core," vol. 2006, 2014.

[10] S. B. Ryzhov *et al.*, "VVER-Type Reactors of Russian Design," *Handb. Nucl. Eng.*, pp. 2249–2320, 2010. https://doi.org/10.1007/978-0-387-98149-9_20

[11] T. Vver, "The VVER today."

[12] V. G. Asmolov, I. N. Gusev, V. R. Kazanskiy, V. P. Povarov, and D. B. Statsura, "New generation first-of-the kind unit- VVER-1200 design features," *Izv. Wysshikh Uchebnykh Zawedeniy, Yad. Energ.*, vol. 2017, no. 3, pp. 5–21, 2017. https://doi.org/10.26583/npe.2017.3.01

[13] "Unit 2 Design," no. v, p. 2012, 2012.

[14] S. A. Hosseini, A. S. Shirani, M. Zangian, and A. Najafi, "Re-assessment of accumulators performance to identify

VVER-1000 vulnerabilities against various break sizes of SB-LOCA along with SBO," *Prog. Nucl. Energy*, vol. 119, no. August 2019, p. 103145, 2020. https://doi.org/10.1016/j.pnucene.2019.103145

[15] Iaea, "Best Estimate Safety Analysis for Nuclear Power Plants: Uncertainty Evaluation; Safety Reports Series 52," pp. 1–211, 2008.

[16] T. Bajs and N. Debrecin, "Development of the Qualified Plant Nodalization for Safety and Operational Transient Analysis," pp. 219–226.

[17] IAEA, "Standard Format and Content for Safety Related Decommissioning Documents," p. 75, 2005.

Proceedings of the European Nuclear Young Generation Forum
ENYGF'21
September 27-30, 2021, Tarragona, Spain

Very high temperatures (1500-2500 °C) measurements using the pyroreflectometry technique for nuclear applications

Turquais, Benjamin[1,2*], Davoust, Laurent[2], Sans, Jean-Louis[3], Delacroix, Jules[2], Journeau, Christophe[2], Piluso, Pascal[2] and Chikhi, Nourdine[4]

[1] CEA, DES, IRESNE, DTN, Cadarache F-13108 Saint-Paul-Lez-Durance, France; [2] Grenoble-INP/Grenoble Alpes University/CNRS, SIMaP Laboratory, EPM Group, 38402 Saint Martin d'Hères, France; [3] Laboratoire PROMES-CNRS, 7 rue du four solaire, 66120 Font-Romeu Odeillo, France; [4] CEA, DES, IRESNE, DEC, Cadarache F-13108 Saint-Paul-Lez-Durance, France

*Corresponding author: *benjamin.turquais2@cea.fr*

I. INTRODUCTION

A severe accident in a nuclear reactor may result in the formation of a molten pool made of steel and corium, melt composed by molten elements present in a reactor core, such as uranium dioxide (UO_2), zirconium (Zr), zirconium dioxide (ZrO_2), steel from internal structures and fission products. Thermohydraulics and thermochemistry effects describe the phenomenology of the molten pool [1]. These effects are governed by thermophysical properties such as density, surface tension and viscosity. It is therefore prior to get an ever better knowledge of these thermophysical properties in order to perform accurate modelling of severe accident scenarios.

Due to the lack of thermophysical properties of corium and steel at very high temperature (1500-2500°C) and at liquid state, the VITI (VIscosity Temperature Installation) facility is used to measure these properties. VITI is part of the PLINIUS (PLatform for Improvements in Nuclear Industry and Utility Safety) severe accident platform [2]. The uncertainties on these properties have to be reduced as low as reasonably achievable for the reliability of the results. Due to a significant temperature dependence, the uncertainty on the thermophysical properties related to the temperature could be preponderant. On the VITI facility, the thermophysical properties are measured by sessile drop [3], maximum bubble pressure [4] or levitation [5] techniques. Due to the aggressive conditions, the temperature is measured remotely through bichromatic pyrometers. This method might lead to uncertainties of 5 to 10%.

The objective of the present work is to reduce as low as reasonably achievable the overall uncertainty on the measurement of very high temperature (1500-2500°C), especially for measurement on liquid surfaces. An experimental prototype, a pyroreflectometer, has thus been implemented in the VITI facility. This prototype is based on previous development [6] and should give theoretically temperature measurement with an uncertainty of 1 to 2 %.

In the next section, some theoretical elements are introduced devoted to radiation, pyrometry and pyroreflectometry techniques. Then, some results concerning typical experimental applications are detailed and discussed.

II. FUNDAMENTALS

A. Theory of radiation

A body at a temperature T radiates energy towards space in all directions and for all wavelengths. The radiation depends only on the temperature of the body and its surface emissivity. The body temperature may be estimated by detecting the radiation on a given solid angle and for given wavelengths. A directional spectral radiance L_λ is defined, which depends only on the temperature T and the spectral emissivity ϵ_λ [7]. The Planck law, in equation (1), gives the dependence of the spectral directional radiance on the temperature T and the wavelength λ. The two Planck constants are $C_1 = 1.19104 \cdot 10^{-16}\, W.m^2.sr^{-1}$ and $C_2 = 0.014388\, m.K$.

$$L_\lambda = \epsilon_\lambda \frac{C_1}{\lambda^5} \cdot \frac{1}{\exp\frac{C_2}{\lambda T} - 1} \qquad (1)$$

The emissivity is a coefficient comprise between 0 (case of a fully reflective surface, like a mirror) and 1 (case of a fully absorptive surface, like a black body). The spectral emissivity ϵ_λ of a surface depends on several parameters (temperature, rugosity …) and is generally unknown. Some hypotheses on the emissivity are thus taken.

B. Pyrometry

The monochromatic pyrometry consists in measuring the spectral radiance at a given wavelength. A monochromatic temperature T_λ (see equation (2)) is given by the monochromatic pyrometer, which is equal to the

thermodynamic temperature T if the emissivity is equal to one, as for a black body:

$$\frac{1}{T} = \frac{1}{T_\lambda} + \frac{\lambda}{C_2} \ln \epsilon_\lambda. \qquad (2)$$

The monochromatic temperature could be representative of the thermodynamic temperature if the surface emissivity is close to one. However, surfaces with unknown emissivity make this technique not suitable for precise temperature measurement.

The bichromatic pyrometry consists in measuring the spectral radiance at two wavelengths. A bichromatic temperature T_c (see equation (3)) is given by a bichromatic pyrometer, and is equal to the thermodynamic temperature T if the emissivities at both wavelengths are equal.

$$\left(\frac{1}{T} - \frac{1}{T_c}\right)\left(\frac{1}{\lambda_1} - \frac{1}{\lambda_2}\right) = \frac{1}{C_2} \ln \frac{\epsilon_{\lambda 1}}{\epsilon_{\lambda 2}}. \qquad (3)$$

The bichromatic temperature may thus be far from the thermodynamic temperature if the emissivity on the considered wavelength range varies significantly. It might be indeed the case for some metals, as tungsten, where the emissivity variation can lead to a bichromatic temperature hundreds degrees greater than the thermodynamic temperature. The bichromatic temperature may be an overestimation of the thermodynamic temperature, for metal for example, or an underestimation.

C. Pyroreflectometry

To overcome the lack of knowledge about emissivity, the pyroreflectometry technique has been developed. This technique combines two monochromatic pyrometers and a reflectometer working at the wavelengths of the monochromatic pyrometers [6]. The two monochromatic temperatures are then corrected by the measured monochromatic reflectivities, which leads to a temperature, called the convergence temperature T^*. A bichromatic temperature may also be determined using the two monochromatic temperatures. The hypothesis is made on a diffusion coefficient η [6, 8], which is supposed to be equal at both wavelengths. This hypothesis is much less stringent than the equality of the emissivities used for bichromatic pyrometry. The convergence temperature may be calculated with a monochromatic temperature T_λ and a spectral reflectivity ρ_λ. Measurements at both wavelengths and the hypothesis on the diffusion coefficient lead to equation (2) valid at both wavelengths.

$$\frac{1}{T^*} = \frac{1}{T_\lambda} + \frac{\lambda}{C_2} \ln(1 - \eta\rho). \qquad (2)$$

III. EXPERIMENTAL APPROACH AND RESULTS

A. Experimental conditions

Very high temperature measurements (1500-2500 °C) are carried out in the inductive furnace of the VITI facility. The system is described in the figure 1. The material (2) to be characterized is place in a crucible (3), surrounded by the inductor (1), the heater – the so-called susceptor (4) in dense graphite, and the thermal shield (5) in porous graphite, according to figure 1. All the elements lay on a support (6) made with dense graphite. They are placed in a cooled vessel filled with argon. The bichromatic pyrometer and the pyroreflectometer focus from the top on the solid/liquid surface of the solid/melted sample. These temperature sensors are first calibrated and then finely adjusted (distance, angle, size of spot view). The calibration of the temperature sensors is performed on the range [1500-2500°C] using three eutectic fixed point cells of metrological quality [9, 10] with a known emissivity.

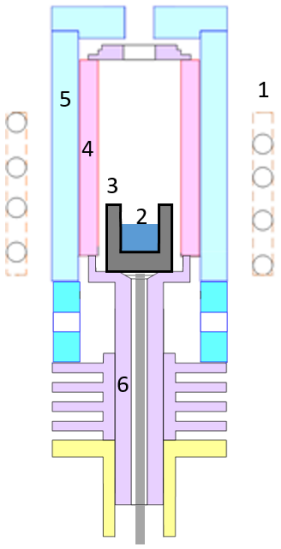

Figure 1: Experimental configuration. 1: Inductor. 2: Sample. 3: Crucible. 4: Susceptor. 5: Thermal shield. 6: Support.

B. The eutectic mixture ruthenium-carbon

The feasibility of the pyroreflectometric measurement on a liquid surface has been first demonstrated directly on a eutectic mixture, ruthenium-carbon, which has a melting temperature of 1953°C but an unknown emissivity unlike the eutectic cells. The eutectic mixture with a slightly hypoeutectic composition is placed within a graphite crucible. The system is heated at the mean rate of 25°C/min. Several thermal cycles are performed around the melting temperature to remove the contribution of possible impurities.

The eutectic mixture ruthenium-carbon has been heated up to 2200°C. The convergence temperature (see figure 2) given by the pyroreflectometer has been evaluated on the liquid surface from 2000 to 2200 °C, even though the spectral reflectivities (see figure 3) are small. As expected, the monochromatic temperatures (T 1.3 µm and T 1.55 µm on figure 2) are underestimations and the bichromatic temperatures (Tc on figure 2) are overestimations of the thermodynamic temperature. The convergence temperature (T^* on figure 2) ranges in between the monochromatic and the bichromatic temperatures, as expected. The convergence temperature of the pyroreflectometer is compared with the temperature given by a standard bichromatic pyrometer (T pyro on figure 2).

Every temperature (monochromatic, bichromatic and pyroreflectometric) is close to each other due to the high apparent emissivity of the susceptor cavity. However, the measurement of the reflectivities has to be improved. We suspect that the reflectivities measured on the eutectic mixture are too low. The thermal expansion of the system might explain the low reflectivity signals that are observed, due to the decreasing of the distance between the sample and the detector. This decreasing of the distance could be enough to reduce drastically the signals in reflectivity. The experimental method is going to be improved in order to obtain reliable reflectivity data.

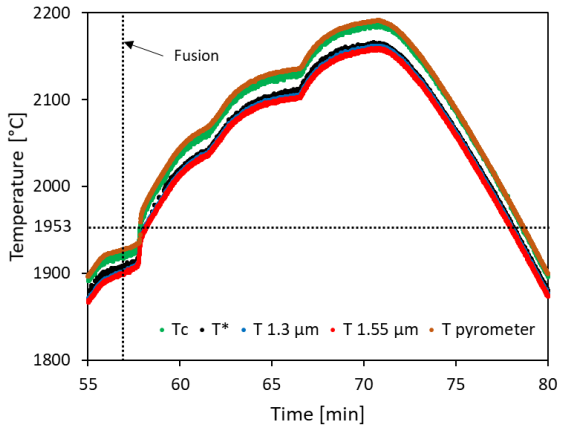

Figure 2: Temperature of the eutectic mixture ruthenium-carbon.

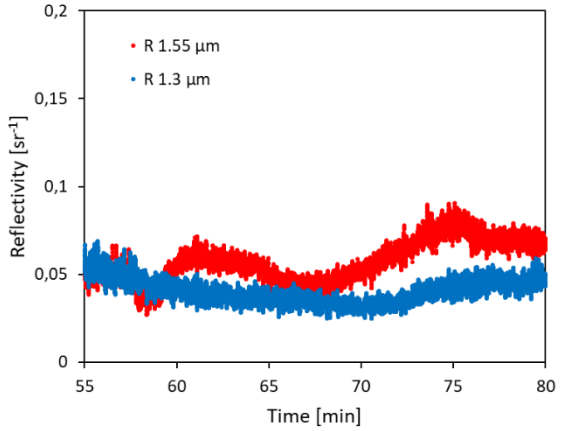

Figure 3: Reflectivity of the eutectic mixture ruthenium-carbon.

C. Liquid iron

Now, a high-purity iron sample is placed within an alumina crucible, according to the general configuration described figure 1. Measurements have been performed up to 1700°C by heating the iron sample at the mean rate of 20°C/min.

The convergence temperature is evaluated between the monochromatic and the bichromatic temperature as expected and explained in section II. However, for the case of melted iron, it happens that the convergence temperature (see figure 4) can not be evaluated every time. The possibility to evaluate the convergence temperature is determined from the order of magnitude of the reflectivities. For the case of iron, the reflectivity at 1.55 µm has to be higher than the reflectivity at 1.3 µm. The inversion of the reflectivities (see figure 5) leads to a non-physical temperature T^* or even to the impossibility to evaluate a temperature T^*. The resulting data points are removed from figure 4. Another case may prevent from a proper evaluation of the convergence temperature. When both reflectivities are close to each other, even in the right order, the convergence temperature can be evaluated mathematically but leads to an absurd value. It may be seen on figure 4, where the convergence temperature presents strong variation below and above the bichromatic temperature. This behaviour is typical of a change in the surface state, which can affect strongly the reflectivities and thus the evaluation of the convergence temperature.

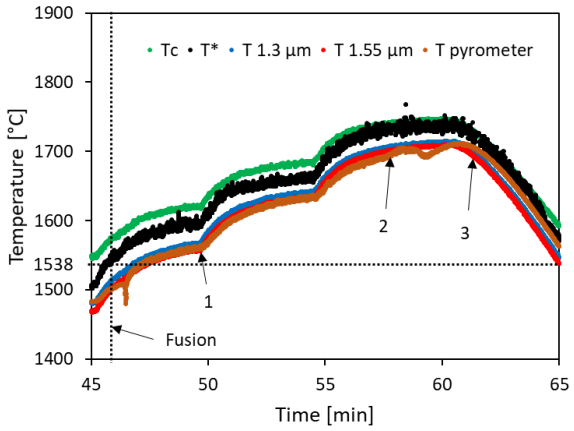

Figure 4: Temperature of liquid iron.

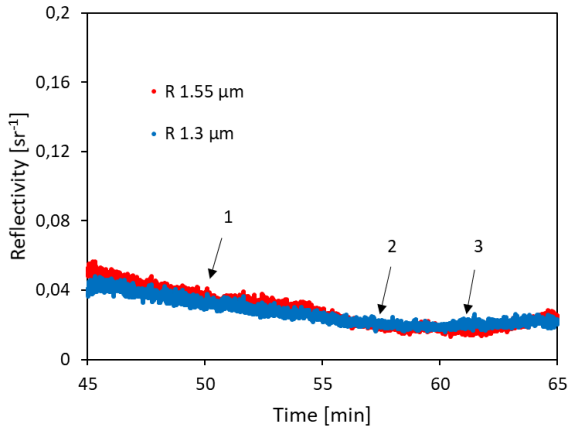

Figure 5: Reflectivity of liquid iron.

It is also suspected that the remaining oxygen, which is present inside the VITI high temperature chamber, may oxidize the surface of liquid iron – whose affinity with oxygen is known. The temperature difference between the bichromatic temperature and the other temperatures is decreasing, which could signify that the emissivity has increased due to the surface oxidation [11]. Three pictures (see figure 6) have been selected at three different times indicated in figures 4 and 5. These pictures show the liquid surface from the top. On the first picture, a mirror-like surface reflecting the surrounding windows (dark patches) can be observed. It is typical of a specular surface, as

expected for liquid metal. Within a time lap of only a few minutes, the shadow completely disappears and a diffuse surface takes place. This diffuse surface seems to be solid and can be seen as the result of metal oxidation under remaining oxygen.

The formation of an oxide crust modifies the measured reflectivities. Figure 4 shows that the convergence temperature can not be evaluated properly for a few minutes. The oxide layer could be semi-transparent at the wavelengths of the pyroreflectometer, which might lead to interferences between reflectivity signals since the thickness of the oxide crust is of the order of the wavelength. However, after a while the convergence temperature could be evaluated again even if the surface was still oxidised. The growth of the oxide crust and thus the disappearing of the interferences could explain the possibility to evaluate again a convergence temperature.

The experimental conditions will be improved in the near future, in order to control the amount of residual oxygen and to monitor the possible oxidation of the liquid surface.

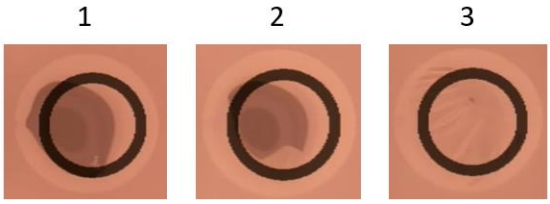

Figure 6: Surface change for the test on liquid iron.

D. Application to severe accident

Such materials as stainless steel, ferritic steel or corium, should be characterized as much as possible to improve the modelling of severe accident scenarios. Some thermophysical properties of these materials may vary strongly with the temperature, especially the surface tension [3]. The uncertainty on the measurement of the temperature might thus be significant in the evaluation of the uncertainty on the measurement of the thermophysical properties, especially at liquid state. The bichromatic pyrometry may lead to uncertainty up to ten percent, i.e. to the order of hundreds of degrees. The method of the pyroreflectometry may reduce the uncertainty on the temperature at one to two percent, i.e. to the order of tens of degrees.

The overall uncertainty on the thermophysical properties may be strongly dependent on the uncertainty on the temperature. The use of the pyroreflectometry can thus provide better estimation of the thermophysical properties.

IV. CONCLUSION

Considering the difficulty and the aggressive conditions of thermophysical properties measurements in the area of nuclear severe accidents, remote and contactless temperature measurements are favoured. The classical technique of the bichromatic pyrometry may lead to uncertainties to the order of 5 to 10%, depending on the radiative knowledge of the liquid material. To optimise the thermophysical properties measurements, the pyroreflectometry technique has been recently implemented in the VITI facility, leading to uncertainties of the order of 1 to 2% [12]. The feasibility of the pyroreflectometry technique on liquid materials has been demonstrated for the first time in this article on two different materials: a eutectic mixture made of ruthenium and carbon and a pure iron sample. This method has been applied using a pyroreflectometer calibrated on the temperature range (1500-2500°C). Some improvements in the reflectivity measurements are still on going in order to be able to perform more accurate temperature measurements by pyroreflectometry. This improvement in temperature evaluation suggests the possibility to deliver in future of more accurate measurements of the thermophysical properties of melted materials, especially in the area of nuclear severe accidents. This method may also be applied in reactor environment, as a tokamak for example [13].

V. REFERENCES

[1] R. Le Tellier, L. Saas, S. Bajard, “Transient stratification modelling of a corium pool in a LWR vessel lower head”, Nuclear Engineering and Design, vol. 287, pp 68-77, 2015.

[2] C. Journeau et al., “Upgrading the PLINIUS platform toward smarter prototypic-corium experimental R&D”, ATH20, 2020.

[3] N. Chikhi, P. Fouquart, J. Delacroix, P. Piluso, Measurement of Type 304L Stainless Steel and 16MND5 Ferritic Steel Density and Surface Tension: Possible Impact for Stratified Molten Pool, Nuclear Technology, vol. 205, no. 1-2, pp 200-212, 2019.

[4] J. Delacroix et al., Measurements of MCCI corium surface tension and density in the VITI facility: synthesis of tests performed within ALISA project, ICONE Proceedings, 2019.

[5] D. Grischenko et P. Piluso, Recent progress in the gas-film levitation as a method for thermophysical properties measurements: application to ZrO2–Al2O3 system, High Temperatures. – High Pressures, vol. 40, no. 2, pp 127-149, 2011.

[6] D. Hernandez et al., Experimental validation of a pyroreflectometric method to determine the true temperature on opaque surface without hampering reflections, Measurement, vol. 42, pp 836-843, 2009.

[7] F. Incropera et D. DeWitt, Fundamentals of heat and mass transfer, seventh edition, I. John Wiley & Sons, Éd., 2011.

[8] J.L. Gardner, T.P. Jones, Multi-wavelength radiation pyrometry where reflectance is measured to estimate emissivity, J. Phys. E: Sci. Instrum, vol. 13, pp 306-310, 1980.

[9] M. Sadli et al., Collaboration Between UME and LNE-INM on Co-C Eutectic Fixed-Point Construction and Characterization, International Journal of Thermophysics, vol. 30, pp 36-46, 2009.

[10] M. Sadli et al., Construction and in-situ characterisation of high-temperature fixed point cells devoted to industrial applications, EPJ Web of Conferences, 77, 00018, 2014.

[11] L. Barka et al., Influence of oxidation and emissivity for metallic alloys space debris during their atmospheric entry, 7th European Conference on Space Debris, vol 7 (1), 2017

[12] B. Turquais et al., Metrology at very high temperature (1300-2500°C) in pyroreflectometry for nuclear applications (in French), Congress of SFT, 2021.

[13] E. Delchambre et al., Performance of pyroreflectometry in a reflective environment, Physica Scripta, 014078, 2011

Proceedings of the European Nuclear Young Generation Forum
ENYGF'21
September 27-30, 2021, Tarragona, Spain

The necessity and benefits of PSA application in NPP design.

Sergey Makukhin[1], Aleksey Sobolev[1]

[1] JSC ATOMPROEKT, Rosatom, Russia

*Corresponding author: SSMakukhin@atomproekt.com

I. INTRODUCTION

Probabilistic safety assessment (PSA) application in the design of NPPs is becoming more and more relevant every year and gaining in significant practical meaning. In parallel to the design process, PSA provides a fully integrated model of the entire plant that can be used to examine the risk from a variety of possible initiating events (e.g. transients, leakages, support system failures, etc.). The PSA consistently accounts for both the event frequency and the potential consequences from equipment failures or human errors.

The PSA model combines front-line safety systems and support systems in a manner that allows designers to identify the risk significance of important intersystem dependencies. The PSA allows designers to quantify the probability of "passive" and "active" failure modes, to examine the significance of single failures and multiple failures, and to determine the risk importance of "safety", "safety related" and "non-safety" systems. Consideration of only a limited set of design basis accidents and application of traditional deterministic design criteria for individual safety functions, systems, and components does not provide the same benefits as the combination of traditional approaches and PSA [1].

A new approach to the risk significance assessment of systems, structures and components (SSC) is also considered in this article. This method can be used for identification of the most significant aspects of plant operation in terms of their impact on safety.

Risk-informed assessment of the deterministic safety classification of structures, systems and components (SSCs) implies the use of the PSA model and is an PSA application, which in this research with using a new method for Paks II NPP is considered.

From the point of view to reduce unnecessary burdens, the NPP licensee may request the change to reduce unnecessary burdens in complying with current technical specifications (TS) requirements based on the operating history of the plant or industry in general. For example, in specific instances, the repair time needed may be longer than the completion times defined in the TS. The required surveillance may lead to plant transients, result in unnecessary equipment wear, result in excessive radiation exposure to plant personnel, or place unnecessary administrative burdens on plant personnel that are not justified by the safety significance of the surveillance requirement. In some cases, the change may provide operational flexibility; in those cases, the change might allow an increased allocation of the plant personnel's time to more safety-significant aspects [2].

II. PSA application

It seems reasonable to divide the PSA application into two types:

A. PSA application to justify the safety of the project as a whole, as well as the assessment of proposed design changes or design options in terms of impact on the safety of the project;
B. PSA application for identification of the most significant aspects of plant operation in terms of their impact on safety.

In practice, the PSA is used to select design options in the course of risk-informed decision-making based on comparative analysis of the design options.

A. Design decisions assessment

The PSA should be used during the lifetime of the plant to provide an input into decision-making in combination with the results and insights of deterministic safety analyses and considerations of defence in depth [3].

Besides the full-scope PSA, which shall confirm the fulfillment of probabilistic safety criteria, the PSA methods should be used during the design process in order to approve that:

- the reliability level of safety-related systems and their protection against CCFs and human errors are sufficient;
- the safety measures provided for accident management (prevention and mitigation of SA consequences) are adequate.

B. A new method for risk significance assessment

PSA importance measures can be used to assess risk (probability-based) importance. These metrics place the equipment importance on a continuous scale. However, for practical use, it is more appropriate to define a limited number of categories (classes), similarly to the deterministic classification. Importance measures to be calculated for the equipment are:

- fractional contribution (FC) or a measure with an essentially equivalent role (e.g. Fussell–Vesely importance or risk decrease factor);
- risk increase factor (RIF) [4].

In international practice [4], typically three levels of risk significance are applied using the threshold values of FC = 0.005 and RIF = 2:

1. Equipment is of High Risk Significance, if
   - its fractional contribution is higher than 0.005 (regardless of the value of its risk increase factor).
2. Equipment is of Medium Risk Significance, if
   - its fractional contribution does not exceed 0.005, and
   - its risk increase factor is higher than 2.
3. Equipment is of Low Risk Significance, if
   - its fractional contribution does not exceed 0.005, and
   - its risk increase factor does not exceed 2.

The main feature and benefit of the proposed classification assessment method is the use of the single significance measure – the conditional fractional contribution (CFC) of the component failure to the probability of nuclear fuel damage (or large release). This approach allows the use of a one-dimension scale (see Figure 1) for the CFC measure to categorize SSC according to the significance of risk, while in international practice, a two-dimensional scale of categorizing according to two indicators of significance is usually used: FC and RIF.

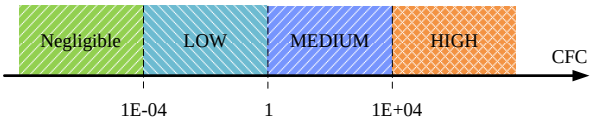

Figure 1. Categorization scale.

For the calculation of CFC relation for RIF [5] is used as a basis, which, using simple transformations based on the physical meaning, makes it possible to evaluate the values of CFC from two sides. As a result, the expression for determining the CFC:

$$\frac{FC_i}{P_i} = RIF - 1 + FC_i \quad (1)$$

Below are the formulas for calculating these indicators for components:

$$CFC_i = RIF - 1 + FC_i \quad (2)$$

$$CFC_i = \frac{FC_i}{P_i} \quad (3)$$

For failures that are initiating events (IEs) or directly lead to IEs, CFC is calculated as the ratio of the IE contribution to the total nuclear fuel damage frequency NFDF (or criterion of limited impact excess frequency CLIEF) to the IE frequency:

$$CFC_i = \frac{FC_{IE}}{f_{IE}} \quad (4)$$

III. RESULTS AND DISCUSSION

In this section, the most significant examples of PSA application to determine the best design options from the point of view of the designed Paks II NPP safety are presented. Also, the preliminary results of risk-informed assessment of the deterministic SSC safety classification are presented here.

A. PSA application for KAC system

The intermediate cooling circuit for essential consumers ventilation system (KAC) is designed for cooled water supply to cool loads of equipment of chilling medium supply systems and ventilation systems in rooms safety trains 1, 2, 3, 4 of Nuclear Island buildings.

Preliminary calculations of the PSA model based on the Paks II NPP Basic Design showed that the design does not meet the safety requirements.

Two design options of KAC system from the point of view of NPP safety were considered (see Figure 2):

- all trains (KAC10/20/30/40) perform heat removal function via the common manifold. The success criterion is 2 out of 4 operating trains. Failure 3 out of 4 trains lead to loss of all 4 safety trains;
- the KAC system is divided into two subsystems (KAC12/34). Each subsystem performs heat removal function from two adjacent safety trains. The success criteria are 1 out of 2 operating trains in each subsystem. Failure 3 out of 4 trains allow to safe 2 out of 4 safety trains.

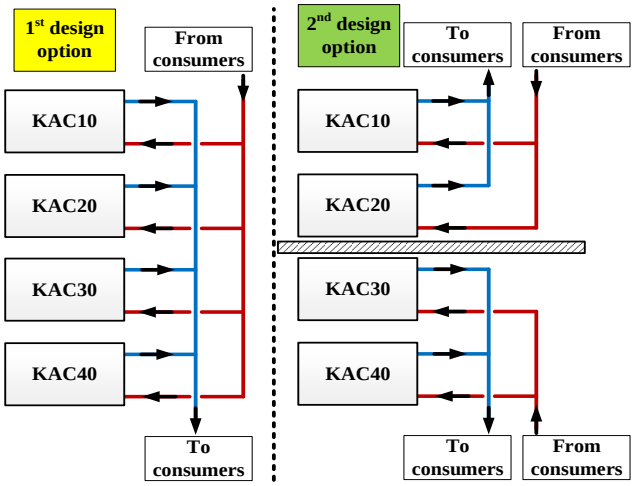

Figure 2. Two design options of KAC system.

For the first option, the contribution of failures associated with the KAC system makes about 60% to the nuclear fuel damage frequency. The failure of the KAC system leads to a complete failure of the emergency power supply system, which in turn leads to the failure of all four safety trains. Based on the results of the Risk benefits assessment, the second design option was chosen from the point of view of NPP safety.

B. PSA application for combination of SDGS buildings

Using the PSA, the qualitative and quantitative analysis of the influence on safety and cost characteristics of Paks II NPP Units 5 and 6 of the design solution related to combination of the standby diesel-generator station (SDGS) buildings was carried out.

Since the assessment of quantitative safety parameters can only be performed by means of PSA, a comparative analysis of probabilistic safety indices for the original and suggested designs was performed.

Failure of all safety trains inside the building is possible only in case of catastrophic external hazards. The only type of external hazard that can cause destruction of only one of the two buildings is the large commercial aircraft crash.

Probabilistic safety parameters were calculated for the original and proposed (including additional modification of normal operation reliable power supply system NORPSS) designs. Cut-off criterion for insignificant cut-sets was 1E-14.

Results of reliability comparative analysis of two UBS buildings and combined UBS (SDGS) building are presented in Table 1.

Table 1. Comparative analysis of reliability for two UBS buildings and combined UBS.

Probabilistic safety indices (PSI)	Freq., 1/year (two UBS)	Freq., 1/year (combined UBS)	Freq. change, %
Total CDF for Full Scope PSA-1	1.63E-07	1.51E-07	-7.36
Total CDF in shutdown modes	3.28E-08	2.12E-08	-35.37
LHR – Failure of function of heat removal to ultimate heat sink	2.79E-08	1.64E-08	-41.22

The analysis results are as follows:

5. Project modification results in significant reduction of frequency of loss of the function of residual heat transfer to the ultimate heat sink, together with total core damage frequency;
6. Design modification allows reducing the construction period for the power unit by 12 months;
7. Design modification allows reducing the operational costs.

According to the results of the PSA calculation and cost-benefit assessment, it was decided to use one SDGS building instead of two.

C. PSA application for I&C system

An analysis of the design modification impact on probabilistic safety indices was performed to justify the exclusion of the second diversity of Reactor Trip System and Engineered Safety Feature Actuation System (RTS-ESFAS).

RTS-ESFAS consists of two sets (diversities), further called sets A and B, in order to meet the design criteria. Each set consists of four redundant trains (further called channels 1,2,3 and 4). The equipment of these four redundant channels is placed in physically separated rooms for I&C of Safety Systems. Sets A and B are not connected with each other functionally. The data between four redundant channels of sets A and B are transmitted via Profibus fibre optic buses. The simplified diagram is shown in Figure 3.

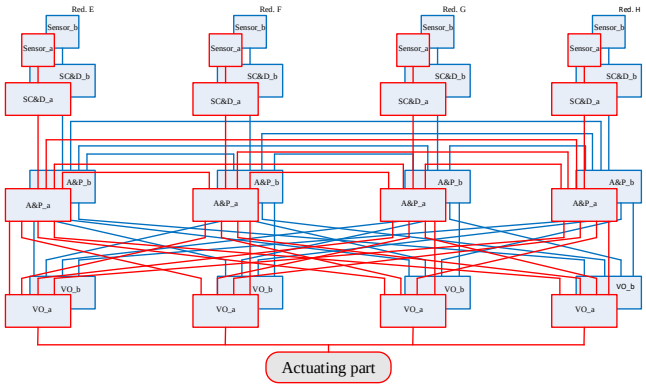

Figure 3. Simplified diagram of RTS-ESFAS with two diversities.

In case of exclusion of the one RTS-ESFAS set:

- probabilistic safety indices (NFD and CLIE) do not change;
- the probability of the RT functions failure does not change;
- the probabilities of failure to generate control signals acting on the equipment of all safety system channels do not change;
- the probability of failure to generate control signals acting on the equipment of a particular SF channel and for which the signals from the sensors enter the processor for processing the input data of the corresponding train (for example, CD14) increase by 40-50 times. In this case, the probabilities of failure of signal generation simultaneously in three or more channels do not change.

The results of the PSA calculation showed that the change in the number of RTS-ESFAS diversities does not affect the probabilistic safety indices of the unit. Thus, from the point of view of PSA, the second diversity is unnecessary. At this stage of the Paks II NPP design implementation, the decision to use one diversity has not yet been made, but if it is adopted, economic costs can be significantly reduced.

D. PSA application for risk-informed assessment of the SSC classification

The Nuclear Safety Commission (NSC) in its volume 3a emphasizes in several paragraphs that the primary basis of the safety classification of the SSCs shall be the deterministic analysis, however, some modification or tuning is allowed to be applied on the basis of the results of the probabilistic analyses.

At this stage of Paks II NNP design, the risk-informed assessment of the SSC safety classification was carried out.

The main purpose of the risk-informed classification assessment is to identify possible discrepancies between probabilistic and deterministic safety classes of SSC.

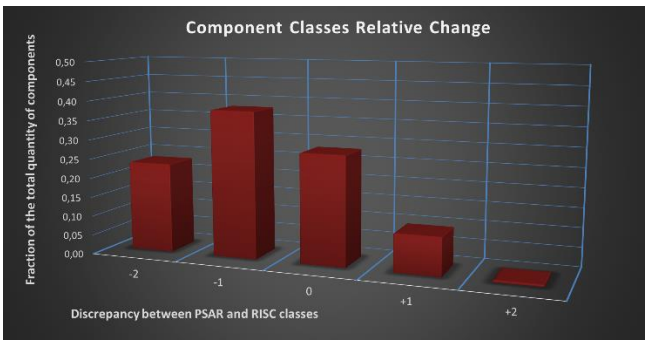

Figure 4. Component Classes Relative Change.

The results shown that significant proportion of changes are attributable to class downgrades (see Figure 4), which is associated with a large quantity of components of the same type, which make an insignificant contribution (the significance of the components is below the sensitivity of the PSA model) to the PSI of NDF and CLIE.

Key preliminary findings:

1. This assessment of the classification is intended for designers of SSC with the aim of familiarization and consideration in the work with a possible revision of safety classes at the next stages of the design;
2. The preliminary risk-informed assessment of the SSC classification carried out according to the developed methodology, showed a high level of correspondence between the estimated and assigned safety classes. Significant class differences (± 2) have a rationale in terms of the PSA model and are of greatest interest for revising the classification;
3. Upgrading is typical for 10 kV NOPSS switchgear and systems supporting their operation (ventilation, cooling, transformers, etc.);
4. Downgrade is typical for components with a high degree of redundancy;
5. The obtained estimates of the most significant components in systems can be used to classify systems for safety.

E. Discussion

Deterministic methods continue to be very effective to ensure safe plant designs. Risk-informed methods should be used to complement, enhance, and validate conclusions that are based on well-established deterministic design principles. It should be noted that when using risk-informed methods, different limitations must be considered in the analysis. Neglecting this can lead to underestimation of important NPP systems and other inadequate results.

The most important benefits from PSA are the added perspectives that are provided by an integrated risk model for the entire plant and a consistent evaluation of both the frequency and consequences of possible accident scenarios.

The main benefits of the use of PSA during the design process are:

- identification and resolution of plant vulnerabilities;
- identification of important intersystem dependencies and potential CCFs;
- examination of risk benefits from different design options;
- qualitative knowledge and understanding of the contribution of components and systems to accident sequences.

The main advantages of the proposed method for risk-informed assessment of the SSC classification with comparision with others are:

- the possibility of SSC categorization by their risk significance into a different number of categories;
- CFC is practically independent of the failure probability;
- the categorization of passive SSC that are not considered in the PSA can be performed, for example, containment, pipelines, etc. (SSC can be introduced into the model with arbitrary reliability parameters);
- the categorization of human actions can be performed;
- the limits for categorization are the same for all probabilistic indices of PSA levels 1 and 2 (the same scale is used).

IV. CONCLUSIONS

Considering results and discussion above, it has been confirmed that during the design process, PSA is successfully and effectively applied to determine the best design options. Some of the PSA-based proposals have already been implemented in the Paks II NPP design, which significantly reduced time, labor and money resources.

The proposed new approach to risk significance assessment of systems, structures and components (SSC) in Paks II NPP design has been used for risk-informed review of safety classification, but also will be used to determine the most significant human errors (for which a more detailed elaboration of accident management guidelines is required), as a tool to justify the frequency of testing safety systems, as well as for risk-informed pre-service and in-service inspection, etc.

V. References

[1] INTERNATIONAL ATOMIC ENERGY AGENCY, Applications of Probabilistic Safety Assessment (PSA) for Nuclear Power Plants, IAEA, Vienna, 2001.

[2] U.S. NUCLEAR REGULATORY COMMISSION, An approach for plant-specific, risk-informed decision-making: technical specifications, Regulatory guide, 2011.

[3] INTERNATIONAL ATOMIC ENERGY AGENCY, Safety Assessment for Facilities and Activities, IAEA Safety Standards Series No. GSR Part 4 (Rev. 1), IAEA, Vienna, 2016.

[4] 202-2009-00/1 “Technical Report. Guidelines for Integrated (Risk-Informed) Safety Classification”, NRSI NUBIKI, 2020.

[5] RiskSpectrum Analysis Tools. Theory Manual. Lloyd's Register Consulting7 – Energy AB, Version 3.2.5.

Proceedings of the European Nuclear Young Generation Forum
ENYGF'21
September 27-30, 2021, Tarragona, Spain

The stress test aproach for safety assessment

Korolev Viktor

[1] JSC Atomenergoproekt, Russian Federation

*Corresponding author: *viktor.korolev.a@gmail.com*

I. INTRODUCTION

On March 11th 2011, a magnitude 9.0 earthquake struck some 80 km off Japan's Tohoku coast. The ensuing tsunami and the subsequent accident at the Fukushima Dai-ichi Nuclear Power Plant (NPP) triggered the core melt of three reactors at the site. It was the worst emergency at a nuclear power plant since the Chernobyl disaster in 1986.

The analysis of the Fukushima accident revealed quite substantial, well-known and recurring technical issues: natural phenomena of a critical nature not being considered, faulty design, insufficient backup systems, failure to introduce safety improvements to operating reactors, human error, inadequate contingency plans, confusion in the response to a severe accident and poor communications. These points are clearly described in the International Atomic Energy Agency (IAEA) comprehensive report on Fukushima published in September 2015.

Against the background of Fukushima and based upon a mandate given by the European Council at its meeting on 24-25/03/2011, the European Commission (EC) – together with the European Nuclear Safety Regulators Group (ENSREG) – launched in 2011 EU-wide comprehensive risk and safety re-assessments of all EU NPPs (hereinafter referred to as "stress tests") [1].

The European Council invited the EC and ENSREG to develop the scope and modalities for the stress tests with the support of the Western European Nuclear Regulators' Association (WENRA). WENRA drafted the preliminary stress tests specifications. Consensus on these specifications, the so-called "EU-STs specifications"

The EU-stress tests specifications, which were the basis of the safety track of the stress tests, defined three main areas (topics) to be assessed: extreme natural events (earthquake, flooding, extreme weather conditions), response of the plants to prolonged loss of electric power and/or loss of the ultimate heat sink (irrespective of the initiating cause) and severe accident management.

The assessments were organised in three phases:

- Self-assessments by nuclear licensees. Licensees were asked to submit stress tests reports covering all their Nuclear Power Plants to the national regulators
- National review of the self-assessments. The National regulator reviewed the ST reports supplied by the licensees and prepared a National Report;
- European Peer Review of National Reports.

A considerable effort was made, in terms of human resources, to analyse the safety of all NPPs and spent fuel storage facilities of all 17 countries in a short time. In each of the 17 countries the review team conducted a NPP visit. The total number of reactor units on the sites visited during the originally scheduled visits in March 2012 was 43 (approximately 30% of all the units in operation). The plant visits confirmed the details of the prior analyses and in some cases have led to additional recommendations. [1]

Additional visits were performed to eight reactor sites by the peer review teams in September 2012, in order to gain additional insight on different reactor types, to discuss implementation of the identified improvements and in order to alleviate concerns relating to installations in areas bordering other Member States. Thus, all operating reactor types in Europe have been visited by peer reviewers.

While the Stress Tests confirmed the high standards of nuclear safety in the EU, the reports also identified a number of improvements that could enhance safety. To ensure an appropriate follow-up, Member States developed National Actions Plans for the implementation of the identified recommendations.

In its meeting on 24-25 March 2011, the European Council mandated that the outcome of the Stress Tests and the information on any subsequent selected safety improvement measures should be provided to the public. Therefore, from the very beginning full transparency was a key issue of the EU-stress tests and its follow-up activities. The ability to become involved, by raising questions on the National Reports and later the National Action Plans and to have public access to all reports of the reviews conducted, illustrates the extent of transparency achieved. [7]

The stress tests highlighted best practices as well as shortcomings in Member States. These are detailed in the Staff Working Document. The following key issues have emerged from the stress tests and from other reports on the Fukushima investigations:

• There is a lack of consistency with respect to assessing and managing external hazards to plant safety. For example, the International Atomic Energy Agency guidance for seismic loads or the guidelines for flooding are not implemented by all Member States

• The scope and depth of the Probabilistic Safety Assessment (PSA) used to characterise the safety of nuclear reactors differ significantly and in some Member States there is an urgent need to bring them up to accepted international standards.

• Severe Accident Management Guidelines covering all types of situations have to be available in all NPPs. The stress tests have shown that Severe Accident Management Guidelines need to be updated and fully implemented as soon as possible in a number of Member States.

• Improvements in safety culture are needed. There are gaps in ensuring comprehensive and transparent identification and management of key safety issues. A glaring lesson from Fukushima is that the tsunami hazard was underestimated, mostly due to human, systemic and organisational factors.

Findings on the legal framework for safety and its implementation A number of weaknesses in the existing nuclear safety framework at the European and the Member States level have been identified.

• The key finding relates to continuing differences between Member States resulting in the absence of a consistent approach to nuclear safety regulation. There are no codified EU mechanisms to agree on technical standards and ways to conduct safety reviews. The Nuclear Safety Directive does not have any provisions to this end.

• The provisions covering the independence of the national regulatory authorities and the means to ensure their effectiveness are minimal and not necessarily sufficient for preventing situations where the regulatory responsibility is split between several entities or is included directly in Ministries (Economy, Environment, etc.). Moreover, the existing catalogue of regulatory competencies is not sufficiently explicit.

• Transparency is essential in ensuring that the best possible safety practices are used, as shown by the stress tests. However, the Nuclear Safety Directive contains only generic requirements on public information.

• The monitoring and verification mechanisms at EU level are limited to the peer review of the national nuclear safety framework.

All participating countries have begun to take operational steps to improve the safety of their plants. These measures include additional mobile equipment to prevent or mitigate severe accidents, the installation of hardened fixed equipment, and the improvement of severe accident management, together with appropriate staff training measures.

Regarding safety, the ENSREG peer review Board report identified four main areas for further improvement across Europe:

• European guidance should be developed on the assessment of natural hazards, including earthquake, flooding and extreme weather conditions, and safety margins, in order to increase consistency between Member States. The Western European Nuclear Regulators' Association, involving the best available expertise from Europe would be well placed to carry out this task.

• Periodic Safety Review of each NPP should be carried out at least every 10 years, to maintain and improve the safety and robustness of plants and revaluate the natural hazards to which plants may be subject to.

• Recognised measures to protect containment integrity as the last barrier to protect people and the environment against radioactive releases must be implemented.

• Accidents resulting from natural hazards should be prevented and/or mitigated so as to limit their consequences. Measures to be considered include bunkered equipment to prevent and manage a severe accident, mobile equipment protected against extreme natural hazards, emergency response centres protected against extreme natural hazards and contamination, rescue teams and equipment rapidly available to support local operators in long duration events. [1, 6, 7]

II. LESSONS OF FUKUSHIMA

This section describes several lessons learned from an analysis of events during the accident at the Fukushima Daiichi Nuclear Power Station.

Lesson 1: Relocation of switchboards and other important equipment to better sites, utilize portable equipment, and ensure access. Waterproofing important equipment and installing it at as elevated a location as possible is an effective countermeasure against tsunamis or floodings.

Lesson 2: Configuration and deployment of isolation valves.

It was reported that isolation valves could not be opened during the accident. While keeping isolation as the top priority, provide ways of opening the most important isolation valves remotely or manually (by locating isolation valves outside the containment vessel and providing backups including for electric power and pneumatics).

Lesson 3: Provision of backup DC power supply for important equipment.

Determining the status of plant was made difficult by the loss of instrumentation functions due to the lack of a DC power supply, there was insufficient time to line up the low-pressure water injection system due to the loss of high-pressure functions [isolation condenser and high-pressure coolant injection system] that require a DC power supply, and reducing pressure via the safety relief valves was delayed. Accordingly, provide portable or backup DC power supplies for this important equipment.

Lesson 4: Instrument reliability and credibility, and measures for dealing with this situation.

For those plant monitoring items that are critical to accident management, review the environmental conditions for instruments (considering the harsh conditions that occur during an accident), provide alternative means for verifying the credibility of instrument readings, and provide measures for dealing with the situation when the plant status cannot be monitored due to lack of faith in these readings.

Lesson 5: Provision of wider range of water injection and cooling systems.

There is a need for greater diversity in the ways of dealing with a loss of functionality in excess of the design assumptions (including the provision of a long-term water source), including with regard to the response and assistance from off-plant. In addition to providing greater protection through measures such as improving the water tightness of key on-site equipment and building layout, there is a need

to ensure the flexibility to deal with a wide range of scenarios though greater diversity, including portable equipment.

Lesson 6: Provision of alternative means for protecting containment vessel.

It is possible that the interior of the containment vessel overheated due to insufficient core cooling, causing degradation of non-metallic components and the potential release of radioactive material. Accordingly, while keeping core cooling as the top priority, there is a need to protect the containment vessel by cooling it on the inside and by providing cooling from outside the containment vessel. [4, 6]

III. STRESS TESTS OF BELARUSIAN NPP

Belarus voluntarily conducted stress tests of the Belarusian NPP in 2016-2018 according to the EU methodology. The General Contractor of the NPP, JSC Atomenergoproekt, takes an active part in the development and peer-review of stress tests. In this paper, the stress-tests and their outputs of the Belarusian NPP were considered. Taking into account that the Belarusian NPP belongs to the generation 3+, has passive core cooling system and four-channel safety systems, according to the results of stress-tests, there are still ways to improve the safety.

The design of the Belarusian NPP from type AES 2006 V-491 is the result of an evolutionary development process of the Russian VVER (Vodo - Vodyanoi Energetichesky Reaktor) type Pressurized Water Reactor (PWR) family. The operating experience within the VVER-type plants amounts to about 1300 reactor-years, among them a great number of plants from the VVER-440 power plants in Russia and eastern Europe as well as the VVER-1000s operating in the Czech Republic, Bulgaria, China, India, Russia and Ukraine.

For the preparation for the Belarusian NPP stress tests, the Ministry of Emergency Situations of the Republic of Belarus has established their regulatory framework.

To improve the stress tests regulatory requirements taking into consideration international recommendations in 2017, norms and regulations on nuclear and radiation safety “Requirements to stress tests (objective safety reassessment) of a nuclear power plant” approved by the Resolution of the Ministry of emergency situations of the Republic of Belarus were adopted. This document was developed with the support of the European Union International Technical Assistance Project.

Under the guidance of the above technical regulatory legal acts, the operating organization (Belarusian NPP State Enterprise) performed stress tests and prepared a relevant report.

The safety systems of the Belarusian NPP are designed with comprehensive consideration of the external, and the buildings, structures and equipment of the Belarusian NPP are designed with account for the design impacts specified in the report in accordance with the current regulatory framework.

The buildings and structures have a significant safety margin in relation to the design seismic impact. Threshold effects for the buildings and structures do not occur at seismic impacts.

There are no radiation consequences of design basis earthquake and safe shutdown earthquake, and no additional improving measures are required. The assessment of the load-bearing capacity reserves available in the building structures (security of strength characteristics, reserves due to elastoplastic behavior of the structures, etc.) showed that for the structures of seismic category I the reserve relative to the safe shutdown earthquake level adopted in the design is not less than 4.9 times (0.62 g), for the inner containment – not less than 4.3 times (0.51 g).

The threshold value of the accelerations specified above for the structures of seismic category I is determined with a sufficient degree of conservatism. If the conservatism is not considered, the threshold level can be further increased. The structures are made of cast-in-situreinforced concrete, which excludes the brittle instantaneous failure (cliff-edge effect) in case of increased seismic impact.

The strength threshold value for the equipment and pipelines under seismic impact is the safe shutdown earthquake level of 7 points adopted in the Belarusian NPP design with an acceleration of 0.12 g.

Taking into account the adopted safety margin for the equipment and pipelines, the maximum permissible acceleration is 0.12x1.07 = 0.13g. With a further increase of stresses, areas of significant plastic deformation can be expected in the equipment and pipelines. The NPP site is not exposed to flooding caused by the surrounding rivers and water basins, as the grading elevation of the site (179.3 m BES) is 51.5 m higher than the water rise level with 0.01% probability. This scenario takes into account breakthrough of dams, the highest levels of seasonal floods and rainfall floods, ice blocking, wind surges and other dangerous factors.

Upstream water drainage systems (stratum drainage, storm water sewerage and catch drain) are designed with account for extreme precipitation.

The maximum values of extreme climatic conditions determined for the site are much lower than those used in the design.

In order to avoid fuel damage in the reactor in an accident involving the loss of all AC power supplies at the NPP during the power operation of the reactor plant, it is required to take measures to restore and maintain the water reserve in the emergency heat removal tanks not later than within 72 hours from the beginning of the accident (provided that the water reserves of the four emergency heat removal tanks are used) in order to ensure the operation of the Passive Heat Removal System.

In order to avoid fuel damage in the spent fuel tank in case of an accident with loss of all AC power supplies at the NPP during the power operation of the reactor plant, it is required to supply water to the spent fuel tank at a rate of not less than 7 kg/sec within not more than 41 hours.

The stress-tests confirm the NPP safety at the initiating events related to the loss of power supply and the loss of the ultimate heat sink, including the combination of the initiating events which occurred at the Fukushima-1 NPP. Efficiency of the measures to limit emergency releases was confirmed within the framework of implementation of Probabilistic Safety Analysis-2 (based on the results of full-scale Probabilistic Safety Analysis-1), where the probability of large radiation releases leading to global contamination of the area around the NPP set as the target criteria is not more than 10-7 (reactor/year).

The stress-test report of the Belarusian NPP also presents the implementation of FLEX approach. That approach is to develop flexible and diverse strategies for increased defence-in-depth for extended loss of AC power with a loss of normal access to the ultimate heat sink, which occurs simultaneously at both units on the site. By providing multiple, diverse methods to supply power and water to support key safety functions, FLEX is intended to mitigate the consequences of a Beyond Design Basis Earthquake [9].

For the accident management at the Belarusian NPP Emergency Operation Procedure, Beyond Design Basis Accident Management Guidelines and Severe Accident Management Guidelines (symptomoriented) are developed and introduced. These manuals include the procedure and criteria of transfer from one manual to the other, as well as scopes of their application and mutual links.

As additional technical means to manage accidents involving loss of power supply exceeding the design requirements (more than 72 hours from the beginning of the accident with the loss of all power supplies), the design provides for a make-up system for the Steam Generator Passive Heat Removal System water tanks and spent fuel pool. Making-up of the Passive Heat Removal System tanks and spent fuel pool is provided by low-power highpressure pump JNB50AP001 of the make-up system for the emergency heat removal tanks. This pump unit is located in the steam chamber and connected to the tanks of the LCU system and to the sump tanks of the containment. The pump is powered from the Beyond Design Basis Accident power supply channel (from the connected mobile Diesel Generator set of power supply channel 7). The Beyond Design Basis Accident power supply channel is designed for 24 hours of independent operation and allows for connection of a mobile Diesel Generator set for recharging the batteries and further operation of the system. In accordance with the recommendations resulting from development of the Stress Test Report (target reassessment of safety) for Belarusian NPP, two mobile Diesel Generator sets (one per NPP Unit) with a power of 500 kW will be provided, which presumably will be located outdoors at the NPP site.

In addition, the spent fuel pool makeup can be implemented by connecting non-routine emergency resources (a fire engine with a pump set with a capacity of 40 l/s and a head of 100 m) to the two process connectors of the JNB50 system. [8]

On January 2017, an IAEA mission for the safety assessment of the Belarusian NPP(SEED-mission) was held in the Republic of Belarus. In the course of the mission, both natural and man-caused external impacts were analyzed and characterized, the design parameters of the construction site were studied, the site and the environment were monitored and the lessons learned at the Fukushima NPP accident were taken into account.

Based on the results of the mission, IAEA experts noted that the NPP design parameters take into account external threats typical for the site such as earthquakes, floods and extreme weather conditions, as well as man-caused events. International experts noted that the threat monitoring programs to be implemented throughout the life cycle of the Belarusian NPP are sufficient and properly provided in the NPP design. It was also noted that the Belarusian side took additional measures related to external events in view of the lessons of the Fukushima NPP accident.

The peer review of the stress-tests report was completed in 2018.

The Peer Review Team identified seven high priority issues which were considered both important for safety and implementable in the short term.

- For natural hazards, the high priority issue was related to the evaluation of the adequacy of design basis earthquake and verifying that this design basis earthquake and the underlying Probabilistic Seismic Hazard Assessments are used as basis for evaluating seismic margins to cope with the seismic design extension conditions. Based on the available information this high priority issue has been adequately addressed provided that the National regulator GAN endorses an updated design basis earthquake based on the review and assessment of the available Probabilistic Seismic Hazard Assessments.

- For loss of safety systems, there were two high priority issues. The first related to enhancing the water supply to the passive heat-removal systems with additional redundant pumping capability. The second related to enhancing the reliability the of power supply of mobile diesel generator by establishing a permanent connection to the Channel 7 busbar. Based on the available information both high priority issues have been adequately addressed provided that the availability of the mobile equipment can be ensured in all conditions.

- For severe accident management there were four high priority issues. The first was related to the development, validation and implementation of symptom-based Emergency Operation Procedures and Severe Accident Management Guidelines. The second was related to the reliability of depressurisation of the primary system to prevent high- pressure core melt scenarios. The third priority issue was related to potential improvements to the habitability of main and emergency control rooms to ensure operators can work in the control rooms during a severe accident combined with a station blackout. The fourth was related to capabilities to prevent and mitigate severe accidents under open reactor conditions.

In addition to the evaluation of the implementation of recommendations related to the seven high priority issues, the Peer Review Team evaluated the comprehensiveness of the Belarusian Action Plan against Peer Review Team recommendations and other sources of relevant information.

Based on the available information, it can be concluded, that the Action Plan has addressed all PRT recommendations related to the high priority issues.

As a result of the evaluation of the stress tests of the Belarusian NPP, special advantages were also identified that exceed the post-Fukushima requirements of the IAEA, which it makes sense to take into account at European nuclear power plants. Such as:

Particular strengths of the Belarusian NPP include a passive residual heat removal system through the steam generators and passive system for heat removal from the containment atmosphere. Both systems are capable to operate passively and automatically even during station black-out conditions at least for 24 hours in the stand-alone mode. In addition, there is a core catcher capable of capture, cool down and stabilize the molten corium preventing a direct challenge to the containment boundary.

The training centre is equipped with the full scope simulator with rather unique capabilities to also simulate severe accidents, thus providing additional features for effective staff training.

The design of the main components allows a “smooth” behaviour in case of transients, especially the steam generators (greater water inventory in the horizontal steam generators compared with Western style reactor designs).

Well-developed countrywide radiation monitoring system represents an important element for effective overall emergency response. [2, 3, 8]

IV. CONCLUSIONS

The ongoing nuclear stress tests are unprecedented in terms of scale and cooperation among the countries involved. The European Commission, together with the European Nuclear Safety Oversight Group, is currently closely monitoring the implementation of the national nuclear safety action plans of the EU Member States and neighbouring States. The European stress test criteria are used internationally by some countries as the basis or benchmark for nuclear power plant safety assessments.

Since 2013, stress tests have been conducted in EU countries on a regular basis, as an ongoing process to improve nuclear safety at nuclear power plants, in close cooperation with national regulatory authorities, together with ENSREG, WENRA and the IAEA.

After analyzing the 2011-2012 stress tests. Euratom has taken initiatives to improve the international legal framework of the IAEA on nuclear safety of nuclear power plants. In 2014, Euratom took into account all the conclusions, recommendations and assessments that were made at the end of the 2011-2012 stress tests and revised the European law on nuclear safety of nuclear power plants, developing a unified European approach to the problem of nuclear safety of nuclear power plants, including issues of responsibility, emergency preparedness and response.

The stress tests and related activities are a major achievement for the EU and the regulatory authorities in the Member States and have led to tangible results:

• Significant and tangible plant improvements have been identified in all participating countries, and are being implemented or planned.

• Weaknesses in frameworks and procedures, as well as gaps in the legal arrangements, have been identified and proposals to improve these are on the drawing board.

• First bridges have been built between authorities dealing with safety and those dealing with security. Improving the dialogue between them on topics that reside at the safety/security interface is essential to respond to citizens' concerns.

In the context of the sustainable development of nuclear power, stress tests provide opportunities for the exchange of best practices for improving the safety and resilience of nuclear power plants to beyond-design accidents, and the principles of transparency and public access to the results of stress tests allow a wide range of stakeholders to participate in the safety assessment, which increases confidence in the nuclear industry [1, 5, 7].

V. References

[1] European Commission, “Communication from the commission to the council and The European Parliament on the comprehensive risk and safety assessments ("stress tests") of nuclear power plants in the European Union and related activities”, Brussels, 4.10.2012

[2] The European Nuclear Safety Regulators Group, “EU Peer Review Report Implementation of Belarusian Stress Test National Action Plan,” HLG_p(2021-42), 2021.

[3] The European Nuclear Safety Regulators Group, “EU Peer Review Report of the Belarus Stress Tests”, HLG_p. (2018-36), 2018.

[4] Masayoshi Matsuura, Kohei Hisamochi, Shinichiro Sato, Kumiaki Moriya, “Lessons Learned from Fukushima Daiichi Nuclear Power Station Accident and Consequent Safety Improvements,” Hitachi Review Vol. 62, No. 1, 2013.

[5] The European Nuclear Safety Regulators Group, “Compilation of recommendations and suggestions,” HLG_p(2012-20)_101, 2012.

[6] International Atomic Energy Agency, The Fukushima Daiichi Accident “Technical Volume 2/5 Safety Assessment,” IAEA, 2015.

[7] The European Nuclear Safety Regulators Group, “Summary report. ENSREG national action plans workshop”, ENSREG, 2012.

[8] National Report of the republic of Belarus on the Belarusian NPP objective safety reassessment (stress tests), Gosatomnadzor, Minsk, 2017.

[9] “Developing the FLEX plan“, Mike Powell, Jeff Taylor, Susan Baier, 2013.

Proceedings of the European Nuclear Young Generation Forum
ENYGF'21
September 27-30, 2021, Tarragona, Spain

Numerical modelling of thermo-kinetic processes in the trap of corium melt during severe accidents at NPPs

Anatoliy Kovalenko[1], Artem Koptuykhov[2], Dmitriy Mescheryakov[3] and Alexey Schuklinov[4*]

[1] Ioffe Physical-Technical Institute, Russian Federation; [2] Petersburg Nuclear Physics Institute named B.P. Konstantinov of National Research Centre "Kurchatov Institute", Russian Federation; [3] Peter the Great Saint-Petersburg Polytechnic University, Russian Federation, [4] JSC ATOMPROEKT, Russian Federation

*Corresponding author: *mupol@mail.ru*

I. INTRODUCTION

The open literature on the progression of hypothetical ssevere accidents at NPPs indicate its connection with a critical disruption of heat removal from the reactor core, causing overheating and melting of its elements. Additional restraining concept of ex-vessel devices for localization of molten accident products has been developed to restrain the spread of the formed radioactive melt into the environment if reactor vessel is disrupted. Its technical implementation for powerful WWER-type Russian reactors is based on the use of an under-reactor cooling trap – a crucible-type heat exchanger [1] filled with a sacrificial material (SM) contributing to withholding of controlled corium thermal and phase state until fully crystallized. SM consisting of a mixture of light iron oxides Fe_2O_3 and aluminum Al_2O_3

The general approach, the physico-mathematical formulation of the problem, as well as computing software (COMSOL) can be applied to similar devices for melt localization (not only for crucible-type melt localization devices for NPP with VVER).

This solution is based on the physicochemical interaction effects between SM and corium melt, which were detailed in Proceedings of the previous conference [2] for selected structural element of SM at the initial state of the melt entering the trap. This article carries out the general synergistic effect on the subsequent stages of processes in the melt localization device, taking into account the design features of the placement of the liquid metal elements in the corium melt pool, as well as heat transfer to the cooling water from the outer side of the reactor vessel.

The performed numerical studies are based on the generalized formulation of the Stefan problem [3], embodied in the developed shock-capturing computer system using COMSOL Multiphysics [4]. This approach enables automation of the conditions for pairing the thermal, hydrodynamic and chemical components of the model, unitizing the discretization of computational domains and their nodalization schemes [5].

II.PROBLEM DEFINITION AND SOLUTION METHODS

A. General model description

Modelling of thermo-kinetic processes of thermal and phase interactions in a cooled ex-vessel device for localizing a corium melt is based on the generalized formulation of the Stefan problem with free phase boundaries:

$$C_{eff}\,\rho\left(\frac{\partial T}{\partial \tau} + v\ grad\,T\right) = div\,(\lambda\ grad\,T) + f, \qquad (1)$$

where ρ – density of the material medium component; T – temperature; τ – time; v – local velocity of the medium; λ – coefficient of thermal transmittance; f – the power of internal heat sources; C_{eff} – the effective specific heat capacity of the medium the heat of the phase transition at its moving boundary in a concentrated form.

Heat conductivity metering during natural convection in a melt is based on the Reynolds-averaged unsteady Navier-Stokes equations and the standard (low Reynolds k-ε) turbulence model.

This model supplemented damping functions give a very accurate description of the boundary layer. The sharp gradients close to walls do, however, require very highly anisotropic meshes. These elements are needed because of the boundary layers that typically form at no-slip walls. The equations are solved along with the continuity equation:

$$\nabla \cdot(\rho\, v) = 0, \qquad (2)$$

Three-stage processes are considered, reflecting the sequence of physicochemical interactions in a multicomponent system of variable composition, including

- the "pre-inverse" front-end stage of gravitational stratification of the lighter metal and heavier oxide component of the corium melt with a decrease in its temperature due to heat consumption for heating and sacrificial material melting;

- the stage of "inversion" of the corium melt oxide and metal components with the transition of molten oxides to the upper part of the basin, and molten metals to the lower due to the changes in their densities ratio;

- the “post-inverse” stage of subsequent cooling and crystallization of the corium melt, considering its natural convection, external vessel cooling of the melt localization device vessel and heat transmission by radiation above the bath surface.

The general model takes into account the residual radioactive heat release from the corium, the heat effects of the sacrificial material melting and the chemical reactions of the oxides repair during the oxidation of under-oxidized melt elements, heat transmission by natural convection in the melt, heat transfer to the cooling water through the walls of the vessel, and thermal radiation in the interior space.

Phase diagrams emulate the phase states of the envisaged system under its composition change in chemical reactions of the sacrificial material’s oxide components with melt metal components.

B. Model numerical implementation

Fig. 1 shows a three-dimensional model of a melt localization device filled with sacrificial material. The generated grids of the computational 3D domains for the problems under consideration are shown in Fig. 2. Discretization was carried out using an anisotropic grid, the step of which decreased at the boundaries of the contact between the sacrificial material and the corium melt. Boundary layer resolution was carried out using an anisotropic grid, the step of which decreased at the boundaries of the computational domain.

a b

Figure 1. The arrangement of the structural elements of the sacrificial material along the tiers (a) in their common basket (b) of the corium localization device

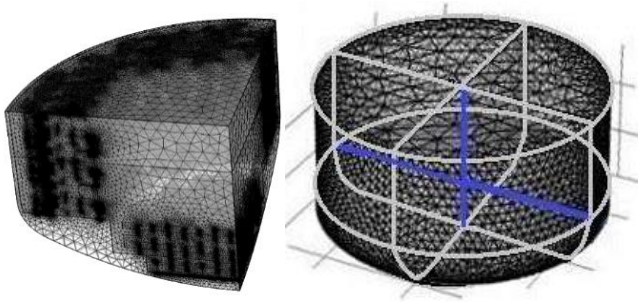

a b

Figure 2. Generated finite element grids for the basket filled with a sacrificial material (a) and for the vessel of the corium localization device (b).

III. SURVEY RESULTS

Calculation data for the “pre-inverse” stage on the presented model are shown in Fig. 3.

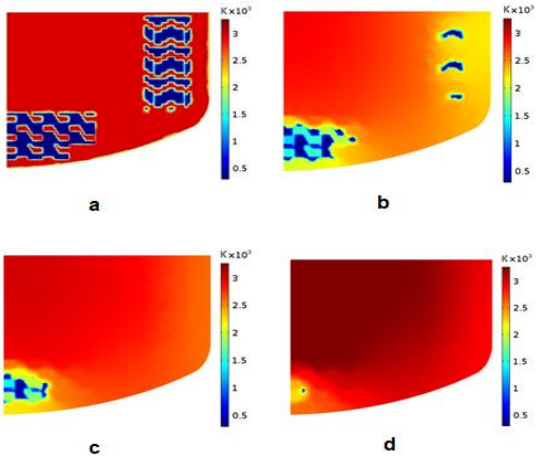

Figure 3. Temperature fields along the central section of the melt bath in its localization device at the “pre-inverse” stage at different times: a-1, b- 20, c- 40 minutes, d- at the end of the “pre-inverse” stage.

As can be seen, the initial period of the “pre-inverse” stage is accompanied by a decrease in the corium temperature due to the heat consumption for sacrificial material heating and melting, despite the residual heat release. Gravity separation of the heavier oxide component of the melt in the lower part of the basin and the lighter metal component in its upper part is observed. Chemical interaction with the sacrificial material leads to a noticeable decrease in the density of the initially heavier oxide components of the melt in comparison with the metallic ones. This causes the transition to the next stage of their "gravitational inversion" with a simultaneously increased melt temperature under the action of the residual energy release of radioactive elements.

The results of numerical simulation of the melt temperature fields at the stage of gravitational inversion of its oxide and metal components are shown in Fig.4. After their inversion, a lighter hot oxide layer is located in the upper part of the melt pool, and a heavier metal layer in the lower part.

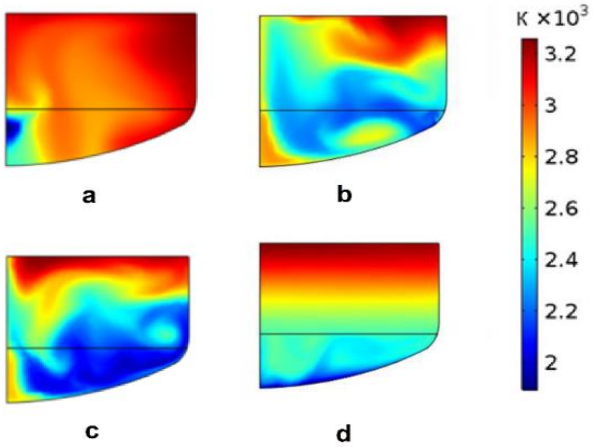

Figure 4. Temperature fields of the melt bath at different moments of the “inverse” stage: a-10, b- 30, c- 40, d- 90 seconds.

The calculations results of the melt temperature fields for the “post-inverse” stage are shown in Fig. 5 and 6.

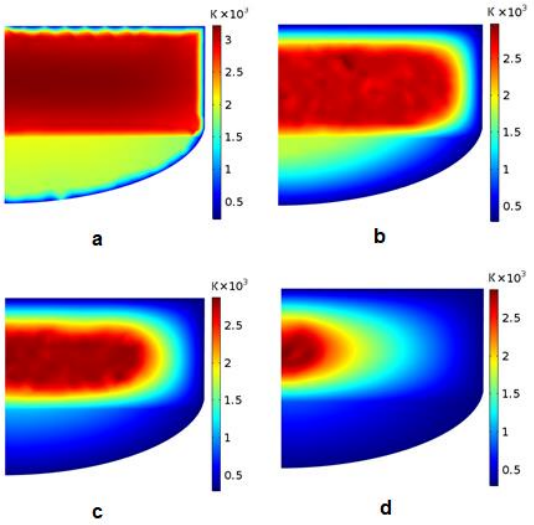

Figure 5. Temperature fields along the central section of the melt bath in the device for its localization at different times of the "post-inverse" stage: a-10 h, b- 50 h, c- 100 h, d- 210 h.

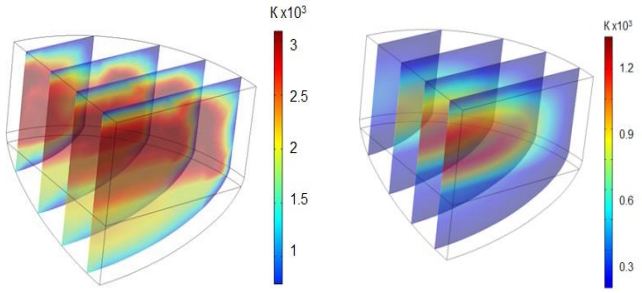

Figure 6. Temperature fields in the characteristic sections of the corium localization device according to the 3D model at the beginning (a) and the end (b) of the "post-inverse" stage.

The spatial 3D model considers crust formation, which prevents heat and mass transfer both on the surface of the corium melt and between its immiscible oxide and metal components.

During the study, a significantly uneven distribution of heat fluxes on the inner side of the vessel walls of the corium localization device was noted, especially in the first hours of the arrival of the high-temperature corium melt with the initial temperature significantly higher than the melting point of the wall metal (Fig. 7).

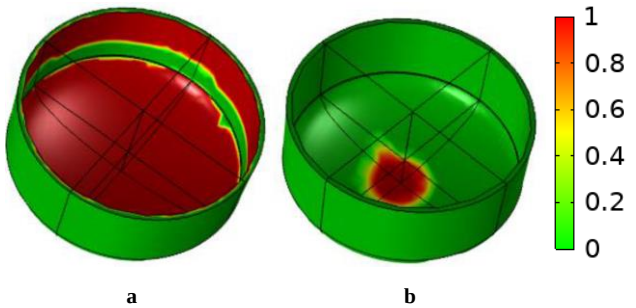

Figure 7. The melting nature of the vessel of the melt localization device at the beginning of its filling with corium (a) and after 40 minutes (b). 0 - solid phase, 1 - liquid phase.

Melting starts 1 hour after the accident. The case heats up unevenly. therefore the melting process initially covers the bottom and top of the wall. Number the melting metal decreases with decreasing heat release. 49 minutes after heating walls, the maximum temperature of the body is less than the melting temperature T = 1688 K the body melting process stops completely.

The melt localization device allows the corium melt to be retained until the melt crystallizes. Melting 1.5-2 mm (2% from wall thickness) is not a significant factor for reducing the device's performance.

According to the results of model calculations, during the first hour after this, there is a partial melting of the vessel walls from the inner side with a depth of up to 1.5 - 2 mm in the bottom area of the trap and in the area of the shell at the boundary of its filling with the incoming melt, which stops after lowering its temperature.

IV.FINDINGS AND CONCLUSIONS

Based on the generalized formulation of the Stefan problem with free phase boundaries, a model for calculating the thermo-kinetic processes of the three-stage interaction of the sacrificial material and the corium melt in the under-reactor device for its localization in severe accidents at NPPs has been developed. The model is implemented in the created end-to-end computing complex using the COMSOL Multiphysics package. It includes the influence of the design features of the sacrificial material placement in the corium localization device, the conditions of residual heat generation and turbulent heat and mass transfer in the melt, as well as heat removal to the cooling water from the outer side of the vessel. The numerical survey results of these processes are presented, including the stage of the sacrificial material melting with chemical reactions of its oxides repair during the oxidation of under-oxidized melt elements, the stage of gravitational inversion of the initial stratification of the oxide and metal components, as well as the stage of melt cooling and crystallization.

The results obtained generally indicate the efficiency of the melt localization device in maintaining the corium melt in a controlled thermal and phase state until complete crystallization, as well as the need to intensify the external water cooling of the trap vessel in the first hours of the high-temperature corium melt entering there.

IV. ACKNOWLEDGMENT

The reported study was funded by RFBR, project number 19-08-01181 A.

V. References

[1] Pat. No. 2514419, Russian Federation, MPK G21C 9/016; SPb., OAO «Golovnoy Institut "VNIPIET"», publ. 27.04.2014, Bull. No. 23 (II Ch.). 11 p.

[2] V.G. Golovacheva, A.N. Kovalenko, A.O. Koptyukhov, D.K. Meshcheryakov, A.P. Schuklinov. "Correlation between Heat-Mass Transfer, Chemical Reactions and Phase Transformations in Corium Melt Localization Devices during Severe Nuclear Power Plant Accidents". Sydney, Australia, International Youth Nuclear Congress, 2020.

[3] A.A. Samarskiy, P.N. Vabishevich, "Computational heat transfer". Moscov, Editorial URSS, 2003.

[4] COMSOL Multiphysics, Software products, Burlington, MA. https://www.comsol.ru/products

[5] A.N. Kovalenko, A.O. Koptyukhov, D.K. Meshcheryakov, A.P. Schuklinov. “Thermo-kinetic processes in the corium traps of high-temperature melt during the reactor accidents at an a-plant: simulation”. St.Petersburg Polytechnical State University Journal. Physics and Mathematics, 2020, v. 13, No 4, pages 46-58.

Proceedings of the European Nuclear Young Generation Forum
ENYGF'21
September 27-30, 2021, Tarragona, Spain

ASVAD
A new safety element to keep Nitrogen-Free Reactors

Arnaldo Laborda* Senior Engineer, ASVAD Inventor & CEO

[1] ASVAD INTL SL Tarragona (Spain)

*Corresponding author: alaborda@asvad-nuclear.com / www.asvad-nuclear.com

I. INTRODUCTION

There is a serious complication which has high probability of occurrence during a Station Blackout (SBO) or a Loss of Coolant Accident (LOCA). This complication is the nitrogen inflow to RCS from the accumulators.

This nitrogen inside the system can seriously disturb the core cooling stopping the natural circulation in the Steam Generators (SG's) besides other complications.

The current strategies to avoid this injection are based on active elements and the organization effort:

- Closing the accumulator output isolation valve.
- Opening the accumulator relief valve.
- Maintaining the RCS pressure over the nitrogen residual pressure.

The ASVAD valve [21] is an innovative safety valve that can avoid this problem in an easy way. This valve is a **passive** and **automatic** element which can precisely detect the correct moment to act seeing the residual pressure in the accumulator. Only when the accumulator gets empty, the valve opens and vents the nitrogen to the containment. This way the nitrogen never will reach the RCS pipes.

The ASVAD Valve provides these main advantages:

- It is a passive device and does not require any external energy to actuate.
- It is fully automatic and does not need any operator assistance.
- It actuates at the required moment; just when the accumulator is nearly depleted.
- It is available all the time, protecting the RCS from nitrogen.
- Allows to depressurize the RCS to lower pressures thus diminishing the leakage rate and facilitating the recovery.

II. THE NITROGEN THREAT

Nitrogen is a gas broadly used in the PWR pressurized accumulators, make-up tanks or similar equipment systems. It allows the passive water injection to the RCS when a LOCA depressurizes the system. But when its function is done, it has to be isolated to avoid from entering into the RCS pipes. If this isolation is not done on time, this gas can seriously threat the core cooling and the fuel integrity.

Once the nitrogen reaches the RCS, this nitrogen unleashes some complications (see refs [3] to [20]):

- The natural circulation **diminishes or even stops** in the SG's, and the **heat transfer is seriously diminished** by the nitrogen presence.
- The RCS pressure **rises -and remains high-** due the nitrogen heating. This will hinder or even impede the low pressure pumps to inject to RCS.
- This nitrogen even can reach the Residual Heat Removal (RHR) pumps making them inoperable.
- If the temperature raises enough, this nitrogen **will accelerate the fuel cladding oxidation** [8].

In the event of an SBO accident, nearly all the plant equipment is lost. In these circumstances only the passive elements work. The principal way to maintain the core cooling is across the SG's by "natural circulation".

Unfortunately this SBO accident triggers other serious accident: The LOCA accident. As this leak is permanent, sooner or later the water in these accumulators ends, and at this moment, the nitrogen threat starts. If the RCS pressure can't be maintained over the nitrogen pressure, this nitrogen start to get into the RCS pipes and soon reach the core and will disseminate across the system reaching the SG's making them useless to cool the RCS.

Why this nitrogen injection has **high probabilities to happen?** :

- Because the LOCA is permanent and the RCS pressure will drop constantly (unless operator actions could stop this drop during some time).
- This nitrogen is already inside the system (and there are big quantities!).
- It has an open & direct path to the reactor.
- During all the time is trying to get into the RCS. It just needs a low pressure moment in the RCS.

- The unique element able to stop it -the accumulator isolation valve- is an active element and needs energy to be closed.

So it's just a question of time to have the nitrogen inside the RCS and disturbing the core cooling. There are not just assumptions or opinions; there were some noticeable events in the past related to nitrogen intrusion in the pipes [7].

III. CURRENT STRATEGIES.

To prevent this nitrogen from reaching the RCS pipes, only three strategies may be taken [1], [2]:

1. Closing (on time) the accumulator output isolation valve.
2. Venting (on time) the residual nitrogen to the containment building.
3. Maintaining the RCS pressure over the nitrogen pressure.

All these strategies have common drawbacks or weakness during an SBO accident:

It needs the deployment and the proper actuation of some active elements as the FLEX AC generators, FLEX pumps or compressors, the isolation or venting valves, and all its support systems. As all these elements are active elements, so they need energy to work.

It also needs the operators work. All these elements are not automatic. They have to be deployed and operated by the recovering operators. So they need not only the organization efforts, but also good procedures and a trained team to develop the recovery strategies.

These strategies have other important drawback: TIME. It's not easy to know WHEN the isolation has to be done. If done too soon, it will be some water wasted in the accumulator. If done too late, it will be the nitrogen injection. And these strategies have to be done simultaneously for ALL the accumulators, as they work in parallel. So these strategies are TIME CRITICAL.

All these strategies rely on a long chain of active components (operators included). If something fails in this chain, it will be the nitrogen injection. A good example is the isolation valves: Even closed, they will leak nitrogen during all the recovery as they are not gas leak-proof.

The last strategy maintaining the RCS pressure is just a temporary strategy. Sooner or later, the RCS will be fully depressurized. Then, one of the two previous strategies has to be taken (with all its drawbacks).

IV. THE ASVAD VALVE.

The (ASVAD) **A**utomatic **S**afety **V**alve for **A**ccumulator **D**epressurization [21] is the response to deal with the Nitrogen Injection Issue. It is a unique kind of safety valve, with a main difference with the standard safety valves: ASVAD only actuates when the pressure drops below a preset level. This level can be adjusted to the point when the accumulator gets empty of water.

The Figure 1 is an inner view of the valve internal elements. Figure 2 is a simplified representation of the ASVAD Valve. It has a pressurized chamber (1) connected to the accumulator nitrogen side. This chamber is sealed by a hollow obturator (2) and a gasket. There is a preloaded spring (3) by an adjustment disc (4) threaded over the obturator.

The basis of the ASVAD valve operation is the imbalance between the forces exerted over the obturator. On the bottom side, there is the force exerted by the accumulator internal pressure. This force firmly pushes up the obturator keeping it closed. On the upper side, there is the force exerted by a preloaded spring. This force is constant and pushes the obturator down trying to open it. While the force exerted by the accumulator normal pressure (thick arrow) is greater than the force exerted by the spring (thin arrow), the obturator remains firmly closed. During normal operation, the force ratio is 3:1.

The spring is preset to the same force of the nitrogen pressure when the accumulator gets empty. So when these circumstances are reached, the spring can overcome the force done by the residual pressure and suddenly pushes down the obturator. This opens the communication from the pressure chamber (1) across the obturator holes and its hollow body, to the outside. Once the obturator has left its seat, the pressure in the chamber will fall even more, leaving the valve permanently open due to the continuous spring action.

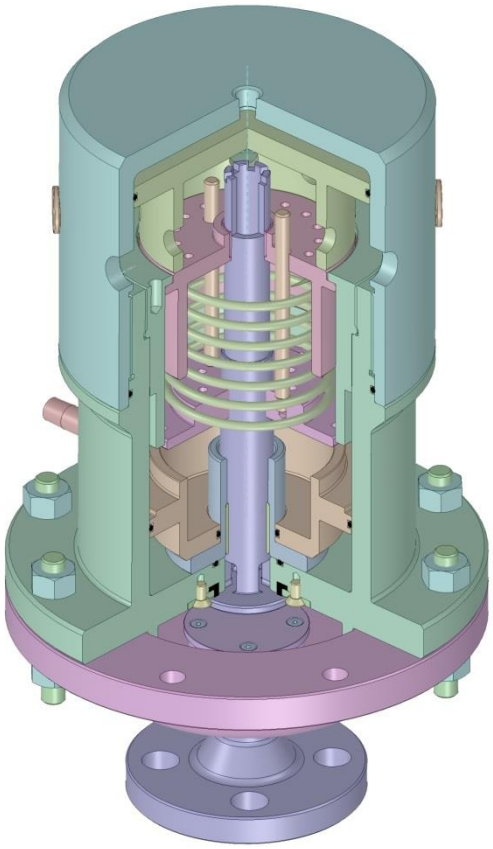

Figure 1. Inner view of the valve internal elements.

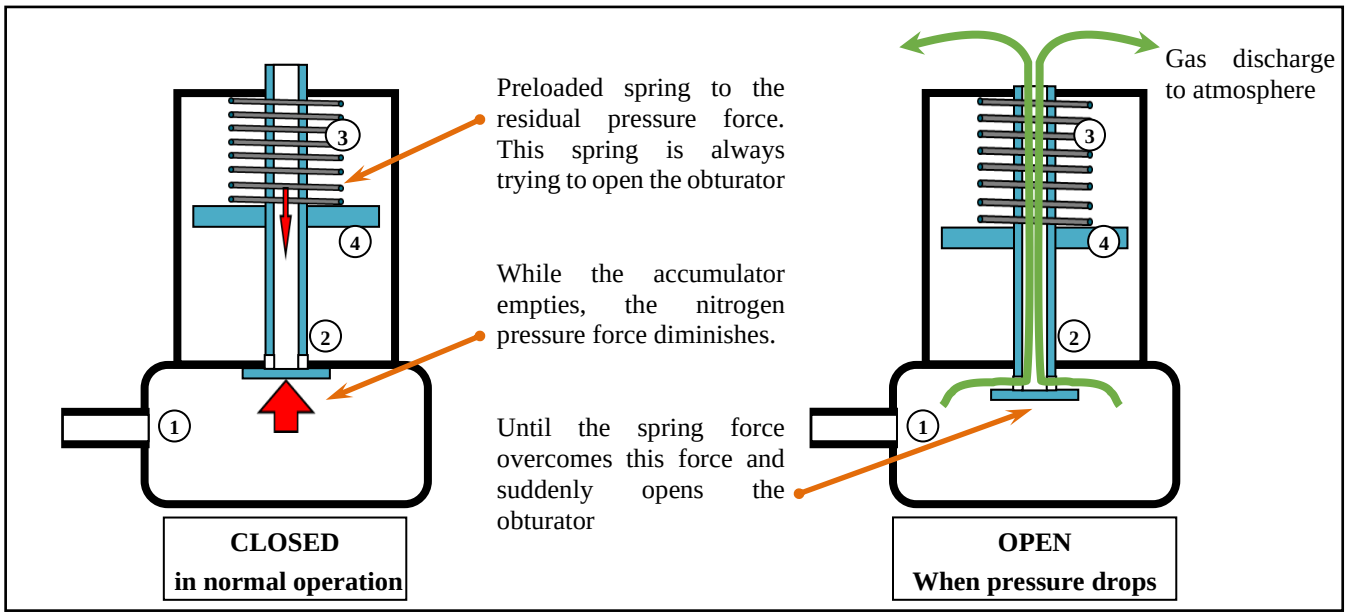

Figure 2. ASVAD valve simplified operation diagram.

The ASVAD Valve has the following advantages:

Main advantages:

1. The ASVAD Valve will be available **all the time** after its installation. Waiting its moment to act.
2. **It completely avoids** the nitrogen injection.
3. It is based on two simple and universal physical principles (force & pressure).
4. **It is fully passive**. It does not require any external energy.
5. **It is fully automatic.** It does not need any operator assistance.
6. It acts at **the right time** and **over all the accumulators**. No time critical operations are needed. It does it automatically by sensing the accumulator pressure. It is also able to self-adapt its opening point to the existing environmental conditions maximizing the accumulator's water volume injected.
7. **It completely vents** the accumulator. No further nitrogen injections will be possible.
8. It allows depressurizing the RCS to LOWER PRESSURES, which will **greatly facilitate the further accident recovery** (This could be its best advantage).
9. It will **save the organization's efforts**, allowing to be focused on other recovery tasks.
10. **It does not interfere** with the normal operation.

Secondary advantages:

1. It is highly **reliable** due to its **simple and robust design** and physical working principle.
2. It is **hard** enough to withstand the post-LOCA environment. It is made on Stainless Steel.
3. It is very **easy to be installed** in the system. It does not require a big modification.
4. It **does not add any new failure mode** different from those already analyzed.
5. It is **intrinsically safe**. No electromagnetic compatibility problems. No-necessary software. Cyber-attack proof. Fire proof. It does not add any fire load. It is not sensitive to radiation, nor sensitive to moisture or even to flooding.
6. It has also a manual operation feature. It can be remotely actuated when required.
7. Its maintenance is simple. **There is no wear**. It just needs a few spare parts. Minimum maintenance cost: "Install & Forget".
8. The desired actuating pressure is **easy to be adjusted and checked**.
9. **It is economic**. It does not need a complex and expensive system modification.
10. **Its qualified life is very long**. Future investments will not be needed. **"Buy once & use it forever".**

About the ASVAD Valve problems:

No specific problems are known yet. A possible problem during operation can be if the valve leaks nitrogen to the atmosphere. But this kind of problem is very rare, and can be similar to any other element in the circuit. It must be taken into account that while there is enough pressure in the accumulator, the pressure closing force will kept the obturator firmly closed. Other possible problem is if the obturator gets stucked in the closing state. But this problem is the same as there is now with the valve not installed.

V. CONCLUSIONS.

The nitrogen Injection to RCS is a complication that **can seriously threat the core cooling** and the **fuel integrity** during an SBO/LOCA accident. **It has high probabilities to happen** during a SBO.

The current strategies to avoid it are **too weak to rely on them**. All of them use active components which needs energy, needs multiple **operator's efforts** doing **time critical actions simultaneously** over different elements. And this is like a chain. Just a fail in the chain, means the complete operation fail.

Using the ASVAD, the RCS nitrogen injection **can be avoided in an easy way**. With ASVAD, the operators will not be burdened coping with the nitrogen injection, and can remain focused in the core cooling, or other recovering tasks. Allowing further RCS depressurization, **it can facilitate the accident recovering**, giving a longer coping time.

ASVAD is **a passive element**, which **automatically vents the nitrogen at the correct moment**. The overall plant safety will be improved installing ASVAD on each accumulator.

VI. REFERENCES

1. VARIOUS AUTHORS, *WCAP-17601-P Rev.1, Reactor Coolant System Response to the Extended Loss of AC Power Event for Westinghouse, Combustion Engineering and Babcock & Wilcox NSSS Designs*, Westinghouse Proprietary Class 2, (2013).
2. VARIOUS AUTHORS, *FSG-10 Rev.1, Passive RCS injection isolation*. Background information for Westinghouse Owners Group Emergency Response Guidelines, PWROG, (2014).
3. CHRISTINE SARRETTE, *Effect of Noncondensable Gases on Circulation of Primary Coolant in Nuclear Power Plants in Abnormal Situations*, Lappeenranta University of Technology (Finland), (2003).
4. TAKASHI NAGAE, TOSHIAKI CHIKUSA, MICHIO MURASE & NORITOSHI MINAMI, *Analysis of Non-condensable Gas Recirculation Flow in Steam Generator U-Tubes during Reflux Condensation Using RELAP5*, Journal of Nuclear Science and Technology, 44:11, 1395-1406 (2007).
5. LI YUQUAN, HAO BOTAO, ZHONG JIA, AND WANG NAN, Comparative Experiments to Assess the Effects of Accumulator Nitrogen Injection on Passive Core Cooling During Small Break LOCA, Nuclear Engineering and Technology 49 54-70 (2017).
6. TAKESHI TAKEDA, AKIRA OHNUKI, DAISUKE KANAMORI, AND IWAO OHTSU, *ROSA/LSTF Tests and RELAP5 Posttest Analyses for PWR Safety System Using SG's Secondary - Side Depressurization against Effects of Release of Nitrogen Gas Dissolved in Accumulator Water*, Science and Technology of Nuclear Installations Volume 2016, Article ID 7481793.
7. VARIOUS AUTHORS, *Various incidents in the US plants related with nitrogen*. NRC GL-2008-01, IN-97-40, IN-89-67, ML031050497, ML031060539, ML031180745, ML090980303.
8. MARTIN STEINBRUECK, FABIO OLIVEIRA DA SILVA, MIRCO GROSSE, *Oxidation of Zircaloy-4 in steam -nitrogen mixtures at 600-1200ºC*, Journal of Nuclear Materials 490 226-237 (2017).
9. GALLARDO, S., ABELLA, V., VERDU, G., 2011. *Assessment of TRACE 5.0 against ROSA Test 6-2, Vessel Lower Plenum SBLOCA*. Tech. Rep. February.
10. KANG, J., YUN, B., 2019. *An experimental study of steam condensation with the presence of air under free convection condition*. In: Nureth-18. pp. 1893{1906.
11. LEE, J., PARK, G.-C., CHO, H. K., 2016. *Validation of wall film condensation model in the presence of NC gas for two-fluid model*. In: NUTHOS-11. pp. 1{15.
12. LEE, K.-W., NO, H. C., CHU, I.-C., MOON, Y. M., CHUN, M.-H., jun. 2006. *Local heat transfer during reflux condensation mode in a U-tube with and without noncondensible gases.* International Journal of Heat and Mass Transfer 49 (11-12), 1813{1819.
13. LIU, T.-J., feb 2001. *Reflux condensation behavior in a U-tube steam generator with or without noncondensables.* Nuclear Engineering and Design 204 (1-3), 221{232.
14. NAGAE, T., CHIKUSA, T., MURASE, M., MINAMI, N., 2007. *Analysis of noncondensable gas recirculation ow in steam generator U-Tubes during reflux condensation using RELAP5*. Journal of Nuclear Science and Technology 44 (11), 1395{1406.
15. PARK, H.-S., NO, H. C., BANG, Y. S., nov. 2003. *Analysis of experiments for in-tube steam condensation in the presence of noncondensable gases at a low pressure using the RELAP5/MOD3.2 code modified with a non-iterative condensation model*. Nuclear Engineering and Design 225 (2-3), 173{190.
16. RIIKONEN, V., KOUHIA, V., KAUPPINEN, O., SJOVALL, H., HYVARINEN, J., 2018. *Experimental observation of adverse and beneficial effects of nitrogen on reactor core cooling.*
17. TAKEDA, T., OHNUKI, A., KANAMORI, D., OHTSU, I., 2016. ROSA/LSTF *Tests and RELAP5 Posttest Analyses for PWR Safety System Using Steam Generator Secondary-Side Depressurization against Effects of Release of Nitrogen Gas Dissolved in Accumulator Water*. Science and Technology of Nuclear Installations 2016.
18. TAKEDA, T., SUZUKI, M., ASAKA, H., NAKAMURA, H., 2006. *Quick-look Data Report of OECD/NEA ROSA Project Test 6-2 (0.1% 15 Pressure Vessel Bottom Small Break LOCA Experiment).* Tech. Rep. JAEA-Research 2006-9002, Japan Atomic Energy Agency.
19. YEONG-JUN, J., DONG-JAE, C., YEON-GUN, L., SIN, K., DONG-WOOK, J., 2015. *Experimental study of condensation heat transfer in the presence of noncondensable gas on the vertical tube*. International Topical Meeting on Nuclear Reactor Thermal Hydraulics 2015, NURETH 2015 7, 6096{6109.
20. The ASVAD Valve: visit www.asvad-nuclear.com.
21. J.FREIXA, A.LABORDA, V.MARTINEZ. Effectiveness of the ASVAD valve in a RPV bottom leak. 2021 Annals of Nuclear Energy. ELSEVIER

Proceedings of the European Nuclear Young Generation Forum
ENYGF'21
September 27-30, 2021, Tarragona, Spain

The potential effect of radiolyzed superplasticizers contained in cement-based materials on europium uptake

Solène Legand[1*], Nathalie Macé[1], Benoist Muzeau[1], Philippe Letutour[1], Sandrine Therias[2], Pascal E. Reiller[3]

[1] Université Paris-Saclay, CEA, Service d'Etude du Comportement des Radionucléides, 91191, Gif-sur-Yvette, France.

[2] Université Clermont Auvergne-CNRS-SIGMA Clermont, ICCF F-63000 Clermont–Ferrand, France

[3] Université Paris-Saclay, CEA, Service d'Études Analytiques et de Réactivité des Surfaces, 91191, Gif-sur-Yvette, France.

* Corresponding author: *solene.legand@cea.fr*

I. INTRODUCTION

In the French nuclear waste management context, most of the intermediate-level long-lived waste will be stabilized in mortar or concrete packages. The cement-waste forms are used to immobilize radionuclides (RN) and provide a protection from radiations. In such cement-based materials, superplasticizers (SP) are used as admixtures to increase the workability of the early-age cement-water-aggregate mixture. In a deep geological repository situation, SP undergo coupled effect from both radiolysis and hydrolysis in the pore solution of cement-based materials leading to the formation of potentially complexing degradation products. Determining the impact of SP degradation products on RN transfer through cementitious materials is important for assessing the disposal concept [1]. This study is focused on two major families of SP used by French nuclear industry: polycarboxylate ether (PCE) and polynapthalene sulfonate (PNS) in the presence of europium(III) taken as chemical analogue of trivalent actinides. The main objectives of this work are i) a better understanding of the sensitivity of SP, and degradation products, to the coupled effect of radiolysis and alkaline hydrolysis; ii) to describe the interactions between Eu(III) and ligands resulting from the degradation of SP by radiolysis and alkaline hydrolysis; and iii) to evaluate the impact of these interactions on the reactive transport of Eu(III) in a compact cementitious matrix after radiolysis [2]–[4]. The study presented hereafter is more particularly focussed on parts i) and ii).

II. RESULTS AND DISCUSSION

A. Materials and method

The experimental part is focused on interactions between Eu(III) and ligands resulting from degradation of SP. SP alkaline solutions are prepared with respectively 1 and 2%w of PCE and PNS in alkaline medium under anaerobic conditions. The SP are commercial products whose density and dry extract are (1.05 ± 0.02) g cm^{-3}, (19.9 ± 2.0)% for PCE and (1.15 ± 0.03) g cm^{-3}, (32.5 ± 1.6)% for PNS. The alkaline medium contains 0.15 mol L^{-1} NaOH, 0.12 mol L^{-1} KOH and 10 g L^{-1} of crush mortar (CEM I 52.5 N - SR 5 CE PM-CP2 NF HTS Le Teil; water/cement ratio = 0.4; 2.51%w PCE or 5.03%w PNS). The SP alkaline solutions are at pH value of 13.3 ± 0.1. The SP alkaline solution are degraded by gamma-radiolysis, which is performed by Poséidon irradiator (LABRA, CEA). The irradiator is equipped with a ^{60}Co source: irradiation doses are 0, 50, 100, and 250 kGy, and the dose rate is 1 kGy h^{-1}. SP alkaline solutions are filtered through Thermo Scientific Nalgene syringe filters equipped with PES membrane (0.2 µm size pore × 25 mm ∅). SP degradation products are characterized by gas spectrometry, infrared spectroscopy, ionic chromatography (IC), size exclusion chromatography (SEC), and total organic carbon content (TOC). The interaction of Eu(III) by SP degradation products is investigated by the measurement of Eu solubility.

The TOC measurement is done with Elementar Vario TOC cube analyzer. The measuring principle is the oxidation of bound carbon and CO_2 measurement with IR detection. The total inorganic carbon (TIC) is measured by acidifing the sample with a 5% H_3PO_4 (85%, Merck). The total carbon (TC) is obtained by combustion of samples at high temperature catalytic combustion up to 850°C. The TOC is obtained by the difference between TC and TIC. The calibration is done using potassium hydrogen phthalate (Elementar S35.00-0151) for TOC and sodium carbonate (Elementar S35.00-0152) for TIC (from 1 to 25 mg_C L^{-1}). The SP alkaline solutions are diluted by 100 and 300 for PCE and PNS alkaline solutions, respectively, to remain in the calibration concentrations range. The injected volume is 0.1 mL and each sample is replicated 3 times. A blank is inserted between each sample to check the background and the system is rinsed with the sample prior to each injection.

The IC system used is an Integrion Ion Chromatography System (Thermofisher, Dionex) controlled by the Chromeleon software. The acetate, SO_4^{2-} and SO_3^{2-} anions

are detected by conductivity. The employed guard column is a Hydroxide-Selective Anion-Exchange Dionex IonPac AG15 RFIC 2 mm ∅ × 50 mm L and the column is an AS15 2 mm ∅ × 250 mm L, both maintained at 30°C. The elution is obtained by isocratic method at 38 mmol L^{-1} of KOH from 0 to 40 min. The flow rate is 0.3 mL min^{-1} and the sample injection volume is fixed at 10 µL. The calibration is performed by a acetate standard solution for IC TraceCERT at 1000 mg L^{-1} in water (Sigma-Aldrich 51791), a sulphate standard solution for Ion Pair Chromatography at 1000 mg L^{-1} in water (Fisher Chemical J/4564/05) and a power of anhydrous Na_2SO_3 (Sigma-Aldrich 31454). Standards are obtained from dilution of the standard solution to the following concentrations: 50; 30; 10; 5; 2; 1 and 0.5 mg·L^{-1}. Standards solutions are injected in triplicates and blanks of pure water are injected before each sample. Samples are also injected in triplicates to estimate measurement standard deviations (σ) and are diluted in pure water with a dilution factor from 0 to 50. The uncertainty is estimated as 2σ.

The SEC system used is U3000 Chromatography System (Thermofisher, Dionex) controlled by the Chromeleon software. The PCE is detected by ERC refractoMax 520 refractive index detector (RI) and the PNS by Dionex PDA-100 Photodiode Array Detector (UV-visible detector at 290 nm. The employed guard column is a Tosoh TSKgel superAW-L 4.6 mm ∅ × 3.5 cm L and two columns in series are Tosoh TSKgel superAW4000 6.0 mm ∅ × 15 cm L × 6 µm particle size, all maintained at 35°C. The elution is obtained by isocratic method at 10 mmol L^{-1} of ammonium acetate from 0 to 40 min. The flow rate is 0.2 mL min^{-1} and the sample injection volume is fixed at 20 µL. The standard calibration, although widely spread, is not applicable to SP so the irradiated samples are compared to each one.

The operational solubility of Eu(III) is measured as a function of SP degradation products. The Eu solubility limit in the medium is estimated at $10^{-(6.1 \pm 0.9)}$ mol L^{-1} at pH 13.3 by PhreeqC software using the PSI database [5] considering amorphous $Eu(OH)_3$; the formation of $Eu(OH)_4^-$ is not considered as explained elsewhere [6]. A total Eu concentration of 10^{-4} mol L^{-1} including a spike of radioactive ^{152}Eu solution (2 Bq g^{-1}) in anoxic conditions is added to SP alkaline solutions. After equilibration of one hour, solutions are ultra-centrifuged at 20,000 rpm for 1h (36,400 g), and aliquot of the supernatant are sampled. The supernatants are analysed by gamma counting in order to determine the residual amount of radioactive tracer dissolved in solution. At this initial concentration of Eu (10^{-4} mol L^{-1}), the Eu wall sorption is considered negligible.

B. Results

The TOC is quantified in SP alkaline solutions. The initial PNS alkaline solutions contains in average 3600 mg_C L^{-1}, *i.e.* three times more TOC as PCE alkaline solutions (1200 mg_C L^{-1}). These initial concentrations are not impacted by irradiation.

The average molecular weight of polymers is measured by SEC. The observed modifications of the average molecular weight of the polymers in solution after irradiation are for both SP as a function of the dose: a degradation by chain scissions for PNS (Figure 1) and also cross-linking for PCE (Figure 2).

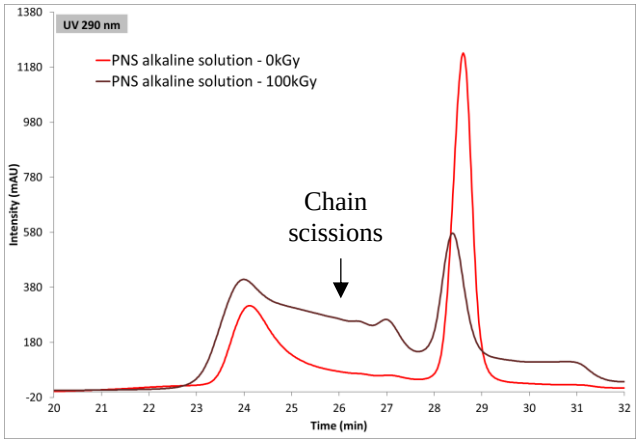

Figure 1. SEC chromatograms of PNS alkaline solution before (0 kGy) and after (100 kGy) irradiation – UV detection at 290 nm.

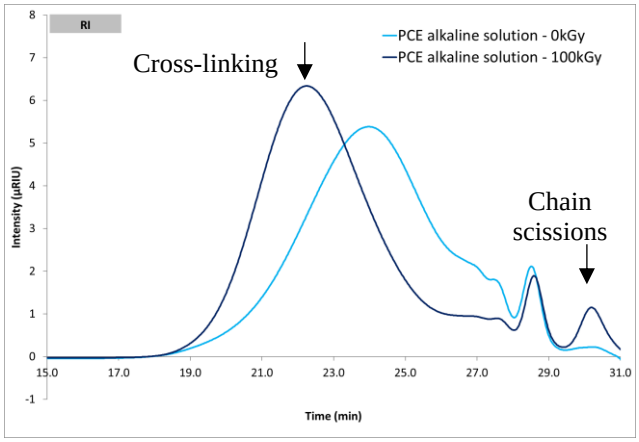

Figure 2. SEC chromatograms of PCE alkaline solution before (0 kGy) and after (100 kGy) irradiation – RI detection.

The SP alkaline solutions are analyzed by IC. Two SP degradation products are characterized in solution as marker of degradation: SO_3^{2-} (and SO_4^{2-}) for PNS, and acetate for PCE. Sulphate come from oxidation of sulphite. The formation of sulphites was also demonstrated without irradiation for PNS proving that this SP is sensitive to alkaline hydrolysis degradation. Formation yields are obtained, (0.017 ± 0.008) µmol J^{-1} and (0.061 ± 0.018) µmol J^{-1} in solution for sulphite and acetate, respectively. These yields, compared to polymer quantity, reach (2.7 ± 1.2) µmol J^{-1} and (30 ± 9) µmol J^{-1} for PNS and PCE, respectively. The corresponding conversion rates at 100 kGy are (11 ± 1.5)% for the two SP. As these values are too high to correspond to primary effects, we conclude that SP degradation products result mainly from the attack of oxidizing radicals resulting from the radiolysis of water [7].

Operational solubility shows a significant increase of dissolved Eu in presence of SP (Figure 3) compared to already available data without SP [3]. Eu solubility seems to increase further significantly after radiolysis degradation at 100 kGy for the PNS. This increase can be attributed to SP radiolysis degradation products.

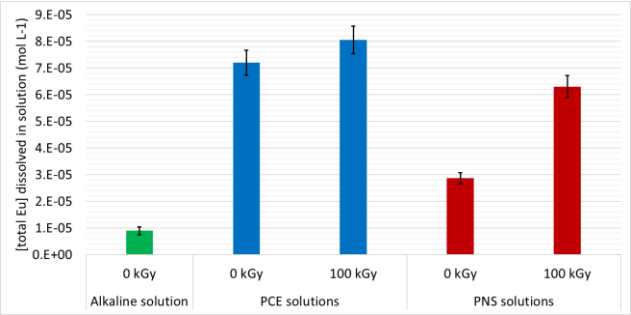

Figure 3. Concentration of total Eu dissolved (mol L^{-1}) in alkaline solution (without SP), PCE alkaline solutions and PNS alkaline solutions in function of dose (0 and 100 kGy) – solutions are without SP, 1 and 2 %w of PCE and PNS respectively in 0.15 mol L^{-1} NaOH, 0.12 mol L^{-1} of KOH and 10 g L^{-1} of crushed mortar (pH 13.3) – $[Eu]_{total} = 10^{-4}$ mol L^{-1}.

III. CONCLUSIONS

The main objectives of this work is to understand interactions between Eu(III) and ligands resulting from sensitivity of SP to the coupled effect of radiolysis and alkaline hydrolysis. These tests will make it possible to interpret the reactive transfer tests in progress on the cement matrices. The first experiments have shown a modification of the average molar weight of the polymer and the formation of SP degradation products in solution after irradiation for both SP as a function of the dose. The presence of SP seems to affect significantly Eu solubility. The degradation by chain scissions seems to affect more the Eu solubility in the case of PNS. Operational solubility measurements will be completed with those for SP alkaline solutions irradiated at 50 and 250 kGy, and for pore solution obtained by pressing of CEM I grout. The complexation of Eu(III) by SP and his degradation products will be investigated in detail using time-resolved laser-induced fluorescence spectroscopy. Eu(III)-sorption/desorption experiments will also be performed in order to highlight the impact of complexes on the uptake of Eu(III) in the cementitious matrix.

IV. ACKNOWLEDGMENT

The authors are grateful to Andra, CEA, EDF and Orano for financial support and F. Carpentier, S. Esnouf, and J. Page for their contributions to this study.

V. References

[1] Andra, 'Tome évolution phénoménologique du stockage géologique', 2005. [Online]. Available: https://www.andra.fr/sites/default/files/2018-02/269.pdf

[2] D. M. García, M. Grivé, L. Duro, S. Brassinnes, and J. de Pablo, 'The potential role of the degradation products of cement superplasticizers on the mobility of radionuclides', *Appl. Geochem.*, vol. 98, pp. 1–9, 2018, doi: 10.1016/j.apgeochem.2018.09.004.

[3] P. Reiller *et al.*, 'Complexing power of hydro-soluble degradation products from γirradiated polyvinylchloride: influence on Eu(OH)3(s) solubility and Eu(III) speciation in neutral to alkaline environment', *Radiochimica Acta*, vol. 105, no. 8, pp. 665–675, Jan. 2017, doi: 10.1515/ract-2016-2691.

[4] E. Fromentin, D. Lebeau, A. Bergounioux, M. Ferry, and P. E. Reiller, 'Interactions between hydro-soluble degradation products from a radio-oxidized polyesterurethane and Eu(III) in contexts of repositories for low and intermediate level radioactive waste', *Radiochimica Acta*, vol. 108, no. 5, pp. 383–395, May 2020, doi: 10.1515/ract-2019-3122.

[5] T. Thoenen, W. Hummel, U. Berner, and E. Curti, 'The PSI/Nagra Chemical Thermodynamic Database 12/07', 2014, [Online]. Available: https://www.lib4ri.ch/archive/nebis/PSI_Berichte_000478272/PSI-Bericht_14-04.pdf

[6] W. Hummel, U. Berner, E. Curti, F. J. Pearson, and T. Thoenen, 'Nagra/PSI Chemical Thermodynamic Data Base 01/01', *Radiochimica Acta*, vol. 90, no. 9–11, Jan. 2002, doi: 10.1524/ract.2002.90.9-11_2002.805.

[7] E. Bjergbakke, K. Sehested, O. L. Rasmussen, and H. Christensen, 'Risø National Laboratory, DK-4000 Roskilde, Denmark April 1984', p. 27, https://core.ac.uk/download/pdf/13751125.pdf 1984.

Proceedings of the European Nuclear Young Generation Forum
ENYGF'21
September 27-30, 2021, Tarragona, Spain

Analysis of venting strategies and hydrogen concentration evolution during a Station Blackout in a BWR-6 containment using GOTHIC 8.3

Diez Alvarez-Buylla, Pino[1*], Estévez-Albuja, Samanta[2], Jiménez, Gonzalo[2] and Gavilán, Carlos[1]

[1] Iberdrola, Spain; [2]Universidad Politécnica de Madrid, Spain

*Corresponding author: pdab@iberdrola.es

I. INTRODUCTION

After the Fukushima accident, the interest on hydrogen combustion hazard management has increased considerably. Many European nuclear plants reinforced their strategies for severe accident management with the installation of Passive Autocatalytic Recombiners (PARs) and Filtered Containment Venting Systems (FCVS), among others. In this study, the hypothesis of considering a preventive venting to try to reduce the hydrogen combustion risk is analyzed for a BWR-6 Mark III containment. The scenario chosen was the in-vessel phase of a Station Blackout (SBO) accident. Cases with and without PARs have been tested.

The venting action has been tested at different conditions to clarify its impact on the hydrogen concentration in the containment. One novelty of this study is to consider the difference between measuring the hydrogen concentration values present in the containment in the venting pipe rather than in the instrumentation position. The purpose is to try to understand the decisions that an operational crew can take with the instrumentation available and analyze the differences by modifying the location of the plant instrumentation.

For the numerical analysis, numerous simulations have been carried out using a BWR containment model with GOTHIC 8.3. It has been observed that hydrogen concentration depends to a great extent on the containment venting strategy. The main conclusion is that the venting strategy, if properly performed, can reduce the risk associated with hydrogen for BWR-6 containments. During a SBO scenario, an early venting increases considerably the hydrogen combustion hazard, even in the cases with PARs.

A. BWR-6 3D Containment model

The three-dimensional model of the BWR-6 Mark III containment was developed at the Nuclear Safety and Thermo-hydraulic group at the UPM with GOTHIC 8.0 [1], [2] . For the development of this work, this prior GOTHIC model was converted from GOTHIC 8.0 to GOTHIC 8.3 Q.A. Some modifications have been performed to adapt them to the new version, e.g. Control Volumes characteristics or thermal conductors and Control Variable options.

The containment is represented using the "Nesting Dolls" approach, extensively explained in [1]. Using this approach, the full containment is modeled with eleven Control Volumes (CVs) and one CV represents the atmosphere. A diagram of the CVs used to model the Mark III containment BWR-6 is presented in Figure 1. These CVs are used to represent the regions of the containment that are occupied by a fluid e.g. steam, air, hydrogen, water, etc.

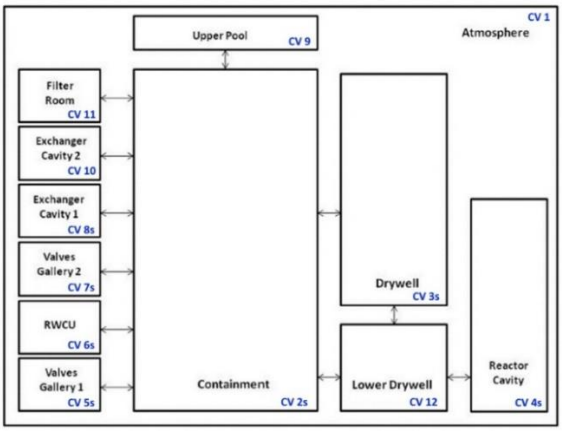

Figure 1 BWR-6 Mark III "nesting dolls" diagram.

B. Accident progression phenomenology

An event results in a loss of offsite power and improvements resulting from the Fukushima accident are not considered, so the extensive damage procedures and guidelines are not simulated.

First, the Reactor Cooling Isolation System (RCIC) and all diesel generators fail to start. As a consequence of the loss of onsite AC power are not available the following systems:

- High Pressure Core Spray (HPCS)
- Low Pressure Core Spray (LPCS)
- Residual Heat Removal (RHR) in all the operational modes. Low Pressure Core Injection System (LPCI)

mode, Containment Spray mode, suppression pool cooling, etc.
- Standby liquid control system (SBLC),
- Condensate, Containment Cooling system
- The Control Rod Drive Hydraulic System (CRDH)

During the first 4 hours of the transient the DC power (station batteries) and associated emergency buses are available.

II. RESULTS

In this section the results from the different sets of cases are presented. Due to the high detail of the model, the results obtained comprehend a large amount of data, having made necessary the development of a tool that allows processing the results and facilitate their interpretation. For this purpose, it was used a program to post process the data obtained from the model developed in GOTHIC: PREDICTORV10 [2]

A. Set 1: Cases without PARs

Several cases with different vent openings depending on the hydrogen concentration measured at the instrumentation have been created. The studied range goes from 1 % to 13 % of hydrogen concentration, since it is the highest value reached in the measurement cell (in the base case), going in 1 % increments. The vent is closed when the containment pressure reaches 102 kPa, equaling the atmospheric pressure.

The case without containment venting, is also included as a base case.

An evaluation of the combustion hazard associated with the evolution of hydrogen concentration has been made, based on the sum of the numerical results obtained with PREDICTORV10 of the cells in the containment, thus ordering the runs from lowest to highest risk. These time results have been normalized against a base case, for without PAR cases Equation 1 and for PAR cases Equation 2.

$$Hydrogen\ Combustion\ Hazard\ Index_{no\ PAR} = \frac{t_{DDT} + t_{SD} + t_{FD}}{t_{(DDT)BL-NO\ PAR} + t_{(SD)BL-NO\ PAR} + t_{(FD)BL-NO\ PAR}} \quad (1)$$

$$Hydrogen\ Combustion\ Hazard\ Index_{PAR} = \frac{t_{DDT} + t_{SD} + t_{FD}}{t_{(DDT)BL-PAR} + t_{(SD)BL-PAR} + t_{(FD)BL-PAR}} \quad (2)$$

where t_{DDT}, t_{SD} and t_{FD}, are the time the cell has spent in detonation, slow deflagration or rapid deflagration regime, respectively; and subindex BL-PAR, BL-NO PAR refers to the times in the base cases without and with PARs.

Figure 2 shows a comparison between the different cases normalized with the base case, which has the value of 1. Values above 1 have a higher hydrogen combustion hazard, versus not venting. therefore, values below 1, have lower hydrogen combustion hazard.

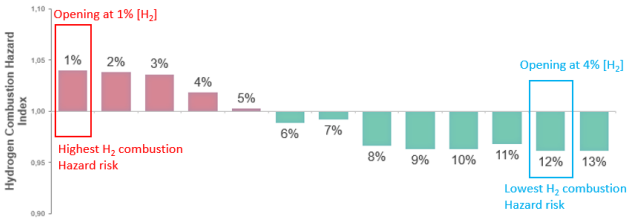

Figure 2 Hydrogen Combustion Hazard Index. Cases vs a normalized hydrogen with the base case having a value of 1.

Venting the containment excessively early, with concentrations less than 5 % registered by the instrumentation, increases hydrogen combustion hazard. On the other hand, venting with concentrations higher than 6 % registered by the instrumentation reduces the hazard associated with hydrogen versus not venting. The case with lower combustion hazard is where venting occurs when there is 12 % H_2 concentration.

The cases where the venting starts too soon, the gas that is mainly vented is steam, increasing the hydrogen combustion risk in the containment. When the venting system is actuated later in the transient, the venting is more effective as it also vents more hydrogen, so the hydrogen combustion risk is reduced. These results were found similar for a PWR Westinghouse containment in previous research works [4]

a. Analysis of the optimum case Lower Risk of combustion)

The results after post-processing the v61 [0.12 H_2] case is presented. In this case venting starts when a 12 % hydrogen concentration is reached. Venting at this concentration corresponds to the lowest hydrogen combustion hazard case.

For each cell in the containment, the most unfavorable results are shown graphically during the time executed where Red cell means that there has been detonation at some point in the transient; Orange cell means that there has been a rapid deflagration at some point in the transient; Yellow cell means that there has been a slow deflagration at some point in the transient; and Green cell means that nothing has happened. There is no ignition of the mixture in any case.

The results presented in Figure 3 shows the results in the containment volume (2s) at each elevation (2sx#). Analyzing these results, it can be appreciated that at the bottom of the containment because of the suppression pool there is no ignition risk (it is full of water). The levels where the risk increases are above the suppression pool, and the risk decreases while ascending to the upper dome, where there is rapid deflagration risk, but no detonation risk. The cells with the highest hydrogen combustion hazard are located on level 5, about 3 meters above the surface of the suppression pool.

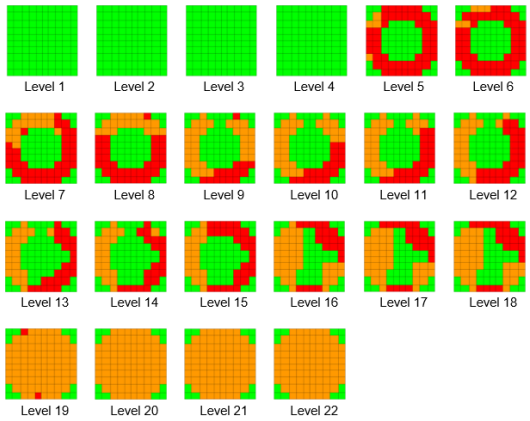

Figure 3 Hydrogen combustion hazard by levels in the containment volume.

Figure 4 represents the behavior of hydrogen along the transient of level 5 cells. It is also shown the hydrogen response in the vent suction cell, and in the cell where the primary containment atmosphere mixing system, AMS, instrumentation is located. It shows the two hydrogen concentration peaks already shown in Figure 4 coming from the SRVs. It is detected that these maximum hydrogen concentrations are attenuated in the control room instrumentation.

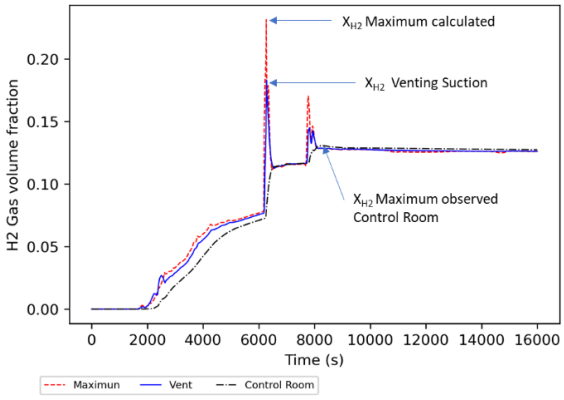

Figure 4 Comparison of the maximum value obtained from hydrogen volume fraction at level 5 versus the value observed in the control room and the value observed in the venting suction cell.

Due to this discrepancy in hydrogen measurements, a new sensitivity analysis has been developed in a containment with PAR, in which the vents have been made according to the measurements at different points of the containment

B. Set 2: Cases with PARs

The PAR performance is based on hydrogen recombination with the oxygen present in the containment atmosphere using certain metals as catalysts. The methodology posed herein establishes the PAR installation, answering the regulatory requirements emerged after Fukushima Daiichi accident [3].

The opening of the containment vent has been simulated when a certain volumetric concentration of hydrogen is reached. Cases have been executed with openings from 1 % to 6 %, since this is the highest value reached in the measurement cell, in 1 % increments. Containment closure is simulated when the containment pressure drops to 102 kPa.

Figure 5 shows a comparison between the different cases normalized with the base case, which has the value of 1. Values above 1 have a higher hydrogen combustion hazard, versus not venting. therefore, values below 1, have lower combustion hazard associated with hydrogen. As happened with the no PAR cases, venting the containment excessively early, with concentrations less than 3 %, increases the hazard associated with hydrogen, and with concentrations higher than 4 % reduces the hazard associated with hydrogen versus not venting.

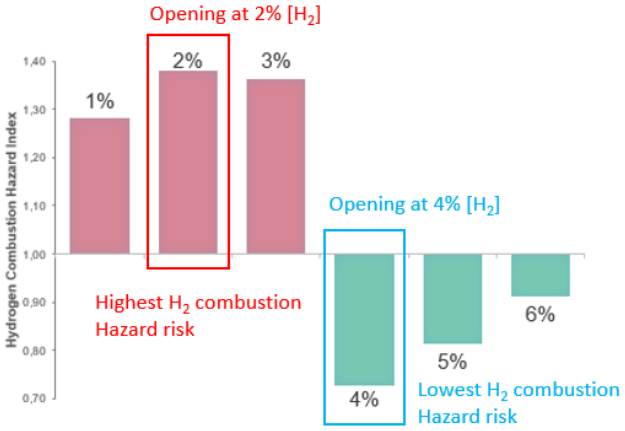

Figure 5. Hydrogen Combustion Hazard Index. Cases vs a normalized hydrogen with the base case having a value of 1.

The main difference between venting at 3% or 4% concentration lies in the timing of venting. At 3% concentration, venting occurs between 4100 seconds (opening) and 4900 seconds (closing). Venting at 4% concentration opens at 6100 seconds and closes at 6950 seconds.

Therefore, during venting at 3% concentration, the massive discharge of hydrogen has not yet occurred, so mainly steam is vented, which is against the inertization of the containment and increases the hydrogen combustion hazard.

On contrary, when venting occurs at 4 % concentration, it is coincident with the first rapid discharge of hydrogen, favoring the elimination of a large amount of hydrogen.

a. Analysis of the optimum case (Lower risk of combustion)

The results after post-processing the v46 [0.04 H_2] case is presented. In this case venting starts when a 4 % hydrogen concentration is reached at the instrumentation location. Venting at this concentration corresponds to the lowest hydrogen combustion hazard case.

The results presented in Figure 6 show the results in the containment volume (2s) at each elevation (2sx#). Analyzing these data, it can be appreciated that as we ascend, the risk associated with hydrogen is reduced. There is not detonation risk above 14 m, and rapid deflagration risks are maintained mostly by the equipment gap, where the flow ascends. The cells with the highest risk are located on level 5, about 3 meters above the surface of the suppression pool.

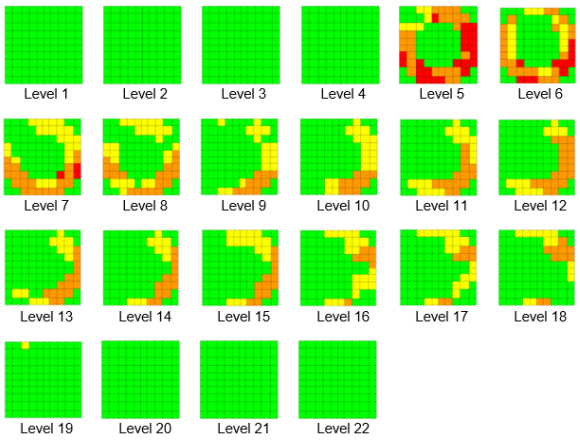

Figure 6. Hydrogen combustion hazard by levels in the containment volume.

Figure 6 presents for each level 5 cells the behavior of hydrogen along the transient. It also shows the hydrogen response in the vent suction cell, and in the cell where the primary containment atmosphere mixing system, AMS, instrumentation is located. It is detected, Figure 7, that these maximum hydrogen concentrations are attenuated in the control room instrumentation, as occurred in the no PAR cases.

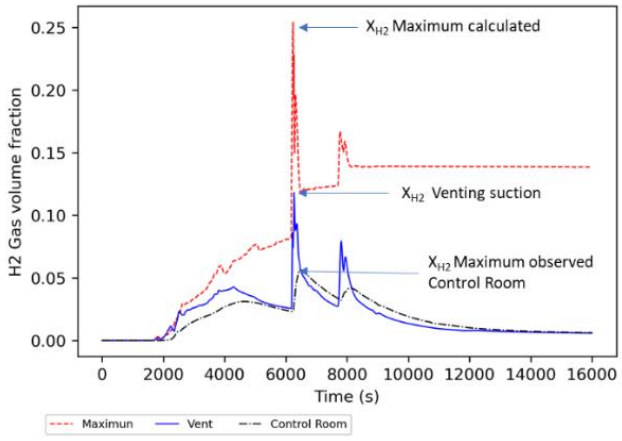

Figure 7. Graphic representation of the Level 5 cells of the Containment volume with the highest hydrogen combustion hazard, comparing it with the measures observed in the Control Room.

Due to this discrepancy in hydrogen measurements, a new sensitivity analysis has been performed, were the vents have been made according to the measurements at different points of the containment.

III. CONCLUSIONS

Hydrogen generated during a SA can be a threat on the containment integrity. The venting strategy to reduce hydrogen combustion hazard has been studied but has not been quantified in a BWR Mark III until now.

The results of the analysis have shown the following:

• Preventive venting in containments without PAR is not recommended since the hydrogen combustion hazard versus non-venting is not significantly improved. The variation in risk depends largely on where the hydrogen is located. Depending on the timing and duration of the vent, one gas or the other will be removed resulting in a higher or lower risk of hydrogen. Due to the high number of hydrogen release points through the SRVs, it is difficult to predict.

• The cells where the hydrogen concentration measurement instrumentation is located, mark lower readings than other cells in the containment. However, despite plant instrumentation does not indicate existing maximums, there are no significant differences in the results regarding the risk of hydrogen.

• Venting the containment too early, with concentrations lower than 5 % without PAR and 3 % with PAR, increases the hydrogen combustion hazard versus not venting at all, considering the hydrogen concentration observed in the control room. However, it has been observed that at equal hydrogen concentration in different points of the containment, the result can be quite different.

• Changing the plant instrumentation location, it is not possible to reduce the total hydrogen combustion hazard concentration, but, knowing the location it is necessary to determine the best optimal moment for venting.

• It is proposed to vent when the hydrogen concentration is high enough to ensure that not only steam is vented. For the geometry analyzed, venting at a hydrogen concentration of 6 % would ensure hydrogen combustion hazard is lower.

Summarizing all the results, it has been found that the venting strategy, if properly performed, can reduce the hydrogen combustion hazard for BWR-6 containments. During a SBO scenario, an early venting increases considerably the hydrogen combustion hazard, even in the cases with PARs. This knowledge could help in the future development of the power plants procedures for hydrogen management.

Being aware of the discrepancy between the maximum hydrogen concentration values and those observed in the control room can help nuclear power plants to implement new instruments in those places where the hydrogen combustion hazard is greater.

IV. References

[1] G. Jimenez *et al.*, "BWR Mark III containment analyses using a GOTHIC 8.0 3D model," *Ann. Nucl. Energy*, vol. 85, pp. 687–703, Feb. 2015, doi: 10.1016/j.anucene.2015.06.025.

[2] C. Serrano *et al.*, "Proposed methodology for Passive Autocatalytic Recombiner sizing and location for a BWR Mark-III reactor containment building," *Ann. Nucl. Energy*, vol. 94, pp. 589–602, Aug. 2016, doi: 10.1016/j.anucene.2016.03.022.

[3] OECD-NEA, "Stress test carried out by the Spanish nuclear power plant. Final Report," 2011.

[4] Fernández-Cosials, Kevin, et al.. 2017. "Study of Hydrogen Risk in a PWR-W Containment during a SBO Scenario; Tau Parameter Definition and application on Venting Strategy Analysis." *Nuclear Engineering and Design* 325 (December): 164–77. https://doi.org/10.1016/j.nucengdes.2017.10.012

Proceedings of the European Nuclear Young Generation Forum
ENYGF'21
September 27-30, 2021, Tarragona, Spain

Trillo NPP full scope PRA

Calvo, David[1*], Osorio de Rebellón, Francisco Javier[1] and Ontoso, Nuria[2]

[1] Iberdrola Generación Nuclear, Spain; [2] Centrales Nucleares Almaraz-Trillo (CNAT), Spain

*Corresponding author: d.calvo@iberdrola.es

I. INTRODUCTION

Probabilistic Risk Assessment (PRA) is a risk analysis technique through which a quantitative estimate of the risk of accidents is reached, and a modeling of the installation that consists of the breakdown of the possible sequences of events that can lead to an accident and, within each sequence, of the possible combinations of elementary events that may cause the sequence.

The main objectives of the PRA will be:

a. Identify the main contributors to risk, verifying that all potential risk scenarios (including multiple failures, common cause failures, and human errors) have been properly selected from their expected frequency and estimated severity, existing adequate preventive or mitigating measures in order to face them.
b. Provide an assessment of the level of safety based on the current design and operation of a Nuclear Power Plant
c. Become a useful technical advisory tool in the decision-making process related to the design and operation of the plant, largely thanks to the PRA applications such as the risk monitor, possible design modifications, operating procedures, etc.

In order to achieve these goals, operators of nuclear power plants around the world are required to carry out these PRA. Each country develops its PRA based on a specific local regulation, whose inception is in the regulations of the US Nuclear Regulatory Commission (NRC), and in the particular case of Spain, taking into account the work carried out in this field by the Western European Nuclear Regulators Association (WENRA), the Spanish Nuclear Safety Regulator (CSN) released the safety instruction IS-25 in 2010 [1], which established the scope to be covered by the owners of the Spanish Nuclear Power Plants in relation to PRA developments.

In particular, Spanish PRA requirements cover a very complete scope that must include the following modes and sources, as depicted in Figure 1:

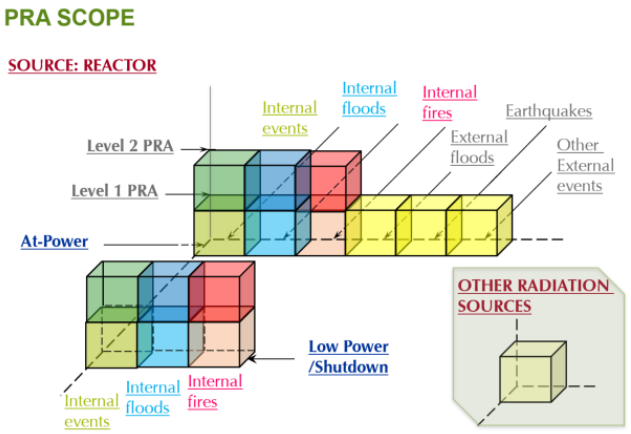

Figure 1. Spanish PRA scope

II. OBJECT

The purpose of this article is to collect the most notable results of the Trillo NPP PRA full scope, according to the Spanish regulation, as shown the figure 1.

This work began in 1992 with the development of the initial tasks of the internal events PRA level 1, and was completed in 2021 after issuing the internal floods shutdown level 2 PRA.

Trillo NPP is a PWR reactor with a German (KWU) design, and its PRA has been reached such level of detail that the created internal events PRA model, with three loops and four safety trains, includes approximately 10,000 basic events and 9,800 gates. Likewise, for the development of the fires PRA model, it is relevant to highlight that due to the great automation of the KWU design, it has been necessary to analyse more than 30,000 cable connections associated with the PRA models.

Therefore, due to the high level of quality attained, it is possible to assure meeting the requirements of Regulatory Guide 1.200 [2] (similar requirements than those included in International Atomic Energy Agency (IAEA) TECDOC 1804 [3]).

III. RESULTS AND ANALYSIS

According to Spanish regulator safety guide GS 1.15 [4], some of the PRA developed at Trillo NPP are required to be reviewed in 5 years (first-level PRA: Internal events Level 1, Internal events Level 2, Internal fires, Internal floods, Shutdown Level 1), whereas others within 10 years (second-level PRA: Internal fires L2, Internal floods L2, Shutdown internal fires, Shutdown internal floods, Shutdown internal fires L2, Shutdown internal floods L2, Shutdown L2 and Other radiation sources).

Regarding to the first-level PRA, the risk contribution for each PRA is shown in the next pie chart (Figure 2).

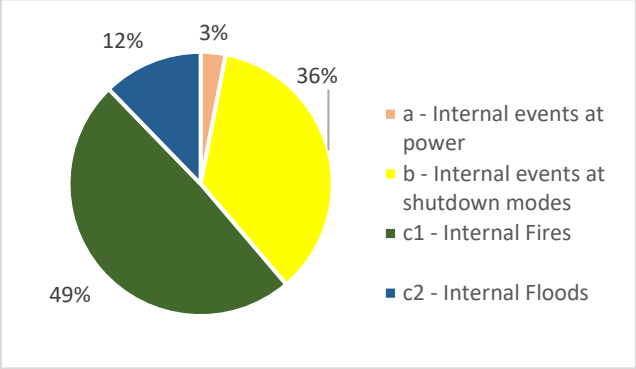

Figure 2. Contribution to CDF

Fire PRA is the greatest contributor in most NPP PRA, especially in those that, as in Trillo NPP, have followed the NUREG-CR-6850 methodology [5], which has been considered excessively conservative. The next contributor is the shutdown PRA, mainly due to the greater contribution of human actions. This fact is caused by the fact that at Trillo NPP most of the potential accidents are mitigated without the need of human actions in the short term, because of the automatic action of the limitation system and the reactor protection system, whereas in shutdown state, the automatic protection systems are unavailable most of the time, therefore arising scenarios are mitigated with manual actions, with the consequent increase in terms of risk. In addition, during the longer periods of shutdown there could be a safety train unavailable due to maintenance. The low contribution of the internal events PRA can also be explained because the model has improved over the past 11 revisions. In addition, it is noteworthy that the plant had an excellent performance, which, as well as other things, it has not trip automatically since 2007.

A. Internal events level 1 PRA

In the last revision, the most significant accidents are LOCA and other pipe breaks, due to the fact that after the implementation of the primary Feed & Bleed, the loss of offsite power (LOOP) and the generic transients such as the reactor trip or the loss of heat sink have decreased sharply.

The most significant components based on their CDF contribution are:

a. Functional groups for tripping the feedwater pumps after reactor trip
b. Control valve for supplying water to the seals of the start and stop pumps

Due to their contribution to the CDF, next common cause failures in equipment are considered important:

a. Failure to open 3/3 isolation valves of the main steam relief valves
b. Failure to open 4/4 emergency feed water valves

The most risk significant human actions failures are carrying out the primary and secondary Feed & Bleed, and making up the pools of the emergency feedwater system

After identifying the most significant human actions, both the simulator sessions for operators and the personnel retraining actions are focused on them.

B. Internal fires PRA

This analysis indicates which are the fire zones and the reason causing the fire, that may ultimately cause core damage. In the last review, the areas with the greatest contribution to the CDF are, on the one hand, those in the annulus reactor building where the borated water tanks of the safety injection system are located, because there are located cables of two out of four safety redundancies (separated 10 m), and on the other hand, the area where the cables that supply information to the main control room are located, inside the electrical building.

In the last revision, there was an 80% reduction, mainly due to the implementation of a series of design modifications aimed to meet an Spanish regulation (IS-30 regarding fire protection requirements), like the automation of the fixed extinction system in the cable rooms inside the electrical building, and especially to the implementation of the design modification, supported by PRA after the analysis of the initial results, which aims to guarantee the protection functions of the reactor coolant pumps (tripping and closing of leakage of high pressure seals) against spurious actions in case of fire.

The process followed for calculating the Fire PRA core damage frequency (CDF) is embraces NUREG/CR-6850 [5] methodology that includes the next tasks: defining the plant boundary and partitioning, selecting components and cables associated with components that could be affected by each fire source and its consequences, then fire frequencies are determined for each group of origins, defining different fire sources, screening out of risk negligible fire compartments, fire growth modeling, fire detection and extinction systems are analyzed, human actions are recalculated bearing in mind the fire effects, performing detailed fire analysis and the multicompartment analysis. These tasks form the input to carry out the quantification of the fire PRA, which uses the EPRI Software FRANX [6]. In this software it is included the relations between basic events and the cables that fails the event, cables and raceways, raceways and zones, and zones and scenarios. Using these relations and the values for scenario fire frequency, scenario severity factor, scenario non suppression probability and the induced PRA initiator, FRANX calculates the CDF for each scenario and the global CDF.

In this case, the most significant components based on their CDF contribution are:

a. Control valves of the emergency supply water system
b. Emergency diesel generators

Due to their contribution to the CDF, next common cause failures in equipment are also considered important:

a. Those common cause failures related to the loss of all the trains of the emergency supply water system
b. Failures in the opening of 3/3 level regulating valves in steam generators (SG) and the failure of 4/4 flow limitation valves to SG

Human actions are particularly important in their contribution to the core damage equation. Among the most significant risk due to failures of human actions, there would be the same as those indicated for internal events.

C. Internal floods PRA

This analysis shows the contribution to the core damage frequency of the different internal floods that occur inside the plant. The scenarios that account for almost the entire frequency of core damage, are flooding in the electronic cabinets and AC bus rooms in the electrical building, and, to a lesser extent, a flooding in the annulus reactor building.

In this case, some of the most significant components have already been indicated for fires PRA, such as:

a. Control valve for the supply of water to the seals of the start and stop pumps
b. Emergency and Safeguard diesel generators

Due to their contribution to the CDF, next common cause failures in equipment are also considered important:

a. Failures in the opening of 3/3 level regulating valves in steam generators (SG) and the failure of 4/4 flow limitation valves to SG
b. Failure in the operation of safeguard emergency diesel generators as well as their online maintenance

Among the most significant risk due to failures of human actions, there would be the same as those indicated for internal and fire events.

D. Shutdown PRA

This analysis shows the contribution to the core damage frequency of the different operating states of the plant (between the residual heat removal system start, and until the residual heat removal system stops at restart). The initiating event that contributes the most to the frequency of core damage is loss of primary inventory, followed to a lesser extent by LOOP.

In this case, the most significant components based on their CDF contribution are:

a. Emergency and safeguard diesel generators
b. RHR pumps

Due to the contribution to the core damage, next common cause failures in equipment are also considered important:

a. Failures in the 24V backup and emergency batteries
b. Failures in the opening of 2/3 and 3/3 level regulating SG valves

The most significant risk human actions are the operations on the nuclear components cooling system valves and operations on the RHR system valves.

E. Internal Events LEVEL 2 PRA

This analysis shows the capabilities of the reactor containment and existing systems in order to mitigate Level 1 sequences that result in core damage. In this way, it can be estimated a probability of failure of the containment during the progression of an accident, causing significant offsite releases.

This PRA concludes that the release frequency is dominated by an induced rupture event in high pressure steam generator tubes when containment is bypassed, and recirculation systems are available. Likewise, the analysis shows an excellent response of containment to short and medium period phenomena, finding almost unique failures in the integrity of the containment after 48 hours.

F. Second-Level PRA

This group of analyzes is composed by other derivatives of first level PRA, such as those that analyze possible emissions outside containment (Level 2), those developments already analyzed but in other modes of operation of the plant (shutdown), and other radiation sources.

The latter is a significant analysis where the events affecting the spent fuel pool are analyzed in detail. In the infrequently case of Trillo NPP, the spent fuel pool is located within the containment, next to the zone where the reactor vessel is located. The results obtained shows that the most significant initiators are the loss of coolant from the spent fuel pool through the auxiliary spent fuel pool cooling system, and the loss of the auxiliary spent fuel pool cooling system together with its electrical support systems. It should be considered that the plant state that is the greater contribution to the CDF, two out of four redundancies are unavailable.

The most significant components, based on their CDF contribution, are the loss of spent fuel pool level instrumentation and isolation valves of the auxiliary spent fuel pool cooling water system

Among the most risk significant human actions failures, the auxiliary spent fuel pool cooling system isolation operation and the spent fuel pool cooling system makeup operation, can be found.

Another second-level PRA is the fire shutdown PRA, where unlike the internal fires PRA, the main difference in the contribution to the CDF consists in the main control room (MCR) area, due to the greater number of manual actuations that are necessary to perform while shutdown mode from the MCR. Both analyses do agree on the importance of fires in the annulus reactor building (specially in areas containing RHR equipment), and fire areas within the electrical

building (mainly those where a fire can cause loss of inventory during the low-level operation mode).

Regarding flood shutdown PRA, the scenarios that account for almost the entire frequency of core damage are the same than those found for internal floods PRA, and, with a greater extent, a flooding in the annulus reactor building.

Floods and fires level 2 PRA results show that the frequency is dominated in both cases by scenarios where a transient takes place with intact containment and recirculation systems are available. Both differ from the internal level 2 PRA, because some scenarios that directly bypasses containment, like steam generator tube rupture, cannot be produce by the fire or flood.

Both floods and fires shutdown level 2 PRA results match internal events and shutdown level 2 PRA results, since release frequency is dominated by scenarios where containment is bypassed, but for both shutdown L2 PRA the main inducer is the loss of instrumentation level when reactor is closed and during low-level operational state, and for the shutdown L2 PRA the main inducer is a RHR LOCA.

IV. PRA APPLICATIONS

PRA studies have become a magnificent tool for improving the design and operation of the plant, and in risk informed decision making process that complements the deterministic defense in depth and safety margins analyses. The most important PRA applications carried out in Trillo NPP were:

a. Risk Monitor: based on PRA models, helps to optimize the operation of the plant by minimizing the risk levels over the operating time, and avoids or controls high-risk configurations. It was installed in main control room to evaluate the risk of maintenance activities and is being updated each year with the new PRA models.
b. AOT extension: Diesel generator allowed outage time extension was approved by the regulator after submitting a risk informed evaluation. This application permits to carry out long term maintenance activities at power operation while reduces the risk during the outage and enables more effective maintenance and better utilization of critical resources.
c. On-line maintenance activities on safety related trains was also approved with a risk informed application. This operation keeps safety systems operable during outage, and enables more effective maintenance and better utilization of critical resources.
d. Mitigation System Performance Index (MSPI) is helpful tool, quantified by the PRA models, to monitor the performance of selected systems based on their ability to perform risk-significant functions. This index was implemented in Trillo NPP and is controlled by the Regulator. After a full PRA revision, this index is updated.
e. Maintenance Rule is a tool for monitoring the performance of the important components against specific criteria of failures and hours of unavailability. The selection of important components was made with the PRA support.

V. CONCLUSIONS

Once all the PRA studies required by the safety instruction IS-25 [1] (that covers all possible risk insights including internal events, fires and floods, both for at power and shutdowns operating modes) have been completed, according to the results, it can be ensured that Trillo NPP shows an excellent low risk levels that place it among the best nuclear power plants in the world, and without significant plant weaknesses.

PRA has proven to be an excellent tool to assess NPP operation and maintenance, as it suggests design changes, evaluates the significance of events, and determines the overall safety performance of the Plant. By developing a full scope PRA, Trillo NPP can now evaluate the risk impact of any event from every point of view, and so balance the risk insights with the deterministic design criteria.

Trillo NPP has deeply used PRA insights to improve nuclear safety. Figure 3 shows the decrease of the at-power internal events CDF (taking the 2005 CDF value as the starting point), which has been achieved thanks to the plant design modifications, (some of them motivated by the PRA), the reduction of reactor trips (no SCRAM since 2007), the optimal balance between reliability of components and their unavailability, and a reduction of 37% in the number of PSA components failures during the last decade compared to the previous one.

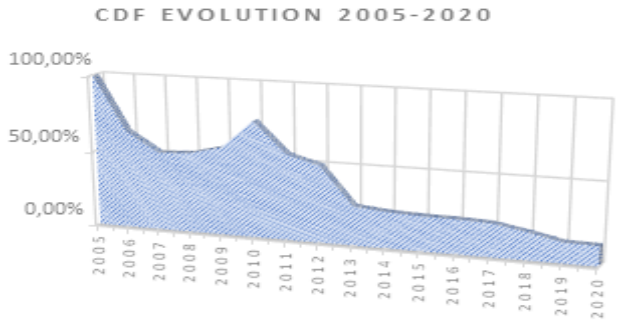

Figure 3. At-power internal events CDF evolution (2005-2020).

VI. References

[1] CSN, "Instrucción IS-25, criterios y requisitos sobre la realización de los análisis probabilistas de seguridad y sus aplicaciones a las centrales nucleares," June, 2010.

[2] US NRC. Regulatory Guide 1.200, "An approach for determining the technical adequacy of probabilistic risk assessment result for risk-informed activities," June, 2008.

[3] International Atomic Energy Agency (IAEA) TECDOC 1804, "Attributes of Full Scope Level 1 Probabilistic Safety Assessment (PSA) for Applications in Nuclear Power Plants," October, 2016.

[4] CSN, "GS-01.15, Actualización y mantenimiento de los Análisis Probabilistas de Seguridad," January, 2017.

[5] US NRC, NUREG/CR-6850 "EPRI/NRC-RES Fire PRA Methodology for Nuclear Power Facilities: Detailed Methodology, Final Report," September, 2005.

[6] FRANX Software Risk and Safety Management Program. Electric Power Research Institute (EPRI).

[7] CAFTA. Risk and Safety Management Program. EPRI.

Proceedings of the European Nuclear Young Generation Forum
ENYGF'21
September 27-30, 2021, Tarragona, Spain

EMERGENCY PREPAREDNESS AND RESPONSE IN BUILD-OWN-OPERATE PROJECTS ON THE BASED ON AKKUYU NPP

Serkan Aslankan

Akkuyu Nuclear JSC, Turkey

Serkan Aslankan: *s.aslankan@akkuyu.com*

I. INTRODUCTION –

After commissioning the first commercial nuclear power plant in Obninsk, Russian Federation, many countries desired to get this new level energy source to use for their needs to energy. USA, UK, Switzerland, Spain, Pakistan, India, Italy and many countries had followed the path of the Nuclear Energy. Especially 1972 oil crises stimulated the transition to the Nuclear Energy from fossil fuels all around the World. [1]

In the beginning of this era, precautions for the preventing nuclear accidents in nuclear power plants were not taken seriously, as it needs. Density of the design basis accidents and the beyond design basis accidents were high. In the 34 years between 1952-1986 years, 8 accidents seen on NPPs above 4th level on the International Nuclear and Radiological Event Scale (INES). After the 1986 Chernobyl disaster to the now, similar accidents prevented except 2011 Fukushima Daichi Disaster. [2]

From this aspect, aviation industry and the nuclear industry have similarities. After the every cases of incidents new measures, orders and regulations came into effect. Over time nuclear and radiation safety has become primary priority for the all Nuclear Power Plants in the World.

There are many business models for nuclear power plants around the world. The first BOO (build-own-operate) project for a NPP still ongoing in Turkey as Akkuyu NPP.

II. EFFECTS OF BEYOND DESIGN BASIS ACCIDENTS TO THE ENVIROMENT AND POPULATION

After the nuclear fission reaction, various types of radionuclides releasing from the fuel elements. iodine-131 (half-life 8.02 days), caesium-137 (half-life 30 years) and caesium-134 (half-life 2.06 years), but many other fission products such as (half-life 33.6 days), Tellurium-129 (half-life 69.6 months), Cesium-136 (half-life 35 days), Silver-110 (half-life 250 days), Zirkonium-96 (half-life 64 days), Niobium95 (half-life 35 days), Barium-140 (half-life 12.7 days) and Lanthanum-140 (half-life 1.68 days). [3]

Iodine-131 (with a short half-life of 8 days) and caesium-137 are remains greatest radiation healt threat to the public. For those two radionuclides, the affected tissues and the time span of the exposure were quite different. Iodine-131 tended to accumulate in the thyroid gland for a few weeks after the release and delivered a dose primarily to that organ. Caesium-137 was deposited on the ground; it delivers a dose to the whole body over many years following the release.

Iodine is found in the structure of the hormones secreted by the thyroid glands. The thyroid gland is an organ that can take the necessary iodine from the free air as well as from the food. The inclusion of radioactive iodine in the hormone structure can cause many cancers, especially thyroid cancer. Studies carried out after the Chernobyl disaster have revealed this issue. [4] For this reason, it is necessary to have iodine tablets in an area of at least 25 km around the NPP in order to meet the iodine need of the body. It is essential that the evacuation process takes place as soon as possible within this period.

Considering the meteorological and landforms of the region, the land area to be purified should be determined, and then the environment in the region should be purified.

A hospital with specialists in the treatment of radiation intake should always be alert to the treatment of both emergency workers and the local population.

In beyond design basis accidents, accident intervention has to be fast and organized by a single management. Therefore, it is a necessity for the managers and teams to intervene in the accident to be pre-trained according to various accident scenarios.

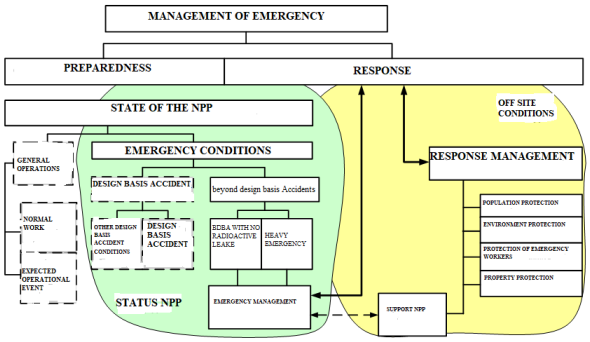

Figure 1. Structure of Management of Emergency (IAEA)

III. Emergency Preparedness in Republic of Turkey

The Republic of Turkey has signed several agreements related to emergency preparedness, including of beyond design basis accidents results:

- Convention on Environmental Impact Assessment in a Transboundary Space, 1991
- Convention on Assistance in the Case of a Nuclear Accident or Radiological Emergency, 1987
- Convention on Early Notification of a Nuclear Accident, 1986
- Convention on Nuclear Safety,1994[5]

Republic of Turkey enacted required laws, regulations and plans:

- National Radiation Emergency plan, TENMAK (Turkish energy, nuclear and mining research institution), 2019
- Regulations of National preparedness to Nuclear and Radioactive emergencies, TAEK (Turkish Nuclear Energy Agency), 15 January 2000
- Establishment of the leadership of AFAD (Disaster And Emergency Management Presidency), Official newspaper of Republic of Turkey No: 2761, 17 July 2009.
- Regulation on the management of radiation emergencies, Official newspaper of Republic of Turkey No: 31159, 06 June 2020

Republic of Turkey have been trying to build nuclear power plants since the 1970s, but due to various reasons, could not fulfill this request. In 12 May 2010, between Russian Federation and Republic of Turkey signed international agreement for the construction of Nuclear power plant based Russian pressured water reactor VVER-1200 in south of Turkey. After the agreement, ROSATOM founded a company in Turkey to run new NPP: Akkuyu Nuclear JSC.

Due to its organizational structure, Akkuyu Nuclear JSC also uses the emergency regulations of Russian Federation:

- Standard Content Protection of personal In Case of Emergency in NPP, Management of Nuclear and radiological safety of Russian Federation,2000
- Regulation about Order Notification and transformation information Order in case of emergencies in NPP, Rosatomnadzor, 2002

In case of beyond design basis emergency, the three parties do management of response to emergency jointly: Akkuyu Nuclear JSC, Rosatom and NDK (Nuclear Regulatory Authority) (with AFAD).

While countries that build their own power plants or countries that have nuclear power plants in the form of a build-operate-transfer project takes the responsibility of the first response after the accident. For the Akkuyu which building in BOO model, Rosatom has taken the shared responsibility of the necessary engineering and first emergency responses [6].

Regional crisis centre is already is currently operational for other nuclear power plants in the region.

IV. RESULTS AND DISCUSSION

In this case, following question arises. How will AFAD and NDK, which acting in accordance with Turkish laws and norms, and regional Crisis Centre's first response initiative can be coordinated to make fast and final decisions?

When we examine the regulations written earlier, one can see that the notable part is that decisions about population and health that occur after a national emergency will mostly be taken domestically; technical decisions will be taken by a structure consisting of NDK, Rosatom and the IAEA.

Although the theoretical and practical aspects do not always coincide, the fact is that the best way to make quick and correct decisions in beyond design basis accidents is to combine the expertise of all institutions. In the current situation, Akkuyu NPP prepared for emergencies with the skilful hands of Ankara, Moscow and Vienna.

V. CONCLUSIONS

Therefore, the problem only can be solve jointly. The best solution would be to create an interdepartmental organization that could make final decisions in the light of the recommendations of these organizations and the IAEA and use the abilities of both the Turkish and Russian sides only in the event of beyond design basis accidents at the Akkuyu NPP.

Given that the BOO project is being carried out in countries without a nuclear base, it is a fact that it would be the most appropriate solution to act in the same way in these projects.

VI. References

[1] Dorothy Nelkin, M. P. “Political parties and the nuclear energy debate in France and Germany”. Comparative Politics, 127-141 (1980)

[2] AP Moller, T. M. Conservation consequences of Chernobyl and other nuclear accidents. Biological Conservation, 2787-2798 (2011).

[3] Mclaughlin P.D., Jones B., Maher M.M “An update on radioactive release and exposures after the Fukushima Dai-ichi nuclear disaster”. The British Journal of Radiology, 85, 1222–1225, (2012)

[4] Brenner AV, Tronko MD, Hatch M, Bogdanova TI, Oliynik VA, Lubin JH, Zablotska LB, Tereschenko VP, McConnell RJ, Zamotaeva GA, O'Kane P, Bouville AC, Chaykovskaya LV, Greenebaum E, Paster IP, Shpak VM, Ron E. I-131 dose response for incident thyroid cancers in Ukraine related to the Chornobyl accident. Environ Health Perspect. 2011 Jul;119(7):933-9.

[5] https://cnpp.iaea.org/countryprofiles/Turkey/Turkey.htm

[6] International agreement between the government of the Russian Federation on cooperation in relation to the construction and operation of a nuclear power plant at the Akkuyu site in the Republic of Turkey

Proceedings of the European Nuclear Young Generation Forum
ENYGF'21
September 27-30, 2021, Tarragona, Spain

Feasibility of the last reactor core discharge of a PWR with three years cooling after shutdown

Sánchez Fernández, Rafael[1] and González Gandal, Rosa[2]

Naturgy Ingeniería Nuclear, Spain[1,2]

rsanchezfe@naturgy.com

I. INTRODUCTION

At the present time, several Spanish NPPs have or will have their spent fuel pools close to saturation. To unload the spent fuel, double-purpose spent fuel casks for dry storage and transportation will be provided.

The container considered in this study for PWR plants has a capacity of 32 fuel assemblies, with several loading schemes and with burn-up credit. Together with this, the licensed thermal and radiological limits require 3 years cooling time prior to be loaded in the container.

II. OBJECTIVE

The study is developed from a theoretical point of view and analyses the feasibility of unloading the last core of a PWR plant, with three years cooling time after the final shutdown of the reactor. The scope of the study is to establish a consistent methodology that can be easily applied.

To achieve the studies' objective, we have studied a strategy of mixing the 'hot' fuel assemblies (high thermal power) of the last core with the 'cold' (low thermal power) theoretically available in the pools. As an initial hypothesis, the fuel assemblies discharged from the first core are considered available. Thermal, source and shield calculations have been performed with different mixing strategies. No structural modifications have been considered in this study.

III. CONTEXT

The NPP chosen for the study had 1392 Spent FA by 2015. Figure 1 shows the Spent fuel cask's loading acceptance criteria for the inventory available after the last reactor core discharge. As seen in the figure, there are a series of spent fuel assembly batches that are in the non-accepted region.

This study aims to prove those non-accepted region fuel assemblies potentially accepted to loading with another loading pattern.

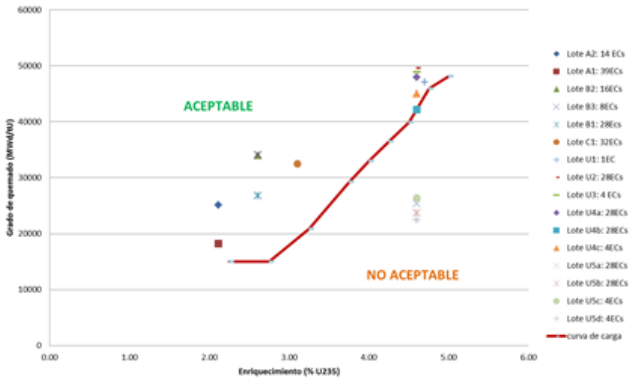

Figure 1. Spent fuel cask's loading acceptance criteria for the inventory available in the last operation cycle. Green region (above red curve) – Acceptable. Orange region (below red curve) – Not acceptable.

IV. METHODOLOGY

Methodology is divided in two distinguished steps. Model validation and customized study for Almaraz NPP.

A. Model validation

To be confident with the results, the first step is to validate that the model developed by the authors represents and reproduces the phenomenology of the spent fuel cask.

Validation has been performed in three fields: sources, shielding and thermal.

The purpose in each of the validation exercises was to quantify the error achieved comparing the cask supplier's base case against our own model.

B. Almaraz NPP customized study

The goal of the second step is to verify that the cask can hold a FA with just 3 years cooling time. For this purpose, FAs from the last reactor core (only 3 years cooling time) and from the first reactor core (around 34 years cooling time) have been selected. This configuration, mixing the coldest FAs with the hottest, is thought to be the most appropriate.

20 cold FAs of around 0.37 kW and 12 hot FA of around 2.2 kW were selected for the study.

The overall power (kW), the neutronic emission rate (n/s) and the gamma emission rate (ph/s) was checked to be below the suppliers' figures as show in Table 1.

	Almaraz NPP ad-hoc study	**Suppliers' limits**
Overall power (kW)	35.0	36.2
Neutron emission rate (n/s)	7.22E+09	2.64E+10
Gamme emission rate (ph/s)	9.93E+16	1.92E+17

Table 1. Almaraz NPP ad-hoc study vs. suppliers' limits

Regarding the thermal model validation, a broader development has been accomplished to verify that not just the peak cladding temperature is not exceeded, but the temperature of each component of the cask. For this, a finite element 3D model has been developed as show in Figure 2.**Figure**

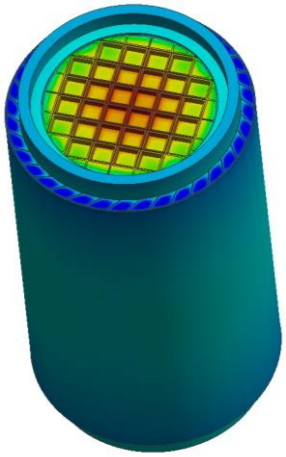

Figure 2. 3D finite element model of the spent fuel cask.

V. CONCLUSIONS

As a result of this work, Naturgy Ingeniería Nuclear has detailed and contrasted models of neutron source, shielding and thermal disciplines of the spent fuel cask. These models will allow, among other things, to carry out analysis of specific loads in reasonable time, which could be necessary to justify real margins of said loads.

In the same way, the experience acquired in this project would allow to approach the modeling of other containers in relatively short times.

It has been proven that the studied spent fuel cask would allow the discharge of the last core with three years of cooling by mixing the hottest FAs with the coldest of the first core.

It hasn't been necessary to modify the loading schemes, checking that the hot FAs of the last core can be loaded in the interior region, without modifying their capacity or their geometric arrangement, that is, it has not been necessary to mix hot and cold FAs between regions. This possibility remains as a margin in case the FAs of the first core are not available.

The total thermal load (35.0 kW) has been kept below design (36.2 kW). The FAs of the last core that go to the interior region have a maximum power of 2.26 kW, exceeding the licensed residual thermal power of 1.35 kW. Therefore, in any case it is necessary to present a modification of the spent fuel cask license to the Spanish regulatory body (CSN).

It is important to point out that in any case it will be necessary to re-license the cask for the loading of the last core regardless of the cooling time since when giving credit to the burnup there will always be FAs of the last that will not comply with the licensed load curve.

VI. References

[1] ANSYS Mechanical 17.2. User's Manual, ANSYS Ltd., 2016.

[2] ANSYS SpaceClaim R17.2. User's Manual, ANSYS Ltd., 2016.

Technical Track 3 – Radioactivity and Radiation Protection

After-Installation Qualification of Commercial Off-The-Shelf Software Linked to Spreadsheet Exports And the Everyday User - Fatal Subtraction or Easy as π?
Authors: Hylko, James M.

Characterisation of radioactive particles via electron microscopy and synchrotron-based techniques.
Authors: Okeme, Ilemona Cornelius; Martin, Peter George; Scott, Thomas Bligh

Conceptual design study and gamma ray shielding analysis of a spent fuel transportation cask for TRIGA Mark II research reactor.
Authors: Borhan, Ridhita Binte

Analysis of a wide range neutron monitor made up of two-spheres from an extended-range Bonner Sphere Spectrometer.
Authors: García-Baonza, Roberto; Gallego, Eduardo; García-Fernández, Gonzalo F.; Lorente, Alfredo; Ibáñez, Sviatoslav

Compton imaging to support a new robotic platform for mapping nuclear decommissioning sites.
Authors: Simons, Mattias; Brabants, Lowie; De Schepper, David; Demeester, Eric; Schroeyers, Wouter

Estimation of exposure to radon and the doses received by the occupants of a dwelling located in a site with a high concentration of radon.
Authors: Trull Hernandis, Cristina, Sancho Fernández, María, Arnal Arnal, José Miguel, Verdú Martín, Gumersindo1 and García Fayos, Beatriz

Radiological characterization for dismantling through robots and drones.
Authors: Fuentevilla Blanco, Eduardo

Analysis of the influence of sampling procedure in water radon measurements.
Authors: Noverques Medina, Aina; Sancho Fernández, María; Juste Vidal, Belén; Verdú Martín, Gumersindo

Development of a method for radiological characterization of airborne dust in the ceramic industry.
Authors: Sáez Muñoz, Marina; Sevilla Terrasa, Aixa; Ortiz, Josefina; Martorell, Sebastián

Portable boron meter, a non-destructive technique proposed to detect boron plugs in NPP pipes without necessity to remove heat insulators and tubes.
Authors: Karst, Maxime; Piette, Ludivine; Cerna, Cédric; Le Noblet, Thibaud; Mathieu, Ludovic; Zongo Sitrougne, Soufian; Van Dendaele, Cédric; Saintamon, Fabrice

Comprehensive management for international transport of activated components of a Cyclotron.
Authors: Rivero Torres, Javier; Arribas Sahuquillo, Juan Antonio; Mora Bastida, Benjamín

Upgrade of Radiation Protection equipment al Cofrentes NPP.
Authors: Vázquez Mora, Mª Carmen; Pedron Hernández, Enrique

Web software for assessment of individual dose to exposed type B category workers without individual monitoring.
Authors: Rivero Torres, Javier; Guardia Almenar, Vicent; Mora Bastida, Benjamín

Development of a thermodynamic sorption modelling database (TSM-DB) of radionuclide sorption on clay systems.

Authors: Castaño, Davor ; López-García, Marta; Valls, Alba; Pérez, Darío; Brassinnes, Stéphane; Duro, Lara; García, David

ADSORPTION OF 99mTcO4- ON SOLID MATRIX: HYDRODYNAMIC BEHAVIOR IN MIXING PROCESSES.

Authors: Llanes Montesino, Luis Enrique

Estimation of exposure to radon and the doses received by the occupants of a dwelling located in a site with a high concentration of radon.

Authors: Sancho, María; Trull-Hernandis, Cristina; Arnal, José Miguel; Verdú-Martín, Gumersindo; García-Fayos, Beatriz

Proceedings of the European Nuclear Young Generation Forum
ENYGF'21
September 27-30, 2021, Tarragona, Spain

After-Installation Qualification of Commercial Off-The-Shelf Software Linked to Spreadsheet Exports *And* the Everyday User - Fatal Subtraction or Easy as π?

Hylko, James M.*

JJE, LLC, USA

*Corresponding author: *JHylko1@msn.com*

I. INTRODUCTION – WHY SPREADSHEETS MATTER

Commercial off-the-shelf (COTS) software is a generic term for task-specific computer codes (e.g., bioassay calculations, evaluating environmental impacts) used in connection with accepted nuclear and non-nuclear industry practices and customarily endorsed by government agencies. Procuring qualified COTS software [1] instead of developing an in-house software coding department maximizes flexibility by obtaining the needed item or service quickly.

Raw data generated from COTS software is often exported to spreadsheets for regulatory reporting customization providing a convenient method for organizing information; from sorting relevant entries or displaying charts to calculating final results using auto-functions, formulas, and standard tools already provided in the software.

Compared to safety system software in nuclear plants having the highest level of programming requirements and the greatest need for rigorous assessment [2], modern spreadsheet calculation applications provide users having minimal programming experience with the capability to build complex program applications. However, overconfidence by the user can prevent taking steps to implement proper controls. As a result, a spreadsheet error, for example, consisting of an unchecked, incorrect formula or a broken link from multiple copy-and-paste modifications are common vulnerabilities that can negatively impact a regulatory decision. Over the past 20+ years, many universal examples have been reported across a variety of industries (e.g., medical, financial, pharmaceutical, nuclear) illustrating unfortunate consequences from uncontrolled spreadsheets [3].

- Data not controlled, 16,000 Covid-19 test results lost for a week, 08 October 2020. Risk: Contact-tracing process delayed. Discrepancy: 16,000 test cases in a week.
- Spreadsheet error led to hospital opening delay, 26 August 2020. Risk: Financial loss. Discrepancy: £16M GBP.
- Submitted bid nearly $3 million USD lower than it should have been, 27 March 2019. Risk: Bid rejection. Discrepancy: $3M USD.
- Unofficial spreadsheets land pharma plant with regulatory warning, 31 January 2017. Risk: Uncontrolled electronic spreadsheet. Discrepancy: Regulatory sanction.
- The misuse of safety critical data using spreadsheets in the nuclear fuel industry, September 1999. Risk: Nuclear site licence noncompliance. Discrepancy: Record falsification.

Therefore, user-developed spreadsheets are not just personal productivity tools, but can become important organizational assets subject to the entire software quality assurance (SQA) lifecycle process.

For the purposes of this paper, if the spreadsheet is a standard package available to every user on the desktop as a utility application and involves, for example, work-related calculations supporting a regulatory metric, the spreadsheet shall be evaluated according to:

A) Spreadsheet Application and Risk Level
B) Applying SQA Spreadsheet Export Qualifiers

Recommended headings establish structural and content consistency making it easier to understand, maintain and provide for future modifications when developing complex spreadsheets. These recommended headings are presented in:

C) Establishing Spreadsheet Consistency

C. Spreadsheet Application and Risk Level

The SQA process begins with a graded approach, defined as ensuring the spreadsheet application is commensurate with risk level expressed by:

- The relative importance to safety, safeguards, and security.
- An association with and magnitude of industrial, radiological and non-radiological hazards.
- The programmatic mission of a facility or activity.
- The particular characteristics of a facility or item.

D. Applying SQA Spreadsheet Export Qualifiers

The software user then determines if the spreadsheet meets one or more of the SQA Spreadsheet Export Qualifiers:

- Calculations or formulas used for work-related purposes where the spreadsheet is relied upon for reporting data or calculational results.
- Tracking, scheduling or status information that is relied upon for regulatory requirements or compliance.
- Relationships such as inputs / outputs or interfaces with databases or systems that perform regulatory or quality-related functions.
- Spreadsheet use impacts legal, regulatory, external milestone, or safeguards and security activities.
- Spreadsheet is the sole source of quality-related information that is required to be provided to external customers (e.g., public, stakeholder, regulator).
- Safety, operations, and / or design-related purposes that generate a quality assurance record.

This documented evaluation is then followed by classifying the spreadsheet using terms and / or letters to identify grade level, thereby distinguishing safety significance:

- Safety Related (A, B, C) - Performs a safety function as part of a structure, system, or component (SSC), or supports facility licensing conditions.
- Non-Safety Related (D) - Does not support or perform a safety function, but is still considered essential to support mission activities (e.g., regulatory reporting).
- Exempt (E) - Embedded application delivered as an integral part of an item that cannot be accessed or modified; or failure would result in negligible project risk. If the spreadsheet involved is low risk (i.e., used for convenience and efficiency) and does not meet an SQA qualifier, the user can exit the SQA process, unless entry is required for other purposes.

It is presumed that the purchased COTS software has already been evaluated for risk level and classification as part of procurement process. However, the user may still need to consider reevaluating the COTS software and linked spreadsheet export together if there are fundamental changes to the original COTS software application, thereby potentially causing changes to the original risk level and classification.

E. Establishing Spreadsheet Consistency

Generating spreadsheets are often self-taught with no formal methodology regarding structure and content. While an informal spreadsheet design may not create an immediate output error, it may cause problems later involving data entry or modifications. Recommended headings are provided that establish structural and content consistency making it easier to understand, maintain and provide for future modifications when developing complex spreadsheets.

Introductory File Information – Entering the file name, author(s), and approving authorities in the spreadsheet avoids searching for that information either electronically or viewing hardcopies.

Access Control – This limits access to spreadsheet files on a central server and assigns appropriate rights to specific departmental employees. Spreadsheets can also be password protected to restrict access and / or designated as "read only" to prevent changes to input files and formulas.

Change and Version Control – Authorized changes are controlled by the software owner and other authorized signatures. A date and revision number allows the user to know that the e-version or printout is the most recent or desired version.

Instructions – Information that details the purpose and operational points of the spreadsheet.

Table of Contents - Identifies the topics covered, including cell / tab locations to move efficiently to desired spreadsheet sections.

Modular Design and Longevity – A flowchart can be used to develop the spreadsheet. The actual electronic version of the spreadsheet should read top-to-bottom and left-to-right; identify inputs, auto-functions, formulas and macros; decision-making outputs; assumptions and error conditions. Group related topics together using titles, bolding, shading and color coding to improve spreadsheet readability. Also, design spreadsheets for longevity by having the capability to revise individual modules only when adapting to future changes.

Data Input, Cell Format Schemes, Ranges, Locations and Protection – Data may be entered into spreadsheets manually or through downloads. Define input, formula and output cell schemes and formats to reduce the probability of cell reference errors caused by moving a column or row to another position. Isolating input cells allows for changes without altering spreadsheet formulas. Locking data input and formula cells prevents inadvertent changes or modifications.

Long-Formula Decomposition - Model simplification consists of having two smaller formulas in two different cells, rather than a complicated formula in a single cell. Also, never embed constants in formulas since they can hide model assumptions and difficult to revise. Apply edit or limit checks, if applicable, to verify that the assumptions or data entered are valid and that calculated values appear reasonable. For example, [= IF (D18 > 0.50, "CHECK"," ")] which reads, if cell D18 calculates to greater than 50

percent, write CHECK in the cell, else write nothing. This improves spreadsheet integrity and confidence of results.

Test as You Go and After the Spreadsheet is Completed – Verify repeated-use, cut-and-paste formulas, templates and overall spreadsheet results match hand calculations. This establishes confidence that the sections and final product are linked correctly when combined to produce the required output. Use automated formula auditing tools that: a) trace and verify all precedent and dependent cell locations are in the formulas; b) show formulas; c) conduct error checking; and d) evaluate formulas.

Boundary Testing – This establishes application-specific upper and lower spreadsheet boundary limits (e.g., extreme inputs, 5-100x above and 0.5-0.01x below an expected application-specific value) allowing you to use the spreadsheet within those limits. Plausible changes across a set of inputs should yield expected, plausible changes in outputs, such as a 5-100x increase to a value in a linear formula should equal a 5-100x increase in the result.

Fault Injection – Purposely enter negative numbers and deliberate incorrect entries to check and correct automatic error notifications (e.g., faults, failures, overflows) and messages. Answers, such as ##### — indicates cell is to narrow; #DIV/0! — indicates a division by 0; and #VALUE! — indicates an incorrect type of argument in a function, such as a letter instead of a number has been entered into the cell.

Verification & Validation Process - Identify how the data are verified and documented using a test plan or your departmental verification and validation process (e.g., calculational peer checks) to bracket all credible capabilities and limitations.

Operating System / Software Failure – Identify proposed corrective actions ahead of time if either the operating system executing the software fails, or the software itself fails, producing an incorrect result causing, for example, a regulatory limit to be exceeded and permit violation.

Conclusions / Output – Results and any key outputs (e.g., numbers, text, files, graphs, tables, etc.) are identifiable and placed in a logical location.

SQA Lifecycle Documentation – The associated forms and authorized approval signatures certify appropriate level of documentation is maintained according to the spreadsheet application, risk level, grade and export qualifier:

- Classification / Grade
- Project Management Plan
- Verification & Validation Report
- User's Manual
- Change Request / Modifications

II. CONCLUSION

COTS software and customized spreadsheet exports have become key components of a company's reporting and operational processes. However, failing to properly evaluate a spreadsheet's application, risk level, and lacking structural and content consistency can yield incorrect results leading to unfortunate consequences. Furthermore, as processes change and new COTS software versions are issued, spreadsheet exports can potentially change the capabilities and limitations of the previously procured and evaluated COTS software requiring a reassessment of risk level and grade. Therefore, controlling spreadsheets should be equivalent to controlling procedures by providing templates and instructions for consistency. This paper provides the everyday user a consistent easy-as-π framework for developing and maintaining both COTS software and complex spreadsheet exports, thereby confirming data integrity and confidence to prevent a fatal subtraction when reporting results.

III. REFERENCES

[1] Systems and Software Engineering – Software Lifecycle Processes, International Organization for Standardization, Geneva, Switzerland, ISO/IEC/IEEE 12207:2017.

[2] Dependability Assessment of Software for Safety Instrumentation and Control Systems at Nuclear Power Plants, International Atomic Energy Agency, Vienna, Austria, IAEA Nuclear Energy Series No. NP-T-3.27, 2018.

[3] The European Spreadsheet Risk Interest Group (EuSpRIG), http://www.eusprig.org/index.htm, [Accessed April 7, 2021].

Proceedings of the European Nuclear Young Generation Forum
ENYGF'21
September 27-30, 2021, Tarragona, Spain

Characterisation of radioactive particles in coal fly ash using electron microscopy and synchrotron-based techniques

Okeme, Ilemona C.[1]; Martin, Peter G.[1] and Scott, Thomas B.[1]

[1] School of Physics, University of Bristol, United Kingdom.

*Corresponding author: ilemona.okeme@bristol.ac.uk

I. INTRODUCTION

An inherent issue that is associated with coal fly ash is the significantly-elevated level of naturally-occurring radioactive material (NORM), otherwise referred to as Technologically-Enhanced NORM (TENORM) [1]. These radio- and chemo-toxic NORMs (^{238}U and ^{232}Th, plus their decay products) occur as µm-sized particulates and constitute a commensurate human health and environmental hazard [2], making coal fly ash disposal a major global concern. Studies on the human and environmental hazards associated with NORM have been largely associated with bulk radiological characteristics - traditionally based on average bulk specific activity concentrations of the radionuclides [3]. However, this does not account for inter particle heterogeneities, leading to significantly biased inventories and risk assessments [4]. Within radiation protection and radioecology, information (at the micro and nano scales) on the form of occurrence, size, morphology and species is of utmost importance for the assessment of the source, transport, deposition, fate and the long-term environmental and human health impact of natural and anthropogenic radioactive materials [5]. Though suitable for the determination of mass concentration and specific activity of bulk radioactive materials, the traditional Inductively Coupled Plasma-Mass Spectrometry (ICP-MS) and gamma-ray spectrometry techniques do not yield this micro- and nano-scale information.

To evaluate the human and environmental risks of NORMs in coal fly ash and to demonstrate the complementarity of scanning electron microscopy (SEM) with energy dispersive spectroscopy (EDS), and synchrotron-based techniques (micro-x-ray fluorescence (µ-XRF), µ-XRF tomography and micro-x-ray absorption near edge spectroscopy (µ-XANES)) in the characterisation of radioactive materials in natural environmental system, an assessment of radioactive particles in Nigerian simulant coal fly ash was performed.

II. MATERIALS AND METHODS

Materials

The simulant coal fly ash samples characterised in this study were prepared from coal sourced from three open-pit coal mines located in Kogi state, Nigeria: the Omelewu (OM) coal mine, located in Imane, within the Olamaboro Local Government Area (LGA), and the Okaba (OK) and Odagbo (OD) mines both located in Okaba and Odagbo, respectively, within the Ankpa LGA. Fifteen coal samples were collected from each mine using a stratified random sampling methodology to ensure that samples collected were representative of the full variability within the mine. Prior to simulant fly ash preparation, the coal samples were crushed, oven-dried at 100°C, and subsequently pulverised using agate mortar and pestle and sieved using a 150 µm stainless steel sieve. To simulate coal fly ash within the laboratory, sub-samples of each pulverised and sieved coal sample (between 200 g and 400 g) in crucibles were combusted at 1,100°C using a Lenton™ muffle furnace. The simulant coal fly ash OMA, OKA and ODA were prepared from OK, OD and OM coal, respectively.

Methods

A. SEM-EDS

SEM-EDS was used to study the actinide-bearing micro-mineral phases in the simulant fly ash samples. To do this, representative composite simulant coal fly ash (OMA, OKA and ODA) bulk ash samples were prepared by depositing a fine layer of fly ash (<1 g) onto a 12 mm adhesive carbon (Leit) disc mounted on a standard SEM pin-stub. Ten subsamples, each for the simulant coal fly ash samples, were prepared in this way for analysis. The samples were then examined using a Zeiss SIGMA™ field emission SEM fitted with secondary electron (SE) (Everhart Thornley SE2) and backscattered electrons (BSE) (AsB) detectors. SEM analysis was performed at a voltage of 20 keV using a 120 µm aperture. EDS analysis

was performed at a voltage of 30 keV using a 120 µm aperture (in high current mode) and an acquisition time of 200 s; the whole surface of each identified REE and actinide mineral particle was raster-scanned, and data analysis undertaken using the associated EDAX (AMETEK Inc.) TEAM™ software. Samples examination was performed using the instrument's Variable Pressure (VP) mode, thereby avoiding the need for a conductive coating to negate surface charging that distorts the generated signal.

Using the AsB BSE detector, actinide-bearing mineral particles containing high-Z elements (e.g. U and Th) in the samples appeared as bright (white) spots against the otherwise dark (low Z) sample background. Actinide-bearing mineral particles were then identified based on their characteristic elemental composition following confirmatory EDS analysis. The elemental composition was determined using an EDAX™ Octane Plus high-resolution EDS system comprising an electronically-cooled silicon drift detector, SDD.

B. Synchrotron radiation analysis

Synchrotron radiation techniques were used to study the distribution and chemical oxidation state of uranium in the identified uranium-bearing particles, at the United Kingdom's synchrotron facility - Diamond Light Source. Synchrotron radiation µ-XRF and µ-XANES were performed on uranium-bearing particles P1 and P2 (uraninite) identified in OMA and OKA simulant fly ash samples. Out of the three monazite particles (**A**, **B** and **C**) identified in OMA, OKA, ODA, respectively, µ-XRF tomography analysis was performed on **A**. Prior to analysis, in-situ isolation of P1, P2 and monazite particle **A** from the bulk simulant coal fly ash was performed using a Kleindiek MM3A micromanipulation system installed within the SEM instrument. This system is able to significantly enhance the resolution and quality of the results obtained when compared to conventional speciation analysis of radioactive particles within 'bulk' coal fly ash materials. This device was used to control an extruded glass capillary with a tip diameter of approximately 1 µm. To negate the effects of electron beam induced charging effects, the non-conductive extruded glass capillary was coated with approximately 2 nm of sputter-deposited gold.

The lift-out process reported in Martin et al [6] was used in this work to extract the radioactive particles, utilising the electron-beam hardening adhesive SEMGlu™. A schematic of the isolation process is presented in Figure 1. Each of the particles extracted from the bulk simulant coal fly ash (still adhered to a glass capillary needle) was securely enclosed in Kapton™ tape in preparation for subsequent synchrotron radiation analysis.

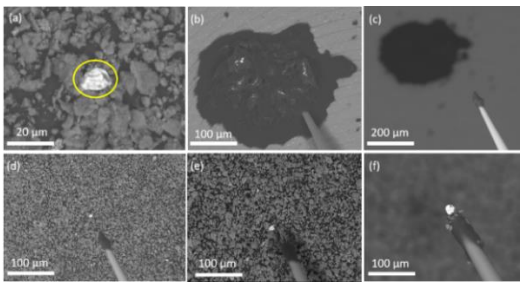

Figure 1. In-situ mineral particle isolation process performed within Zeiss SIGMA VP SEM using Kleindiek MM3A micromanipulator: (a) locating particle using BSE detector and co-incident EDS; (b) and (c) applying small quantity of electron-beam-hardening SEMGluTM to extruded tip of glass capillary; (d) and (e) progressively lowering glass capillary to approach particle; (f) removing particle from surrounding bulk material, attached to capillary tip.

III. RESULTS AND DISCUSSION

A. SEM-EDS

Figures 2, 3 and 4 show the results of SEM-EDS analysis of uranium-bearing particles (P1 and P2), thorium-bearing (thorite) particle (P3) and monazite particle (**A**, **B** and **C**), respectively. These particles existed in discrete form (with sizes between 10 µm and 80 µm), dispersed within the fly ash samples. The weathered, pitted and cracked surface morphologies of these radioactive particles indicate the tendency to further fragment into more smaller fragments (particulate matter with diameter ≤2.5, PM2.5), thereby increasing the risk of inhalation and the localised radiation dose, if particulates should be carried into the air. Trace amounts of Th and U were found in the monazite particles **A** (4.0 ± 0.2, 1.3 ± 0.12), **B** (2.67 ± 0.24, 0.93 ± 0.09) and **C** (2.53 ± 0.31, 0.52 ± 0.06).

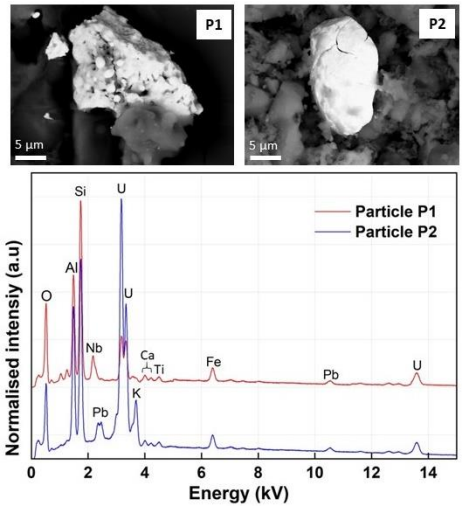

Figure 2. (top) Backscattered electron images of two uranium-bearing particles (P1 in OKA, P2 in OMA). (bottom) Associated EDS spectra with emission peaks identified.

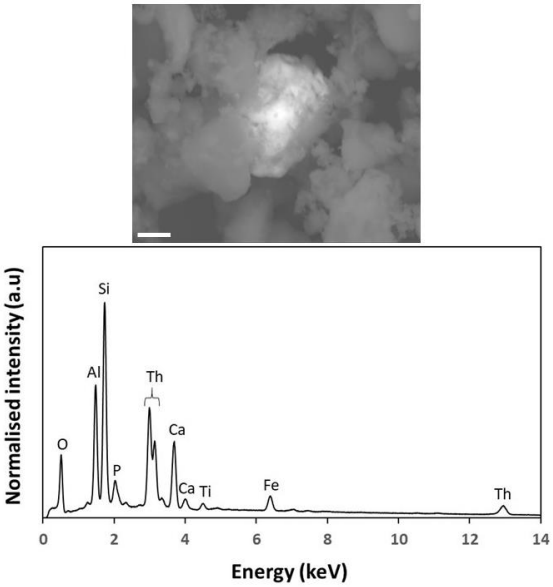

Figure 3. (top) Backscattered electron image of Thorite particle (P3 in OMA). (bottom) Associated EDS spectrum with emission peaks identified. Scale bar = 2 µm.

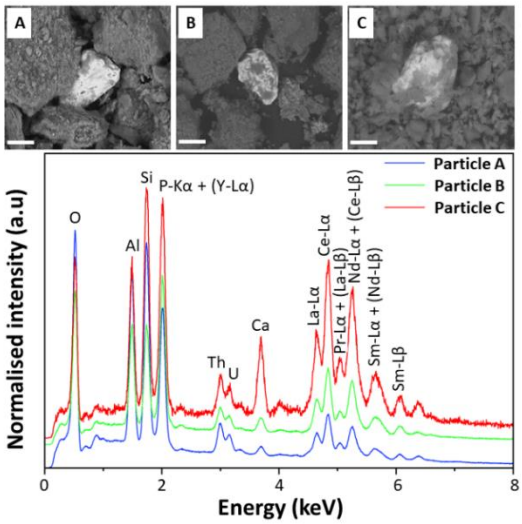

Figure 4. (top) Backscattered electron images of monazite particles (A, B, C) in OMA, OKA, ODA, respectively; (bottom) Associated EDS spectra, with emission peaks identified. Scale bars = 50 µm.

B. Synchrotron analysis

The µ-XRF analysis of P1 (Figure 5) shows the particle matrix to be composed of a homogenous distribution of U, with regions of higher U concentration (brighter regions); this is as a result of the botryoidal surface morphology of P1. Similarly, µ-XRF analysis of P2 (Figure 6) showed a homogeneous distribution of U (red region), colocalising with low levels of Th (indicated by the yellow region). The implications of the homogenous distribution of U in P1 and P2 is the expectedly high leaching rate of surface-bound U due to the high surface area to volume ratio of the micro-scale particles.

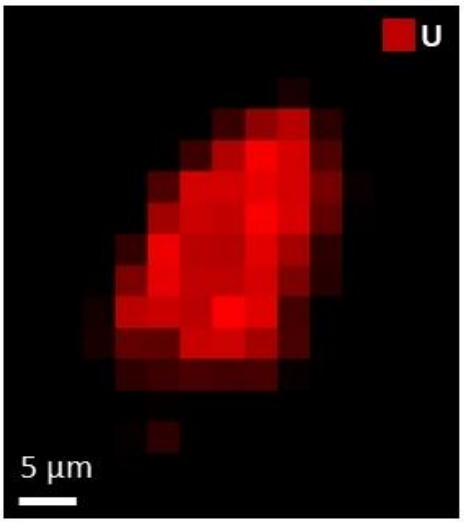

Figure 5. µ-XRF plot of particle P1.

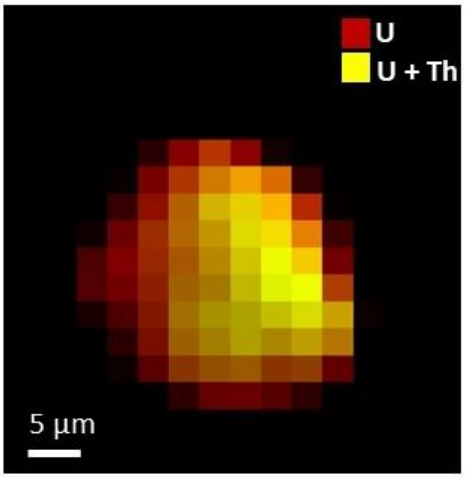

Figure 6. µ-XRF plot of particle P2.

From the µ-XANES spectra of P1 and P2 alongside the spectrum of a UO_2 reference material (Figure 7), the spectra of both P1 and P2 show a main peak at 17,176 eV (labelled as point X), with a subtle peak at 17,216 eV (point Y). These peaks match perfectly with the UO_2 standard spectrum [7], which shows that U exists in the IV oxidation state in both particles. In studies of bulk UO_2 in the environment, the existence of U in the IV oxidation state typically implies low mobility and solubility of U. However, the fact that UO_2 in the coal fly ash is micro-scale means that when it is exposed to rain, meteoric waters and oxidising environmental conditions, changes in the oxidation state could quickly result.

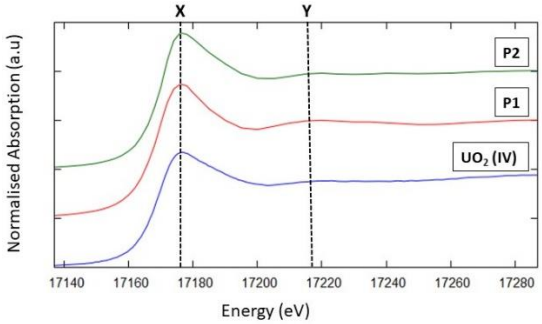

Figure 7: XANES plot of P1 and P2 alongside UO_2 reference spectrum.

From the result of μ-XRF tomography of the monazite particle A (Figure 8), both, Th and U, were observed to exist strongly colocalised in the interior of the monazite particle, while being simultaneously depleted around its surface, with the rare earth elements Ce, La concentrated on the particle surface - surrounding the Th and U. The implication of surface depletion of U and Th in monazite particles is that leaching of both elements into the environment from these resistate monazite particles would be insignificantly very low.

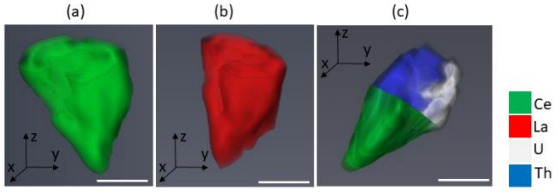

Figure 8: Cut sections of 3D volumetric renderings of monazite particle A showing the core-shell pattern. (a) and (b): hollow interior within Ce and La volumetric renderings. (c): Ce outer shell with U and Th components within the core. Scale bars = 25 μm.

IV. CONCLUSION

This work has determined the occurrence of actinide-bearing particles and the distribution and oxidation state of U in simulant coal fly ash. Microparticles of uraninite, thorite and monazite were found within the simulant fly ash, with the tendency to disintegrate into the more harmful PM2.5. The concentration of U and Th in the interior of monazite particles implies insignificant leaching of both elements into the natural environment. U was found to be homogeneously distributed in the uraninite particles, existing in the insoluble and immobile IV oxidation state. Though, U(IV) oxide mineral species is recognised to be relatively immobile due to low solubility, the homogenous distribution of U in microparticles P1 and P2, alongside their high surface area to volume ratios, has the consequence of high risk of localised radiation dose delivery (when inhaled or in contact with the body) and a high leaching rate of surface bound U, polluting drinking waters. Based on the analysis presented herein, it is strongly recommended that the coal fly ash derived from burning these Nigerian coal types should be carefully managed to limit meteoric leaching.

V. REFERENCES

[1] NORM.https://www.world-nuclear.org/information-library/safety-and-security/radiation-and-health/naturally-occurring-radioactive-materials-norm.aspx (2020).

[2] USGS. Radioactive Elements in Coal and Fly Ash: Abundance, Forms, and Environmental Significance. Fact sheet FS-163-97, 4 pages, 1997.

[3] N.E. Lauer, J.C. Hower, H. Hsu-Kim, R.K. Taggart, A. Vengosh. NORM in coals and coal combustion residuals in the United States. Environ. Sci. Technol., vol. 49, pp. 11227-11233, 2015.

[4] IAEA. Radioactive particles in the environment: Sources, particle characteristics and analytical techniques. IAEA-TECDOC-1663 Vienna, page 2, 2011.

[5] B. Salbu et al. Challenges associated with the behaviour of radioactive particles in the environment. J. Environ. Radioact., vol. 186, pp.101-115, 2018.

[6] P.G. Martin et al. In-situ removal and characterisation of uranium-containing particles from sediments surrounding the Fukushima Daiichi Nuclear Power Plant. Spectrochimica Acta Part B: Atomic Spectroscopy, Vol. 117, pp. 1-7, 2016.

[7] International X-ray Absorption Society, XAFS materialsdatabase. http://ixs.iit.edu/database/data/Farrel_Lytle_data/RAW/U/index.html.(Accessed 6 March 2019).

Proceedings of the European Nuclear Young Generation Forum
ENYGF'21
September 27-30, 2021, Tarragona, Spain

Conceptual Design Study and Gamma-ray Shielding Analysis of a Spent Fuel Transportation Cask for TRIGA Mark II Research Reactor

Borhan, Ridhita*, Hossain, Hasibul and Mollah, A.S.

Department of Nuclear Science and Engineering

[1]Military Institute of Science and Technology (MIST), Dhaka Bangladesh

*Corresponding author: *ridhitabinte@gmail.com*

I. INTRODUCTION

The TRIGA Mark II of the BAEC (Bangladesh Atomic Energy Commission)- the only research reactor of Bangladesh has been operating since 1986, without any reshuffling or reloading till the present day. The reactor is designed for continuous operation at a steady thermal power level of 3 MW. Since commissioning, the total burnup of the reactor has been approximately 850 MWD. For the continuous operation of a nuclear reactor, burnt fuel needs to be replaced with fresh fuel, where appropriate fuel transfer device is required. The current TRIGA core filled with spent fuels must be emptied before fresh fuels take in place. The spent fuels will be transferred from current reactor core into spent fuel pool using fuel transfer cask to provide a safe transfer operation. The process of transferring spent fuels into Spent Fuel Pool requires a fuel transfer cask. The purpose of a fuel transfer cask is to provide a short-term safe storage of an irradiated fuel and a safe container for transportation of the fuel outside TRIGA reactor site. A fuel transfer cask, for transferring the spent nuclear fuel element within the reactor hall, is still unavailable at the TRIGA reactor facility. A conceptual design study has been made of a spent fuel transfer cask for the TRIGA spent fuel [1].

The conceptual cask in this paper has been designed keeping the ALARA principle and the attenuation co-efficient in mind. The objectives of this work have been:

i. To perform the conceptual design study of BAEC TRIGA spent fuel transfer cask by using a designing software;

ii. To simulate the conceptual design cask for gamma-ray dose calculation based on multi-layer concept by using Monte Carlo GEANT4 code developed by CERN;

iii. To compare the dose rate with regulatory dose limits as per ALARA principle.

II. METHODOLOGY

Many countries have conducted their research work on designing and modifying transportation casks. These casks have been used simply for moving the spent fuel from the reactor core to the spent fuel pools (SFP) or to carry the spent fuel to reprocessing plants; in addition to that, they are utilized as temporary spent fuel storage. Most of these research works are mainly focused on the spent fuel that are originated from commercial nuclear power plants (NPPs). Only a handful number of studies have acknowledged the handling of spent fuel that are produced from research reactors.

This study is mainly focused on the gamma-ray shielding analysis of a coneptual Transportation cask for the spent fuel of BAEC TRIGA Reactor. A brief description of the cask design and gamma-ray shielding analysis is given in the following sub-section:

A. Source Term

The source term of the BAEC TRIGA Mark-Ⅱ reactor was evaluated using an ORIGEN 2.1 code, which lead to a total core inventory of 2.76E+18 Bq [4]. There are 95 fuel rods in the core of BAEC TRIGA Reactor. Among these, "C08" fuel rod has the highest burnup [5] of 23.84% [1], (of its initial U-235 content) which yields a total activity of 2.4E+16 Bq. So, C08 fuel rod will have to be replaced first and it is going to pose maximum dose to the workers compared to other Spent fuel rods. Shielding calculation for this fuel rod will ensure maximum radiation protection. The standard TRIGA fuel element contains homogeneous 20% enriched U-ZrH mixture as shown in Figure 1. The fuel section of the fuel elements is 38.1 cm (15 inches) in length and outer diameter is 3.63 cm (1.43 inch).

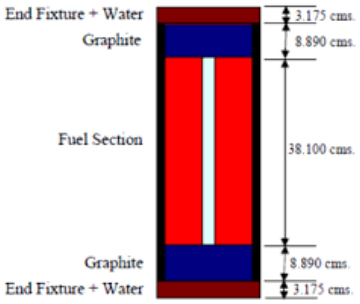

Figure 1. TRIGA Fuel Element.

The average photon energy of the fission products is 0.752 MeV which was evaluated using the ICRP database [6] and the activity of fission products from the source term calculation. This calculated result is in well agreement with other literature values [7-8].

B. Shielding Material Selection

If the cask can be manufactured domestically using indigenous materials then the expenses will be much lower compared to an imported cask from a foreign company. Importing raw materials for the cask will also increase the expenses, so local availability of the shielding materials of the cask is a major factor. Shielding properties such as density and linear attenuation co-efficient are also vital in the selection of a material for gamma-ray shielding. A number of materials were considered for this study; but based on the cost, density and attenuation properties, Aluminium (Al), Iron (Fe) and Lead (Pb)were selected.

Attenuation properties for these three shielding materials have been shown in Table 1. From this table, it can be seen that, 1 cm of Pb is equivalent to 1.98 cm of Fe, and 5.67 cm of Al. Keeping this equivalency of thickness in mind, the thickness of the three layers has been iteratively increased in table 3 to find out the optimum size of the cask.

Table 1. Attenuation properties of shielding materials at 752 keV photon energy.

Material	μ/ρ (cm^2/gm)	μ (cm^{-1})	mfp (cm)
Al	0.0704	0.190	5.26
Fe	0.0691	0.544	1.84
Pb	0.0949	1.08	0.928

C. Simulation Setup

Geant4 which stands for "Geometry and Tracking" is a toolkit for the simulation of the passage of particles through matter using Monte Carlo methods. It uses object-oriented programming (C++). It offers its users a set of functionalities including tracking of particles, physics models, varied types of sensitive detectors etc. [9]

The setup of the simulation for this study has been shown in figure 1. A cylindrical volumetric source has been used in the simulation to replicate the spent fuel rod. A standard ICRU sphere of 30 cm diameter has been used as the phantom for measuring the ambient equivalent dose, H*(10). Figure 2 demonstrates a typical multilayer shield that has been used in the simulation. In case of single and double layer shields the multilayer shield was replaced by a single or double layered slab. The distance of the detector and source from the shield has always been kept constant.

The equivalent dose at a distance of 2 meter from the source has to be within 0.1 mSv. Without any shielding, the equivalent dose at 2m distance from the source is 420 mSv; so, the cask must reduce the equivalent dose by a factor of 4.2E+4.

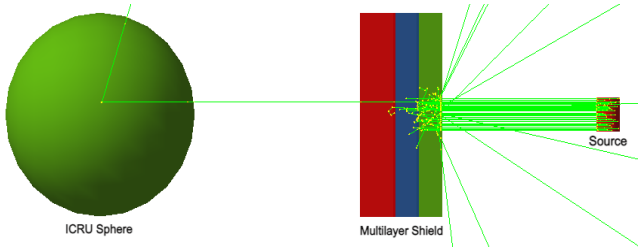

Figure 2. Simulation setup in GEANT4 for gamma-ray shielding analysis of a typical multilayer shield.

III. RESULTS AND DISCUSSION

To check whether the simulated results are conforming to experimental results within an acceptable limit or not, a comparison study has been conducted before performing the simulation of the gamma-ray shielding analysis. After it was ensured that GEANT4 provided results within an acceptable limit of uncertainty, gamma-ray shielding analysis has been performed for single, double and multi-layered shields. After finding out the most optimum arrangement of layers in the cask, multiple runs were performed in the GEANT4 to find out the overall thickness and height of the cask that would meet the required dose limits.

A. Comparison Study of Shielding Property

Geant4 (ver. 10.7) along with "G4EmLivermore" physics model has been used in this work. To validate the setup of the simulation, the linear attenuation coefficient of different materials have been calculated and compared with the standard values from NIST database [10]. The deviation between the two data has been shown in Table 2.

Table 2. Comparison between simulation result and standard value of linear attenuation coefficient for varied energy sources.

Energy (keV)	Linear attenuation coefficient (cm^{-1})					
	Aluminium		Iron		Lead	
	Geant4	Std.	Geant4	Std.	Geant4	Std.
59.5	0.69	0.76	9.25	9.69	55.63	58.16
279.1	0.27	0.29	0.82	0.90	4.99	5.32
662	0.193	0.202	0.547	0.578	1.17	1.25
1173	0.14	0.15	0.38	0.44	0.63	0.70
1274.5	0.132	0.146	0.37	0.42	0.59	0.66
1332	0.135	0.144	0.384	0.407	0.598	0.634

From Table 2, it can be seen that the results of the simulation are in well agreement with the standard ones. The setup of the simulation for the comparison study has been shown in figure 2. Instead of an ICRU sphere, a NaI scintillation detector was used for this simulation to record the absorbed dose.

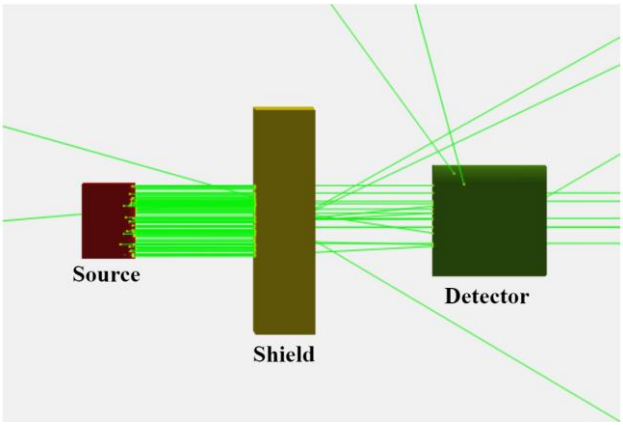

Figure 3. Simulation setup in GEANT4 for the comparison study of shielding property.

B. Simulation of conceptual design cask

Shielding effectiveness of single, double and multilayer shielding has been compared in this study. From Geant4 simulation, it has been found that triple layer shielding is more effective tan double and single-layer shielding; specially the Fe-Pb-Al arrangement is more effective than other shielding arrangements. The ambient equivalent dose, H*(10), for all types of shielding arrangements has been normalized and is shown in Figure 3. Fe-Pb-Al shield is almost 2 times more effective tan traditional single layer Pb shielding and 1.2 times more effective than Fe-Pb double layer shield.

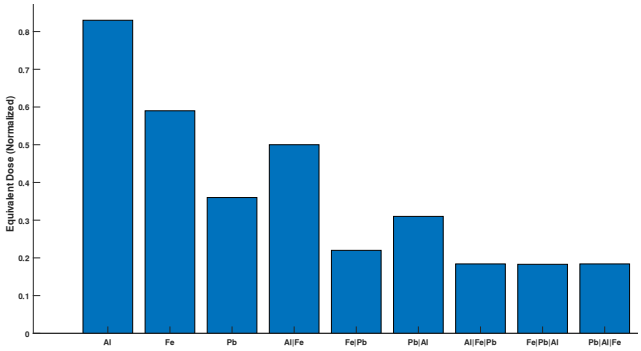

Figure 4. Normalized equivalent dose for different arrangements of single, double and triple layer shielding.

A simple iterative technique has been used to find out the optimum size of the cask where the thickness of different layers is increased in every run of Geant4. The ambient dose equivalent for each run is shown in Table 3. In each run, 10^9 particles are simulated.

Table 3. Dose obtained from Geant4 for different arrangements of Fe-Pb-Al shield and error in results

Thickness (in mfp)	Ambient Dose Equivalent, H*(10) (mSv)	Error (%)
No shield	5.72E-6	0.00058
1 Fe+1 Pb +1Al	3.96E-7	0.0042
2 Fe+1 Pb+1 Al	1.62E-7	0.0066
3 Fe+1 Pb+1 Al	6.69E-8	0.0103
3 Fe+2 Pb+1 Al	2.59E-8	0.0165
3 Fe+3 Pb+1 Al	1.04E-8	0.0262
3 Fe+4 Pb+1 Al	4.02E-9	0.0421
3 Fe+5 Pb+1 Al	1.66E-9	0.0663
3 Fe+6 Pb+1 Al	5.49E-10	0.114
3 Fe+6 Pb+2 Al	3.11E-10	0.146
4 Fe+6 Pb+2 Al	1.03E-10	0.26

It can be concluded that, a cylindrical cask with a radius of 27.1 cm would be enough to reduce the gamma-ray radiation dose by a minimum factor of 4.2E4; where, the thickness of Al, Fe and Pb will be respectively 10.52 cm, 7.36 cm and 5.57 cm and the diameter of the fuel rod is 3.63 cm. The height of the fuel rod is about 38.1 cm, so the overall height of the cask will be 85 cm.

C. Conceptual Design

Based on simulation by GEANT4, a conceptual transport cask has been designed with the total height and width of the proposed layers in this work. Figure 5 provides an overall view of the conceptual design of the cask.

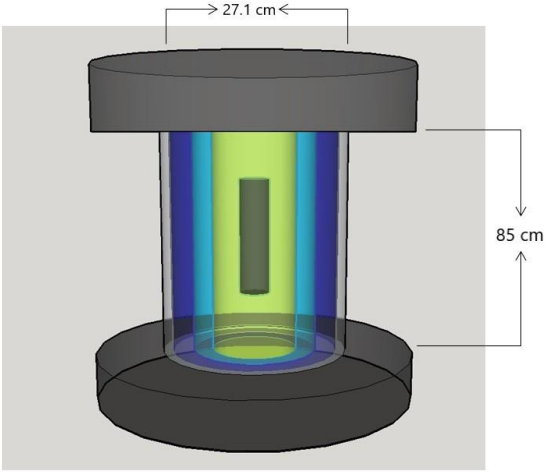

Figure 5. Outer layers of the transportation cask designated by different colors.

Figure 6 provides a cross- sectional view of the transport cask. As it can be seen from the figure, the yellow color denotes an iron metal layer, the green layer is lead, the blue one is aluminium, and the outermost layer is made of stainless steel. A cylindrical shaped fuel basket is also provided keeping in mind the single fuel rod arrangement

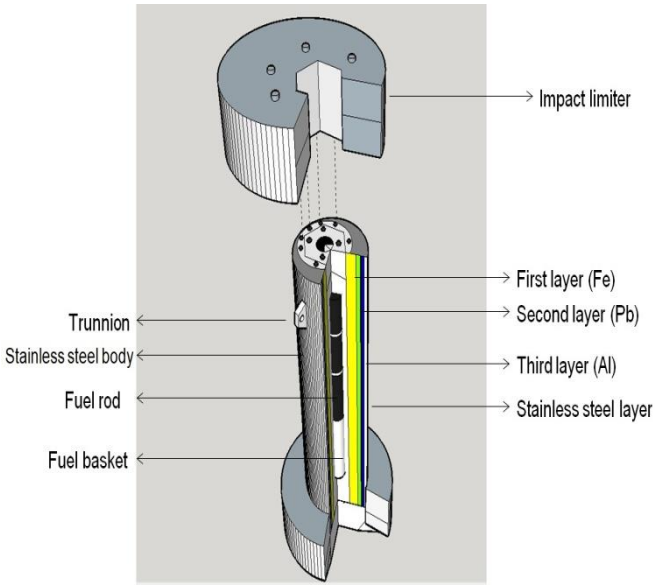

Figure 6. Cross-sectional view of the spent fuel transportation cask.

IV. CONCLUSION

For in-core fuel management of BAEC TRIGA reactor, high burn-up fuels would need to be replaced with fresh fuels in order to maintain the criticality condition for smooth operation of the reactor. The process of transferring spent fuels from TRIGA reactor into Spent Fuel Pool requires a fuel transfer cask. A fuel transfer cask, for transferring the spent nuclear fuel element within the reactor hall, is still unavailable at the TRIGA reactor facility. A conceptual design study based on multilayered shielding concept has been made of a spent fuel transfer cask for the TRIGA spent fuel. The radiation shielding analysis of the TRIGA spent fuel transfer cask was carried out using the Monte Carlo code GEANT4 developed by the CERN. Shielding materials used in the calculations were lead (Pb), iron (Fe) and aluminium (Al). It is found that the total dose rates are below the normal transport criteria that meet the standards specified. This cask holds one spent fuel element for the TRIGA reactor. This conceptual cask design can be modified to accommodate more tan one spent fuel element. However, the conceptual design will remain the same as that of multilayered based concept.

It is recommended that the design should be verified by other computer codes [10-11] before the detailed design of the cask is finalized due to sizing issues. In future, thermal performance analyses with a standard code and verifying tests should be carried out to improve the structural integrity of the cask. Further studies are needed to check radiation exposure level after the spent fuel is in the cask so that a best dimension can be proposed.

V. REFERENCES

[1] Borhan R., Hossain H. and Mollah A.S., "Conceptual Design Study and Gamma-ray Shielding Analysis of a Spent Fuel Transportation Cask for 3 MW TRIGA MARK II Research Reactor", B.Sc. Thesis, Dept. of Nuclear Science and Engineering, MIST, 2021.

[2] A. Mohammadi, M. Hassanzadeh and M. Gharib, "Shielding calculation and criticality safety analysis of spent fuel transportation cask in research reactors", *Applied Radiation and Isotopes*, vol. 108, pp. 129-132, 2016.

[3] K. S and D. I, "Cask Selection for Spent Nuclear Fuel Shipment from Research Reactor", *Journal of Nuclear Energy Science & Power Generation Technology*, vol. 06, no. 02, 2017.

[4]Rahman, M., Jahan, N. and Huda, M., "Source Term Evaluation for the TRIGA Mark-II Research Reactor of Bangladesh Using ORIGEN 2.1 Code," *NUCLEAR SCIENCE AND APPLICATIONS*, vol. 26, pp. 33-37, 2017.

[5] ICRP Publication 107, "Nuclear Decay Data for Dosimetric Calculations", *Annals of the ICRP*, vol. 38, 2008.

[6] Lamarsh, J. and, Baratta A., "Introduction to nuclear engineering*"*, 3rd ed., pp. 84, 2009.

[7] Schaeffer, N. M., "Reactor Shielding for Nuclear Engineers", U. S. Atomic Energy Commission of Information Services, pp. 52, 1973.

[8] Agostinelli, S., Allison, J., Amako, K. and Apostolakis et. al.,"Geant4—a simulation toolkit", *Nuclear Instruments and Methods in Physics Research Section A: Accelerators, Spectrometers, Detectors and Associated Equipment*, vol. 506(3), pp. 250-303, 2003.

[9] Hubbell, J. and Seltzer, S., "Tables of X-Ray Mass Attenuation Coefficients and Mass Energy-Absorption Coefficients 1 keV to 20 MeV for Elements Z = 1 to 92 and 48 Additional Substances of Dosimetric Interest," http://physics.nist.gov/PhysRefData/XrayMassCoef/cover.html, [online], (Accessed March 10, 2021)

[10] Chaobin Chen, Qi Yang, Bin Wu, Yuncheng Han, Jing Song, FDS Team, Validation of Shielding Analysis Capability of SuperMC with SINBAD, EPJ Web of Conferences 153, 02009, (2017).

[11] LA-UR-03-1987, MCNP – A General Monte Carlo N Particle Transport Code, Version 5, Release 1.40, (2005).

Proceedings of the European Nuclear Young Generation Forum
ENYGF'21
September 27-30, 2021, Tarragona, Spain

Analysis of a wide range neutron monitor made up of two-spheres from an extended-range Bonner Sphere Spectrometer

García-Baonza, Roberto[1*], Gallego, Eduardo[1], García-Fernández, Gonzalo F.[1], Lorente, Alfredo[1] and Ibáñez, Sviatoslav[1]

[1] Departamento de Ingeniería Energética, ETSI Industriales, Universidad Politécnica de Madrid, Spain

*Corresponding author: *roberto.gabaonza@upm.es*

I. INTRODUCTION

The large variability of dose quantities with neutron energy [1] obliges the use of reliable monitoring systems of neutron radiation with radiation protection purposes. The stray neutron radiation is very important in medical facilities like radiotherapy or protontherapy facilities, where neutron energies cover a wide range of energies [2-3].

In compact protontherapy facilities, the main concern about radiological protection is stray radiation from high energy neutrons [4]. This high energy neutron radiation must be monitored using wide range rem-meters [5] and extended-range Bonner Sphere Spectrometers (BSS) [6-7].

The lack of extended-range BSS in Madrid, and the installation of the two first Spanish protontherapy facilities in this region [8], promoted the idea of Universidad Politécnica de Madrid (UPM) of designing and constructing an own system of extended-range BSS (UPM-BSS), modifying a previous BSS system [9]. The design and the preliminary characteristics and considerations of this extended-range BSS can be consulted in [10].

The construction of the extended-range UPM-BSS was successfully completed in the last quarter of 2020, and the first experimental tests are already being carried out at the UPM neutronics hall (LMN-UPM) [9].

This communication pretends to cover another field of application of this UPM-BSS. Apart from neutron spectrometry, this system of spheres can also be used in the design of a wide range neutron monitor made up of two-spheres. This kind of systems, formed by more than one sphere/monitor or active volume, have been widely studied in the last decade, with great interest in neutron dosimetry.

According to the above, the objective of this work was the development of a wide range neutron monitor based on the new UPM BSS. Nowadays, there is a substantial increase of technological applications where neutron fields of a very wide range of energies are generated, from thermal to high energies with hundreds of MeV.

II. MATERIALS AND METHODS

The extended-range UPM BSS is constituted by 6 conventional HDPE spheres [9] plus two of the extended-range spheres proposed in [10], both with a lead spallation layer, copper is not a viable option [10]. In these spheres, the detector is a ^{6}LiI(Eu) crystal scintillator, although it is also possible to replace this crystal with gold foils for neutron detection. The nuclear reaction of interest, for neutron detection, in this cylindrical crystal scintillator (0.4 cm x 0.4 cm Ø) is the reaction $^{6}Li(n,\alpha)^{3}H$.

The two extended-range spheres are modifications to the 7.62 cm and 12.7 cm diameter conventional HDPE spheres of the UPM BSS. The modifications of these two spheres are summarized in Table 1, and an illustration to visualize the design of these spheres is shown in [10].

Table 1. Modifications to the 7.62 cm and 12.7 cm diameter conventional HDPE spheres of the UPM BSS.

Internal sphere of 7.62 cm (8''(1''Pb))	Internal sphere of 12.7 cm (12''(1''Pb))
Addition of a 7.62 cm i.d. and 12.7 cm o.d. shell composed by lead (11.25 g/cm^3) and a 12.7 cm i.d. and 20.32 cm o.d. shell of HDPE.	Addition of a 12.7 cm i.d. and 17.78 cm o.d. shell composed by lead (11.25 g/cm^3) and a 17.78 cm i.d. and 30.48 cm o.d. shell of HDPE.

Note: i.d. – internal diameter / o.d. – outer diameter

The shells of lead of these two extended-range spheres (Table 1) are not bordered by a thin aluminum layer, as was proposed in the preliminary design [10].

The response functions of these two extended-range spheres have been recalculated for this work using the MCNP6.1 code [11]. Moreover, the response functions of two conventional HDPE spheres, 7.62 cm (3''HDPE) and 30.48 cm (12''HDPE) diameter spheres, have also been recalculated with MCNP6.1. All the calculi have been carried out using the methodology expressed in [10] for obtaining these functions, but changing the irradiation model. Hence, the number of counts has been estimated

imposing a tally multiplier (MT105) in the calculus of the neutron fluence on the ^{6}LiI(Eu) crystal scintillator.

In the present work, the ENDF/B-VII.1 nuclear-data library [12] has been used for defining all the nuclides, except for hydrogen (ENDF/B-VI.8). Thermal scattering law S(α,β) has been taken into account in polyethylene through the ENDF71SaB thermal cross-section library card poly.20t.

The simulation with MCNP6 of the response of the 4 spheres mentioned above has been carried out for 56 neutron energies, between 10^{-9} MeV and 230 MeV, following the irradiation model described in [13] (disk monoenergetic neutron source). A spline interpolation technique has been used in this work for constructing the response function of each sphere from the 56 points of these functions calculated by MCNP6.

The simulation of neutron transport with MCNP6 [14] up to neutron energies of 230 MeV requires the use of physics models (intra-nuclear cascade models + evaporation models). This fact is a consequence of the limited energy at which many libraries are processed (20 MeV or 150 MeV in this case).

The intra-nuclear cascade model applied in this work for neutron energies higher than 20 MeV, through the MCNP6 mix & match capability, has been the CEM03.03 with its GEM evaporation model associated by default in MCNP6. The application of different physics models can be an origin of discrepancies in Monte Carlo simulations [10][15]. Another source of uncertainty, apart from the physics models, are the nuclear data libraries used in the calculi [3].

The simulations have been performed with a number of histories enough to obtain relative statistical uncertainties lower than 1%. Hence, all the simulations have passed the MCNP 10 statistical checks for the tally fluctuation chart bin result.

The algebraic methodology described in [16] for an accurate and portable solid state neutron rem-meter has been implemented for this work in MATLAB [17], to combine the response functions. This methodology has allowed calculating a theoretical calibration factor for each sphere in each combination of two spheres, which allows obtaining a dose response function for each combination of spheres.

Moreover, a theoretical calibration factor, for an ^{241}Am/^{9}Be neutron source, has been estimated for the two extended-range spheres, 8''(1''Pb) and 12''(1''Pb), in order to determine their theoretical dose response functions. The ^{241}Am/^{9}Be neutron source has been defined in MCNP following the MCNP definition for this source employed in [9], which is a benchmarked simulation model.

The relative dose response functions of the best combination of spheres and of the sphere 12''(1''Pb) have been obtained to quantify how good is this best combination of spheres. These functions have been obtained by dividing the values of their dose response functions into the values of the ICRP74 fluence-to-ambient dose equivalent conversion function [1], which have been calculated by MCNP6.1 for the same neutron energies.

III. RESULTS

The response functions, of the different spheres mentioned before and analyzed in this work, are shown in Figure 1.

The dose response functions obtained combining the response functions of two spheres, using the methodology described in [16] and implemented for this work in MATLAB, are shown in Figure 2. In Figure 2, these dose response functions are compared with the calculated dose response functions of spheres 8''(1''Pb) and 12''(1''Pb), the ICRP74 fluence-to-ambient dose equivalent conversion function [1] and the WENDI-II [18] dose response function calculated in [19]. A comparison of the WENDI-II dose response function with other commercial monitors can be found in [20].

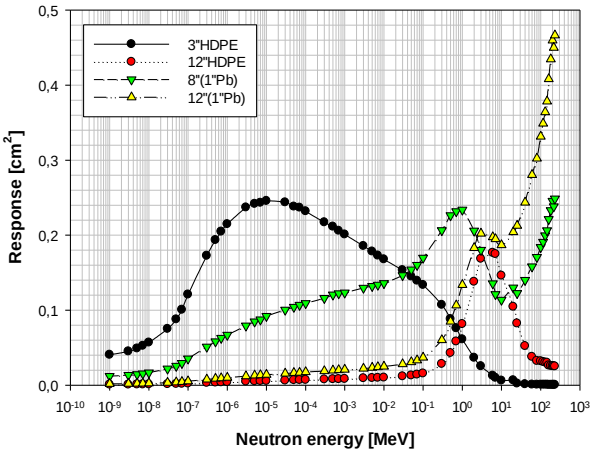

Figure 1. Calculated response functions of the different spheres.

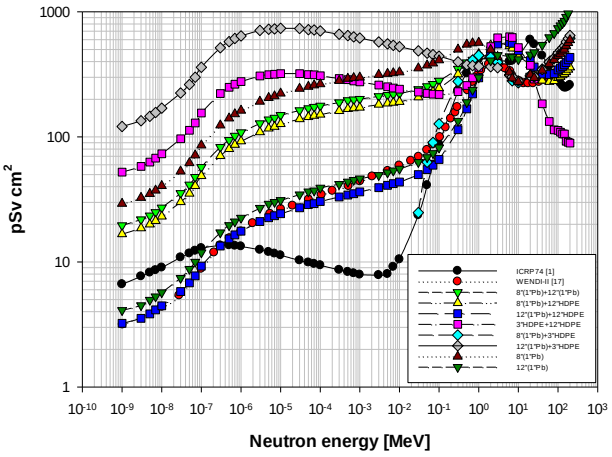

Figure 2. Dose response functions of different two-spheres neutron monitors, of the extended-range spheres, and the WENDI-II rem-meter, together with the ICRP74 fluence-to-ambient dose equivalent conversion function.

The relative dose response functions obtained for the best combination of spheres (12''(1''Pb) + 12''HDPE), and the sphere 12''(1''Pb), are shown in Figure 3, between 10^{-9} MeV and 200 MeV. This graph also shows a baseline, equal to 1 for all the neutron energies, in order to help to quantify the deviations of the dose response functions with respect to the ICRP74 fluence-to-ambient dose equivalent conversion function.

The dose response function of this combination (12''(1''Pb) + 12''HDPE) presents the lowest levels of overestimation in the thermal and epithermal ranges of energy, and this function also has a very interesting similarity to the WENDI-II dose response function calculated in [19]. These reasons and its best adjustment to the ICRP74 function motivated the selection of this combination.

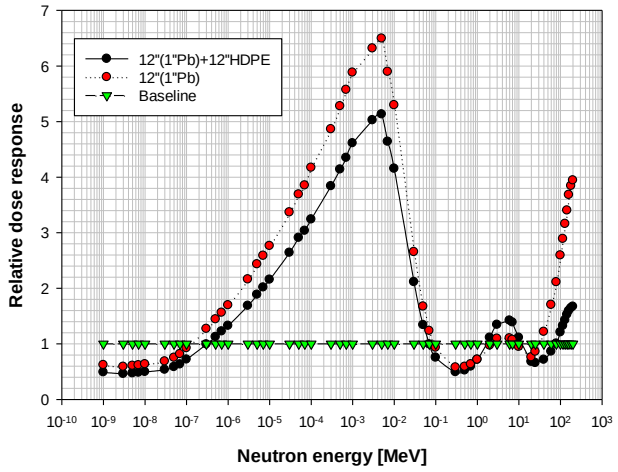

Figure 3. Relative dose response functions of the best combination of spheres (12''(1''Pb) + 12''HDPE) and the sphere 12''(1''Pb).

IV. DISCUSSION

The similarity of the response functions obtained in this work (Figure 1), and the response functions obtained in [10], demonstrates how for the analysis of Bonner spheres the irradiation model used in this work and the irradiation model employed in [10], based on [5], are equivalent. Both irradiation models provide practically the same results because, for Bonner spheres, the cone irradiation models are able to fit their neutron emissions to the dimensions of the spheres, the same does not happen for cylindrical monitors.

The response functions of the two extended-range spheres (Figure 1) confirm the range extension of these spheres, a consequence of the lead spallation layer introduced in their configurations. This range extension is not observed for the rest of the spheres (conventional HDPE spheres), their response functions for neutron energies higher than 10 MeV do not have a positive slope due to the lack of a spallation layer.

The results shown in Figure 2 demonstrate how the conceptual idea proposed in this work of using the extended-range UPM BSS for constructing a wide range neutron monitor made up of two-spheres is viable. The dose response function obtained by the combination of one of the extended-range spheres (12''(1''Pb)) and one conventional sphere (12''HDPE) can be compared with the WENDI-II function [19] in all the range of neutron energies. Thus, this idea is viable for its experimental application, providing an alternative to the use of commercial and expensive monitors. Sphere 8''(1''Pb) does not show a good adjustment to the ICRP74 function, and sphere 12''(1''Pb) presents a better dose response than the best combination up to 40 MeV. However, for energies higher than 80 MeV, sphere 12''(1''Pb) presents important overestimations.

The dose response functions of (12''(1''Pb) + 12''HDPE) and WENDI-II are very close for neutron energies lower than 10^{-5} MeV and higher than 50 MeV. For neutron energies between 10^{-5} – 0.07 MeV and 2-50 MeV, the two-spheres monitor studied in this work presents a better behavior than WENDI-II, whose dose response is better between 0.07 MeV and 2 MeV.

On the other hand, this second figure also demonstrates how the combination of a small sphere and a big sphere is not a good option, in this case. The dose response functions have very high values, overestimations with respect to the ICRP74 fluence-to-ambient dose equivalent conversion function, in the thermal and epithermal ranges (3''HDPE + 12''HDPE / 12''(1''Pb) + 3''HDPE), and even a function has negative values (8''(1''Pb) + 3''HDPE). This last fact, the negative values in a dose response function of a two-spheres monitor made up of a small sphere and a big sphere, is in accordance with the results achieved in [21].

The combinations of the sphere 8''(1''Pb) with the spheres 12''HDPE and 12''(1''Pb) are not a good option, important overestimations in the thermal and epithermal ranges can be appreciated in Figure 2, with respect to the ICRP74 fluence-to-ambient dose equivalent conversion function. The combination of the two conventional spheres, 3'' HDPE and 12''HDPE, does not have a positive slope for neutron energies higher than 10 MeV, following this fact the explanation given in the second paragraph of this section, there is a lack of spallation layer in both spheres.

The combinations of a higher number of spheres, 3 spheres, or even the combination of the 4 spheres analyzed in this work, have also been studied. These combinations of a higher number of spheres have not provided remarkable results, with worser results than the combination 12''(1''Pb) + 12''HDPE. A higher number of spheres in the combination means more experimental requirements, in terms of time-consuming and positions with similar neutron fluxes and spectra.

Finally, the relative dose response function of 12''(1''Pb) + 12''HDPE (Figure 3) demonstrates how this combination presents a robust and good behavior in all the evaluated range of energies (10^{-9} MeV – 200 MeV). The introduction of the sphere 12''HDPE in this combination allows to control overestimations at energies higher than 80 MeV, these overestimations can be observed in Figure 3 for the sphere 12''(1''Pb).

V. CONCLUSIONS

The results achieved in the present work have shown as viable the possibility of constructing a passive wide range neutron monitor made up of two-spheres of the extended-range UPM BSS. This monitor would be formed by one extended-range Bonner sphere (12''(1''Pb)) and a conventional HDPE sphere (12''HDPE) of the extended-range UPM BSS. Another passive wide range neutron monitors, with spherical geometries, can be found in the literature [22-24].

The idea of this kind of monitors, with more than one element, seems really interesting in order to find solutions for getting cheap and tuneable monitors for different

facilities, being able to cover different needs with simple modifications of the constituent elements. Moreover, the algebraic methodology used in this work, based on [16], has demonstrated to be valid for the design of these monitors, being this methodology very simple to implement for different combinations in a numeric computing platform like MATLAB.

Sphere 12''(1''Pb) has also shown an interesting response, although its significant overestimations at high energies recommend the combined use of (12''(1''Pb) + 12''HDPE) for neutron monitoring in protontherapy facilities.

In the near future, when the preliminary tests of the new spheres of the UPM BSS have been successfully completed at the LMN-UPM [9], the theoretical idea proposed in this work pretends to be tested, comparing its experimental results, at the UPM irradiation bench [9], with other wide range monitors: WENDI-II [18] and LUPIN-II [25].

VI. REFERENCES

[1] ICRP, Conversion Coefficients for use in Radiological Protection against External Radiation, ICRP Publication 74. 1996.

[2] H. R. Vega-Carrillo, S. A. Martínez-Ovalle, A. M. Lallena, G. A. Mercado, and J. L. Benites-Rengifo, "Neutron and photon spectra in LINACs," Appl. Radiat. Isot., vol. 71, pp. 75–80, 2012.

[3] G. F. García-Fernandez et al., "Neutron dosimetry and shielding verification in commissioning of Compact Proton Therapy Centers (CPTC) using MCNP6.2 Monte Carlo code," Appl. Radiat. Isot., vol. 169, 109279, 2021.

[4] H. Paganetti, Proton Beam Therapy. IOP Publishing, 2017.

[5] G. F. García-Fernández et al., "Monte Carlo characterization and benchmarking of extended range REM meters for its application in shielding and radiation area monitoring in Compact Proton Therapy Centers (CPTC)," Appl. Radiat. Isot., vol. 152, pp. 115–126, 2019.

[6] R. M. Howell and E. A. Burgett, "Secondary neutron spectrum from 250-MeV passively scattered proton therapy: Measurement with an extended-range Bonner sphere system," Med. Phys., vol. 41, no. 9, 2014.

[7] K. Amgarou et al., "Measurement of the neutron fields produced by a 62 MeV proton beam on a PMMA phantom using extended range Bonner sphere spectrometers," Nucl. Instruments Methods Phys. Res. Sect. A Accel. Spectrometers, Detect. Assoc. Equip., vol. 654, pp. 399–405, 2011.

[8] G. F. García-Fernández et al., "Intercomparing of stray neutron fields produced by synchrocyclotrons and synchrotrons used in Compact Protontherapy Centers (CPTC)," in 45º Reunión Anual de la Sociedad Nuclear Española, Vigo, Spain, September 25th-27th, 2019.

[9] H. R. Vega-Carrillo, E. Gallego, A. Lorente, I. P. Rubio, and R. Méndez, "Neutron features at the UPM neutronics hall," Appl. Radiat. Isot., vol. 70, pp. 1603–1607, 2012.

[10] R. García-Baonza, G. F. García-Fernández, L. E. Cevallos-Robalino, and E. Gallego, "Analysis by Monte Carlo methods of the response of an extended-range Bonner Sphere Spectrometer," Appl. Radiat. Isot., vol. 163, 109196, 2020.

[11] T. Goorley et al., "Initial MCNP6 release overview," Nucl. Technol., vol. 180, no. 3, pp. 298–315, 2012.

[12] M. B. Chadwick et al., "ENDF/B-VII.1 nuclear data for science and technology: Cross sections, covariances, fission product yields and decay data," Nucl. Data Sheets, vol. 112, pp. 2887–2996, 2011.

[13] R. Bedogni, P. Ferrari, G. Gualdrini, and A. Esposito, "Design and experimental validation of a Bonner Sphere Spectrometer based on Dysprosium activation foils," Radiat. Meas., vol. 45, pp. 1201–1204, 2010.

[14] D. Pelowitz and G. Fallgreen, A McMath, "MCNP6™ User's Manual Code Version 6.1.1 beta". Los Alamos National Laboratory, Report LA-CP-14-00745, 2014.

[15] V. De Smet et al., "Secondary neutrons inside a proton therapy facility: MCNPX simulations compared to measurements performed with a Bonner Sphere Spectrometer and neutron H*(10) monitors," Radiat. Meas., vol. 99, pp. 25–40, 2017.

[16] T. M. Oakes et al., "An accurate and portable solid state neutron rem meter," Nucl. Instruments Methods Phys. Res. Sect. A Accel. Spectrometers, Detect. Assoc. Equip., vol. 719, pp. 6–12, 2013.

[17] Mathworks, "MATLAB R2018a." 2018.

[18] R. H. Olsher et al., "WENDI: An improved neutron rem meter," Health Phys., vol. 79, no. 2, pp. 170–181, 2000.

[19] V. De Smet, I. Gerardy, F. Stichelbaut, and S. Tolo, "MCNPX simulations of the response of the extended-range rem meter WENDI-2," Nucl. Technol. Radiat. Prot., vol. 29, pp. 25–30, 2014.

[20] N. Dinar et al., "Instrument intercomparison in the high-energy field at the CERN-EU reference field (CERF) facility and comparison with the 2017 FLUKA simulations," Radiat. Meas., vol. 117, pp. 24–34, 2018.

[21] L. G. Beskrovnaia, S. V. Guseva, and G. N. Timoshenko, "Method for Monitoring of Neutron Fields near High-Energy Accelerators," Phys. Part. Nucl. Lett., vol. 15, no. 3, pp. 336–341, 2018.

[22] G. Fehrenbacher et al., "Measurement of the fluence response of the GSI neutron ball in high-energy neutron fields produced by 500 A MeV and 800 A MeV deuterons," Radiat. Prot. Dosimetry, vol. 126, no. 1–4, pp. 497–500, 2007.

[23] G. Fehrenbacher et al., "Measurement of the fluence response of the GSI neutron ball dosemeter in the energy range from thermal to 19 MeV," Radiat. Prot. Dosimetry, vol. 126, no. 1–4, pp. 546–548, 2007.

[24] S. Agosteo, M. Caresana, M. Ferrarini, and M. Silari, "A passive rem counter based on CR39 SSNTD coupled with a boron converter," Radiat. Meas., vol. 44, pp. 985–987, 2009.

[25] M. Caresana et al., "A new version of the LUPIN detector: Improvements and latest experimental verification," Rev. Sci. Instrum., vol. 85, 065102, 2014.

Proceedings of the European Nuclear Young Generation Forum
ENYGF'21
September 27-30, 2021, Tarragona, Spain

Estimation of exposure to radon and the doses received by the occupants of a dwelling located in a site with a high concentration of radon.

Trull Hernandis, Cristina[1], Sancho Fernández, María[1*], Arnal Arnal, José Miguel[1], Verdú Martín, Gumersindo[1] and García Fayos, Beatriz[1]

[1]Instituto Universitario de Seguridad Industrial, Radiofísica y Medioambiental (ISIRYM), Universitat Politècnica de València, Camí de Vera s/n. 46022, Spain

*Corresponding author: *msanchof@iqn.upv.es*

I. INTRODUCTION

An 80 % of the radiation exposure that population receives comes from natural sources, constituting a threat to the public health, coming in a 16% from the soil, 13% from the cosmic rays, 9% from food intakes and 42% due to radon presence [1]. Uranium-238 contained in soils and rocks disintegrates into radon-222 and, due to its gaseous nature, this radioisotope is capable to emanate from the rocks and enter into enclosed areas, where it tends to accumulate. The exposure risk generally comes from inhaling radon gas and its descendants. Disintegration products tend to deposit in the respiratory tract, emitting charged particles which interact with the organism. Radioactive interactions with the body cause cellular damage, leading to alterations in the DNA of the tissues, entailing carcinogenic problems. In fact, radon exposures represent the second reason for lung cancer deaths in the world, only preceded by smoking [2].

According to the risks that radon exposure involves, radon concentrations inside dwellings need to be controlled. Directive 2013/59/EURATOM regulates the basic safety standards for protection against the dangers arising from exposure to ionizing radiation. Therefore, current legislation establishes 300 Bq/m^3 as the reference level in relation to the annual average activity of radon concentration in air [3]. When these standards are exceeded, action policies have to be acquired due to the public hazard implications. Nevertheless, limits exceeded or not, recommendations and guidelines are essential to prevent the occupants from the adverse effects derived from radon exposure.

Exposure levels and the radiation absorbed by the occupants may differ substantially for the same dwelling. Different radon concentrations can be reached in a building, depending on several factors, among them the type of construction materials, soil composition, presence of cracks in the slab of the building, etc. For a specific building, with its features, the concentrations are affected and vary depending on relevant factors as the ventilation and the air fluxes behaviour, as well as dwellers may receive distinct doses depending on their habits and routines [2]. The difference in the exposures must be characterized to comprehend the potential harmful derived and to ensure the integrity of the tenants' health.

The objective of this work is to reproduce a dwelling situation with radon in air that propitiates high exposure levels for its occupants. Subsequently, to characterize different exposure profiles that could occur in a site, estimating the dose received, taking into consideration the exposure conditions and the occupants' daily habits.

II. PROCEDURE

The work procedure has consisted in the following stages:

a) Dwelling location. The dwelling object of this work is located attending to emulate a situation capable to reach high radon in air concentrations. To this effect, potential radon cartographies [4][5] are used in combination with weather reports [6]. The dwelling is placed in a location that combines high potential radon values with weather conditions that tend to increase the concentration indoors.

b) Dwelling description. Once the emplacement is defined, the building specifications are designated. The features that alter the radiological situation in a dwelling are studied, considering for this air flow simulation studies [7][8][9]. Then the disposition of the dwelling spaces is provided.

c) Occupants and habits description. After the description of the dwelling features, the occupants' profiles are designated. Their daily routines and habits performed throughout the day are described, considering for this the difference in the respiratory rates of the individuals [10][11][12].

d) Dose estimation. Measuring devices and their internal disposition are suggested based on CSN measuring guideline specifications [13]. Then, an estimation of the radon concentrations per room is provided, in view of the air flow simulation studies [7][8][9], for their later use in the dose exposure calculations and their consequent analysis.

III. RESULTS AND DISCUSSION

The themes proposed for evaluation in the Procedure are discussed in this section, including the results obtained as the dwelling location and features, as well as the occupants' description and their dose exposure estimation.

A. Dwelling location

In Spain there are quite different radon in air concentrations, depending on the geographical area. The potential radon in air Spanish cartography points the different zones of the territory that are feasible to achieve high concentrations, exceedingly at least at the 10% of the cases values of 400 Bq/m^3 [4]. The dwelling location is placed in Galicia, one of the communities that shows higher potential radon levels.

Precipitation and humidity are environmental factors with a great impact on radon in air concentrations. Soil permeability decreases when the weather is rainy and humidity levels are high [14]. The radon dissolved in the soil can reach the surface throughout the dry part of the ground, which corresponds to the bottom of the dwellings, accessing to the enclosed spaces, and concentrating inside them. During a five-year period, from 2013 to 2017, the zone that accumulates more precipitations, propitiating the radon entry in the residences, was the western part of the territory, as it is deduced from the accumulated rainfalls reports [6].

The radon presence in Galicia in each township is considered to locate the dwelling within the western part [5]. The towns identified by the presence of at least 300 Bq/m^3 in more than 10% of the dwellings are selected for the final location. The emplacement is based in the province of A Coruña, in the town of Outes.

B. Dwelling description

The disposition of the different rooms limits in every home the draft of natural air due to the presence of walls [7]. Depending on the distribution of the ventilation elements, as windows, doors, and the space communications, the air stagnation can be prevented. Furthermore, radon tends to accumulate in lower floors, due to its density, and reaches higher concentrations in small spaces. The radon transfer to spaces with lower concentration is limited when great humidity values are present, as could occur in kitchens and bathrooms. The diffusion coefficient decreases and, therefore, these areas tend to achieve larger radon levels [8][9]. When these situations are combined, as in a single ground floor house, with small rooms and poor ventilation standards, the spaces are no longer homogeneous and the exposure levels in a house oscillate depending on the room.

The building under study corresponds with a standard single house at ground floor level, whose rooms disposition does not allow the natural passage of the air fluxes throughout the house. Locating the dwelling at ground level leads to reproduce adverse radon concentrations, due to the radon tends to accumulate near to the ground [14]. The arrangement of the rooms, presented in Figure 1, is disposed, accordingly with the computational fluid dynamics, to prevent the air homogenization in the dwelling.

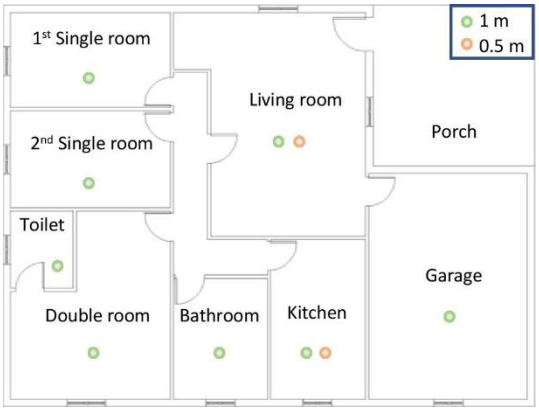

Figure 1. Layout of the house and provision of the measuring devices.

C. Occupants and habits description

The group of dwellers who occupies the described residence has five members: two middle-aged adults, one 10-year-old child, a baby, and an elderly person with a reduced mobility condition. From the profiles described above, it is possible to characterize distinct exposure situations that could happen in a dwelling.

The daily routine defined for each tenant considers the time consumed in each room of the house, and the habits that can affect their respiratory rhythms. The amounts of air inhaled differ depending on the age as a function of the frequency and their inhalation capacity. During resting periods, a grown-up person can inhale between 12 and 20 times per minute [10]. Therefore, it is considered that each adult breathes 15 times per minute, inhaling 12 liters of air per minute. Whereas, if the adult is under prolonged effort conditions, the respiratory rhythm can reach the amount of 100 liters, equivalent to 60 breaths per minute [11] From these values, and with the aim to emulate the most adverse conditions, 60 liters are assigned for intermediate situations, equivalent to inhaling around 30 times per minute.

A child respiratory frequency is comprised between 18 to 25 breaths per minute [10]. In addition, the normal values of air inhaled by a child round between 7 and 7.5 milliliter per kilogram [12]. For the 10-year-old child it is considered 21 breaths during resting periods, 30 for middle efforts and 60 during periods of physical activity. Considering a weight of 33.5 kg, the air amounts inhaled are from 5.276 liters, during quietness, 7.537 liters during medium efforts, and 15.075 liters during prolonged activities.

On their behalf, infants breathe about 25 to 36 per minute [10]. Hence, it is established for the estimations that the infant breathes 31 times per minute during quiet periods. Considering the normal children respiratory values mentioned above, and being the infant's weight 8.41 kg, the volume inhaled per minute is 1.955 liters. For periods of continuous crying, it is settled that the respiratory rhythms increase in a 50 %, being the amount inhaled 2.933 liters.

Daily routines of each dweller and the different spaces occupied during the day are defined [15] and sum up below.

a) Elderly person. Due to the dweller mobility limitations, the elder spends most of the day in the building, occupying the living room, bathroom, and the 1st single room. Most of

this time is spent resting, except during rehab exercises in the living room, reaching medium respiratory rates.

b) Adult number 1. This tenant spends the least amount of time in the dwelling, due to work responsibilities. All the rooms are frequented in quietness by the dweller, except the single dormitories. The execution of daily tasks in the garage propitiates periods of medium effort. High respiratory rhythms are achieved due to physical training practice, performed in the living room.

c) Adult number 2. This dweller frequents all the rooms of the dwelling, except the garage. The homemaker daily tasks, performed in most of the rooms, propitiate medium respiratory levels. In addition, the exercise practice in the living room carries an increase in the respiratory rates to high levels.

d) Baby. The infant frequents all the rooms, except the garage and the single dormitories. The respiratory rhythms of the baby alternate between resting and prolonged crying, consequently increasing the respiratory rates, differentiating the periods spent on the floor highchair from the others.

e) Child. The dweller occupies the 2nd single dormitory, bathroom, living room, and the garage. While the kid is playing in the living room or the garage, the respiratory rhythms vary from calmness to high levels, with medium rhythms at the bathroom and the living room activities.

D. Dose estimation

The devices suggested to use for evaluating the radiological situation, chosen considering cost and uncertainty linkage, are passive long-term measuring devices, gauging during a 3-months period, meanwhile the dwelling remains closed [16]. Electret ionization chambers are selected for the dosimetry, due to their medium cost, and its standard uncertainty from 8 to 15% for 200 Bq/m^3 exposure [2].

The location of the measuring devices is presented in Figure 1. The detectors should be situated at 1 m from the ground, far from the ventilation elements, and maintaining 30 cm to the external walls, and 10 cm to other objects [13], one per each space considered homogeneous. Two additional devices should be disposed closer to the floor level, at the minimum height recommended in guidelines [13]: 0.5 m, since radon tends to accumulate near to the ground level. Differences in exposure when a baby spends time in a floor highchair, are characterized by these two additional devices. When the measuring periods are finalized, the devices are collected for later study in the laboratory, obtaining the corresponding concentration per measuring device.

Concentrations per room, presented in Table 1, are assumed with the aim to reproduce a dwelling situation that would exceed the reference level of 300 Bq/m^3 of average activity radon concentration in air [3]. The concentrations allocation is based on the computational fluid dynamics [7][8][9]. The main factor assessed is the dimension of the rooms. The smaller spaces correspond to higher radon concentrations. In addition, larger values are assigned when humidity is present. Due to radon is eight times heavier than air, for the same room, higher values are assigned to the devices nearest to the floor, corresponding to the floor highchair location.

Table 1. Radon concentration per room.

Room		Bq/m^3	Room		Bq/m^3
Living room	1 m	189.4	Kitchen	1 m	335.6
	0.5 m	228.6		0.5 m	376.9
1st Room		228.2	Bathroom		424.6
2nd Room		228.6	Toilet		512.8
Double room		196.3	Garage		313.6

In all the rooms the concentrations exceed 100 Bq/m^3, reaching in an occasion a value up to 500 Bq/m^3. The presence of rooms which exceed the 300 Bq/m^3, established by the legislation as the reference level [3], specially entails a risk for the occupants. Considering the concentration values assigned per room, the levels of exposure are estimated for each occupant.

The daily accumulated activity to which the dwellers are exposed ($A_{accu-exp}$) is obtained as the sum of the product of the concentrations assumed for each measuring device ($[Rn]_{room}$) multiplied by the time, which the tenant has spent in the room (t_r), and the air volume inhaled, varying with the respiratory rates (V_{air}), according to Equation 1.

$$A_{accum-exp} = \sum [Rn]_{room} \cdot t_r \cdot V_{air} \qquad (1)$$

Starting from the accumulated activity exposition values and knowing the time per day that each occupant spends in the dwelling (t_{day}), the activity average exposure per hour (A_{av-exp}) is obtained by Equation 2).

$$A_{av-exp} = A_{accum-exp}/t_{day} \qquad (2)$$

Current legislation dictates the reference levels referring to radon in air concentrations, which in this case are exceeded. Since the total activity exposure is related to the radon in air concentrations, and there is no established reference level for this radon exposure, the exposition that the occupants suffer will entail a risk to their health. Both accumulated activities exposure, daily and the average spent per hour, are calculated for each occupant, and presented in Figure 2.

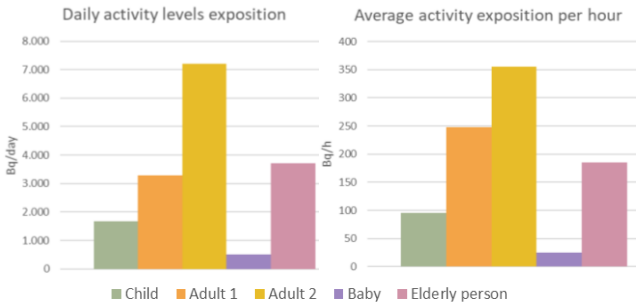

Figure 2. (A) Daily activity levels occupants exposition; (B) Activity exposition average received per hour when in the dwelling.

As it is observed in Figure 2 (A), the dweller with higher daily exposure is the adult number 2, due to the large amount of time spent in the dwelling, combined with periods of physical exertion. The elderly person is the following tenant who receives a bigger amount daily, since the elder spends a substantial part of the day inside the building. The adult

number 1 presents an accumulated activity exposure per day closer to the elderly person, although is who spends less time in the dwelling, but in periods of high physical activity. The activities to which the child and the baby are exposed, correspond to lower values, this variation comes from the remarkable difference between their inhalation capacities with the volumes that the adults inhale. Nevertheless, accordingly to WHO, low concentrations do not mean an exposure level that ensures the integrity of the health of the individual, since there is no level below which the exposures can be considered safe [2].

When the different times spent in the dwelling are considered, some differences appear in terms of the activity exposition, Figure 2 (B). The adult number 2 remains with the highest value. However, adult number 1 becomes the second occupant receiving highest activity exposure per hour spent, exceeding the elderly person exposure. This variation is a consequence of the different nature of the activities performed in the dwelling.

Conforming to the given results, the activities to which the occupants of the same dwelling are exposed differ depending on the exposure times, and the radon concentration of the room, varying with the activities carried out. Consequently, the exposition suffered from a dweller during a narrow period, but a higher respiratory frequency, can overtake the activity exposition levels that another tenant receives, even if the staying periods are greater.

In addition, the dose received by the Adult 2 is calculated (Equation 3) due to it presents the higher activity exposition levels. For this purpose, depending on the time spent annually at each room (t) and the radon concentrations ($[Rn]_{room}$), the total activity exposition has been obtained for its further conversion to dose exposition. Conversion factor for radon and its progeny, when evaluating at home environments, corresponds with 1.1 Sv per Jhm^{-3}, which means effective dose per unit of potential exposure of alpha energy, $F_{D.ef}$, [17]. $F_{Bq/J}$ corresponds to conversion factor from Bq/m^3 to J/m^3[18], being the radon secular equilibrium factor for radon in dwellings, F_{eq-sec}, 0.4 [2].

$$Dose = \sum [Rn]_{room} \cdot t \cdot F_{eq-sec} \cdot F_{Bq/J} \cdot F_{D.ef} \quad (3)$$

Effective dose estimated for the dweller corresponds to 4.24 mSv per year, level which would exceed the 1 mSv per year established as a dose limit recommendation for the members of the public [17].

According to these estimation results, mitigation measures may be applied in the dwelling to preserve the health of occupants from radon exposure [15].

IV. CONCLUSIONS

A radiological evaluation of a dwelling, whose features propitiate high radon in air concentrations, has been performed. For this purpose, the meteorological conditions in the area and the geographical location of the dwelling have been considered. The exposures of the dwelling occupants to different levels of activity concentration have been estimated, considering meanwhile their habits and daily routines performed in the different stays of the building.

According the European Council Directive and WHO, the dwellers are residing in a house with radon concentrations which entail a risk for their health, due to exceeding the 300 Bq/m^3. Considering the variations of exposure that can arise in the same building, the radon concentrations must be considered together with the corresponding exposure levels, and the effective dose. All of this to evaluate the radiological situation suffered by each occupant, then manifest the risks that the presence in the dwelling may entail and be able to undertake the corresponding measures to preserve the health integrity of the occupants.

V. References

[1] PNUMA, “Radiación. Efectos y fuentes,” 2016.

[2] OMS, “Manual de la OMS sobre el radón en interiores,” 2015.

[3] European Union, “Council Directive 2013/59/EURATOM,” 2014.

[4] CSN, “Cartografía del POTENCIAL DE RADÓN en España,” 2017.

[5] Universidad de Santiago de Compostela, “Porcentaje de medidas de más de 300 Bq/m^3 por municipio,” 2018.

[6] Xunta de Galicia, “Informe climatológico anual. Mapa de precipitación acumulada no anos 2013-2017,”

[7] K. Akbari, and J. Mahmoudi, “Numerical simulation of radon transports and indoor air conditions effects,” IJSER, vol. 3(6), 2012.

[8] K. Akbari, J. Mahmoudi, and J. Ghanbari, “Influence of indoor air conditions on radon concentration in a detached house,” Journal of Environmental Radioactivity, vol. 116, pp. 166-173, 2013.

[9] R. Rabi, and L. Oufni, “Study of radon dispersion in typical dwelling using CFD modeling combined with passive-active measurements,” Radiation Physics and Chemistry, vol. 139, pp. 40-48, 2017.

[10] J. López Chicharro, and A. Fernández Vaquero, “Fisiología del Ejercicio,” 3e, V, 2006.

[11] Breathe (Sheff), “Your lungs and exercise,” 12(1), pp. 97-100, 2016.

[12] J. López-Herce, M. Rupérez Lucas, C. García Sanz, and E. García Sánchez, “IV Curso sobre la Función Pulmonar en el Niño (Principios y Aplicaciones),” 2013.

[13] CSN, “Directrices sobre la competencia de los laboratorios y servicios de medida de radón en aire,” 2010.

[14] CSN, “Protección frente a la inmisión de gas radón en edificios,” 2010.

[15] C. Trull Hernandis, “Desarrollo de las medidas necesarias para la reducción y el control de la concentración de radón en el aire interior de una vivienda unifamiliar localizada en la comunidad de Galicia,” TFG, Ingeniería Química, UPV, 2018.

[16] CSN, “Metodología para la evaluación de la exposición al radón en los lugares de trabajo,” 2012.

[17] Ministerio de la Presidencia, “Real Decreto 783/2001,” 2001.

[18] ICRP, “Protection Against Radon222.,” Publication 65, 1990.

Proceedings of the European Nuclear Young Generation Forum
ENYGF'21
September 27-30, 2021, Tarragona, Spain

Compton imaging to support a new robotic platform for mapping nuclear decommissioning sites

Simons, Mattias[1*], Brabants, Lowie[1], De Schepper, David[2], Demeester, Eric[2] and Schroeyers, Wouter[1]

[1] Uhasselt – Hasselt University, CMK, NuTeC, Nuclear Technology- Faculty of Engineering Technology, Agoralaan H, 3590 Diepenbeek, Belgium; [2] KU Leuven, ACRO, Department of Mechanical Engineering, Wetenschapspark 27, 3590 Diepenbeek, Belgium

*Corresponding author: *mattias.simons@uhasselt.be*

I. INTRODUCTION

A nuclear decommissioning environment requires the characterisation of hotspots in a high dose rate environment. The current practice to identifying hotspots is for human operators to enter the facility and manually localise and characterise these hotspots. As a result, operators that carry out these measurements are exposed to dose uptake, which implies that special safety measures are necessary to protect the workers performing these measurements.

In these situations, where operators are exposed to high dose rates, the time available to perform the mapping measurements is limited to keep the dose uptake as low as reasonably achievable. This, however, introduces the risk of an incomplete characterisation, where sources are missed or inaccurately characterized. Instead of using human interventions, an alternative approach could be to use a robotic platform to automate the repetitive measurement procedures of localising hotspots [1]. Not only does the use of a robot minimise human radiation exposure by reducing the need for human presence and thus reducing unnecessary dose uptake. The use of robots also takes away the time limitation, leading to more accurate measurements.

In the ARCHER project (Autonomous Robotic platform for CHaractERization), a robotic system is being developed to perform mapping and characterisation measurements in a nuclear decommissioning environment. One of the applications of this platform is the localisation and characterisation of radioactive hotspots inside tanks or pipes larger than 60cm.

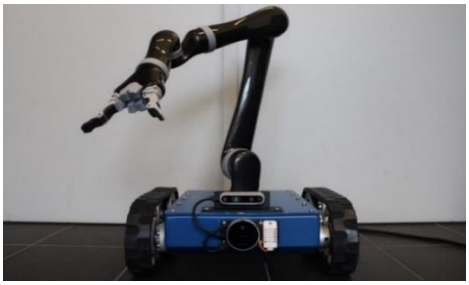

Figure 1. Picture of the ARCHER robotic platform

Figure 1 shows a picture of the robotic platform that is currently being developed in the ARCHER project. This platform is equipped with a robotic arm that is used to perform the necessary movements and manipulations of the detector. The measurements aim at identifying and characterizing hot spots.

In literature, different methods have been proposed to localise hotspots. Two categories of approaches that are frequently reported are i) [2] performing multiple measurements in a scanning approach and apply interpolations to determine the source location or, ii) [3]–[5] using a gamma or Compton camera that can directly give spatial information in a single measurement. Selivanova et al. [2] demonstrated the capabilities of a scanning approach by using a CloPema dual-arm robot in combination with a kromek-GR1-A+ CZT (Cadmium Zinc Telluride) spectrometer. By measuring spectrums with a detection time of one second per spectrum and scanning performed in a serpentine pattern with a scanning speed of 5 cm/s, heatmaps were created based on the measured total counts per spectrum. Selivanova et al. proved a scanning approach to be a feasible method for localising standard point sources with activities of hundreds of kBq. Selinova et al. achieved minimal detectable activities (MDA's) in the order of kBq to tens of GBq, depending on the amount of shielding between source and detector.

Due to the repetitive nature of a scanning pattern, measuring with a robotic arm remains a time-intensive method. As the measurements are performed in close proximity to the hot spots, every executed movement has a risk of contaminating the robotic platform or detector. The alternative approach, (approach ii) of using a gamma camera (with physical or electronic collimation) has the advantage that direct spatial information about the source location can be extracted. This minimizes the need for movements and manipulations of the robot and therefore reduces the risk of contaminating the robot. Carrel et al. [4] proposed the gampix gamma camera that performs spatial localisation of a source in a single measurement. This system utilises a Timepix readout chip in combination with a 1000 µm thick CdTe (Cadmium

Telluride) semiconductor crystal and a coded aperture or multi-pinhole collimator. By introducing a decoding step, sources with varying energy were successfully localised. However, at higher gamma energies, e.g. ^{60}Co, the efficiency significantly dropped for this system. Additionally, when a collimator would be used in a high background environment, also shielding needs to be added to limit incident radiation from outside the field of view of the collimator. This would significantly increase the weight and make it too heavy to use on a small robotic platform, such as ARCHER, which needs to be able to manoeuvre inside tanks or pipes.

Contrary to the approach of using a gamma camera equipped with a physical collimator and shielding, electronic collimation can be used. A Compton camera makes use of the kinematics of Compton scattering to calculate the possible directions of incident gamma radiation. Therefore, a Compton camera can directly extract geometric information about the location of hotspots. This limits the need for manipulations and movements of the robotic platform and arm while also limiting the needed weight for the detector. Also, the weight will be kept low as no physical collimator is needed. Sato et al. [3] proved this concept of using a Compton camera to localise sources. In his research, the Compton camera with a total weight of less than one kg was mounted on a drone. This camera consisted of two detectors, one scatterer and one absorber detector, both made from Ce-doped GAGG ($Gd_3Al_2Ga_3O_{12}$) scintillators with a distance of 23.5 mm between the two. Instead of using two detectors for the Compton camera, as was the case during the research of Sato et al., in this work only one detector was used. This was done using a method similar to the method proposed by Turecek [5] to operate an advapix TPX3 as a single layer Compton camera. This eliminates the need for multiple detectors, which reduces costs and simplifies the setup.

The ARCHER platform in the current state makes use of a lightweight spectrometer to map a nuclear environment by repeating multiple measurements in a scanning pattern. However, using a Compton camera or a combined approach including both a CZT spectrometer and a Compton camera could highly optimise the time needed for the measurement process to localise hotspots. This paper focuses on the comparison of both approaches individually as the hybrid approach of combining CZT spectrometer with Compton camera will be researched in a later stadium in the project. Using a Compton camera on the ARCHER robotic platform to localise sources is compared to the currently used method of repeating measurements in a scanning pattern. Lab-scale tests were performed to evaluate the time needed to localise the sources for both methods.

II. METHODS AND MATERIALS

In order to compare A) measuring in a scanning pattern with B) using a Compton camera to localise sources, an **Epson c3a601s robotic arm** with **RC6+ controller** was used. In the current setup, the arm has a reach of about 40 cm by 20 cm with a maximum payload of 3 kg for the detector and mounting hardware. The same sources were used during the tests of both methods, a ^{137}Cs source with an activity of 168 kBq and a ^{60}Co source with an activity of 23 kBq.

A. Scanning pattern measurements

The detector used in the scanning setup was a **25S25 BriLanCe 380 $LaBr_3$ scintillator** connected to an **osprey multi-channel analyser** with an integrated power supply was used with a bias voltage of 650V.

To measure the different spectra, the commercial software **Genie gamma analysis and acquisition** was used. Different measuring times were used, with varying grid sizes of 100 mm by 100 mm, 50 mm by 50 mm and 25 mm by 25 mm. Table 1 shows the different settings used to perform the scanning measurements with the spectrometer. The listed heights correspond to the distances between the table surface and detector. This was done in natural background.

Table 1. Different configurations of measured grids with corresponding height, source and measuring time for each spectrum.

Test case	Total area	Grid size	Height	Source	Source location	Measuring time
nr	cm	mm	mm		mm,mm	s
1	40 x 20	100 x 100	100	^{241}Am	200,100	60
2	40 x 20	100 x 100	100	^{241}Am	250,150	60
3	40 x 20	100 x 100	50	^{241}Am	200,100	60
4	40 x 20	100 x 100	50	^{241}Am	250,150	60
5	40 x 20	100 x 100	100	^{137}Cs	200,100	60
6	40 x 20	100 x 100	100	^{137}Cs	250,150	60
7	40 x 20	100 x 100	50	^{137}Cs	200,100	60
8	40 x 20	100 x 100	50	^{137}Cs	250,150	60
9	40 x 20	100 x 100	100	^{137}Cs	250,150	5
10	40 x 20	100 x 100	100	^{137}Cs	250,150	10
11	40 x 20	100 x 100	50	^{137}Cs	250,150	5
12	40 x 20	100 x 100	50	^{137}Cs	250,150	10
13	40 x 20	50 x 50	50	^{137}Cs	250,150	5
14	40 x 20	50 x 50	50	^{137}Cs	250,150	10

After measuring a spectrum at a certain coordinate, the total counts were calculated. Also, the number of counts within 3 regions of interest (ROI) in the spectrum was calculated. These ROI's correspond to the energies emitted by ^{137}Cs, ^{60}Co and ^{241}Am. Next, the background spectrum of $LaBr_3$ was subtracted from the data and heatmaps were created using **SAGA gis geostatistics** software [6]. This software was used to interpolate the values of total counts and counts per ROI for each measuring point with the use of a thin-plate spline interpolation method with a cell size set to 1 mm. The expected location of the source was defined by the location of the maximum value in these heatmaps. The different configurations of measured grids will be evaluated on the accuracy of the source location and measurement time.

B. Compton camera

A single **advapix TPX3 detector** with 1000 µm CdTe semiconductor crystal was mounted on the Epson robotic arm. This detector will be used as a lightweight Compton camera which makes use of the Timepix3 readout chip. This chip has an event-based readout for a total of 65k pixels and can simultaneously register the time of arrival and energy for each pixel [7].

From a Compton event that is in coincidence with a photoelectric absorption, it is possible to reconstruct a cone that contains possible locations of the source. To do this, the following information is needed: the coordinates of the

Compton interaction, the coordinates of the photoelectric absorption and the energy of the incident gamma.

Depth reconstruction of coincident pixels and events was used to determine the depth across the z-axis between two coincident interactions. This was done by reconstructing the height based on the small difference in time of arrival for pixels where interactions occur at a different height, according to the method described by Bergmann et al. [8].

To be able to reconstruct the depth difference between two interactions, a correction for time-walk is necessary. Time-walk is an effect that results in a slower detection of arrival time for, lower energy pixels in a gamma camera and if not corrected, it will result in a wrong calculation of the z coordinates. The correction was performed according to the method proposed by Turecek by making a calibration, using the 59 keV gamma peak of ^{241}Am [9].

After applying this correction, adjacent pixels are grouped into clusters and the mean x, y and z values of the interactions were calculated. From these coordinates, the axis of each cone is calculated. After this, the opening angle of each cone is calculated from the energy of the two coincident interactions, according to the Compton formula. This results in cones where the surface of a cone represents all possible locations of the source. The cones where the total energy corresponds to the 662 keV gamma of ^{137}Cs are then summed and expressed in spherical coordinates. The location of the source is then defined at the intersection of these cones. Figure 2 shows a simplified illustration of the used method.

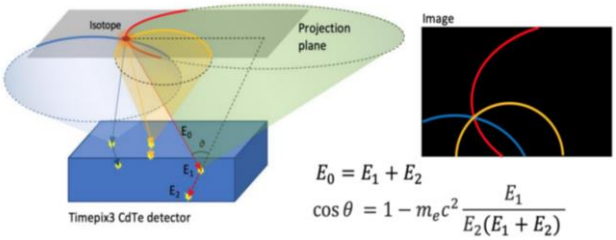

Figure 2. Illustration of the principle of reconstruction of a gamma source (left) with the reconstructed image of the Compton cones(right) [5]**.**

A ^{137}Cs source was used to simulate a hotspot and was placed on the table 10 cm below the detector and with a distance of 12 cm between the table surface and detector. Additionally, a ^{60}Co source was placed on the table to simulate an increased background.

III. RESULTS AND DISCUSSION

Measurements with point sources were performed with both discussed techniques and the same sources were used in both measurements.

A. Scanning pattern measurements

Table 2 shows the results of the errors made on the localisation of the measured test cases. When a grid size of 5 cm by 5 cm is used, ^{137}Cs sources can be localised with an accuracy up to 5.8 mm for the worst-case scenario, which is when a source is in the middle of four measuring points. It can be noted that when heatmaps are made based on the total number of counts in a spectrum, the achieved accuracy is generally higher. However, when the total number of counts is used, it is not possible to directly perform identification of the used sources, as is the case for heatmaps based on only the number of counts inside a ROI.

As expected, reducing the distance between measurements will improve the accuracy of retrieving the source, but this will also increase the time needed to scan the surface and manoeuvre the robot or robotic arm so a trade-off will be needed.

Table 2. Results of the localisation of point sources by using the scanning method with the $LaBr_3$ connected to osprey.

	nuclide energie thin-plate spline			Total counts thin-plate spline		
Test case	*Δx*	*Δy*	Δtotal	*Δx*	*Δy*	Δtotal
nr	mm	mm	mm	mm	mm	mm
1	0	0	0,0	1	0	1,0
2	0	3	3,0	1	3	3,2
3	0	0	0,0	0	0	0,0
4	6	-1	6,1	6	-1	6,1
5	1	0	1,0	1	0	1,0
6	9	-4	9,8	7	-4	8,1
7	0	0	0,0	0	0	0,0
8	9	-4	9,8	7	-4	8,1
9	2	16	16,1	3	7	7,6
10	-1	4	4,1	-1	4	4,1
11	9	-1	9,1	3	-5	5,8
12	6	-3	6,7	5	-2	5,4
13	1	-1	1,4	1	-1	1,4
14	1	-1	1,4	1	-1	1,4

Figure 3 shows the heatmap interpolated with the thin-plate spline method of test case number 8 where the source was located in the middle of 4 measuring points. The source was found on the green dot with an error of 8.1 mm compared to the actual source location. With a total of 15 measuring points of one minute and the movement of the robotic arm, it took about 25 minutes to complete this scan.

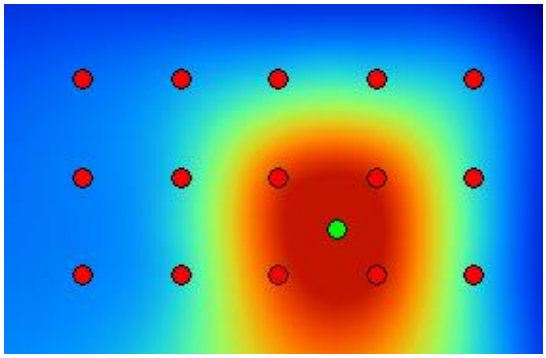

Figure 3. Interpolated heatmap based on the total counts of a ^{137}Cs source placed in the middle of four measuring points on a 10 cm by 10 cm scanning grid with a measuring time of 60 seconds. Red dots indicate the points where measurements are performed and the green dot indicates the estimated position of the source.

An additional measurement with two sources was performed to check the ability to distinguish multiple sources. This scan was performed with a grid size of 25 mm by 25 mm. The upper left source located on the table was a ^{60}Co source and the lower right source was a mixed source with ^{60}Co and ^{137}Cs. The measuring times for this grid were 60 seconds per measurement. This mixed source had an activity of 7.3 kBq for ^{60}Co and 9.1 kBq ^{137}Cs.

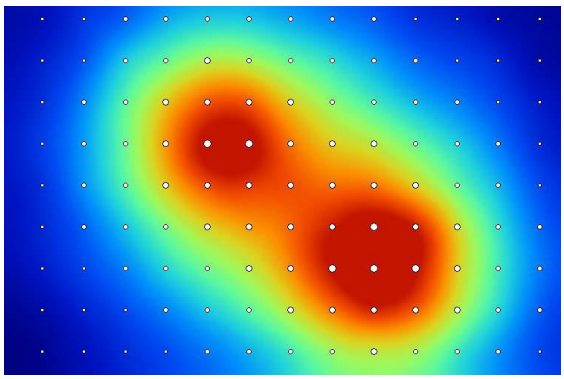

Figure 4. Measuring points and heatmap interpolated by thin-plate spline method of a 25 mm by 25 mm scanning grid with ^{60}Co and mixed ^{60}Co/ ^{137}Cs source.

Figure 4 shows the interpolated heatmap based on total counts for each measuring point. Two clear hotspots can be distinguished. However, it took several hours to complete this scan and map a surface of 40 cm by 20 cm.

B. Compton camera

The measurement with a measuring time of 15 minutes was performed to localise a ^{137}Cs source located at 10 cm below the detector with a detector to surface distance of 12 cm. A ^{60}Co source was used to simulate a background.

Figure 5 shows the reconstructed image where cones are accumulated in spherical coordinates. This reconstruction can then be used to localise the source. It can be seen that a hotspot is being identified at the location with a polar angle of 35 degrees.

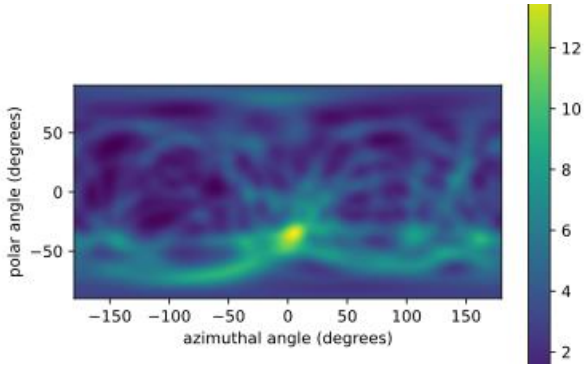

Figure 5. spherical back-projection of a 15-minute measurement with a detector to table distance of 12 cm. The colourmap represents an arbitrary unit that indicates the overlap between cones.

The algorithm in its current state was able to successfully localise ^{137}Cs without significant interference of ^{60}Co in the background. The Compton camera indicates the region where hotspots or sources are located without the need for movement of the robotic platform or manipulations of the robotic arm. However, one of the use cases of the ARCHER project is the characterisation of sources. Therefore, a combined approach where the Compton camera is used to indicate the region of the hotspots followed by a very local scanning pattern is suggested to optimise the time to localise hotspots and characterize this hotspot. The advantage of using a spectrometer for this local scanning is its better performance in the characterisation of the present radionuclides while limiting the time needed to localise sources by using the Compton camera.

IV. CONCLUSION AND FUTURE WORKS

Using a robotic arm to scan surfaces by performing measurements on multiple points proves to be a valuable approach to localise hotspots. However, it is time-consuming. Our experimental results demonstrated that a measurement of an area of 40 cm by 20 cm took 25 minutes (test case 8). In the current setup, when a 5 cm by 5 cm grid size is used, accuracy could be achieved of up to 5 mm to localise point sources.

The use of a Compton camera has been found to be an added value. The Compton camera reduces the time needed to localise hotspots compared to using the scanning approach with a spectrometer and limits the necessary movements of the robotic platform. It should, however, be noted that this paper only compares on measurement time. Future works will also include other factors such as sensitivity limits.

Both the methods for hotspot localisation will go into further development. For the approach of repeating spectrometric measurements in a scanning pattern, further research will focus on improving the necessary measurement times. For the Compton camera, developments will focus on improving its efficiency by optimising the used algorithm for reconstruction.

ACKNOWLEDGEMENTS

This work was supported by the Fund for Scientific Research Flanders (FWO) scholarship nr 1SA2621N hosted by the University of Hasselt.

The ARCHER project is carried out by academic research partners UHasselt and KU Leuven in collaboration with the industrial partners Tecnubel (Engie) and Magics instruments. This project is funded by the energy transition fund of FOD economy (federal government Belgium)

REFERENCES

[1] OECD & NEA, "R&D and Innovation Needs for Decommissioning Nuclear Facilities," p. 318, 2014.
[2] A. Selivanova *et al.*, "The use of a CZT detector with robotic systems," *Appl. Radiat. Isot.*, vol. 166, p. 109395, Dec. 2020.
[3] Y. Sato *et al.*, "Development of compact Compton camera for 3D image reconstruction of radioactive contamination," in *Journal of Instrumentation*, 2017, vol. 12, no. 11, pp. C11007–C11007.
[4] H. Lemaire, F. Carrel, M. Gmar, V. Schoepff, and M. Trocme, "GAMPIX: a new generation of gamma camera based on the Timepix chip," *15th Int. Work. Radiat. Imaging Detect.*, pp. 3–4, 2013.
[5] D. Turecek, et al., "Single layer Compton camera based on Timepix3 technology," in *Journal of Instrumentation*, 2020, vol. 15, no. 1, p. 17.
[6] O. Conrad *et al.*, "System for Automated Geoscientific Analyses (SAGA) v. 2.1.4," *Geosci. Model Dev.*, vol. 8, no. 7, pp. 1991–2007, 2015.
[7] T. Poikela *et al.*, "Timepix3: A 65K channel hybrid pixel readout chip with simultaneous ToA/ToT and sparse readout," *J. Instrum.*, vol. 9, no. 5, 2014.
[8] B. Bergmann, et al., "3D reconstruction of particle tracks in a 2 mm thick CdTe hybrid pixel detector," *Eur. Phys. J. C*, vol. 79, p. 165, 2019.
[9] D. Turecek, et al., "USB 3.0 readout and time-walk correction method for Timepix3 detector," *J. Instrum.*, vol. 11, no. 12, 2016.

Proceedings of the European Nuclear Young Generation Forum
ENYGF'21
September 27-30, 2021, Tarragona, Spain

Radiological characterization for dismantling through robots and drones.

Eduardo Fuentevilla Blanco[1*], Ángel Ramos Gallardo[1], Sergio Segovia González[1]

[1] ENUSA Industrias Avanzadas S.A., Spain

*Corresponding author: *fbe@enusa.es*

I. INTRODUCTION

In the 40s, teleoperated arms (waldos) [1] were used for the manipulation of dangerous nuclear materials. Since this milestone, the nuclear industry opposed to carry on with this sort of technology. Despite being one of the pioneers using robots, the nuclear industry did not continue betting on it and let other industries such as the aerospace or manufacturing one to take the lead [2].

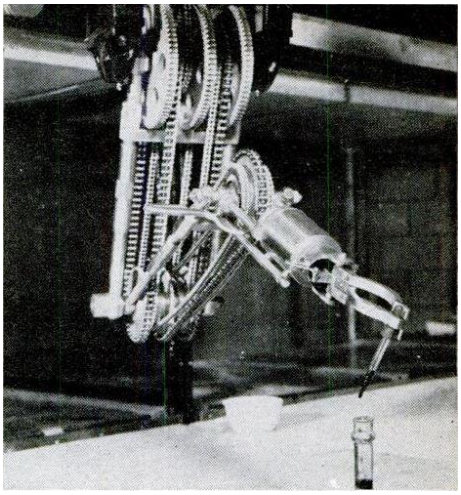

Figure 1. Arm manipulator "waldo".

It is true that today's accessibility to new technologies has allowed other industries to enter the world of robotics in an easier and more affordable way. Likewise, the evolution of the components used on the manufacturing of robots; more precise and lighter sensors and more powerful electronics have enabled applications to be accomplished more effectively and efficiently than ever before.

However, the nuclear industry continues to detect practices that we can consider archaic today. The radiological characterization on dismantling tasks is a clear example, where in many cases the taking of measurements keeps being manual; it is the operator who physically accesses the radiated area with a radiation detector and obtains the measurement. Therefore, this implies:

- Exposing a human to a radioactive environment.
- Long setup times; protection measures and radiological monitoring, structures or tools to reach difficult accessibility areas or meshing for the radioactive levels location.
- Errors in measurement due to human factors; inaccurate distances and orientations on the detector positioning.

With the aim of addressing these deficiencies and in search of a more effective, efficient and safe dismantling, ENUSA is currently developing automatic inspection equipment based on these new possibilities, bifurcating its efforts into two lines of action: Dismantling in outdoor and indoor areas.

II. OUTDOOR DISMANTLING

Currently, the procedure to control environmental gamma radiation rates at the Saelices mine is carried out manually. Qualified personnel move through the terrain and position themselves, with the help of GNSS (Global Navigation Satellite System) [2], at predetermined points on which a radiation measurement is made at a height of one meter above the soil with a portable equipment. Every year environmental rates are mapped, counting several thousand points, in a process that takes weeks.

In addition, in the conditioning processes of the lands which undergoes rehabilitation, it is planned to monitor the environmental rates after each stage of the process. Four or five stages are contemplated in which layers of different materials are arranged on the surface to be rehabilitated, being the number of points to be sampled on each stage also numerous.

For this reason, ENUSA started a development project to automate these measurements on the mine grounds by using drones, in order to free the personnel from these routine measurement tasks, obtaining a faster mapping and also being able to make a simple monitoring of environmental rates control in the successive stages of soil conditioning.

Figure 2. Outdoor drone.

Therefore, a drone has been developed whose automatic procedure for taking measurements consists of:

1. Reaching a height (safety height) to avoid collision with the ground or any obstacle. It is important to know the highest elevation of the terrain to be inspected as well as the height of the highest obstacle.

2. Going to the point of interest from where obtaining a radiation measurement is required while maintaining the safety height. The drone has the ability to receive multiple coordinates at once and automatically reach them.

3. Once the drone is located at the desired point, going down to a height such that the detector is 1 meter from the ground.

4. Taking the radiation measurement for as long as it is required.

5. Repeating the previous step until all the desired points are covered.

In terms of location, the drone is positioned using the same system which is currently being used in the mine; a GNSS system. To improve positioning accuracy, the drone relies on an RTK (real-time kinematic) station that serves as a reference to correct its position. This type of method makes possible to obtain a precision of centimetres [4].

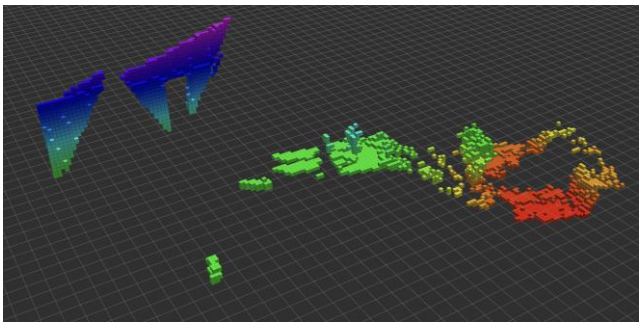

Figure 3. Closest points mapping generated by the sweep sensor.

A great handicap on this development is to avoid that the measurement is taken on an obstacle and not on the ground directly. The possibility may arise that a tree or bush is found at the point of interest in such a way that the detector is taking the radiation of 1 meter plus the height of the obstacle as this is mistaken as if it were the ground. Due to this, a sweep sensor has been developed that scans the area near the point of interest so the distance from the drone to the closest points is known. Knowing the elevation of the point of interest, it can be deduced if what the drone detects is an obstacle or not.

This laser scan also serves as a security method for the drone. It is important that the drone descends to the desired height when the area is clear of any obstacle which could interfere with the propellers, hence, avoiding a possible collision. In this way, the sweep sensor also allows you to know if the site where the measurement is to be taken is safe or not.

When an obstacle is detected at the point of interest, the drone is programmed to continue in a straight line towards the next point of interest, until it finds an area free of obstacles. Therefore, a safe area for the drone to approach the ground at the appropriate height and take the measurement.

Regarding the detector, the drone uses a "Geiger-Müller" type detector with an energy range of 40 KeV – 1.3 MeV, a measurement range between 0.5 µSv/h – 10 mSv/h, a sensitivity of 750 CPS/mSv/h and a total weight of 700 g approximately. Under this payload the drone can measure close to 30 minutes without stopping to replace its batteries.

III. INDOOR DISMANTLING

In the decontamination of nuclear power plants undergoing dismantling, an identification and characterization of the radiated areas are carried out in order to be decontaminated later on. This operation is carried out manually and requires personnel staying under radioactive environments for a long period of time, hence, the measurements are sensitive to human factors.

The use of automated systems capable of operating effectively in indoor areas with difficult access presents an interesting alternative to the current manual inspections. It implies firstly a drastic reduction in the exposure of inspectors to radioactive environments and secondly, it would allow greater automation of the process that entails less variability and greater reliability in the measurements.

Therefore, ENUSA together with Hovering Solutions saw the opportunity to investigate the possibilities of carrying out this type of alternative inspection system, leading to the development of prototypes to evaluate these capabilities. The objective was to develop prototypes of both a drone and a climbing robot which complements each other allowing the incorporation of the required radiation detectors and measurement equipment. As of now both platforms use a CZT type detector with 32 cm^3 volume detection, an energy range of 50keV – 1.5 MeV, energy resolution of less than 7.2% FWHM [5] at 662 keV and a total weight of 300 g. Considering this payload they can measure for around 20 to 25 minutes wirelessly without stopping. However, they are meant to work connected by wire which makes them capable of taking measurements as long as it is needed.

F. Drone

The drone is an agile system that allows you to reach difficult to access areas with relative ease.

Figure 4. Indoor drone.

It has two inspection modes:

- Sweep: The drone approaches the wall to be measured, keeping a fixed distance from it. The drone then begins taking measurements as it moves along the wall. This method makes it possible to take a measurement of the general radiation, allowing the areas of greatest radiation to be detected quickly.

- Spot: The drone approaches a specific point on the wall where it remains stable for a certain time until the detector takes a spectrum of the radiation present. This mode allows to know the radiation more precisely from a point of interest.

Unlike the outdoor drone, the indoor drone cannot be helped by the GNSS system for its positioning and therefore presents an added difficulty. For its location it relies on sensors based on laser technology; the light beam bounces off the encountered objects and its distance is calculated by measuring the time it takes to be reflected. Taking an immense amount of references, it is possible to generate a sufficiently precise map of the place, giving the drone the ability to position itself within a centimetre level accuracy.

The detector carried by the drone allows a spectroscopic analysis of the gamma radiation registered, so the main radioisotopes that are present on the surface can be identified. To facilitate the visualization in the dismantling tasks, the drone has a software integrated that allows colouring the measured points according to the radiation level and its energy, linking the position information the laser system provides with the counts per second that the detector reads.

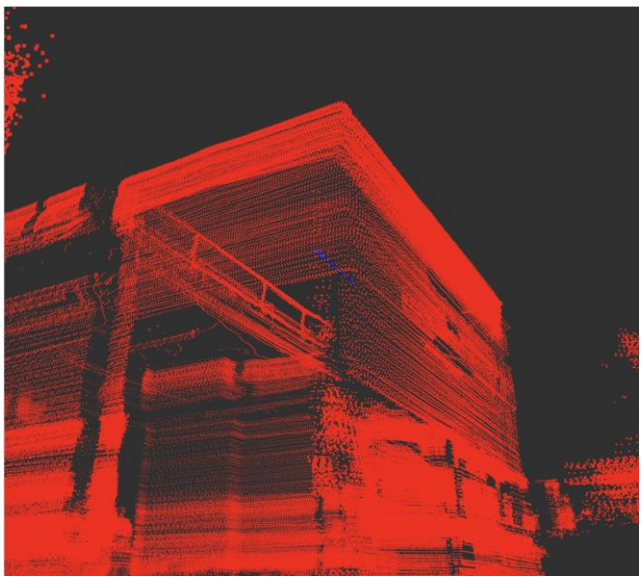

Figure 5. Drone positioning map.

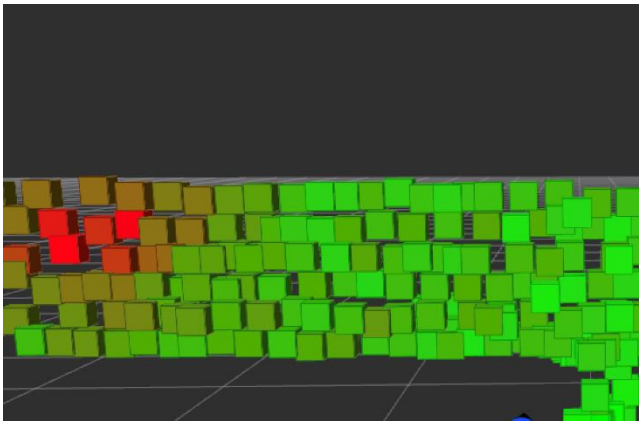

Figure 6. Drone radiation mapping.

G. Climbing robot

The climbing robot emerges as a complement to the task the drone performs. The physical characteristics a drone presents prevent it from accessing areas where the free flow of air is compromised. This is the case of areas close to ceilings or walls, areas populated with excess pipes or dimensionally reduced recesses. On the contrary, the climbing robot allows the characterization of ceilings and achieves more precise detector-point of interest distances due to its greater stability. Likewise, it presents an alternative of less agility than the drone when being transported to the different areas of interest.

The climbing robot is designed with the ability to inspect floors, ceilings and walls. For the latter two, the robot has been supplied with a turbine which generates a vacuum effect, allowing it to adhere to surfaces.

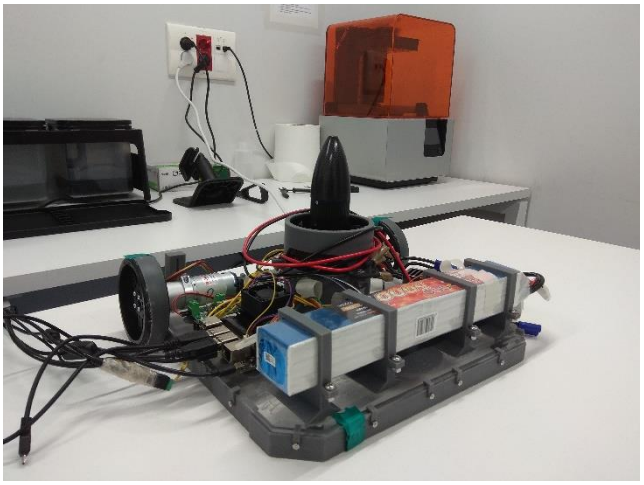

Figure 7. Climbing robot.

Like the drone, its location system is based on laser technology granting the ability to map the place for the robot to be located by itself. As a complement to laser positioning, it is supplied with vision cameras that, through software analysis of the images obtained, allows correcting the final positioning. They also serve to implement avoidance and detection of obstacles such as pipes, protrusions or edges on the surfaces which can difficult the robot stability.

The robot loads a radiation detector which can be automatically positioned at the desired distance from the surface. Being the ultimate objective the performance of radiological characterization tasks, the robot is capable of generating a heat map that will serve as a visual aid to quickly recognize the radiation on the inspected surface.

Figure 8 illustrates a map where the robot position is marked together with the counts per seconds (CPS) measured by the detector and pictures in a colour by counts fashion.

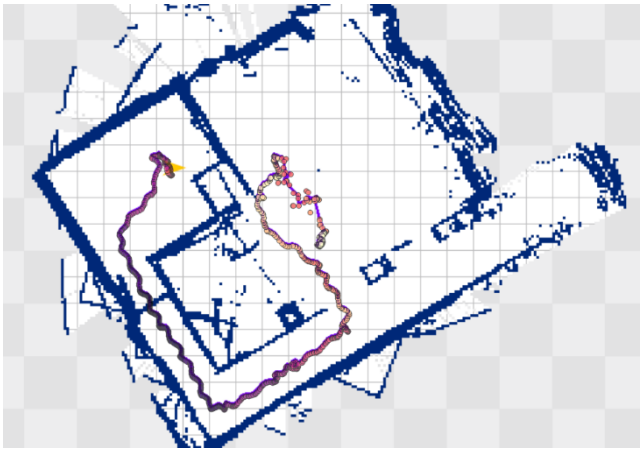

Figure 8. Climbing robot positioning map.

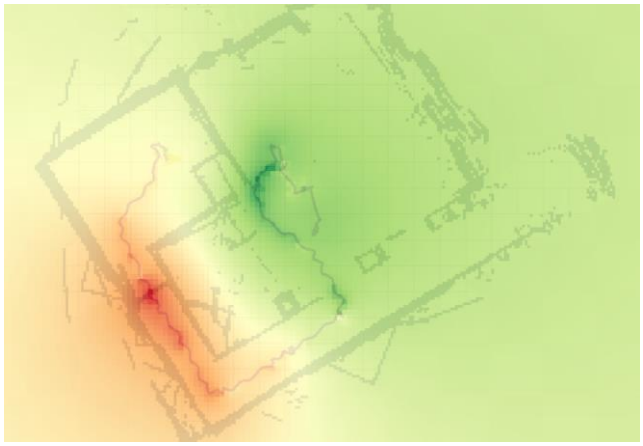

Figure 9. Climbing robot radiation heat map.

In figure 9 an IDW interpolation [6] is applied to generate a heatmap which help to visualize the CPS distribution. It also allows to represents the measurement by radiation channels allowing to identify the radioactive element.

IV. CONCLUSION

The implementation of radiological characterization tasks by using more automated means supposes, in the first place, an increase in operator safety; less time exposed to radiation without the need to access hard-to-reach places with harnesses, scaffolding or other tools. It also guarantees more effective and efficient work; a control in the distance of the detector, measurements in difficult access places, less time of execution, cost savings as well as the gathering and treatment of data in real time.

It stands out in an industry like the nuclear one, where safety is vital, that so little has been invested in more automated procedures which imply a reduction in the dangers that the sector entails.

For this reason, ENUSA is currently developing automated tools for radiological characterization, focused on dismantling procedures.

V. REFERENCES

[1] The first arm manipulators, link: Waldo Archives - cyberneticzoo.com

[2] Susan Goldberg "The robot revolution has arrived", link: National Geographic September edition 2021.

[3] Global Navigation Satellite System (GNSS), Link: What is GNSS? | EGNOS User Support (essp-sas.eu)

[4] RTK precision, Link: Centimeter Precision GNSS explained - RTK Explained - ArduSimple

[5] FWHM definition, Link: FWHM (noao.edu)

[6] IDW interpolation, Link: How inverse distance weighted interpolation works—ArcGIS Pro | Documentation

Proceedings of the European Nuclear Young Generation Forum
ENYGF'21
September 27-30, 2021, Tarragona, Spain

Analysis of the influence of sampling procedure in water radon measurements

Noverques Medina, Aina; Sancho Fernández, María; Juste Vidal, Belén; Verdú Martín, Gumersindo.

[1] Institute for Industrial, Radiophysical and Environmental Safety (ISIRYM). Universitat Politècnica de València. Spain.

*Corresponding author: *ainome@iqn.upv.es*

I. INTRODUCTION

Considered as a carcinogenic element, radon produces in Spain, more than 30% of the total natural radiation to which a person is exposed during a year. This supposes an average of 1.15 mSv per year reaching up to 40 mSv in specific areas whose soils have a high content of radium and uranium. [1, 2].

The main radon generating sources are soil, depending on its uranium content; water, which can carry radium present in sediments and be transported by groundwaters to lakes, rivers or ponds; and building materials, also depending on their radium content.

Both air radon concentration and water radon concentration are controlled according to European legislation: Directive 2013/59/EURATOM and Directive 2013/51/EURATOM, respectively. In both cases, the main objective is to protect people from this gas exposure.

However, since radon is a gas with a high air affinity, it is difficult to measure and control. For this reason, it is important to learn about its behavior in different media (water, air, or soil) and to provide different methodologies and protocols that guarantee its correct measurement.

Some of the current researches are focused on the problems of radon measurements in water: sampling, transport and measurements in the laboratory or in situ. These processes are difficult to carry out due to the loss of radon that occurs. Among the variety of radon in water measuring methodologies, the most important techniques are gamma spectrometry, using the gamma rays of radon and its progeny (Pb-214 and Bi-214); using ionization chambers, or by extraction of radon by organic solvents and measurements by scintillation liquid counters. All three methods are efficient and reliable, and their selection will depend on the required test conditions [3].

The measurement of radon in water using scintillation detectors has been extensively verified by numerous studies showing that it is very useful in the measurement of radon in water [4, 5].

Moreover, it is important to examine the process of water sampling because radon can be released into the air if bubbling of the sample occurs. It has been found that radon concentrations in water, measured on-site, are between 13% and 22% above the same measurements performed in the laboratory and that pipetting the water sample prevents radon loss due to bubbling [5].

Additionally, radon concentration varies enormously depending on the distance to the emitting source that generates it. For example, in surface waters concentrations are generally less than 2 $B \cdot L^{-1}$ while in groundwater they can reach more than 10000 $B \cdot L^{-1}$.

Having a reliable methodology, and knowing the behavior of radon at laboratory scale, would facilitate subsequent radon measurements in groundwaters, lakes and ponds.

For this reason, the main objective of this research is to analyze the behavior of radon in water inside a sealed tank by studying its distribution at different liquid points, as well as using two different methods of water sampling.

II. METHODOLOGY

This section details the experimental procedure developed, including both the detector used and the experimental equipment.

C. Radon source and experimental device

In this research, two natural radium-226 source have been used to analyze radon homogeneity in water. Their activities are about 4.27 kBq and 45 kBq. They have been also characterized to estimate its radon emission rate. These sources make it possible to enrich water: initially it is free of radon and gradually, its concentration increases. The longer the test time, the higher the radon concentration in water.

To carry out the tests, a high-density polyethylene tank, impervious to radon, with a capacity of 120 L was used. Inside, on the base, the sealed radon source, was placed. The tank was filled with 50 L of water, which will gradually be enriched with radon.

The main diagram of the experimental device is shown in Figure 1:

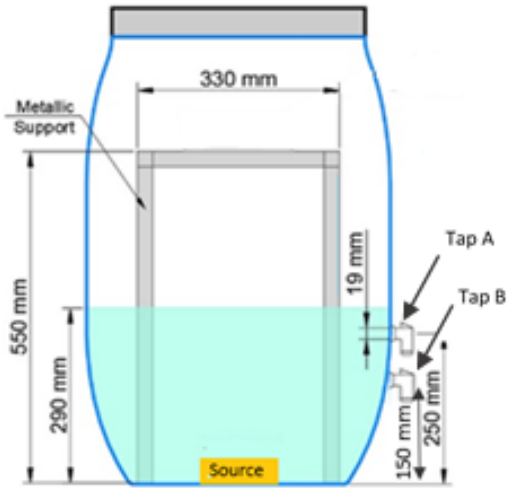

Figure 1. Sketch of the experimental device.

D. Experimental procedure

Two different types of radon-in-water tests were carried out:

1. Study of radon concentration in water at different points of the liquid volume. For this purpose, two taps were installed in the tanks, at the heights shown in Figure 1. Tap A is 25 cm from the base, and tap B is about 15 cm from the base (10 cm below tap A). The two taps are on the same vertical line but at different distances from the source at the bottom.
   In this study the water sampling method is the same: the tap is slowly opened, and the water is collected in a beaker. From there, the water sample required for analysis in the detector is extracted by pipetting and mixed with liquid scintillator cocktail for its measurement.
   For these tests, the source used is the one with lowest activity: 4.27 kBq. Experimental test consisted of a first stage of water enrichment (which lasted 13 days), with the source inside the tank; and a second stage (which lasted 7 days) in which radon source was removed and the radon concentration in water during radioactivity decay was also studied.
   This study allows to analyse the evolution of radon concentration in water during both stages at two different heights in the liquid.
2. Study of the influence of water sampling method on radon concentration measurement. The two different sampling methods were: sampling of the water through the tap and subsequent pipetting from the beaker; and direct sampling of the water by inserting a syringe through the tank.
   For water sampling through the tap, as in the previous section, the tap is opened, the water sample is collected, and tap closed again.
   In this case, the source used has a higher activity, 45 kBq, so the test times can be reduced to 242 hours.

E. Detector for radon in water measurements

The detector used for radon analysis in water is the Hidex 600 SL scintillation liquid counter (Hidex Company). Its principle of operation is based on the property of some substances to emit light when they interact with radiation. These light pulses are collected and converted into an electrical signal that determines the energy of the incident particle and allows to know, in this case, the levels of radon in the water sample.

The measurement method is based on mixing 8 mL of water sample with 12 mL of scintillation liquid cocktail. According to the manufacturer, radon is extracted from the water to the cocktail with an error of less than 10% [6].

III. RESULTS

The results obtained in this research are presented below according to the sequence of tests previously described.

A. Study of radon distribution in water at different heights of the liquid

Radon measurements in water inside the tank have been performed by sampling through two taps (A and B), located at different heights as described in the methodology.

Water enrichment takes places for almost 306 hours. Afterwards, removal of the radon source causes a drop in radon concentration in water up to 495 hours as it is observed in the following Figure 2 that shows the results obtained for both taps:

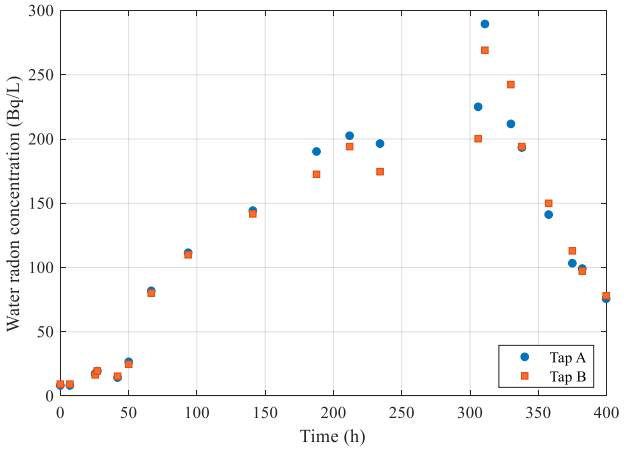

Figure 2. Results obtained from the measurement of radon in water using two taps at different heights: tap A and tap B.

As shown in the figure, initially the amount of radon in water is practically zero, then, water is enriched until it reaches 225.07 $Bq \cdot L^{-1}$ for tap A and 200.26 $Bq \cdot L^{-1}$ with tap B in 306 hours.

Once the source is removed, as there is no longer any radon input, its concentration in the water decreases to 75.70 $Bq \cdot L^{-1}$ for tap A and 78.95 $Bq \cdot L^{-1}$ for tap B, after 187 hours approximately.

Analyzing the dispersion of results between tap A (taking this as a reference) and tap B, it should be noted that, for the first water samples, up to approximately 187 hours, the average dispersion of all values is less than 7%.

From that point until 360 hours, as shown in the figure 2, the dispersion of results at both sampling points increases slightly, ranging between 9 and 14%. In this case, the average value of the dispersion is less than 10%.

In the last test section, from 360 hours to 400 hours, the dispersion is below 1%. In this case, there is a point, at 374 hours, which, as shown in the graph, has a higher dispersion of 9%.

Additionally, the ratio of radon concentration obtained through Tap A and Tap B has been calculated, which is shown in Figure 3.

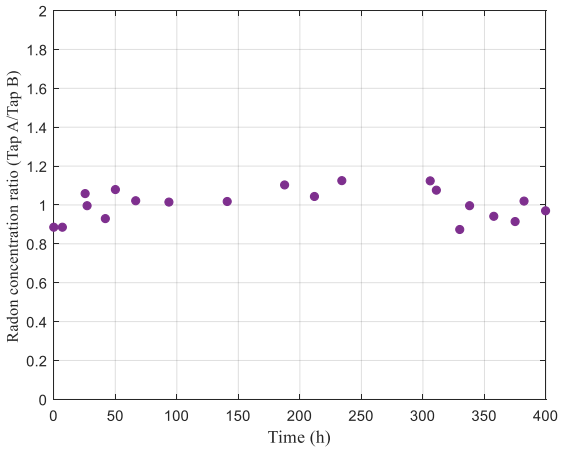

Figure 3. Radon concentration ratio by Tap A and Tap B

As observed in Figure 3, the ratio of radon concentrations in water is around 1, slightly oscillating from 0.88 to 1.12.

The measured radon concentration values in water are similar in both tap A and tap B. This verifies that radon in water is homogeneously distributed inside the tank even in the static state of the water, without agitation.

B. Study of the influence of water sampling method on radon concentration measurement

This section analyzes the radon concentration in water measured by two different samplings: the water is collected in a beaker through a tap and the water is extracted directly from the tank by inserting a syringe inside it. Both tap and syringe are located at the same height.

Results are shown in the following Figure 4:

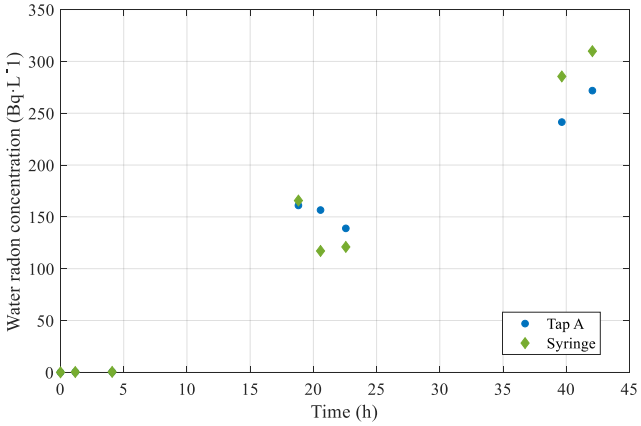

Figure 4. Results obtained from the measurement of radon in water using two different collecting water methods: tap and syringe

Radon values in water enriched with a 45 kBq source range from initially 0 $Bq \cdot L^{-1}$ to 271.79 $Bq \cdot L^{-1}$ for the tap and 309.89 79 $Bq \cdot L^{-1}$ for the syringe at 42 hours.

Initially, for very low radon water concentrations, both sampling methods offer very similar results with a dispersion less than 1%, until 5 hours exposure.

In Figure 4, it is observed that, as the water becomes enriched with radon, the dispersion increases. The average value of the dispersion of results of radon concentration in water is below 20% for all measurements carried out.

These results show differences in radon concentration results mainly due to the water sampling method. In the case of the tap, the water that is collected in the beaker is gently bubbled. However, during the extraction of the sample through the syringe, the water goes directly from the inside of the tank to the syringe and from there to the vial of scintillation liquid, practically without bubbling. In both cases, the way to insert the water sample into the scintillation vial is the same, so that this bubbling condition could be considered negligible.

The ratio of radon concentration in water has also been represented according to the extraction method (Tap A/ syringe) in Figure 5.

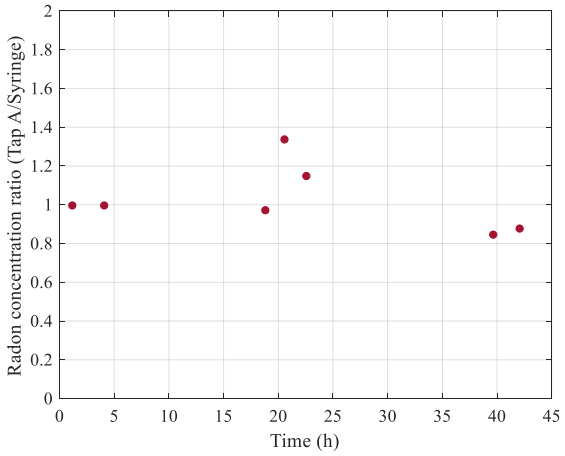

Figure 5. Radon concentration ratio by Tap A and syringe

As observed, radon concentration ratio (Tap A/syringe) ranges between 0.87 and 1.33. The results show ratio values

close to 1 and therefore the difference between the extraction method is small.

The global average of the dispersions in all measurements is less than 20%. Thus, both water extraction methods could be accepted considering that a correction factor of 20% must be applied for the results obtained with the tap.

In other investigations, water sampling through direct extraction and pipetting allows obtaining slightly higher values of radon in water than other methods in which there is a greater degree of bubbling [5]. This is verified by the experimental results obtained in which it is observed that when the water is more enriched, the extraction with the syringe allows measuring higher concentrations. The bubbling produced (tap A) in the collection of water in the beaker causes a slight loss of radon in the sample.

C. CONCLUSIONS

In this research, the distribution of radon in water inside a tank, in steady state, and with two different sampling methods has been analyzed.

From the results obtained from the radon distribution inside the tank, it is observed that through both taps the final concentration reached is practically the same: 225.07 79 $Bq \cdot L^{-1}$ (Tap A) and 200.26 79 $Bq \cdot L^{-1}$ (Tap B). Concentration drops to 75.70 79 $Bq \cdot L^{-1}$ for tap A and 78.95 79 $Bq \cdot L^{-1}$ for tap B after the source removal from inside the tank.

According to the dispersion results calculated between tap A and tap B, 15% is not exceeded at any point of sampling. The low dispersion of the results suggests that the radon distribution inside the tank is taking place in a homogeneous way. These results are verified by calculating the ratio radon concentration which is close to 1.

Once this distribution was known, the water sampling was analyzed by two different methods: water collection from a tap and direct extraction from the tank using a syringe.

After water enrichment, radon concentration reaches 271.79 $Bq \cdot L^{-1}$ for the tap and 309.89 79 $Bq \cdot L^{-1}$ for the syringe in 42 hours.

The results show slightly higher radon concentrations in water if the sample was drawn with a syringe, directly from inside the tank. This could be mainly due to the sampling of the water with tap causes greater bubbling than with the syringe. The dispersion of radon results in water is, on average, 20%. In this case, the radon concentration ratio is slightly away from 1, oscillating between 0.99 and 1.33.

This research has proved, on the one hand, the homogeneous distribution of radon inside the tank according to the sampled conditions. Likewise, according to the dispersion obtained by tap and syringe water sampling results, a correction factor could be used to adjust the achieved values of radon water concentration.

D. References

[1] Cancio Pérez, D. (2010). Impacto radiológico de las fuentes naturales y artificiales de radiación. El informe UNSCEAR 2008. Nucleus, (48), 3-9.

[2] Zeeb, H., & Shannoun, F. (2015). Manual de la OMS Sobre el Radón en Interiores: Una perspectiva de salud Pública.

[3] Pujol, L., & Pérez-Zabaleta, M. E. (2017). Comparison of three methods for measuring 222 Rn in drinking water. Journal of Radioanalytical and Nuclear Chemistry, 314(2), 781-788.

[4] Jobbágy, V., Stroh, H., Marissens, G., & Hult, M. (2019). Comprehensive study on the technical aspects of sampling, transporting and measuring radon-in-water. Journal of environmental radioactivity, 197, 30-38.

[5] V. Gruber, F.J. Maringer, C. Landstetter, "Radon and other natural radionuclides in drinking water in Austria: Measurement and assessment". Applied Radiation and Isotopes, Volume 67, Issue 5, 2009.

[6] Hidex 600SL User Manual. Doc 413-009. Version 1.0. Hidex.

Proceedings of the European Nuclear Young Generation Forum
ENYGF'21
September 27-30, 2021, Tarragona, Spain

Development of a method for radiological characterization of airborne dust in the ceramic industry

Sáez-Muñoz, Marina[1*], Sevilla, Aixa[1], Ortiz, Josefina[1] and Martorell, Sebastián[1]

[1] Laboratorio de Radiactividad Ambiental, MEDASEGI Research Group, Universitat Politècnica de València, Spain

*Corresponding author: *masaemuo@etsii.upv.es*

I. INTRODUCTION

The ceramic industry in Spain is mainly located in the Valencian Community, and it represents 2.7% of the Valencian GDP (*Gross Domestic Product*). Different types of industries participate in this sector: zirconium sand milling plants, frits, pigments and glass production industries, atomizers and ceramic tile producers.

In most of them, some NORM materials (Naturally Occurring Radioactive Materials) are used, such as zirconia sands, which contain natural isotopes of the U-238 and Th-232 chains. Both chains are formed by alpha, beta and gamma emitters, some of them with long half-life ($T_{1/2}$) that can affect to the workers of these industries. In particular, it is important to highlight uranium and thorium isotopes: U-238 ($4.5 \cdot 10^9$ years, $T_{1/2}$), U-234 ($2.5 \cdot 10^5$ years, $T_{1/2}$), Th-232 ($1.4 \cdot 10^{10}$ years, $T_{1/2}$) and Th-230 ($7.5 \cdot 10^4$ years, $T_{1/2}$), all of them alpha emitters. Other important isotopes present in their chains are Ra-226 (1600 years, $T_{1/2}$), Ra-228 (5.8 years, $T_{1/2}$), Pb-210 (22 years, $T_{1/2}$), and Po-210 (138 days, $T_{1/2}$), but they were not considered in this first study.

The zircon sands used in the Valencian Community usually come from Australia or South Africa, which are the main producers. Their activities depend on the origin of the sand and they range between 1000 - 4000 Bq kg^{-1} of U-238 and 400-1000 Bq kg^{-1} of Th-232, and may be even higher in other countries [1]. Therefore, these raw materials and their derivative products usually exceed 500 Bq kg^{-1}, which is the exemption level proposed by the Spanish Nuclear Safety Council (CSN) in its Safety Guide 11.02 "Control of exposure to natural sources of radiation" [2] for the U-238 and Th-232 in secular equilibrium with all their descendants. These exemption levels were also recommended by the European Union in its document RP 122, part II [3], and they should not be exceeded to limit worker and public effective doses to 300 μSv $year^{-1}$.

The production activities carried out in these companies of the ceramic sector (classified as Zirconium industries and therefore are within the scope of the NORM industries) are regulated by the Regulation on sanitary protection against ionizing radiation (RD 783/2001) [4], which transposes the European Directive 96/29/EURATOM [5], and the Technical Instruction of the Spanish Nuclear Safety Council (CSN) IS-33, on radiological criteria for the protection of workers and the population against to the risk of exposure to natural radiation [6]. The radiological impact of these NORM industries must be assessed following the Spanish Nuclear Safety Council (CSN) in its Safety Guide 11.03, "Methodology for the evaluation of the radiological impact of NORM industries" considering both external and internal exposure [7].

Previous studies done by the group revealed that the workers of the ceramic industry are professionally exposed to effective doses lower than the annual limit for the public of 1 mSv (maximum levels of 0.6 mSv), estimating the internal dose as the main contribution [8]. The internal doses were calculated considering the activity of the ceramic materials and the amount of dust inhaled. However, it would be interesting to improve the characterization of the inhaled source term to obtain a less conservative internal dose when the values are close to the limits established in the regulations.

With this objective, the Laboratorio de Radiactividad Ambiental of the Universitat Politècnica de València is working on the project of "Characterization and radiological measurement of airborne dust in the ceramic industry of the Valencian Community" promoted by the Valencian Regional Government (AICO/2020/106).

II. MATERIALS AND METHODS

The methodology used to evaluate the internal dose by inhalation is based on the activity of the ceramic materials and the total amount of dust present in the work environment. However, this is a conservative approximation of the dose received by inhalation, since the real activity of the collected dust is not determined. Therefore, it is intended to improve the characterization of the inhaled source term by means of radiochemical separation procedures of the isotopes of interest.

The radiochemical procedure to separate the isotopes of interest consists of four main steps: sample pretreatment, chemical separation, alpha source separation and the measurement.

In particular, this project has started with the development of procedures for the determination of alpha emitters of uranium (U-238, U-234 and U-235) and thorium (Th-232, Th-230 and Th-228) present in glass-fiber filters of 45 mm with zirconium silicate dust (Figure 1).

Figure 1. Aerosol filter sample with zirconium silicate dust.

Due to the complexity of dissolution of the matrix, the pretreatment of the sample is carried out by fusion technique with borate salts at 1000 ºC for 30 minutes. Then the sample is dissolved in an acidic media (Figure 4). Once the sample is dissolved, uranium and thorium tracers are added (U-232 and Th-229, respectively) to determine the chemical yield of the procedure. Polyethylene glycol (PEG) is added to remove the silicates of the sample and the borates of the fluxer. After that, the actinides are coprecipitated with iron hydroxides and dissolved the proper acidic media for column separation.

Subsequently, two separation methodologies were tested to separate the isotopes of interest: chromatographic extraction resins (UTEVA resin) and ion exchange resins (AG1X8). UTEVA resin allowed the separation of uranium isotopes following the scheme shown in Figure 2.

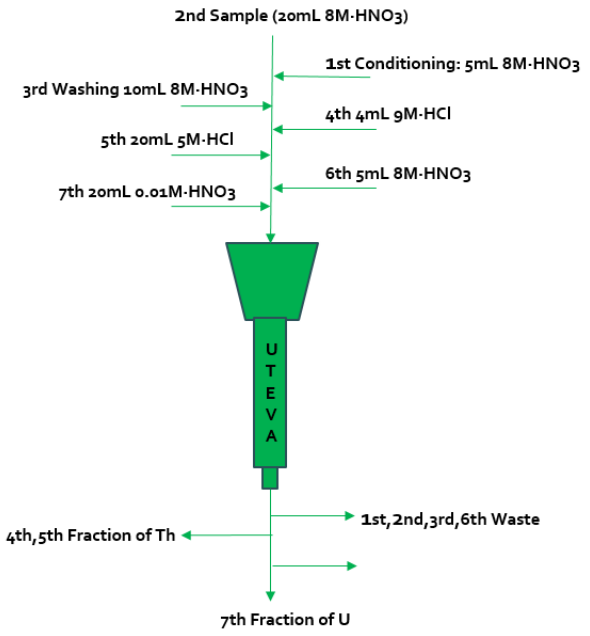

Figure 2. UTEVA separation steps.

However, ion exchange resins were needed to determine thorium isotopes. Two column separation steps were used. The first one allowed the separation of uranium isotopes, (Figure 3) and the second one was used for thorium purification (Figure 4).

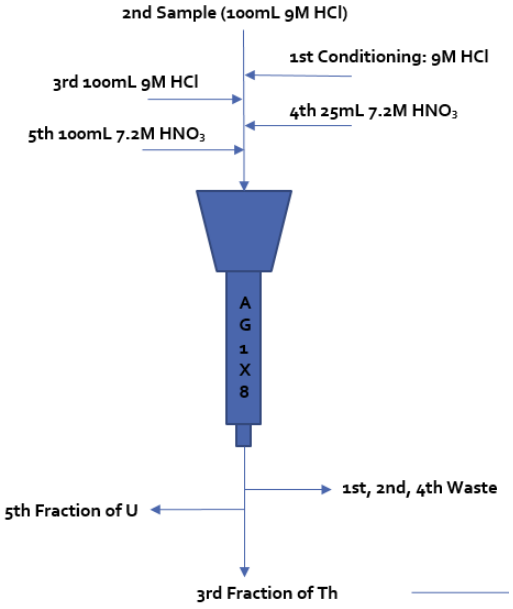

Figure 3. Ion exchange separation steps: first column.

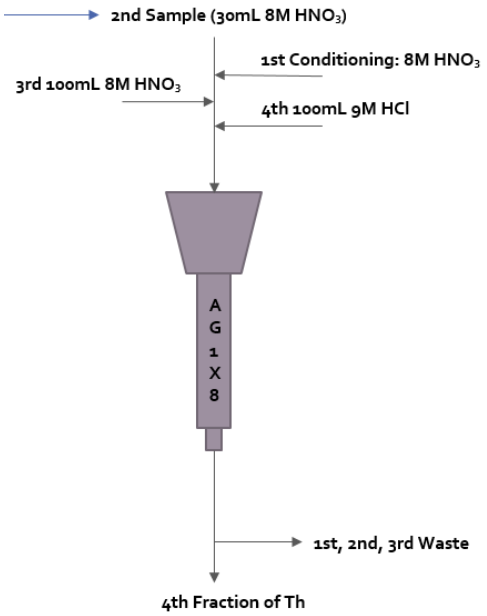

Figure 4. Ion exchange separation steps: second column.

Finally, the alpha sources are prepared by electrodeposition in a stainless steel planchet of 25 mm diameter following the method proposed by Hallstadius [9] and the planchets are measured by alpha spectrometry to quantify uranium and thorium activities. Figure 5 and Figure 6 show an example of both spectra.

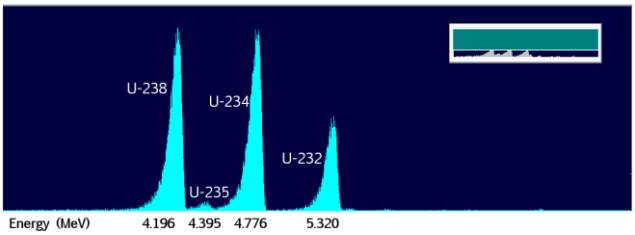

Figure 7. Uranium spectrum by alpha spectrometry.

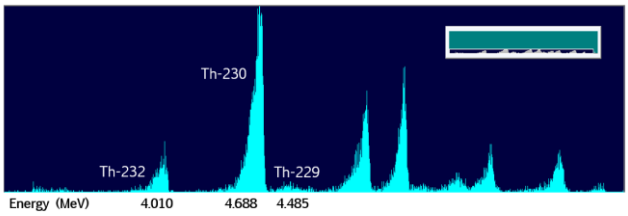

Figure 8. Thorium spectrum by alpha spectrometry.

III. RESULTS AND DISCUSSION

Nine tests were performed with UTEVA resin separation. The average uranium activities and the range of values obtained are shown in Table 1.

Table 1. Average uranium activities obtained with UTEVA resin separation, standard deviation (SD) between replicates and in relative percentage (RSD).

Parameter	U-238	U-234	U-235
$A_{average}$ (Bq kg^{-1})	4747	4687	130
A_{range} (Bq kg^{-1})	4055-5551	3950-5688	106-153
SD (Bq kg^{-1})	600	593	46
RSD (%)	13	13	12

The procedure with UTEVA separation is quite reproducible in the conditions of our laboratory, with deviation below 15% in U-238, U-234 and U-235 activities. In addition, the results proved the secular equilibrium in U-238 chain, with an average ratio U-234/U-238 of 0.99. However, the chemical yield is below 6% in all the tests carried out due to the complexity of the sample, increasing the uncertainty in the determination. Thorium activities were not calculated because it was not possible to electroplate UTEVA thorium fraction. An additional cleaning step would be necessary to quantify thorium.

Six tests with the ion exchange separation were performed and the average uranium activities obtained are shown in Table 2.

Table 2. Average uranium activities obtained with Ion Exchange resin separation, standard deviation (SD) between replicates and in relative percentage (RSD).

Parameter	U-238	U-234	U-235
$A_{average}$ (Bq kg^{-1})	4148	4090	140
A_{range} (Bq kg^{-1})	3921-4383	3773-4445	109-180
SD (Bq kg^{-1})	192	244	29
RSD (%)	4.6	5.9	21.1

As can be seen, this methodology is also reproducible in the conditions of our laboratory, with a relative standard deviation below 6% for U-238 and U-234 activities. The secular equilibrium in the uranium chain is maintained, with an average ratio U-234/U-238 of 0.99. Moreover, chemical yields are still low, but higher than UTEVA separation, ranging from 17 to 31%. Therefore, uranium activities have a lower uncertainty. The thorium fraction was cleaned in other ion exchange resin and their activities obtained are shown in Table 3.

Table 3. Average thorium activities obtained with Ion Exchange resin separation, standard deviation (SD) between replicates and in relative percentage (RSD).

Parameter	Th-232	Th-230
$A_{average}$ (Bq kg^{-1})	836	5101
A_{range} (Bq kg^{-1})	268-1435	1311-8323
SD (Bq kg^{-1})	432	2821
RSD (%)	51.7	55.3

Thorium activities had high variability due to the low chemical yields obtained in the separation. In most cases they were below 10%, except in one case with 55%. The activities obtained in the last case were 662 ± 96 Bq kg^{-1} for Th-232 and 3923 ± 500 Bq kg^{-1} for Th-230, proving again the secular equilibrium in uranium chain due to the similar activities obtained for U-234 and U-238. However, the methodology is going to be improved to increase thorium yields and reduce the activity variability and uncertainty. Th-228 was not calculated because is also present in U-232 tracer.

Moreover, the zirconium silicate sample analysed in this work was previously measured by gamma spectrometry to identify the equilibrium in both chains and the approximately activity of their isotopes. In this case, the amount of sample was enough to be measured by this technique, but it is not possible in real aerosol samples.

HPGe detector was used to measure uranium and thorium chain activities. U-238, U-234 and Th-230 are quantified by its gamma emitter daughter Pb-214 (351,92 keV), and Th-232 by Ac-228 (911,07 keV). Their activities were 4096 ± 21 Bq kg^{-1} and 608 ±17 Bq kg^{-1}, respectively. The activities obtained in the study were compared with the gamma activities. The range and average relative bias obtained for uranium and thorium isotopes are shown in Table 4.

Table 4. Average and range relative bias obtained with UTEVA and Ion Exchange resin separation for uranium and thorium isotopes.

Relative Bias (%)	UTEVA		ION EXCHANGE	
	Average	Range	Average	Range
U-238	16	-1.0 – 40	1.3	0 – 7
U-234	14	0.2 – 40	-0.1	-2 – 9
Th-230	-	-	25	-4 – 103
Th-232	-	-	38	9 – 136

Uranium activities obtained with UTEVA separation were in most cases acceptable (relative bias below 25%). However, in two samples activities were higher, with relative bias close to 40%.

The uranium activities obtained with ion exchange separation are more similar to gamma activities, with all relative bias below 10%. For this reason, ion exchange resins are better to determine uranium activities in this type of samples.

In case of thorium determination, only ion exchange resins were able to separate and quantify thorium fraction. However, chemical yields were very low in most of the cases and relative bias were high. Only in the case of the sample with 55% of chemical yield, the activities were calculated with high accuracy (relative bias below 10% for both isotopes).

IV. CONCLUSIONS

The Laboratorio de Radiactividad Ambiental of the Universitat Politècnica de València is developing radiochemical methods for the determination of the main natural isotopes present in the airborne samples of the ceramic tiles industry.

In the first approach, the laboratory has tested different methods for uranium and thorium determination in aerosol filters with zirconium silicates. The methods tested were based in a pretreatment of the sample by fusion and then a separation by extraction chromatography (UTEVA) or ion exchange resins. Finally, the actinides were electroplated and measured by alpha spectrometry.

According to the results, ion exchange resins are the better option to separate uranium isotopes due to the good reproducibility and accuracy and higher chemical yields than UTEVA resins. However, thorium yields are more variable and high relative deviations were obtained when yields were low. For this reason, the laboratory is working on improving these results modifying some separation steps. In addition, the individual determination of thorium is going to be tested.

Once the final method is developed, the LRA-UPV will determine uranium and thorium activities of the aerosols present in the working areas, and will evaluate more realistically the internal doses received by the workers of the ceramic industry.

V. References

[1] International Atomic Energy Agency (IAEA), Radiation Protection and NORM Residue Management in the Zircon and Zirconia Industries, Safety Reports Series, No. 51, 2007.

[2] Spanish Nuclear Safety Council (CSN), Safety Guide GS-11.02, Control of exposure to natural sources of radiation. CSN, 2012.

[3] RP 122: Radiation Protection 122. Part II. Application of the concepts of exemption and clearance to natural radiation sources, European Commission, 2001.

[4] Spanish Royal Decree 783/2001, which approves the Regulation on Protection against Ionising Radiations, 2001.

[5] Council Directive 96/29/EURATOM, laying down basic safety standards for the protection of the health of workers and the general public against the dangers arising from ionizing radiation, 1996.

[6] Spanish Nuclear Safety Council (CSN), Technical Instruction IS-33, on radiological criteria for the protection of workers and the population against to the risk of exposure to natural radiation. CSN, 2011.

[7] Spanish Nuclear Safety Council (CSN), Safety Guide GS-11.03, Methodology for the evaluation of the radiological impact of NORM industries. CSN, 2012.

[8] Spanish Nuclear Safety Council (CSN), Technical Reports Collection INT-04-33, “Estudio radiológico de la industria cerámica y auxiliaries”. CSN, 2013. (In Spanish)

[9] Hallstadius, L., A method for the electrodeposition of actinides, Nuclear Instruments and Methods in Physics Research 223, 266–267, 1984.

Proceedings of the European Nuclear Young Generation Forum
ENYGF'21
September 27-30, 2021, Tarragona, Spain

Portable boron meter, a non-destructive technique proposed to detect boron plugs in NPP pipes without necessity to remove heat insulators and tubes

Karst Maxime[1*], Piette Ludivine[1], Saintamon Fabrice[1], Le Noblet Thibaud[2], Van Dendaele Cédric[2], Zongo Sitrougne Soufian[3], Cerna Cedric[3], Mathieu Ludovic[3], Stuttge Louise[4], Moukaddam Mohamad[4]

[1] EDF/UNIE/GPEX France

[2]CARMELEC France

[3] Université de Bordeaux, CNRS, CENBG, UMR5797, F-33175 Gradignan, France

[4]IPHC, Université de Strasbourg, CNRS-IN2P3, F-67037 Strasbourg, France

*Corresponding authors: maxime.karst@edf.fr / ludivine.piette@edf.fr

I. INTRODUCTION

Boron, and especially the ^{10}B, is an element with the property of absorbing the neutrons produced by nuclear reactions. It is mixed with the water of the primary circuit and allows to control, and if necessary, to stop the nuclear reaction. At standstill, additional amounts of boron are introduced into the primary circuit to prevent any possibility of inadvertent restart of the nuclear reaction.

In the TWE (Treatment of Waste Effluents), boron is under the form of boric acid which is very sensitive to temperature changes. Under specific circumstances [1], it can crystallize (Figure 1) forming a deposit on the walls of the pipes. This deposit could become a plug and may prevent proper effluent flow. Pinpoint the exact location of the cap is extremely difficult or even impossible.

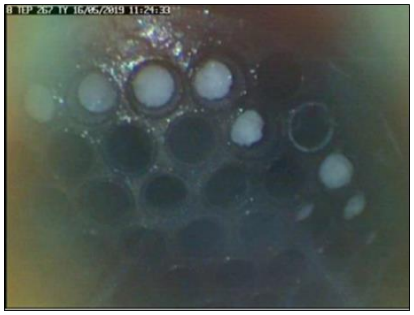

Figure 1: View of boron plug inside pipes

In some cases, the location of the plug can be estimated thanks to a gamma camera, endoscopy or thermal camera but theses technics suffer from a lack of efficiency. As the localization of the plug is not well known, the only solution today consist of removing large portions of pipes by cutting/welding which involves significant costs in time, money and dose.

From this statement, a non-intrusive detection technique has been developed allowing to locate those boron deposits. The solution is based on a regular boron detection method [2]: a standard neutron source of $^{241}Am^{13}C$ is used (available on each EDF NPP) in association with a neutron detector to monitor neutron flux along pipes.

II. TECHNICAL SOLUTION DEVELOPED

A. General method used

The boron detector is composed of a neutron source with thermalizer and a neutron/gamma detector. Neutrons will be first thermalized by about ten centimeters of polyethylene before passing through the pipes. Neutron flux is monitored by a slow neutron detector on the other side of the pipe. Figures 2 and 3 illustrate the detection solution.

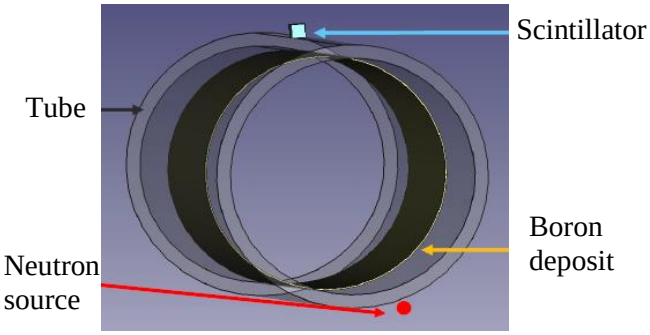

Figure 2: System diagram

All components are maintained with a mechanical structure made with a 3D print for the first prototype.

Figure 3: General view of our detection solution built with a 3D print

B. Neutron/Gamma Detector

The neutron detector is composed by an organic scintillator coupled to a photomultiplier. The signals are acquired, treated and digitalized with a fast dedicated electronics allowing their integration. The neutron/gamma discrimination is based on a Pulse Shape Discrimination (PSD) analysis [3].

As shown in Figure 4a, the fall time of a signal induced by a gamma interaction is faster than the one created by a neutron. By integrating the signals on two different time gates (slow and fast), it is possible to separate the two components. A schematic view of the 2D histogram of the slow gate / total gate charge ratio with respect to the total charge is shown in Figure 4b. The results obtained on the AIFIRA accelerator facility [4] at CENBG are shown in Figure 5.

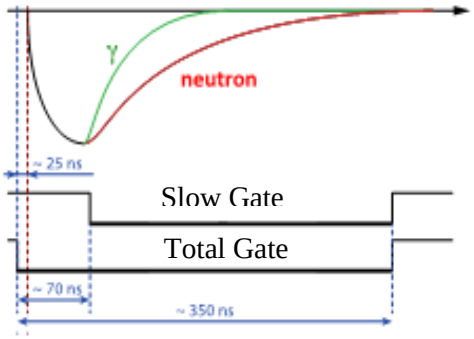

Figure 4a: Discriminant scintillator output signal diagram showing the different slow components of neutron and gamma ray and signal load integration gates

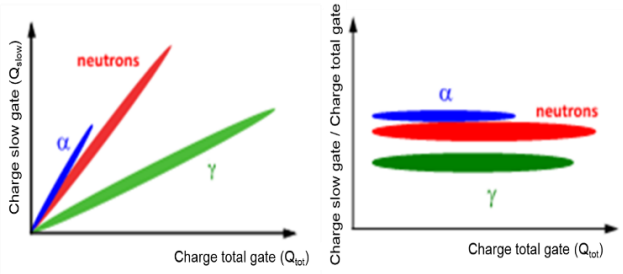

Figure 4b: Principle of Pulse Shape Discrimination

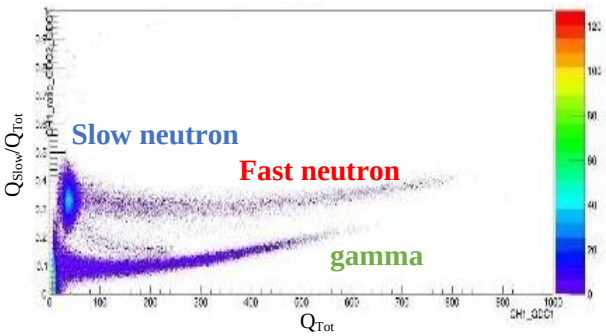

Figure 5: Correlations between Qtot and Qslow/Qtot obtained in the reaction in the compound, experience with the AIFIRA accelerator at CENBG

C. Thermalization

MCNP simulations have been performed to define and optimize the geometry of the device such as the placement of the source and the thickness of the thermalization. An optimum between detection sensitivity and cumbersome has been selected. Pipes are most of the time difficult to access and our solution needs to be really small and light.

On Figure 6, there are simulations about a tube of 5cm internal diameter, with 10cm of HDPE and plug/deposits of 10 cm long. It shows that a boron plug will be detectable in this configuration: there is a factor of 100 difference between black and red lines. Neutron flux would decrease by a factor of 100 if there is a boron plug, and by a factor around 10 in a known range of energy if there is a deposit (blue, orange and green lines).

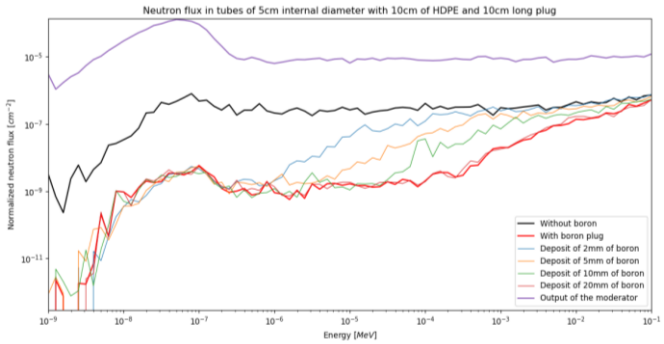

Figure 6: MCNP simulations illustrate neutron flux normalized of different sizes of boron deposits.

III. RESULTS AND DISCUSSION

A first version of the prototype was used in the Fessenheim NPP on TWE system. As the results of the simulations predicted, our system was able to detected boron deposit or plug larger than 6 mm diameter. Boron plug has been detected helping this NPP to repair pipes.

A. Tests configuration - Fessenheim NPP

During those tests, around 40 points of measurements were done to search boron plugs in TWE pipes, in a tube DN15 of 20 mm of external diameter in a gamma atmosphere from 0 to 1 mSv/h.

Measurements at key locations were done. First, reference measurements on a tube assumed to be boron free were done. Then, there were measurements on a tube at the exit

of the room to the glove box (Figure 7a), on a tube downstream of the pump (Figure 7b) and on 2 elbows of TWE room at the top of the room (Figure 7c).

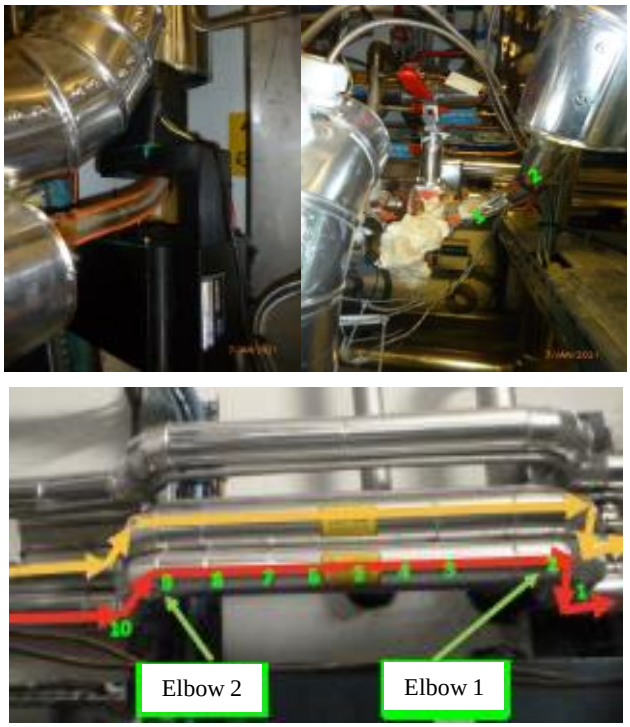

Figure 7a (top left), 7b (top right) and 7c (down): show different configurations of tests at the Fessenheim NPP

B. Results of test campaign

Figure 8 shows the neutron flux measured on the pipe downstream of the pump (Figure 7b). At this location, a deficit of 50 % up to 60 % on the counting rate has been measured compared to the reference pipes. This deficit is interpreted as an increasing of the neutron absorption which is probably induced by the presence of boron inside the pipe (plug/deposit).

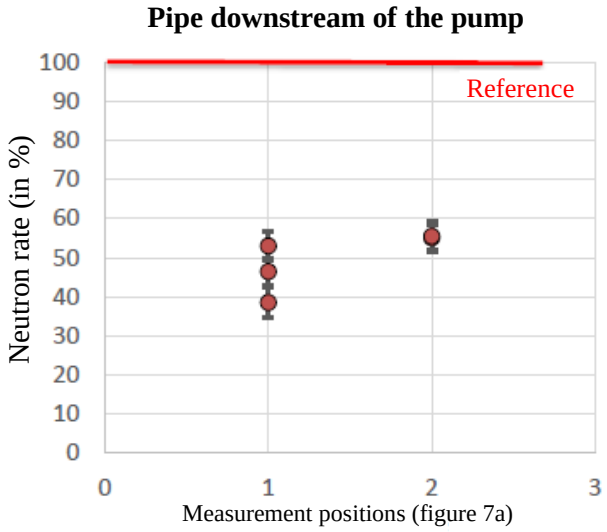

Figure 8: Neutron flux observed on measure points 1 and 2 (see on Figure 7b).

Fessenheim workers could verify the tube downstream of the pump. No boron plug has been found at this place, but a big deposit of boron as shown in Figure 9. Pipe was not completely blocked. This large deposit was due to accumulation of boron just before plug. Total boron plug was at a place inaccessible by the boron detector 20 centimeters lower on this pipe.

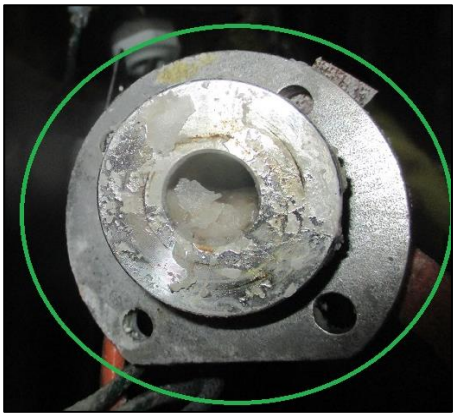

Figure 9: Big deposit of boron just before plug found thanks to our detector

C. Discussion

We had feedback about the gain in time, money and dose with our Fessenheim tests. Local team estimate the gain in time to one week of work with multiple entries in RCA. So we won one week on a critical operation. The gain in dose is near a factor of 5, it will increase with the improvements of the boron meter. We scanned 6 areas for the local team and we validate one. Workers on the field integrated 0,11 mSv for this work. Without our help 5 more areas (and pipes) would have been tested in the same room. At time, money and dose gain, we can also add “social and human factors” gain. Indeed, finding those plugs or deposits is an exhausting work because they are very difficult to find. And now, with this solution, they know where to search, employees are motivated again.

The very interesting results obtained in this test campaign lead us to improve our first prototype.

Several improvements are being studied: the comparison of several slow neutron detectors, the miniaturization of the photodetector, the hardening of the electronics, and the reliability of the online algorithms and analysis. For example, the size of the detector can be reduced by using a SiPM [5] instead of the current photomultiplier.

In case the heat insulator is present, the tube is not visible which could lead to a misalignment between the neutron source, the tube and the neutron detector. The gamma rays of ^{241}Am (around 60 keV) could be used to properly center and verify the alignment as a large part of these gamma rays are stopped by the pipes. To improve placement of our system on pipes we are looking to install two slow neutron detectors instead of one. This solution will be used to increase the sensitivity and improve the placement of the boron detector around the tube.

To decrease dose integrated by workers due to proximity with pipes and hot spots, our detector will be improved with robotic systems (motors and wheels). Two movements are important: linear displacement along pipes and rotation around pipes.

These ideas will be tested this year as part of a national case dedicated to the TWE system on NPP.

IV. CONCLUSIONS

Boron plugs are a problem because of the difficulty to locate them. Knowing boron is neutron-absorbing, the idea of using neutron sources present in NPP as a boron detector has emerged. After simulations, a prototype was created and tested on the Fessenheim NPP. Indeed, they have pipes where deposits of boron are common.

Those tests were a success, and showed gains in dose (gain of 0,55 mSv per worker), time (at least a week) and money. Studies are actually done to improve the boron meter and deploy this solution in French EDF NPP. We also plan to use this system on other systems in NPP, not only TWE. This solution can be use in all nuclear facilities which use boron as moderator.

V. REFERENCES

[1] M. Louis-Louisy, “Fiche MTE n°51: Propriétés physico-chimiques de l'acide borique”, 2020

[2] Mirion Technologies “155780FR-F_BM501”

[3] A Muoio et al 2018 J. Phys.: Conf. Ser.966 012064

[4] P. Barberet, J. Jouve, S. Sorieul, P. Alfaurt, L. Mathieu. AIFIRA: a light ion beam facility for ion beam analysis and irradiation. Eur.Phys.J.Plus, 2021, 136 (1), pp.67

[5] M. Meshkian et all, 2017 IEEE Nuclear Science Symposium and Medical Imaging Conference (NSS/MIC), Atlanta, GA, USA, 2017

Proceedings of the European Nuclear Young Generation Forum
ENYGF'21
September 27-30, 2021, Tarragona, Spain

Comprehensive management for international transport of activated components of a Cyclotron

Rivero Torres, Javier[1], Arribas Sahuquillo, Juan Antonio[1] and Mora Bastida, Benjamín[1*]

[1] GD Energy Services S.A.U. (GDES), Spain.

*Corresponding author: *b.mora@gdes.com*

I. INTRODUCTION

The production and supply of radiopharmaceuticals is one of the main economic activities in the field of Nuclear Medicine and Molecular Imaging. Due to the high cost of the equipment and technology required for the synthesis of radioisotopes, the acquisition of disused or second-hand equipment by companies in the sector is a viable and common option.

The challenge presented by our client consisted of the comprehensive management of the radioactive transport of the activated components of a disused cyclotron from Spain to a French radiopharmaceutical company where it would be reinstalled. In general terms, this project should include the following stages:

d. Characterisation of the cyclotron's components, in order to estimate the activity of the objects with the objective of complying with European regulations on transport of dangerous goods by road (ADR) [1].
e. Conditioning of all the components to enable them to be handled and transported safely, in compliance with radiological protection criteria.
f. Full transport of the cyclotron from Spain to the destination facility in France, according to all the transport requirements of the ADR agreement.

The cyclotron was disassembled by the acquirer's technicians, who also transported the non-activated components by conventional means.

The elements to be subjected to radioactive transport were some of the external and internal components of the cyclotron, most of its pieces and equipment were made up of metallic materials susceptible to present radioisotopes produced by activation during the period of use of the cyclotron. Due to the uncertainties provided by the origin of the radioisotopes, the characterization process had to be qualitative as well as quantitative, so gamma spectrometry was selected as the ideal method to achieve both objectives.

II. METHODOLOGY AND RESULTS

A. Prior Radiological Verification

In order to perform the characterisation of the components, the pieces were weighed and a prior radiological verification was carried out using portable radiation detectors on all parts and equipment of the cyclotron object of the project. The table 1 shows the results of the measurements performed on each component of the cyclotron.

Table 1. Prior measurements of the equipment.

Component	Weight (kg)	Dose Rate (µSv/h)	
		Contact	1 meter
Beam probe (3 pieces)	2	221	0.7
F18 cell nº1	0.5	26	0.34
Small beam collector	2	4.8	<0.10
Avar leaves	0.1	0.4	<0.10
Cell 11	0.2	9.3	0.10
Beam collimator	0.1	0.15	<0.10
B. collimator/adapter	2	1.36	0.12
Paper burn nº2	0.2	0.50	<0.10
Large beam colector nº1	2	<0.10	<0.10
F-18 cell nº2	0.5	<0.10	<0.10
F-18 cell adapter	2	0.25	<0.10
Paper burn nº1	0.2	0.15	<0.10
Dame	0.2	0.22	<0.10
Adapter 100/63	2	<0.10	<0.10
Beam collector	3	<0.10	<0.10
Injector protector	2	<0.10	<0.10
Cryostat	4500	2.5	0.25
Pump	30	<0.10	<0.10
Beam line	50	1.5	<0.10
Cell changer	172	0.40	<0.10
Sheet changer 1	30	5	0.10
Sheet changer 2	30	4.8	0.10

Removable contamination was evaluated by means of smear tests and a surface contamination detector. The results in all the components were negative.

B. Activity assessment

As previously discussed, activity estimation of each part and component was carried out using a gamma acquisition system:

- Multichannel Detector and Amplifier
  Type: 2" NaI
  Brand: Canberra
- Spectrometry software
  Brand: Canberra.
  Model: Genie 2k.

Figure 1. Characterization of the cyclotron's cryostat.

In order to assess individual efficiency curves, each piece of the cyclotron was modelled using the Geometry Composer Software by Canberra.

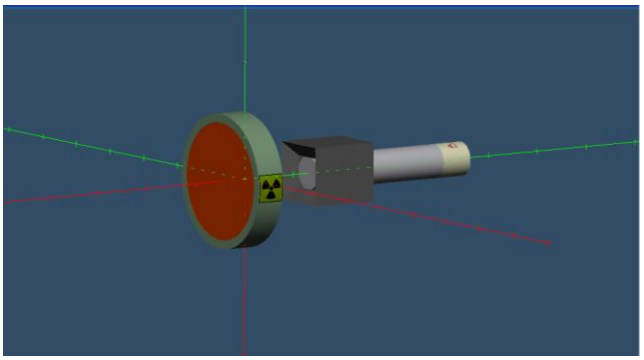

Figure 2. Modelling of component.

The specific activities of the components of the cyclotron are reported in table 2.

Table 2. Estimated activity of the components.

Component	Isotopes	Activity (Bq/g)	Activity (Bq)
Beam probe (3 pieces)	Zn-65	1.76E+03	3.51E+06
F18 cell nº1	Co-56	9.66E+02	4.83E+05
Small beam collector	Co-56,	4.88E+01	9.75E+04
	Zn-65	2.22E+01	4.43E+04
Avar leaves	Zn-65	1.12E+02	1.12E+04
Cell 11	Co-57	4.32E+02	8.63E+04
Beam collimator	Zn-65	1.76E+0.1	1.476E+03
B. collimator/adapter	Zn-65	1.94E+02	3.87E+05
Paper burn nº2	Zn-65	1.25E+01	2.50E+03
Large beam colector nº1	--	--	--
F-18 cell nº2	Co-56	3.26E-01	1.63E+02
F-18 cell adapter	Zn-65	8.45E-01	1.69E+03
Paper burn nº1	Co-57	1.20E+00	2.40E+02
Dame	Co-56	6.10E+00	1.22E+03
Adapter 100/63	--	--	--
Beam collector	--	--	--
Injector protector	--	--	--
Cryostat	Co-60	1.36E-01	6.10E+05
Pump	--	--	--
Beam line	Co-56,	6.58E-02	3.29E+03
	Zn-65	6.70E-02	3.35E+03
Cell changer	--	--	--
Sheet changer 1	Zn-65	2.09E+00	6.26E+04
Sheet changer 2	Zn-65	1.72E+00	5.15E+04

C. Conditioning and transportation.

The conditioning consisted mainly of preparing the correct packaging for each of the parts and elements of the cyclotron, to guarantee their integrity during transport, as well as compliance with European regulations for the transport of dangerous goods by road (ADR) [1].

The equipment was split into two groups:

- Components with specific activities below the exemption limit were packaged to be shipped on a lorry.
- The activities of the rest of the components accomplished the requirements to be transported together into a metal box classified as Excepted packaged (Figure 3).

Figure 3. Excepted package.

The two vehicles conveyed the equipment by road to its destination in France. To guarantee the integrity of the materials, some accelerometers were installed in the packages to record possible impacts during loading, transport and unloading operations. All the results recorded were satisfactory and, consequently, the safe transport of the components was guaranteed.

III. CONCLUSIONS

GDES carried out the characterisation of 22 pieces in total, 14 of which were classified as exempted material for road transport, while 8 pieces presented an activity above the ADR exemption limit.

The pieces that exceeded the exempted material criterion could be packed together in an excepted package.

The accurate radiological characterisation of the components of the cyclotron provided useful information to perform their transport safely and efficiently.

IV. References

[1] European Agreement concerning the International Carriage of Dangerous Goods by Road (ADR). 2019

Proceedings of the European Nuclear Young Generation Forum
ENYGF'21
September 27-30, 2021, Tarragona, Spain

Upgrade of Radiation Protection equipment at Cofrentes NPP

Vázquez Mora, Mª Carmen and Pedrón Hernández, Enrique

[1] Iberdrola Generación Nuclear, Spain

*Corresponding author: cvmo@iberdrola.es ; epedronh@iberdrola.es

I. INTRODUCTION

Cofrentes Nuclear Power Plant sits next to the Jucar River, in the municipality of Cofrentes, province of Valencia (Spain). The station is equipped with a Nuclear Steam Supply System (NSSS) comprised of a boiling water reactor of the BWR-6 type designed and supplied by General Electric.
The containment building is of the MARK-III type, combining the inherent advantages and safety of pressure suppression systems with the simplicity of a dry Containment Building.

Information of Interest about Cofrentes NPP

Reactor Type:	BWR/6
Type of Containment Building	MARK-III
Thermal Power	3,237 MWt
Electric Power	1,092 MWe
First Connection to the Grid	October 14, 1984
Duration of Operating Cycles	24 months
Number of Refueling Outages Completed	22

Around 700 individuals, including both IBERDROLA staff and contractors, work every day at the station.

Spain's Regulation on Health Protection against Ionizing Radiations [1] establishes that the Regulator (*CSN*), depending on the radiological risk of onsite activities, shall decide when radiation protection responsibilities fall on the licensee, on an in-house Radiation Protection Unit (RPU) or on a contracted Technical Radiation Protection Unit.

In the case of Spanish nuclear power plants, they all have in-house Radiation Protection Units [2]. Generally speaking, activities covered and developed by RPUs are mainly aimed at complying with the Regulation on Health Protection against Ionizing Radiations, with applicable European Union Provisions and Directives [3], Regulatory Safety Guides [4,5] and with specific requirements by the *CSN*.

The Radiation Protection Unit has to enforce compliance with the annual dose limits laid down in EURATOM's Directive 2013/59 [3], which establishes basic safety norms for protection against ionizing radiation exposure risks.

Activities covered and developed by the RPU integrate at last the following aspects:

- Design, assembly, installation, operation, modification and decommission of systems and equipment.
- Procurement of materials and equipment.
- Radiological site-associated risks.
- Classification of work areas and radiologically-exposed workers.
- Access, stay and work in areas with radiological risk.
- Radiation and contamination surveillance.
- Radwaste and effluent monitoring.
- Maintenance, verification and calibration of ionizing radiation measurement and detection systems.
- Dosimetric surveillance.
- Radiological site impact during normal operation and under accident conditions.
- Personnel qualification and training.
- Radiation protection optimization.

To comply with some activities assigned to the RPU, it is necessary to have equipment which ensures correct radiation and contamination surveillance.

Cofrentes NPP has a large variety of radiation and contamination monitoring equipment to guarantee compliance with applicable requirements at all times, for both workers exposed to ionizing radiations, as well as for the public and the environment.

Following usage of off-site exposure and contamination monitoring equipment, Cofrentes NPP established a gradual upgrade plan for the following equipment:

- Official Thermoluminescent Dosimetry System (TLD).
- Personal contamination gate monitors.
- External Personal Dosimetry System (EPD).

Upgrade of above-mentioned equipment was carried out sequentially by Cofrentes NPP's RPU between 2016 and 2021.

Upgrading this equipment ensures RPU capabilities to further perform activities described in Spain's Regulation on Health Protection against Ionizing Radiation [1], more specifically Cofrentes NPP's Operating License and a number of official production documents, including the site's Radiation Protection Manual [6].

II. UPGRADE OF RADIATION PROTECTION EQUIPMENT

A. Official Thermoluminescent Dosimetry System (TLD).

A role of the RPU is to ensure dosimetric surveillance of workers who carry out activities at the station's controlled area. To do that, the *CSN* authorizes the Offsite Personal Dosimetry Service to perform official dosimetry surveillance activities at Cofrentes NPP.

Ever since the station was commissioned, the Offsite Personal Dosimetry Service has used a thermoluminescent dosimetry system (TLD) to measure equivalent doses at different tissue levels. The most interesting depths in terms of personal dosimetry are 7 mg/cm^2 (depth to assess superficial dose), Hp (0.07) and 1000 mg/cm^2 (depth corresponding to initial body mass), Hp (10).

It is important to mention that thermoluminescence is the property of some substances which heat up and emit light after having been exposed to ionizing radiation. Light emission is proportional to incident radiation.

The dosimetry system selected as radiation-sensitive material to measure personal dose is comprised of copper-doped lithium borate thermoluminescence material (Li2B4O7:Cu), (elements 1 & 2 in the dosimeter) and thulium-doped calcium sulfate thermoluminescence material (CaSO4:Tm), (elements 3 & 4 in the dosimeter).

The following table shows general dosimeter characteristics [7]:

Element	Phosphorus	Sensitivity	Measurement Range	Purpose
1	$^{n}Li_2{}^{n}B_4O_7$:Cu	B, γ	100µSv ~ 10Sv	Skin dose
2	$^{n}Li_2{}^{n}B_4O_7$:Cu	B, γ	100µSv ~ 10Sv	10keV ~ 10MeV
3	$CaSO_4$:Tm	B, γ	10µSv ~ 500mSv	25keV ~ 10MeV
4	$CaSO_4$:Tm	γ	10µSv ~ 500mSv	25keV ~ 10MeV

According to the previous table, the dose range covered by the TLD is between 10 µSv and 10 Sv.

In 2016 Cofrentes NPP began to roll out a test program for commissioning of a new TLD dosimetry system, as specified in Regulatory Safety Guide 7.1 (Rev. 1) "Technical-administrative requirements for personal dosimetry services", with the aim to request CSN approval of the new thermoluminescent dosimetry system.

In 2019, following favorable approval by the CSN, the old dosimetry system was replaced with the new one,

which at Cofrentes NPP is comprised of the following elements:

- 1 TLD dosimeter reader device by Panasonic, model UD-7900M2N.
- 1 TLD dosimeter reader device by Panasonic, model UD-716AGL.
- 1 TLD dosimeter irradiating device by Panasonic, model UD-794D2NCE.
- 3 PCs, each associated to a previous computer and equipped with the software needed for equipment management and control.
- 6000 TLD dosimeters by Panasonic, model UD-802AT.
- 6000 dosimeter-holders by Panasonic, models UD-874ATM1.

Figure 1: Panasonic UD-7900M reading device.

The main advantages of the new dosimetry system compared to the previous one are as follows:

- The external personal dosimetry system is technologically up-to-date.
- Information on the type of incident radiation is provided, discriminating between X, ɣ and β rays and even neutrons, thus favoring a dose calculation algorithm adjustment commensurate with the incident radiation type.
- Reduced person-hour rate for TLD reading (reader can process 500 TLDs at once).
- Nitrogen usage is not required, thus reducing equipment operation costs and risks.

- Economic savings, as no corrective maintenance by external personnel is required.

In 2020, the Offsite Personal Dosimetry Service participated in the 6th Edition of "Intercomparison of Offsite Personal Dosimetry Services" (organized by the CSN), where it satisfactorily presented its new dosimetry system, concluding that:

"All Hp (10) & Hp (0.07) measurements comply with ISO 14146 criteria".

This thermoluminescent dosimetry system meets RPU targets relating to dosimetric surveillance of radiologically-exposed workers, thus meeting short- and long-term accuracy and quality targets.

Figure 2: Dosimeter model UD-802AT with dosimeter-holder.

B. Personal Contamination Gate Monitors

Another task assigned to the RPU is to ensure that professionally exposed workers are contamination-free. To do that, the RPU continuously monitors the contamination of all personnel at Cofrentes NPP

using "Personal Contamination Gate Monitors" capable of detecting superficial beta/gamma contamination in people and small objects exiting the Controlled Area.

This type of gate monitor is equipped with a number of scintillating fiber detectors distributed inside the monitor to perform whole-body measurements (head, thorax, limbs, hands and feet) and detect beta and gamma radiation.

These large monitors are designed for permanent installation, work totally autonomously and are always ready to measure.

The personal contamination gate monitor analyzes superficial contamination in people, rejecting any worker whose measured value exceeds the setpoint.

The previous gate monitor model used by Cofrentes NPP was in service continuously for a number of years. Although it worked properly, maintenance become increasingly difficult mainly due to a lack of original spare parts and to manufacturers being out of business.

Thus, in 2018 six new TwoStep™-Exit II contamination gate monitors by Mirion Technologies were purchased to replace old monitors.

Technologically speaking, the new gate monitors are a considerable improvement. Their main characteristics are as follows [8]:

- Fiber plastic scintillator detectors for beta radiation (gas not required).
- Fiber plastic scintillator detectors for gamma radiation (gas not required).
- 10-mm lead shielding for gamma detectors.
- Enclosure for measurement of small objects.
- Barcode reader for measurement management.
- Exit barrier.
- Touchscreen.
- Data management software.
- UPS (Uninterruptible Power Supply).

In 2019, works to replace old gate monitors with new ones were undertaken. These works involved removing old gate monitors, transporting new monitors to their installation point, performing the mechanical installation, completing functional tests and commissioning them.

Figure 3: Personal contamination gate monitor TwoStepTM-Exit II.

The main advantages of new gate monitors compared to old ones are as follows:

- Enhanced efficiency of Co-60 energy measurements.
- Significant reduction of person-hour ratio for preventive and corrective maintenance tasks, i.e., in 2017 Cofrentes NPP allocated 775 person-hour to corrective tasks on gate monitors, which once replaced allowed the station in 2020 to reduce gate monitor maintenance hours down to 250 person-hour.
- Increased spare part stock to ensure reliable maintenance of old gate monitors still in operation.
- Definitive removal of PR gas, reducing risks and performance costs in new gate monitors.
- Using fiber plastic scintillator technology facilitates probe maintenance and cleaning tasks, reducing gate monitor unavailability due to maintenance.
- Use of a robust internal calculation algorithm which enhances measurement reliability.

- Continuous visualization of gate monitor status and availability of gate monitor measurements from an office PC (via software).
- Possibility of using the reader to associate barcodes to worker measurements.

In short, the purchase of these new personal contamination gate monitors provides the RPU with tools to further guarantee ongoing surveillance tasks and ensure workers exiting the Radiological Control Area at Cofrentes NPP are contamination-free.

C. External Personal Dosimetry System (EPD)

The last upgrade project of Radiation Protection equipment at Cofrentes NPP involved the Electronic Personal Dosimeter (EPD) system,

which together with the official thermoluminescent dosimetry system (TLD), comprise Cofrentes NPP's workforce dosimetry surveillance system.

Electronic Personal Dosimeters (EPD) are used to measure the gamma radiation dose of radiologically-exposed workers inside the Controlled Area.

The following table shows the technical features of this equipment [9]:

Energy Response	Power range. 15 keV to 7 MeV
	Linearity: better than ±20%, from 16 keV to 7 Mev
Measurement Range	Dose: from 1 µSv to 10 Sv
	Dose rate: from 0.1 µSv to 20 Sv/h
Accuracy Hp(10)	<± 5% (137Cs)
	≤ ±10% (60Co)
	≤ ±10% (241Am)
	≤ ±10% 16 keV
Dose Rate Linearity	≤ ±20% to 10 Sv/h (1000 rem/h) (Co-60 & X-Ray H30 of 20 keV)
Dose Display	1 µSv to 10 Sv
Dose Rate Display	10 µSv/h to 10 Sv/h

These devices provide workers with real-time dose information and feature warning alarms in case dose and dose rates are exceeded.

On the other hand, the Electronic Personal Dosimeter (EPD) system allows the RPU to assess, control and limit the doses of radiologically-exposed workers, as well as to radiologically monitor them online, thus ensuring compliance with administrative dose limits at Cofrentes NPP.

The new Electronic Personal Dosimeter (EPD) system was purchased in 2019 with the aim to replace the former system, which was replaced mainly due to the following reasons:

- Constant reduction in the number of available EPDs.
- Not possible to procure old EPDs as they were discontinued by the manufacturer.
- Not possible to buy spare parts to repair dosimeters.
- Limited in-house stock of parts to repair dosimeters.
- High amount of resources (person/hour) allocated to dosimetry system maintenance (i.e., in 2019, 250 repair requests were issued in Cofrentes NPP, with a work load of 350 person/hour).
- Reduced time allocated to administrative tasks to analyze deteriorated dosimeters (i.e., in 2019, a total of 90 analyses were performed, for a work load of 50 person/hour).

The new system consists of the following elements:

- 1,500 electronic personal dosimeters (EPD).
- 7 input readers.
- 7 exit readers.
- 1 input/output reader.
- Dosimeter setup and management software.

Figure 5: EPD model DMC-3000.

Compared to the previous system, the main advantages of the new EPD system are as follows:

- Significant reduction of person-hour ratio for corrective maintenance tasks and associated administrative proceedings.
- Elimination of electromagnetic interferences from electrical and electronic equipment affecting dosimeters.
- Enhanced user interface, as dosimeters are equipped with sound, light and vibration alerts.

- Availability of a large number of dosimeters to cover periods of large demand.
- Equipment largely used in other national and international stations, meaning their performance and usage is known by workers from other facilities.

Figure 6: EPD reader, model LDM 2000.

After tests performed at Cofrentes NPP to confirm correct performance of the EPD dosimetry system and adaptation of the station's radiological management software (AGER) with the operational dosimetry management software (REMI), the new system was commissioned in early 2021.

The new EPD dosimetry system, together with the new official dosimetry system (TLD) commissioned in early 2019, provide Cofrentes' RPU with the tools needed to confidently undertake dosimetric surveillance of all personnel. In addition, dosimetry systems were upgraded with the latest technology and maintenance guarantees, thus ensuring the RPU at Cofrentes NPP can reliably perform dosimetry surveillance activities.

III. CONCLUSIONS

Over the last 5 years, Cofrentes NPP made significant efforts, both financial and technical, to upgrade TLD and EPD dosimetry surveillance systems and personal contamination monitoring equipment at the station's controlled area exit.

This upgrade was a significant improvement compared to equipment previously used, both in terms of technology (new equipment uses the latest high-tech available) and reliability (new equipment requires less maintenance, spare parts are available on the marketplace and suppliers provide technical support if needed).

With this new equipment, the RPU will continue to perform their surveillance of personal dosimetry and superficial contamination with full guarantees in the short- and long-term and in compliance with existing radiation protection regulations.

IV. References

[1] Spain's Royal Decree 783/2001 dated July 6, approving Spain's Regulation on Health Protection against Ionizing Radiations

[2] "Permit for the Radiation Protection unit at Cofrentes Nuclear Power Plant". CNCOF/COF/01/34.

[3] Directive 2013/059/EURATOM BY THE COUNCIL, dated December 5, 2013.

[4] Regulatory Safety Guide 7.3 (Rev.1), "Bases for establishment of technical radiation protection services or units".

[5] Regulatory Safety Guide 7.6 (Rev.1), "Content of radiation protection manuals for nuclear facilities and radioactive facilities of nuclear fuel cycle".

[6] DOE 06 "Cofrentes NPP Radiation Protection Manual".

[7] UD-7900M TLD Reader Operation Manual.

[8] Checkpoint: Body TwoStep™-Exit II. Technical handbook. MIRION TECHNOLOGIES.

[9] "DMC 3000 User´s guide". MIRION TECHNOLOGIES. 151153EN-F.

Proceedings of the European Nuclear Young Generation Forum
ENYGF'21
September 27-30, 2021, Tarragona, Spain

Web software for assessment of individual dose to exposed type B category workers without individual monitoring.

Rivero Torres, Javier[1], Guardia Almenar, Vicent[1] and Mora Bastida, Benjamín[1*]

[1] GD Energy Services S.A.U. (GDES), Spain.

*Corresponding author: *b.mora@gdes.com*

I. INTRODUCTION

According to Spanish regulation framework [1], for the purposes of monitoring and surveillance, a distinction is made between two categories of exposed workers:

a. category A: those exposed workers who are liable to receive an effective dose greater than 6 mSv per year or an equivalent dose greater than 15 mSv per year for the lens of the eye or greater than 150 mSv per year for skin and extremities;
b. category B: those exposed workers who are not classified as category A workers.

Individual doses of occupationally exposed type B category workers may be estimated by area monitoring. For this purpose, the facilities must have a procedure for assigning doses based on working environmental monitoring results. This procedure must arise an annual dose record for all type B category workers.

To harmonize these procedures, the Spanish Forum on Radiation Protection in the Healthcare Environment has developed a protocol [2], where guidelines are provided when passive dosemeters are used for monitoring of working environment with the objective to forecast doses to type B category workers.

The experience of GD Energy Services (GDES) as both Approved Dosimetry Service (ADS) and Radiation Protection Service has shown that radiological control of type B workers performed by area dosimetry not always concludes on the proper evaluation of individual doses. For this reason, a web application has been drawn up by GDES that applies the Spanish Forum protocol to the assignment of doses to type B workers, based on the data provided from the monthly dosimetry readings of thermoluminescent area dosemeters.

II. DOSE ASSIGNMENT

The assignment of doses is automatically performed by the application using an algorithm depending on the use of the dosemeter. There are two categories of dosemeters that may be selected according to the special features of the facility:

a. Personal Used Workstation dosemeter (DPT). These dosemeters are assigned to all workers sharing an exposure area (e.g. X-ray equipment), and will be worn by individual workers when operating on that equipment as if it were a personal dosemeter.
b. Fixed area dosemeter (FAD). These dosemeters are used as conventional area dosemeters, located at a measurement point (e.g., the control station of an X-ray machine).

In both cases, each dosemeter is assigned to an independent workstation, nevertheless, DPTs are shared by workers who wear in the same way they would wear individual dosemeters, whereas FADs are located in a fixed place.
Workers may be assigned to one or several dosemeters belonging to one facility. This information will be used by the application to calculate the doses of each worker based on the doses quantified by the dosemeters. Individual doses are calculated with the following expression:

$$H_{Worker} = \overline{(H_{Dosemeter}} + 2\sigma_H) \cdot t$$

Where H_{worker} is the individual dose, calculated from the doses registered by the dosemeters ($H_{dosemeter}$), the standard deviation (σ_H) and the full-time/part-time coefficient (t).
In case of one person working at more than one facility, the process of dose calculation is performed individually for each facility, and the records belonging to different facilities will be stored independently.

III. STRUCTURE OF THE APPLICATION

The application developed by GDES allows the allocation of each task of the procedure of dose assignment to the proper entity which has the information, avoiding unnecessary data transmission and redundant work. The figure 1 shows a flowchart of the application.

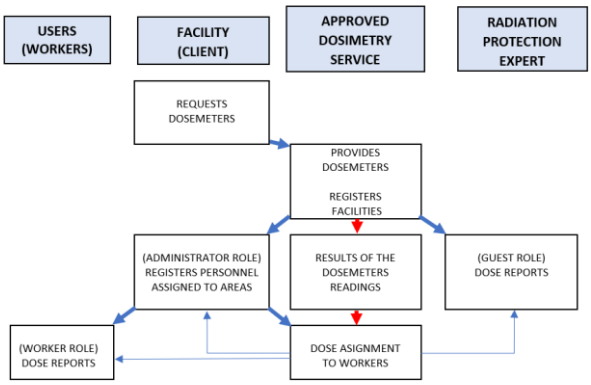

Figure 1. Software's flowchart

The process begins when the client requests the service to the ADS by communicating their necessities. The ADS may give advice on the number and category of dosemeters depending on the type of facility and equipment, number of exposed workers, etc.

Using the information supplied by the client, the ADS registers the facility on the application, assigning the dosemeters and introducing the category and identification of the dosemeters in the database. The ADS provides the client with authorized users to manage the data of their facility.

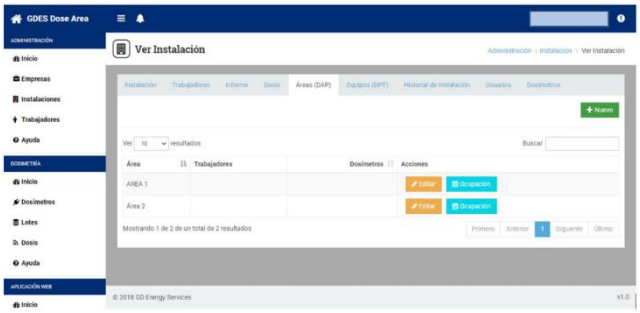

Figure 2. User's view of the application

The authorized users of the facility can access the application and, through a web environment manage the workers of their installation, generating records, cancellations, and assigning them to each dosemeter of the installation on a full or part-time basis.

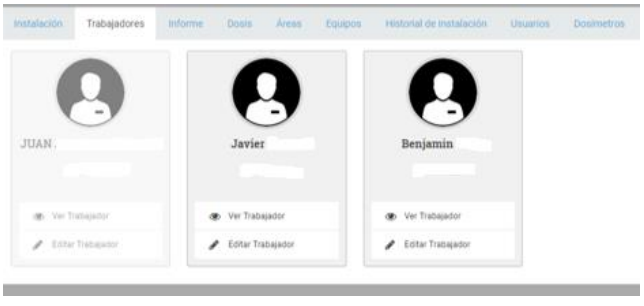

Figure 3. User's view of the application

Once the registration process of the facility has been completed, the ADS will upload the readings of the dosemeters generated monthly to the application. The application may be adapted to directly import the file format generated by de TLD reader (e.g ASCII).

This information will be used by the application to calculate the doses of each worker based on the procedure previously discussed. Consequently, each worker will have an individual report of dose created monthly (figure 4).

Figure 4. Individual dose report

The individual dosimetry reports will be available to the authorised users of the installation, as well as to the workers themselves, who have access to the doses assigned to them at any time in all the facilities in which they are registered.

IV. OTHER FUNCIONALITIES

Additional functionalities have been implemented in the application, to simplify the management of the dosimetry to both the ADS and the facility's Radiation Protection Officer:

- The application generates an exportable file with the necessary information for its implementation in the facility's annual report.
- Control of non-replacement of the dosemeter, as well as the possible loss of dosimetry information.
- Establishment of dose values that warn in case of a potential dose threshold exceeding and/or an overexposure.

V. CONCLUSION

The application developed by GDES allows the assignment of doses to type B category workers who do not use individual dosimetry, in a simple, reliable, updated and systematic way; based on the "Protocol for dosimetry surveillance by means of area dosimetry of exposed workers classified as type B in the health sector".

VI. References

[1] Spain, "Real Decreto 783-2001, de 6 de julio, por el que se aprueba el Reglamento sobre Protección Sanitaria contra radiaciones ionizantes," Boletín Oficial del Estado no. 178.

[2] Foro sobre Protección Radiológica en el Medio Sanitario, "Protocolo para la Vigilancia dosimétrica mediante dosimetría de área de los trabajadores expuestos clasificados como categoría B en el ámbito Sanitario."

Proceedings of the European Nuclear Young Generation Forum
ENYGF'21
September 27-30, 2021, Tarragona, Spain

Development of a thermodynamic sorption modelling database (TSM-DB) of radionuclide sorption on clay systems

D. Castaño[1], M. López-García[1], Pérez, D.[1], Valls, A.[1], S. Brassinnes[2], L. Duro[1]., D. García[1]

[1]Amphos21, Carrer Veneçuela 103, 08019, Barcelona, Spain.
[2]Belgian Agency for Radioactive Waste and Enriched Fissile materials (ONDRAF/NIRAS), Belgium.

*Corresponding author: *david.garcia@amphos21.com*

I. INTRODUCTION

Sorption is one of the most effective mechanisms retarding the migration of radionuclides (RN) through engineering and natural (i.e. host-rock) barriers of geological repositories of radioactive waste [1]. This term refers mainly to chemical interactions, although Van der Waals physical interactions are also included. There is a complete body of scientific literature on this subject, accompanied by a large set of data of the sorption of different radionuclides onto different solid substrates of interest, specifically clays and cementitious materials. During the last 3 years, NIRAS-ONDRAF, the Belgian radioactive waste management organisation has been developing a sorption database (SDB) of radionuclides with a first focus on clays and cement phases that will be eventually extended to other materials. The added value of the SDB relies not only on the experimental raw data contained, but on how the DB is structured and the associated software tools developed to help in feeding, analysing and extracting the sorption data. The structure and contents of the database are presented in Figure 1.

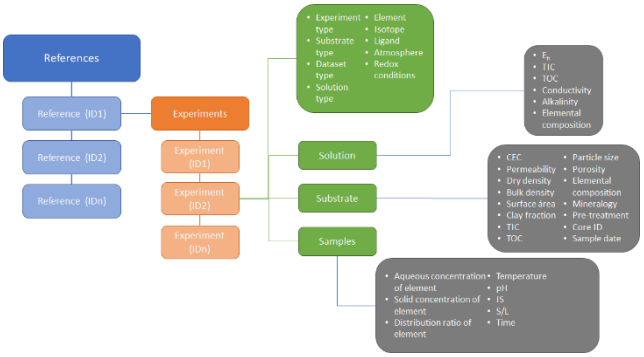

Figure 1. Scheme of data structure in the sorption SDB.

Together with the development of the SDB, ONDRAF/NIRAS is now working on developing a complementary database focused on the modelling of adsorption data. Several thermodynamic sorption models (TSM) have been applied for predicting the sorption behaviour of radionuclides onto different materials. The main aim of the present work was to develop a database of radionuclide sorption models for illite and montmorillonite. These solid phases are two of the most relevant phases when studying clay systems as they are main clay components. To do so, a sorption model selection from literature was performed, selecting the most relevant information for modelling purposes.

II. METHODOLOGY

The literature review and data compilation were performed analysing the open scientific literature as well as thermodynamic sorption databases such as RES3T [2]. Original publications were selected to avoid model reinterpretations and/or possible errors in model compilations. Specifically, the following information has been evaluated for each revised reference:

- Surface characteristics of the solids:
  - Specific surface area (SSA).
  - Site type and site density.
  - Cationic exchange capacity (CEC).
- Type of interaction for RN adsorption (accompanied by their respective constants log(K)):
  - Surface complexation (SC).
  - Ionic exchange (IE).
- Electrostatic approach used in the model:
  - Non electrostatic (NEM).
  - Constant capacitance (CCM).
  - Double diffusive layer (DLM).
  - Triple diffusive layer (TLM).

In a later project step this information will be introduced in the TSM-DB with the final target of linking the experimental results, already compiled in the SDB, with the models included within the TSM-DB, refining the models (when possible) and to check the experimental datasets with

well-documented and published sorption models automatically.

III. RESULTS AND DISCUSSION

The literature review encompassed 105 publications from 1994 to 2019 including thermodynamic sorption models (Figure 2). 39 of these publications refer to illite as the main clay phase and 66 of them to montmorillonite. The evolution on the number of publications during the last years clearly evidenced the increasing interest on the topic and give an overview on the amount of models available to be of use to the radioactive waste management community.

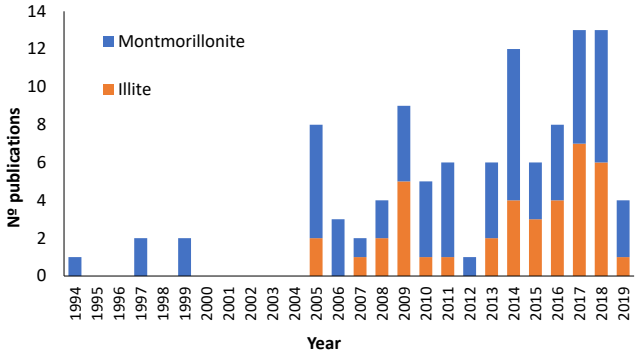

Figure 2. Temporal distribution of the selected publications.

The radionuclides studied in the revised references are: alkaline metals (Rb, Cs), divalent (Ni, Sr, Co…), trivalent (Eu, Cm, Am…), tetravalent (Th, Np, Pu…), pentavalent (Np, Pa, Pu…) and hexavalent (U) radionuclides as well as oxoanionic species (Se(IV), Nb(V) and Cr(VI)), being divalent radionuclides the ones with most investigations (Figure 3).

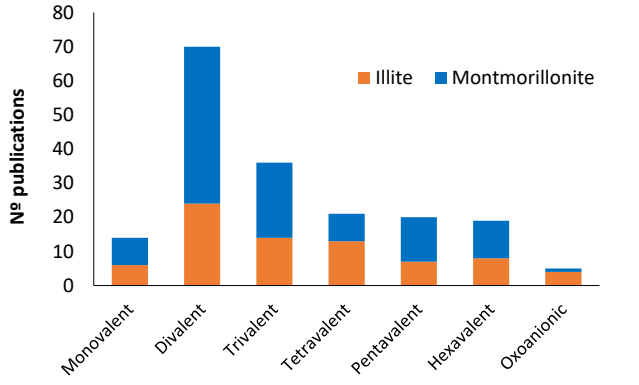

Figure 3. Radionuclide sorption modelling exercises reported in the selected publications.

From the data compiled, a brief summary follows:

- IE models are mostly used for alkaline-alkaline earth elements and divalent metals, as expected by its ability to substitute interlayer ions.
- SCM models are mostly for oxoanionic species, Ln/Ac elements and metals, as expected by their higher tendency to hydrolysis.
- Most of the models developed do not consider electrostatic effects, i.e. NEM is the most common model used (82 references). CCM is used in 2 references for illite and 5 for montmorillonite, DLM is used in 2 references for illite and 14 for montmorillonite and TLM is used in 1 reference for montmorillonite.
- It is also relevant to highlight that a large proportion of the models in the literature build upon the wellknown Baeyens and Bradbury [3] approaches, taken as "reference model" for sorption of radionuclides on clays

The two databases (SDB and TSM-DB) itself and the tools under development to manage the database will be very useful for the forthcoming calculations in support of safety/performance assessments exercises of radioactive waste management agencies. It is important to highlight that this kind of tools are essential to support the knowledge management of sorption data, being of utmost importance to rationalize models, to assess data gaps, and to establish a priority list for future investigations.

IV. REFERENCES

[1] RETROCK, 2005, Treatment of radionuclide transport in geosphere within safety assessments. EC Project RETROCK (C.No.: FIKW-CT-2001-20201).

[2] https://www.hzdr.de/db/RES3T.login.

[3] Bradbury, M. H., & Baeyens, B. (2005). Modelling the sorption of Mn(II), Co(II), Ni(II), Zn(II), Cd(II), Eu(III), Am(III), Sn(IV), Th(IV), Np(V) and U(VI) on montmorillonite: Linear free energy relationships and estimates of surface binding constants for some selected heavy metals and actinide. Geochimica et Cosmochimica Acta.

Proceedings of the European Nuclear Young Generation Forum
ENYGF'21
September 27-30, 2021, Tarragona, Spain

Adsorption of $^{99m}TcO_4^-$ on solid matrix: hydrodynamic behavior in mixing processes

Llanes-Montesino, Luis Enrique[1*], Espino-López, Raquel[2], Aguilera-Corrales, Yuri[2], Domínguez-Catasús, Judith[3]

Higher Institute of Technologies and Applied Sciences of University of Havana (InSTEC), Cuba.

*Corresponding author: enrique@instec.cu

I. INTRODUCTION

Radiotracers as a tool for various applications in the industry allow to carry out studies without stopping the technological flow of processes. Moreover, its high sensitivity allows the addition of small amounts without creating disturbances in the system [1], [2]. Studies which expand the potentialities of ^{99m}Tc eluted from ^{99}Mo/^{99m}Tc generator to label silts, silica (FS) and zeolite (FZ) supported ferragels have been carried out in our country [3]. The adsorption process of ^{99m}Tc into lateritic ore have been studied in order to obtain a solid radiotracer for applications in nickel industry. The obtaining of nickel and cobalt occupies one of the most important places in the cuban economy [4], [5]. On the other hand, mechanical mixing is one of the most common operations in the chemical and nickel industries. It is frequently used for homogenization of miscible liquids. The colorimetry, thermometric, pH-metric and conductivity methods have been widely used for investigation and analysis of the nature of homogenization by means of the classical impulse-response technique [6]. All of these methods require the inclusion of the sonde inside the reactor, which cause disturbances to the liquid movement.

Different models have been developed for describing mixing characteristics in batch reactors. Khang and Levenspiel used the tanks-in-series with recycle model to study the homogenization of a NaCl-saturated solution in turbine and propeller agitated batch mixing tanks, using the conductivity method [6]. According to Khang and Levenspiel model, the impulse response generated by a system represented by N tanks in series with recycle is:

$$y(t) = 1 + 2\exp\left(-\frac{2\pi^2}{NT}\cdot t\right)\cos\left(\frac{2\pi t}{T} + \frac{2\pi}{N}\right) \qquad (1)$$

where

$$A = 2\exp\left(\frac{-2\pi^2\cdot t}{NT}\right) \qquad (2)$$

is the decaying amplitude of response signal, and $K=2\pi^2/NT$ is the decay rate constant [s^{-1}], which express the rate to approach to uniformity in the mixing tank and it can be found from the magnitude of the slope in the plot of lnA vs. t. (lnA=ln2-Kt).

From dimensional analysis, we can show that the decay rate constant, K, is related to the system variables by the dimensionless group:

$$\left(\frac{n}{K}\right)\left(\frac{d}{D}\right)^c = f\left(\frac{nd^2\rho}{\mu}\right) \qquad (3)$$

where n, ρ, μ, d and D, are the rotational speed [s^{-1}], density [kg/m^3], viscosity [Pa·s], diameter of stirrer [m] and diameter of tank [m] respectively, and c is a fitting parameter. The dimensionless group n/K represents the mixing-rate number, N_{mix}.

Each agitated system has a value of Reynolds number after which the mixing-rate number, remains constant. In this Reynolds range is easier to control the system parameters, so it is very important to know it.

The relationship between the mixing-rate number (N_{mix}) and the Reynolds number (Re) characterizes the mixing inside the reactor and allows to fit different parameters such as: stirrer rotational speed and mixing time, according to cost-benefit ratio [7].

In this study the laterite samples obtained from the nickel industry were characterized, labeling of treated and untreated laterites using ^{99m}Tc was evaluated, adsorption of ^{99m}Tc in laterites was theoretically studied, desorption of labeled laterites at different values of pH was evaluated and the hydrodynamic patron in the mixing process in a batch reactor at laboratory scale was characterized.

II. EXPERIMENTAL

1 g of laterite and 1 mL of $^{99m}TcO_4^-$ (ac) eluted from the ^{99}Mo/^{99m}Tc generator with 3 MBq of ^{99m}Tc activity were added in a tube for centrifuge. The mixture was stirred for a period of 15 min. Soon afterwards 2 mL of SnF_2 or $SnCl_2$ solution (pH = 5) of varying concentration according to experiment, was added. The solution was stirred for a reaction time which varies in each experiment and it was centrifuged for 1 min. Three aqueous phase samples of 0.2 mL were taken and were measured three times with a radiometric system SRN1C-02, coupled to a NaI (Tl) detector. To evaluate ^{99m}Tc

retention in the silica sand, the retention degree ($R_{ret\%}$), was determined indirectly as:

$$R_{ret\%} = \left(\frac{A_b - A_l}{A_b}\right) \times 100 \qquad (4)$$

where, A_l (cps mL^{-1}) and A_b (cps mL^{-1}) are the radioactive concentrations of ^{99m}Tc solutions, after and before the contact with the silica sand, respectively. Each experiment was repeated three times for error estimation. Some studies were carried out using experimental designs. In these cases, the error was calculated from three experiments in the center of the experimental plan.

For the study of the possible interactions among the species of ^{99m}Tc and the laterite, and the capacity of adsorption of the radioisotope on the solid the mathematical model of Dubinin-Radushkevich (D-R) was used. This theoretical model was evaluated according to experimental equilibrium being based on the magnitude of the coefficient of determination for the lineal regression (R2) after express the isotherm in their lineal form:

$$ln\, q_{eq} = ln\, q_{max} - B_D \left[RT\, ln\left(1 + {}^{1}/_{C_{eq}}\right)\right]^2 \qquad (5)$$

The adsorbed ^{99m}Tc for unit of mass of substrate in equilibrium was calculated according to the equation 6.

$$q_{eq} = \frac{(C_0 - C_{eq}) \cdot V}{M} \qquad (6)$$

where Co is the initial radioactive concentration of ^{99m}Tc (MBq/L), Ceq is the radioactive concentration in equilibrium (MBq/L), M is the mass of laterite (g), V is the volume of solution (L) and q_{eq} is the adsorbate concentration in the adsorbed phase (MBq/g).

The energy average of adsorption for adsorbate mol was determined starting from the parameter B_D of the Dubinin-Radushkevich model through the following expression:

$$E\ (kJ/mol) = \frac{1}{\sqrt{2 \cdot B_D}} \qquad (7)$$

To evaluate the influence of the agitation speed and the initial pH of the solution in contact with the radiotracer on the stability of the ^{99m}Tc-laterite solid radiotracer, 0.5 g of labeled laterite and 10 mL of each solution were put in contact during 10 min on Heidolph PROMAX 2020 horizontal agitator according to the speed executed design. Labeling of the laterite was carried out following the procedure described previously. To evaluate the solid radiotracer stability, desorption of ^{99m}Tc was determined in each solution after the contact with the solid phase, as:

$$^{99m}Tc_{ac}(\%) = \frac{A_{ac}}{A_s} \times 100 \qquad (8)$$

where, A_{ac} (cps) is the ^{99m}Tc total activity in solution and A_s (cps) is the activity of the laterite using as target.

The mixing experiments were carried out under the experimental conditions showed in Table 1. The schematic experimental apparatus is shown in Figure 1. The stirrer shaft was driven by a variable speed electric motor, which controls the agitation rate in the range from 13 rpm to 73 rpm.

Table 1. Experimental conditions for the hydrodynamic characterization.

Parameter	***Value***
Tank diameter (m)	0.5
Stirred diameter (m)	0.2
H/D (reaction zone)	1
Material of construction	Stainless steels (thickness: 0.0015 m)
Impeller position (both setups)	L=D/3
Propeller type with 3 paddles	

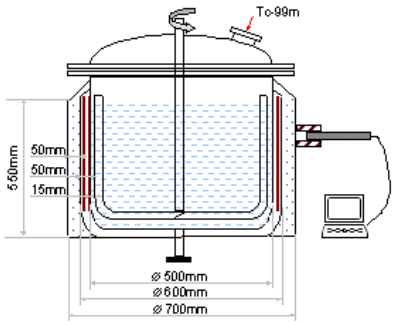

Figure 1. Schematic diagram of the experimental apparatus.

A small volume of radiotracer (^{99m}Tc) was rapidly added, lightly under the liquid surface and the mixing processes was monitored by a scintillation detector placed outside the tank, near the injection point. The volume "seen" by the sonde was controlled by placing it in a ring of lead with a 2 cm diameter hole. The recorded impulse responses were normalized by dividing by their final values.

The tanks-in-series with recycle model was evaluated by comparing normalized experimental curves with the ones predicted by equation 1. The mean return time was calculated from the experimental curves for each rotational speed, while the number of tanks was the visual fitting parameter.

The basic information needed to establish the relationship between the mixing-rate number and the Reynolds number was obtained from the curves that record the variation of the counting rate of the radiotracer with time, during the mixing process. Therefore the homogenization experiments were repeated 10 times for each rotational speed.

According to the tanks-in-series with recycle model, the normalized counting-rate amplitude decays exponentially with time. In order to calculate the decay rate constant, K, the maximum values of counting rate from the peaks of the normalized curve were recorded, and these were changed into the amplitudes from the final value, A. The decay rate constant for each rotational speed were founded from the slopes of the corresponding lnA vs. t plots. Finally, the values of mixing-rate number, n/K, were plotted vs. the Reynolds number and the mean value of the mixing-rate number in the range of $4{,}78 \times 10^4 < Re < 2{,}68 \times 10^5$ was calculated.

III. RESULTS AND DISCUSSION

Wet granulometric separation techniques as per Taylor's series, and X-ray fluorescence (XRF) have been used to characterize the laterite ore. Results are shown in Tables 2 and 3.

Table 2. Results of the X-ray fluorescence.

Oxide	NiO	CoO	Fe_2O_3	MnO	MgO
%	1.730	0.189	65.46	1.394	1.193
Oxide	**Cr_2O_3**	**Al_2O_3**	**SiO_2**	**CuO**	**ZnO**
%	2.951	6.441	8.470	0.021	0.057

Table 3. Results of granulometric characterization of the laterite.

Size (mm)	Weight percent (%)
> 2.00	1
[0.20 ; 2.00]	10
< 0.20	87

The metals Ni (1.35 %), Co (0.145 %), Fe (44.2 %), Mg (0.57 %) and Al (4.38 %) were determined by XRF. It was concluded that the ore feed essentially contains iron oxides (goethite) and that most metals contained in the laterite have a specific granulometry of concentration. Size fractions of mineral particles above 2 mm are enriched with magnesium silicates (olivine and serpentine) and aluminium hydroxide (gibbsite); whilst iron oxides (gibbsite) are concentration in particles lesser than 0,075 mm.

Labeling studies results of treated and untreated laterites using ^{99m}Tc are shown in Table 4.

Table 4. Retention degree of 99mtc in two samples of lateritic ores.

Lateritic ore	R_{ret}%
Untreated	89.80 ± 0.20
Treated (reducing conditions, H_2 + CO)	81.04 ± 0.10

Retention degree of ^{99m}Tc in treated laterite (reduced) was 8 % higher. The iron present in the surface is reduced after the previous treatment, which is favorable to the formation of bonds Fe-O-Tc.

The experimental data was adjusted to the lineal model of the Dubinin-Radushkevich isotherm (equation 5). Figure 2 show the dependence between $\ln(q_{eq})$ and ε^2 for the adsorption of ^{99m}Tc on laterite. The parameters of the Dubinin-Radushkevich model according to the carried out regression analysis are shown in Table 5.

The bonding energy (E), calculated starting from B_D using the equation 7 was equal to 9.46 kJ/mol, and it is in the typical range of the bonding energy for mechanisms of ionic interaction (8-16 kJ/mol) [8]. This energy value indicates that the chemisorption plays a significant role in the mechanism of ^{99m}Tc adsorption on the laterite, that which coincides with another authors [9].

To evaluate the stability of the solid radiotrazador after the contact with the solution for different pH conditions according to the executed experiment, ^{99m}Tc desorbed percent was determined. This results are shown in Table 6.

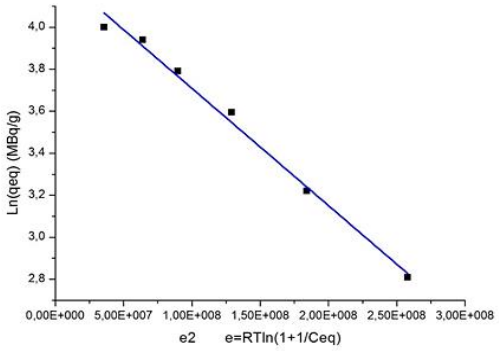

Figure 2. Dubinin-Radushkevich isotherm for the adsorption of ^{99m}Tc on laterite.

Table 5. Dubinin-Radushkevich adsorption parameters.

Parameter	$B_D(mol^2/J^2)$	2.04E(-8)
Maximum adsorption capacity	q_{max} (MBq/g)	77.6

Table 6. Desorption of 99mtc from laterite. contact time: 20 minutes.

Laterite	Desorption of ^{99m}Tc (%)	
	pH=4	**pH=10**
Treated	1.49	4.39
Untreated	2.14	2.96

The desorption of ^{99m}Tc from laterites at pH 4 and 10 showed that for untreated laterite the values were 2.1 % and 3% respectively, while for the treated material were 1.5% and 4.4 %. Results show high values of ^{99m}Tc sorption yields on laterites.

This solid radiotracer (^{99m}Tc-laterite) can be used to understand the hydrodynamic behavior in mixing process. Labeled laterites was evaluated in the leaching process of lateritic ore with an acid solution in a batch reactor at laboratory scale, using a propeller with three paddles impeller.

The experimental and theoretical curves are shown in Figure 3.

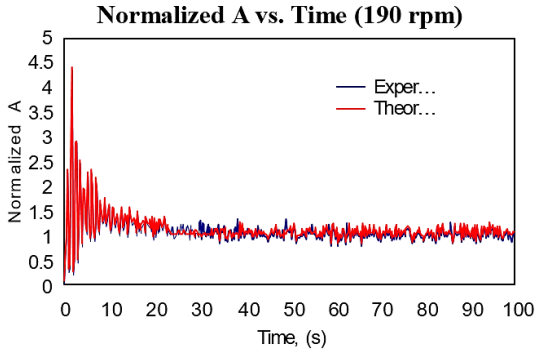

Figure 3. Experimental and theoretical curves for 190 rpm rotational speed.

As can be appreciated in Figure 3, the minimum value on the experimental curve never coincide with the theoretical curve. This could be consequence of the of the activity picks overlapping, which becomes more critic for the higher rotational speeds, because the return time diminishes and approaches to the fixed measure time.

From the comparison of the experimental and theoretical curves, one could affirm that the behavior of the fluid in the reactor fits to the tanks-in-series with recycle model. Thus we conclude that it could be used for fluid mixing characterization.

After analyzing the whole experimental data was founded an exponential relationship between rotational speed (n) and the rate to approach to uniformity in the mixing tank (K):

$$K=0{,}0211e^{0{,}0324\cdot n} \quad (9)$$

In the other hand the homogenization time (t_{hom}) is exponentially related with the rotational speed, too:

$$t_{hom} = 87{,}814e^{-0{,}0301\cdot n} \quad (10)$$

The last relationship allows to establish the rotational speed critical value, for specifically characterized mixing system, after which does not make sense to increase the rotational speed because, the decreasing of homogenization time does not justify the corresponding energy consumption.

The relationship between the mixing-rate number and Reynolds number is shown in Figure 4.

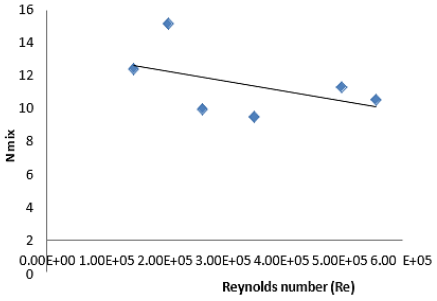

Figure 4. Mixing-rate number (Nmix) vs. Reynolds number (Re).

The mean value of the mixing-rate number in the range of $4{,}78x10^4 < Re < 2{,}68x10^5$ is 7,8 ± 0.9. It was an expected behavior. In most of the cases the mixing-rate number remains constant in the turbulent region ($Re>10^4$).

Anyway, the mean value can be used for calculating the rotational speed necessary at a given time or the mixing time under different conditions (rotational speed, density, viscosity, etc.), in order to achieve the required homogenization degree.

IV. CONCLUSIONS

The characterization of the lateritic ore shows the high iron content which is favorable to the formation of Fe-O-Tc bonds. The laterite treated is more promising to be used as a support in obtaining ^{99m}Tc solid tracers. The untreated laterite have higher ^{99m}Tc retention yields than the treated one and can be an attractive support for ^{99m}Tc solid radiotracer. The Dubinin-Radushkevich model provides a good description of the adsorption process of ^{99m}Tc on untreated laterites and suggests chemisorption mechanisms between the ^{99m}Tc and the laterite surface. The maximum adsorption capacity of ^{99m}Tc in this sample is 77.6 MBq/g. The solid radiotracer obtained from laterite ore labeled with ^{99m}Tc can be used to understand the mixing process in simulated acid leaching (pH=4) of laterite at laboratory scale. The tanks-in-series with recycle model fits well for the mixing in agitated batch reactors with propeller impeller. The homogenization time can be used as well as the relationship between the mixing-rate number and Reynolds number in the scale up methodology.

V. ACKNOWLEDGMENT

We wish to thank the IAEA for supporting this work under the Coordinated Research Project (CRP) Radiometric Methods for Measuring and Modeling Multiphase Systems towards Industrial Processes.

VI. REFERENCES

[1] IAEA, *Guidebook on radioisotope tracers in industry*. Technical Report S. N. 316. Vienna, International Atomic Energy Agency (1990).

[2] IAEA, *Radiotracer applications in industry – a guidebook*. Technical Report. S. N. 423. Vienna, International Atomic Energy Agency (2004).

[3] Martínez, E., *Síntesis y evaluación de Ferrageles como perspectivos radiotrazadores sólidos de ^{99m}Tc.* Tesis presentada en opción al grado científico de Licenciado en Radioquímica, InSTEC, Radioquímica, *J. Domínguez* (2013).

[4] Gavin M. Mudd. *Global trends and environmental issues in nickel mining: Sulfides versus laterites*. Ore Geology Reviews. Volume 38, Issues 1–2. Pages 9–26, October (2010).

[5] Dr. Ashok D. Dalvi; Dr. W. Gordon Bacon; Mr. Robert C. Osborne. *The Past and the Future of Nickel Laterites*. PDAC 2004 International Convention, Trade Show & Investors Exchange March 7-10 (2004).

[6] Domínguez, J., Abreu, A.M., *Mixing characterization in batch reactors using radiotracer techniques*. J. Radioanal. Nucl. Chem Vol. 241: 337-340 (1999).

[7] Blet, V., et al., *Radioactive Tracing as Aid for Diagnosing Chemical Reactors.* Oil and Gas Science and Technology. 55(2): p. 171-183 (2000).

[8] Dubinin, M.M. and L.V. Radushkevich, *Equation of the Characteristic Curve of Activated Charcoal.* Proc. Acad. Sci. Phvs. Chem. (1946).

[9] Jaroniec, M. and R. Madey, *Physical Adsorption on Heterogeneous Solids*. Elsevier: 6.20 (199

Proceedings of the European Nuclear Young Generation Forum
ENYGF'21
September 27-30, 2021, Tarragona, Spain

Estimation of exposure to radon and the doses received by the occupants of a dwelling located in a site with a high concentration of radon.

Trull Hernandis, Cristina[1], Sancho Fernández, María[1*], Arnal Arnal, José Miguel[1], Verdú Martín, Gumersindo[1] and García Fayos, Beatriz[1]

[1]Instituto Universitario de Seguridad Industrial, Radiofísica y Medioambiental (ISIRYM), Universitat Politècnica de València, Camí de Vera s/n. 46022, Spain

*Corresponding author: *msanchof@iqn.upv.es*

VI. INTRODUCTION

An 80 % of the radiation exposure that population receives comes from natural sources, constituting a threat to the public health, coming in a 16% from the soil, 13% from the cosmic rays, 9% from food intakes and 42% due to radon presence [1]. Uranium-238 contained in soils and rocks disintegrates into radon-222 and, due to its gaseous nature, this radioisotope is capable to emanate from the rocks and enter into enclosed areas, where it tends to accumulate. The exposure risk generally comes from inhaling radon gas and its descendants. Disintegration products tend to deposit in the respiratory tract, emitting charged particles which interact with the organism. Radioactive interactions with the body cause cellular damage, leading to alterations in the DNA of the tissues, entailing carcinogenic problems. In fact, radon exposures represent the second reason for lung cancer deaths in the world, only preceded by smoking [2].

According to the risks that radon exposure involves, radon concentrations inside dwellings need to be controlled. Directive 2013/59/EURATOM regulates the basic safety standards for protection against the dangers arising from exposure to ionizing radiation. Therefore, current legislation establishes 300 Bq/m^3 as the reference level in relation to the annual average activity of radon concentration in air [3]. When these standards are exceeded, action policies have to be acquired due to the public hazard implications. Nevertheless, limits exceeded or not, recommendations and guidelines are essential to prevent the occupants from the adverse effects derived from radon exposure.

Exposure levels and the radiation absorbed by the occupants may differ substantially for the same dwelling. Different radon concentrations can be reached in a building, depending on several factors, among them the type of construction materials, soil composition, presence of cracks in the slab of the building, etc. For a specific building, with its features, the concentrations are affected and vary depending on relevant factors as the ventilation and the air fluxes behaviour, as well as dwellers may receive distinct doses depending on their habits and routines [2]. The difference in the exposures must be characterized to comprehend the potential harmful derived and to ensure the integrity of the tenants' health.

The objective of this work is to reproduce a dwelling situation with radon in air that propitiates high exposure levels for its occupants. Subsequently, to characterize different exposure profiles that could occur in a site, estimating the dose received, taking into consideration the exposure conditions and the occupants' daily habits.

VII. PROCEDURE

The work procedure has consisted in the following stages:

a) Dwelling location. The dwelling object of this work is located attending to emulate a situation capable to reach high radon in air concentrations. To this effect, potential radon cartographies [4][5] are used in combination with weather reports [6]. The dwelling is placed in a location that combines high potential radon values with weather conditions that tend to increase the concentration indoors.

b) Dwelling description. Once the emplacement is defined, the building specifications are designated. The features that alter the radiological situation in a dwelling are studied, considering for this air flow simulation studies [7][8][9]. Then the disposition of the dwelling spaces is provided.

c) Occupants and habits description. After the description of the dwelling features, the occupants' profiles are designated. Their daily routines and habits performed throughout the day are described, considering for this the difference in the respiratory rates of the individuals [10][11][12].

d) Dose estimation. Measuring devices and their internal disposition are suggested based on CSN measuring guideline specifications [13]. Then, an estimation of the radon concentrations per room is provided, in view of the air flow simulation studies [7][8][9], for their later use in the dose exposure calculations and their consequent analysis.

VIII. RESULTS AND DISCUSSION

The themes proposed for evaluation in the Procedure are discussed in this section, including the results obtained as the dwelling location and features, as well as the occupants' description and their dose exposure estimation.

E. Dwelling location

In Spain there are quite different radon in air concentrations, depending on the geographical area. The potential radon in air Spanish cartography points the different zones of the territory that are feasible to achieve high concentrations, exceedingly at least at the 10% of the cases values of 400 Bq/m^3 [4]. The dwelling location is placed in Galicia, one of the communities that shows higher potential radon levels.

Precipitation and humidity are environmental factors with a great impact on radon in air concentrations. Soil permeability decreases when the weather is rainy and humidity levels are high [14]. The radon dissolved in the soil can reach the surface throughout the dry part of the ground, which corresponds to the bottom of the dwellings, accessing to the enclosed spaces, and concentrating inside them. During a five-year period, from 2013 to 2017, the zone that accumulates more precipitations, propitiating the radon entry in the residences, was the western part of the territory, as it is deduced from the accumulated rainfalls reports [6].

The radon presence in Galicia in each township is considered to locate the dwelling within the western part [5]. The towns identified by the presence of at least 300 Bq/m^3 in more than 10% of the dwellings are selected for the final location. The emplacement is based in the province of A Coruña, in the town of Outes.

F. Dwelling description

The disposition of the different rooms limits in every home the draft of natural air due to the presence of walls [7]. Depending on the distribution of the ventilation elements, as windows, doors, and the space communications, the air stagnation can be prevented. Furthermore, radon tends to accumulate in lower floors, due to its density, and reaches higher concentrations in small spaces. The radon transfer to spaces with lower concentration is limited when great humidity values are present, as could occur in kitchens and bathrooms. The diffusion coefficient decreases and, therefore, these areas tend to achieve larger radon levels [8][9]. When these situations are combined, as in a single ground floor house, with small rooms and poor ventilation standards, the spaces are no longer homogeneous and the exposure levels in a house oscillate depending on the room.

The building under study corresponds with a standard single house at ground floor level, whose rooms disposition does not allow the natural passage of the air fluxes throughout the house. Locating the dwelling at ground level leads to reproduce adverse radon concentrations, due to the radon tends to accumulate near to the ground [14]. The arrangement of the rooms, presented in Figure 1, is disposed, accordingly with the computational fluid dynamics, to prevent the air homogenization in the dwelling.

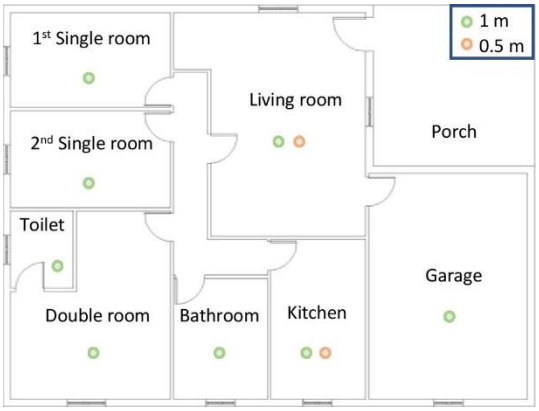

Figure 1. Layout of the house and provision of the measuring devices.

G. Occupants and habits description

The group of dwellers who occupies the described residence has five members: two middle-aged adults, one 10-year-old child, a baby, and an elderly person with a reduced mobility condition. From the profiles described above, it is possible to characterize distinct exposure situations that could happen in a dwelling.

The daily routine defined for each tenant considers the time consumed in each room of the house, and the habits that can affect their respiratory rhythms. The amounts of air inhaled differ depending on the age as a function of the frequency and their inhalation capacity. During resting periods, a grown-up person can inhale between 12 and 20 times per minute [10]. Therefore, it is considered that each adult breathes 15 times per minute, inhaling 12 liters of air per minute. Whereas, if the adult is under prolonged effort conditions, the respiratory rhythm can reach the amount of 100 liters, equivalent to 60 breaths per minute [11] From these values, and with the aim to emulate the most adverse conditions, 60 liters are assigned for intermediate situations, equivalent to inhaling around 30 times per minute.

A child respiratory frequency is comprised between 18 to 25 breaths per minute [10]. In addition, the normal values of air inhaled by a child round between 7 and 7.5 milliliter per kilogram [12]. For the 10-year-old child it is considered 21 breaths during resting periods, 30 for middle efforts and 60 during periods of physical activity. Considering a weight of 33.5 kg, the air amounts inhaled are from 5.276 liters, during quietness, 7.537 liters during medium efforts, and 15.075 liters during prolonged activities.

On their behalf, infants breathe about 25 to 36 per minute [10]. Hence, it is established for the estimations that the infant breathes 31 times per minute during quiet periods. Considering the normal children respiratory values mentioned above, and being the infant's weight 8.41 kg, the volume inhaled per minute is 1.955 liters. For periods of continuous crying, it is settled that the respiratory rhythms increase in a 50 %, being the amount inhaled 2.933 liters.

Daily routines of each dweller and the different spaces occupied during the day are defined [15] and sum up below.

a) Elderly person. Due to the dweller mobility limitations, the elder spends most of the day in the building, occupying the living room, bathroom, and the 1st single room. Most of

this time is spent resting, except during rehab exercises in the living room, reaching medium respiratory rates.

b) Adult number 1. This tenant spends the least amount of time in the dwelling, due to work responsibilities. All the rooms are frequented in quietness by the dweller, except the single dormitories. The execution of daily tasks in the garage propitiates periods of medium effort. High respiratory rhythms are achieved due to physical training practice, performed in the living room.

c) Adult number 2. This dweller frequents all the rooms of the dwelling, except the garage. The homemaker daily tasks, performed in most of the rooms, propitiate medium respiratory levels. In addition, the exercise practice in the living room carries an increase in the respiratory rates to high levels.

d) Baby. The infant frequents all the rooms, except the garage and the single dormitories. The respiratory rhythms of the baby alternate between resting and prolonged crying, consequently increasing the respiratory rates, differentiating the periods spent on the floor highchair from the others.

e) Child. The dweller occupies the 2nd single dormitory, bathroom, living room, and the garage. While the kid is playing in the living room or the garage, the respiratory rhythms vary from calmness to high levels, with medium rhythms at the bathroom and the living room activities.

H. Dose estimation

The devices suggested to use for evaluating the radiological situation, chosen considering cost and uncertainty linkage, are passive long-term measuring devices, gauging during a 3-months period, meanwhile the dwelling remains closed [16]. Electret ionization chambers are selected for the dosimetry, due to their medium cost, and its standard uncertainty from 8 to 15% for 200 Bq/m^3 exposure [2].

The location of the measuring devices is presented in Figure 1. The detectors should be situated at 1 m from the ground, far from the ventilation elements, and maintaining 30 cm to the external walls, and 10 cm to other objects [13], one per each space considered homogeneous. Two additional devices should be disposed closer to the floor level, at the minimum height recommended in guidelines [13]: 0.5 m, since radon tends to accumulate near to the ground level. Differences in exposure when a baby spends time in a floor highchair, are characterized by these two additional devices. When the measuring periods are finalized, the devices are collected for later study in the laboratory, obtaining the corresponding concentration per measuring device.

Concentrations per room, presented in Table 1, are assumed with the aim to reproduce a dwelling situation that would exceed the reference level of 300 Bq/m^3 of average activity radon concentration in air [3]. The concentrations allocation is based on the computational fluid dynamics [7][8][9]. The main factor assessed is the dimension of the rooms. The smaller spaces correspond to higher radon concentrations. In addition, larger values are assigned when humidity is present. Due to radon is eight times heavier than air, for the same room, higher values are assigned to the devices nearest to the floor, corresponding to the floor highchair location.

Table 1. Radon concentration per room.

Room		Bq/m^3	Room		Bq/m^3
Living room	1 m	189.4	Kitchen	1 m	335.6
	0.5 m	228.6		0.5 m	376.9
1st Room		228.2	Bathroom		424.6
2nd Room		228.6	Toilet		512.8
Double room		196.3	Garage		313.6

In all the rooms the concentrations exceed 100 Bq/m^3, reaching in an occasion a value up to 500 Bq/m^3. The presence of rooms which exceed the 300 Bq/m^3, established by the legislation as the reference level [3], specially entails a risk for the occupants. Considering the concentration values assigned per room, the levels of exposure are estimated for each occupant.

The daily accumulated activity to which the dwellers are exposed ($A_{accu-exp}$) is obtained as the sum of the product of the concentrations assumed for each measuring device ($[Rn]_{room}$) multiplied by the time, which the tenant has spent in the room (t_r), and the air volume inhaled, varying with the respiratory rates (V_{air}), according to Equation 1.

$$A_{accum-exp} = \sum [Rn]_{room} \cdot t_r \cdot V_{air} \qquad (1)$$

Starting from the accumulated activity exposition values and knowing the time per day that each occupant spends in the dwelling (t_{day}), the activity average exposure per hour (A_{av-exp}) is obtained by Equation 2).

$$A_{av-exp} = A_{accum-exp}/t_{day} \qquad (2)$$

Current legislation dictates the reference levels referring to radon in air concentrations, which in this case are exceeded. Since the total activity exposure is related to the radon in air concentrations, and there is no established reference level for this radon exposure, the exposition that the occupants suffer will entail a risk to their health. Both accumulated activities exposure, daily and the average spent per hour, are calculated for each occupant, and presented in Figure 2.

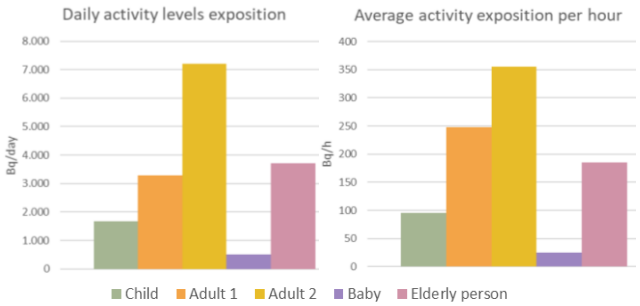

Figure 2. (A) Daily activity levels occupants exposition; (B) Activity exposition average received per hour when in the dwelling.

As it is observed in Figure 2 (A), the dweller with higher daily exposure is the adult number 2, due to the large amount of time spent in the dwelling, combined with periods of physical exertion. The elderly person is the following tenant who receives a bigger amount daily, since the elder spends a substantial part of the day inside the building. The adult

number 1 presents an accumulated activity exposure per day closer to the elderly person, although is who spends less time in the dwelling, but in periods of high physical activity. The activities to which the child and the baby are exposed, correspond to lower values, this variation comes from the remarkable difference between their inhalation capacities with the volumes that the adults inhale. Nevertheless, accordingly to WHO, low concentrations do not mean an exposure level that ensures the integrity of the health of the individual, since there is no level below which the exposures can be considered safe [2].

When the different times spent in the dwelling are considered, some differences appear in terms of the activity exposition, Figure 2 (B). The adult number 2 remains with the highest value. However, adult number 1 becomes the second occupant receiving highest activity exposure per hour spent, exceeding the elderly person exposure. This variation is a consequence of the different nature of the activities performed in the dwelling.

Conforming to the given results, the activities to which the occupants of the same dwelling are exposed differ depending on the exposure times, and the radon concentration of the room, varying with the activities carried out. Consequently, the exposition suffered from a dweller during a narrow period, but a higher respiratory frequency, can overtake the activity exposition levels that another tenant receives, even if the staying periods are greater.

In addition, the dose received by the Adult 2 is calculated (Equation 3) due to it presents the higher activity exposition levels. For this purpose, depending on the time spent annually at each room (t) and the radon concentrations ($[Rn]_{room}$), the total activity exposition has been obtained for its further conversion to dose exposition. Conversion factor for radon and its progeny, when evaluating at home environments, corresponds with 1.1 Sv per Jhm^{-3}, which means effective dose per unit of potential exposure of alpha energy, $F_{D.ef}$, [17]. $F_{Bq/J}$ corresponds to conversion factor from Bq/m^3 to J/m^3[18], being the radon secular equilibrium factor for radon in dwellings, F_{eq-sec}, 0.4 [2].

$$Dose = \sum [Rn]_{room} \cdot t \cdot F_{eq-sec} \cdot F_{Bq/J} \cdot F_{D.ef} \quad (3)$$

Effective dose estimated for the dweller corresponds to 4.24 mSv per year, level which would exceed the 1 mSv per year established as a dose limit recommendation for the members of the public [17].

According to these estimation results, mitigation measures may be applied in the dwelling to preserve the health of occupants from radon exposure [15].

IX. CONCLUSIONS

A radiological evaluation of a dwelling, whose features propitiate high radon in air concentrations, has been performed. For this purpose, the meteorological conditions in the area and the geographical location of the dwelling have been considered. The exposures of the dwelling occupants to different levels of activity concentration have been estimated, considering meanwhile their habits and daily routines performed in the different stays of the building.

According the European Council Directive and WHO, the dwellers are residing in a house with radon concentrations which entail a risk for their health, due to exceeding the 300 Bq/m^3. Considering the variations of exposure that can arise in the same building, the radon concentrations must be considered together with the corresponding exposure levels, and the effective dose. All of this to evaluate the radiological situation suffered by each occupant, then manifest the risks that the presence in the dwelling may entail and be able to undertake the corresponding measures to preserve the health integrity of the occupants.

X. References

[1] PNUMA, “Radiación. Efectos y fuentes,” 2016.

[2] OMS, “Manual de la OMS sobre el radón en interiores,” 2015.

[3] European Union, “Council Directive 2013/59/EURATOM,” 2014.

[4] CSN, “Cartografía del POTENCIAL DE RADÓN en España,” 2017.

[5] Universidad de Santiago de Compostela, “Porcentaje de medidas de más de 300 Bq/m^3 por municipio,” 2018.

[6] Xunta de Galicia, “Informe climatológico anual. Mapa de precipitación acumulada no anos 2013-2017,”

[7] K. Akbari, and J. Mahmoudi, “Numerical simulation of radon transports and indoor air conditions effects,” IJSER, vol. 3(6), 2012.

[8] K. Akbari, J. Mahmoudi, and J. Ghanbari, “Influence of indoor air conditions on radon concentration in a detached house,” Journal of Environmental Radioactivity, vol. 116, pp. 166-173, 2013.

[9] R. Rabi, and L. Oufni, “Study of radon dispersion in typical dwelling using CFD modeling combined with passive-active measurements,” Radiation Physics and Chemistry, vol. 139, pp. 40-48, 2017.

[10] J. López Chicharro, and A. Fernández Vaquero, “Fisiología del Ejercicio,” 3e, V, 2006.

[11] Breathe (Sheff), “Your lungs and exercise,” 12(1), pp. 97-100, 2016.

[12] J. López-Herce, M. Rupérez Lucas, C. García Sanz, and E. García Sánchez, “IV Curso sobre la Función Pulmonar en el Niño (Principios y Aplicaciones),” 2013.

[13] CSN, “Directrices sobre la competencia de los laboratorios y servicios de medida de radón en aire,” 2010.

[14] CSN, “Protección frente a la inmisión de gas radón en edificios,” 2010.

[15] C. Trull Hernandis, “Desarrollo de las medidas necesarias para la reducción y el control de la concentración de radón en el aire interior de una vivienda unifamiliar localizada en la comunidad de Galicia,” TFG, Ingeniería Química, UPV, 2018.

[16] CSN, “Metodología para la evaluación de la exposición al radón en los lugares de trabajo,” 2012.

[17] Ministerio de la Presidencia, “Real Decreto 783/2001,” 2001.

[18] ICRP, “Protection Against Radon222.,” Publication 65, 1990.

Technical Track 4 – NPP Engineering, operation, maintenance, and digitalization

Experience of digital transformation applied to P&IDS and its application to main control room and engineering.

Authors: Barroso, Javier

BIM digital twin associated with the design of passive fire protection.

Authors: Sabater Sancho, Ignacio; Pascual Rubio, Arturo;Real Soler, Juan Pedro

Vigia project: system based on UHF RFID technology to optimise control&monitoring in FME zones.

Authors: Arnaldos Gonzalvez, Adoracion; Minguez Muñoz, Alberto; Roselló Garcia, José Ignacio

Innovative technology and O&M solutions for NPPs.

Authors: Arnaldos Gonzalvez, Adoracion; Roselló Garcia, José Ignacio; Alcaraz Pieters, Daniel; Minguez Muñoz, Alberto

Non essential Chilled Water Refrigeration Unit Installation

Authors: Deltoro, Javier; Flores, Raquel

Corrosion monitoring in steel structures of the reactor´s vessel at the Vandellós I Nuclear Power Plant – Dormancy period.

Authors: Durán López, Javier

Advantages of implementing computer-based procedures.

Authors: Barroso, Javier

Suitability of Small Two-Bar Test for estimation of tensile test parameters.

Authors: Joshi, Aniket; Forsey, Alex; Moat, Richard; Güngör, Salih

An Assessment of the functional reliability of the control and protection system in the type of reactors WWER.

Authors: Yılmazer, Samed Tugrul

A complex for localization and repair of the fuel pool cladding for NPP-2006 project.

Authors: Tikhonov, Aleksandr

Proceedings of the European Nuclear Young Generation Forum
ENYGF'21
September 27-30, 2021, Tarragona, Spain

The Importance of Synthetic Viewing for Teleoperation Tasks in Hazardous Environments

Pacheco-Gutierrez, Salvador[1*], Caliskanelli, Ipek[1] and Skilton, Rob[1]

[1] UK Atomic Energy Authority – Remote Applications in Challenging Environments (UKAEA-RACE), United Kingdom

*Corresponding author: *salvador.pacheco-gutierrez@ukaea.uk*

I. INTRODUCTION

Nuclear power, conceived during the second world war as a mass destruction technology, has now become the primer technology aiming at low-carbon emission source of energy. Furthermore, the joining of the once divided West and East has led to a worldwide research ground that involves not only physics or chemistry but many other engineering fields, such as robotics, programming, and more recently artificial intelligence (AI) to make fusion energy a reliable source.

Recent advances in robotics and communications have allowed performing risky tasks such as handling, maintenance and decommissioning using teleoperation, applying unilateral or bilateral control. Unilateral control refers to a situation where one side follows the position or forces of the other. Typically, this would be a remote manipulator following a human-interface device (HID)[1]. Bilateral control is a scheme where both, HID and remote manipulator, follow each other in a closed loop. Moreover, teleoperation helps saving time, effort and most importantly lives.

With recent developments in graphics processing, together with highly accurate 3D sensing devices capable of providing high-quality point cloud[2] data at high frame rates, the creation of live virtual environments for aiding remote handling, maintenance and inspection is now a possibility at a cheaper cost. However, in a nuclear teleoperation scenario, the real-time transmission of large high-resolution point cloud data still represents a challenge due to bandwidth limitations combined with far geographical locations. To counteract this challenge, the information gathered can be processed using computer vision and deep learning algorithms to compress, segment, filter and effectively transmit only important information. Moreover, current development of 5G technologies appears to be promising in solving latency related problems [1].

This manuscript is structured as follows: Section II addresses the challenges in teleoperation with regards to its viewing systems. Section III discusses what virtual reality and synthetic viewing are, and how these technologies can be used to improve the user experience of remote operators in the nuclear industry. Lastly, in Section IV we discuss current work conducted in the UKAEA to address the challenges of integrating real-time synthetic viewing into teleoperated systems.

[1] Due to the political incorrectness of the master-slave terminology, in this paper we refer human interface device (HID) to that is known as master, and the remote manipulator to what is refereed as the slave.

II. VISION SYSTEMS FOR ROBOTIC TELEOPERATION IN NUCLEAR

A fundamental aspect for successful teleoperation tasks is the knowledge of the inner state of the remote system and its surroundings in real-time; this is achieved using exteroceptive and proprioceptive sensors, respectively. For the former, joint positions and velocities can be obtained through optical encoders attached to each joint. The latter lies in gathering real-time information using video and/or 3D cameras as well as any other external sensing device. As can be inferred, the accurate and fast transmission of this information is crucial for an adequate functioning of any teleoperation system. With focus on vision, we briefly describe a few of the systems utilised in nuclear applications, their importance, and current challenges associated with those systems.

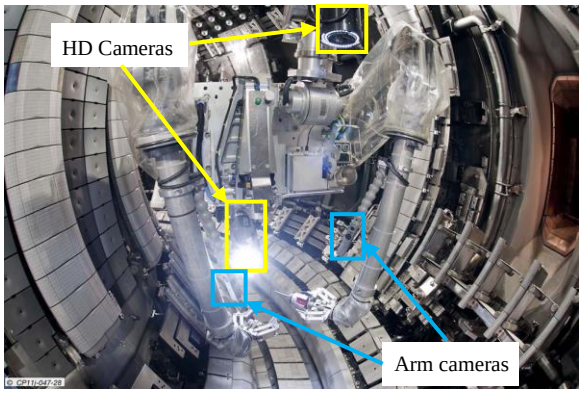

Figure 1. Remote Handling MASCOT Manipulator inside the JET Vacuum Vessel (May 2011).

In the case of fusion reactors, metallic tiles containing lithium are used, together with cooling systems and complex magnetic coils, to contain the plasma within the vacuum

vessel [2]. This results in radiation damage to the tiles that require adequate inspection and regular replacement (Figure 1). The maintenance activities are extremely dangerous for human beings due to the high radiation not only inside the vessel but on its near surroundings.

The robotic device shown in Figure 1 called MASCOT (Italian: MAnipulatore Servo COntrollato Transistorizzato) is a 1960's built teleoperated dual arm robotic manipulator with 7 degrees of freedom currently used for maintenance tasks inside the JET vessel using a bilateral control [3]. The vision system of MASCOT consists of two high definition cameras mounted above and behind the operative area. Two extra cameras are mounted on each one of the arms assisting the operator with close-up views. This vision setup provides remote operators with live image/video feed of MASCOT's surroundings (Figure 2).

However, regardless of the quality of the cameras and the flexibility on its positioning, this solution fails to provide the operator with a sense of depth and volume (3D) in real-time. This is particularly important when performing grasping, bolting and other related tasks, and can drastically affect operators training time. A partial solution to this consists on integrating a virtual reality scenario together with the vision system (see Section III).

Figure 2. JET Remote Handling Control Room and MASCOT vision system.

Another application is the decommissioning of gloveboxes containing radioactive material. Although, usually they represent a low risk for operators, legacy or damaged gloveboxes can represent a high risk and a key challenge in reduction of hazardous waste. The need for a solution to this is such that recently Sellafield LTD granted a multimillionaire contract to a UK-based firm to tackle this problem [4]. Moreover, the National Nuclear Laboratory (NNL) recently released a UKRI funded challenge for the decommissioning of alpha-contaminated gloveboxes [5]. Such task consisted in utilising novel robotic-aided cutting technologies.

As the need for decommissioning appears obvious, a reliable and robust vision system providing the operators with an adequate insight of the contents of the gloveboxes is required. A potential solution to this problem is the usage of 3D cameras. This would enhance the experience of the remote operator drastically by providing a sense of depth, texture, and even haptic feedback [6, 7].

III. VIRTUAL REALITY AND SYNTHETIC VIEWING

Virtual reality (VR) consists of an interactive computer simulation that enhances sensory, usually visual, feedback in such a way that the operator perceives the feeling of being immersed in the simulation [8]. VR applications in industry are various: simulation of mechatronic systems, prototype testing and training, assembly tasks assessment, to mention a few [9]. In the UKAEA, VR has been used as an approach trying to solve the lack of depth perception when performing remote operations and training inside JET. This consists in including a real-time VR replica of the teleoperated system interacting with JET's inner vessel (environment) on the operator's vision system [10] (Figure 3). Furthermore, the dynamic effects of VR simulation on the operators are currently being investigated and considered for improvement and verification of future reactors such as ITER [11]. Moreover, an extension of VR called Augmented Reality (AR), consisting in the superposition of virtual objects over a real scenario, is currently under development for applications on ITER [12].

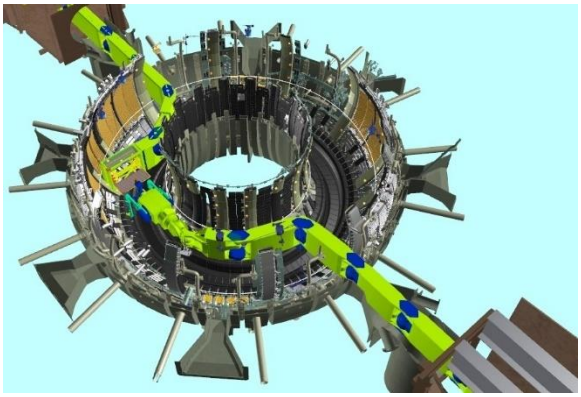

Figure 3. Simulation of two booms operating in the JET Tokamak.

The models of objects in VR and AR systems are required to encompass a description of its dynamic behaviour [8]. Such behaviour can be static or Newtonian. The first consist of stationary objects lacking interaction (visualisation purposes only) and the latter on objects that are ruled by real-world physics laws. In VR applications, these objects must be known in advance, which means that any sudden changes on the real scenario may not be captured in the virtual replica leading to potential collisions or unexpected behaviours. It is then necessary to utilise 3D feedbacked information to update or augment the virtual world accordingly.

Synthetic viewing is proposed as a tool to provide an enhanced environment state estimation. Synthetic viewing consists in combining data from the model and information gathered from multiple sensors to estimate the state of an environment with aims at real-time viewing. The fusion of this information allows to generate an up-to-date virtual environment, and due to the 3D nature of the information, it is possible to visualise the environment from multiple points of view avoiding occlusions and interferences typically present on video-only viewing systems. Although synthetic viewing is currently under assessment for applications in ITER [13], a large amount of research is being conducted to prove and demonstrate its capabilities for remote handling applications [14].

[2] A 3D point cloud is a set of points in $\mathbb{R}^3$ usually consisting of multiple attributes such as colour, texture, normal, etc.

Recent developments on 3D cameras, also known as RGB-D sensors, allow to gather point clouds with millions of points with ~0.06mm precision at high rates. On one hand, the accuracy and density of this data can provide and outstanding insight of the remote environment, on the other hand, this data can be extremely large to achieve desirable transmission rates, particularly in remote operation.

Multiple approaches have been investigated to improve latency in point cloud data transmission. Some of them rely on performing object detection on the remote side (on-the-edge) aiming at transmitting only analytical parameters of the objects located on the scene. Methodologies vary from deep learning [15, 16] to classical fitting approaches such as RANSAC [17]. Computational time, detection accuracy and a priori model availability represent some of the drawbacks on this approach. For instance, in partially known scenarios such as decommissioning of gloveboxes, accurate 3D or analytical models of the objects are not always available.

Other techniques are focused on the compression of point cloud raw data using tree-like structures [14], video compression formats [18] among others [19]. The most important advantage of these methods is that there is no need for an a priori knowledge of the scene. However, even after compression, the transmitted data can still be large and bandwidth consuming. Moreover, compression may represent a loss in accuracy and resolution. To this end, a combination of object detection and point cloud data compression can represent a good trade-off between computation and transmission time, and quality.

The ultimate goal of the integration of synthetic viewing in teleoperation tasks, is to contribute in the development of a robust and reliable remote handling system by providing an intuitive vision system. This with aims at reducing training and operation times. In turn, this translates into shorter and more productive shutdown periods optimising operational costs.

IV. UK-ROK: SYNTHETIC VIEWS FOR A DIGITAL TWIN-BASED SYSTEM FOR REMOTE OPERATION

The UK-ROK project is a collaboration between the UK and the Republic of Korea (ROK) aiming to establish a digital-twin based teleoperation system operated between the two countries. This is a cross-institutions project having the University of Manchester and the Remote Applications in Challenging Environments (RACE) department of the UKAEA on the UK side, and the Korea Atomic Energy Research Institute (KAERI) on the ROK side.

Considering a traditional unilateral controlled teleoperation system, this project is focused on enhancing operator's performance by providing physical models of the remote environment, consisting of the remote manipulator and 3D cameras gathering information of their surroundings (Figure 4). The operator in front of the HID is set to use a digital twin that is replicating the remote manipulator and overlaying the point cloud data gathered from the remote environment on the real-time VR setup.

The information consisting, but not limited to, point cloud and robot joint positions, is then transmitted to the digital twin using the communications channel. Similarly, control commands (joint positions and velocities) are also send from the HID to the remote robot using the same communication channel. Hence, the communication is bidirectional.

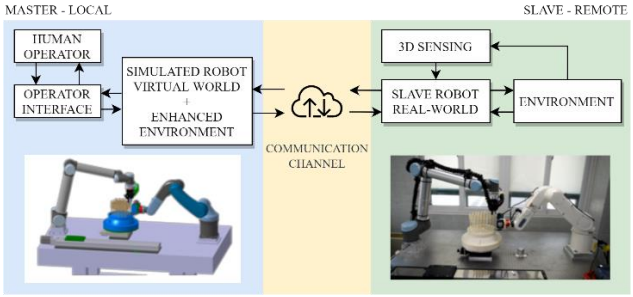

Figure 4. High-level teleoperation system architecture.

The communication channel is a virtual private network which tunnels the data transmitted from one end to the other over the internet. In terms of control, the framework of operation is expected to be: i) manual, ii) human planned and iii) human supervised. Due to limitations in this paper's scope, the control aspects of the manipulator will be kept to a minimum.

A. Point Cloud Data Compression using Tree-like Structures

As mentioned in the previous section, the efficient and fast transmission of point cloud data plays a key role in adequate functioning of the vision system. Hence, one of the most important research topics in this project relate to the compression, transmission, and decompression of point cloud data. In this research, the compression of point clouds is conducted using tree-based structure codification, more specifically octrees and kd-trees. Octrees and kd-trees perform a recursive decomposition which partitions space into cells of a determined size. Then, points lying within each cell are combined to generate a single data point. In the case of octrees, the size and number of cells is defined a priori, whereas on the kd-trees, the size is defined using hyperplanes defined by the median value computed for each axis recursively [14] (Figure 5).

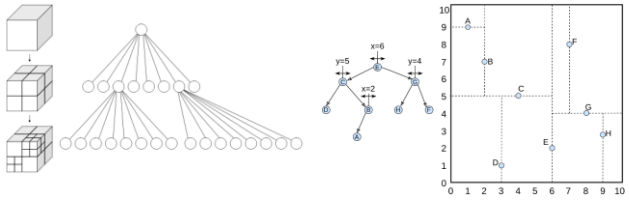

a) **b)**

Figure 5. Tree structures for point cloud data codification: a) octree and b) kd-tree [14].

B. 3D Enhanced Digital Twin for Improving Operators Performance

Initial point cloud data transmission experiments were conducted between two remote locations in the UK: Oxford and Manchester. The remote UR5 Robot manipulator with a RobotiQ Gripper for object manipulation (Figure 6b) is used for the teleoperation. The digital replica of the UR5 robot manipulator (Figure 6a) consisted in a VR representation. As can be observed in Figure 6a, with the

integration of live point cloud data on the digital twin, the remote environment is visualised for the operator in a 3D fashion. Such enhancement allows the operator to perceive depth and colour, which improves the handling of objects. It is important to mention that prior to the integration of the 3D vision system onto the teleoperation system, the operator was only able to visualise image (video-like) feed from the remote environment. This created a burden to an adequate manipulation of objects and in some cases causing collisions and undesired behaviours.

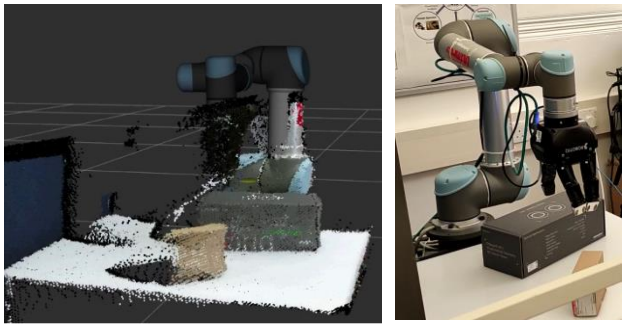

a) **b)**

Figure 6. RGB-D enhanced master side. a) master side enhanced with live RGB-D data gathered from b) slave manipulator.

Initial tests showed that it is possible to update the reconstructed digital replica at a frame rate of ~11 frames per second, approximately one frame every 90 milliseconds. Even though this copes with expected update rates [13], the aim is to reduce even more this delay. To do so, we are currently investigating smarter ways to filter down the information we transmit to the remote side.

Object classification techniques based on deep learning appear to be a promising research path to identify relevant objects on the scene and to prioritise the transmission of those. KAERI has got a vast knowledge and experience in object segmentation from point cloud data and we are currently working on enhancing the proposed vision system. Another research path being explored relies on performing multiple levels of compression. This consists on dynamically variate the amount of data transmitted on a single frame based on the priorisation of elements on that frame. Likewise, we are focusing on a user-defined multiple-level compression system that would allow the user to manually prioritise the quality and transmission on certain objects on the scene. Both techniques aim at reducing the amount of data, hence reducing bandwidth consumption. With this, we predict and improvement on 3D data transmission times. Current work is expected to be integrated as a first trial on the decommissioning of contaminated gloveboxes in the near future.

V. Conclusions

This paper presented a general overview of current viewing technologies and existing challenges in the nuclear industry for remote handling. Since the need for 3D vision on next generation remote handling systems appears obvious, the research here conducted aims at enhancing the operator with real-time 3D views of the remote environment. To achieve low latency, a novel technique for 3D data transmission was described as well as its integration within a teleoperation system controlled from two remote locations in the UK.

VI. Acknowledgements

This work is funded by the UK Engineering & Physical Sciences Research Council (EPSRC) Grant No. EP/S03286X/1. The authors would like to thank Michael Hellebrand and National Nuclear User Facility for Hot Robotics project (Grant No. EP/T011432/1) for leasing hardware to support this research.

VII. References

[1] F. Hu, "A Vision of an XR-Aided Teleoperation System toward 5G/B5G," in IEEE Communications Magazine, Vol 59, 2021.

[2] R. Buckingham, “Remote-handling challenges in fusion research and beyond”, Nature Phys 12, 391–393, 2016.

[3] B. Haist, “Remote handling preparations for JET EP2 shutdown”, Fusion Engineering and Design, 2009.

[4] UK Government, “Sellafield Contract Win for UK Firm”, Department of Climate Change and Energy, Online report, 2017.

[5] National Nuclear Laboratory, “Alpha Glovebox Decommissioning Feasibility Study”, UKRI Project 104068.

[6] F. Ryden, “Proxy method for fast haptic rendering from time varying point clouds”. In IEE/RSJ, San Francisco, USA, 2011.

[7] L. Niu, O. Suominen, “Eye-in-Hand Manipulation for Remote Handling: Experimental Setup”, in Proc. of MS&E, 2018.

[8] M. Matjaz, “Haptics for Virtual Reality and Teleoperation”, Series: Intelligent Systems, Control and Automation, Springer Dordrecht, 2012.

[9] D. Ma, X. Fan, J. Gausemeier and M. Grafe, “Virtual Reality & Augmented Reality in Industry”, Springer, Heidelberg, 2011.

[10] S. Sanders and A.C. Rolfe, “The use of virtual reality for preparation and implementation of JET remote handling operations”, Fusion Engineering and Design, Volume 69, 2003.

[11] C.J.M. Heemskerk, M.R. de Baar, et al, “Extending Virtual Reality simulation of ITER maintenance operations with dynamic effects”, Fusion Engineering and Design, 2011.

[12] ITER newsline, “Augmented reality - Assessing the future work environment”, https://www.iter.org/newsline/-/3509, 2020.

[13] ITER newsline 273, “The promises of ‘synthetic viewing’”, https://www.iter.org/newsline/273/1613, June 2013.

[14] S. Pacheco-Gutierrez, I. Caliskanelli and R. Skilton, “Point Cloud Compression and Transmission for Remote Handling Applications”, Journal of Software, Vol 16, Number 1, 2021.

[15] C. R. Qi, Li Yi, at al., “PointNet++: Deep Hierarchical Feature Learning on Point Sets in a Metric Space”, In Proc. of the 31st Int. Conf. on Neural Information Processing Systems, USA, 2017.

[16] Y. Guo, H. Wang, Q. Hu, H. Liu, L. Liu and M. Bennamoun, "Deep Learning for 3D Point Clouds: A Survey," in IEEE Transactions on Pattern Analysis and Machine Intelligence, 2020.

[17] M. A. Fischler and R. C. Bolles, “Random Sample Consensus: A Paradigm for Model Fitting with Applications to Image Analysis and Automated Cartography”. Comm. of the ACM, Vol 24, 1981.

[18] S. Schwarz, M. Preda, V. Baroncini, et al., “Emerging MPEG Standards for Point Cloud Compression”, IEEE Journal on Emerging and Selected Topics in Circuits and Systems 9, 2019.

[19] C. Cao, M. Preda, “3D Point Cloud Compression: A Survey”, 24th International Conference on 3D Web Technology, 2019.

Proceedings of the European Nuclear Young Generation Forum
ENYGF'21
September 27-30, 2021, Tarragona, Spain

CORDEL: Harmonizing reactor designs and licensing

Tanguy, Ronan[1*] and Na, Byung-Chan[1]

[1] World Nuclear Association (WNA), United Kingdom

*Corresponding author: *ronan.tanguy@world-nuclear.org*

I. INTRODUCTION

The role of nuclear energy is becoming increasingly important to meet energy security goals and climate change targets. Nuclear new build projects however currently face many challenges that are reducing the competitiveness of nuclear power. Long construction times, high capital costs along with national political situations and regulatory approaches are major barriers for companies seeking to develop new power plants. The licensing and permitting activities that must take place before construction not only take up a considerable amount of time and expense but must also be repeated each time a reactor vendor seeks to export their design into another country, as designs are currently only approved for a given regulatory regime. Not only does this mean that multiple design assessments are needed but also that designs must be adapted for given regulatory regimes. The international standardization of reactor would allow vendors and operators to enjoy the plethora of benefits including improved safety, decreased cost and faster construction that result from a large fleet deployment.

The World Nuclear Association's Cooperation on Reactor Design Evaluation and Licensing (CORDEL) working group has been striving towards the goal of establishing an internationally accepted nuclear reactor design approval and certification process through the harmonization of approaches to licensing and worldwide convergence of safety standards for reactor designs since it was established in 2007. CORDEL is split into six task forces that work together to achieve these goals as detailed in Table 1 below.

Table 1. CORDEL Task Forces

Task Force	Role
Licensing & Permitting	Identifying good practices in licensing and permitting for nuclear new build
Mechanical Codes & Standards	Pursue harmonization of mechanical codes and standards used in nuclear component and facility designs
Digital Instrumentation & Control	Increasing awareness of inconsistencies in licensing requirements for I&C systems and promoting convergence of the requirements
Small Modular Reactors	Establishing a path towards harmonized global small modular reactor deployment
Design Change Management	Analysing and determining potential enhancements to international institutional mechanisms to maintain standardization during the lifetime of a standardized nuclear fleet
Nuclear Safety Standards	Providing industry feedback on the work being performed by the IAEA Nuclear Safety Standards Committee to ensure that industry concerns are included.

This report will outline the work of the Mechanical Codes and Standards Task Force and touch upon the Licensing and Permitting Task Force to present the scope and breadth of the activities undertaken by CORDEL.

II. CORDEL ROADMAP

The six task forces collaborate to achieve the goals set out in the CORDEL roadmap [1] that provide a pathway to full standardization and harmonization of reactor designs and licensing with contributions from all stakeholders; industry, regulators and international institutions. The three main roadmap steps are presented in the following sections.

A. Step 1: Sharing of Design Assessments

The first step within the roadmap concerns the sharing of design assessments. No change to existing regulatory frameworks is expected during this period but the focus is instead on the sharing of knowledge and lessons by stakeholders. Collaborative networks are to be formed to allow regulators and reactor designers to share their experiences of respectively assessing designs and having their designs assessed. In this phase, CORDEL will work to highlight areas in which industry would benefit from greater harmonization and standardization and those in which equivalence currently exists by reviewing and commenting

on codes and standards with a view to convergence. At the end of this step, high level safety goals would be understood by all regulators and designers. CORDEL will then compile the lessons learnt by regulators and industry during the first phase of the process which is to be used going forward into the second step Regulators should also have started work on the alignment of the content and structure of their licensing documents where possible to enable actions in the second phase to take place.

B. Step 2: Instituting Common Design Approval Processes

The second step of work focuses on the validation and acceptance of design approval across multiple regulatory regimes. The first objective within this step is to have multiple national regulators agree to collaborate on safety reviews. This action should be assisted by industry with designers working to support the establishment of multi-national reviews. The lessons learnt during the first step of work will enable regulators to gain insight into multi-national reviews on both aspects for which approaches are aligned but also for those where approaches significantly diverge. The lessons learnt from undertaking reviews on these two types of topics are essential in enabling progress on alignment as they will identify areas in which resolution is required and allow CORDEL to produce a plan towards an agreement on such topics.

C. Step 3: Issuing International Design Certification

Once regulators have undertaken joint reviews and plans have been put in place to resolve areas of misalignment, work can move onto the third step which focuses on the validation of designs by an international framework of experts from national regulators from both established and emerging nuclear nations. The committee will validate chosen designs so that they can be provided with an international design certification acknowledging that the design has met the requirements for licensing throughout the nations that are members of the committee. During this third step of the roadmap, CORDEL will work to support the licensing reviews through the development of lessons learnt which will feedback to industry enabling it to produce designs that be more readily accepted by the licensing committee. This iterative positive feedback loop should enable much faster licensing of new nuclear power plants.

III. MECHANICAL CODES & STANDARDS TASK FORCE

The Mechanical Codes and Standards Task Force (MCSTF) was established in 2010 with a mandate to pursue the harmonization of mechanical codes and standards used in the design of nuclear components and facilities. Its work focuses on the comparison of requirements defined in the principal international nuclear mechanical design codes published by Standard Development Organisations (SDOs) such as AFCEN (France), ASME (USA), CSA (Canada), JSME (Japan), KEPIC (South Korea) and NIKIET (Russia). In line with the CORDEL roadmap, the efforts of the MCSTF are concentrated on identifying areas of equivalence and divergence in the aforementioned design codes through comparison and benchmarking. Recommendations for harmonization and alignment and proposed common codes are then put to relevant SDOs and the SDO Convergence Board based upon the task force's findings.

A. Previous MCSTF Achievements

The Task Force's initial work proposed a harmonized international alternative for the certification of Non-Destructive Examination (NDE) personnel [2]. Harmonization of this certification would improve nuclear supply chains as workers who are trained according to an internationally consistent set of requirements need not be retrained when a component is manufactured for a plant within a new regulatory regime. This would give reactor vendors the confidence that certified personnel have a broad knowledge of NDE methods allowing better international transferability of personnel thereby reducing lead times for the manufacture of nuclear components and increasing the number of potential manufacturers for their components. Following a study of existing code requirements for the certification, the MCSTF proposed that such a harmonized international alternative of NDE personnel be included in all the nuclear mechanical codes. The MCSTF also identified the need for a third part to undertake the certification process to firstly prevent potentially unscrupulous companies using the certification process as a rubber stamp for their personnel to be able to conduct a test but also to assist inexperienced companies in following best practice. This third part should follow ISO 9712:2012 for their certification process.

The second report produced by the MCSTF was written in conjunction with and published by ASME. This report [3] compared the requirements of major nuclear codes and standards for welding qualifications. A high level comparison structure was used for this analysis featuring ASME Boiler and Pressure Vessel Code (BPVC) as the baseline against the other codes and standards would be evaluated. Sections of the codes to be compared were mapped against their ASME BPVC counterparts where possible and assigned a classification according to their similarity to the BPVC baseline. The report examined three main sections of the codes; welder and welding operator qualifications, technical content of welding procedure specifications and qualification of procedures, and technical management and supervision of welding and a manufacturing/construction tool.

B. Non-Linear Analysis

The MCSTF focused its recent efforts on the requirements for Class 1 nuclear components and the rules that govern their design. Non-linear analysis is used as part of these rules for complex geometries that conventional linear elastic methods are unable to adequately assess. The MCSTF developed a project to investigate differences between codes for non-linear analysis and propose recommendations for

harmonization. The codes require that Class 1 components be protected against three major failure modes (excessive deformation, plastic instability and fracture-decohesion), two major degradation mechanisms (fatigue and ratcheting) and two types of loading conditions (monotonic and cyclic) for both thermal and mechanical loads.

The MCSTF produced a series of reports on this topic. The first of these [4] compared the existing codes to find areas where the methodologies differed. Four main areas were identified; limit analysis associated with perfectly plastic materials, monotonic elastic-plastic analysis associated with material stress-strain curve, cyclic elastic-plastic analysis associated with material cyclic stress-strain curves for the fatigue plasticity correction factor and material constitutive equations for shakedown and ratcheting analysis.

Once the areas of divergence were identified, a series of benchmarks were carried out on two typical Class 1 nuclear components by a group of ten international experts from WNA member organisations. The first of these benchmarks featured a large low alloy steel vessel nozzle and the second was based on a reinforced steel piping tee. These benchmarks aimed to compare different practices between codes then assess and analyse the results obtained through the use of the different codes. The first benchmark examined elastic stress, plastic collapse, plastic instability and local failure whereas the second benchmark investigated the effects of cyclical mechanical and thermal loads to perform fatigue assessment. The loads applied to the components and their material properties were constant across each given benchmark. These benchmarks and their results are presented within the second CORDEL report on non-linear analysis [5].

The benchmarking exercises revealed that differences in results arose as a consequence of three principal factors; modelling assumptions made by the analysts, the analysis and assessment methods adopted by the analysts and finally differences in the design code rules [6]. These factors enabled the identification of several areas in which no guidance is provided within the design codes for analysts, leading to a variation in results due to the different individual approaches. It is these areas that were then focused upon and further developed in the final report in the Non-Linear Analysis series [7] to provide recommendations for industrial practice to harmonize and converge analysts' approaches.

The recommendations covered all aspects of performing a non-linear analysis, from the initial problem definition, set-up of the geometry and choice of finite element parameters to post-processing and interpretation of the simulation's results. Locations of special interest during post processing are highlighted along with procedures for stress classification and linearisation. The benchmarks that were presented in the previous reports enabled recommendations to be provided for plastic analysis with multiple methods presented for calculating collapse loads and guidance as to which method to select for a given analysis. Non-linear analysis of elastic and plastic fatigue are also covered with a particular emphasis placed upon the calculation of the elastoplastic concentration factor. As fatigue analysis examines the behaviour of the material over many cycles, the treatment of time dependent variables is key, as such it was recommended that all time-steps include stress linearization and that they be refined enough to capture maximum stresses. It was also recommended that variable material properties be used for such an analysis, notably those that are temperature dependent.

The conclusions within the report principally focus on differences between codified approaches and recommended the most suitable code for a given analysis. The benchmarks did however also employ non-codified approaches, notably for plastic analysis. These results will be taken to SDOs for consideration in future code development.

C. Fatigue Life Analysis

Extending the lifespan of existing plants has been determined by the International Energy Agency to be one of the most cost-effective ways of generating electricity [8]. Proving that components can withstand the demands of increased loading cycles is an essential part of making the case for a licence extension. Fatigue analysis is employed to determine how materials fail under repeated loading from both mechanical and thermal stresses and therefore justify the lifespan of a given component.

The MCSTF has worked to review and compare the current requirements of major nuclear design codes and standards with regards to fatigue analysis with a view to proposing common/harmonized rules for design and analysis. The codes and standards considered for this project are the American ASME BVPC, French RCC-M, Japanese JSME S NC1 and Korean KEPIC MN MNB. A series of reports has been proposed as part of this study, the first of which reviews and compares the aforementioned codes applicable to Light Water Reactor (LWR) plants [9].

This first report used the ASME BPVC code as a baseline as the other three codes were originally developed from it. The report examined how the codes approached eight different parameters (temperature limit, applicable materials, stress, effect of elastic modulus, cumulative usage, plasticity, design curve and fatigue strength reduction factor) and assigned a classification to each code/standard in function of its similitude to ASME BPVC for a given parameter. These classifications ranged from "Same" for technical identical criteria to "Technically Different" for cases in which either code's requirements required either higher or lower thresholds, such differences are typically due to differences in regulatory requirements between the countries of code origin. The report found that the vast majority of codes/standards had either the same or equivalent requirements for the vast majority of parameters. Areas of dissimilitude with ASME BPVC were observed within the JSME S NC1 code for the plasticity factor and the fatigue strength reduction factor and within RCC-M for the plasticity factor.

The findings from this first report will be built upon in three further reports in the Fatigue Life Analysis series that will propose common/harmonized approaches for the pressure vessel and piping fatigue design rules, fatigue crack growth analysis and analysis of environmental effects on fatigue.

IV. LICENSING & PERMITTING TASK FORCE

The Licensing and Permitting Task Force (LPTF) was jointly established in 2011 by the WNA to identify good practices in licensing and permitting for nuclear new build projects. The LPTF is key to achieving CORDEL goals as it promotes dialogue between industry and regulators and seeks to capitalize on opportunities to contribute to licensing processes for all existing nuclear technology and emerging designs, in both established and newcomer nuclear countries. The work undertaken by the LPTF complements the efforts of the MCSTF, as the harmonization of licensing frameworks along with the alignment of technical requirements increases confidence on both sides of regulatory acceptance procedures. This dual approach should result in faster design licensing due to increased familiarity with the design for regulators and fewer design modifications to be made by the vendor.

The LPTF's work has examined licensing processes across ten countries to assess the relationship between the various regulatory regimes and commercial project decisions. The report [10] identified three main areas in which standardization of licensing processes would bring the greatest benefit to nuclear new build projects. This work paves the way for the facilitation of the licensing of First in a Country new build projects once a standardized reactor design has been licensed in another country.

V. CONCLUSION

The harmonization and standardization of nuclear reactor designs and licensing are key to improving the competitiveness of nuclear power as the world transitions away from fossil fuels and seeks zero carbon energy sources. CORDEL plays a vital role in achieving this goal through its Task Forces that work to align stances across the world on a wide range of subjects, from mechanical non-linear analysis to proposing alternative licensing international frameworks. Deep decarbonization will require the deployment of both gigawatt scale reactors and small modular reactors (SMR). The success of SMRs will largely depend on harmonization efforts as the economic model of factory based production lines for widespread export will only work if the same design can exported to multiple countries. The work performed by the MCSTF will enable this standardization, which will have benefits for reactor vendors who can be confident that their design meets the technical safety standards required by regulators throughout the world. Looking to the future, the MCSTF will work to ensure the incorporation of upcoming technologies such as advanced manufacturing and AI into codes and standards is undertaken in a harmonized manner from the start.

The success story of harmonization in the transport of nuclear materials along with experiences in other industries (notably pharmaceutical with the development of COVID-19 vaccines) demonstrate that the goal can be achieved when there is a sufficient and pressing global need.

There is arguably no greater current worldwide need than that to confront climate change by reducing and halting greenhouse gas emissions. Nuclear power is uniquely placed to rise up to the challenge of decarbonization but the effectiveness of its contribution depends on a coordinated international strategy. The CORDEL roadmap outlines the key steps that must be taken by the nuclear industry and its stakeholders to succeed in this international effort and bring the power of the atom to the fight against climate change.

VI. REFERENCES

[1] World Nuclear Association, "CORDEL Strategic Plan 2019-2023," World Nuclear Association, London, 2019.

[2] World Nuclear Association, "Certification of NDE Personnel Harmonization of International Code Requirements," World Nuclear Association, London, 2014.

[3] ASME, "STP-NU-078 Comparison Report on Welding Qualification and Welding Quality Assurance," ASME, New York, 2016.

[4] World Nuclear Association, "Non-Linear Analysis Design Rules Part 1: Code Comparison," World Nuclear Association, London, 2017.

[5] World Nuclear Association, "Non-Linear Analysis Design Rules Part 2a: Specification of Benchmarks on Nozzles under Pressure, Thermal and Piping Loads," World Nuclear Association, London, 2019.

[6] World Nuclear Association, "Non-Linear Analysis Design Rules Part 2b: Assessment of Non-Linear Benchmark Results," World Nuclear Association, London, 2020.

[7] World Nuclear Association, "Non-Linear Analysis Design Rules Part 3: Recommendations for Industrial Practices," World Nuclear Association, London, 2021.

[8] International Energy Agency, "Projected Costs of Generating Electricity 2020," International Energy Agency, Paris, 2020.

[9] World Nuclear Association, "Comparison of Fatigue Life Analysis Methods, Comparison of Pressure Vessel Fatigue Codified Design Rules Based on S-N Approach," World Nuclear Association, London, 2020.

[10] World Nuclear Association, "Licensing and Project Development of New Nuclear Plants," World Nuclear Association, London, 2013.

Proceedings of the European Nuclear Young Generation Forum
ENYGF'21
September 27-30, 2021, Tarragona, Spain

BIM as a way to be one step further

Dzhabarov Dmitrii [1]

[1] RAOS Project Oy, Finland

*Corresponding author: dmitrii.dzhabarov@rosatom.fi

I. INTRODUCTION

The term BIM stands for Building Information Model. The main difference between BIM and 3D Models is that Building Information Model contains a lot of information and/or attributes on objects, which are linked with the project database.

In the present work, the experience of utilizing BIM in the project design of NPP "Hanhikivi-1" in Finland will be exposed.

NPP "Hanhikivi-1" is a nuclear power plant proposed for construction on the Finnish Hanhikivi peninsula, in the municipality of Pyhäjoki. It is to house one Russian-designed WWER-1200 pressurized water reactor, with a capacity of 1200 MW.

Figure 1. NPP "Hanhikivi-1"

- Customer: Fennovoima Oy
- General contractor: RAOS Project Oy
- Number of units: 1

The unique nature of the project is growing out from Finish regulation requirements (e.g. see YVL B7 below) and EPC contract's requirement, e.g. all drawing shall be elaborated from the 3D Model.

Deep experience of ROSATOM in design opens possibility to create high-level detailed 3D Model already at Basic Design stage.

Example of YVL B7 requirements (Finnish Regulatory Guides on nuclear safety) regarding BIM:

- **343a**
  "The license applicant shall submit to STUK for the review of the construction license application a 3D computer model (building information model).
  It shall include a preliminary presentation of buildings, and systems, structures and components to the extent necessary for assessing the layout design of the plant, space reservations, the implementation of separation requirements and protection against internal hazards.
  Systems, structures and components in Class EYT shall be presented extensively enough so that the significance of their positioning to systems, structures and components important to safety can be assessed.
  A description of the 3D computer model (information model description) shall be submitted as an appendix to the model." [2019-12-15]
- **345a**
  "The license applicant shall maintain the documents, analyses and 3D computer model presented in requirements 342–345 during the construction of the nuclear facility.
  The updates to the 3D computer model shall be delivered to STUK sufficiently often in order to implement regulatory oversight". [2019-12-15].

The BIM information databases of the project contain information from different perspectives and suppliers, e.g.:

- **JSC Atomproekt** – General designer
- **JSC OKB Gidropress** – Reactor Plant equipment supplier
- **GE Steam Power** – Turbine equipment supplier
- **JSC CONCERN TITAN-2** are responsible for site preparation, for construction and installation works (e.g. 3D model of pit excavation)
- **Fennovoima Oy** – Owner's Scope buildings integration

Some practical benefits of implementing BIM in the project are mentioned hereinafter:

- **Integration of all involved parties**

When all disciplines works in the same virtual space and sees objects of all other specialists it allows to avoid clashes/issues during design work.

Integration of work results of different companies allows easily review interface points and avoiding collisions.

- **Clash review**

Autodesk Navisworks provides tools for clash search based on rules, which user can specify by using unique attributes of objects, e.g:

We can specify two groups of objects based on unique values of attributes.
After these two groups will be specified – we can create a clash search only between these two groups of objects.
And such kind of rule will work in all buildings of the project because the unique attributes of those groups remain the same in each building of the project.

This method saves time on the review of buildings and allows to keep track of statistics of the number of clashes in the building.

- **Fulfillment of layout related requirements, concepts and etc.**

There are many requirements, which regulate a minimum safe distance between different types of objects. To demonstrate that these requirements taken into account in some cases used specific space reservations together with clash rules, in other cases software provides tools for measuring distance during a visual check. It allows solving possible issues even before 2D drawings will be produced.

- **Verification of physical separation**

Rooms have attributes of Safety Divisions (1- 4), objects have Functional Train attributes (1-10), by the coloring of rooms and objects in the specific colors based on these 2 attributes it possible to make a fast visual check that all objects belong to the correct premises.

- **Maintainability & Constructability demonstration**

Space reservation for maintenance together with a visual check of 3D allows verifying maintainability and constructability of equipment (e.g. that space around the equipment is sufficient, size of doors during transport route bigger than the size of parts of equipment). Elaboration of 2D drawing directly from 3D;

- **Hazard analysis**

Developed 3D model used as input for different types of Hazard analysis, e.g. flooding analysis, fire safety analysis.

- **Detecting of design issues in early project stages**

Review of a 3D model together with system design documentation allows agree on future layout solutions even before building documentation will be elaborated.

II. BIM development at Basic Design

The 3D Model elaboration process using several design tools, as shown in figure 2.

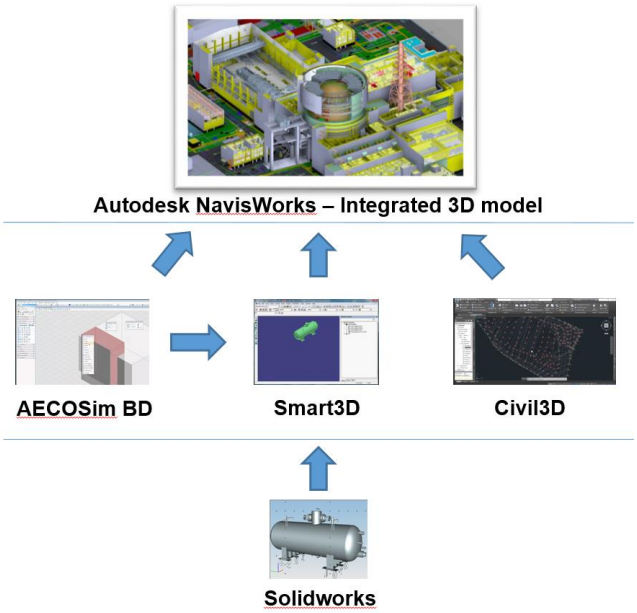

Figure 2. 3D Model elaboration process

1. General Designer design tools:
   - **Intergraph Smart 3D** – Process, HVAC, Electrical disciplines
   - **Bentley AECOsim Building Designer** – Civil, Architectural disciplines
   - **Autodesk Civil3D** – General layout
2. Supplies:
   - **Dassault Systemes Solidworks** – e.g. JSC OKB Gidropress for Reactor Plant equipment
3. **Autodesk NavisWorks –** Integration of discipline level 3D models from Design tools with custom tool of General Designer.

BIM shall be corresponding with Plant Database, to accomplice it in the project were elaborate documents which describe rules based on which shall be designed BIM and Plan Database.

3D Model Description – the main document describes rules by which 3D Model of the project shall be elaborated:

- Level of detailing of 3D model by disciplines;
- Language;
- Design coordinate systems;
- Structure (hierarchy) of objects;
- List of used objects;
- List of used attributes.

List of NPP Information Model (IM) objects – the document describes objects, which planned and allowed to use in the project, each object has a unique Object ID based on its type.

The Glossary of Information Model (IM) Attributes – the document describes attributes, which planned and allowed to use in the project, each Attribute has a unique Attribute ID.

Each object has a limited amount of attributes, which applies to it.

Additionally, Information Model Database has a much wider scope of objects and attributes than it would necessary to present in BIM. That is why 3D Model Description chooses only relevant and important ones to be presented in BIM.

Corresponding and consistency between IM objects, Attributes in BIM and Project database managed by utilizing same objects ID and attributes ID, examples shown in table 1 and 2.

Table 1. IM Objects examples

Object ID	IM Object
id_obj_00001	Room
id_obj_00007	Concrete Wall
id_obj_00033	Isolation valve

Table 2. Attributes examples

Attributes ID	Attribute
id_atr_00001	Name (KKS code)
id_atr_00412	Safety division
id_atr_00012	Safety class

Additionally to the civil structures and process equipment in the elaboration of BIM, space reservations are employed for different purposes, e.g.:

- Escape route and Passage Way – to verify safe access;

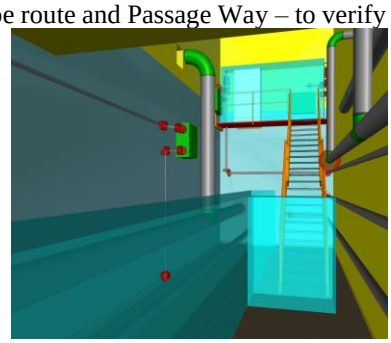

Figure 3. Passage Way (blue space reservation)

- Doors openings;

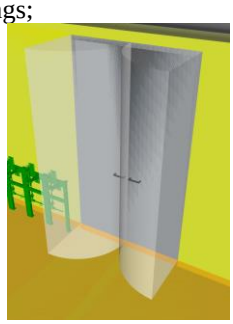

Figure 4. Doors openings

- Insulation – effects external diameter of pipelines;

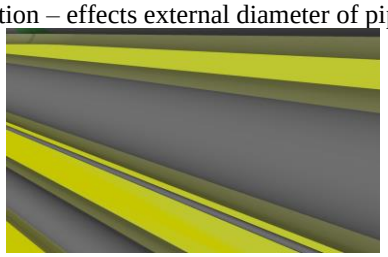

Figure 5. Pipes Insulation

- Measurements – to verify free space around welding points;

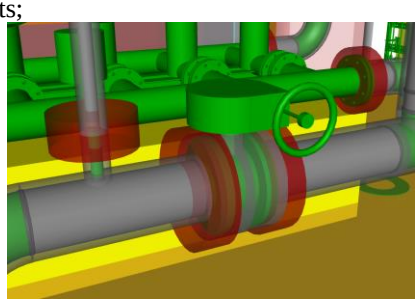

Figure 6. Measurements (red space reservation)

- Fire resistance construction – for hazard analysis;
- Fire damage zone – for hazard analysis;
- Equipment operation and maintenance;

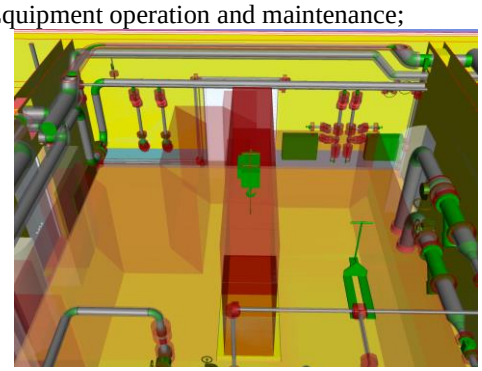

Figure 7. Maintenance routes of equipment (red space reservation)

- Transport way of lifting equipment.

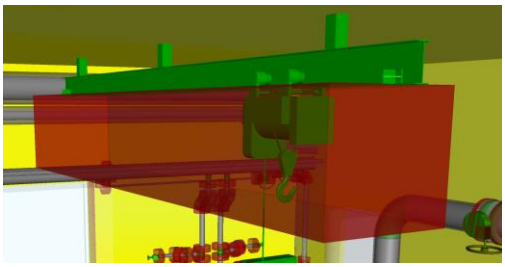

Figure 8. Maintenance equipment

III. Review process benefits

Autodesk Navisworks software provides a user-friendly tool for reviewing clashes based on the rules by what kind of objects has a collision, e.g.:

01. Escape Routes/Passage Way - Pipe Run/Duct Run/Pipe Support/Cableway/Cable Tray Support/E
02. Door/Window - Pipe Run/Duct Run/Cableway/Cable Tray Support/Equipment/Concrete Stair(Co
03. Pipe Run - Pipe/Duct Run/Cableway/Cable Tray Support/Equipment/Concrete Stair(Column,Bean
04. Duct Run - Duct/Pipe Support/Cableway/Cable Tray Support/Equipment/Concrete Stair(Column,
05. Cableway - Pipe Support/Cableway/Equipment/Concrete Stair(Column,Beam)/Steel Beam(Stair)
06. Equipment - Pipe Support/Equipment/Concrete Stair(Column,Beam)/Steel Beam(Stair)
07. Steel Beam/Steel Stair - Concrete Stair/Concrete Column/Concrete Beam/Pipe Support
08. Maintenence - Pipe Run/Duct Run/Cableway/Cable Tray Support
09. Concrete Wall/Slab - Pipe Run/Duct Run/Cableway (just for information)

Figure 9. Example of clash rules

RAOS Project Oy as well have in house developed plugins for Navisworks, which allowed to prepare automatically reports from BIM:

- Report of consistency of IM objects and attributes with 3D Model Description;
- Report of data comparison between versions of models;
- Object data reports in order for a fast overview of all data presented in the BIM in excel format.

Attributes in BIM allowed make an easy visual check by changing colours of the object based on selected attributes, e.g. cable trays based on their functional train:

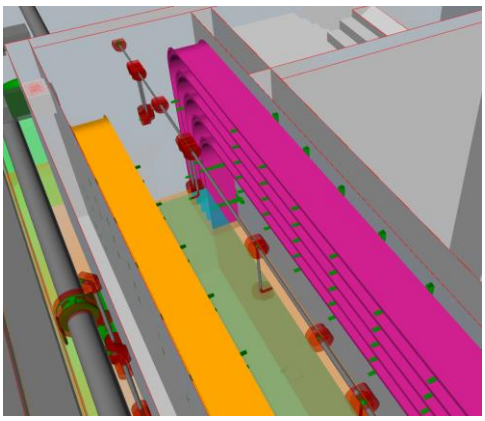

Figure 10. Electrical cable trays

Elaboration of 2D drawing significantly speeds up the working process and ensures that different chapters of basic design have a unique source without any differences.

2D drawing are easy to attach to the 3D model in order to compare by visual check to ensure that no changes were done in drawing (against the agreed design in 3D model).

IV. Positive effects of detailed BIM

- The location of buildings on the site justified and optimized.
- Buildings' dimensions justified and optimized.
- Minimizing risks of changing buildings' dimensions after CLG.
- Justified the effect of the location of each building on the safety and security of NPP.
- Management of internal interfaces, as well as interfaces between RAOS and Owner scope.
- Implement strict requirements of EPC contract to the internal buildings' layout.
- Fixing and avoiding more than 100.000 clashes already at the Basic Design stage.
- Implement lessons learned from databases CONEX (NEA/CNRA/R(2012)2 First Construction Experience Synthesis Report and NEA/CNRA/R(2015)4 - Second Construction Experience Synthesis Report).
- Implement requirements of EPC contract regarding Operation & Maintenance, Occupational safety and health and Plant Availability Factor (92-93%).
- At the next stage of the project, the detailed 3D model will allow to speed up analysis of supplied equipment and its influence on buildings' dimensions.

Proceedings of the European Nuclear Young Generation Forum
ENYGF'21
September 27-30, 2021, Tarragona, Spain

Environmental safety justification in the design of NPP

Daniil Kolesov[1]

JSC "Atomenergoproekt", Russia

I. Introduction

The electrical power demand as well as the number of consumers is growing day by day, all over the world. This is also the case for Russia. Since 2008, the electrical power production in the Russian Federation has grown by 5.3%. At the same time, the consumption has increased by 5.4%. The growing demand comes from the transport, housing and utilities sectors; in addition, energy-intensive industries are developing both inside the country and in countries consuming the exported electricity, as presented in [10].

The thermal power plant share in electricity generation in Russia is 59.3%, according to data for year 2020. The share of hydroelectric power plants together with other power production based on renewable energy sources is 20.1% of the total, and that of nuclear power plants reaches 20.6% [9].

By 2040, the power consumption is expected to grow by 60% compared to 2017. In this regard, non-carbon resources should provide more than 40% of the production increase.

The nuclear power generation has grown by 25% since 2008. New technologies are being created, which allow for the minimization of radioactive waste, discharges and emissions, while relevant requirements are constantly becoming more stringent. The share of generation 3+ nuclear power plants and upgraded existing power units is growing; besides, we expect an increase in the power of fast reactors for which the closed nuclear fuel cycle is used [10].

II. Environmental safety justification

According to the basic Russian sanitary regulations governing the radiation safety [11, 12], the radiation safety of personnel, public, and environment is considered to be ensured if it complies with the main radiation safety principles: justification, optimization, regulation. The justification principle is implemented by comparing the benefits and hazards of a radiation source while taking into account various factors: radiological criteria, environmental, social, economic, psychological, and other indicators. The optimization principle is applied to normal operation of ionizing radiation sources. The optimization should be used in case of exposure levels ranging from the appropriate dose limits to a negligible level of 10 μSv/year for the individual dose. The regulation principle is used to prevent exceeding the dose limits established by the Russian legislation. Besides, a system of additional standards derived from dose limits has been introduced, and the possibility of multiple-factor effects due to ionizing radiation sources is taken into consideration.

The basis for ensuring the nuclear, radiation, and environmental safety of a nuclear power plant consists of reactor plant environmental impact assessment documents which are part of the design documentation in accordance with the requirements of the Russian environmental legislation and standards based on the IAEA recommendations [3].

The restrictions on NPP pollutant release into the environment, established by the sanitary requirements, preclude the possibility of severe disturbances in the functioning of biogeocenoses in the NPP region and a significant accumulation of radioactive contaminants in environmental objects [2]. Critical ecosystems in the NPP region should be selected and justified in the course of environmental safety justification activities. It allows reducing both the scope of research in the region and the volume of assessments and forecasts of NPP natural environment condition and changes in this condition due to the NPP operation. Critical ecosystems also serve as a biological indicator of all biogeocenoses in the region.

Critical ecosystems are those ecosystems which due to their biological characteristics and location in the region are the most sensitive to hazards arising from the NPP or from other causes. For the same reasons, as a consequence of changes in their life processes, they can adversely affect the human health, living conditions in the region, and economic activity conditions to a greater extent than other ecosystems. Accordingly, the well-being of critical biogeocenoses guarantees the well-being of other (non-critical) biogeocenoses and the absence of indirect influence of the NPP or other hazards on the NPP region population [5].

The site to be selected for the NPP construction should meet specific requirements which along with engineering and administrative measures implemented at the NPP shall ensure the radiation safety of population during NPP normal operation and possible emergencies which cannot

be completely excluded. According to the Russian Federation legislation [12], NPPs must be located in sparsely populated, non-flooded areas with a stable wind regime and limiting the possibility of radioactive substance spread outside the facility site owing to their topographic and hydrogeological conditions. These requirements are determined by the concern for the population and natural area protection in case of unforseen accidents at the NPP. Moreover, they are associated with the need to maintain a low risk level for the population during the NPP operation under conditions of widespread development of nuclear power industry. No hazardous natural phenomena, accidents at enterprises of other industries or transport accidents shall lead to an increased risk for the population, and accordingly, they shall not result in a decreased NPP safety.

A. Hazards for the environment of NPP site regions

Radionuclides from the NPP can enter the environment with process and ventilation gases and aerosols, with NPP heat-transfer equipment cooling water, sometimes with residual water. Water bodies are contaminated from the NPP emission cloud and directly, i.e. with NPP liquid discharges. As shown in the diagram (Figure 1), radionuclides from the emission cloud fall onto the surface of water objects and onto their water catchment areas, become involved in biological cycles and ecosystems, and are accumulated, among other things, in biological objects consumed as food by people, cause the external exposure of humans, and also the internal and external exposure of vegetation and animals [2]. It should be taken into consideration that the nuclear power plant radiation effect is lower than that of coal-fired power plants [3]. For example, according to data for year 1990 collected by Badyaev [2], radioactive fallouts from the atmospheric air in the Beloyarsk NPP area are due only to global fallouts, since the NPP influence in the region does not exceed background fluctuations. The same data were confirmed in 2020 by Mikhailovskaya [8]. Over the period from 2002 to 2013, a decrease has been observed in radioactive substance emissions and radionuclide discharges into water bodies. At the same time, these values do not exceed 20% of the established standards for permissible emissions and discharges, according to [3].

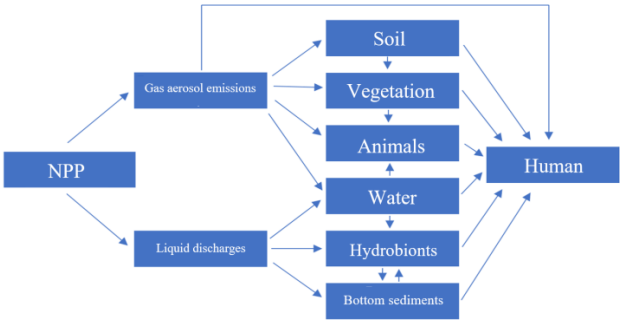

Figure 1. Human exposure to radiation due to radionuclides released from the NPP into the environment.

Radionuclides fall onto the soil surface from the NPP emission cloud. Most radionuclides are well sorbed by soils and move into the depths over time. The radionuclide vertical movement along the soil profile is determined by the precipitation filtration deep into the soil, capillary moisture volume, ion diffusion, soil particle mechanical transfer, microorganism activity, etc. [2].

In NPP normal operation mode, radionuclides from the emission plume are deposited directly on the above-ground part of plants and assimilated through the root system from the soil. The forest, namely, the pine forest is the most radiosensitive of all possible biogeocenoses. The Scotch pine is one of the vegetation types that rather effectively accumulates radioactive pollutants from the nuclear power plant release into the atmosphere [2]. Therefore, obtaining information about the response of the forest cenosis to small but long-term radiation effects is one of the important tasks of radioecology. This task is solved by organizing and carrying out the environmental radiation monitoring in the NPP region.

Animals living in the soil, insects, birds, amphibians, reptiles, and vertebrates represent the fauna in the NPP region. However, from the human protection viewpoint, farm animals are primarily considered, since they represent the main radionuclide transmission link in the human food chain. The issue of radionuclide consumption and accumulation by other animal groups is considered either as the radionuclide transformation and transfer links in the NPP region ecosystems, or as an issue related to the assessment of radiation effects directly on representatives of these groups themselves.

Regarding the NPP region hydrology, the design stage includes the development of water intake design and the assessment of how its operation is affected by the interrelation between surface and ground waters, the investigation as to how the pumping-out mode influences the soil engineering and geological properties, and the assessment of karst-suffusion process development. The use of inland water bodies and their outflowing rivers for NPP water supply should mandatorily take into account the aquatic ecosystem preservation requirements and, for this purpose, provide for appropriate river runoff conditions, prevent lake water depletion below the natural minimum and lake water overheating exceeding permissible temperatures [1]. Liquid radioactive waste discharge or their dilution with the subsequent discharge into open water bodies is prohibited by the Russian Federation legislation [2].

B. Hazards for the population and NPP personnel

Sanitary rules represent the implementation of the sanitary principle of human protection from the effects of radiation. The task of ensuring the NPP radiation safety for the population is solved by designers, developers, and operating personnel. The critical population group concept is used for assessing the radiation burden on the NPP region population. This is a limited population group consisting of people who, due to their living conditions, food, or other reasons, are exposed to radiation from radionuclide emission (or discharge) more than other NPP region population groups. If the critical population group is protected from radiation effects from the NPP, then one can conclude that the entire region population is protected, as

shown by Egorov [6]. The individual dose for the population living near a nuclear power plant with a capacity of 4 to 5 GW does not exceed 5 mrem/year at a natural background dose of 60 to 70 mrem/year [3].

C. Hazards due to non-radioactive contamination sources

In addition to radioactive discharges, emissions and waste, a nuclear power plant during normal operation is also a source of thermal pollution and chemical emissions from facilities located at the NPP site.

The design sections provide the results indicating that non-radiological hazards have no above-standard effects on the population and environmental objects of the NPP regions, as shown by Babina et al. [1], [4], [7], [8].

III. Conclusion

Nowadays, the nuclear energy is an environmentally safe energy source. The issues of NPP impact on the region enviroment are solved at the design stage. Many factors are taken into account to ensure the environmental safety and the population and personnel well-being.

IV. REFERENCES

[1] T. Babina, N. Del'vin, V. Pisarev. Hydrothermal situation in cooling ponds located in different latitudinal zones of the European part of the Soviet Union. In Radioecological research in the NPP zone: collection of scientific works, N. Kulikov and M. Chebotina, Eds., Sverdlovsk, USSR: UrO AS USSR 1988, pp. 49-52.

[2] V. Badyaev, Yu. Egorov, S. Kazakov. Environmental protection during NPP operation. Moscow, USSR, Energoatomizdat, 1990.

[3] V. Grachev. Environmental safety of nuclear power plants. In Ecology and industry of Russia, vol. 24, No. 3, pp. 44-50, 2020. doi: 10.18412/1816-0395-2020-3-44-50.

[4] Yu. Egorov, S. Leonov, D. Meshcheryakov. Main results of radiation environmental monitoring of Lake Druksiai – a reservoir for cooling the Ignalina NPP. In Ecology of regions of nuclear power plants (ERAS-1), vol. 1, Yu. Egorov, Ed., Moscow, Russia: GNIPKII – NIOEAS, 1994, pp. 144-170.

[5] Yu. Egorov, V. Kocher'yan, D. Lyuri, F. Tikhomirov, V. Chionov. Critical ecosystems of the Kursk NPP region. In Ecology of regions of nuclear power plants (ERAS-4), vol. 4, Yu. Egorov, Ed., Moscow, Russia, NIOEAS GNIPKII – Atomenergoproekt, 1995, pp. 55-77.

[6] Yu. Egorov, S. Ryabov, V. Chionov. Dose load on the population living in the Kursk NPP region. In Ecology of regions of nuclear power plants (ERAS-5), vol. 5, Yu. Egorov, Ed., Moscow, Russia, NIOEAS GNIPKII – Atomenergoproekt, 1996, pp. 31-43.

[7] S. Lyubimova, O. Sitnikova, A. Trapeznikov. Some questions of the hydrochemistry of the Beloyarsk reservoir. In Radioecological research in the NPP zone: collection of scientific works, N. Kulikov and M. Chebotina, Eds., Sverdlovsk, USSR, UrO AS USSR 1988, pp. 60-62.

[8] L. Mikhailovskaya, V. Guseva, O. Rukavishnikova, Z.Mikhailovskaya. Technogenic radionuclides in soils and plants of terrestrial ecosystems in the zone of influence of nuclear enterprises. In Ecol Rus. Sci. Acad., no. 2, pp. 110-118, Mar-Apr 2020, doi: 10.31857/s0367059720020092.

[9] Analysis of electric energy and power balances indicators in the UES of Russia for the IV quarter of 2020, SO UES Accessed: Mar. 27, 2021. [Online]. Available: JSC https://www.so-ups.ru/fileadmin/files/company/reports/ups-review/2021/ups_ balance _analysis_2020q4.pdf

[10] Energy strategy of Russian Federation for a period till 2035, approved by order No. 1523-r dated June 9, 2020 of the government of the Russian Federation, Accessed: Mar. 20, 2021. [Online] Available: http://publication.pravo.gov.ru/ Document/View/0001202006110003

[11] Engineering surveys for nuclear power plants construction SP151.13330.2012, approved by order of the Federal Agency for Construction and Housing and Utilities (Gosstroy) dated December 25, 2012 N 110 / GS, Accessed: Mar. 20, 2021. [Online] Available: https://minstroyrf.gov.ru/docs/1935/

[12] Sanitary rules and regulations SanPiN 2.6.1.2612-10, approved by Resolution of the Chief State sanitary doctor of the Russian Federation dated July 7, 2009 N 47, Accessed: Mar. 20, 2021. [Online] Available: http://13.rospotrebnadzor.ru/ sites/default/files/2.6.1.2612-10.rt

Proceedings of the European Nuclear Young Generation Forum
ENYGF'21
September 27-30, 2021, Tarragona, Spain

Performance evolution of ENUSA PWR fuel assembly

Lucile, Fallot[1*] and Elena, Botica[1]

[1] ENUSA Industrias Avanzadas S.A., S.M.E (ENUSA), Spain

*Corresponding author: lcjf@enusa.es

I. Introduction

At the beginning of the commercial operation of the Pressurized Water Reactors (PWR), it was quite common that fuel was subjected to a wide variety of failures and operational issues. Nevertheless, the industry breakthroughs allowed to keep improving fuel behaviour over the last decades, until failures in the fuel become occasional.

However, the more demanding operational conditions in the current Nuclear Power Plants (NPPs) have led to keep working on enhancing fuel performance. Therefore, the fuel assembly product and fabrication procedures have been continuously reassessed with the objective to boost plant operation while preventing the occurrence of failures, those which are mostly mitigated and those which still occur punctually. Moreover, the operational conditions have a huge impact on the fuel behaviour, and for this reason ENUSA works closely with PWR utilities, providing them recommendations to guarantee the optimal fuel performance, considering the more demanding operational conditions that are planned to be implemented in the NPPs in the coming years.

Fuel failures can be divided into two categories: the fuel rod failures and their consequent fission product release; and fuel assembly failures that are produced when the integrity of the fuel skeleton and/or the mechanical structures of the fuel assembly is affected, which could drive to safety or fuel handling issues.

This paper will present the evolution of the performance of the PWR fuel fabricated by ENUSA, focussing on each one of the fuel failure categories over the last decades.

II. Fuel rod failures

Fuel rod failures are commonly characterized by a hole in the cladding, which leads to fission product release to the primary system coolant. In order to have a proper surveillance and detect this type of failures during operation, ENUSA performs monthly analyses of the primary coolant activity [1]. Once a failure is confirmed, it is monitored until the cycle ends, later a root cause analysis and inspections are usually performed to identify the mechanism of occurrence of this failure. Moreover, ENUSA manages a database with all the fuel rod failures occurred on its fuel since the first deliveries. Despite there have been no failures in the fuel rods fabricated by ENUSA since 2016 (see Figure 1), improvements on fuel design, fabrication processes and changes in reactor operation and in the activities of the facilities have allowed to reduce the high rate of failures observed in the first decades of the commercial operation of the NPPs.

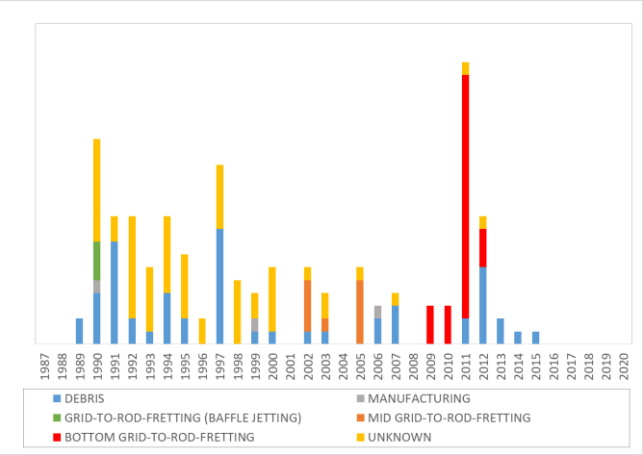

Figure 1. ENUSA's fuel rod failures since 1989

The several causes of fuel rod failures are described hereafter, along with some examples of actions implemented on the fuel design and on the activities of ENUSA and PWR utilities for mitigating them.

A. Manufacturing

Just three failures in ENUSA fuel rods were caused by manufacturing flaws. This type of failures can be caused by primary contamination, weld defects, end plug defects, clad flaws, and gaps in the pellet column that lead to the collapse of the rod, among others [2].

On the basis of the international nuclear industry and ENUSA data, ENUSA's manufacturing division constantly upgrades its Manufacturing and Quality Plans (MAQP) and reinforces the quality controls through the implementation of new technologies (use of a laser micrometre incorporated

in the pressurization equipment to detect helium leak, automatic visual inspection of pellets to detect cracks and excessive porosity, for example) [3]. Other improvements in the fabrication processes will be explained later along this paper, within the description of other specific failure mechanisms.

B. Grid-To-Rod Fretting

The grid-to-rod fretting (GTRF) occurs because of the vibrations between the rods and the springs and dimples of the grids. GTRF failures were observed in the fuel supplied by ENUSA in 1990 and between 2002 and 2012 (see Figure 1).

They are produced due to the cross flows within the fuel assembly and can be accentuated by baffle jetting in downflow reactors. Baffle jetting can be mitigated by modifying the barrel and the former plates of the reactor vessel to convert a downflow plant into an upflow plant. In fact, in a downflow plant, the direction of the coolant flow between the barrel and the deflector is downwards and opposite to the flow within the core, creating an elevated pressure difference through the deflector. This pressure difference triggers water jetting through the baffle-former bolts that impacts the fuel rods facing the deflector, causing a failure by fretting. If the conversion of the vessel to an upflow design is not possible, clips between fuel grids can reduce the vibration, and the peripheral fuel rods facing the deflector can be extracted to be replaced by steel rods. Failures in fuel rods supplied by ENUSA because of baffle jetting only occurred in 1990 (see Figure 1).

Although the baffle jetting can be eradicated, the cross flows within the fuel assembly can be reduced but not eliminated. These flows and rods vibrations can be potentially controlled by the grids designs. Firstly, the Robust Protective Grid was introduced on top of the bottom nozzle for debris retention purposes mainly, nevertheless, it also gave rod support that led to decrease rod vibration, and therefore minimize lower grid-to-rod fretting events. Later, the introduction of Intermediate Flow Mixing (IFM) grids in the fuel design and the changes on the mixing vanes structures of the different grids allowed to re-distribute the flow, which was previously oriented towards the centre of the fuel assembly. Moreover, another example of changes consisted in increasing the contact area between grid springs and dimples and the fuel rods in order to extend the GTRF margin. These changes have allowed to eliminate GTRF failures in the fuel fabricated by ENUSA since 2003.

C. Debris fretting

As it can be seen on Figure 1, failures by debris constitute the primary source of failures and since the beginning of the commercial operation of the NPPs they have been present. Moreover, evaluating globally the last decade of failures, debris abrasion is the main leakers' mechanism. Debris sources are diverse within the primary system, however, during the last decade there is an increasing trend where the principal source of debris is the reactor ageing.

The two main solutions for mitigating debris abrasion consist in ensuring the absence of debris within the vessel and avoiding the debris to reach the fuel rods. The first one is covered by the Foreign Material Exclusion (FME) procedures during the manufacturing of the fuel assemblies and during the refuelling activities in the core facilities. The second one can only be achieved by modifying the fuel assembly design, which now includes several barriers against debris (see Figure 2): incorporation of additional filters in the fuel assembly skeleton and the pre-oxidation of the lower part of the cladding to strengthen fuel rod resistance against impacts.

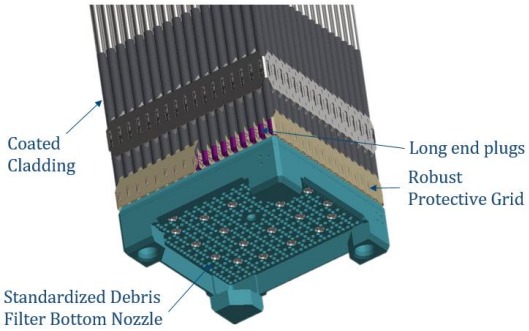

Figure 2. Anti-debris barriers in the current fuel fabricated by ENUSA

D. Fuel rod cladding corrosion and crud deposition

Corrosion products, also known as "crud", are constantly released into the primary coolant system. They come from the surfaces of the different components of the primary loop, mainly from steam generators, but also from the pipes and the skeleton of the fuel itself, and then can be deposited on the fuel rods within the core. In fact, crud deposition on fuel rods could have some associated problems, the most known is Crud-Induced-Localised Corrosion (CILC), since the phenomena involved in the corrosion of the cladding material are accelerated due to crud concentration on the cladding. To mitigate localized corrosion and large crud deposition on the rods due to an excessive local power, the enrichment, the absorber concentration and the pellet-to-pellet gaps are controlled during the manufacturing in ENUSA's factory, using a gamma scanner [3]. Despite the corrosion of the cladding and the deposition of crud have never caused failures in the fuel supplied by ENUSA, it has always been a concern for the PWR utilities. Breakthroughs in the fuel cladding materials [4], improvements of the manufacturing processes [3] and the reactor operating activities allowed to decrease even more the probability of corrosion and crud related issues.

In order to counteract any type of localized corrosion, minimize the amount of corrosion products deposited on the fuel surface and ensure cladding integrity, an optimized chemistry is required. The optimized chemistry consists in pH optimization, follow up of chemical parameters and the use of computational tools and codes.

Regarding the corrosion, the most important modification was the change of the cladding material for new zirconium alloys that demonstrated their better behaviour regarding the resistance against corrosion, as well as other materials

properties where a compromise was reached [4]. This change in fuel cladding has been checked along all the oxide thickness measurements and visual inspections evaluations carried out by ENUSA in several reactors, moreover it has been a key assessment of the fuel behaviour to ensure the design safety criteria are met along the several cycles of irradiation.

E. Pellet-Cladding Interaction

Pellet-Cladding Interaction (PCI) failures occur when cladding experiences high local stresses due to pellet expansion with the chemical action of aggressive fission products, like iodine, on the cladding's inner surface at the same time. This phenomenon is amplified if there are anomalies on the pellet surface (missing pellet surface area, see Figure 3) or on the inner part of the cladding. PCI failures usually happen during startups and mid-cycle power maneuvering.

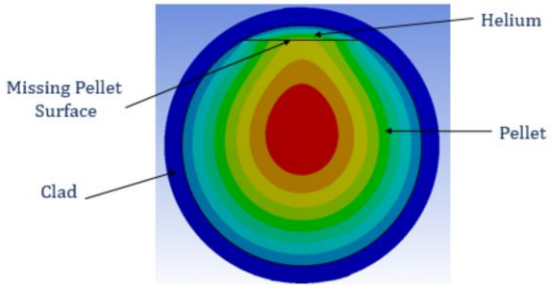

Figure 3. Modelization of missing pellet surface area

The fuel fabricated by ENUSA has been free of PCI failures, thanks to several reactor operating and manufacturing activities.

To avoid Missing Pellet Surface Area (MPSA) (see Figure 3), ENUSA's factory uses Pellet Automatic Inspection machines which have a LED light system and a CCD linear camera that scans around 20 pellets in a row [3]. The system identifies the defect and compares it with visual standards to reject the abnormal pellets.

Regarding the operating conditions of the reactors, ENUSA provides to the PWR utilities recommendations about the maximum power rates during power transients, in order to limit the stresses in the cladding. These actions have allowed the fuel to face the more challenging conditions of operation along the nuclear industry history, like the increase of maximum burnup limits and the Flexible Power Operation conditions, for instance.

III. Fuel assembly mechanical failures

Despite excessive geometric distortion can lead to safety concerns during the operation of the reactor when occurs an Incomplete Rod Insertion (IRI), most of the fuel assembly skeleton failures do not. They rather imply fuel handling issues during loading and unloading the core and during the irradiated fuel storage.

The evolution of the fuel assembly design and the fabrication processes allowed to mitigate most of the skeleton failures, as described hereafter.

A. Manufacturing

Manufacturing failures related with the fuel assembly skeleton gathers defaults in the components (grids, nozzles, guide thimbles) and defective assembling [2]. To mitigate defaults in the components and early fuel assembly bow, the processes for inserting of the rods within the skeleton were optimized to impede the push of the rods. Additionally, the fabrication and control processes were improved to avoid defects while assembling the product and in case they are produced, to better identify them and introduce corrective solutions [3]. ENUSA's factory manages a database with the notifications of the deviations from the normal processes, in order to better analyse them and find solutions not to repeat them.

B. Excessive geometrical deformation

Because of the creep, the neutronic fluence and the hold down spring force, the fuel assembly skeleton (grids and guide thimbles above all) grows and suffer geometric deformations (bow, tilt and distortion, see Figure 4) along its cycles of irradiation. Depending on the stiffness of the fuel assembly structure and operational conditions, some fuel designs can suffer excessive deformations and lead to fuel handling problems and safety issues. In fact, the AEF fuel, the previous design to the current range fuels supplied by ENUSA, was affected by IRI issues in 23 occasions. Besides the difficult insertion of the control rods within distorted guide thimbles, an excessive geometric deformation of the fuel assembly implies larger fuel assembly gaps in some areas respect to its neighbours, commonly known as water gaps issues, which will impact the neutronic fluence and the local power density, affecting the operation of the reactor.

Some modifications on the next fuel design fabricated by ENUSA allowed to reduce significantly the IRI risk, through an increased stiffness of the fuel assembly compared to the AEF design, as it has been observed in the dimensional inspections. These modifications consisted in changing the material of the guide thimbles, increasing their thickness, reducing the hold down spring force and introducing IFM grids which enhanced the geometry stability, although they are not structural grids.

Besides the reduction of IRI risk, the increased stiffness of the fuel assembly also allowed to mitigate the fuel handling issues, because an excessive distortion of the fuel assembly complicated the core loading and unloading, as well as the spent fuel handling for the storage in containers.

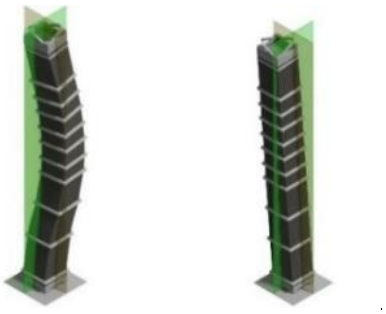

Figure 4. 3D Modelization of a distorted fuel assembly (distortion and bow on the left, tilt on the right) (see Note below)

Note: On Figure 4, the deformation scale is enlarged, whereas the axial scale (length of the fuel assembly) is reduced, in order to see the distortion effect.

C. Stress Corrosion Cracking

Stress Corrosion Cracking (SCC) is a phenomenon that appears under the combination of three conditions: a corrosive atmosphere, a susceptible material and a tensional state applied on the material, causing a failure by an induced crack. In the 90s' decade, this phenomenon used to happen in two components of the fuel assembly: the head spring bolts and the expansion couplings between the top nozzle and the guide thimbles. More recently, it was also observed SCC on the dimples of the protective grid, which could lead to the release of debris into the core.

To reduce the SCC risk in the head spring bolt, which appeared at the end of the 90s' decade, several solutions were implemented along the years. The first ones consisted in changing the material heat treatment, and then in changing the bolts material. To completely mitigate this issue, a new top nozzle design was introduced, where there is no bolt to maintain the spring, since it is integrated within the nozzle. Currently, if the spent fuel stored in the pool is susceptible to suffer head spring bolt SCC, the top nozzle can be replaced by an integrated top nozzle, or handled according to specific processes.

The SCC that occurs in the expansion couplings between the top nozzle and the guide thimbles (see Figure 5) is initiated by inter-granular cracks within the material during the expansion process. The chemical atmosphere in the reactor and spent fuel pool help these cracks to expand until breaking the coupling. This phenomenon leads to the separation of the top nozzle from the fuel assembly, which implies a fuel handling issues. To reduce the SCC risk in this component, the coupling material between the top nozzle and the guide thimbles, usually stainless steel, must contain very low carbon concentration and the heat treatments need to be very well controlled to avoid sensitization. In addition, the chemistry of the spent fuel pools must be optimized to minimize the corrosive environment.

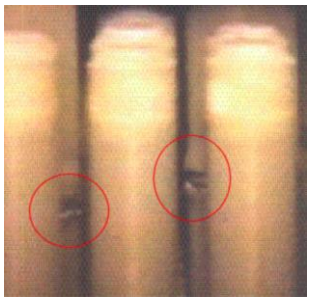

Figure 5. Stress Corrosion Cracking in the coupling between the top nozzle and the guide thimbles

Regarding the SCC issue in the protective grid dimples, the thermal treatment of this grid was modified so that the protective grid is more ductile.

D. Mechanical failures during fuel handling

As the grids grow and the fuel assemblies suffer geometrical distortion during the irradiation in the core, the handling of the fuel assemblies results in a difficult activity during core loading and unloading or during the handling for fuel storage. It has been observed in various occasions that the grids of several fuel assemblies could interact between them and the movement of the fuel assembly could lead to their break. Moreover, the springs of the grids also could be damaged in case of impact. Regarding the other components of the fuel assembly, the bottom nozzle of some former fuel designs could be broken if, during handling operations, the fuel assembly laid on one side supporting the handling utility weight.

In order to mitigate such mechanical failures, chamfers were added to every components corners that constitute the fuel assembly. Moreover, grids and bottom nozzle were strengthened (implementation of a skirt between the legs of the bottom nozzle and reinforcement of the grid welds, for example).

IV. Conclusions

Along the nuclear industry history, both fuel rod failures and fuel skeleton failures have been investigated to find solutions to mitigate them and boosting fuel performance. On the basis of the root cause analyses, improvements not only in fuel design but also in fabrication and reactor operating activities were implemented to upgrade fuel reliability. Nowadays, few failures occur sometimes, and most of the failure mechanisms have been mitigated, compared to the numerous fuel failures that used to happen at the beginning of the commercial operation of the PWR reactors.

Despite no fuel failures have occurred in the fuel supplied by ENUSA since 2016, the more and more challenging operating conditions have done fuel behaviour keep improving, so that the fuel can withstand future more demanding operating conditions without failing. The final objective consists in achieving an Accident Tolerant Fuel (ATF) able to cover the future reactor ambitious operational conditions.

V. References

[1] Fuel Reliability Monitoring and Failure Evaluation Handbook: Revision 3. EPRI, Palo Alto, CA: 2019. 3002016031

[2] Critical Fuel Reliability Attributes for Fuel Fabrication surveillance, EPRI, Palo Alto, CA: 2015. 3002005549

[3] Y. Romero, M. Aulló, J. A. Herrero, "Manufacturing improvements for fuel reliability", Top Fuel 2018, Prague, Czech Republic, September and October 2018.

[4] G. Pan, D.B. Mitchell, A.M. Garde, J.L. Norrell, A.R. Atwood, M. Limbäck, "Advantages Gained by Optimized ZIRLO™ and AXIOM™ PWR Cladding Materials", Top Fuel 2016, Boise, Idaho, USA, September 11-15, 2016.

Proceedings of the European Nuclear Young Generation Forum
ENYGF'21
September 27-30, 2021, Tarragona, Spain

MBIR project is mega-science class installation. Multipurpose fast neutron research reactor.

Stepanova Elena Olegovna[1 *], Agapov Artem Anatolyevich[1], Parfenchikov Ilya Sergeevich[1], Malyshev Victor Valerievich[1], Dorovskikh Boris Vasilievich[1]

JSC Atomtechenergo[1], Russia

**Corresponding author*: *stepanovaeo@cate.ru*

I. INTRODUCTION

Research reactors have contributed substantially to the development of nuclear science and technology for the last half-century.

We have now reached of the moment when most of the research carried out at the level of existing reactors has been completed. Innovation and new research require new instruments and more powerful complexes based on high-flux reactors with laboratories for post-irradiation examination.

The creation and the future operation of a multipurpose fast neutron research reactor (MBIR) is considered as one of the strategically important innovative projects for the nuclear energy development. This RF project is focused on solving the problems of resource provision, economic security and increasing the branch enterprises competitiveness.

Figure 1. MBIR. [1]

II. INTERNATIONAL RESEARCH CENTER

A research reactor may be constructed to meet the requirements of a single Member State or serve as a regional or international center of excellence, helping to meet the needs of both the initiating Member State and its neighbors or collaborators.

The structural framework is two-component: a reactor complex owned by the Russian Federation and technically managed by the authorized Russian organization SSC RIAR. A creative research component goes to the International Research Centre on a long-term agreement.

The MBIR's Steering Committee will be responsible for the programs formation, approval and implementation as national as international scientific research.

RIAR will be bearing direct responsibility for liabilities, operation, and maintenance and the program's technical execution. RIAR will also provide extra laboratory services on site.

Consortium Leader of MBIR Reactor International Research Centre will manage the budgeting process, including consortium share (administrative costs of the consortium management) and the irradiation service budget, which will define the pricing model for the irradiation contracts. [2]

The reactor is designed to provide a wide range of research and experimental work using reactor radiation in the following areas:

Structural elements materials research:

– research of the structural materials for the research of promising types of nuclear fuel and absorbing materials;active zones for the new types of reactors, fuel elements tests under high dose fast neutrons irradiation with different temperature regimes;
– research & development of the radiation, temperature, and corrosion resistant materials for the fusion and other advanced types of reactors.

Fuel and fuel rods research:

– testing of different types of fuel, fuel rods, and cladding for the new generation of reactors;
– closed fuel cycle technologies design;
– long living radioactive elements handling;
– testing of the dense fuel containing minor actinides;
– radioactive waste and spent fuel management;
– development and safety recommendations for fuel fabrication and FA design.

Coolants performance:

– research in the independent loop-channels;

– simulation of the active zones elements behavior with different coolants.
– other research

Isotope technology & production:

– experimental validation and development of the radionuclides production technologies
– silicon doping technology research;
– production of large diameter silicon ingots;
– new materials research;
– high dose irradiation & research of new advanced structural materials: high flux = accelerated doze accumulation = reduction of the research timeframe.[2]

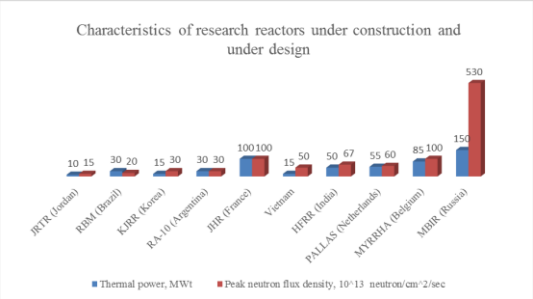

Figure 2. Characteristics of research reactors under construction and under design.

Competitive advantages of MBIR:

– Fast neutron spectrum;
– High flux neutron;
– Wide experimental possibilities, including three independent loop installations;
– Up-to-the-mark safety level (passive SS: 2 ERS loops);
– Technological solutions are referent to the Fast Reactor BOR-60.
– Professional team of the operating organization;
– Possibility of commerciality the MBIR use (isotopes, NDS. NAA, electricity generation);
– High utilization factor (0.65);
– Design lifetime - 50 years;
– Provision of the fuel cycle by RIAR.

III. DESIGN SOLUTIONS

The maximum possible use of reference solutions is envisaged to ensure reliable and safe operation of the MBIR reactor. The MBIR design project is based on the positively proven technologies of the BOR-60 reactor plant.

MBIR includes a reactor unit with two sodium cooling circuits and a third steam-water circuit, a steam turbine unit, transport and technological schemes, loop installations, vertical and horizontal test hole, a complex of research shielding chambers and a laboratory complex.

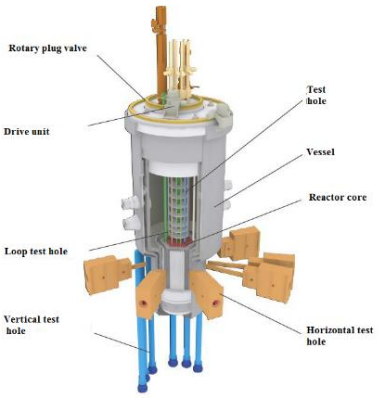

Figure 3. Reactor configuration. [2]

RF MBIR consists of two independent loops, each of which contains pipelines and equipment of the I, II and III circuits. The three-loop circuit provides heat transfer from the operating reactor through two loops to the steam turbine unit. The RF MBIR also provides for an emergency heat removal system (EHRS) circuit. It is constantly in working condition in the mode natural circulation, while heat from the I circuit is removed by an air heat exchanger (AHE).

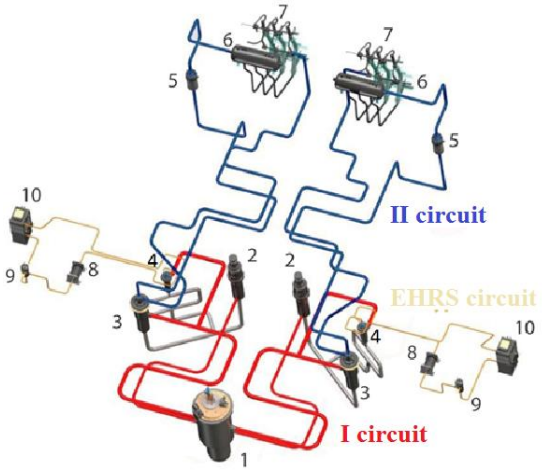

Figure 2. I and II circuits.
1- reactor; 2-RCP; 3- intermediate heat exchanger; 4- emergency heat exchanger; 5- electromagnetic pump of II circuit; 7-inverse steam generator; 8- electromagnetic pump of EHRS circuit; 10-air heat exchanger. [1]

Sodium is used as the coolant for the I and II circuits, water-steam is the coolant for the III circuit (and in the AHE EHRS). There are two symmetrically located blocks of the emergency heat removal system.

The three-circuit heat transfer scheme is optimal for fast neutron reactors, preventing the ingress of radioactive sodium into the steam-water circuit in the event of a steam generator leak. The two-loop layout of the installation ensures safety in the event of a possible failure of one loop (depressurization of equipment, pipeline). In this case, the reactor is shut down by a signal generated in the integrated control and safety system (CSS), and the residual heat output is removed by the operable loop and the EHRS channel.

The first circuit of the MBIR reactor is designed to remove heat from the reactor by circulating a liquid metal sodium coolant in the I circuit and transferring it to the II circuit and

the EHRS circuit through an intermediate and emergency heat exchanger. Each loop removes 50% of the power from the reactor.

The II circuit is designed to remove heat from the I circuit in intermediate heat exchangers and transfer it to the III circuit to steam generators. In addition, the II circuit is designed to avoid contamination of the III circuit with radionuclides of the I circuit when the intermediate heat exchangers tube bundle of is decompressed, i.e. to improve the radiation safety of the MBIR. This goal is achieved by the layout of the II circuit in relation to the the I circuit, and by increased pressure of II circuit against the pressure of the I circuit: (the pressure from the side of the I circuit is not more than 0.07 MPa, and from the side of the II circuit is 1.0 MPa).[3]

Induced radioactivity and fission products are absent in the sodium of the II circuit.

The II circuit is a normal operating system important to safety. It has two symmetrical loops of the same power (72 MW).

The symmetry of the loops allows the use of the same type of thermal mechanical equipment. The EHRS circuit is a safety system and is designed both for emergency cooling of the reactor and for scheduled heat removal from the core. in the amount of 4% of the reactor thermal. Thus each EHRS loop removes 3 MW of thermal power.[4]

The MBIR reactor consists of the following main elements:

- main vessel with the guard vessel and leakage monitoring sensor of the sodium and the vessel thermal movement;
- rotary plug valves;
- reactor vessel internals (in-vessel storage, basket with core assemblies, reflectors);
- in-vessel fueling machine;
- instrumentation and automated control systems;
- cable trends;
- block insulation;
- upper and low supports of reactor;
- thermal shield;
- crown sheet;
- CPS actuator including emergency shutdown element, automatic control element, reactivity compensation element, manual control element.

Fuel assemblies, control rods of CSS are placed in core, as well as experimental assemblies and devices. The core and reflector of the MBIR reactor are formed by the following assemblies:

- 93 fuel assemblies;
- 8 CR CSS with their sleeves;
- 26 nuclear power simulators;
- 278 reflector assemblies;
- 74 packages of in-reactor storage protection assemblies;
- 38 spent fuel assemblies in the in-vessel storage.

Dangerous consequences of non-project accident are excluded by a special protective structure over the reactor shaft, the guard vessel of the reactor, housing enclosure for equipment and pipelines of the I circuit, the emergency cooling system of the reactor, which localize the consequences of internal accidents and protect the reactor from external influences.

Nuclear safety is achieved by the design and reactor neutronics of fuel assemblies and the core, as well as by appropriate organizational and technical measures.

The loop equipment and pipelines of the MBIR, which are in contact with the sodium coolant, are equipped with an electric heating and thermal insulation system. It needs for the possibility of heating and maintaining the temperature in the loops within (225 ± 25) ºC. The set of electric heaters allows indirect monitoring of sodium leakage by closing the electric heater to the vessel.[4]

The buildings and structures layout is based on the modular principle. The layout of the RF includes the physical separation of equipment (the reactor, IHE, the I circuit pumps, sodium purification systems, etc.). The presence of the II intermediate circuit with a non-radioactive sodium coolant excludes the possibility of dangerous chemical interaction of the radioactive coolant (the sodium of I circuit with water-steam of the III circuit). Such technical and design solutions reduce personnel doze rates during operation the RF.

The following requirements were taken into account when assembling master layout plan of the MBIR:

- zoning of the territory according to the buildings of the main production purpose and auxiliary buildings;
- optimal planning of buildings and structures of the main production and service one
- provision of straight-line main routes for laying engineering communications;
- reduction of technological, transport and pedestrian connections.

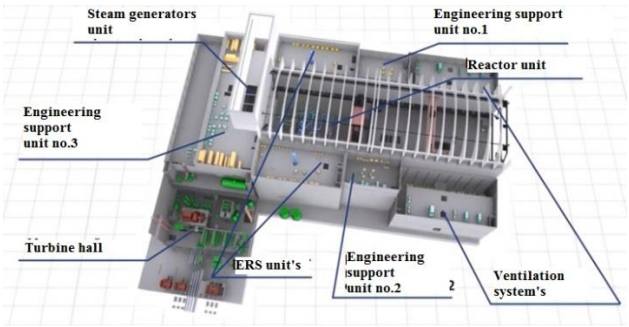

Figure 5. Systems and units in the main building. [1]

IV. ATE. PARTICIPATION IN THE PROJECT

JSC Atomtekhenergo is an engineering company of Rosatom Corporation, which commissions NPP in the Russian Federation and foreign NPP based on Russian project. Also ATE is actively developing in adjacent markets (research reactors, traditional energy and gas industry facilities).

ATE has competence in the design and construction of nuclear facility (structures and complexes with research nuclear reactors) in terms of:

– systems for checking equipment operability and testing for compliance with project characteristics;
– control room (unit conrol room, emergency control room, local control room);
– human-machine interfaces;
– special software;
– modernization of monitoring and control systems;
– electricity supply systems (internal and external electricity grids, low-current systems).

JSC Atomtechenergo is one of the main members in the MBIR commissioning.

Organization of the commissioning process for MBIR:

– development and adoption of the organization structure;
– intra-group collaboration;
– organization and management of commissioning works in accordance with project management standards;
– planning of commissioning works, adoption of the portal for supporting the commissioning works;
– technical guidance and coordination of the commissioning works;
– weekly planning, control and reporting;
– development of commissioning, operational and training documentation;
– consulting the customer's personnel;
– training of operating personnel.

JSC Atomtechenergo, as the general contractor for commissioning, will ensure a phased safe commissioning of all systems and equipment of the international center MBIR.

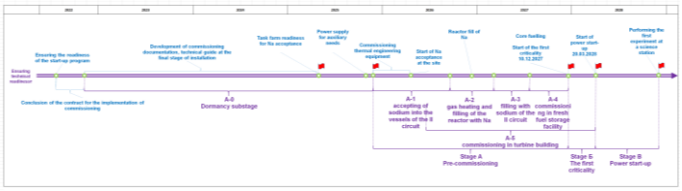

Figure 6. Commissioning schedule of MBIR.

Important key events are highlighted in the table 1.

Table 1. Milestone event.

No.	Milestone event	Deadline
1.	Delivery of the reactor vessel	08.2023
2.	Completion of the overhead traveling crane installation	10.2023
3.	Installation of reactor vessel in design position	11.2023
4.	Completion of the turbine set installation	06.2025
5.	Completion of the III circuit systems installation	08.2025
6.	Power supply for auxiliary needs according to the design scheme	09.2026
7.	Completion of the reactor facility equipment installation	12.2026
8.	Completion of construction and installation jobs and commissioning	06.2027
9.	First criticality	12.2027
10.	Power start-up	03.2028
11.	Signing of the acceptance commission certificate	05.2028
12.	Operational commissioning	11.2028

A. Design features of MBIR for commissioning

The presence of an intermediate sodium circuit gives some features for the MBIR reactor commissioning, in contrast to other types of reactor. The sodium circuit leads to an increase metal consumption, installation and commissioning works.

On the reason the length of the sodium accumulation period for filling the reactor, sodium acceptance will begin long before the end of installation work on the main equipment of the unit. Thus, there will be a combination of the started operation of a part of the block equipment and the continuation of construction and installation work on the rest of the block equipment. So there is a need to separate the start-up complex. This entails the priority release of the necessary working documentation, the corresponding commissioning documentation, the adoption of organizational and technical measures to combine operational and construction and installation works, priority material and technical support.

The number of ventilation systems is increasing, which is associated with ensuring a normal temperature regime in sodium rooms, as well as with the requirements of a fire regime. In addition, part of the ventilation systems are involved in the Sodium Acceptance Complex, while the construction part is not yet ready for them. Thus, it will become necessary to crush large ventilation systems into parts, which entails an increase in the volume and duration of commissioning.

It will also be difficult to carry out commissioning work on the core refueling system. It is due to the technology of reloading: under a layer of sodium, which makes it impossible to carry out visual control of the fuel-charging gears. Preliminary complex commissioning on the bench, in the reactor tank before filling with sodium in the simulated core are required to fettle the refueling system

Because of the need to combine the work of in-core and ex-core refueling mechanisms, it is inevitable to combine "clean" work in the reactor with construction and installation work in the central hall.

The first heating of MBIR cooling circuits, including equipment, occurs gradually within 15 or more days. The heating rate of the above equipment should be no more than 30 ° C / h.

Also it is necessary to provide heating for the initial filling with sodium:

– pipelines of the I, II circuits and EHRS circuit - up to 250°C;

– casings of RCP-1,IHE, EHE - up to 250°C;
– -drainage pipelines of the I and the EHRS circuits - up to 250°C;
– drainage pipelines of the II circuit - periodically up to 450°C;
– the first heating of reverse steam generator modules is carried out by electric heaters with
– temperature of 20°C to 350°C at a rate not exceeding 10°C / h in steps of max. 50° C with a stop for 3 hours at each stage;
– armature enclosed in a casing - up to 250°C.

V. References

[1] “About MBIR”, Electronic resource // URL: http://mbir-rosatom.ru ,date of the application April, 2021

[2] “Let's give the world MBIR”.REA – Monthly journal of nuclear energy of Russia.Manufacturing Science. March, 2021

[3] V.V. Kalygin, “Scientific and methodological support for the operation of MBIR”. Dissertation, Russia, Dmitrovgrad, 2014

[4] “Reactor facility MBIR”. Design document, Russia, Moscow, 2019

List of abbreviations

NPP Nuclear power plant

ATE Atomtechenergo

CSS control and safety system

SSC RIAR. State Scientific Center – Atomic Reactor Research Institute

NRI Nuclear Research Installation

IAEA International Atomic Energy Agency

MBIR Multipurpose Fast Neutron Research Reactor

NAA Neutron Activation Analysis

RF Reactor facility

EHRS Emergency heat removal system

SS Security System

NDS Nuclear-doped silicon

Proceedings of the European Nuclear Young Generation Forum
ENYGF'21
September 27-30, 2021, Tarragona, Spain

A digital tool and methodology to increase safety and efficiency in NPP

Viamonte, Borja[1*], García, Oscar[1] and Recasens, Francesc[1]

[1] IDOM, Spain

*Corresponding author: *borja.viamonte@idom.com*

I. INTRODUCTION

In this era of digital transformation, where many applications (computers and the Internet) emerge in a new environment, they allow us to access a considerable amount of information and services due to the data they manage. The main goal is to optimize the processes, automatize repetitive tasks and reduce the human factor error.

If we analyse the digital transformation applied to the industrial world, in particular the nuclear sector, we can affirm that managing huge quantities of data will help in most processes, but also, we need to ensure the safety and the security of the new environment in the aforesaid sector.

Nuclear plants built in the 70's-80's handle a number of records, which are stored in complex databases and systems. The documentation associated to these records (manuals, instructions, procedures, inspections, etc.) is also stored in complex databases, which requires to ensure the integrity of the information and that all links are correctly stored, so all information is available for the appropriate personnel. There could be a lot of physical elements not properly configured in digital support (e.g. drawings) [1], that require on-site accesses and inefficient personnel hours for determine 'the gaps' between the aforementioned existing physical reality and the configured information (plant documentation). This gives rise to the imperative need for optimum configuration management.

If we want to ensure the nuclear safety culture (operating in a reliable and environmental friendly manner with the attitude, approaches and commitment of individuals), we need to analyse the economic impact of the inefficient hours when we are looking for specific information in case it is not configured as expected. We also need to take into consideration there are zones with radioactive dose rate that requires a pre-job activity (e.g.: ensure where is the item you need to locate, analyse if you need scaffolding, etc.) and a huge coordination across different departments/teams/specialities. Finally, it is also necessary to consider the high time requirements spent in multiple on-site accesses to prepare this works involving all these different units (in man-hours terms).

In this line of safety and efficiency, the need to optimize prior planning of the work to be undertaken gains importance, considering aspects such as radiological and operational risks, coordination between the different Operational Units, the need for auxiliary means (scaffolding, thermal insulation removal, storage areas...), calculation and preparation of maneuvers, etc.

Therefore, it can be considered that the use of digital transformation methodologies and tools make the difference when it comes to optimizing and undertaking continuous improvement in the work.

II. TOOL AND METHODOLOGY

Due to the knowledge acquired after many years working in projects related to Plant Life Management, Periodic Safety Review, etc. IDOM is very concerned of how useful is to use a good configuration management methodology [2], identify people with expertise in different fields within the organization and prepare every action with the required care and time in the most efficient possible way.

Plantview™, is the software chosen tool for visually organizing, viewing, annotating and sharing 3D laser scans, 360° panorama images, photos and documents.

Figure 1. Plantview™ project main window (orthophoto of the NPP and the structure with main buildings in scope)

In a first step, it's very important to define the scope and the main goals so that the level of information required can be decided. This will determine aspects such as the degree of precision required in the scans, the percentage of shadow points (areas out of scanner range) that can be found in order to minimize them (or that those shadow areas do not impact on the capture of relevant areas/objects), the use of other information formats such as photos or videos to complement or supplement this physical reality, the degree of detail

required on areas of particular interest for their purpose, etc. [3]

In these terms, we can distinguish different approaches of use, since it is not the same to use it for operational focus (e.g.: in training or querying elements), or engineering, which would require greater precision for taking measurements in design modifications, maneuvers, physical interferences, etc.

In a second step, taking advantage of different existing technologies and bearing in mind the previously considerations, capture the physical reality of the plant (e.g.: laser scanning, 360° pictures, 360°videos) [4].

After that, it is important to define the information layers we want to add over the multimedia (different than BIM dimensions). We can consider them as individual modules which allow us to manage different aspects of the daily work (i.e. manufacturer component info, radiological area aspects, replacement stock info, etc.).

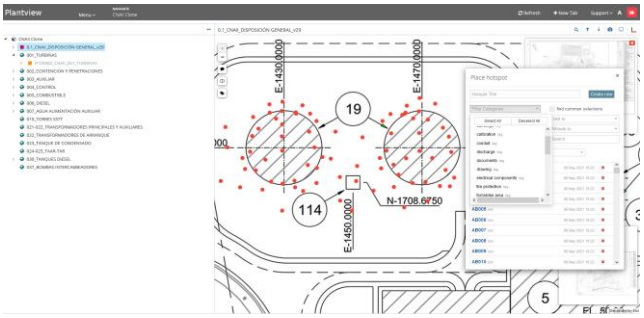

Figure 2. Plantview™ project categories example

To keep the pictures, scans and videos of the plant updated, it is key to maintain the added value of the tool, this way the users would be able to take out the most of it. Otherwise, their work may be compromised.

This way, every time a new installation, refurbishment or revamping is done, new pictures, scans and videos of the zone must be taken take and updated it in our tool.

Once the multimedia has been updated and the information layers configured, users can access to this information (it can be documents, drawings, pictures, scans, videos, links to external information, etc.) in a visual and very intuitive way, avoiding a tricky user experience.

In order to achieve that, it is very important to have that structure well defined from the beginning, having these inputs by the customer since the start of the project.

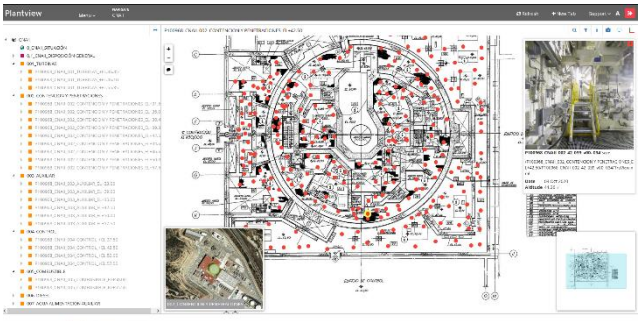

Figure 3. One of the ANAV NPP plantview™ project structure with the buildings, elevations and scanning positions

It is important to remember that despite of this tool helps us with configuration management, this is not their main goal. Even though it includes linked information to the physical reality of the plant, its main goal is to complement the existing information as a remote visualization tool.

Depending on the client expectations, this methodology can be used as is, being a quick win because of its fast return of investment and its many benefits as we will see later on, or can also be used as a first step, being a proof of concept for a bigger initiative as could be a digital twin.

When running within the plant system it allows to access different data sources of the plant (databases, Information Management System of the plant, etc.) being a smooth connection between the configuration management and a remote visualization tool.

Figure 4. Containment building remote navigation example

III. MAIN BENEFITS AND ADVANTAGES

The main results obtained from the application of this methodology and use of the tool leads to a substantial improvement in safety and efficiency, the latter being closely linked to the economic aspect. All this is materialized through:

- An improvement in the coordination of the different units/departments involved in the work. In the preparation and planning of work, whether in pre-job or post-job meetings, the professionals have a tool at their disposal that allows them to consult the plant remotely, being able to focus each of them on their particular area (prevention of occupational risks, radiological protection, maintenance units, etc...). This makes it more efficient to deal with all aspects of the work in an open environment and debate, reducing doubts, achieving consensus that increases safety in their performance and reducing the time needed to invest during the same.
- The minimization of doses and reinforcement of the ALARA criterion application, making it possible to visualize areas with high radiological risk. In the NPP's there are areas in which access is highly or completely conditioned by the radiological status of the plant. For example, in a PWR plant, information on the physical reality of the sealing table could be consulted at any time during the operation.
- Improve efficiency and productivity by minimizing the man-hours spent on low value-

added walkdowns. Throughout the operating life of a plant, a large number of hours are spent on access prior to the start of work to check certain aspects (feasibility and location of storage areas, the need to install scaffolding, dismantling of thermal insulation, calculation and measurements taking for maneuvers, etc.). These accesses, although completely necessary in many cases, can be minimized by remote consultation with the tool, considerably reducing the associated costs.

- Improvements in the design aspect, being able to contrast and/or consult information that is not configured or contained in documentation without physically accessing the plant. Likewise, by carrying out specific campaigns to capture the physical reality (at a reduced cost), they guarantee an improvement in configuration control and traceability of the different design modifications carried out during the plant's operating period.
- Optimization of access to information, linking different complex databases through a very intuitive and visual interface. This means a reduction of ineffective time spent navigating between different sources.
- The use of the tool in staff training, with a significant impact on plant safety. With all the configured information available, specific training plans for personnel can be implemented. As an example, videos can be used as e-manuals to train certain profiles in the specific maintenance of equipment, use of VR and/or AR, etc.

IV. CONCLUSION

The main results that are being obtained from the application of this methodology and use of the tool are basically an increase in efficiency (based on the optimization of resources and time), as well as an increase in safety through the minimization of radiological risk and the indirect integration of techniques and means for the prevention of human error.

At the same time, the cost-benefit and time required for the implementation of this methodology are the keys that makes it very competitive in comparison with other alternatives which, although they may be much more complex, are far away from the quick win that this one represents.

Lessons learned have shown that in already built plants where a BIM model has not been made from the beginning, this tool and technology brings an efficiency benefit with a minimum investment and guarantees optimal adaptability thanks to its easy handling and fast transition to change.

V. REFERENCES

[1] IAEA, TECDOC-1335 "Configuration Management in NPP", January 2003.

[2] INPO, AP-929 "Configuration Control Process Description", May 1998.

[3] T. a. L. -. S. P. R. LLC, "3D Laser Scanning: Benefits and Paybacks for Industrial Plant Design, Construction and Operation", 2009.

[4] IFF, Fraunhofer Institute for Factory Operation and Automation, "Laser Scanning Guidelines for Plant and Industry. Preparation and Execution of Laser Scanning Projects for Industrial Plant Design and Documentation", 2015.

Proceedings of the European Nuclear Young Generation Forum
ENYGF'21
September 27-30, 2021, Tarragona, Spain

Fast neutron reactors with sodium coolant. Competitiveness and prospects.

Smelov, Andrey*

[1] Beloyarsk NPP, Russian Federation

* Corresponding author: *andreysmelov88@gmail.com*

I. INTRODUCTION

In 1942, under the leadership of E. Fermi, the world's first nuclear reactor operating on thermal neutrons was launched. It was Fermi who proposed to develop the power industry on the basis of fast-neutron reactors. He suggested that such reactors could produce more fuel than they consumed, opening the way to a new energy industry with virtually inexhaustible resources. He presented his calculations at the meeting "Discussion of the Problem of Reproduction" held in the United States on April 26, 1944. From that moment on, active work on the creation of the experimental American breeder began.

The first demonstration fast reactor EBR-I was launched on December 20, 1951 in Idaho (USA). The coolant was sodium and potassium eutectic.

In 1955, the first research fast reactor of zero power was launched in the USSR, at the Institute of Physics and Power Engineering (Obninsk), under the leadership of A.I. Leypunsky. The same institute two years later launched the BR-2 research reactor with mercury coolant. In 1954-1955 the ZEUS and ZEPHYR reactors were tested in Great Britain. The fast French RAPSODIE reactor started operating in 1967 and the Japanese JOYO in 1977.

It should be noted that the development of fast reactor technology will mean a transition to a closed nuclear fuel cycle and more efficient use of uranium reserves. This is an important issue for the rapidly developing economies of China and India, because it is these countries that are experiencing the greatest growth in energy consumption.

The lack of large-scale implementation of fast-neutron reactors is due not so much to underdeveloped technology as to a lack of large-scale SNF reprocessing facilities. Such facilities are needed to extract both uranium and plutonium from fuel; they are an important link to ensure the closure of the nuclear fuel cycle. To date, only four countries (France, Great Britain, Russia, and Japan) have industrial reprocessing of spent nuclear fuel. [1]

II. FAST REACTORS WITH SODIUM COOLANT

Fast reactors with sodium coolant:

- The only type of fast reactor created in the world to date;

- The only type of fast reactor that can be proposed for commercial use in the coming decades;

Table 1. List of sodium-cooled fast-neutron reactors, including those that have been decommissioned and are in the commissioning phase.[2]

Reactor	Country	Site	Operated from	Shut down	Heat capacity MWt
BN-350	Kazakhstan	Aktau NPP	1973	1999	1000
Phénix	France	Marcoule	1973	2009	563
Superphénix	France	Creys-Malville	1985	1998	3000
Monju	Japan	Monju NPP	1994	2016	714
PFR	UK	Dounreay	1974	1994	650
Fermi-1	USA	Enrico Fermi NPP	1963	1972	200
KNK-I	Germany	RC Karlsruhe	1971	1974	
KNK-II	Germany	RC Karlsruhe	1976	1991	
BN-600	Russia	Beloyarsk NPP	1980	Active	1470
BN-800	Russia	Beloyarsk NPP	2014	Active	2100
PFBR	India	Madras NPP	2004	Under construction	1250
CFR-600	China	Xiapu	2017	Under construction	1500

At the moment Russia is generally acknowledged as a world leader in the development of fast neutron reactor technology, with two operating industrial reactors at the Beloyarsk NPP site - BN-600 and BN-800.

III. SODIUM TECHNOLOGY

Some metals (sodium, potassium, lead, bismuth) and gases (e.g., helium) that are not neutron moderators can be used as coolants for fast reactors. The greatest use is for sodium.[3]

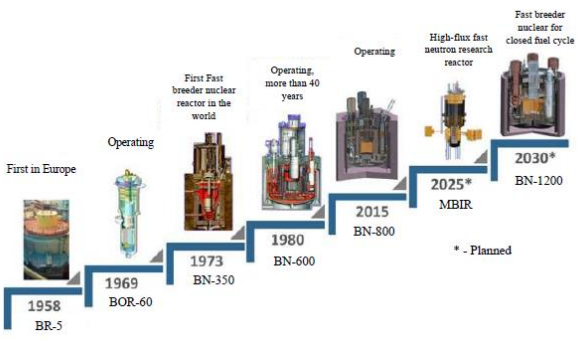

Figure 1: Stages in the development of BN technology in Russia

Table 2. Main advantages of sodium coolant

The benefits	Features of technology
Sodium is not a neutron moderator	Possibility of application in fast reactors
High boiling point (~880 ^{0}C)	It allows high sodium temperature at the reactor outlet (547 ^{0}C for BN-800) and pressure close to atmospheric in the reactor circuits (0.054 MPa for the 1st circuit of BN-800). For VVER-1200 the reactor outlet water temperature is 330^{0}C , at a pressure of 16.2MPa
High heat capacity (~ 30 J/mol*K) and high thermal conductivity (~ 80 W/m.*K), ability to operate at high temperatures	Allows to reduce the size of the core, due to high energy release (~ 450 MW/m3). Possibility to use leakage neutrons for fuel reproduction, in the reproduction shield containing depleted uranium
High electrical conductivity of sodium;	Sealed electromagnetic pumps can be used
Low corrosiveness	

Table 3: Main disadvantages of sodium coolant.

Disadvantages	Features of technology
High chemical activity of sodium in relation to water, air, aqueous acid solutions, fire hazard of sodium in contact with air in case of depressurization of circuits	Necessity of application of inert gases for protection of sodium surface in compensation volumes of circuits. Provision of main equipment and pipelines with safety covers.
Possible formation of explosive mixtures in chemical reactions of sodium with water and aqueous solutions	Providing rooms with sodium-water heat exchangers with hydrogen control system
Relatively high temperature of transition from liquid to solid state (97.8 ^{0}C)	the need for electric heating systems for equipment and pipelines (before commissioning - operation, some equipment is heated by gas with the help of compressors);
The need for cleaning, laundering, and, for primary circuit equipment, decontamination, when carrying out repair work	Increasing the complexity of repair work
Heat transfer fluid is unchangeable over the entire life of the unit	High requirements for sodium purity. Availability of sodium purification systems.
Inaccessibility to personnel for 10-12 days of the premises with the equipment of the 1st circuit, due to the duration of decay of radioactive isotopes	Increasing the complexity of repair work, increasing the dose load of personnel

IV. COMPETITIVENESS OF FAST REACTORS

An analysis of current forecasts for the development of the electric power industry in Russia and the world according to authoritative expert organizations (International Energy Agency, U.S. Energy Information Administration, INEI RAS, etc.) shows that the share of nuclear power in the generation structure on the horizon of 2040 practically does not change. Globally, the share of nuclear generation will remain at ~12% (a drop in the share in Europe and the US is offset by growth in China and India), and in Russia it will be no more than 20%.[4]

The basic condition for a noticeable increase in the share of NPPs in the total energy balance is to ensure competitiveness, which is directly related to the solution of systemic problems of nuclear power.

Figure 2 shows the results of calculations of Levelized cost of electricity (LCOE) indicator of competing energy technologies in relation to conditions of Russia. Calculation for FR-1200 is carried out under condition of fuel overloading of 13 t.m./year (average burnup of SNuP-fuel is 8% t.a.) [5].

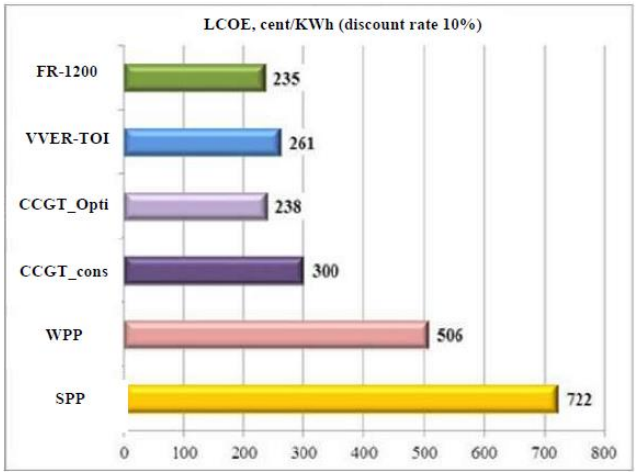

Figure 2. LCOE of competing generation types in the Russian context

Based on the results of LCOE calculation, the following main conclusions can be made:

- the requirements set to the LCOE of industrial energy complex with FR-1200 guarantee the provision of competitiveness by the LCOE indicator;

- deviation of LCOE indicator of industrial energy complex with FR-1200 according to the basic variant in comparison with the requirements of competitiveness is ~ 4%

V. PROJECT BN-1200

Power unit with BN-1200 reactor is a key element of two-component nuclear power system with BN and VVER reactors in closed nuclear fuel cycle.

The experience and competence, gained during the creation and commissioning of the BN-800 reactor, the BN-600 reactor operation and new technical solutions have improved the main

technical and economic performance of the BN-1200 power unit and made it comparable to the VVER reactor not only in terms of safety, but also in terms of specific capital costs and LCOE in relation to the VVER-TOI.

Developers of the BN-1200 project managed to significantly reduce construction volumes compared not only to their predecessor projects, but also to VVER-1200 and allow the BN-1200 project to be competitive in the market of prospective power units due to application of new technical and design solutions.

Table 4: Changes in construction volumes of BN-1200M

Characteristics	BN-1200	BN-1200M*
Building area of the reactor building, m^2	10452	6658 (-36,2 %)
Construction volume of the reactor building with the building envelope, m^3	620 700	409 410 (-34,0%)
Specific indicators of the building volume of the reactor building, m^3/MW	508,770	327,528 (-35,6 %)

The results of the evaluation of BN-1200 concept according to the methodology of the Generation IV International Forum show that the BN-1200 project has a good potential in terms of compliance with the parameters for nuclear power systems of the fourth generation.

Thanks to improvement of safety systems (increase of reliability of the emergency heat removal systems and implementation of additional bars of passive emergency thermal protection) a considerable safety level increase in the BN-1200 design was achieved. The probability of severe core damage for internal events during reactor power operation for BN-1200 is 5x10-7. [6]

Generation IV International Forum (GIF) defines the main requirements for Generation 4 nuclear power systems, which are broken down into four areas: stability of energy development, non-proliferation of nuclear materials and physical protection, safety and reliability, and competitiveness (economy) [7].

At the September 2017 meeting of the GIF Project Agreement Governing Board on System Integration and Assessment of the Fast Sodium Reactor, the BN-1200 concept was formally accepted and approved by all Governing Board members as meeting the GIF requirements for Generation IV fast reactors.

VI. HAS THE TIME OF FAST REACTORS COME?

The answer to the question "Is it time to make a decision on the development/commercialization of the BN technology" lies in the comparison of BN projects not only with PWR, but also with other energy sources (combined cycle plants (CCPs), renewable energy sources (RESs)), including resource availability and other factors characterizing the long-term development of the technology.

In addition, it is worth taking into account the fact that about 370 thousand tons of spent nuclear fuel was formed in the world at the beginning of 2014 (not including India and Pakistan), of which about 250 thousand tons are in storage, and only one-third is reprocessed [8]. The annual rate of SNF production is about 10.5 thousand tons of spent nuclear fuel, and there is no growth in SNF reprocessing.

At the same time the light water reactor technology consumes natural uranium resources, loads enrichment facilities, increases the volume of depleted uranium hexafluoride, SNF with plutonium and other minor actinides (MA), and has limitations on the temperature potential of the generated heat.

In fact, the uranium supply-demand balance projection to 2035 characterizes the risks of light water thermal reactor resource availability and the need for a more focused and efficient transition to the closed fuel cycle(CFC).[9]

On the other hand, there are different opinions today about which CFC and fast-neutron reactor technologies should be created and when and how to transition to these technologies in a nuclear power industry that started with thermal reactors

A comparison of innovative nuclear power systems was carried out using the KIND methodology for two scales of nuclear power: small -20 GW and large -100 GW.[10] Application of the developed mathematical model showed that for most countries not planning to develop nuclear power on a significant scale it is reasonable to develop nuclear power plants on the basis of an open nuclear fuel cycle with thermal neutron reactors. Calculations performed using the developed mathematical model for countries planning the development of nuclear energy on a significant scale showed that in this case the model gives preference to systems including fast reactors. For countries seeking high rates of nuclear power development and expecting a shortage of nuclear fuel, such as India and China, the best of the alternatives considered is a two-component system with sodium fast reactors, which have a short fuel doubling time and high reproduction rate.[10]

Multicriteria scenario analysis work considered alternative scenarios with different nuclear and non-nuclear system structures. The results showed that among all scenarios the options with a two-component nuclear power structure had a higher rating. Among the variants with a two-component structure the highest rating has the scenario, in which the growth of nuclear power is realized ahead of non-nuclear power ("RO_wBN"). [10]

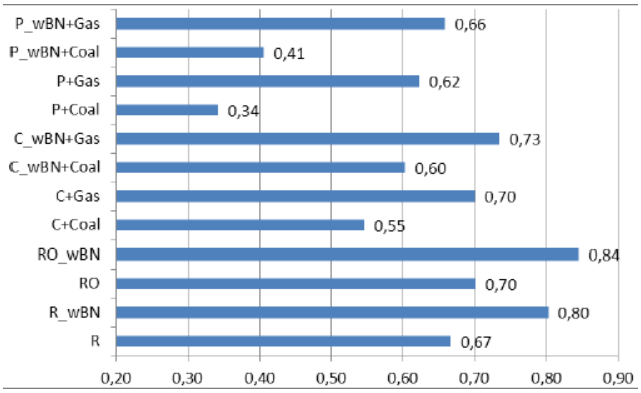

Figure 3. Comparison of alternative energy scenarios

Thus, it is shown that the advanced development of two-component nuclear power with fast and thermal neutron reactors increases the fuel resource of energy carriers, improves the environmental impact on nature, population and personnel, increases export opportunities in nuclear and non-nuclear power and reduces gas and coal consumption.

VII. REFERENCES

[1] Akatov A.A., Koryakovsky Yu. Fast Neutron Reactors," 2012.

[2] Fast Neutron Reactors // WNA, 2013-03-15

[3] Lecture course, "Sodium technology", Institute of Physics and Power Engineering FEI, 1993.

[4] A.A. Makarov, L.M. Grigoriev, T.A. Mitrova, «Forecast of the development of the energy world and Russia 2016», INEI RAS-

AC under the Government of the Russian Federation - Moscow, 2016.

[5] Tolstoukhov D.A., Panov S.A., Presnyakov I.V. (Private Institution "ITCP "PRORYV", Moscow) "Competitiveness of NPP projects with RBN".

[6] V.P. Ershov (JSC Atomproject, St. Petersburg), S.F. Shepelev (JSC Afrikantov OKBM, Nizhniy Novgorod) "Power Unit with BN-1200M Reactor Plant" [

[7] E.V. Nalichev (VNIIA, Moscow), E.V. Marova, S.F. Shepelev, Y.M. Ashurko, V.M. Dekusar, V.V. Korobeinikov, B.B. Tikhomirov, "Results of the assessment of BN 1200 project compliance with Generation IV and INPRO requirements," IAEA CN 245 399, international conference FR-17, 2017

[8] IAEA nuclear energy series "Status and trends in spent fuel and radioactive waste management" No.NW-T-1.14, 2018

[9] A Joint Report by the Nuclear Energy Agency and the International Atomic Energy Agency, NEA No. 7301 "Uranium 2016: Resources, Productionand Demand", OECD 2016

[10] P.N. Alekseev, V.Yu. Blandinsky, A.L. Balanin, A.V. Grol, A.V. Gulevich, V.M. Dekusar, A.F. Egorov, V.V. Korobeinikov, E.V. Marova, A.M. Maslov,A.L. Moseev, V.D. Nevinitsa, P.S. Teplov, M.R. Farakshin, P.A. Fomichenko, S.F. Shepelev, A.V. Shirokov, "Multifactor evaluation of competitiveness of a commercial BN type power unit in the Russian energy system", 2018

Proceedings of the European Nuclear Young Generation Forum
ENYGF'21
September 27-30, 2021, Tarragona, Spain

Issues of improving procedures for accounting and control of radioactive waste using a software tool

Arsen Dzhamavov[1]*

[1] The FEDERAL STATE UNITARY ENTERPRISE «NATIONAL OPERATOR FOR RADIOACTIVE WASTE MANAGEMENT» - Russian National Operator

*Corresponding author: *darsen52096@yandex.ru*

I. INTRODUCTION

Today, the safe handling of radioactive waste (RW) and their final isolation are topical issues for states that use atomic energy to develop energy, science and healthcare.

In the process of handling radioactive waste, there is a need for documentary control of information submitted in various paper and electronic formats. In view of the variety of documents, a large amount of manual labor and routine operations arise, which, in turn, does not exclude the occurrence of errors in the conduct of documentary control.

In these conditions, it seems appropriate to use a specialized software tool. Software Tool should ensure a reduction in the number of "manual" control operations; reduction and subsequently termination of the use of paper data carriers; creation of a single array of electronic files, which includes all acts, contracts, certificates; maintaining and improving existing administrative processes and implementing external transfers of service files while maintaining a high level of overall security.

An important priority of the State Corporation "Rosatom" is digitalization basic internal processes and corporate functions. Enterprises using digital technologies have significant competitive advantages. The degree of control over the processes and the availability of the results for all interested parties are also increasing. Digitization allows enterprise professionals to make more informed decisions, make transformations to quickly implement certain solutions to incoming problems, ensure enterprise security and improve operational efficiency.

FSUE "NORWM", ensuring the safe handling of RW accepted for disposal, is guided by the criteria for the acceptability of the specified RW for disposal. The software will allow making timely organizational and technical decisions and promptly assessing the compliance of the accounting data of RW packages with the acceptance criteria.

II. SOFTWARE CAPABILITIES

Class 3 and 4 radioactive waste is sent for disposal at near-surface disposal facilities (Figure 1).

Figure 1. Near-surface disposal site in Novouralsk

The criteria for the acceptability of radioactive waste for disposal are established by federal rules and regulations, and design documentation for radioactive waste disposal facility. Confirmation of RW compliance with the acceptance criteria is as follows [1-4]:

- a passport is issued for the RW transferred for disposal, including information on their isotopic composition and specific activity. The passport is drawn up by the organization, as a result of which the radioactive waste was formed, or the organization that carries out processing and conditioning;
- at the reception of RW transferred for disposal, the National Operator monitors their characteristics, which includes the attributes of the transferred packages;
- RW compliance with the acceptance criteria for disposal should be confirmed by experimental (instrumental) and calculation methods, provided that they are based on the results of preliminary direct and (or)

indirect measurements of the values of controlled parameters of the technological process (including those performed by RW suppliers);

- the characteristics and properties of RW sent for disposal must be determined in the volume and with an accuracy that allows confirming compliance with the criteria for the acceptability of RW for disposal.

The software tool will allow you to implement the following digital capabilities, such as:

- automation of procedures for incoming control of RW accepted for disposal;
- uniform methodological support when interacting with third-party counterparties;
- maintaining an archive of documentation for accounting and control of radioactive substances and radioactive waste;
- maintaining an electronic form of the RW accounting journal;
- maintaining reporting forms;
- formation of layouts for RW packages in radioactive waste disposal facility based on accounting data;
- formation of a logbook for recording technological parameters (including the surface density of nuclear fissile materials (NFM) in RW storage facilities);
- generation of a QR code for marking RW packages and radioactive waste disposal facility sites;
- maintenance of other analytical reports for submission to the employees of the enterprise, the atomic energy management bodies, state regulatory bodies in the field of atomic energy use, etc.

Within the framework of the software tool, as a "central" entity, an electronic copy of a passport for a RW package will be maintained, containing information on the main characteristics of a RW package and confirmation of the compliance of this RW package with the established acceptance criteria for disposal.

The substation by uploading data from passports to radioactive waste packages will allow automating control of such parameters as:

- assignment of solid waste to RW and determination of the RW class in accordance with the criteria established in the Decree of the Government of the Russian Federation [5];
- RW code, consisting of 11 characters and generated in accordance with tables 6 “RW code” and 7 “RW type code” of the Order of the State Corporation [6];
- determination of the RW category on the basis of the basic sanitary rules for ensuring radiation safety [7];
- the density of the contents of the RW package and the degree of filling of the RW package in accordance with the established acceptance criteria for a specific disposal facility to be filled;
- compliance of the weight and volume of the gross (net) packaging with the requirements of technical documentation and operational documentation.

It is expected that the use of the software tool in the future will improve the quality of filling out passports, and will make it possible to verify the information of the documents transferred together by packages of radioactive waste.

The organizational structure of the interaction of software modules is shown in Figure 2.

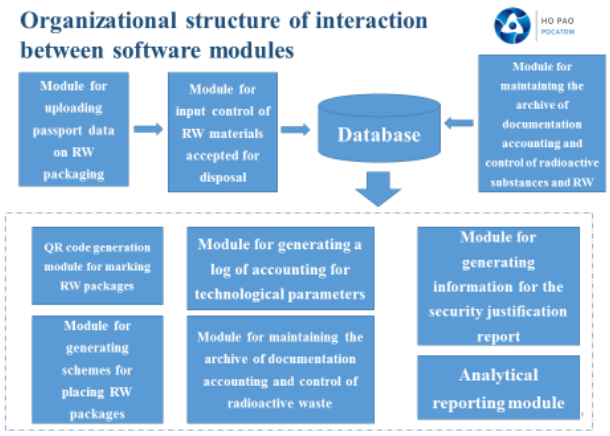

Figure 2. Organizational structure of interaction between software modules

Keeping an archive of documentation for accounting and control of radioactive substances and radioactive waste should provide access to accounting documentation and, if necessary, its submission.

Keeping a register of radioactive waste in electronic form will ensure the versioning of its data - ensuring that the relevant requirements for information protection are met, control of making corrections to accounting data only with the preservation of information about the date and persons who made such changes, as well as about the initial data before corrections are made requires normal rules.

Also, the software tool will provide the ability to promptly draw up reporting documents established by regulatory and legal acts in the field of accounting and control of radioactive waste State accounting and control System radioactive waste, in strict accordance with the accounting data.

III. CONCLUSIONS

The development of software tools to automate accounting and control procedures is an important step towards the creation of an automated tool for solving problems in the field of accounting and control of radioactive waste, including their incoming control during acceptance for disposal. The software tool will make it possible to make timely organizational and technical decisions and quickly assess the compliance of RW packages with the acceptance criteria, monitor the technological parameters of the radioactive waste disposal facility operation.

Automation of the described processes, in addition to clear advantages, will allow for more transparent and operational management of radioactive waste disposal facility activities, verification of the possibilities of implementing individual proposals, etc.

Further steps in the development of the software tool can be:

1. Automation of the technologist's workplace for managing the production process, including the targeted placement of packages based on their properties.
2. Collecting data to substantiate the composition of radioactive waste by methods of the radionuclide vector and quality control of filling out passports by organizations.
3. Development of a system for managing the rules for checking the compliance of radioactive waste with requirements and restrictions, based on the management system for "big data" or semantic networks.

IV. References

[11] Federal norms and rules in the field of atomic energy use "Criteria for the acceptability of radioactive waste for disposal" (NP-093-14);

[12] Federal norms and rules in the field of the use of atomic energy “Near-surface disposal of radioactive waste. Safety requirements "(NP-069-14);

[13] Federal norms and rules in the field of the use of atomic energy “Disposal of radioactive waste. Principles, criteria and basic safety requirements” (NP-055-14);

[14] Recommendations on the order, volume, methods and means of radioactive waste control in order to confirm their compliance with the acceptance criteria for disposal (RB-155-20);

[15] Decree of the Government of the Russian Federation of October 19, 2012 No. 1069 (as revised on February 4, 2015) "On criteria for classifying solid, liquid and gaseous waste as radioactive waste, criteria for classifying radioactive waste as special radioactive waste and for removable radioactive waste and criteria classification of removed radioactive waste ";

[16] Order of the State Atomic Energy Corporation "Rosatom" dated September 28, 2016 No. 1/24-NPA "On Approval of Report Forms in the Field of State Accounting and Control of Radioactive Substances, Radioactive Waste and Nuclear Materials Not Subject to Accounting in the State accounting and control of nuclear materials, the activity of which is greater than or equal to the minimum significant activity or the specific activity of which is greater than or equal to the minimum significant specific activity established by federal norms and rules in the field of atomic energy use, the procedure and deadlines for submission of reports ”;

[17] Basic Sanitary Rules for Ensuring Radiation Safety of Russia Federation;

Proceedings of the European Nuclear Young Generation Forum
ENYGF'21
September 27-30, 2021, Tarragona, Spain

Physical startup tests for VVER-1200 of Belarussian NPP: technique, some results and nuclear safety

Priputnev, Aleksandr[1*]

[1] JSC "Atomtechenergo" , Russia

*Corresponding author: pexapexb@gmail.com

I. INTRODUCTION

The Belarussian nuclear power plant (NPP) is the first nuclear power plant built under the Russian VVER-1200 project outside of Russia. The Belarussian nuclear power plant is located in close proximity to such EU countries as Poland, Latvia, Estonia and Lithuania. On November 3, 2020, the NPP started generating electricity.

On February 9 and 10, the European Nuclear Safety Regulators Group (ENSREG) paid an expert visit to the Belarussian nuclear power plant. In its preliminary report [3], ENSREG concluded that, based on the NPP visit and the information, the visible progress is made in implementing the ENSREG recommendations issued in 2018 and related to priority safety issues.

Before that, in the period from 10.10.2020 to 19.10.2020, one of the most important tests confirming the safe operation of the nuclear power plant was carried out at the unit No. 1 of the Belarussian NPP - tests to verify the neutron-physical characteristics (NPC) of the core of the nuclear reactor.

The main purposes of tests were:

- confirmation of the safe operation of NPP;
- confirmation of the safety of the implemented fuel loading;
- confirmation of the correctness of NPC performed in support of fuel loading;
- obtaining information for improvement (adjustment) of calculation programs for fuel cycle modeling.

For the project of power units with the VVER-1200 reactor plant new methods and programs of physical tests were developed. They took into account the design features of the new reactor, the properties of the control and protection system, the capabilities of modern measuring systems, as well as the needs for justifying modern calculation codes used in safety analyses.

The test programs were carried out in full, in accordance with the working programs and test methods, with full compliance of the requirements of nuclear safety.

The results of experimental determinations of NPC were analyzed for compliance with the project and the performed safety analyses by checking the fulfillment of the established success criteria.

The following NPCs were conducted to confirm the safe operation of the Belarussian NPP [4]:

1) reaching first criticality and minimal controlled power of reactor;

2) testing for controls coupling with the drives of control and protection system absorbing rod (CPS AR);

3) determining of maximum allowed current of the ionization chambers programme measurement complex hardware (PMCH);

4) determining of the temperature and density reactivity ratios;

5) determining the effectiveness of CPS control rod and determination of asymmetry of core multiplication behavior distribution;

6) determination of control and protection system control rod (CPS CR) groups integrated serviceability, alternately submerged in a core free of other absorbers;

7) determination of CPS CR groups differential and integrated serviceability submerged and retrieved in the regular sequence and reactivity coefficient by boric acid concentration;

8) determining the effectiveness of the accelerated preventative protection (APP) group;

9) determination of the effectiveness of individual CPS CR from the submerged regulatory groups of CPS CR;

10) determination of the full efficiency of emergency protection, including without the one of the most effective control rods;

11) determining the power effect and the power reactivity coefficient.

The specified above tests were nuclear hazardous because they are not provided in the Technical Specifications of Safe Operation.

During the tests, reactivity was the main parameter to be monitored and changed.

During testing, PMCH was used, consisting of current measurement system (IPT-4) equipment for measuring the currents of the boron-lined gas-filled ionization chambers (KNK-17-1) and the KNK-17-1 ionization chambers themselves. Using these currents, the PMCH software module calculated the reactivity values.

The properties of the PMCH equipment are such that even with a low initial power, it was possible to collect experimental data sufficient for correct processing.

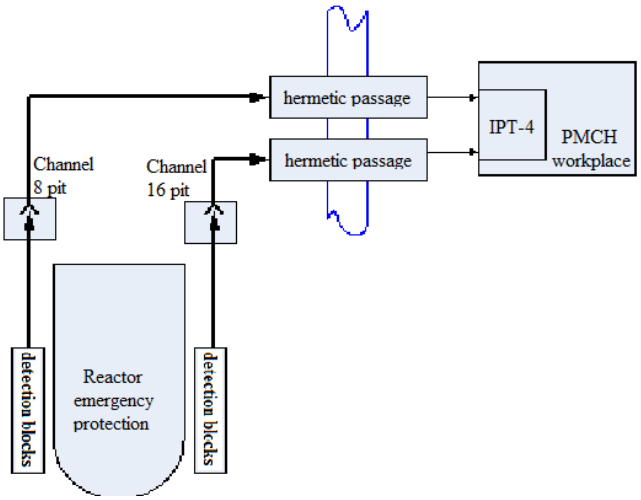

Figure 1. PMCH block diagram.

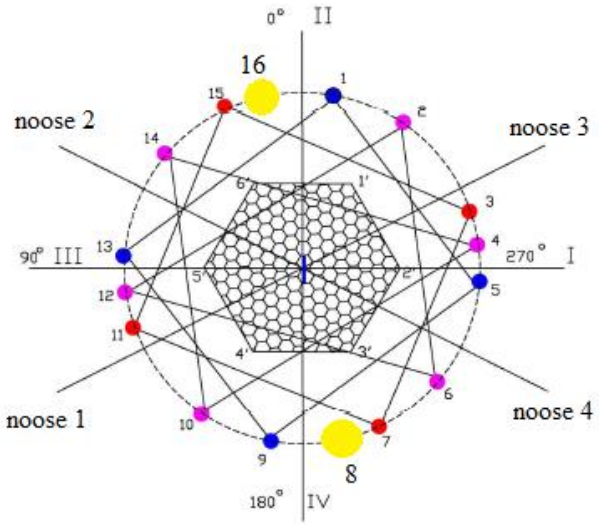

Figure 2. Placement of 8 and 16 IC channels relative to the core.

II. NPC HIGHLIGHTS AND RESULTS

Due to the limited scope, the report contains the main points and results of the following tests: determining of the temperature and density reactivity ratios; determining the power reactivity coefficient; determination of the full efficiency of emergency protection (EP).

A. Determining of the temperature and density reactivity ratios

The most important parameters of the core are the temperature coefficient of reactivity and density coefficient of reactivity of the coolant. They determine the safety of reactor operation (self-regulation and stability).

The test purposes were the following:

– to determine the temperature coefficient of reactivity ($\partial\rho/\partial T$) for conditions with different values of the critical boric acid concentration for the first fuel loading;

– to determine the density reactivity ratio ($\partial\rho/\partial\gamma$) of the coolant.

The test was considered successful with the following conditions:

– reactivity coefficient per a coolant temperature ≤ 0;

– density coefficient ≥ 0.

The tests for determining reactivity ratios were performed at critical concentrations of boric acid in the reactor, corresponding to the four different CPS CR groups position.

The temperature coefficient was determined when the temperature of circuit 1 changed (increased or decreased) by changing (increased or decreased) the steam extraction from the steam generator (SG).

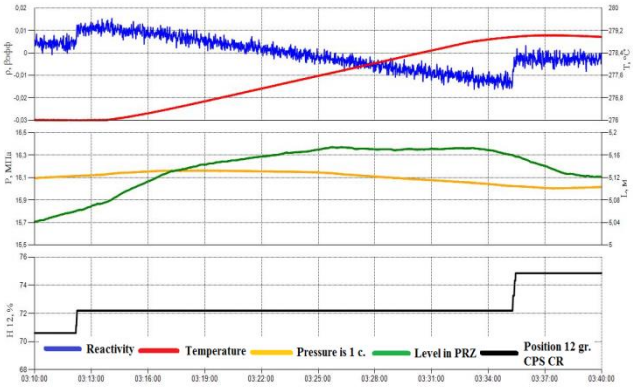

Figure 3. Parameters of the core during the first temperature coefficient measurement (here one can see the dependence of reactivity on temperature)-

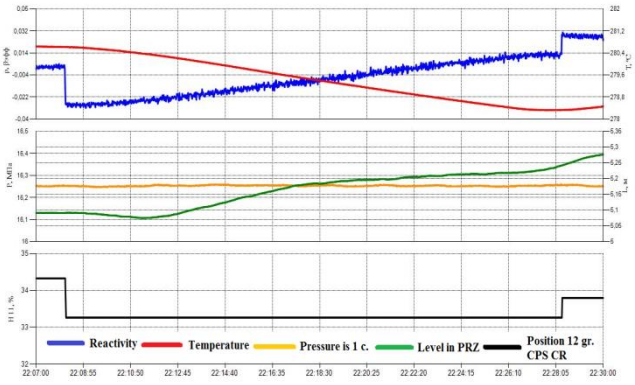

Figure 4. Parameters of the core during the third temperature coefficient measurement (here one can see the dependence of reactivity on temperature).

According to the rules of nuclear safety of reactor installations of nuclear power plants NP-082-07 [2], the values of the reactivity coefficients for the temperature of

the coolant and the temperature of the fuel, reactor power, should not be positive in all critical states.

Table 1. Results of the evaluation of the temperature and density coefficients of reactivity.

№	Height of CPS group H12,%	Test result $\partial\rho/\partial\gamma$, %/ g/cm^3	Test result $\partial\rho/\partial T$, *10^{-3} ,%/ ^{o}C
1	72,2	1,78	-5,9
2	38,6	7,33	-15,9
3	33,8	5,79	-13,2
4	14,6	4,19	-10,2

All the values of the temperature coefficient of reactivity are negative, and coincide with the calculated values. The density coefficient of reactivity is positive in all states. Obtained results comply with success criteria.

B. Determining the power reactivity coefficient

The purpose of the tests was to determine the power reactivity coefficient and its compliance with the design confirmation.

The test was considered successful with the following conditions:

– differences in the obtained value of the power reactivity coefficient from the design value are not more than 0.25×10^{-3} %/MW;
– negative power reactivity coefficient.

To determine the power reactivity coefficient with an increase in the reactor power to ~1% Nnom, two tests were provided by introducing a positive reactivity into the core by moving the 12 group of CPS CR up: in the first test - with the constant extraction of steam from the Steam Generator (SG), in the second - with the complete cessation of steam extraction from the SG.

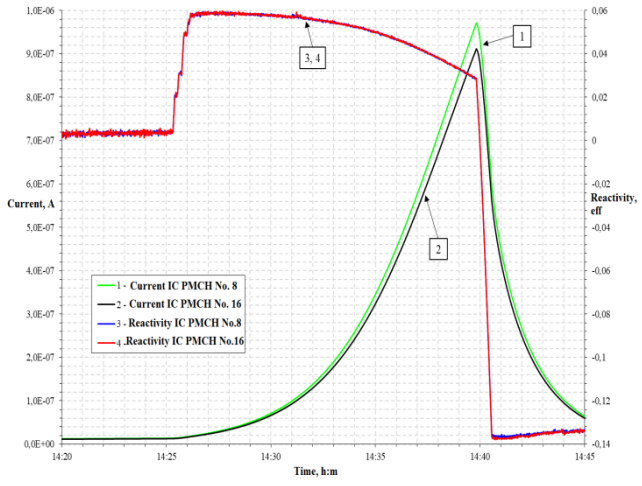

Figure 5. Parameters (current and reactivity) of the core during the first the power reactivity coefficient measurement (with the constant extraction of steam).

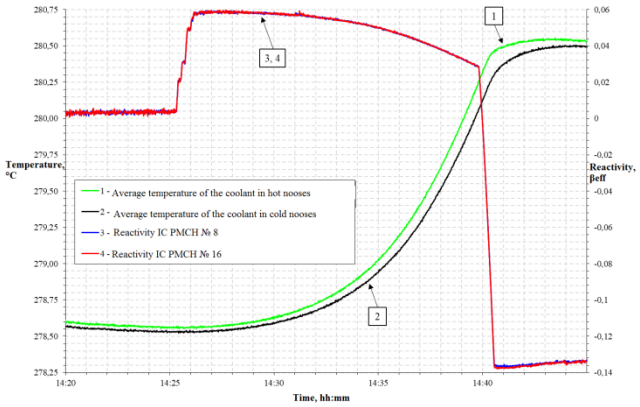

Figure 6. Parameters (temperature and reactivity)of the core during the first the power reactivity coefficient measurement (without the extraction of steam).

Figs. 5, 6 show that the positive reactivity introduced into the core is compensated by the action of negative feedbacks in power and temperature of the coolant due to an increase in the reactor power and heating of the coolant.

Table 2. Values of the power reactivity coefficient.

	The power reactivity coefficient, $\alpha N \cdot 10^3$ %/MW	
	Test result	design value
First test	-(0,78±0,18)	-0,58
Second test	-(0,83±0,23)	

Table 2 shows that the obtained value of the total power reactivity coefficient is negative. Obtained results comply with success criteria.

C. Determination of emergency protection efficiency

One of the most important tests, which traditionally completes the NPC at the stage of "Physical start-up" is to determine emergency protection efficiency.

The objective of the tests was confirmation of the compliance of the actual values of the EP efficiencies with the design, namely:

– emergency protection efficiency of the most effective control rod;
– full emergency protection efficiency.

The tests were considered successful if:

– the difference between the obtained EP efficiency and the calculated values was not more than 15% (relative);
– the EP efficiency without one of the most effective CPS CR was more than 7.0%.

At the beginning of the test, a positive reactivity about +0.06 βeff was introduced into the core. The neutron power increased to approximately 0.3%Nnom, after which the EP was reset, while measures were taken "jamming" of CPS CR 14-33, located near PMCH measuring channel No. 16. After that in about 60 seconds, the command was given to reset the held CPS CR. Figure 7 shows the main parameters of the core during the test, here the reset of the CPS "jamming" CR is seen well.

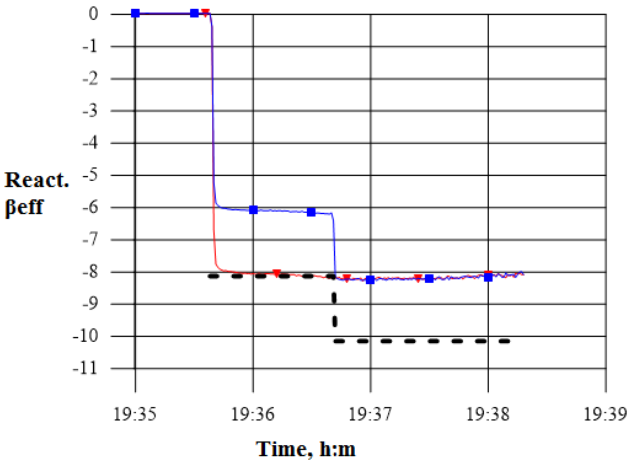

Figure 7. Reactivity during the by resetting the EP with "jamming" AR №14-33 (red line - IC №8, blue line - IC №16 (closer to AR№14-33), dashed line - calculated value)

The values obtained as a result of the processing of the full efficiency of the EP and the efficiency EP without one CPS CR coincided with the design values presented in the project. This can be seen in Tables 3 and 4.

Table 3. The efficiency EP without CR №. 14-33, H12 = 65.8%.

Test result, %	design value (H12=80%), %	Calculated deviation, % rel
7.9	8.13	±2.8

Table 4. The full efficiency EP, H12 = 65.8%.

Test result, %	Design value (H12=80%), %	Calculated deviation, % rel
9.9	10.15	±2.5

This fact confirms the requirement of the NP 082-07 [2], according to reactor shutdown systems that perform the function of EP, without one most effective EP, have:

– response time sufficient to render the reactor subcritical without violating safe operation limits in case of operational events;

– worth sufficient for rendering the reactor subcritical and maintaining it in this state in case of operational events, including design basis accidents.

III. THE MAIN CONCLUSIONS

In the course of all physical tests at the Belarussian NPP unit No. 1, it was confirmed that the established success criteria were complied. The accordance of the implemented fuel load with the design is demonstrated. During the tests, new experimental data were also obtained for the verification and validation of design codes used in the design; for the analysis and improvement of physical testing programs for new VVER power units.

The results of traditional tests confirmed the self-protection characteristics of the core by showing negative temperature, power, and positive density reactivity coefficients. The necessary effectiveness of emergency protection has been confirmed, including without one of the most effective CPS CR.

In support of the above conclusions it is necessary to give the results of the OSART pre-operation mission [5] conducted at the Belarussian Nuclear Power Plant in August 5 to 22, 2019. IAEA. The report on the results of the mission states that the leaders of the Belarussian NPP are committed to improve the operational safety and reliability of their plant. The OSART team found good performance areas of the Belarussian NPP.

The results of the tests presented in this article to verify the NPC of the first fuel loading of the Belarussian NPP unit No. 1 at the commissioning stage confirm the compliance of the NPC with the design values and requirements [2] and guarantee the design level of safe operation. These tests were carried out with strict compliance with nuclear safety measures and in the time optimal to reduce the period of commissioning and to obtain correct data.

IV. References

[1] F.Malin, "Control rod drop during hot zero power", pp. 46, 2013.

[2] "Nuclear Safety Rules for Reactor Facilities of Nuclear Power Plants". NP 082-07, 2007.

[3] "Preliminary EU Peer Review Report Implementation of Belarusian Stress Test National Action Plan", pp. 58, 2021.

[4] "Report on performance of commissioning activities the Belarusian NPP unit No. 1 at the stage «PHYSICAL START-UP»", 2020.

[5] "The results of the Pre-Operational OSART mission". Available: https://www.iaea.org/node/41549, pp. 3, 2019

Proceedings of the European Nuclear Young Generation Forum
ENYGF'21
September 27-30, 2021, Tarragona, Spain

Life of PIE (Post Irradiation Evaluation)

Preston, Henry[1*]

[1] UK National Nuclear Laboratory (NNL), United Kingdom

*Corresponding author: *henry.preston@uknnl.com*

I. INTRODUCTION

The National Nuclear Laboratory (NNL) is a UK government owned and operated nuclear services technology provider covering the whole of the nuclear fuel cycle. With a unique set of skills, facilities and capabilities – including four world-leading laboratories in North West England – NNL aims to harnessing nuclear science to benefit society, as laid out in the recent strategic plan [1]. Established in 2008, the National Nuclear Laboratory brought together the UK's nuclear research and development capability into one organisation. Our workforce represents a combined 10,000 years of expertise in nuclear science and technology and we're continuing to grow.

Post Irradiation Evaluation (PIE) is a key aspect of continued safe operation of nuclear reactors. The area has been crucial to understanding fuel behaviour throughout the fuel cycle and central to demonstrating the safety of reactors and fuel management facilities. In the UK, NNL has decades of experience overseeing PIE campaigns for multiple customers - From the original Magnox reactors to the current Advanced Gas-cooled Reactor (AGR) fleet, as well as nuclear submarines and other novel reactor designs. PIE involves performing a variety of measurement, assessment and analysis techniques on fuel and other nuclear materials in hot cells and underwater.

The future of PIE at NNL will see a transition, over the next decade, from servicing UK AGR power stations to increasing support for spent fuel management and future UK reactor requirements.

This short article aims to provide a flavour of PIE at NNL; both at our active handling facility and on customer sites; with a particular focus on underwater PIE and how it benefits Nuclear Power Plant operation; and how we are striving to innovate and digitise for current and future requirements.

II. Current PIE

NNL's PIE capability collectively has over 100 years of experience in a variety of Post Irradiation Evaluation (PIE) techniques. The capability is comprised of 5 main areas which are involved in the entire PIE process from underwater inspection of fuel in-pond, to non-destructive and destructive examination of nuclear fuel in-cave, together with the measurement of the graphite core material properties and other irradiated reactor components. PIE is integral to safe operation of current reactors and also to spent fuel management and future reactor designs. Although there are 5 main areas of capability, this article will only look at irradiated fuel characterisation, which takes place in hot cells at our Active Handling Facility (AHF) and underwater in fuel cooling ponds at our customer sites.

A. Windscale Active Handling Facility

The Windscale Active Handling Facility (AHF) operated by NNL, consists of thirteen heavily shielded hot cells, a number of fumehoods, open labs and decontamination facilities. A video of the AHF facility at Windscale can be seen in [2].

Generally, each hot cell has five workstations with two manipulators. These cells are approximately 11 metres in length and contain a variety of analysis equipment for performing routine PIE, one off experiments and processing waste materials. The cells are connected on one end by a transport system allowing the movement of equipment and active material. These hot cells (or 'caves') are designated as highly active (HA) cells, and are used to process and characterise spent fuel and irradiated reactor components. The cells are specially designed to support the processing and examination of highly active gamma emitting materials, and as such are fabricated with thick concrete walls and equipped with either lead glass or zinc bromide viewing stations. Many of the cells have a designated purpose within the PIE lifecycle, ranging from dismantling of a fuel assembly, visual inspection and welding up of waste components, to small sample preparation for optical and electron microscopy. The majority of the equipment used is heavily modified for use within the hot cell, to allow it to be easily transported throughout the hot cell system and be operable with manipulators as well as resilient to the highly active environment. **Figure 13** offers an example image of inside a hot cell at AHF, with remote manipulator arms operating the gamma spectroscopy rig.

Figure 13: Gamma spectroscopy rig installed in a hot cell.

More information about experimenting on irradiated nuclear fuel at NNL's Windscale Laboratory can be found in Dr Matthew Barker's TEK Talk on "The Life of PIE" [3].

B. Underwater PIE

In addition to hot cell work at AHF, the NNL underwater inspection team has provided on-site PIE to the fleet of UK AGR stations over several decades, and considerable operational experience has been amassed. Examining thousands of AGR fuel pins a year, and latterly using in-cave condition monitoring examinations as a data comparison. **Figure 14** provides an example setup of the underwater inspections team examining AGR fuel in a power station cooling pond.

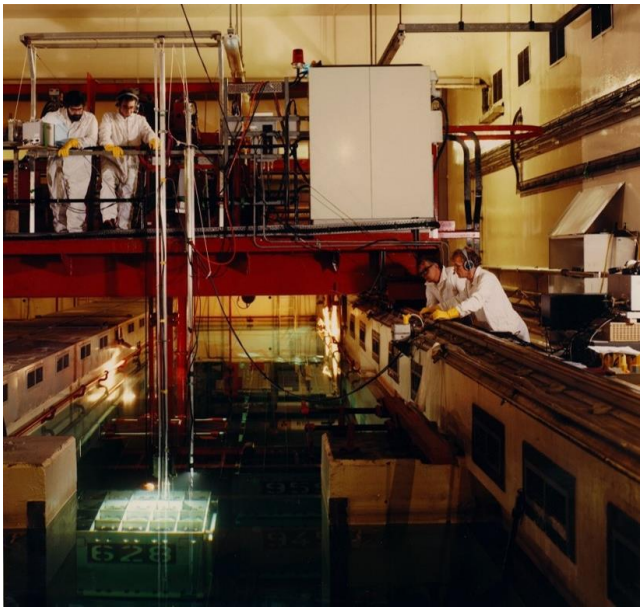

Figure 14: Example setup of underwater inspections team on a customer site.

Underwater inspections of AGR fuel are to provide condition monitoring, assessing the levels of carbonaceous deposit that has formed on fuel pin surfaces during operation and for any other observations. Carbonaceous deposit can impair heat transfer between the fuel and coolant during operation in an AGR, therefore understanding its properties is crucial for continued safe operation and for optimising fuel performance.

III. Innovation

NNL has fostered a strong innovation culture, which has been applied to the underwater PIE area to great effect. Recent case studies offer great examples of collaboration focused on bringing about improved digital data recording and analysis, as well as investigating the feasibility of new in-pond techniques beyond visual examination. This includes: the acquisition of tablet computers and the development of a data recording app to replace hand written notes, improving data processing; investigating the use of machine learning algorithm Computer Vision to aid inspection footage interpretation and assessment; and a feasibility study into underwater sampling of carbonaceous deposits from the surfaces of spent AGR fuel pins [4].

IV. Future of PIE

Irradiated fuel characterisation has formed the backbone of NNL's commercial operations over the last two decades. The team involved in irradiated fuel characterisation have demonstrated focus and resilience towards delivering results in support of the UK's AGR reactor fleet. The area has been crucial to understanding fuel behaviour throughout the fuel cycle and central to demonstrating the safety of reactors and fuel management facilities. The team hold a depth of experience in irradiated fuel characterisation relating to AGR, with a number of individuals possessing wider experience – based primarily around LWR and some fast reactor fuel.

The future of PIE at NNL will see a transition, over the next decade, from routine servicing of UK AGR power stations, to increasing bespoke support for spent fuel management and future UK reactor requirements. The knowledge acquired from irradiated fuel behaviour through PIE has been crucial for continued safe operation and extending the life of ageing nuclear power stations. This knowledge can be utilised to further improve the monitoring and management of spent fuel and can aid the development of future UK reactors.

V. References

[1] UKNNL, Strategic Plan, https://www.nnl.co.uk/strategicplan, June 2021.

[2] UKNNL, "NNL Windscale Laboratory Overview", https://youtu.be/l1YrLxQwapo, July 2015.

[3] UKNNL, "Matthew Barker: The Life of PIE", https://youtu.be/YTKd7STLvZ4, June 2017.

[4] Game Changers, "Fuel pin remote sampling tool" https://www.gamechangers.technology/challenge/Fuel_pin_remote_sampling_tool, November 2020

Proceedings of the European Nuclear Young Generation Forum
ENYGF'21
September 27-30, 2021, Tarragona, Spain

Fuel Assembly Protective Grid Design Considerations to Deal with Fibres in the Coolant Flow during Accident Cases

Redlinger-Pohn, Jakob D. [1*] and Lundell, Fredrik[1]

[1] Department of Engineering Mechanics, KTH Royal Institute of Technology, Sweden

*Corresponding author: edu.redlinger@gmail.com

I. INTRODUCTION

Given the potential risks with nuclear energy, accident scenarios and operational challenges need to be reviewed and discussed to allow for preparation and risk mitigation. The risk discussed in this paper is the deposition of fibres (for example from insulation, or air filters) on screens and fuel assemblies potentially leading to an increased pressure loss and a drop in coolant flow rate [1,2].

The retention of fibres on screens is dependent on the two parameters fibre length l to the screen opening size D, i.e., l/D, and the spacing between the openings S, i.e., l/S (the parameters are defined in Figure 2). In a recent publication, we documented four distinct fibre deposition regimes [3,4], shown in Figure 1. Fibres deposit on screens with relatively small openings, i.e., $l/D > 1$, through retention (Figure 1c): long fibres are unable to pass through the hole. The process is fast and only a few fibres leak through the screen before it is covered by fibres. However, the velocity at the screen opening, i.e., holes, scales with the inverse of the screen open area, i.e., the ratio of the hole are to the total screen area. Increased acceleration into small openings, i.e., $l/S < 1$ (Figure 1d) leads to high hydrodynamic forces, which we documented hindering the deposition of fibres.

Fibres deposit on screens with relatively large openings, i.e., $l/D < 1$, via stapling (Figure 1a). Fibres pass through the opening, but can deposit at the spacing if $l/S > 1$ where they are retained by friction. A fibre mat is then formed from the edge and will eventually cover the screen. The process is slow, and a significant number of fibres can leak through the screen. If the spacing is large, i.e., $l/S < 1$ (Figure 1b), fibres are hindered from deposition at the spacing, and effectively no screen covering mat can be formed. Consequently, the fibres leak through the screen indefinitely.

Fibres leaked through the screen can potentially deposit on downstream equipment, for example, a second screen or the fuel assembly. We have documented previously [3], that the chance of downstream fibre collection by a second screen is dependent on the collection rates k. The collection rate k is here defined as the inverse of the specific filtration volume v, which describes the suspension volume per area [m³/m²] passed through the screen or fuel assembly until coverage is reached. The collection rate can then be calculated as: $k = v^{-1} = (u_n t_c)^{-1}$, with u_n being the approach velocity upstream the screen (i.e., ratio of the flow rate F and the screen area A, F/A) and t_c being the time passed until full coverage is reached.

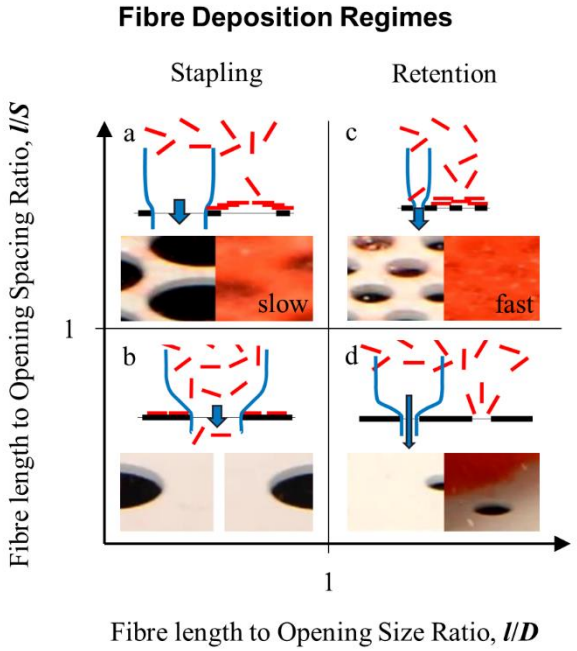

Figure 1. Collection regimes (adapted from [3]) of fibres on screens in dependence on the fibre length l to the opening size D, i.e., l/D and fibre length l to the opening spacing S, i.e., l/S. a: stapling with the collection of fibres. b: hindered stapling. c: fibre retention. d: hindered fibre retention.

For the case of an efficient upstream screen with a high collection rate k_{up} compared to the downstream screen with a low collection rate k_{down}, i.e., $k_{up}/k_{down} > 1$, the number of fibres leaked through the upstream screen was insignificant and the downstream screen remained unclogged. For the case of $k_{up}/k_{down} < 1$, the number of fibres that leaked through the upstream screen was significant and a fibre mat could be formed on the downstream screen, which can also be the fuel assembly.

The latter scenario was documented by Suh [2] for an APR1400 experimental model. Approximately 25% of the fibrous material was documented to have leaked through the Emergency Core Cooling System (ECCS) screen. The leaked fibres deposited in the fuel assembly and triggered an increase of the pressure loss after filtering suspended fine particles. The focus of Suh [2] was on the documentation of the fibre deposition in the fuel assembly and expectable pressure drop. However, they do not provide any insights on the deposition mechanism and collection rate k. Further, they treated the fibre collection at the ECCS screen and fuel assembly independently. As we have shown in our previous work [3], the likelihood of a downstream screen, here the fuel assembly, being covered by fibres depends on the upstream screen efficiency in relation to the downstream screen efficiency, as can be attained by a comparison of the fibre collection rates k.

In this publication, we will describe the fibre deposition on fuel assemblies of two designs, PLUS7 P-Grid and Guardian P-Grid [5]. The observations will be discussed in light of follow our previous work on fibre collections on screens. This will allows us to make conclusions on the chance of fibres depositing in the fuel assembly after leakage from the ECCS screen.

II. Experimental Setup

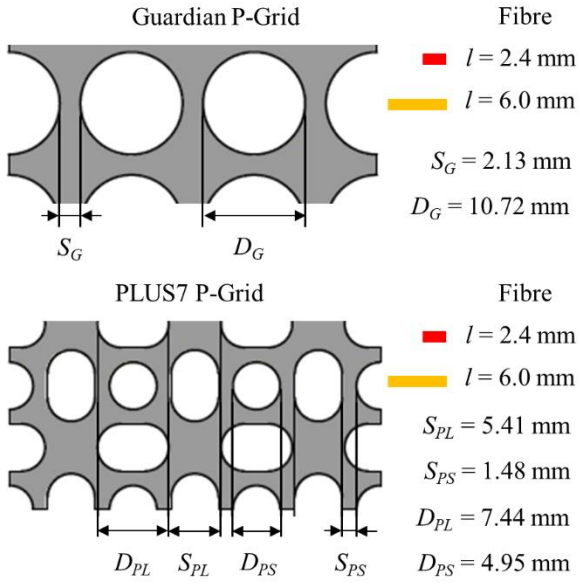

Figure 2. Dimensions of the Guardian P-Grid (opening D_G and spacing S_G) and PLUS7 P-Grid (large opening D_{PL}, small opening D_{PS}, large spacing S_{PL} small spacing S_{PS}) and the 2.4 mm (in red) and 6.0 mm (in yellow) fibre in relation.

We used the same experimental setup as in our previous study [3]; a filtration column with an exchangeable screening section of 100 mm square and optical access at the screening zone. The fibre deposition on the screen was recorded with a Nikon D7100 (Nikon Corporation, Japan). In this study, we used two types of polyamide fibres. The red fibres have a length of 2.4 mm and the yellow fibres have a length of 6.0 mm. The fibre concentration was ~ 3 g/L what corresponded to a dilute suspension, i.e., with no significant interaction of the fibres upstream the screen. The volume flow rate was set to 20 L/min, being comparable to Suh [2] (who used a 16-by-16 rods PLUS7 grid and ours corresponds to 7-by-7 rods) and calculating to to an upstream velocity u_n of 33.3 mm/s.

The fuel assembly protective grids, shown in Figure 2, were reproduced from literature specifications [5] and 3D printed with a height of 10 mm to fit into the screening section of the filtration column. The Guardian P-Grid is of a simple hole-plate design with comparable large openings. The red fibres are at the border of stapling and the yellow fibres are within the stapling regime (see Figure 1a). The PLUS7 P-Grid is of a more complex design and consists of larger elliptical openings and smaller circular openings. Based on the smaller dimensions, red fibres are within the stapling regime and yellow fibres are within the retention regime (compare to Figure 1c).

III. Results and Discussion

In the following, we first present the deposition of fibres on the fuel assembly protective grid and estimate the collection rate k. Secondly, we compare the collection rate k of the fuel assembly to screens, determined in our earlier work [3] and discuss the likelihood of fibre collection at either equipment.

A. Fibre Deposition on Fuel Assemblies

The PLUS7 P-Grid (Figure 3) successfully collected the shorter 2.4 mm (red) and longer 6 mm fibres (yellow).

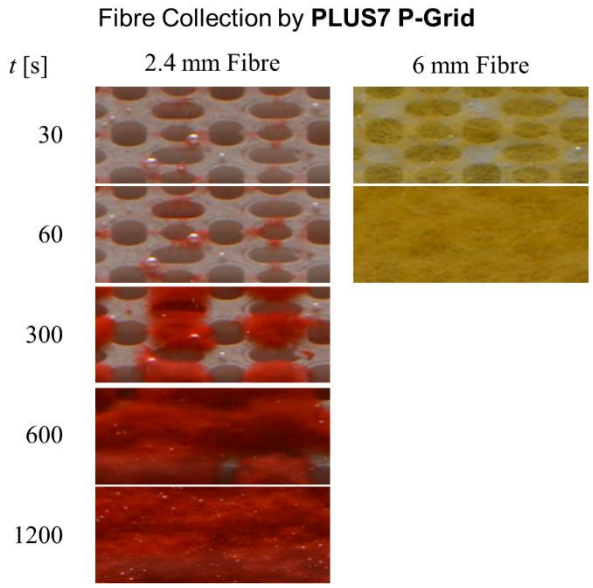

Figure 3. Snapshots of the fibre collection on the fuel assembly PLUS7 P-Grid. Note that the red fibres first collect on the spacings and the yellow fibres bridge the holes.

The 2.4 mm fibres were collected via stapling starting from the spacing at the smaller openings S_{PS} (t = 60 s). Following the smaller openings D_{PS} were covered by the fibre mat growing from the spacing into the hole (t = 300 s). The collection rate for the partial coverage calculates to $k_{P,2.4,small}$ ~ 0.1 m^{-1}. From the established deposition, the fibre mat continued to grow by collected fibres, covering the whole screen after about 900 s. The corresponding collection rate is $k_{P,2.4}$ = 0.033 m^{-1}. The 6 mm fibres were collected via retention. The screen openings were covered within the first t = 30 s (see the image at t = 30 s). Coverage of the fuel assembly solid part lagged and the screen was

fully covered by a fibre mat after $t = 45$ s, yielding a collection rate $k_{P,6} = 0.667$ m^{-1}.

The Guardian P-Grid (Figure 4) collected shorter 2.4 mm fibres on the spacing, which was anticipated since $l/S_G = 1.13 > 1$ at $l/D_G = 0.22 < 1$. In previous experiments, we documented the coverage of screens by stapling with a similar spacing S but smaller opening D compared to the Guardian P-Grid [4]. Here, the Guardian P-Grid remained uncovered, and the holes remained open for the maximum observation time of $t = 1200$ s. Eßl [6] documented the coverage of openings with $l/D_G = 0.18$, i.e., smaller than for the Guardian P-Grid. There a fibre mat first grew in height until it collapsed and covered the openings. We did not run our experiment for that long but noted a continuous growth of the fibre mat for 1200 s. Coverage of the Guardian P-Grid is hence conceivable, but as shown here, not within the initial stage of an event that introduces fibres to the coolant flow, for example a loss of coolant accident. The long-term behavior, however, remains to be investigated. In any case, a significant number of fibres of 2.4 mm length will leak through the protective grid which, potentially, can deposit on small flow obstructions such as the mixing vanes of a fuel assembly.

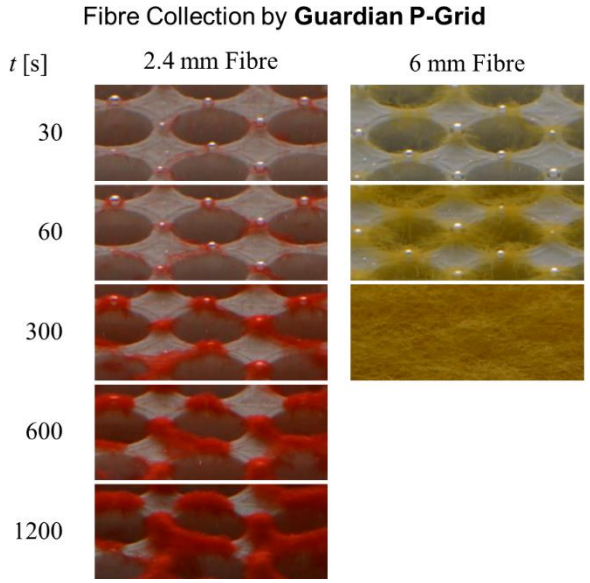

Figure 4. Snapshots of the fibre collection on the fuel assembly Guardian P-Grid. Note that the red fibres collect on the spacings only and the yellow fibres cover the holes with time.

The 6 mm fibres were collected via successful stapling, starting from the fuel assembly solid part (Figure 4, $t = 30$ s) and growing inwards (Figure 5, $t = 60$ s). After $t \sim 80$ s, the screen was covered by a fibre mat what yields a collection rate $k_{G,6} = 0.375$ m^{-1}.

B. Towards an Estimation of the Fuel Assembly Coverage

In our previous work, we documented the collection of 2.4 mm fibres (the same as used here) by retention and stapling on screens of various design. The screen area and upstream velocity u_n were identical with the settings in this study. The associated specific filtrate volume v and the collection rate k as its inverse are listed in Table 1. The collection rate k is seen to decrease with (i) an increasing opening size D, especially when crossing from retention to stapling, and (ii) an increasing spacing between the holes S (see the hole plates in Table 1).

The collection rate k of M10 and M4 (Table 1) was high and only a few fibres would leak through these screens. The collection rate k of Rv6-7.5 and Rv6-8 (Table 1) was higher than what we measured for the fuel assembly at identical settings (i.e., same flow rate and fibre type, $l = 2.4$ mm).

Table 1. Geometrical specification filtrate volume v and collection rate $k = v^{-1}$ of screens of various design from our previous work [4]. The settings were comparable; fibre $l = 2.4$ mm and $u_n \sim 33.3$ mm/s.

Type	Mesh		Hole Plate		
ID	M10	M4	Rv6-7.5	Rv6-8	Rv6-9
l/D	1.2	0.5	0.4	0.4	0.4
l/S	4.2	2.0	1.6	1.2	0.8
Mode	Retention	Stapling	Stapling	Stapling	Uncovered
v [m]	0.45	1.27	4.07	11.17	-
k [m^{-1}]	2.22	0.79	0.25	0.09	-

Hence, fibres leaking through these screens can be assumed to deposit on the fuel assembly without being large enough in numbers to cover the fuel assembly fully. Specifically, the Guardian P-Grid would only collect 2.4 mm fibres by stapling on the solid spacing with the openings remaining uncovered. For the PLUS7 P-Grid we expect a more complicated behavior. We compare the Rv6-8 collection rate $k = 0.09$ m^{-1} to the measured collection rate for the small openings only which was $k_{P,2.4,small} \sim 0.1$ m^{-1} and the total fuel assembly which was $k_{P,2.4} = 0.033$ m^{-1}. Likely, the fuel assembly will be partly covered with the small openings being blocked by a fibre mat. It is conceivable, that these blocked openings will pose a local flow restriction with a redirection of the coolant flow through the larger openings. A partial coverage might consequently affect the coolant flow distribution, whilst the total flow rate might be less affected.

Stapling was hindered on Rv6-9 (Table 1) and basically, all suspended fibres leaked past the screen. These fibres can consequently deposit on downstream equipment, for example at the fuel assembly protective grid. That is likely if the downstream equipment has smaller dimensions than the upstream hole screen (discussed in the next section), what would be the case for the PLUS7 P-Grid with $l/S_{PS} = 1.62$ but not for the Guardian P-Grid.

C. Discussion and Outlook

Two principal design considerations can be drawn from our observations of fibre deposition on fuel assembly protective grid in combination with our previous observations of screen coverage by fibres [3]:

(1) The paring of the fibre length l to the opening D and spacing S determines the chance for fibre deposition and the collection rate. Suspended fibres will pass the screen and the fuel assembly given they are smaller than the geometry without covering the surface (see Figure 1b and Figure 4, 2.4 mm fibre). For an unknown fibre length, as it can be

anticipated for glass fibres dispersed from insulation material during a Loss of Coolant Accident, it may be difficult to a priori estimate the chance of screen coverage. The same equipment, for example, Guardian P-Grid, will remain uncovered for long time if the suspended fibres received have a length $l < 2.4$ mm whilst being covered quickly by fibres having a length $l = 6$ mm. We used in our experiment a mono-disperse model system, i.e., one fibre length. In a real case, the fibre length will be a distribution and we expect the larger fibres in the distribution to determine the coverage probability. The quantification of the effect of long fibres on the screen deposition is the subject of a current study of ours.

(2) We have shown in our previous work, that the downstream equipment will be covered by fibres if $k_{up}/k_{down} < 1$ (Figure 5a) whilst remaining uncovered if $k_{up}/k_{down} > 1$ (Figure 5b). That is most likely the case, if the dimensions of the downstream equipment (fuel assembly), i.e., opening size D and/or opening spacing S, are smaller than for the upstream equipment (ECCS screen). That allows a simple approach to mitigate the threat of fibre deposition on the fuel assembly protective grid by an efficient collection at the ECCS screens. For that, the ECCS screens should be equipped with hole plates having small openings and a large open are, or be complemented with an additional screening layer, for example a mesh added on top of the hole plates.

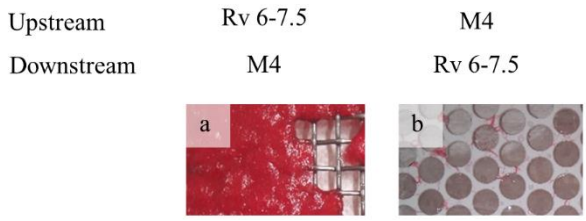

Figure 5. Adapted reproduction from [4] of the downstream screen coverage in dependence on the screen efficiencies. M4 is more efficient than Rv 6-7.5 (Table 1). Consequently, a: M4 as downstream screen is covered whilst b: Rv 6-7.5 as downstream screen remains uncovered.

Shown in our previous work [3] is the sensitivity of the collection rate on the upstream velocity u_n. With increasing u_n, more fibres can leak past the screen (especially in the stapling regime) and deposition of fibres can be hindered. The flow rate F in a system of ECCS screens followed by a fuel assembly is constant and the screen area A, which may differ, sets the upstream velocity $u_n = F/A$. The dependence of the filtrate volume v until coverage is however not linear with u_n. Paradoxically, in total more fibres may leak through ECCS screens operating in the stapling regime [3] with a larger screening area (which were installed in some plants [7]) compared to a smaller screening area. For a general statement, we will probe the impact of u_n on the PLUS7 P-Grid and encourage for a closer-to-the-application test including variations of ECCS screen size and design in series with fuel assembly section.

IV. Conclusion

Fibres, for example from insulation material, need to be accounted for as debris during accident cases such as a Loss of Coolant Accident. Given their slender shape, these fibres can deposit on ECCS screen, fuel assemblies and other structures by retention, i.e., size exclusion and stapling, i.e., frictional immobilization. In a previous work [3,4] we documented the coverage of screens of various design that were sensitive on the pairing of the fibre length l to the opening size D and opening spacing S. In this study we extended the deposition of fibres onto fuel assemblies, which were reported to collect fibres that leak through the first ECCS screen [2]. We reproduced the protective grids PLUS7 P-Grid (irregular openings) and Guardian P-Grid (large openings) from the literature [5] and probed the deposition of two types of fibres.

In accordance with our previous findings [3], fibre deposits on the screen if $l/S > 1$, whereby the Guardian P-grid at $l/S \sim 1$ remained open for the studied time t of 1200 s, i.e, 20 min. The PLUS7 P-Grid with irregular openings had two distinguishable coverage phases: (1) first the smaller openings were covered, in case of 2.4 mm fibres by stapling, and (2) after their blockage the larger elliptical openings were covered. This can lead to a partly covered fuel assembly with varying blockage for the coolant flow past the screen, potentially impacting the core cooling. These aspects should receive attention in future work.

Coverage of the fuel assembly reported here is comparable to the coverage of screens in general [3]. That allowed us to comment on the expected likelihood of the fuel assembly coverage by fibres in dependence on the ECCS screen design. In summary, we expect an insufficient leakage of fibres past the ECCS screens if the screen geometry, i.e., D and S, is smaller than for the fuel assembly. The statement is based on an equal screen area of the ECCS screen A_{Screen} and fuel assembly A_{AF} and needs to be re-evaluated for differing screen areas, for example $A_{Screen} < A_{FA}$, especially when the ECCS screen is operating in the stapling regime.

V. References

[1] G. H. Hart, A short history of the sump clogging issue and analysis of the problem, Nucl. News 47, 2004, 24-34.

[2] J.K. Suh, Evaluation of Long Term Core Cooling Capability Considering LOCA-generated Debris, PhD Thesis, 2015, Seoul National University.

[3] J.D. Redlinger-Pohn, et al., Parameter Regimes and Rates of Fibre Collection on Screens of Various Design, Sepur, 259, 118053.

[4] J.D. Redlinger-Pohn, et al., Fibre Clogging in Nuclear Power Plants, Swedish Radiation Safety Authority SSM Report 2020:07, 2020.

[5] M.-S. Jung, and K.-T. Kim, Debris Filtering Efficiency and its Effect on Long Term Cooling Capability, Nuc. Eng. Res. Des. 261, 2013, 1-9.

[6] M. Eßl, Design of a Distributor for Fibre Suspensions, Master Thesis, 2017, Graz University of Technology.

[7] OECD, NEA/CSNI/R(2002)6: Knowledge Base for Strainer Clogging - Modifications performed in different countries since 1992.

The authors thank Dr. Nils Tillmark for the design of the filtration column and the Swedish Radiation Safety Authority (Strålsäkerhetsmyndigheten, SSM) for funding.

Proceedings of the European Nuclear Young Generation Forum
ENYGF'21
September 27-30, 2021, Tarragona, Spain

Maintenance needs and power losses identification through heat rate monitoring systems

García Salmerón, María[1], González Pindado, Francisco Javier[1*], Martín García, Mariano[1*], Barroso Martín, Javier[1*]

[1] Tecnatom, Spain

*Corresponding author: *mgs@tecnatom.es; jgp@tecnatom.es; mmg@tecnatom.es; jbarroso@tecnatom.es*

I. INTRODUCTION

TecOS SOLCEP is a software tool to monitor, diagnose and quantify performance deviations in power plants. Additionally, its customization to each generation unit and its detailed scope makes a TecOS SOLCEP model a digital twin of the performance status of a power plant. The methodology, definition of indicators and nomenclature follows ASME standards. Although it was initially created to be applied in coal power plants, its applicability has been widened to combined cycles, solar-thermal and nuclear power plants. TecOS SOLCEP is currently being used in 59 plants on several continents, where 17 years of success stories have resulted in economic benefits for plants.

II. BENEFIT-BASED MAINTENANCE (BBM)

The implicit concept within TecOS SOLCEP is "Benefit-based Maintenance" (BbM) as an addition to common maintenance strategies such as time-based, condition-based, or predictive. These last three maintenance strategies are aimed at achieving the safety and reliability objectives shared by all electricity generation technologies, understanding safety as people, both outside and inside the plant, the environment and the equipment, in this order. BbM is focused towards getting the maximum economic benefit by taking care of efficiency, which has historically not been a plant priority.

Improving or maintaining efficiency, and therefore the maximum achievable power, is one of the main challenges of this era for power plants, and especially nuclear power plants that usually operate at maximum load. Therefore, the BbM concept applied with the help of monitoring tools is expected to play an important role in improving efficiency which, in plants operating mainly at full power, is equivalent to increasing or maintaining the maximum power.

Power plants aiming to life extension can also leverage the identification and quantification of equipment inefficiencies to better address the needed investments.

BbM shall tell us when a maintenance action to restore the efficiency of an equipment is economically beneficial. This equation has three terms: first, losses associated with a particular deviation; second, the cost of the equipment maintenance or replacement actions, which may also include the need to stop the plant and its production; and third, the estimated degradation rate after restoration. TecOS SOLCEP provides information on the first and third terms, helping to make the best decision. The second term can be evaluated and scheduled well in advance because maintenance actions are usually addressed only during major outages.

Monitoring tools, along with the BbM application, shall add two additional functionalities: support the decision making process of operational optimization, which is particularly important for plants operating at variable loads, with different possible configurations, or that stop and start frequently; and assisted diagnosis, to help identify the root causes of a given deviation.

III. PURPOSES OF MONITORING TOOLS

In the authors' view, the main purposes of a performance monitoring tool, applicable to any power generation technology, should be as follows.

The first purpose should be to obtain a quantification, as accurate as possible, of the current situation of the plant, using only process instrumentation. This includes evaluating the thermodynamic status and mass flow at each relevant point of the process circuits.

Thermodynamic states and flows are obtained using power balances on the turbine shaft along with global and partial mass and energy balances in the Rankine cycle and heat exchangers. This procedure allows to obtain the values of non-instrumented variables such as moisture in the exhaust of steam turbines, and at other points of the cycle in nuclear power plants.

Non-instrumented flows can be estimated from valve opening position using their characteristic curves, or by performing field measurements during specific tests.

The performance status of the plant is finally represented by the key performance indicators (KPIs) of the plant, each system and each equipment, which monitoring facilitates the alert of deviations and the diagnostic process. Figure 1 shows the calculation flow for a nuclear power plant.

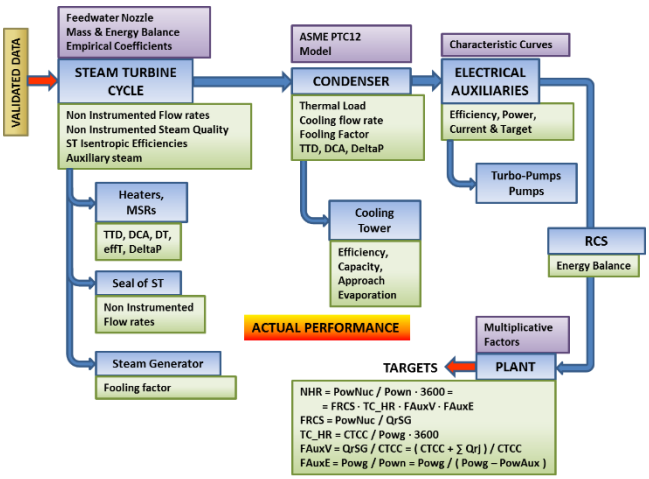

Figure 1. Block diagram of the current performance calculation for a nuclear power plant.

The second purpose should be the determination, as precisely as possible, of the individual objectives for each parameter, equipment and system, which deviation significantly affects the specific consumption and maximum achievable power. These objectives should be obtained for the current operational and boundary conditions of the plant: load level or downtime, start-up situations, system coupling situations, environmental conditions and fuel.

The objectives, to be representative, shall be obtained from various sources: steam turbine design data, design balances at different loads, acceptance test results, equipment design data and their characteristic curves, statistical regression of the best historical data records (e.g. electrical auxiliaries or makeup water), and specific simulation models of the most influential components (e.g. condenser and cooling tower).

The objectives should also consider the non-recoverable and recoverable degradation of existing equipment, or be updated if some equipment was replaced by a more efficient one. The steam turbine is the main equipment where degradation is to be considered. The target values of any monitoring system should be updated after each major outage, since the condition of the plant after maintenance usually reflects the best achievable values.

And the third purpose should be to calculate the contribution of each system, component and operational parameter, to the deviation of specific consumption and maximum power. This is the primary set of values for BbM. The impact or contribution of each of the deviations should be expressed in energy units for specific consumption, in MW for power, and also in monetary units for both. Figure 2 shows all the primary parameters considered in a generic nuclear power plant model.

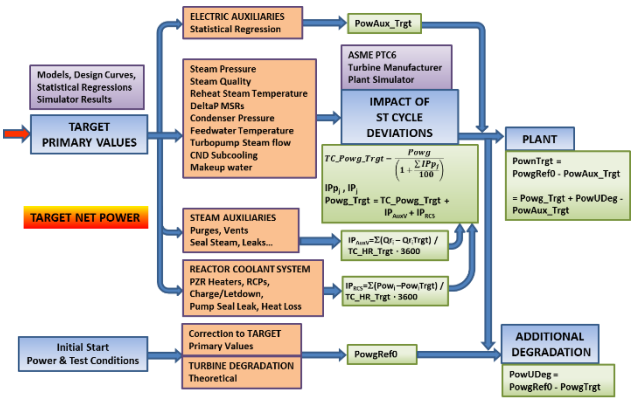

Figure 2. Block diagram for calculation of the maximum target power in a nuclear power plant.

The impact of a single deviation on the specific consumption and/or maximum power is mainly obtained from the technical documentation provided by the steam turbine suppliers that typically use stationary state simulators adjusted to the design characteristics of plant equipment. Nevertheless, this is not the only source, properly validated simulators (against actual plant behavior and transients) should be one of the preferential sources for impact functions.

The use of parametric impact functions, compared with the direct use of real-time simulation models, has great advantages: including the speed of calculation and the ease of interpretation of the results.

The results of the monitoring tool should be collected on displays for online visualization and early warning of deviations, and in reports for average and cumulative results, used for accounting and diagnosis of medium and long-term deviations. Figures 3 and 4 show the main displays for deviations from specific consumption and maximum power.

Figure 3 shows the application of human factor engineering and high-performance displays in a monitoring tool. Other important features include focusing the user's eyes on the elements that require their attention, without overloading with an excess of information; and to use elements with a high degree of abstraction such as the deformable polygon and variable ring in size and color.

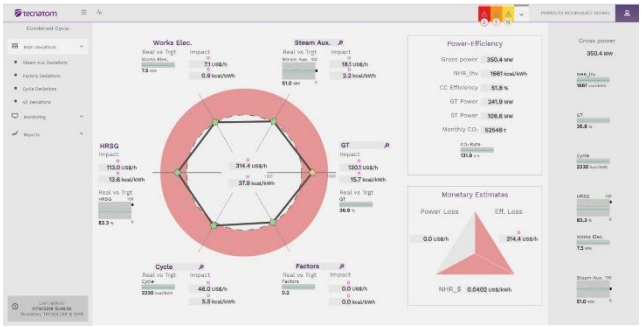

Figure 3. Specific consumption deviations display.

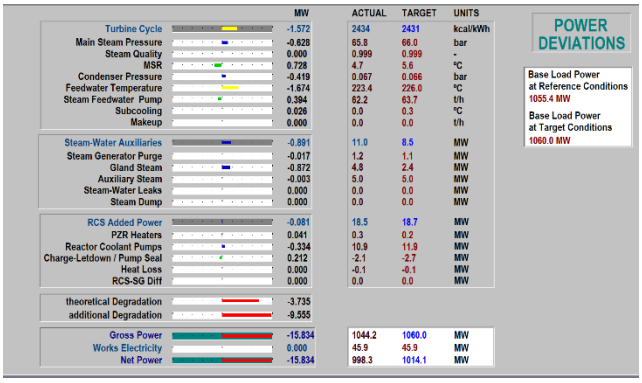

Figure 4. Maximum power deviations display.

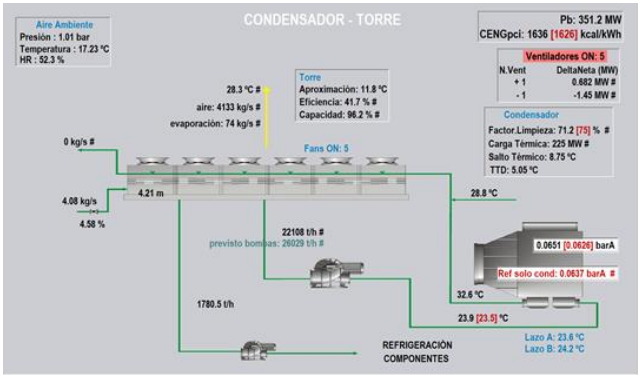

Figure 5. Condenser-tower display: optimization of the number of fans.

IV. OPTIMIZING THE OPERATION

To ensure that an Operation Optimization tool is accurate when evaluating different alternatives and making future projections, you need to gather information not only from performance monitoring tools, but also from market applications that provide pricing and load demand projections, and from weather forecasting applications.

The advantages of this exchange of information are: the use of current values of equipment and systems performance, information about the evolution of the degradation of certain equipment, and the best predictions regarding boundary conditions.

Operational or maintenance decision-making based on the results of these optimization tools can, depending on the reliability of the projections, bring significant economic benefits and a competitive advantage.

Monitoring tools should include optimization elements for individual equipment or systems within their structure. TecOS SOLCEP includes several of these operation optimization elements that are helping plants on the decision-making process. Examples include: optimal number of operating cells in a cooling tower, optimal number of running water pumps, selection of the running pump when redundant.

Figure 5 shows the support screen for the optimal number of towers in a real case. The model uses a simulation system for the condenser-tower assembly and a parametric impact curve for the influence of the condenser pressure on turbine power. The calculation of the impact of start or stop a fan in the tower is evaluated by considering its electrical consumption, and then calculating successively the outlet water temperature change, the condenser pressure change and the steam turbine change. In the case presented in the figure, for the condenser thermal load and environmental conditions, it is recommended to start one more fan, with an improvement of the net power of 0.68 MW. Once the fan is started, if the plant is at maximum load, it would translate directly into a net power increase.

To answer questions regarding the overall behavior of the plant in terms of maximum power, it is also advisable to have a Balance of Plant simulation model. This simulator should be a flexible tool that allows calculations to be performed with different options: current or reference environmental boundary conditions, current or equipment design performance, and different plant configurations.

Figure 6 shows one of the displays of such a stationary simulator that is independent from TecOS SOLCEP, even though connected.

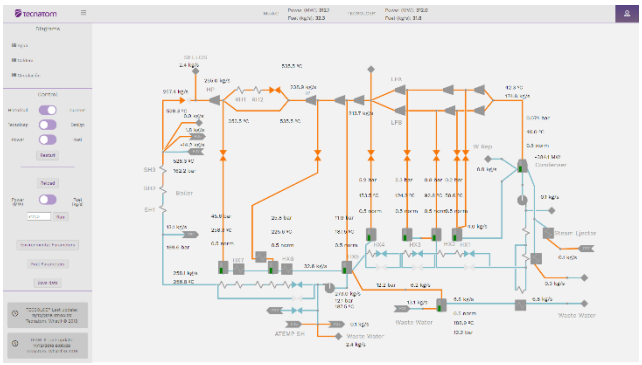

Figure 6. Stationary simulator for operation optimization: Rankine Cycle.

V. ASSISTED DIAGNOSIS

A monitoring tool should include a diagnostic functionality for the identification of the origin of performance deviations for individual components. This functionality gives the user-engineer the ability to identify, in a guided way, the root cause and make decisions regarding maintenance or repair, or redundant equipment selection. Decisions may sometimes be related to changes in the operational configuration of the plant, or variation of setpoints, intended to restore or minimize the effect of a given degradation or malfunction.

This functionality is called Assisted Diagnostics. The main motivation of this application is to capture the knowledge and diagnostic experience of professionals dedicated to performance monitoring.

In general, assisted diagnosis of a component is based on four concepts:

- the values of the instrumentation related to the equipment,

- the expected values for each instrumented variable,
- logical rules for diagnosis and recommended verifications,
- the results of recommended inspections and field measurements.

All these concepts are combined in the formulation of a particular diagnostic model for each equipment, the results of which are listed on the diagnostic display of the equipment, one of whose examples is shown in Figure 7.

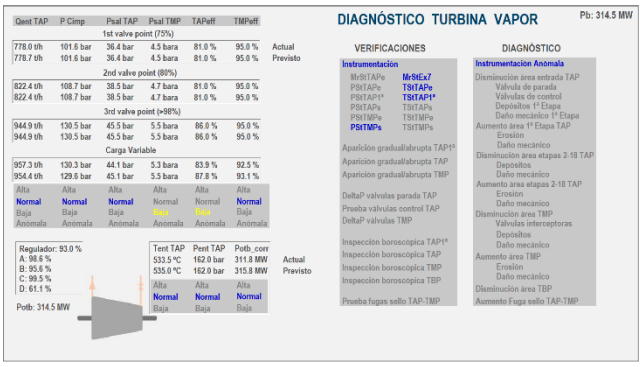

Figure 7. Assisted diagnostic display for a steam turbine.

The diagnostic display will generally consist of the following elements:

- current and expected values of the most relevant instrumentation and derived indicators,
- instrumentation status based on deviations between current values and expected values,
- process diagram and instrumentation of the equipment with the values and location of the instruments associated with the equipment,
- result of Diagnosis, in which several possible causes may occur explaining deviations,
- recommended checks to focus and reject or confirm diagnosis.

The expected values for the instrumentation and indicators of each instrumented variable are generally obtained from historical periods, stored in the database, where the equipment was in a perfect condition; for example, at the beginning of the plant operation or after the maintenance of a particular equipment.

Logical rules allow to identify instrumentation anomalies and to relate the deviations, and combinations of both, to the originating causes. These rules have generally been obtained from the guiding document "ASME PTC-PM 2010", but also from the intensive use of Dynamic Plant Simulators and lessons learned from real operational experiences.

Once the initial diagnosis of a component has been checked online, in which several possible causes appear for the deviations detected, or after being alerted by the "alarm buttons", a "Diagnostic Session" shall be initiated to advance the discrimination or confirmation of the causes.

During a Diagnostic Session of a component, recommendations for checking instrumentation, inspections, field measurements, testing, or trend charting should be followed. Once these checks are performed, the result will be feedbacked to the Diagnostics application. In this way the recommendation already executed would disappear and in the Diagnostics table some of the probable causes could disappear or be confirmed.

The dynamics of Diagnostics require the execution of each and every one of the recommendations in order to confirm the final diagnosis. For this reason, a session can take several hours, or even days, until all recommendations are covered, and the diagnosis is confirmed.

The equipment that shall include an Assisted Diagnostics application are the main ones of a plant where there is usually enough instrumentation, such as: Heat Exchangers, Condenser, Cooling Tower, Pumps and Fans and Steam Turbine.

VI. CONCLUSIONS

This article reflects the authors opinions on the features and functionality that a performance monitoring tool should possess in today's digital environment. This point of view is based on years of experience in tracking and diagnosing performance deviations in power plants and developing solutions and simulation models. The information provided by these tools to the professionals of the plants and monitoring centers has served to take the best decisions regarding the maintenance of equipment and optimization of the operation.

TecOS SOLCEP, is the monitoring tool developed by the authors that has the characteristics described in this document and is integrated into the TecOS "suite" of the company Tecnatom, which is an integrated set of solutions, designed to manage the assets of the energy and industrial sectors.

The use of these monitoring systems in a fleet of plants, with their component of standardization of visualization, operation, and nomenclature, allows the interchangeability of monitoring and diagnostic professionals, and the optimization of the number of specialists needed in the monitoring centers. The use of TecOS SOLCEP in a fleet also allows comparative evaluation between units of the same technology, and identification of best practices, which can thus be more easily shared between operators and technicians.

VII. REFERENCES

[1] ASME PTC PM-2010, Performance Monitoring Guidelines for Power Plants, (2010)

[2] EPRI 1020645, Plant Support Engineering: Guideline for System Monitoring by System Engineers, (2010)

[3] ANSI/ISA-101.01, Human-Machine Interfaces, (2015)

[4] Vicente and Rasmussen, Ecological Interface Design: Theoretical Foundations, (1992)

Proceedings of the European Nuclear Young Generation Forum
ENYGF'21
September 27-30, 2021, Tarragona, Spain

Experience of Digital Transformation Applied to P&IDs and its Application to Main Control Room and Engineering

Barroso, Javier [1], Ramos, Mateo [1], Gil, Javier [1],

[1] Tecnatom, Spain

*Corresponding author: *jbarroso@tecnatom.es, mramos@tecnatom.es, jgil@tecnatom.es*

I. INTRODUCTION: CURRENT SITUATION AND ITS CHALLENGES

The nuclear power plants fleet that is currently in operation, has been mostly designed and constructed before the introduction of Building Information Modeling (BIM) methodologies, integrated design software or even 3D modelling tools. This means that the Piping and Instrumentation Diagrams (P&IDs) of such plants can only be found either in paper or pdf formats. Efforts to digitalize nuclear power plants drawings and schematics have been limited to the use of CAD software for design modifications, and even though technologies such as Laser Scanning and Photogrammetry has been successfully applied to build digital models of the plants buildings and spaces, its application to P&IDs has been challenging.

During the Operation and Maintenance (O&M) of a nuclear power plant, it is necessary to know at all times the real status of all assets since alignments, work orders, working permits, clearance orders… will vary over the time and therefore will have an impact on the operation of the power plant and in the planning of the next activities.

Plant personnel that want to check such information need to navigate and search throughout the P&IDs on one hand and through the different management system applications on the other, leading to cross checking the information between different formats, interfaces and platforms. Information available within the management system does not include any kind of graphical representation in the P&IDs, which generates inefficiencies and human-error risks when checking different information sources in order to know the actual status of the plant. This situation applies to different roles within the nuclear power plant organization such as operators, engineering, maintenance, radiological protection…

II. CENTRALIZED VISUALIZATION

A. Proposed Solution

The optimal solution to solve the abovementioned problems would be the centralization of information in a visual application that allows the display of the relevant data over the plant diagrams and building plans. This would allow the user to access only one application to check the real plant status and, in a layout, already familiar, which includes all the needed information needed to be able to plan, execute and follow the upcoming works.

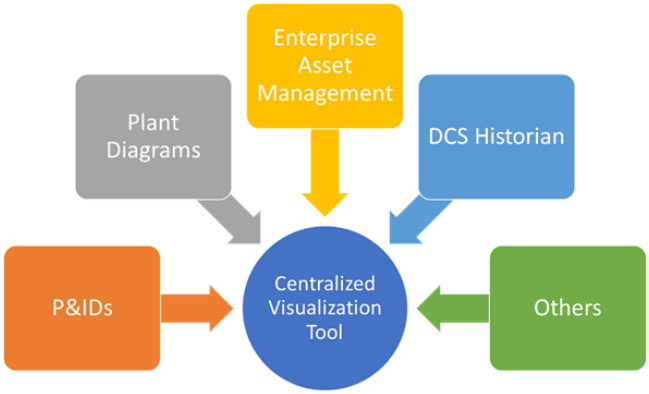

Figure 1. Centralized Visualization Concept.

TecOS VIEW ™ is an application that allows the visualization of the management systems information over the plant diagrams and building plans in an interactive way. TecOS VIEW ™ integrates the data needed from the different sources, through the communication with third party solutions, and allows its visualization in layers over the diagrams more familiar to the user which enhances the performance and situational awareness.

Figure 2. Artificial Intelligence to process drawings into interactive P&IDs.

TecOS VIEW ™ builds up its capabilities from the original documentation, typically the P&IDs and other diagrams and schematics, in the format currently archived in the document management system. These formats range from pdf to CAD

and even images, which will be processed to identify the equipment tags. Therefore, it is not necessary to modify, draw or pre-process the currently available diagrams and ensures the compliance with the latest official version. TecOS VIEW ™ leverages Optical Character Recognition (OCR) and Machine Learning techniques to identify and position within the diagram the different components, instrumentation and rooms tags. These tags will be the base for information representation and since they are used across the different management systems, tags will be the cornerstone for data integration.

B. P&IDs in most nuclear power plants

Piping and Instrumentation Diagrams (P&IDs) are easily managed by nuclear workers and they are comprehensive and supportive while preparing and executed their tasks.

Most nuclear power plants worldwide have been designed and constructed before the introduction of integrated design software and 3D modelling, which limits the Piping and Instrumentation Diagrams (P&IDs) to paper copies or pdf files in the best case and therefore its use and connectivity. Those new plants are following a more structured way to design the plants as it can be noted in references [1] and [2]. We have tried to apply some of these lessons into this approach that is focused for older plants where migrating into a BIM system may be too complicated.

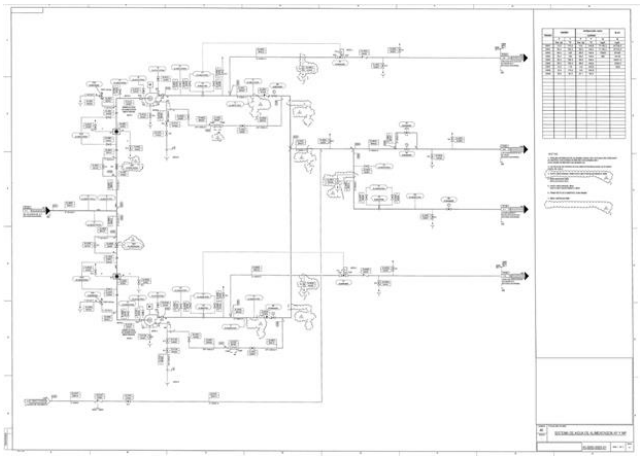

Figure 3. Example of a NPP P&ID.

C. Interactive P&IDs

As the P&IDs and other building drawings are managed often and easily by the nuclear workers, we considered that they could be used as the basis for representing the information about the components. After a deep research, we conceptualized a system that could manage different layers of information over the drawings having a concept similar to the BIM (Building Information Model) systems used in new industries or the more widely extended Google Maps.

In order to have interactive P&IDs, the following points need to be addressed:

- Digitize the current P&IDs (or other drawings)
- Integrated database correlated with the components identification
- HMI that represents the P&IDs and the layers of information and allows the user to interact
- Connect with the sources of information

D. Description of TecOS VIEW ™ as Interactive P&IDs system

From the conceptual design, Tecnatom built an application called TecOS VIEW ™ as interactive P&IDs system.

Figure 4. TecOS VIEW ™ application.

It is an application that can be used on desktop and tablets with all the operating systems (iOS, Windows or Android). The system is able to work in online and offline mode so it can be used to support the field tasks in areas where no WiFi is available.

It has an user-friendly and simplified interface. The user can easily navigate through the drawings including the P&IDs but also building diagrams, electric wiring diagrams among others. A hierarchy of drawings can also be established to simplify the navigation.

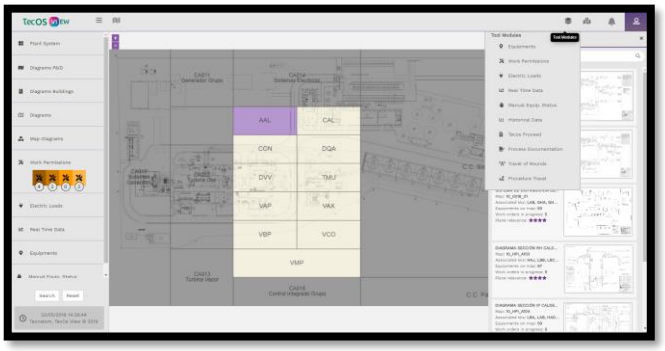

Figure 5. TecOS VIEW ™ interface. Navigation.

The user can search components obtaining the list of drawings where this component is represented and navigating through them.

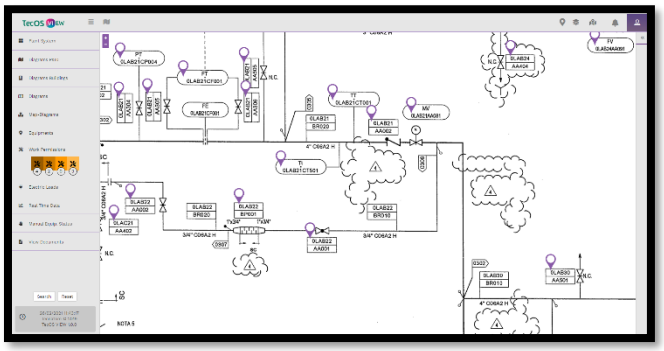

Figure 6. TecOS VIEW ™ interface. Components search.

TecOS VIEW ™ can also integrate over the diagram different layers of information. For that purpose, it is needed to connect the solution to the sources of information such as the document management system, asset management system or real-time data systems. The user can easily select which layer of information is to be represented over the drawing.

Users can get visualize the information they need in a comprehensive format that they are used to manage having interactive P&IDs.

III. USE CASES

A. Components Identification and Location

The first and more basic use case of TecOS VIEW ™ is the identification and location of tags throughout the plant. Taking advantage that all labels within the diagrams have been processed and characterized, plant personnel can now search for any tag and the system will provide a list of diagrams where such tag can be found.

Even though basic, this feature has been proven useful to a wide range of plant personnel roles. Some practical applications where this functionality has been proved useful are plant modifications, where engineering can easily limit the drawings revision scope based on the impacted components.

B. Work Permissions and Administrative Clearance

TecOS VIEW ™ provides the capability of visualizing over the plant diagrams all the open work permissions and the active administrative clearances. Additionally, the user can check all of those that apply to a certain component or working space.

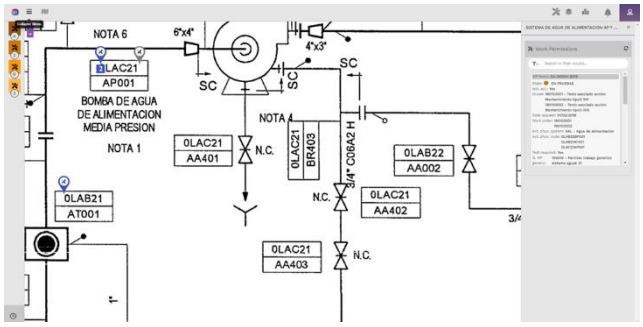

Figure 7. TecOS VIEW ™ interface. Work Permission.

This functionality allows the operation crew not only to focus on the information available in the DCS, but also have an overview of the plant and the related local works performed at any time. Considering the planification of works, the user can optimize such planning by easily checking the status of the applicable components and providing the best possible sequencing according to the location. This is achieved thanks to displaying the information of the components in the P&IDs.

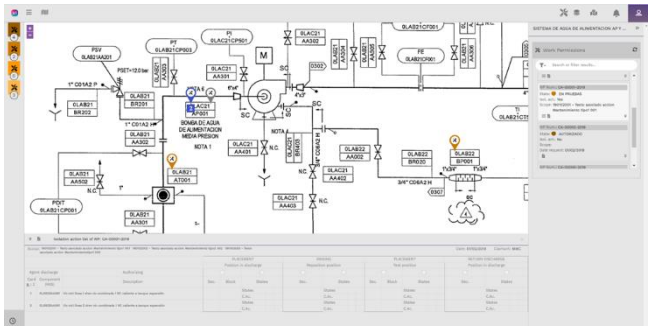

Figure 8. TecOS VIEW ™ interface. Work Permission Details.

C. Electric Loads Identification

During the planning of maintenance works, one of the most time consuming and prone to error is the identification of the power supply related to the components affected by the works. Using TecOS VIEW ™, the applicable power supply box for any component can be easily identified together with all the affected components.

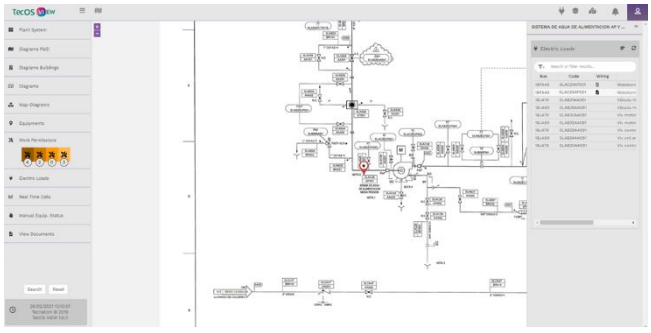

Figure 9. TecOS VIEW ™ interface. Electric Loads.

D. Plant Data Connection

The possibility of accessing plant process data when planning works is another of TecOS VIEW ™ capabilities. The user can see the process values such as temperatures, pressures, … in an easy way before authorizing any work.

Additionally, during the follow-up of the works, the diagrams will show how the different variables are being affected without the need to access the DCS or SCADA.

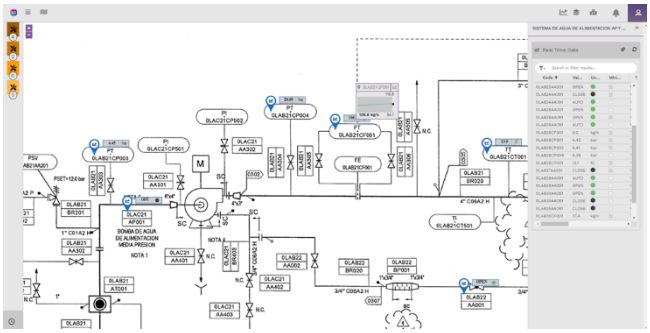

Figure 10. TecOS VIEW ™ interface. Process Data.

IV. IMPLEMENTING AN INTERACTIVE P&IDS SYSTEM AT NUCLEAR

Tecnatom is currently launching an implementation project of interactive P&IDs at a nuclear facility using TecOS VIEW ™ technology.

The project strategy agreed with the plant is starting with a Proof-of-Concept (PoC). The scope is optimized and the PoC focuses the efforts on validating the value contribution of the tool and the user experience.

The scope includes:

- Processing P&IDs and building drawings
- Searching components in drawings
- Navigation through drawings
- Easy view of clearances
- Access to information associated with the components
- Online and offline mode

The aim of the PoC includes identifying the best tablets to enhance user experience in the field; WiFi area needs and user experience in no WiFi areas. Also, during the PoC possible improvements to the tools may be identified from users' feedback and will be identified potential use cases that add more value.

This approach allows minimizing the effort required to make the best decision on the final installation in the plant. The results and conclusions of the proof-of-concept experience will be presented during the conference.

V. CONCLUSIONS

Interactive P&IDs like TecOS VIEW ™ is a promising technology which help the users at control room, field and the office to increase the efficiency while reducing the time needed for their tasks by having the information integrated, available and comprehensive. Getting an easy visualization of the information improves the decision-making process. As it is a collaborative tool, it enhances the coordination among the different departments and workers.

TecOS VIEW ™ is a flexible and scalable system with several different use cases and applicable to different departments within a nuclear power plant. The system can first be deployed working as a stand-alone solution leveraging a simple use case with the idea of increasing the number of use cases over time, as it is integrated with different sources of information.

Tecnatom is currently launching an implementation project of interactive P&IDs at a nuclear facility using TecOS VIEW ™ technology. Preliminary results and conclusions are promising that this approach may support the different use cases identified. However, the presentation should include more updated information including more solid results and conclusions of the proof-of-concept experience after the first months of user experience.

Proceedings of the European Nuclear Young Generation Forum
ENYGF'21
September 27-30, 2021, Tarragona, Spain

BIM digital twin associated with the design of passive fire protection

Sabater Sancho, Ignacio[1*], Pascual Rubio, Arturo[2], Real Soler, Juan Pedro[3]

[1] Grupo Dominguis Energy Services (GDES), Spain; [2] Grupo Dominguis Energy Services (GDES), Spain; [3] Grupo Dominguis Energy Services (GDES), Spain

*Corresponding author: i.sabater@gdes.com; a.pascual@gdes.com; j.real@gdes.com

I. INTRODUCTION

Since the implementation of Appendix R of the 10 CFR 50, some Nuclear Power Plants have been forced to install passive fire protection systems to reach and keep plants in safe shutdown conditions.

Particularly as far as fire protection rules is concerned, Spanish Nuclear Power Plants are subjected to IS-30 Safety Instruction which is mandatory. This instruction establishes the requirements for fire protection in Nuclear Power Plants in a deterministic way.

Due to the huge economic effort of reaching the requirements of the IS-30, several measures were put in place to adopt a risk-informed, performance-based Fire Protection License Base, according to NFPA 805.

The need to comply with the regulations described above forces Nuclear Power Plants to make a lot of design modifications, with the great complexity that this entailed.

Specifically, this regulation implied various design modifications related to the separation of redundant trains by RF-60 or RF-180 fire barriers from safety-related and non-safety-related electrical circuits that, due to a fire, may adversely affect the safe shutdown of the NNP. These modifications present a great challenge when designing the different protection configurations and obtaining their measurements due to the infinite number of interferences that exist and the difficult access to these trains in most cases, that makes the design process an inefficient and not very accurate work.

As a result of the process of continuous improvement and optimization of the different processes, Grupo Dominguis Energy Services (GDES) introduced for the first time at Vandellós II Nuclear Power Plant the process of digitization of nuclear facilities for the generation of the BIM digital twin associated with the design of passive fire protection. This implied the implementation of a new standard engineering design that has been spreading throughout the remaining Spanish nuclear plants.

Figure 1. Darmatt KM1 passive protection installed by GDES Auxiliary +108 Vandellós II NNP (Spain)

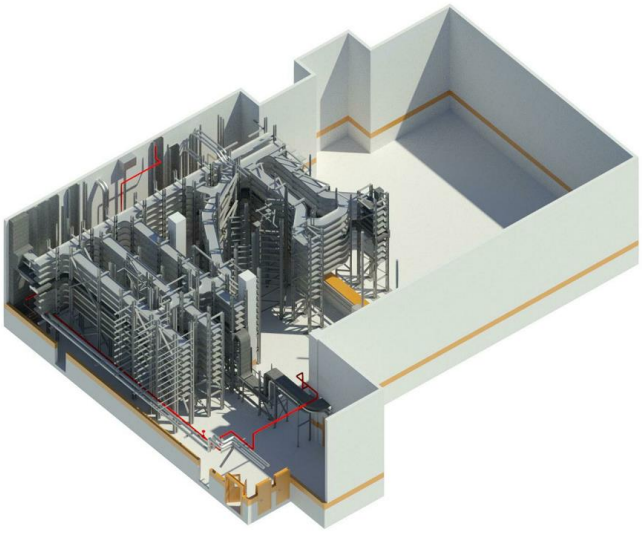

Figure 2. Digital twin for RF-60 passive fire protection design at Vandellós II NNP (Spain) Control Building, Elevation +100

II. DIGITAL TWIN

The term Digital Twin refers to the virtual reproduction of an installation and all the elements that it is made up of, both in geometric aspects and properties of each element. This definition is applicable either to the drafting of new construction projects or, in our case, to the existing installations such as Nuclear Power Plants.

The creation of the digital twin of the Nuclear Power Plants should be based on the generation of an As-Built LOD-500 BIM model from the installation`s points cloud obtained by a 3D Scan.

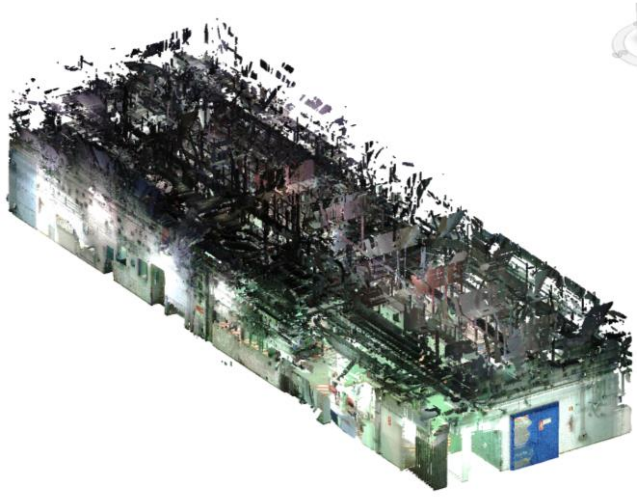

Figure 3. Remote Shutdown Panel Room Points Cloud Almaraz I NPP (Spain).

The methodology used by GDES in the Design Engineering phase of the "design, supply and installation of passive fire protection RF-60 and RF-180 projects" is based on the generation of the BIM digital twin on which the protections to be installed are designed.

III. DATA COLLECTION

The objective of data collection is to obtain the points cloud of the electrical conduits to be protected and their possible interferences. Then, subsequently process the data and join the different scanning points, generating a single points cloud over which the protection is modelled.

The methodology used in data collection represents an innovative and differentiating element with respect to that used in design modification projects in Nuclear Power Plants and more specifically in those related to passive fire protection, providing some competitive advantages.

E. Safety

The main objective of the nuclear industry is to guarantee the safety of the facility, people, and the environment. Data collection by 3D Laser Scanner is perfectly aligned with this objective since it reduces the risk to people by completely preventing work at heights, measurement of electrical conduits at heights and the assembly and disassembly of scaffolding.

F. Cost reduction

The use of the Scanner contributes to cut costs by eliminating the ones associated with the assembly of scaffoldings to get the accurate measurements. At first glance, this would seem a negligible cost. Nothing could be further from the truth, as there are hundreds of metres of piping, most of which are located at great heights, which entails an enormous cost, both in terms of material resources and staff, as well as economic resources. Using this technology, Almaraz I and II and Vandellós II Nuclear Power Plants have prevented the installation of a total volume of scaffolding of 450 m^3 and 125 m^3 respectively, in the last projects carried out, and have been able to assign these material and staff resources to other tasks.

Just as important as the economic costs are the costs in terms of the dose received by the staff during data collection. Traditionally, data collection in passive fire protection projects involved long periods of time on site measuring electrical conduits and their possible interferences, transferring them manually to CAD models and then verifying the measurements again. This methodology, besides being inefficient, involves long periods of time exposed to ionizing radiation and contamination risks. The use of this technology makes it possible to reduce costs in terms of dose to negligible levels, transferring the measurement process from the plant to the office thus, it is only necessary to be present inside the installation to place the scanner, allowing us to operate it remotely from points with a low dose rate.

Room	NPP	Scans	Volume
EK158	Almaraz Unit I	13	2980 m^3
EK158	Almaraz Unit II	22	2980 m^3
S20	Vandellós II	42	5760 m^3

Table 1. Volume of scaffolding saved on different projects

G. Accuracy

Traditionally, data collection is based on the preparation of dimensioned diagrams which in turn are based on the measurements obtained using a flexometer, which is an inefficient and inaccurate process making it difficult to accurately reproduce the installation due to the huge number of elements and measurements to be considered. The 3D laser scanner allows us to solve all these problems by obtaining a points cloud with all the elements of the installation with point position discrepancies of less than 2mm, something unthinkable to achieve manually.

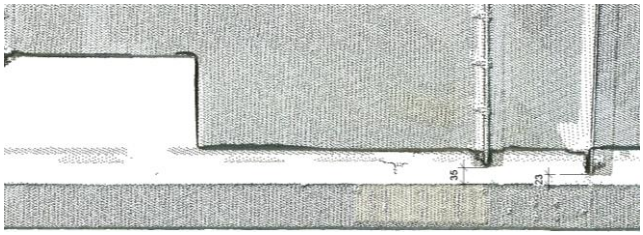

Figure 4. Point cloud of the detail of the distance between cable tray and HVAC. Almaraz I NPP (Spain)

IV. BIM MODEL

From the point cloud obtained, an As Built model of the installation is generated, focusing especially on the electrical conduits to be protected, as well as those elements that could interfere.

A. Passive protection design

The BIM As Built model of the installation allows us to design the passive fire protection having a global vision of the project and all its elements, verifying the necessary spaces due to the thickness of the protections, proposing alternative solutions in those places with insufficient spaces, allowing the design of alternative solutions.

Modelling the passive protections on the digital twin of the installation makes it possible to know with high reliability the material needs required for the design modification, thus reducing cost overruns associated with material over-ordering.

In the same way, knowing each of the configurations that make up the protection and their dimensions makes it possible to establish the execution time necessary to carry out the design modification, thus adjusting the necessary staff to meet the deadlines, therefore preventing cost overruns due to overstaffing.

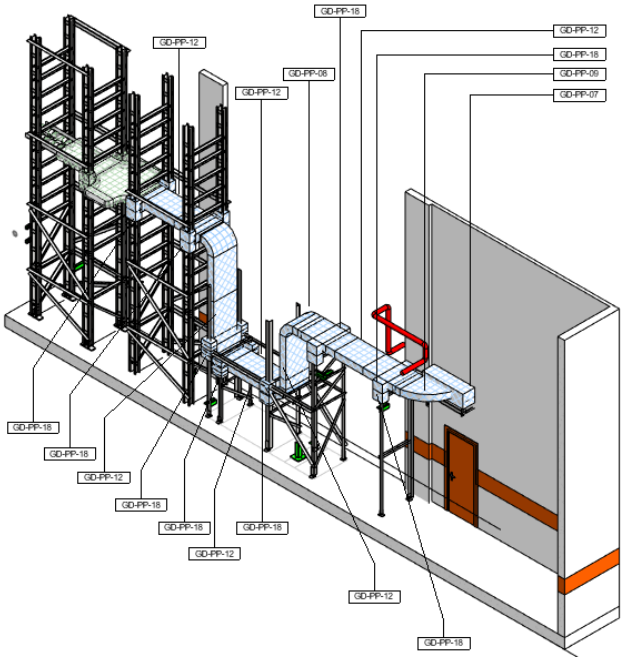

Figure 5. Modelling of electrical cable tray protections. Control Building, Elevation +100 Vandellós II NNP (Spain)

B. Manufacturing sheets

As a result of the modelling of the passive protections on the digital twin, we obtain the manufacturing sheets.

These are a set of exploded drawings of each of the elements that make up the protection and are made up of a series of sheets. The first of these refers to aspects related to traceability, indicating the exact location of the configuration to which the manufacturing sheet refers to. A control code is assigned, and it indicates both the traceability of the materials used at that point and the operations carried out by each worker.

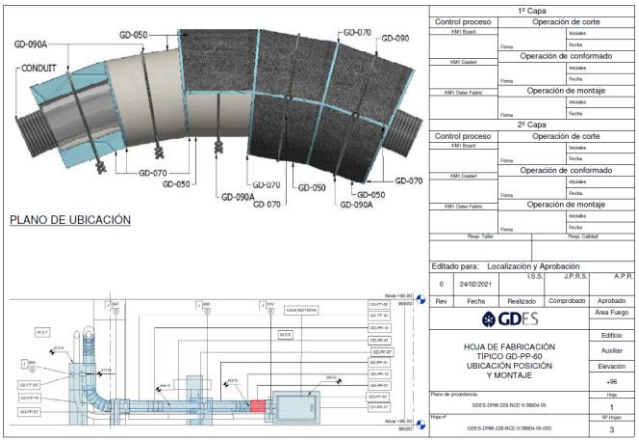

Figure 6. Cover sheet of fabrication sheet NCD V/36604 Auxiliary Building Elevation +96 Vandellós II NPP (Spain)

Due to the scale of passive protection installation projects and the large number of operations involved, it is often difficult to keep track of the actual state of execution. Thanks to the manufacturing sheet, we divide the total scope into small configurations to which we assign a code according to their state of execution, allowing us to keep a real and precise control.

The following sheets indicate the dimensions of the parts to form the protection allowing the operator to carry out the cutting tasks in a workshop area preventing the necessary dose associated with taking measurements of the parts to be manufactured.

C. Options

There are many options offered using this methodology: highlighting the possibility of modelling new elements to be installed in the floors from 2D plans and inserting them on the BIM digital twin or on the points cloud, allowing the analysis of the project feasibility, verifying interferences and realistically projecting the necessary design modifications.

Figure 7. MSR modelling. Turbine Building Vandellós II NPP (Spain)

V. RESULTS

As a result of this methodology, a digital twin of the installation is obtained, which includes all the elements identified according to plan coding and the modelling of the passive fire protection.

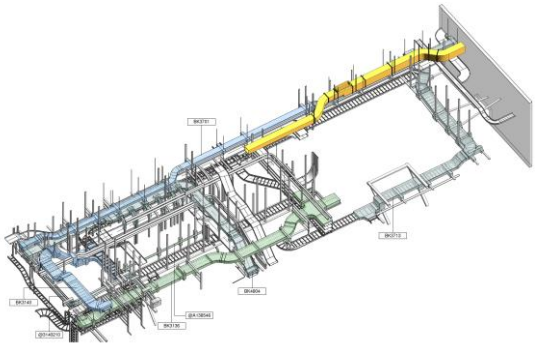

Figure 8. Digital twin of Remote Shutdown Panel Room Almaraz I NPP (Spain)

The model also allows NPPs to obtain 3D engineering drawings with a level of detail that would be difficult to achieve using other techniques.

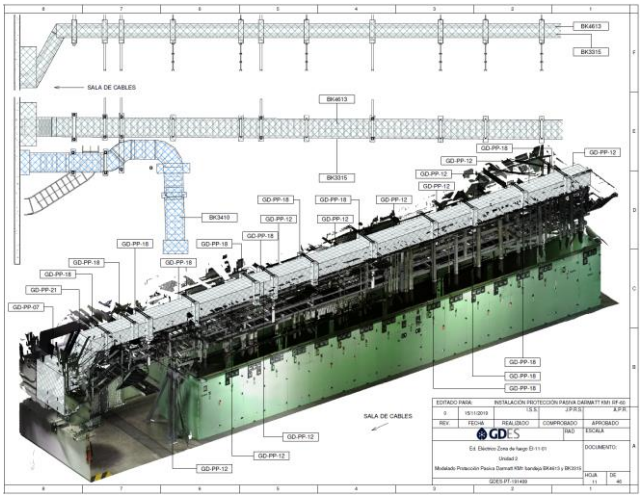

Figure 9. 3D plan combining the points cloud with the protection Almaraz I NPP (Spain)

In addition, 2D plan and elevation drawings combining the point cloud together with the protection modelling including the typical configurations to be installed on that section together with the surface area of each of one can be generated from the model.

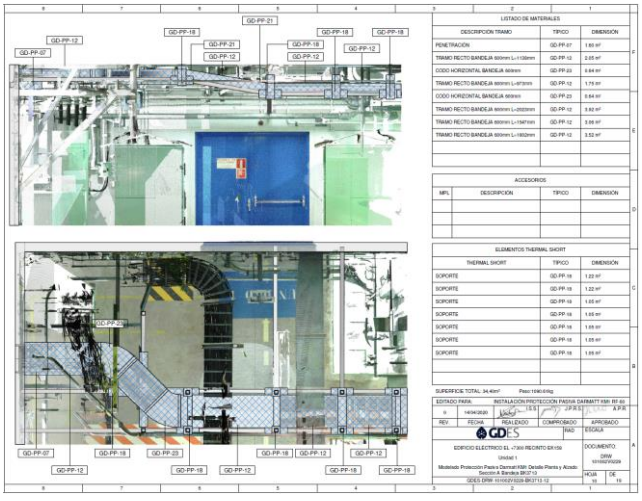

Figure 10. 2D plan combining the points cloud with the protection Almaraz I NPP (Spain)

This type of documentation is highly valued by Nuclear Power Plant engineers as it facilitates their understanding of the design modification, giving them confidence in the feasibility of the solutions adopted.

Valuable information in the form of measurement tables can be obtained from the BIM model of the installation. This methodology makes it possible to obtain measurements of any element in the plant either it is duct lengths, support element type and dimensions or the surface area required for the installation of passive fire protection.

Obtaining reliable data on the surface area required for the protection of the pipelines is essential both for the supplier when stockpiling materials and for the plant, as it allows the structural department to verify the validity of the support elements and/or to plan modifications whenever is deemed.

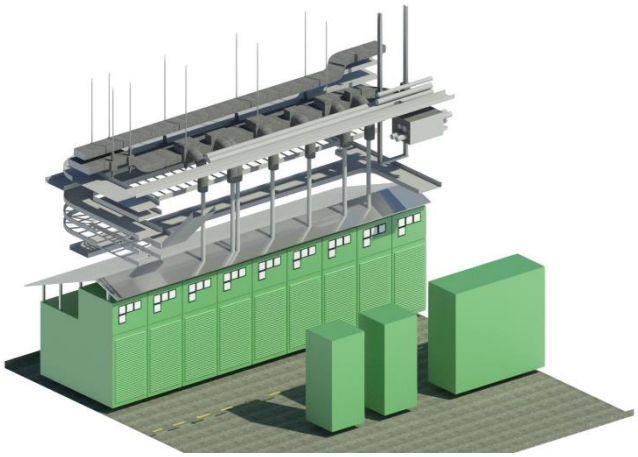

Figure 11. Digital twin of Remote Shutdown Panel Room Almaraz I NPP (Spain)

As an additional value, the use of the 3D Laser Scanner facilitates to generate a very useful photorealistic and virtual reality model of the installation, on which Pre-Jobs meetings, inspections, measurements of distances, surfaces, and volumes, identifying elements. Thus, reducing the dose received by the staff to 0 and without any risk to either people or to the plant.

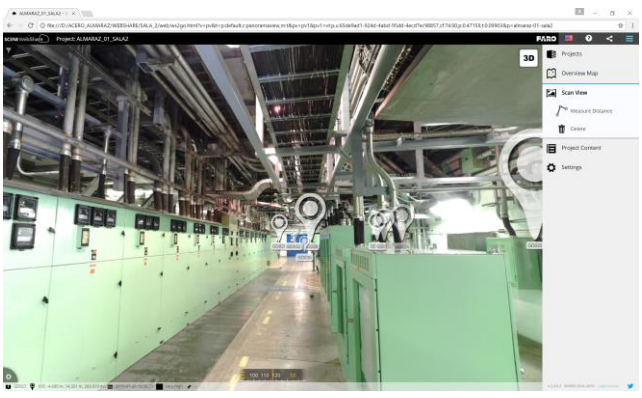

Figure 12. Photorealistic model of Remote Shutdown Panel Room Almaraz I NPP (Spain)

Proceedings of the European Nuclear Young Generation Forum
ENYGF'21
September 27-30, 2021, Tarragona, Spain

Vigia project: system based on UHF RFID technology to optimise control&monitoring in FME zones.

Mínguez Muñoz, Alberto*[1] , Roselló García, José Ignacio[1] , Concejal Bermejo, Alberto[2] and Pérez Tejedor, Porfirio[2]

[1] GD Energy Services, Spain; [2] Iberdrola Generación Nuclear, Spain

*Corresponding author: *a.minguez@gdes.com*

I. INTRODUCTION

GD Energy Services (GDES) is a Spanish family-owned Group with international presence, providing services for energy industry: nuclear services, decommissioning services, surface treatments, logistics, wind energy services and emergency response services.

The development of equipment for specific uses, together with the trials of GDES 's own staff during the testing stage, allows GDES to know how that equipment works. GDES with its client's orientation is committed to solve any kind of problems since it has a Technological Development area for the development of measured solutions (GDES Innovation), and a high number of experimented technical staff in continuous training.

VIGIA project belongs to nuclear services area, specifically to the Operation&Maintenance support business, one of the GDES key areas with over 85 years of experience (maintenance services, support for refueling services, radiological emergencies, waste management, decontamination, etc.).

In nuclear sector preventing foreign material presence in certain zones is highly important. An undesirable presence of an object in a specific zone could develop considerable damages to the NPP equipment (for example, to fuel rods). To manage it, NPPs are organized in levels of FMEZs (Foreign Material Exclusion Zones) depending on their implicit risks.

Nowadays, although the FME control plans are improving in NPPs, they are still based on manual controls. In the FMEZ, materials are tracked and identified manually, which, in many cases, is time-consuming, requires a lot of manpower and involves a high risk of human error.

Introducing processes and procedures digitalization in FMEZs management is an innovation initiative with exponential benefits regarding to the needed investment. GDES analysed the opportunity and decided to introduce wireless technology (UHF RFID) in this scenario [1] [2] [3]. UHF RFID technology reduces the spent time on material monitoring and tracking tasks and brings down both the number of staff assigned to the tasks and the possibility of error. At the same time, it provides added value to this activity, since it gives greater control over aspects such as verification that tools are appropriate to the task in hand, their correct use, their condition and/or calibration, and their radiological characterisation. It also makes it possible to easily locate lost tools anywhere in the FME work areas.

VIGIA is a combined hardware and software system to control and monitor materials in FMEZs using RFID (Radio Frequency Identification) wireless technology. The requirements to be met were specified by IBERDROLA GENERACION NUCLEAR:

- Compliance with electromagnetic interference regulations.
- Tags must not interact with the use of MTE (Material Tool Equipment).
- Tags must not become foreign materials in the FMEZ.
- Mobile, autonomous and modular system.
- Future-proof and user-friendly.

II. DESCRIPTION

During the 22nd refuelling outage at Cofrentes Nuclear Power Plant (Valencia, Spain), GDES implemented its innovative technological system: Vigia. A combined hardware and software system to control and monitor materials in FMEZs using RFID (Radio Frequency Identification) wireless technology. This project was designed with the aim of optimising the time that workers spend in the FMEZ with or without MTE (Material Tool Equipment). It also introduces functionalities that complement current MTE monitoring and tracking tasks, such as time spent by workers in specific zones, calibration status of equipment, and intensity of use of specific tools and equipment.

The Vigia system is made up of several mobile beacons for tracking PMTE (Person Material Tool Equipment), programmable tags adapted to PMTE and portable units for both logging the tags and checking&monitoring MTE.

The mobile beacons consist of a reader that can be attached to several antennas. These antennas can cover a wide-ranging area, over 3 meters. The range is adjustable and can be adapted to the environment in which each beacon is set up, allowing compliance with electromagnetic interference regulations.

Figure 1. Vigia System at Cofrentes NPP.

In turn, each beacon has presence-sensing features within the field of action of the antennas, which enable them to be shut down and automatically reset if necessary. This system of sensors boosts efficiency and reduces false positives and incidents. It is also capable of determining whether the user is entering or exiting an FMEZ.

Beacons have a GUI (graphical user interface) that enables the user to interact with the Vigia system. The GUI connects to a database containing information on all tagged PMTE, which is updated in real time with the portable units. In addition, each beacon stores all the information on the sensors, reader status, operation of the antennas, and movements detected by it, both by logged PMTE and tags that have not been logged. The beacons have a UPS capable of keeping them running for one hour in the absence of a power supply, which means they can be relocated within the plant without having to be switched off. Each beacon measures 30 cm x 30 cm x 130 cm and weighs less than 20 kg, has in-built wheels and can be moved without any auxiliary aids.

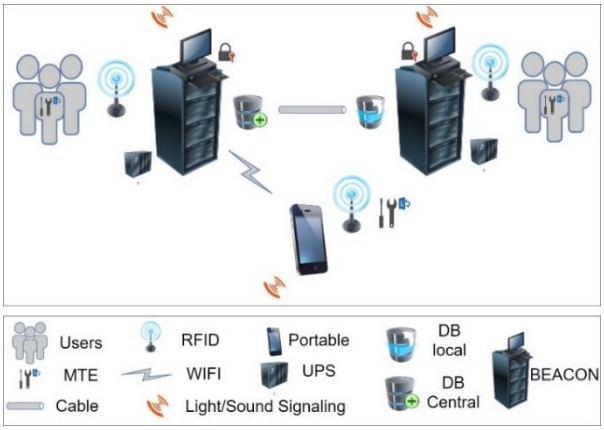

Figure 2. System Overview.

In addition to the mobile beacons, Vigia has battery-powered portable units for logging all new material and for monitoring the real-time status of PMTE in the FMEZ. This unit is synchronised with the mobile beacons, thus streamlining the process of logging PMTE. Another feature of Vigia's portable units is the search for lost or misplaced MTE. It has several operating modes, which include indiscriminate or selective MTE searches.

Figure 3. Components. Mobile beacons and portable reader.

One of the most relevant aspects of the design and development of Vigia was the selection and installation of MTE tags. For this purpose, a market study was conducted. The first step was to note the different materials on which they were to be installed, the use of the MTE by operators

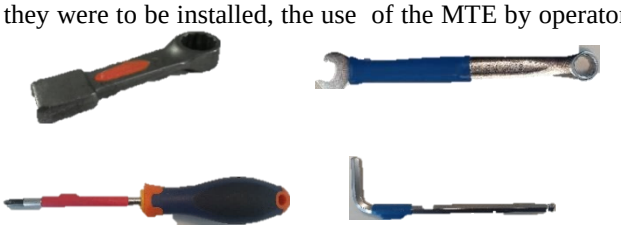

Figure 4. Tagged tools.

and the size of the MTE.

Five models of tags were selected, adapted to metallic and non-metallic materials. Their size ranges from 0.5 to 2 cm^2, with a volume less than 3 cm^3. The MTE selection criteria were: resistance to wear and tear, best coverage/tag size ratio, maximum available memory in the tag and reliability in repetition test in the use of MTE.

To facilitate installation of the tags and to prevent them from detaching, including in the event of improper use of the MTE, durability tests were carried out on products that had been tagged.

Figure 5. Refuelling Outage Tools.

III. RESULTS AND DISCUSSION

Vigia was implemented at the Cofrentes Nuclear Power Plant during the 22nd scheduled refuelling outage, which took place between 3 November and 6 December 2019. Prior to the refuelling outage, the tools in the different trolleys serving the tasks performed on site were tagged. Along with the tools, material and equipment within the FMEZ or that those were expected to be introduced to the zone later on were also tagged. People were also monitored with the same UHF RFID technology, to track the MTE along with the people associated with the MTE.

To monitor PMTE, two Vigia beacons were installed at the FMEZ access points. These beacons acted as entrance/exit barriers to the FMEZ.

The use of this technology provided real-time control of PMTE in zone. Vigia boasts various functions. It can be used to produce reports, detect MTE or work-related incidents, view PMTE inside the FMEZ, alongside a wide range of options for instantly acquiring and processing associated data, leading to greater, more flexible and higher-quality control over the FMEZ supervision tasks.

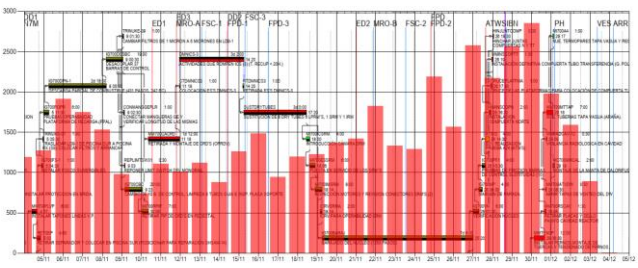

Figure 6. PMTEs detected during refuelling.

In Figure 6, the vertical columns are the quantity of inputs and outputs in beacons during all days of the refuelling outage. During the Vigia system operation, 790 hours uninterrupted, 1.000 MTEs and 250 persons were tracked generating 16.000 and 45.000 records respectively.

After completing all the works of the refuelling outage, the MTEs were examined to check the integrity of the RFID tags and the coating applied to hold them. During the inspection, no anomalies were detected on either the tags or the coating.

IV. CONCLUSIONS

The implementation of VIGIA had some demonstrated advantages such as:

- Real-time control of PMTE in the FME zone.
- Reduction of time spent on material monitoring and tracking tasks.
- Reduction of the staff assigned to activity control in FMEZs.
- More flexible and higher-quality control over the FMEZs supervision tasks.
- Enhances tasks&incidents control during periods of burdened work, such as refuelling outages.
- Instantly acquiring and processing associated data: use of tools, calibration date, radiological characterisation, time spent in specific areas…
- Reduction of potential human errors.
- Locate lost MTE easily.
- Automatic report generation.
- Eliminates paperwork.

In conclusion, although this was the first time that this system had been implemented at Cofrentes Nuclear Power Plant, and therefore had no prior experience to draw from, this project has demonstrated that RFID technology enables supervisors conducted through an FMEZ to respond quickly and specifically to real incidents that may occur during periods of complex work, such as refuelling outages. The digitization of the information from the tags enhances decision-making, provides automated control of on-site tools and eliminates paperwork – and the potential for human error – from the monitoring and logging processes. This technology also enables complementary functionalities to be added to current MTE monitoring and tracking tasks, such as time spent in specific areas, equipment calibration status, intensity of use of specific tools and equipment and, in general, a wide range of use options thanks to its tailor-made software.

The future development involves new technologies like Artificial Intelligence, Deep Learning and Machine Vision to improve the input and output process. The stored data during the 22nd refuelling outage is being used to make prediction models to help FME human supervisors to schedule future tasks.

V. REFERENCES

[1] *Radio Frequency Identification (RFID) Technology Trends and Power Plant Applications* EPRI, Palo Alto, CA:2004. TR-1003733

[2] *NRC, 2003, "Guidelines for Evaluating Electromagnetic and Radio-Frequency Interference in Safety Related Instrumentation and Control Systems," 1.180, U.S. Nuclear Regulatory Commission, Rev. 1.*

[3] *Guidelines for Electromagnetic Compatibility Testing of Power Plant Equipment: Revision 4 to TR-102323. EPRI, Palo Alto, CA:2013. TR-102323-R4.*

Proceedings of the European Nuclear Young Generation Forum
ENYGF'21
September 27-30, 2021, Tarragona, Spain

Innovative technology and O&M solutions for NPPs

Roselló García, Jose Ignacio[1*], Alcaraz Pieters, Daniel[1], and Mínguez Muñoz, Alberto[1]

[1] GD Energy Services S.A.U. (GDES), Spain

* Corresponding author: j.rosello@gdes.com

I. INTRODUCTION

GD Energy Services (GDES) is an international service provider to the energy industry, leader in nuclear services and decommissioning, surface treatment, industrial maintenance, renewable energies and emergencies.

Operation & Maintenance Support (O&M) is one of the main service areas of GDES, including, among other activities: maintenance services, waste management, fuel movement support, support for refuelling services, radiological emergencies, and decontamination. In this regard, GDES has been undertaking industrial cleaning and radiological decontamination services since its creation in 1977, with the aim of being able to handle materials while reducing the risk of contamination dispersion, the radiological cost of operations with affected materials, the volume of radioactive waste, and confining contamination. Outstanding among GDES's specialist services are those of radioactive decontamination and maintenance, an activity that is currently carried out in Spain, France and UK.

The previous experience acquired in radioactive decontamination and maintenance has allowed GDES to accumulate the necessary knowledge to develop procedures, equipment and systems, that allow the optimization of the work in terms of time, dose and safety and security. In this paper we present several of these developments, as well as the benefits obtained after their implementation.

II. DESCRIPTION

Thanks to its strong commitment to research development and innovation, GDES delivers innovative technology and tailored solutions for Nuclear Power Plants operation and maintenance.

Innovation at GDES is developed by, and for, all its stakeholders, staff, partners and customers.

Hereinafter the main areas of activity of GDES Innovation area, and some of its main exponents, are exposed.

A. FME: Equipment for Removal, Collection and Characterisation of Debris in the NPP's Pools

Since long time Nuclear Industry has been applying dedicated politics to prevent Foreign Materials reaching equipment and systems of NPP's. FMs can easily reach the bottom of NPP's pools due to falls during maintenance works or because of materials handling in the primary circuit.

FM presence can result in damage of components in the pools, increased radiation levels, degradation of systems and their performance, unscheduled outages or outage extension.

Despite constant efforts to apply and improve FME procedures, in some isolated cases FM's get to NPPs pools and must be retrieved.

GDES has developed dedicated equipment for object retrieval (Reshand© and Demos©), as well as equipment for debris analysis (Filtrabris©), providing innovative technology to FME issues: mitigation (avoiding damage by debris) and correction (allowing root cause removal). All this equipment can work in combination, thus enhancing its effectiveness and allowing a wider range of application.

Reshand© is a robotic arm for objects retrieval in NPPs' pools:

- Semi-automatic, remotely operable by one single worker by means of an electronic control glove.
- Mounted at the extremity of a pole and equipped with 2 cameras, it easily allows to recover objects of different kind, size, and geometry.
- Wide range of applications: modular system with different easily setup configurations, completed with a set of interchangeable tools (clamps, pliers, etc).

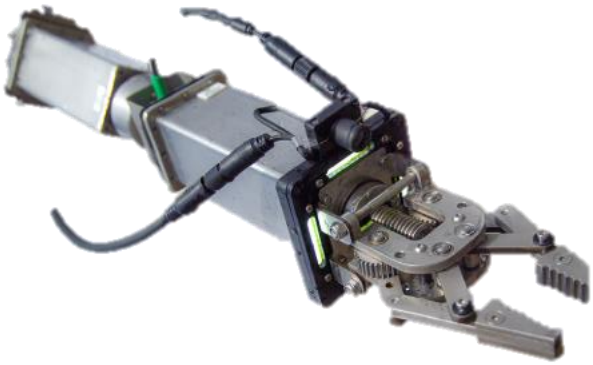

Figure 1. Reshand©, remote operated robotic arm for objects retrieval

Filtrabris© is an aspiration and filtration system for the analysis of debris accumulated in NPPs' spent fuel elements:

- It couples to the lower end of the fuel element; debris filter removal, in fuel elements equipped with this element, is not required.
- Vacuum debris is collected into a canister filter equipped with camera and lights for visual inspection.
- Fuel channel crud is collected into a second cartridge filter of high filtering capacity to prevent from spreading it in the pool.
- Debris captured in the canister filter of the Filtrabris can be remotely manipulated and collected by Reshand. Reshand also supports localized aspiration in inaccessible areas.

Figure 2. Filtrabris©, aspiration and filtration system for the analysis of debris accumulated in spent fuel elements

Demos© is a Remotely Operated Vehicle (ROV) for the mechanical cleaning and decontamination of floor and walls of NPPs' pools:

- Decontamination by brushing and vacuuming, operating in conjunction with a water filtering system.
- Operational doses reduction during decontamination works in NPPs' pools.
- Decontamination with the reactor cavity flooded, allowing critical path schedule compression.
- Remote control operation with on-line viewing and video recording of the activity, allowing the inspection of the reactor's pools to find FM.
- Demos© robot can work alone or in combination with Filtrabris© (after the scrubbing, the vacuumed particles are filtered, inspected, and collected for further analysis and disposal).

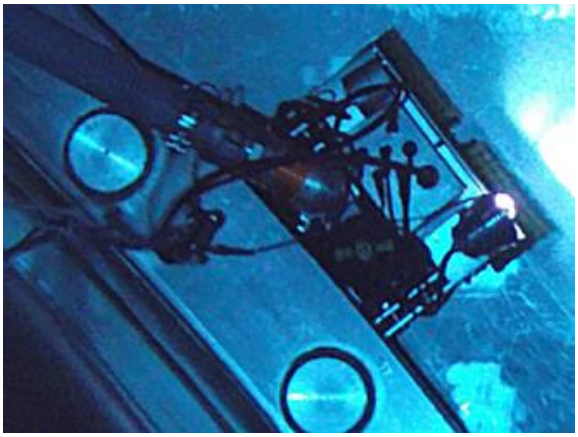

Figure 3. Demos©, ROV for underwater mechanical cleaning and decontamination of NPPs' pools

B. Remote Systems and Automation to Reach Higher Safety Levels, Schedule Compression and Operational Dose Reduction

Maintenance and inspection of equipment and components in nuclear power plants often entail high radiation exposures. Most of these tasks are carried out during shutdowns, during which it is also required to minimize actuation times to reduce the critical path.

Pre-decontamination works reduce final operational doses. If, in addition, the tasks are carried out remotely, operational doses are minimized, and times are shortened. Finally, the execution of certain applications under water allows to carry out the works without entering the critical path.

In this sense, GDES develops customized equipment for improvement of specific processes, automating tasks and allowing their execution remotely, to reach higher safety levels, reduce operational doses and shorten schedules. As examples, TrackRing©, LD4+©, Tirant© and Drumcar© are described below.

TrackRing© is a ROV for underwater cleaning and decontamination of the reactor vessel flange:

- Adaptability to the flange of any NPPs, even with guide pins, caps housings or upper internals present.
- Minimize operational doses to workers during this activity.

- Elimination, by brushing, vacuuming and filtering the remains of the seal without damaging the surface of the flange.
- Perform cleaning under water, reducing critical path schedule.
- Ability to view online and video signal recording.

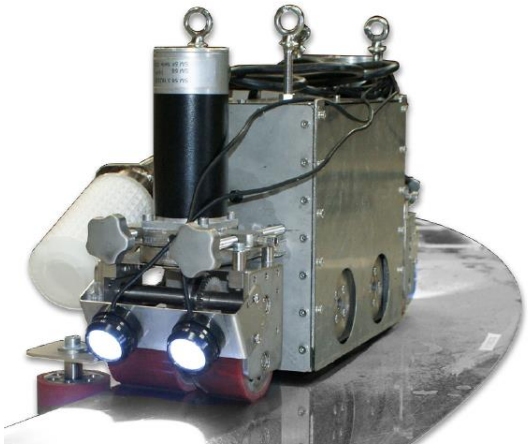

Figure 4. Track Ring©, ROV for the underwater cleaning and decontamination of the reactor vessel flange

LD4+© is a robot for mechanical cleaning of reactor vessel bolt housings:

- Decontamination and cleaning of reactor vessel bolt housings in any LWR, regardless of vessel or bolt diameter.
- Can be either autonomous or remotely operated, with or without the reactor head in place.
- Remote control operation: on-line viewing and video recording of the activity.

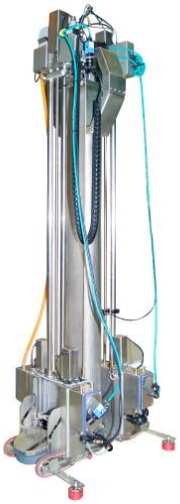

Figure 5. LD4+©, robot for mechanical cleaning of reactor vessel bolt housings

Tirant© is a robot for arc-spry metallization of large bore pipes:

- Automatic arc-spray metallisation process of the inner surfaces of pipes.
- The resulting coating has anticorrosion properties, as well as increased hardness and therefore abrasion resistance.
- Minimises radiation dose and other operational risks workers might otherwise be exposed to.

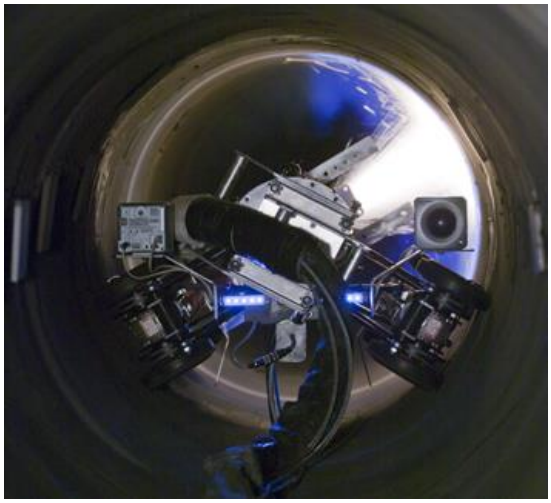

Figure 6. Tirant©, robot for the arc-spry metallization of large bore pipes

Drumcar© is a radioactive waste drum characterizer:

- Optimization and Automatization of drum characterization process.
- Process scanning, information traceability, paper removal.
- Dose reduction, safety improvement and human error reduction.
- Acquisition of radiological and dimensional data with plant equipment.
- Compliance with the cybersecurity procedures of the installation.

Figure 7. Drumcar©, radioactive drum characterizer

III. RESULTS AND DISCUSSION

The described equipment has been developed by GDES Innovation as tailored solutions for specific O&M support activities. In this sense, GDES has carried out the following services and implementations over the last few years:

- Reshand© implementation in Cofrentes and Almaraz NPPs (2017 and 2018 outages), both for objects retrieval in the containment pools and for handling radioactive waste and moving materials in areas of difficult access or with risk of radiation and contamination, such as a solid waste interim storage facility.
- Underwater decontamination of containment pools with Demos© ROV in Cofrentes, Trillo and Laguna Verde NPPs, during different outages (2013-2021). Common operations:
    a. Elimination of solids accumulated in the reactor pool during fuel change operations.
    b. Decontamination of NPPs' pools prior to refuelling outage.
    c. Inspection of NPPs' pools to find FM.
- Underwater decontamination of reactor vessel flange with Track Ring© ROV in Trillo NPP, during different outages (2015-2021).
- Arc-spry metallization of the Cross-Under's inner walls in Laguna Verde NPP (2010).
- Drumcar© implementation in a Spanish NPP (2020), for radiological characterization of nuclear waste drums stored in the temporary solid waste warehouse (ATRS).

The benefits of previous interventions and implantations are summarized in:

- Reach of higher safety levels.
- Minimization of operational doses, optimizing ALARA practices.
- FM inspection and retrieval, preventing their entry into the systems.
- Reduction of critical path activities times, during outages.

Proceedings of the European Nuclear Young Generation Forum
ENYGF'21
September 27-30, 2021, Tarragona, Spain

Non-essential chilled water refrigeration unit installation.

Deltoro-Deltoro, Javier[1*], Flores-Martín, Raquel[1]

[1] Iberdrola Generación Nuclear, Spain

*Corresponding author: *jdeltoro@iberdrola.es*

I. INTRODUCTION

Cofrentes NPP Non-essential chilled water System (P44) was originally designed with two redundant 100% capacity units (4200 KW) to supply 7 ºC water for several Plant's HVAC. Some of this equipment are the responsible to maintain the regulated temperature in the Primary Contention or in the Main Turbine Hall.

The two refrigeration units of the P44 were oversized so from the beginning of the Plant operation some other consumers were added to the System. The following figure shows the original and added consumers to the System.

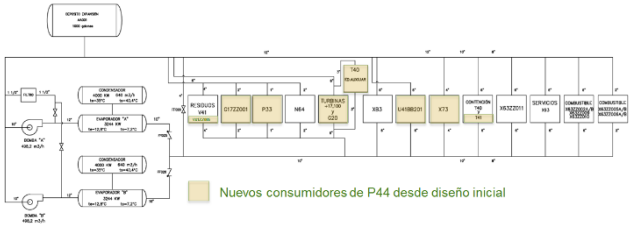

Figure 1. Original and new consumers of the System

The refrigeration units were designed in the mid 70's with the refrigeration gas R22. The European Rule 2037/2000 prohibited the use of the R22 gas from January the 1st 2014, so Cofrentes executed a Project for substituting the R22 for the R507. This Project was made in just one of the two units with the aim of evaluating the results. The result was a 30% loss of performance compared to the originally refrigeration power. Consequently, the other unit remain with the R22.

In 2014, the Rule 517/2014 was developed by the European Commission, prohibiting the use of any gas higher Global Warming Potential (GWP) than 2500. The R507 has a GWP of 3985.

The situation of the new consumers added to the System and the Regulation status made Cofrentes to take action.

II. ALTERNATIVE ANALYSIS

In 2018 a detailed analysis of different alternatives was fulfilled to recover the original refrigeration power and comply with the European Rules.

Two main alternatives were stablished: either the replacement of the existing Units or the installation of a third Unit.

The replacement of existing Units was discarded since:

- During the execution time estimated in 4 months, the System would dependent of just one Unit. Any problem with the running Unit would cause a complete loss of the System.
- Both Units are physically near, so there would be a risk of affecting the running Unit during the substitution works of the other.
- Access to the room were the Units are located is relatively small. This would compromise the manoeuvres and hinder the substitution.

The installation of a third Unit alternative was the selected. It could be fulfilled by two options:

- Installation in the Main Turbine Building
- Installation in the Electrical Building Roof

The Main Turbine Building option was discarded because there would be a long distance to the existing Units. Thus the new piping isometric to install would be longer than 150 meters, which would difficult the System operation from a hydraulic point of view.

Consquently, the chosen option was the Electrical Building Roof installation, since the existing Units are located just below the roof and this location was empty. This resulted in a somehow easy and hydraulically convenient installation.

Once a third Unit installation was the chosen alternative, the next step was the selection of the type of refrigeration technology. The first decision were to keep the gas refrigeration technology, but with a four-generation gas (HFO) that complies with the European Rules, avoiding the restrictions imposed.

The third Unit selected was a two stages centrifugal compressor, liquid condensing, 5000 KW refrigeration

power (30 % higher than the existing), with a R1233zd gas (GWP of 7).

III. DESIGN

With the new third Unit installation in a two units System design, it was necessary to develop numerous series of calculations.

The new Unit must be inserted in the hydraulic circuit of the non-essential chilled water System and added as a new consumer of the Service Water System (P41) as the Unit condenser would be fed from this System.

From a civil point of view the Electrical Building Structure also needed to be analysed as the new Unit weighed near 30 tons.

From an electrical point of view there was the need to enlarge one of the Plant main electrical 6,3 KV frames to feed the 1 MW power consumption.

The mechanical piping design scope changes included ten 12" butterfly valves, six 10" butterfly new valves, 35 small diameter valves, more than 220 piping fittings, 39 meters 12" pipe and more than 100 meters of small diameter pipe.

The electrical design scope changes included more than 2,5 kilometers of wiring.

The civil design scope included the following modifications:

- Pillar's reinforcement
- New Unit housing. The new machine was not permitted to be placed outside.
- Improved access to the Electrical roof. The existing access to this location was by a vertical ladder from inside the Building.

The following figure shows a scheme of the new Unit Housing.

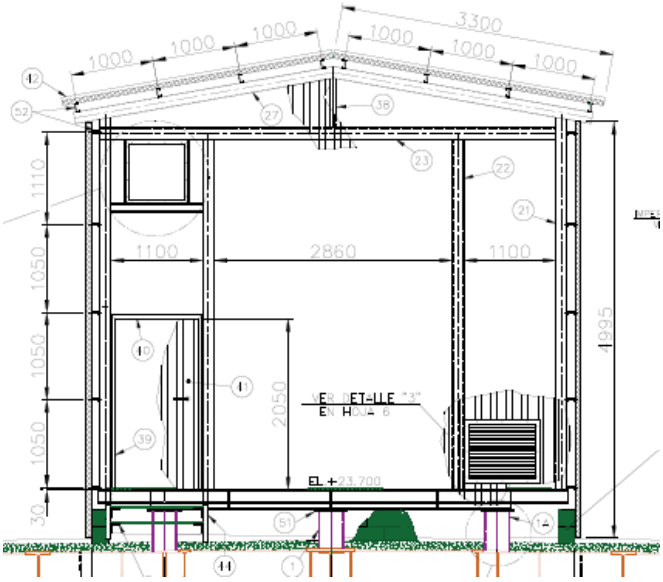

Figure 2. New Unit Protection housing

The necessary modifications defined previously were documented in four Plant Modification Packages:

- OCP 5464: New refrigeration Unit Installation
- OCP 5487: Plant interfaces
- OCP 5494: Fire Protection modifications
- OCP 5488: Plant Electrical Frame enlargement

IV. EXECUTION

The Project execution began in the 22th outage in 2019. The 6,3 KV Electrical Frame enlargement was not compatible with the Plant operation as this Frame already feeds many others equipment.

At the beginning of 2020 the Plant Interfaces were executed. These Plant interface modifications that is, the hydraulic connections to the existing P44 and P41 system were executed. Once these connections were established, the rest of the Project could be developed with no interference with the Plant normal Operation.

The following pictures show details of the Electrical Frame modification and existing System interface connections.

Figure 3 and 4. Electrical and interface modifications

The new Unit installation works began in April 2020. The execution conditions were:

- Four main disciplines involved and related: Mechanical, Electrical, I&C and Civil.
- Environmental conditions.
- Large interferences with existing installations.
- Execution with the Plant operating.
- Installation of the new Unit in a location at 23 meters from the ground.
- COVID-19 pandemic.

The tasks began with the pillar's reinforcement. The reinforcement was made in the different Building elevations. An example is shown in the following picture.

Figure 5. Pillars reinforcement (before and after)

Afterwards, the civil works in the roof were fulfilled. A new concrete basement for the equipment was built and once it was finished the new Unit was lifted from the ground. To do so, two cranes were needed: one of 130 tons and other of 500 tons.

The following pictures shows the Unit basement and the lifting of the Unit.

Figure 6. New Unit basement

Figure 7. New Unit lifting

Simultaneously electrical and instrumentation wires and equipment were installed and tended. One of the main instrumentation tasks was installing a local control unit of the new Unit inside the Plant to ease the operation. By this means, Operation Staff could operate the new Unit without accessing to the Roof.

Figure 8. Redundant Local Control Unit

Finally, the New Unit Housing were built and the mechanical piping was connected to the existing systems.

Figure 9. New Unit Housing

The execution process took five months involving more than 16 companies and 80 professionals. The tasks were developed under the strict sanitary conditions imposed by the COVID 19 pandemic with no infection.

V. COMMISSIONING

Once the installation of the new Unit was finished a numerous series of tests were fulfilled by the Operation Staff to assure the new Unit could be declared operable, as:

- New Unit operating in pararel with an existing one
- Stop of an operating Unit and automatic start of a the new Unit
- New Unit operation with the two System Pumps

These tests took approximately two weeks and were successfully passed.

VI. OPERATION

In late July 2020 the new Unit was put in operation as main System Unit, supplying chilled water to all the System consumers. The most demanding conditions happened during August 2020 with outside temperatures higher than 40 ºC. In this condition the new Unit worked with no failure producing approximately a 70% of its rate refrigeration

power. This 30 % margin in the worst condition, assure the proper performance of the Unit.

VII. CONCLUSIONS

Developing and fulfilling the Project took two years and a half took from the Analysis phase till the end of the Commissioning. The Project involved a series of difficulties summarized in modifying an originally two Unit System to implement a third one, execution works with the Plant in operation in a location at 23 meters from the ground and with the sanitaria restrictions due to the COVID 19 pandemic.

Nevertheless, the Project complied with schedule and budget and the new Unit performance was even better than predicted.

VIII. GRATITUDES

This Project could not has achieved successfully without the strong effort of Simón Olivera Carbonell responsible of the design area, Raquel Flores responsible of the execution and Evaristo Pitaluga as responsible of Operation and Commissioning

Proceedings of the European Nuclear Young Generation Forum
ENYGF'21
September 27-30, 2021, Tarragona, Spain

Corrosion monitoring in steel structures of the reactor´s vessel at the Vandellós I Nuclear Power Plant – Dormancy period

Durán López, Javier[1*]

[1] ENRESA, Spain

*Corresponding author: jdul@enresa.es

I. INTRODUCTION

Vandellós I ended its activity in October 1989 after 17 years of operation due to the effects of a fire that significantly affected the site, although there were no environmental consequences regarding radioactive emissions. The proprietor (Hifrensa) decided to proceed with shutdown in view of the elevated cost of restarting activity after the fire, in compliance with the requisites established by the Spanish Nuclear Safety Council (CSN).

During the second stage, entrusted to the National Radioactive Waste Company (Enresa), all installations, buildings and structures outside the reactor´s vessel were dismantled, and the reactor´s vessel was confined. On June 30th 2003, Enresa completed dismantling.

During 2004 the site was prepared for the dormancy period (for a duration of 25 years), both from the functional and organizational/personnel structure point of views. Once the reactor was sealed, most of the location was recovered.

Since then, and after the favourable assessment of CSN on December 15th 2004, the site is licensed to remain in a passive state, with the corresponding surveillance to guarantee its safety, store certain radioactive materials and to ensure the confining of remaining structures. This license will be valid until the next stage of dismantling, the documentation for which must be presented to CSN at least one year in advance.

The dormancy period lasts approximately 25 years, which allows a significant reduction of radiological levels. After this period ends in 2028, dismantling of the remaining installations will be carried out in more favourable conditions. This basically will involve the building that houses the reactor, which is complete shutdown, and all the auxiliary buildings remaining.

Every five years, tests are carried out to ensure the reliability of the static confinement of the reactor´s vessel, which ensure the correct state of conservation of the vessel's internal structures. These tests were carried out throughout the 2020.

II. SURVEILLANCE OF METALLIC STRUCTURES

Within the five-year tests that were carried out throughout 2020, the corresponding ones were carried out to determine the degrees of corrosion of different structures and components associated with the reactor´s vessel. For this presentation, those reports corresponding to the inspection of the internal structures of the reactor´s vessel, as well as the reinforcements that are embedded in the reinforced concrete that makes up the main structure of the reactor´s vessel, and the inspection of the metal structure of the Weather Protection Building, which is attached to the reinforced concrete structure of the reactor vessel, will be analysed.

All tests and inspections are carried out within the framework of the Surveillance Plan and the Technical Specifications that are in force at the facility, and which are mandatory.

After carrying out the tests and inspections, different forms are filled in and the corresponding reports are drawn up showing the results obtained.

A. Atmospheric corrosion monitoring inside the Reactor´s Vessel

As previously mentioned, in application of the Surveillance Plan and the Technical Specifications in the latency phase of the Vandellós I NPP, it is necessary to carry out an evaluation of the possible risks of corrosion of the interior materials of the reactor´s vessel, including the original materials of the installation and the control elements introduced later.

Studies carried out on the conservation of the internal structures of the reactor´s vessel establish that the effects of corrosion will not compromise its general behaviour, although it may lead to the detachment of certain pieces, especially those of small size. Therefore, it is necessary to

carry out a periodic monitoring program of these structures in order to avoid this situation.

In 2000 an "R&D Study for the monitoring of the corrosivity of the internal atmosphere of the reactor´s vessel" was prepared. From the conclusions of this study and since 2002, the temperature and relative humidity inside the reactor´s vessel are being monitored and the atmospheric corrosivity towards different types of structural steels is being evaluated.

The tasks that are included are the following:

-Semester collection of electrical resistance data in the three test wells.

-Temperature (T) and Relative Humidity (RH) data collection inside the reactor´s vessel, which can justify differences in atmospheric corrosivity, between the three wells in the reactor´s vessel through which the corrosion rate is measured.

-Execution of the gravimetric measurements plan, so it will be necessary to remove specimens that have already completed their cycle inside the reactor´s vessel and install other new gravimetric specimens to replace the withdrawn ones.

For the execution of the gravimetric measurements plan started in 2002, three types of steel were chosen: ASTM A516 Gr.60, ASTM C1035 and F1252 as representative of the existing structures inside the reactor´s vessel, exposing a total of 162 specimens (54 of each type of steel).

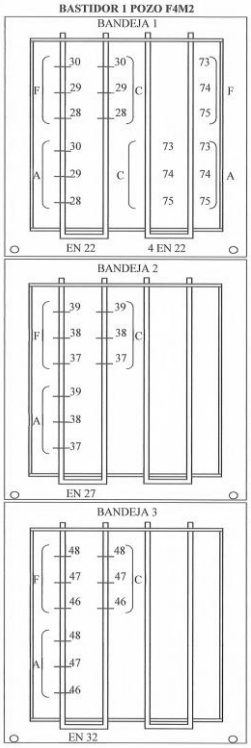

Figure 1. Distribution of the gravimetric specimens currently installed in the three trays of the frame located in well F4M2

Specifically, in 2020, several gravimetric specimens were removed. Some of them have been exposed for a total of 18 years, while others have been exposed for 5 years. Simultaneously, that same day, a new series of specimens of the three steels were installed, together with three relative humidity and temperature sensors for the fifth study period.

The study is carried out in triplicate, by exposing three specimens of each steel in each of the three wells and exposure time. Specifically, the UNE-EN ISO 11844-2 standard is followed.

The removed specimens have been weighed, after carefully cleaning them to eliminate adhering dust, and the increase in mass due to the formation of corrosion products has been obtained.

Subsequently, a pickling is performed, which causes a loss of mass that must be taken into account to correctly evaluate the loss of mass due exclusively to the corrosion process.

Therefore, the difference in mass that has occurred before and after exposure is measured, determining the corrosion rate that this steel has suffered during the exposure time.

B. Corrosion monitoring in reinforced steel in the reactor´s vessel

According to what is established in the Latency Phase Surveillance Plan of the facility, a five-year monitoring of the behaviour of the concrete and the reinforcement of the reactor´s vessel must be carried out.

After the study of the previous reports and the preparation of the measurement equipment, an inspection was made for the location of the reinforcements, the concrete surface and the electrical connections with the reinforcement embedded in the concrete were checked. This was done to carry out electrochemical measurements and make a record of environmental parameters.

To carry out this control, eighteen points are measured at three different levels, specifically at levels 16, 30 and 47, taking a minimum of two measurements, at two different locations, within each point.

In this way, the corrosion potential, the intensity of the corrosion (by the modulated confinement method) and the resistivity of the concrete (by the galvanostatic pulse method) are checked.

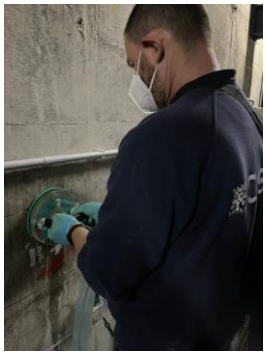

Photography 1. Taking measurements on site

Corrosion potential

The measurement of the corrosion potential consists of determining the electrical potential difference between the steel of the reinforcement and a reference electrode that is placed in contact with the concrete surface. For this,

different types of reference electrodes are used, the most common being copper / copper sulfate reference electrodes for field measurements.

Resistivity

The measurement of the resistivity of the concrete helps to interpret the value of the corrosion rate, since it is closely related to the humidity content of the concrete.

It is measured by the method of "current interruption" by which the instantaneous voltage drop is recorded when an electrical signal is imposed and then it is cut. In this way the calculation of electrical resistivity is obtained from known geometric parameters.

Corrosion intensity

Corrosion intensity is the only electrochemical parameter that allows the kinetics of the corrosion process to be quantified. Polarization resistance is the technique that has been used the most to measure the corrosion rate in reinforced concrete reinforcements.

C. Weather Protection Building inspection

The purpose of the inspection is to evaluate the state of the building and indicate the proposals for action if necessary, based on the evolution of the damage found in the inspection.

• Exterior Inspection, which affects elements only accessible from outside the building.

• Interior Inspection, which will be carried out from inside the building.

From the development of the inspection, a report is generated with the following content:

• Form with general inspection information.

• Conclusions: depending on the damage observed and its estimated evolution, it is indicated if special studies are necessary or if an action on the building and the action period is necessary.

• Annexes with the damage files in the elements inspected by each area. Includes photographs of the observed deterioration.

To carry out the inspection, the criteria established in the standards UNE-EN ISO 4628 “Evaluation of the degradation of Coatings” and UNE EN ISO 12944 “Protection of structural steel” have been followed.

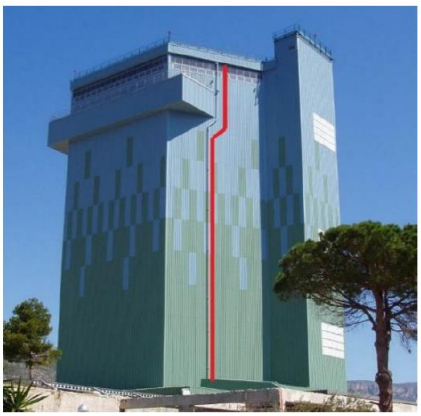

Photography 2. Exterior appearance of the Weather Protection Building

Metal structure evaluation criteria

The number of evaluation points adopted correspond to the approximate criteria of one evaluation point per 100 m2 of total structure, approximately equivalent to the criteria of evaluation points separated every 9.00 - 10.00 m, whether it is in vertical or horizontal walls. The distribution of the number of evaluation points between the different areas has been carried out in proportion to the evaluated area, trying to round to multiples of 10.

The evaluation points will be chosen in such a way that they represent as closely as possible the state of the area. All evaluation points will be uniquely identified by alphanumeric coding, so that the traceability of the evaluation carried out is never lost.

Enclosure panels evaluation criteria

The following evaluations were carried out on each panel (4x1 meters):

• 2 evaluations of the degree of oxidation in areas away from folds

• 2 evaluations of the degree of blistering in areas away from folds

• 2 evaluations of the degree of incision corrosion in the bending area of the panels

III. RESULTS AND CONCLUSIONS

A. Atmospheric corrosion monitoring inside the Reactor´s Vessel

The visual appearance of the specimens at the time of removal indicates the formation of few corrosion products. Obviously, a greater abundance of corrosion products is also observed as the exposure time increases to 18 years.

In the same way, the average increase in mass due to the formation of corrosion products is measured for each type of steel as a function of the exposure time. Below is an example of these graphs:

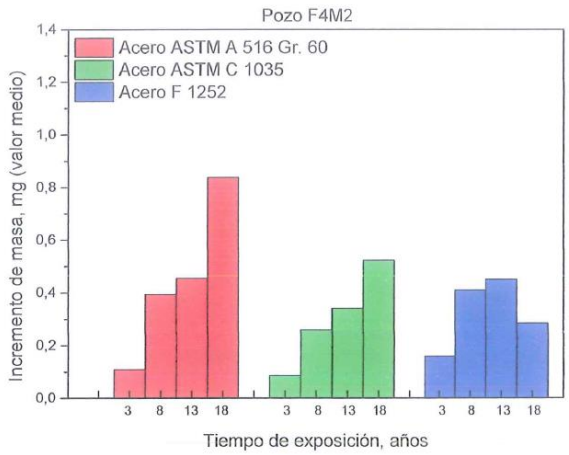

Figure 2. Mass increase data (mean value), in mg, of the three steel in well F4M2

From the observation of these graphs, it can be deduced that, due to the low corrosion rates obtained both by electrical resistance measurements and by the gravimetric method, the possible corrosion suffered by the internal structures of the reactor´s vessel is negligible.

B. Corrosion monitoring in reinforced steel in the reactor´s vessel

Once the results of the electrochemical measurements have been obtained, it was observed how all the evaluated parameters are within the limits established as negligible corrosion or low risk, according to the given interpretation criteria.

No signs of corrosion are detected in any of the evaluated areas, which indicates that the structure is still in what is called the initiation period (prior to the depassivation of the reinforcement), without having reached at this time the propagation stage.

Table 1. Summary of the results obtained in the field evaluation by electrochemical techniques.

	MEDIDAS PUNTUALES		PROMEDIO MAPEOS	
	Icorr(uA/cm2)	Ecorr(mV)	Ecorr (mV)	Resistividad (KΩ.cm)
A1	0,001	13,6	76,0	338,9
A2	0,035	47,8	112,3	174,6
A3	0,017	62,4	94,2	317,9
A4	0,001	89,8	99,7	312,8
A5	0,003	116,2	103,4	213,9
A6	0,009	29,7	-7,6	189,6
B1	0,018	130,1	133,0	226,7
B2	0,015	141,4	156,3	275,7
B3	0,048	128,3	137,6	236,5
B4	0,037	116,1	120,1	269,1
B5	0,034	100,7	110,7	206,5
B6	0,025	-53,4	120,5	391,1
C1	0,067	45,5	131,9	209,4
C2	0,002	121,2	114,3	293,7
C3	0,002	169,5	151,9	260,3
C4	0,015	76,9	5,9	280,4
C5	0,016	92,5	103,5	181,8
C6	0,012	79,1	34,2	308,8

C. Weather Protection Building inspection

As a result of this inspection, it is concluded:

• The metal structure shows a high degree of oxidation in the area of elevation +16.00, especially in the profiles located in a horizontal position, due to the accumulation of dust and other aggressive environmental agents.

• In the rest of the structure there are only specific areas with low degree of oxidation.

• In any case, a general cleaning of the metal structure is recommended to remove dust and dirt.

• The condition of the cladding panels is acceptable on the outside, not being significantly affected by corrosion or fatigue processes. Only two panels have been detected in an unsatisfactory state, with a local loss of the coating paint, probably due to being badly applied in the factory, but without affecting the galvanic protection.

• The interior face of the panels does not show atmospheric corrosion. Its appearance is good.

• From the fastening screws of the enclosure panels to the metal structure, a representative sample has been collected to measure their loss of mass. The conclusion is that the loss is less than 3%. Therefore, the advance of corrosion in the screws will not be a problem during the Latency Phase and it is not foreseen that it will be necessary to implement additional maintenance measures, except the periodic replacement of some lost screws.

• Nor have fatigue problems been detected in the cladding panels

• The downspouts show occasional deteriorations, which must be repaired as part of the routine maintenance of the installation.

IV. FINAL CONCLUSIONS

The results obtained in the tests of surveillance and structural control of the reactor´s vessel have shown its integrity and good condition.

In addition, even though the weather protection building has suffered at some points the action of corrosion, this will not affect its structural integrity. Only minor repairs will be necessary.

The next tests will be held in 2025.

V. REFERENCES

[1] Empresa Nacional de Residuos Radiactivos, S.A. S.M.E., “ESTRATOS” magazine, number 124, April 2021.

[2] https://www.enresa.es/eng/index/activities-and-projects/dismantling-and-environmental-restoration/dismantling-of-vandellos-i-nuclear-power-plant

Proceedings of the European Nuclear Young Generation Forum
ENYGF'21
September 27-30, 2021, Tarragona, Spain

Advantages of Implementing Computer-Based Procedures

Barroso, Javier [1], Ramos, Mateo [1], Gil, Javier [1],

[1] Tecnatom, Spain

*Corresponding author: *jbarroso@tecnatom.es, mramos@tecnatom.es, jgil@tecnatom.es*

I. INTRODUCTION: CONTEXT

The majority of today's nuclear power plants fleet is still running its operation and maintenance using paper-based procedures (PBP) and therefore incurring in a great number of inefficiencies such as the cost associated to the management of the paper records and the difficulty to know the progress of the executions.

In order to prove the value and cost reduction to a nuclear power plant site, Tecnatom has been working together with the site management to define the best possible deployment strategy of TecOS PROCEED ™, Tecnatom Computer-Based Procedures (CBP) system specifically designed and developed for the nuclear sector, and to quantify the cost reduction impact of such change.

A. Deployment Strategy Evaluation

One of the main challenges when deploying a new system that covers such a wide scope and implies so many changes in the organization processes, is to define the right deployment strategy for the nuclear facility that generates quick wins and adds value from the very beginning of the process. Additionally, as any relevant modification of the working processes, it shall be executed incrementally and focusing on the higher impact areas first.

Considering such approach and with the idea of providing a sound plan to the nuclear power site, the conversion of procedures was identified as the bottleneck and cornerstone for a successful deployment of the system. Even though TecOS PROCEED ™ has been developed considering this fact and therefore one of its characteristics is that procedures are edited and converted using Microsoft Word, there are still many tasks and steps until each procedure can be placed into production in the platform. These tasks range from document formatting to aids definition and insertion to consistency verification with the master copy of the procedure.

Evaluating the strategy from the benefits perspective, the implementation of CBP systems provides the strongest advantages from the paper management side. This means that the greater impact generated by the digitalization of procedures is related with the optimization and / or elimination of printing, transporting, scanning, reviewing and archiving of the paper records. Therefore, there is a direct relationship between the number of executions of a procedure and the cost and manpower reductions produced by the digitalization of it.

Besides the paper management improvement, CBP systems that do not rely on PDF as the digitalization format have other benefits that increase exponentially with the number of executions of each procedure. Systems such as TecOS PROCEED ™, which allow the input, archiving and processing of data during the normal execution of the procedures, enable the application of online data verification, simple historic data comparison and advanced data analytics. This is another factor to weight in the deployment strategy definition and that supports the idea of beginning with those procedures that accumulate a larger number of executions over time. For a certain site with three reactors, the distribution of procedures execution is as shown below in Figure 1 where more than 70% of procedure executions by Operations are related with surveillance procedures ("PV" in the figure), when compared with the other types of procedures (the other acronyms in the figure).

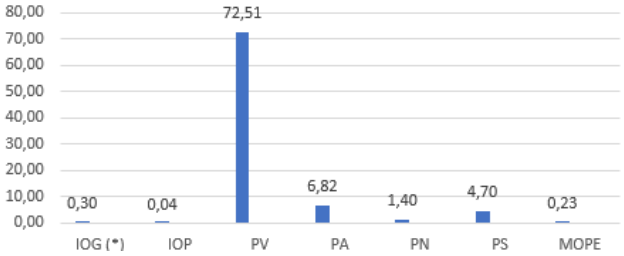

Figure 1. Distribution of executions among procedures types.

B. Procedures Digitalization Prioritization: Surveillance Procedures

Once the strategy is clear, converting first those procedures with more executions, an evaluation of plan procedures historic data is needed in order to identify which are the more often executed procedures. When tackling a task like this, the first thing one realizes is that there are no clear and accessible records of the procedures execution and therefore it is necessary to review the procedures archives and count the executions within the period of time. In case the power plant has had a CBP solution implemented, such query would have been rather simple and definitely cheaper to execute.

Based on the data collected from the nuclear power plant site, a basic analysis was done showing that Surveillance Procedures are those more frequently executed with a big difference compared to the rest of procedures as shown in Figure 1 and Figure 2. This result, even though surveillance procedures are not the type of procedures that would come up to your mind when thinking about CBP systems, is totally obvious considering that some of these procedures are executed on a daily basis and even more often. In case the desired scope is even narrower, eighteen procedures gather almost 75% of the total procedures' executions as it clearly seen in Figure 2 below.

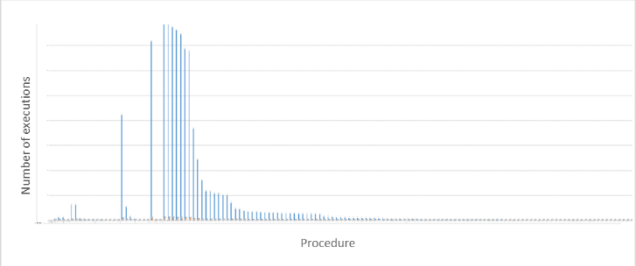

Figure 2. Distribution of executions by procedure.

Additionally, the digitalization of Surveillance Procedures and its integration in a CBP system not based on PDF, such as TecOS PROCEED ™, has further benefits derived from the nature of these procedures. As Surveillance Procedures include the registry of many values from readings to parameters gathered during tests execution, they open the potential application of execution aids and data analytics.

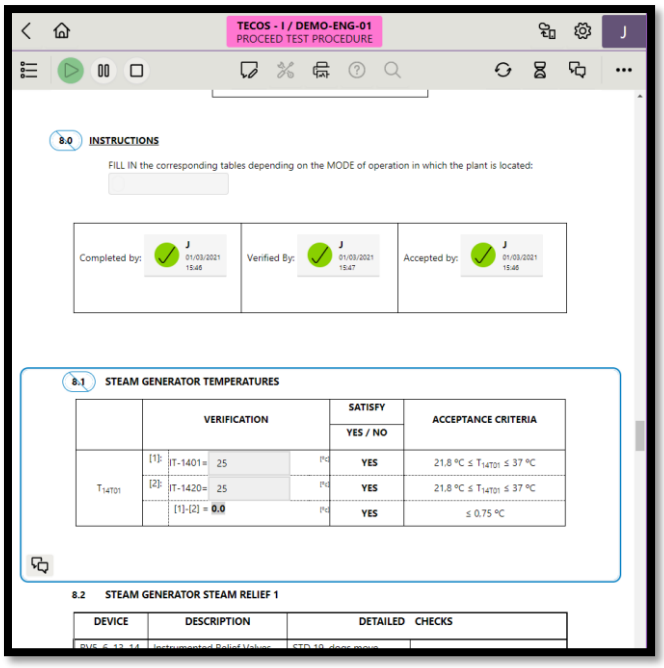

Figure 3. Procedures execution aids applied to acceptance criteria.

Procedure execution aids in CBP systems that allow data entry, recording and management can be applied in different ways, being available in TecOS PROCEED ™ the following ones:

- Dynamic limits, which alert the user if the entered value is outside of the limit
- Automatic formulas that avoid the need of manually calculating the formulas taking advantage of the processing capabilities and reliability of the computing device.

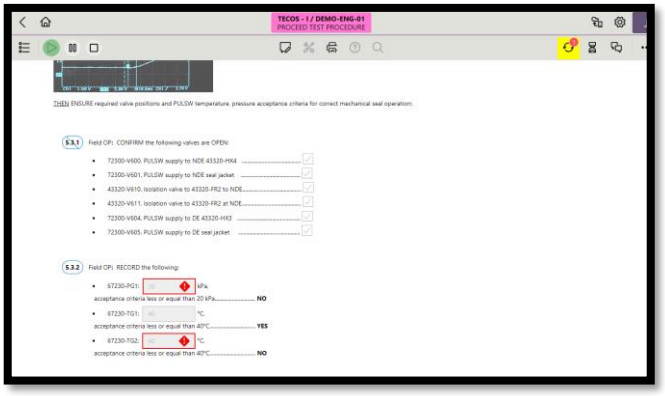

Figure 4. Dynamic limits and auto-verification surveillance requirement.

These aids enhance the correct execution of the procedures and streamline the review process.

Data analytics is the other application enabled by the availability of historic records of the execution. TecOS PROCEED ™ allows access to data, which was before only available on paper and that took a huge effort to extract to a digital file where it could be processed, with no additional effort. The data can be processed not only to show trends on the readings and values, but also high added value information such as components degradation indications by comparing the performance over different tests.

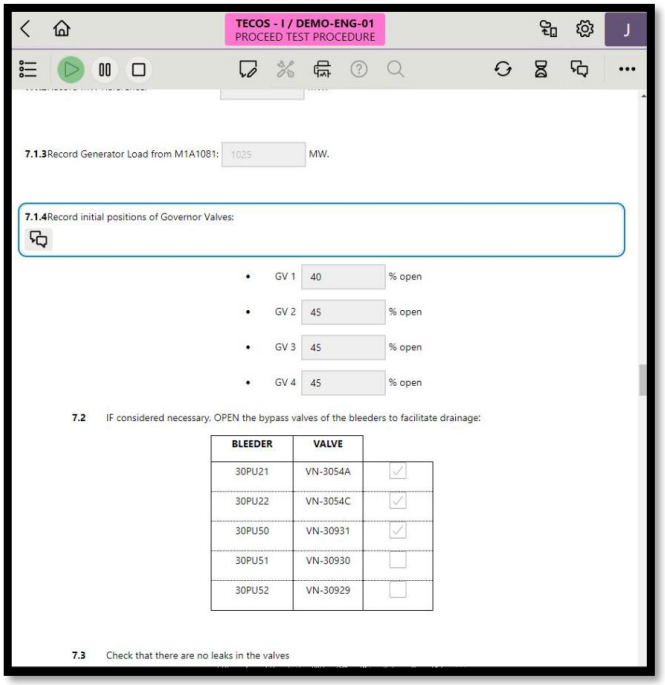

Figure 5. Analytics can be performed on all entry records.

II. BUSINESS CASE ANALYSIS

Taking the deployment strategy and prioritization defined in the previous section, a business case is built over that base. This business case is developed together with the operator

of two nuclear sites and covers the main benefits identified during the Proof of Concept and the subsequent clarification meetings. These benefits can be both tangible and intangible, meaning that such business case needs to be tailored and adapted to each case.

A. Economic Savings

Direct economic savings may be the center piece of any business case. In this area, there is a list of administrative processes associated to the management of paper-based procedures, which is clearly optimized thanks to the implementation of a digital solution. The processes where these economic savings can be seen due to the deployment of a CBP system are:

- Planning
- Movement of procedures around the facility
- Reviewing of the execution
- Scanning
- Archiving and registry

Once the processes are identified, it is also necessary to work to quantify how much manpower is spent on those tasks and what would be the difference once the new system is in service and has been running for several months, that is, once the learning curve has flattened and the new processes are solid within the organization. The result of such evaluation was that, from a conservative perspective and for a site with two reactors, at least five thousand hours (5,000 h) would be saved from low added value tasks. Besides the tangible side, these new processes would bring some other indirect advantages such as the paper and printing cost reduction, not to mention the positive environmental impact of paper use reduction. Those savings only consider operations procedures. If the scope includes maintenance procedures, the savings would be much higher.

Another positive impact when accounting economic cost savings is the reduction of delays during refueling outages. During such time, there is a higher number of activities within the facility and more personnel, both internal and external which has a high risk of resulting in delays and therefore affect the availability of the nuclear power plant. The impact associated to the verification of the execution of the procedures and the compliance with the surveillance requirements, the interruptions during the operations to check the planification and the search for registries are the higher impact areas during an outage. It is estimated that delays can account up to five fours of unavailability along the overall refueling outage.

B. Procedure execution aids

When considering the implementation of a Computerized Based Procedures system, one of the intangibles that shall be considered is the benefits that such system has over the safety of the facility. Advanced CBP systems that allow the user to input, register and manage data have the capability of limits verification, formulas calculation and image attachment to the records. These functionalities optimize the execution of the procedures and reduce errors.

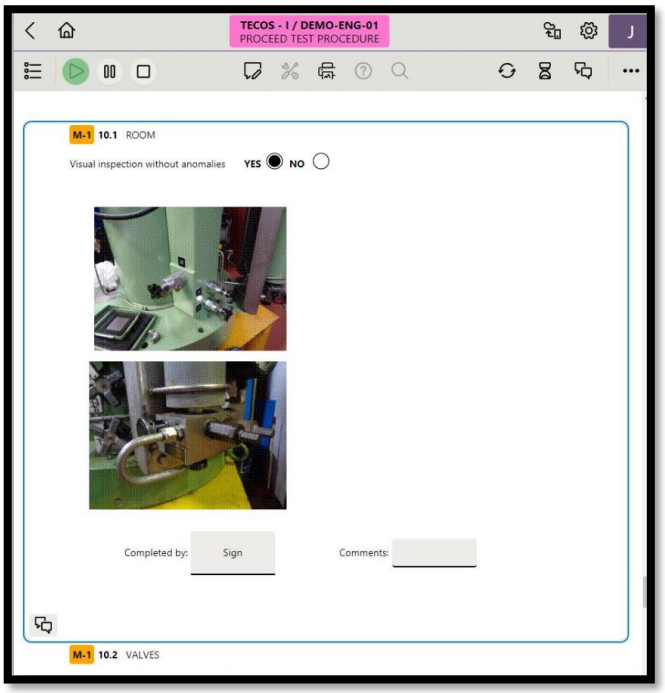

Figure 6. Attachment of pictures to the execution.

C. Data availability and usage

The implementation of advanced CBP systems support the digital transformation of the organization, pushing it to be more data driven. Availability of data recorded during the execution of the procedures and its readiness to be consumed without any additional cost, has a value in itself. From data availability point of view, the benefit is related with:

- More data available to be processed without any additional cost
- Data is in context and allows comparison between different executions of the same procedure
- Data analytics, where data can be processed to evaluate equipment degradation, plant personnel performance or deviations from the expected values
- Dashboards and advanced visualizations to support the decision-making process

Having data available is the first step towards a data driven organization, which subsequently supports informed decisions and more accurate risk management.

Figure 7. Dashboards with TecOS PROCEED ™ data.

III. CONCLUSIONS

Implementing a Computer Based Procedures system is a relevant challenge for any organization since it covers such a wide scope and implies so many changes in the processes, therefore a clear deployment strategy focused on adding value from the beginning is needed. Through this paper, we have described how Tecnatom has accompanied an operator of two nuclear sites in the strategy definition and subsequent business case for the deployment of TecOS PROCEED ™ for operating procedures. Such deployment has been planned and defined to maximize TecOS PROCEED ™ use and take advantage of its related economic benefits as soon as possible by prioritizing the inclusion of the Surveillance Procedures in the system.

TecOS PROCEED ™ and its capabilities as an advanced Computer Based Procedures system have been designed and developed having in mind the needs and use cases of nuclear power plants. Additionally, the benefits and advantages not only focus on what can be done today, but on what will the organization need tomorrow to be more efficient, more reliable and safer.

Proceedings of the European Nuclear Young Generation Forum
ENYGF'21
September 27-30, 2021, Tarragona, Spain

Suitability of Small Two-Bar Test for Estimation of Tensile Test Parameters

Joshi, Aniket[1*]; Forsey, Alex[1]; Moat, Richard[1]; and Güngör, Salih[1]

[1] Department of Materials, School of Engineering & Innovation, The Open University, Milton Keynes MK7 6AA, United Kingdom

*Corresponding author: *aniket.joshi@open.ac.uk*

I. INTRODUCTION

The tensile test is widely used to gather insight into a material's basic mechanical properties. This testing methodology for materials has been codified into standards. The ASTM E8/E8M standard [1] is one such example. These tests are routinely used to examine structural integrity for the life extension of reactors. Its utility is even more pronounced as the current Gen-III reactors begin to reach the end of their lifecycle.

The ASTM E8 standard recommends various gauge lengths for tensile testing. Gauge length refers to the length of the specimen expected to undergo deformation. This varies from 200 mm for a plate-type standard specimen to a 25 mm gauge length for a "sub-size" specimen. However, this gauge length is exclusive of the overall specimen length. This, in turn, means that a sub-size specimen, which has the smallest dimensions according to the E8/E8M standard, can be as long as 100 mm.

The E8 standard is not the only one that codifies sample dimensions. With similar dimension ranges proposed by various standards worldwide, the constraints arise in the gauge length availability when not enough material is available.

On another spectrum of materials' testing, residual creep life tests require similar specimen dimensions for their analysis. The ASTM E139 standard [2] is one of the numerous standards that provide specimen dimension guidelines. The specimen dimensions are similar to those suggested for tensile testing as well.

Due to the long durations involved in creep testing, novel methods have been proposed to scale down the size of the specimens involved, thereby reducing the amount of material used, in addition to the decreased time required for testing. The benefits of a miniaturized specimen are numerous. As mentioned by Hyde et al [3], there are strong driving forces for the development of these techniques, such as (a) to make effective use of limited material, especially from reactors to irradiate the least amount of sample possible; (b) extract the least amount of material possible so as to not tamper with the structural integrity; (c) More tests can be performed where material is scarce, such as in weldments.

The Small Punch Test (SPT), which was pioneered on the work by Manahan et al's [4] 'Miniature Disk Bend Test', is codified in the European Code of Practice [5] for tensile and creep testing. It uses a disc of diameter 8 mm and thickness 0.5 mm for its test.

Another recently developed testing methodology, the Small Two-Bar Test (S2BT), for miniaturized specimens has shown promise [6]. The S2BT was first proposed by Hyde et al [6] in 2012. A schematic of this test is shown in Fig. 1 [7].

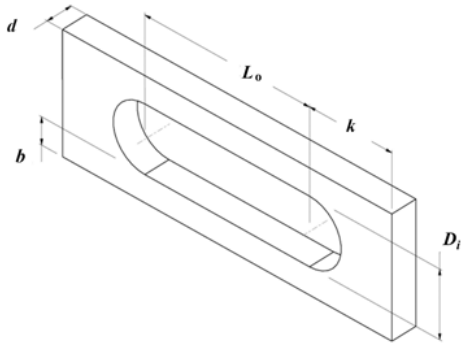

Figure 1. Schematic of the S2BT specimen. Adapted from [7]. '*d*' is the thickness, '*b*' is the width, 'D_i' is the diameter for loading pins, 'L_0' is the loading bar length, and '*k*' is the length of the loading pin's end.

Ali et al [8] analysed the effect of variation in the specimen size on the reference parameters for creep testing and proposed a range of dimension ratios in their study. The output of this test is close to a uniaxial creep test due to both the S2BT's bars undergoing a largely uniaxial state of stress.

This study aims to put forth initial results from using the S2BT for tensile testing. It is hypothesized that the results obtained could be comparable to a standard sub-size tensile test. The unique geometry has the potential advantage of being insensitive to slight misalignments during loading since they can be self-aligned upto a certain degree. This makes it more robust than scaling down a sub-size specimen to its corresponding size.

Additionally, due to the availability of two-bars, two datasets can potentially be obtained from a single specimen. Effectively, this would make it more efficient than the SPT or a miniaturized version of the sub-size specimen test.

Compared to the SPT, the S2BT does not involve recommendations of the test to be performed in an inert atmosphere. Thus, this improves the accessibility of the test and brings down the testing costs. The SPT also needs data conversion since it's a different form of loading (biaxial stress state) but the S2BT's loading geometry negates this requirement (laregely uniaxial stress state).

To assess preliminary feasibilities of this test for tensile testing purposes, we perform tensile tests on SS316L– a widely used material in the nuclear industry. To analyse any strain rate dependencies that may be introduced due to the miniaturization of the specimen, various strain rates are tested on the S2BT specimen. Strain within each arm is captured with the help of 2D DIC (Digital Image Correlation), which allows for non-contact measurement of strain. This is vital given the size of the specimens involved in S2BT, because even small stresses applied by a contact extensometer can affect the test.

Lastly, the S2BT test is then simulated via FEA (using Abaqus/Explicit) and these results are then compared to a sub-size test.

II. METHODOLOGY

The specimens were manufactured from virgin SS316L. The parent bar was solution annealed, cold-rolled, and heat treated subsequently at 1060ºC. The grain size was observed to be 33 μm (± 6 μm). A sample micrograph is also shown in fig. 4. The specimen dimensions used for the entirety of the study are depicted in Fig. 2. The dimensions are based on the ratios proposed by Ali et al [8]. The experimental setup is shown in Fig. 3.

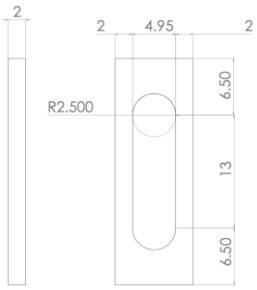

Figure 2. Specimen dimensions for S2BT samples used. All dimensions are in mm.

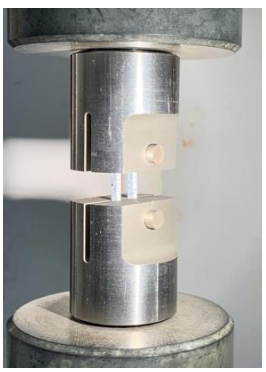

Figure 3. Specimen mounting for S2BT experiments.

Micro-hardness tests were performed on the samples and the average Vicker's Hardness was found to be 217.5 ± 2.57 HV.

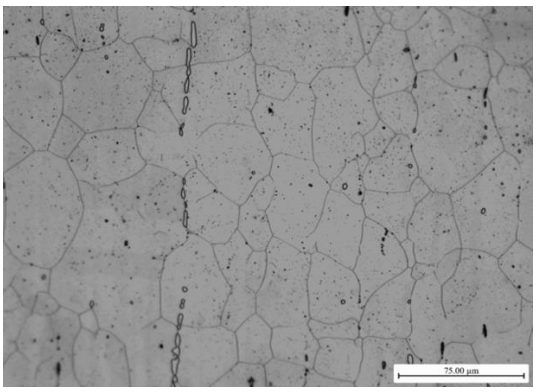

Figure 4. Micrograph of S2BT specimen.

The strain rates used for the tests, represented as mm/min of travel, were 0.1, 0.3, 0.5, and 0.8. The force reading from the Instron 50 kN universal tesing machine is used to calculate the total stress borne by the two arms. However, it is not possible to determine the load partitioning between the specific arms if one of the arms begins to preferentially deform plastically and eventually fracture.

Thus, the force readings were used to calculate the stress in each arm individually by dividing the force reading by the cross-sectional area of the arm under consideration. Due to the size of the specimens, the strain readings obtained from the Instron testing machine are not used to obtain stress-strain curves.

Strain is obtained with the help of DIC. The samples are painted in a black and white speckle pattern before being loaded. The cameras capture the image of the sample every 5 seconds during the test. These images are then loaded onto the LaVision GmbH DaVis 8.3 DIC software to calculate the displacement vectors. These displacement vectors are subsequently used to calculate the strain within the sample.

Micro-hardness tests performed on a reference sub-size specimen showed a mean hardness of 231 ± 3.24 HV. DIC was also performed on the sub-size specimen to ensure consistency in strain measurement.

The results from the sub-size test was then fed into Abaqus/Explicit for finite element analysis. C3D8R element formulation was used to simulate the S2BT specimen while the pins were modelled as a rigid body. The rigid body assumption was taken into account since it decreases the computation time and the pins, made of Hastelloy X in the experiment, were not deformed during the S2BT experiments. A mass scaling factor of 1000 was also used to increase the computational speed while the "Step" used 'Dynamic, Explicit' to simulate specimen fracture. The FEA setup is shown in fig. 5. Mesh size convergence study indicated that a hex mesh of size 0.3 mm is adequate for FEA.

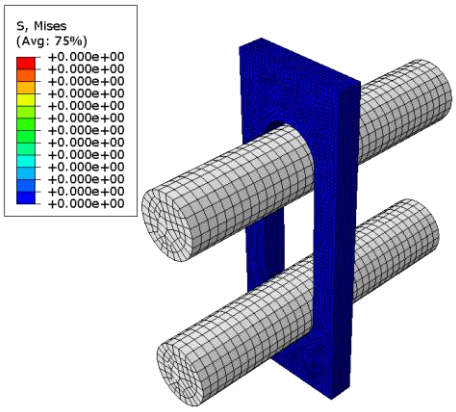

Figure 5. FEA setup (0.5 mm/min strain rate).

Thus, the results from S2BT, Sub-size, and FEA tests are all compared. This is discussed in the next section.

III. RESULTS

Fig. 6 shows the cracked specimen (on the left) in contrast to an untested S2BT specimen (on the right).

Fig. 7 depicts the comparison of the S2BT tests at various strain rates, while fig. 8. compares the mean values of the S2BT tests (shown in fig. 7) to the sub-size specimen's results and the FEA result.

Figure 6. Failed vs new S2BT specimen.

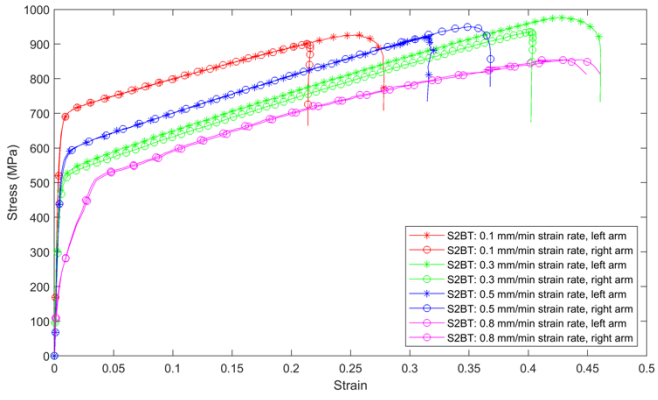

Figure 7. True stress-strain graphs for individual S2BT arms.

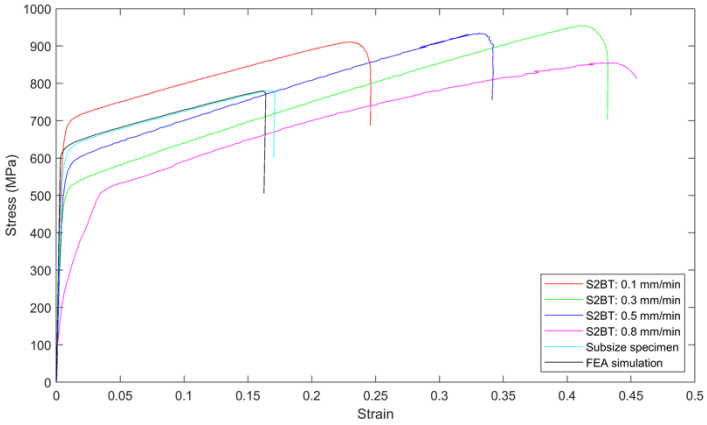

Figure 8. Comparison of true stress-strain curves for S2BT, Subsize test, and FE simulation.

Based on the stress-strain curves that are obtained from these tests, the elastic modulus can be estimated for each sample as well. This is enumerated in Table 1.

Table 1. Elastic modulus values for S2BT and sub-size specimens

Sample type and strain rate	Elastic Modulus (GPa)
S2BT (0.8 mm/min)	140.54
S2BT (0.5 mm/min)	133.46
S2BT (0.3 mm/min)	154.69
S2BT (0.1 mm/min)	166.98
Sub-size	151.86
FEA simulation	156.54

A mean elastic modulus of 148.91 GPa was found for the S2BT samples, compared to the 151.86 GPa value observed for the subsize specimen.

Fig. 7 and 8 are indicative of the potential offered by the S2BT technique. Prior to the initiation of plasticity, there is a close match of all S2BT results with the subsize test and the FE simulation except for the S2BT performed at 0.1 mm/min strain rate. This is potentially an unexplored research avenue and is currently being investigated. It is not clear why the behaviour at this strain rate should be different than in other strain rates and is subject to investigation in our future studies. For the remaining tests, there is an arguably close match, but not at in the plastic region. The ultimate tensile strength varies too dramatically to conclusively recommend it as a benefit of the S2BT.

A slight variation in results can also be observed within an S2BT sample. This could be due to the minute variations in the arm thicknesses and the microstructure. Thus, each arm bears a slightly different load and this may explain the variations.

It can also be noticed that despite the slight variations, fig. 7. shows that two samples can be extracted from a single specimen. As hypothesized, this is an additional benefit as compared to shrinking down a sub-size specimen in size.

Additionally, deliberate misalignment (of 3º) was also introduced in the specimen loading to test the self-centering

property of S2BT. Fig. 9 shows the sample (S2BT at 0.8 mm/min strain rate) in its initial state and and fig. 10. shows the same specimen at failure. If a miniaturized sub-size specimen had experienced a misalignment, it would not have experienced uniaxial loading.

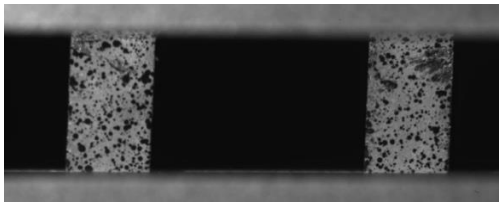

Figure 9. S2BT sample with deliberate misalignment (0.8mm/min strain rate) during loading.

Figure 10. S2BT sample (0.8 mm/min strain rate) at fracture.

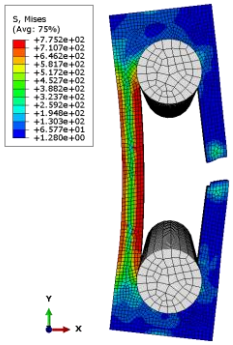

Figure 12. FEA simulation of S2BT (0.5 mm/min) depicting specimen rupture.

Thus, based on the results depicted, the following points can be concluded from the study:

- S2BT in tensile is potentially insensitive to loading misalignment at strain rates greater than (and including) 0.3 mm/min of travel.
- S2BT tensile test results do not not need a conversion factor for comparison to sub-size tests.
- FEA results show a good match with the S2BT test done at 0.5 mm/min. Fig. 12 shows the FEA specimen at rupture. The observed yield strength for the FEA result was approximately 615 MPa while for the S2BT it was approximately 595 MPa.
- S2BT tensile test results match well with sub-size tests with respect to the general trend of the stress-strain curves, elastic modulus, and yield strength.

However, it must also be mentioned that the necking of the specimen, and by extention the ultimate tensile strength, was not a focus of this study. A significant variation is observed in these parameters. Due to the size of the specimens involved, numerous tests would be needed before establishing a procedure to estimate the ultimate tensile strength from S2BT.

IV. FUTURE WORK

This study was the first of its kind to evaluate the S2BT for tensile tests. The following future work directions are proposed by the authors in efforts of test standardisation:

- Testing with more materials, such as SS316H, etc.
- Testing at more strain rates to establish strain rate dependency.
- Testing more samples to establish a procedure for estimation of the ultimate tensile strength.
- Compare with the SRT and SPT.
- Vary the thickness of the specimen in efforts of dimension standardization.A standardized testing procedure can help extend reactor lifetime in a sustainable manner while also providing an avenue for the development of new alloys for next generation reactors.

V. REFERENCES

[1] *Test Methods for Tension Testing of Metallic Materials*, E28 Committee Technical report, ASTM International, 2013.

[2] *ASTM E-139/83*, American Society For Testing And Materials, 1990, Surface Engineering, v. 5, Philadelphia.

[3] T. H. Hyde, W. Sun, and J. A. Williams, “Requirements for and use of miniature test specimens to provide mechanical and creep properties of materials: a review,” in *International Materials Reviews*, vol. 52(4), pp. 213–255, July 2007.

[4] MP Manahan, AE Browning, AS Argon, and OK Harling, “Miniaturized disk bend test technique development and application,” in *The Use of Small-Scale Specimens for Testing Irradiated Material*. ASTM International, 1986.

[5] *Small punch test method for metallic materials*, European Committee for Standardization, Technical Report CWA 15627:2007, European Committee for Standardization, 36 rue de Stassart, B-1050 Brussels, 2007.

[6] Thomas H Hyde, Wei Sun, and Balhassn SM Ali, “A small creep test specimen for use in determining uniaxial creep rupture data,” in *2nd international conference SSTT determination of mechanical properties of materials by small punch and other miniature testing techniques*, Ostrava (CZ), pp. 261–270, 2012.

[7] Balhassn S. M. Ali, Tom H. Hyde, and Wei Sun, “Small Two-Bar Specimen Creep Testing of Grade P91 Steel at 650°C.” in *High Temperature Materials and Processes*, vol. 35(3), January 2016.

[8] Balhassn SM Ali, Terry YP Yuen, and Mohamed Saber, “Creep evaluation of traditional and nuclear power plant high-temperature components, using small pin- loaded one-bar and two-bar specimens,” in *Nuclear Technology*, vol. 196(1), pp. 130–140, 2016.

Proceedings of the European Nuclear Young Generation Forum
ENYGF'21
September 27-30, 2021, Tarragona, Spain

An Assessment of the functional reliability of the control and protection system in the type of reactors WWER

Yilmazer Samed Tugrul, Akkuyu NPP Turkey, *st.yilmazer@akkuyu.com*

I. INTRODUCTION

The use of nuclear technologies, such as in nuclear power plants, requires the inclusion of safety systems in the equipment that implements these technologies. The purpose of the security system is to transfer emergencies in the event of a violation of the normal functioning of the object of protection to the rank of non-dangerous, i.e., parrying failures of the object of protection. Thus, the security system has an important role to play in ensuring the safe operation of the object of protection, but it is not a means of ensuring its reliable operation.

The main purpose of the control and protection system is to ensure the nuclear safety of the reactor and control its power capacity by the regulations. The reactor control and protection system is not only a system that is important for safety but also the main system for operational nuclear safety, along with the liquid control system. Therefore, at the beginning of the work, we need to be sure and evaluate the reliability of this system.

Any such complex consists of a protection object (PO) and a security system (SS). Security systems consist of several protection channels (PC), each of which has designed to fend off a certain type of protection object failures. Each protection channel, in turn, has a complex structure. The emergency of the complex occurs at the time when the corresponding protection channel of the security system does not perform its functions. By an accident, we mean an event that involves a major violation of the operating modes of the system, leading to the creation of dangerous conditions for human life and the environment.

There are various types of monitoring of the serviceability of the elements of the security protection channel of the security system. The state of some elements can be monitored continuously, while the state of others is monitored periodically, and the control takes some finite time. The readiness of a periodically monitored element is significantly different from the readiness of the same element that is continuously monitored, so there is a need to take into account periodic monitoring in the safety analysis.

II. OVERVİEW OF THE RESEARCH PROBLEM

There is lot of specialized software systems, which can make us ensure the readiness and the functional reliability of the control and protection system. The main question is which one we need to choose. I'd like to show you some of options and which difficulties could we face during the researches.

As many of you know, there is a type of analysis called 'probabilistic risk analysis'.

Ensuring the safety of nuclear power plants is one of the most important tasks in the development of nuclear energy in the country. The Chernobyl tragedy has shown all too clearly the cost of neglecting this factor. Therefore, in the process of designing, building, and operating a nuclear power plant, it is necessary to make great efforts to ensure that the nuclear power plant complies with very strict international standards. Following these standards, the probability of severe damage to the core of nuclear power plant should not exceed 1x10-5 per reactor per year. The probability of radioactive substances leaving the sealed shell 1x10-7 per reactor per year, the radiation impact of a nuclear power plant on the population and the environment should not exceed approximately 1% of the dose received from natural radiation sources.

To implement these requirements, the plant design process is accompanied by several serious studies, during which the safety of nuclear power plants is justified. An important place in this is occupied by the procedure of probabilistic risk analysis. When performing this analysis, the value of the safety indicators of alternative NPP structures is calculated based on a priori initial information about the reliability of the equipment and the optimal structure of the plant systems is selected in terms of reliability and safety. A strategy for maintenance and repair, monitoring and diagnosing the technical condition of the equipment are developed to ensure the required level of safety.

When performing probabilistic risk analysis, event trees and fault trees have found the greatest use. They have led to their use as part of many codes for this security analysis, some of which are listed below;

CAFTA +/ETA-II developed by SAIC Corporation USA

SAPFIRE developed by the U.S. nuclear regulatory commission

Risk Spectrum developed by the company Relcon Teknik AB Sweden

CRISS developed by the experimental design bureau of mechanical engineering named I.I. Afrikantov (Experimental Design Bureau of Mechanical Engineering Rosatom)

Among them, the most widespread in Russia during the probabilistic risk analysis NPP were two codes: CRISS and Risk Spectrum.

The disadvantages of failure tree/event tree are:

-bulkiness (the number of elements failure tree to N always exceeds the number of elements of the circuit diagram n and in general tends to the value $N=2^n$)

-it's unacceptable (from the point of view of the subsequent modelling stage) to have the same elements in different branches;

-inability to display non-monotonic structures;

-difficulty or inability to display the conditions for connecting reserves;

-the inability to image logical loops

An attempt to overcome these shortcomings is the introduction of additional elements in addition to the three main ones, although this immediately removes the corresponding fault trees from the category of simple graphs. In our opinion, the big flaw lies in the fault trees/event trees methodology itself. It is known to be based on reverse logic (fault trees are focused on failure). It is quite difficulty for a researcher to use this type of logic. The number of ways in which an accident can develop with a large number of system elements is very large. The probability of each path being implemented depends on a variety of reasons and conditions. Even the most obvious and repeatedly recorded in practice variants of system degradation, as a rule, are very poorly documented. And the presence of such documents does not guarantee that in the next case, the accident will not develop in a different scenario.

As a result, the researcher requires very high qualification and experience in the development of fault trees and when switching to modelling technical systems built on different physical principles, it is often necessary to learn again. The disadvantage of the method is that the specialist conducting the research must adapt to the method, and not focus on the physical picture of the processes. In our option, mathematics should be hidden from the researcher as much as possible, and the method itself should be adapted to the features of ordinary, direct, human logic to the highest possible extent.

It is these considerations that have led to the development of modelling methods based on alternative approaches. In the US, this is the method of GO-schemes, in Russia-a general logical-probabilistic method involving the use of functional integrity schemes.

A. Software system "CRISS 4.0"

This software designed to simulate and analyse safety systems and a nuclear installation as a whole while performing probabilistic safety analysis.

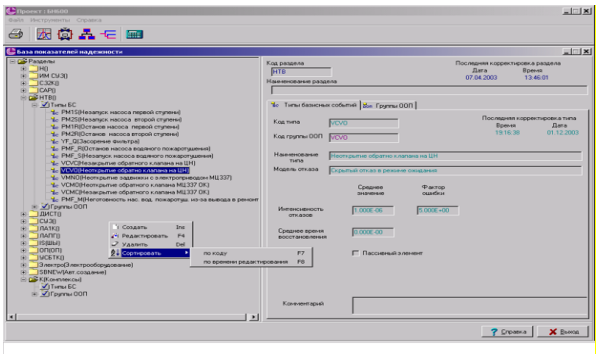

Figure 1. Working window of the software "CRISS 4.0"

The most common among foreign software systems are Risk Spectrum to calculate the reliability of REE (Radio-electronic equipment) and ERP (Electro radio products), the automated system (ASCR), the automated system for calculating the reliability of ERP and REE are widely used.

The CRISS 4.0 version of the program has intended for use in the educational process and has the following limitations:

- The number of inputs of the logical operator of the failure tree-no more than five

- The total number of logical operators in the failure tree is no more than ten

- When creating bounce trees, it is possible to use a single transition operator (transfer)

- The number of functional events in the event tree is no more than five

The training version of the program requires an annual update of the executable module.

B. Software system "Risk Spectrum"

The Risk Spectrum software system is used for probabilistic analysis of nuclear power plant safety.

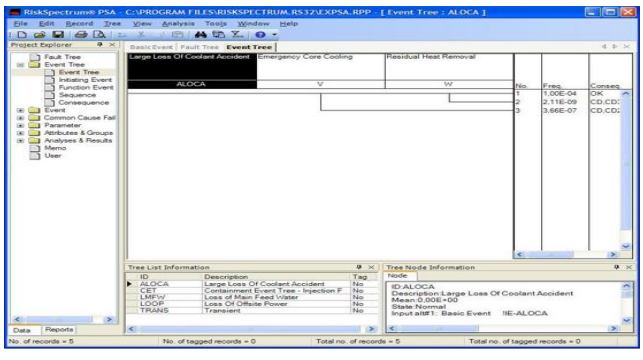

Figure 2. Working window of the software "Risk Spectrum"

Disadvantages and limitations of the RISK-Spectrum code:

- The possibility of obtaining only conservative (sometimes excessively) estimates of the NPP, which leads to an underestimation of the actual level of nuclear power plant safety and the adoption of incorrect design decisions;
- Highly inflated estimates of the CDF (core damage frequency), etc. Indicators when taking into account personnel errors (the contribution of personnel errors in the CDF in 'standby modes' is 96% - for Tianwan NPP, about 100 % - for the 3rd unit of the Kaliningrad NPP). Risk spectrum gives the NPP safety indicators deteriorated several times in the case of PRA (personnel reliability analysis)
- The core of the code runs in the MS DOC OS environment; this imposes strong restrictions on the dimensionality of the models and leads to gross calculation errors associated with cutting off "insignificant sections"
- Models are developed based on the assumption that the duration of the post-accident event is 24 hours. Up-to-date IAEA documents and the world practice of implementing the WAB require consideration of post-accident periods of at least 72 hours. Under these conditions, the use of Risk Spectrum is highly undesirable, since it does not contain "programming" errors in the code.

C. ASRN – The automated reliability calculation system

The automated reliability calculation system (ASRN) developed based on the reference book "Reliability of electrical radio components". It allows you to calculate the total failure rate of modules of the 1st and 2nd levels without redundancy, which are equipped with domestic and imported electric radio products in operation and storage mode (only for domestic electric radio products) as part of mobile and stationary objects.

For this work, we reviewed and were acquainted with the software programs that support work on the probabilistic risk analysis, among which we highlighted the ASRN as the most suitable for our work.

III. Using accident-free operating experience

The use of accident-free experience in the operation of nuclear technology facilities for assessing their reliability indicators is justified, since this is also an experience that can help in a situation where the object was operated for a sufficiently long (representative) time, and its failures were not observed.

In this case, possible to make the following assumptions:

1) the time to object failure (regardless of its causes) is distributed exponentially;
2) there should have been at least one bounce with a high probability, but we were "lucky".

IV. Approaches to the structural assessment of reliability indicators

The structural reliability of a system (device) is the resulting reliability of a system (device) with a given structure (*Source of given structure cannot be shared due to strictly information privacy) and known values of the reliability of all its parts (blocks, elements)

A. Serial connection

In case where the system consist of several parts, the failure of at least one of which leads to the failure of the entire system. It said that these parts connected in series. Depict such a connection, as shown in the figure 3.

Fig. 3 Serial Connection of elements

If the failures of each part are independent of the state of the other parts, i.e. failure of one part does not change the reliability of others, and then the reliability of such a system has defined as the product of the reliability of individual parts, i.e.

$$P(t) = \prod_{i=1}^{N} P_i$$

Where;

P(t) is the probability that the object will not fail by time t, or the probability of no-failure operation during time t,

N is the number of system elements.

The reliability of a serial connection is always no higher than the reliability of the most unreliable element.

B. Parallel connection

In case where the system consist of several parts and the failure of only all parts leads to the failure of the system as a whole, it has said that these parts has connected in parallel. The figure 4 shows a parallel connection of the elements.

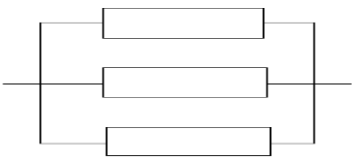

Fig. 4 Parallel connection of elements

If the failures of each part are independent of the state of the other parts, then the probability F(t)=1-P(t) of a system failure is equal to the product of the failure probabilities of all its parts.

$$F(t) = \prod_{i=1}^{N} F_i = \prod_{i=1}^{N} (1 - P_i(t))$$

Hence the reliability of the parallel connection is

$$P(t) = 1 - \prod_{i=1}^{N} \left(1 - P_i(t)\right)$$

Thus, the reliability of the parallel connection is always higher than the reliability of the most reliable element. Parallel connection of elements has often called hot redundancy, because such a connection has used to increase the reliability of system due to the simultaneous operation of several elements of the same type, when at least one of them is sufficient to perform the function.

When determining the "P" with the help of the software program "ASRN", we had to select some elements in the program that are located on the electrical circuit.

V. Reliability Assessment

We need to obtain numerically the values of the probabilistic characteristics for the elements included in the electrical part of the automatic control system AP1 and AP2.

A general reliability scheme for the electrical part of the automatic power control system of the reactor plant is presented (*source of given structure cannot be shared due to strictly information privacy)

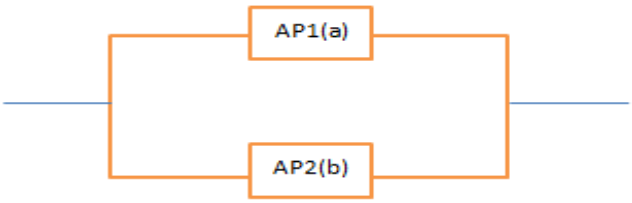

Fig. 5 General reliability scheme for the automatic control system

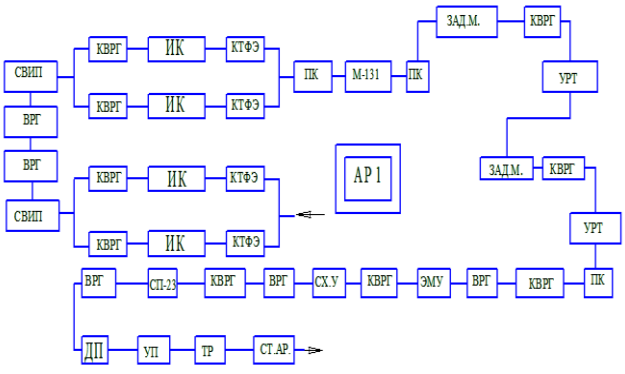

Fig. 6 Reliability scheme for the automatic control channel AP1 (Channel elements are specified in Russian as in the original source)

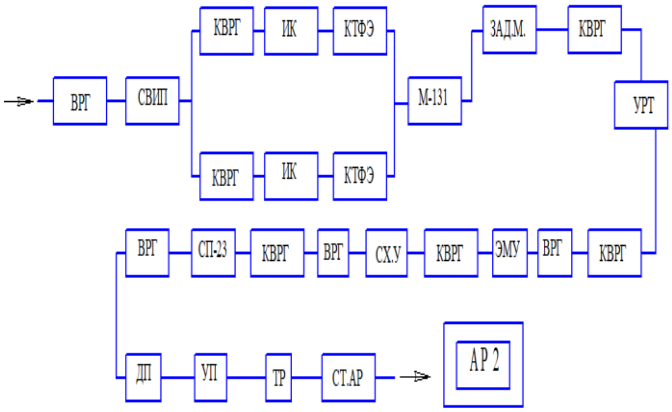

Fig. 7 Reliability scheme for the automatic control channel AP2 (Channel elements are specified in Russian as in the original source)

At the beginning of calculating the probability of failure free operation of the electrical circuit, we need to determine the failure rates ($\lambda_{э_1}$) each element. We have four sources of information with which we have determined or "manually" calculated the failure rates of electrical elements.

The probability of failure-free operation estimated for 1 year, which corresponds to the hourly equivalent of 8760 hours. This value helps us to find out the reliability of the system under study for the entire year using the following formula:

$$P(t) = e^{-\lambda.t}$$

λ- failure rate (1/h)

t- is the time for which the probability of failure-free operation of the electrical radio device is estimated (h). The results of the failure rate and the probability of failure of each element has shown in table 1.

After finding the results, we can then evaluate the reliability indicators of the scheme, which has shown in fig. 5. In the scheme, some elements have connected on a parallel and some on a sequential principle, so we need to use the formulas for serial and parallel connections when calculating the reliability of the system under study.

To calculate the total probability of failure-free operation, we decided to decompose the reliability scheme. Therefore, we divide the schemes AP1 and AP2 into ten parts and start separately calculating the probabilities of failure-free operation of each part. After performing the calculation, we will determine the probability of failure-free operation of each circuit separately. As indicated in the general diagram fig.5 AP1 and AP2 connected in parallel. Therefore, to find the final probability of failure, we need to use formulas for parallel connections using the results of the probability of failure of AP1 and AP2.

Methods for evaluating reliability indicators in the decomposition of the product circuit are shown in fig.8 and fig.9

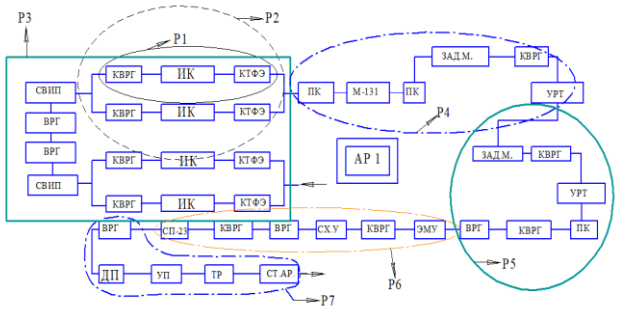

Fig.8. Decomposition of the reliability scheme of the electrical part of AP1

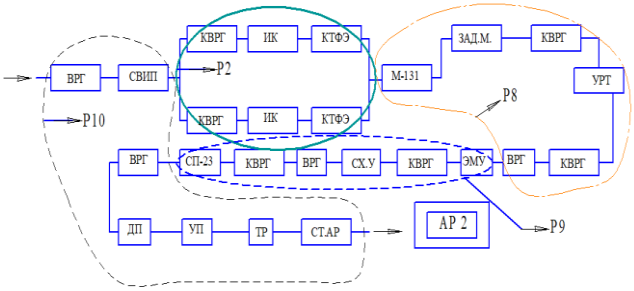

Fig.9. Decomposition of the reliability scheme of the electrical part of AP2

Calculation for table 1.

We determine the probability of failure-free operation for each part using the values of the probability of failure-free operation of each element.

Calculate the probability of failure-free operation for AP1 using this formula

$$P(AP1) = P_3 \times P_4 \times P_5 \times P_6 \times P_7 = 0{,}6649691.$$

Let's calculate the probability of failure-free operation for AP2 using the formula

$$P(AP2) = P_8 \times P_9 \times P_{10} \times P_2 \quad = 0{,}6653976\ .$$

In the general diagram (fig.5), AP1 and AP2 connected in parallel. Therefore, we should use the formula for parallel connections and the total probability of failure has calculated as follows:

$$P_{\text{система}} = 1 - (1 - P(AP1)) \times (1 - P(AP2)) \quad = 0{,}8878978.$$

Calculation for table 2.

Calculate P for each part using the values of the probability of failure-free operation of each element.

For AP1

$$P(AP1) = P_3 \times P_4 \times P_5 \times P_6 \times P_7 = 0{,}224232$$

For AP2

$$P(AP2) = P_8 \times P_9 \times P_{10} \times P_2 \quad = 0{,}304047$$

In the general diagram (fig.5), AP1 and AP2 connected in parallel. Therefore, we should use the formula for parallel connections and the total probability of failure has calculated as follows:

$$P_{\text{сумма}} = 1 - (1 - P(AP1)) \times (1 - P(AP2)) = 0{,}4601018$$

VI. Conclusion

In any case, we cannot be hundred percent sure that the item or equipment is completely reliable. When calculating reliability, all parameters and all probabilities must be included to calculation. Therefore, at this point the experience of operation and the opinions of experienced specialists who have devoted their many years to this industry will be incredibly invaluable.

In this technological era, there is a big task ahead of us. We have to find the optimal solution and combine our experience with new technologies.

VII. References

[1] D.S. Samokhin, "Evaluation of reliability indicators of equipment elements and personnel of nuclear technology facilities using fuzzy probabilistic models," Obninsk, Russian Federation, 2009, 43-44, 49-50.

[2] Y.V. Volkov, N.L. Salnikov, "Report on research work on the topic "Evaluation of the functional reliability of the control and protection system of the AM installation," MEPhI. Obninsk, vol. 1994, p:53.

[3] A. Stroganov, V. Zhadnov, S. Polessky, "Review of software systems for calculating the reliability of complex technical systems, 2007, p: 183-190.

[4] GOST 26843-86, Nuclear power reactors. General requirements for control and testify systems

№	Elements	Quantity	*$\lambda_{э_1}$[1/h] Operating time-8760 hours	Reference of literature	P
1	Дп	2	$0{,}126.10^{-6}$	ASRN	0,998896
2	Зад.М.	3	$0{,}00032.10^{-6}$	ASRN	0,999997
3	Врг	9	$0{,}00026.10^{-6}$	ASRN	0,999997
4	Кврг	12	$0{,}00026.10^{-6}$	ASRN	0,999997
5	Ктфэ	3	$0{,}00026.10^{-6}$	ASRN	0,999997
6	Свип	3	$0{,}03800.10^{-4}$	[2]	0,999667
7	Сп-23	2	$0{,}08500.10^{-4}$	[1]	0,928244
8	Ст. Ар.	2	$0{,}1.10^{-4}$	[4]	0,916127
9	Сх-у	2	$0{,}08500.10^{-4}$	[1]	0,928244
10	Пк	3	$0{,}00409.10^{-6}$	ASRN	0,999964
11	М-131	2	$0{,}01000.10^{-4}$	[2]	0,991278
12	Ик	3	$0{,}01600.10^{-4}$	[2]	0,986081
13	Тр	2	$0{,}08500.10^{-4}$	[1]	0,928244
14	Уп	2	$0{,}01469.10^{-6}$	ASRN	0,999871
15	Урт	3	$0{,}00032.10^{-6}$	ASRN	0,999997
16	Эму	2	$0{,}09800.10^{-4}$	[2]	0,917733

Table 2 – Results of the evaluation of the reliability indicators of the elements

№	Elements	Quantity	*$\lambda_{э_1}$[1/h] Operating time-8760 hours	Reference of literature	P
1	Дп	2	$0{,}003.10^{-4}$	[2]	0,974062
2	Зад.М.	3	$0{,}058.10^{-4}$	[2]	0,950461
3	Врг	9	$0{,}085.10^{-4}$	[1]	0,928244
4	Кврг	12	$0{,}085.10^{-4}$	[1]	0,928244
5	Ктфэ	3	$0{,}085.10^{-4}$	[1]	0,928244
6	Свип	3	$0{,}038.10^{-4}$	[2]	0,967260
7	Сп-23	2	$0{,}085.10^{-4}$	[1]	0,928244
8	Ст. Ар.	2	$0{,}1.10^{-4}$	[9]	0,916127
9	Сх-у	2	$0{,}085.10^{-4}$	[1]	0,928244
10	Пк	3	$0{,}0005.10^{-4}$	[2]	0,999562
11	М-131	2	$0{,}01.10^{-4}$	[2]	0,991278
12	Ик	3	$0{,}016.10^{-4}$	[2]	0,986082
13	Тр	2	$0{,}085.10^{-4}$	[1]	0,928244
14	Уп	2	$0{,}01.10^{-4}$	[2]	0,991278
15	Урт	3	$0{,}054.10^{-4}$	[2]	0,953795
16	Эму	2	$0{,}098.10^{-4}$	[2]	0,917734

Table 3 – Reliability characteristics of elements according to the report data (2)

Proceedings of the European Nuclear Young Generation Forum
ENYGF'21
September 27-30, 2021, Tarragona, Spain

A complex for localization and repair of the fuel pool cladding for NPP-2006 project

Tikhonov, Aleksandr[1]

[1] Rosatom, Russia

*Corresponding author: *TikhonovAI@nvnpp1.rosenergoatom.ru*

I. INTRODUCTION

The fuel pool, filled with a water solution of boric acid, is the main construction of the system for storing radiationexposed nuclear fuel at the NPP

According to the technical requirements and to ensure optimal economic characteristics, in the NPP-2006 project the fuel pool (FP) is designed with one compartment. This allows to significantly decrease the diameter of the containment and the dimensions of the reactor building in general.

The volume of the FP allows to store spent fuel assemblies in the course of 10 years of energy production and to reload all the fuel assemblies from the reactor core to the FP at any time. [1]

The NPP-2006 project has a device for repairing the claddings, which allows not to separate the FP into compartments (a deviation from the requirements of sec. 4.3.5 of NP-061-05 must be justified) and to ensure repair without unloading the fuel. [2-6].

II. THE PROBLEM OF REPAIRING THE FUEL POOL JOINTS WITHOUT DRAINING

1. The level of reliability of localization of revealed leaks of tanks, reservoirs, pools does not meet the requirements and safety standards.

2. Risk of discharge or leakage of hazardous or radioactive media and/or their impact on the environment.

3. Violation or termination of the technological process due to exceeding the design limits connected with the formation of a leak in the FP.

4. Unloading of nuclear fuel and emptying of the tank is required.

5. Unscheduled repairs to eliminate defects.

6. Contact with surface preparation products, deviation from the requirements of the water chemistry mode.

In accordance with the requirements of the "Working process regulations for the safe operation of unit № 1 of Novovoronezh NPP-2":

a. the reactor plant should be brought to "Cold" state in case of a leak of more than 1 m3/day in the cladding of the FP for its repair;

b. in case of a decrease in the FP level to +25.350 m restore the level within 72 hours, if the level is not restored, unscheduled transfer the power unit to "Hot" state;

c. provided that the nominal level in the FP is maintained at a leak rate of less than 1 m3/day, it is allowed to repair the cladding during the next SPM.

One day of idling of the power unit is estimated at 1,7 million US dollars. In Russia there are 19 VVER type power units.

III. THE ESSANCE OF THE PROJECT

A. The first stage is localization:

Localization of leaks of tanks, vessels and reservoirs, the design features of which do not allow to carry out repairs without partial or complete emptying of the tank.

This stage is necessary for the time of delivery and installation of an automated device for repair.

A high level of localization reliability eliminates the necessity for draining or the possibility of leakage of hazardous or radioactive media, environmental impact, disruption/shutdown of the process, or unplanned repairs to equipment.

Localization of leaks of containers and reservoirs is carried out by installing a metal patch followed by creating a vacuum in the formed closed cavity due to work a water-jet pump. The working medium that creates the vacuum is the boric water of the FP. It needs for hold the metal patch on the FP wall and limit the leak to a value not exceeding the safety limits Figure 1.

Before installing the localization device, the fuel cell racks are rearranged. This is permitted by nuclear safety documents and design.

1. There is no need to empty the vessel or to prepare the surface around the leak beforehand.
2. Does not decrease the quality of media in the vessel (does not affect water chemistry).
3. Almost no restrictions on the duration and conditions of use.

Calculations (in an ANSYS program) were performed with a small leak (less than 1.0 m3/day) for different depths of the leak (up to 19 m). It was also calculated that the minimum mass flow rate of water to the ejector of the device should be more than 4 kg / s.

The calculation results show that the leak localization device successfully copes with its functions. There is a result of tests in situ at Unit 1 of Novovoronezh NPP-2.

Figure 1. General form of a localization device.

B. The second stage is repair:

An automated remote device is installed, which allows to carry out the whole complex of measures for repairing the cladding, which include surface preparation and applying a composite lining.

To select the reference technology for repairing the FP of power units № 1 and № 2 of the Novovoronezh NPP-2, an analysis was made of the technology used worldwide for repairing tanks' and structures' cladding. According to the results of the analysis, the gluing technology was chosen as the technology for repair Figure 2.

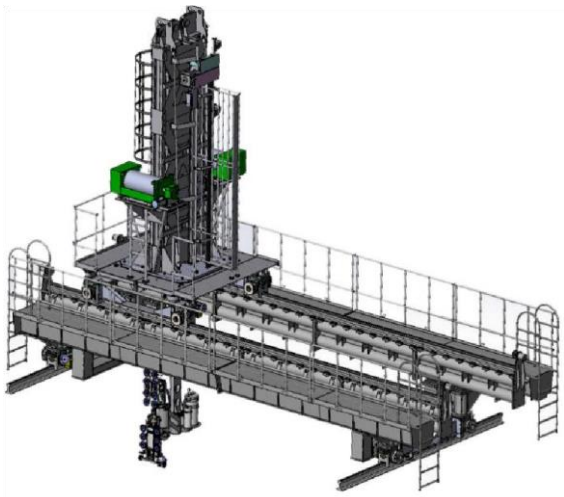

Figure 2. General form of an automated remote device.

The developed device allows you to perform the following works:

1. To detect leaks, repair the cladding of the walls of FP and monitor the tightness of the repaired place.
2. To detect leaks and repair the FP floor cladding.
3. To detect leaks and repair the FP cladding in the wall-wall, wall-floor zones.

The choice of materials from which the device for repairing the FP cladding is made was carried out taking into account its functions and was determined by the working conditions similar to equipment operating in the FP (refueling machine, system for detecting defective FAs, inspection stand and repair of fuel assemblies).

The device is a frame which can move on the rails of the refueling machine. A telescopic rod with a winch and a overhead manipulator are installed on the trolley. Diagnostic, repair and grinding modules can be installed on it Figure 3.

Before installing the protective plate, the surface is ground, using a suction device, it eliminates the ingress of metal elements into the FP.

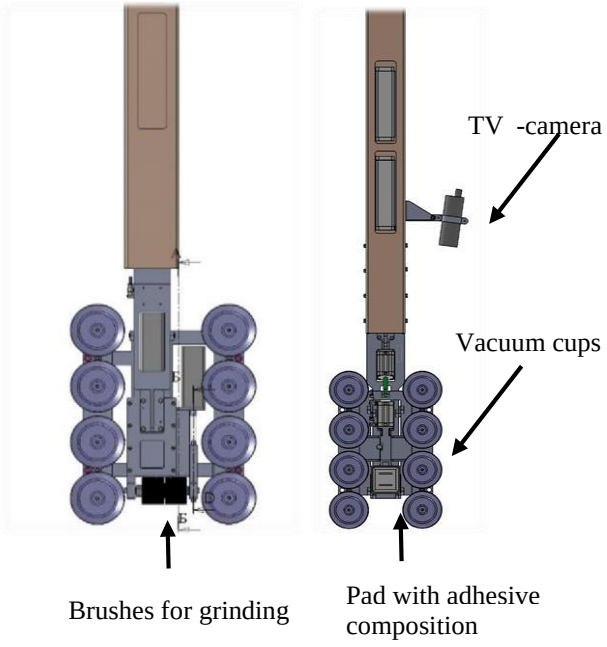

Figure 3. The repair modules.

Sealing is carried out by applying a stainless steel protective plate with an epoxy-based adhesive layer applied to it. The composition of the glue allows you to repair under water into account the chemical composition, temperature and radiation dose.

C. Choise of adhesive composition

To select the adhesive composition, tests were carried out which copy the actual operating conditions as close as possible:

1. The metal plate is made of austenitic corrosionresistant steel 08H18N10T, as well as the FP cladding.

2. The composition of the medium corresponded to the media in FP.

3. The composition was cured in a solution of boric acid for 18 hours at 20°C, for 12 hours at 28°C, for 6 hours at 45°C and for 4 hours at 60°C. [8]

4. Exposure to ionizing radiation up to an absorbed dose of 20 MGy at an absorbed dose rate of 5.5 kGy/h (for 152 days). [9]

5. Tensile strength test ≥8 MPa. [10]

IV. RESULTS OF THE COMMISSIONING

This set of measures was taken at the Novovoronezh NPP-2 site and its effectiveness was confirmed. The application procedure was approved by the regulator in the field of nuclear and radiation safety. [11, 12] The complex allows you to:

1. Minimize the risk of discharge or leakage of hazardous or radioactive media and/or their impact on the environment.
2. Exclude violation or termination of the technological process due to exceeding the design limits connected with the formation of a leak in the FP.
3. Unloading of nuclear fuel and emptying of the tank is not required.
4. There is no need for unscheduled repairs to eliminate defects.
5. Minimize contact with surface preparation products, deviation from the requirements of the water chemistry mode.

V. REFERENCES

[1] Povarov V. P., Fedorov A. I., Statsura D. B., Topchiyan R. M. The head unit of the new generation VVER-1200. Features of commissioning / Tenth International Scientific-Technical Conference “Safety, Efficiency and Economics of Atomic Energy”, Moscow, 25 – 27 May 2016.

[2] Federal Safety Regulations in the Field of the Use of Atomic Energy. Safety Rules for Storage and Transportation of Nuclear Fuel at Nuclear Facilities. NP-061-05: Approved by Ordinance of the Federal Environmental, Industrial and Nuclear Supervision Service No. 23, dated of December 30, 2005. Introduced in May 01, 2006.

[3] The head unit of the new generation – features of the VVER1200 project. Asmolov V. G., Gusev I. N., Kazansky V. R., Povarov V. P., Statsura D. B. // Nuclear power. 2017. № 3.

[4] Fuel overload system. Explanatory note. OKB “Gidropress”. 2008.

[5] Novovoronezh NPP-2, Unit 2. Security justification report. NW2O.W.120.2. &&&&&&. &&&&. 000.HD.0001. Moscow, “Atomenergoproekt”, 2015.

[6] Thematic report. On the substantiation of the availability of free volume for unloading spent nuclear fuel for the repair of a cooling pool. NW2O.B.120. &. &&&&&&. &&&&. 022.HF.0010. Moscow, “Atomenergoproekt”, 2016.

[7] S. A. Andrushechko, A. M. Afrov, B. Yu. Vasiliev, V. N. Generalov, K. B. Kosourov, Yu. M. Semchenkov, V. F. Ukrainians. NPP with a VVER-1000 reactor. From the physical basis of operation to the evolution of the project. – Moscow: Logos. – 2010.

[8] Annotation report on the device for the repair of lining the pool exposure. Moscow, JSC “NIKIMT-Atomstroy”, 2018.

[9] Program and methods of testing МИ СМ 03-NIKIMT -072014.

[10] Notification No. 3225-18 of December 14, 2018 on the amendment of Chapter 9 of Book 1 of the Report on the safety justification of power unit No. 1 of Novovoronezh NPP-2.

[11] Program and methods for the commissioning of the device for the repair of the lining of the pool NW2O.T.189.2.0UJA &&. FAB && 060.PA.0001.

[12] The protocol of comprehensive testing of the device for the repair of the lining of the exposure pool No. MND-39545/2018.

Technical Track 5 – Communication, teaching & learning, and knowledge management

Jansen, Rob (11); Khamaza, Alexander (12); Knochenhauer, Michael (13); Mackey, John (14); Meloni, Paride (15); Mistryugov, Denis (12); Nitoi, Mirela (16); Pinel, Cyril (2); Power, Steve (14); Puska, Eija-Karita (17); Rimkevicius, Sigitas (18); de los Reyes, Afredo (3); Shevchenko, Igor (19); Turcu, Ilie (16); Volant, Philippe (2); Yesypenko, Yuliya (19)

Knowledge transfer in FEA trainings: ROSATOM’s modern approach.

Authors: Roskoshnaya, Maria; Tkachenko, Evgeniia

Educational strategy for the management of nuclear knowledge.

Authors: Llanes Montesino, Luis Enrique

RADIOMON – Isotopes, radiation and nuclear technologies in a new game for the i-Generation.

Authors: Nouchy, Fabio

Proceedings of the European Nuclear Young Generation Forum
ENYGF'21
September 27-30, 2021, Tarragona, Spain

"Climate change, safety, and facts galore": A critical review of nuclear communications for the future

Lindberg, John C.H. [1, 2*]

[1] Department of Geography, King's College London, United Kingdom; [2] Department of Cancer and Surgery, Imperial College London, United Kingdom

*Corresponding author: john.lindberg@kcl.ac.uk

I. INTRODUCTION

At the time of its inception as a power source in 1951, nuclear energy was endorsed by many as the future of energy supply, enabling everything from flying cars to the colonisation of space. However, the utopian visions did not last, and by the 1970s, the nuclear discourse had shifted considerably - away from the promises that could be brought by nuclear energy and towards a discourse firmly centred on risks, accidents, and radiation. The courts of public opinion sentenced nuclear power to an existence in the fringes of the energy sector, to be neither seen, nor heard. Today, nuclear power is often viewed with scepticism by policy makers and the public alike, and much of the narrative continues to focus on safety, rather than the many positive attributes it possesses in relation to *e.g.* addressing energy poverty or meeting the Sustainable Development Goals. Despite major efforts, the nuclear industry's communications strategies have largely failed to deliver the promise of nuclear energy. To unlock the potential of nuclear energy, the industry must seize back the narrative, but doing so will require a fundamental communications reform. For such reforms, however, to be successful, it is crucial to firstly review the current strategies. This paper will, therefore, offer a critical review of the nuclear industry's communications efforts, and provide some insights as to the way forward.

II. THE ROLE OF EMOTIONS AND IMAGERY

All communication and messaging are inherently value-laden [1], but historically, the role of emotions have been regarded as merely irrational gut reactions, and been positioned in a dichotomous relationship against rationality. Reviewing the nuclear industry's historical communication strategies, it is clear that the dismissal of nuclear ambiguity or opposition as being "irrational" is deeply ingrained within the industry. However, emotions are central to decision making, as noted in research on individuals with certain types of brain damage, who struggle to make appropriate decisions when their emotional capacity has been damaged [2,3]. Indeed, the human brain is hard-wired to place emotions and imagery at the heart of our engagement with the surrounding environment [4]. Images, both actual, created, and recalled from memory, are the basic building block for human consciousness, and play an important role in cognitive and perceptual-motor tasks [8, 9]. The "library" of mental imagery which we all possess is predominantly populated by either experiential ("lived") experiences, or by learning. In the nuclear case, people predominantly rely on the imagery they are provided with through e.g. media depictions.

Our ability to create visual imagery is crucial *"whether it is the everyday problem-solving required for stability, safety, and survival at home, in the workplace, or in the community"* [10]. Imagery, however, does not exist in a vacuum, and they acquire "somatic markers", (i.e., feelings) – either positive or negative – which are linked to bodily reactions. Once judged, the images and their somatic markers are pooled, and are consulted when making a judgment or when encountering an issue again [11]. This associative pool and its imagery "*…come laden with associations in the form of feelings, e.g., attraction, calm, tranquility, fear, anger, or anticipation* [10] and upon subsequently encountering an image, different emotions would be triggered. A negative marker would, upon the encounter with a previously known image, raise awareness and alarm, whereas an image with a positive marker would, conversely, act as an incentive [2, 3].

Imagery and its emotional markers, once implanted, have a significant impact on how risks and events are perceived [15]. The images and their somatic markers are likely similar regardless of the probability of the outcome, pointing towards the idea that it is the possibility, rather than the probability, which drives the somatic markers, and by extension, the perception of a specific activity [12]. This has found support elsewhere [11, 13]. If the imagery is deemed credible or reliable, coupled with strong somatic markers, probability plays very little in role, and strong affect towards a specific outcome was insensitive to the actual probability of the event happening. This is clearly the case with nuclear accidents, which receive considerable media coverage,

resulting in an over-estimation of any consequences and probability, whereas more deadly activities (*e.g.* car accidents) receive less attention and thus its consequences are often underestimated [11, 14]. This is crucial in the nuclear context, as the most common image associations with nuclear energy were negative, connected with nuclear weapons, nuclear war, accidents, uncleanliness, and waste [16]. When asked to describe what a worst-case nuclear power accident would look like, the description offered by respondents was very similar to the perceived aftermath of nuclear war [17]. Without replacing this imagery, nuclear power's unique risk perception will likely linger.

III. REVIEWING THE STATUS QUO

Despite the crucial role that imagery and emotions play, the nuclear industry continues to focus on the dissemination of facts as its main raison d'être, communications-wise. However, is there evidence to support this strategy?

A. The (limited) role of knowledge

The nuclear industry's communication strategy has largely been driven by the idea that public opinion towards nuclear power is driven by a knowledge deficit. A commonly voiced opinion within the nuclear industry is the notion that *"[a] low level of public acceptance of nuclear power is usually due to a lack of knowledge"* [18]. Indeed, for a considerable part of the history of nuclear energy, the industry's mantra has been based on the notion that *"tell them the facts and they will love nuclear power"*. This is likely a response to surveys consistently showing that public understanding of radiation is either incomplete and/or incorrect [19].

However, even early nuclear-specific studies found no relationship between knowledge and opinions towards nuclear energy [20, 21]. When reviewing 38 different studies relating to women's risk perception of nuclear facilities and/or nuclear power generally, it was found that there was no support for the notion of increased knowledge resulting in decreased concern [22]. This has been supported elsewhere, showing that prior attitudes to nuclear energy play a major role in determining trust towards nuclear, whereas familiarity and knowledge of nuclear and radiological science played only a weak role [25]. Indeed, knowledge does not really shape views or alter opinions, but rather merely serves to confirm already-held views [23, 24]. This exemplifies the importance of confirmation bias in decision-making, and the human tendency towards reducing cognitive dissonance. Furthermore, the failure of facts to drive opinion change is the result of a simple fact: These factors must be reflected in any communications strategy, and for a very simple reason: 95% of our interactions with the world are processed in an automatic, involuntary, intuitive, nonverbal, narrative and experiential fashion [6, 7]. The way we think and interact with the environment can be divided into two different modes, or systems [5]. The dominant system, which Kahneman dubbed "System 1" relies heavily on images, narratives and metaphors to encode reality [7] whereas "System 2", being analytical, effortful, deliberative, and "rational" [6], has a proclivity towards facts. However, the nuclear industry has focused almost exclusively on "System 2", even if it is only responsible for a sliver of our decisions.

Despite the fact the evidence clearly highlights that the dissemination of facts as a strategy stands on very shaky grounds, it continues to be a cornerstone for the industry. As noted earlier, it is emotions and imagery, not facts, that are the key drivers behind people's perceptions generally, and this is very much the case for nuclear as well. A clear example of this that the nuclear sector can learn from is the way renewables have fundamentally shaped the clean energy narrative. Indeed, as a sector they have by and large been able to shape a narrative of hope for a better tomorrow surrounding their technology, directly driven by very powerful (and positive) imagery and associated emotions. Therefore, the nuclear industry should abandon knowledge dissemination as its guiding principle as far as communication is concerned, and rapidly move to align itself with a strategy that embraces emotions and provides positive imagery, to create positive associations with nuclear energy. However, this would require revisiting another key outreach cornerstone for the industry: safety.

B. Safety, safety, and more safety?

Since the 1960s, safety has been a central narrative in nuclear discourse. In many ways, this is paradoxical, as nuclear energy is not only the safest energy source available [26], but the use of nuclear energy is also estimated to have prevented considerable air pollution-related premature deaths worldwide [27]. The health risks posed by nuclear energy under both normal operating conditions and accident conditions have been extensively studied, finding that nuclear power plants have no material impact under normal operations. However, whilst the safety narrative was initially conceived and promoted by the anti-nuclear movement, the nuclear industry has directly and indirectly adopted it as a cornerstone of its own narratives. There is also ample evidence that the safety narrative has become internalized within the nuclear industry's modus operandi, with many of the next-generation developments of nuclear reactor designs being sold as "safer", offering "passive safety" or to be "walk-away safe" features, trying to sooth public concern about nuclear accidents. However, as Abdulla et al. [28] highlights *"[m]any of the strategies employed by the [nuclear] industry to defuse the dread seem likely to fail. The development of actuarially ever-safer reactors will not allow nuclear power to gain the level of acceptability required for substantially increased deployment, unless those developments erode the dread associated with the technology".*

The fundamental problem with the safety paradigm is the fact it gives rise to the so called "boomerang effect", whereby communication intended to decrease anxiety about a subject (e.g. nuclear power) results in an increase in anxiety [44]. There are many empirical examples of that, were communication has resulted in public mistrust and anxiety about nuclear energy, when the intention was to promote it [29-30]. Furthermore, by bringing attention to safety, the nuclear industry invites the negative imagery and emotions often associated with nuclear accidents, which directly undermines any positive messages. Indeed, the industry's refusal to move away from safety as a

communications strategy plays into the hands of its detractors. However, attempts to reframe nuclear power as a key technology for mitigating climate change has taken place since the late 1990s. Has this worked?

C. Climate change

The intersection between nuclear power and climate change in terms of public opinion is an avenue well-travelled. Several studies have found that those who are more concerned about climate change mitigation are also critical towards nuclear power because of general concerns about different environmental risks [32-36]. Interestingly, de Groot et al [37] found that those who identified most strongly with environmental values also did not acknowledge the environmental benefits of nuclear energy, and overall perceived nuclear energy's risks to be much higher than benefits. Similarly, the more serious a risk people considered climate change to be, the stronger in favour they were of renewables, but also led to a lowering in preference for nuclear power [38]. Indeed, Pidgeon et al. [34] found that a simple reframing of nuclear energy as a solution to climate change would, at best, result in what they dubbed "reluctant acceptance", with very few of the respondents actively favouring nuclear energy over renewables. In a similar vein, Bickerstaff et al. [33] found that very few of the focus group attendees genuinely favoured nuclear energy as a means of addressing climate change, and that only after discussion accepted nuclear energy as a "lesser of two evils". A strong reluctance amongst the focus group attendees to accept nuclear was noted, and acceptance only voiced after respondent had clearly stated their dislike for the nuclear. This notion has been supported elsewhere [39], which likely plays an important role in explaining why nuclear power struggles in the current renewables-dominated discourse. Similarly, Corner et al. [32] concluded that changing the framing of nuclear into being a solution to climate change did very little to increase public support for nuclear energy. Keller et al.'s [40] in-depth study of affective imagery and its impact on public support or opposition towards new nuclear found that the association between nuclear energy and climate change did not occur spontaneously, further suggesting that the climate change pivot has had very limited impact.

It is possible that anecdotal evidence of climate change leading to people becoming more pro-nuclear is driving the pivot towards climate change as the main communications frame. There have been cases of individuals from the anti-nuclear environment (e.g. Stephen Tindale) which cited the need for nuclear energy in combatting climate change as the reason for their change in opinion. However, given the findings discussed earlier, the evidence suggests a highly limited role for climate change in changing public opinion regarding nuclear energy. Evidence even suggests that a substantial part of the public perceives nuclear energy as a contributor to climate change - 69% of respondents in France [41] and 49% in Belgium [42]. Truelove & Greenberg [43] similarly found that more than 50% of their sample believed nuclear contributed to climate change.

These findings reinforce the notion that the industry's climate pivot has yielded very little success. Whilst pursuing widespread adoration might be unrealistic, the nuclear industry will likely struggle to attract support if only aiming for "reluctant acceptance". That is not a long-term solution, and undermines the rationale for the industry's climate change pivot, especially as those most concerned about climate change are also those least in favour of nuclear.

IV. COMMUNICATIONS FOR THE FUTURE

Nuclear power and technology have a very important role to play in the upcoming decades. It will help combat air pollution, provide clean drinking water, fight starvation, eliminate energy poverty, and help decarbonise our energy system. However, this role will be squandered if the public does not support nuclear energy, and the nuclear industry has a bit of an uphill battle in that department. The nuclear sector must find the courage to slam the reset button on its communications activities, and fundamentally change its approach. Focusing on "correcting misunderstandings" to win over the public and policy makers has never worked, and never will. It simply does not appeal to our nature.

We have seen that the most successful communication strategies are those that appeal to our human nature by telling stories, using powerful imagery and emotions. As Storr eloquently summarises it, there is *"…simply no way to understand the human world without stories. They fill our newspapers, our law courts, our sporting arenas, our government debating chambers, our school playgrounds, our computer games, the lyrics to our songs, our private thoughts and public conversation and our waking and sleeping dreams. Stories are everywhere. Stories are us"* [31]. In many ways, nuclear power has an immensely powerful story to tell, not dissimilar to that of David (nuclear) and Goliath (fossil fuels). Indeed, with nuclear power having the potential to fundamentally revolutionise life as we know it, the messages of "hope" and building a stronger tomorrow should likely find favour with the public. It is, however, crucial that the nuclear industry starts a sustained campaign, centred on positive imagery and emotions, to start and replace the multi-decade anti-nuclear master narrative that still surrounds nuclear power. If successfully done, the future for nuclear power will likely be very bright indeed.

V. REFERENCES

[1] Fahlquist, J. N. & Roeser, S., 2015. Nuclear energy, responsible risk communication and moral emotions: a three level framework. *Journal of Risk Research,* 18(3), pp. 333-346.

[2] Damasio, A. R., 1996. The Somatic Marker Hypothesis and the Possible Functions of the Prefrontal Cortex. *Philosophical Transactions: Biological Sciences,* 351(1346), pp. 1413-1420.

[3] Damasio, A., 2006. *Descratre's Error.* London: Vintage.

[4] Reynolds, B. J., 2011. When the facts are just not enough: Credibly communicating about risk is riskier when emotions run high and time is short. *Toxicology and Applied Pharmacology,* 254(2), pp. 206-214.

[5] Epstein, S., 1994. Integration of the Cognitive and the Psychodynamic Unconscious. *American Psychologist,* 49(8), pp. 709-724.

[6] Kahneman, D., 2011. *Thinking, Fast and Slow.* New York: Farrar, Straus and Giroux.

[7] Slovic, P., et al., 2004. Risk as Analysis and Risk as Feelings: Some Thoughts about Affect, Reason, Risk, and Rationality. *Risk Analysis*, 24(2), pp. 311-322.

[8] Marks, D. F., 1999. Consciousness, mental imagery and action. *British Journal of Psychology*, Volume 90, pp. 567-585.

[9] Damasio, A., 2000. *The Feeling of What Happens.* London: Vintage.

[10] Marks, D. F., 2019. I Am Conscious, Therefore, I Am: Imagery, Affect, Action, and a General Theory of Behavior. *Brain Sciences*, 9(107), pp. 1-27.

[11] Slovic, P., et al., 2005. Affect, Risk, and Decision Making. *Health Psychology*, 24(4 (Suppl.)), pp. S35-S40.

[12] Loewenstein, G. F., et al., 2001. Risk as feelings. *Psychological Bulletin*, 127(2), pp. 267-286.

[13] Rottenstreich, Y. & Hsee, C. K., 2001. Money, Kisses, and Electric Shocks: On the Affective Psychology of Risk. *Psychological Science*, 12(3), pp. 185-190.

[14] Lichtenstein, S., Slovic, P., fischhoff, B. & al., e., 1978. Judged frequency of lethal events.. *Judged frequency of lethal events. Journal of Experimental Psychology: Human Learning and Memory*, 4(6), pp. 551-578.

[15] Peters, E. & Slovic, P., 1996. The Role of Affect and Worldviews as Orienting Dispositions in the Perception and Acceptance of Nuclear Power. *Journal of Applied Social Psychology*, 26(16), pp. 1427-1453.

[16] Slovic, P., et al., 1985. Characterising Perceived Risk. In: *Perilous progress: Managing the hazards of technology.* Boulder, CO.: Westview, pp. 91-125.

[17] Slovic, P., et al., 1991. Perceived Risk, Trust, and the Politics of Nuclear Waste. *Science*, Volume 254, pp. 1603-1607.

[18] World Nuclear News, 2020. *The barrier to nuclear is perception, says panel*. Available at: https://www.world-nuclear-news.org/Articles/The-barrier-to-nuclear-is-perception,-says-panel.

[19] Henriksen, E. K., 1996. Laypeople's understanding of radioactivity and radiation. *Radiation Protection Dosimetry*, 68(3/4), pp. 191-196.

[20] Sundstrom, E., et al., 1977. Community attitudes toward a proposed nuclear power generating facility as a function of expected outcomes. *Journal of Community Psychology*, 5(3), pp. 199-208.

[21] Clelland, D. & Bremseth, M., 1977. *Student Reactions to Breeder Reactors.* Chicago: Department of Sociology, University of Tennessee, Knoxville.

[22] Davidson, D. J. & Freudenburg, W. R., 1996. Gender and environmental risk concerns. *Environmental Behavior*, 28(3), pp. 302-339.

[23] Visschers, V. H. M. & Wallquist, L., 2013. Nuclear power before and after Fukushima: The relations between acceptance, ambivalence and knowledge. *Journal of Environmental Psychology*, Volume 36, pp. 77-86.

[24] Kasperson, R. E., et al., 1980. Public Opposition to Nuclear Energy: Retrospect and Prospect. *Science, Technology, & Human Values*, 5(31), pp. 11-23.

[25] Oltra, C., et al., 2019. Trust perceptions among residents surrounding nuclear power plants: A descriptive and explanatory study. *Progress in Nuclear Energy*, Volume 113, pp. 1-6.

[26] Markandya, A. & Wilkinson, P., 2007. Electricity generation and health. *The Lancet*, 370(9591), pp. 979-990.

[27] Kharecha, P. A. & Hansen, J. E., 2013. Prevented Mortality and Greenhouse Gas Emissions from Historical and Projected Nuclear Power. *Environmental Science & Technology*, 47(9), pp. 4889-4895.

[28] Abdulla, A., et al., 2019. Limits to deployment of nuclear power for decarbonization: Insights from public opinion. *Energy Policy*, Volume 129, pp. 1339-1346.

[29] Novikau, A., 2017. What is "Chernobyl Syndrome?" The Use of Radiophobia in Nuclear Communications. *Environmental Communication*, 11(6), pp. 800-809.

[30] Grimston, M., 2016. *The Paralysis in Energy Decision Making.* Dunbeath: Whittles Publishing.

[31] Storr, W., 2019. *The Science of Storytelling.* London: William Collins.

[32] Corner, A. et al., 2011. Nuclear power, climate change and energy security: Exploring British public attitudes. *Energy Policy*, 39(9), pp. 4823-4833.

[33] Bickerstaff, K. et al., 2008. Reframing nuclear power in the UK energy debate: nuclear power, climate change mitigation and radioactive waste. *Public Understanding of Science*, 17(2), pp. 145-169.

[34] Pidgeon, N. F., et al., 2008. Climate change or nuclear power—No thanks! A quantitative study of public perceptions and risk framing in Britain. *Global Environmental Change*, 18(1), pp. 69-85.

[35] Vainio, A., Paloniemi, R. & Varho, V., 2017. Weighing the Risks of Nuclear Energy and Climate Change: Trust in Different Information Sources, Perceived Risks, and Willingness to Pay for Alternatives to Nuclear Power. *Risk Analysis*, 37(3), pp. 557-569.

[36] Kahan, D., 2014. *Who fears what & why? Trust but verify!* Available at: http://www.culturalcognition.net/blog/2014/3/10/who-fears-what-why-trust-but-verify.html.

[37] de Groot, J. I. M., Steg, L. & Poortinga, W., 2013. Values, Perceived Risks and Benefits, and Acceptability of Nuclear Energy. *Risk Analysis*, 33(2), pp. 307-317.

[38] Chung, J.-B. & Kim, E.-S., 2018. Public perception of energy transition in Korea: Nuclear power, climate change, and party preference. *Energy Policy*, Volume 116, pp. 137-144.

[39] Venables, D., et al., 2009. Living with Nuclear Power: A Q-Method Study of Local Community Perceptions. *Risk Analysis*, 29(8), pp. 1089-1104.

[40] Keller, C., Visschers, V. & Siegrist, M., 2012. Affective Imagery and Acceptance of Replacing Nuclear Power Plants. *Risk Analysis*, 32(3), pp. 464-477.

[41] World Nuclear News, 2019. *French public sees continued use of nuclear energy.* [Online] Available at: https://www.world-nuclear-news.org/Articles/French-public-sees-continued-use-of-nuclear-energy [Accessed 1 January 2021].

[42] World Nuclear News, 2019. *Belgian support for keeping reactors running beyond 2025 rises.* Available at: https://www.world-nuclear-news.org/Articles/Nuclear-upport-grows-in-Belgium.

[43] Truelove, H. B. & Greenberg, M., 2013. Who has become more open to nuclear power because of climate change?. *Climatic Change*, Volume 116, pp. 389-409.

[44] Hart, P. S., 2014. “Boomerang effects in risk communication” in *Effective Risk Communication*, Arvai J. & Rivers III, L. Eds, Abingdon: Routledge, ch. 18, pp. 304-318.

Proceedings of the European Nuclear Young Generation Forum
ENYGF'21
September 27-30, 2021, Tarragona, Spain

#NetZeroNeedsNuclear: Mobilising the nuclear community and beyond to influence change at COP26

Thomas, Saralyn[1*] and Khuttan, Arun[2]

[1] Abbott Risk Consulting Ltd, Nuclear Institute Young Generation Network, UK; [2] Magnox Ltd, Nuclear Institute Young Generation Network, UK

*Corresponding author: *Saralyn.thomas@consultarc.com*

I. INTRODUCTION

2021 is a pivotal year for the climate. In November, Glasgow will host the United Nations (UN) Climate Change Conference, COP26. The climate talks will be the biggest international summit the UK has ever hosted, bringing together over 30,000 delegates including heads of state, climate experts and campaigners to agree coordinated action to tackle climate change. Although these talks are held every year, COP26 is particularly important as progress on the commitments made in the Paris Agreement at COP21 will be a key part of discussions. It is also highly anticipated having been postponed by a year due to the COVID-19 pandemic and represents an opportunity to collaborate globally on a green recovery plan.

This year, the Nuclear Institute (NI) Young Generation Network (YGN) has a unique opportunity to make waves at the conference. The NI, as the learned society for the UK nuclear sector, is a member society of the European Nuclear Society (ENS), a learned society representing over 12,000 professionals from the academic world, research centres, industry and authorities. ENS is also a United Nations Framework Convention on Climate Change (UNFCCC) accredited Non-Governmental Organisation (NGO) and a founding member of Nuclear for Climate, a grassroots initiative gathering over 150 associations, including the NI, with the goal of educating policymakers and the public about the necessity of including nuclear energy among carbon-free solutions to climate change.

For each Conference of the Parties (COP), Nuclear for Climate partners with the young generation association from the hosting country to coordinate presence in the UN zone. As a result, the UK YGN set up a team of volunteers, their vision and mission for 2021 being:

•Vision: To have a clean, sustainable and abundant low-carbon future for all

•Mission: To accelerate the ability of the world to achieve Net Zero by 2050, by driving collaboration between nuclear and renewable technology.

A key aspect of the mission is to collaborate with other clean energies to communicate with people beyond the nuclear community, with the aim of educating others about nuclear's clean energy credentials.

II. NET ZERO NEEDS NUCLEAR CAMPAIGN

In order to achieve the above vision and mission, the UK YGN launched the #NetZeroNeedsNuclear campaign in February 2021. The campaign aims to:

- Promote and raise awareness of nuclear as a low-carbon energy source;
- Drive support for nuclear as a key part of our path to Net Zero;
- Influence policymakers who are involved in COP26 to take a scientific and technology neutral approach to energy policy and financing; and
- Envision sustainable collaboration between nuclear and renewables.

Key aspects of the campaign are discussed in more detail in the below sub-sections.

A. Nuclear for Climate Position Paper

The heart of the campaign lies in a position paper written by the UK YGN on behalf of Nuclear for Climate. The position paper has been written using reputable references from a range of source such as the International Energy Agency, Intergovernmental Panel on Climate Change, International Atomic Energy Agency and many more. The scientifically underpinned position paper summarises why Net Zero Needs Nuclear in the following five points [1]:

- Nuclear is a proven low-carbon source of energy which reduces greenhouse gas emissions and can replace our current reliance on polluting fossil fuel sources.
- Nuclear is available, scalable and deployable: New nuclear needs to be deployed at scale and urgently, along with renewables, in order for Net Zero targets to be achievable.
- Nuclear is a flexible and affordable source of clean energy: Nuclear can integrate with an increasing

supply of variable renewables to deliver efficient and affordable clean energy systems.
- Nuclear can deliver more than just low-carbon electricity: Nuclear is also capable of supporting the decarbonisation of other sectors, such as heating and transport.
- Nuclear supports inclusive and sustainable global development: Nuclear promotes global socio-economic benefits and is strongly aligned to the UN Sustainable Development Goals (SDGs).

The position paper presents the scientific justification on why Net Zero Needs Nuclear and asks the following from policymakers:

"We are calling on all negotiators and policymakers who are involved at COP26 to take a scientific and technology neutral approach to energy policy and financing that can promote sustainable collaboration between nuclear and renewables."

As a result of feedback from the World Nuclear Association, the team intends to approach these international policy makers with the position paper in May as many key decisions that will be finalised at COP26 will be discussed well in advance of the conference in November.

B. Call to Action

Alongside the position paper is a petition which was set up on change.org [2]. This was created as the team wanted to demonstrate the level of support globally for the campaign. A target of 10,000 signatures on the petition has been set and the petition will be referred to when approaching policy makers to evidence the support for nuclear energy.

C. Social Media Campaign

A social media campaign was developed for the launch of the campaign in order to create some buzz online. Social media is an incredibly powerful tool in campaigning – social media posts, with the right hashtags, have the potential to show the world both the importance of nuclear along with the people behind the messages.

Humanising the nuclear community through the campaign was key. Individuals were encouraged to join the social media campaign in the following ways:

- Taking a short video answering the prompt "Net Zero Needs Nuclear because …";
- Taking a selfie with a #NetZeroNeedsNuclear poster;
- Adding a photo and a quote about why Net Zero Needs Nuclear to a social media template (see Figure 1 for an example);
- Using the #NetZeroNeedsNuclear social media frame for your profile picture.

To encourage more people to get involved, people were asked to nominate at least three other people to sign the petition and get involved in the social media campaign. In order to take advantage of our collective network, people were encouraged to nominate a diverse range of people in their posts, such as contacts that work outside the nuclear industry or those who live in a different country.

Hashtags were also incredibly important for the social media campaign. Although a range of hashtags were encouraged, the following hashtags were prioritised: #COP26, #NetZero, #TogetherForOurPlanet and #NetZeroNeedsNuclear.

The first two hashtags were adopted as these were generic hashtags that those interested in COP26 and clean energies would likely follow. #TogetherForOurPlanet was a particularly key hashtag as this was adopted by the COP26 Presidency in the UK for their social media posts [3]. Using this hashtag on our posts meant that the #NetZeroNeedsNuclear campaign then featured heavily when following that hashtag. Use of the #NetZeroNeedsNuclear hashtag allowed us to keep track of additional social media activity.

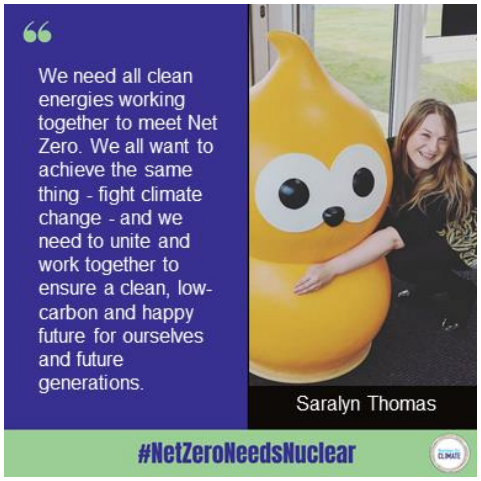

Figure 1. Example of the social media template being used

III. MOBILISING THE NUCLEAR COMMUNITY AND BEYOND

An early activity undertaken by the team was identifying a variety of stakeholders. This was imperative to getting our message out and gaining support for the campaign. The following high-level stakeholders were identified as important to engage with:

- Nuclear professionals and advocates;
- Clean energy industries;
- UNFCCC NGOs and wider groups with shared values;
- International policymakers.

It was agreed that the earlier stages of the campaign would concentrate on engaging with nuclear professionals and advocates as they are already passionate about nuclear's role in meeting net zero. As support was gained from the nuclear community, engagement would then progress to the clean energy industries and NGOs/wider groups, until approaching international policymakers when the campaign was well established with a large presence online and many signatures on the petition.

It was recognised that a different approach would need to be taken with each type of stakeholder. The approach taken with each of these stakeholders is explained in the below sub-groups.

A. Nuclear Professionals and Advocates

As the team was mostly UK based, stakeholder engagement primarily started with those based in the UK. The UK YGN worked very closely with the NI, which has over 4,000 members with nine regional branches across the UK. Each of the branches were contacted with details of the campaign while a variety of communications to NI members were written, e.g. newsletters, articles in the NI bi-monthly journal, social media posts. The NI website was also updated so that the campaign was showcased prominently.

The team was largely supported by the Nuclear Industry Association, the trade association for the civil nuclear industry in the UK. The NIA represents more than 250 companies across the supply chain and were able to contact their company members about the campaign.

Soon after launch of the campaign, our efforts turned to our international colleagues. Nuclear for Climate was key to ensuring international presence in the campaign as they were able to contact all the associations under Nuclear for Climate, such as the American Nuclear Society, French Nuclear Energy Society (SFEN), JAIF and many more. A Nuclear for Climate Steering Committee was also set up where we were able to inform Nuclear for Climate of our activities and ask for their support promoting the campaign.

Another powerful international stakeholder for the team was Women in Nuclear (WiN) Global and the newly established WiN Global Young Generation. WiN currently has approximately 35,000 members including chapters' members and individuals from 129 countries. In total there are over 42 national, regional and international chapters throughout the world. Hence, collaboration with WiN Global represented a significant opportunity to the team to promote the campaign internationally.

International conferences also represented an opportunity to promote the campaign. For instance, organisers for the 54th JAIF Annual Conference, the 40th Annual Conference of the Canadian Nuclear Society and ENYGF 2021 itself were contacted asking for the campaign to be promoted during the conference.

It was important also to engage with those outside the nuclear industry who were passionate about nuclear energy. Periodic meetings were set up with various nuclear campaigners and influencers to understand how to amplify and accelerate messages to non-traditional audiences. This included meetings with Eric Meyer, Founder of Generation Atomic, Zion Lights, science communicator and ex-Extinction Rebellion spokesperson and Brazilian Model Isabelle Boemeke.

Such campaigners and industry leaders were asked to formally support the campaign by becoming an envoy, with the responsibility of promoting the campaign in their companies, while speaking at events, etc.

B. Clean Energy Industries

The next step was to engage with the wider clean energy industry. Our message here was that greater collaboration was required across the energy sector in order to achieve our common goal of meeting net zero.

As the NI is the professional membership body for the UK nuclear sector, a natural ally outside the industry were other professional institutes representing individuals working in the wider energy sector. Institutes such as the Energy Institute, Institute of Physics and Institution of Chemical Engineers were contacted.

The team was also recommended to contact trade unions. A particularly successful collaboration was with Prospect, a trade union for professionals working in science, energy and beyond. The team was given the opportunity to write a guest blog [4] about the campaign which was shared with their 150,000+ members.

As part of the #NetZeroNeedsNuclear campaign, the team planned to organise a series of webinars. The clean energy industry was identified as our preferred collaborator for such events so we could share our messages to a new audience, i.e. the wider low-carbon energy industry.

One successful example of this was a webinar, "Engineering for the Energy Transition" we collaborated on with COP26 and Beyond and Global Engineering Futures [5]. A full list of collaborators can be seen in Figure 2. The webinar featured a panel discussion, and interactive question and answer sessions with industry, academic experts and early-career engineers from many of the sectors crucial to the energy transition such as renewables, nuclear, aviation and industry. The webinar itself was well attended, primarily by those working outside the nuclear industry.

Figure 2. Collaborators for the "Engineering for the Energy Transition" webinar

C. UNFCCC NGOs and Wider Groups with Shared Values

UNFCCC NGOs were an important ally as they will have access to the UN zone at COP26, alongside ourselves. Early collaboration with these NGOs could maximise our impact at the conference itself. A list of UNFCCC accredited NGOs can be found online [6]. The list was reviewed and refined by the team to include NGOs related to sustainable energy, renewables, youth groups and hard to decarbonise industry groups.

A list of other groups with shared values was also produced from a wider web search. Examples of these groups are Freeport East Hydrogen Hub, the Clean Air Task Force, Mothers for Lungs.

Our approach in such communications was to put our shared values at the forefront, similar to the approach taken with the clean energy industry. UNFCCC accredited NGOs are passionate about the climate and want to help save our planet. This is exactly what we want to do as part of the #NetZeroNeedsNuclear campaign and our wider vision and mission statements. Highlighting nuclear's role in fulfilling

several of the UN's SDGs was also an important part of this approach.

D. International Policymakers

The key aim of the campaign was to influence the decision making of policymakers in the run up to COP26. This activity was scheduled towards the end of the campaign in the hopes that the petition would have gained a large number of signatures by this point in the campaign.

Although the UK YGN had a good understanding of its own Government and who would be representing the UK at COP26, we were not knowledgeable on other Governments across the world. It was decided early in our planning that the international YGNs would be integral to this activity.

The UK YGN worked closely with the International Youth Nuclear Congress (IYNC) to organise an advocacy workshop about the #NetZeroNeedsNuclear campaign.

The aim of the workshop was to brief all YGNs about the campaign and ask for their support in writing a letter to their own Government. The intent was that Governments and UN representatives across the world would be contacted by 40+ YGNs across the world, imploring them to consider nuclear energy in their decision making at COP26.

IV. MEASURING SUCCESS

Success can be achieved in a variety of ways. Our vision of success was for nuclear to be included in discussions at COP26. At the time of writing, COP26 has not taken place and it remains to be seen whether a successful outcome will have been achieved.

In the event that nuclear does have a good outcome at COP26, it is also difficult to determine whether that outcome can be attributed in any way to the #NetZeroNeedsNuclear campaign.

In order to measure the success of the campaign, a variety of metrics were tracked. Below are some of the more important ones:

- Number of signatures on the petition;
- Social media impressions;
- Number of media articles.

The clearest measure of success was the number of signatures on the petition. Figure 3 shows the number of signatures gathered throughout the campaign to date. An increase in the number of signatures could generally be seen following activities from the team, such as social media posts, articles being published, the campaign being promoted during an event. The comments section of the petition was also a useful indication of reach due to comments making references to certain countries or different languages being used.

Social media impressions were a useful metric. Social media activity on each post was monitored to identify what type of posts worked well and should be repeated. Generally, the team found that posts which included animations and featured people were popular.

Another priority for the team was to engage with the media; hence, the number of media pieces was another important indication of success. To date, the campaign has featured in three different media pieces online.

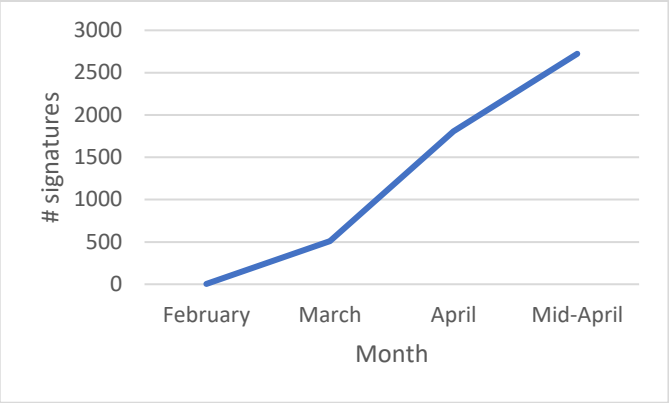

Figure 3. Number of signatures gathered throughout the campaign.

V. CONCLUSION AND NEXT STEPS

COP26 is an international gathering of people who are passionate about saving our planet. Collaboration between countries and different sectors will be key to meeting net zero and such collaboration is also key to the success of the #NetZeroNeedsNuclear campaign.

Seven months remain until COP26 and our next step is to start formally engaging with international policymakers. Working with other YGNs will be key to this – our collective young voices will send a much stronger message to the UN. ENYGF 2021 takes place just a weeks before COP26 and we will be using the conference as one last opportunity to gather international support for the campaign and present a united front.

VI. References

[1] Nuclear for Climate, Position paper "Net Zero Needs Nuclear 2021 Position Paper", https://www.euronuclear.org/wp-content/uploads/2021/02/COP26-Position-Paper.pdf (accessed 11/04/21).

[2] "Save our Climate – Acknowledge that Net Zero Needs Nuclear at COP26", https://www.change.org/p/save-our-climate-we-need-your-signatures-acknowledge-that-net-zero-needs-nuclear-at-cop26 (accessed 11/04/21).

[3] UK Cabinet Office, "Together for our planet – The UK's year of climate action", https://together-for-our-planet.ukcop26.org/ (accessed 11/04/21).

[4] Prospect, "Young clean energy heroes set out on COP26 campaign trail", https://prospect.org.uk/news/young-clean-energy-heroes-set-out-on-cop26-campaign-trail/ (accessed 11/04/21).

[5] COP26 and Beyond, "Engineering for the Energy Transition - An Online Event", https://www.cop26andbeyond.com/blog/engineering-for-the-energy-transition (accessed 11/04/21).

[6] UNFCC, "Admitted NGOs", https://unfccc.int/process/parties-non-party-stakeholders/non-party-stakeholders/admitted-ngos/list-of-admitted-ngos (accessed 11/04/21).

Proceedings of the European Nuclear Young Generation Forum
ENYGF'21
September 27-30, 2021, Tarragona, Spain

Novelties in Teaching and Learning. Process and systematic approaches harmonization.

Vladislav Cherdantsev

Rosatom Technical Academy (Rosatom Tech), Russia

*Corresponding author: *cherdantsewva@gmail.com*

I. INTRODUCTION

To ensure the long-term, successful and failure-free operation of nuclear power plants, it is necessary to make the safety of nuclear power plants a top priority, especially in relation to the economic one. The operating personnel, just like the administrative personnel, having constant direct contact with the equipment is an integral part of ensuring the reliable and safe operation of the nuclear power plant. That is why **the main task of training centers** (which we build on the sites of our customers' NPPs on a "turnkey" basis), as an end-product of the personnel training process, **is** precisely **qualified personnel** capable of thinking, taking clear actions and deliberate decisions in short periods of time.

Before I proceed, I'd like to mention that the initiating event for creation of Nuclear Power Plant training centers was, unfortunately, nothing else but a set of disasters at both Three Mile Island and Chernobyl that we will remember forever. In next two years after the accidents a decree was issued in USSR that obliged operating organizations to enhance the equality of personnel training and also it became mandatory to include training centers in NPP design.

Since then we, fortunately, haven't come across accidents with such devastating consequences which literally shows the effectiveness of measures taken way back then.

In this work, I would like to share our experience, breakthrough technologies and methods of increasing the efficiency of training of nuclear power plants operating personnel.

II. TEACHING AND LEARNING NOVELTIES

In this section, our teaching technologies, novelties and breakthroughs in teaching and learning sphere are described.

A. Instructors of new generation

Currently, the foreign portfolio of the state corporation "Rosatom" encounters just about 36 orders for the nuclear power plants construction in various countries. In order to effectively train such a volume of foreign personnel it is necessary to have a pool of new generation instructors who must have excellent knowledge of technology, fluent English, psychological and pedagogical skills, as well as know the cultural characteristics and mentality of the peoples.

To solve this task, we have developed an ambitious project involving the training of over 120 instructors of a new generation.

The project started in 2018. It refers to a two-year training program. The training is carried out in 12 directions: from the shift supervisor of the radiation safety department to the shift supervisor of the power unit. As part of the curriculum, graduates of advanced technical universities master the technological aspects, issues of safe operation of nuclear power plants, instructor skills, undergo training at innovative power units of generation 3+ - VVER-1200 and in international training centers.

Figure 1. Instructors of new generation graduation.

Talking about English, it is obvious that free communication without the need for translation contributes to better mutual understanding between the student and the teacher. To this end, Rosatom Technical Academy has developed a unique English language program, organized as a continuous and intensive process. It includes:

- Classes with Rosatom Tech teachers in technical English
- Development of speech skills in the classroom on the general communication course

- Preparation and defense of presentations according to specialties.

The first 39 nuclear knowledge ambassadors completed a 2-year training cycle in 2020 and have already started training the Rooppur NPP personnel.

The “new generation instructors” project also became a finalist at the “People investor - 2020” forum held in Russia.

B. “Turnkey” Training Centers

To ensure the start-up and safe operation of nuclear power plants in the country of a foreign customer, we offer a unique product called "Turnkey" Training Center.

Turnkey training center - is a comprehensive solution, a full-fledged training center that includes not only infrastructure, but also a whole training management system. The training center allows initial training and continue training of NPP operating personnel throughout the entire period of NPP operation. A huge advantage of this approach is that there is no need to send foreign personnel to the Russian Federation for training.

Figure 2. A turnkey training center design.

The training centers that we offer are unique because of two reasons:

1. The TC includes not only the infrastructure design, but also the whole training management system
2. It harmonizes the 2 well-known approaches:
    a. Process approach to Quality Management System (QMS)
    b. Systematic approach to training (SAT).

Let’s take a closer look at the 2nd advantage.

As TC operating experience showed, the implementation of only one quality management system standards ISO 9001-2015 [1] to improve the quality of personnel training at the training center is not enough. And not only does a successful application of systematic approach to personnel training along with the process approach of the QMS pose the problem, but also real confirmation of the application, a graphical description of the very harmonization of SAT and the process approach in QMS. What customers really need is a precise description of interactions between the components of the process called "personnel training". This is what confirms the fact of a real harmonization of the methods I mentioned that improve the quality of provided services.

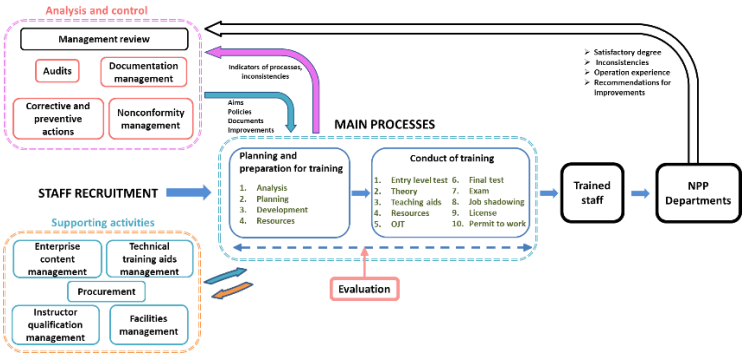

Figure 3. Processes and main activities interaction diagram.

In accordance with Ref. [1], to implement the process approach, an organization must “identify” and manage “multiple and interrelated activities”. An activity that uses resources and is managed to transform inputs into outputs can be considered as a process.

The main processes are depicted in the center of the Figure 3 and since a TC mostly performs teaching activity, let’s take a closer look at a “personnel training” process.

As I have already noted, a systematic approach to training, described in [2] has been implemented in the training center for personnel training. The personnel training process conventionally consists of two stages:

1. Planning and preparation for training. The following SAT stages are carried out here:
    a. Analysis
    b. Design
    c. Development.

Based on the results of the development stage, an intermediate assessment of the learning process is carried out, after which the second stage of the personnel training process begins:

2. Conduct of training,

including an entry level test, theoretical training using teaching aids and resources, on the job training, final test, exams, job shadowing, obtaining a license (if necessary) and subsequent admission to work.

For the successful implementation of these stages, the departments of the TC, involved in their implementation, send requests, interact with TC supporting activities. The result of such interaction is the allocation of **resources** by the departments which perform supporting activities, such as: material and technical support, computer support for training process, technical training aids, etc.

The analysis and control block, in turn, provides:

a. quality of normative, educational, methodological and production documentation
b. records management
c. audits conduction
d. development of corrective and preventive actions.

Having studied the diagram, it is easy to see that we not only continuously improve the quality of the provided personnel

training services (in accordance with [1]) implementing SAT, but also successfully demonstrate this harmonization on the diagram, describing all the interactions between the main TC processes and activities.

C. Integrated Information System (IIS)

Before we move to our next novelty in teaching and learning, let's first consider the main TC components:

a. Resources (instructors, technical teaching aids, teaching materials, full-scale simulator, etc.)
b. Training management system
c. Integrated information system

Thus, along with the resources and the training management system (which was discussed in section II.B), the TC includes the so-called Integrated Information System.

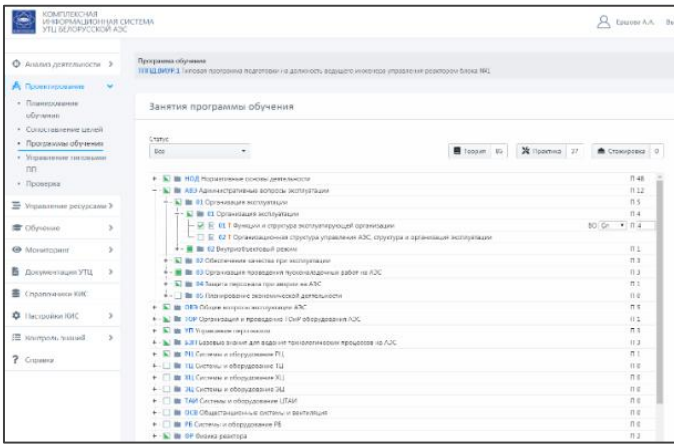

Figure 4. IIS user interface.

IIS is a set of subsystems used to automate the main processes of the nuclear power plant TC. The system is implemented in the form of web applications that can be easily installed on the software platform in the training center. IIS automates the following activities:

- Implementation of SAT methodology
- Planning and organization of training
- Teaching and knowledge control
- Computer-based training and tests

IIS is comprised of the following subsystems:

1. Main activities analysis and training programs development support system
2. Training materials development support system
3. Support for organization of training
4. Automated training and knowledge control system
5. NPP personnel qualification data accounting system
6. Monitoring and analysis of training processes
7. Integration of information services and their management resources

Subsystems #1-6 ensure the complete implementation of SAT.

Receiving this system as part of our turnkey TC product, the customer almost completely automates the process of training NPP personnel in accordance with the latest methodologies and international IAEA requirements in the field of teaching and learning. This, in turn, has a positive effect on the general level of NPP safety culture, which directly affects its safe operation.

Over and above, what concerns cyber security: the software we implement is stored locally within a training center and since only authorized personnel can enter the TC the leak of secret information can't happen.

D. Computer-based training system (CBTS)

And the last novelty I'd like to tell you about is a Computer-based training system. In 2020 the pandemic has led to a drastic growth in remote learning. And since classroom sessions were not allowed we decided to apply CBTS in full scope so as to meet personnel training deadlines.

Thus, a CBTS is a software complex (integrated into IIS) designed for personnel training and testing and evaluation of training.

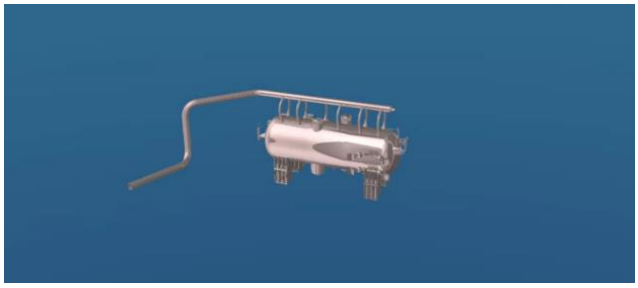

Figure 5. CBTS screenshot. Steam generator 3D model.

By this time, we have developed CBTS for almost every NPP system, as well as for such NPP processes as:

1. transitions from cold to hot state and back
2. transitions from hot state to operation at minimum controlled level of power and back
3. transitions from operation at minimum controlled level of power to operation at power and etc...

Information content of CBTS comprises:

- 3D models
- Drawings and pictures of system components
- Animated schemes of fluids flows and equipment operation
- Photos of equipment
- Hyperlinks to the operational documents

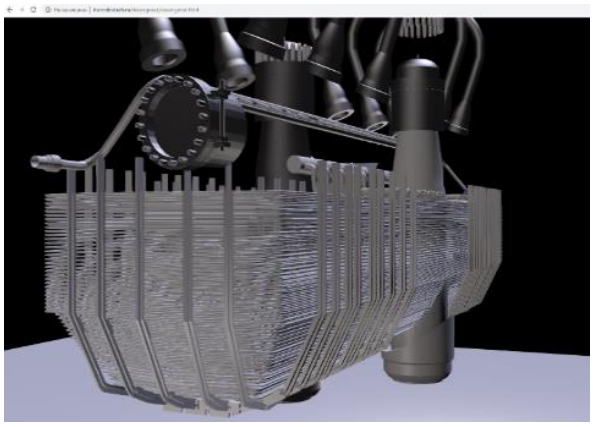

Figure 6. CBTS screenshot. Steam generator internal structure.

Along with online classes implementation of CBTS gives personnel an opportunity to study materials themselves

more detailed even without a presence of an instructor since it provides a very precise description of every single detail of main NPP equipment. It also teaches you how to operate NPP systems: start-ups, shutdowns, procedures for taking equipment out of service for maintenance, possible malfunctions are mentioned in CBTS.

3D models are also useful for those who struggle with spatial thinking.

III. CONCLUSIONS

The novelties in teaching and learning that I reported on today are absolutely vital for those who particularly work in nuclear sphere. One of the indicators that proves the effectiveness of our teaching methods is the fact that even the pandemic hasn't broken our foreign personnel education plans. Our novelties in teaching and learning not only make the education process efficient (since even without a direct contact with lecturers, students are still being explained the information they study via CBTS) but also extremely convenient for both sides. Additionally, a great role in teaching of foreign personnel plays communication without interpreters, which accelerates the education processes by twice.

Over and above that an implementation of visual education (Computer Based Training System) going with a simultaneously pronounced lecturer speech allows personnel to study materials themselves as if they are still in a classroom.

Fluent in English instructors of new generation, whose training program takes maximum 2 years literally break language borders between students and them. According to feedbacks given by our foreign customers, they are completely satisfied with the education quality we provide.

All of the foreigners who undergo our training are broken down into groups according to the position they will take.

Initially they are given a **theory course** (which is carried out in classrooms in a form of lecture where students may interrupt lecturer and ask anything) which is followed by an **evaluation stage** goes which is aimed at revealing strong and weak sides of future personnel (all of the results and recorded and furtherly taken into consideration so as to implement necessary changes into training programs for the following groups).

Those who successfully pass theory then pass **on the job training** at a corresponding position where specially appointed power plant operators explain the operation of one or another NPP system or equipment.

The combination of the following training steps shows incredibly high degree of knowledge which is proved by the final tests and exams.

And of course, what I'd like to highlight the most is a "Turnkey" Training Center, which is a great invention. It comprises not only the infrastructure design, but also the whole personnel training management system. The harmonization of process approach in QMS and systematic approach to training, which is undoubtedly an innovation, lets us to even more enhance the quality of service we offer.

The presence of such a training center gives the customer a guarantee in the service provider. It also contributes to a continuous safety culture improvement along with a reduction of a human factor at NPP.

IV. References

[1] ISO 9001, Quality management systems— Requirements, 2015.

[2] IAEA, Experience in the use of systematic approach to training (SAT) for nuclear power plant personnel, pp. 1-3, 1998

Proceedings of the European Nuclear Young Generation Forum
ENYGF'21
September 27-30, 2021, Tarragona, Spain

Analysis of the impact of the COVID-19 pandemic on the Spanish Radiation Protection Professionals

García-Baonza, Roberto[1], Sáez-Muñoz, Marina[2*], Candela-Juan, Cristian[3], Rozas, Saroa[4], Camp, Anna[5] and Andresz, Sylvain[6]

[1] Departamento de Ingeniería Energética, ETSI Industriales, Universidad Politécnica de Madrid, Spain

[2] Laboratorio de Radiactividad Ambiental, MEDASEGI Research Group, Universitat Politècnica de València, Spain

[3] Centro Nacional de Dosimetría (CND), Instituto Nacional de Gestión Sanitaria, Spain

[4] Department of Energy Engineering, Faculty of Engineering in Bilbao, University of the Basque Country (UPV/EHU), Spain

[5] Institut de Tècniques Energètiques, Universitat Politècnica de Catalunya (UPC), Spain

[6] Nuclear Protection Evaluation Center (CEPN), France

*Corresponding author: *masaemuo@etsii.upv.es*

I. INTRODUCTION

The pandemic situation originated due to the appearance of the SARS-CoV-2 virus has changed many aspects of our lives and work, especially from the moment in which the World Health Organization (WHO) declared as a global pandemic the widespread presence of this coronavirus in the world (March 11th, 2020) [1].

Before this pandemic, the use of surveys for analysing the impact of regulations on radiation safety [2], the knowledge of radiation protection among radiology professionals and students [3], or the perspectives and opinions of young professionals in radiation protection [4] was already a common via to obtain important data, for reinforcing the radiation protection systems and the radiation safety culture.

For this reason, and due to the useful information obtained in the past with different surveys, the Young Generation Network of the International Radiation Protection Association (IRPA-YGN) carried out a preliminary assessment of the impact of COVID-19 in the work of radiation protection experts. This first assessment collected the testimonies of 30 young professionals involved in this organization, showing a significant impact on the working conditions of radiation protection experts, especially of those from hospitals [5]. This first survey was very preliminar and short.

Many other testimonies and communications about the impact of COVID-19 in health physics and radiation protection have also been reported in the last months [6–8]. However, as far as the authors know, this impact has not been deeply evaluated in Spain for the different sectors of the radiation protection system. For this reason, the Youth Committee of the Spanish Society for Radiological Protection (J-SEPR), supported by the SEPR and the IRPA-YGN, launched an online survey to evaluate the impact and the consequences of this crisis in the daily job of the SEPR members.

The survey has tried to cover many aspects related to the work developed by the Spanish professionals: the possibility of teleworking, virtual or hybrid inspections/measurements/calibrations/quality controls, changes in the workload, change of the work role, labor productivity, main difficulties found as a consequence of the COVID-19, and many others. The data have been analysed taking into account the age of the participants.

According to the above, this communication shows some preliminary results obtained by the SEPR about the impact of the COVID-19 pandemic on the Spanish radiation protection professionals. Therefore, a first analysis is carried out in order to analyze the adaptation capacity of this sector and its professionals, showing the improvement essential points that ought to be taken into account in the future to reinforce the Spanish radiation protection system in extreme situations.

Moreover, this evaluation tried to be an example and a guide for other national societies, following the proposal, promoted by the IRPA-YGN, for the implementation of this kind of studies about the impact of COVID-19 in the radiation protection professionals in different countries.

The same survey could be launched by other youth committees of RP (Radiation Protection) societies.

II. MATERIALS AND METHODS

The survey designed for this study about the impact of COVID-19 on the Spanish radiation professionals was implemented in Google Forms. This free online platform for surveys was chosen due to its simplicity and easy editing. Besides, the use of an online platform has allowed promoting this survey among SEPR members by digital media, such as private and institutional social networks (Twitter, LinkedIn, or Facebook) or institutional forum, website and newsletter. The use of digital media allows collecting easily more data, and overcome restrictions associated with the COVI-19 pandemic, but these media can suppose a barrier to the participation of some senior members.

One of the key points of all the surveys for getting a significant number of answers is the number of questions, the type of question and the brief time required for completing the survey. For this reason, the survey was designed with a limited number of questions (40) distributed in 5 pages, with only 5 open questions. The estimated time needed to complete it was 15 min.

The first page of the survey was focused on obtaining data about participants: age category (18-35 / 36-55 / +55), institution or area of work, and region where the job is developed. Moreover, it was mandatory to introduce an e-mail on the first page, which allowed detecting duplicate entries.

The next three pages of the survey included the same 10 multiple choice questions, all of them related to the impact of COVID-19 in the day-to-day labor of radiation protection professionals. These same 10 questions were designed in order to evaluate the evolution of the COVID-19 impact in three different periods in Spain:

- 15/03/2020 – 21/06/2020: First alarm state
- 21/06/2020 – 26/10/2020: Period between the first and the second alarm states
- 26/10/2020 – End of the survey (05/04/2021): Second alarm state

The last page of the survey was dedicated to evaluate, with multiple-choice questions, the labor productivity and workload during the pandemic, and the possibility of teleworking in this sector even after the pandemic situation. Moreover, this last page included 5 open questions related to the main difficulties found by the professionals, and the lessons and initiatives promoted and developed by the participants and their institutions to overcome these difficulties.

This survey was opened for the participation of all the members during two weeks and a half, getting to collect data about the impact of COVID-19 in the day-to-day work of 35 radiation protection experts, which represents around 5 % of the SEPR members.

III. RESULTS

The characteristics of the sample in terms of areas of work and age categories can be found in Figure 1 (areas of work) and Figure 2 (age categories).

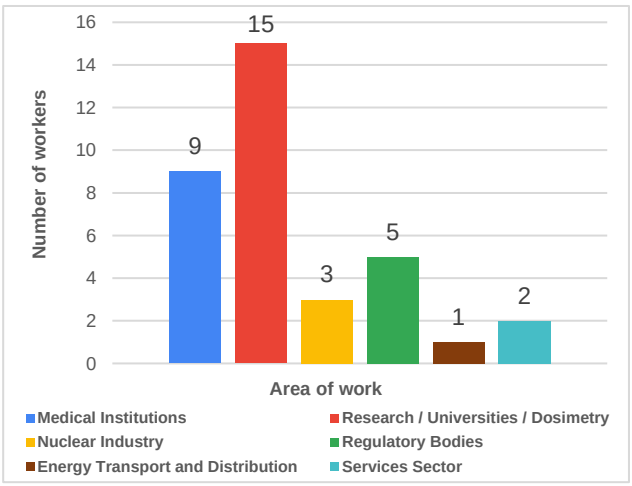

Figure 1. Areas of work of the survey participants.

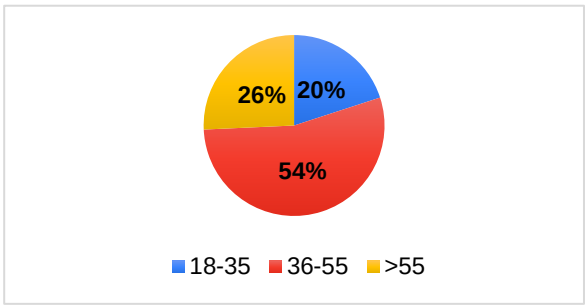

Figure 2. Distribution by age categories, in years, of the survey participants.

The answers came from 8 different Spanish regions, notably from Madrid and Cataluña, and most of the answers were from workers related to medical institutions, and research/academic and dosimetry areas (Figure 1). Hence, Figure 1 gives an idea about the areas of work of the Spanish radiation protection professionals. Moreover, these preliminary data also reflect the age distribution of the SEPR members and Spanish radiation protection professionals (Figure 2). This distribution is approximately in accordance with the Spanish population pyramid [9] and shows a good balance between youth and very experienced professionals.

The results about the capacity of the Spanish radiation protection workers for changing their work modality are shown in Figure 3. This figure shows the evolution of the number of workers in different modes of work in the three different periods previously defined in section 2. These data demonstrate the high impact of COVID-19 in the first period of the pandemic, where all 100 % of on-site activities were related to the health sector (hospitals) and the nuclear industry, plus some employees of the regulatory bodies.

Therefore, most of those activities non-related to hospitals and the nuclear industry have shown good flexibility for adapting their modes of work to teleworking or mixed-modalities, research and routine lab works were the most affected works (many of them were postponed). The

stability of the number of workers in non-on-site modalities in the last two periods indicates that these modes of work will keep on up to the end of the pandemic.

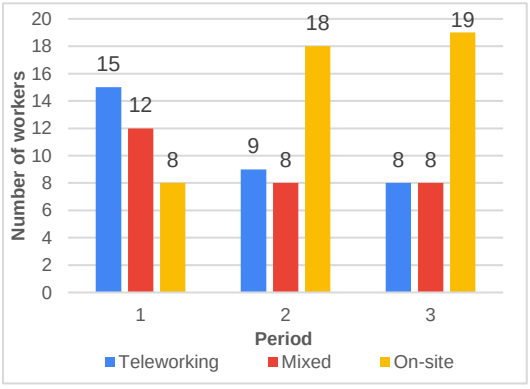

Figure 3. Number of workers in the different modes of work during the 3 periods of time evaluated.

These non-on-site modes of work will not completely disappear from the Spanish radiation protection system after COVID-19 pandemic. The data acquired in this survey show how 56 % of the participants that have not been working 100 % on-site think that their institutions will keep on the possibility of teleworking, with more or less flexibility, after COVID-19. This important data demonstrates that this pandemic has accelerated the introduction of new modes of work in those activities non-related to the health systems and the nuclear industry in the Spanish radiation protection system.

All the participants have indicated that their institutions promoted teleworking and different hygiene measures (use of personal protective equipment, disinfection of surfaces, or interpersonal distance were the most common) to reduce biological risks associated with COVID-19.

The workload and the labor productivity of the Spanish professionals, from the beginning of the pandemic, have also been affected by the new modes of work and the pandemic evolution, which has postponed many radiation protection activities. Table 1 shows the data collected in this work about workload and labor productivity.

Table 1. Workload and labor productivity of the Spanish radiation protection professionals from the beginning of the COVID-19 pandemic.

	Higher	Same	Lower
Workload	19	14	2
Labor Productivity	11	12	12

These data about the labor conditions of the Spanish professionals show how the workload over these workers has remained constant and even it has increased for the 54 % of the participants. Hence, this sector has shown to be very resilient to this extreme situation. On the other hand, the labor productivity has varied during this period among the participants. One of the common points found in the answers to the survey is that many operations such as quality control, calibration, commissioning and inspections suffered delays due to the pandemic.

The last point to analyse is the impact of COVID-19 on the Spanish radiation protection system in terms of dosimetry activities. One of the most important points for evaluating the impact of COVID-19 in the dosimetry of the Spanish radiation protection professionals is the evaluation of the possible temporary extension of the use of dosimeters. This analysis is shown in Figure 4 for the three time periods considered.

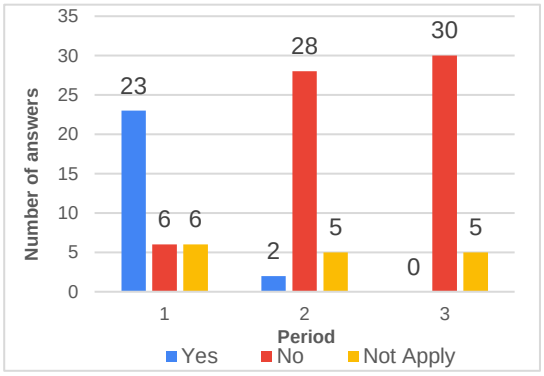

Figure 4. Extension of use of monthly dosimeters in the Spanish radiation protection due to the COVID-19 impact.

According to the data shown in Figure 4, the reading period of many dosimeters was extended due to the pandemic situation. However, these data are not critical or dangerous if are compared with the data shown in Figure 3. This is because most of the dosimeters lecture extensions took place in the first period, and in this same period most of the Spanish professionals were teleworking or reduced their on-site activity (Figure 3), so the dosimetry control of these professionals might not be compromised by this extension. Besides, it is important to point out that the Spanish dosimetry centers have implemented new modes of work, so these changes could also have introduced certain delays in the lecture of dosimeters in the first period.

The amount of data collected in this survey from dosimetry centers is low, but these data seem to point out that these centers have been working in mixed-modalities during these periods. Hence, the work developed by these centers has been continuous and the new modalities have not harmed the dosimetry control of radiation protection professionals.

The data shown in Figure 4 about the second and third periods are in accordance with data in Figure 3 and are really similar, so it looks like from the second period the radiation protection professionals already have a clear framework for developing their tasks up to the end of this pandemic. In the last period, the participants did not report any delay in the lecture of dosimeters.

Other variables that affected worker's dosimetry during these three periods were the introduction in some cases of new inspection/test modalities (hybrid modalities) and the prioritization of teleworking as a measure for reducing the impact of COVID-19.

These variables reduced the presence of professionals in on-site tasks. Figure 5 shows the evolution in the three time periods of the amount of on-site and hybrid inspection tasks developed by the Spanish professionals.

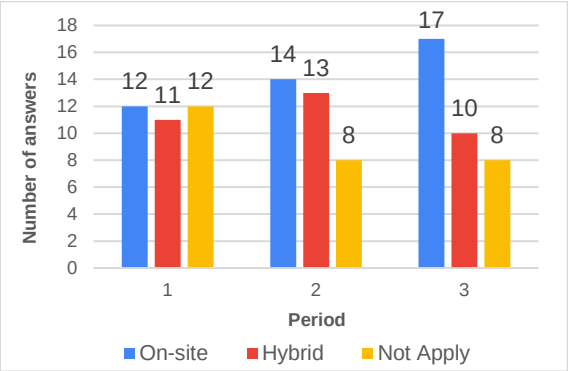

Figure 5. Implementation of hybrid inspections and tasks in the Spanish radiation protection system.

Figure 5 shows how the number of inspections and tests carried out in the first period were lower than in the rest of the periods, so probably some inspections were postponed to other periods, in the last two periods the same number of inspections were carried out. However, the most relevant information provided by Figure 5 is related to the introduction of hybrid modalities in the inspections and tests in the Spanish radiation protection system.

Hence, these last results show how the introduction of these hybrid modalities will persist on time at least up to the end of this pandemic. In the first two periods, the hybrid inspections represented 48 % of the inspections, almost half of the test tasks, and in the last period, this percentage was reduced to 37 %. Therefore, the reduction and flexibility of mobility and capacity measures reduced the percentage of hybrid inspections, but these inspections probably persist on time, like the possibility of teleworking in many positions non-related to the health sector and nuclear industry.

A deep analysis of the results obtained in this survey will be presented in future studies, including the data from the open questions related to the main difficulties found by the professionals, and the lessons and initiatives promoted and developed to overcome them.

IV. CONCLUSIONS

The main conclusion of this preliminary study is that the appearance of COVID-19 has modified deeply the labor conditions and modalities of the Spanish radiation protection professionals. The impact of COVID-19 on daily RP labor was much more significant at the beginning of the pandemic (first period). The results, in terms of labor modality and lecture of dosimeters, seem to point out that from the second period the professionals have had clear and direct instructions about how to adapt their jobs to the new situation, and many institutions will remain using teleworking as a job modality (100 % or mixed) even after this pandemic.

The extension of the lecture periods of the dosimeters was only important in the first period, the period in which most of the professionals were in alternative modes of work to on-site working. Hence, this extension did not generally affect the dosimetry of these workers. The implementation of hybrid inspections and tests also supposed a change for the Spanish workers, and this option will probably remain up to the end of the pandemic.

The health sector and the nuclear industry are the sectors of the Spanish radiation protection system with lower capacity and flexibility for changing their modes of work, among other reasons, because their activities were considered essential by the Spanish Government, so the professionals of these two sectors are the most exposed to COVID-19. The workload over the Spanish professionals has been in general the same or higher than before the appearance of COVID-19, so this sector seems not to have suffered the general activity plummet suffered by the Spanish economy.

The balance between youth and very experienced professionals indicates that SEPR is in the right direction for assuring generational replacements in the future.

REFERENCES

[1] WHO Director-General's opening remarks at the media briefing on COVID19 – March 2020

[2] T. Berris, D. Žontar, and M. M. Rehani, "Survey on impact of regulations on radiation safety and development of radiation safety culture in 25 countries," *J. Med. Imaging*, vol. 4, no. 3, p. 031204, 2017.

[3] S. Maharjan, K. Parajuli, S. Sah, and U. Poudel, "Knowledge of radiation protection among radiology professionals and students: A medical college-based study," *Eur. J. Radiol. Open*, vol. 7, p. 100287, 2020.

[4] S. Andresz, P. Bryant, J. Heaps, T. Beaumont, S. Vecchiola, and P. Caldeira Ideias, "Young professionals in radiation protection: Challenges and perspectives - Outcomes of an international survey," *Radioprotection*, vol. 54, no. 1, pp. 35–40, 2019.

[5] S. Andresz, F. Kabrt, O. Nusrat, and C. Papp, "Impact of the Covid-19 Pandemic on the Young Generation in Radiation Protection, Synthesis of Testimonies and Experiences," 2021.

[6] M. Ku, T. Morgan, A. Malbon, T. Bartram, J. Cavanagh, and B. Halvorsen, "Provision of a consistent national approach to radiation therapy workforce protection measures in Australia during the COVID-19 pandemic," *Aust. Heal. Rev.*, vol. 44, pp. 535–539, 2020.

[7] R. Meades, G. Gnanasegaran, and D. McCool, "Radionuclide therapy services in an era of COVID-19: The radiation protection challenges, opportunities and considerations," *Nucl. Med. Commun.*, 2020.

[8] M. Portaluri, S. Bambace, F. Tramacere, A. Errico, S. Carbone, and T. Portaluri, "Staff and Patient Protection in Radiation Oncology Departments During Coronavirus Disease 2019 (COVID-19) Pandemic," *Adv. Radiat. Oncol.*, vol. 5, no. 4, pp. 628–630, 2020.

[9] Instituto Nacional de Estadística, "Pirámide de la población empadronada en España," 2020. [Online]. Available: https://www.ine.es/covid/piramides.htm. [Accessed: 13-Apr-2021].

Proceedings of the European Nuclear Young Generation Forum
ENYGF'21
September 27-30, 2021, Tarragona, Spain

Digital Twin on nuclear energy

Torres Márquez, Rafael Antonio[1*] and Romero Martín, Patricia[2*]

[1/2] Tecnatom S.A., Spain

Corresponding author: 1 ratorres@tecnatom.es 2* promero@tecnatom.es

I. What is a digital twin?

The concept of digital twin that emerged in the simulation world in the late 1970s associated with the race for space conquest is making great strides in its implementation in all types of industrial environments, and nuclear power plants are not an exception. The plants benefit in countless areas from what this tool contributes to the daily work carried out in the context of a plant.

But what is a digital twin? Well, a digital twin is nothing more than a part of the reality that we represent, with greater or lesser accuracy in an electronic device. The how and what we represent in that piece of reality are their great differentiators, while their applications will be shared among them.

Table 1. What do we represent?

Information	Description
Simulator	Data & behaviour from de simulation engine
IoT	Additional signal sampling data of quantities or systems not related to the operation of the plant
BIM, PIM & PLM	Collaborative methodologies data: • **B**uilding **I**nformation **M**anagement • **P**roduct **I**nformation **M**anagement • **P**roduct **L**ifecycle **M**anagement
Big Data	Offline data from the operation of the plant over the years and their intelligent analysis
Online Data sampling	Online data from existing plant signage

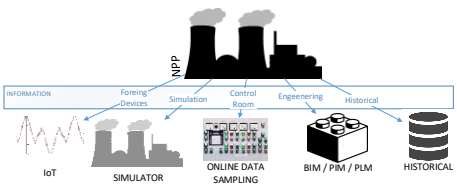

Schema 1. Model "as-built"

The maxim: "80% of the information is given to us visually" is the main reason because this concept is growing on this way, we would represent the full plant with an accuracy of millimeters and accessing to all this information from our desk, even from home. This is the reason why how do we represent the information is so important.

I. WHAT DO WE REPRESENT?

Some of the first digital twins are simulators, flight, driving, instrumentation management ones, etc. and surprisingly among all these, the simulators of the main and emergency control rooms of a nuclear power plant stand out. Control room simulators have evolved in many of their aspects, from the virtualization / digitization of their interfaces to the incorporation of new modeling tools.

Figure 1. Control room simulator by Tecnatom

The incorporation of information into the simulators generates a wide range of applications and improves the representation of reality. For example, Big Data is being incorporated into the simulation through intelligent analysis for the generation of systems simulation models, allowing the definition of the behavior of the mentioned systems through the analysis of the data collected throughout the system's operating time in plant, however, this mechanism can be applied both at a macro level (a full system or even a plant) and at a micro level (behavior of a valve, sub-chiller, or turbine).

Figure 2. Valve sensorization by Tecnatom

This information at micro level is usually incorporated by means of sensorization that with IoT techniques allow us to have real-time measurements of magnitudes related to their behavior, which, as an usual rule, are not commonly measured for plant operation and which can be of very heterogeneous in origin and format (we are talking about environmental measures, video surveillance systems, active security systems, on-site control systems, etc.).

Figure 3. Tecnatom Monitoring and diagnostic tool

The incorporation of all this information helps us with the application of digital twins, in this way the intelligent analysis of Big Data allows us to have predictive models that together with expert systems and information from IoT define security, safety and operation monitoring applications, decision-making applications and predictive maintenance applications.

The grouping of all this information allows us to use collaborative work methodologies, for example BIM, PIM and PLM which are nothing more than tools that centralize information regarding a specific aspect and allow orderly and completely access to it.

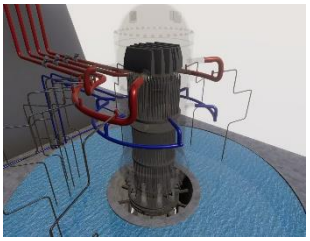

Figure 4. Marketing information in Tecnatom simulator

In the case of PIM/PLM, the aspect in which it focuses is the product, for PIM specifically the product features and for PLM specifically the lifecycle of product.

These methodologies help us with the management of the resulting products or those necessary in a central, by managing information such as technical characteristics, multimedia and marketing information, videos, descriptive data, maintenance data, etc. and they can be input and output for digital twins and they are endorsed by the definition of digital twin (digitization of a part of reality).

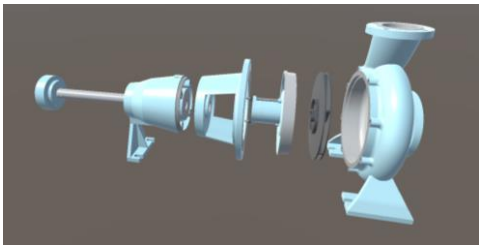

Figure 5. Product information

Digital twins supported by PIM/PLM tools have a series of applications whose main focus is information, in such a way that, if we consider the digital twin as the source of that information, we will have applications in which instead of going to reality, we present the information from its digital twin where you can find marketing information, documentation, maintenance data, engineering information...

Similarly, if the PIM/PLM information enters the digital twin, we will have augmented reality applications.

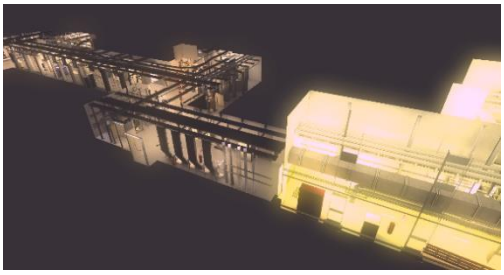

Figure 6. Model "as-built"

On the other hand, BIM tools focus on construction / building and allow the creation and management of an entire building project of a building or group of them, including information from design plans, building plans, the elevation of these, engineering plans and successive scanners in time of the buildings already built, generating a history of the "as-built" models of these.

All this data allow us to build an entire digital twin of the building and that covers from the first conceptual design phases to the decommissioning phase, identifying the evolution or drift in time from reality to the expected according to planimetry.

Figure 7. Tecnatom Digital twin embedded on a simulator control room

Digital twins based on BIM methodologies have a wide range of applications, due to the features of the tool, they are usually applications focused on buildings, in this way, areas such as maintenance and engineering are the great beneficiaries, but there are other areas and phases of the lifecycle of an industrial plant that also benefit from them thanks to the visual information they provide, in fact, they are tools that are becoming essential in the design, construction and decommissioning phases, but also, we must not lose sight of the applications in the framework of training and virtual commissioning.

Figure 8. BIM from AtuchaII NPP

In the simplest terms, virtual commissioning is the practice of using "virtual simulation technology" for "commission"—design, install or test— modifications over a system, component or structure over virtual model before you implement it to the real system. This "virtual simulation technology" is a digital twin.

For example, suppose that we want to introduce a modification in the control room panels, adding a series of registers, indicators and / or buttons, the best way to do it according to Human Factor Engineering premises is to have a virtual control room in which you can perform those modifications. Likewise, if the modifications are in the behavior of a system, in which we have added a series of redundant lines, the best way to test it is by means of a simulator, in this case, that we know as an engineering simulator and, as we have already said, it is one of the first digital twins. Obviously, we cannot lose sight of the applicability that all these digital twins have in the broader framework of training.

II. HOW DO WE REPRESENT?

The "as-built" models are the main support for a visual digital representation of reality, giving way to the more widely known digital twins, VR, which in all its forms (immersive systems, MR, AR, realistic 3D, virtual tours, etc.) endorse the maxim that ***"80% of the information is given to us visually"*** which is what makes digital twins so powerful since they provide visual information that we can define as real.

Table 2. How do we represent?

Representation	Description
eXtended Reality(xR)	xR is a superset which includes the entire spectrum from "the complete real" to "the complete virtual"
VR	Virtual Reality
AR	Augmented Reality
XR/MR	Cross-Reality or Mixed Reality
CR	Cinematic Reality
AI	Artificial Intelligence
Immersive system	Immersive VR
Realistic 3D	3D realistic modeling
Virtual Tours	360 images chains

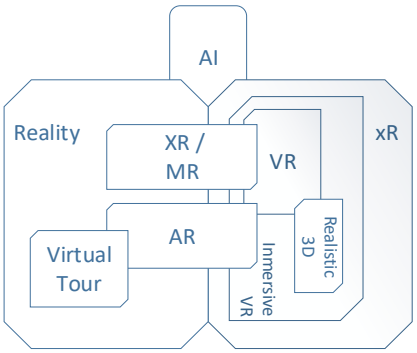

Schema 2. xR components

We will be taking another step towards digital reality if at the same time this VR is fed with "real" digital behaviors thanks to AI.

Figure 9. Almaraz VR developed by Tecnatom

There are many applications of these digital twins, mainly highlighting training in the broadest sense of the definition, the availability of visualizing the behavior of an entire plant in the face of a series of operations / actions; the possibility of training in the handling or use of machinery through MR or CR; training in operation through the virtualization of interfaces, safety training with a guidance system, even visual training or knowledge of the environment that allows a person who has to enter an industrial building to know the facilities long before its access.

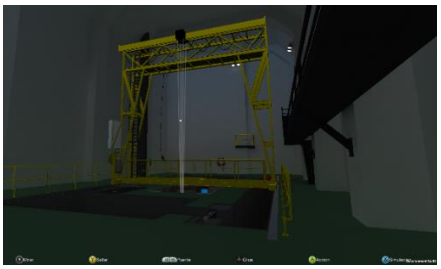

Figure 10. VR for operational training for the control crane of used fuel pool developed by Tecnatom

In fact, a digital twin can be part of another digital twins, in such a way that, for example, we can add to a control room simulator another twin of an independent system, such as a crane or a refueling machine or we can add the information from a PIM/PLM in a VR.

Figure 11. Digital twin of refuelling engine embedded on simulator control room developed by Tecnatom

An AR, the digital presentation of information over a "reality", can be by itself a digital twin that is projected in any space of reality, in fact, it would be as if we represent a document, model or information coming from reality against reality itself (the most common functionality of AR) but we can add an AR again within a higher-level representation digital twin, in this way we have VR applications in which information can be presented in AR mode, assembly procedures, documentation from a PIM or BIM, responses from an expert system, etc.

Figure 12. Tecnatom Augmented reality

But the applications of these digital twins do not end there. Mainly those based on "as-built" models, normally built from laser scanning or high resolution photogrammetry that allow precision in the models of even microns, these models serve perfectly for work planning, you could avoid entering a restricted or controlled area by previously collecting requirements from the environment sitting in front of the computer screen (there is space for a scaffold, what tools are needed, there is room for the component, etc.); and most importantly for engineering jobs, such as engineering studies or component replacement.

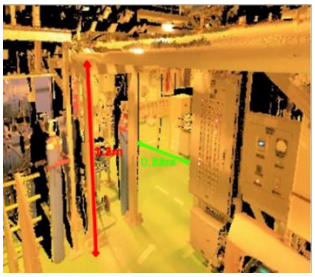

Figure 13. 3D Measurement tool on cloud of points

III. NEXT STEPS

In this way, if we go back to the beginning and pick up the simulation-based digital twin, replace its interface with an immersive VR, and add the information from the plant in real time, we will be able to compare simulation and reality, evaluate possible drifts of one of them and through AI and Big Data analysis predict possible both abnormal or normal behaviors, recommend procedures, and make decisions.

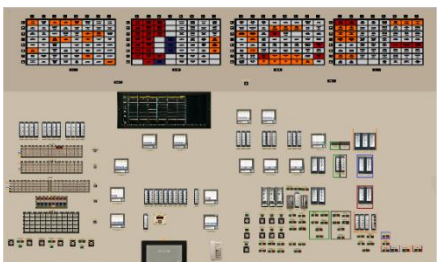

Figure 14. Virtual panel developed by Tecnatom

All this from your desktop computer or your own mobile phone. But this tool does not stop in its evolution, flexibility and modularity, the integration of new technologies will make it possible to improve in the efficiency of the processes in the industrial companies which will implement the use of digital twins.

Plants are using long simulators and have perfectly understood that digital twins are that tool from the point of view of the tests that make good the maxim **"Virtual tests do not entail costs or losses, but they do have benefits." (Virtual Commissioning)**

Figure 15. Digital twin with AR of documentation and MR in simulator control crane of used fuel pool inside a CR developed by VirtualWare

There are many plants and companies that are assuming this challenge and that consider the digital twin as a fundamental tool evolving in parallel to how this technology is doing, the first steps are already being taken to achieve the total integration of all technologies.

IV. References

[1] F. Ortega, P. Rey, N Jung and M. Rovaglio "Process simulation and virtual reality coupling. an approach to reduce dose and improve the training of NPP field operators," presented at the NESTet2011, Prague, Czech Republic, 15-18 May, 2011, A0014.

[2] J. Angás, X. Jardi, A. Pontes, I. Mach, F. Tarrasa, y M. García. "Determinación de elevaciones reales de tuberías para ANAV y CNAT mediante tecnología de escaneado láser 3D". Revista de la Sociedad Nuclear Española, 310: 58-61.

[3] R. Torres y P. Rey "Simulación con realidad virtual de la máquina de recarga de la CN Atucha II" presented at the 41 Reunión anual de la SNE, 23-25 Sept., 2015,

[4] P. Rey, N. Rivero y S. López "New simulation tools acting like a magnet to attract young engineers", presented at the NESTet2013, Madrid, Spain,17-21 Nov.,2013

[5] J. de Ramón, J. Angas, "Consolidación y perspectivas de la tecnología láser escáner 3D en el sector nuclear." Año 2011.

[6] V. Cheutet, A. Sekhari, N. Corbeaux. "PLM and BIM approach to support information management in nuclear decommissioning: a synthesis." presented at the 15th IFIP International Conference on Product Lifecycle Management (PLM 2018), Jul 2018, Turin, Italy. pp.104-114. ffhal-01847842f

[7] P. Morilhat "Digitalization of Nuclear Power Plants at EDF" presented at the Energiforsk Annual Nuclear Conference 2018, January 2018, Stockholm, Sweden.

[8] U. Serna "Una nueva relación con las máquinas" article from enerTIC, *https://enertic.org/una-nueva-relacion-con-las-maquinas/* Mar. 2021

Proceedings of the European Nuclear Young Generation Forum

ENYGF'21

September 27-30, 2021, Tarragona, Spain

Development of a simulator of a PBMR nuclear reactor as a means of strengthening skills and knowledge of its operation, based on free software

Alvarado Patricio, Rodrigo Neri.

[1] Universidad Nacional Autónoma de México (UNAM), México.

*Corresponding author: *nerialvarado.327@gmail.com*

I. INTRODUCTION

When we use IAEA (International Atomic Energy Agency) simulators in the course on nuclear reactor technology [1] we found that there is no way to change model parameters representing plant characteristics, and the textbooks in general do not consider the use of personal computers for power plant development using both good numerical software and easy to use graphical interfaces. The use of spreadsheets is attractive because graphs, diagrams and simple calculations can be used for the modelling of plant components, however, they do not have a programming language that allows for reliable revisions and improvements to the models. Nor do they have algorithms for solving differential equations or modelling control systems; revision of any slightly detailed model is practically impossible [2]. The power to do complex analysis is very limited if not specialized software is available. In addition, the experience on nuclear systems analysis is distributed among several members of the academic staff. A specific simulation-based system design tool could help join efforts and fill this gap. A software hides the complexity of the model from the system designer and allows you to configure parameters and analyse results in a single application [3]. Therefore, it was decided to carry out the modelling of the PBMR (Pebble Bed Modular Reactor) reactor, based on previous knowledge.

During the learning of a nuclear reactor operation, such as the PBMR (Pebble Bed Modular Reactor), the future nuclear engineer usually has access to specialized software and classical texts that detail important operational aspects of the plant. The problem when wanting to build a simulator without those tools begins with the definition of the development platform and eventually the graphical interfaces because they require licenses and cost learning processes that are not always accessible to students. To investigate the benefit of developing your own models for the learning process improvement, this project has been proposed, having as main goal a basic principles simulator of the PBMR on a free software platform that allows the schematic visualization of the plant evolution during transient and permanent conditions. The basic requirements for this project begin with the ability to review and update the component models and their graphical user interfaces to sequentially achieve better plant representations. The programming process forces the student to solve difficulties that perhaps otherwise would not have even been raised, in addition to now having the possibility of changing initial and boundary conditions as well as being able to modify system characteristics.

The challenge to carry out an analysis of the nuclear reactor response to expected events, in this case PBMR using its own models arises from the problem of not having the software for the development of the simulator and/or easy to use GUI software. Not having the software or simulators limits you to carry out steady state or transient analysis, since many of these programs are not freely accessible or do not have the necessary scope to carry them out. Another problem maybe students' approach to free software programming, since many of the current nuclear engineering courses do not help the student to you see beyond the exercises that are solved in textbooks.

To carry out this project, a combination of different free-use programs is proposed in LINUX, Gnu Octave, Open Office Calc, Bash, etc., in which the programming and scope of each modeled element of the nuclear plant are detailed. During the joint execution of these programs on a personal computer, the results obtained from the simulation are stored in a database that the student can access by different means, and can also modify some elements of the program.

Although the software is free to use, it follows the standards of other tools for commercial use, in addition to making use of different programming languages, it helps to have a better administration, presentation and graphs of results.

II. PBMR REACTOR DESIGN

The simulator design begins with the definition of a graphical interface for the simulator, which is fundamentally established as an Open Calc file that becomes an electronic book (E-book) which can have as many pages as required. A page for the particular simulator purposes, another for model requirements, one more for plant control system models, and user visualization. On the first page, the user has basically available the parameters and quantities that control the simulation process, such as integration intervals, display time intervals, convergence criteria of the dynamic and steady-state models. On the next page the user can access geometric, nominal operation and physical parameters such as reactor core heat transfer, component time constants, etc., which define PBMR reactor processes models. On this same page, the user determines the initial conditions or the operating values for both the steady state simulations and those for the simulation of expected operational transients. The results of the simulations are generated in time intervals defined on the first page. Pressing a button on the control page signals the execution of a script to initiate information transfers from Calc to Octave where the required calculations are carried out for each simulator component model and consequently updates the results files in csv format; which are read periodically and automatically by the spreadsheet. In the case of steady-state simulations, there are pages where the main variables, of the plant components operation, are displayed. There are different spreadsheet pages for the reactor, the heat exchanger, recuperators, etc., but there are also other pages where plant component efficiencies can be seen, as well as the rates of entropy generation and exergies destruction for each stage of the thermodynamic cycle.

For plant transient simulations there are other pages where the user can modify operating conditions either by controlling the reactor power, open and close valves that represent deviations or leaks of the working fluid. Changes in the conditions of the equipment can also be made in the diagrams by means of the previously established buttons, which in turn change the parameters of the models. These changes execute orders transferred by macros, which in turn are reflected in the values that are being simulated in the octave program.

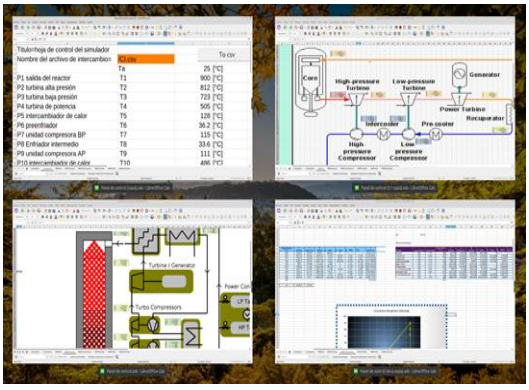

Figure 1. PBMR simulator e-book

Currently the simulations are continuous during time intervals but require the user to press a key to continue the simulation for another period of time delimited and defined on page 1.

It should be noted that this simulator has a set of specific tables of thermodynamic properties (obtained from NIST) for helium, which is the working fluid. This can be modified to consider other types of refrigerant with the same structure of the PBMR, for example carbon dioxide, among others.

.

III. PBMR'S MODELING IN STEADY AND TRANSIENT STATE

The modeled PBMR is based on the "evolutionary design of the German AVR, THTR and HTR-Modul designs" [4], where the power generation of this reactor starts in the fuel spheres in the core by the nuclear fission of uranium and The refrigerant used is Helium, which is forced through that configuration where it heats up as it passes around the spheres. The heat removed there is forced from the reactor (1 in figure 2) to the high pressure turbine, passing through the low pressure turbine (2) and then to the power turbine (3) by the recuperator that acts as a main heat sump. The initially hot helium (4) transfers heat through the recuperator to the cooled helium returning from cycle (10) to restart the process. The helium that is still hot (5) goes to additional cooling processes (6 and 8) to improve its pumping conditions and then on the secondary side of the recuperator it is preheated to re-enter the reactor. The power turbine is the generator drive to obtain electricity.

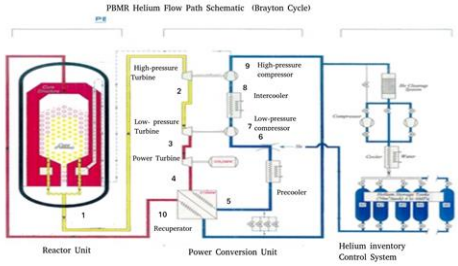

Figure 2. Thermodynamic cycle of PBMR.

A. The steady state PBMR

The modeling of the PBMR in steady state, makes an element by element study of the nuclear plant denoting each change of inputs and outputs of the components numbered in figure 2. To facilitate modeling, the location of the equipment, turbines, compressors, generator, etc., the mass flow is usually kept constant throughout the thermodynamic cycle but it can also be modified to simulate leaks for example. This model is also based on previous studies [5] and comparison can be made.

Each component calculation begins with pressure and temperature update, where Octave, element by element, evaluates other variables throughout the entire cycle, for example entropies, exergies, power output, heat generated, etc., are obtained. When the user modifies component input

values, he can observe the resulting changes in the cycle graph.

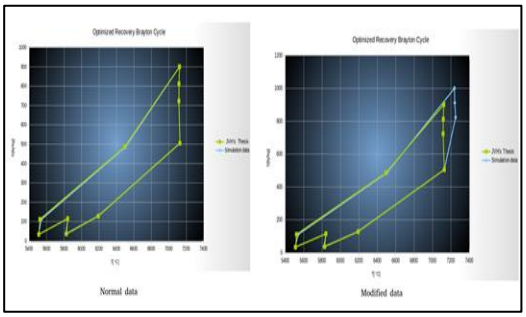

Figure 3. Steady-state T-s graph.

B. The transient state PBMR

For the transient state calculation, the enthalpy change over time is taken into account through a series of first-order differential equations that are shown in the following table

Table 1. Differential Equations of Transient Reactor Modelling

Plant Element	Diferential Equation
nuclear power	$\frac{dn}{dt} = \frac{(r-1)*\beta}{\Lambda} n + \sum_{i=1}^{6} \lambda_i c_i + S_0$ $\frac{dc_1}{dt} = \frac{\beta_i}{\Lambda} n - \lambda_i c_i$ $\phi_{c0} \cos(\frac{\pi z}{H_e}) J_0(\frac{2.405 r}{R_e}) * n(t)$
Neutron Poisoning	$\frac{dX}{dt} = 0 = Y_{Te}\Sigma_f \phi + Y_X \Sigma_f \phi - \lambda_X X - \sigma_X X \phi$ $\frac{-dI}{dt} = Y_{Te}\Sigma_f \phi - \lambda_I I - \sigma_I I \phi$
Heat transfer in the reactor	$\rho c_p \frac{d\bar{T}}{dt} = q''' + \lambda_f [b_f \bar{T} - a f \bar{T}_w]$ $\frac{\rho c_p}{k_g} \frac{d\bar{T}_c}{dt} = \lambda_c [\bar{T}_c - b_c T_p + a_c T_\infty]$
Reactivity	$r = r_{crod} + \alpha_T * (\bar{T}_f - \bar{T}_0) + \alpha_x * (\overline{Xe} - \overline{Xe}_0)$ $\frac{dh_1}{dt} = \frac{h_1 - h_{10}}{T} - \frac{Q_{react}}{mT}$
Reactor cooling	$\frac{\rho c_p}{k_g} \frac{dT_\infty}{dt} = mAh_c(T_w - T_{infinito}) - m(T_{\infty e} - T_{\infty s})$
High-Pressure Turbine	$\frac{dh_2}{dt} = \frac{h_1 - h_2}{T} - \frac{W_{Tap}}{mT}$
High-Pressure Compressor	$\frac{dh_9}{dt} = \frac{h_8 - h_9}{T} - \frac{W_{Cap}}{mT}$
Low Pressure Turbine	$\frac{dh_3}{dt} = \frac{h_2 - h_3}{T} - \frac{W_{Tbp}}{mT}$
Low-Pressure Compressor	$\frac{dh_7}{dt} = \frac{h_6 - h_7}{T} - \frac{W_{Cbp}}{mT}$
Power Turbine	$\frac{dh_4}{dt} = \frac{h_3 - h_4}{T} - \frac{W_{TG}}{mT}$
Recuperator primary circuit	$\frac{dh_5}{dt} = \frac{h_4 - h_5}{T} - \frac{Q_{prim}}{mT}$
Recuperator secondary circuit	$\frac{dh_{10}}{dt} = \frac{h_9 - h_{10}}{T} - \frac{Q_{abs}}{mT}$
Precooler	$\frac{dh_6}{dt} = \frac{h_5 - h_6}{T} - \frac{Q_{pre}}{mT}$
Intercooler	$\frac{dh_8}{dt} = \frac{h_7 - h_8}{T} - \frac{Q_{eni}}{mT}$

With the results obtained from the previous equations, the new parameters are calculated under the disturbance conditions that are added by the user from the simulator spreadsheet and then Octave reads these data through csv files and calculates all nuclear and thermodynamic parameters under transient states.

For the operation of the reactor, the calculation of the point kinetic equation is made, solving the differential equation with integrated methods in the same programming system. In addition to this calculation, the radial and axial potential distribution is obtained from the solution of the neutron diffusion equation in steady state considering a homogeneous reactor [6].

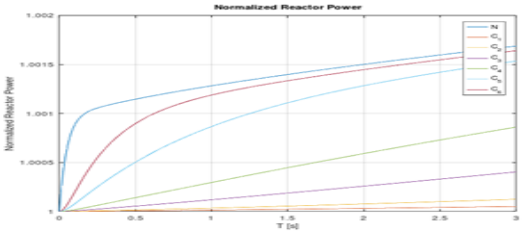

Figure 4. Normalized reactor power

$$\phi_{c0} = \frac{3.63P}{VE_R\Sigma_f} \cos(\frac{\pi z}{H_e}) J_0(\frac{2.405 r}{R_e}) * n(t)$$

$$B^2 = (\frac{\pi}{H_e})^2 + (\frac{2.405}{R_e})^2$$

n (t) is the solution of the point kinetic equation.

The heat transfer in the fuel is modeled considering an average sphere where the radial temperature distribution is fundamentally quadratic in the nuclear fuel region and linear in the outer shell of the sphere. This allows using only two ordinary differential equations to obtain the temperatures at any point on the sphere [2].

$$\lambda_f = \frac{3k_g R_w}{R^2(R_w^2 - R^2)} \qquad b_f = \frac{5k_f(R - R_w)}{5k_f(R - R_w) - k_g R_w}$$

$$a_f = \frac{k_g R_w}{5k_f(R - R_w) - k_g R_w}$$

$$\rho c_p \frac{d\bar{T}}{dt} = q''' + \lambda_f [b_f \bar{T} - af \bar{T}_w]$$

The amount of heat that flows from the surface of the fuel sphere of radius R to the cover surface with radius Rw, passing through the fuel-free zone, is equal to the heat removed by convection from the outer surface of the sphere by the Helium coolant.

$$\lambda_c = \frac{3Rw}{R_w^3 - 1.5R_w(R_w^2 - R^2)} \quad b_c = \frac{k_g R}{k_g R - h_c R_w (R - R - w)}$$

$$a_c = \frac{h_c R_w (R - R - w)}{k_g R - h_c R_w (R - R - w)}$$

$$\frac{\rho c_p}{k_g} \frac{d\bar{T}_c}{dt} = \lambda_c [\bar{T}_c - b_c T_p + a_c T_\infty]$$

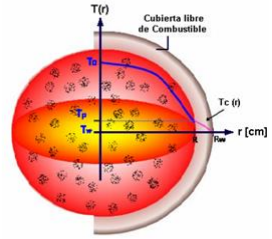

Figure 5. PBMR Fuel.

The general equation that defines the heat transfer from the spheres to helium, and which is going to be simulated is:

$$\frac{\rho c_p}{k_g} \frac{dT_\infty}{dt} = mAh_c(T_w - T_{infinito}) - m(T_{\infty e} - T_{\infty s})$$

Table 2. Basic nuclear data of PBMR

Parameter	Value
Thermal Capacity	300 [Mwt]
Gross Electrical Capacity	144 [Mwe]
Moderator an Reflector	graphite
Primary coolant	Helium
Helium inlet Temperature	486 [ªC]
Helium outlet Temperature	900 [ªC]
Helium Average Pressure	7 [MPa]

IV. CONCLUSIONS

This work has been a magnificent opportunity to explore possible benefit that may be obtained from using several GNU free software platform components in a coordinated way, so that graduate students can enhance the learning process. The goal was to numerically simulate the behavior of a nuclear power plant, its physical processes with a user friendly GUI. Although spreadsheets have the ability to do complex calculations, possibly solve differential equations, and handle macros to embed or modify graphics or other objects; the development and review process is extremely complicated by the syntax they use for numerical calculations. They have not methods for ODE numerical integration and control systems modeling, which are basic features in octave, matlab, scilab, etc. For this reason, routine scripts were developed and tested successfully for the transfer of information between these programs. Results are very encouraging and improvements to this modeling processes and the incorporation to other programs such as TRAC-BF1 for the modeling of nuclear power plants are currently being considered.

V. Acknowledgment

I thank Dr. Jaime Morales my thesis advisor and the group of the nuclear reactor engineering laboratory of UNAM for giving me advice, I also thank CONACYT for the support provided.

VI. References

[1] E.Salazar, “TECNOLOGÍA DE REACTORES NUCLEARES (TRN)”master's course, Universidad Nacional Autónoma de México, CDMX, México 2020.

[2] T. Jungebloud, “Untersuchungen zur Integration von algorithmischen und Datensichtmethoden fur die Systemanalyse” Thesis,Technische Universit¨at Ilmenau, Ilmenau, Germany 2009.

[3]S. Jäger “Model-Driven Development of Simulation-Based System Design Tools”2016 IEEE 14th International Conference on Software Engineering Research,Towson, MD, USA July 2016

[4]ARIS “ Pebble Bed Modular Reactor (PBMR)”,IAEA ,Status report 70 augost 2011

[5] J. Valle. “Modelado y Simulación Dinámica de un Reactor PBMR Optimizado con Módulos de Generación de Hidrógeno y Desalinización de Agua de Mar” M.S Thesis , Universidad Nacional Autónoma de México, CDMX, México 2007.

[6] M.M. El-Wakil, *Nuclear Heat transport.*4th Printing, Pensylvania. EU.,International textbook company, 1971.

[7] F. Gou. “Dynamic response of the HTR-10 under the control rod withdrawal test without scram” International Youth Nuclear Congress 2016, IYNC2016, Hangzhou, China, July 2016, pp. 247-254.

Proceedings of the European Nuclear Young Generation Forum
ENYGF'21
September 27-30, 2021, Tarragona, Spain

New Generation Instructors Training Program

Feofanova, Angelina[1*] and Feofanov, Roman[1]

[1] Rosatom Technical Academy, Russian Federation

*Corresponding author: *angrid7787@ya.ru*

I. INTRODUCTION

Nuclear industry evolves rapidly since there is a considerable need of thermal and electrical energy production. Nowadays, a significant part of energy is produced at nuclear power plants in the following countries: USA, Russian Federation, France, etc. These countries extensively operate NPPs to generate heat and energy, constantly upgrade and improve the technology of energy production at nuclear power plants and, most importantly, contribute to the improvement of nuclear power plants safety.

At the same time, some countries are at the beginning of nuclear energy use and development. The nuclear facility design, construction and operation is quite a complex task requiring irreproachable attention of every member taking part in this process. For this reason, it is vital to ensure operating NPPs and NPPs under construction with highly professional personnel in order to provide effective, reliable and safe operation.

Getting experience in the field of atomic energy use and learning from countries that actively operate nuclear facilities is an appropriate and the most efficient way to solve the problem of safety provision and reliable operation of innovative nuclear technologies. Currently, Russian Federation has agreements (contracts) with the following countries: Bangladesh, Belarus, Finland, Turkey, Hungary, Egypt, Uzbekistan. In accordance with these agreements nuclear power plants are designed and constructed (using Russian Federation projects) in the aforementioned countries. Furthermore, Russian Federation has an obligation to provide training for foreign operating personnel.

It is forecasted a growth of NPP operating personnel which needs training and, moreover, by 2025, the number of trainees will have increased up to 1050 people (Figure 1).

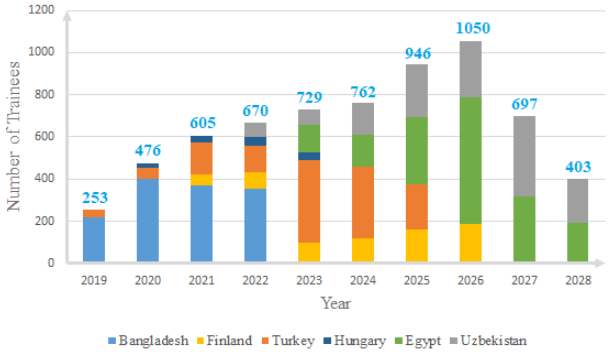

Figure 1. NPP Personnel Training Forecast.

As a result, State Atomic Energy Corporation Rosatom has created an ambitious project of new generation instructors training for teaching NPP operating personnel. Many years of organization experience, latest approaches to the educational process and international standards were taken into account to create this program. The program has been developed specially for the effective training of specialists in the field of nuclear industry. By 2025, there will be a need for approximately 180 new generation instructors due to the fact that it is predicted a growth of operating personnel for NPPs (Figure 2).

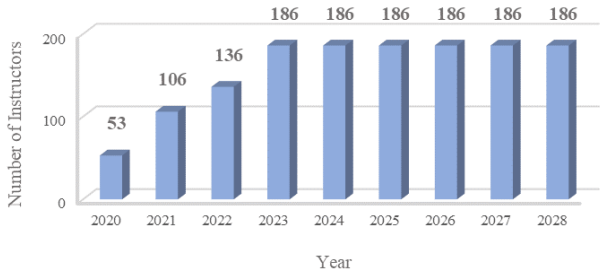

Figure 2. Projected Growth of New Generation Instructors.

An overview of new generation instructors training program developed by Rosatom for training operating personnel of NPPs is shown in this article. The main steps of the training are mentioned in the next section. The instructors are obliged to take all the stages in accordance with their individual syllabus. Thereafter, the instructors

training results are exposed showing actual efficiency of the project.

II. TRAINING PROGRAM

The main stages of new generation instructors training program are given below in accordance with the Rosatom project.

E. Training Program Stages

First of all, the instructors training process is divided into the following steps:

- Theoretical training
- Practical training
- On-the-job training
- Technical English study

The instructors take the program and study independently, however, each instructor is controlled by a mentor (expert). The expert is a former highly qualified employee of an NPP, who has been worked at a nuclear power plant for a considerable amount of time. The expert is an excellent professional who knows the technology of energy production at NPP in perfection. The expert shares experience and contributes to the instructor study during the whole training period.

The new generation instructors training is carried out in the following specialties:

- Unit shift supervisor
- Shop shift supervisor (reactor shop, turbine shop, chemical shop, electrical shop, instrumentation and control shop, etc.)
- General training instructor (federal rules and regulations, occupational safety, nuclear safety provision, radiation safety provision, regulatory framework, etc.)

The training duration depends on the chosen specialty. For instance, unit shift supervisor training program lasts 24 months, whereas shop shift supervisor program lasts 17 months or a trainee has to study 9 months in order to become general training instructor.

The aforementioned training stages are examined below in more detail.

First of all, during the theoretical training the instructors are supposed to study technology of electricity generation at NPPs designed by Rosatom. The theoretical training is based on current regulatory and operation documentation including operation manuals, project reports, process regulations for NPP safe operation, job descriptions and others. Therefore, the instructors gradually study equipment and systems of corresponding shops, regulatory basis of the operational activities, NPP operation administrative issues, NPP operation modes.

The instructors learn and get knowledge sequentially. They start with basic principles of NPP functioning and, eventually, by the end of the training program the instructors gain essential amount of knowledge required for performing duties of a shop shift supervisor. For example, taking the reactor shop shift supervisor program, the instructor studies the senior reactor shop operator course, then the reactor control lead engineer course, and, finally, the reactor shop shift supervisor course.

In addition to this, the instructor is obliged to take the course of systematic approach to training in order to learn necessary competencies in the area of personnel training and essential instructor skills. Upon completion of this course the instructor will get knowledge of organizing and managing methods of the educational process.

The second stage of the new generation instructors training program is practical training. For specialties such as unit shift supervisor, reactor shop shift supervisor and turbine shop shift supervisor the practical training includes training with use of a full-scope simulator (a full-scope model of the real main control room). The use of the full-scope simulator gives an opportunity to simulate NPP normal operation modes, abnormal operation modes, design basis accidents, beyond design basis accidents and others. The instructors training sessions on the full-scope simulator are performed using a complex all-mode mathematical model of a power unit functioning in real time and confirmed training session scenarios developed to teach the operating personnel of NPPs (for example, reactor control lead engineer, turbine control lead engineer, unit shift supervisor, etc.).

One more step of the new generation instructors training is on-the-job training at an NPP. At this stage the instructors are sent to a new operating power unit (for instance, VVER-1200) after receiving theoretical knowledge required to work at NPPs. After that, they return back and proceed theoretical training. For example, after passing a part of theoretical training the instructor taking the reactor shop shift supervisor specialty is sent at an NPP to carry out on-the-job training of a senior reactor shop operator. He consolidates theoretical knowledge, receives a vast amount of experience and understands NPPs operation features.

During on-the-job training the instructor has a mentor who shares the experience and help the instructor to comprehend equipment and systems operation features of the corresponding shop in a short period of time. The mentor is a person from among the operating personnel working at an NPP and belonging to the corresponding shop. Additionally, the instructor works morning, day and night shifts in order to be with the same mentor all the time.

Having gained necessary experience, the instructor returns back and continues theoretical training.

The instructor takes the technical English course simultaneously with all the stages mentioned above. Taking into account tight deadlines and importance of the instructor set objectives, the technical English training is organized as an intensive and continuous process. The technical English course includes technical english classes with high qualified teacher, general communication course developed for improving speech skills, self-study, rehearsal and practice of delivering a lecture, thorough and productive self-study of English during on-the-job trainings. All the learning types listed above increase the level of English and consequently prepare the instructors for their future specialization and position.

Assuming that subsequently the new generation instructors will teach NPP personnel in English, it is vital for them to have high level of English language proficiency, extensive base of technical terms, and what is equally important, to be capable of delivering lectures in English.

Consequently, during the technical English language course instructors are obliged to conduct plenty of preliminary lectures on the topics corresponding to the field of their training program. Furthermore, the instructors must practice making the required training materials.

The instructors have to select a topic and prepare the necessary training aids (a handbook, a session plan and a presentation) in English as well as to present it in front of the audience, teaching the latter this topic. The preliminary lectures are appraised by high-qualified English tutors, professional translators and experts in the field of NPP operation. It is not only knowledge of English language that is evaluated, but also proficiency in the technical specialty and teaching skills.

Additionally, during the whole period of training, the instructors practice translating technical literature and developing training aids. Thus, they regularly create handbooks and presentations in both Russian and English languages on the certain topics related to their specialties as well as the glossaries to the handbooks. These works are also assessed by translators and technical English tutors.

Thereby, the technical English course enables instructors to enhance required skills that will let them perform work with high quality in the future.

The duration of each stage in the instructors training is determined by the field of study and specified in the individual syllabus, e.g. for the unit shift supervisor program each stage constitutes (Figure 3):

- Theoretical training 1680 hours
- Practical training 280 hours
- On-the-job training 920 hours
- Technical English 874 hours

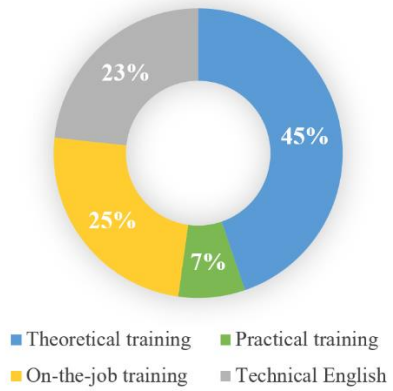

Figure 3. Ratio of Stages in USS Training Program.

F. Instructor Training Completion

When completing the training, the instructors are obliged to take the examination of their knowledge, skills and abilities and have the appraisal in Russian and English. This assessment encompasses three stages. First, the instructor has to pass the exams that reaffirm the qualification in the field of nuclear power plant operation and maintenance. The second stage is intended to confirm the instructor competencies and thereby it implies that the instructor conducts the final lecture in Russian. During this lecture, the trainee has to demonstrate not only the teaching skills, but also knowledge received throughout the theoretical and practical training, as well as the ability to develop the training materials (a handbook, a session plan and a presentation) correctly. In the ultimate stage of the certification the instructor is obliged to deliver a lecture in English and prepare the necessary training materials.

Consequently, this three-stage examination following the completion of the training evaluates three aspects of the instructor education: knowledge in the field of nuclear power plant operation and maintenance, teaching skills and English proficiency.

Having passed all final examinations successfully, the instructors receive diplomas in the specialty “Nuclear Power Plant Personnel Training Instructor”.

III. INSTRUCTOR ROLE

After completing the training and passing the examination, the new generation instructors commence their job responsibilities:

- Development of training aids
- Translation of training aids into English
- Training of NPP personnel by means of diverse approaches (lectures, seminars, etc.)
- Conduction of practical classes (using full-scope simulator)

The new generation instructors training program is versatile and unique since a considerable number of university graduates (applicants) from many different types of educational background is united to carry out and lead future projects consolidated by one idea. However, not everyone has an opportunity to take part in this project due to the fact that the number of specialties (training programs) is quite exiguous. Furthermore, if the graduates have applied for a certain program (for example, turbine shop shift supervisor program), they are ought to have a relevant education. In addition to this, it is also crucial for the future instructors to have an appropriate education and high grades. The obstacles such as limited knowledge, lack of learning skills will definitely increase training time, expenses on the education and slow down the training progress.

More importantly, the instructors have to understand how to use and analyze the regulatory and operation documentation, especially the information received by using the full-scope simulator. If the instructors do not have a sufficient base of knowledge, it is likely that they will get stuck for a solution while executing complicated tasks. Occasionally, they search the required information for a long period of time and simulate various operation modes several times to define mistakes, resolve the problem and create correct training materials.

Nevertheless, by the end of the program the new generation instructors have already gained essential amount of knowledge, experience and practice required for delivering lectures and creating the training materials. And as the instructors continue encourage themselves to explore new, immerse deeper into the field of atomic energy use, solve complex tasks and achieve ambitious goals, they will, without a doubt, become professionals very soon.

IV. PROGRAM EFFICIENY ASSESSMENT

Currently, the ambitious project for training the young instructors presents its first outcomes. Having completed the education and successfully passed the exams, approximately seventy employees have been qualified as the first category NPP personnel training specialists. Now they are actively involved in the training aids development and commence teaching. Above ninety employees still proceed education under the Rosatom program. Moreover, every year the best university graduates are selected to participate in this project.

According to the results of the instructors examination and appraisal, it is possible to conclude that the organization and structure of the training process is qualitatively performed and does not require alterations. The majority of trainees have received the highest grades (Figure 4).

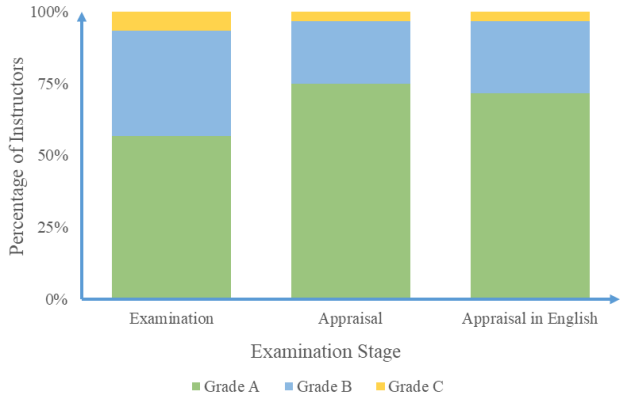

Figure 4. Results of Instructors Examination and Certification

It is also possible to evaluate the current efficiency of the instructors work. Plenty of them are already teaching aspiring personnel of the nuclear power plants. The feedback questionnaires filled out by the audience provide the information on the proficiency of the instructors in conducting lectures. Furthermore, experienced translators and tutors have assessed English language skills of the instructors. The survey results are high: prevailing number of the trainees are satisfied with the qualification, professionalism and expertise of the new generation instructors (Figure 5).

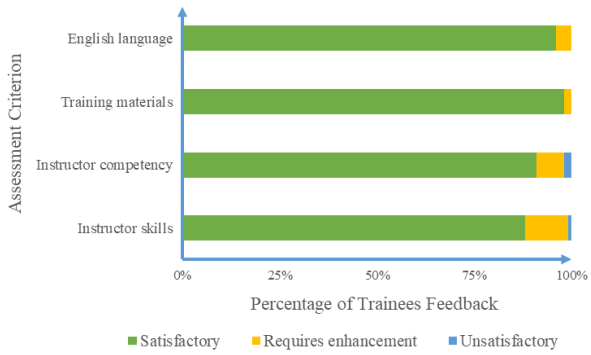

Figure 5. Upshot of Trainees Feedback

Despite the high results, like any project, the instructors training program requires continuous enhancement and advancement in order to keep this approach at the forefront. The ongoing improvement of this program is ensured by getting a feedback not only from the audience, but also from the experts in the field of atomic energy and the professional translators. The presence of the latter at the instructors lectures is crucial for making the program better and advanced. The feedback lets the instructors to correct their mistakes, eliminate imperfections and evolve their teaching skills. Furthermore, receiving the feedback from the instructors themselves is a significant component for improving this ambitious project. Their opinion and viewpoint can enhance some aspects of the approach to training.

V. CONCLUSION

The new generation instructors training project allows to reduce time and expenses on the education of NPP international personnel since there is no need to employ professional translators and highly qualified staff with extensive work experience.

Furthermore, it is sufficient to employ a few new generation instructors in order to develop a necessary number of training aids and to resolve the issue related to teaching a large number of NPP personnel.

All of the above indicates that the new generation instructors training program is effective and specially devised for the most productive training of specialists in the atomic industry with regard to many years of operational experience, current approaches to educational process and international standards.

VI. References

[1] International Atomic Energy Agency, “Development of Instructors for Nuclear Power Plant Personnel Training”, IAEA TECDOC, no. 1392, Rev. 1, 2018

[2] International Atomic Energy Agency, “Use of control room simulators for training of nuclear power plant personnel”, IAEA-TECDOC-1411, September 2004

[3] International Training Center for Nuclear Power Plant Personnel, Rosatom Technical Academy, September 2019. – URL: https://new.rosatomtech.ru/activity/international-training-center-for-nuclear-power-plant-personnel/

Proceedings of the European Nuclear Young Generation Forum
ENYGF'21
September 27-30, 2021, Tarragona, Spain

Scientific dissemination in the Time of COVID

García, Pablo; Durán, Luis Felipe; Noverques, Aina; Vázquez, Carlos

Jóvenes Nucleares (JJNN), Spain

*Corresponding authors: pablo.garcia@jovenesnucleares.com; luisfelipe.duran@jovenesnucleares.org; a.noverques@jovenesnucleares.org; c.vazquez@jovenesnucleares.com

I. INTRODUCTION

Scientific dissemination activities of Jóvenes Nucleares (JJNN) have traditionally been divided into two tracks: a face-to-face one, for which content and formats have been developed over the last 20 years, such as talks, courses and seminars already consolidated, and a second digital way, in which the experience and the contents of the first group activities have been disseminated in our social networks' profiles (Twitter, Facebook, Instagram and YouTube).

However, the impact of COVID 19, through the lockdown imposed to protect the health of the population, has forced JJNN to transform our face-to-face activities.

This paper presents the JJNN strategy to adapt our traditional activities to streaming and the digital environment, from the changes in the approach and logistics to the results of audience and interaction with the public, particularizing the examples of the 2020 edition of the Advanced Reactors Seminar and the growth of our YouTube channel.

The results obtained by JJNN have been highly satisfactory, with audience rates much higher than usual and a significant percentage of Latin American attendees, consolidating our network as a benchmark in nuclear science and technology dissemination in Spanish.

II. TRADITIONAL SCIENTIFIC DISSEMINATION ACTIVITIES

Within the first group of dissemination activities of JJNN, three levels of depth can be distinguished in terms of how the knowledge transferred by our volunteers is adapted according to the target audience, from basic talks in high schools to seminars in specialized technical schools, passing through basic courses on nuclear science and technology.

As an example, the following table summarizes the dissemination activities carried out in 2019 by JJNN.

Table 1. JJNN's scientific dissemination activities in 2019

Face-to-face	Virtual
26 basic talks in high schools 7 basic courses 1 technical seminar 4 debates and technical conferences 5 talks in Pint of Science Spain	1 basic course (IAEA translators)

The ratio between face-to-face and virtual activities in the table above clearly indicates that streaming disclosure has never been a goal for JJNN, but just a tool to use in case there was no other choice.

On the other hand, where the digital route had yet started was in our Social Networks (SNs). In 2019 JJNN's Twitter profile was the most followed Nuclear Young Generation account in the world, thanks to the development of disclosure threads and the use of this material for other SNs (FB, LkIn and Ig) used to give very good results.

Additionally, and fortunately, in 2019, JJNN decided to take a step forward with their own YouTube channel by creating the #FiveMinutesWith (#CincoMinutosCon) in which an expert on a topic related to nuclear technology responds in five minutes, briefly, to five questions from the public.

In this way, planned activities for 2020 basically consisted of continuing to develop our face-to-face activity.

Table 2. JJNN's scientific dissemination activities planned for 2020

Face-to-face	Virtual
20 basic talks in high schools 7 basic courses 1 technical seminar 2 debates and technical conferences 3 talks in Pint of Science Spain	1 basic course (IAEA translators)

That is, with small nuances and, of course, maintaining the great work of the SNs team, JJNN did not have in February 2020 neither a plan nor a digitization strategy for its disclosure activities.

III. VIRTUAL SCIENTIFIC DISSEMINATION ACTIVITIES IN 2020

When the State of Alarm was declared in Spain in March 2020, all the people who did not perform essential tasks in the management of the health emergency were confined to their homes. Consequently, all JJNN face-to-face activities were cancelled, and our Board of Government found it necessary to rethink the entire calendar approved just a month before at the JJNN's General Assembly.

The following is the strategy developed by JJNN's Board of Directors, in three steps:

A. Identify which activities were easier to bring to streaming

Between March and June 2020 JJNN broadcast, both through the recently discovered YouTube channel and through Zoom, a series of disclosure talks and basic courses in nuclear science and technology.

In this case, it is worth highlighting two milestones in the scientific dissemination of JJNN, having developed two activities for the public outside of Spain, such as our first basic course in English, organized in collaboration with the ENS-YGN, and the first virtual edition of our Advanced Reactors Seminar, with a great reception in Latin America.

B. Promote brainstorming

Given that the traditional outreach activities of JJNN had been canceled, part of our Board of Government started a working group of new activities to develop new ideas, or those ideas that in another context would have been brazen for not being able to carry them out:

- A series of interviews with young professionals from the nuclear industry began, in collaboration with WiN Spain, with a very good reception from the public.

- Participation in new forums and invitations that, in previous years, due to workload and unavailability of schedules, had been missed, such as a talk for the IEEE Engineering Society at the National University of Paraguay.

- JJNN's participation in RASNE was updated by organizing a digital round table to discuss what the future of our industry will be like.

C. Creation of a content generation group for SNs

The results of the working group have been satisfactory, with a growth of 27% in followers in RRSS, as seen in the figure below, positioning JJNN as a reference for dissemination of nuclear science and technology in Latin America and having known to generate diverse disclosure and debate contents.

Figure 1. Growth of followers in SNs in 2020

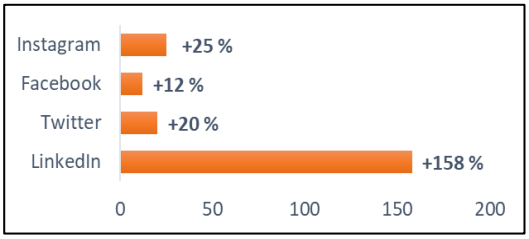

IV. 2020 RESULTS

Although the previous image already reflects some of the results of this year and anticipates that it was not, finally, the disaster that our Board of Government anticipated at the beginning of the pandemic, in this specific section of results we will highlight, among all the information analysed, the two aspects that we have best been able to parameterize.

A. First virtual edition of the Advanced Reactors Seminar

The 2020 edition of the Advanced Reactors Seminar, the first in digital format, attracted 200 attendees, 90% of whom attended all sessions. In previous editions, due to its rigid format, the Seminar usually had about 90 attendees and just 60% retention.

In addition, we were able to organize an additional debate session which was joined by 40 people, half from Latin America, who spent 2 hours talking about the current and future state of advanced reactors, something unthinkable in the traditional face-to-face format of the Seminar.

Finally, the feedback on this edition has been tremendously positive, having improved in all the assessment indicators compared to previous years.

B. JJNN's YouTube channel

The JJNN's YouTube channel data is presented in the figure below.

Figure 2. Growth of JJNN's YouTube channel in 2020

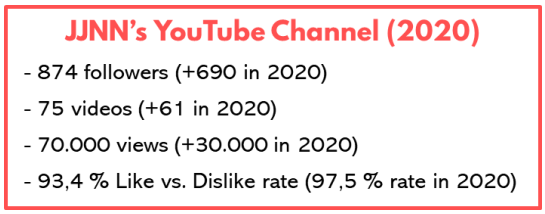

It must be recognized that the statistics that appear in the figure are misleading, since although the channel had existed since 2015, its use as a disclosure tool began at the end of 2019, so it is logical that the channel soared in the last year.

However, the data that is relevant and can help to understand why, from JJNN, we consider that our YouTube channel has worked very satisfactorily, is our most viewed videos ranking, in which we find very interesting things, like the Introduction to Nuclear Physics video of the Basic Course on Nuclear Fusion, in which such interesting things as the standard model of particles are explained: more than 1,200 people have seen the video and not a single person has disliked the video.

Table 3. JJNN's Youtube channel TOP videos

Video	Published	Total views	2020 views	L. vs DL. Rate	Retention (%)	Followers generated
What is nuclear energy?	Apr. 2016	46,353	5,405	81,60 %	49,70 %	70 (8,0 %)
Nuclear fission in two minutes	Mar. 2020	9,458	9,458	98,80 %	81,90 %	51 (5,8 %)
#FiveMinutesWith Eduardo Gallego	Apr. 2019	1,280	537	100 %	64,40 %	21 (2,4 %)
BCNF - Introduction to Nuclear Physics	Mar.2020	1,231	1,231	100 %	72,30 %	23 (2,6 %)
Chernobyl. The series seen by a nuclear engineer	Apr. 2020	1,170	1,170	97,80 %	81,10 %	23 (2,6 %)

And finally, we come to the part of the results where we consider that, in 2020, in such a strange context for everyone, we cannot rely solely on metrics.

C. SWOT analysis

In 2020 the feedback has been more important than ever and, therefore, at JJNN we have taken all those non-measurable impressions and we have done an analysis with them.

Figure 3. SWOAT analysis of JJNN's virtual disclosure activities in 2020

Strengths	Weaknesses
1. Financial savings	1. Loss of closeness to the public
2. More effective management	2. Dilution of the target audience
3. Greater depth in interaction	3. Can't get direct feedback
Opportunities	**Threats**
1. Access to new audiences	1. Stable connection dependency
2. Access to TOP speakers	2. Loss of public interest
3. Access to relevant topics	3. Networking deficit

V. FUTURE OF JJNN DISSEMINATION ACTIVITIES

After analyzing the results, both measurable and subjective, JJNN's conclusion regarding the future of our disclosure activity is that we really want to return, BUT we are NOT in a hurry.

We are aware that face-to-face disclosure is one of our strengths and we love it, but we consider that we have solved the situation we were facing very well and, therefore, while it is not completely safe and desirable to return to the normality, to the dynamic and close formats, we are not going to expose our speakers or our audience to any unnecessary risk.

For this reason, from JJNN we have decided to continue with our digital activities at least until the end of 2021 and, in addition, we have taken advantage of the total stoppage of some activities, such as talks in high schools and basic courses, to rethink its long-term management strategy. Over 2021 we will launch the new hybrid approaches between the digital format, with great potential, and the face-to-face one, our greatest value.

Proceedings of the European Nuclear Young Generation Forum
ENYGF'21
September 27-30, 2021, Tarragona, Spain

Spanish Nuclear Society STEM Program: science face-to-face

García, Pablo [1]; Gala, Laura [2]; García, José [3]; Palacio, Teresa [4]

[1] Jóvenes Nucleares (JJNN), Spain; [2] Foro Nuclear, Spain; [3] Endesa, Spain; [4] Enresa, Spain

*Corresponding authors: pablo.garcia@jovenesnucleares.com; lgala@foronuclear.org; jose.garciala@enel.com; tpaa@enresa.es

I. INTRODUCTION

The Spanish Nuclear Society (SNE), through the work of its committees and with help from its corporate members, has taken the initiative to include, in the days prior to its Annual Meeting, a STEM program oriented to secondary school students, with the aim of promoting dissemination and knowledge of nuclear science and technology to society in an open way.

This paper will present how the STEM program of the SNE Annual Meeting aims to give added value to the Congress and to bring the SNE closer to society through information and training of students in technical concepts and scientists related to science and technology.

This program has been implemented in the last two face-to-face editions of the Annual Meeting with a great success of participation and an enormously positive evaluation among the more than 1000 students and the teaching staff who participated in the 9 proposed workshops.

II. STEM METHODOLOGY

STEM is the acronym for four academic disciplines: Science, Technology, Engineering, and Mathematics. STEM-based education is a learning approach that removes traditional barriers that separate these disciplines and integrates them into real, rigorous, and relevant experiences for students [1]. In other words, STEM methodology is practice-based learning.

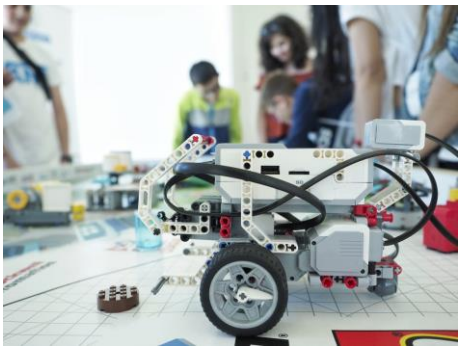

Figure 1. SNE's STEM Program 2018 edition.

Currently, society is facing a growing demand for technical and scientific talent capable of generating new ideas and being at the forefront of innovation. It is necessary to train more technical and scientific profiles that have the academic tools and vision to be able to identify opportunities for technological development [2]. Therefore, it is necessary to motivate young people to pursue careers in science and technology areas, and this is precisely the goal of STEM Programs.

III. THE STEM PROGRAM OF THE SPANISH NUCLEAR SOCIETY

The Spanish Nuclear Society (SNE) is a non-profit association, declared of Public Utility, which brings together professionals in the nuclear sector in Spain, who carry out their activity in all areas of science and technology: electricity companies and engineering, capital goods, nuclear fuel manufacturing, radiation protection and specialized services, as well as universities, research centers and regulatory bodies. One of the fundamental objectives of the SNE is the dissemination and knowledge of nuclear science and technology.

For more than 45 years, the SNE has held its Annual Meeting in different cities of Spain, with a duration of three days. The central axis is an intense Technical Program, complemented with the collective participation of the attendees in social and cultural events in emblematic places of the city.

Additionally, the Meeting also includes activities open to society in general, such as the Basic Course on Nuclear Science and Technology taught by Young Nuclear, the conference organized by WIN (Women in Nuclear) or the course for teachers organized by Foro de la Spanish Nuclear Industry, with the aim of disseminating the concepts of nuclear science and technology.

It is, therefore, within these open activities, where the STEM Program of the Annual Meeting of the Spanish Nuclear Society is included.

A. SNE's STEM Program Purpose

The STEM program organized by the SNE within the activities of its Annual Meeting is an open and free event aimed at students at secondary high schools in their last two years.

With this activity, the SNE aims to give added value to its Annual Meeting by providing information and training for secondary students in technical and scientific concepts related to science and technology in general and with ionizing radiation applications.

B. Organization and content of the program

The organization of the STEM program consists of five workshops in parallel, over two days, each lasting 1.5 hours, which are repeated in three shifts, during school hours. The groups of students can choose which workshops they prefer and, if there are enough places available, each group can carry out more than one workshop on the same day.

Table 1. STEM Program daily schedule

Turn	Workshop 1	…	Workshop 5
1st	20-30 students	…	20-30 students
2nd	20-30 students	…	20-30 students
3rd	20-30 students	…	20-30 students

IV. STEM WORKSHOPS

All the workshops carried out during the program have in common the dissemination of STEM materials in a practical way.

Below are some of the workshops held in the two editions of the program by way of example.

D. The Circular Challenge

"The Circular Challenge" is a technological and participatory experience that, through app gaming, allows the students to discover how renewable gas is a key source of energy to curb climate change and promote the circular economy. Students will understand how renewable gas is created, the uses it enables, and its critical role in the future as clean and sustainable energy, together with nuclear power and other renewable sources.

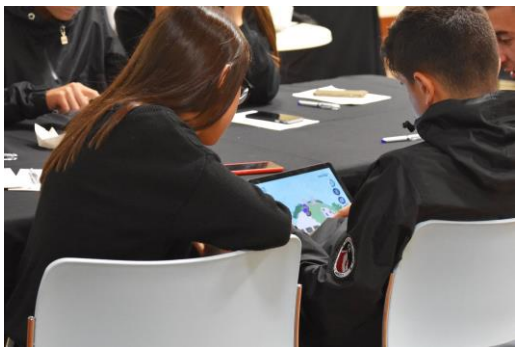

Figure 2. SNE's STEM Program 2019 edition. The Circular Challenge workshop.

This proposal, an excellent tool to transfer expert knowledge to high school students, in addition to dealing with technical issues, raises work on values, the development of critical sense, civility and social commitment.

E. DiY Holograms

This workshop is presented in two parts, with an initial introduction to the concepts of optics, electromagnetic radiation, ionizing radiation and the visible spectrum, lasers and holograms, and a second practical part that consists of the elaboration of a plastic prism with which to they will be able to visualize hologram simulations through devices.

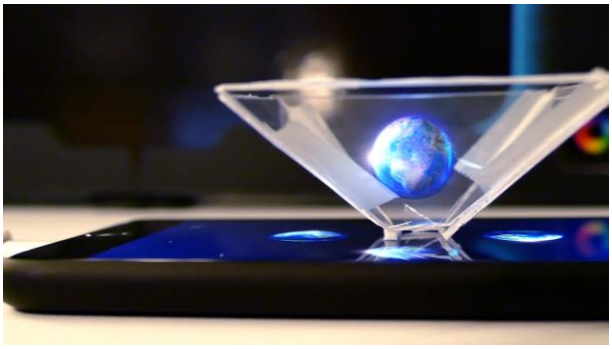

Figure 3. DiY hologram demonstration.

Finally, a pooling is carried out between the speaker and participants to clarify doubts and provide additional teaching resources. Additionally, an explanatory video is projected through the prisms about what nuclear fission is and how a nuclear power plant works for the generation of electricity free of emissions.

F. Energy in the Classroom

Through a series of simple experiments and with materials that can be found in everyday life, the aim is to show students the processes of transformation of different raw materials or natural resources into electrical energy.

Figure 4. SNE's STEM 2019 edition. Energy in the Classroom workshop.

Figure 4. SNE's STEM 2019 edition. Energy in the Classroom workshop.

These activities will allow them to establish the knowledge acquired in the classroom and see its application in a practical way, know the technology used, the advantages and disadvantages that each of the sources entail and be able to compare them.

G. Sustainable Chemistry

This workshop begins with a general presentation to introduce the concept of sustainability, as well as the twelve

principles of sustainable chemistry, and to raise examples of environmental problems, such as energy abuse or the misuse of water, which can be partially solved through change of performance.

Figure 5. SNE's STEM Program 2019 edition. Sustainable Chemistry workshop.

Finally, the practical part of the workshop invites students to carry out experiments to deal with topics such as: what is a catalyst and what advantages can it bring from a sustainable point of view, how much electricity is consumed in the world and why is it? a problem? Why is the use of renewable energy interesting in the future? or what are electromagnets used for and how can you make them with conventional materials?

H. Radioactive waste

After a presentation on what radioactive waste is, how it is generated, how it is classified, how it is managed and who takes care of this work, two monitors - a scientist and an assistant - present the activity.

Figure 6. SNE's STEM Program 2019 edition. Radioactive waste workshop.

Figure 6. SNE's STEM Program 2019 edition. Radioactive waste workshop.

In the first place, the aim is for students to understand what radioactivity is with the help of a radiometer. Then, through a group of card game, one delves into what is a waste, and what is a radioactive waste, where it is produced and where it is managed. Once the above is understood, it is shown how radioactive waste is managed with an experiment in which, with a syringe with a tube of chemical light, the students simulate the management of low and medium level waste: the students must have the syringe in the drum for three days simulating the 300 years that waste remains in a storage center and, later, in class they will open the drum and the chemical light will no longer shine. Finally, to fully understand the engineering barriers that isolate the waste, the concept is reinforced with a sound player, whose beep will be attenuated as the barriers are implemented, until it can no longer be heard. This module is completed with environmental integration and surveillance of the environment.

The activity ends with a board game on the transport of low and medium level radioactive waste in which, through 40 questions to 4 teams, all concepts are reviewed.

V. RESULTS AND CONCLUSIONS

The STEM program has been implemented in the last two face-to-face editions of the Spanish Nuclear Society Annual Meeting (2018 and 2019) with a great success of participation and an enormously positive evaluation among the more than 1000 students and the teaching staff who participated in the 9 proposed workshops.

In addition to the positive feedback received from participating students and teachers, the STEM program has had great visibility in the local press [3, 4, 5] in the cities of Ávila and Vigo, thus helping the SNE to (i) meet its objective of disseminating nuclear science and technology and (ii) open the Annual Meeting to the public.

After two years of development, the three most important points have been identified to ensure that the program develops satisfactorily:

- A strict planning of the specific resources of each workshop is necessary, as well as the schedule of the development days to be able to coordinate well the transit of the students, as well as that the workshops are developed in their time.

- The participation of the collective partners of the SNE as sponsors of the workshops has notably helped the program, both in its planning and in its development and visibility.

- The program must be attractive to make public administrations, in charge of facilitating interaction with the centers, be interested in it.

For this reason, considering the identified improvement points and the lessons learned implemented, the Spanish Nuclear Society has decided to go on with its STEM Program in upcoming face-to-face editions of its Annual Meeting.

Therefore, after a year in which this program has not had a place in the Virtual Meeting of the SNE, the STEM Program will resume, at the end of 2021, in the next Annual Meeting of the Spanish Nuclear Society, with a restricted capacity to be able to fulfill all health measures and recommendations and guarantee the protection of speakers and students while they share this STEM experience.

VI. References

[1] Takeuchi, M. et al. Transdisciplinarity in STEM Education: A Critical Review. Studies in Science Education. April 2020.

DOI 10.1080/03057267.2020.1755802

[2] Capraro, R, Capraro, M, Morgan, J. STEM Project-Based Learning. An Integrated Science, Technology, Engineering, and Mathematics (STEM) Approach. Sense Publishers (2013)

ISBN-13: 978-9462091412

[3] Jóvenes preparados para el futuro. 2018. El diario digital de Ávila.

[4] La cumbre de la Sociedad Nuclear Española reunirá en Vigo a 600 expertos. 2019. Faro de Vigo.

[5] El sector nuclear español se reúne en Vigo para presentar sus novedades. 2019. Energética XXI.

Proceedings of the European Nuclear Young Generation Forum
ENYGF'21
September 27-30, 2021, Tarragona, Spain

How to talk to the ordinary citizen: Social Media Strategies for the Nuclear Sector

Ortega, Laura*

IE University,Spain;

*Corresponding author: lauraortegap99@gmail.com

I. INTRODUCTION

In our hyperconnected technological world, it is rare to find a company or project that doesn't have an online presence. At times, we even find that there is an oversaturation of content and accounts communicating the same information. Other times, we find that there is a disconnection between what the public wants and the content that companies send. For this reason, any account must learn how to prioritize, synthesize, and always offer valuable information for the users. More specifically, how to offer a real bidirectional communication channel, and not only use their channels for informational purposes.

To explain the next social media practices, I will consider the target audience, as the ordinary citizen – in other words, not from the scientific community. And the goal as creating awareness of the benefits of nuclear energy, positive sector recall, and positioning when considered for the energetic mix. Hence, I will make some recommendations on how to offer the communication with them, by proposing new directions for their channels and influencer marketing through YouTube or streaming platforms.

II. THE ORDINARY CITIZEN

It is common knowledge that the nuclear sector and the science community's social media channels have been growing in the past years [1], however, these accounts are still very under the radar for the "normal" citizens. This means that we still encounter the problem of communicating and building trust relationships between the sector and citizens. We must aim to provide clear, easy, and transparent information that they can understand to build a trust relationship with the science/nuclear community. And for this, we have to think about how to stop the cycle of being both the communicators who put out the content and information, and the receivers - as currently, we are only speaking from and to ourselves - so we can open it up to the wider community.

A. Where to find them

People are lazy by nature. Therefore, one must go to the channels where they are most active in because they are not going to proactively search for you. They will only do so for specific actions, and consultation.

Current trends suggest that the best channels to communicate with younger audiences are Instagram, Twitter, and Tik Tok [2]. For these last ones, the company Iberdrola has already launched its channel and has obtained some positive and negative results in relation to their communication strategy. On another hand, LinkedIn and Twitter are for professional and educated profiles, but since the nuclear sector is already established in those areas, they should try other platforms or give those another use. This goes in the same way as to how they take advice and inspiration like scientific influencers Operador Nuclear (106k Followers, Twitter) [3], and Deborah Ciencia (51.9k Followers, Twitter) [4]. Their practices work for the nuclear sector audience – a very niche audience - and what they need is a broad one.

Instead, because the current issue is not a corporate one but a sector one, companies must collaborate with each other by sharing information and resources to change people's perceptions of nuclear energy. To then generate general nuclear energy awareness and exposure, so it can later lead to trust relationships and open channels of communication and information flow with ordinary citizens.

It has been proved that communication by a group of companies is taken better than by individual ones, as the message won't be disregarded because someone had a problem with one of the companies and instead, they will focus on the greater message [5]. The goal should be to attract new audiences and retain the current ones. This means nuclear energy awareness and exposure, which would then lead to a greater trust relationship and would open a new channel of communication and information flow. It is important to consider all generations for this.

III. SOCIAL MEDIA STRATEGIES

Following with the above mention, we need to investigate new channels and actions.

We must remember that different platforms attract different audiences. Therefore, is not advisable to cross-share content in between platforms, because often they will not be used to its full potential.

As well, anytime we create actions in social media, KPIS (Key Performance Indicators) must be considered. From our point of departure, scoping KPIS like Impressions and Reach, are the best as what we want is for the greatest amount of people to get to know about the sector. Then metrics like shares, comments, and mentions or hashtag tracking would allow us to evaluate the positive brand associations.

A new channel to consider is "Clubhouse", an invitation-only social media app that works through live audio-dropping chat rooms of up to 5,000 people [6]. Its audio format has great potential for the nuclear community, linking professionals and ordinary citizens in a more private setting where doubts and concerns can be addressed in live discussions.

However, the most promising channel and format right now is video streaming. 80% of customers now say that they'd rather watch a live video than read a company's blog [7]. Companies produce eye-catching content that catches the interest of users through live streaming on platforms like YouTube, Instagram, Twitch, or Facebook Live. Customers and prospects will also respond and ask questions in real time by watching live streams.

B. Campaigns

Along with educational content that can help the citizens understand the sector. A way to positioning nuclear energy as a key player in the energy mix, is through short-term campaigns with high impact, long-term campaigns with micro-influencers, events, video streaming, appearances in the media and social listening answering to Q&A both online and face-to-face.

When the goal is awareness and engagement, short-term strategies or punctual campaigns can have more impact.

One of the ways that is gaining popularity to generate that effect is through Influencer Marketing. According to Tomoson study, is estimated that businesses make an average of $6.50 USD for every 1$ spent on influencers [8], and, that a whopping 74% trust on influencers to take their purchasing decisions. Influencer marketing is defined as a type of social media marketing that uses sponsored content and product mentions from content creators. Depending on their follower base they are categorised in different tiers, nano, macro, top…etc.

In this frame of work, Micro-influencer marketing and Macro Influencers will be the best. Why?

Micro-influencers like; educational leaders, scientist, technological peers are capable to penetrate trust circles in their network, something which in communication is gold. By using these types of profiles, you can focus your network where your core audience is already active.

Macro-influencers: have a big audience base, but not as big as top influencers, therefore they provide reach and they can still provide a sense of proximity with the audience, which is what we want.

These influencers could take several actions. An idea to generate this effect is by allowing people to experience the product, in this case the nuclear energy. Because access to nuclear plants is restricted, a way to give that opportunity to the ordinary citizen is through influencers. First, it would be easier to give that access to one person, and secondly, they already have an established audience the nuclear company can use to its advantage. Influencers can develop and cultivate stronger, more authentic relationships with their audience, and that is why, the audience is more trusting. Further on, this could help in the efforts of trying to make nuclear energy be considered in people's minds as an energy source.

Ways in which this could be done, is by taking some influencers and do a vlog around the plant, interviews, and social media challenges if permitted by security. The key to success so all parties win is that the content is informative and entertaining. Imagine you want to show a new nuclear facility in construction, which always has some controversy depending on who you ask. A corporate video from the company might not have much effect on an ordinary citizen, because the relationship of trust is not established, and it might be seen as greenwashing. However, if it were to be done by an influencer they like, they trust and that has their own style of presenting things, they would accept it and be more receptive to take it into a positive way.

Figure 1. Twitch Session with Spanish Biggest Influencer 2020 Ibai Llanos and Football Player Piqué

Figure 2. Twitch Session with Nuclear Influencer Operador Nuclear, Sciene Influencer, La Gata de Schrodinger and Orbytal (Chemistry Science Channel)

C. What content works

First, a point to consider is format. Then, it will all depend on the purpose, goals, or if it's a short-term strategy or long-term. Considering our target and the goal of awareness, and engagement. The most popular formats are as follows.

Instagram stories and time-sensitive posts - This is easier to consume, casual, and reminds users about the existence of your page daily.

Then, ***short-form video***, especially more with the rise of TikTok and Instagram Reels. Video is social media's best friend.

Content must be "on their level", and ***human, real***. Sometimes we believe we are being simplistic, but we aren't. One must tailor the message to the specific audience, so they understand what they get from it and how it is beneficial to them. For example, a person complains on social media because an increase in the invoice of electricity, there, she doesn't care if the company is sorry or that everyone else is going through the same, she cares about why this happened, if it can be revised, and how can she pay that new fee.

Being said that, it is crucial to ***respond to user questions and shout-outs***, regularly and as soon as possible. Is rare for ordinary citizens to engage in nuclear sector, so when they do, we cannot miss the opportunity.

Lastly, ***emotional content.*** A study of 1,400 successful advertising campaigns, showed that those with emotional content performed about twice as well (31% vs. 16%) [9]. Emotional marketing helps people decide with their hearts, even when the sector is something that doesn't interest them. For this reason, showing the people that work every day in the sector, their stories, and not only the corporate side, has great potential for the ordinary citizen to find a point of connection and trust.

IV. Conclusion

Nuclear companies may use social media listening to find industry influencers with which to collaborate and boost their marketing messages. Even if social media strategies are not the only ones that need to be considered when approaching the ordinary citizen, they offer a direct channel of communication with them, and it should be exploited to the maximum. Therefore, the best use of these channels is to have collaborations in between companies, innovate with its practices so it overcomes the content saturation, and most importantly be there for the audience. Listen to their concerns, questions, and do not bombard them with content that they didn't ask for. Is more about being available, than being a push over – in communication strategy this is when you use various activities to get your message in front of your audience, by contrast pull marketing is when the company offers content that is valuable to the audience, gets involved in the community that they are in, and the audience is drawn into the company voluntarily because of the value they offer [10].

Nevertheless, since the sector is still widely unknown for this target, it will need to make some practices to seem attractive and position itself as someone that ordinary citizens could approach, trust and like. As has been established this can be done, through influencer marketing, but other measures in a wider scheme of things is simplifying messages, adapting to the social media channels that "ordinary" citizens use, and adapt it to its capability, use the most attractive content possible, and then be available both online and offline.

V. References

[1] "Nuclear Communicator's Toolbox,"IAEA, 31-Jan-2019. [Online] Available : https://www.iaea.org/resources/nuclear-communicators-toolbox/tools/social-media

[2] "5 Emerging Marketing Channels You Should Prioritize in 2021." Raitses,R. 5-Oct-2020. [Online] Available : https://www.linkedin.com/pulse/5-emerging-marketing-channels-you-should-prioritize-2021-roie-raitses/

[3] Operador Nuclear Twitter. 31 -May- 2021. [Online] Available : https://twitter.com/OperadorNuclear

[4] Deborah Ciencia Twitter. 31-May- 2021. [Online] Available : https://twitter.com/deborahciencia

[5] "Group Decision Making," Principles of Social Psychology. 26-Sept-2014. [Online] Available : https://opentextbc.ca/socialpsychology/chapter/group-decision-making/

[6] "Clubhouse app : what is it and how do you get an invite to the exclusive audio app?", The Guardian. 17-Feb-2021. [Online] Available : https://www.theguardian.com/technology/2021/feb/17/clubhouse-app-invite-what-is-it-how-to-get-audio-chat-elon-musk

[7] "5 Social Takeaways for Tech Companies," Sporut Social. NDA. [Online] Available : https://sproutsocial.com/insights/guides/social-for-tech-companies/

[8] "20 Surprising Influencer Marketing," Digital Marketing Institute. 25-Oct- 2018. [Online] Available : https://digitalmarketinginstitute.com/blog/20-influencer-marketing-statistics-that-will-surprise-you

[9] "The Ultimate Guide to Emotional Marketing ", Decker, A. Hubspot. 20-Aug-2018. [Online] Available : https://blog.hubspot.com/marketing/emotion-marketing

[10] "Push vs. Pull Marketing ," Murphy,D. Social Media Today. May, 13, 2008. [Online] Available : https://www.socialmediatoday.com/content/push-vs-pull-marketing

Proceedings of the European Nuclear Young Generation Forum
ENYGF'21
September 27-30, 2021, Tarragona, Spain

EUROSAFE: Fostering the sharing of nuclear expertise

Cozzo, C.[1*], Allagbe, C.[2], Alonso, J. R[3], Ben Ouaghrem, K[2], Cizelj, L.[4], Degueldre, D.[5], Eibl-Schwäger, C.[6], Faye, H.[2], Fukasawa, M.[7], Glevarec, J.[2], Hatala, B.[8], Horvath, A.[9], Hrehor, M.[10], Jansen, R.[11], Khamaza, A.[12], Knochenhauer, M.[13], Mackey, J.[14], Meloni, P.[15], Mistryugov, D.[12], Nitoi, M.[16], Pinel, C.[2], Power, S.[14], Puska, E.-K.[17], Rimkevicius, S.[18], de los Reyes, A.[3], Shevchenko, I.[19], Turcu, I.[16], Volant, Ph.[2], Yesypenko, Y.[19]

[1]Paul Scherrer Institut (PSI), Laboratory for Reactor Physics and Thermal-Hydraulics, Forschungsstrasse 111, 5232 Villigen, Switzerland
[2]Institute for Radiological Protection and Nuclear Safety (IRSN), 31 ave de la Division Leclerc, 22260 Fontenay-aux-Roses, France
[3]Consejo de Seguridad Nuclear (CSN), Pedro Justo Dorado Dellmans 11, 28040 Madrid, Spain
[4]Jožef Stefan Institute (JSI), Jamova cesta 39, 1000 Ljubljana, Slovenia
[5]Bel V, Rue Walcourt 148 Walcourtstraat, 1070 Brussels, Belgium
[6]Global Research for Safety (GRS), Forschungszentrum, Boltzmannstr. 14, 85748 Garching, Germany
[7]Nuclear Regulatory Authority (NRA), 1-9-9 Roppongi, minato-ku, Tokyo 106-8450, Japan
[8]VUJE,a.s., Okruzna 5, Trnava, Slovak Republic
[9]Centre for Energy Research (EK-CER), Konkoly Thege M. út 29-33., H-1121 Budapest, Hungary
[10]Státní ústav radiační ochrany v.v.i. (SURO), Bartoškova 28, 140 00 Praha 4, Czechia
[11]Authority for Nuclear Safety and Radiation Protection (ANVS), Koningskade 4, 2596 AA Den Haag, Netherlands
[12]Scientific and Engineering Centre for Nuclear and Radiation Safety (SEC NRS), Malaya Krasnoselskaya st. 2/8, bld. 5, 107140, Moscow, Russia
[13]The Swedish Radiation Safety Authority (SSM), SE-171 16 Stockholm Solna strandväg 96, Sweden
[14]Jacobs RSD, 305 Bridgewater Place, Warrington WA3 6XF, United Kingdom
[15]Italian National Agency for New Technologies, Energy and Sustainable Economic Development (ENEA), via Martiri di Monte Sole 4, 40129 Bologna, Italy
[16]Technologies for Nuclear Energy (RATEN ICN), Campului Street no.1, Mioveni, Arges, 115400, Romania
[17]VTT Technical Research Centre of Finland, Kivimiehentie 3, 02150 Espoo, Finland
[18]Lithuanian Energy Institute (LEI), Breslaujos 3, 44403 Kaunas, Lithuania
[19]State Scientific and Technical Center for Nuclear and Radiation Safety of the State Nuclear Regulatory Committee of Ukraine (SSTC NRS), 35-37 Vasylya Stusa Street, 03142, Kyiv, Ukraine

*Corresponding author: *cedric.cozzo@psi.ch*

VII. ETSON AND EUROSAFE

Nuclear energy not only allows for the production of a reliable, economic and carbon-free energy; it also holds an excellent safety and security record. To achieve this, every nuclear safety authority benefits from the technical and scientific expertise provided by their respective Technical Safety Organisations (TSOs) [1]. In 2006, most of the European TSOs (see Figure 1) have regrouped under the European Technical Safety Organisation Network (ETSON) that serves as a common platform to its member organisations to foster technical exchanges, to share best practices in nuclear safety, to plan and implement nuclear safety research programmes, to facilitate the application of the European directive on nuclear safety and to work together in safety assessment and research projects [2]. Nowadays, ETSON with its 16 members is also represented beyond Europe thanks to its associated members of Russia, Ukraine and Japan (Figure 1). The EUROSAFE Forum, 'EUROSAFE' for short [3], is organised in order to bring together experienced and young experts and representatives in the fields of nuclear safety and security, radioactive waste management, radiation protection and emergency preparedness & response, thus providing ETSON with an annual event fostering more in-depth knowledge exchange and discussion on ongoing developments in research, technology and regulatory related activities. The organization of EUROSAFE is incumbent upon the EUROSAFE Programme Committee (EPC), which includes also the Regulatory Bodies of Sweden, The Netherlands and Spain with their internal TSO unit, currently composed of this paper's authors.

With the aim of performing high-quality experts-gathering events, the EPC is looking at attracting the audience with an exciting and innovative programme. This is mostly achieved by *i)* identifying the positive features in the past events and *ii)* dealing with innovative topics and introducing new concepts. With this paper, the EPC would like to share their experience related to the successful organization and realisation of the EUROSAFE important conference series.

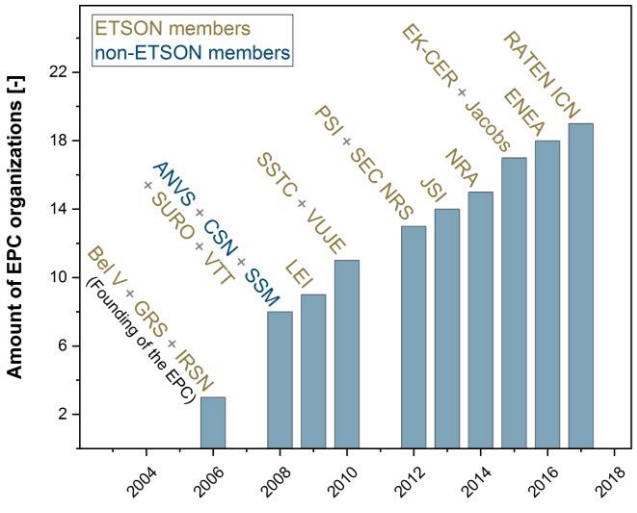

Figure 1. Evolution of the EUROSAFE Programme Committee. The acronyms of each institution are described in the affiliation section.

I. KNOWLEDGE DISSEMINATION FRAMEWORK

A. Technical Sessions

The latest technical-scientific activities and findings of ETSON members are presented and discussed in several technical sessions. These are generally regrouped around the three topics: *1)* nuclear installations safety and security, *2)* waste management and decommissioning & disposal, *3)* radiation protection, environment and emergency preparedness & response. This spectrum of topics allows EUROSAFE to bring together experts and representatives from different organisations: research institutes, public authorities, regulatory bodies & safety authorities, power utilities, the nuclear industry and non-governmental organisations from all over Europe and beyond to inform about and discuss current developments in research and technology. Technical sessions can be opened with an impulse speech given by an external specialist, which provides a different perspective or new understanding on the research or developments. The duration of EUROSAFE (plenary + technical sessions) is usually limited to two full days, and a poster session is organised to accommodate the numerous paper submissions that are not accepted as presentations.

A feedback of the event is provided at different levels. First, a summary of the technical sessions is given by their respective chairman. Then, the experience from each institution is share during the EPC meetings. Finally, it is planned in the future to make use of the mobile application of the conference in order to collect feedback from the participants.

B. ENSTTI

Founded in 2010 by four ETSON member organisations, the European Nuclear Safety Training and Tutoring Institute [4], ENSTTI for short, aimed to transfer the knowledge and know-how of the European nuclear safety organizations (TSOs) in the fields of nuclear safety and radiation protection. ENSTTI offers a wide portfolio of technical trainings and provided great career boasts for both junior and senior staff in regulatory bodies and TSOs in European and worldwide. In the last years, EUROSAFE has been the seat of the EU Training & Tutoring award, granted by the Directorate-General for International Cooperation and Development of the European.

C. Publications

The magazine "EUROSAFE Tribune" [3] was published twice a year between 2001 and 2016, providing the readers with articles about key issues in the world of nuclear safety and radiological protection. In an alternating sequence, the editions focussed on the respective EUROSAFE Forum´s main subject and on special topics. From 2017, the EUROSAFE proceedings, abstracts and presentations are published on the ETSON website [3].

II. OPTIMISATION OF THE RESOURCES

This section provides additional considerations that allow for a better management of the resources.

A. Rotation of the organization lead

As founding members and given their central location in Europe, the EUROSAFE conferences are alternatively hosted by Bel V, GRS and IRSN on behalf of ETSON. This rotation brings diversity in the cultural background while not burdening every year the same institution with the organisation costs and logistics.

B. Complementarity and support to IAEA international conference on TSO

Every four years since 2007 (three years for the first interval), the IAEA is organising an international conference on Challenges Faced by Technical and Scientific Support Organizations [4]. Since the objective of EUROSAFE partially overlap those of this conference series, EUROSAFE did not take place in 2010, 2014 and 2018. Rather than competing with the IAEA conferences dedicated to TSOs, the EPC is supporting their organisation. Contributing to these events allows ETSON to increase its visibility beyond Europe. It should be noted that earlier this year, ETSON has expressed its support at the IAEA to maintain the next IAEA TSO conference as planned in 2022 in Russia [5].

III. MAJOR NETWORKING EVENT

Since the EPC values the outcome of informal discussion, it aims to make EUROSAFE a vibrating event where the audience can enjoy a relaxed atmosphere in addition to the high quality technical presentations. Therefore, the EUROSAFE programme is rhythmed with technical and networking sessions such as, but not limited to, the typical dinner or coffee breaks that can be found in most

conferences. This sections describes several additional features providing significant added value to EUROSAFE.

A. TSO Café

What makes EUROSAFE very prone to exchange is a concept called the TSO Café. TSO Café is a networking-oriented concept that takes place between sessions, during the break. The staff of each TSO can present the activities of their institution in their respective booth. In addition, local specialties are distributed in order to complement the technical interactions with cultural exchange.

First introduced in Munich, Germany, in 2016, the TSO Café was very well received by the audience and especially the young experts with its relaxed atmosphere, and was recently extended to the concept of the ETSON Marketplace.

B. ETSON Marketplace

During the whole event, the ETSON Marketplace provides a space for networking and relaxing. First introduced at EUROSAFE 2019, the ETSON Marketplace includes the TSO Café and a Speakers' Corner (Figure 2) for the full duration of the event. The Speaker's corner is a multi-purpose area that can be used for general communication such as an information session of the ETSON Junior Staff Programm [6], panel discussions and award ceremonies.

Figure 2: ETSON Marketplace at the EUROSAFE 2019

C. ETSON Science Slam

The ETSON Science Slam (Figure 3) is a yearly competition aiming to promote outstanding work performed by junior scientists within the ETSON institutions. Upon acceptance of the paper, a limited amount of candidates is invited to present their work to the EUROSAFE audience in a succinct manner. Not only the technical achievements (judged by a jury), but also the degree of collaboration and the communication skills are weighted to determine the winner of the slam. The audience is also asked to participate in the voting process. The ETSON award ceremony takes place at the end of the conference and is organised by the ETSON Junior Staff Programm (JSP) [8].

Figure 3: ETSON Science Slam at the EUROSAFE 2019

D. Guest lectures

During the plenary session, two types of guest lectures are taking place. On one hand, prominent persons in the nuclear field are invited to share their current view and perspective with respect to their activities and the nuclear context. On the other hand, distinguished persons, unrelated to nuclear activities, present their activities and experience. This insightful and inspiring external presentation is an excellent way to broaden the vision of the audience and allows drawing similarities in the challenges faced by completely different businesses. Among the most appreciated ones were the talk 'Man, Risk and Rescue – Flight Safety Research in Civil Aviation' given by Manfred Müller from the Deutsche Lufthansa AG and 'Ebola health crisis management in Guinea' by Antoine Peigney, a former humanitarian manager at the French Red Cross.

IV. FINAL REMARKS

Based on the successful logistical, technical and networking concepts, the EPC will organise the EUROSAFE 2021 on November, 22-23rd in Paris, France [3]. It will integrate all the aforementioned concepts and will also further promote an open dialogue by inviting the representatives of the (civil) society and strengthen its position as an important event in Europe and beyond. Moreover, having in mind the focus on the young generation, the EPC is looking forward to interacting with the Nuclear Young Generation at the next EUROSAFE Forum.

V. REFERENCES

[1] Technical and Scientific Support Organizations Providing Support to Regulatory Functions, IAEA-TECDOC-1835, 2018.

[2] ETSON, http://www.etson.eu/About

[3] Publications ETSON and EUROSAFE http://www.etson.eu/publications

[4] EUROSAFE 2021 http://www.etson.eu/eurosafe

[5] ENSTTI, https://enstti.eu/wp/

[6] International Conference on Challenges Faced by Technical and Scientific Support Organizations (TSOs) in Enhancing Nuclear Safety and Security: Ensuring Effective and Sustainable Expertise, 15–18 October 2018, Brussels, Belgium

[7] SEC NRS news 24.06.2020 “The 2022 IAEA International TSOs Conference is planned to take place in Russia in 2022” https://www.secnrs.ru/en/news/index.php?ELEMENT_ID=6671

[8] ETSON Junior Staff Programm, http://www.etson.eu/jsp

VI. ACKNOWLEDGEMENTS

The authors would like to acknowledge the support of C. Hommers (GRS) for providing information and reviewing the article.

The EPC is thankful to EC DG Devco for the staging of the T&T award ceremony at the EUROSAFE.

Proceedings of the European Nuclear Young Generation Forum
ENYGF'21
September 27-30, 2021, Tarragona, Spain

Knowledge transfer in FEA trainings: ROSATOM's modern approach: theory and practice

Roskoshnaya Maria[1] and Tkachenko Evgeniia[2*]

[1] Rusatom Service JSC (RusAS), Russia; [2] Rusatom Service JSC (RusAS), Russia

*Corresponding author: *evstkachenko@yandex.ru*

I. INTRODUCTION

Foreign economic activity is an essential part of working process of many companies in nuclear industry. Even though nuclear industry is mostly focused inside country-owner of a nuclear power plant (NPP), global cooperation is still inevitable.

As foreign economic activity (FEA) is implemented globally and not only in nuclear, but in each and every industry and business area, we may have misguiding thinking, that skills and knowledge related to FEA are easy to obtain and easy to develop. Unfortunately, FEA processes may be quite complicated which may lead to personnel errors during the implementation of these processes (supply, logistics, export control, contract drafting and signing, etc.).

This paper focuses on how to provide knowledge and develop skills for the company personnel involved in foreign economic activities, what are the main issues that may be faced by the personnel and how knowledge transfer may eliminate risks of those issues come true.

II. ROSATOM STATE ATOMIC ENERGY CORPORATION

State Atomic Energy Corporation Rosatom or ROSATOM is one the global technological leaders. It is a multi-industry holding comprising assets in power engineering, machine engineering and construction, among others. Having competencies across the entire nuclear fuel cycle, the corporation boasts the largest foreign project portfolio in the world with 35 power units at different stages of implementation in 12 countries. ROSATOM is the largest producer of electricity in Russia, ensuring over 20% of the country's energy needs. ROSATOM also ventures into manufacturing equipment and isotopes for nuclear medicine, does research, materials studies, digital products, manufactures various innovative nuclear and non-nuclear products. ROSATOM is engaged into low-carbon generation, including wind energy. The corporation includes about 400 enterprises and organizations employing a total of more than 250,000 people. Since October 2020, ROSATOM has been a member of the United Nations Global Compact, the largest corporate social responsibility and sustainable development initiative for businesses across the world.

Rusatom Service Joint Stock Company is a part of Rosatom Group and a corporate service integrator for foreign NPP support. The company offers wide range of services for NPP operation support, including consulting services related to export control issues. Rusatom Service not only assists with obtaining permitting documents for nuclear industry enterprises or with setting up business processes related to export control and foreign trade, but also conducts large personnel trainings. Rusatom Service leads projects with 16 foreign customers supporting 16 units in 38 countries.

The variety of activities and the focus on bringing new products to international markets leads to the urgent need to form diverse teams that quickly adapt to changing conditions and are able to transfer large amounts of information to new employees and project teams in a short time. To successfully achieve business goals and adapt personnel to the change of teams and functions – there must be a method for accumulating and transferring knowledge within ROSATOM (and Rusatom Service JSC).

III. RUSATOM SERVICE JSC FOREIGN ECONOMIC ACTIVITY

As Rusatom Service JSC is a decent player on the global market in nuclear, the company carries out a great amount of export annually.

Table 1. Export activity dynamics

Criteria	Rate / Description
The appearance of new export products, the expansion of the export nomenclature for the previous reporting year or	Implementation of the NPP commissioning activities (Republic of Turkey, Republic of Belarus); Implementation of the E-Learning course "Fundamentals of

types of work (services)	Modern Russian-designed NPPs with VVER-1200" (People's Republic of China) Republic of Turkey – implementation of activities in the areas of commissioning and training of operating personnel of Akkuyu NPP;
The appearance of new countries for export in the previous reporting year	People's Republic of Bangladesh – training of Ruppur NPP personnel; Republic of Belarus – commissioning of the Belarusian NPP;
Availability of export volume growth dynamics	The average annual absolute growth of exports over the past 5 years amounted to 21.95 million USD with an average annual growth rate of 48.5%

To carry out this amount of export successfully Rusatom Service needs highly qualified personnel. However, it is quite difficult to find one-hundred-percent matchable employee. That is why Rusatom Service JSC implements different knowledge transfer techniques, approved by the State Atomic Energy Corporation Rosatom as well as human resources (HR) management within the organization.

Since 2018 Rusatom Service JSC has faced significant growth of number of personnel. Volume of orders from the foreign customers increased which lead to the necessity of the employment of new personnel and development of new functions within the company. The graph below shows the growth of number of personnel.

Graph 1. Rusatom Service number of personnel growth

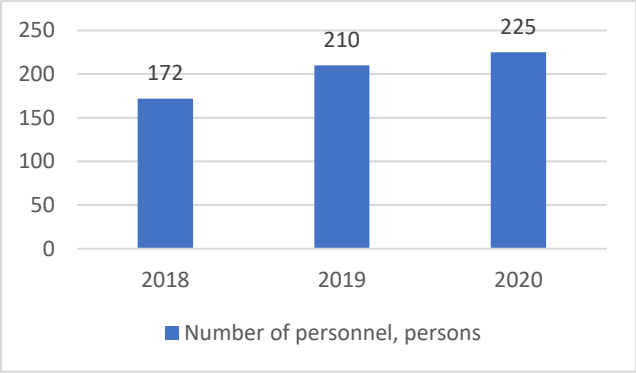

To adapt to the changing circumstances and to respond market demand Rusatom Service JSC uses human resources management technique – so called teams shuffle. A strong project lead can be switched to another function and a new team around this project lead is formed. For example, in 2019 due to the intention of the company to provide training services for NPP personnel, the Head of Division for supply of equipment, spare parts and technologies for Western and Central Europe was appointed to the position of Head of Training Projects Department. Since 2019 the team has grown up to 15 people, several large projects have been implemented including training for personnel of Akkuyu NPP (Turkey), Ruppur NPP (Bangladesh), Hanhikivi NPP (Finland). The urgent need of training was fully covered by the newly created team, so the new branch of services was implemented.

Another good example of implementation of mentioned HR management technique is transfer of the Head of Division for supply of equipment, spare parts and technologies for Western and Central Europe (was appointed right after the mentioned transfer of previous Head of Division) to the position of Head of Marketing and Development Division. Since 2020 Rusatom Service JSC has been actively promoting its new products on the international market. Now Marketing and Development Division includes 10 people, support in sales has been strengthened decently.

IV. KNOWLEDGE TRANSFER IN FEA IMPLEMENTED IN ROSATOM AND RUSATOM SERVICE

ROSATOM pays close attention to the professional development of the employees. The Corporation supports national universities, create corporate training organizations (Rosatom Corporate Academy), supports internal trainings on enterprise level, promotes mentioned trainings in case they may be useful for the Russian nuclear industry.

ROSATOM has built a training system, following the best international practices, and put in operation internal educational clusters. The main corporate institution is the Rosatom Academy with a developed training system for industry personnel. For training of foreign contractors, there is a Technical Academy, mainly focused on hard skills development.

A. Rosatom Corporate Academy

The Rosatom Academy has been in existence since 2012. During this time, the Academy has grown from an industry-wide educational organization to a reliable partner of Rosatom in implementing projects in support of business and has trained more than 496,000 employees. The key activities of the Academy are determined by the strategic priorities of the development of the nuclear industry.

Areas of expertise of the Rosatom Academy:

- change management
- corporate culture management
- career and succession management
- Rosatom production system
- work with young people
- executive development
- competencies of working and engineering personnel
- digital competencies and culture
- development of business competencies

Today, the Academy's portfolio includes 430 training programs that are aimed at solving specific industry

problems. In addition to training managers and specialists, employees, attracting talented graduates to the industry, as well as training a new generation of workers and engineers according to WorldSkills standards. the Academy implements projects aimed at developing the corporate culture, building the leadership potential of personnel.

B. Project Office “Fabrika”

On December 1, 2017, the company (Rusatom Service JSC) launched the "Fabrika" project, which aims to systematically train specialists with the appropriate set of skills and competencies.

"Fabrika" is an industry project for the training of novice specialists in the field of project management in the nuclear industry, which provides:

- participation in international projects;
- training at the Rosatom Corporate Academy;
- mentoring of experienced project managers;
- 2-year development program;
- at the end of the program – building a career in the Rusatom Service JSC.

The development of the project participants is organized according to the 70/20/10 talent management model, where 70 is development through direct implementation of tasks, 20 is training through exchange of experience, and 10 is training through trainings. In accordance with this model, a key role in the development of project participants is given to mentors – current managers and/or project managers of Rusatom Service JSC, to whom the interns are "transferred" to direct subordination.

Important aspect of the project is the ability to transfer from one department to another (rotation). Such a move provides an opportunity to get to know the company better, gain new knowledge and skills, and look at other business processes. The frequency of rotation is from 3 to 6 months. The project participants learn in practice the processes of participation in international tenders, contracting and management of small and medium-sized projects in the field of nuclear energy.

"Fabrika" project provides young specialists with opportunity to develop skills related to FEA by their direct involvement in RusAS FEA. Interns carry out supplies for foreign NPPs and implement all the supporting processes (negotiations with contractors, export control procedures, contract drafting, procurement, tax refund, etc.)

C. Rusatom Service JSC internal training

Rusatom Service JSC has internal trainings for its employees (both new and experienced), which are performed by the representatives of different departments and offices.

Firstly, for new employees RusAS has monthly “Newbie day” which includes several trainings related to basic FEA procedures and processes: procurement, contract drafting and signing, agreement development, work with primary accounting documentation.

Secondly, RusAS requires all the Project Managers and Project Leads involved in supply project complete training on export control. This training is offered in e-learning format (theory) and short practice days with the coach (practice), where the participators may ask question and study difficult cases in the field of export control. This training is offered once in a half a year.

Thirdly, Rusatom Service holds same training for procurement procedures (for experienced employees). The training is carried out in ZOOM (or similar app) or in training class with the coach.

Finally, Project Leads are responsible for the knowledge transfer in their teams, so they ensure that Project Managers, that they work together with, are familiar with the processes of supply chain in RusAS.

D. “FEA Specialist” training institute (Rusatom Service JSC)

Since 2021 Rusatom Service has been updating all the existing internal trainings and has been forming universal training for FEA specialist development. The program of this training consists of several topics:

- export control
- international transport logistics
- negotiations
- contract work support
- currency control
- financial and tax support

The training aims to deepen knowledge of the experienced employees in the field of foreign economic activity and to help new employees become involved in the company’s processes.

The training program is being created by the representatives of functional departments of RusAS as well as partners’ companies.

E. Gamification in trainings (Rusatom Service JSC)

To make trainings more effective and easier to understand Rusatom Service JSC implements gamification in learning process.

For example, to help RusAS employees understand the full supply chain and its compliance with the export control requirements Rusatom Service Export Control Department has created a board game.

The goal of the game is to be the first to implement a transaction with controlled goods and technologies, taking into account the requirements of export control.

The players will have to answer questions about export control and perform tasks on the board cells related to the supply of equipment or the implementation of services.

The game helps the players to understand what are the main stages of supply chain are and how to work with controlled goods and technologies legally.

The game mechanics is based on the Monopoly board game, players use dice and do rounds to finish the foreign economic deals. They move on the board and do the tasks provided on the board or answer questions in the field of export control. The goal of the game is to complete the foreign trade deal faster than other teams (teams play the role of an exporter of a particular goods/services).

F. Rusatom Service external trainings

The developed training system within the organization and the training circuit, as well as the available tools, allowed Rusatom Service to share its practices in a business way – as a result, the company has commercial projects: training external clients (starting from industry organization with ROSATOM to foreign customers).

Table 2. Training services growth

Criteria	Rate / Description
Annual growth of number of projects	11 projects for 2019 23 projects for 2020 Total: 34 projects for 2 years
Annual growth of trainees	15 trainees for 2019 83 trainees for 2020 Total: 98 trainees for 2 years
Annual growth of number of sold keys for distance training	50+ keys for 2020

Rusatom Service created several types of trainings related to export control. These trainings are:

- webinars
- workshops
- large training programs

Training structure as following:
- entry test (or interview): tricky topics are discovered; the trainer is aware what will need more attention.
- basic topics: each course program is formed before the training and is offered as a product.
- custom topics: are developed before the training according to the customer needs.
- final examination: test and interview before the certificate is granted.
- mentoring: after-course support offered after the graduation to maintain knowledge of the customers.

Training is offered in various formats:
- full-time training: lectures are given in a training class with the participation of a trainer, practical classes are held in a training class with the participation of a trainer. The final test is conducted in the classroom and includes written assignments and interviews with the trainer.
- online training: training is conducted in the online format; the lecture part is presented in the form of video recordings. The practical part is held as a video conference with the participation of the trainer. The final testing is conducted in the online format.
- combined training: the lecture part is presented in the format of video recordings. The practical part is held in the classroom with the participation of a trainer. The final test is conducted in the classroom and includes written assignments and interviews with the trainer.

Rusatom Service conducts trainings related to export control topics and foreign economic activity support:
- online training "Basics of export control"
- online training "International transport logistics"
- training Program: "Specialist in the field of export control"
- export control as compliance tool for international commitments and foreign economic activity
- export control: intangible transfer of technology. Organization of international educational and scientific activities in compliance with EC requirements
- export control: organization of an institution of certified export control specialists and independent identification centers
- foreign economic activity: rules of cross-border logistics and major customs procedures. Tools for compliance with international requirements.

V. Conclusion

This report shows that ROSATOM implements integrated approach for the development of training and knowledge transfer on the corporate management level as well as on the level of any industry organization under its governance. Organizations develop their own trainings and knowledge transfer systems according to the industry standards. ROSATOM successfully implements foreign best practices as well as shares its own. Internal training development leads to creation of new products, which will cover market demand, and increase of total revenue.

VI. References

[1] Rosatom Atomic Energy State Corporation website (www.rosatom.ru).

[2] Rusatom Service JSC website (www.rusatomservice.ru)

[3] Rosatom Academy website (www.rosatom-academy.ru)

Proceedings of the European Nuclear Young Generation Forum
ENYGF'21
September 27-30, 2021, Tarragona, Spain

Educational strategy for the management of nuclear knowledge

Llanes-Montesino, Luis Enrique[1*], López-Núñez, Arnaldo[2], García-Rodríguez, Berta[2], Meneses-López, Serguei[3]

Higher Institute of Technologies and Applied Sciences of University of Havana (InSTEC), Cuba.

*Corresponding author: *enrique@instec.cu*

I. INTRODUCTION

Nuclear knowledge management is a systematic and integrated method applied to all stages of the nuclear knowledge cycle, including its identification, sharing, protection, dissemination, preservation and the corresponding transfer to achieve specific objectives [1]. This management seeks to make explicit the greatest amount of implicit and tacit knowledge to safeguard information, protect institutional memory, train people and produce innovative knowledge, increasing the value of the organization [2]. The creation of networks constitutes a fundamental tool to achieve a better management of nuclear knowledge and in the case of Cuba it was defined, since mid-2018, as one of the national actions planned to fulfill the work commitments of the regional project with the International Atomic Energy Agency (IAEA), RLA 0057: *Improvement of Teaching, Training, Dissemination and Knowledge Management in the Nuclear Sphere*.

With the collaboration of the Higher Institute of Technologies and Applied Sciences of the University of Havana (InSTEC) and the Agency for Nuclear Energy and Advanced Technologies (AENTA), the impact that the foundation of a network that would promote a more active participation of young students and professionals in the sector in the promotion and development of nuclear applications was evaluated. This organization, in addition, would achieve progress towards integration to the nuclear activity of the latin-american region. Within this framework, and as our country is a member of the Latin American Young Nuclear Association (AJNL), the Cuban Youth Nuclear Network (JovNuC) was created in January, 2019, whose fundamental objective is to provide a space for the exchange of knowledge for dissemination and development of nuclear science and technologies for peaceful purposes, which allows integration among members from all over the country, as well as the implementation of projects and actions that result in benefits for cuban society and the region. The JovNuC network then identified the fundamental elements for the design of an educational strategy for nuclear knowledge management and a biannual action plan was conceived that responds to the needs of said strategy.

The scientific novelty is given by the very fact of the practical and effective application of said strategy based on the results that were verified after executing the action plan from the JovNuC Network during the years 2019 and 2020, including the challenges imposed by the COVID-19 in the last year.

II. DEVELOPMENT OF THE STRATEGY AND THE ACTION PLAN

A. Basic elements of the strategy

An effective knowledge management strategy combines three basic elements: people, processes and tools, operating within an organizational culture that recognizes the value of core knowledge [3, 4]. When designing the strategy, one of the key factors in its success is that its purpose responds to the challenges and objectives of the organization itself, but without forgetting the dynamics of exchange and collaboration with the environment that pose significant operational and cultural challenges. That is why it is necessary to articulate knowledge management strategies in a dynamic context that allow them to be adapted to the purpose, focus, reality and maturity of the organization [5, 6].

If the existing literature is reviewed, there are multiple criteria when defining the types of strategies, but in general they can be grouped into 8 large strategic groups depending on the objective they are aimed at and the characteristics of the organization (figure 1).

Figure 1. Strategy types in function of the objective and the characteristics of each organization.

Additionally, it must be added that, in general, the objectives to be achieved are only achieved with a mixed strategy, either because it changes in the type moving from one group to another, or simply because one serves as a support to another [2].

B. From the strategy to the national action plan proposed within the network

From the combination of the groups exposed above, the strategy proposal was based on the matrix described by García B. in 2017 as part of the development of a knowledge management strategy within the framework of technical cooperation [2]. This has as its final objective the creation of competences in specialists linked to the introduction of new technologies in an efficient manner, meaning "efficient" to achieve the result in the shortest possible time with a shortening of the learning curve, without geographical limits within the country and with a rational use of financial, human and technological resources. Taking as a basis the represented matrix, the national action plan was prepared, which was carried out by the JovNuC Network in 2019 and 2020. The essential aspects included in this action plan are presented below:

1.- Provide spaces for exchange for the dissemination of knowledge and the development of nuclear science and technology for peaceful purposes, which allows integration among members without gender distinction from an entire country, as well as the implementation of projects and actions that result in benefits for all.

2.- Carry out open house activities at cuban nuclear centers for 12th grade students and for those with a nuclear profile in their university studies.

3.- Articulate a network of circles of interest in various primary schools in the capital, as well as at other educational levels.

4.- Create digital platforms and social networks for the dissemination of knowledge and the promotion of events, workshops and the use of new nuclear technologies.

5.- Connect the work of the JovNuC with the fundamental communication media at the country, to offer more information and scientific dissemination to all types of public.

6.- Launch the bulletins of the JovNuC in printed and digital formats.

7.- Develop leadership and nuclear knowledge management workshops in universities and centers linked to the AENTA, which allow its participants to appropriate the basic tools of knowledge management.

8.- Promote events such as the International Youth Nuclear Congress (IYNC) 2018 and the 26th Women in Nuclear (WiN) Global Annual Conference, at the regional, national and rural and urban levels, which allow creating synergies between the most diverse members.

9.- Develop vocational guidance activities from an early age in schools, and in exact sciences pre-universities as the main quarries of the future nuclear generation.

10.- Conclude the development of a multimedia on nuclear applications for peaceful purposes in Cuba and in the world.

11.- Promote the implementation of monitoring and remediation activities on beaches, rivers and other ecosystems through the use of nuclear techniques.

III. RESULTS AND DISCUSSION

With the support of several cuban specialists and the leading role of a group of young people from both the nuclear sector and other areas that support the objectives of the network (communicators, designers, journalists), the implementation of the proposed actions was achieved. In this way, the official JovNuC pages on Facebook, Instagram and Twitter were concluded under a youth-friendly design, which have been highly useful for scientific spreading and interaction with various types of public. Currently these platforms exceed 700 followers and the publications that are uploaded reach more than 1,100 views. Also, the *Atoms for Peace* and *40th anniversary of InSTEC* competitions were launched, with the objectives of generating informative materials on nuclear applications and promoting scientific research in young people for the benefit of cuban society, respectively. Both contests had a high participation of young nuclear professionals and of other related sciences in the modality of informative and scientific poster.

On the other hand, links with the country's news media, among them Canal Educativo, Agencia Cubana de Noticias (ACN), Semanario Tribuna de La Habana, Revista Juventud Técnica were established, as well as with spaces for scientific dissemination that operate on Telegram such as *El Radical Libre*, *ConCienciAndo*, *Revista Encuentro con la Química* and the *Radioactive* podcast. These media have served as tools to disseminate and share information, allowing the people to whom they reach to appropriate knowledge and motivation, especially in the midst of the current conditions of isolation that COVID-19 has imposed; in addition, they have disclosed the winners of the competitions launched by JovNuC and have published interviews with young students and professionals in the sector, where their most diverse experiences are exposed.

Likewise, an open-door program was developed for the nuclear centers for twelfth-grade students, which positively awakens interest in nuclear sciences, which together with the InSTEC university extension project to increase the vocational orientation of the pre-university education students in the social contribution weeks demonstrated the network's ability to integrate and enrich the existing vocational structures and activities that reach the entire country. During 15 days each year in April, the university students are distributed by provinces and they are sent to carry out this task of orientation towards nuclear careers in pre-university schools. As a result, old stereotypes that cast doubt on the suitability of women to study a nuclear career have been broken. It was found that InSTEC received enrollments with the same or greater number of women than men in the last two academic courses.

During the 2018-2019 and part of the 2019-2020 periods several editions of the experiment fairs were held during which the institute (InSTEC) becomes a public space for exchange on the ways, ways and means of transmitting the scientific-technical work in the sector; an announcement is usually made through National Television and that weekend

many parents drive their children and also receive the information and talks. The day includes: exhibitions and surprising science experiments (physics and chemistry), talks and debates (for parents and children), cultural activities, launching and selling books, contests and participation games for the little ones and for adolescents and young people.

University fostered new spaces for discussions with specialists from the AENTA to offer updated information about nuclear networks and repositories, as well as the state of the art of the main nuclear techniques, taking advantage of the knowledge of cuban experts (figure 2). Knowledge fairs with physicochemical experiments were held, as well as a scientific forum in which young graduates from the nuclear sphere shared experiences and collective research. Documentaries and films by Marie Curie were screened: "Marie Curie, passages from her story" and "Marie Curie, a woman in the front line", which brings students closer to the life of the eminent scientist, and highlights the role of women in science.

Figure 2. Session of debate "nuclear knowledge transfers" with the expert Ing. Berta García (AENTA).

Circles of interest were created in 4 primary schools in the cuban capital, to awaken interest in science from an early age, specifically nuclear science. The smallest nuclear-themed puzzles and role-plays with the girls and boys were brought into the classroom, promoting the role of women in the scientific field (figure 3).

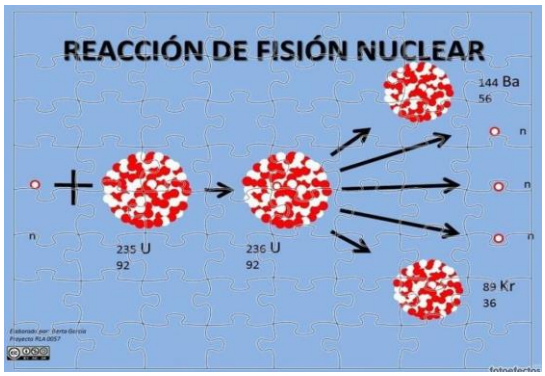

Figure 3. Puzzle example used in the circles of interest in primary schools of the cuban capital.

Young people from the nuclear sector had the opportunity to participate in the Workshop for New Leaders from Latin America and the Caribbean in fields related to nuclear technology, held in October-2019, where they received talks and conferences from renowned regional experts; the First National Workshop for Young People about Nuclear Applications was also held, within the framework of the first anniversary of JovNuC, in January-2020, which fulfilled one of the objectives of the network referred to creating spaces for young cubans (students and professionals) can develop and grow in the field of nuclear applications. That same year, on September, the network collaborated with the cuban chapter of WiN in organizing the "Stand up for Nuclear" event, allowing the online participation of various members of the network.

In the midst of the current epidemiological situation in Cuba and the rest of the world, whatsapp groups were created that bring together members of the network, students from 12th grade university colleges and other young people interested in supporting the work of JovNuC. These spaces function as types of work communities and in one of them the first multimedia on nuclear applications in our country is designed and assembled, taking advantage of ideas and collective knowledge. Additionally, news and information about foreign and international nuclear activities are shared, and enriching debates are held about new "ways of doing", more creative and more adapted to the changing scenarios in which we develop.

IV. LOOKS WITH FUTURE PERSPECTIVES

The Cuban Young Nuclear Network will continue to adapt its strategy in correspondence with the growing needs for a more active participation of our young students and professionals in the sector in the promotion and development of nuclear applications. In the immediate future, the actions are aimed at achieving the preparation of webinars, courses and other interactive online activities, together with InSTEC, AENTA and other centers in the sector, as well as creating a coordinated integration agenda with other nuclear youth networks of the Latin American region and the design of new digital materials (mobile applications) for nuclear science dissemination.

Looking to the future, the JovNuC network has identified as goals to be achieved in the coming years those related to strengthening the actions of the network in the Central and Eastern provinces of the country, generating the development of cooperation projects between centers and members. These projects would result benefits for all, promote the organization and development of informative campaigns at the national level on the peaceful uses of nuclear energy, among other issues, establish new alliances with universities, research centers, science-technology parks and other working groups that support the efficient actions of JovNuC.

V. CONCLUSIONS

Aware of the importance of nuclear knowledge management, the JovNuC network develops methodologies and collaborates with InSTEC, AENTA and other institutions to plan, design and implement nuclear knowledge management strategies and promote nuclear education in Cuba. The described strategy and the actions developed to execute it have a direct impact on the more active participation of young students and professionals in the sector in the promotion and development of nuclear applications. It connects the three basic elements involved in making knowledge management more effective, considering all the actors that make it possible from their experience. The results of the application of the action plan

proposed in the 19-20 period show the relevance of this strategy to achieve the objectives set by the JovNuC network. It is recommended to continue refining the strategy, adapting it to new scenarios.

VI. REFERENCES

[1] IAEA, "Managing Nuclear Knowledge"; Pocket Reference for Executives. IAEA, Vienna, Austria (2009).

[2] García Rodríguez, B., "Estrategia de gestión del conocimiento en el marco de la cooperación técnica", Segundo Simposio Internacional sobre Educación, Capacitación, Extensión y Gestión del Conocimiento en Tecnología Nuclear, Buenos Aires, Argentina (2017).

[3] IAEA, "Knowledge Management and Its Implementation in Nuclear Organizations", Nuclear Energy Series No. NG-T-6.10. Accessed on: June 20, 2021. [Online]. Available: http://www.iaea.org/Publications/index.html (2016).

[4] Martín del Campo, C., "La importancia de la gestión del conocimiento nuclear en la formación de profesionales", Simposio Internacional sobre Educación, Capacitación y Gestión del Conocimiento en Energía Nuclear y sus Aplicaciones, Facultad de Ingeniería, Universidad Nacional Autónoma de México (2015).

[5] IAEA, "Interactive Training Course on Nuclear Knowledge Management", Part 1. Training Course Series 43, Vienna, Austria (2010).

[6] Yanev Y-Head KM Unit, "Nuclear Knowledge Management. A review of achievements, recommendations and framework for future development". Prepared for WATEC 2005 meeting. IAEA, Vienna, Austria (2005)

Proceedings of the European Nuclear Young Generation Forum
ENYGF'21
September 27-30, 2021, Tarragona, Spain

RADIOMON – Isotopes, radiation and nuclear technologies in a new game for the i-Generation

Nouchy, Fabio[1*], Dandoy, Florence[1] and Coeck, Michèle[2]

[1] Tractebel Engie, Belgium; [2] Belgian Nuclear Research Centre (SCK CEN), Belgium

*Corresponding author: *fabio.nouchy@tractebel.engie.com*

I. INTRODUCTION

In these last decades, the word "nuclear" has often been connected to negative connotations by the general public in a popular thinking. The use of nuclear technology for warfare purposes has not yet been forgotten, and the many benefits brought by its peaceful use for electricity production are overshadowed by accidents [1]. As an additional factor, nuclear physics and associated technologies are seldom easy to understand; whilst sciences of macroscopical phenomena can often be spectacular, the effects of decay, fission, fusion or other nuclear phenomena are intangible, odourless and not even visible with microscopes. These characteristics demand even more abstract thinking, which can be, without appropriate guidance, a difficult exercise for many students. The already small population of potential STEM (Science, Technology, Engineering, and Mathematics) pupils and students are often left unaware of this field as they are not broadly introduced to nuclear science and technologies in their secondary school studies and do not have means to visualize the physics. These youngsters would rather turn their attention to either more popular technologies for the same purpose, e.g. wind turbines, which is socially accepted as a good technology to combat climate change, or more sensational, e.g. rocket engineering if they are attracted by exciting challenges.

Nowadays, innovative video materials succeed in visualizing nuclear phenomena and more investment could be allocated for developing these tools into teaching means for complex concepts. Indeed, the target group of these media is intended to be large and in certain cases they succeed in reaching a large population, as for example [2].

Nonetheless, within the large amount of media material available on the social networks, the impact is not enough and cannot be compared to the direct effect that the perspective of a Mars exploration can have on a young mind.

The authors of this paper share a wish to attempt broadening the circle of people that could have an interest in nuclear physics while rendering the topic more popular. The objective is to find a way to reach a large population among those promising young pupils and students that still have to choose their study and career path.

The possibilities to integrate nuclear phenomena into a videogame have been explored. The direct objective is therefore to teach to the younger generations basic nuclear and radiation physics and to let them discover nuclear technologies in the fun environment of a videogame, without stressing the learning possibilities when distributing the product but accurately integrating them and declaring them as such. The primary target group are teenagers, for which videogames are an effective means to reach a large population, but by extension the game can be played by all age categories. The other reason for which videogames are chosen is their potential to visualize phenomena such as radiation decay and elements such as radionuclides in an attractive and accessible way, as they benefit from artistic freedom. At the same time the player learns-by-doing, if the game is designed such that the game's objectives are aligned with the learning objectives.

II. DISCUSSION ON EXPLORED OPTIONS

One of the most popular options to attempt a connection between the subject and the mean is to insert the danger of radiations into a realistic **action game** (i.e. games with one main character in first person carrying out different tasks/quests), which would make an interesting concept allowing to discover technologies and learn radiation protection in a simulated environment. Nonetheless, it remains a limited approach, highlighting the negative effects of radiations, which we do not strive for, and moreover it has already been adopted in the past. The most significative and popular game that has already integrated the danger of radiations is undoubtedly Fallout, where the main character would roam in areas that may be highly radioactive, measuring the radiation levels with a Geiger counter and collect a radiation dose (fairly measured in *rad*) that affects the skills of the character. To render the concept "playable" though, several features were invented, as the possibility to remove *rad* by taking medicines, or that

people, instead of dying of radiation sickness, would become ghouls, zombie-like creatures that may even glow. Indeed, the whole environment was reflecting a post-nuclear-war apocalypse wasteland.

Besides the simplifications, that are justified for playability reasons, this sort of apocalyptic vision created by Fallout is feeding the common negative perception on nuclear, which we intend to counteract.

Therefore, we discarded any inclusion of radiation into post-apocalyptic scenarios.

Some games were specifically created to simulate nuclear reactor functioning or the environment of Chernobyl after the accident, with a concept similar to Fallout. These games remain for niche public and most present the negative connotation too. The desired setup is rather the one of a more casual game, which is accessible for all and especially for those who desire to have some fun without investing too much time in the game.

Theoretically, any action game could host radiations, even **platform games** as Super Mario or **sandbox games** as Minecraft, and indeed choosing a successful franchise would maximize and guarantee the reach. The obstacle found on this path is to contact the major producers of such videogames and, even if we surmounted such obstacle, convincing them of the added value of integrating radiation for the game itself and avoiding another title as “Fallout” (especially in terms of invented facts) are even bigger risks that we cannot face at this stage.

Developing an original game is the best solution to avoid unwished twists of reality. The option of realistic action games becomes though unaffordable, as such games require a big effort in terms of resources. Qualitatively, the cost of a game as a function of the development complexity follows an exponential trend [3].

A more abstract and artistic idea consists in the attempt to visualize nuclear phenomena and give a face to radionuclides. As each radionuclide has its own characteristics (atomic number, size, half-life, decay types, energies of emitted particles, cross-sections) one can imagine that each of them represents a separate character, with its own features and personality. This leads to a direct association to a very popular franchise that also produced videogames, i.e. Pokémon.

Pokémon is categorized as a “**monster-collection Role Playing Game (RPG)**” and it has inspired similar concepts along the years. We argue here that their success is connected to the aspect of collection. At the light of this incredible success, the following question was raised: why inventing imaginary characters when nature offers us the chart of nuclides?

Radiomon is a concept loosely inspired by Pokémon, that will probably become a mix between a monster-collection RPG and a strategy game, as the player will have to choose in advance the best Radiomons from the collection.

Lastly, the choice of the platform on which the game will be developed is driven by the wish of greatest accessibility to a large audience, which nowadays is guaranteed on mobile applications for free download. This is supported by the data retrieved from the gaming industry [4], that indicate an important rise in the mobile gaming section of the market, leading us to focus on a game supported by a mobile app.

III. Retained approach

In Pokémon the characters are evolving thanks to the experience gained in battles: each of them has one or more types of attack, with associated attack points, and to protect itself from the adversary it has defence points and, together with its life points, the resilience to the adversaries’ attacks is determined.

Few of these properties can be associated to Radiomon properties: types of attack are decay types and attack points are decay energies. Their evolution occurs via decay after a specific time or particle capture, which is intrinsically defined by a property called the "cross-section". These three properties (decay time, decay energy and cross-section) make the concept viable for a time-driven game in which the mastery of the cross-section will allow the player to trigger the best physical effects to win the game. Indeed, it is by activating Radiomons that decay energy is emitted against the target.

With this basic concept, the purpose can be flexible, let it be a fight between two teams of Radiomons or a task of sending the decay energies towards a target as a tumour cell in the allotted time. At this stage, the project is consulting with game developers to determine the best goal for the player.

As the concept should be synonymous of fun, consistently with a casual game, we identify here below the elements that we think will bring joy to the player:

- Collection: there are more than 100 elements and potentially hundreds of radionuclides – the objective to have a full collection of characters can be the main drive for the player.

- Hitting the spot: sending a ball to a goal is the most popular form of entertainment in the world. In this game: the ball is the incoming particle and the goal is the cross-section.

- Fun visuals: all nuclear phenomena being invisible, they can be visualized in an entertaining manner without restrictions associated to reality.

- Storytelling: we are preparing to important discussions with the developer to include a story-telling that may link the game to the discovery of technology and history, through dedicated missions to accomplish or modes of collecting the Radiomons.

In the most basic concept of the game, the player can carry out the following actions: the choice of the Radiomons based on the acquired collection, their activation by “feeding” them a neutron and the use of shielding equipment, which is consistent with the concept of a casual game. Nonetheless, to be more successful in the game, the knowledge of the three properties (decay time, decay energy and cross section) is a must. This has the purpose of stimulating the curiosity of all the players which, in order to win, will gladly try to remember by heart which Radiomon

has a higher fission cross-section or most energetic gamma rays, for example.

G. Learning objectives

This leads us to list the learning objectives of the basic concept into 3 categories:

- nuclear physics, the properties of the Radiomons.

- radiation protection: as the decay particles are sent, they can be stopped interacting with the environment, which will be used to let the player learn basic concepts of radiation protection in the game.

- chemical compositions: one last important aspect to be addressed by this game is the association of the Radiomons to the reality. The player should not lose contact with the context of the game, lest he/she will start thinking about magics rather than nuclear physics. The collection method within the game will therefore be linking real-life objects, either common or specific technologies, with the Radiomons. E.g., from water one can extract two hydrogens and an oxygen, while inside a nuclear fuel pellet the same oxygen can be found together with uranium.

To assess if the player actually learns the three aspects (nuclear physics, radiation protection and chemical composition), we will use the game prototype together with a "before and after" test.

IV. Challenges

The main challenge identified for this project is the market competition: a game has to be a flawless, attractive and engaging product and many other games in the market have these characteristics. The necessary condition is therefore to achieve a high quality gameplay within the final product. In fact, although the game concept is rather unique, the choice of mobile games in the app store is such that the average player will tend to choose only the most popular options, i.e. high rating and number of downloads. The associated risk of a failure is the loss of investment and a lower-than-expected reach among players.

Among the major goals of the concept there is to visualize the radionuclides in an impactful way: inspiration for this goal is the famous cartoon series "Il était une fois…la vie" from 1987 [5], where the human cells were "humanized" to explain how the human body works. The challenge here is to create meaningful representations of the Radiomons, easily recognizable, and conceptually consistent with their nature: all gases shall have similar look, all metals shall have a shiny appearance, stable nuclides will look dormant while radioactive ones distressed, the cross-section can represent a visual feature of the nuclides, and so on.

Simplification of reality is inevitable in games and this concept is not left untouched. For playability purposes, the following points are necessary simplifications:

- the decay time is a fixed time rather than a half-life,
- decay particles don't scatter in air and travel "forward" undisturbed in a straight line until the target,
- the number of decay and capture modes will be limited and the energy dependence minimized,
- sizes and distances are adapted to the dynamics of the game.

For each of these points additional media material, e.g. edutainment videos, should be created to explain the reality and why it has been modified within the game.

Finally, the objective to realize a profitable product which is educative and realistic on one hand while presented as a casual game on the other hand does not have many precedents and it will require a good and balanced effort between conceptualization, development, marketing and dissemination.

V. Roadmap and long term vision

The project has concluded an exploration phase where the interest of nuclear organisations was confirmed and possible developers were consulted.

In the current phase, the definition phase, the high level concept has been completed and presented for discussion to stakeholders and developers, with the objective to obtain a prototype version to be tested before proceeding into the full development of the product.

During an acceleration phase we will therefore determine the basis for the product that will be commercialised at the end of the next phase.

The flexibility of the concept proposed allows a scaling-up of the concept, where we could twist or adapt the product into other versions with a more educational purposes or other dedicated tasks. The long term vision is therefore not limited to one videogame but rather a properly developed franchise to open up infinite possibilities of different story lines where all the different facets of nuclear science and technologies could be addressed.

VI. Conclusion

Having debated the possible benefits that a game for a broad population would bring to both the society and the nuclear scene, this project is of high interest. The major challenge being found within the market competition, the necessary condition for a success is the high quality of the product. We call for an extended collaboration among the nuclear organisations to share the risks as the benefits will be common for all. Our original approach relies on the support of experienced game developers and, most importantly, the cooperation of numerous nuclear stakeholders for this effort of creating, branding and spreading a product that would have the ambition of "giving a face" to all the radionuclides and decay particles and give visibility to nuclear technologies to benefit the whole nuclear industry, healthcare and research organisations.

Acknowledgement

This project could not be started without the Innovation Lab within Tractebel, nor without the first interest shown by, in chronological order, Foratom, the Belgian Nuclear Forum, the Nuclear Skills Strategy Group (UK), the SCK CEN Academy, Engie Talent development and Gaston Meskens and Adrian Bull for their precious insights, the SFEN-JG together to all the individuals that showed interest in the development of such concept. Last but not least, the

European Enterprise Network allowed us to get in contact with more than 30 videogame developers, that may one day develop the first version of the game.

VII. References

[1] Y. Yan, F. Lu, "A Survey and Analysis on the Sense of Nuclear Safety & Security for the Public: A Chinese Perspective", in *Sustainability* **2018**, 10, 2495; doi:10.3390/su10072495

[2] M. Anticole, *Is radiation dangerous?*, TED-Ed, March 14, 2016. Accessed on: June 9, 2021. [Online]. Available: https://www.youtube.com/watch?v=zI2vRwFKnHQ

[3] D. Tryfanava, *How much does it cost to make a video game?*, VironIT, June 19, 2018. Accessed on: June 9, 2021. [Online]. Available: https://vironit.com/how-much-does-it-cost-to-make-a-video-game/

[4] ISFE, *Key Facts 2020*, ISFE Europe's Video Games Industry, 2020. Accessed on: June 9, 2021. [Online]. Available: https://www.isfe.eu/wp-content/uploads/2020/08/ISFE-final-1.pdf

[5] Hello Maestro, *Once upon a time... Life*, Hello Maestro!, 2021. Accessed on: June 9, 2021. [Online]. Available: http://www.hellomaestro.fr/en/all-hello-maestro-videos-are-here

Proceedings of the European Nuclear Young Generation Forum

ENYGF'21

September 27-30, 2021, Tarragona, Spain

Energy Transition: The Role of Nuclear Education

Di Trapani, Antonella[1*], Obisesan, Kathryn[1*] and Solà Martínez, Roger[1*]

[1] Organisation for Economic Co-operation and Development Nuclear Energy Agency (OECD NEA), France

*Corresponding authors: *Antonella.Ditrapani@oecd-nea.org; Kathryn.Obisesan@oecd-nea.org; Roger.SolaMartinez@oecd-nea.org*

I. INTRODUCTION

Global demand for energy is increasing rapidly, because ofpopulation and economic growth, especially in emerging market economies. While accompanied by greaterprosperity, rising demand creates new challenges [1].

Energy security concerns can emerge, as more consumers require ever more energy resources. In addition, higher consumption of fossil fuels leads to higher greenhouse gas emissions, particularly carbon dioxide (CO2), which contribute to global warming. At the same time, the number of people without access to electricity remains unacceptably high.

However, such challenges can create opportunities. A sustainable energy future will require new thinking and new systems – essentially a transformation in the way we produce, deliver and consume energy. If our goal is to raise living standards, provide access to modern energy services, use energy more efficiently, protect the global environment and ensure reliable energy supplies, green growth must playa key role.

Access to affordable, reliable and clean energy is crucial for achieving sustainable development goals, from eradicating poverty through to advancing health and education, to facilitating industrial development and reducing greenhousegas emissions. Nuclear power — alongside other technologies — can provide the energy to ultimately achieve high living standards, good health, a cleanenvironment, and a sustainable economy [2].

With the recognition of the role of nuclear in the de-carbonization and in view of the 26th UN Climate Change Conference of the Parties, COP26, nuclear is back on the agenda of many governments and policymakers. And because of this, it is becoming even more important to maintain the expertise to understand the old technologies and cultivate experts who will foster new innovation in light of these challenges, even for countries with no nuclear power.

In 2000, the Organisation for Economic Co-operation and Development Nuclear Energy Agency (OECD NEA) published *Nuclear Education and Training: Cause for Concern?*, which, for the first time, drew attention to the likelihood of insufficient human resources to support nuclear power plant operations, the decommissioning of existing nuclear facilities and foreseeable developments [3].

In other words, nuclear energy is an indispensable tool for achieving the global sustainable development agenda [4], and skilled human resource is a vital first step in ensuring asustainable supply of qualified personnel for the safe, responsible and sustainable use of nuclear technologies [5].

Academic institutions across NEA member countries play an important role in this regard, not only nurturing the next generation of nuclear experts and creating the talent pipeline necessary for the sustainability of the nuclear sector, but also providing solutions to complex and emerging issues and challenges, which affect the nuclear energy sector through their research and expertise.

However, NEA member countries have expressed concerns about lack of graduates with the required skills to enter the job market and difficulties in transferring the knowledge, which have been accumulated by the current workforce.

In this paper, we will present the main instruments developed by the NEA to address the challenges of NEA member countries in developing nuclear experts and stress the important role of nuclear education towards the energy transition.

II. CURRENT STATUS AND DEVELOPMENT

The NEA launched the Nuclear Education, Skills and Technology (NEST) Framework, in partnership with its member countries, to help address important gaps in nuclear skills capacity building, knowledge transfer and technical innovation in an international context. It entered into force on the 15 February 2019.

The NEST Framework is a multilateral initiative, which, through international collaborative research projects, trains and facilitates the skills development and training of the next generation of nuclear professionals.

This framework brings together a variety of pertinent actors in nuclear including but not limited to academia, research institutions, technical support organizations (TSOs), regulators and industry. The main objective of NEST is to foster a new generation of nuclear experts and leaders by transmitting practical knowledge and offering hands-on training in several nucleardisciplines and fields. The young generation of Fellows (Master, PhD students and young professionals) could gain skills and competences related to reactor safety, small modular reactor (SMR) design, decommissioning and radioactive waste management to nuclear medicine and radiological protection.

At the heart of the NEST Framework are multinational and multidisciplinary projects. NEST projects should meet specific education and skills development needs and be embedded into real-world context as well as addressing challenging problems of industry and/or regulatory bodies. A NEST project has to involve Fellows from at least three different NEST countries. Fig. 1 illustrates the main principles of the NEST Projects.

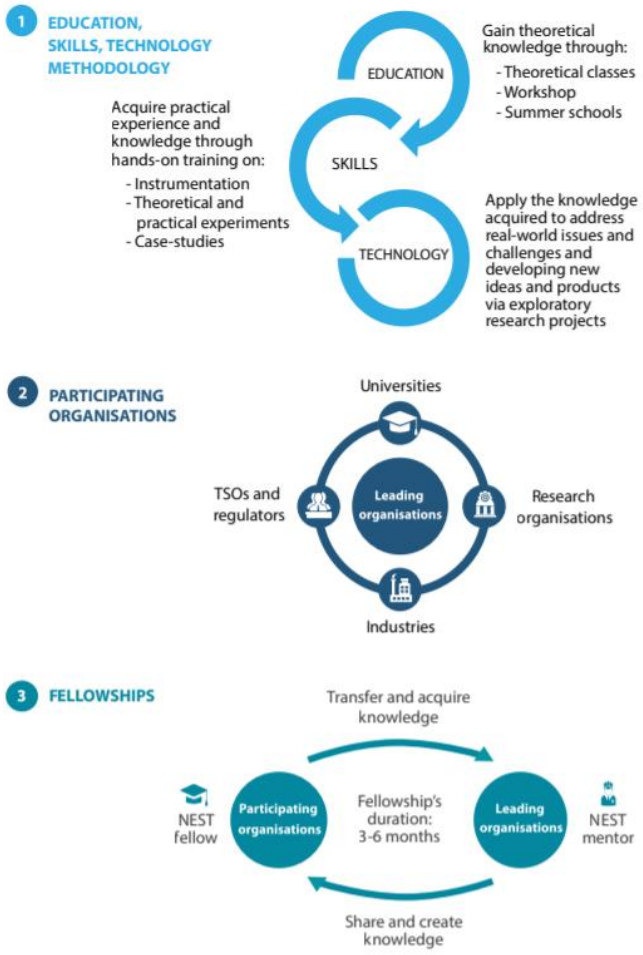

Figure 1. NEST: how it works [6].

Each NEST Fellow is assigned a NEST Mentor, who is an expert and leader in the field, from whom the knowledge will be transferred from.

Once the fellow goes back to their own home institution, they continue to work under adequate mentorship on an exploratory research project. The research activity will be developed in the home organisation in tight connection with other fellows working in the same NEST Project along with mentors from the participating organisation to provide necessary guidance and develop new skills and competences. That could eventually lead to new ideas and new technologies. The Fellows will also participate in educational activities such as workshops and summer schools to broaden their knowledge of the nuclear field.

On another note, over the years, the NEA has had little direct engagement with academic institutions that are responsible for developing the next generation of nuclear science and technology experts. Furthermore, these academic institutions lack a global platform to exchange experiences and co-operate towards common goals.

To address these gaps, the NEA has recently established the NEA Global Forum on Nuclear Education, Science, Technology and Policy, which entered into force on 28 January 2021.

The Global Forum on Nuclear Education, Science, Technology and Policy is led by a Council of Advisors comprised of representatives from approximately 20 academic institutions in NEA member countries. The Council of Advisors' role is to define the programme of work and working areas for the Global Forum, identify good practices, facilitate shared activities, co-ordinate joint programmes of educational innovation, and oversee the work and outputs of the Working Groups.

These two education activities at the NEA aim to recognise and cultivate the important of human capacity building and knowledge management for the continued development and advancement of nuclear.

III. RESULTS

NEST and the Global Forum are at the forefront of the co-operation in nuclear education and capacity building required to address the most important challenges society is facing today: fostering a new generation of nuclear leaders and to engage with them in topics of relevance such as the climate change mitigation.

While the NEST Framework will work more on developing skills for the young generation, the Global Forum will promote and develop policies related to global challenges.

The NEST Framework, albeit in its early stage, has already achieved international recognition as the main instrument for NEA member countries to train a new generation of leaders and experts. Thirteen Fellows participated in NESTFellowships in 2019-2020 and thirty-two Fellows attended the NEST online SMR Hackathon in August 2020.

Among all the NEST Projects, the NEST Small Modular Reactors Project plays an important role in the energy transition and the future deployment of SMR technologies globally. In the SMR Hackathon, the Fellows examined innovative aspects of SMR technology. What was unique, within this event, was that the Hackathon brought together the traditional science and engineering technologies with social and political science aspects.

Building on the success of the 2020 SMR Hackathon, this year will take place the 2021 SMR Prize Competition, where

the ultimate goal of the students is to create a novel, optimised deployment scenario for using an advanced reactor (any reactor design newer than Generation II/III Light Water Reactors) to support an industrial use that requires combined heat and power.

The benefits offered by the NEST Framework have been lately discussed during a NEA WebChat with NEST Fellows organised on 8 April 2021. The WebChat highlighted the importance of cultivating the next generation of nuclear experts. The discussion focused on the important role of education, training, and knowledge management to the nuclear sector. NEST Fellows shared the value of their experience and remarked that its main benefit was "achieving a better understanding of the international nuclear community and the career opportunities in the global nuclear sector." [7]

The Global Forum on Nuclear Education, Science, Technology and Policy has already identified areas of work: education, society, innovation, and gender balance. In addition, it has proposed to further investigate the integration of disruptive technologies as a working area of the Forum.

On June 4, 2021, the first official Global Forum event was held to celebrate and recognise students for their accomplishments. The NEA under the auspices of the Global Forum hosted the Global Commencement for Nuclear Science and Engineering under the theme ''the role of early nuclear graduates in addressing climate change''. The Commencement featured nuclear professionals and experts to share their insights with students and offer them recognition for the completion of their nuclear degree. The event had 300 individuals signed up and featured renowned and young generation speakers who delivered lectures stressing the important role nuclear energy has, together with variable renewables, in addressing climate change mitigation if the Paris Agreement goals have to be met. It was stressed how nuclear energy is also a safe, secure source of energy and provides stable career paths and opportunities for young graduates. Attracting the future young generation to nuclear degrees and careers is a major challenge for all countries. Dr James E. Hansen sent a powerful message to the class of 2021 advising young students who are uncertain about their future career path to consider choosing nuclear degrees in order to contribute to ''making life better for people, and helping restoring a healthy climate''. [8]

There was a common thread running through all the speakers: today's graduates in the nuclear science and technology fields will play a large role in decarbonising the electricity sector and paving the way for a clean energy future.

NEST and the Global Forum are two new NEA initiatives but have collectively already hosted a number of impactful events, and activities. In the future, they will continue to co-ordinate collaborative work to advance the education of the future nuclear work force.

IV. CONCLUSIONS

In this paper we examined how the role of nuclear education is vital to the energy transition and building a talent pipelinein any sector requires long-term investment and strategic vision. Both NEA initiatives contribute greatly to promote nuclear education and capacity building as a driver for the energy transition. Experts are necessary to develop new technologies and maintain long-term understandings for long-term operations. Thus, each country, independent of their nuclear power status, needs qualified personnel, experts and leaders. None of this will be possible without strengthening the countries' nuclear education and capacity building systems. NEA, through these initiatives, is helpingits member countries to achieve these goals.

NEST, in particular, has shown that it helps the young generation, who is quintessential in nuclear future role in global energy systems, with the opportunity to build their international network, develop important technical and non-technical skills and apply nuclear knowledge to address real-world issues.

The Global Forum will help to shape policies to addressing collectively global challenges society is facing, such as climate change, and where the contribution nuclear education will have an important role to play.

V. ACKNOWLEDGEMENTS

We would like to offer our thanks to NEA member countries in acknowledging the important role nuclear education has in the nuclear energy sector. A particular thank goes to the NEST Management Board and to the Global Forum Council of Advisors in leading these initiatives.

VI. References

[1] OECD, IEA "OECD Green Growth Studies – Energy," 2011

[2] IAEA, "Nuclear Power for Sustainable Development" 2017

[3] OECD/NEA, "Nuclear Education and Training: Cause for Concern?" 2000

[4] UN "Application of the United Nations Framework Classification for Resources and the United Nations Resource Management System: The Role of Nuclear Energy in Sustainable Development - Entry Pathways" 2020

[5] F Alam, R Sarkar, H Chowdhury, "Nuclear Power Plants in Emerging Economies and Human Resource Development: A review" 2019

[6] OECD/NEA, "Strategic Plan 2019-2021 and Beyond" 2021

OECD/NEA, "NEA WebChat with NEST Fellows Larissa Shasko and Stephen King" 2021*INTRO*

Dfjskj

ENYGF
TARRAGONA '21